Comparative Analysis of Microwave Link Using Space and Hybrid Diversity Configuration on Mountain Topography Area

Ade Wahyudin[1], Alfin Hikmaturokhman[2]
[1]*Sekolah Tinggi Multi Media Yogyakarta*
[2]*Institut Teknologi Telkom Purwokerto*
[1]*Jalan Magelang Km. 6 Yogyakarta 55284, Indonesia*
[2]*Jl. D. I. Panjaitan No. 128 Purwokerto 53147, Jawa Tengah, Indonesia*
Email: [1]adew001@kominfo.go.id, [2]alfin@ittelkom-pwt.ac.id

ARTICLE INFORMATION

Received on 27 December 2020
Revised on 8 August 2021
Accepted on 13 August 2021

Keywords:
Space Diversity
Hybrid Diversity
Availability
Microwave
Mountain

ABSTRACT

The penetration of telecommunication infrastructure in Indonesia is growing significantly every year. However, this growth is not comparable to the technology distribution in remote areas, especially areas with mountainous contours. So it takes a proper backhaul network design to deploy telecommunication services in remote areas. Microwave transmission technology is widely used as a backhaul network in mountainous areas. However, multipath fading becomes a problem in microwave communication, so we use the diversity configuration approach to solve it. Space diversity configurations are the system most often used, but in more extreme conditions it can use a hybrid diversity configuration, a combination of space and frequency diversity. In this study, we design and compare the performance of two types of diversity configurations, namely space and hybrid diversity in cross-mountainous areas using simulation software Pathloss 5.0. Before comparison, these paths are tested with a point-to-point configuration to assess the communication performance using a microwave link. Based on the simulation, the resulting cross-mountain microwave communication performance using point-to-point configuration results in 99.98179% availability and 5742.79 seconds unavailability in one year. These values are still far from the ITU-T G.821 standard, namely 99.99% availability. In the configuration using Space Diversity, the quality has increased. Still, it cannot meet ITU standards because it can only produce 99.98333% to 99.98943% availability or comparable to un-availability for 5255.53 to 3332.48 seconds/year. Meanwhile, the hybrid diversity configuration can produce a performance that meets ITU standards with availability of 99.99122% or equivalent to un-availability for 2769.79 seconds per year.

1. Introduction

The growth of telecommunication and ICT infrastructure and services in Indonesia increasing rapidly, resulting in the need for adequate infrastructure both in quality and capacity. This is due to the growth of ICT service users in Indonesia, which is increasing significantly up to 10.12% per year (Badan Pusat Statistik, 2018). Therefore, the development of telecommunications infrastructure is the key to the increasing penetration and equitable deployment of ICT infrastructure and services in all regions of Indonesia.

In terms of deploying ICT infrastructure, geographically, Indonesia has an archipelago as well as a row of hills and mountains, so it requires good planning. Palapa Ring is expected to support the access network, backhaul to the backbone of ICT services throughout Indonesia (Kementerian Komunikasi dan Informatika, 2013). However, not all areas in Indonesia can be supported by fiber optics. Mountainous and remote areas still use other suitable communication media such as satellites and microwaves. Microwave communication has an important role in ICT infrastructure deployment, especially remote and extreme topology areas that are impossible to reach by fiber optic (Hikmaturokhman & Wahyudin, 2018). So that to overcome the obstacles caused by geographical conditions, a proper microwave link design is needed.

This technology uses electromagnetic waves that have micro wavelengths or are called microwaves and antennas as a means to transmit signals so they can be used to communicate (Hikmaturokhman et al., 2017). Microwave radio communication systems play an important role in cellular communication systems, especially in point-to-point backhaul communication between Base Stations or Base Stations Towards a Radio Access Network (RAN). The basic configuration of a microwave communication system is point-to-point, which consists of a transmitter and a receiver as a medium for sending and receiving signals (Kizer, 2013). The process of propagating from the transmitting antenna to the receiving antenna, radio waves through various paths with some propagation paths. The basic mechanism of microwave communication is the Line of Sight (LOS), a condition where the transmitter and the receiver can be directly connected without any obstacles, as illustrated in Figure 1.

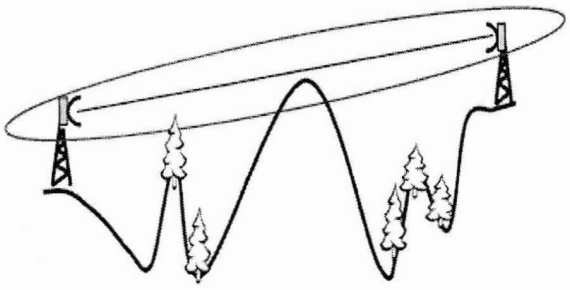

Figure 1. Line of sight communication (Hikmaturrokhman & Wahyudin, 2018)

In this research, the microwave link deployed across a mountain range on South Sulawesi Province, connecting a network between the Kaleakan site in North Toraja District to the Walenrang site in Luwu District. Because this communication path is in a mountainous area with an average altitude range from 2000 to 3000 meters above sea level, the possibility of disturbance is very high. The most likely disturbance is transmitted signal allows for transmission loss due to multipath fading. Multipath fading is a disturbance caused by multiple signal trajectories caused by reflection, refraction, diffraction, and scattering in signal propagation (Dewanti et al., 2017).

The method to anticipate multipath fading is space diversity, which is one of several wireless diversity schemes that use two or more antennas to increase the quality and reliability of the system (Freeman, 2007). The conventional space diversity configuration uses one additional antenna that acts as a receiver, which is used to amplify the signal received from multipath. In addition to the Space Diversity configuration, there is a Hybrid Diversity configuration that combines Space Diversity and Frequency Diversity. So, it can amplify the signal and has a longer range, but Hybrid Diversity has very expensive costs to deploy (Wahyudin & Hikmaturokhman, 2021).

The main indicator of microwave implementation is system reliability, represented in the value of availability or unavailability (Oktaviasari et al., 2018). This indicator can determine the condition of system performance and can see the system's reliability. The greater the availability value obtained, the better the quality given. So, if observed from a geographic point of view, it is also very necessary to select and use a good antenna and system design (Lehpamer, 2010).

So based on the background, the author is interested in studying the research with the title "Comparative Analysis of Microwave Link Using Space and Hybrid Diversity Configuration on Mountain Topography Area", where the authors designed a microwave radio transmission network in remote areas in the mountains, Toraja, South Sulawesi. The point-to-point antenna configuration is designed in advance to show the performance of microwave radio transmission networks without diversity. The diversity configuration is

designed to compare the performance of two antenna diversity configurations, namely Space diversity and Hybrid Diversity, then compare and analyze the design simulation results and parameters such as Availability, Unavailability, Free Space Loss, EIRP, RSL, and Fading Margin.

2. Literature Review

2.1. Previous Works

Based on previous research about the use of space diversity in a suburban area, conclude the availability of microwave links can increase up to a value of 99.9999%. Also, the highest diversity receives signal was obtained at 200λ, with the value of diversity receive signal is -83.94 dBm. Thus, the further distance between the antennas, the higher diversity of receive signal (Pradana & Wahyudin, 2018). In another study about the use of frequency diversity in the ocean's topology concluded that the value of reliability or system availability that uses frequency diversity is 99.96879%, with an outage time of 8603.03 seconds/year (Rahmawati & Wahyudin, 2018). While the research on the use of space and hybrid diversity in the ocean shows that both of the configurations resulting in an excellent quality of communication in terms of availability and fading margin (Wahyudin & Hikmaturokhman, 2021).

2.2. Atmospheric Effect in Microwave Communication System

The atmospheric effect such as temperature, humidity, and rain are the effects that occur in the earth's atmosphere. Raindrops cause attenuation to electromagnetic waves. The heavier the rain, the greater the attenuation. The consequence of the atmospheric effect in microwave communication is the occurrence of absorption, refraction, and ducting (Hikmaturokhman et al., 2017). Absorption is caused by oxygen in the atmosphere, rain, and fog. It causes the energy propagated to experience attenuation. The oxygen in the atmosphere absorbs some of the energy from the microwaves, but this attenuation has little effect. While refraction is the deflection of radio waves due to changes in atmospheric characteristics (changes in temperature, atmospheric density, humidity). Changes in atmospheric density also affect the speed of propagation of the waves. Then, ducting is the phenomenon of trapping microwaves in an atmospheric waveguide. The ducting phenomenon usually occurs at low altitudes with a very dense layer of the atmosphere and occurs near or above the water surface (Winch, 1998).

2.3. Terrain Effect in Microwave Communication System

Terrain effect is an effect caused by a barrier or object that obstructs the Line of Sight, such as are reflection and diffraction. Reflection causes the beam to change its phase angle, a microwave beam that changes the phase angle can cause an amplification or attenuation of the beam energy. One example of reflection is, for example, ground reflection (Freeman, 2007). Diffraction is a characteristic of electromagnetic waves that occurs when a beam hits a barrier. Diffraction occurs when radio waves hit objects or obstructions in the form of sharp edges, corners, or a surface edge. The diffraction of radio waves will break down and reach the shadowed region. Waves with high frequency tend to follow LOS and do not experience diffraction to the area behind the shadowed region. While, for lower frequencies, diffraction occurs more frequently and results in more shadowed region loss (Hikmaturokhman & Wahyudin, 2018).

2.4. Fresnel Zone

Fresnel zone or fresnel area is an ellipsoidal region formed from radiation emitting from the transmitter antenna and receiver antenna. The Fresnel zone size is determined by the frequency of operation and the

distance between the two sites. Fresnel zone is obtained by the following formula (Hikmaturokhman & Wahyudin, 2018),

$$Fn = 17{,}3\sqrt{\frac{n\,d_1 d_2}{f\,d}} \quad \text{..... 2)}$$

Where, F_n is n^{-th} fresnel area radius (km); d_1 and d_2 are the distance between the transmitter and the barrier, and vice versa (km); d is the sum of d_1 and d_2; f is the frequency (GHz).

2.5. Diversity Antenna Method

a. Space Diversity

In this system, the receiver uses two antennas that are installed vertically at a certain distance. To get optimal performance, the spacing between two vertically separated antennas is the following formula (Kizer, 2013),

$$s = \frac{3\times\lambda\times R}{D} \quad \text{..... 3)}$$

Where, s is spacing between antennas (m), λ is the wavelength (m), R is the radius of the earth (6370 km), and D is path length (km).

If the transmission system uses space diversity techniques to overcome fading, an improvement factor will be obtained with the following equation,

$$I_{sd} = \frac{1.2\times10^{-3}\times\eta\times s^2\times f\times10^{(FM-v)/10}}{D} \quad \text{..... 4)}$$

Where I_{sd} is the improvement factor, η is the switching diversity coefficient (ideally is 1), s is spacing between antennas (m), FM is fading margin, v is the difference in gain of the two antennas.

The equation can be converted into decibels with the following equation,

$$I_{sd} = 20\log s + 10\log f - 10\log D + FM - v - 29.1 \quad \text{..... 5)}$$

After that, the fading margin equation for space diversity configuration can be calculated with the following formula,

$$FM = 20\,log\,D + 5\,log(a\,x\,b\,x\,2{,}5) - 5\,log\,UnAvpath - 10\,log\,s + \frac{1}{2}v - 15{,}4 \quad \text{..... 6)}$$

b. Frequency Diversity

In the frequency diversity technique, the system uses an antenna with two different frequencies. The frequency difference (Δf) between the two frequencies is 2%-6% to avoid interference. If the transmission system uses the frequency diversity technique to overcome fading, then the improvement factor will be obtained with the following formula (Hikmaturokhman & Wahyudin, 2018),

$$I_{fd} = \frac{0.8\times\Delta f}{f^2\times D}\times 10^{FM/10} \quad \text{..... 7)}$$

Where Δf is the difference in frequency diversity.

The equation can be converted into decibels with the following equation,

$$I_{fd} = 10\,log\,\Delta f - 20\log f - 10\log D + FM\ 0.9 \quad \text{..... 8)}$$

After that, the fading margin equation for frequency diversity configuration can be calculated with the following formula,

$$FM = 20\log D + 5\log(a\times b\times 2.5) + 15\log f - 5\log UnAv_{path} - 5\log\Delta f - 29.5 \quad \text{..... 9)}$$

c. Hybrid Diversity

Hybrid diversity combines space and frequency diversity configuration. The system improvement is determined by the mechanism of selecting the highest improvement factor between space and frequency diversity (Kizer, 2013).

$$I_{FF-HD} = I_{FF-SD} \text{ or } I_{FF-FD} \text{ , select the highest score} \quad \text{..... 10)}$$

I_{FF-HD} = Hybrid Diversity Flat Fading diversity improvement factor

$$I_{DF-HD} = I_{DF-SD} \text{ or } I_{DF-FD} \text{ , select the highest score} \quad \text{..... 11)}$$

I_{DF-HD} = Hybrid Diversity Diverse Fading diversity improvement factor

2.6. Availability

Availability affects system reliability. The system reliability measure is often referred to as availability. Availability is often referred to as reliability which is defined by the system's ability to provide services. The opposite of availability is unavailability or outage time, which means the system fails to provide services (Lehpamer, 2010).

To get diversity availability, calculate the unavailability diversity with the following equation,

$$UnAvpath_{diversity} = \frac{UnAvpath}{I_{diversity}} \quad \text{..... 12)}$$

Where diversity availability is a division between unavailability non-diversity and diversity improvement factors so that availability space diversity can be calculated with the following equation,

$$\text{Avpath}_{\text{diversity}} = (1 - \text{UnAvpath}_{\text{diversity}}) \text{ x } 100\% \quad \text{..... 13)}$$

2.7. Link Budget Calculation

a. Microwave Transmission Path

The distance between sites can be calculated by determining the nominal position of two points on the earth line and calculating the distance. The nominal location of a point is usually expressed in terms of latitude and longitude. Each point of latitude and longitude is expressed in degrees, minutes, and seconds. The value needs to be converted first in units of degrees and converted into km. So, to change the nominal point from hours minutes to seconds to hour values only is to use the equations (Hikmaturokhman et al., 2017).

$$Latitude \text{ and } longitude = derajat + \frac{menit}{60} + \frac{detik}{3600} \quad \text{..... 14)}$$

$$Latitude\ Distance = |Latitude\ of\ Site\ 1 - Latitude\ of\ Site\ 2| \text{ x } 110{,}33 \quad \text{..... 15)}$$

$$Longitude\ Distance = |Longitude\ of\ Site\ 1 - Longitude\ of\ Site\ 2| \text{ x } 111{,}32 \quad \text{..... 16)}$$

So the Path length is,

$$Pathlength = \sqrt{(Latitude\ Distance)^2 + (Longitude\ Distance)^2} \quad \text{..... 17)}$$

b. Antenna Gain

The antenna gain is responsible for measuring the ability of an antenna to transmit information to the destination. The amount of antenna gain can be determined by the equation,

$$G = 20 \log f + 20 \log d + 10 \log \eta + 20.4 \quad \text{..... 18)}$$

Where G is antenna gain, η is antenna efficiency, d is antenna diameter, and f is frequency.

c. Free Space Loss (FSL)

FSL is the attenuation that exists along with the space between the transmitting and receiving antennas. In this space, no obstructions are allowed because the transmission is a line of sight. The amount of FSL can be calculated by the equation (Azhar et al., 2018),

$$FSL = 92.45 + 20\log D(km) + 20\log f(GHz) \quad 19)$$

Where D is path length, and f is frequency.

d. Effective Isotropic Power (EIRP)

EIRP is the maximum power of the microwave signal that comes out of the transmitting antenna or to show the effective value of the power emitted by the transmitting antenna. In other words, the power has been strengthened. EIRP is obtained by adding up the power and gain and reducing the transmission loss(Hikmaturokhman & Wahyudin, 2018),

$$IRP = P_{TX} + G_{antena} - L_{TX} \quad 20)$$

e. Isotropic Received Level (IRL)

Isotropic Received Level (IRL) is the value of the isotropic power level received by the receiving station. IRL is obtained using the following equation (Hikmaturokhman & Wahyudin, 2018),

$$IRL = EIRP - FSL \quad 21)$$

f. Received Signal Level (RSL)

Received Signal Level (RSL) is the power level received by the receiver antenna device. RSL is obtained from the sum of the IRL with the receiver antenna gain and reduced loss line receiver. (Pramono, 2014),

$$RSL = IRL + G_{RX} - L_{RX} \quad 22)$$

g. Hop loss (L_h)

Hop loss is the difference between gain and loss on a microwave communication link. The loss value is referred to the sum of free space loss and atmosphere effect. Hop loss is expressed by the equation (Attamimi & Rachman, 2014),

$$L_h = FSL + L_{Tx} + L_{Rx} + L_{Atm} - (G_{Tx} + G_{Rx}) \quad 23)$$

h. Fading Margin (FM)

The calculation equation is used to get the fading margin value by entering the received signal level and the threshold value on the receiving side. The fading margin can be calculated with the following equation (Kizer, 2013),

$$FM = RSL - RxThreshold \quad 24)$$

i. Availability

Availability paths are expressed by equations,

$$Av_{path} = (1 - UnAv_{path})x\ 100\% \quad 25)$$

$$UnAv_{path} = a\ x\ b\ x\ 2.5\ x\ f\ x\ D^3 x\ 10^{-6}\ x\ 10^{-\frac{FM}{10}} \quad 26)$$

Coefficient a is the earth's roughness factor, where the value of is 4 for subtle regions, seas, lakes, and deserts; 1 for areas of average roughness, plain; and ¼ for mountains and plateaus. While coefficient b is climatic factors, where the value of is ½ for hot and humid areas; 1/4 for normal areas; and 1/8 for mountains (very dry).

2.8. Standard ITU-T G.821

The ITU-T G.821 standard is a reference for the availability of two parameters to determine the available quantity in the form of Availability Ratio (AR), which is the ratio of time available for communication to the total operating time, Outage Intensity (OI), which is the number of outages in the communication system in total operating time. OI can be referred to as the average time for each outage that occurs during an operation. Operation time is usually 1 year (Kizer, 2013). Table 1 shown the standard of availability based on ITU-R (ITU-T G.821).

Table 1. Standard of availability based on ITU-R (ITU-T G.821) for availability two-way objectives

No	Link Grade	Availability Condition
1	High-Grade Circuit	99.997 % for 46.7-Km hop in 2500-Km Hypothetical Reference Digital Path (HDRP)
2	Medium-Grade Circuit	
	• Class 1280-Km radio section	99.997% for 46.7-km hop
	• Class 2280-Km radio section	99.996% for 46.7-km hop
	• Class 350-Km radio sub-section	• 99.98% for 50-km hop • 99.995% for 10-km hop
	• Class 450-Km radio sub-section	• 99.95% for 50-km hop • 99.99% for 50-km hop
3	Local-Grade Link	• Commonly used for high frequency (>17-GHz) hops • No availability objectives

Source: ITU-T (2002)

3. Method

This study analyzes the microwave link performance of two different types of diversity configurations, namely space diversity and hybrid diversity in the mountain topography area. But, before design a microwave link using diversity configuration, the microwave link was configured with a point-to-point antenna between two sites. This is done to assess the microwave link performance without using a diversity configuration.

The microwave link design simulation uses Pathloss 5 software. The data used to simulate microwave networks consists of sites data, antenna type data, and microwave radio. Meanwhile, The microwave link performance indicators such as availability, un-availability, and fading margin, as illustrated in Figure 2.

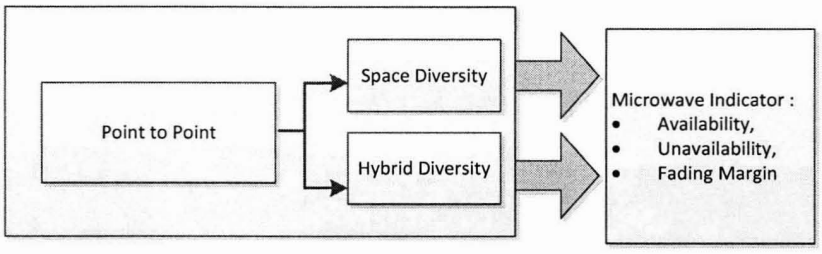

Figure 2. Research variable

Microwave design simulations are carried out by performing various configurations, including:

3.1. Digital Maps Configuration

In the early stages of the simulation, the digital map format used in the study is Shuttle Radar Topographic Mission (SRTM). Then at this stage, the Geographic Information System in the software is

generated by submitting the latitude and longitude of the research area. So, the determined site is at the right coordinates and generates a real contour map like the reality in the field, as shown in Figure 3.

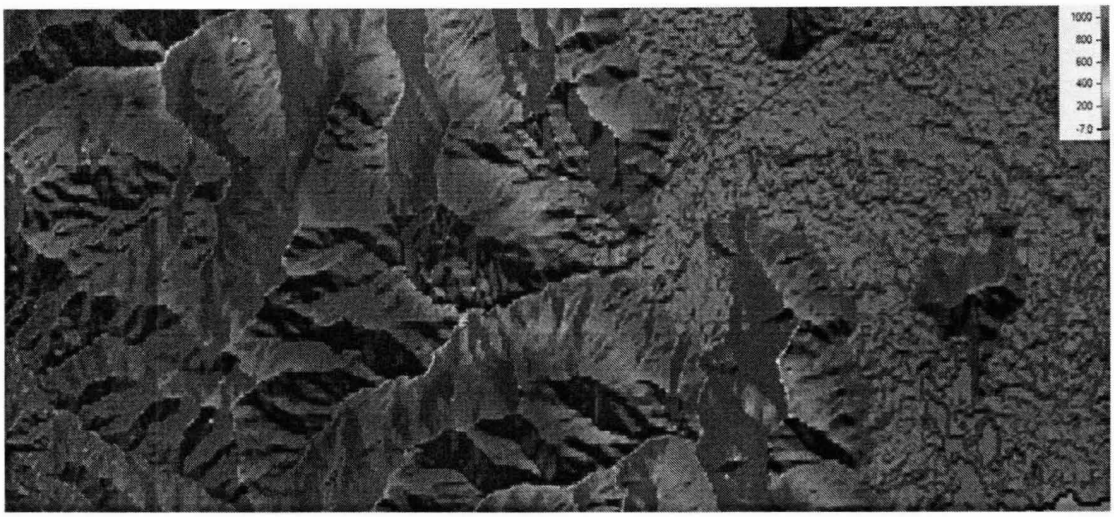

Figure 3. Mountain terrain digital map (Kaleakan - Walenrang)

3.2. Site Configuration

At this stage, arrangements are made for the site that has been determined. These arrangements include the site coordinates location, the site height, the site shape, and others. Table 2 describes the location of the research site. The sites used are Walenrang and Kaleakan in South Sulawesi with a link length of 17 km with the use of 26,000 MHz frequency with vertical polarization. The use of the 26,000 MHz frequency is due to the short-haul length so that high frequencies are needed to reach short-distance microwave links.

Table 2. Site parameters across the Kaleakan and Walenrang mountains

Parameter	Kaleakan	Walenrang
Latitude	02 57 13.00 S	02 51 43.30 S
Longitude	120 03 01.00 E	120 10 24.80 E
True azimuth (°)	53.54	233.54
Vertical angle (°)	-4.04	3.93
Elevation (m)	1209.11	31.65
Path length (km)	17.08	
Frequency (MHz)	26,000	
Polarization	Vertical	

Source: Data processed by researchers

3.3. Terrain and Atmosphere Factor Configuration

The software generates earth contour or terrain conditions from two connected microwave links. Furthermore, various obstacles that may exist in the field can be added, such as trees, forests, buildings, towers, and others. In mountainous areas, it has extreme terrain because the land area has hilly contours from one side to the other with a terrain roughness of 42.67 meters. Another thing to note is that the contours of mountainous

terrain can cause multipath fading caused by the reflection of electromagnetic waves hitting the earth's surface, as shown in Figure 4.

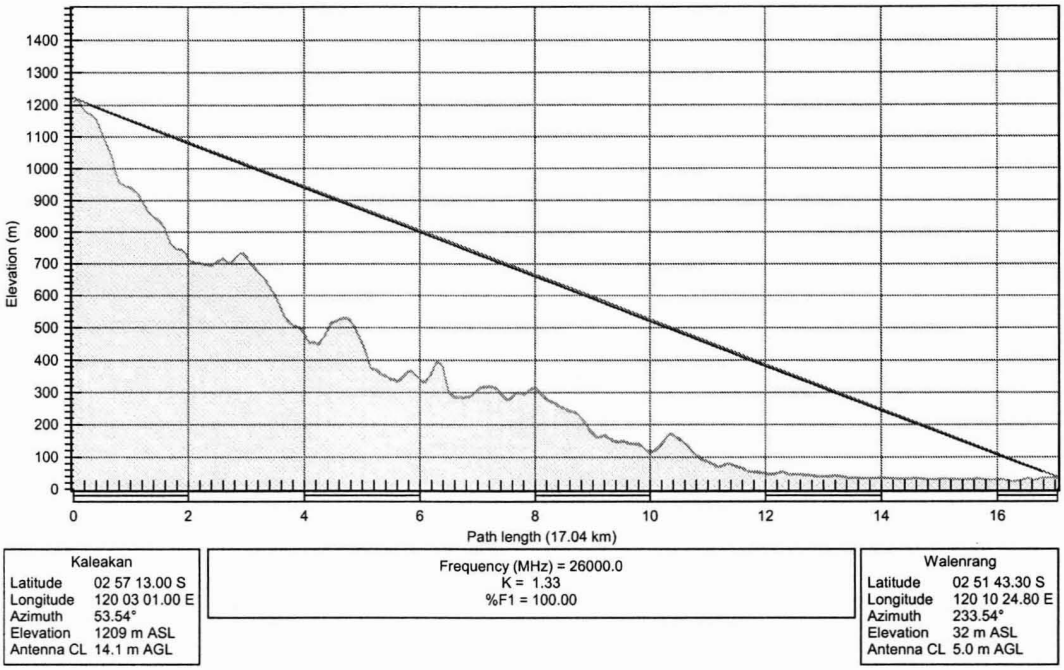

Figure 4. Path profile of microwave communication across mountains

Atmospheric and rain data uses reference ITU-R P.837.5, as described in Table 3.

Table 3. Atmospheric parameters across the Kaleakan and Walenrang mountains

Parameter	Value
Climatic factor	2
Terrain roughness (m)	42.67
C factor	0.52
Average annual temperature (°C)	18.21
Fade occurrence factor (Po)	4,078E-002
0,01% rain rate (mm/hr)	79.70

Source: ITU-R P.837.5

3.4. Radio Transmission

Various microwave radio link settings are carried out at this stage, including antenna settings, radio equipment settings, frequency spectrum settings, and transmission loss.

a. Antenna

The antenna used in the cross-mountain microwave transmission system is the VHLP2-26 model manufactured by Andrew. This antenna operates at a frequency of 24,250 – 26,500 MHz with a diameter of 0.6 meters, an antenna gain of 41.2 dBi, and is capable of transmitting electromagnetic waves with a wide beamwidth of 1.5^{o}. Based on the antenna height calculation that considers the Fresnel Zone and the

curvature of the earth, it is found that the height of the antenna installed in Kaleakan is as high as 14.14 meters, while in Walenrang is 5 meter, as described in Table 4.

Table 4. Antenna parameters point to point cross mountains

Parameter	Kaleakan	Walenrang
Antenna model	VHLP2-26 (TR)	VHLP2-26 (TR)
Antenna file name	7020	7020
Antenna gain (dBi)	41.2	41.2
Antenna height (m)	14.14	5
Antenna diameter (m)	0.6	0.6

Source: Data processed by researchers

The diversity antenna is installed with a space diversity coefficient range between 100 - 200 with an interval of 25. In Kaleakan, the antenna and line transmission diversity are installed at the height of 11.79 to 12.95 meters with an interval of 0.3 meters. Likewise, the Walenrang antenna and line transmission diversity are installed at the height of 2.7 - 2.85 meters with an interval of 3.75 meters.

The length of line transmission causes TX line loss, where the greater the diversity coefficient, the lower the resulting loss. Likewise, in Diversity net path loss, although the value at both sites is the same, the effect of antenna diversity has an impact on net path loss, where the farther the antenna diversity from the main antenna, the lower the resulting loss, as shown in Table 5.

Table 5. Diversity Tx line loss (dB) and net path loss in cross mountain microwave communication

Antenna spacing configuration	Diversity Height		Diversity TX line loss		Diversity Net Path loss	
	Kaleakan	Walenrang	Kaleakan	Walenrang	Kaleakan	Walenrang
Space diversity (ρ = 100)	12.95	3.85	4.26	1.27	74.99	75.01
Space diversity (ρ = 125)	12.66	3.56	4.17	1.17	74.90	74.91
Space diversity (ρ = 150)	12.37	3.27	4.07	1.08	74.80	74.81
Space diversity (ρ = 175)	12.08	2.99	3.98	0.98	74.71	74.72
Space diversity (ρ = 200)	11.79	2.70	3.88	0.89	74.61	74.63

Source: Data processed by researchers

b. Line Transmission

The line transmission for the cross-mountains microwave communication system is the EW240 model produced by CommScope, which is an elliptical waveguide for frequency of 22,000 MHz – 26,500 MHz and has 32.91 dB/100 m unit loss.

c. Transmission Loss

Based on the simulation, it is found that the total net path loss for the cross-mountain microwave transmission system is 75.38 dB. Meanwhile, the free-space loss is 145.42 dB which is because although the length of the link is quite close, the use of high frequency and rough terrain contours results in a large Free Space Loss. Atmospheric absorption loss occurs quite high. It is because high-frequency use has high atmospheric absorption characteristics, as described in Table 6.

Table 6. Transmission loss in cross-mountain microwave communications

Parameter	Kaleakan	Walenrang
TX line loss (dB)	4.65	1.65
Circulator branching loss (dB)	2	2
Free space loss (dB)	145.42	
Atmospheric absorption loss (dB)	2,07	
Net path loss (dB)	75.38	75.38

Source: Data processed by researchers

d. Parameter Radio

The radio device used on the cross mountains microwave communication is the ML26E HP manufactured by Ericsson. The device uses the CQPSK modulation. This device is capable of radiating an EIRP of 52.55 dBm and has a threshold at the receiver of 10-6 BER with a level of -79 dBm, as described in Table 7.

Table 7. Radio parameters on cross mountains microwave communication

Parameter	Kaleakan	Walenrang
Radio model	ML26E HP 17E1,raf	ML26E HP 17E1,raf
Radio file name	ml26e hp 17e1	ml26e hp 17e1
TX power (dBm)	18.00	18.00
Emission designator	28M6G7W	28M6G7W
EIRP (dBm)	52.55	55.55
RX threshold criteria	1E-6 BER	1E-6 BER
RX threshold level (dBm)	-79.00	-79.00

Source: Data processed by researchers

e. Transmission Channel Frequency Settings

The frequency channel used in point-to-point and space diversity uses a frequency of 26,173 MHz, vertical polarization in Kaleakan, and 25,165 MHz in Walenrang. While hybrid diversity configuration using two frequency channels. The frequency channel used for cross-mountain transmission system uses a frequency of 26,173 MHz and 25,277 MHz with vertical polarization in Pekajang Village while in Air Jukung Village using a frequency of 25,165 MHz and 26,285 MHz with vertical polarization.

3.5. Simulation Report

The last stage is to get a report from the simulations that have been carried out. The resulting reports include transmission summary reports and transmission detail reports.

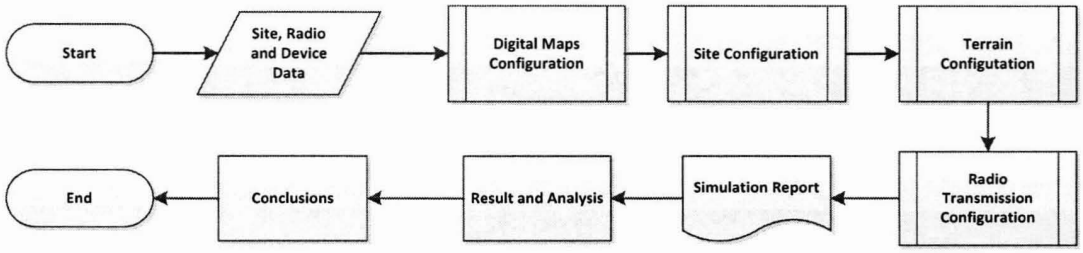

Figure 5. Research flowchart

4. Result and Discussion

4.1. Point-to-Point Configuration

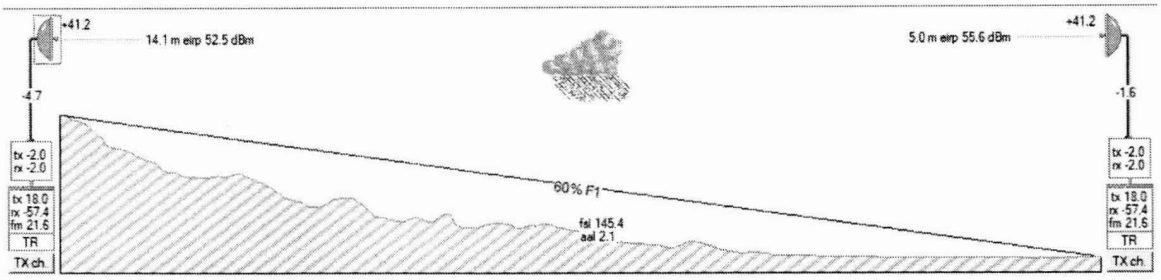

Figure 6. Point-to-point microwave radio transmission configuration over mountains

According to the simulation results, the fading margin on a cross-mountain microwave link using a point-to-point antenna reaches 21.62 dB. This is because the received signal is quite low at -57.38 dBm while the receiver threshold level on the radio device reaches -79 dBm. The result of the annual multipath availability is 99.98179%, and the annual multipath un-availability is 5742.79 seconds per year. Meanwhile, in rainy conditions, the annual multipath availability is 99.85763%, and the annual multipath un-availability is 748.27 minutes per year, as described in Table 8.

Table 8. Point to point microwave link performance on mountain ranges

Parameter	Kaleakan	Walenrang
Receive signal (dBm)	-57.38	-57.38
Thermal fade margin (dB)	21.62	21.62
Worst month multipath availability (%)	99.97189	99.97189
Worst month multipath unavailability (sec)	738.80	738.80
Annual multipath availability (%)	99.99089	99.99089
Annual multipath unavailability (sec)	2871.39	2871.39
Annual 2-way multipath availability (%)	99.98179	
Annual 2-way multipath unavailability (sec)	5742.79	
Polarization	Vertical	
0,01% rain rate (mm/hr)	79.70	
Flat fade margin - rain (dB)	21.62	
Rain attenuation (dB)	21.62	
Annual rain availability (%)	99.87585	
Annual rain unavailability (min)	652.56	
Annual rain + multipath availability (%)	99.85763	
Annual rain + multipath unavailability (min)	748.27	

Source: Data processed by researchers

4.2. Radio Transmission Configuration Microwave Space Diversity in Cross Mountains

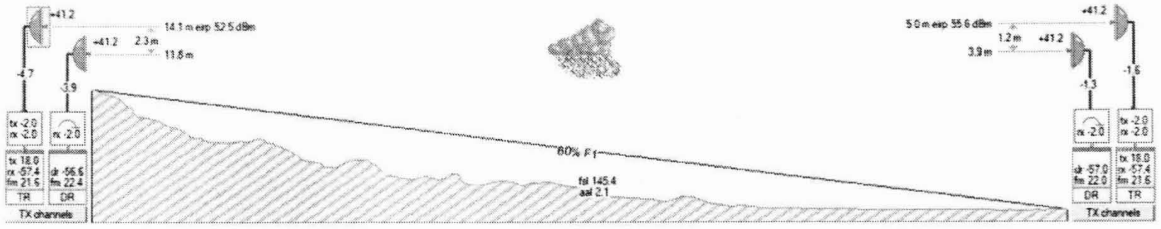

Figure 7. Radio transmission configuration microwave space diversity in cross mountains

According to the simulation, the fading margin in the cross-mountain microwave communication system, the Kaleakan site is 22.01 dB - 22.39 dB, while the Walenrang site is 21.99 dB to 22.37 dB, as shown in table 10. The calculation of the fading margin is obtained from the reduction of the Received Signal Level by the Receiver Threshold, where the receiver threshold is based on the radio parameters shown in Table 9.

Table 9. Fade margin space diversity in cross mountains microwave communication

Antenna Spacing Configuration	Kaleakan	Walenrang
Space diversity (ρ = 100)	22.01	21.99
Space diversity (ρ = 125)	22.10	22.09
Space diversity (ρ = 150)	22.20	22.19
Space diversity (ρ = 175)	22.29	22.28
Space diversity (ρ = 200)	22.39	22.37

Source: Data processed by researchers

Table 10. Space diversity improvement factor in cross mountains microwave communication

Antenna Spacing Configuration	SD Improvement factor	
	Desa Pekajang	Desa Air Jukung
Space diversity (ρ = 100)	1.00	1.00
Space diversity (ρ = 125)	1.00	1.00
Space diversity (ρ = 150)	1.00	1.00
Space diversity (ρ = 175)	1.13	1.08
Space diversity (ρ = 200)	1.47	1.42

Source: Data processed by researchers

Then, the annual multipath availability in cross-mountain microwave communication systems has a value range of 99.98333% to 99.98943%, or in one year, there is a transmission failure on both uplink and downlink lines for 5255.53 seconds to 3332.48 seconds, such as described in Table 11. While it has the same annual multipath availability value in rainy conditions, this is due to the annual rain availability of 99.87938% and unavailability conditions for 721 to 671 minutes in one year, as in Table 12.

Table 11. Availability and un-availability of space diversity in cross-mountain microwave communication

Antenna Spacing Configuration	Annual 2-way multipath availability (%)	Annual 2-way multipath unavailability (sec)
Space diversity (ρ = 100)	99.98333	5255.53
Space diversity (ρ = 125)	99.98370	5141.29
Space diversity (ρ = 150)	99.98405	5029.53
Space diversity (ρ = 175)	99.98590	4447.82
Space diversity (ρ = 200)	99.98943	3332.48

Source: Data processed by researchers

Table 12. Availability and un-availability + rain space diversity in cross mountain microwave communication

Antenna Spacing Configuration	Flat fade margin - rain (dB)	Annual rain + multipath availability (%)	Annual rain + multipath unavailability (min)
Space diversity (ρ = 100)	21.99	99.86271	721.58
Space diversity (ρ = 125)	22.09	99.86394	715.11
Space diversity (ρ = 150)	22.19	99.86516	708.73
Space diversity (ρ = 175)	22.28	99.86782	694.72
Space diversity (ρ = 200)	22.37	99.87220	671.70

Source: Data processed by researchers

4.3. Radio Transmission Configuration Microwave Hybrid Diversity in Cross Mountains

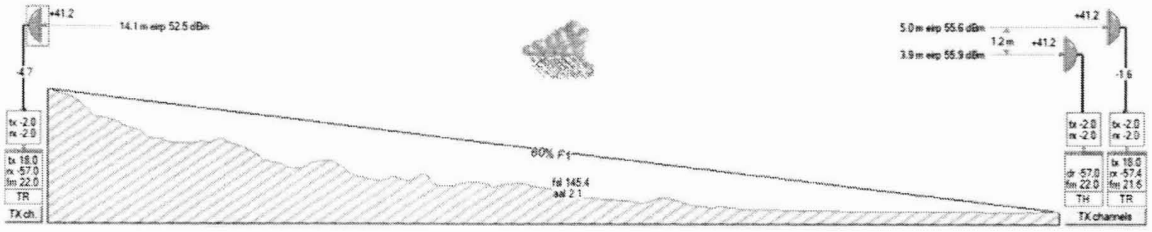

Figure 8. Radio transmission configuration microwave space diversity in cross mountains

Based on the simulation results, the resulting fading margin hybrid diversity in the cross-mountain microwave communication system, the Kaleakan site is 21.99 dB - 22.37 dB while the Walenrang site is 21.99 dB to 22.37 dB, as shown in Table 13.

Table 13. Fade margin hybrid diversity in cross mountains microwave communication

Antenna Spacing Configuration	Fade margin (dB)	
	Kaleakan	Walenrang
Hybrid diversity (ρ = 100)	21.99	21.99
Hybrid diversity (ρ = 125)	22.09	22.09
Hybrid diversity (ρ = 150)	22.19	22.19
Hybrid diversity (ρ = 175)	22.28	22.28
Hybrid diversity (ρ = 200)	22.37	22.37

Source: Data processed by researchers

Table 14. Hybrid diversity improvement factor in cross-mountain microwave communication

Antenna Spacing Configuration	SD Improvement Factor		FD Improvement Factor		Quad Diversity Improvement Factor	
	Kaleakan	Walenrang	Kaleakan	Walenrang	Kaleakan	Walenrang
Hybrid diversity (ρ = 100)		1.00	1.23	1.00		2.00
Hybrid diversity (ρ = 125)		1.00	1.26	1.00		2.00
Hybrid diversity (ρ = 150)		1.00	1.28	1.03		2.03
Hybrid diversity (ρ = 175)		1.08	1.31	1.05		2.13
Hybrid diversity (ρ = 200)		1.42	1.34	1.07		2.49

Source: Data processed by researchers

Then, the annual multipath availability in cross-water microwave communication systems has a value range of 99.98903% to 99.99122%, or in one year, there is a transmission failure on both uplink and downlink lines for 3458.99 seconds to 2769.79 seconds, such as is described in Table 15. While it has the same annual multipath availability in rainy conditions, this is due to the annual rain availability of 99.87938% and unavailability for 691 to 662 minutes in one year, as in Table 16.

Table 15. Availability and un-availability of space diversity in cross-mountain microwave communication

Antenna Spacing Configuration	Annual 2-way multipath availability (%)	Annual 2-way multipath unavailability (sec)
Hybrid diversity (ρ = 100)	99.98903	3458.99
Hybrid diversity (ρ = 125)	99.98942	3335.51
Hybrid diversity (ρ = 150)	99.98984	3205.56
Hybrid diversity (ρ = 175)	99.99036	3038.74
Hybrid diversity (ρ = 200)	99.99122	2769.79

Source: Data processed by researchers

Table 16. Availability and un-availability + rain space diversity in cross mountain microwave communication

Antenna Spacing Configuration	Flat fade margin - rain (dB)	Annual rain + multipath availability (%)	Annual rain + multipath unavailability (min)
Hybrid diversity (ρ = 100)	21.99	99.86841	691.64
Hybrid diversity (ρ = 125)	22.09	99.86967	685.02
Hybrid diversity (ρ = 150)	22.19	99.87094	678.33
Hybrid diversity (ρ = 175)	22.28	99.87229	671.23
Hybrid diversity (ρ = 200)	22.37	99.87399	662.32

Source: Data processed by researchers

4.4. Discussion

In the mountains terrain, the fading margin of a point-to-point configuration produces 21.62 dB. This value results in the availability of 99.98179% or un-availability for 5742.79 seconds/year. This value does not meet the standards set by the ITU-R (ITU-T G.821), where for microwave communication with a distance of 10 km – 50 km, a minimum availability is 99.99%. So to solve it, the microwave communication system uses a diversity, space, and hybrid configuration approach.

In the microwave communication configuration using space and hybrid diversity, the fading margin is almost the same for all the spacing between antennas setting (ρ = 100 to ρ = 200). This is because some hybrid diversity configurations are looking for the best performance between system space or frequency diversity. Then, based on the simulation results, space diversity produces the best fading margin value in some

conditions. Even though overall, the fading margin on both the space and the hybrid almost has the same value. Also, the further the space between antennas, the bigger the fading margin value, as shown in Figure 9.

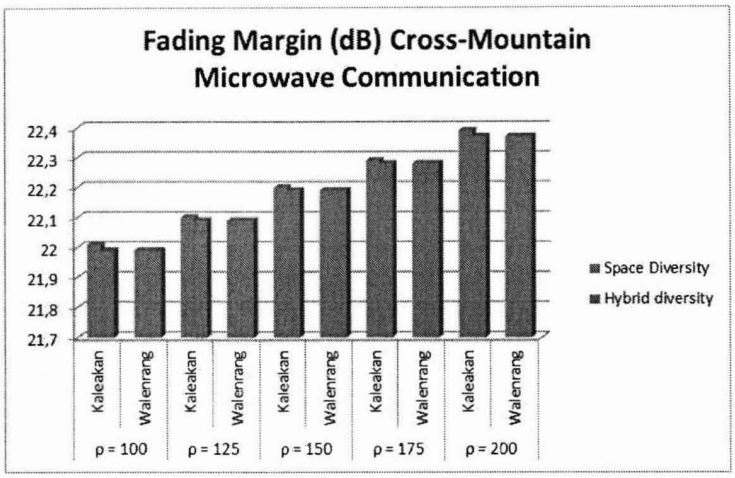

Figure 9. Comparison of fading margin on space configuration and hybrid diversity in cross-mountain microwave communication

Overall, using the diversity configuration has not been able to produce a performance above the standard set by ITU. In space diversity with the closest spacing ($\rho = 100$), the availability is 99.98333% to 99.98943% or comparable to un-availability for 5255.53 to 3332.48 seconds per year and increases significantly in proportion to the distance between antennas. Even the hybrid diversity configuration has not been able to produce values above 99.99%, except at the farthest antenna distance, it results in the availability of up to 99.99122% or equivalent to un-availability for 2769.79 seconds per year at all antenna distances, as shown in figure 10. It is due to the use of high frequencies that are susceptible to attenuation, such as multipath and the influence of the atmosphere and hilly contour conditions that cause diffraction.

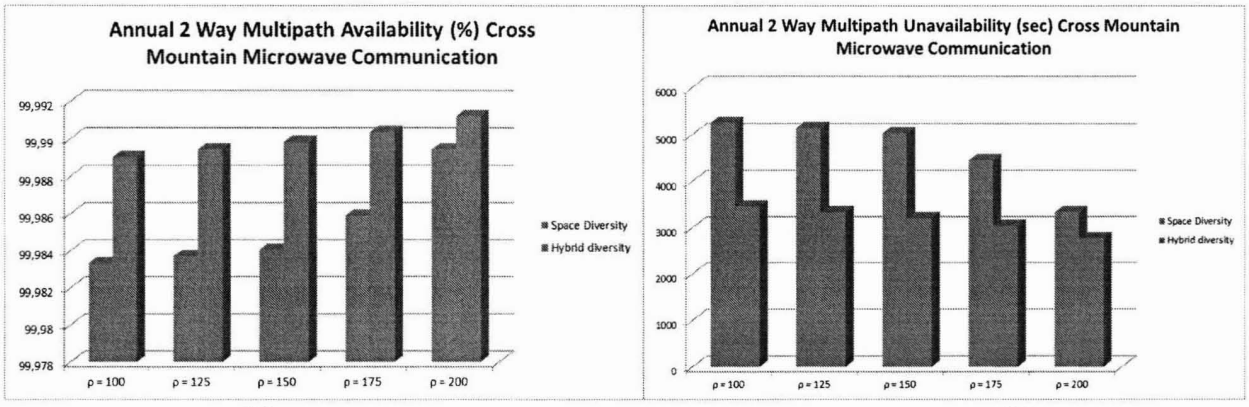

(a) (b)

Figure 10. Comparison of annual 2-way multipath availability (a) and unavailability (b) on space configuration and hybrid diversity in cross-mountain microwave communication

Even though it produces different meter values in rainy conditions, overall results in worse performance because none of the configurations produce the above standard conditions set by the ITU, as shown in Figures 11. Several solutions to overcome microwave communication quality problems are The worst thing in mountainous areas is to use a lower frequency or to use a repeater in the middle of the track.

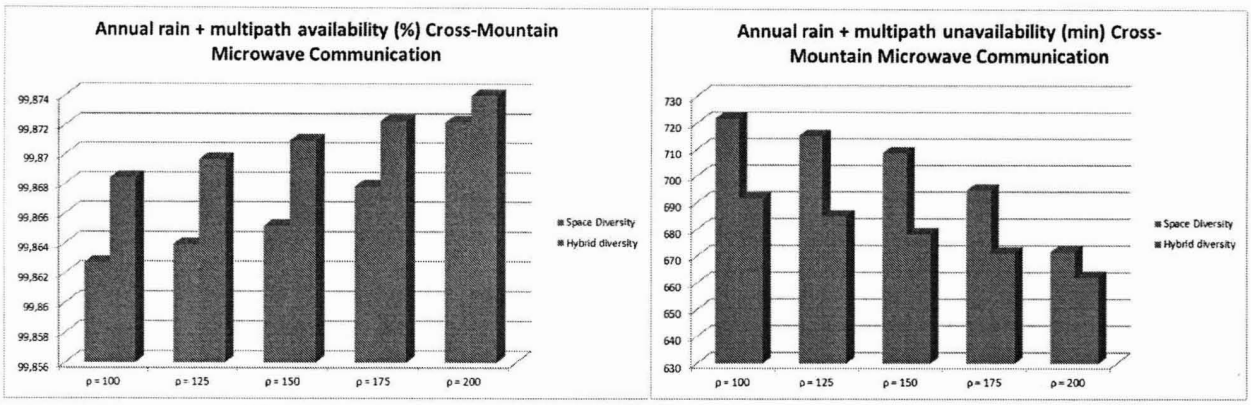

(a) (b)

Figure 11. Comparison of annual rain + multipath availability (a) and unavailability (b) configuration of space and hybrid diversity in cross-mountain microwave communication

5. Conclusion

Based on the results and discussion, it can be concluded that the microwave communication system can implement point-to-point configurations, space diversity, and hybrid diversity both across mountains. The fading margin of Cross-Mountain Microwave Communication with a point-to-point configuration produces a value of 21.62 dB. However, when using space diversity and hybrid diversity, it increases from 21.99 dB to 22.37 dB.

In the cross-mountain communication system using point-to-point configuration, result in the availability is 99.98179% or un-availability for 5742.79 seconds in one year. This value does not meet the standards set by the ITU-R (ITU-T G.821), where for communication with a distance of 10km - 50km, a minimum availability value must be 99.99%.

Overall, cross-mountain communication systems using diversity configurations have not been able to produce values above the standards set by the ITU. In space diversity with the closest antenna space ($\rho = 100$), the availability is 99.98333% to 99.98943% or comparable to un-availability for 5255.53 to 3332.48 seconds/year and increases significantly in proportion to the distance between antennas space. Even the hybrid diversity configuration has not been able to produce values above 99.99%, except at the farthest antenna distance, it results in the availability of up to 99.99122% or equivalent to un-availability for 2769.79 seconds per year at all antenna distances.

6. References

Attamimi, S., & Rachman, R. (2014). Perancangan Jaringan Transmisi Gelombang Mikro Pada Link Site Mranggen 2 Dengan Site Pucang Gading. *Jurnal Teknologi Elektro*, *5*(2). https://doi.org/10.22441/jte.v5i2.764

Azhar, M., Pradana, Z. H., & Wahyudin, A. (2018). Analisa Perencanaan Backhaul Untuk Jaringan Long Term Evolution (LTE) Dikota Yogyakarta. *Techno (Jurnal Fakultas Teknik, Universitas Muhammadiyah Purwokerto)*, *19*(2), 103. https://doi.org/10.30595/techno.v19i2.3010

Badan Pusat Statistik. (2018). *Statistik Telekomunikasi Indonesia*. Badan Pusat Statistik.

Dewanti, I. E., Wahyudin, A., & Hikmaturrokhman, A. (2017). Analisis Perbandingan Passive Repeater Back-To-Back Antenna Dan Passive Repeater Plane Reflector Menggunakan Pathloss 5 . 0 Comparative Analysis of Passive Repeater Back-To-Back Passive Repeater Antenna and Plane Reflector Using the. *Senatek (Seminar Nasional Teknik) 2017*, 1–8.

Freeman, R. L. (2007). *Radio System Design For Telecommunications* (3rd ed.). John Wiley & Sons.

Hikmaturokhman, A., & Wahyudin, A. (2018). *Perancangan Jaringan Gelombang Mikro Menggunakan Pathloss 5* (U. K. Usman (ed.)). Pustaka Ilmu.

Hikmaturokhman, A., Wahyudin, A., Yuchintya, A. S., & Nugraha, T. A. (2017). Comparison analysis of passive repeater links prediction using methods: Barnett Vigants & ITU models. *Proceedings of 2017 4th International Conference on New Media Studies, CONMEDIA 2017, 2018-Janua*, 142–147. https://doi.org/10.1109/CONMEDIA.2017.8266046

Hikmaturrokhman, A., & Wahyudin, A. (2018). *Perancangan Jaringan Gelombang Mikro Menggunakan Pathloss 5* (Vol. 53, Issue 9). https://doi.org/10.1017/CBO9781107415324.004

ITU-T. (2002). *ITU - T Recommendation G.821 Series G: Transmission Systems And Media, Digital Systems And Networks.*

Kementerian Komunikasi dan Informatika. (2013). *Sekilas Palapa Ring*. Kominfo.Go.Id. https://kominfo.go.id/content/detail/3298/sekilas-palapa-ring/0/palapa_ring

Kizer, G. (2013). *Digital Microwave Communication Engineering Point-to-Point Microwave Systems*. John Wiley & Sons. https://doi.org/10.1037/0003-066X.45.9.1018

Lehpamer, H. (2010). *Microwave Transmission Networks Planning, Design and Deploymeny* (3rd ed., Vol. 53, Issue 9). McGraw-Hill. https://doi.org/10.1017/CBO9781107415324.004

Oktaviasari, E., Wahyudin, A., & Hikmaturokhman, A. (2018). Analisis Perbandingan Interferensi Link Gelombang Mikro pada Daerah Urban dan Rural Menggunakan. *Conference of Electrical Engineering, Telematics, Industrial Technology, and Creative Media*, *1*, 178–183.

Pradana, Z. H., & Wahyudin, A. (2018). Analisis Optimasi Space Diversity pada Link Microwave Menggunakan ITU Models. *Jurnal Elektro Dan Telekomunikasi Terapan*, *4*(2), 586. https://doi.org/10.25124/jett.v4i2.1148

Pramono, S. (2014). Analisa Perencanaan Power Link Budget untuk Radio Microwave Point to Point Frekuensi 7 GHz (Studi Kasus : Semarang). *Politeknik Negeri Semarang, Jurnal Teknik Elektro Terapan*, *3*(1), 27–31.

Rahmawati, Y. Y., & Wahyudin, A. (2018). Perancangan Jaringan Backhaul Sistem Transmisi Gelombang Mikro Digital Menggunakan Frequency Diversity dan Tanpa Diversity di Wilayah Kepulauan Riau. *Techno (Jurnal Fakultas Teknik, Universitas Muhammadiyah Purwokerto)*, *19*(2), 63. https://doi.org/10.30595/techno.v19i2.3178

Wahyudin, A., & Hikmaturokhman, A. (2021). Analysis of cross-ocean microwave communication systems using point-to-point, space diversity and hybrid diversity configurations. *Journal of Communications*, *16*(8), 331–340. https://doi.org/10.12720/jcm.16.8.331-340

Winch, R. G. (1998). *Telecommunication Transmission Systems, 2nd edition* (2nd ed.). McGraw-Hill.

Slow Frequency Hopping for Mitigating Tidal Fading on Rural Long Distance Over-Water Wireless Links

Alex Macmillan, Mahesh K. Marina and Jhair Tocancipa Triana

Informatics Research Report 1365

SCHOOL *of* INFORMATICS
Institute for Computing Systems Architecture
March 2010

A shorter version of this paper will appear in *Proc. IEEE INFOCOM 2010 Conference — Work-in-Progress (WiP) Track*, San Diego, USA, March 2010.

Abstract : We consider the scenario where long-distance point-to-point wireless links are established over tidal estuaries to bring Internet access to rural communities living in coastal villages. Using real signal strength measurements from links in the Tegola network testbed in northwest Scotland, we highlight the significance of the tidal fading problem, which we reason using a simple geometric model and simulation using the well-known Pathloss radio link planning tool. We propose slow frequency hopping as a cost-effective, software-only alternative to the commonly used space-diversity approach for mitigating tidal fading, and demonstrate its effectiveness using Pathloss simulation.

Keywords : Frequency diversity, Wireless, Community broadband, Link planning, Fading, Over-water, Over-sea, Tide

Copyright © 2010 University of Edinburgh. All rights reserved. Permission is hereby granted for this report to be reproduced for non-commercial purposes as long as this notice is reprinted in full in any reproduction. Applications to make other use of the material should be addressed to Copyright Permissions, School of Informatics, The University of Edinburgh, Informatics Forum, 10 Crichton Street, Edinburgh EH8 9AB, UK.

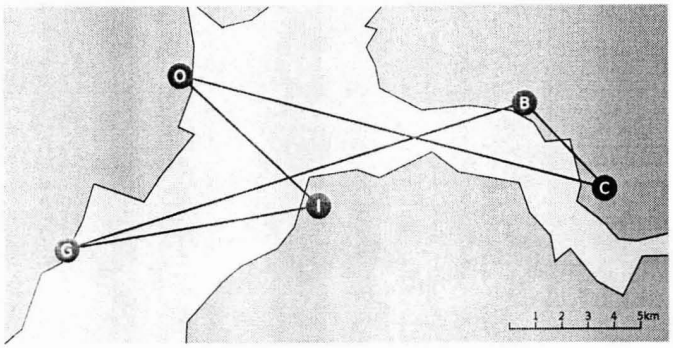

Figure 1: The six over-water links in the Tegola network.

1 Introduction

For rural and remote areas that are plagued by lack of wired broadband infrastructure, poor mobile phone network coverage, and expensive and high latency satellite coverage, WiFi-based long distance wireless mesh networking has emerged in recent years as a cost-effective approach for enabling Internet access to communities (see [1, 2] and references therein). This has led to considerable work from the research community looking at a range of issues, including the understanding of long-distance wireless link characteristics in rural settings, notably by Brewer et al. [3] and Raman et al. [4]. The main conclusion from these link characterization studies is that rural long-distance wireless links experience negligible link quality variations and that they function as planned with a strong correlation between received signal strength and link quality.

One conclusion from previous work that is of particular relevance to this report is that long, line-of-sight links in rural networks experience very low multipath interference and delay spread [3]. This conclusion may not always hold. We consider one such exceptional yet common scenario where point-to-point wireless links are deployed at low altitudes over tidal estuaries and as a result, multipath interference from reflections over tidal water can be significant. In regions such as the Scottish Highlands and Islands where most rural communities (representing 90% of the population, about a quarter million people) live in coastal villages, this can present a major obstacle to reliable Internet service delivery. In fact, there have been media reports of unreliable broadband service and ensuing public dissatisfaction with a commercial long-distance wireless deployment in the Western Isles of Scotland that was primarily attributed to wireless signal propagation over tidal waters [5]. The extent of this problem in general can be appreciated by considering areas with tidal estuaries and archipelagos worldwide (e.g., Japan, Indonesia, United Kingdom).

In this report we revisit wireless transmission over tidal water by showing the significance of the problem using signal strength measurements taken from over-water links in the Tegola network, a long-distance WiFi mesh network testbed deployed in northwest Scotland connecting several remote communities to the Internet [2]. All of the links in the network are at least partly over-water (See Figure 1). We reason about tidal fading effects by developing a simple geometric model. We also perform simulations using a more realistic and well-known radio link planning tool called Pathloss [6].

More crucially, we propose a slow frequency hopping[1] technique to mitigate tidal fading. The essential idea is to exploit the frequency dependence of the two-ray interference pattern and adaptively switch to a frequency (channel) that is not currently experiencing fading. Compared to the commonly employed spacial diversity approach, our proposal is cost-effective as it does not require additional hardware and straightforward to deploy since it is a software-only solution.

The remainder of this report is organised as follows. In Section 2, we explore the tidal fading problem in detail using a geometric model, the pathloss simulation tool and real-world data gathered from the Tegola testbed; we also briefly review related work in the field of over-water wireless communication. Section 3 describes the commonly used space-diversity solution, and introduces our proposed slow frequency

[1]Our use of the term frequency hopping is more akin to that of link layer channel hopping techniques such as SSCH [7] and different from that of physical layer frequency hopping in the spread spectrum context.

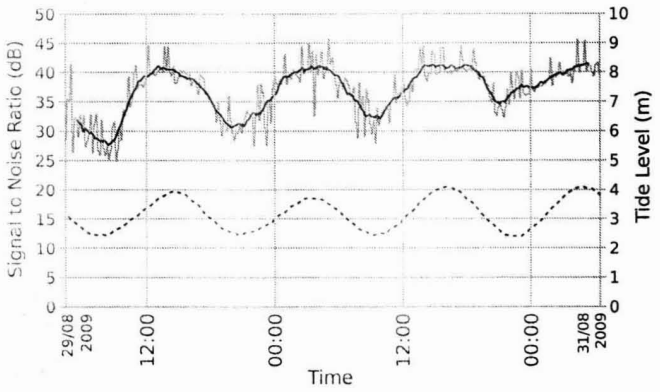

Figure 2: Signal strength data collected from the Ornsay–Corran link in the Tegola network — the thin (thick) line corresponds to measured signal strength (two hour box-car average). The dashed line shows the tide height data as recorded at a nearby location (Ullapool) for the same time period.

hopping approach. Finally we conclude in Section 4.

2 The Problem

Wireless links over estuaries experience time-varying fading that is dependent on the height of the tide. This is a problem because links experiencing such fading can degrade in quality or fail altogether when the fade margin is insufficient. We have observed this form of fading on almost all point-to-point links in the Tegola network. As an illustration of the tidal fading effect, Figure 2 shows the *measured* signal strength for the Ornsay–Corran link (between 'O' and 'C' in Figure 1), a 15.9 km link almost entirely spanning water between the Isle of Skye and the Scottish mainland. We will use the Ornsay–Corran link in the rest of this paper in reasoning about this problem and the relative merits of various mitigation techniques; this is done for ease of exposition and does not limit the generality of our arguments.

Tidal fading occurs as a result of the interference between the direct line-of-sight path from the transmitter antenna to the receiver antenna and the indirect path that reflects on the water plane (Figure 3). As the tide rises and falls, the length of the reflected path changes. This in turn causes a change in the phase difference between the two paths. As the phase difference approaches 180 degrees, the interference between the paths will be increasingly destructive, resulting in a deeper fade (also referred to as a *null*). As sea-water acts as a very good reflector at near-grazing angles, the fading due to destructive interference can be significant. In practice, we have recorded fades in excess of 30dB.

2.1 Geometric Model

A simple geometric model can be used to determine the extent of signal fading due to tidal variation. Our model (elaborated in the Appendix) computes the difference in path length between the direct and indirect rays, the resulting phase difference between the rays and thus the amplitude of the received signal relative to the case when only the direct path is present.

Figure 4 shows the relative received signal strength for links of various lengths using our geometric model. The characteristic nulls (deep fades) that occur at specific tide heights are evident from this plot. A link with an insufficient fade margin is likely to fail when it experiences a null. Thus, for such a link, breaks in service can be expected to occur periodically in relation to the rise and fall of the tide.

Further modelling allows us to determine the kind of effects we would expect to observe given the specific tidal height variation. These effects are graphed and explained in Figure 5. In particular, we see that for a given link, the same amount of tidal variation at different tide heights can result in radically different responses in the relative received signal strength (RSS). Note that the measured signal strength for the Ornsay–Corran link in the Tegola network shown in Figure 2 can be characterised as a "positive"

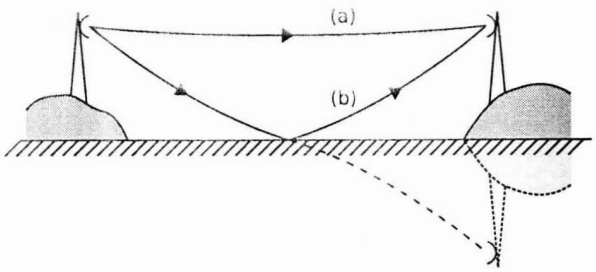

Figure 3: The two ray model, showing (a) the direct path and (b) the indirect path reflected off the water plane. The reflected path is longer, and so may interfere destructively with the direct path. Refraction is neglected in this diagram. The ray paths are curved due to the flat-earth representation used to clarify the reflection.

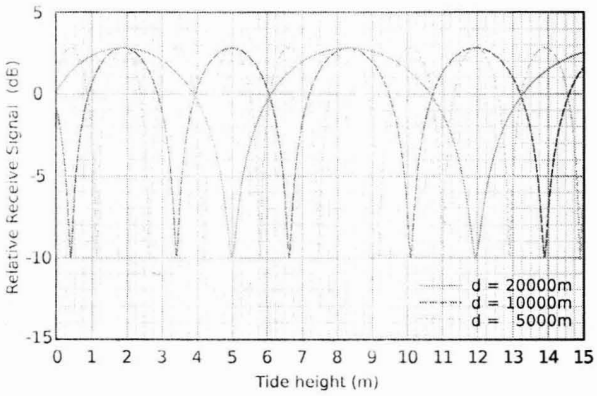

Figure 4: Relative received signal strength vs. tidal height for links with both antennas 50m above sea level calculated using the geometric model for three link lengths. The reflection coefficient is 0.9. The frequency of operation is 5.180GHz (at 2.4GHz the null spacing would approximately double). Atmospheric effects and earth curvature are neglected.

response.

2.2 Pathloss Tool

Now we use a more realistic simulation to demonstrate the effect of tidal variation on the received signal strength. Specifically, we use Pathloss [6], a well-known radio link planning tool from Contract Telecommunication Engineering (CTE). Pathloss accepts input regarding the locations of link endpoints, frequency and mode of operation of the planned link. It uses terrain data to determine the link profile, and then performs calculation using the Longley Rice model [8] in order to determine the expected fading. It also considers environmental factors and earth curvature. We use Pathloss version 4.0.

Figure 6 shows the expected fading with varying tide heights for the Ornsay–Corran link obtained using the Pathloss tool. We see a similar characteristic behavior to that predicted by the simple geometric model. Note that propagation of radio waves is also affected by change in air pressure, which causes rays to diffract. This effect is usually modelled using a *k-factor*, which specifies a gradient change in air pressure with respect to altitude. A k-factor of 1 models no gradient and 1.33 models a "normal" gradient likely in real-world environments. An air-pressure gradient has an approximately constant effect on the two-ray model, causing the direct and reflected rays to travel via longer, curving paths. As a result, the shape of the graph shown in Figure 4 will remain essentially the same, though it may be shifted along the horizontal axis. This similarity in shape means that conclusions from the geometric model will still apply under moderate atmospheric conditions. This argument is validated by the Pathloss simulation of the Ornsay–Corran link for two different k-factor values (see Figure 6).

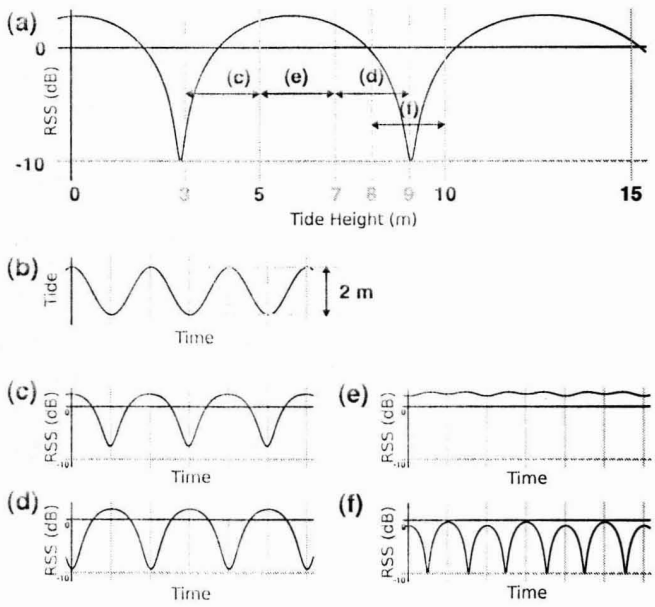

Figure 5: Modelling the effect of the tide-RSS transfer function on four tidal variations of 2 m. **(a)** A typical transfer function. (b) The simulated tidal variation. (c) A "positive" response, where increase in tidal height results in increased signal strength. (d) A "negative" response, where increase in tidal height results in decreased signal strength. (e) A "flat" response, where the signal strength is stable to within approximately 2 dB throughout the tidal cycle. (f) A "cross-null" response, which has two minima for every tidal period.

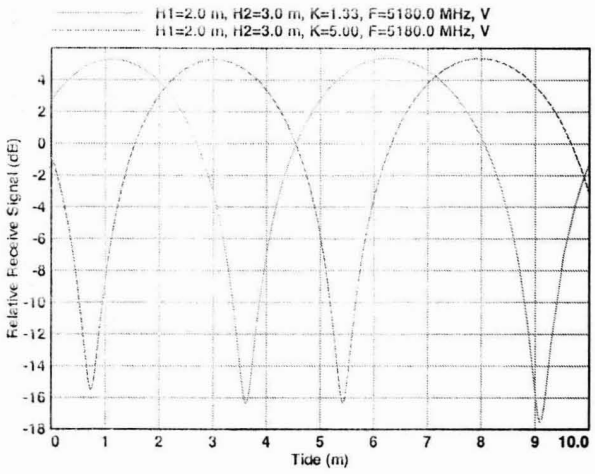

Figure 6: Signal strength against tide height for the Ornsay–Corran link, simulated using CTE Pathloss 4.0. H1 and H2 refer to the heights of the antennas above land height, as determined by the link profile — the antenna heights can be very low as they are positioned on the sides of hills.

2.3 Related Work

While many works have studied propagation of microwaves over water, only a small number have studied the effect of variations in water level on signal fading, or the mitigation thereof [9, 10]. Haslett [11] discusses propagation over water, noting the tidal effect on signal strength and suggesting spacial diversity as a common and robust mitigation technique.

Other studies have observed atmospheric conditions such as ducting [12, 13, 14] or more general distur-

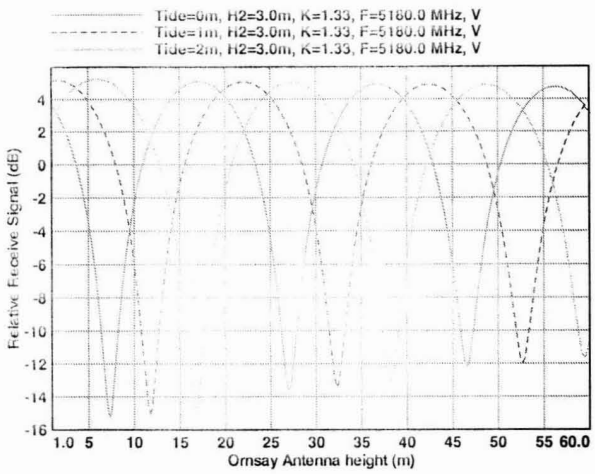

Figure 7: Path loss simulated using CTE Pathloss 4.0 for varying height of the Ornsay antenna on the Ornsay–Corran link. The graph shows that nulls occur approximately every 20 m.

bances at altitude [15]. Extreme conditions over water can have a radical effect. At low altitudes above the water surface the pressure gradient can invert [12, 13, 14] causing ducting. When ducting occurs, multiple rays may reach the receiver after several reflections. The phase of the arriving rays is difficult to predict, and the two-ray model becomes invalid. However, ducting is more likely to occur in some climates than in others, and has not been observed to date in the Tegola network.

3 Solution Approaches

In this section, we present our proposed frequency diversity based technique for countering tidal fading. We begin by discussing the commonly employed spacial diversity solution to motivate our approach.

3.1 Spacial Diversity

Based on our discussion in Section 2, we know that multipath interference at the receiver changes with the height of the tide as a result of phase changes between the direct and reflected rays, causing nulls when both rays are out of phase by 180°. In fact, the interference pattern is dependent on the relative height difference between antenna heights and water level (tide height) at any given point in time. Figure 7 shows this relationship for the Ornsay–Corran link for three different tide heights (with respect to the sea level) by varying the antenna height (with respect to the ground level) at Ornsay (assuming it is the receiver). From this figure, we can make a few observations.

Firstly, one could identify an antenna height at the receiver for a given height of the reflecting plane so as to avoid nulls.

Secondly, when the level of the reflecting plane varies, as is the case with tidal water, any specific antenna height will experience a null at some point in the tidal cycle.

Thirdly, the tide height changes merely have the effect of the shifting the signal strength versus antenna height curve along the horizontal axis — separation between nulls and their depth remain practically unchanged.

Finally, the depth of the nulls reduces with the antenna height, which suggests that links with antennas mounted close to the water level are more severely affected by tidal fading.

The commonly used spacial diversity solution to mitigate tidal fading exploits the combined effect of antenna height and tide height on the received signal strength. Specifically, the idea is based on the third observation above, using two receiving antennas vertically separated by a distance equal to half the separation between the nulls. This ensures that both antennas do not ever experience a null at the same

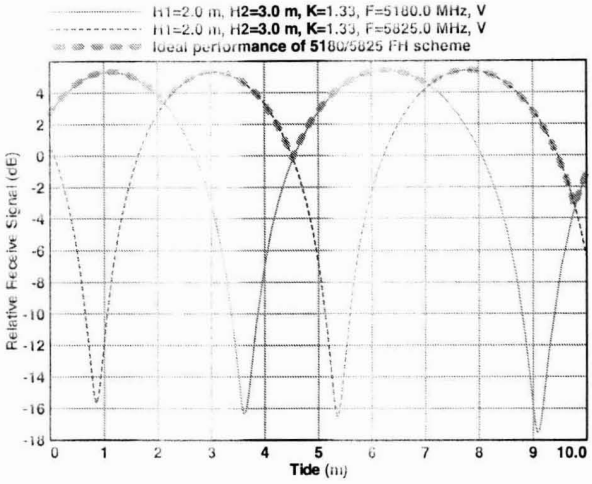

Figure 8: Simulated tidal fading when operating at 5180MHz and 5825MHz for the Ornsay–Corran link using CTE Pathloss 4.0. The fading that would be experienced by a slow frequency hopping system using these two frequencies is also shown.

time. As an example, for the Ornsay–Corran link the vertical antenna separation in a spacial diversity system would be around 10m as the null separation is approximately 20m.

While spacial diversity is a robust and popular solution, it has a couple of major drawbacks in terms of deployment complexity and cost, especially from the perspective of community deployed wireless networks in rural areas.

Firstly, employing spacial diversity requires accurate measurement, planning and tools in order to determine the appropriate antenna separation. These may not be readily available to a community looking to install an over-water link.

The second antenna (dish) also substantially increases the overall cost of the installation. For community installations, the antenna can be among the most expensive pieces of equipment.

Additionally, the cost of the mast increases rapidly with respect to mast height [16]. A single antenna can be easily and inexpensively mounted just a few metres above the ground, but the cost and complication of installing a mast for an additional 10m-spaced diversity antenna will be much greater.

3.2 Our Proposal: Slow Frequency Hopping

Our proposal, termed Slow Frequency Hopping (SFH), exploits the frequency dependence of the two-ray model by switching channels (frequencies) to avoid nulls. The two-ray model is frequency dependent because the amplitude of the received signal is governed by the phase difference between the direct and indirect rays. As the frequency increases, the wavelength decreases, and so the phase difference will change as well. Thus, while for one frequency the two rays may be 180° out of phase resulting in a null, at another frequency the two rays will be in phase.

Figure 8 shows potential gains from our SFH proposal, again using the Ornsay–Corran link in the Tegola network as an example. For instance, when operating at 5.825 GHz, reflections from a tide height of 3.6 m would cause a 16 dB fade. Hopping to 5.180 GHz would instead provide a 4-5 dB enhancement to signal strength due to constructive interference, a net improvement of more than 20dB. The heavy dashed line shows that an optimal frequency hopping scheme using just these two frequencies would prevent signal degradation due to tidal fading altogether for tides between 0 and 9.4 m on the Ornsay–Corran link. The ideal frequency separation for this link (where nulls at one frequency are maxima at the other) is approximately 800MHz. Hopping between more than two frequencies is expected to provide further improvement by delivering the 4-5 dB enhancement over a wider range of tide heights.

Crucially, the SFH technique does not require any additional hardware. The technique can be implemented solely in software by relying upon channel switching features that already exist in virtually all

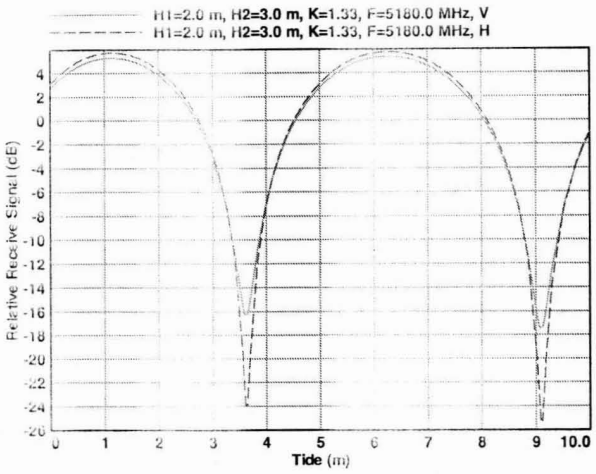

Figure 9: Path loss against tide height simulated using CTE Pathloss 4.0 for vertical and horizontal polarisations on the Ornsay-Corran link. The graph shows that horizontally polarised waves experience deeper fading at nulls than vertically polarised waves.

commodity 802.11 wireless radio cards and driver software. Since channel switching in our case needs to only happen at a slower time scale (in the order of minutes at best), channel switching overheads and the ability to switch quickly are non-issues.

Various types of strategies can be employed to realize SFH in practice. A *reactive* strategy would consider switching to a different channel if the link performance on the current channel becomes unacceptable. An *active* strategy would continuously measure performance at other channels so as to pick the best channel at a given time (akin to 802.11 rate adaptation algorithms like SampleRate). A *proactive* strategy would go a step further by incorporating prediction and link modelling to estimate the performance on each channel in the near future.

Note that the available frequencies for switching need to be sufficiently far apart in order to fully realize the benefits of the SFH technique. This would have been seen to be difficult in the past with the traditional rigid command-and-control spectrum regulatory approach that assigned narrow spectrum bands, each for a specific purpose [17]. With spectrum regulatory reform underway worldwide and technological advances in the form of cognitive radios, a specific spectrum band need no longer be coupled to a specific purpose. As we have demonstrated, even with minor changes to the current regulatory structure, the SFH technique can still be quite effective. Specifically, allowing greater portion of the 5GHz unlicensed spectrum supported by 802.11a devices for fixed wireless access in rural areas with more uniform and relaxed EIRP limits would be sufficient, as 802.11a devices can hop between 24 non-overlapping 20MHz-wide channels in the 5.15-5.85 GHz range.

3.3 Discussion

Here we briefly discuss other possible approaches to mitigate tidal fading.

3.3.1 Polarisation Diversity

Horizontally polarised waves reflect better than vertically polarised waves [18]. As a result, simulation shows that vertically polarised waves experience less deep fades but horizontally polarised waves experience greater (but virtually insignificant) enhancement at peaks. This is illustrated in Figure 9. Our earlier investigation [2] suggests that this approach yields only marginal gains.

3.3.2 Circular Polarisation

Helical antennas operating in axial mode can be used to transmit circularly polarised (CP) waves. CP may be either left-hand polarised or right-hand polarised. Helical antennas are receptive to CP waves with the same handedness, but reject CP waves of the wrong handedness with a significant ratio. This effect can be exploited in order to reject reflections — after reflection the handedness of a CP wave is reversed [18]. This means that a right-handed CP wave will become a left-handed CP wave after reflection, and will thus be rejected by the receiving antenna. Preliminary experimental results [19] appear to corroborate this theory.

A circular polarisation based approach, however, has some limitations: CP antennas for frequencies in the 5GHz range are less compact than their linearly polarised counterparts for the same gain (equivalently, beam width) as the beam width must be traded off against the length of the helix. Commercially available helical antennas, while being compact and with similar cost, have comparatively wide beam widths and low effective gain, thus making them unsuitable for long-distance wireless links (around 10km). Additionally, CP antennas are typically limited to operating effectively in a narrow frequency range of around 100MHz.

3.3.3 MIMO

The 802.11n (MIMO) standard [20] specifies two spatial diversity modes — Transmit Beamforming (TxBF) and Space-Time Block Coding (STBC). These modes may be able to mitigate tidal fading effects, but their benefits remain unproven, for long-distance point-to-point links in rural environments.

In the future, we plan to study the effectiveness of 802.11n in comparison with the proposed SFH technique.

4 Conclusions

4.1 Preliminary Findings

Our findings show that there is a significant relation between tide height and signal strength for over-sea wireless links, that deep fades due to tidal effects can have a significant impact on link quality, and that unlike over-land rural networks, tidal effects may be the primary cause of performance degradation.

We propose a software-only solution called slow frequency hopping to effectively mitigate tidal fades without requiring expert knowledge from network installers and maintainers. Our proposed solution can be implemented using features that already exist in all 802.11 devices, and is a cost-effective alternative to the industry solution based on spacial diversity.

4.2 Planned Work

We plan to continue to collect data from links in the Tegola network in order to verify conclusions drawn from modelling and simulation in this paper. This data will be correlated with available weather information in order to better characterise the effect of adverse conditions such as rain and humidity on the accuracy of the geometric model.

More crucially, we plan to develop a prototype implementation of the proposed slow frequency hopping mitigation technique and conduct a measurement-based evaluation on the Tegola network to experimentally validate our simulation results and compare with the spacial diversity solution. We also plan to design, implement and evaluate reactive, active and proactive frequency hopping strategies.

Acknowledgments

This work was supported in part by The Royal Society. We would like to thank Peter Buneman and Mino Bernardi for helpful discussions, and British Oceanographic Data Centre (BODC) for the tidal data.

RECOMMENDATION ITU-R P.838-3

Specific attenuation model for rain for use in prediction methods

(Question ITU-R 201/3)

(1992-1999-2003-2005)

The ITU Radiocommunication Assembly,

considering

a) that there is a need to calculate the attenuation due to rain from a knowledge of rain rates,

recommends

1 that the following procedure be used.

The specific attenuation γ_R (dB/km) is obtained from the rain rate R (mm/h) using the power-law relationship:

$$\gamma_R = kR^{\alpha} \tag{1}$$

Values for the coefficients k and α are determined as functions of frequency, f (GHz), in the range from 1 to 1 000 GHz, from the following equations, which have been developed from curve-fitting to power-law coefficients derived from scattering calculations:

$$\log_{10} k = \sum_{j=1}^{4} \left(a_j \exp\left[-\left(\frac{\log_{10} f - b_j}{c_j} \right)^2 \right] \right) + m_k \log_{10} f + c_k \tag{2}$$

$$\alpha = \sum_{j=1}^{5} \left(a_j \exp\left[-\left(\frac{\log_{10} f - b_j}{c_j} \right)^2 \right] \right) + m_\alpha \log_{10} f + c_\alpha \tag{3}$$

where:

f: frequency (GHz)

k: either k_H or k_V

α: either α_H or α_V.

Values for the constants for the coefficient k_H for horizontal polarization are given in Table 1 and for the coefficient k_V for vertical polarization in Table 2. Table 3 gives the values for the constants for the coefficient α_H for horizontal polarization, and Table 4 gives the values for the constants for the coefficient α_V for vertical polarization.

TABLE 1

Coefficients for k_H

j	a_j	b_j	c_j	m_k	c_k
1	–5.33980	–0.10008	1.13098	–0.18961	0.71147
2	–0.35351	1.26970	0.45400		
3	–0.23789	0.86036	0.15354		
4	–0.94158	0.64552	0.16817		

TABLE 2

Coefficients for k_V

j	a_j	b_j	c_j	m_k	c_k
1	–3.80595	0.56934	0.81061	–0.16398	0.63297
2	–3.44965	–0.22911	0.51059		
3	–0.39902	0.73042	0.11899		
4	0.50167	1.07319	0.27195		

TABLE 3

Coefficients for α_H

j	a_j	b_j	c_j	m_α	c_α
1	–0.14318	1.82442	–0.55187	0.67849	–1.95537
2	0.29591	0.77564	0.19822		
3	0.32177	0.63773	0.13164		
4	–5.37610	–0.96230	1.47828		
5	16.1721	–3.29980	3.43990		

TABLE 4

Coefficients for α_V

j	a_j	b_j	c_j	m_α	c_α
1	–0.07771	2.33840	–0.76284	–0.053739	0.83433
2	0.56727	0.95545	0.54039		
3	–0.20238	1.14520	0.26809		
4	–48.2991	0.791669	0.116226		
5	48.5833	0.791459	0.116479		

For linear and circular polarization, and for all path geometries, the coefficients in equation (1) can be calculated from the values given by equations (2) and (3) using the following equations:

$$k = [k_H + k_V + (k_H - k_V)\cos^2\theta \cos 2\tau]/2 \quad (4)$$

$$\alpha = [k_H\alpha_H + k_V\alpha_V + (k_H\alpha_H - k_V\alpha_V)\cos^2\theta \cos 2\tau]/2k \quad (5)$$

where θ is the path elevation angle and τ is the polarization tilt angle relative to the horizontal ($\tau = 45°$ for circular polarization).

For quick reference, the coefficients k and α are shown graphically in Figs. 1 to 4, and Table 5 lists numerical values for the coefficients at given frequencies.

FIGURE 1

***k* coefficient for horizontal polarization**

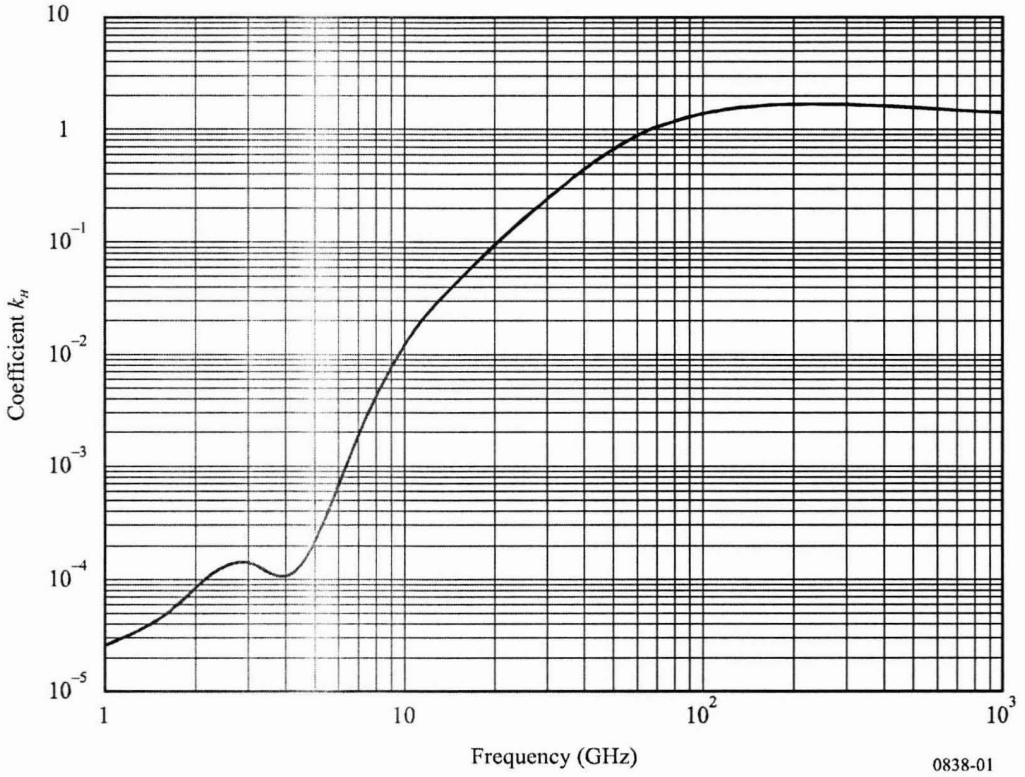

FIGURE 2

α coefficient for horizontal polarization

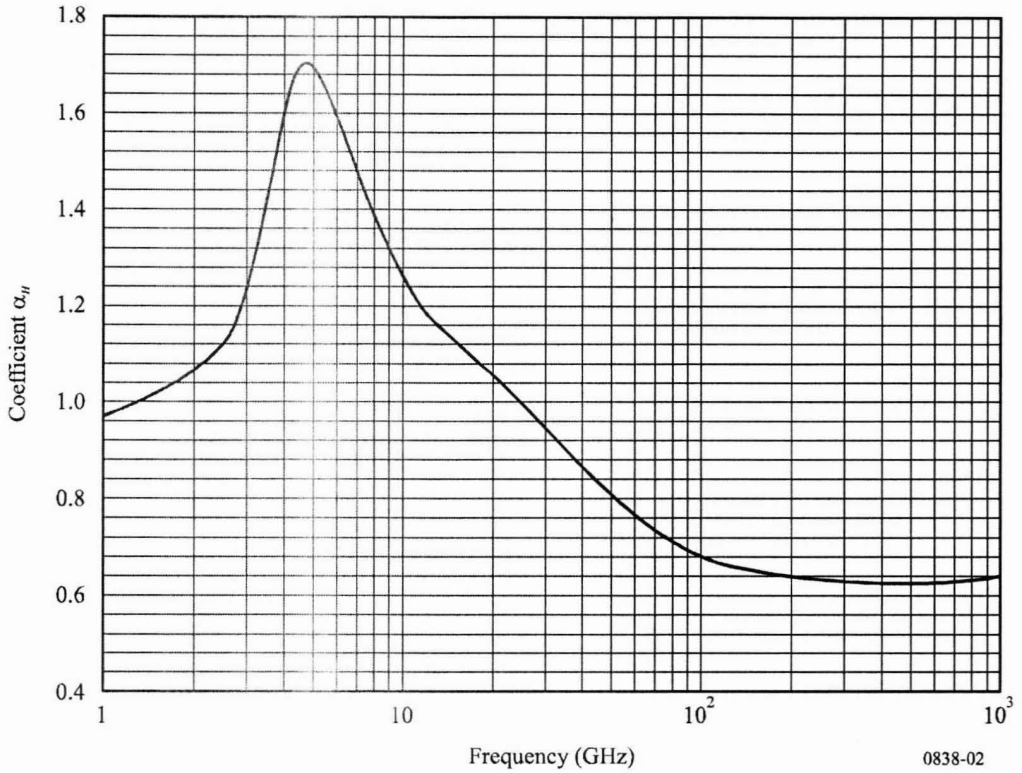

FIGURE 3

***k* coefficient for vertical polarization**

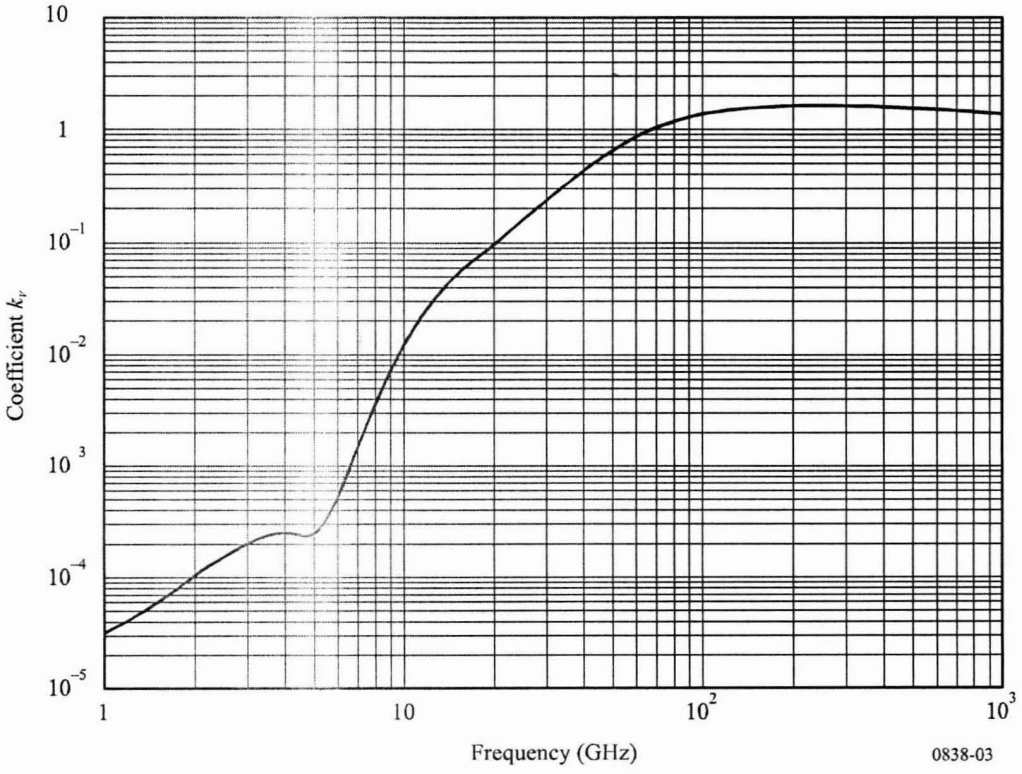

FIGURE 4

α coefficient for vertical polarization

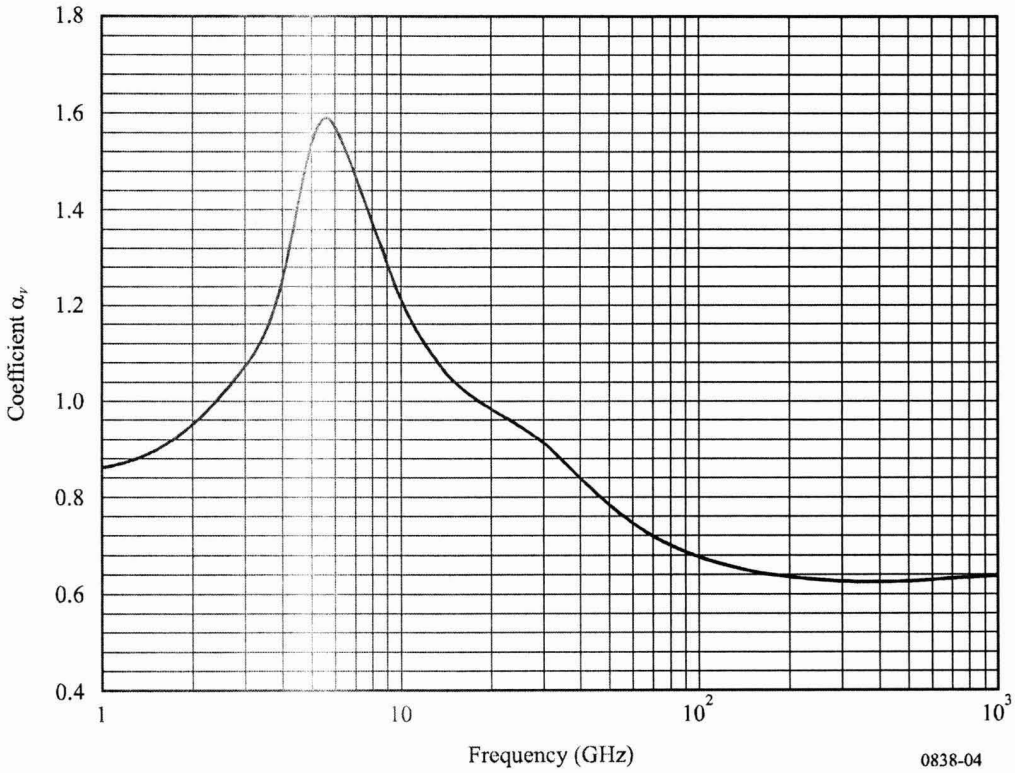

TABLE 5

Frequency-dependent coefficients for estimating specific rain attenuation using equations (4), (5) and (1)

Frequency (GHz)	k_H	α_H	k_V	α_V
1	0.0000259	0.9691	0.0000308	0.8592
1.5	0.0000443	1.0185	0.0000574	0.8957
2	0.0000847	1.0664	0.0000998	0.9490
2.5	0.0001321	1.1209	0.0001464	1.0085
3	0.0001390	1.2322	0.0001942	1.0688
3.5	0.0001155	1.4189	0.0002346	1.1387
4	0.0001071	1.6009	0.0002461	1.2476
4.5	0.0001340	1.6948	0.0002347	1.3987
5	0.0002162	1.6969	0.0002428	1.5317
5.5	0.0003909	1.6499	0.0003115	1.5882
6	0.0007056	1.5900	0.0004878	1.5728
7	0.001915	1.4810	0.001425	1.4745
8	0.004115	1.3905	0.003450	1.3797
9	0.007535	1.3155	0.006691	1.2895
10	0.01217	1.2571	0.01129	1.2156

TABLE 5 (*continued*)

Frequency (GHz)	k_H	α_H	k_V	α_V
11	0.01772	1.2140	0.01731	1.1617
12	0.02386	1.1825	0.02455	1.1216
13	0.03041	1.1586	0.03266	1.0901
14	0.03738	1.1396	0.04126	1.0646
15	0.04481	1.1233	0.05008	1.0440
16	0.05282	1.1086	0.05899	1.0273
17	0.06146	1.0949	0.06797	1.0137
18	0.07078	1.0818	0.07708	1.0025
19	0.08084	1.0691	0.08642	0.9930
20	0.09164	1.0568	0.09611	0.9847
21	0.1032	1.0447	0.1063	0.9771
22	0.1155	1.0329	0.1170	0.9700
23	0.1286	1.0214	0.1284	0.9630
24	0.1425	1.0101	0.1404	0.9561
25	0.1571	0.9991	0.1533	0.9491
26	0.1724	0.9884	0.1669	0.9421
27	0.1884	0.9780	0.1813	0.9349
28	0.2051	0.9679	0.1964	0.9277
29	0.2224	0.9580	0.2124	0.9203
30	0.2403	0.9485	0.2291	0.9129
31	0.2588	0.9392	0.2465	0.9055
32	0.2778	0.9302	0.2646	0.8981
33	0.2972	0.9214	0.2833	0.8907
34	0.3171	0.9129	0.3026	0.8834
35	0.3374	0.9047	0.3224	0.8761
36	0.3580	0.8967	0.3427	0.8690
37	0.3789	0.8890	0.3633	0.8621
38	0.4001	0.8816	0.3844	0.8552
39	0.4215	0.8743	0.4058	0.8486
40	0.4431	0.8673	0.4274	0.8421
41	0.4647	0.8605	0.4492	0.8357
42	0.4865	0.8539	0.4712	0.8296
43	0.5084	0.8476	0.4932	0.8236
44	0.5302	0.8414	0.5153	0.8179
45	0.5521	0.8355	0.5375	0.8123
46	0.5738	0.8297	0.5596	0.8069
47	0.5956	0.8241	0.5817	0.8017
48	0.6172	0.8187	0.6037	0.7967

TABLE 5 (*continued*)

Frequency (GHz)	k_H	α_H	k_V	α_V
49	0.6386	0.8134	0.6255	0.7918
50	0.6600	0.8084	0.6472	0.7871
51	0.6811	0.8034	0.6687	0.7826
52	0.7020	0.7987	0.6901	0.7783
53	0.7228	0.7941	0.7112	0.7741
54	0.7433	0.7896	0.7321	0.7700
55	0.7635	0.7853	0.7527	0.7661
56	0.7835	0.7811	0.7730	0.7623
57	0.8032	0.7771	0.7931	0.7587
58	0.8226	0.7731	0.8129	0.7552
59	0.8418	0.7693	0.8324	0.7518
60	0.8606	0.7656	0.8515	0.7486
61	0.8791	0.7621	0.8704	0.7454
62	0.8974	0.7586	0.8889	0.7424
63	0.9153	0.7552	0.9071	0.7395
64	0.9328	0.7520	0.9250	0.7366
65	0.9501	0.7488	0.9425	0.7339
66	0.9670	0.7458	0.9598	0.7313
67	0.9836	0.7428	0.9767	0.7287
68	0.9999	0.7400	0.9932	0.7262
69	1.0159	0.7372	1.0094	0.7238
70	1.0315	0.7345	1.0253	0.7215
71	1.0468	0.7318	1.0409	0.7193
72	1.0618	0.7293	1.0561	0.7171
73	1.0764	0.7268	1.0711	0.7150
74	1.0908	0.7244	1.0857	0.7130
75	1.1048	0.7221	1.1000	0.7110
76	1.1185	0.7199	1.1139	0.7091
77	1.1320	0.7177	1.1276	0.7073
78	1.1451	0.7156	1.1410	0.7055
79	1.1579	0.7135	1.1541	0.7038
80	1.1704	0.7115	1.1668	0.7021
81	1.1827	0.7096	1.1793	0.7004
82	1.1946	0.7077	1.1915	0.6988
83	1.2063	0.7058	1.2034	0.6973
84	1.2177	0.7040	1.2151	0.6958
85	1.2289	0.7023	1.2265	0.6943
86	1.2398	0.7006	1.2376	0.6929

TABLE 5 (*end*)

Frequency (GHz)	k_H	α_H	k_V	α_V
87	1.2504	0.6990	1.2484	0.6915
88	1.2607	0.6974	1.2590	0.6902
89	1.2708	0.6959	1.2694	0.6889
90	1.2807	0.6944	1.2795	0.6876
91	1.2903	0.6929	1.2893	0.6864
92	1.2997	0.6915	1.2989	0.6852
93	1.3089	0.6901	1.3083	0.6840
94	1.3179	0.6888	1.3175	0.6828
95	1.3266	0.6875	1.3265	0.6817
96	1.3351	0.6862	1.3352	0.6806
97	1.3434	0.6850	1.3437	0.6796
98	1.3515	0.6838	1.3520	0.6785
99	1.3594	0.6826	1.3601	0.6775
100	1.3671	0.6815	1.3680	0.6765
120	1.4866	0.6640	1.4911	0.6609
150	1.5823	0.6494	1.5896	0.6466
200	1.6378	0.6382	1.6443	0.6343
300	1.6286	0.6296	1.6286	0.6262
400	1.5860	0.6262	1.5820	0.6256
500	1.5418	0.6253	1.5366	0.6272
600	1.5013	0.6262	1.4967	0.6293
700	1.4654	0.6284	1.4622	0.6315
800	1.4335	0.6315	1.4321	0.6334
900	1.4050	0.6353	1.4056	0.6351
1 000	1.3795	0.6396	1.3822	0.6365



Planning, Designing and Performance Evaluation of Micro Wave Link Case Study from Wegeda to NefasMewucha

Gashaw Mihretu[1(✉)], Pushparaghavan Annamalai[1], and N. Malmurugan[2]

[1] Faculty of Electrical and Computer Engineering,
Bahir Dar Institute of Technology, Bahir Dar University, POB 26, Bahir Dar, Ethiopia
gashite2009@gmail.com, aprshamu@gmail.com
[2] Mahindra College of Engineering, Salem, Tamilnadu, India
n.malmurugan@gmail.com

Abstract. The Microwave link is an alternative link for fiber optics or for the area which is difficult to practically implement fiber optics and satellite link access. It has different properties like line of sight, environmental constraints, including rain fade and many obstacle issues such as hills, buildings and trees. In Ethiopia, Amhara region, South Gondar, currently the hill station in between Wegeda Amanuel areas, microwave link severely affected and equipment failure due to the environmental interferences. Because of interruption of this link, most of the times stop the connection of this area. Due to the above limitation of the rural access to this area, this paper is specially intended to provide and fulfill the needs by planning and designing microwave link between NefasMewucha to Wegeda. The traffic from and to Wegeda is likely to increase in future as it is one of the important potential area in Amhara region. Hence, it needs reliable and efficient alternate communication link. In overall, this paper deals the site survey, system margins, frequency planning, power budget calculation and performance evaluation activities and the results are simulated using Global mapper 12.

Keywords: Path clearance · Signal Radiation Loss · System Margin · Power budget · Link reliability

1 Introduction

Microwave link is very important in the Ethiopia Amhara region because most of the geographical areas are not suitable for wired communications systems. Wegeda is one of the most inconvenient areas for copper wire and optical fiber link, but these areas are highly productive and it should have an uninterrupted telecommunication network to access these products and increase the development. An alternative link has required to connect Wegeda to other parts of Amhara region and whole country. Preferably, micro wave link is a choice to achieve this objective in appropriate way for the cost effective, more convenient for the proposed link access better than optical link [7].

© ICST Institute for Computer Sciences, Social Informatics and Telecommunications Engineering 2020
Published by Springer Nature Switzerland AG 2020. All Rights Reserved
N. G. Habtu et al. (Eds.): ICAST 2019, LNICST 308, pp. 337–354, 2020.
https://doi.org/10.1007/978-3-030-43690-2_23

The following Fig. 1 illustrates the flow chart approach for the proposed microwave link system and its design process. Mainly, the proposed link focus on the path performance for stage by stages per the system design process [2].

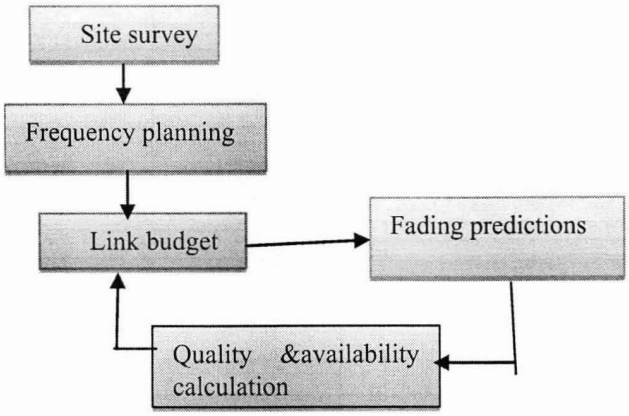

Fig. 1. System design process flow chart

2 Site Planning and Selection

The two sites of proposed link are, one is NefasMewucha and the other is Wegeda. From these sites, most of the real time data are collected by pilot surveying approach. These data are helped to know the path clearance, the coordinates of the sites, distance between path link, antenna height and the location and height of obstacles [3].

2.1 Path Wegeda to NefasMewucha

Figure 2 shows a geographical map of the two proposed terminals (Wegeda to NefasMewucha).

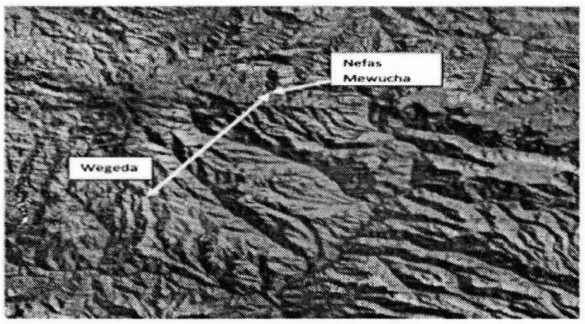

Fig. 2. Map of area of interest of the link

The proposed link is from Wegeda to NefasMewucha and its coordinate is measured at the presently existing tower of the two sites by using Global Positioning System (GPS) receivers and possible hop distance is determined by Global mapper 12 software by using these coordinates. Table 1 given below shows the coordinates and possible hop distance of the proposed link.

Table 1. Co-ordinates and hop distance of Wegeda and NefasMewucha

Path profile	Radio terminals sites	
	Wegeda	NefasMewucha
Latitude	11°23′50.0580″N	11°44′505″N
Longitude	38°14′18.173″E	38°28′665″E
Elevation	2560.84 m	3010 m
Maximum Hop length	45.1 km from NefasMewucha	45.1 km from Wegeda

Note: the hop length from the above Table 1 is line of sight length not road distance.

Based on the above data, path profile between two sites, the maximum hop length, elevation of the two sites and the maximum height of obstacles are obtained and shown in Fig. 3.

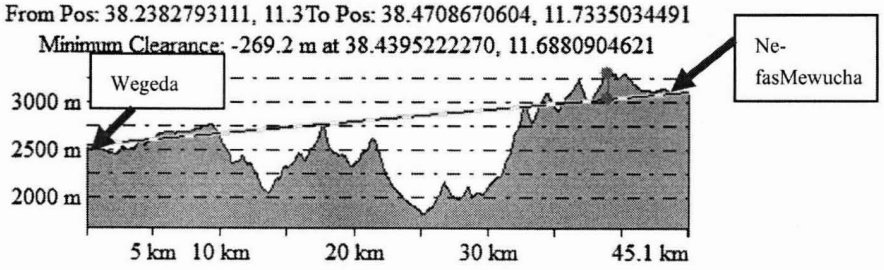

Fig. 3. Path distance from Wegeda to NefasMewucha

As shown in Fig. 3. It is observed that the link is not a clear line of sight. So an alternative link is required.

2.2 Recommended Hop Link: Wegeda to Guna and Guna to NefasMewucha

The two recommended hop links are from Wegeda to Guna and from Guna to Nefas-Mewucha with repeater at Guna. The map shown in Fig. 4 illustrates the two alternative links.

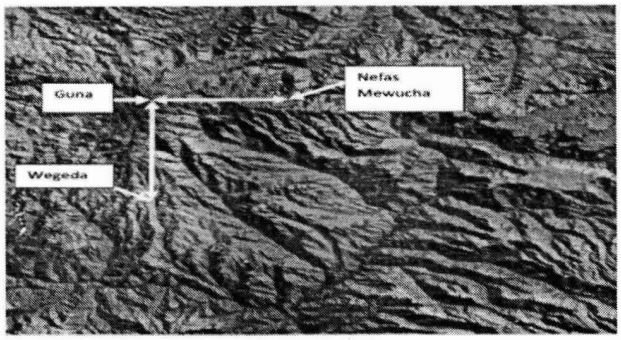

Fig. 4. Illustrate the hop from Wegeda to Guna and Guna to NefasMewucha

Coordinates of the two hops such as latitude, longitude and elevation are measured using GPS receivers at the existing towers (Table 2).

Table 2. Co-ordinates of sites and their path length

Path profile	Link sites		
	Wegeda	NefasMewucha	Guna
Latitude	11°23′50.0580″N	11°44′505″N	11°42′39″N
Longitude	38°14′18.173″E	38°28′665″E	38°14′31.9605″E
Elevation	2560.84 m	3010 m	4122 m
Maximum hop length	35.0 km from Guna	25.5 km from Guna	35.0 km to Wegeda & 25.5 km from NefasMewucha

Note:- The hop distance in the above table is line of sight distance.

The path profile of the two alternative links, from Wegeda to Guna and Guna to NefasMewucha are shown in Figs. 5 and 6 below. The path profile of the hop from Wegeda to Guna and Guna to NefasMewucha needs minimum 28.8 m and 21.4 m height antennas respectively for line of sight.

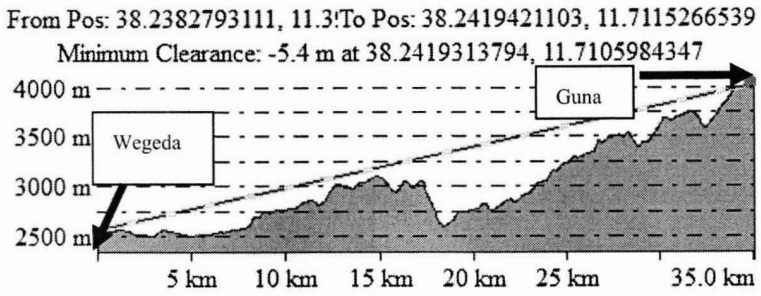

Fig. 5. Path profile from Wegeda-Guna

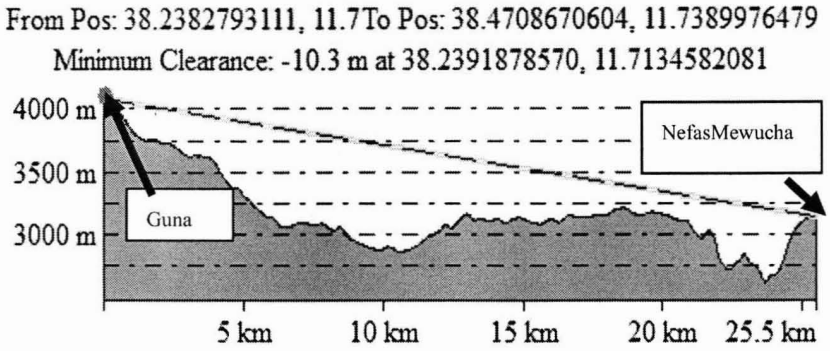

Fig. 6. Path link length from Guna to NefasMewucha

2.3 Frequency Planning

The operating frequency bands of existing link at the Guna station in the direction of the proposed link is 8 GHz. So, that the frequency to be selected should be different from this band. In the design link 7 GHz frequency band is used for both transmitter and receiver frequency for each hop as per Table 3 shown below

Table 3. Frequency arrangement

Station	Unit	Tx module	Rx module	LO	IF (Tx/Rx)	T/R (Duplex)
Guna	MHz	7550	7850	5550	2000/2161	161 MHz
NefasMewucha to/from Guna	MHz	7850	7550		2161/2000	
Guna to/from Wegeda	MHz	7125	7425	5125	2000/2161	161/154 MHz
Wegeda	MHz	7425	7125		2161/2000	

3 Use of Repeaters

As shown in Fig. 3 below, it is already seen that there is no possibility of establishing the direct microwave link between the stations Wegeda to NefasMewucha due to LOS obstruction. Hence a repeater station in Guna is suggested in between [11].

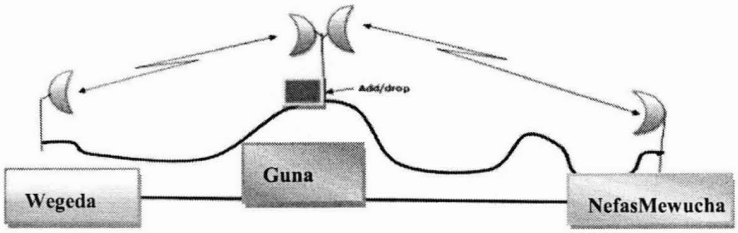

Fig. 7. Repeaters between Wegeda and NefasMewucha

At Guna station adds/drops of data, voice and videos are done by using ADM equipment.

4 First Fresnel Zone (FFZ)

After getting a feasible link, the next step in the microwave link design is calculating the (FFZ) radius, in order to know at least 60% of the FFZ free from any type of obstruction in the hop [6].

It depends on the hope length and the operating frequency [1]. For no obstructions between two sites, the maximum first Fresnel zone radius is calculated using the following formula [6].

$$F = 8,657\sqrt{l/f} \tag{1}$$

Where

F = first Fresnel zone
l = the maximum hop length in meter
f = operating frequency of the link

4.1 FFZ –Wegeda to Guna

The maximum 60% FFZ of this path is calculated using Eq. (1) with,

l = Hop length from Wegeda to Guna in meter = 35 km = 35000 m
f = operating frequency of link = 7.125 GHz

$$F = 8,657\sqrt{35000/7.125 * 10^9} = 19.187$$

4.2 FFZ– Guna to NefasMewucha

The 60% radius of the FFZ for the above link is calculated using Eq. (1) with,

l = Hop length from Guna to NefasMewucha 25.5 km = 25500 m
f = operating frequency of path = 7.55 GHz

$$F = 8,657\sqrt{25500/7.55 * 10^9} = 15.9\,\text{m}$$

5 Antenna Height Calculation

Antenna height of the microwave link is calculated based on the Rec. ITU-R P.530-14 [10]. For the first hop antenna height, $(A_h) = 1.0 * F_1 = 1 * 19.187$ m = 19.187 m, we must consider the height of trees and growth of vegetables 12 m and 3 m respectively. Where F_1 is First Fresnel Zone radius, so the antenna height, $(A_h) = 19.187$ m + 12 m + 3 m = 34.187 m (this is the minimum antenna height for the first hop).

Similarly, the same procedure can be repeated for the second hop.

Antenna height, $(A_h) = 1.0 * F_1 + 12$ m + 3 m = 15.9 m + 12 m + 3 m = 30.9 m (this is the minimum antenna height for the second hop). In the two hops, the antenna should not be mounted less than the calculated height.

In our design, the antennas can be mounted at 40 m and 35 m for the first hop and the second hop on the existing tower heights respectively to have more clearance.

The first and second hop path profiles with the recommended antenna heights have 34.6 m and 24.7 m give clearance from any obstacle and they are shown in Figs. 8 and 9 respectively. These indicate the feasible path of the two hops.

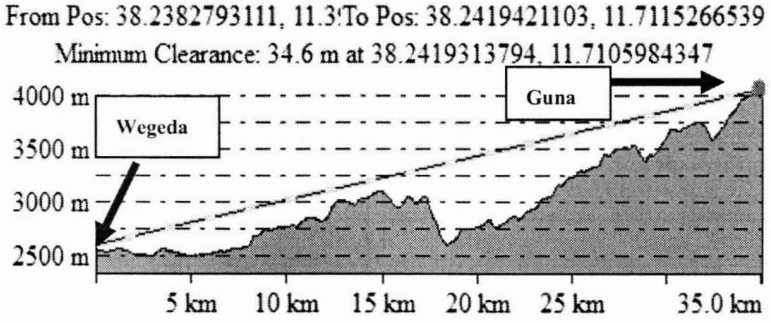

Fig. 8. Path clearance from Wegeda to Guna with 40 m antenna height

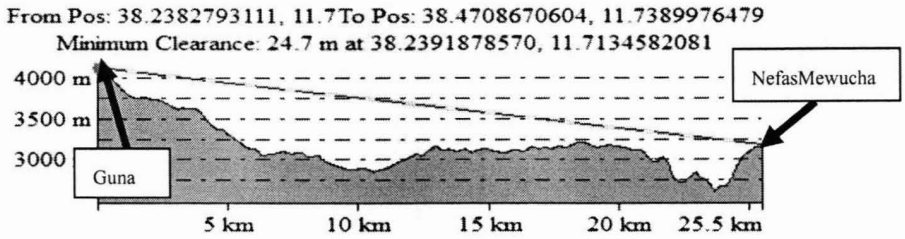

Fig. 9. Path from Guna to NefasMewucha with 35 m antenna height

6 Micro Wave Link Path Analysis

Microwave link path analysis is carried out to dimension the link and it is a calculation involving the gain and loss factors associated with the antennas, transmitters, transmission lines and propagation environment [2].

6.1 Signal Radiation Losses (SRL)

Signal radiation loss is the degradation of transmitting signals, when it propagates through a free space. This loss depends on the length of links and the operating frequency of path [4].

If the frequency and the distance are expressed in terms of Kilometer and Giga Hertz, the signal radiation loss is given by the following equation [6, 8].

$$L_{SRL} = 92.45 + 20\log(f) + 20\log(d)\,[\text{dB}] \tag{2}$$

Where

f = frequency (GHz)
d = distance of hop between transmitter and receiver (Km)

6.2 Power Received (P_r)

The receive power is the amount of power reached at the receiver unit after the transmitted power pass through a free space [5]. To assure the link feasibility the received power magnitude must be greater than or equal to the Receiver sensitivity threshold. P_r can calculate using the following formula [8].

$$P_r = P_t - L_{ctx} + G_{atx} - L_{crx} + G_{arx} - SRL - R_t\,[\text{dBm}] \tag{3}$$

Where

P_r = Power received
P_t = Output power of the transmitter (dBm)
$L_{ctx,}$ = Connectors, branching Loss (cable unit) b/n Transmitter and Transmitter antenna (dB)
L_{crx} = Connectors, branching Loss (cable unit) b/n Receiver and Receiver antenna (dB)
G_{atx} = Gain of transmitter antenna (dBi)
G_{arx} = Gain of receiver antenna (dBi)
SRL = Signal Radiation Loss (dB)
R_t = Rain attenuation (dB)
$P_r \geq R_s$ (receiver sensitivity threshold)

6.3 Rain Attenuation Calculation for the First Hop (Wegeda to Guna)

The rain data were taken from National Metrology Agency Bahir Dar branch which is collected from NefasMewucha, Simada (Wegeda) and Gassay rain fall sites.

The rain attenuation calculations are calculated based on ITU-R Model of Rain Attenuation because the rain attenuation is minimum in this model when compare to other methods. It is calculated by using the following steps [9].

Step 1: Obtain the rain rate R0.01 exceeded in 0.01% of the time (with an integration of 1 min) [9]. The maximum rain rate at the two sites are taken from the collected data. But in Guna there is no rainfall station, we use the rainfall data from Gassay station, which is near to Guna and it has almost the same rain data. The maximum rain rate at Wegeda and Gassay record in July 2013 and mar 2014, and the values are 444.9 mm/h and 719.6 mm/h respectively. The average rain ratings are used.

$$\begin{aligned} \text{Average rain rate} &= (444.9\,\text{mm/h} + 719.6\,\text{mm/h})/2 \\ &= 582.25\,\text{mm/h} \\ R_{0.01} &= 582.25\,\text{mm}/60\,\text{min} = 9.7\,\text{mm/min} \end{aligned}$$

Step 2: Compute the specific attenuation, γ (dB/km) for 7 GHz frequency band, vertical polarization and the above rain rate. It can be expressed as follows [9].

$$\gamma = KR^{\alpha} \tag{4}$$

Where

γ = rain rate at p% of probability
K, α = functions of frequency, f (GHz) in the range 1 to 1000 GHz.

The specific attenuation is computed by using k = 0.00265 and α = 1.312, these values are tabulated values by different publications for 7 GHz frequency. Therefore, specific attenuation is calculated by using Eq. (4).

$$\gamma = KR^{\alpha} = 0.00265 * 9.7^{1.312} = 0.0522\,\text{dB/km}$$

Step 3: Compute the effective path length, d_{eff}, of the link by multiplying the actual path length (1) by a distance factor(r). Before computing effective path length, distance factor is given by [9].

$$r = 1/1 + l/d_0 \tag{5}$$

Where

r = distance factor
l = path length

Where, for $R_{0.001} \leq 100$ mm/h [10].

$$d_0 = 35e^{-0.015R}_{0.01} \tag{6}$$

With actual path length of 35 km and d_0 is calculated by Eq. (6)
But in our design 0.01 R ≥ 100 mm/h, we use the value 100 mm/h in place of 0.01*R*.

$$d_0 = 35e^{-0.015*100} = 3.448\,\text{km}$$

Therefore, distance factor and effective distance become.

$$\text{And} \quad d_{\text{eff}} = 35\,\text{km} * 0.0897 = 3.1395\,\text{km}$$

Step 4: An estimate of the path attenuation exceeded in 0.01% of the time is given by [9]

$$A_{0.01} = \gamma d_{\text{eff}} = \gamma l.r\,(\text{dB}) \tag{7}$$

Where

l = path length
r = reduction factor

By using the values of effective distance and specific attenuation from the above analysis the estimated path attenuation exceeded 0.01% becomes

$$A_{0.01} = 0.0522 * 3.1395 = 0.164\,\text{dB}$$

6.4 Rain Attenuation Calculation for the Second Hop (Guna to NefasMewucha)

The rain attenuation calculations are calculated based on ITU-R Model of Rain Attenuation because the rain attenuation is minimum in this model when compare to other methods [9]. It is calculated by using the following steps.

Step 1: The rain rate R0.01 exceeded in 0.01% of the time (with an integration of 1 min) [9]. The data were collected by the national metrology agency, Bahir Dar branch. We take the maximum rain rate at the two sites from the collected data. But at Guna there is no rainfall station, we use the rainfall data from Gassay station which is near to Guna. The maximum rain rate at Guna and NefasMewucha are recorded in March 2014 and July 1998, and the values are 719.6 mm/h and 510.0 mm/h respectively. The average rain ratings are used.

$$\begin{aligned}\text{Average rain rate} &= (510.0\,\text{mm/h} + 719.6\,\text{mm/h})/2\\ &= 614.8\,\text{mm/h}\\ R_{0.01} &= 614.8\,\text{mm}/60\,\text{min} = 10.25\,\text{mm/min}\end{aligned}$$

Step 2: Computation of the specific attenuation, γ (dB/km) for 7 GHz frequency band, vertical polarization and the above rain rate. The specific attenuation is computed by using $k = 0.00265$ and $\alpha = 1.312$, these values are tabulated values by different publications for 7 GHz frequency. The calculation is done by using Eq. (4) as follow.

$$\gamma = KR^{\alpha} = 0.00265 * 10.25^{1.312} = 0.056\,\text{dB/km}$$

Step 3: Computation of the effective path length, d_{eff}, of the link by multiplying the actual path length (l) by a distance factor *r*. Before computing effective path length, we must calculate the distance factor by using Eq. (5) with actual path length of 25.5 km and d_0 is calculated by Eqs. (6).

But In our design $0.01\,R \geq 100$ mm/h, we use the value 100 mm/h in place of $0.01R$.

$$d_0 = 35e^{-0.015*100} = 3.448\,\text{km}$$

Therefore, distance factor and effective distance become.

$$\begin{aligned}r &= 1/(1 + 25.5\,\text{km}/3.448\,\text{km}) = 1/8.3956 = 0.119\\ \text{And}\quad d_{eff} &= 25.5\,\text{km} * 0.119 = 3.037\,\text{km}\end{aligned}$$

Step 4: An estimate of the path attenuation exceeded in 0.01% of the time is calculated by using Eq. (7)

$$A_{0.01} = 0.056 * 3.037 = 0.17\,\text{dB}$$

The rain attenuation of the first hop and the second hop are 0.164 dB and 0.17 dB respectively. This result shows the rain attenuation is directly proportional to the rain rate because the rain rate in the second hop is greater than the first hop.

6.5 System Margin (SM)

System margin is an essential parameter in microwave link path which is to evaluate the performance of the link to be established and it can be expressed as

$$SM = P_r - R_{th} \tag{8}$$

Where

SM = System margin
P_r = Received Signal Level
R_{th} = Receiver threshold

7 Power Budget of the Proposed Link

Before establishing the path of the proposed link we should determine the equipment's used at the transmitter and the receiver site and select that equipment's with appropriate ratings to have a reliable system [2].

The specification of the equipment's used at the transmitter and receiver site is shown in Table 4 below.

Table 4. Rating of equipment used in transmitters and receivers site

Frequency bands (GHz)		7
Full-duplex		FDD
Operating frequency		7125 MHz to 7900 MHz
Standby mode configuration		1 + 0 or 1 + 1
Power supply (V)		DC: −48 V (+24 V), 10%
RF output power (dBm)		27
Receiver threshold (dBm)		−84
Antenna gain (dBi) medium (0.9 m diameter)		34.8
Type of cable	Operating frequency	Loss in dB per 100 feet
LMR-900	7 GHz	2.9

7.1 Power Budget from Wegeda to Guna

In order to calculate the Power budget, we use the specifications of the equipment given in Table 4.

Signal Radiation Loss *(SRL)*
Signal Radiation Loss in free space *is* calculated using Eq. (2) with f = frequency (GHz) = 7.125 and d = distance of the hop between *Wegeda to Guna* (Km) = 35

$$L_{SRL} = 92.45 + 20\log(7.125) + 20\log(35)\,[\text{dB}]$$
$$= 92.45 + 17.055 + 30.88 = 140.386\,\text{dB}$$

Power Received P_r
Received power at the receiver side can be calculated using Eq. (4) with P_t = output power of the transmitter (dBm) = 27 and Lctx, = Loss (cable, connectors, branching unit at Tx) = 5.766 dB + 0.025 dB = 5.79 dB, because the cable length at the transmitter side is 60 m, it has 5.766 dB loss and 0.025 dB is connector loss.

L_{crx} = Loss (cable, connectors, branching unit at Rx) 5.766 dB + 0.025 dB = 5.79 dB, because the cable length at the receiver side is 60 m, it has 5.766 dB loss and 0.025 dB is connector loss between transmitter/receiver and antenna.

G_{atx} = Gain of transmitter antenna (dBi) = 34.8
G_{atx} = Gain of transmitter antenna (dBi) = 34.8
G_{arx} = Gain of receiver antenna (dBi) = 34.8
L_{SRL} = Signal Radiation Loss (dB) = 140.386
R_t = Rain attenuation (dB) = 0.164

$$P_r = 27\,\text{dBm} + 34.8\,\text{dBi} - 5.79\,\text{dB} + 34.8\,\text{dBi} - 5.79\,\text{dB} - 140.386\,\text{dB} - 0.164\,\text{dB}$$
$$= -55.53\,\text{dBm}$$

System Margin (SM)
The system margin of the above path can be calculated as follows using Eq. (8).

With P_r = power Received = −55.53 dBm and R_{th} = Receiver threshold = −84 dBm

$$SM = P_r - R_{th}$$
$$= -55.53\,\text{dBm} - (-84\,\text{dBm}) = 28.47\,\text{dB}$$

7.2 Link Budget from Guna to NefasMewucha

In order to calculate the power budget, we use the specifications of the equipment given in Table 4.

Signal Radiation Loss (SRL)
Signal Radiation Loss in free space *is* calculated using Eq. (3) with f = frequency (GHz) = 7.55 and d = distance of the hop between Guna to NefasMewucha (Km) = 25.5

$$\begin{aligned} L_{SRL} &= 92.45 + 20\log(7.55) + 20\log(25.5)\,[\text{dB}] \\ &= 92.45 + 17.559 + 28.13 = 138.14\,\text{dB} \end{aligned}$$

Power Received (P_r)
Received power at the receiver side in the second hop can be calculated using Eq. (4) with P_t = output power of the transmitter (dBm) = 27, L_{ctx}, = Loss (cable, connectors, 55 m, it has 5.23 dB loss and 0.025 dB is connector loss between transmitter/receiver and antenna (dB) = 5.23 dB + 0.025 dB = 5.255 dB, L_{crx} = Loss (cable, connectors, branching unit at Rx) 5.23 dB + 0.025 dB = 5.255 dB, because the cable length at the transmitter side is 55 m, it has 5.23 dB loss and 0.025 dB is connector loss between transmitter/receiver and antenna, G_{atx} = gain of the transmitter antenna (dBi) = 34.8, G_{arx} = gain of receiver antenna (dBi) = 34.8, L_{SRL} = Signal Radiation Loss s (dB) = 138.14 and R_t = rain attenuation (dB) = 0.17 dB.

$$\begin{aligned} P_r &= 27\,\text{dBm} + 34.8\,\text{dBi} - 5.255\,\text{dB} + 34.8\,\text{dBi} - 5.255\,\text{dB} - 138.14\,\text{dB} - 0.17\,\text{dB} \\ &= -52.22\,\text{dBm} \end{aligned}$$

System Margin
The system margin of the above path can be calculated as follows using Eq. (8) with P_r = power Received = −52.22 dBm and R_{th} = Receiver threshold = −84 dB.

$$\begin{aligned} SM &= P_r - R_{th} \\ &= -52.22\,\text{dBm} - (-84\,\text{dBm}) = 31.78\,\text{dB} \end{aligned}$$

Note: in the power budget analysis of the above two hops, Wegeda to Guna has system margin of 28.47 dB and the second Guna to NefasMewucha has 31.78 dB. These results are greater than 10 dB (threshold value) which shows the link has the ability to provide guaranteed quality of service.

8 Link Availability

The path availability also called link reliability is the percentage of time that the received signal is above the required threshold, P_{req}. It is sometimes expressed as the expected minutes of outage per year and the percentage of time represents the outage time for a given link budget [8]. The path availability is function of the radio frequency, diversity, fade margin, path length, and local climate. The International Telecommunication Union publishes reports with empirical models of required fade margin for different parts of the world [10].

The percentage of time (P_w) that fades depth (A) (dB) is exceeded in the average worst month is calculated by using the following equation [10].

$$P_w = k * l^{3.6} * f^{0.89}(1 + |\varepsilon_p|)^{-1.4} * 10^{-A/10} \tag{9}$$

Where

k = geoclimatic factor
l = path length in km
f = frequency in GHz
ε_P = path slope
A = fade margin [dB]

The path inclination $|\varepsilon_p|$ (mrad) of the link is calculated from the antenna heights of the transmitter and receiver (above sea level or some other reference height) and it is calculated as follows [10],

$$\varepsilon_p = (h_A - h_B)/l \tag{10}$$

Where

h_A = antenna height + ground elevation at the transmitter in m
h_B = antenna height + ground elevation at the receiver in m
l = path length in Km

Another parameter that determines the percentage of the time average worst month is geoclimatic (k) factor.

It can be calculated using

$$K = 10^{-(6.5-Clat-Clon)} P_L^{1.5} \tag{11}$$

The above equation is because of that the proposed link is Overland links for which the lower of the transmitting and receiving antennas is less than 70 m above mean sea level.

ITU recommendation calculations for K, there are four K categories, two of which are for overland inks and two for over-water links. K can be estimated from the contour maps given in Figures of ITU-R PN.453-4, from Figs. 7, 8, and 9. For the percentage of

time P_L that the average refractivity gradient in the lowest 100 m of the atmosphere is less than 100 N-units per km [8].

The value of P_L is determined by using figures of ITU-R PN.453-4. From these figures the value of P_L is determined to be 5, 20, 10 and 1 for the months of November, August, May and February respectively and we take the highest value. Hence 20 is used as P_L value, and 0 (dB), and 0.3 (dB) are taken as the value of C_{Lat} and C_{Lon} respectively.

By using Eq. (11).

$$K = 10^{-(6.5-0-0.3)}20^{1.5} = 5.64 * 10^{-5}$$

8.1 Link Availability from Wegeda to Guna

After we determine geoclimatic (k) factors, path inclination will be calculated by using Eq. (10) with $h_A = 2610.08$ m, $l = 35$ km and $h_B = 4162$ m

$$\varepsilon_p = (2610.08 - 4162)\ \text{m}/35 = -44.34$$

Hence, the percentage of time (P_w) can be calculated by using Eq. (9) with fade depth (A) = 28.47 dB

$$\begin{aligned} P_w &= 5.64 * 10^{-5} * 35^{3.6} * 7^{0.89}(1 + |-44.34|)^{-1..4} * 10^{-28.47710} \\ &= 77.45 * 10^{-5} = 0.0007745\% \end{aligned}$$

We can consider the above outage (unavailability) is due to equipment failure and propagation outage. The outage is expressed in terms of hour, minute and second. Let us consider a 1-year or 8760-h interval. A year has 525,600 min or 31,536,000 s. Then the annual expected outage of this link with unavailability of 0.0007745% is

$$\begin{aligned} &8760\,\text{h} * 0.000007745 = 0.06784\,\text{h} \\ &525,600\,\text{min} * 0.000007745 = 4.070772\,\text{min} \\ &31,536,000\,\text{s} * 0.000007745 = 244.2463\,\text{s} \end{aligned}$$

Therefore, unavailability occurs in this hop 0.06784 h, 4.070772 min or 244.24632 s annually.

The availability of this link is determined based on the outage of the worth month or time percentage and it can be calculated as follows.

$$\begin{aligned} \text{Link availability } (P_A)\,\% &= 100\% - P_W\% \\ &= 100\% - 0.0007745 \\ &= 99.9992255\% \end{aligned}$$

From the above unavailability and availability values we can say the link is reliable.

8.2 Link Availability from Guna to NefasMewucha

After we determine geoclimatic (k) factors, path inclination will be calculated. By using Eq. (10) with $h_A = 4157$ m, $l = 25.5$ km and $h_B = 3045$ m

$$\varepsilon_p = (4157\,\text{m} - 3045\,\text{m})/25.5 = 43.6$$

Hence, the percentage of time (p_w) can be calculated by using Eq. (9) with fade depth (A) = 31.78 dB

$$P_w = 5.64 * 10^{-5} * 25.5^{3.6} * 7^{0.89}(1 + |43.6|)^{-1..4} * 10^{-31.78/10} = 8.51 * 10^{-5}$$
$$= 0.0000851\%$$

We can consider the above outage (unavailability) is due to equipment failure and propagation outage. The outage is expressed in terms of hour, minute and second. Let us consider a 1-year or 8760-h interval. A year has 525,600 min or 31,536,000 s. Then the annual expected outage of this link with unavailability of 0.0000851% is

$$8760\,\text{h} * 0.000000851 = 0.007455\,\text{h}$$
$$525,600\,\text{min} * 0.000000851 = 0.447286\,\text{min}$$
$$31,536,000\,\text{s} * 0.000000851 = 26.837\,\text{s}$$

Therefore, unavailability occurs in this hop 0.007455 h, 0.447286 min or 26.837 s annually.

The availability of this link is determined based on the outage of the worth month or time percentage and it can be calculated as follows.

$$\text{Link availability } (P_A)\,\% = 100\% - P_W\%$$
$$= 100\% - 0.0000851\%$$
$$= 99.9999149\%$$

From the above unavailability and availability values we can say the design system is reliable.

9 Conclusion

A direct microwave link between Wegeda to NefasMewucha was initially proposed because of the importance of Wegeda as one socioeconomic growth area in Amhara region. This direct link could not be designed due to Non-clear line of sight propagation. An alternative proposal consisting of two paths from Wegeda to Guna and from Guna to NefasMewucha has been considered and power budget, signal radiation loss, rain attenuation, system margin and reliability of the link are calculated and simulated. The results are found to be consistent with practice.

The link availability of the two hops was calculated based on ITU recommendations, which is 99.9992255% in the first hop and 99.9999149% in the second hop. The fade margin is 28.47 dB and 31.78 dB in the first and second hop respectively which are greater than the recommended fade margin, in other words as the outage or unavailability percentage is very small, the designed link is more reliable and quality of service will be established.

References

1. Moreno, L.: Point-To-Point Radio Link Engineering (2001–2010)
2. Freeman, R.L.: Telecommunication System Engineering, 4th edn. Wiley, Hoboken (2004)
3. Balanis, C.A.: Antenna Theory, Analysis and Design, 3rd edn. Wiley, Hoboken (2005)
4. Young, M.F.: Planning a Microwave Radio Link (2002)
5. Garlington, T.: Microwave Line-of-Sight Transmission Engineering (2006)
6. Lehpamer, H.: Microwave Transmission Networks, Planning, Design and Deployment, 2nd edn, p. 106. McGraw-Hill Professional Engineering, New York (2004)
7. Rakib Al Mahmud, M.D., Khan, Z.S.: Analysis and planning microwave link to established efficient wireless communications. Blekinge Institute of Technology, September 2009
8. Ul Islam, M.R., et al.: Fade margins prediction for broadband fixed wireless access (BFWA) from measurements in tropics. Prog. Electromagn. Res. C **11**, 199–212 (2009)
9. Rec. ITU-R p.530-12: Propagation data and prediction methods required for the design of terrestrial line-of-sight systems. ITU, Geneva (2007)
10. ITU-R P.530-14: Propagation data and prediction methods required for the design of terrestrial line-of-sight systems. ITU, February 2012
11. Shaoying, C.:Digital Microwave Communication Principles V1.1. Huawei Technologies Co., Ltd., Shenzhen (2006)

CenturyLink

Microwave Radio Systems Overview

Search

Welcome
Benefits of Microwave Backhaul
Radio Frequency Safety
Microwave Radio and Transmission Line Theory
▽ Radio Types
Lynx.sc Radio
Stratex Velox LE Radio
Ericsson Mini-Link Radio
Alcatel MDR-7000 Radio
Alcatel MDR-8000 Radio
Harris MicroStar Radio
Harris Constellation Radio
Harris TRuepoint Radio
Maintenance Responsibilities
Trouble Resolution
Glossary
Post Test

Radio Types: Lynx.sc Radio

Proxim Inc. is the manufacturing company that owns and produces the Lynx line of microwave radios. Lynx radios labeled Western Multiplex Corporation and Glenayre are radios produced prior to March 2003. The Western Multiplex Corporation separated from its parent company Glenayre in 1999, and merged with Proxim in 2003.

The Lynx.sc radio is a low-cost, efficient microwave point-to-point radio system that operates license-free in either the 2.4 GHz or 5.8 GHz Industrial, Scientific, and Medical (ISM) bands. The Lynx.sc series offers one or two DS-1 capacity models.

A Lynx.sc is an indoor-only system that combines data interface, signaling andcontrol, and RF functionality in a single 19-inch rack mounted unit. The unit connects to the outdoor antenna by way of a half-inch diameter 50 Ohm coaxial connector terminated by an N-type RF connector. The 5.8 GHz radios should use elliptical waveguides for feeder lengths in excess of 200 feet.

The Lynx.sc offers a craft interface function that is accessed either locally with a computer by way of a serial port or remotely through an RJ-11 modem jack. The craft interface also provides extended information including some advanced diagnostics and configuration information. Any information that is available on the far-end terminal is also available at the near-end craft interface.

The following graphic shows the controls, connectors, and indicators on the front of the Lynx.sc. Click **next** to view the rear panel.

Activity

Review the following manuals:

- Lynx.sc Installation and Maintenance Manual
- Lynx.hd Installation and Maintenance Manual

Contact Site Owner: Feedback
Page Updated December 2009

© 2011 CenturyLink, Inc. All rights reserved.
The name CenturyLink and the pathways logo are trademarks of CenturyTel, Inc.

Print This Page

Trouble Resolution: Bit Error Rate (BER) Type Alarm
A local BER alarm generally indicates that the aggregate baseband signal the radio is receiving is taking errors. In most cases this eliminates the distant end tributary DS-1 inputs as a probable cause. The elements of the radio system that might affect the aggregate baseband are likely between the IF circuitry and the antenna.

The first step in the troubleshooting process is to verify that you are receiving an adequate signal level. In most systems, you can use alarm LED conditions to make a determination of your troubleshooting path. If your assessment indicates a receive signal issue, here are a few things to check.

Things to Check	Action
Receive Signal Level (RSL)	Depending on the radio system, you can determine RSL by either taking a DC voltage measurement at the RSL test point, view it through the craft interface, or both.
Transmission and Waveguide Connections	Visually inspect the RF cables, waveguides, and connectors for serviceability.
Proper Radio Settings	Make sure that the radio frequency and operating parameters are correct.
Antenna	If you are tracking an RSL loss, the antenna is very often going to be the trouble. Antenna problems could be caused by misalignment, path interference, and antenna polarization.

If your RSL is within established parameters, you can make use of the craft interface functionality to do loopback testing. If the link is established between both radio stations, you may be able to at least isolate the issue to which station is faulted.

Actual Scenario
A field operations technician is dispatched to a microwave site pursuant to a path failure between a Base Transceiver Station (BTS) and the Mobile Switching Center (MSC). Upon arriving at the site, he makes an initial assessment of RSL and discovers that it is 20 dB below tolerance. He immediately contacts his tower support vendor and arranges to troubleshoot at the antenna. He assesses the path for interference and has the antenna swept across the specified azimuth and declination; the RSL does not recover. The technician then has the polarity of the antenna at the feed-horn checked and discovers a mismatch. The polarity is set to specification and the path recovers.

Trouble Resolution: Data Loss Type Alarm
This type of alarm generally indicates an error condition in the tributary DS-1 signal or signals. The cause may be external to the radio system or as a result of a failure within the radio system. It is likely that if the failure is in the radio that it occurs before the IF and RF circuitry. Most systems have multiplexing circuitry to aggregate tributary signals prior to IF up-converting and down-converting.
If your assessment points to a data loss type failure, the radio system, in most cases, provides specific failure data that allows you to determine which tributary circuit is in

trouble. If your assessment indicates a tributary data loss issue, here are a few things to check.

If your assessment points to a data loss type failure, the radio system, in most cases, provides specific failure data that allows you to determine which tributary circuit is in trouble. If your assessment indicates a tributary data loss issue, here are a few things to check.

Things to Check	Action
Connections	Perform a visual inspection of the DS-1 connection.
Data	Verify that the DS-1 line has data active at the radio connection.
Loopbacks	You can use of the craft interface functionality to do loopback testing to isolate the fault.

Actual Scenario
A field operations technician is dispatched to a microwave site pursuant to path degradation between a BTS and the MSC. Upon arriving at the site, he makes an initial assessment of the alarm indications and discovers a synchronization loss on a multiplexer card within the radio. He conducts a visual inspection and discovers a damaged cable between the modem and the radio assembly. The cable damage was caused by mice chewing on the cable.

With most microwave radio systems, a far end failure alarm indication is provided. In many cases, you do not know which station has failed, and will probably go first to the closest site. At that site you either discover the problem, or observe indications that requires you to travel to the distant site. Most systems offer far end troubleshooting capabilities through the craft interface. This functionality is only available if the RF link is still established.

If you suspect a distant end issue, verify the following before you leave to go to the other site.

Things to Check	Action
Link	Determine if the RF link is established between both stations.
Troubleshoot Remotely	If you have a link to the remote site, attempt to use the remote troubleshooting functionality. You may be able to isolate the problem and speed the restoration time.

Actual Scenario
A field operations technician is dispatched to a microwave site pursuant to path failure

between several BTSs and the MSC. Upon arriving at the site, he makes an initial assessment of the alarm indications and discovers a far end radio failure condition. He checks the RSL and discovers that no receive signal is present. He travels to the distant site and discovers the DC power supply in a fault condition. He replaces the power supply and restores the circuits.

Microwave Radio and Transmission Line Theory: Waveguide Theory

The quality and effectiveness of the antenna is equally as important as the quality of the radio. The critical link between these two is the transmission line. Very often a radio is located remotely from its antenna. Effectively bridging that electrical and physical gap can be challenging. Lower frequency radios make use of coaxial cable to connect a transceiver—a contraction of transmitter and receiver. A transceiver contains both transmit and receive circuitry with the antenna. Higher frequency microwave radio systems must overcome an additional challenge—the skin effect.

The skin effect is the tendency of high-frequency electric current to flow at much higher rates near the surface of a conductor than near its core. Because microwave frequencies are subject to the skin effect, they experience major attenuation when applied to a conventional coaxial cable. To overcome this problem the waveguide was invented. The waveguide is essentially a hollow metal tube used to transfer microwave radio frequencies. Because the interior of the tube offers a great deal more surface area than the center conductor of a coaxial cable, the attenuation of the signal is far less. Waveguides may be either rectangular, elliptical, or circular in shape. The physical dimensions of the waveguide selected are very specific to the wavelength of the operating frequency of the radio.

Because the waveguide is a rigid or semi-rigid metallic tube, it presents greater expense and difficulty of installation. Most of the systems our company has deployed have overcome that difficulty by using an innovative method. The radio system is split into two parts—an indoor unit and an outdoor unit.

By creating only the lower frequency Intermediate Frequency (IF) signal indoors, you can use coax cable to span the distance to the outdoor unit. The outdoor unit produces the RF signals and is mounted adjacent to the antenna on a pole or tower. This allows for a very short waveguide interface between the RF portion of the radio and the antenna. Power for the outdoor unit, control signals, and the IF can all traverse the coaxial cable connecting the two units.

The following graphic shows is an example of our typical radio configuration to reduce the length of the waveguide.

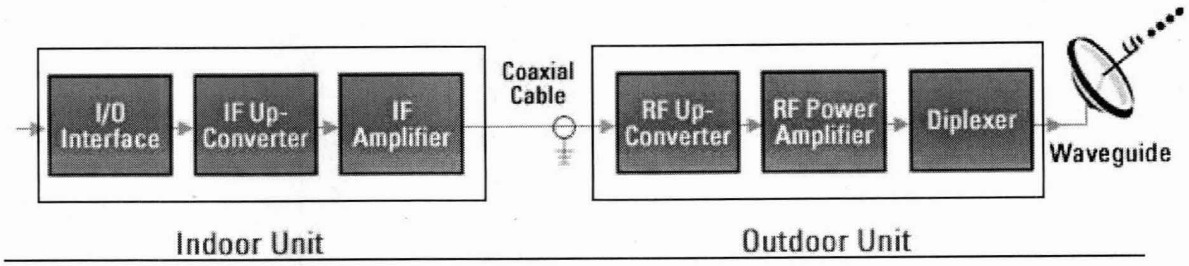

Radio Types

The FCC requires that microwave radio links that fall within certain frequency ranges be licensed. The licensing process ensures that CenturyLink is protected from frequency interference. Extensive study of coordination is accomplished before submitting for the license. This ensures that there are no interference issues or objections from any existing licensees near the area of the proposed microwave radio link.

The license specifies site name, site coordinates, frequencies, polarization, equipment type, stability, output power, type of modulation, path azimuth, distance, antenna types, model, gain, and if required, a radiation pattern provided or certified by the manufacturer.

Typical CenturyLink wireless markets layout in three areas, metro, suburban, and rural. We follow these general guidelines when deploying licensed systems in these areas.

- Metro area radios generally are 18 GHz, use two-foot diameter antennas, and paths are less than four miles.
- Suburban area radios generally are 11 GHz, use four-foot diameter antennas, and paths are less than eight miles.
- Rural area radios are usually 6 GHz, and use six-foot diameter antennas. Path length is dependent on too many design characteristics to state a standard but is generally between eight and 25 miles.

Microwave radio systems operating in the 18 GHz, 11 GHz, and 6 GHz ranges are required by the FCC to be licensed. CenturyLink has deployed a great many unlicensed microwave radio systems. These systems typically operate in either the 2.4 GHz or 5.8 GHz range, and are not required by the FCC to be licensed. An unlicensed deployment offers the advantage of increasing speed to market, and has in the past offered significant equipment cost savings. We have opted to license all new microwave backhaul deployments, but will continue to deploy unlicensed systems in certain situations:

- To meet increased capacity needs in an existing unlicensed system.
- To replace failed system components in an existing unlicensed system.
- Any condition that prevents the link parameters from meeting FCC licensing specifications.

License renewals are the responsibility of the Microwave Regulatory Engineer. Field Operations must post a copy of the FCC Microwave License at each permanent microwave site. This insures that frequency, emission, and transmit power requirements

are met during maintenance. Any discrepancies such as antenna type, height, polarization, or azimuth must be reported to the Microwave Engineering Regulatory Engineer

Radio Types: Harris Constellation Radio
The Constellation™ radio is a scalable low, medium, and high capacity digital radio. The radios are available in 6, 7, 8, 10, and 11 GHz frequency bands. The Constellation platform includes both terminal and repeater configurations.

The repeater configuration radio supports an add or drop of up to 16 DS-1 signals from each direction. The DS-1 signals must be dropped in groups of four.

Low and medium capacity radios are configured for the following data capacities:
• 8 and 16 DS-1s
• 1 DS-3

The Constellation Radio is comprised of the following major sub-assemblies:

- Signal processing section
- Radio frequency section
- Antenna coupling unit (ACU)

The Signal Processing Section (SPS) serves as the signal interface for payload data sources. The SPS is comprised of the following components.

Component	Function
M12 Multiplexer Cards	The M12 multiplexer cards are used for DS-1 level interface. The M12 interfaces with the DS-1 payload data and outputs a multiplexed DS-2 to the High Level Multiplexer (HLM).
Service Channel Card	The service channel card provides service channel interface for order wire functions and enhanced operations data sharing between radio units. Its output is applied to the Modem.
High Level Multiplexer Card	The high level multiplexer card interfaces with the output of the M12 cards and the modem.
Modem Card	The modem card combines all signals for transmission into a modulating IF signal for application to the transmitter. In the receive mode, the modem demodulates the received IF signal from the receiver.
Signal Processing Unit (SPU) Controller Card	The SPU controller card is responsible for operations, administrations, maintenance, and performance monitoring and interface for the radio system.

The Radio Frequency Section handles all RF level functions for the radio. It is comprised of the following components.

Component	Function
Power Supply	The power supply provides filtered and regulated power to all of the system cards and modules.
Transmitter	The transmitter takes in the transmit IF from the modem, up-converts it to the desired output frequency and power level, then applies the signal to the ACU.
Receiver	The receiver takes in the received RF from the ACU, down-converts it to an IF level, and applies the signal to the modem for demodulation.

The ACU serves as the interface between the radio and the antenna system. The ACU provides only waveguide flange connections for the transmission line.

Radio Types: Alcatel MDR-8000 Radio

The MDR-8000 family of microwave digital radios provides an RF telecommunications link for short-haul, medium-to-high capacity digital transmission systems using 4QAM coded or Trellis Coded Modulation schemes for transmission capacities of two DS-1s to one OC-3. The signals are transmitted in the 2–16 GHz frequency bands. The radio is an indoor only assembly that provides payload data interface, signal processing, RF power, and diplexer functionality. Coax cable or waveguide assemblies connect the system to an external antenna. The system is a standard 19-inch rack mount assembly, occupying seven rack height increments. Up to four MDR-8000 systems can be housed in a single 7-foot rack.

The MDR-8000 family of radios supports three basic configurations:

- Non-standby—available in all frequency bands—stand alone transmitter and receiver combination.
- Hot-standby—available in all frequency bands—pair of transmitters and receivers, both pairs operating on the same set of go and return frequencies.
- Frequency diversity—pair of transmitters and receivers, each pair operating on a different set of go and return frequencies.

The MDR-8000 common shelf assembly consists of the shelf assembly wired (SAW), shelf internal RF cables, front cover, and modules. The MDR-8000 SAW consists of backplane assembly, card cage assembly, front cover, heat sinks, brackets, and mounting hardware.

The following graphic shows the controls, connectors, and indicators on the MDR-8000 components. Click **next** to view specific components.

Radio Types: Harris MicroStar Radio

MicroStar® is a family of point-to-point digital microwave radios designed for rapid deployment of short, medium, and long links.

This core radio platform is designed to provide reliable link data rates of 2, 4, 8, and 16 DS-1s or one DS-3. A radio system includes an Indoor Unit (IDU) and an Outdoor Unit (ODU). A MicroStar terminal in an unprotected configuration consists of one IDU and one ODU. The ODU contains the RF transceiver and is connected to the IDU through a coaxial cable.

The ODU is a weatherproof housing designed to mount on a mast or tower with an antenna in a separate or detachable mount. The IDU shelf can be mounted in the standard 19-inch radio relay rack.

The MicroStar supports an interface with the Network Management System (NMS) and element management system with Simple Network Management Protocol (SNMP).

The following graphic shows the controls, connectors, and indicators on the front panel of the MicroStar.

Radio Types: Alcatel MDR-7000 Radio
The MDR-7000 family of microwave digital radios provides an RF telecommunications link for short-haul, low-to-medium capacity digital transmission systems using 4Quadrature Amplitude Modulation (4QAM) coded modulation for transmission of 2, 4, 8, or 16 DS-1 or E1 signals or one DS-3 signal. The signals are transmitted in the 15, 18, 23, and 38 GHz frequency bands. Center frequency increments and channel bandwidths are selectable. The radio assemblies, including interface capabilities at the DS-1, E1, or DS-3 level, consist of an outdoor unit (ODU) for pole mounting and an indoor unit (IDU) for mounting in a standard 19-inch radio rack or stand-alone rack. A coax cable (up to 1,000 ft) connects the IDU to the outdoor equipment.

The main purpose of the IDU is to process DS-1, E1, or DS-3 data, depending on the configuration, and monitor and control the MDR-7000 radio. The IDU supplies the outdoor unit with multiplexed data, operating power, and overhead through a single coaxial cable. Control data in the overhead is used to control outdoor unit operation.

The ODU performs modulation, demodulation, up and down conversion to IF and RF, amplification, filtering, and antenna functions. It is both frequency and capacity dependent. ODUs are available for DS-1, E1, and DS-3 capacities and 15, 18, 23, and 38 GHz frequency bands. There is no maintenance required and the complete ODU must be replaced if it fails.

The MDR-7000 IDU is available in three radio configurations: non-standby, wired hot-standby equipped non-standby, and hot-standby. The non-standby system consists of the IDU and the ODU connected together with a single RF cable. The hot-standby system consists of a double-height IDU and two ODUs.

A laptop computer is required to access provisioning, alarm information, and troubleshooting functions within the radio. These functions are performed through the Alcatel User System Interface (USI) maintenance program software. The computer must be MS-DOS based and IBM compatible.

Radio Types: Ericsson Mini-Link Radio

The Ericsson Mini-Link radio system consists of an indoor access module and an outdoor radio unit with antenna. The outdoor part contains all frequency dependent units. All traffic capacity dependent units are located indoors. The indoor access module comprises a magazine with different plug-in units providing modem, switching, and optional service functions. The indoor part is connected to the radio unit with a single coaxial cable.

The compact antennas are normally installed integrated with the radio unit, but a separate installation is also possible. A 6-feet antenna for separate installation is offered as well. All antennas are easily adjustable for fine alignment of both azimuth and elevation.

The Mini-Link radio system supports the standardized Simple Network Management Protocol (SNMP) interface. Local setup, configuration, and supervision are performed using the PC-based Mini-Link Service Manager (MSM) software.

A terminal consists of an indoor and an outdoor part:

- The outdoor part is fully independent of traffic capacity and supplied for various frequency bands. It consists of an antenna, a radio unit (RAU), and associated installation hardware. The antenna and the radio are either integrated or installed separately. For protected systems (1+1), two radio units and one or two antennas are used.
- The indoor part, the access module, is fully independent of frequency band and supplied in different versions for various traffic capacities and system configurations. It consists of a modem unit (MMU) and a switch multiplexer unit (SMU), as well as an optional service access unit (SAU), all housed in one common shelf called an access module magazine (AMM). An additional MMU is required for protected systems. The radio cable connects the outdoor part to the indoor part.

Radio Types: Stratex Velox LE Radio

Stratex Velox LE 2400 and 5800 series radios are ISM band digital radio systems that provide short-to-medium range, point-to-point digital communication with high data security at rates of one, two ,or four DS-1s. The data rates scale depending on the number of enabled DS-1 tributaries. The systems make use of spread spectrum technology and may be operated license-free in the 2.4 GHz and 5.8 GHz ISM bands.

For Velox LE operation, the ISM bands are divided into upper and lower frequency sub-bands. A Velox LE high-band Outdoor Unit (OU) transmits in the higher frequency sub-band and receives in the lower frequency sub-band, while a low-band OU transmits in the lower sub-band and receives in the higher sub-band. A Velox LE radio link uses a low-band OU on one end of the link to communicate with a high-band OU on the other end.

A Velox LE digital radio link consists of a pair of Velox LE radio stations. Each Velox LE radio station consists of two main parts:

- An Outdoor Unit (OU) operating in the 2.4 GHz or 5.8 GHz ISM frequency bands. The OU provides the radio transceiver functionality by accepting radio link data from the Indoor Unit (IU) and converting it to the 2.4 GHz or 5.8 GHz ISM frequency band using spread-spectrum modulation. The received signal is de-spread and transmitted to the IU in a digital format.
- An Indoor Unit (IU) available with 1, 2 or 4 E1 and 1, 2 or 4 T-1 data interfaces (choice of E1 or T-1 is software-selectable). The IU combines nE1 or nT-1 data with Wayside Service Channel serial data and link Internet Protocol (IP) data to be transmitted across the radio link. The IU also provides power to the OU.

Interconnection between the OU and IU is achieved using UV-protected STP (Screened Twisted Pair) cable.

The Velox system also offers the following benefits:

- No loss of performance with long cable runs, and few limitations on bend radius.
- Built-in Spectrum Analyzer for detection interference.
- Craft interface.

The craft tool application provides extensive management functions on site, and through the microwave radio link, can be used to access the station on the opposite side of the link. The craft tool is a software application that runs on a computer that is connected to a IU serial port (DB-9) or an Ethernet connection (10Base-T). Both are accessed from the IU front-panel.

The Velox LE product range is a split-architecture radios system with two installation options.

- All indoor option consisting of a Digital Unit (DU) and Indoor Radio Frequency Unit (IRFU) both one rack unit (RU) high and 19-inch rack mountable.
- Indoor/Outdoor option consisting of a one RU high 19-inch rack mountable DU and a mast/pole mountable Outdoor Radio Frequency Unit (ORFU).

Radio Types: Lynx.sc Radio

Proxim Inc. is the manufacturing company that owns and produces the Lynx line of microwave radios. Lynx radios labeled Western Multiplex Corporation and Glenayre are radios produced prior to March 2003. The Western Multiplex Corporation separated from its parent company Glenayre in 1999, and merged with Proxim in 2003.

The Lynx.sc radio is a low-cost, efficient microwave point-to-point radio system that operates license-free in either the 2.4 GHz or 5.8 GHz Industrial, Scientific, and Medical (ISM) bands. The Lynx.sc series offers one or two DS-1 capacity models.

A Lynx.sc is an indoor-only system that combines data interface, signaling andcontrol, and RF functionality in a single 19-inch rack mounted unit. The unit connects to the outdoor antenna by way of a half-inch diameter 50 Ohm coaxial connector terminated by an N-type RF connector. The 5.8 GHz radios should use elliptical waveguides for feeder lengths in excess of 200 feet.

The Lynx.sc offers a craft interface function that is accessed either locally with a computer by way of a serial port or remotely through an RJ-11 modem jack. The craft interface also provides extended information including some advanced diagnostics and configuration information. Any information that is available on the far-end terminal is also available at the near-end craft interface.

NAD83

Microwave path design: The basics

Part 1 — This four-part primer on propagation-related basics, for those learning about microwave communications, begins with "line-of-sight" determinations and the evaluation of path clearances with regard to refractive effects.

By Jeff Ashley

Microwave communications path design poses many challenges. In addition to *static gain and loss* considerations, *terrain* and *propagation dynamics* can play a large role in determining whether a proposed path will have the required signal levels, clearances and reliability.

This four-part series will only scratch the surface with regard to these considerations, and it is not intended to cover *all* aspects of path design or any one in great depth. The primary focus of the series is to serve as a primer on some of the propagation-related basics for those who may be new to the microwave communications field.

Given this disclaimer, the following tasks are some of the fundamental components of microwave path design:

- ❑ determining whether a proposed path is "line-of-sight."
- ❑ evaluating path clearances with regard to refractive effects.
- ❑ evaluating path clearances with regard to Fresnel zones.
- ❑ considering path reflections.
- ❑ deriving a power budget and the fade margin.
- ❑ path reliability.

Part 1 of this series deals with the first two components; the others will be discussed in Parts 2, 3 and 4.

Determining line-of-sight

Although there are situations where microwave paths are designed to work without line-of-sight conditions, they would not be considered the "norm" for industrial microwave systems and therefore will not be dealt with here. In most situations, if a prospective path is not line-of-sight, then an alternate route is considered.

Determining whether a path is line-of-sight can be partially accomplished with the aid of a *topographical map*. This type of map will show the various elevations along the length of the path between proposed endpoints. Plotting these elevations at intervals will produce a path profile showing terrain relative to the antenna elevations, as shown in Figure 1 below left. This graphical representation aids in determining not only whether a line-of-site condition exists between endpoints but also in measuring clearances between the main beam (center) of the path and the surrounding terrain.

Topographical information for many areas throughout the world is now available on CD-ROM. Various software applications have been developed to design microwave paths based on this information. Since this option can be a bit "pricey," many opt to use inexpensive topographical maps, which may be used with the same success.

When evaluating a proposed path, the *path profile* should be developed first. This will identify path obstructions from terrain features. A field survey should follow, which offers the necessary visual confirmation that the height of foliage or of man-made objects (which are not indicated on a topographical map) will not be located in or too near the proposed path.

If visual confirmation is difficult because of the distance between path endpoints, a mirror can be used to reflect the sun's light from one path endpoint back toward the other. If the mirror's flash of reflected sunlight is seen back at the opposite endpoint, the path is line-of-sight. This is referred to as "flashing" a path. Alternate methods

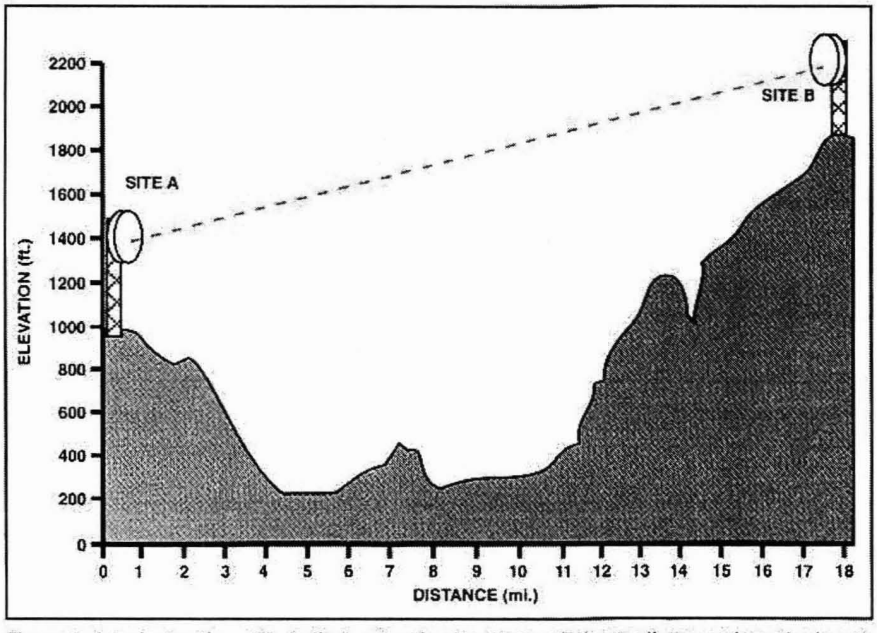

Figure 1. A typical path profile indicates terrain elevations relative to distance along the length of the path.

Ashley is a communications technician in Los Angeles.

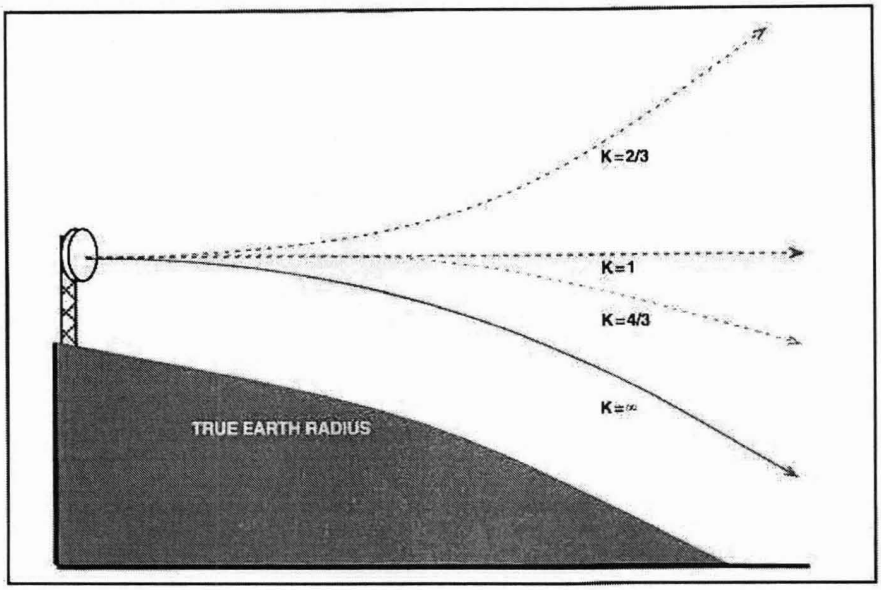

Figure 2. Where *K* equals infinity, the wavefront parallels the radius of the true earth. When no refractive effects are present ($K = 1$), no bending of the wavefront occurs.

might include the use of high-intensity search or strobe lights.

Evaluating path clearances—refraction

When the *dielectric constant* of the atmosphere changes with height-above-ground, the *refractive index* will also change. This refractive variation in turn causes the propagating wavefront to effectively "bend." If a condition exists where the dielectric constant of the atmosphere is constant with height-above-ground, no refraction will occur and the wavefront will travel in a straight line. This is not the "norm," however. Because of dielectric variations typically present, a wavefront usually will be refracted so that it will follow a path somewhere between a straight line and the true curvature of the earth (referred to as R). A wavefront propagating through the environment will be slowed by, and be effectively bent toward, an atmosphere that is more dense, such as one with a high water-vapor content (dense clouds or fog). That is why, rather than traveling in a straight line, the wavefront is normally bent earthward—which serves to extend its horizon.

Because atmospheric conditions are dynamic, the bending effect of the propagating wavefront will vary. To provide a simple model describing the path traveled by a wavefront for a particular refractive condition, engineers have developed a factor, K, where KR is considered the *"equivalent" earth radius*. This equivalent radius describes the bending of the wavefront relative to the *true earth radius*, as shown in Figure 2 on page 28.

The refractive index can change

ALL THE COMMUNICATION EQUIPMENT YOU NEED. . . *IN ONE CATALOG!*

For over 20 years, Marketronics has provided you with quality communication equipment at very competitive prices. Now, we bring you our **NEW Product Selection Guide.** It's packed with cutting edge products from many new manufacturers as well as expanded offerings of existing product lines.

When you select Marketronics as your provider, you're guaranteed to receive quality equipment, excellent service, and great prices!

Contact us today to request your ***FREE*** copy of our catalog and also to learn how you can start saving money today!

- tel: 800 845 1230 or 954 846 1011
- fax: 954 846 1672
- email: sales@marketronics.com

- More than 10,000 items
- Over 120 Manufacturers
- Lowest Total Cost

Marketronics CORPORATION

VISIT OUR ONLINE CATALOG - www.marketronics.com

PLEASE DROP BY BOOTH #1308 AT IWCE

World's Leading Distributor of Quality Telecommunication Equipment

drastically with time. This means the microwave beam between path endpoints will "bow" to a greater or lesser extent. In fact, it may "bow" in an upward *or* a downward direction, depending on the value of K at the time. It is therefore important to evaluate clearances from path obstructions over a wide range of K in order to determine whether adequate path clearances are maintained under various degrees of refraction. Often, three values of K are used in the calculations. Two of the three values describe the *limits* or boundaries of refraction that might occur (although with anomalous conditions, values exist outside these limits), while the third describes what is considered "normal" or expected. The value of $K = \infty$, also known as "super-standard" atmosphere, is one extreme where the wavefront follows the true curvature of the earth. The other extreme value of K typically used is 2/3 and is termed "substandard" atmosphere. It is also a condition commonly referred to as "earth bulge." The median value of $K = 4/3$ is used to evaluate the path under "normal" atmospheric conditions in temperate climates.

There are two methods of graphically displaying the various *equivalent* earth radii with respect to the terrain between path endpoints: the "flat earth" method and the "curved earth" method. Figure 3 above is an example of a "flat earth" path profile. It is called "flat earth" because the horizontal axis (or baseline) has been kept flat and

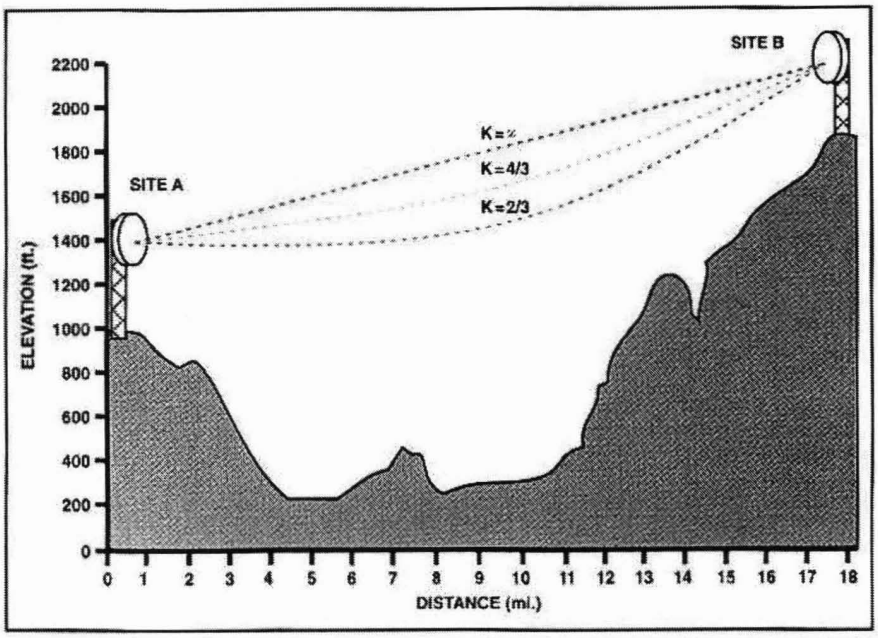

Figure 3. This is a 'flat-earth' profile. Terrain features become more of an obstruction consideration when $K = 2/3$.

Here's a Family that Keeps its Secrets

Introducing Selectone's Full Line of Voice Encryption Products

Today more than ever, the world of two-way communications needs the advantage of secure voice. The Selectone family of voice encryption products offers you **a clear choice at affordable prices.**

From the low-end inversion scramblers, the **ST-22** and **ST-20B**; to our mid-range scramblers, the **ST-25B** with digital rolling code security; to the state-of-the-art **Advantage-Plus** encryption series with time domain scrambling and digital signal processing, Selectone will provide the right product match for your specific security requirements. ***No hassles. No overselling. No kidding!***

We're confident that our product line is exactly what you're looking for, and we'll provide you with a personalized quote to prove it. Simply give us a call, send us a fax or write to us with your requirements, and **we'll provide you with a customized quote at no cost.** It's simple. It's free. And best of all, it introduces you to the finest family of encryption products in the world. You have our name on it.

See us at IWCE, Booth 935.

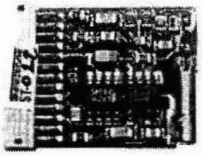

Low-end inversion scramblers. ST-22, ST-20B

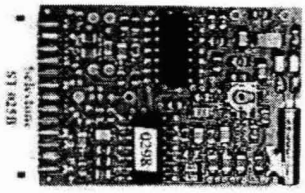

Mid-range scramblers. ST-25B

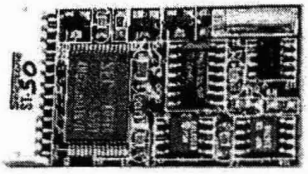

State-of-the-Art Advantage-Plus series. ST-50, ST-51, ST-52

CUSTOM QUOTES AVAILABLE

1-800-227-0376

Selectone

Selectone, Inc. • 3501 Breakwater Ave. • Hayward, CA 94545 USA
Phone: 510-781-0376 • Fax: 510-781-5454 • Internet: www.selectone.com

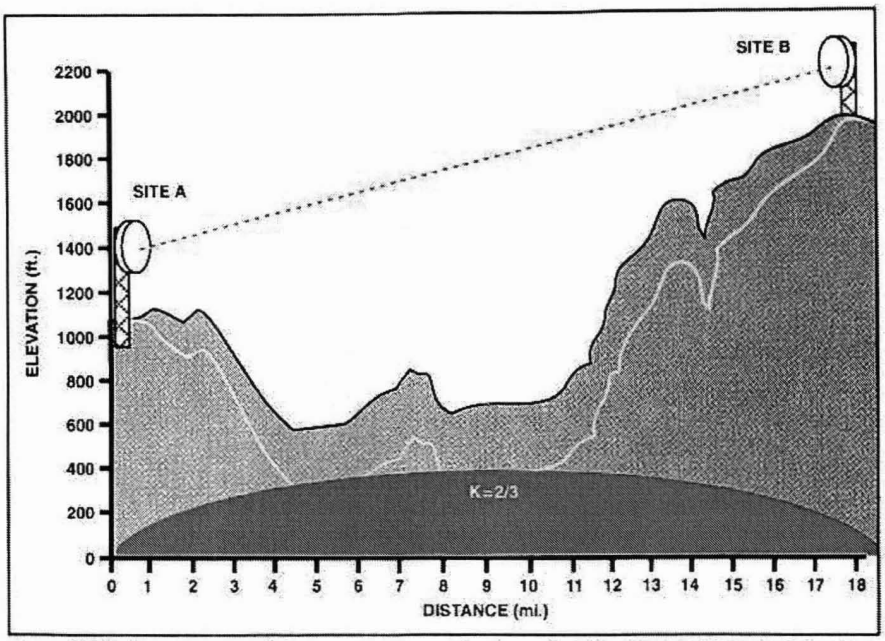

Figure 4. This is an exaggerated curved-earth profile where $K = 2/3$, with identical terrain features as shown in Figure 3. (Figure 3 elevations are represented by the yellow line.) Because the equivalent earth radius 'bulges up' in the center, the elevations of the terrain features increase, *reducing* path clearances. When $K = 4/3$, the earth bulge is less severe, resulting in greater path clearances. The greatest clearance is realized when $K = \infty$.

represents the earth's curvature as a flat line. The various equivalent earth radii represented by the different values of K are shown by bending the path beam line between antennas. The three lines shown in Figure 3 correspond to the refractive conditions where $K = \infty$, $K = 4/3$ and $K = 2/3$.

Elevations of terrain features between path endpoints are plotted using the flat baseline as a reference. The profile allows one to see if there is sufficient path clearance over the terrain for each value of K.

The curved earth approach, as shown in Figure 4 on the left, leaves the beam line between antennas straight and instead bows the horizontal baseline to correspond to one particular value of K. Elevation of all terrain features must be added to that of the bowed baseline reference. The straight beam line between antennas must now be checked for sufficient clearance from all terrain features for that value of K.

With the curved earth profile, the one limit of $K = \infty$ would be shown with the baseline flat. Here (as with the flat-earth approach) is the one "extreme" condition where the wavefront (shown as a straight line) follows

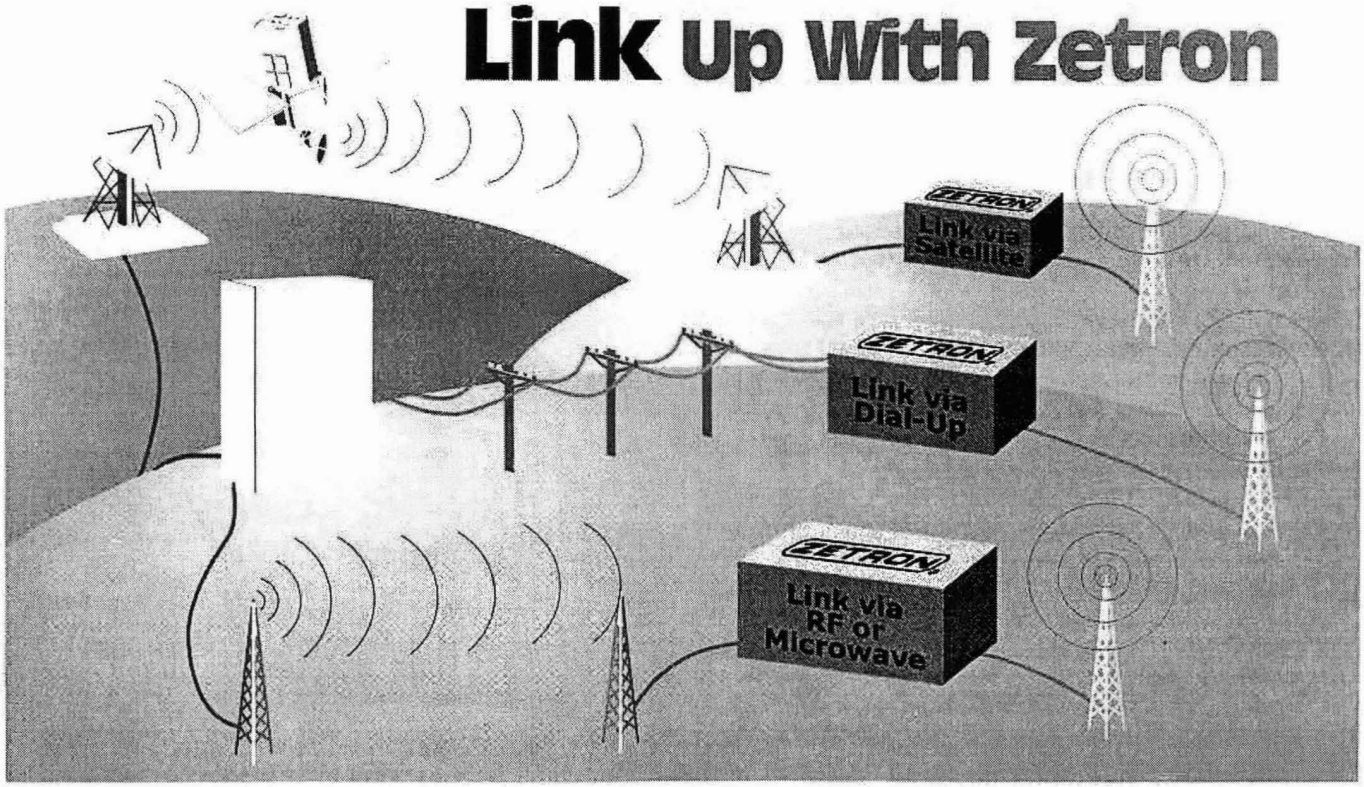

Zetron, Inc. PO Box 97004, Redmond WA 98073-9704 USA

ZETRON®

Ph: (425) 820-6363 Fax: (425) 820-7031 Email: mps@zetron.com Web: http://www.zetron.com

European Office: Zetron, Inc. 27-29 Campbell Court, Bramley, TADLEY, Basingstoke, RG26 5EG,UK Phone: +44 1256 880663 Fax: +44 1256 880491

the true curvature of the earth (also shown as a straight line). As the value of K gets smaller and reaches the other limit of K=2/3, the equivalent earth radius bulges upward more in the center, hence the term "earth bulge." As these profiles show, paths with values of $K = 4/3$ and $K = 2/3$ have less path clearance with respect to terrain features than when $K = \infty$.

The following equation can be used to calculate how much the horizontal axis (or baseline) of a "curved earth" profile will bow upward at any point along the path for a particular value of K:

$$h = \frac{d_1 \times d_2}{1.5 \times K}$$

where h is the vertical variation in height (ft.).

d_1 is the distance (mi.) from one end of the path to the point being considered.

d_2 is the distance (mi.) from the point considered to the other end of the path.

With the "flat earth" profile, h is subtracted from the direct ray ($K = \infty$) reference line (for positive values of K) at various distances along the path in order to develop a graphical representation of the amount of wavefront bowing that will occur for the value of K under investigation.

With the "flat earth" profile, the wavefront, rather than the baseline, is shown "bowed," and the amount of bowing changes as the value of K changes. The distance between the bowed wavefront and the terrain features can be measured graphically to determine path clearances for each value of K.

Whichever profiling method is used ("curved earth" or "flat earth"), it can be seen graphically that smaller values of K result in greater bulging or "bowing." This in turn results in less path clearance with regard to terrain features.

... Smaller values of K result in greater bulging or 'bowing.' This in turn results in less path clearance ...

Because the microwave path has *radial dimension*, the clearances considered are not only those above and below the center of the path, but also to either side.

Initially, these graphical methods allow path clearances to be measured as distances, *in feet*. Once this information has been obtained, it is however, typically converted to a more meaningful design measurement, called the *Fresnel zone*.

The next article in this series will discuss path clearances with regard to Fresnel zones.

References

Laine, R.U., *Determining Antenna Heights for Coastal Areas*. Lenkurt Electric, Monograph 197.

"Microwave Systems, Microwave Path-Testing," *Bell Systems Practices*, AT&T Standard, September 1962.

"Microwave Transmission Engineering (Part One and Two)," *GTE-Lenkurt Demodulator*, July/August, 1972.

White, R.F., *Engineering Considerations for Microwave Communications Systems*, 4th Ed., GTE-Lenkurt, San Carlos, CA, 1983.

Now you can have the convenience of a belt clip & protection of a BEE® Case

New from BEE®

Clip-on Cases

Available in Leather or Durus® Nylon

If you love the convenience of a belt clip on your portable, but hate the way plastic always seems to break... BEE® has a solution for you!

Introducing the first belt clip available on a top quality leather or nylon case. Our clip is formed from heavy gauge, heat treated, powder coated spring steel and is securely riveted to the back of the case. You'll never have to worry about radio damage again.

GIVE US A BUZZ 1-800-336-3115

Now your choice of three convenient ways to carry your radio case:

Our new spring steel belt clip mounted on the back of either leather or Durus® cases.

or

Our famous quick disconnect swivel option.

or

Regular snap down belt flap.

See us at IWCE Booth 300.

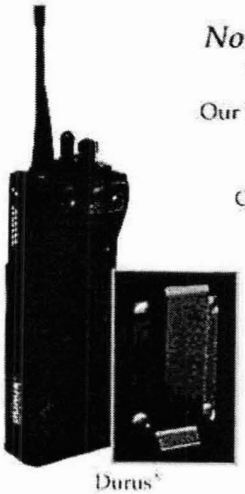

Durus®

BEE® PRODUCT DURUS® MADE IN THE U.S.A.

BEE®

2120 Roberts Drive, Broadview, IL 60153
Tel: (800) 336-3115 • Fax: (800) 345-2091
E-Mail: beecase@aol.com

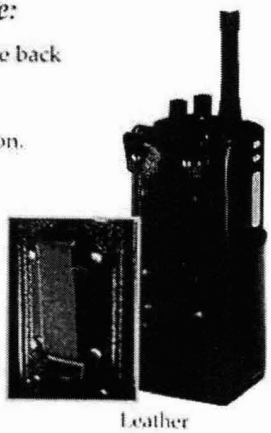

Leather

BEE® and Durus® are registered trademarks of BEE Electronics, Inc.

Microwave path design: The basics

Part 2 —This four-part primer on propagation-related basics, for those learning about microwave communications, continues with a discussion of path clearances and Fresnel zones.

By Jeff Ashley

In Part 1 of this series (*MRT* May), two of the basic propagation-related considerations in the microwave path design process were discussed:

- ❑ determining whether a proposed path is "line-of-sight."
- ❑ evaluating path clearances with regard to refractive effects.

Remaining fundamental design components to be discussed are:

- ❑ evaluating path clearances with regard to Fresnel zones.
- ❑ considering path reflections.
- ❑ deriving a power budget and the fade margin.
- ❑ path reliability.

This article will briefly cover item three, path clearances and Fresnel zones. The remaining items will be dealt with in the concluding parts of this series.

Evaluating path clearances—Fresnel zones

If one were to look directly into the center beam of a microwave path (gazing directly into the dish), the Fresnel zones could be defined as an infinite number of circles centered around the center beam, each having a larger radius than the previous one, as shown in Figure 1 below. The Fresnel zones get closer as they expand further away from the center. The radii of these zones reach a maximum at mid-path and diminish on either side of mid-path.

From a side view of the path, as shown in Figure 2 on page 30, one can see the creation of ellipsoids between path endpoints, centered around the main beam. Each ellipse represents the boundary of a particular Fresnel zone.

Fresnel zones are numbered from the center of the path out. The boundary of the first radius out from the center represents the first Fresnel zone, which contains all wave components whose distance traveled to the far-end is exactly 1/2 wavelength (λ)greater than the direct ray. The boundary of the second radius out from the center represents the second Fresnel zone, which contains all wave components whose distance traveled to the far-end is exactly 1λ greater than the direct ray. Each integer increase of Fresnel zone number represents an increase of 1/2λ to the distance traveled to reach the other end of the path.

The equation that determines the radius of the first Fresnel zone (in feet) at any particular distance along the path is:

$$F_1 = 72.1\sqrt{\frac{d_1 \times d_2}{f \times D}}$$

where

F_1 = the first Fresnel zone radius (ft.).
d_1 = distance (mi.) from one endpoint to the point being considered.
D = total path length (mi.).
$d_2 = D - d_1$.
f = frequency (GHz).

The radius of *any* Fresnel zone number can be calculated by the following equation once the radius of the *first* Fresnel zone has been determined:

$$F_n = F_1\sqrt{n}$$

where n = the Fresnel zone number being evaluated.

When examining path profiles, if one wishes to know what Fresnel zone is represented by a particular clearance (in feet), the

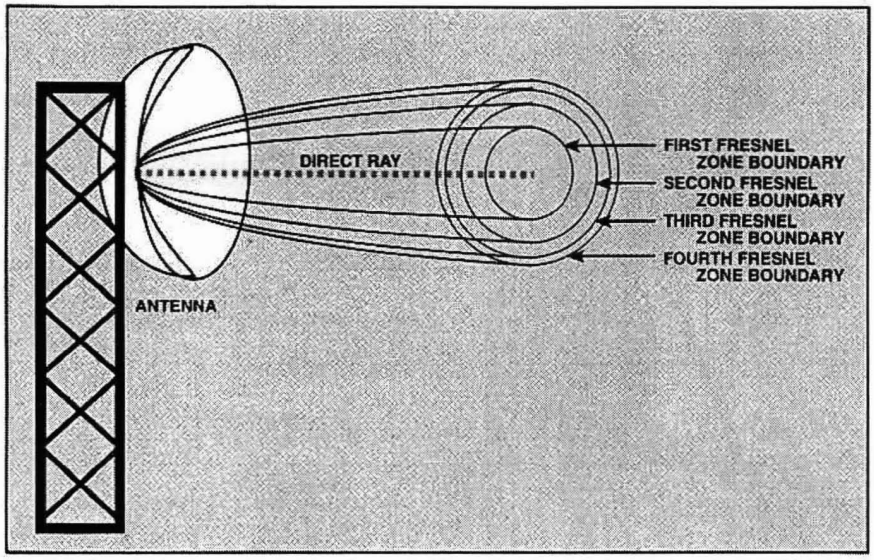

Figure 1. Fresnel zones could be viewed as an infinite number of circles centered around the direct ray, each circle having a larger radius than the previous one. Fresnel zones get closer together as they expand out further from the center.

Ashley is a communications technician in Los Angeles.

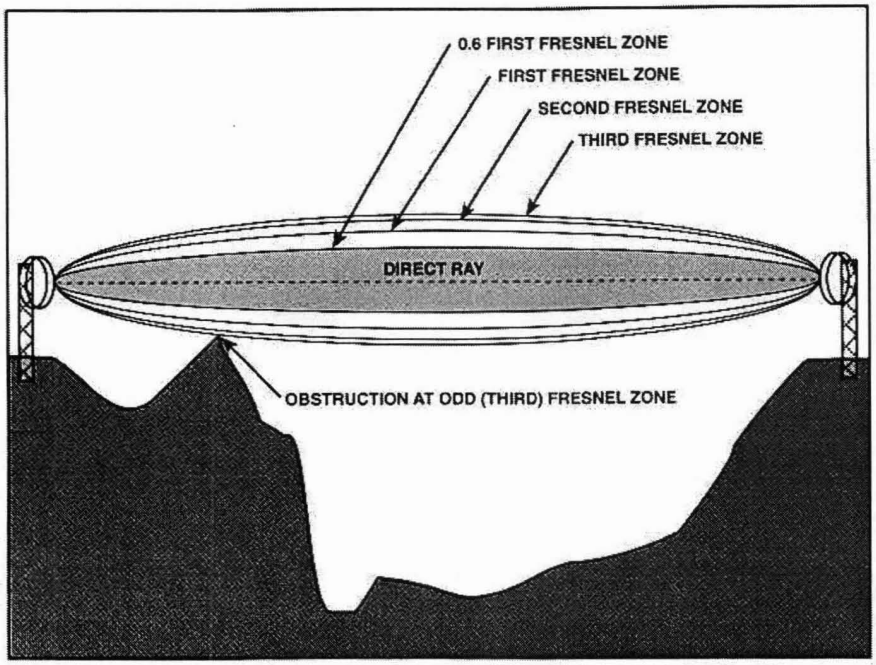

Figure 2. The Fresnel zone radii decrease with distance from mid-path. The Fresnel zone boundaries are defined by ellipsoids around the direct ray. Here, a path obstruction is shown with third Fresnel zone clearance. Because this is an odd Fresnel zone, signal energy reflected by the obstruction surface will be in phase and will add with the energy from the direct ray as it arrives at the far-end receiver. How much energy is reflected depends on the coefficient of reflectivity of the obstructing surface.

following form comes in handy:

$$\text{Fresnel zone } \# = \frac{\text{clearance}^2(\text{ft.}) \times f \times D}{72.1^2 \times d_1 \times d_2}$$

In general, if the path is line-of-sight with adequate clearance, the loss in RF signal between one end's transmitter and the other end's receiver will merely be that of free space, as described by the equation:

$$FSL\ (\text{dB}) = 96.6 + 20 \log_{10} F + 20 \log_{10} D$$

where
FSL (dB) = Free Space Loss (dB).
F = Frequency (GHz).
D= Distance (mi.).

As indicated in Figure 3 on page 32, if a path has less than 0.6 first Fresnel zone clearance, there will be more loss than merely that of free space, even though a line-of-sight condition may exist. With *odd* Fresnel zone clearances something *less* than free space losses may be realized, while with *even* Fresnel zone clearances losses may be quite significant. This is because of the phase relationship between the direct and reflected

Intelligent Power Management....

...hardware and software solutions for wireless devices, phones and radios; notebook, palmtop and desktop PC's; handheld devices, PDA's, and portable electronics.

Our patented *QuickSaver*® Intelligent Charge Solution ICS17XX family of battery charge control ICs are unsurpassed in providing:

- **Highest level of charge acceptance**
- **Consistent peak run time and standby time**
- **Greatly extended cell replacement life**
- **Lower internal pressure buildup and temp rise**
- **Greatly suppress the onset of capacity fade**

For the best power management solutions for MRT products, contact us at (610) 676-0188, or visit us on the internet at http://www.galaxypower.com.

P.O. Box 890 • 2500 Eisenhower Avenue • Valley Forge, PA 19482-0890
Ph: (610) 676-0188 • Fax: (610) 676-0189

Attention System Engineers:
Solve Voter System Problems Fast!

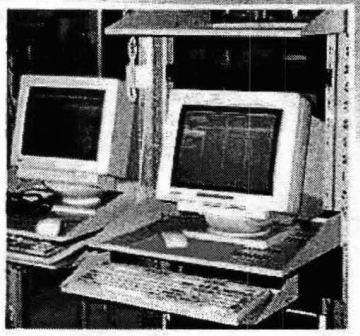

Remote Comparator Display

* Control Your Voters from a Remote PC
* Cuts Costly Maintenance Time
* Finds Intermittent Problems Fast
* Reduces Receiver Downtime
* Logs Receiver Failures
* Modular & Expandable

Call or Write for our **FREE** System Planner!

CTI Products Inc.
Land Mobile Radio Solutions

1211 West Sharon Road, Cincinnati, Ohio 45240
(513)595-5900
info@ctiproducts.com
www.ctiproducts.com/landmobile

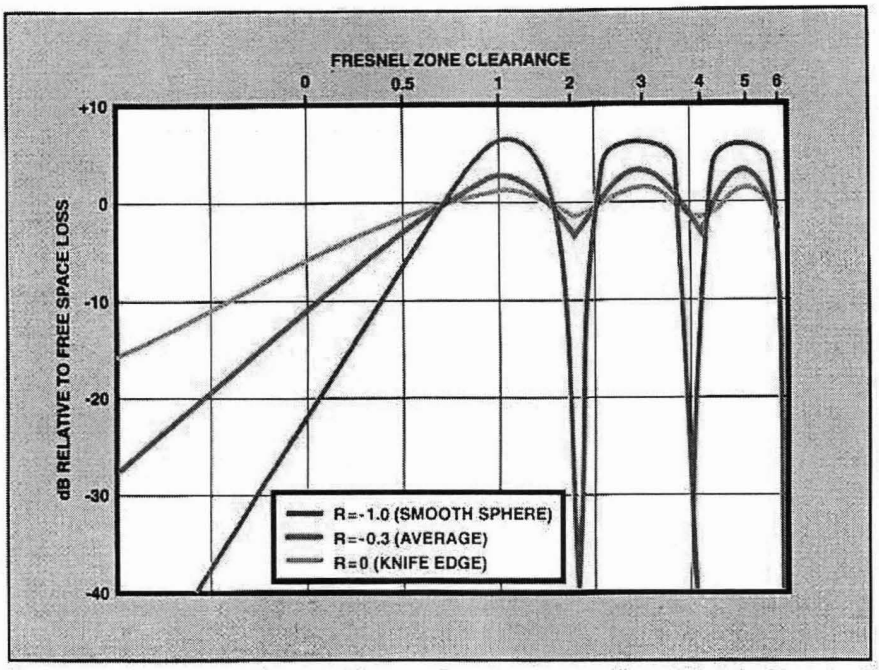

Figure 3. Deep fades result when out-of-phase reflected energy combines with the incident signal at the receiver, increasing the cancellation of the RF receive signal.

signal at the receiving antenna.

When the signal is reflected, it undergoes a 180° phase lag (equivalent to 1/2λ delay) referenced to the incident wavefront. (Although, as will be mentioned in Part 3 of this series, wave *polarization* and grazing angle can affect this). If the reflective surface is located at the first Fresnel zone, the reflected signal will arrive at the receiver delayed by another 1/2λ, for a total delay of 1λ. Signals reaching the receive antenna are therefore in phase and additive.

If the reflective surface is located at the boundary of the second Fresnel zone (which by definition, delays the signal by two 1/2 wavelengths) the wavefront, when reflected, reaches the receiving antenna delayed by a total of 1.5λ. This means it will be out of phase relative to the incident wavefront, and signals reaching the receiver will cancel to some extent.

This effect repeats for each odd and even Fresnel zone, which explains the slight rises and very deep nulls in signal level for the *even* and *odd* Fresnel zone clearances (as shown in Figure 3). Raising one or both antennas is one method of altering the Fresnel zone clearance. As the clearance increases to higher order Fresnel zone numbers, the intensity of this problem diminishes because the magnitude of the coefficient of reflection with regard to the reflecting surface diminishes.

Paths are usually designed to meet specific Fresnel zone clearance criteria for one or more values of *K*. "Heavy route"

VSWR BRIDGES & TEST CABLES

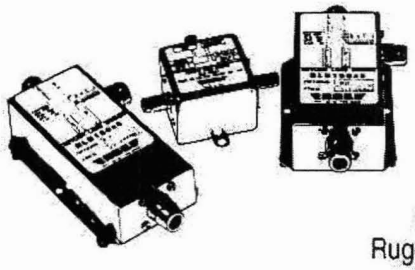

FEATURES:

5 watt power
High directivity
RF reflected port
Rugged construction

Using the EAGLE return loss bridge allows frequency domain reflectometry tests to be made easily and inexpensively. There is no need to spend thousands of dollars on a dedicated antenna tester. Simply use the EAGLE bridge with your present spectrum analyzer and tracking generator. This technique is described in our free application note. See offer below.

Price: $469.00 for a 1.0 GHz bridge.

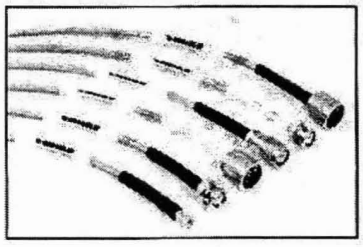

FEATURES:

Low loss
Low Cost
Custom labels
Swept to 3.0 GHz
Rugged! 60 lb. pull
Excellent return loss

Are you frustrated with cable assemblies that break easily, are lossy at low microwave, or work intermittantly? Our bridge customers had the same problem. At EAGLE we now manufacture low-cost rugged test cables! Each one is tested on a vector network analyzer to 3.0 GHz. Our custom labeling makes cable ID a snap. Excellent return loss reduces disturbances to combiners and filters.

Price: $29.00 1-4 quantity with "N" connectors.

Call for FREE application note: "Antenna and Feedline Measurements"

EAGLE

P.O. BOX 4010 ▼ SEDONA, AZ ▼ 86340 ▼ VOICE: (520) 204-2597 ▼ FAX: (520) 204-2568

New Design For Low Band VHF Repeaters

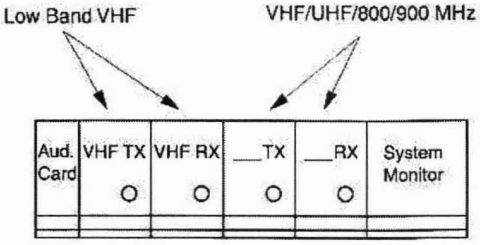

Solves Your Interoperability Problems

If your organization uses a low band VHF system, an MT-3 Cross-Band Repeater from Daniels Electronics could be configured to allow you to talk with agencies using AM, FM, VHF, UHF, or 800/900 MHz equipment.

Call Toll Free 1-800-664-4066

43 Erie St. Victoria BC
CANADA V8V 1P8
U.S.A. Fax: (360) 738-2230
Phone: (250) 382-8268
Email: sales@danelec.com
Web: http://www.danelec.com

DANIELS® ELECTRONICS LTD.

Circle (28) on Fast Fact Card

Interference Patrol

Responsibility for controlling interference on shared channels lies *first* with radio users:



☆ Listen before you transmit on a shared channel. Learn how to disable the squelch to listen for other users.

☆ Use your call sign whenever you use the radio.

☆ If you use a scrambler for privacy on a shared channel, sign off "in the clear" so other users know you are finished.

☆ Have your radio serviced periodically to be sure it is on frequency.

☆ Keep communications brief to promote harmony with other users who share the channel.

☆ Use the minimum transmitter power and antenna height you need to cover your area. That might be less than the power and antenna height specified on your license.

System operators:

☆ Post the name and 24-hour phone number of the site manager at the access point for each antenna site.

A public service message from

Mobile Radio Technology.

requirements dictate that there must be at least 0.3 first Fresnel zone clearance when $K = 2/3$, and 1.0 first Fresnel zone clearance when $K = 4/3$, whichever is greater. "Light route" requirements dictate at least 0.6 first Fresnel zone clearance plus ten feet when $K = 1$.

Another important consideration here is what *type* of reflecting surface is being evaluated. In general, three categories of surfaces are defined, each with its own reflection coefficient: $R = 0$ (a sharp or "knife" edge), $R = -0.3$ ("average" roughness) and $R = -1.0$ (a smooth spherical surface). (The reflection coefficient will be described in more detail in the third article of this series.) The type of surface makes a big difference with regard to attenuation on the even Fresnel zone clearances because obstructions with larger, smoother surface areas reflect more energy. With more out-of-phase reflected energy combining with the incident signal at the receiver, greater cancellation of RF receive signal will be realized, resulting in deep fades as shown in Figure 3.

The next article in this series will briefly discuss path reflections, the power budget and the fade margin.

References

Laine, R.U., *Determining Antenna Heights for Coastal Areas*, Lenkurt Electric, Monograph 197.

"Microwave Systems, Microwave Path-Testing," *Bell Systems Practices*, AT&T Standard, September 1962.

"Microwave Transmission Engineering (Part One and Two)," *GTE-Lenkurt Demodulator*, July/August, 1972.

White, R.F., *Engineering Considerations for Microwave Communications Systems*, 4th Ed., GTE-Lenkurt, San Carlos, CA, 1983.

Microwave path design series

Part 1: "Microwave path design: The Basics," May 1998.

Part 2: "Microwave path design: The Basics," June 1998.

Back issues printed within the past two years can be ordered for $10 each, postpaid. Call Intertec Publishing customer service at 800-441-0294. Issues printed more than two years ago and individual article photocopies are not available from the publisher. Individual photocopies of articles printed since January 1983 can be ordered from the UMI Information Store, 800-248-0360.

Microwave path design: The basics

Part 3—This series of four articles is a primer on some of the propagation-related basics of microwave path design. This month's installment explains the effect of path reflections on fading, how to derive a power budget and the fade margin.

By Jeff Ashley

In the first two parts of this series (*MRT* May and June), the microwave path design process was described in terms of:

- ❑ determining whether a proposed path is "line-of-sight."
- ❑ evaluating path clearances with regard to refractive effects.
- ❑ evaluating path clearances with regard to Fresnel zones.

This section covers path reflections and how to derive a power budget and fade margin. The concluding installment will examine path reliability.

Considering path reflections

A point of reflection will exist somewhere along the length of the path where (with regard to the reflecting plane and antennas at both ends) the angle of incidence equals the angle of reflection (see Figure 1 below). If antennas at each end of the path are at the same height above a flat, reflecting surface, the reflection point will be located halfway between the two. However, if antenna elevations are different, the reflection point will be closer to the lower antenna and will move along the length of the path, toward one endpoint or the other as K varies ("K" was defined in Part 1 of this series). If sufficient out-of-phase signal from the reflection point is received at the far-end receiver, catastrophic fading may occur.

In some cases the reflection point will be blocked naturally by terrain features. Manipulation of antenna heights is a method of moving the reflection point to a different spot along the length of the path so that it can be blocked by an obstruction or perhaps so that it may fall on a less reflective surface. Rough surfaces do not reflect as well as smooth, flat surfaces, such as water.

The magnitude of the reflection coefficient (amount of "reflectivity") also increases as the angle of incidence decreases. Because of this, short paths with endpoints at a considerable height above the reflecting surface will be affected less than those with endpoints barely higher than the reflective surface itself (a microwave link between two offshore oil platforms, for example). The magnitude of the reflection coefficient can vary from 0 to −1.0, the latter corresponding to 100% reflection. The negative sign refers to a 180° phase reversal at the point of reflection.

There is an advantage to using vertical polarization when the grazing angle on a reflective surface is a couple of degrees or greater. The magnitude of the reflection coefficient with vertical polarization is much less than that of horizontal polarization. Less reflected signal will be present at the receive antenna on the other end of the path. In fact, with a grazing angle of 6.5°, the magnitude of the reflection coefficient for a vertically polarized wave is only about −0.08 compared to about −1.0 for horizontal polarization. The magnitude rises as the grazing angle increases above 6.5° until it finally meets the same value of the horizontally polarized signal (at 90°).

The phase change (or lag) at the point of reflection for a vertically polarized signal is also significantly affected at low grazing angles as compared to the practically uniform 180° phase reversal for a horizontally polarized signal. As the angle increases from 1° to 30°, the phase change of a vertically polarized signal drops quickly from about 180° to 4°. With only a 4° phase lag, the reflected signal that reaches the receive antenna on the other end of the path would have more of an additive, rather than canceling effect.

The distance to the reflection point can be calculated using the equation

$$d_1 = nD \qquad \text{[Eq. 1]}$$

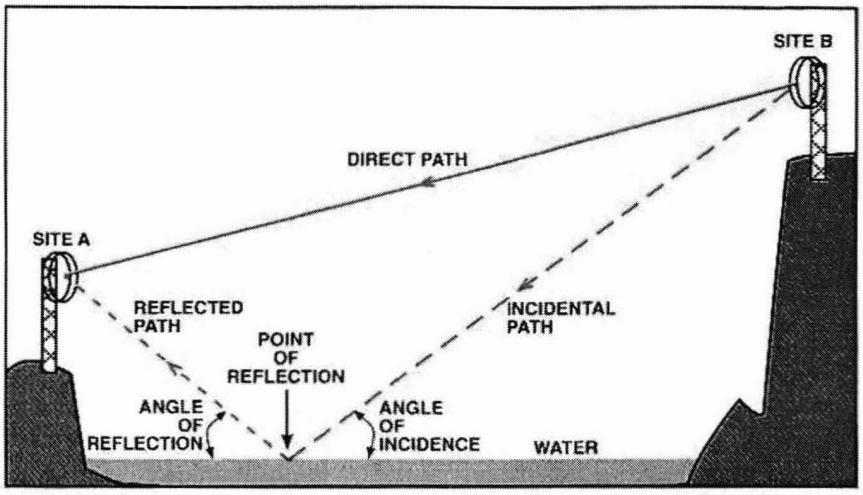

Figure 1. At the point of reflection, the angle of incidence equals the angle of reflection.

Ashley is a communications technician in Los Angeles.

where (for $K = \infty$ *only*):

$$n = \frac{h_1}{h_1 + h_2}$$

and

h_1 = the elevation of the lower antenna above the reflecting surface.

h_2 = the elevation of the higher antenna above the reflecting surface.

d_1 = the distance (mi.) to the reflection point from the h_1 end.

D = the total path length.

Because calculations for n, where $K = 2/3$ and $K = 4/3$, get a bit involved, estimated values can be obtained from graphs offered in R.F. White *(see references)*.

As refractive conditions change, the degree of bowing that occurs on the wavefront will change. As the amount of bowing changes, the location of the reflection point will vary in relative distance between the two path endpoints. In designing a path, it is useful to analyze the overall range of movement (or distance of travel) that can occur for this reflection point. The design engineer must determine whether (in its range of movement) it may wander onto a highly reflective surface (such as a body of water) that lies between path endpoints. In such an undesirable situation, measures might be taken to move the reflection point elsewhere by changing antenna heights, or by attempting to block the reflection.

To determine the practical limits of travel for the reflection point, two values of K are typically used that would describe limits of refractive conditions. One limit is when refractive conditions correspond to a value of $K = \infty$. The other extreme limit will be the value of K that would bend the path downward to the point of grazing the ground. Beyond this grazing point, no reflection can exist because the path itself is being obstructed by the earth.

The value of K that corresponds to "grazing" can be calculated from the equation:

$$K = \frac{1}{1.5\left(X + Y + 2\sqrt{XY}\right)} \quad \text{[Eq. 2]}$$

where

$$X = \frac{h_1}{D^2} \quad \text{and} \quad Y = \frac{h_2}{D^2}$$

(h_1, h_2 and D are already defined in Equation 1).

The distance to the grazing point is calculated from Equation 1, where:

$$n = \frac{1}{1 + \sqrt{\frac{Y}{X}}}$$

Deriving a power budget

A path power budget is nothing but an itemized list of all system losses and gains (in decibels) from the transmitter on one end of the path to the receiver on the other end, and everything in between.

For example, if starting with the transmitter on one end of the path, one would note transmitter output power (+dBm), then subtract all the losses in subsequent connectors and circulators external to the radio assembly, along with waveguide losses (−dB) until the antenna is reached. The gain of the antenna would be added to that value (minus the loss in the radome, if used) to give the resultant effective radiated power (ERP.). This is the available RF signal that will be propagated through the atmosphere to the other

RF Site Monitoring Made Simple!

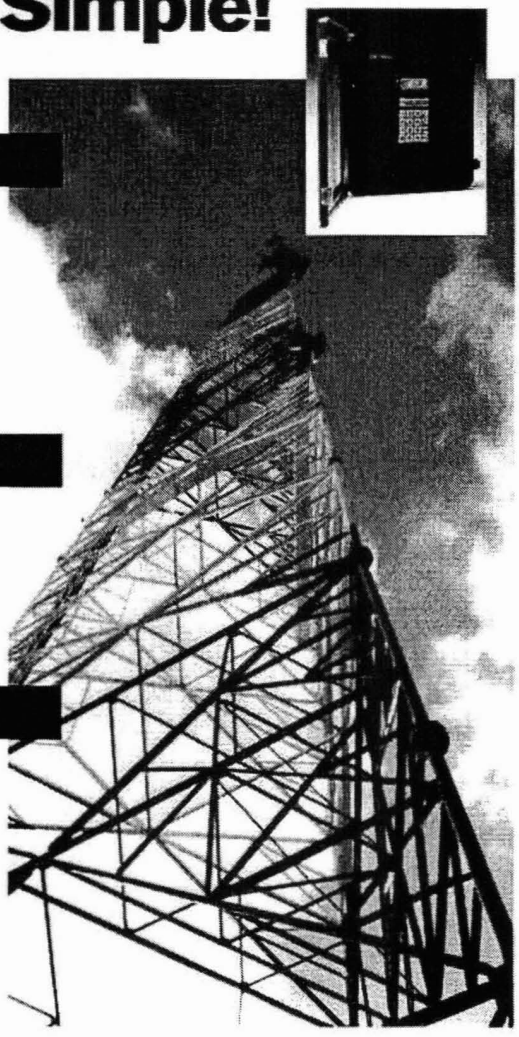

Monitor
- Security
- Battery Power
- Tower Lights
- RF Power

Control
- Generators
- Transmitters
- HVAC

Alarm
- Telco\Cellular
- Voice\Message Pages

Call 425.820.6363 FAX 425.820.7031
Email zetron@zetron.com today!

ZETRON

Zetron, Inc. PO Box 97004 Redmond, WA 98073-9704 USA
Web: http://www.zetron.com

Circle (23) on Fast Fact Card

end of the link. As the signal makes its way through the atmosphere to the receiving site, free space loss (−dB) (the formula for this was given in Part 2, *MRT* June), in addition to atmospheric losses (−dB), would then be subtracted from the ERP value.

The term *atmospheric loss* or "absorption" pertains to effects that atmospheric gases, primarily oxygen and water vapor, have on microwave propagation. These effects are calculated separately from free space losses. Attenuation figures are directly proportional to path length and increase with frequency (0.0002 dB/mi. at 2GHz, 0.002 dB/mi. at 8GHz and almost 0.2dB/mi. at 20GHz).

At the receiving end of the link, the considerations are the same as on the transmitter end, only in reverse order (radome loss; antenna gain, waveguide, connector and hybrid/coupler losses), with the remaining signal level being applied to the receiver (−dBm).

Fade margin

The receiver manufacturer will offer a *noise threshold specification* (expressed in −dBm) which, simply stated, is the sensitivity of the receiver. It is considered to be the lowest receive signal level at which the receiver will still be considered "unusable." There are variations in the definition of the term "unusable," which means the use of different standards in determining how a particular receiver threshold specification will be obtained. For example, on most industrial analog microwave systems the practical threshold of the receiver is considered the absolute RF signal level (−dBm) injected into the receiver that will establish a 30dB (flat) signal-to-noise ratio (58dBrnc0) as measured in a discriminated baseband noise slot. The telephone companies, however, have used a 33dB (flat) signal-to-noise ratio (55dBrnc0). (The baseband frequency of this noise slot will typically be specified by the equipment manufacturer and is dependent on the particular channel loading of that equipment. It is usually assigned somewhere above the highest occupied frequency slot on the baseband. Because noise effects are worst on the high end of the baseband, this slot would offer a worst case scenario for the signal-to-noise measurement.)

The threshold specification on digital microwave receivers makes reference to the bit-error rate (BER) of the recovered data rather than to a discriminated analog noise measurement. The old Bell standard for digital systems is the RF signal level injected into the receiver that will produce a BER that exceeds 10^{-3}. This is typically referred to as the "outage" threshold. Often, however, a BER of 10^{-6} (referred to as the operating point threshold) is used because this is a more common T-1 level standard. (As a note, the difference between these two bit-error rates relates to a change in RF receive level of only 2dB–3dB. This is because BER performance on digital radios degrades rapidly after the 10^{-6} point.) As long as the BER is defined along with the threshold specification, no confusion over terms should exist.

On analog microwave systems, the difference between the receiver threshold value (−dBm) and the receive signal level (RSL) being applied to the receiver (−dBm) under normal path conditions is referred to as the *fade margin* (expressed in dB). This is a "safety margin" of excess signal that the path can fade before the receiver becomes "unusable" due to

NEW SOLUTIONS

You know our products. For 25 years, we have introduced innovative designs to the land-mobile radio industry. For the last fifteen years, our company has been synonymous with reliable, quality, customer-focused products under our customers' labels. We're Instrument Associates, a leading name in the future of wireless infrastructure products. And we're joining forces with our parent company to provide new solutions. "Reintroducing" an expert in wireless solutions—with new products and a new name: GAI-TRONICS.

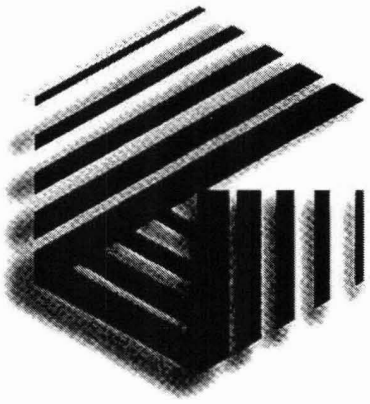

DESKTOP CONTROLLERS
TELEPHONE INTERCONNECTS
REPEATER CONTROLLERS
DISPATCH SOLUTIONS

GAI-TRONICS® CORPORATION
Instrument Associates Division

2455 Harbor Avenue • P.O. Box 11127 • Memphis, Tennessee 38113
901 947 4000 • FX 901 948 8855 • www.instrumentassociates.com

GAI-Tronics Corporation is an operating subsidiary of Sensorial® Communications, Inc.

Circle (25) on Fast Fact Card

noise. The same general definition could be used for digital microwave systems, although in this case it might be termed "flat" or *thermal fade margin* (TFM). Other terms applicable to digital systems are *dispersive fade margin* (DFM), *adjacent channel interference fade margin* (AIFM), and *external interference fade margin* (EIFM). *Composite fade margin* (CFM) is a term used to describe the composite affects of TFM, DFM, AIFM and EIFM. Typical receiver threshold levels for digital or analog commercial microwave receivers are usually in the ballpark area of −70dBm to −85dBm.

It should be noted that microwave receivers have a specified range of RF input signal level over which they should properly detect and decode modulated information. This means not only that there is a *minimum* signal level (receiver "threshold") but also a *maximum* signal level that can be applied to the receiver input without expecting distortion or data errors in the recovered signal. This restricts the path designer from creating a huge fade margin by applying excessively high RF levels to the receiver under normal path conditions. Additionally, a path phenomenon referred to as "up-fading" can occur (particularly around the end of a period of severe multipath activity) where the microwave link receivers realize an extreme increase in RF signal level (relative to normal RSL). Up-fading is thought to be the result of an anomalous "lens" effect in the atmosphere. For such reasons, the design engineer should leave a margin of at least 10dB between normal path RSL and the receiver's upper RF input limit. The typical design RSL for a microwave receiver is about −35dBm.

The next and final article in this four-part series will discuss microwave path reliability.

References

"Atmospheric Effects on Microwave," Technical Note TN-5.0, Digital Microwave, Aug. 1986.

Hartmann, P.R., J.A. Crossett and E.W. Allen, "Propagation and Countermeasures in Line of Site Digital Transmission Systems," Rockwell International, Collins Transmission Systems Division, Technical Bulletin 523-0609099-011A3J.

Laine, R.U., "Determining Antenna Heights for Coastal Areas," Lenkurt Electric, Monograph 197.

Llanes, Cesar L., "6-Gigahertz Space-Diversity Digital Microwave Test Link," Los Angeles County Internal Services Department, ITS Engineering Study, Los Angeles, CA, Nov. 1989.

"Microwave Transmission Engineering (Part One)," *Demodulator*, GTE-Lenkurt, July 1972.

"Microwave Transmission Engineering (Part Two)," *Demodulator*, GTE-Lenkurt, Aug. 1972.

"Multipath Fading," *Demodulator*, GTE-Lenkurt, Nov. 1967.

White, R.F., *Engineering Considerations for Microwave Communications Systems*, 4th Ed., GTE-Lenkurt, San Carlos, CA, 1983.

Microwave path design series

Part 1: "Microwave path design: The Basics," May 1998.
Part 2: "Microwave path design: The Basics," June 1998.
Part 3: "Microwave path design: The Basics," July 1998.

Back issues printed within the past two years can be ordered for $10 each, postpaid. Call Intertec Publishing customer service at 800-441-0294. Issues printed more than two years ago and individual article photocopies are not available from the publisher. Individual photocopies of articles printed since January 1987 can be ordered from the UMI Information Store, 800-248-0360.

AEA NEW!

GRAPHICAL ANTENNA & CABLE ANALYZERS



The complete line of AEA antenna and cable anlyzers are now available **FACTORY DIRECT** at the lowest possible cost. Each antenna analyzer gives a **graphical display of SWR** curves with variable sweep width and center frequency. The **30-150, 150-525,** and **806-960** MHz antenna analyzers are each **$499.95** plus $7.50 shipping and handling. The **SWR-121 HF** analyzer covers 1-30 MHz and is priced at **$299.95** plus $7.50 shipping and handling.

We are pleased to announce the **NEW** AEA **CIA-HF** Complex Impedance Analyzer that features all the features of the above SWR Analyst products. In addition, the CIA-HF gives graphical displays of impedance, reactance, resistance and relative phase angle with a vector display mode. Automatically display the 2:1 SWR points or any two other user selectable bandwidths. Display reactance and the conjugate match value of inductance or capacitance necessary to resonate a mis-tuned antenna. The CIA-HF covers a frequency range of 400kHz to 54 MHz and has a low introductory factory direct price of **$359.95** plus $7.50 shipping & handling in CONUS.

The **AEA CableMate™** graphical Time Domain Reflectometer **(TDR)** is packaged in the same style package as the SWR analyzers. The CableMate shows multiple faults in a cable on the graphical display. Virtually any multi-conductor cable may be **tested for shorts, opens or impedance lumps**. The CableMate is an **excellent** device for **measuring the length of most any cable** for inventory purposes. It will also directly show the 25 MHz return loss. An RJ-45 switch adapter allows easy testing of LAN cables. The CableMate is priced at **$359.95** plus $7.50 shipping and handling in CONUS.

All AEA analyzer products come standard with a **serial computer interface**. Optional DOS applications software (except CIA-HF) with interface cable is **$29.95** each. With this software you can store the graphical data for your antennas or cables for future reference.

For more information on this exciting new product or for our catalog, contact AEA at the numbers listed below.

MasterCard VISA

AEA

Orders: 1-800-258-7805

Tech Info: 760-598-9677 • Fax: 760-598-4898 • www.aea-wireless.com
Division of TEMPO RESEARCH CORPORATION
1221 Liberty Way • Vista, CA 92083
Prices and Specifications subject to change without notice or obligation.

Circle (27) on Fast Fact Card

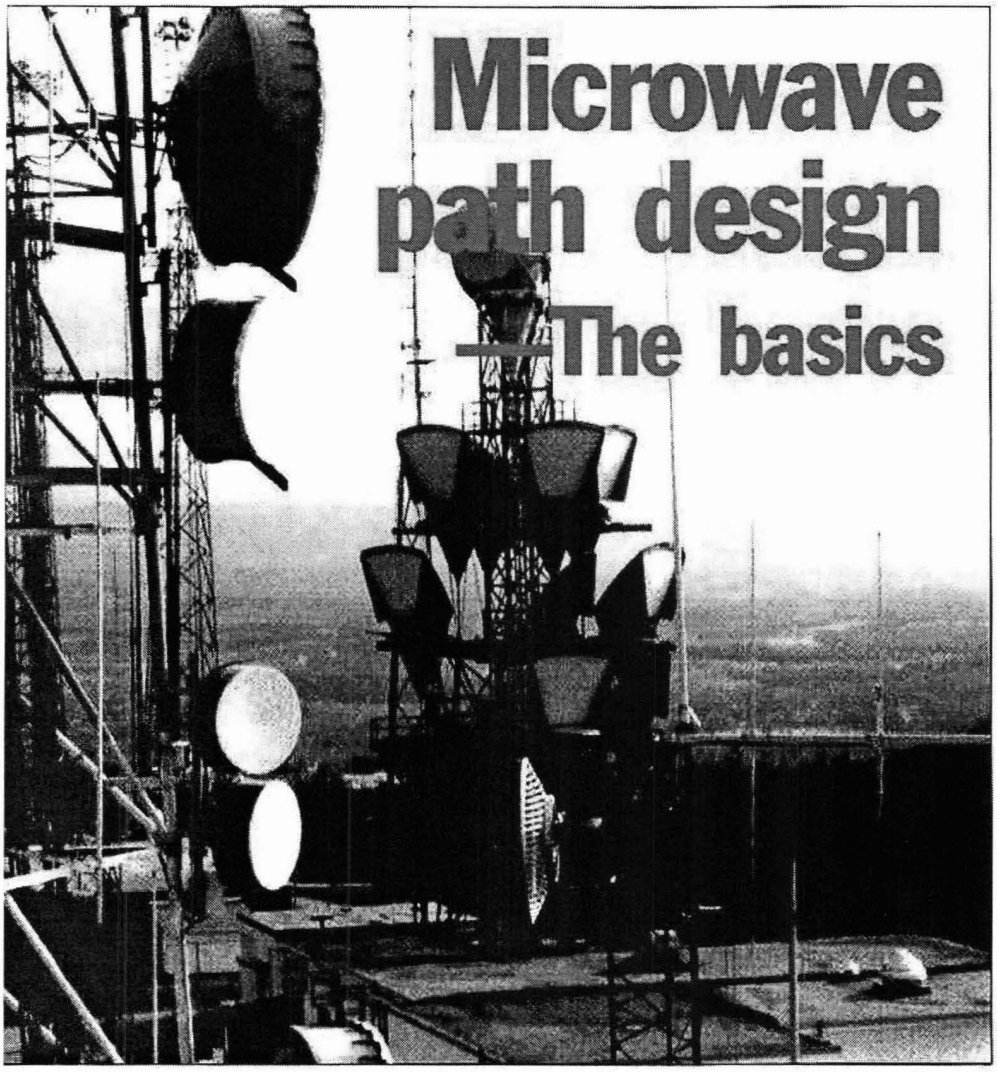

Microwave path design — The basics

Part 4—This series of four articles is a primer on some of the propagation-related basics of microwave path design. This last installment discusses path reliability.

By Jeff Ashley

Preceding installments in this series have described basic considerations:

- Determining whether a proposed path is "line-of-sight."
- Evaluating path clearances with regard to refractive effects.
- Evaluating path clearances with regard to Fresnel zones.
- Considering path reflections.
- Deriving a power budget and fade margin.

This concluding article covers path reliability.

Path reliability

Usually, microwave links are designed to meet a specific reliability factor. Reliability may also be termed "availability" and is expressed as a percentage. It represents the percentage of time the link is expected to operate without an outage caused by propagation conditions. The Bell standard for short-haul propagation reliability is 99.995% (minimum), while requirements for high-capacity, long-haul may be 99.9999%. "Unavailability" or the probability of an *outage* (because of propagation conditions) is often referred to and, if expressed in percentage, the value is determined by subtracting the availability (expressed as a percentage) from 100. For example, a short-haul reliability (availability) factor of 99.995% can also be expressed as an *unavailability* factor of 0.005%.

Availability and unavailability are referenced to a year. In other words, if the unavailability is 0.001%, it could also be stated there will be:

$$365.25\ (\text{days / yr}) \times 24\ (\text{hr / day}) \times 60\ (\text{min / hr}) \times \frac{0.001}{100}$$

= 5.26 minutes of unavailability (outage) *per year.*

The propagation-related unavailability is derived from Equation 1 below. This equation is used as an approximation for the one-direction effects of multipath fading with various terrain and atmospheric conditions.

$$P_m = a \times b \times 2.5 \times 10^{-6} \times f \times D^3 \times 10^{-F/10} \qquad \text{[Eq. 1]}$$

where

P_m = Outage probability (unavailability) due to multipath fading.
D = path length (in miles).
f = frequency (in GHz).
F = fade margin of the path (in dB).
a = one of the following generalized terrain factors:
- 4: very smooth (including water).
- 1: average, some roughness.
- 1/4: very rough.

b = one of the following generalized climate factors:
- 1/2: hot, humid.
- 1/4: normal, temperate.
- 1/8: very dry.

(Note that the result of this equation must be multiplied by 100 in order to be expressed as a percentage.)

Another factor that can affect path reliability is rain attenuation, particularly past 10GHz. At these higher frequencies, the wavelength becomes short enough that rain droplets (depending on their size and shape) can present themselves as obstructions to the path. This occurs when the diameter of the droplets approach 1/4 wavelength of the frequency being used. The maximum instantaneous intensity of the rainfall and the percentage of the total path within the rain cell are other factors to be considered.

Because rain rates differ by geographic location, statistics for the particular area of interest must be obtained. Commercial path design software typically has this information in tables, requiring the user simply to select the geographic location of the proposed path. The values for that area are then accessed. The National Weather Bureau also maintains this information for various cities throughout the United States.

Increasing path reliability

One method of increasing path reliability is to increase the fade margin. If the

Ashley is a communications technician in Los Angeles.

design engineer dictates a particular fade margin requirement from the start, the power budget can be determined in a particular sequence. Knowing the noise threshold of the receiver being used (-dBm) and the required fade margin, the nominal signal level into the receiver can be determined (noise threshold [-dBm] plus fade margin [+ dB] = nominal receive level [-dBm]). The difference in decibels between the transmitter RF output level (+ dBm) on one end of the path and the desired receive signal level (RSL) on the other end of the path will be the maximum allowable net path loss. Because path distance and antenna heights are known, free space and atmospheric losses, along with all hardware losses on both ends, can be determined and will exceed this allowable net path loss by some amount (measured in decibels). The amount by which it is exceeded will be the necessary combined gain of the antennas on each end of the path. To achieve this required gain, proper antenna reflector diameters must be selected.

Parabolic ("dish") antennas typically have gain efficiencies of 55% to 65%. Using an efficiency of 55%, the gain of a parabolic antenna can be calculated as follows:

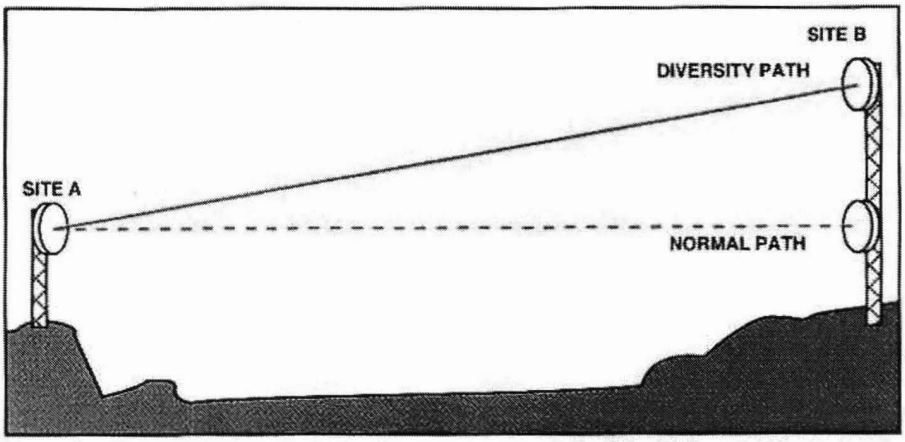

Figure 1. With adequate spacing between antennas, there should be little correlation between paths with regard to fading.

$$G = 20 \log_{10} B + 20 \log_{10} F + 7.5 \quad \text{[Eq. 2]}$$

where

G = gain over an isotropic antenna.

B = parabola diameter in feet.

F = frequency in GHz.

After a proposed microwave path has been evaluated with regard to reliability, the calculations may show that it will not meet the required standards. In such situations, additional techniques known as *diversity* methods may be employed.

One such technique is *space diversity*, which involves the addition of another receive antenna, separated in distance from the first, as shown in Figure 1 above. An additional receiver and associated switching/combining equipment will also be needed. The additional "diversity" antenna is usually mounted on the same tower structure, yet vertically separated from the site's original receive antenna. This diversity antenna is connected to the diversity receiver. This additional equipment essentially creates another microwave path between the two sites. Receiver switching and combining equipment then senses which receiver has the troubled signal (if fades occur) and switches that receiver "off-line."

Constructing a UHF Trunking System?

Build it "Smart" with the Ritron RRX-450 Synthesized Repeater.

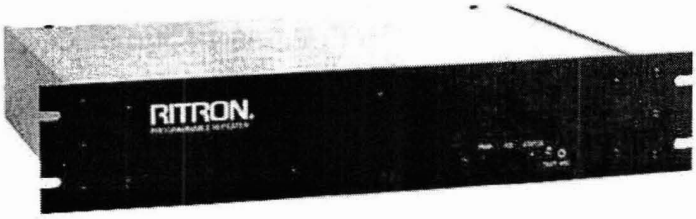

Call us at 800-USA-1-USA or FAX 800-251-RFAX and find out about the smart solution for your UHF trunking system.

Easy Interface to Trunking Controllers!

RITRON, INC.
Wireless Communications Products and Systems

UHF trunking is a smart idea. It's spectrum efficient and has plenty of profit potential for an operator. But don't stop there. If you're constructing a system or planning to soon, build your system "smart" with Ritron's RRX-450 synthesized repeater.

The RRX-450 repeater is the intelligent choice because it offers so much for so few dollars. For starters, it easily connects to trunking controllers through a dedicated internal connector, eliminating interface hassles.

The RRX-450's superior technical performance is well suited for trunking environments. It has excellent transmit modulation bandwidth and linearity, allowing trunking control data to pass through cleanly without any distortion. And it can easily drive a 100 Watt power amplifier with 6 Watts of input and still operate at continuous duty.

All of these features make Ritron's RRX-450 the competent choice for your trunked radio system at a cost that's hundreds of dollars below the competition:

- 10 pin trunking controller interface
- Ventilated rack mount enclosure with cooling fan
- UHF and VHF* Models
- 8 & 30 Watts output power
- 110/220 VAC operation
- CTCSS/DCS Signalling
- 12 VDC trickle charge w/Auto cutover
- Flexible PC Programming

* *FCC type acceptance pending (available for international sale)*

MADE IN THE USA

One drawback of space diversity is increased cost. Tower heights must be greater to achieve sufficient vertical antenna separation. In some cases, the existing tower structure might have to be retrofitted to handle the additional wind loading created by the diversity antenna. The diversity antenna, receiver and combining and switching equipment create additional cost.

When spacing is adequate between antennas, there should be little correlation between the two paths with regard to propagation characteristics. Improvement in reliability comes from the reduced probability that both paths will be adversely affected by fading at the same time.

In general, more vertical spacing between antennas offers less path correlation and better path reliability. The rule of thumb for antenna spacing is as follows: 60–80 feet at 2GHz, 45–50 feet at 4GHz, 30-40 feet at 6GHz and 25–30 feet at 11GHz.

The following modified form of Arvids Vigants' fade reduction factor equation can be used to estimate the improvement offered by space diversity:

$$I_{sd} = \frac{7.0 \times 10^{-5} \times f \times s^2 \times 10^{F+10}}{D}$$

[Eq. 3]

where

I_{sd} = improvement factor (space diversity).

f = frequency in GHz.

s = vertical antenna spacing, in feet, between centers.

D = path length in miles.

F = path fade margin (if one antenna's path has a smaller fade margin, use that figure).

Frequency diversity is another method used to increase path reliability. Microwave transmitters operating on two frequencies (with a typical in-band diversity spacing of about 2%), and sometimes in two frequency bands (called crossband diversity), are used to transmit the same information to separate receivers at the other end of the path.

Reliability improvement comes from the reduced chances of fading occurring on both frequencies (or frequency bands) at the same time.

Frequency diversity does not require the vertical antenna spacing used in space diversity, and therefore reduces tower cost. It does, however, require the use of more spectrum because it uses two sets of frequencies.

Because available frequencies are in limited supply, the FCC disallows the use of frequency diversity except under certain conditions. Test comparisons between space and frequency diversity indicate that improvements realized with space diversity are generally greater than those achieved with frequency diversity.

A general formula to calculate the improvement factor given by frequency diversity is as follows:

$$I_{fd} = K \times \left(\frac{\Delta f}{f}\right) \times 10^{F+10}$$

[Eq. 4]

where

I_{fd} = frequency diversity improvement factor.

$\frac{\Delta f}{f}$ = frequency diversity spacing (*percent* ÷ 100).

F = fade margin.

K = 1/2 for 4 GHz band.
1/4 for 6 GHz band.
1/8 for 8 GHz band.
1/12 for 12 GHz band.

(The values of K shown above for the 8GHz and 12GHz bands are GTE-Lenkurt engineering estimates based on work from

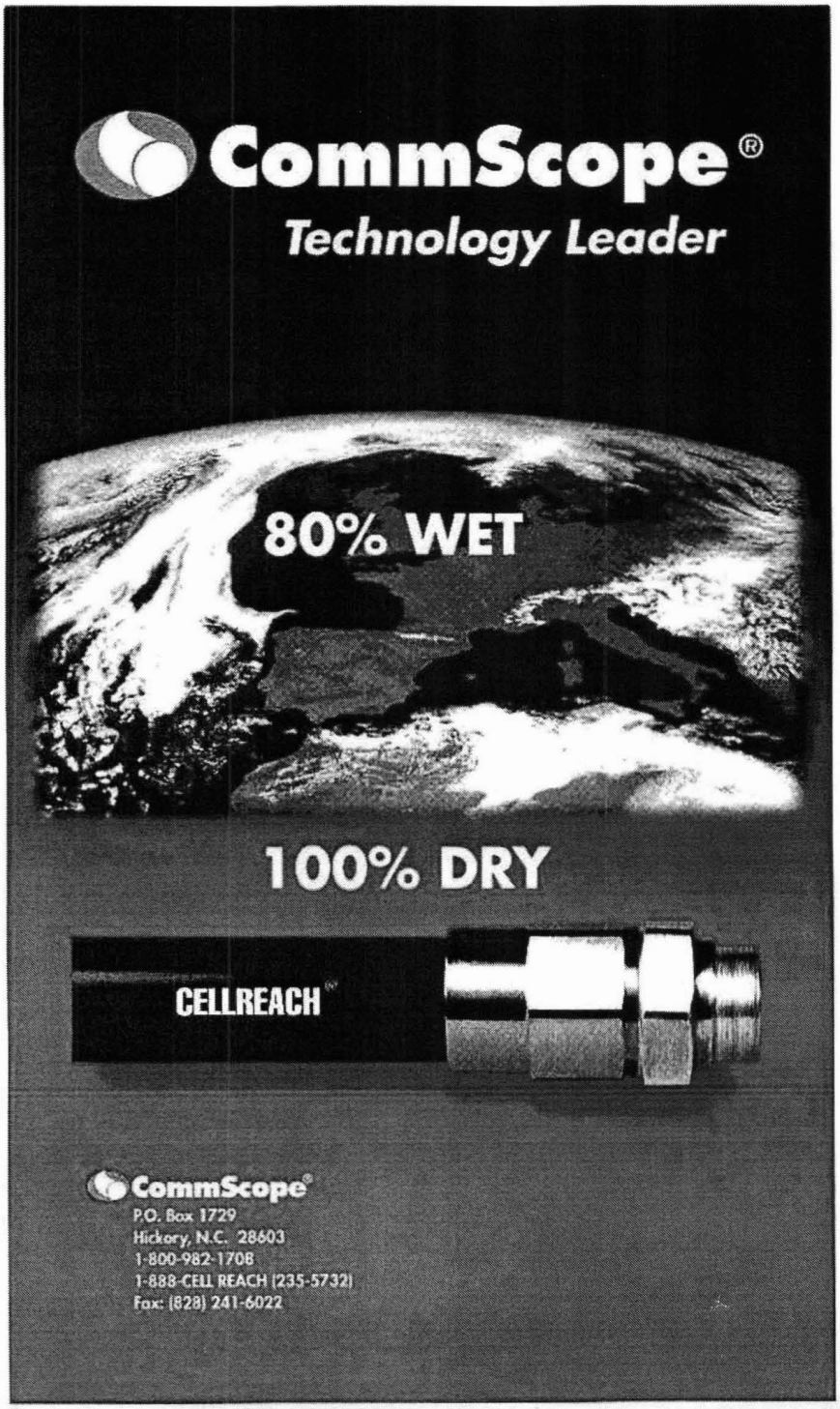

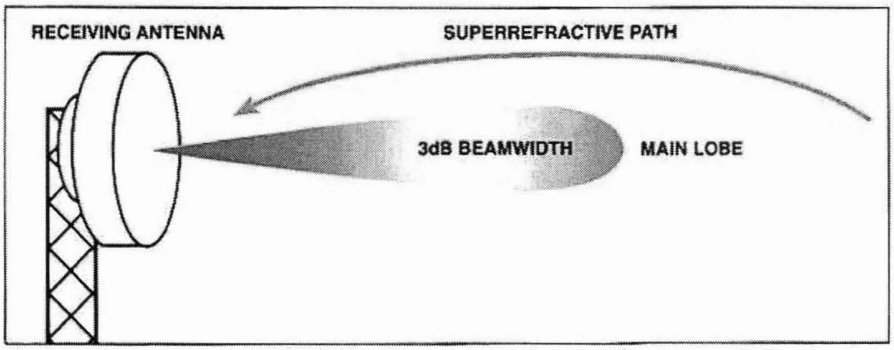

The increased vertical angle of arrival under superrefractive conditions may cause the incoming wavefront to fall outside the beamwidth of the antenna. This is called 'antenna decoupling' and can cause a significant reduction in receive levels.

W.T. Barnett that dealt strictly with the 4GHz and 6GHz bands.)

Neither space diversity nor in-band frequency diversity provide improvement against rain attenuation, although out-of-band frequency diversity (such as 6GHz/12GHz) does.

Under superrefractive atmospheric conditions, negative values of K can exist where the path bows skyward at mid-path and comes downward at the ends. This will create a wavefront that will arrive at the antenna with a greater vertical angle than normal (see Figure 2 above). Because microwave antenna beamwidths can be small, this increased vertical arrival angle may be outside the antenna's half-power beamwidth. The received signal level realized may be sufficiently low to cause noise problems or even an outage. This has been termed "antenna decoupling." A method of reducing this effect is to use a special *angle diversity* feed horn arrangement that essentially creates two vertically separated main lobes, so that if the signal level from the lower (normal) main lobe diminishes sufficiently because of the wavefront's increased arrival angle, the other (upper) lobe will be better oriented. Because most fades are due to reflections and multipath effects rather than this anomalous superrefractive condition, angle diversity offers only a limited improvement factor over that of a non-diversity path under typical path conditions.

Hybrid diversity is where both frequency *and* space diversity are employed simultaneously. However, most of the improvement comes from the effect of the space diversity.

The following equation is used when calculating fade probabilities with various methods of diversity:

$$U_{div} = \frac{P_m}{I} \qquad \text{[Eq. 5]}$$

where

U_{div} = unavailability or probability of outage (using some diversity method).

P_m = annual unavailability (non-diversity) due to multipath (Eq. 1).

I = diversity improvement factor (Eq. 3 and Eq. 4).

In multiple-hop microwave systems, the overall reliability figure (expressed as a percentage) is obtained by taking the sum of the unavailability figures (as a percentage) for each hop, and subtracting that figure from 100.

Conclusion

Many other considerations go into the complete design of a microwave path and communications link. Additionally, each of the points discussed can be taken in much greater depth. Volumes of information are available to the interested reader from many of the large communications companies, both past and present.

This series of articles has offered a glimpse into some of the more fundamental propagation-related design considerations and will be of value to those just getting their feet wet in the microwave communications field. ■

References

"Antenna Decoupling," GTE-Lenkurt *Demodulator*, March/April 1978.

Laine, R.U., "Determining Antenna Heights for Coastal Areas," Lenkurt Electric, Monograph 197.

Llanes, Cesar L., "6-Gigahertz Space-Diversity Digital Microwave Test Link," Los Angeles County Internal Services Department, ITS Engineering Study, Los Angeles, Nov. 1989.

"Multipath Fading," *Demodulator*, GTE-Lenkurt, Nov. 1967.

"Space Diversity," GTE-Lenkurt *Demodulator*, May 1973.

White, R.F., *Engineering Considerations for Microwave Communications Systems*, 4th Ed., GTE-Lenkurt, San Carlos, CA, 1983.

Acknowledgments

A special thanks to Cesar Llanes for answering so many questions through the years.

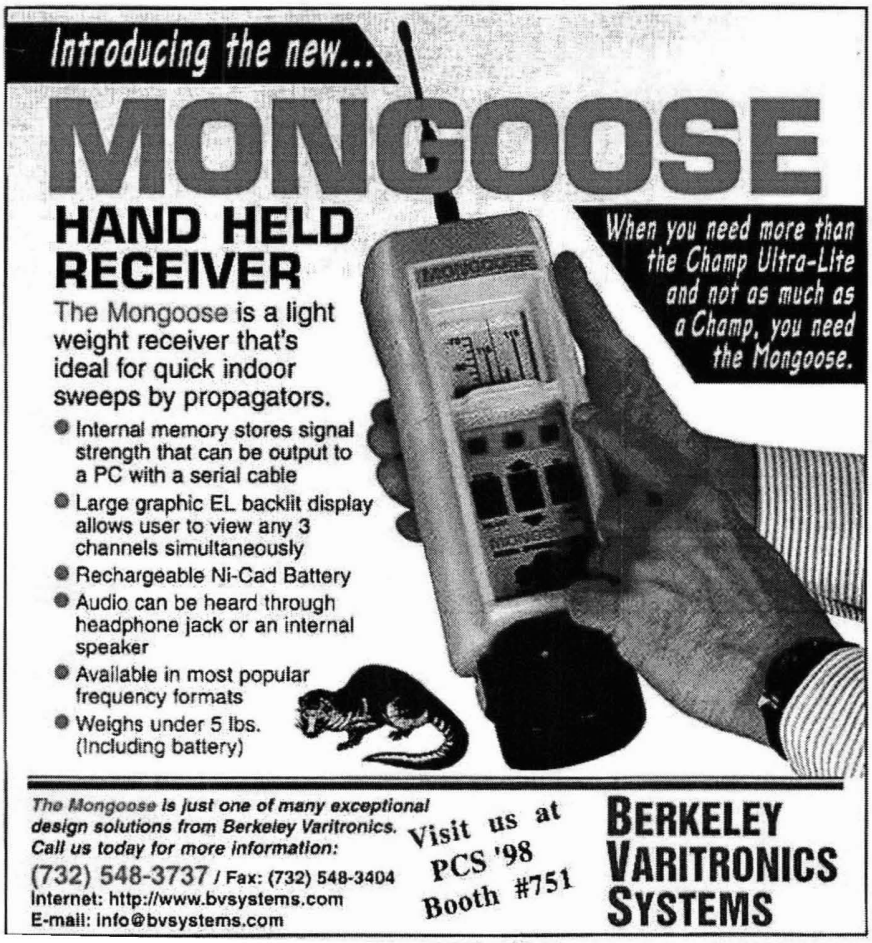

Atmospheric Refraction

Speed of radio wave:

$$c = \sqrt{\frac{\mu}{\varepsilon}} = \sqrt{\frac{\mu_0}{\varepsilon_0}}\sqrt{\frac{\mu_r}{\varepsilon_r}} = c\sqrt{\frac{u_r}{\varepsilon_r}} \propto c\sqrt{\frac{1}{\varepsilon_r}}$$

Snell's Law

$$\frac{n_1}{n_2} = \frac{\sin\theta_2}{\sin\theta_1}$$

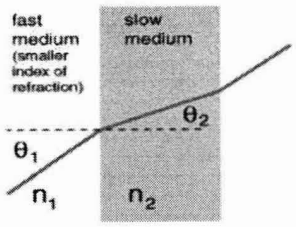

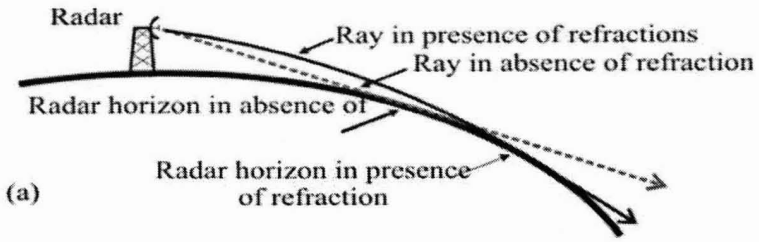

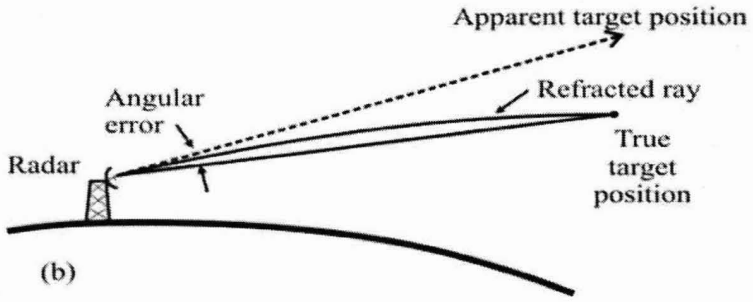

Refractivity

$$N = (n-1)\cdot 10^6$$

Pressure and water-vapor content decrease rapidly with altitude, while temperature decreases slowly, refractivity and decreases with altitude. Thus, velocity increases with altitude, and rays bend downward. Dominant change in refractivity occurs with along vertical. **Key point: not the actual refractivity, but changes (gradient) in refractivity cause rays to bend.**

Earth's Effective Radius Linear Model (a = 3440 nmi = 378.137 km)

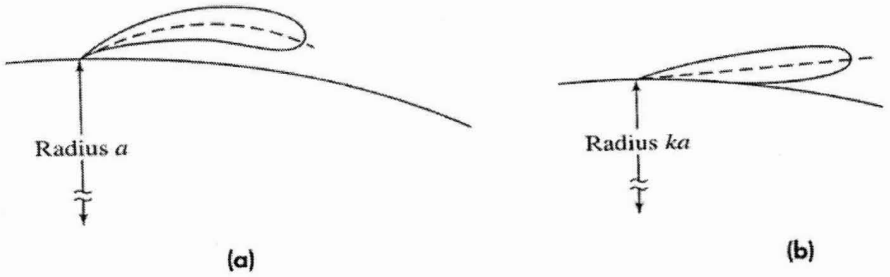

Value for k to get straight-line propagation:

$$k = \frac{1}{1 + a(dn/dh)}$$

Where dn/dh is the change is refractive index as a function of height. The long-term average refractivity for the U.S. is about. -39N/km. After converting to n and we find k = 4/3. What does this mean?

Distance to Horizon (antenna height =)

$$d = \sqrt{2kah_a} \text{ (Consistent Units)}$$
$$d(km) = 4.12\sqrt{h_a}(m)$$

Exponential Model of Refractivity: $N = N_s \exp(-h/H_s)$, were N_s = refractivity at surface of earth, h = height above sea level, and Hs = scale height.

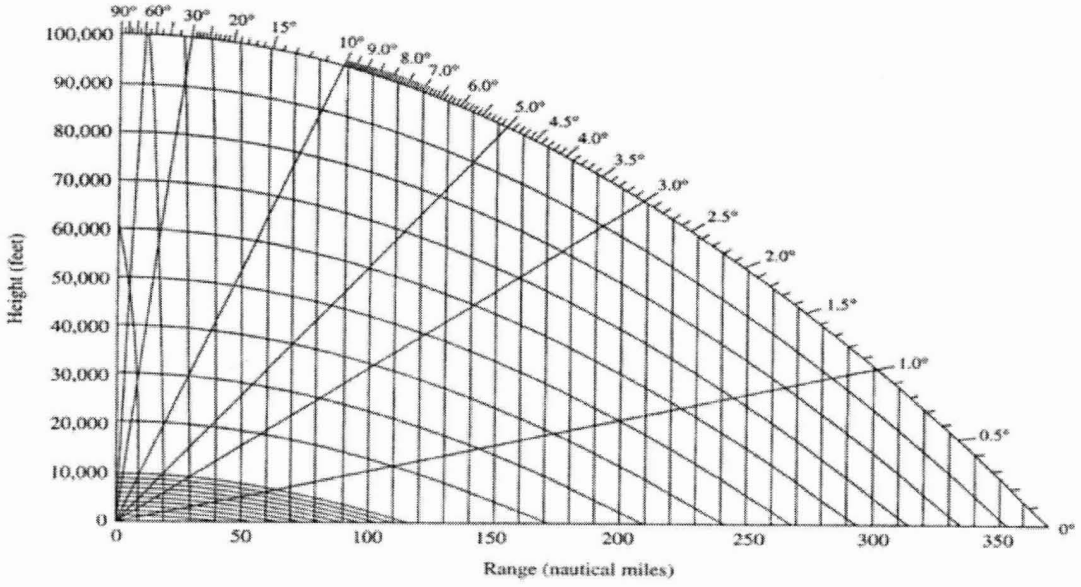

Radar range-angle-diagram used to plot antenna coverage, based on exponential model of refraction with = 313.

Standard Atmosphere: $N = 316\exp(-Z/26.5) \quad Z \le 25$, Where Z = altitude in thousands of feet.

Radar Measurement Errors Due to Refraction

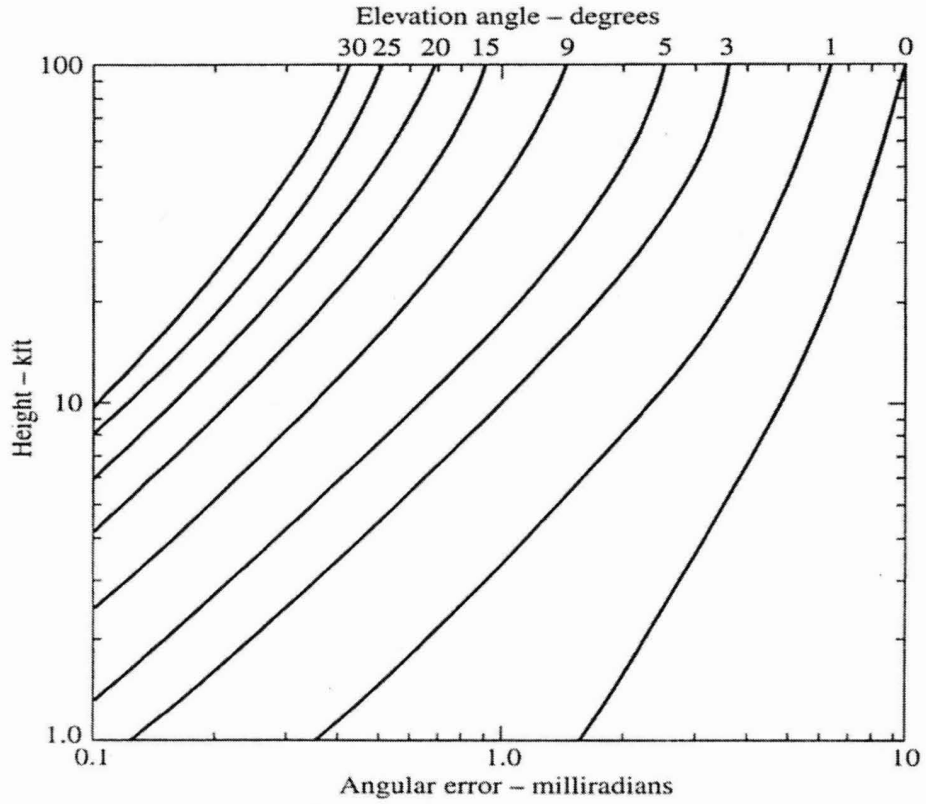

Calculated angle error (abscissa) due to atmospheric refraction for a standard atmosphere as function of elevation angle and target height (ordinate)

Refraction also caused range errors:

$$R_c \cong 0.42 + 0.0577 R_t \sqrt{\frac{N_s}{h}}$$

Where R_c = range correction (m), R_t is radar range (km), N_s is surface refractivity in N-units, and h = radar altitude in kft.

Measurement of Refractivity: Radiosonde, aircraft, helicopters, small rockets, refractometer

Anomalous Propagation (AP)

If a strong low-level inversion exists, the radar beam may be refracted such that it strikes the ground some distance from the radar.

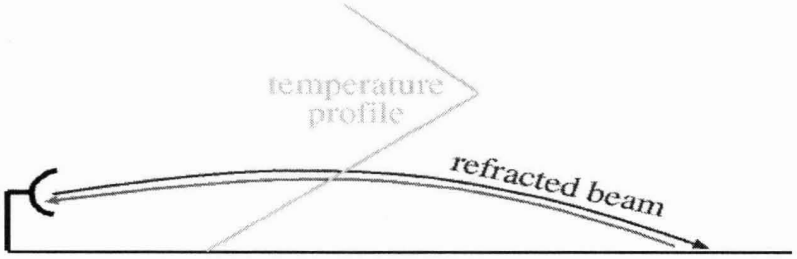

Question: What time of day do you expect AP more likely?

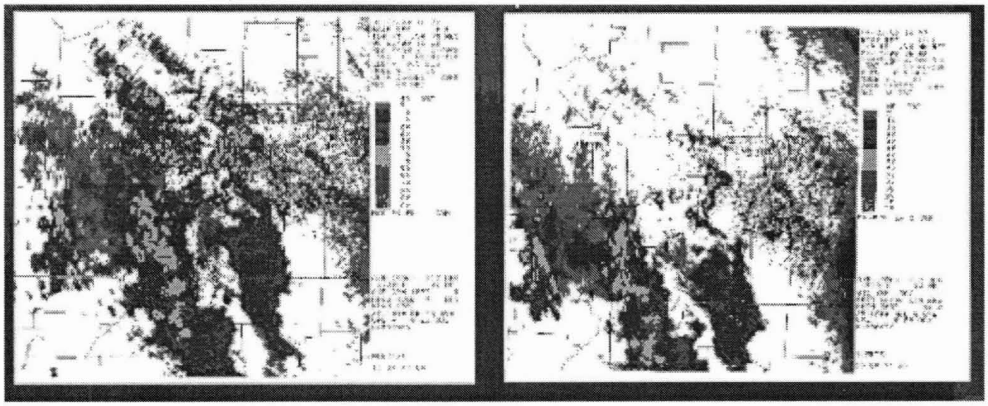

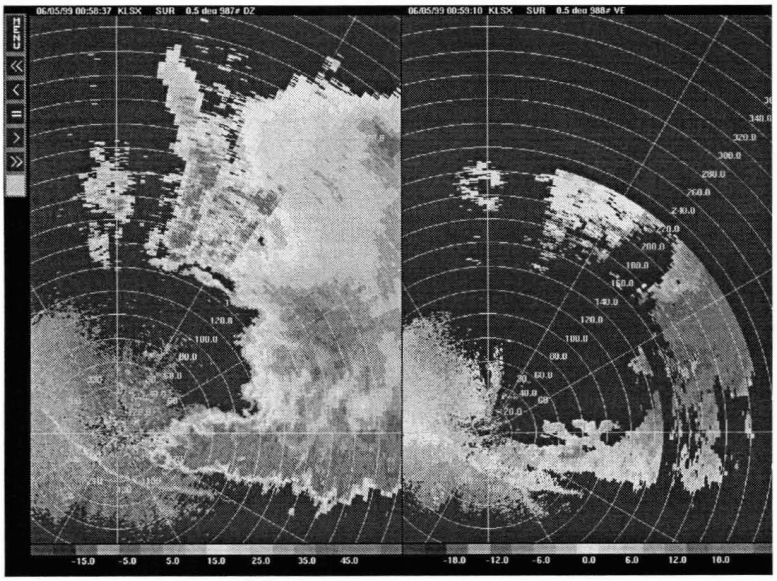

Atmospheric Attenuation

Attenuation of electromagnetic energy in the atmosphere. Solid curve is due to absorption by oxygen. Dashed curve is due to absorption by water vapor.

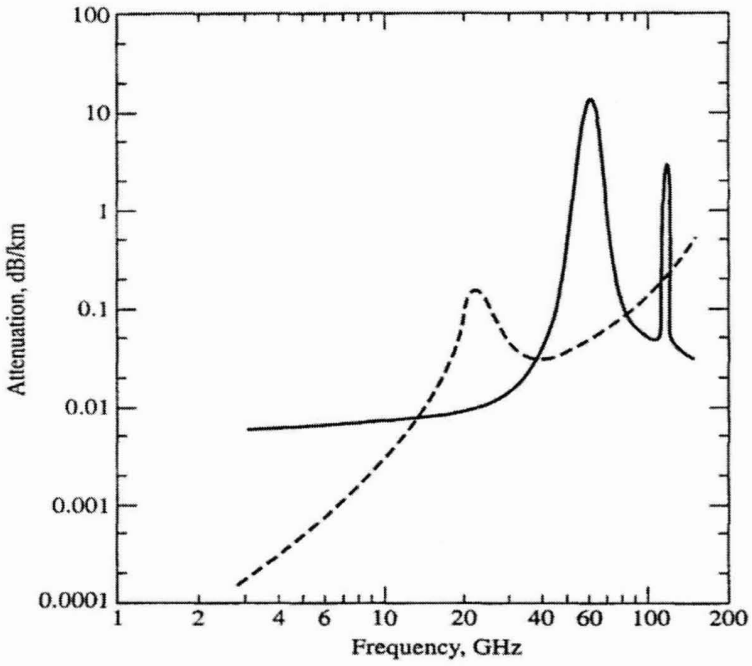

We modifying radar equations to account for attenuation by multiplying numerator with factor $\exp(-2\alpha R)$ where α is the one-way the attenuation coefficient in the same units of distance^{-1}, and R is the range to the target. For example, the radar equation for distributed targets:

$$P_r = \left(\frac{G^2 \lambda^2 P_t \theta \phi c \tau}{1024 \ln(2) \pi^2} \right) \frac{\eta}{R^2} = C \frac{\eta}{R^2}$$

becomes:

$$P_r = \left(\frac{G^2 \lambda^2 P_t \theta \phi c \tau}{1024 \ln(2) \pi^2} \right) \frac{\eta}{R^2} e^{-2\alpha R} = C \frac{\eta}{R^2} e^{-2\alpha R}$$

The other radar equations are modified the same way. If α is not constant, but a function of distance, then we use $\exp(-2\int \alpha(R) dR$.

Important Note: The figure above is the attenuation and **not** the attenuation coefficient α. What is plotted in the figure is equivalent to 4.34α.

Problem. Show that the relationship between attenuation in dB/km and attenuation coefficient is

Attenuation in dB per unit distance = 4.34×attenuation coefficient

Question. Using the figure above, what is the one-way total atmospheric attenuation for a K-band radar at 22 GHz? over a distance of 20 km?

Answer. At 22 GHz there is a peak in the water vapor absorption and the attenuation (broken curve) is about 0.2 dB/km. The attenuation due to oxygen is about 0.01 dB/km. The attenuation total is then 0.21 dB/km or 0.21×20 = 4.2 dB or a factor 1/2.63 = 0.38. Alternatively, 0.21 dB/km is equivalent to an attenuation coefficient $\alpha = 0.21/4.34 = 0.04839$ km $^{-1}$. The attenuation is then exp(-0.04839×20) = 0.38.

Effect of Elevation Angle

Two-way atmospheric attenuation as a function of range and frequency for (a) 0° elevation angle and (b) 5° elevation angle.

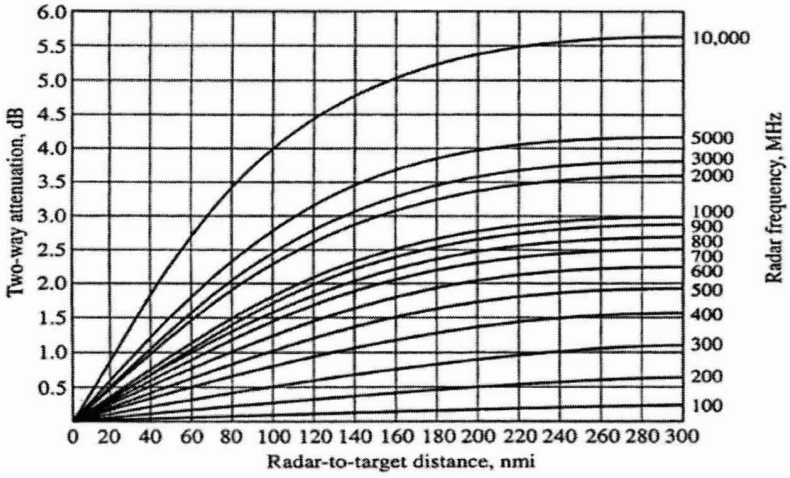

(a)

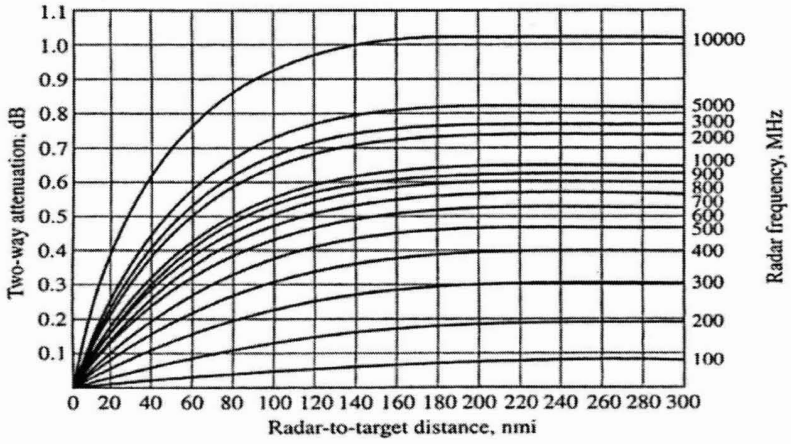

(b)

International Journal of Multidisciplinary Research and Modern Education (IJMRME)
ISSN (Online): 2454 - 6119
(www.rdmodernresearch.org) Volume II, Issue I, 2016

DESIGN OF DIGITAL MICROWAVE RADIO LINK BY MATLAB

Ghasan Ali Hussain
Assistant Lecturer, Department of Electrical Engineering,
University of Kufa, Iraq

Abstract:

Generally, Digital microwave radio (DMR) offers solving for connecting, it provides enable and grow communication networks for public and private networks to a wide range of applications and for environments. The principle of DMR system and design parameters, influencing factors for its performance have been presented. The performance calculations of the system are developed, and the design steps to satisfy quality and reliability objectives have been given. Typically, to design any DMR Link needs to committee of engineers and technicians to scan the earth between two sites that will establish this system, then study of geometry properties of this region and the height of obstacles if exist to design the height towers, power and another parameters, that may happen mistakes which need to solve it after finishing of establishment system and it needs to a big time and hard work. Developing a computer program using MTLAB has been suggested to obtain tower heights at different sites of the link in the first, then getting performance calculation, system configuration that satisfies the reliability and quality objectives specified by ITU. The results proves that the lowest time and easy way have been achieved by using the Matlab software program. Comparison between of the developed software with other sources (such as Alcatel Company which established a system of DMR between Libya and Algeria countries) has been discussed. The results confirms capability of using software program to design and test any DMR system.

Key Words: DMR, Matlab Software, Digital Microwave, LOS & C/N

Introduction:

It is true to say that the future of almost all communications mediums is in the transmission of digits. In general, digital transmission offers the end user better quality and the provider more capacity for a given transmission resources [1]. A DMR link is similar to an analogue microwave link with the exception of calculating the desired C_{min}/N. For digital links, the required carrier power is a function of the desired performance (i.e. probability of error) and the noise power [1]. In the recent years, the development of a digital modulation radio increased for telecommunication radio system, since it is used for the private and government sectors, and the demand for new types of services is also increasing. An electronic digital switching is used for voice and data switching. The new central office switching equipment is a computer based machine that is vastly superior to the earlier electro-mechanical switching. These switching operate with PCM voice circuits (64 Kbps per 4 KHz voice channel).

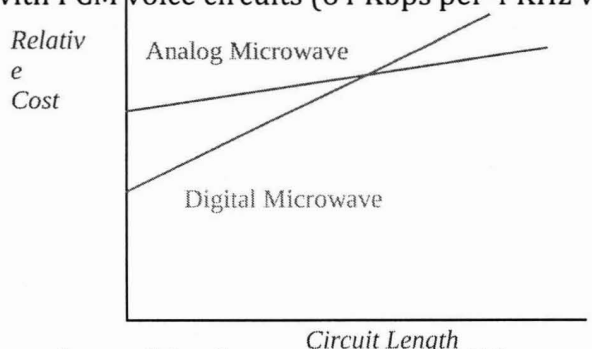

Comparison of Analogue and Digital Microwave Radio Costs [2]

Since the trunk connections to the switches are digital signals, the lowest multiplexing costs are achieved by utilization of digital transmission. DMR tend to cost more than FM radios but the overall transmission cost, including multiplexing costs is usually lower than analog transmission systems. The figure above shows comparison of the relative transmission costs of analog and digital microwave radio systems [2].

DMR offers significant advantages over analog transmission. DMR with regeneration per repeater has no build-up of noise and the system noise performance is independent of the number of hops, where as the total noise in analog system builds up as the log of the number of repeaters [3].

Line of Sight (LOS) Propagation [4]:

The propagation of any two antennas consists of LOS path with other waves that comes from ground or any other surface which parallels the earth's surface and a sky waves that comes from the components of signal reflected off the troposphere or ionosphere, a waves that reflected off obstacle in the terrain, and a ground reflected path. The existence and advantages of these modes depend on the link geometry, the operating frequency, terrain and distance between both antennas. For frequencies mode is the predominant mode available for use; the other modes may cause interference with the stronger LOS path. Line-of-sight links are limited in distance by the curvature of the earth, obstacles along the path, and free space loss. Average distances for conservatively designed LOS links are 30 to 48 Km.

Path Profile [5]:

In path profile we must take into considerations all obstacles along the Line-Of-Sight radio path including trees and vegetation, earth curvature, and fresnel zone.

Path profile is performed according to the following steps [5]:

1. Get obstacle information from topo-graphical maps scale 1:25,000 or 1:50,000, to now the height and position for earth obstacle.
2. Setup a graph paper and indicate obstacle height on Y-axis and the distance from both sites on X-axis. Trace all obstacles as shown in figure 1. Where d_{A1} represent the distance from the A site to the first obstacle and d_{A2} it is from the A site to the 2nd obstacle, and the same for the other site, since d_{B1} it is the distance from the B site to the first obstacle and which is the second obstacle for A site, so d_{B2} is the distance from the B site to the second obstacle so it is first obstacle for A site. h_1 and h_2 are the heights for both obstacle respectively [3].

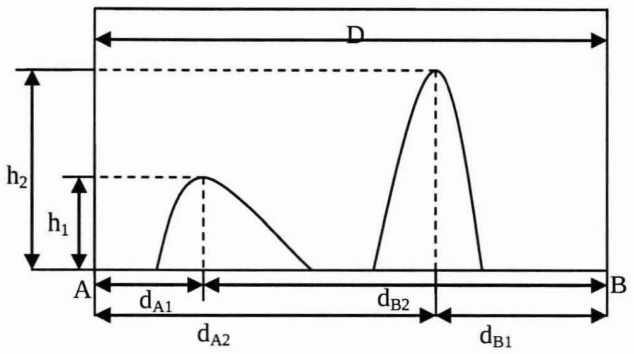

Figure 1: Obstacle between the Two Sites

3. Determine Earth Curvature (E.C) [5]:

Earth curvature or it is called earth bulge in some books, since it is the bending density of the earth and it is the ratio of the effective earth radios to the true earth radius. In order to draw the line of sight straight in a path profile, the ray bending due to

variation in K-value is added to the terrain height. The modification of the terrain height is given by:-

$$\mathbf{E.C = \frac{0.078 d_1 d_2}{k}} \quad \text{In meter} \qquad (1)$$

Where k is the K-value as shown in figure 2 and the other parameters have their previous definition.

The value of k in Libya is taken greater than 1, typically k=4/3.

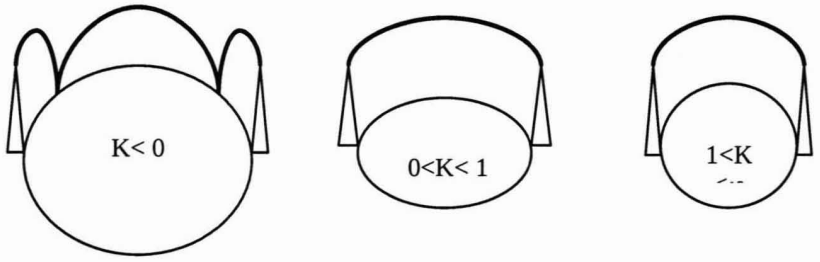

Figure 2: Various Forms of Atmospheric Reflection [3]

It is clear from figure 2 that the heights are obtained when 0<k<1.

4. Determine Fresnel Zone Clearance [5]:

An EM wave front has expanding properties as it travels increases or decreases of signal level of reflection or phase transmission will occurred.

The first Fresnel zone is defined as the locus of points where $d_3-(d_1+d_2) = \lambda/2$. This equation describes an ellipse, but for practical applications the radius F_1 may be approximated by the formula:-

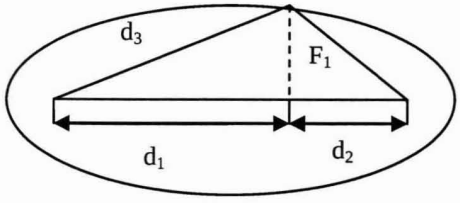

$$\mathbf{F_1 = 17.3\sqrt{\frac{d_1 . d_2}{f . d}}} \quad \text{Meter} \qquad (2)$$

In general the nth Fresnel zone radius (when $d_3-(d_1+d_2) = n\lambda/2$) is given by:-

$$\mathbf{F_n = 17.3\sqrt{\frac{n d_1 d_2}{f . D}}} \qquad (3)$$

Where f =frequency (GHz).
D = path length (Km) ($D=d_1+d_2$).
d_1= distance from transmitter to a given point along the path (Km).
d_2=distance from receiver to the same point along the path (Km).

The impact of diffraction and reflection on the radio waves can be seen easily by using the model developed by A. fresnel for optics. Fresnel accounted of the diffraction of light by assuming that the cross section of an optical wave front is divided into zones of concentric circles separated by half- wave lengths [4]. Optimum clearance of on obstacle defined as 0.6 of (1st fresnel zone clearance).

5. Setup table showing obstacle distances d_1& d_2 and calculated E.C and F_1 for each obstacle as shown below:-

Obstacle location	d_1	d_2	E.C	Fresnel zone Radius
Obstacle #1	~	~	~	~
Obstacle #2	~	~	~	~
~	~	~	~	~

6. For each obstacle add it's earth curvature E.C, $0.6F_1$ it is height, and in case of vegetation and trees between the heights add an average value of 12 meters for trees and 3 meters for average growth as shown in fig 3.
7. Repeats step 6 for each obstacle and draw the results on a graph paper. Then draw straight line connecting the top heights obtained in step 6 for each obstacle as shown in fig 4. More than one possibility may result, and the best choice minimum tower heights are selected.

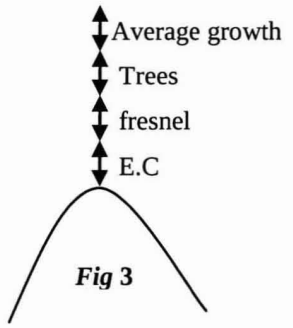

Fig 3

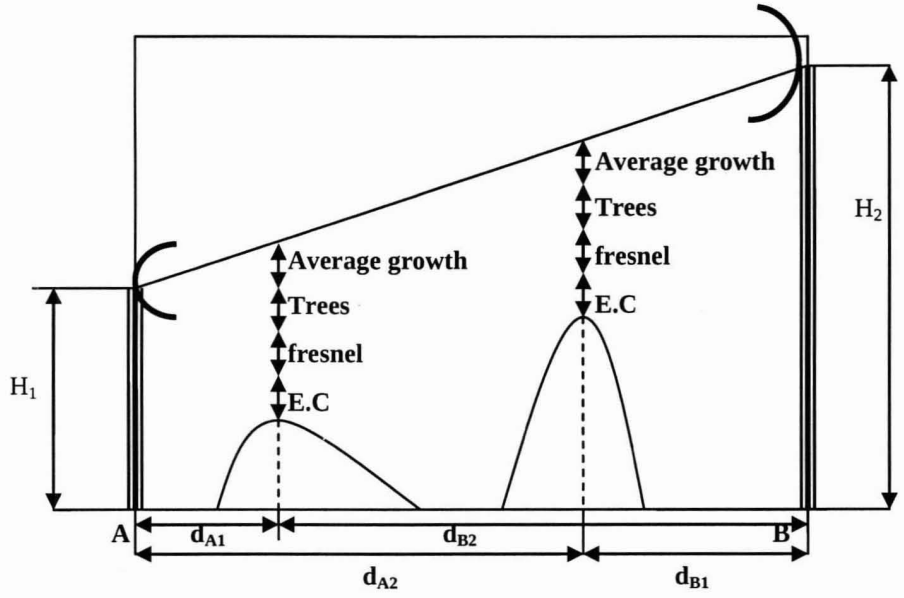

Figure 4: Radio system performance Design [6]

1. Determine C/N Requirement

We can determine C/N by assuming certain BER, and then from bit rate, and BW, C/N is obtained.

2. Get receiver noise figure, and noise power as

$$N=KTBF \quad (4)$$

Where

N = is the noise power.
F = is the noise figure.
B = is the receiver BW.
T = is effective noise temperature.

3. Get C_{min} that is required receiver carrier level then

$$C_{min}=N_{total} + C/N \quad (5)$$

4. Get transmit power, use given value or assumed, value
5. Get system gain (G_s) as

$$G_s= P_t - C_{min} \quad (6)$$

6. Repeater spacing

$$G_s = P_t - C_{min} \geq F + L_s + L_f + L_b - G_t - G_r \quad (7)$$

Where F is Hope fade margin (dBs) of a non-diversity system required meeting the reliability objective, and it is have the following expression

$$F = 30\log D + 10\log 6ABf - 10\log(1-R) - 70 \quad (8)$$

Where :- (1-R) is the reliability objective.

A is roughness factor and it is equal (4) for very smooth terrain, equal (1) for equal average terrain with some roughness, and equal (1/4) for very rough terrain.

B is factor to covert worst month probability to annual prob. Since it is equal (1/8) for mountainous or very dry area, equal (1/4) for average terrain with some roughness, equal (1/2) for hot or humid areas, and equal (1) on worst month basis.

L_s = is the free space loss

$$L_s = 92.4 + 20\log D + 20\log f \quad (9)$$

For f in GHz, and D in Km

L_f = is feeder loss, and L_b is branching loss.

G_t, G_r is the gain of transmitter and receiver respectively.

Note: If we have (R=99.9%) that is give (1-R) =0.001, then (-10log (1-R)) =+30dBs. But if the (R=99.99%), then (-10log (1-R)) =+40dBs.

Therefore F is increased by 10 as a result of improving reliability by adding extra "9" to the decimal point. This extra 10dBs on fade margin will require extra 10dBs in power to keep a constant G_s (system gain) or in other words to meet C/N requirement which again is being selected to satisfy the desired BER.

Link Calculation Procedure [4]:

The following assumptions are made:-

1. An adequate path clearance is provided on the path under consideration.
2. Rain attenuation and atmospheric absorption have been ignored, which is appropriate for frequencies below 10GHz. These two effects are easily added for use of higher frequencies.
3. As often the case, antenna size is the final design parameter. Hence antenna size is calculated from other design parameters whose values are already selected.
   The procedure shown can be rearranged to make any design parameter the last value to be determined. Often iteration is required in order to determine the best combination of design values. The following design changes are commonly made to meet performance objectives:-

- Increase transmitter power.
- Use lower loss transmission line.
- Use lower noise receiver.
- Add diversity path to the unprotected path.
- Increase antenna spacing for existing space diversity or frequency spacing for existing frequency diversity.
- Increase antenna size.
- Add an amplitude equalizer or, for greater improvement, add an adaptive transversal equalizer.

Design of Tower Heights:-

The methodology of program is, in the first will calculate the Fresnel zone (F_R) and earth curvature (E.C), then increase 12 meters for trees and 3 meters for average growth to the E.C, F_R, height of obstacle, then will again the process for all obstacles, by the breath of the time the program will find the bigger height of obstacles, then it works

to find all possible of ways to send and receive the signal with ensure don't crossing the path any obstacle. In the last, the program will choosing the lowest cost of the towers.

The Link Design and Parameters:

In the beginning, when the program execution will ask to insert the input data, then it will star to calculate the required data automatically. When calculated the outage by program, it will calculate the unprotected probability of outage and compared with Severely Error Second (SES) for availability case or Degraded Minutes (DM) for quality case. If the probability less than it, the program will tell that "Here we get a good performance" otherwise the program will using all the possible solutions such as (space diversity, frequency diversity, combine diversity, equalization,....etc) until getting a good performance and then, the program will tell "Here we get a good performance". If still the probability bigger than SES, then it well tell that "You must change design parameters".

Results & Discussion:

- **Determination of Tower Heights:-**

Scenario 1:-

A system of digital radio link that established among three sites and two hops; the data available is given in table 1

TOWER DESIGN (Two Hop)

Radio frequency (f) = 6 GHz. K= 4/3

FIRST HOP

Path length (D) = 30 Km

- Site A = 30m over MSL

First obstacle:-

Distance (d_{A1}) =10 Km

Height (h_1) =45 m

Second obstacle:-

Distance (d_{A2}) = 15Km

Height (h_2) = 60 m

Third obstacle:-

Distance (d_{A3}) =20 Km

Height (h_3) =40 m

- Site B =40m over MSL

SECOND HOP

Path length (D) =60 Km.

- Site B = 40m over MSL.

First obstacle:-

Distance (d_{B1}) =20 Km.

Height (h_1) =40 m.

Second obstacle:-

Distance (d_{B2}) =35 Km.

Height (h_2) =35 m

Third obstacle:-

Distance (d_{B3}) = 50 Km.

Height (h_3) =50 m.

- Site C =30m over MSL.

The Developed Program Results:

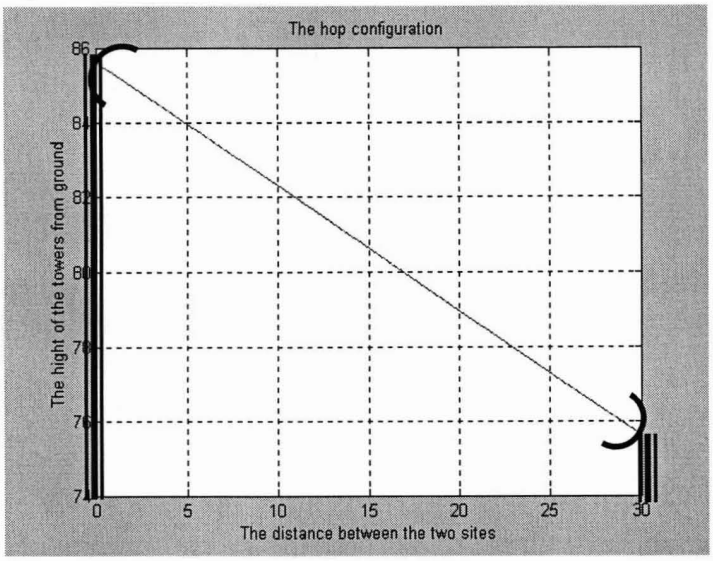

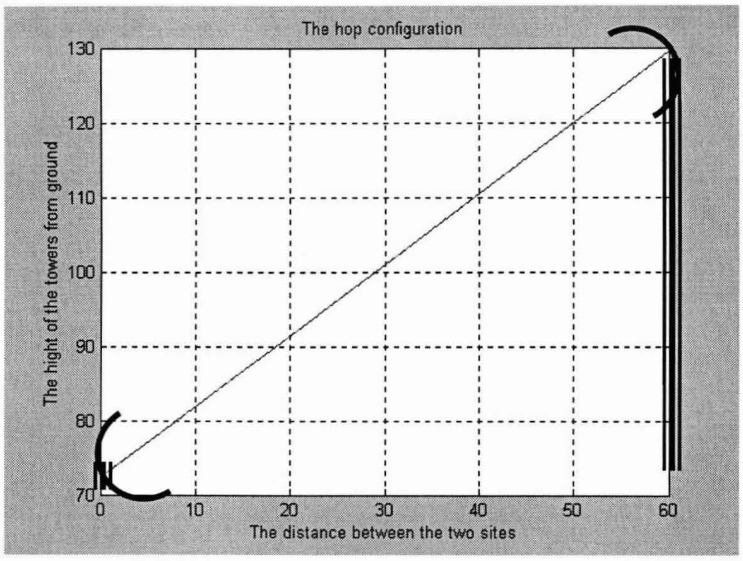

Comparison between the Results of This Program and Other Results of Sources

Results of The Computer Program	*Results Obtained By Manual Calculation*
Hop #1 h_1= 85.6326m h_2=75.6326m	Hop#1 h_1=85m h_2=75m
Hop#2 h_1=72.2966m h_2=129.4162m	Hop#2 h_1=73m h_2=128.8m

Note: - From the comparison table it is clear that the two results are almost identical.

- **Link Design And Performance Calculation:**

To perform link design and performance calculation, we will consider two examples one system uses M-PSK modulation, and other system uses M-QAM modulation respectively, as shown below:-

Scenario 2:

A system of digital microwave radio link between two sites firs called repeater B and another called Harash is utilizing Q-PSK modulation technique and it has the following data:-

Bit Rate (R) =34 Mbps
Radio Frequency (f) = 2.203 GHz
Path Length (D) = 79 Km
Power Options (P_t) =30 dBm
Antenna Diameter Options (Dia) =3.7 m
Antenna Efficiency Options (eff) =0.5
W/G Loss Factor Options (W/G) =3.4983799E-02 dB/m
Receiver Noise Figure Options (NF) = 4 dB
Antenna Spacing (SD) = 20 m
Frequency Spacing (FD) = 6.6090003E-02 GHz

Modulation Type:

The Spectral Efficiency (Se) = 1.7 bps/Hz
CQ =1E-03
Wx=3.090946

QPSK

RF-Channel Bandwidth (BW) =20 MHz

CCIR Outage Objectives:

1. Availability (BER=1.0E-03) Objectives (SES)= 1.7064001E-03%
2. Quality (BER=1.0E-06) Objectives (DM) = 1.264E-02 %

Path Losses:

Site (A) Repeater ***B***

Transmitter line losses

a. antenna Height Above Ground (HT) =149m
b. horizontal Transmission Line Length (U) = 10 m

Site (B) ***Harash***

Receiver Line Losses

a. Antenna Height Above Ground (Upper Antenna if SPACE DIVERSITY is Used) (HR) =212 m
b. Horizontal Transmission Line Length (C) =10 m

Branching Loss (Lb) =4.7dB
Atmospheric Absorption Losses (Lg) =0 dB
Miscellaneous Losses (Lm) =0 dB
Terrain Factor (a) =1
Climate Factor (b) =0.25
Modulation Implementation Loss (MIL) = 2 dB
Dispersive Fade Margin (DFM) = 39.9 dB
Interference Fade Margin (IFM) = 57.5 dB
The AEQ Improvement Factor (AEQIF) = 1.5
Combiner Hysteresis Loss (H) = 3 dB
CQ = 1E-06
WX = 4.744944
Modulation Implementation Loss (MIL) = 2 dB
Dispersive Fade Margin (DFM) = 37.8 dB
Interference Fade Margin (IFM) = 55.5 dB

The Requirement:

1. E_b/N_o.
2. RSLm.
3. G_s.
4. PUL.

5. The link performance and configuration.

Scenario 3:

A system of digital microwave radio link between two sites, first called sim sim and another called vert designed (16-QAM modulation technique is selected) and it has the following data:-

Bit Rate (R) = 140 Mbps
Radio Frequency (f) = 6.77 GHz
Path Length (D) = 92.4 Km
Power Options (Pt) =30 27.0 dBm or (0-3 dBW)
Antenna Diameter Options (Dia) =3.7 m
Antenna Efficiency Options (eff) =0.5
W/G Loss Factor Options (W/G) =4.4771198E-02 dB/m
Receiver Noise Figure Options (NF) = 4 dB
Antenna Spacing (SD) = 5 12 m
Frequency Spacing (FD) = 0.2708 0.3385 GHz

Modulation Type:

The Spectral Efficiency (Se) = 3.5 bps/Hz
CQ =1.3333334E-03
Wx=3.004823

16-QAM

RF-Channel Bandwidth (BW) =40 MHz

CCIR Outage Objectives:

3. Availability (BER=1.0E-03) Objectives (SES)= 1.9958401E-03%
4. Quality (BER=1.0E-06) Objectives (DM) = 1.4784001E-02 %

Path Losses:

Site (A) Sim *Sim*

Transmitter line losses

c. antenna Height Above Ground (HT) =26 m
d. horizontal Transmission Line Length (U) = 19 m

Site (B) *Vert Pre*

Receiver Line Losses

c. Antenna Height Above Ground (Upper Antenna if SPACE DIVERSITY is Used) (HR) =29 m

Branching Loss (Lb) =4.5 dB
Atmospheric Absorption Losses (Lg) =0 dB
Miscellaneous Losses (Lm) =0 dB
Terrain Factor (a) =4
Climate Factor (b) =0.125

AVAILABILITY CALCULATIONS (BER=1.0E-03)

Modulation Implementation Loss (MIL) = 3 dB
Dispersive Fade Margin (DFM) = 26.8 dB
Interference Fade Margin (IFM) = 57dB
The AEQ Improvement Factor (AEQIF) = 6.6
Antenna Spacing (S) =12 m
Combiner Hysteresis Loss (H) = 0 dB

QUALITY CALCULATIONS (BER=1.0E-06)

CQ= 1.3333333E-06
WX= 4.689944
Modulation Implementation Loss (MIL) = 3 dB

Dispersive Fade Margin (DFM) = 24.1 dB
Interference Fade Margin (IFM) = 54.3 dB

The Requirement:

6. E_b/N_o.
7. RSLm.
8. G_s.
9. PUL.
10. The link performance and configuration.

Comparison among of our Program and Other Sources:

Q-PSK (Availability)

	Outage Time (%)		
Source	***Computer Output***	***Alcatel ATFH***	***Another Program[7]***
Unprotect System	*123.0E-4*	*95.96E-4*	*124.4E-4*
With Adaptive Equalization	*82.0E-4*		*82.93E-4*

Q-PSK (Quality)

	Outage Time (%)		
Source	***Computer Output***	***Alcatel ATFH***	***Another Program [7]***
Unprotect System	*278E-4*	*272.54E-4*	*280.7E-4*
With Space Diversity	*44.5E-4*		*44.68E-4*

16-QAM (Availability)

	Outage Time (%)		
Source	***Computer Output***	***Alcatel ATFH***	***Another Program[7]***
Unprotect System	*3584E-4*	*1649E-4*	*3574E-4*
With Space Diversity & Equalization	*14E-4*	*6.5E-4*	*14.32E-4*

16-QAM (Quality)

	Outage Time (%)		
Source	***Output Computer***	***Alcatel ATFH***	***Another Program[7]***
Unprotect System	*6789E-4*	*3250E-4*	*6783E-4*
With space Diversity & Equalization	*52E-4*	*39.3E-4*	*51.6E-4*

Conclusion:

In the recent years, the development of a digital modulation radio is increased for telecommunication radio system, since it used for the private and government sectors, and the demand for new types of services is also increasing. DMR it provides enable and grow communication networks for public and private networks to a wide range of applications and for environments. Design DMR link by MAtlab software and compare among own results and other results have been done. The results were symmetrical, the results of the developed computer program conform to the result obtained from other sources. Modulation techniques which are widely used in digital microwave radio are Q-PSK and M-QAM. The steps of path profiles are :-

a. Get obstacle information from topo-graphical maps.

b. Setup a graph paper and indicate obstacle height on Y-axis and the distance from both sites on x-axis.
c. Determine Earth Curvature.
d. Determine Fresnel Zone Clearance.
e. Setup table for obstacle distances, clearance and fresnel zone.
f. For each obstacle add its earth curvature E.C, 0.6F1, 12 for trees and 3 for the growth.
g. Repeats step (f) for each obstacle and draw the results on a graph paper.

Diversity is used to improve the performance of the radio which is affected by objective fading the terrain, atmosphere, and precipitation. Availability objective is used to measure the availability of the link such as the BER performance when it isn't greater than 1E-03 for a specified period. It is specified as severely errored seconds (SES). The quality objective of a link is the percentage of time the BER is more 10^{-6}. It is specified as degraded minutes (DM). The results of the developed computer program package conforms to the results obtain by the other references.

References:

1. http://www.google.etidweb.tamu.edu/faculity/mcdougall/455/handouts/455lec14.pdf
2. Neil F. Dinn," Digital Radio its Time has Come," IEEE Comm Mag, Nov, 1980
3. Harold Sobol, "Progress in Microwave Communication Systems" Microwave Journal, Jan 1983
4. D. R. Smith, "Digital Transmission Systems" (New York: Nostrand Reinhold, 1985).
5. Ingvar Henne per Thorvaldsen, "Planning Of Line-Of-Sight Radio Relay Systems" (second Edition 1999).
6. D/ A. S. Akki & D/ M. M .Musa, "The Notes of Lecture".
7. Salah Al-Akkari "From Analogue to Digital Microwave Radio Systems"EE Department – Alfateh University, BIC Project 1993.
8. Stephen B, Wicker, "Error Control Systems for Digital Comm & Storage".
9. T. Noguchhi, Y. Daido, and J, A, Nossek, "Modulation Techniques for Microwave Digital Radio", IEEE Comm, Mag. 24, no. 10. Oct. 1986.
10. Recommendation and Reports of the CCIR, Fixed "Service Using Radio-Relay Systems", Vol, IX-Part 1, XVIth Plenary Assemply Dubrovnik, 1986.
11. Peter J. Maclane , Marvin K, Simon , "Introduction To Trellis-Coded Modulation With Applications"
12. Roger L. Freeman, "Radio System Design for Telecommunications "(New York: Widely, 1987).
13. Roger L. Freeman, "Telecommunication Transmission Hand Book", 2nd (New York:Widely, 1981).

International Journal of Information and Communication Sciences
2017; 2(2): 15-23
http://www.sciencepublishinggroup.com/j/ijics
doi: 10.11648/j.ijics.20170202.11

SciencePG
Science Publishing Group

Path Profile for Terrestrial Line of Site Microwave Link in the C-Band

Enyenihi Henry Johnson[1], Okoye O. Jude[2], Obinwa Christian Amaefule[3]

[1]Department of Electrical/Electronic Engineering, Akwa Ibom State University, Mkpat Enin, Nigeria
[2]Department of Electrical/Electronic and Computer Engineering, University of Uyo, Uyo, Nigeria
[3]Department of Electrical Engineering, Imo State University (IMSU), Owerri, Nigeria

Email address:

gentlejayy@yahoo.com (E. H. Johnson)

To cite this article:

Enyenihi Henry Johnson, Okoye O. Jude, Obinwa Christian Amaefule. Path Profile for Terrestrial Line of Site Microwave Link in the C-Band. *International Journal of Information and Communication Sciences.* Vol. 2, No. 2, 2017, pp. 15-23. doi: 10.11648/j.ijics.20170202.11

Received: October 16, 2016; **Accepted**: December 27, 2016; **Published**: April 26, 2017

Abstract: In this paper, development of path profile for 6GHz C-band terrestrial line-of-site microwave link is presented. The path (elevation) profile data set is obtained using Geocontext online elevation software. With the path profile, the minimum antenna elevation and the minimum antenna mast heights for effective line of site installation are determined. According to the results, when path inclination is greater than zero, antenna elevation is 105.873m and 88.528m at the transmitter and receiver respectively, with antenna mast height of 36.712m at both the transmitter and the receiver and critical clearance of 4.787m at a distance of 1897.626m from the transmitter. However, when path inclination is equal to zero, antenna elevation is 88.528m at both the transmitter and receiver with antenna mast height of 19.367m and 36.712m at the transmitter and receiver respectively. In this case, the critical clearance is 0 m (zero meter) at a distance of 686.641m from the transmitter.

Keywords: Path Profile, Microwave Link, Line-of-Site, C-Band, Path Inclination, Fresnel Zone, Earth Bulge

1. Introduction

At high frequencies such as the microwave frequencies, adequate planning is required to ensure line-of-site between the antennas at two distant communication link endpoints [1-5]. In this case, some factors must be taken into consideration in order to ensure clear line-of-sight; among the factors are, the earth curvature, the Fresnel Zone clearance, the atmospheric refraction and possible obstacles on the path of the communication link [6-9]. However, "in order to determine tower heights for suitable path clearance, a pat profile must be plotted" [10-12].

According to Standard (1996), path profile is a graphic representation of the physical features of signal propagation path; the path profile contains both endpoints of the path and shows the elevations in the vertical plane of points between the endpoints. The path profile also shows the Earth surface along with buildings, trees, and other features that may block the radio signal [13]. Importantly, proper planning of microwave and cellular path profile can help network planners to determine accurate tower heights for the antenna in order to achieve Line-of-Sight (LOS) clearance of the first Fresnel Zone or Fresnel Radius from obstacles that are along the radio propagation path and this will improve the Quality of Service (QoS) delivery of deployed systems [1, 14-15].

In this paper, approach for generating and plotting the path profile for terrestrial line of site microwave link in presented. In order to generate the path profile for terrestrial line of site microwave link, the elevation data along the signal path is required. The elevation data is used in conjunction with the signal frequency to generate and plot the various components of the path profile. The components of the path profile includes amongst others; elevation profile, earth bulge, Fresnel zone ellipsoid, minimum transmitter antenna height, minimum receiver antenna height and the location of the critical point for maintaining clear line of site. Sample path profile data set for a C-band link at 6GHz is generated and plotted for two cases, when the path inclination is equal to zero and when the path inclination is greater than zero. The signal path (or link) elevation profile (that is, elevation and distance) are obtained using Geocontext Online Elevation software [16]. With the path profile data and graph plots, the minimum antenna elevation and the minimum antenna mast heights for effective line of site installation are determined. The path profile ideas presented in this paper is very useful for

terrestrial line of site microwave network designers and researchers.

2. Methodology

The following steps are used in generating the path profile for a C-band terrestrial line of site microwave link between University of Uyo Town Campus at Ipka Road and the Main Campus of University of Uyo which is at Use Offort:.

Step 1: The Signal Frequency

The radius of the Fresnel Zone is a functions of frequency. As such, in this study the 6 GHz (in the C-Band) is considered.

Step 2: The Location (Longitude and Latitude) Of The Transmitter and The Receiver

Let $LONG_{tx}$ and LAT_{tx} be the longitude and attitude of the coordinates of the Let $LONG_{rx}$ and LAT_{rx} be the longitude and attitude of the coordinates of the receiver respectively. transmitter respectively.

University of Uyo

Step 3: The Distance Between The Transmitter and The Receiver

The path length (or distance), $\boldsymbol{d}$ in Km between the transmitter and receiver is determined by using the Haversine formula and the coordinates (longitude and the latitude) of the transmitter and receiver. The Haversine formula is given as:

$$d = 2R\left\{\sqrt[2]{\sin\left(\frac{LAT_{rx}-LAT_{tx}}{2}\right)^2 + \cos(LAT_{rx})\cos(LAT_{tx})\sin\left(\frac{LONG_{rx}-LONG_{tx}}{2}\right)^2}\right\} \quad (1)$$

$$\text{Where LAT in Radians} = \frac{(\text{LAT in Degrees} * 3.142)}{180} \quad (2)$$

$$\text{LONG in Radians} = \frac{(\text{LONG in Degrees} * 3.142)}{180} \quad (3)$$

Where

- LAT_{tx} and LAT_{rx} are the latitude of the coordinates of point1 and point 2 respectively
- $LONG_{tx}$ and $LONG_{rx}$ are the longitude of the coordinates of point1 and point x respectively
- R = radius of the earth = 6371 km. R varies from 6356.752km at the poles to 6378.137 km at the equator.
- d = the distance in Km between the two coordinates

Step 4: The Elevation Data and the Elevation Profile Between The Transmitter and Receiver

The Elevation Data set for the given location is generated using an Geocontext Online Elevation software [15].

The elevation data is generated by entering the longitude and latitude of the transmitter ($LONG_{tx}$ and LAT_{tx}) and the longitude and latitude of the receiver ($LONG_{rx}$ and LAT_{rx}) into the source and destination coordinates textboxes on the Geocontext Online Elevation software. The elevation data set generated by the Geocontext Online Elevation software [15] includes:

i. Points specified by their longitudes and latitudes,
ii. The start point at the transmitter (transmitter location is the first point)
iii. The end or the last point at the receiver (receiver location is the last point)
iv. Distance of each of the points from the starting point's longitude and latitude
v. The elevation at each point above sea level as the reference plane.

Step 5: The Earth Bulge

The formula for calculating the Earth bulge at a distance d_1 from the transmitter and distance d_2 from the receiver is given as follows:

$$H_{b(x)} = \frac{1000(d_1)(d_2)}{8(E_r)} \quad (4)$$

where,

- $H_{b(x)}$ =Height difference of Earth's Curvature at the point x between the transmitter and the receiver (m)
- d_1 = Distance between the point and the transmitter (km)
- d_2 = Distance between the point and the receiver (km)
- E_r = Effective Radius of Earth (km) Note: Usually taken as $\frac{4}{3}$ (1.333 rec.)actual radius to account for atmospheric refraction i.e. E_r = 8,504km

Step 6: The Radius of the First Fresnel Zone

The radius of the kth Fresnel zone at point x is given as;

$$r_{fk(x)} = \sqrt[2]{\left(\frac{k(\lambda)(d_1)(d_2)}{(d_1)+(d_2)}\right)} = \sqrt[2]{\left(\frac{k(\lambda)(d_1)(d_2)}{d}\right)} \quad (5)$$

where k = 1,2,3,…

$r_{fk(x)}$ is the radius of the kth Fresnel zone at point x.

d_1 is the distance of the point from the transmitter

d_2 is the distance of the point from the receiver

d is the distance between the transmitter and the receiver where

$$d = d_1 + d_2 \quad (6)$$

λ is the wavelength of the signal, where;

$$\lambda = \frac{c}{f} \quad (7)$$

where,

- C =Speed of light in a vacuum ($3x10^8 ms^{-1}$)
- d =Total Distance (m)
- f = Signal frequency (Hz)

Step 7: The Maximum Height Of Obstacle In The Terrain

The maximum height of obstacle ($H_{obstacle(x)}$) is estimated from the knowledge of the terrain. In this research, the terrain within which the link is located is in Uyo metropolis. The obstacles expected in the terrain are mainly buildings. The buildings within the signal path in Uyo are mainly two storey buildings. As such, the obstacle height is estimated as 10 meters.

Step 8: The Minimum Height of Antenna For Line of Sight Installation

The theoretical minimum height of antenna ($H_{antenna(minimum)}$) for line of sight installation is calculated

with respect to elevation, radius of first Fresnel zone, height of obstacle and earth bulge, as follows:

$$H_{antenna(minimum)} = \text{maximum}_{x=1,2,3,\ldots n_e}(E_x + r_{fk(x)} + H_{b(x)} + H_{obstacle(x)}) \quad (8)$$

where

$r_{fk(x)}$ is the radius of the kth Fresnel zone at point x.

$H_{b(x)}$ =Height difference of Earth's Curvature at the point x between the transmitter and the receiver (m)

$H_{obstacle(x)}$ is the maximum height of obstacle

E_x is the elevation in meter at point x

Step 9: The Minimum Height Of Transmitter Antenna and The Minimum Height Of Receiver Antenna

The effective minimum antenna height with respect to the elevation of the transmitter (E_{tx}) and elevation of the receiver (E_{rx}).

$$H_{effant(minimum)} = H_{antenna(minimum)} - \text{minimum}_{x=1,2,3,\ldots n_e}(E_{tx}, E_{rx}) \quad (9)$$

Let H_{tx} be the Height of Transmitter antenna and let H_{rx} be the Height of Receiver antenna, then

$$H_{tx} = E_{tx} + H_{effant(minimum)} \quad (10)$$

$$H_{rx} = E_{rx} + H_{effant(minimum)} \quad (11)$$

Step 10: Generate the Fresnel Ellipsoid

The Fresnel ellipsoid if formed around the centre of the Fresnel zone. In order to generate the Fresnel Ellipsoid, the centre line (line-of-sight) through the Fresnel zone is first generated. Then the radius of the first Fresnel zone is added to the value of the elevation at the centre line of the Fresnel zone (for the upper part of Fresnel ellipsoid) and subtracted from the value of the elevation at the centre line of the Fresnel zone (for the lower part of Fresnel ellipsoid).

Step 11: The Centre Line (Line-Of-Sight) Through The Fresnel Zone

Let the elevation at the transmitter is E_{rx} and the Elevation at the receiver be E_{rx}, respectively.

Let the distance of the transmitter from the transmitter is d_{tx} and the distance of the receiver from the transmitter be d_{rx}.

Let the gradient (m_{txrx}) of the line linking the transmitter and the receiver be defined as;

$$m_{txrx} = \frac{(E_{rx} - E_{tx})}{(d_{rx} - d_{rx})} \quad (12)$$

The equation for the transmitter to receiver line that passes through the point (d_x, E_{xf}) is given as:

$$\frac{(E_{xf} - E_{tx})}{(d_x - d_{tx})} = \frac{(E_{rx} - E_{tx})}{(d_{rx} - d_{tx})} = m_{txrx} \quad (13)$$

$$E_{xf} - E_{tx} = m_{txrx}(d_x - d_{tx}) \quad (14)$$

$$E_{xf} = m_{txrx}(d_x - d_{tx}) + E_{tx} \quad (15)$$

Now, $d_{tx} = 0m$ and $d_{rx} = 6379.51952869827\ m$. Also, E_{tx} =69.16137695 m and $E_{rx} = 51.8163147\ m$.

$$m_{txrx} = \frac{(E_{rx} - E_{tx})}{(d_{rx} - d_{rx})} = \frac{(51.8163147 - 69.16137695)}{(6379.51952869827 - 0)} = -0.00271887 \quad (16)$$

$$E_{xf} = -0.00271887\ (d_x - 0) + 69.16137695 \quad (17)$$

$$E_{xf} = -0.00271887 d_x + 69.16137695 \quad (18)$$

Step 12: The Elevations for the Fresnel Zone Ellipsoid

The Fresnel zone ellipsoid is formed around the centre line of the Fresnel zone defined in equation 3.26. Let $E_{fu(x)}$be the elevation for the upper part of the first Fresnel ellipsoid at point x and let $E_{fd(x)}$ be the elevation for the lower part of the first Fresnel ellipsoid at point x, then;

$$E_{fu(x)} = E_{xf} + r_{fk(x)} = -0.00271887 d_x + 69.16137695 + r_{fk(x)} \quad (19)$$

$$E_{fd(x)} = E_{xf} - r_{fk(x)} = -0.00271887 d_x + 69.16137695 - r_{fk(x)} \quad (20)$$

Where $r_{fk(x)}$ is the radius of the kth Fresnel zone at point x.

Step 13: The Path Inclination

Path inclination ε_p is given as follows;

$$\varepsilon_p = \frac{|H_{tx} - H_{rx}|}{d} \quad (21)$$

where d (in Km) is the distance between the transmitter and the receiver while H_{tx} and H_{rx} are in meters are the height of the transmitter and the receiver respectively.

3. Results and Discussions

A sample microwave link is used to demonstrate the effectiveness of the path profile algorithm presented in paper. The path profile data set and graph plots are presented for two cases; when the path inclination is equal to zero and when the path inclination is greater than zero. The results for the sample path profile studied are presented in this section 4.

Step 1: The Signal Frequency

In this study, the C-band is considered and the frequency selected is 6 GHz.

Step 2: The Location (Longitude and Latitude) Of The

Transmitter and The Receiver

The transmitter is located at University of Uyo Town Campus at Ipka Road. Then, in Figure 1. $LONG_{tx} = 7.919108$ and $LAT_{tx} = 5.042362$. Also, the receiver is located at the Main Campus of University of Uyo which is at Use Offort.. Then, in Figure 1. $LONG_{rx} = 7.976615$ and $LAT_{rx} = 5.040823$.

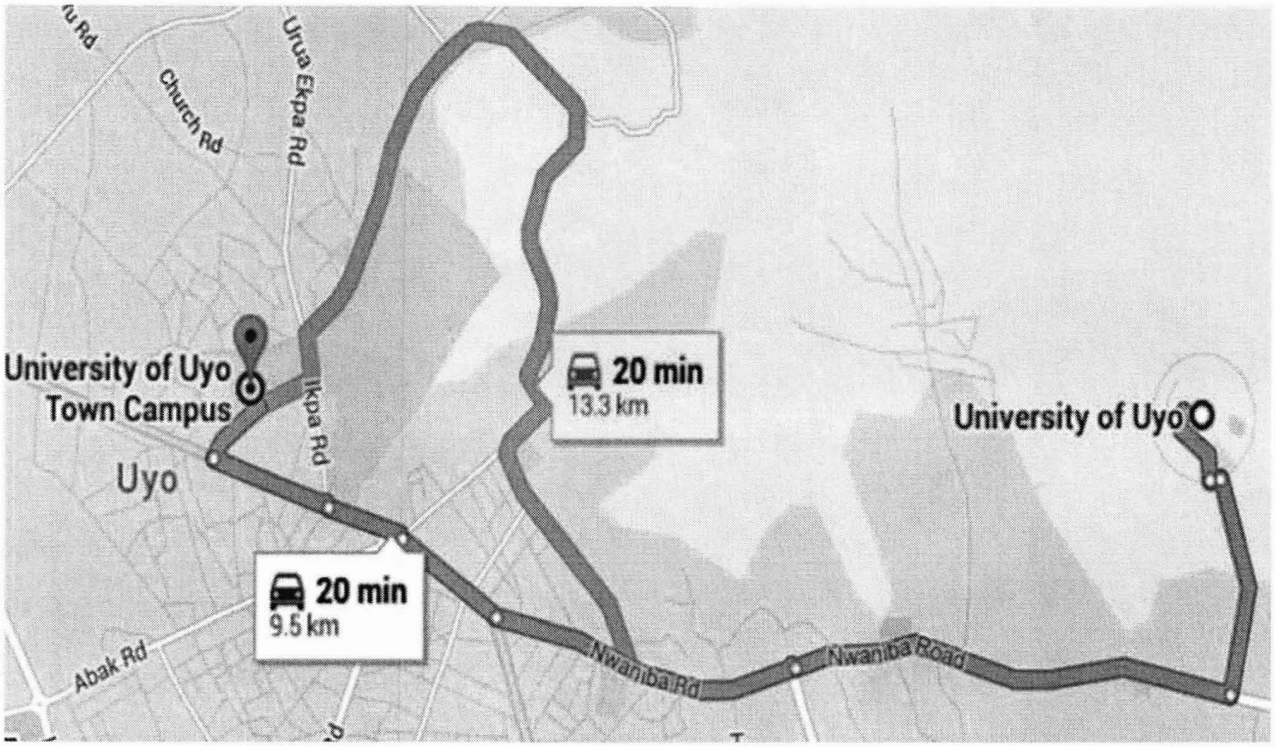

Figure 1. *Screenshot of The Google Map View Of The Location Of The Transmitter at University of Uyo Town Campus and The Receiver at the Main Campus of.*

Step 4: The Elevation Data and The Elevation Profile Between The Transmitter and Receiver

Some portions of the 512 records in the elevation dataset for the given transmitter and receiver location are given a in table 1. The dataset is generated using a Geocontext Online Elevation [15]. As shown in Figure 1, the transmitter is located at University of Uyo Town Campus, Ikpa Road with longitude of 7.919108 and latitude of 5.042362 while the receiver located at the Main Campus of University of Uyo, Use Offort at longitude of 7.976615 and latitude of 5.040823. The elevation profile plot for all the 512 data points in the full dataset is given in Figure 2. From Table 1 and Figure 2, the elevation at the transmitter is 69.161m (Column 5, Data Point Number 1) whereas the elevation at the receiver is 51.816m (Column 5, Data Point Number 512).

Table 1. *Selected Portion of the 512 Data Points In The Elevation Profile Dataset.*

Column 1	Column 2	Column 3	Column 4	Column 5	Column 6	Column 7
Data Point Number	Latitude	Longitude	Distance (m)	Elevation (m)	Distance in Mile	Elevation (ft)
1	5.04236	7.91911	0.000	69.161	0.0000	226.907
32	5.042266719	7.922598873	387.016	69.183	0.2405	226.979
64	5.04217041	7.926200289	786.516	68.964	0.4887	226.260
96	5.042074081	7.929801704	1186.016	31.262	0.7370	102.565
128	5.041977732	7.933403117	1585.517	56.770	0.9852	186.254
192	5.041784975	7.940605942	2384.517	58.895	1.4817	193.224
224	5.041688567	7.944207353	2784.017	29.950	1.7299	98.263
256	5.041592138	7.947808762	3183.518	43.500	1.9781	142.717
288	5.041495691	7.951410171	3583.018	37.450	2.2264	122.866
320	5.041399223	7.955011578	3982.518	34.161	2.4746	112.077
352	5.041302735	7.958612984	4382.018	49.212	2.7229	161.458
384	5.041206228	7.96221439	4781.519	56.030	2.9711	183.826
416	5.041109701	7.965815794	5181.019	50.308	3.2193	165.054
448	5.041013154	7.969417197	5580.519	52.172	3.4676	171.169
480	5.040916587	7.973018599	5980.019	51.368	3.7158	168.531
512	5.04082	7.97662	6379.520	51.816	3.9640	170.001

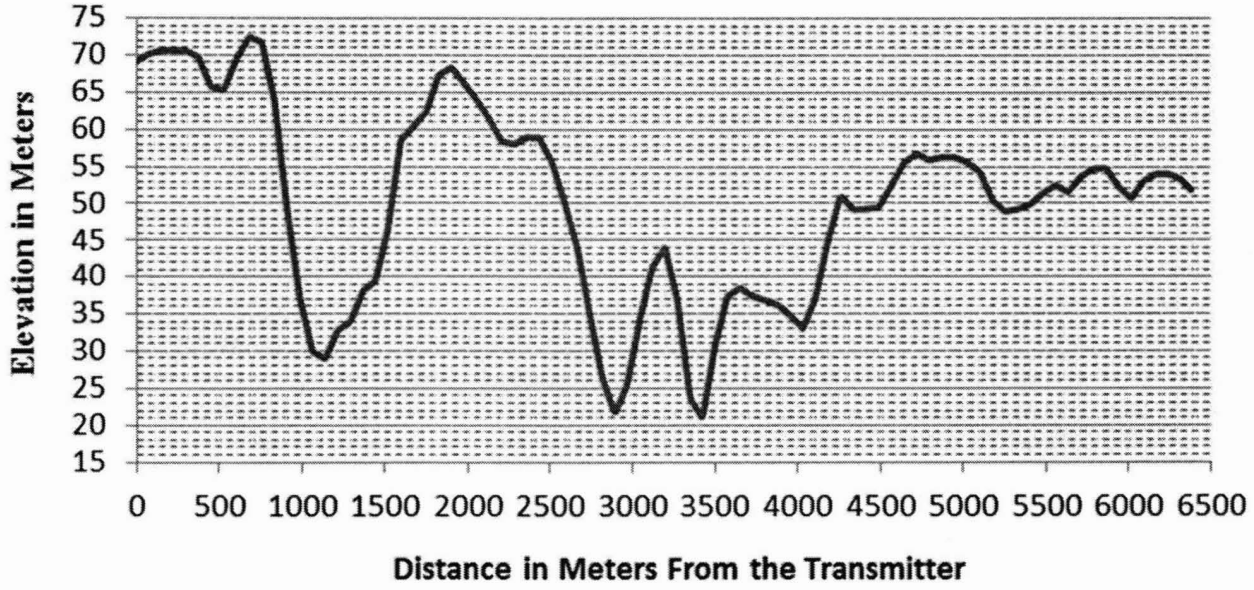

Figure 2. *Elevation Profile (Elevation Versus Distance).*

Some portions of the 512 records in the complete path profile dataset for the given transmitter and receiver location and microwave signal at 6GHz are given in Table 1. The path profile plot for all the 512 data points in the full path profile dataset is given in Figure 3. For Path Inclination (εp) >0 and in Figure 4. For Path Inclination (εp) = 0.

Table 2. *Selected Portions of the 512 Data Points in the Path Profile Dataset for 6 GHz Signal For Path Inclination (εp) = 0 and Path Inclination (εp) > 0.*

Column 1	Column 2	Column 3	Column 4	Column 5	Column 6
Data Point Number	Distance (m) from the Transmitter	Elevation (m)	Radius of the First Fresnel Zone (in Meters)	Earth Bulge (in Meters)	Line Of Site Elevation (εp > 0)
1 (Transmitter)	0	69.161	0	0	105.873
32	387.016	69.183	4.263	0.341	104.821
56	686.641	72.419	5.535	0.575	104.006
128	1585.517	56.77	7.718	1.117	101.562
153	1897.626	68.348	8.164	1.25	100.714
160	1985.017	66.004	8.269	1.282	100.476
192	2384.517	58.895	8.641	1.4	99.39
224	2784.017	29.95	8.857	1.471	98.304
250	3108.611	40.23	8.927	1.495	97.421
251	3121.096	41.313	8.928	1.495	97.387
256	3183.518	43.5	8.93	1.494	97.218
288	3583.018	37.45	8.862	1.473	96.132
320	3982.518	34.161	8.65	1.403	95.045
352	4382.018	49.212	8.283	1.287	93.959
384	4781.519	56.03	7.739	1.123	92.873
416	5181.019	50.308	6.976	0.913	91.787
448	5580.519	52.172	5.912	0.655	90.701
480	5980.019	51.368	4.327	0.351	89.614
512 (Receiver)	6379.52	51.816	0	0	88.528

Table 2. *Continue.*

Column 1	Column 7	Column 8	Column 9
Data Point Number	Line Of Site Elevation (εp = 0)	Clearance Distance (in meters) Between Obstacle and Fresnel Zone (εp > 0)	Clearance Distance (in meters) Between Obstacle and Fresnel Zone (εp = 0)
1 (Transmitter)	88.528	26.712	9.367
32	88.528	16.77	4.741
56	88.528	9.943	0
128	88.528	18.238	12.922
153	88.528	4.787	0.766
160	88.528	6.653	2.974
192	88.528	11.814	9.593
224	88.528	39.167	38.249
250	88.528	27.843	27.877

Column 1	Column 7	Column 8	Column 9
Data Point Number	**Line Of Site Elevation (εp = 0)**	**Clearance Distance (in meters) Between Obstacle and Fresnel Zone (εp > 0)**	**Clearance Distance (in meters) Between Obstacle and Fresnel Zone (εp = 0)**
251	88.528	26.724	26.792
256	88.528	24.362	24.602
288	88.528	29.485	30.744
320	88.528	32.182	34.314
352	88.528	16.895	19.747
384	88.528	10.243	13.636
416	88.528	16.613	20.331
448	88.528	16.05	19.789
480	88.528	19.241	22.482
512 (Receiver)	88.528	26.712	26.712

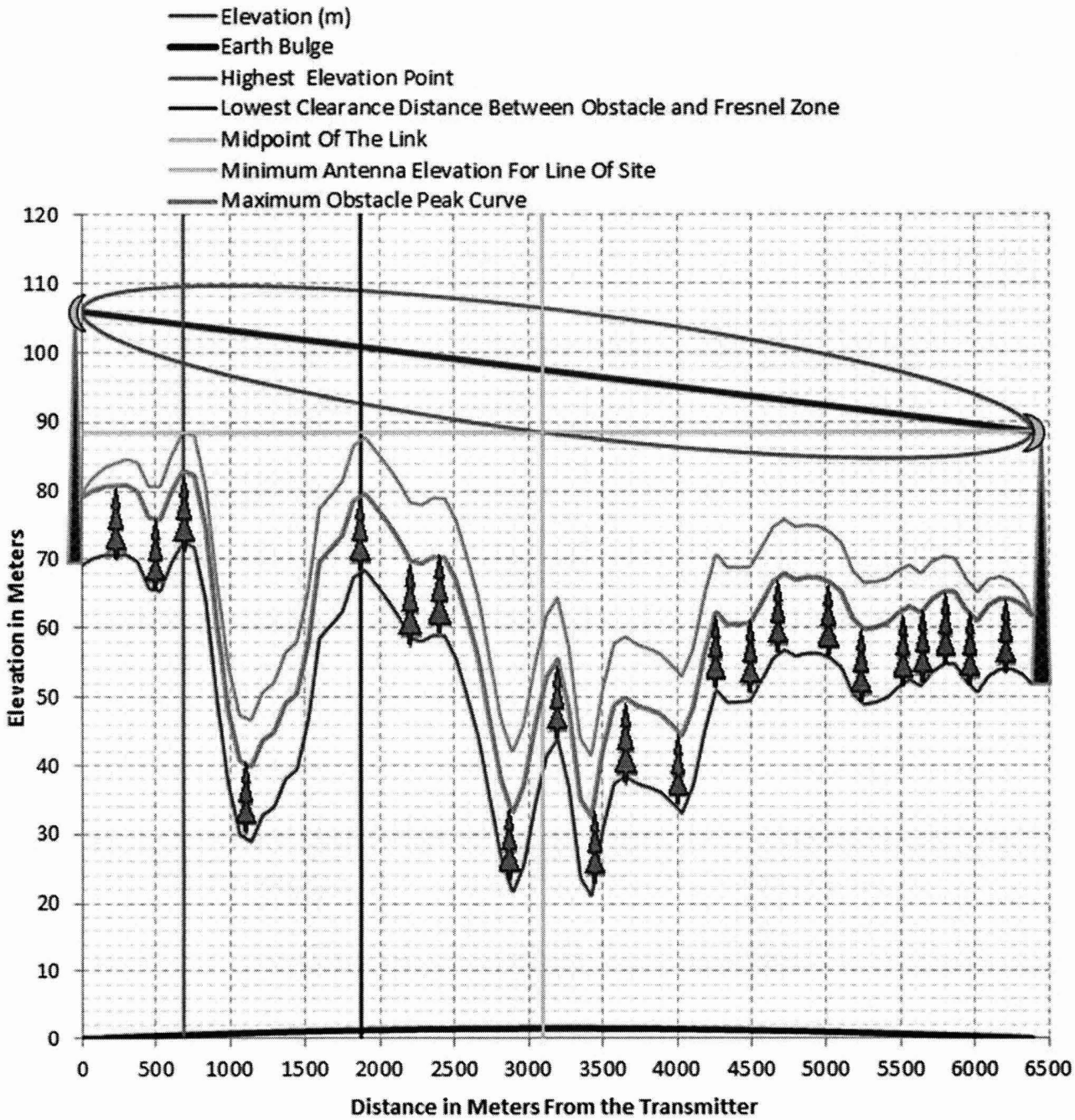

Figure 3. *Complete Path Profile: Elevation Versus Distance For 6GHz Signal and With Path inclination Greater Than Zero.*

According to Table 2, when the path inclination is (εp) > 0, the line of site is a line with negative gradient, sloping from line of site elevation of 105.873m (column 6 and row Data Point Number 1 of table 2) at the transmitter, down to line of site elevation of 88.528m (column 6 and row Data Point Number 512 of table 2) at the receiver. Furthermore, in column 8 and column 2 of row Data Point Number 153 in table 2, the critical point for line of site has 4.787m clearance distance (in meters) between obstacle and the first Fresnel zone and it is located at a distance of 1897.626 m from the transmitter.

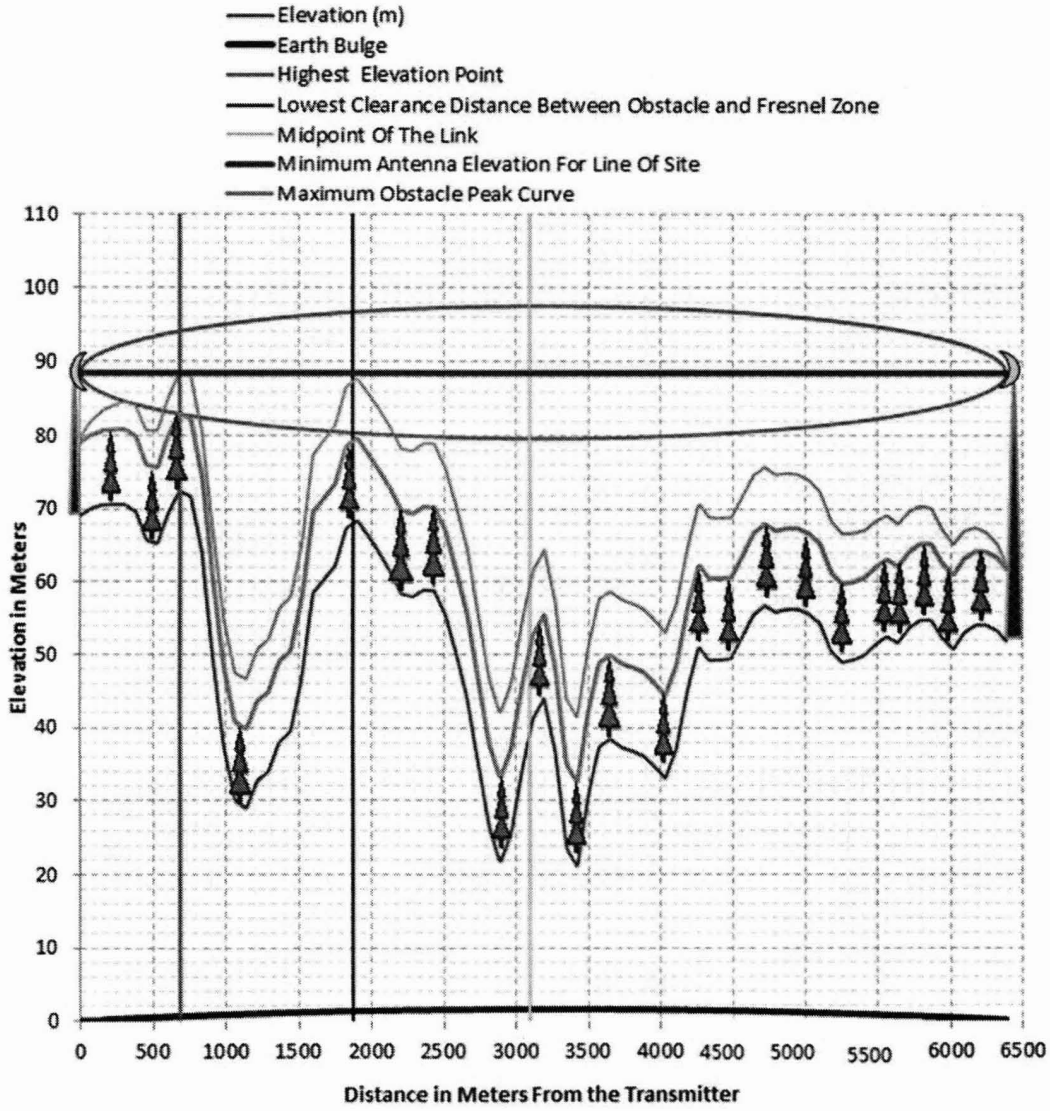

Figure 4. *Complete Path Profile : Elevation Versus Distance For 6GHz Signal and With Zero Path inclination.*

The critical point for line of site is indicated as the vertical black line in Figure 3. The clearance distance between obstacle and the first Fresnel zone at the link midpoint (in column 2 and column 8 of row Data Point Number 250 and 251 in table 2) is above 27m. However, the earth bulge is highest at the link midpoint with earth bulge of about 1.495m (column 5 of row Data Point Number 250 and 251 in table 2). The link midpoint is indicated as the vertical green line in Figure 3 and Figure 4.

On the other hand, according to Table 2, when the path inclination is (εp) = 0, the line of site is a horizontal line at line of site elevation of 88.528m (column 7 and row Data Point Number 1 of table 2) at the transmitter and at the receiver as well (column 7 and row Data Point Number 512 of table 2). Furthermore, in column 9 and column 2 of row Data Point Number 56 in table 2, the critical point for line of site has 0m clearance distance (in meters) between obstacle and the first Fresnel zone and it is located at a distance of 686.641m from the transmitter. The critical point for line of site is indicated as the vertical red line in Figure 4. The clearance distance between obstacle and the first Fresnel zone at the link midpoint (in column 2 and column 9 of row Data Point Number 250 and 251 in table 2) is above 27m.

When Path Inclination (εp) > 0, the transmitter and receiver antenna elevation and mast heights can be determined from the data in table 2 as follows;

Transmitter Antenna Elevation = Line of Site Elevation at the Transmitter = 105.873m (22)

Transmitter Antenna Mast Height = Transmitter Antenna Elevation - Elevation at the Transmitter Location = 105.873m - 69.161m = 36.712m (23)

Receiver Antenna Elevation = Line of Site Elevation at the Receiver = 88.528m (24)

Receiver Antenna Mast Height = Receiver Antenna Elevation - Elevation at the Receiver Location = 88.528m - 51.816m = 36.712m (25)

Similarly, when Path Inclination (εp) = 0, the transmitter and receiver antenna elevation and mast heights can be determined from the data in table 2 as follows;

Transmitter Antenna Elevation = Line of Site Elevation at the Transmitter = 88.528m (26)

Transmitter Antenna Mast Height = Transmitter Antenna Elevation - Elevation at the Transmitter Location = 88.528m - 69.161m = 19.367m. (27)

Receiver Antenna Elevation = Line of Site Elevation at the Receiver = 88.528m (28)

Receiver Antenna Mast Height = Receiver Antenna Elevation –

Elevation at the Receiver Location = 88.528m - 51.816m = 36.712m. (29)

Table 3. *The Transmitter and Receiver Antenna Elevation and Mast Heights.*

	Elevation at The Transmitter Location	**Transmitter Antenna Mast Height**	**Line Of Site Elevation at the Transmitter (Or Transmitter Antenna Elevation)**
Path Inclination (εp) > 0	69.161m	36.712m	105.873m
Path Inclination (εp) = 0	69.161m	19.367m	88.528m

Table 3. *Continue.*

	Elevation at The Receiver Location	**Receiver Antenna Mast Height**	**Line Of Site Elevation at the Receiver (Or Receiver Antenna Elevation)**
Path Inclination (εp) > 0	51.816m	36.712m	88.528m
Path Inclination (εp) = 0	51.816m	36.712m	88.528m

In table 3, is can be seen that for Path Inclination (εp) = 0 antenna mast height of 36.712m is required at the transmitter and at the receiver. However, for Path Inclination (εp) > 0 antenna mast height of 19.367m is required at the transmitter and antenna mast height of 36.712m is required at the receiver.

4. Conclusion

The approach for generating and plotting the path profile data for terrestrial line of site microwave link in presented. Sample path profile data set for a C-band link at 6GHz is generated and plotted for two cases, when the path inclination is equal to zero and when the path inclination is greater than zero. The signal path (or link) elevation profile (that is, elevation and distance) are obtained using Geocontext Online Elevation software. With the path profile data and graph plots, the minimum antenna elevation and the minimum antenna mast heights for effective line of site installation are determined. Also, the critical location where the line of site condition can easily be violated is also determined. The path profile tool presented in this paper is very useful for wireless network designers.

References

[1] Okorogu, V. N., Onoh, G. N., Onwujei, A. I., & Oluka, E. C. (2012) A Technique for Planning Microwave and Cellular Path Profile in the Tropics and Determination of Antenna Tower Heights (A Study of Onitsha/Nnewi Axis of Anambra State, Nigeria). International Journal of Engineering Science and Innovative Technology (IJESIT) Volume 1, Issue 2, November 2012.

[2] Hansryd, J., Edstam, J., Olsson, B. E., & Larsson, C. (2013). Non-line-of-sight microwave backhaul for small cells. *Ericsson Review*, *22*.

[3] Matheson, R., & Morris, A. C. (2012). The technical basis for spectrum rights: Policies to enhance market efficiency. *Telecommunications Policy*, *36*(9), 783-792.

[4] Burrell, J. (2003). Disruptive effects of electromagnetic interference on communication and electronic systems (Doctoral. dissertation, George Mason University).

[5] Cordeiro, C., Gossain, H., Ashok, R., & Agrawal, D. P. (2003, May). The last mile: Wireless technologies for broadband and home networks. In *Center for Distributed and Mobile Computing, University of Cincinnati, Cincinnati, OH. Presented at 21st Brazilian symposium on computer networks (SBRC 2003), Natal, Brazil.*

[6] Hassan, A. K. (2011). *Automated Microwave Antenna Alignment of Base Transceiver Station* (Doctoral dissertation, Karlstad University).

[7] Series, M. (2011). Maritime broadband wireless mesh networks.

[8] de Sousa Nunes, T. M. (2012). Microwave radio link between two endpoints.

[9] Arzubi, A. A., Castro Lechtaler, A., Foti, A., Fusario, R., García Garino, C., & García Guibout, J. (2010). Design of a Trans-Horizon radio link for ultra high and super high frequencies. In *XVI Congreso Argentino de Ciencias de la Computación.*

[10] Smith, D. R. (2012). Digital transmission systems. Springer Science & Business Media.

[11] Alcatel-Lucent (2012) Microwave System Path Survey Report. Technical report.

[12] Hufford, G. A., Longley, A. G., & Kissick, W. A. (1982). *A guide to the use of the ITS irregular terrain model in the area prediction mode*. US Department of Commerce, National Telecommunications and Information Administration.

[13] Standard, F. (1996). Telecommunications: Glossary of telecommunication terms. *Retrieved January*, *15*(2004), 69-72.

[14] Sharma, P. K., & Singh, R. K. (2012). Cell coverage area and link budget calculations in GSM system. *International Journal of Modern Engineering Research (IJMER) vol*, *2*, 170-176.

[15] Mahato, S. B. (2007). Performance Evaluation of Six-Sectored Configuration in Hexagonal WCDMA (UMTS) Cellular Network Layout.

[16] Geocontext Online Elevation software available at http://www.geocontext.org/publ/2010/04/profiler/en/ Accessed on July 1o 2016.

THE BELL SYSTEM
TECHNICAL JOURNAL

DEVOTED TO THE SCIENTIFIC AND ENGINEERING
ASPECTS OF ELECTRICAL COMMUNICATION

Volume 60 July-August 1981 Number 6

Copyright © 1981 American Telephone and Telegraph Company. Printed in U.S.A.

Microwave Radio Obstruction Fading

By A. VIGANTS

(Manuscript received February 20, 1981)

The occurrence of obstruction fading on line-of-sight microwave radio paths can require tower heights that are substantially larger than those needed for transmission in a normal atmosphere. In this paper, we show that the occurrence probability of obstruction fading can be estimated from the probability distribution of positive vertical refractivity gradients. The occurrence of positive refractivity gradients is related to general meteorological variables in a companion paper. The work summarized is part of a recent effort that has resulted in a new tower-height design method where tower-height requirements are quantitatively determined from transmission performance requirements.

I. INTRODUCTION

The design and the transmission performance of terrestrial line-of-sight microwave radio paths is greatly influenced by two clear-air propagation phenomena, obstruction and multipath fading. Both types of fading are caused by anomalous stratification of the atmosphere. In the case of obstruction fading, atmospheric stratification temporarily changes the transmission path to such an extent that it becomes blocked by the terrain. In the case of multipath fading, a different type of atmospheric stratification temporarily creates multiple transmission paths that cause destructive interference of a number of waves at the receiving antenna.

Satisfactory transmission performance is attained when the height of microwave radio towers is sufficient to reduce the occurrence of obstruction fading to a tolerable value, and when diversity protection is used to eliminate transmission impairments caused by multipath

fading. Methods for the estimation of multipath fading and the associated transmission performance have been developed, but a similar body of knowledge does not exist for obstruction fading.[1-6] One reason is that the variation of the occurrence of obstruction fading is much larger than that of multipath fading, which implies that the cost for establishing a data base for obstruction fading by direct measurement would be prohibitive.

However, obstruction fading can be related to meteorological variables for which a data base already exists. Recent work on this approach has resulted in a method that permits estimation of obstruction fading for any location in the United States. One part of this work, described in a companion paper, is the determination of probability distributions of positive vertical gradients of atmospheric microwave refractivity.[7] In this paper, we show that the probability of obstruction fading can be determined from probability distributions of the positive refractivity gradients. A mathematical model of obstruction fading is formulated to accomplish this. Obstruction-fading measurements are used to determine an obstruction loss expression for deep obstruction fading. A height interval for the definition of a positive refractivity gradient probability is also determined.

Tower-height requirements follow from transmission performance requirements when we use the mathematical model of obstruction fading. A new tower-height design method incorporating this approach supersedes the historical clearance rules (summarized in Ref. 2) previously used in the Bell System that did not relate performance to height in a quantitative manner. Additional advantages of the new method are geographic resolution and performance-based comparison of designs. We discuss transmission performance requirements applicable to tower-height determination in Section IX.

II. DAYTIME PROPAGATION

Microwave radio propagation on a line-of-sight path in a normal daytime atmosphere can be characterized by the trajectory of a ray that passes from the transmitting antenna to the receiving antenna. The trajectory is curved because the microwave index of refraction of the atmosphere decreases with height. The index of refraction (n) is usually described in terms of refractivity,[8]

$$N = (n - 1)10^6. \tag{1}$$

As an example, a refractivity of 320 N-units corresponds to a value of 1.000320 for the index of refraction. The vertical change of the refractivity can be considered to be a linear decrease with height in the first few hundred feet above ground.[9,10] A single parameter of the atmosphere, the refractivity gradient (N'), determines the trajectory of the

ray under such conditions. An alternate parameter, denoted by K, is frequently used to describe the refractivity gradient.[11-13] The origin of K is a geometric transformation to an equivalent earth without atmosphere and a radius which is K times that of the actual earth. The conversion between the two parameters is

$$N' = -157(1 - K^{-1}), \tag{2}$$

where K is dimensionless, and N' is expressed in N-units per kilometer.[12,13] The daytime "standard" value of K is 4/3, which corresponds to a refractivity gradient of -39.25 N-units/km. Expressed as a function of K, the equation for the trajectory of the ray is

$$H_d = (D_1D_2/1.5)(1 - K^{-1}), \tag{3}$$

where H_d is the vertical deviation of the trajectory from a straight line between the antennas, and D_1 and D_2 are the distances from a point of interest to the ends of the path (Fig. 1). The units of H_d are feet when D_1 and D_2 are in miles.

The nearness of the trajectory of the ray to the terrain is usually described by a normalized vertical distance, which is the vertical distance between a terrain point of interest and the trajectory, divided by the radius of the first Fresnel zone,[11,12]

$$F_1 = 72.1(D_1D_2/fD)^{1/2}. \tag{4}$$

The units of F_1 are feet when the frequency f is in GHz and the path length D is in miles ($D = D_1 + D_2$). The normalization to F_1 introduces

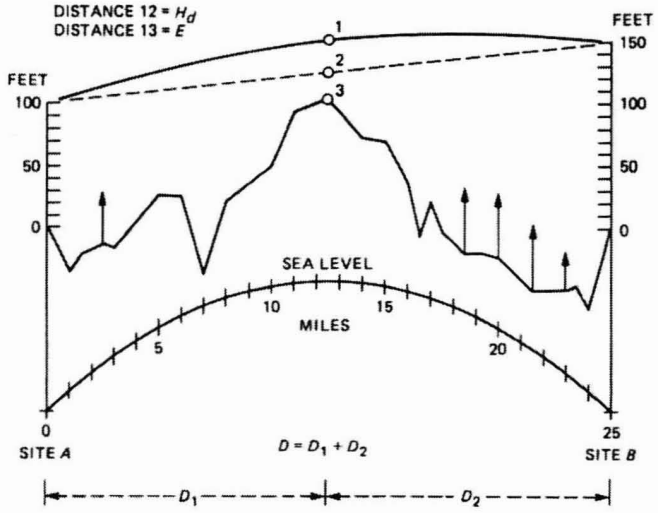

Fig. 1—Example of ray trajectory between antennas when $K = 4/3$ (solid line). In the absence of the atmosphere, or in the case of an atmosphere in which the vertical refractivity gradient is zero, the trajectory would be a straight line (dashed line). Arrows on the path profile denote tree cover.

scaling for frequency and distance that is convenient when signal attenuation due to the proximity of the terrain is considered. The attenuation is controlled by the terrain point with the smallest normalized vertical distance to the trajectory of the ray. This point on the terrain is referred to as the controlling obstruction. Tree cover and buildings must be included in the description of the terrain when the controlling obstruction is determined. The distance from the controlling obstruction to the trajectory of the ray is called clearance (distance E in Fig. 1).

Microwave radio paths are usually designed to avoid daytime attenuation caused by the proximity of the terrain to the trajectory of the ray. This is accomplished by using antenna heights such that the normalized clearance E/F_1 is unity or larger when K is 4/3.[2,12] Normalized clearances on many paths exceed unity at $K = 4/3$ because of antenna heights required to avoid excessive obstruction fading.

III. OBSTRUCTED PROPAGATION

Humid air can become positioned above drier surface-based air as a result of atmospheric stratification (layering).[7] Such stratification, when it occurs, develops gradually during the night and persists until broken up by air turbulence, caused either by a change in wind pattern or by a change in atmospheric conditions associated with sunrise. The resulting increase of refractivity with height causes the trajectory of the ray between the antennas to deviate downward from its normal daytime location. When the refractivity increase becomes sufficiently steep, the trajectory is blocked by the terrain, and the receiving antenna is placed in a shadow zone. The associated reduction in the received signal power is referred to as obstruction fading.

During obstruction fading, the lowest layer of the atmosphere controls propagation. The increases of refractivity with height in this layer are not necessarily linear, but it can be argued that the deviation of the trajectory is determined by a space-averaged gradient. Characterization of obstructed propagation by a single atmospheric parameter, a positive refractivity gradient, is therefore appropriate. This leads to the concept of a virtual trajectory (Fig. 2), which is a trajectory between the antennas that would exist for a particular positive refractivity gradient in the absence of the obstruction. The resulting geometrical description of blockage is similar to that of clearance, except that vertical distances from the terrain to the virtual trajectory are negative to signify blockage. The controlling obstruction in this case is that for which the normalized vertical distance has the largest negative value.

Quantitative description of obstruction fading in terms of the above geometry requires consideration of two topics. First, a relationship

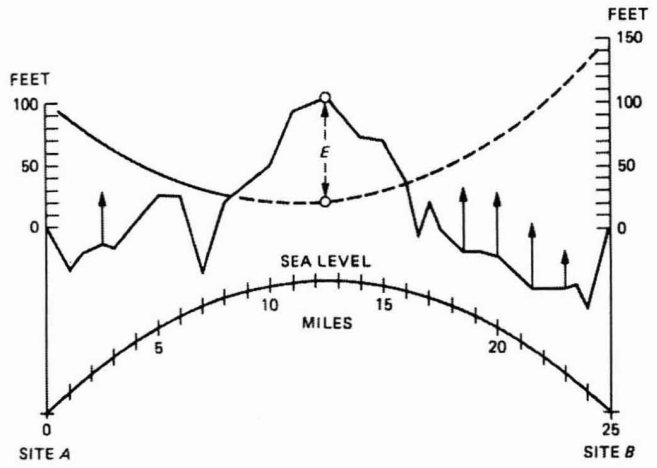

Fig. 2—Example of virtual trajectory between antennas when $K = 1/2$.

between obstruction loss and the normalized blockage E/F_1 at the controlling obstruction must be obtained. Second, probabilities of positive refractivity gradients must be translated into probabilities of blockage. We use the obstruction-fading measurements summarized in Section IV to accomplish this.

IV. MEASURED OBSTRUCTION FADING

We obtained quantitative information on obstruction fading from fading measurements carried out for one year (February 1974–January 1975) at 4.13 GHz on a 24.3-mi path in northeastern Florida where obstruction fading is prevalent. The measurement path was flat with substantial tree cover. At the transmitting site, referred to as station T, the ground elevation was 40 ft relative to the mean sea level. The centerline of the transmitting antenna (10-ft horn reflector) was 270 ft above ground. The controlling obstruction, located at 11.9 mi from the receiving site, consisted of 50-ft tree cover on ground that was 15 ft above the mean sea level. At the receiving site, referred to as station R, the ground elevation was 15 ft above the mean sea level. The centerline of the receiving antenna (10-ft horn reflector) was 220 ft above ground. Reception was also monitored on an antenna (10-ft dish) with a centerline at 185 ft above ground. We adjusted instrumentation gains to simulate operation with equal antenna gains and equal waveguide losses. A third receiving antenna (6-ft dish), added on November 1, 1974, had a centerline height of 73 ft above ground. During substantial fading experienced in November, the presence of the third receiving antenna permitted further verification of earlier conclusions that the amount of fading at station R was inversely

related to antenna height in a manner that indicated the presence of obstruction fading.

We used Portable Propagation Recorders (PPRs) to record the experimental results. These devices sampled the received signals ten times per second and accumulated the time during which the strength of the signals was below a set of levels. The levels for the top antenna were, in dB relative to daytime normal, −10 and then −20 to −40 in 5-dB steps. Limitations of recording capacity forced us to assign a smaller set of levels to the two lower antennas. We transmitted the accumulated data to Bell Laboratories at Holmdel, New Jersey, once every working day. The accumulated data were also automatically punched out on paper tape at station *R* at noon every day. This permitted the signal statistics to be separated into noon-to-noon periods. The interpretation of the statistics was aided by strip charts (3 in/h) that accompanied each 24-h block.

Obstruction fading was present on four nights during 24-h periods that ended at noon on March 8, June 20, November 3, and November 17 in the 1-yr measurement period. We determined the presence of obstruction fading on the basis of three criteria: depressed levels of received signals on a time scale of tens of minutes, increase of fading with decrease of antenna height, and high degree of simultaneous fading on the two upper antennas. The last criterion separates nights with obstruction fading from those with heavy multipath fading.

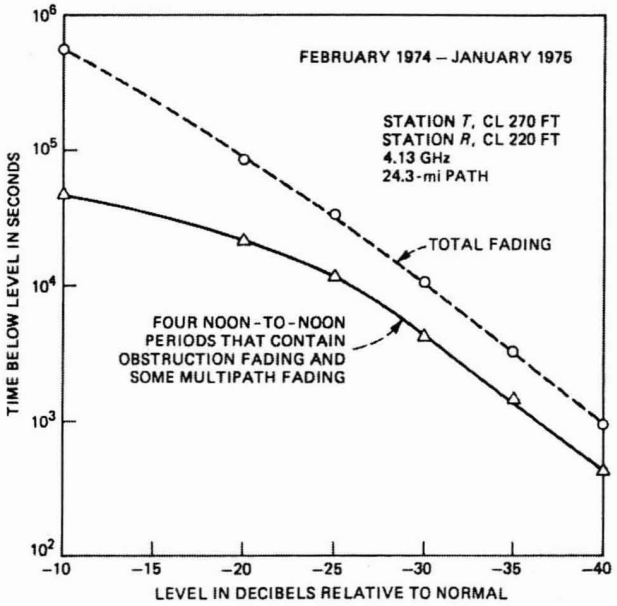

Fig. 3—Measured obstruction fading.

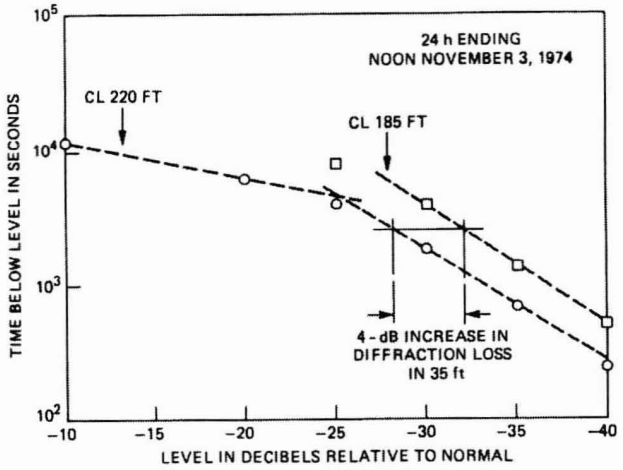

Fig. 4—Variation of obstruction fading with reception height at station *R*.

The measured time below −35 dB on the top antenna during nights with obstruction fading was 1425 s (solid curve in Fig. 3). The corresponding simultaneous time below −35 dB on the two upper antennas was 562 s. The space-diversity improvement is only 2.5 (1425/562), which demonstrates the incapacitation of diversity protection in the presence of obstruction fading.

The measured time below −35 dB on the top antenna caused by all fading was 3217 s (dashed curve in Fig. 3). Subtracting the obstruction-fading dominated time from this yields the amount of multipath fading (1792 s below −35 dB). The corresponding simultaneous time below −35 dB caused by multipath fading on the two upper antennas was 16 s. The space-diversity improvement of 112 (1792/16) is typical of multipath fading.

V. EMPIRICAL OBSTRUCTION LOSS EXPRESSION

We obtain a relationship between obstruction loss and blockage when measurements made at station *R* are related to diffraction theory. The measurements imply a linear relation between large obstruction loss in dB and normalized blockage, with a slope of 20 dB per unit of normalized blockage. This follows from the observation that (Fig. 4), for a given amount of loss larger than about 25 dB on the top antenna at station *R*, the loss on the antenna 35 feet below it is *4* dB larger. From the geometry of the path (specified in Section IV), the vertical offset corresponding to 35 ft at station *R* is 17.9 ft (35 × 12.4/24.3) at the controlling obstruction 11.9 mi from station *R* (12.4 mi from station *T*). The radius of the first Fresnel zone at this point on the path is 87.4 ft. Therefore, the vertical offset is 0.20 (17.9/87.4) in

terms of a change of normalized blockage. This corresponds to a change of 20 dB per unit of normalized blockage (4/0.20).

Large values of the theoretical obstruction loss for extended obstructions, such as large spheres, vary approximately linearly with normalized blockage.[14] The theoretical results suggest that straight-line approximations for large losses intersect zero loss at 0.5 units of normalized clearance. Given this, and the experimentally inferred slope of 20 dB, the loss expression applicable to deep obstruction fading becomes

$$M = -10 + 20(E/F_1), \qquad M < -20, \tag{5}$$

where M is the fade level in dB relative to free space, and the value of the vertical distance E is negative to signify blockage. The term "free space" refers to a signal level that would be attained in the absence of atmospheric effects and without the proximity of the terrain.

The above empirical obstruction loss expression describes diffraction by "large" obstructions in the presence of atmospheric stratification. Paths with obstructions of "smaller" horizontal extent, such as a mountain ridge, may have obstruction losses smaller than those described by the empirical expression. This is suggested by a comparison with the theoretical limiting case of knife-edge diffraction (Fig. 5).[13,14] Such "smaller" obstructions usually occur in mountainous terrain where obstruction fading is not a problem. Based on general scaling

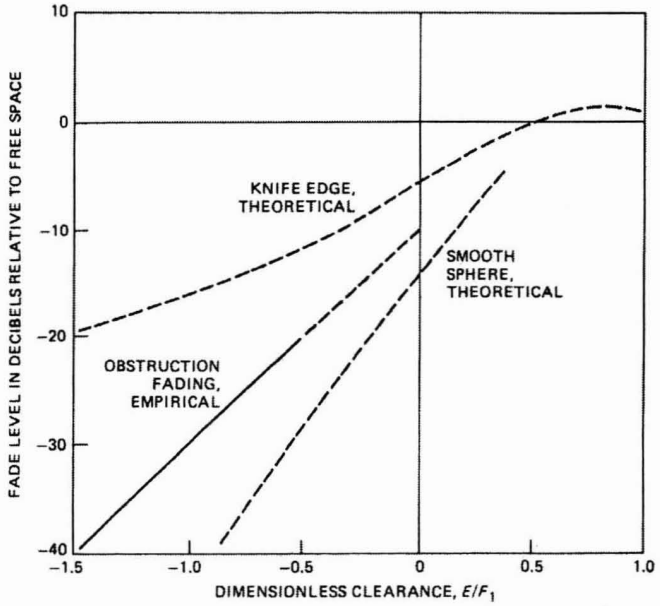

Fig. 5—Obstruction loss for deep obstruction fading on line-of-sight microwave radio paths.

experience in path engineering, the empirical loss expression can be applied at frequencies from 2 to 11 GHz on most practical paths between 20 and 30 mi in length.

VI. PROBABILITY OF OBSTRUCTION FADING

The practical problem in microwave radio path engineering is estimating the amount of time during which obstruction fading causes the received signal to be below a particular fade level. This time can be obtained from the probability of obstruction fading, which can be estimated from the probability distribution of refractivity gradients.

The steps in the procedure for making such an estimation are outlined in a simplified flow chart in Fig. 6. A fade level of interest corresponds to a normalized blockage E/F_1 as specified by the obstruction loss expression in eq. (5). The value of F_1 can be calculated when the radio frequency is specified and the location of the controlling obstruction is determined. This can be an iterative procedure, since the location of the controlling obstruction can change with antenna height and refractivity gradient. When F_1 has been calculated, the vertical distance E can be determined from a rearranged obstruction loss expression

$$E = (F_1/20)(M + 10). \tag{6}$$

Next, given the tentative heights of the transmitting and receiving antennas and the profile of the path, eq. (3) for the trajectory of the ray can be applied to determine a positive refractivity gradient (S) required to produce the value of E determined above.

The annual amount of time during which obstruction fading causes a received signal to be below a particular fade level can then be expressed, in seconds per year, as

$$T = T_0 P(N' > S), \tag{7}$$

where T_0 is the number of seconds in a year and $P(N' > S)$ is the annual probability that the refractivity gradient N' exceeds S.

The annual probability that the refractivity gradient exceeds a particular positive value S is composed of seasonal parts,[7]

$$P(N' > S) = (1/4) \sum_i P_i(N' > S), \tag{8}$$

where the summation extends over the four seasons of the year. Each seasonal probability consists of two components

$$P_i(N' > S) = 0.8P_{m,i} + 0.2P_{s,i}, \tag{9}$$

where the subscript m refers to the mixed (daytime) atmosphere, and the subscript s refers to a stratified (nighttime) atmosphere. Both

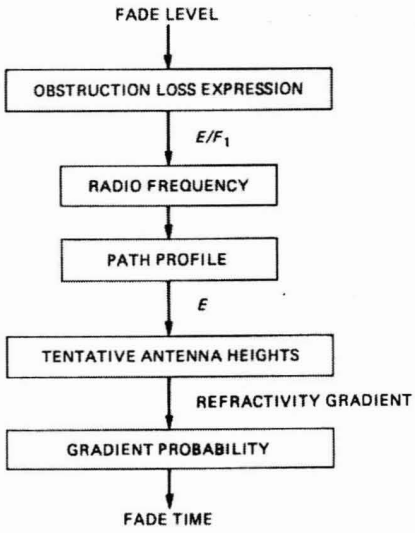

Fig. 6—Obstruction fading calculation.

components are Gaussian probability functions specified by appropriate values of their means and standard deviations.[7] The means vary with geographic locations, but in a given season they are the same for the mixed and stratified regimes in the above mathematical formulation. The standard deviation for the mixed regime is 15 N-units/km for all locations and all seasons of the year in the United States.[7] The amount of obstruction fading is governed largely by the standard deviations for the stratified regime, which exhibit considerable geographic and seasonal variation.[7]

VII. GRADIENT SCALE

Probability distributions of refractivity gradients usually describe the occurrence of increments of refractivity associated with an increment in height.[7,15] A frequently used height increment is 100 m. Analyzing data for other height increments shows that the standard deviation of positive refractivity increments in the stratified regime is inversely proportional to the fourth root of the height increment.[7] This arises because the absolute increase in refractivity that the atmosphere can support is limited. This behavior of the gradient statistics necessitates use of obstruction-fading measurements to determine the height increment (gradient scale) appropriate for microwave obstruction fading.

Simultaneous fading on the upper two receiving antennas at station R is the experimental measurement best suited for the determination of the gradient scale (centerlines of 220 and 185 ft above ground).

Simultaneous fading below the −35 dB fade level was measured on these antennas continuously throughout the experiment. The total simultaneous time below −35 dB was 562 s in the four 24-h periods when obstruction fading was present. This time represents "pure" obstruction fading below −35 dB at the 220-ft height, since the constraint of simultaneity removes multipath effects.

The calculated time below the −35 dB fade level can be expressed as a function of the height increment, or more specifically from eq. (9) in Ref. 7, as a function of the coefficient in the expression that relates the standard deviation of positive refractivity increments to meteorological parameters. This coefficient is inversely proportional to the fourth root of the height increment. The value of the coefficient is 440 when the height increment is 100 m.[7] The corresponding standard deviations for the area where the path is located are, in N-units/km, 71 for winter, 56 for spring, 58 for summer, and 96 for fall.[16] The coefficient that corresponds to the measured 562 s is 540 (Fig. 7). Therefore, the height interval (gradient scale) appropriate for calculation of obstruction fading becomes, as determined from Fig. 4 in Ref.

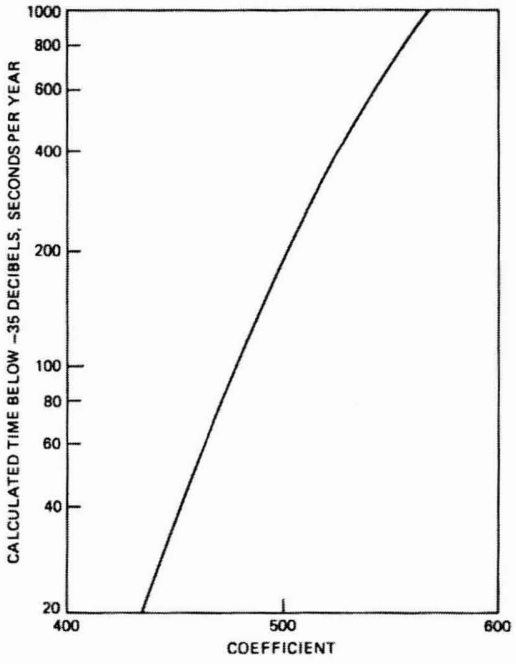

Fig. 7—Calculated obstruction fading as a function of the coefficient in the expression for the standard deviation of refractivity gradient.[7] Measured obstruction fading of 562 s and meteorological parameters for the propagation path between stations T and R determine 540 as the value of the coefficient.[16]

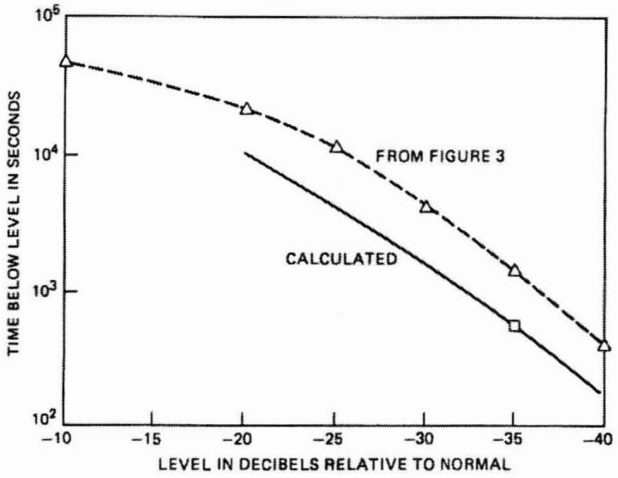

Fig. 8—Calculated obstruction fading at station *R*. Measured fading on nights when obstruction fading was dominant is shown by dashed curve (from Fig. 3), which contains some multipath fading.

7, $(1400/540)^4$ or 45 m. The corresponding standard deviations of the positive refractivity increments are, in *N*-units/km, 87 for winter, 69 for spring, 71 for summer, and 118 for fall.

The mean values of the refractivity gradients do not require scaling, since they describe the daytime reference condition of the atmosphere. The values of the means used in the above calculations are, in *N*-units/km, −46 for winter, −53 for spring, −58 for summer, and −53 for fall.[16]

VIII. CALCULATED OBSTRUCTION FADING

A comparison of calculated and measured obstruction fading at station *R* demonstrates the validity of the mathematical model. The slope of the calculated obstruction fading curve matches the measured results (Fig. 8). The slope is determined by the mathematical model, which has not been forced to conform in any way to slopes of measured fading curves. The calculated curve passes through the simultaneous fading point at −35 dB, which was used to determine the gradient scale and which describes "pure" obstruction fading. The dashed curve (from Fig. 3) describes measured obstruction fading accompanied by some multipath fading. Extension of the calculated curve to fade levels significantly shallower than −20 dB is not appropriate, since the obstruction loss curve incorporated in the mathematical model applies only to deep obstruction fades.

Additional calculated results for station *R* (Figs. 9 and 10) illustrate the variation of obstruction fading with antenna height and radio

frequency. The time below −35 dB varies by more than two orders of magnitude as the receiving height at station R changes 200 ft. When the radio frequency is varied from 2 to 11 GHz, the fade level at 10 s/yr (Fig. 10) varies over a range of almost 20 dB. This variation is a consequence of the frequency dependence of the obstruction loss in eq. (5). The obstruction loss increases with frequency because, as illustrated in Fig. 11, the blockage of Fresnel zones increases with frequency.

IX. DESIGN SPECIFICATIONS

Tower-height design specifications can be derived from Bell System's annual all-cause two-way transmission unavailability design limit of 0.02 percent, which applies to a 4000-mi long-haul circuit or a 250-mi short-haul circuit.[1,2,6] For route engineering purposes, half of this is allocated to multipath fading in the 2-GHz, 4-GHz, and 6-GHz bands where clear-air propagation phenomena are the dominant causes of propagation impairments.[1,2] A new allocation to obstruction fading is 0.005 percent, which is both two-way and one-way, assuming that both directions of transmission use radio channels on the same terrestrial radio route. The other 0.005 percent is allocated to equipment impair-

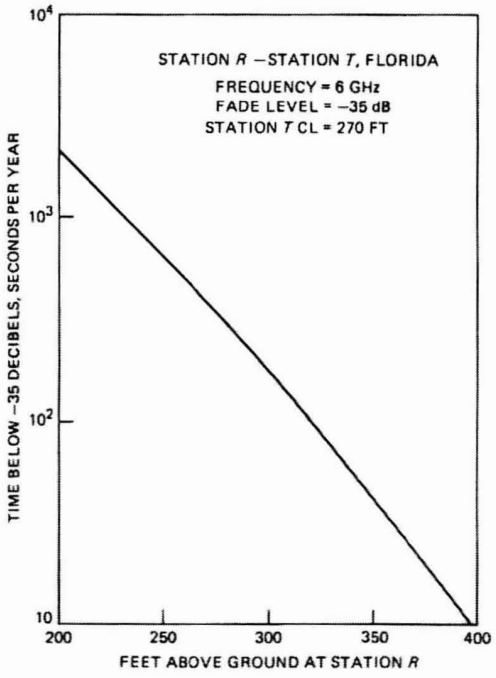

Fig. 9—Variation of obstruction fading with antenna height.

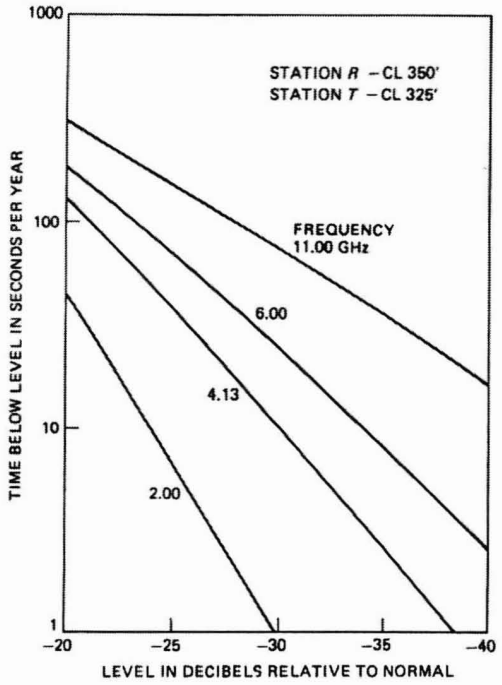

Fig. 10—Calculated obstruction fading for station R – station T.

ments and other causes. These design allocations emphasize that, in modern solid state radio systems, transmission performance is governed by propagation impairments. In the case of short-haul radio, tradeoffs between allocations are frequently invoked, particularly so in the 11-GHz band where transmission unavailability caused by rain can be dominant.

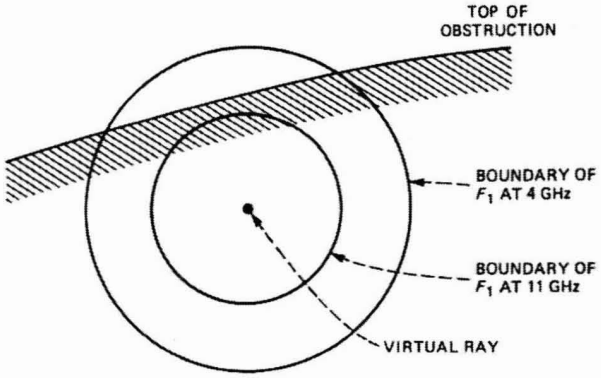

Fig. 11—Illustration of blockage.

The allocations are prorated to distance. For long-haul service, this implies that antenna centerline heights (tower heights) on a 25-mi path have to be such that the annual time below a specified fade level, caused by obstruction fading, is 10 s or less. A fade level of −35 dB is recommended as the obstruction fading outage threshold in tower-height design procedures. The choice of −35 dB as a design value is related to general characteristics of radio systems, interference considerations, and possible joint occurrence of obstruction fading and multipath fading. An advantage of an equipment-independent fade-level specification is design stability, since radio towers are "permanent" parts of the plant that can be expected to be used for a number of future varieties of radio equipment and service. Combined use of the allocation and the −35 dB value is necessary to achieve a balanced design where terrain clearance is adequate and where impairment of diversity protection is minimal when obstruction fading and multipath fading occur jointly.

When used as design criteria, the allocations are prorated to the length of a frequency-diversity switching section or to a route segment between terminals or drop and add points. For example, the allocation to a switching section containing three 25-mi paths (hops) is 30 s. The hops are permitted to contribute unequally to the 30-s total. A design where two hops contribute 5 s each and the third hop contributes 20 s is satisfactory. Design allocations such as these are related to measured performance in an average sense, since fading can vary from year to year, and because interactions of fading, actual fade margins, and protection system operation can be complicated.

Tower heights on radio hops in short-haul service frequently have been determined by clearance rules that are the same as those for hops in long-haul service. This permits flexibility in the routing of communications traffic with differing reliability requirements. Therefore, tower-height requirements for short-haul routes can be determined from the obstruction-fading allocation of 10 s/yr prorated to a 25-mi hop. An option for the determination of short-haul tower heights is an obstruction fading allocation of 160 s/yr prorated to a 25-mi hop. This retains the standard one-to-sixteen ratio of per-mile performance between long-haul and short-haul service. The 160-s option can be used only when reliability requirements are expected to remain constant over the life of the towers. When used as design criteria, these allocations are prorated to the length of a switching section or route segment.

In the case of paths equipped for space-diversity reception, the obstruction fading allocation for the lower antenna prorated to a 25-mi hop is 50 s/yr for long-haul service and for those hops in short-haul service where the height of the upper antenna is determined by the

10-s allocation. We apply the 50-s allocation on a per-hop basis to avoid impairment of space-diversity protection. A separate allocation for lower antennas is not made when we use the 160-s option to design short-haul paths, since this option represents a design limit.

The design criteria outlined above indicate that tower heights larger than previously required can be beneficial in regions where obstruction fading is severe. For example, a previous clearance rule has been grazing (zero) clearance at $K = 1/2$ in difficult propagation areas,[2] which requires approximately 180-ft towers on a 20-mi flat path covered by 50-ft trees. The new criteria indicate that towers on such a path may need to be as high as 250 ft for long-haul service in an area with a high occurrence probability of obstruction fading.

X. CONCLUSION

A new tower-height design method outlined in this paper permits more efficient use of construction funds, since tower heights are quantitatively related to transmission performance. High towers can be constructed where needed, whereas towers of minimal height, determined by daytime clearance requirements, can be used in the cooler regions of the United States.

XI. ACKNOWLEDGMENTS

The work on obstruction fading benefited considerably from interactions with W. T. Barnett. We had many helpful discussions with J. A. Schiavone about the meteorological aspects of radio propagation. Portable Propagation Recorders (PPRs) designed by G. A. Zimmerman made acquisition of the propagation data possible. A number of colleagues at Bell Laboratories, AT&T Long Lines, and Southern Bell provided assistance needed to carry out the propagation measurements.

REFERENCES

1. A. Vigants and M. V. Pursley, "Transmission Unavailability of Frequency-Diversity Protected Microwave FM Radio Systems Caused by Multipath Fading," B.S.T.J., *58*, No. 8 (October 1979), pp. 1779–96.
2. A. Vigants, "Space-Diversity Engineering," B.S.T.J., *54*, No. 1 (January 1975), pp. 103–42.
3. W. T. Barnett, "Microwave Line-of-Sight Propagation With and Without Frequency Diversity," B.S.T.J., *49*, No. 8 (October 1970), pp. 1827–71.
4. W. T. Barnett, "Multipath Propagation at 4, 6, and 11 GHz," B.S.T.J. *51*, No. 2 (February 1972), pp. 321–61.
5. S. H. Lin, "Statistical Behavior of Deep Fades of Diversity Signals," IEEE Trans. Commun., *COM-20*, No. 6 (December 1972), pp. 1100–7.
6. W. Y. S. Chen, "Estimated Outage in Long-Haul Radio Relay Systems with Protection Switching," B.S.T.J., *50*, No. 4 (April 1971), pp. 1455–85.
7. J. A. Schiavone, "Prediction of Positive Refractivity Gradients for Line-of-Sight Microwave Radio Paths," B.S.T.J., this issue.
8. B. R. Bean and E. J. Dutton, *Radio Meteorology*, National Bureau of Standards, U. S. Government Printing Office, 1966.

9. C. L. Pekeris, "Accuracy of the Earth-Flattening Approximation in the Theory of Microwave Propagation," Phys. Rev. *70,* Nos. 7 and 8 (October 1 and 15, 1946), pp. 518–22.
10. D. E. Kerr, *Propagation of Short Radio Waves*, New York: McGraw-Hill, 1951.
11. D. C. Livingston, *The Physics of Microwave Propagation*, Englewood Cliffs, New Jersey: Prentice-Hall, 1970.
12. R. F. White, *Engineering Considerations for Microwave Communications Systems*, San Carlos, California: Lenkurt Electric Co., 1970.
13. M. P. M. Hall, "Effects of the Troposphere on Radio Communications," London: Peter Peregrinus Ltd. on behalf of the Institution of Electrical Engineers, 1979.
14. K. Bullington, "Radio Propagation Fundamentals," B.S.T.J., *36* (May 1957), pp. 593–626.
15. C. A. Samson, "Refractivity Gradients in the Northern Hemisphere," OT Report 75-59, U. S. Department of Commerce, Office of Telecommunications, U. S. Government Printing Office, April 1975.
16. J. A. Schiavone, private communication, 1979.

The basic calculations associated with a Digital Microwave Radio Path Data Sheet are simply the addition and subtraction of relative gains, losses, and power levels, in dB or dBm, to arrive at an expected or desired Composite Fade Margin. The gathering of those numbers and some of the preliminary calculations associated with path length and azimuths is a bit more difficult, depending on access to the correct tables, use of hand-held calculators, and the like. The conversion of the expected or desired Composite Fade Margin into predictable short-term (multipath fade) and long-term (rain fade) Outage Time, SESR, Path Reliability, and Rain Availability requires even more sophistication.

This StarLink 2 Tutorial is intended to provide you a limited overview of the basic calculations associated with the Digital Microwave Radio Path Data Sheet and to compare these results with recognized performance objectives.

StarLink 2's short-term (multipath fade) Probability of Outage (SESR) and Annual Outage Time computations are based upon Vigants' widely-used field-verified model as defined in references [15] for North American links and [6] for International (ITU-R Rep. 338) links.

The ITU-R Rec. P.530-8 [Ref. 16] multipath outage prediction method (with Hosoya's space diversity improvement model) could produce results widely divergent from Vigants' model, especially for flatland paths using space diversity in difficult geoclimatic regions. For this reason, the Rec. P.530-8 short-term outage model is not provided in this version of StarLink.

StarLink 2's long-term (rain fade) outage time computations use the Crane rain model, and access Crane's rain rate tables [8] for North American radio-relay links which are derived from ITU-R but optimized for this region. This Crane model accesses ITU-R rain regions and rain rate tables [5] for international microwave path rain outage calculations.

The new ITU-R Rec. P.530-8 rain availability model is also not used in StarLink 2 rain outage computations. StarLink 2 applies the Crane rain model to all rain outage and link availability calculations worldwide.

HARRIS STARLINK 2

Determining the Free Space Path Loss is the next calculation in the preparation of a Path Data Sheet. Free-space loss is defined as the loss that exists between two isotropic antennas in free space, where there are no ground influences or obstructions; in other words, where losses due to refraction, reflection, and diffraction fade activity and atmospheric absorption do not exist. Radio energy is lost with distance because of the triangular spreading of wavefront energy as it travels through space. In accordance with the inverse-square law, wavefront area quadruples for each doubling of distance, for a 10 log 1/4 = 6 dB increase in path loss.

$10 \cdot \log_{10}\left(\frac{1}{4}\right) = -6$ dB

The derivation of the formula for free-space loss is presented in many other references and will not be repeated here. The formula itself, however, is shown below:

A = 96.6 + 20 log f + 20 log Dmi

where	A	=	free space attenuation between antennas, dB
	f	=	frequency, GHz
	Dmi	=	path length, miles

and **A = 92.4 + 20 log f + 20 log Dkm**

where	Dkm	=	path length, kilometers

The Unfaded Receive Signal Level is computed by introducing the Net Path Loss (NPL), dB, between a radio transmitter output and the following radio receiver's input. The microwave radio transmit power is reduced by the NPL as determined by free space and atmospheric absorption losses, antenna gains, and all the feeder and network losses at both ends of the single radio path, link, or hop, as it is variously called.

RSL = Pt - NPL

= Pt + Gt - Lfs - Labs + Gr - Lf - Lnet

where	Pt	=	transmit power, dBm
	Gt	=	transmit antenna gain, dB
	Lfs	=	free space loss, dB
	Labs	=	absorption loss, dB
	Gr	=	receive antenna gain, dB
	Lf	=	coax or waveguide feeder loss, dB
	Lnet	=	network and other losses, dB

Pt 1A Gt

$(30-5)+10=35$

$35-(FS-Abs)$

$35-75=$

$-40+20$

$-20-7=$

STATIC

The Thermal (or Flat) Fade Margin (TFM) is the difference between the Unfaded Receive Signal Level and the receiver's Static or Dynamic Threshold, as measured with back-to-back digital radios, at a given Bit Error Rate. StarLink 2 provides you with the ability to select either the 10-3 BER Dynamic Threshold for outage computations or the 10-6 BER Static Threshold for other performance and availability computations. This selection adjusts the receiver's threshold to correspond with the selected BER. The threshold RSL values used in the StarLink template are based on Harris MCD's Digital Microwave Radios. The values are located in a table and are accessed via WindowsTM commands based on the data you enter, e.g. threshold BER, frequency, capacity, protection type, etc.

It is important to note that an internationally defined outage in a PDH (asynchronous) digital radio link corresponds to a 10-3 BER severely-errored second (SES) event at the receiver's Dynamic Threshold. This threshold is very near the initiation of a T1 or E1 AIS alarm (loss of frame synchronization) condition in the connected PABX, channel bank, transmultiplexer, etc. trunk port. The digital radio's 10-6 BER Static Threshold or operating point is used for in-service radio and interference measurements (with attenuators) and as a measurement of circuit quality, not outage, although it is sometimes assigned as an "outage" threshold by some users.

The outage threshold of a SONET or SDH (synchronous) digital link, perhaps one using the MegaStar 155 radio, is defined at its SONET/SDH multiplexer's loss-of-pointer synchronization (LOP) point coinciding with a 2x10-5 BER for STM-1 and STS-3 radios. However, only a very small difference, perhaps 0.5 dB, between this LOP and a 10-3 BER threshold point occurs.

Dispersive Fade Margin

A few high-clearance digital microwave radio links with adverse path geometry are susceptible to Dispersive (spectrum-distorting) Fading, and as well as interference and the flat fading mentioned above. Dispersive fading may cause the loss of the digital radio receiver's quadrature lock (synchronization) due to amplitude or group delay slope and notch effects resulting in degraded error performance, including short- or long-term outage. Powerful corrective measures combating dispersive fading include Space Diversity, Forward Error Correction (FEC), Adaptive Time Domain Equalization (ATDE), and Adaptive IF Slope Amplitude Equalization (ASAE). As the RF bandwidth or number of signaling states increases the effect of dispersive fading increases, requiring the more sophisticated countermeasures typical of today's digital microwave receivers.

The robustness of a digital radio to dispersive fading is defined by its Dispersive Fade Margin (DFM), a value found in the radio's data sheets. The DFM for a digital radio is derived from its Signature Curve, derived by moving a high-level multipath notch through the receiver's IF passband at depths increased to cause an outage. This notch results from the canceling null generated by the combining of the transmitter's direct signal with its multipath signal delayed 6.3 nsec (6 feet or 2m).

StarLink 2 adds TFM + DFM (power addition, e.g. 40 dB TFM + 50 dB DFM = 39.6 dB CFM) to derive the link's Composite Fade Margin (CFM) used for multipath outage calculations. Unless very high thermal fade margins result with a short path and/or large antennas, the impact of a modern digital radio's DFM upon CFM, and therefore upon the link design, should be negligible.

However, the radio's DFM could be heavily degraded on some high clearance paths with inadequate antenna discriminations to the resulting very long-delayed (>10 nsec) multipath signal. The radio's DFM could degrade from 50+ dB to 40 dB (or even much lower) with this long-delayed high amplitude multipath signal.

It is essential that the antenna discriminations (antenna's frequency band, sizes, and uptilt) to the long-delayed specular reflection lower the echo's amplitude adequately to meet a minimum 50 dB link DFM objective for no degradation in the link's error performance:

Link DFM = Radio DFM [f(delay time)] + Antenna Discriminations = >50 dB

Intra-station and interlink Interference from other microwave transmitters may also degrade the digital radio's threshold and, therefore, the link's fade margin. Although usually ignored in initial path design, interference is often limited to that level introducing <1 dB threshold (and fade margin) degradation into a link.

Once the Composite Fade Margin has been determined, it is used to compute an expected severely-errored second ratio (SESR) and, in North America, the one-way path reliability based upon annual outage time. Path reliability (from the annual short-term outage time computation) is influenced by the effects of:

- Multipath fading, defined by geographical propagation characteristics (climate and terrain) for given locales, and
- Average Annual Temperature defining the fade season for the same geographical region.

CFM is also an input for computing expected the annual two-way Path Availability in high-frequency links which accommodates all long-term (>10 CSES traffic disconnect) rain outage events. Path availability is computed from:

- Rain attenuation tables which assign coefficients based upon frequency and polarization, and
- Rain rate tables based upon thunderstorm and similar high rain rate activity in all worldwide regions.

Of course, equipment, antenna system, and infrastructure failures and manual intervention (switching, etc.) can also cause long-term outage, but these are not a part of these StarLink 2 two-way availability calculations. Rain outage is considered as a "self-healing" unavailability event, and unlike most other long-term outage events is predictable.

Each of these factors has been the topic of numerous studies and papers, and it is not the intent of this tutorial to provide an in-depth discussion of them. If you desire more information than is presented here, please refer to the References at the end of this tutorial.

The fade margin of a digital microwave radio path provides a "safety margin" to protect the microwave signal from the adverse effects (carrier-to-noise degradations) of multipath fading, interference, and rain attenuation. Digital microwave link fade margins are usually much smaller than for analog radio whose fade margins are often increased to provide baseband quieting (low thermal noise) even in shot and other non-fading links.

The provision of an adequate fade margin and path clearance to protect against CFM degradations and outage due to surface ducting and earth blocking, plus diversity on longer or otherwise vulnerable paths, make it possible to achieve per-hop propagation reliabilities with respect to Rayleigh-distributed multipath fading, exceeding 99.999%.

Path reliability, along with quality (RBER, %EFS, etc.), defines digital radio link performance during traffic availability periods. Path availability relates to the time a given microwave link is operational for a specified period of time, typically a year. With the exception of high-frequency (>10 GHz) microwave links in rain areas, the availability objective of most microwave links is 100%. Predicted (measured) only during available (traffic connected) periods, path reliability is a measure of annual short-term (<10 CSES) one-way multipath fade outage occurring over a 2-4.5 month fade season.

Table 1: Rain Availability, Multipath Reliability, and Outage Time

Annual Rain Availability or Path Reliability, %	Outage Time %	Outage Time* per Year	3 Month Fade Period	Fade Period Month (Avg.)	Fade Period Day (Avg.)
90.0	10.0	876 hrs	876 hrs	292 hrs	10 hrs
95.0	5.0	438 hrs	438 hrs	146 hrs	5 hrs
98.0	2.0	175 hrs	175 hrs	58 hrs	2 hrs
99.0	1.0	88 hrs	88 hrs	29 hrs	1 hr
99.9	0.1	9 hrs	9 hrs	3 hr	6 min
99.99	0.01	52 min	52 min	18 min	35 sec
99.999	0.001	5 min	5 min	106 sec	4 sec
99.9999	0.0001	32 sec	32 sec	11 sec	1 sec

* Rain outage is distributed over an annual period, perhaps averaged over 10 or more years. Multipath outage is assumed to occur during a worst month (ITU) or over a fade season (3 months @ 100C/500F, for North American model calculations).

In this section, the fractional probability of outage, U or SESR (severely-errored second ratio), is used rather than percentage probability. This is the probability of an outage occurrence, known internationally as the Severely-Errored Second Ratio or SESR. The fractional "reliability" parameter, A is equal to (1-SESR). The percent reliability, as used in microwave radio, is equal to 100 (1-SESR). $100 \cdot (1-SESR)$

Availability is sometimes incorrectly expressed as a percentage synonymous with path reliability. A microwave link becomes "unavailable" (or "failed", disconnecting traffic) only after ten seconds of continuous outage (>10 CSES), such as with a typical rain outage event, whereas each second of multipath outage (up to ten continuous SESs) only degrades path reliability. Message (VF or data) traffic is lost or disconnected only with long-term unavailability events, not short-term SES outage events.

North American Outage Calculations

In North America, the equation for the probability of short-term outage in a non-diversity path during the fade season is as follows [10]:

10^{-5} D^3 $10^{-CFM/10}$

Und (SESR) = c f/4 10-5 Dmi3 10CFM/10

where Und = one-way probability of outage (SESR) for a non-diversity path

f = frequency, GHz

Dmi = path length, miles

CFM = composite or thermal (flat) fade margin, dB

c = climate/terrain factor (see c-factor pull-down maps)

= 6: influenced by surface ducting (flat, very humid)

= 4: average terrain, very humid climate

= 2: average terrain, humid climate

= 1: average terrain, average climate

= 0.25: mountainous terrain and dry climate

or **c = x(w/50)-1.3** $C = X \cdot \left(\frac{w}{50}\right)^{-1.3}$ $C = X \cdot \left(\frac{w}{50}\right)^{-1.3}$

$X = 2$ very humid
1.4 humid
1 average
0.5 dry

where x = climate factor: 2, 1.4, 1, or 0.5 for very humid, humid, average, and dry climates

= c½ from map, except when c = 6, x = 2

w = average terrain roughness over a 20-140 ft range, from the path profile (50 ft is average terrain). The tilting ground of a high/low path computes to a large w even if the terrain is smooth, for c = 0.52 maximum even in very humid areas.

Also **Und (SESR) = c f 6 x10-7 Dkm3 10CFM/10**

C climate 0.5 Southwright 2

where Dkm = path length, kilometers

c = either from the above, or computed as c = x (S/15)-1.3

S = terrain roughness, 6-42m range from the path profile

x = climate factor (see following conversion table)

ITU-R REP. 338 Severely-Errored Second Ratio (SESR) Calculations

StarLink 2 computes the probability of outage (SESR) for international non-diversity radio-relay links as follows:

Und (SESR) = K•Q f Dkm3 10CFM/10

where Und (SESR) = one-way probability of outage (SESR) for a non-diversity path

f = frequency, GHz

Dkm = path length, km

CFM = composite or thermal (flat) fade margin, dB

K•Q = geoclimatic factor (see K•Q factors pull-down maps)

= x(S-1.3)

x = climate factor

= 4.1x10-5: Maritime climate, coastal with surface ducting (flat, very humid, high temperature)

= 3.1x10-5: Maritime sub-tropical

= 2.1x10-5: Continental temperate or mid-latitude inland

= 1x10-5: High, dry, mountainous

S = Average terrain roughness, 6-42m (20m average terrain)

ITU-R Climate Regions	ITU-R Climate, x	North American Climate, x
Maritime temperature coastal or high humidity temperature	4.1x10-5	2.0
Maritime sub-tropical	3.1x10-5	1.4
Continental temperate or mid-latitude inland	2.1x10-5	1.0
High-dry mountainous	1.0x10-5	0.5

For microwave systems needing the added protection of diversity (e.g. space diversity) to meet outage objectives, the calculation for Und, the non-diversity outage probability, is identical to that above. Diversity provides an improvement to the path reliability (reduces outage time). The probability of outage (SESR) or "unreliability" for a diversity system is calculated based on the following formula [12]:

Ud (SESR) = Und/Id

where Id = Diversity Improvement Factor

The diversity improvement factor differs for each type of diversity - space, frequency, hybrid, multiline, etc.

Space Diversity Improvement Factor

The diversity improvement factor, Isd for space diversity, is shown below:

Isd = 7x10-5 f s2 10FM'/10 /D

$$\frac{7 \cdot 10^{-5} \cdot f \cdot s^2 \cdot 10^{\frac{FM'}{10}}}{D}$$

$$\frac{7 \cdot 10^{-5} \cdot F_{GHz} \cdot S^2 \cdot 10^{\frac{DIV\ TFM}{10}}}{10}$$

where Isd = space diversity improvement factor

f = frequency, GHz

D = path length, miles

s = vertical antenna spacing, feet

FM'= fade margin associated with the diversity antenna. FM' is introduced when the fade margin differs between the main and diversity paths. In such cases, StarLink 2 will take FM as the larger of the two fade margins used in calculating Und for the path. FM' is then the smaller of the two fade margins used to calculate Isd.

and **Isd = 1.2x10-3 f s2 10FM'/10/D**

where D = path length, kilometers

s = vertical antenna spacing, meters

Angle Diversity Improvement Factor

StarLink 2 diversity improvement calculations do not accommodate Angle Diversity, a method of improving path reliability with a special antenna now rarely used. The angle diversity antenna has two feeds vertically offset by about 1o (the smaller the better) in a single antenna. Angle diversity is occasionally suggested as a substitute for the venerable two-dish space diversity scheme where tower loading, aesthetics, antenna heights, and tower or building space is limited. Angle diversity is most effective when path outages are dominated by dispersive fade activity (dispersive fade outage greater than flat fade outage).

However, digital radios are now far more robust to dispersive fade activity, i.e. have DFMs some 20 dB higher, than the 1980s digital radios which inspired the wide use of angle diversity antennas. When

used, an angle diversity improvement factor Iad may be assigned, but some extended period of exacting antenna alignment to the path's geoclimatic conditions may be required for optimum Iad.

Self-Healing Ring "Route Diversity") Improvement Factors

Ring (loop) systems will automatically route T1 and E1 trunks away from fading microwave paths, and therefore improve the performance (reduce outage) in these networks. While "route diversity" improvements are not in StarLink 2, an Isr = 20 is typical for ring systems.

Frequency and Hybrid Diversity Improvement Factors

Frequency and hybrid diversity improvements are computed in StarLink 2 for links in regions where regulatory rules so permit. The hybrid diversity improvement factor, Ihd, is derived from the space diversity improvement Isd shown above and the frequency diversity improvement factor Ifd described below:

SPACE FREQ

Ihd = Isd + Ifd

$I_{hd} = I_{sd} \cdot I_{fd}$?

Above 3 GHz, Isd is always higher (better) than Ifd unless the diversity spacing, Δf, exceeds about 5% (300 MHz/0.3 GHz in the 6 GHz band, for example). Below 3 GHz, Ifd is usually larger than Isd and is therefore selected by StarLink 2.

The higher T/R frequencies must always be assigned to the upper antenna at the space-diversity (usually the lower) end of each hybrid diversity link for optimum performance.

The frequency diversity improvement factor, Ifd, is as follows:

Ifd = 50 Δf 10CFM/10 /f2 Dmi

where	Δf	=	diversity spacing, GHz
	f	=	frequency, GHz
	Dmi	=	path length, miles
	CFM	=	flat or composite fade margin. dB

and **Ifd = 80 Δf 10CFM/10 /f2 Dkm**

where	Dkm	=	path length, kilometers

$\left(\frac{df}{f}\right) \cdot 10^{\frac{TFM}{10}}$

$I_{fd} = \frac{50 \cdot \Delta f \cdot 10^{\frac{CFM}{10}}}{f^2 D_{mi}}$

The performance objectives are defined as the SESR (severely-errored second ratio) objective for ITU-R links and systems. No further calculation of actual outage time over a measurement period (e.g., month, year) is necessary. As will be discussed later, the ITU any- or worse-month objective [2] for a microwave system is:

SESR Objective = 0.00054 x Dkm/2500

Where Dkm = Path or system length, km

Although it is not required in ITU calculations, the actual outage time over a one-month period can be computed by multiplying the probability of outage, SESR, times the number of seconds in a month (2.6 x106). Annual outage in an ITU link or system amay be computed from the following North American procedure.

In North American calculation procedures, the annual outage time due to multipath fade activity in a microwave link is computed over a one-year period. In this calculation, actual outage is defined as that occurring over a 2-4.5 month "fade season":

T = U To t/50

where T = annual outage, SES/yr

To = fade season taken as three months (a combination of two severe and two moderate fade months, or 8x106 seconds

U = SESR = non-diversity or diversity probability of outage

t = average annual temperature, oF, extends the fade season in warmer areas and shortens it in cooler climates (35o<t<75oF)

North American Multipath Outage (and Path Reliability) Objective

The most common short-term one-way outage objective for a T1/E1 trunk, regardless of system length, is about 1600 outage seconds per year (SES/yr), or 99.995% end-to-end propagation reliability. This is as equally true of a 5-hop short-haul system as a 150-hop long-haul system, except that in a very long-haul (perhaps >50 hop) system, only half of the hops are considered as fading. A 99.999% per-hop reliability (320 SES/yr outage) objective (floor) is often assigned to spur links and short systems of less than about 5 tandem hops.

Although computed over the fade season, this is considered an annual outage compared, perhaps, to Bell short-haul (<400 km/250 mile), Bell long-haul (6400 km/4000 mile), or other end-user objective.

ITU-R SESR (probability of multipath outage) Objective

As discussed in the previous section, the ITU objective [2] is SESR = 0.0054 x Dkm/2500.

Rain Outage and Availability Objective

The long-term rain outage in a high frequency (>10 GHz) microwave link is often engineered to this same 99.995% objective - now an annual two-way rain availability, not one-way multipath reliability, objective. This corresponds to an ITU-R per-hop availability objective since the 60-hop 2500 km ITU-R reference circuit end-to-end two-way availability objective of 99.7% [1] scales to 99.995% availability objective for a typical 40 km link.

The 1600 SES/yr outage objective for a system (one-way T1 trunk) may be over links making up a part or whole of a long-haul system, a short-haul system, or other distance. While the following computations are for link(s) making up a full short- or long-haul system, the 1600 end-to-end SES/yr outage allocation may be proportioned only to the actual number of tandem hops in an actual system. For example, 1600/20 = 80 SES/yr (99.99975% path reliability) per-hop objective for a 20-hop digital microwave system.

The Bell short-haul one-way T1/E1 trunk outage objective (at its 10-3 BER SES outage point) is defined as:

T (short-haul) = 1600 x Dmi/250, SES/yr
= 6.4Dmi

where Dmi = System (T1/E1 trunk) length, miles

T (short-haul) = (1600 Dkm/400), SES/yr
= 4Dkm, SES/yr

where Dkm = System (T1/E1 trunk) length, kilometers

The AT&T long-haul one-way outage is defined as:

T (long-haul) = 1600 Dmi/2000, SES/yr
= 0.8Dmi

where Dmi = System (T1/E1 trunk) length, miles

T (long-haul) = 1600 x Dkm/3200 SES/yr
= 0.5Dkm

where Dkm = System (T1/E1 trunk) length, kilometers

The ITU-R probability of outage (SESR) objective [2] for a high-grade reference 2500 km/1500 mi system (E1 trunk) length is:

U (SESR) = 0.00054 x Dkm/2500

where

U (SESR)	=	Probability of outage
Dkm	=	System (E1 trunk) length, kilometers

Although neither any-month nor annual outage seconds (SES/month or SES/year) are specified as an objective (only U), T may be computed from U:

Tmo = U (SESR) x 2.6x106

Tyr = Tmo 3 t/50

where

Tmo	=	outage objective, SES/month
Tyr	=	outage objective, SES/yr
t	=	average annual temperature, oF
	=	1.8 0C + 32

$U = 0.00054 \cdot \frac{D_{km}}{2500}$

$T_{mo} = U \cdot 2{,}600{,}000$

$T_{yr} = T_{mo} \cdot 3 \cdot \left(\frac{t_F}{50}\right)$

16 SES/yr

1.8 · 15 + 32

15°C

59°F

$T_{mo} = U_{SESR} \cdot 2.6 \cdot 10^6$

$T_{mo} = U_{SESR} \cdot 2{,}600{,}000$

SES per year $= T_{mo} \cdot 3 \cdot \left(\frac{t}{50}\right)$

$T_{mi} = 8.045$ km

ITU = 16 SES

$B_S = 32$

$B_L = 4$

8 km

0.00000172 8

X 260000

4.49 T_m

X T_{yr}

In considering how to establish realistic outage or reliability objectives, several things need to be kept in mind. A single overall design objective for not more than X hours, minutes, or seconds outage over some period such as a year is an over-simplification. The character of the particular kind of outage and its effect on the system should be taken into account, and perhaps there should even be different objectives for different types of outage.

For example, propagation outages due to multipath fading are usually short. An outage of an hour per year due to multipath might represent 1,000 or more individual outages, each averaging 1 second or less (1 SES) on a properly engineered path. On the other hand, propagation outages totaling an hour per hop due to rain attenuation might consist of four or five individual outages averaging ten to fifteen minutes each. The effects of long-term and short-term system outage on message trunks are very different. Short-term "unreliability" outage events do not disconnect circuits nor reduce (in most circuits) data throughout. Long-term "unavailability" events cause both traffic disconnect and loss of data throughput.

A distinction should be made between communication circuits for which an outage of a few seconds or a few minutes is just a nuisance or an inconvenience, and circuits for which such an outage might result in danger to life, great economic loss, or other catastrophic consequences. The suitability or unsuitability of a rain-affected band such as 18 or 38 GHz could differ widely for these two situations.

Even if the maximum possible reliability and availability objectives are established and a path or a system is engineered to the full limit of the state of the art, the probability of outage can never be eliminated but only reduced to a very low value. Thus it is imperative to make any ultra-important services as fail-safe as possible against a loss of the communications channel. Therefore, regardless of the degree of reliability a system should be engineered so that if an outage does occur it can be tolerated or at least its effects at least kept within acceptable bounds.

It seems that in some cases, perhaps many cases, a more relaxed attitude might be taken toward rain-induced outages than toward multipath outages or even equipment outages. In several respects, rain outage is somewhat benign in nature. If the fade margins are kept high and the paths are not stretched out too much, even in less advantageous areas the number of outages per year should not be very large and the length of individual rain outages on a hop should only rarely exceed five to perhaps ten minutes.

Short (less than 2-second) microwave outages, common on a typical longer diversity or a shorter non-diversity digital microwave link with adequate fade margin, will not drop any telephone or data lines. Such outages quickly clear with all circuits remaining connected and little note taken of these transient events. Critical real-time, non-repeatable control or data blocks are usually sent over data circuits that have X.25, X.35, etc. error detection which requests a resend of interrupted data from far-end buffers. Longer outages associated with low fade margins, rain, etc. disconnect all subscribers and may block access to the digital link for at least 10 seconds after each long-term outage event. Such traffic disconnects are unacceptable to most users. These more vulnerable links clearly require diversity or ring protection.

For high reliability links (usually in long-haul systems with a many hops in tandem), the per-hop objective may be approach or exceed 99.9999%, allowing only 20-30 seconds per-hop outage per year. Short-haul systems, up to about ten hops, often have a per-hop design objective of about 99.9995%, for 160 SES/yr outage. Spur legs or short systems with 2-5 hops may be designed for something on the order of 99.999% per-hop path reliability equating to 320 SES (5.3 minutes) outage per year. Such objectives such as these are typical of those used in telephone, utility, and public

safety networks. For other services even dramatically lowered path reliabilities may be acceptable, even approaching 99.99% or about 1 hour outage per year.



It is important to note that StarLink 2 path reliability formulas and methods are for calculating short-term one-way outage. To calculate two-way outage it is necessary to double the calculated multipath outage. Unavailability outages due to rain fading do not have to be doubled since they occur simultaneously in both directions of transmission and are always two way.

The principal gaseous absorption is by oxygen and water vapor. The attenuation due to oxygen is relatively constant in the 2 to 14 GHz frequency range. Water vapor absorption, on the other hand, is highly dependent on the frequency, as well as to the density of the water vapor (absolute humidity, gm/m3) [4]. The following formulas from ITU-R Report 719-1 [3] have been incorporated into StarLink 2 for the purposes of calculating the attenuating effect of oxygen and water vapor within an accuracy of within ± 0.2 dB when compared to later ITU-R models:

Aoxy = [6.6/(f2+0.33) + 9/((f-57)2 + 1.96)] f2 10-3, dB/km

where f = frequency, GHz

Awv = [0.067 + 2.4/((f-22.3)2 + 6.6) f2 p 10-4, dB/km

where f = frequency, GHz

p = water vapor density, gm/m3

= 7.5 (ITU-R typical value corresponding to 50% humidity at 16oC or 75% humidity at 10oC is used in StarLink 2)

Heavy rainfall, usually in cells accompanying thunderstorm activity, has a great impact on path availability above 10 GHz in some areas, and this long-term (5-15 min) outage time causes traffic disconnects. Such long-term outage is never added to short-term multipath outage previously discussed. Rain outage increases dramatically with frequency, and then with path length. Increased outage at 23 GHz can require a 2-to-1 reduction in path length compared to 18 GHz for a given availability, for example. Extended 10-15 minute duration fades to over 50 dB have been recorded on a 5 km/3 mi 18 GHz path in Houston, for example. The predicted annual outage may not occur for years, and then accumulate over a single rainy season for a long-term average.

Early studies, both theoretical and experimental, resulted from the recognition of the importance of rain in designing microwave paths with availability objective in excess of 99.9%. In recent years the emphasis has been on establishing predictive techniques for the statistical estimation of the attenuation probability distribution for a particular path. R. K. Crane [8] has developed a model for determining the attenuation due to rain based on several factors, including path length, frequency, and point rain rates. These have been incorporated into StarLink, with Crane's formulas:

$$A(\%) = aRB(\%)[(euBd-1)/uB) - (bBecBd)/cB) + (bBecBD)/cB]$$

where A(%) = rain attenuation, dB, exceeded (%) of the time
R(%) = rain rate, mm/hr, exceeded (%) of the time
D = path length, kilometers
u = (ln becd)/d
b = 2.3 R(%)-0.17
c = 0.026 - 0.03 ln R(%)
d = 3.8 - 0.6 ln R(%)
a = multiplier, function of frequency and polarization
B = exponent, function of frequency and polarization

A greatly simplified rain attenuation (A%) model has been provided in ITU-R Rec. P.530 with its latest change provided in P.530-8. The highly simplified P.630 model lends itself to calculator methods of computation, and provides A(%) values comparable in most rain regions but widely different in others. StarLink 2 uses the above Crane model, not the ITU-R P.530 model.

$$A = aRB\left[\left(\frac{e^{uBd}-1}{uB}\right) - \left(\frac{bBe^{cBd}}{cB}\right) + \left(\frac{bBe^{cBD}}{cB}\right)\right]$$

$$u = \left(\frac{\ln be^{cd}}{d}\right)$$

Rain attenuation at the higher microwave frequencies has (>10 GHz) been under study for more than 50 years. Much is known about the qualitative aspects, but the problems faced by the microwave transmission engineer - who makes quantitative estimates of the probability distribution of the rainfall attenuation for a given frequency band, polarization, path length, and geographic (rain distribution rate) area - remains more difficult.

In order to estimate this probability distribution, instantaneous rainfall data is needed. Unfortunately, the available rainfall data is usually in the form of a statistical description of the amount of rain which falls at a given measurement point over various time periods - generally at least an hour in length.

The rain-induced attenuation along a given path at a given instant in time is a function of the integrated effect of the rainfall existing at all points along the path. Rain attenuation is affected not only by the total amount of water in the path at that instant, but also by its distribution along the path in volume and drop size. For heavy rain rates, the instantaneous distribution of volume and drop size along the path is highly variable and is difficult to predict with any sort of accuracy from the kind of rainfall data generally available.

One of the earliest and most comprehensive attempts at developing a workable prediction method was carried out by Bell Laboratories in the 1950s, and was described in a classic paper by Hathaway and Evans (1958). A method of predicting annual outages for microwave paths operating in the 11 GHz common carrier band as a function of path length, fade margin, and geographical area within North America was developed in this paper.

This study has proved to be a worthwhile prediction tool and, even considering its limitations, is still one of the best references available for microwave engineers working within the United States. Additional studies have been conducted in Europe and Asia. The combined information has been reviewed and published by R. K. Crane [8] for North American paths and internationally in the ITU-R Recommendations [5]

Increasing the fade margins, shortening path lengths, and increasing antenna sizes are the most readily available tools for reducing the per-hop rain outage in a given area. Route diversity (ring protection) or a lower, less vulnerable frequency band is often considered.

The total annual rainfall in an area has little relation to the rain attenuation for the area. Within the U.S., for example, the northwestern states have the greatest annual rainfall (in excess of 100 inches/2500 mm per year) produced, however, by long periods of steady rain of relatively low intensity at any given time. Other areas of the country with lower annual rates experience thunderstorms and frontal squalls that produce short duration rain rates of extreme intensity. It is the incidence of rainstorms of this type that determines the rain rates for an area and thus the high-frequency microwave link's long-term path outage ("unavailability") characteristics.

Even the rain statistics for a day or an hour have little relationship to rain attenuation. A day with only a fraction of an inch/centimeter of total rainfall may have a path outage due to a short period of concentrated, extremely high intensity rain. Another path that has days with several inches/centimeters of total rainfall may experience little or no path attenuation because the rain is spread over a long time period or area.

The most common reason a preference for lower frequencies is the susceptibility of bands above 10 GHz to rainfall attenuation. Although the effect is present to some degree at lower frequencies, it

increases rapidly with frequency. For example, a raincell intensity causing only a few dB of attenuation at lower frequencies could be sufficient to cause a path outage at 18 GHz.

Although fades caused by raincells are occasionally observed at lower frequencies (10-20 dB fades at 6 GHz have been recorded even in North America), this type of fade generally causes outages only on paths above 10 GHz. The outages are usually caused by blockage of the path by the passage of raincells (thunderstorms, etc.), perhaps 4-8 km/2.5-5 mi in diameter and 5-15 minutes in duration on the path. Such fading exhibits fairly slow, erratic level changes, with rapid path failure as the raincell intercepts the path. The fades are nonselective in that all main and diversity paths in both directions are affected simultaneously.

Vertical polarization is far less susceptible to rainfall attenuation than horizontal polarized frequencies. Increased fade margin is of some help in rainfall attenuation fading; margins as high as 45 to 60 dB, some with ATPC, have been used in some highly vulnerable links for increased availability. When permitted, seldom-used crossband diversity is totally effective - the lower frequency path is stable (affected only by multipath fading) during periods when the upper frequency path is obstructed by raincells. Route diversity (ring-protected paths separated by more than about 8 km/5mi) is also used successfully.

In summary, things to bear in mind in connection with rain attenuation fades are:

- Multipath fading is at its minimum during periods of heavy rainfall with well aligned dishes, so the entire path fade margin is available to combat the rain attenuation (wet-radome loss effects are minimized with shrouded antennas).

- Neither space diversity nor in-band frequency diversity provides any improvement against rain attenuation.

- Vertically-polarized high-frequency link rain outage is 40-60% less than those links horizontally polarized.

1. ITU-R Rec. F.557-4, "Availability Objective for Radio-Relay Systems", Geneva, 1997.
2. ITU-R Rec. F.634-4, "Error Performance Objectives for Radio-Relay Links Forming Part of a High-Grade Circuit", Geneva, 1997.
3. ITU-R Rec P.676-3, "Attenuation by Atmosphere Gases ", Geneva, 1997.
4. ITU-R Rec. P.836-1, "Surface Water Vapor Density", Geneva, 1997.
5. ITU-R Rec. P.837-1, "Characteristics of Precipitation for Propagation Modeling", Geneva, 1997.
6. ITU-R Rep. 338-6, "Propagation Data and Prediction Methods Required for Terrestrial Line-of-Sight Radio-Relay Systems", Geneva, 1990.
7. U.S. Department of Commerce Special Publication No. 8, "Formulas and Tables for the Computation of Geodetic Positions", C&GS, Washington, DC, 1963.
8. R. K. Crane, "Prediction of Attenuation by Rain", Proc. IEEE Trans. on Communications, September, 1980.
9. R. U. Laine, A. Ross Lunan, "Digital Microwave Link Engineering - Performance Definitions and Objectives", ENTELEC '94 Conference, San Antonio, TX, March 1994.
10. R. U. Laine, A. Ross Lunan, "Digital Microwave Link Engineering - Performance Predictions and Path Calculations", ENTELEC '95 Conference, Houston, TX, April 1995.
11. R. U. Laine, A. Ross Lunan, "Digital Microwave Link Engineering - Path Alignment, Testing, and Troubleshooting", APCO '94 Conference, Pittsburgh, PA, August 1994.
12. R. U. Laine, A. Ross Lunan, "Digital Microwave Link Engineering - Protection Schemes and Diversity Arrangements", APCO '95 Conference, Detroit, MI, August, 1995.
13. S. H. Lin, "Measured Relative Performance of Antenna Pattern Diversity, Antenna Angle Diversity, and Vertical Space Diversity in Mississippi", IEEE Globecom '88, Hollywood, FL, November 1988
14. W. D. Rummler, "Advances in Microwave Radio Route Engineering for Rain", ICC 87, Seattle, WA, June 1987.
15. A. Vigants, "Space Diversity Engineering", Bell System Technical Journal, Vol. 54, No. 1, January 1975.
16. ITU-R Rec. P.530-8, "Propagation Data and Prediction Methods Required for the Design of Terrestrial Line-of-Sight Systems", Geneva, 1999.

POINT RAIN RATE (Rp) Distribution Values (mm/hr) versus percent of Year RAIN RATE is Exceeded

RAIN CLIMATE REGIONS

Percent of Year	A(1)	B(2)	C(3)	D1(4)	D2(5)	D3(6)	E(7)	F(8)	G(9)	H(10)
0.0010	28.0	54.0	80.0	90.0	102.0	127.0	164.0	66.0	129.0	251.0
0.0020	24.0	40.0	62.0	72.0	86.0	107.0	144.0	51.0	109.0	220.0
0.0050	12.0	26.0	41.0	50.0	64.0	81.0	117.0	34.0	85.0	178.0
0.0100	**15.0**	**19.0**	**28.0**	**37.0**	**49.0**	**63.0**	**98.0**	**23.0**	**67.0**	**147.0**
0.0200	12.0	14.0	18.0	27.0	35.0	48.0	77.0	14.0	51.00	115.0
0.0500	8.0	9.5	11.0	16.0	22.0	31.0	52.0	8.0	33.0	77.8
0.1000	6.5	6.8	7.2	11.0	15.0	22.0	35.0	5.5	22.0	51.0
0.2000	4.0	4.8	4.8	7.5	9.5	14.0	21.0	3.2	14.0	31.0
0.5000	2.5	2.7	2.8	4.0	5.2	7.0	8.5	1.2	7.0	13.0
1.0000	1.7	1.8	1.9	2.2	3.0	4.0	4.0	0.8	3.7	6.4
2.0000	1.1	1.2	1.2	1.3	1.8	2.5	2.0	0.4	1.6	2.8

Information contained in the table above is from Predictions of Rain Attenuation, by Robert K. Crane for North A.

You can access the **Path Reliability Calculations** form:

- by selecting a path on the **Snapshot** form and clicking the **Path Reliability Calculations** button;
- or by selecting the **Project Menu**, then the **Path Reliability Calculations** submenu.

Path reliability and availability calculations are the main features of StarLink 2. In order to proceed, you will be required to make some choices and input some general and specific information.

All **Required Inputs** appear in white on the form. They are grouped into logical units, within frames that are labeled for easy navigation within the form. Below is a summary list of the inputs:

Radio Equipment

- **Type**
- **Capacity in T1s or E1s**
- **Frequency Band**
- **Protection configuration or non-protected**
- **Power level**

Antennas

- **Size and gain**
- **Centerline**

Transmission lines

- **Type**
- **Length**

Climate-related data

- **Climate-terrain factor: c-factor with or without "w", terrain roughness , in North America; KQ with "S", terrain roughness, in ITU-R regions**
- **Average annual temperature: North American model (for North American or International calculations only), to determine the length of the fade season and therefore the annual outage time and path reliability**
- **Rain zone (Crane or ITU-R)**
- **Path Polarization**

Losses

- **Miscellaneous losses**
- **Negative losses for higher fade margin or system gain in What If studies**

Space diversity protection

- **Diversity antenna(s) centerline(s)**
- **Diversity antenna(s) size(s) and gain(s)**

Frequency diversity protection

- **frequency spacing**

Hybrid (space + frequency) diversity, a very effective and economical three-antenna/path diversity arrangement, is also available for Harris medium and high capacity radios Hybrid diversity requires both space diversity and frequency diversity inputs. The dual antenna end of the path is selected on this form.

All the inputs are not required for all paths. For example, rain-related data (rain region, path polarization, etc.) are required only if transmission frequency is above 10 GHz. Also, the diversity configuration (space, frequency, or hybrid) is not available for all radios nor necessary on all paths.

StarLink 2 has a built-in **AutoCalc** feature: path reliability and rain availability calculations are done as soon as all required data is entered. If any required data is either missing or invalid, a warning is displayed on the form. You may click on the warning button to display what is missing or invalid (if there are many items missing, the first 2 or 3 will be displayed).

If you change the radio equipment or the transmission frequency, some previously entered data may be no longer valid (such as antennas and feeders at the new frequency). StarLink 2 automatically detects this condition, and requires the new input(s).

Micropath® Corporation

P.O. Box 17184
Golden, Colorado 80402

• Tel: 303.526-5454
• Fax: 303.526-0202

• Web: www.micropath.com
• E-Mail: support@micropath.com

True North Azimuth —> Magnetic North Azimuth



The National Geophysical Data Center (NGDC) has an online Magnetic Declination Calculator at:
http://ngdc.noaa.gov/geomag-web

If you know the true north azimuth between two locations, it is a simple matter of adding or subtracting the magnetic declination to the true north azimuth.

Abbreviations:

MagDec	: Magnetic Declination - Degrees
AZ_TN	: Azimuth True North - Degrees
AZ_MN	: Azimuth Magnetic North – Degrees
MN	: Magnetic North
TN	: True North
ABS()	: Absolute Value
<	: Less then
>=	: Greater then or equal

Algorithm:

If MagDec < 0 (WEST) Magnetic Declination is west of 0.0 degrees true north
AZ_MN = AZ_TN + ABS(MagDec) **or** AZ_MN = AZ_TN - (-MagDec)

If MagDec >= 0 (EAST) Magnetic Declination is east of 0.0 degrees true north
AZ_MN = AZ_TN - MagDec

Example:

AZ_TN = 090
MagDec = -7.00 (WEST)
AZ_MN = AZ_TN + ABS(MagDec) **or** AZ_MN = AZ_TN - (-MagDec)
097= 090 + ABS(-7.00) **or** 097 = 090 - (-7.00)

AZ_MN = 097 degrees

If AZ_MN < 0 then AZ_MN = 360 + AZ_MN
If AZ_MN >= 360 then AZ_MN = AZ_MN – 360

References:

http://www.geog.ucsb.edu/~archer/Geog12/Lecture11.pdf

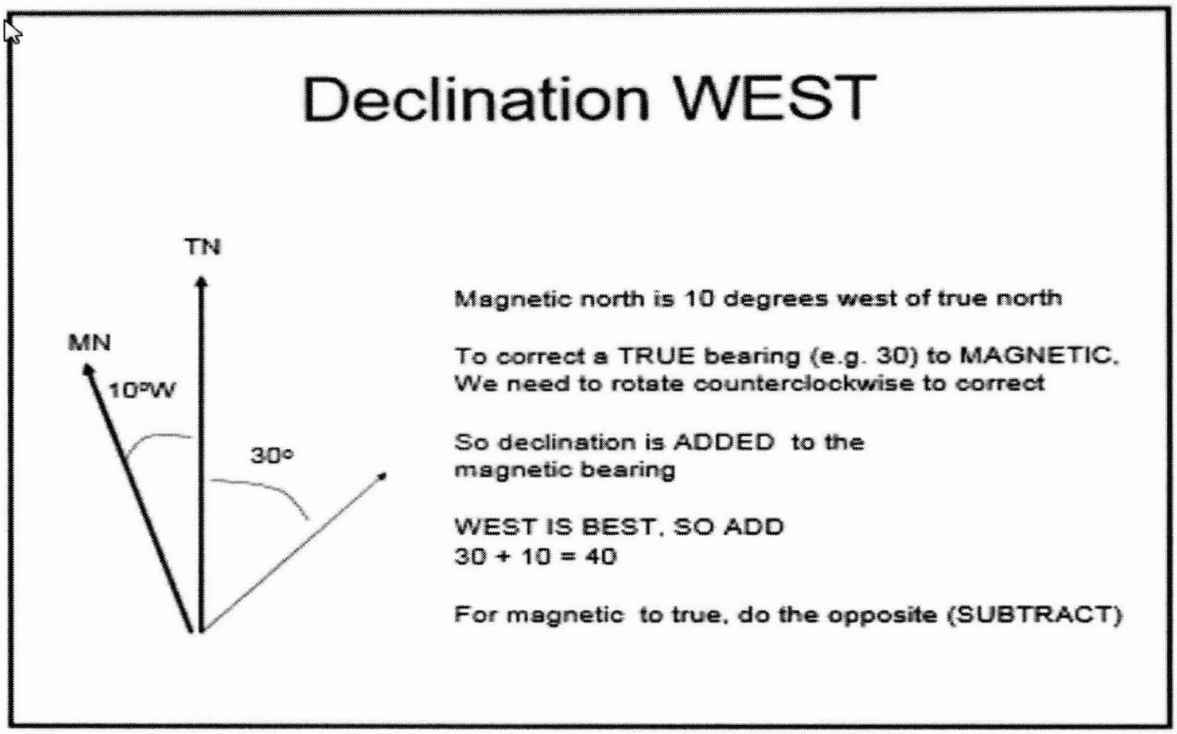

Note: The above picture denotes the Magnetic Declinaton as +10 degrees west.
Decimal magnetic declinations west of 0.0 degrees true north (TN) are negative, i.e., -10 degrees.
Decimal magnetic declinations east of 0.0 degrees true north (TN) are positive, i.e., +10 degrees.

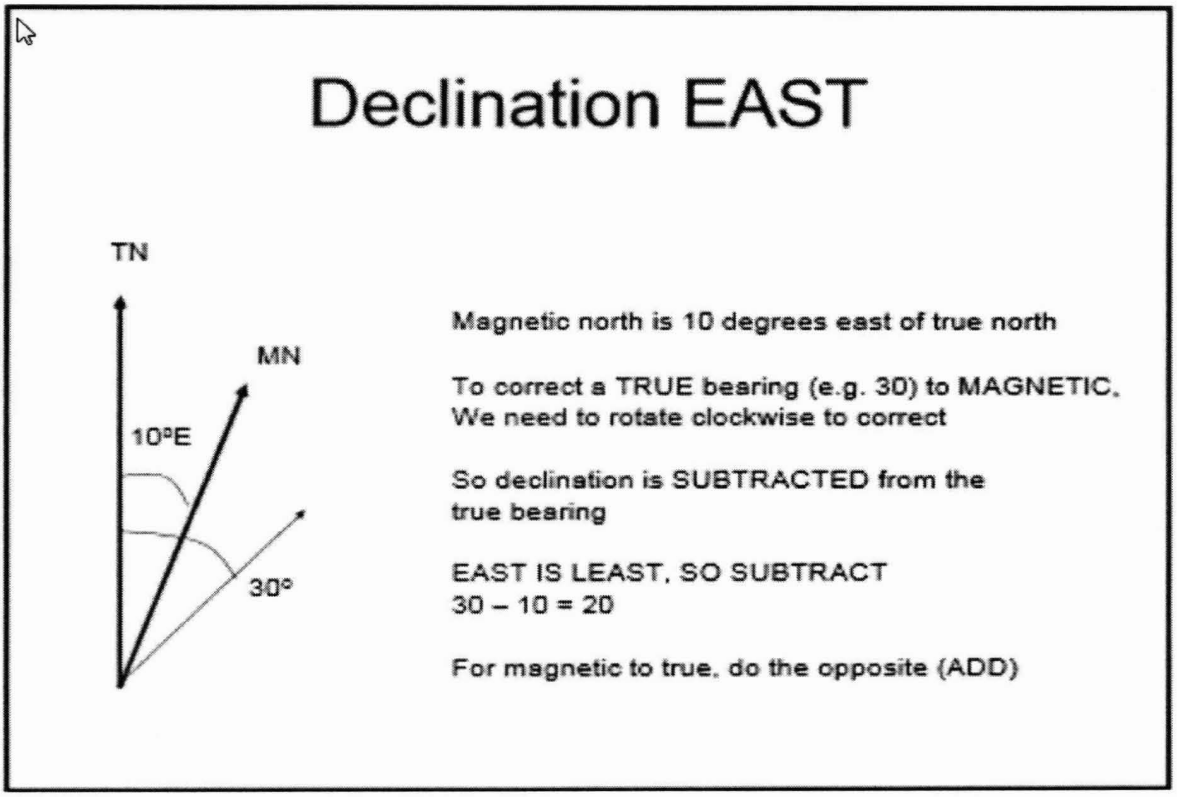

http://www.firefightermath.org/index.php?option=com_content&view=article&id=56&Itemid=70/

The magnetic reference for Earth is north regardless of whether you are traveling north or south. Magnetic declination, or declination, is the difference between the true north reading from the map and the magnetic north reading from a compass. When a compass is used in combination with a map, a correction must be made to allow for declination.

In North America, magnetic declination varies from 30 degrees East in Alaska to 20 degrees West in Labrador, Maine. The degrees of declination for an area are usually located on the bottom margin of the map near the north arrow, or they can be located using a declination chart.

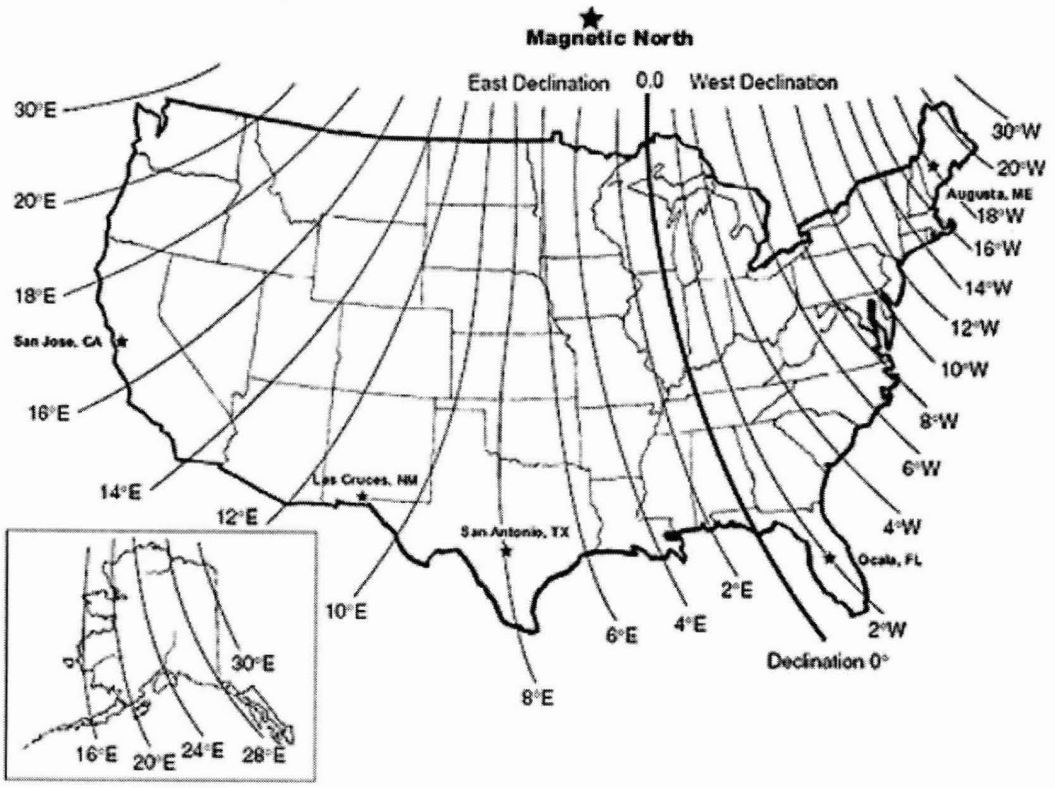

Figure 6.2—Map shows declination of the compass in North America.

The method for correcting for declination is as follows:
1. For Easterly Declination, subtract the declination from the true reading to obtain the magnetic reading. Magnetic = true - easterly declination
2. For Westerly Declination, add the declination to the true reading to obtain the magnetic reading. Magnetic = true + westerly declination

An easy way to remember whether to add or subtract is "West is best and East is least." So for West declination, add to the true reading (West is best, and therefore a larger number) and for East declination subtract from the true reading (East is least, and therefore a smaller number).

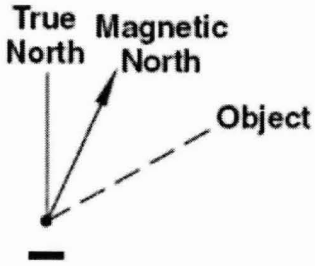

If the arrow *on the compass* is to the right of *true north*, or to the east, **subtract** the declination.

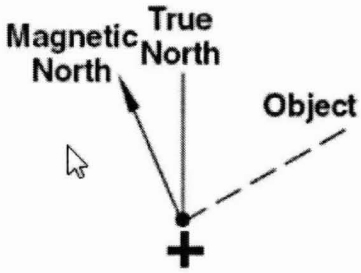

If the arrow *on the compass* is to the left of *true north*, or to the west, **add** the declination.

Example 1 - Paloma is in San Jose, California. The declination is 17°E. Paloma's compass reading from her current location to the mountain range to which she is traveling is 35°. What is her true reading?

Step 1. The declination of 17°E is an **easterly declination**.

Step 2. In this case, True - east = magnetic according to the "East is least" guideline above, so we will solve the equation for the true reading and find that true = magnetic + east. We must **add** the declination to go from the magnetic reading on the compass to the true reading.

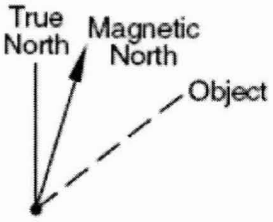

35° magnetic reading
+ 17°E declination
52° true reading

Paloma's true reading is 52 degrees.

Example 2 - Sonia is in Augusta, Maine. She has a compass with a magnetic north reading of 45°. What is her true reading on a map?

Step 1. Look up the declination for Augusta, Maine, on a declination chart. Maine has a declination of 18°W.

Step 2. Because 18°W is a westerly declination, remember "West is best" and that the magnetic = true + west. In this case, to solve for the true reading, we must subtract the declination from the magnetic bearing: true = magnetic - west.

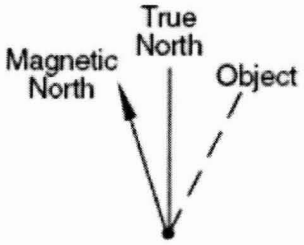

45° magnetic reading
– 18°W declination
27° true reading

Sonia's true reading is 27 degrees.

When traveling in an opposite direction and adjusting map readings for use with compass readings, do the opposite of the above for adding and subtracting the declination.

Example 3 - Roger looks at a map and takes an azimuth reading of 85°, a true reading, off the map from where he is standing to the location of a tower. The declination for the area is 12°E. What is the magnetic reading?

Step 1. In order to find the magnetic reading by using a compass, subtract the easterly declination. Remember, "East is least."

85° - 12°= 73°

Roger's magnetic reading is 73 degrees.

Microwave Link Analysis

			Site A	Site B
Site Name		:	SPAN 1A	SPAN 1B
Location		:		
Call Sign		:		
Coordinates (North American 1927, MEAN FOR CONUS)				
Latitude		:	43° 57' 41.50" N	43° 51' 01.0
Longitude		:	102° 20' 13.30" W	102° 29' 46.7
Elevation		ft/m:	2940.0 / 896.1	2880.0 / 877.
Azimuth		deg:	226.0452	45.93475
Distance		mi/km:	11.06 / 17.8	11.06 / 17.8
Frequency		MHz:	5735.0000	5800.0000
Equipment		:	AFC SSR	AFC SSR
Antenna Height - Tx / Rx / Div		ft:	80.0 / 80.0 / 120.1	50.0 / 50.0 /
Tx Antenna Type		:	Mark	Mark
Tx Antenna Size / Polarization		ft:	6.001 / V	6 / V
Rx Antenna Type		:	Mark	Mark
Rx Antenna Size / Polarization		ft:	6 / V	6 / V
Diversity Antenna Type		:		
Diversity Antenna Size / Polarization		ft:	9.8 / H	10 / H
Tx Transmission Line Length		:	75.0	85.0
Tx Transmission Line Type		:	LDF4-50A	LDF4-50A
Rx Transmission Line Length		ft:	75.0	85.0
Rx Transmission Line Type		:	LDF4-50A	LDF4-50A
Effective Isotropic Radiated Power		dBm:	53.21	53.21
System Gains			**Site A to B**	**Site B to A**
Tx Antenna Gain		dBi:	38.0	38.0
Rx Antenna Gain	Pri / Div	dBi:	38.0 / 20.0	38.0 / 15.0
Transmitter Power		dBm:	20.0	20.0
Total System Gain		dB:	96.0	96.0
System Losses			**Site A to B**	**Site B to A**
Free Space Path Loss		dBi:	132.62	132.72
Atmospheric Absorption		dB:	0.15	0.15
Tx Radome Loss	Pri / Div	dB:	0.5	0.5
Tx Connector Loss		dB:	0.29	0.29
Tx RF Branching Loss		dB:	3.0	3.0
Tx Miscellaneous & Safety Loss		dB:	1.0	1.0
Rx Connector Loss		dB:	0.29	0.29
Rx Transmission Line Loss	Pri / Div	dB:	0.0 / 15.0	0.0 / 10.0
Rx Radome Loss	Pri / Div	dB:	0.5 / 0.0	0.5 / 0.0
Rx Miscellaneous & Safety Loss	Pri / Div	dB:	1.0 / 0.0	1.0 / 0.0
Total System Loss		dB:	139.35	139.45
Path Calculations			**Site A to B**	**Site B to A**
Unfaded Receive Signal Level		dBm:	-43.35 at Site B	-43.45 at Site
Rx Threshold Level		dBm:	-85.0 at Site B	-85.0 at Site A
Fade Margin		dB:	10.48 at Site B	10.48 at Site
Outage		sec/year:	143864.0	143866.5
Rain Outage		sec/year:	0.0	0.0
Propagation Reliability		%:	99.5438104	99.5438024
Diversity			**Site A to B**	**Site B to A**
Type			Space	Space
Reliability		%:	0.0	98.5790254
Outage		sec/year:	2325079.0	448118.6
Improvement Factor		:	0.06	0.32

Outage Parameters: Vigants - Digital

Climate Factor (c)	6.000	Terrain Factor (w)	111.0	Average Temperature	30.0°C / 86.(
CFM	10.48	DFM	11.000	TFM	41.554
BER	1x10E-6	AIFM	0.000	EIFM	20.000

HARRIS

Network Engineering Paper

Digital Microwave Link Engineering – Performance Predictions and Path Calculations

Richard U. Laine, P.E.

Harris Microwave Communications Division
Redwood Shores, CA 94065

rlaine@harris.com

(650) 594-3465 (-3672 Fax)

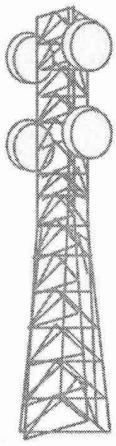

ENTELEC '95 Annual Meeting Conference Paper
Houston, TX
April 4, 1995

Digital Microwave Link Engineering - Performance Predictions and Path Calculations

Richard U. Laine, P.E.
A. Ross Lunan, P.E.

Harris Corporation, Farinon Division
San Carlos, CA 94070

Abstract

Digital microwave radio link performance is highly dependent upon the matching of path geometry (clearance, diversity configurations, and antenna heights, sizes, and alignments) to the diurnal and seasonal climatic and terrain characteristics and variabilities for the area. This paper describes enhanced transmission engineering models and techniques, compliant to newly standardized performance terms and objectives, now resident in user-friendly calculator and computer programs. With improved field survey, path alignment, and degraded performance troubleshooting procedures added to these engineering tools, compliance to user performance (outage and quality) objectives and other design goals is better assured.

This paper is one of three addressing the subject of Digital Microwave Link Engineering. The companion papers, "Performance Definitions and Objectives" [1] and "Path Alignment, Testing, and Troubleshooting" [2], complete the series.

Introduction

The availability and performance of a digital microwave radio relay link is very often contingent upon the successful marriage of robust radio equipments with optimized path engineering techniques which accommodate multipath and power fading along with the other adverse characteristics of a hostile world such as interference and long-delayed echoes. The full benefits of modern state-of-the-art radios in exceeding user expectations is only attained with the optimum selection of antenna heights, sizes, alignments, or diversity spacings matched to path geometry and atmospheric characteristics. The transmission engineer must consider local and synoptic climatic (atmospheric layering, refractive gradients, rain, weather fronts) and terrestrial (reflectivity, obstruction, moisture content) characteristics and configure the antenna systems appropriately.

Multipath Outage Models

Atmospheric and terrestrial characteristics exhibiting localized diurnal and seasonal variabilities are also influenced by weather fronts and other random occurrences. Mathematical models which take into account climatic conditions, terrain roughness, rain area (in availability computations only), path length, frequency band, fade margin, average annual temperature, and diversity arrangements as variables have evolved which accurately predict the availability and performance of microwave links worldwide.

Amongst the many available, Arvids Vigants' 1975 radio-relay link multipath fade outage model [3], based upon the fade activity on many Bell System microwave paths in the U.S. over an extended period in varied climate and terrain ambients, is the norm for most North American (NA) and international (CCIR, now ITU-R) outage prediction calculations. Diverse models proprietary to some countries are shown in CCIR Rep. 338 [4].

North American Calculations

The most simplistic adaptation of Vigants' North American model for short-term (<10 SES/fade event) non-diversity (ND) fade outage in a digital microwave link, in severely-errored seconds (SES, BER>10^{-3}) per year, is (for a 25 mi path):

$$T_{ND} = 0.4\ c\ f\ t\ D^3\ 10^{-CFM/10}$$

where, for example

T_{ND}	=	One-way outage, SES/yr
c	=	NA climate-terrain factor
	=	1 (Fig. 1), or $x(w/50)^{1.3}$
x	=	NA climate factor, 1 (Fig. 2)
w	=	Terrain roughness, 50 ft
f	=	6.7 GHz
D	=	Path length, 25 mi
CFM	=	Composite Fade Margin, 34 dB
t	=	Average annual temperature, 50°F.

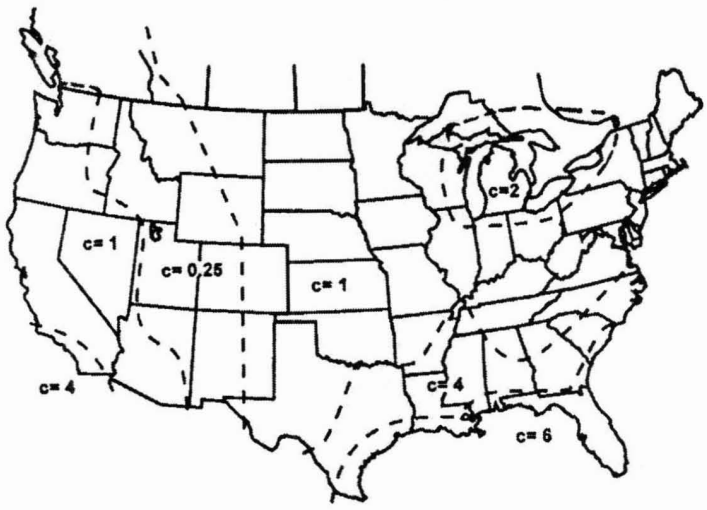

Fig. 1. NA climate-terrain factors, c (U.S.).

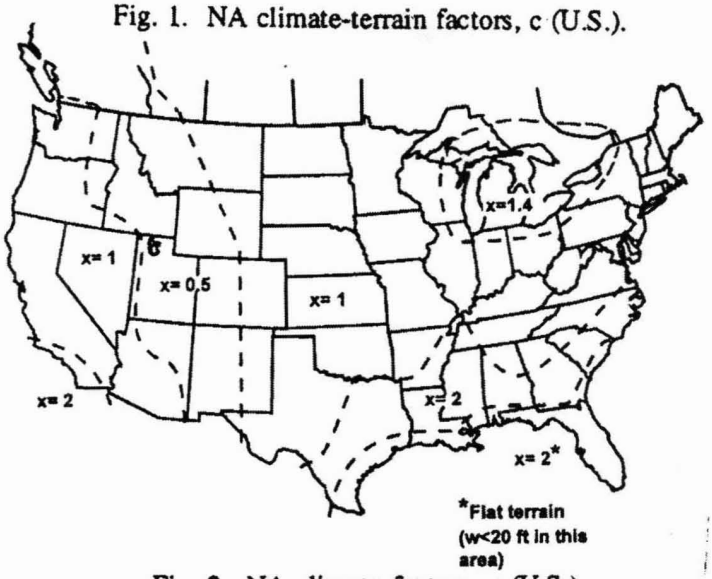

Fig. 2. NA climate factors, x (U.S.).

Therefore

T_{ND} = 834 SES/yr (99.99735% path reliability).

With space diversity (SD), this excessive outage time lowers to 20 SES/yr:

$$T_{SD} = 5.7\times10^{3}\ c\ t\ D^{4}\ 10^{-CFM/5}/s^{2}$$
$$= 5.7\times10^{3}\ 1\ 50\ 25^{4}\ 10^{-34/5}/30^{2}$$
$$= 20\ \text{SES/yr (SD dish separation s = 30 ft).}$$

This SD outage formula may be rearranged to derive the fade margin required to meet a path outage objective (20 SES/yr, in this NA example):

$$CFM = 18.8 - 5 \log (T\ s^{2}/D^{4}\ c\ t)$$
$$= 18.8 - 5 \log (20\ 30^{2}/25^{4}\ 1\ 50)$$
$$= 34\ \text{db (checks).}$$

CCIR Calculations

In CCIR computations, the fade outage in a digital microwave link, in SES/any month, is (for this same 40 km path):

$$T_{ND} = 2.6\times10^{6}\ K{\cdot}Q\ f\ D^{3}\ 10^{-CFM/10}$$

where

T_{ND} = One-way outage, SES/any month
$K{\cdot}Q$ = CCIR climate-terrain factor, $x/S^{1.3}$
x = CCIR climate factor, 2.1×10^{-5} (Table 1)
S = Terrain roughness, 15.2 m
f = 6.7 GHz
D = Path length, 40 km
CFM = Composite Fade Margin, 34 dB.

Therefore

T_{ND} = 270 SES/any month.

Climate Regions	**x (CCIR)**	**x (NA)**
Maritime temperate, coastal or high humidity/temperature	4.1×10^{-5}	2.0
Maritime sub-tropical	3.1×10^{-5}	1.4
Continental temperate or mid-latitude inland	2.1×10^{-5}	1.0
High-dry mountainous	1.0×10^{-5}	0.5
Climate-Terrain Factor (K·Q in CCIR; c in NA)	$x/S^{1.3}$	$x/(w/50)^{1.3}$

Table 1. CCIR climate factors, x, for K·Q computations (and equivalent NA climate factors).

The Model - a Closer Look

If the foregoing NA or CCIR computations meet the user's performance objectives for the link [1], the optimum configuration of the radio equipments and antenna feeder systems is then selected by the transmission engineer. These outage computations are valid only if the fade margin is not degraded by external interference, long-term power fade activity, or antenna misalignment, and that the antenna feeder systems are selected for optimum sizes, heights, diversity spacings, and alignments matched to the path's climatic and terrestrial characteristics. It is the purpose of microwave path engineering to ensure the achievement of this sometimes elusive goal.

Vigants' multipath outage model is universal, with results differing only in the outage period - annual in North American (NA) predictions, and "any month" (usually interpreted as "worst fading month") in CCIR regions (outside of Canada and the U.S.). Whether supporting NA or CCIR, Vigants' outage model yields identical probabilities of outage (U) which, when multiplied times the fade period (8×10^6 t/50 sec/fade season in NA or 2.6×10^6 sec/mo in CCIR), yields the following non-diversity path outage times:

$$U_{ND}\ (NA) = 2.5\times10^{-6}\ c\ f\ D^3\ 10^{-CFM/10}$$
$$= 2.5\times10^{-6}\ 1\ 6.7\ 25^3\ 10^{-34/10}$$
$$= 0.0001042\ (w = 50\ ft)$$

$$\text{Outage (NA)} = 0.00010419\ (8\times10^6\ t/50)$$
$$= 834\ SES/yr$$

$$U_{ND}\ (CCIR) = K{\cdot}Q\ f\ D^3\ 10^{-CFM/10}$$
$$= 2.1\times10^{-5}/15.2^{1.3}\ 6.7\ 40^3\ 10^{-34/10}$$
$$= 0.0001042\ (S = 15.2\ m)$$

$$\text{Outage(CCIR)} = 0.0001042\ (2.6\times10^6)$$
$$= 270\ SES/any\ month$$

The NA climate-terrain (c) factor is either extracted from the wide area (synoptic) map (Fig. 1) or, preferably, computed from $c = x(w/50)^{-1.3}$ where x is from the wide area climate map (Fig. 2) and w is terrain roughness (limited to a 20-140 ft range) computed from the path profile [3]. In CCIR computations, the Vigants K·Q factor in Table 1 is from the CCIR Rep. 338 table of climate-terrain types (2.1×10^{-5} for "continental temperate climates or mid-latitude inland climatic areas with average rolling terrain", for example) and S (the terrain roughness in m) is (like w, over a 6-43 m range) computed from the path profile [4]. Worldwide K·Q maps are available.

Diversity Improvements

Diversity, usually space but often frequency or hybrid diversity in CCIR regions and some NA electrical utilities, must be added to the microwave link if the non-diversity outage exceeds the user's performance objectives [1]. The reduction in non-diversity outage time is the diversity improvement factor. In North America, the computed SD outage reduction with equal gain ($v^2 = 1$) dishes spaced s = 30 ft is

$$I_{SD} = 7\times10^{-5}\ f\ v^2\ s^2\ 10^{CFM/10}/D$$
$$= 7\times10^{-5}\ 6.7\ 1\ 30^2\ 10^{34/10}/25$$
$$= 42.$$

The outage time is thus reduced to 834/42 = 20 SES/yr, as previously computed. With frequency diversity (FD), the improvement factor with $\Delta f = 160$ MHz (0.16 GHz) is reduced to

$$I_{FD} = 50\ \Delta f\ 10^{CFM/10}/f^2\ D$$
$$= 50\ 0.16\ 10^{34/10}/6.7^2\ 25$$
$$= 18\ (834/18 = 47\ SES/yr\ outage).$$

Similar CCIR improvement factors (and resulting any-month outages) are computed below (s = 9.1 m); hybrid diversity (HD) links use only I_{SD}, ignoring I_{FD}.

$$I_{SD} = 1.2\times10^{-3}\ f\ s^2\ 10^{CFM/10}/D$$
$$= 42\ (270/42 = 7\ SES/any\ month\ outage)$$

$$I_{FD} = 80\ \Delta f\ 10^{CFM/10}/f^2\ D$$
$$= 18\ (270/18 = 15\ SES/any\ month\ outage)$$

Outage Model Constraints

It is evident from the foregoing computations that:

- Any loss of fade margin (CFM) due to interference, power fading, antenna misalignment, etc. greatly increases outage time, from x10 (ND) to at least x100 (SD or FD) for a 10 dB loss in CFM.
- Doubling of path length (D) increases multipath outage x8 (ND) to x16 (SD or FD).
- Frequency (f) is irrelevant in SD links; outage time is proportional to f in ND links.
- Outage time (T) is proportional to the annual average temperature (t, NA calculations only) and to the climate-terrain characteristics (c or K·Q).
- Outages due to specular reflections from smooth terrain, exposed bodies of water, etc. are excluded from ND computations and presume optimum dish spacings in SD computations.

The accurate prediction of outage times is thus dependent upon the assignment of path clearances (especially above 3 GHz) adequate to clear atmospheric ducting layers that cause power fading, antenna heights (especially in ND links below 3 GHz) for minimum reflection fading, dish separations for uncorrelative diversity antenna fade activity, and frequency band, dish sizes, and alignments to 1) provide adequate discrimination to multipath and interfering signals and 2) accommodate widely varying incoming ray arrival angles typical of many difficult

24 dB
22 dB

climatic areas.

Path Clearance Considerations

A half-century accumulation of the fading characteristics of countless analog and digital microwave paths scattered around the world with divergent climatic and terrestrial conditions in all frequency bands and varying path lengths and clearances has established effective top-to-top (main path) clearance rules. These rules apply, of course, to "flat land" microwave links; excessive rather than inadequate clearance is the primary cause of much degraded performance between mountain top sites. The main path in these elevated links is (or should be) between the bottom dishes to maximize CFMs. The diversity paths are then to the top dishes.

The minimum clearances assigned to microwave paths are dependent upon the frequency band, a measure of path sensitivity to ground-based atmospheric boundary layering (ABL), and climate-terrain conditions (c-factor, a measure of the recurrence and severity of the ABLs, as shown in Fig. 1 and Table 1). These criteria are shown below.

Main (Top-to-Top) Path Clearance Rules

	Climate-Terrain Factor, c	
Band	<2 (good to average)	≥2 (moderate to very difficult)
Above 3 GHz	$0.6F_1$ @ k = 1	F_1 @ k = 4/3 and $0.3F_1$ @ k = 2/3*
Below 3 GHz	$0.6F_1$ @ k = 1	$0.6F_1$ @ k = 1

*If $0.3F_1$ @ k = 2/3 clearance is controlling, diversity protection is usually required.

Diversity (Top-to-Bottom) Path Clearance Rule

All bands	$0.6F_1$ @ k = 4/3	$0.6F_1$ @ k = 4/3

"Blackout" Area Main Path Clearance Rule

Above 3 GHz (>20 mile path)	N/A	k = 1 grazing over a 150 ft ABL

The purpose of these path clearance criteria is the avoidance of long-term fade margin degradations which, at the least, increase short-term multipath fade outage. In some areas, on longer paths above 3 GHz, non-compliance to these clearance rules may even result in the total entrapment, defocusing, or obstruction of the path, thus precipitating a long-term outage [2, 5].

The imminent transfer of some 2 GHz bands from point-to-point service to PCS (PCN), MSS, BAS, and emerging technologies will result in the migration of many private and public (common carrier) links from these stable bands to higher frequencies more vulnerable to performance degradations due to power fading in difficult propagation areas. Many of these displaced links will be upgraded to digital if not SONET or SDH with evermore demanding performance objectives imposed by new technologies (LAN, teleconferencing, high speed data transport, ATM, network management including SCADA, and other monitoring and control functions, etc.). Considering this, it is even more essential that the clearances and antenna configurations of these new higher frequency links accommodate the climate-terrain characteristics of the area rather than simply matching that of the more stable existing 2 GHz paths. In difficult areas, clearances on longer paths may have to increase (but could lower in other areas or on short paths), diversity dishes may be added, antennas carefully selected and precisely uptilted and, in very rare cases, path lengths shortened or systems rerouted.

The impact upon the performance of longer (>20 mi) higher frequency (usually 6-8 GHz) paths assigned inadequate clearances in difficult propagation (c≥2) areas cannot be overstated. Substandard (k<1) ABLs often accompany cold fronts, with large temperature drops, over areas with warm surface water. Deep obstruction fades may occur in these areas, causing perhaps hours of severe multipath fade activity and even long-term outages.

In other areas with "microclimates" supporting atmospheric entrapment and defocusing or "blackout" layers, the higher frequency microwave signal is not obstructed, but rather refracted away from the distant antenna or defocused (spread) much like a spot-to-flood beam adjustment on a flashlight. A notorious example of this occurs on a 55 mi microwave link across the English Channel. Even though the main (top-to-top) path met the k = 2/3rds "difficult area" clearance criterion with 800/350 ft main dish heights plus SD dishes 30 ft lower, occasional low-level ABL ducts would obliterate these upper paths. Yet, during this time a normally blocked but now high level stable path existed between a third set of diversity dishes positioned low at their 120/60 ft heights [6].

Similar entrapment atmospheres occur, again with a large nighttime temperature drop, over irrigated farmland and swamps, near warm inland lakes, bays, seas and gulfs, and in other areas well known to local microwave link operators. In these areas, some antenna heights have been successfully increased to meet the "blackout" area criterion shown on the clearance rules chart, but only after the incidence of such devastating fade activity was confirmed by operating experience on this or a nearby path similarly configured.

Path Profiles

Antenna heights and diversity dish separations selected to meet the performance objectives are based upon accurate, field-verified profles of the microwave path. In many regions, very detailed up-to-date topographic maps show not only swamps, lakes, terrain features, but also buildings, water and oil storage tanks, forested areas, tall "heritage" cottonwood trees grouped around isolated farmhouses, powerlines, and communications towers. With such accurate contour maps, field surveys often focus more on tree heights and densities (with growth), specular reflection zone characteristics, on-path building heights, atmospheric considerations (ducting caused by local ground water - shoreline, lakes, swamps, etc.), existing microwave/VHF sites (for frequencies and zoning), and building codes than on the precise verification of terrain elevations.

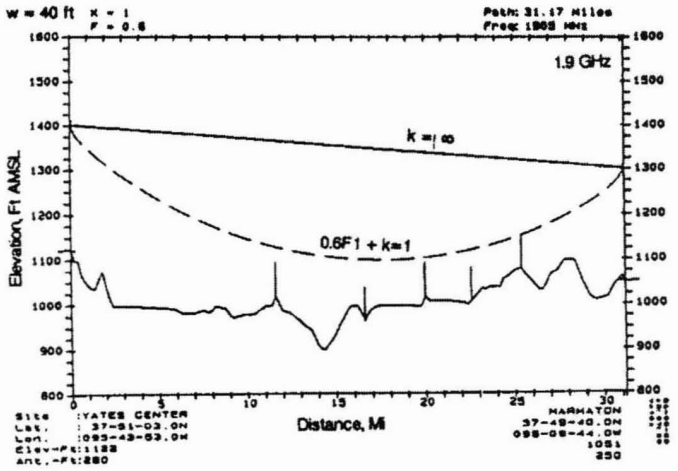

3a. Flat earth path profile.

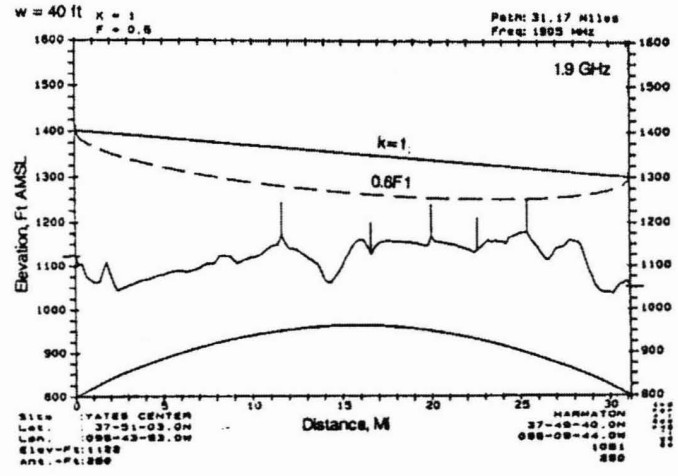

3b. True earth path profile.

Fig. 3. Profiles for a $0.6F_1$ @ k = 1 clearance criterion on a 31 mi/50 km path.

Typical field-verified path profiles in Fig. 3a (on "flat earth" k = ∞ rectangular paper) and 3b (on "true earth" k = 1 curvature paper) show main antenna heights compliant to a $0.6F_1$ @ k = 1 main path clearance criteria over a 31 mi path. These are plotted from a path profile computer program which, like other available programs, show tree growth, man-made obstructions, Fresnel zone clearances, and earth's curvature (k = 1, k = 4/3, k = 2/3, etc.). One important feature of this and some other profiling programs is the automatic computation of terrain roughness (w, over a 20-140 ft range or S, over a 6-43 m range) that could otherwise be time-consuming. Terrain roughness is an important input to the computation of an exacting climate-terrain factor used in Vigants and other microwave path outage models.

Preliminary path profiles are usually from USGS (or country-equivalent) 7.5 minute (or other) topographic maps; county/province and auto society or other local road maps (often providing urban area details down to street and building names) and aeronautical sectional, local, ONC, etc. charts are important supplements to the topographical maps.

Specular Reflections

Path profiles clearly show those terrain characteristics necessary for assigning antenna heights and diversity spacings. In the absence of flat, exposed, reflective terrain (open farmland, wasteland, swamps) or open water (lakes, shorelines, sea) with no obvious specular (mirror-like) reflection zones, "flat land" (as opposed to mountainous or elevated) paths are assigned diversity spacings adequate to meet the outage objectives (usually about 40, 30, and 20 ft in the 2, 6, and 11 GHz bands, respectively). Vigants' model for flatland path engineering limits diversity spacings to 50 ft as specular reflection fades become increasingly

correlated with larger spacings. In the mountains, as on the 60-90 mile (100-150 km) "difficult" inter-island paths in Hawaii, much larger spacings are assigned to accommodate elevated ducting and other atmospheric conditions [5].

Exposed (meaning little terrain blockage or dish discrimination to) specular reflection zones could cause deep multipath fading on each antenna. If the diversity antenna spacing is incorrect, such fading is correlated which increases path outage. Such paths must undergo a geometry analysis, a feature of some newer computer and calculator programs. Harris Farinon's MAGIC and REFL programs are examples.

Path Geometry

Very often, path geometry programs are an essential ingredient in the optimum selection of antenna heights, sizes, and diversity arrangements. Harris Farinon's HP41CX/CV (and others, such as the HP48) calculator programs input dish and reflection heights AMSL, path length, frequency, and k-factors (usually k = 4/3 and k = ∞) to derive the following important data (Fig. 4):

- location of the reflection (dish heights?)
- dish discriminations to the reflection (dish sizes?)
- Fresnel zone clearance at the reflection (diversity?)
- reflection grazing angle (V or H pol.?)
- ray height above the reflection zone
- reflected ray delay, nsec (link's DFM?)
- optimum diversity dish separations
- RSL up- or down-fade depth due to the reflection
- arrival angle change with k-factor variations (sizes?)
- obstruction loss vs. terrain ("knife-edge", etc.)

Impressive new computer profile programs now provide not only much of these data, but will "drag" an antenna up and down a tower (with a mouse-controlled cursor) and interactively display a Fresnel interference pattern vs. k-factor (path clearance) below the profile, as seen in Fig. 5.

With these data, precise antenna sizes, heights, uptilt, diversity spacings, frequency band, polarization, adaptive equalization (dispersive fade) countermeasures, and other parameters impacting upon path performance may be optimized. Some of the possible effects upon

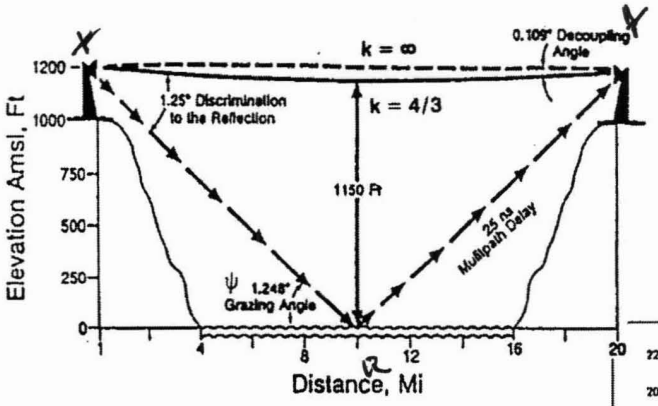

English

```
  REFLECTION OR
OBSTRUCTION, K=1.33
  (FT AMSL, MI)

X ELEV=1,200.
R ELEV=0.
  DISTANCE=20.00
Y ELEV=1,200.
  DIST XR=10.00
  DIST RY=10.00
H(R)=1,150.
ANT. DISC. :
  X,DEG=1.248
  Y,DEG=1.248
FREQ=2.000 GHZ
F(N)=101.76

SD DISH SEP:
  SD(X)=18.3
  SD(Y)=18.3
DELAY,NS=25.44
RSL(R=-1),dB=-11.32
  R,DEG=1.248
```

Metric

```
  REFLECTION OR
OBSTRUCTION, K=1.33
  (M AMSL, KM)

X ELEV=365.
R ELEV=0.
  DISTANCE=32.19
Y ELEV=365.
  DIST XR=16.10
  DIST RY=16.10
H(R)=350.
ANT. DISC. :
  X,DEG=1.246
  Y,DEG=1.246
FREQ=2.000 GHZ
F(N)=101.76

SD DISH SEP:
  SD(X)=5.6
  SD(Y)=5.6
DELAY,NS=25.44
RSL(R=-1),dB=-11.15
  R,DEG=1.246
```

Fig. 4. Geometry sketch and calculator printouts for a short 20 mi/32 km path.

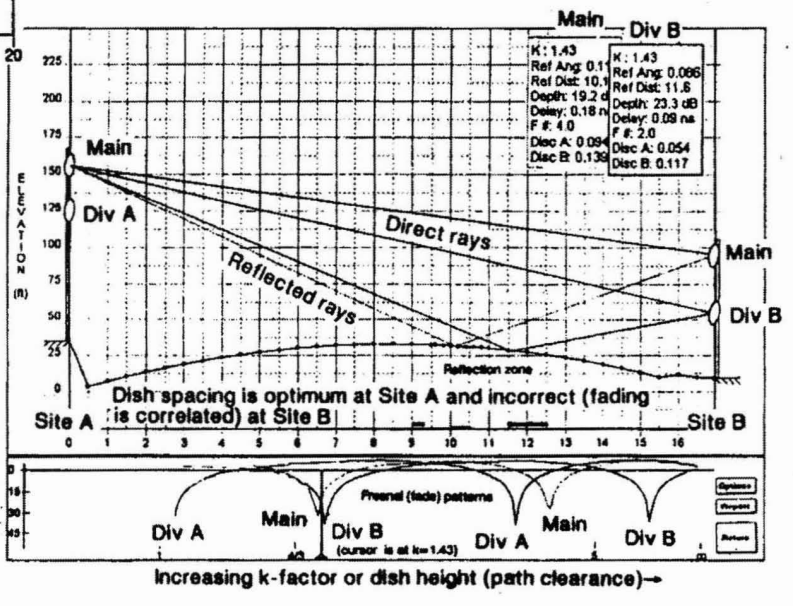

Fig. 5. Computer profile showing the main and diversity antenna Fresnel patterns on a 17 mi/27 km overwater path.

performance if bypassing a geometry study may include the following.

Antenna	Possible Consequence
Too small (for the band)	Inadequate discrimination to the reflection (increased multipath fade outages, degraded DFM)
Too large (and/or not uptilted)	Increased antenna decoupling outages with k-factor variations
Too high	Exposed to the reflection zone
Too low	Possibly obstructed or vulnerable to power fading
Improper diversity dish spacing	Correlated multipath fading and increased outage
Horizontally polarized	Deeper fading compared to V-pol (grazing angle >0.2°)

Polarization Selection

While polarization selection (V- or H-pol) is customarily considered a frequency assignment ("prior coordination") function, the performance of certain microwave links is significantly enhanced using V-pol. The two specific configurations for which this is the case is in

- high frequency (>10 GHz) links, to reduce rain outage ("unavailability") 30-60%, and
- high clearance reflective paths with large (>0.2°) grazing angles, to reduce the reflection coefficient (fade depth).

Intense rain, as often accompanies thundercells, is made up of large drops that are flattened to bean shape (wide horizontal dimension) by air friction. This larger horizontal dimension typically doubles rain outage in high frequency microwave links as compared to vertical. V-pol is thus preferred where rain outage impacts on path availability.

Fig. 6a shows the reduction in the magnitude of the reflection (reflection coefficient, R) as a function of the reflection (grazing) angle at the specular reflection plane. It is not uncommon for the grazing angle on high clearance paths exposed to specular reflections to

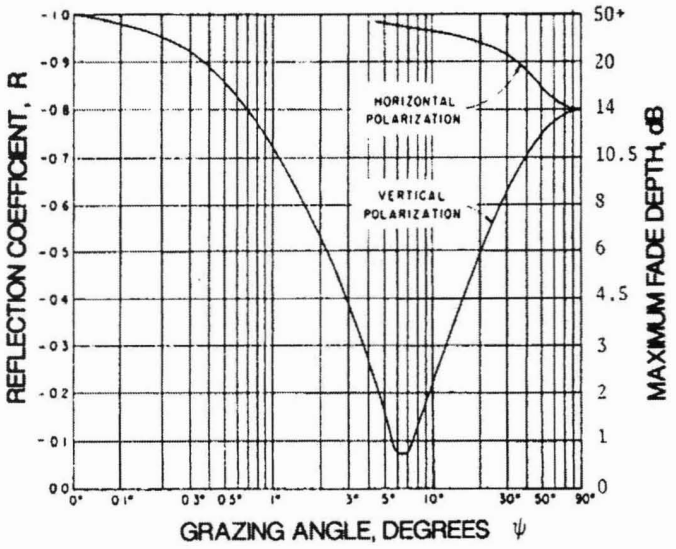

6a. Reflection coefficient vs. grazing angle and fade depth, V- and H-pol.

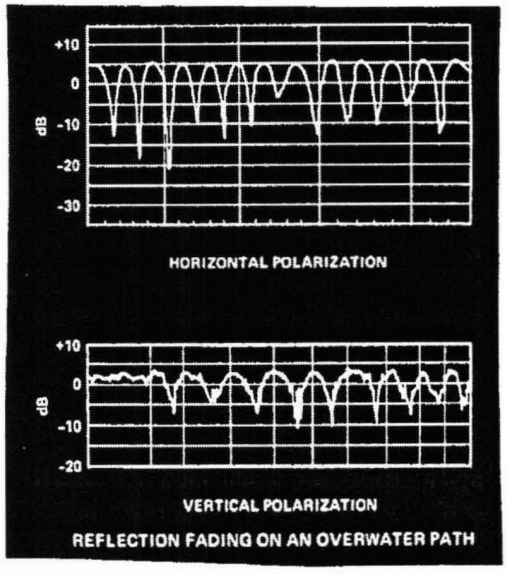

6b. Fade charts, V- and H-pol.

Fig. 6. Reduction of reflection fade depth with V-pol on high clearance paths.

exceed 0.2°, the threshold of a significant lowering of the reflection coefficient with V-pol. If the path geometry analysis (from REFL or other) computes a 0.4° grazing angle, for example, Fig. 6a shows the -1.0 specular reflection coefficient lowered to -0.9, limiting the fade depth to 20 log 1/(1+R) = 20 dB with V-pol compared to >40 dB multipath outage fade depth with H-pol.

Difficult Digital Microwave Paths

Any microwave path is tagged as "difficult" for digital transmission if it easily supports a high capacity analog link, but severely degrades the performance of a medium to high capacity digital microwave link [5]. Difficult digital microwave links typically have one of the two following characteristics:

- Path is long (perhaps >50 mi/80 km) and supports elevated ducting layers that generate deep, fast multipath fades separated <200 msec between diversity dishes. If the quadrature recovery time of the receiver demodulator is insufficient (e.g. >200 msec), excessive SES path outages may occur.

- Path is short (perhaps <25 mi/40 km) but has high clearance over exposed (little terrain blockage and dish discrimination to) terrain supporting long-delayed (>10 nsec/10 ft) multipath reflections. The resulting narrow amplitude notches may stress the digital microwave spectrum beyond the capability of the adaptive equalizers, causing SES outages and degraded quality (burst ES, high BER, etc.).

Difficult digital microwave path geometry must be identified by the transmission engineer and the path configured appropriately with robust radio equipments and antenna systems optimized for the adverse conditions. As adaptive countermeasures in the receivers improve, so often do the transported bits-per-second payloads, RF bandwidths, and modulation complexities increase to continually challenge the system designer.

Path Calculation Sheets

The more routine transmission engineering function involves the selection of antenna sizes, waveguide types, digital radio system gains, radome types, and other hardware to meet the fade margin and, thus, the path probability of outage (U), annual or any month outage time (T), annual path reliability (%), and path availability (in paths affected by long-term rain outage), objectives for the link. This final configuring of the microwave link is after the frequency band, antenna heights, and diversity spacings have been selected to match climatic and terrestrial characteristics (along with any other constraints on dish sizes and types imposed by interference, tower loading, and mounting space and aesthetics).

All of these data are inputted to a path calculation form, usually interactively with a computer program. As the input data (radio system gain, payload, frequency band, antenna sizes, waveguide types and lengths, polarization, etc.) are modified within the aforementioned constraints, outputted performance and availability results appear on the calculation sheet. With a match of these results to the user objectives, the digital microwave path's transmission design is completed.

Conclusions

Digital microwave path engineering, sometimes described as more of art than a science because of the impact of wide variabilities and uncertainties in nature, has evolved significantly over the years, matching similar achievements in robust medium and high capacity digital microwave radio design. A thorough "proactive" transmission study into the climatic and terrain characteristics of the area, with antenna systems appropriately configured, will eliminate nearly all of the uncertainties involved in meeting user performance objectives.

Acknowledgements

The assistance provided by the Harris Farinon Transmission Engineering Department during the preparation of this series is gratefully acknowledged. Bill Musharbash is especially thanked for his radically new computer profiling program (written on Visual C++ running on Windows NT), example of which is seen in Fig. 5.

References

1. R.U. Laine and A. Ross Lunan, "Digital Microwave Link Engineering - Performance Definitions and Objectives", ENTELEC '94 Conference, San Antonio

2. R.U. Laine and A. Ross Lunan, "Digital Microwave Link Engineering - Path Alignment, Testing, and Troubleshooting", APCO 1994 Annual Conference, Pittsburgh

3. Arvids Vigants, "Space Diversity Engineering", Bell System Technical Journal, January 1975.

4. CCIR (ITU-R) Rep. 338-6, "Propagation Data and Prediction Methods for Terrestrial Line-of-Sight Systems", Dusseldorf, 1990.

5. R.U. Laine, "Special Transmission Design Techniques for Difficult 45 Mbps Digital Microwave Links", ENTELEC '91 Conference, Houston

6. S. Zebrowitz, "The Use of Multiple Diversity to Minimize the Effects of Ducting on a Long Path", NTC, 1975

Microwave Path Design - Microwave Engineering Fundamentals Equations

Created: 2024-02-19 09:34:05 Latest reply: 2024-03-25 04:27:54 48 4 4 0 0

View the author 0#



salmaamari MVE Author

597 2508 13

Follow Chat

Post

Frequency

$$f = 1/\tau = c/\lambda$$

Frequency (f) = Number of repetitions (cycles) per second (Hz)
Period (τ) = Duration of a single cycle (seconds)
Wavelength (λ) = Distance wave travels in one period (m)
Speed of Light (c) = 2.99792458×10^8 m/s

Free Space Loss (FSPL)

$$FSPL_{dB} = 96.6 + 20\log[f_{GHz}] + 20\log[d_{mi}] \text{ dB}$$
$$FSPL_{dB} = 92.4 + 20\log[f_{GHz}] + 20\log[d_{km}] \text{ dB}$$

f = frequency (GHz)
d = distance

Friis Transmission Equation

$$P_r = \frac{P_t G_t G_r}{(4\pi d/\lambda)^2}$$

P_r = Power Received (watts)
P_t = Power Transmitted (watts)
G_t = Transmit Antenna Gain
G_r = Receive Antenna Gain
d = Path Distance (m)
λ = wavelength (m)

Fresnel Zone

$$F_n = 72.1\sqrt{\frac{nd_1d_2}{fD}}$$

F_n = n^{th} Fresnel Zone radius (feet)
d_1 = Distance from one end of the path to the reflection point (miles)
D = Total path length (miles)
d_2 = D - d_1
f = Frequency (GHz)

$$F_n = 17.3\sqrt{\frac{nd_1d_2}{fD}}$$

F_n = n^{th} Fresnel Zone radius (meters)
d_1 = Distance from one end of the path to the reflection point (km)
D = Total path length (km)
d_2 = D - d_1
f = Frequency (GHz)

$F_n = 72.1\sqrt{\frac{nd_1d_2}{fD}}$

K Factor (k)

$$k = a_e / a \text{ or } k = 157 / (157 + dN/dh)$$

a = normal Earth radius (6370 km)
a_e = effective Earth radius (km)
dN/dh = refractive gradient value

Earth bulge (h)

$$h(meters) = d_{1km}d_{2km}/12.75k$$

h = 0 for k = infinity
d_1 = Distance from one end of the path to point along the path (km)
D = Total path length (km)
d_2 (km) = D - d_1
k = k factor

Link Budget Equation

$$Rx_2 = P_1 - L_1 + G_1 - FSPL_{1\to2} + G_2 - L_2$$

Rx = Receive signal level (dBm)
P = transmit power (dBm)
L = line loss (dB)
G = gain (dBi)
FSPL = Free Space Path Loss (dB)

Vigants Composite Fade Margin Equation

$$CFM = -10\log_{10}(10^{-TFM/10} + 10^{-DFM/10} + 10^{-EIFM/10})$$

CFM = Composite fade margin (dB)
TFM = Thermal fade margin (RSL - Threshold) (dB)
DFM = Dispersive fade margin (dB)
EIFM = External interference fade margin (dB)

Vigants Multipath Outage Model (predicts Atmospheric Multipath Fading)

FIND

T = Annual outage time (s)
r = Fade occurrence factor
T_0 = (t/50)(8 * 10^6) = Length of the fading season (s)
t = Average annual temperature (F)
CFM = Composite Fade Margin (dB)
I_D = Space Diversity Improvement Factor (1 for non-diversity, >1 for diversity)

Vigants Fade Occurrence Factor

$$r = x \left[\frac{50}{w}\right]^{1.3} \left[\frac{f}{4}\right] D^3 \times 10^{-5}$$

r = Fade Occurrence Factor
x = Climate factor (0.5 - 2 for good - poor areas, see map)
w = Terrain roughness ($20 \le w \le 140$ ft.)
f = Frequency (GHz)
D = Path length (mi)

Vigants Space Diversity Improvement Factor

$$I_D = 7 \times 10^5 s^2 \left(\frac{f}{D}\right) 10^{\left(\frac{CFM}{10}\right)}$$

I_D = Space Diversity Improvement Factor
s = Vertical antenna spacing (ft) ($s \le 50$ ft)
f = Frequency (GHz)
D = Path length (mi)
CFM = Composite Fade Margin (dB)

ITU-R P.530 Method of Calculating Path Reliability (Computes predicted outage due to flat fading and selective fading)

$$P_{total} = (P_{Flat} + P_S) / I_D$$

P_{total} = Total predicted annual outage
P_{Flat} = Probability of Yearly Flat Fading
P_S = Probability of Yearly Selective Fading
I_D = Diversity Improvement Factor

ITU Method Yearly Flat Fading Calculation (PFlat)

$$P_{Flat} = p_w \times 10^{-\Delta G/10} \%$$

ΔG = Logarithmic geoclimatic conversion factor, depends on Latitude, path length, and path inclination factor, $|\varepsilon_p|$
p_w = Worst Month Flat Fading Probability

$$p_w = P_0 \times 10^{-FM/10}$$

P_0 = Fade Occurrence Factor %
FM = fade margin (dB)

ITU Method Fade Occurrence Factor Calculation (P0)

$$P_0 = K d^{3.1} (1 + |\varepsilon_p|)^{-1.29} f_{GHz}^{0.8} \times 10^{-0.00089 h_L} \%$$

$$|\varepsilon_p| = |h_{RLW} - h_{TLW}| / d$$

K = K factor = $10^{-4.0 - 0.0027 dN_1}$
d = Path Length (km)
h_{RLW} = Receiver antenna height above sea level (m)
h_{TLW} = Transmitter antenna height above sea level (m)
h_L = Height above sea level of the lower antenna between transmitter and receiver antenna heights (m)
d_{N1} = Point refractivity gradient found from ITU-R P.453-10 Figure 12
e_p = path inclination (milliradians)

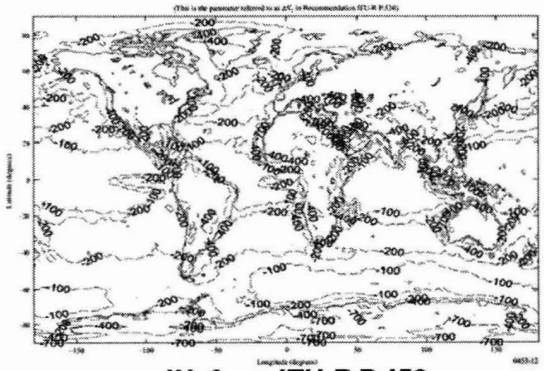

dN_1 from ITU-R P.453

ITU Method Selective Outage Probability Calculation (PS)

$$P_S = 2.15 \eta \left[W_{S1} \times 10^{-B_M/20} \frac{\tau_m^2}{\tau_{SM}} + W_{NM} \times 10^{-B_{MN}/20} \frac{\tau_m^2}{\tau_{SNM}}\right]$$

W_S = Signature Width (GHz)
B_s = Signature Depth (dB)
$\tau_m = 0.7 \left(\frac{d}{50}\right)^{1.3}$ ns
τ_{SA} = Reference Delay (ns) or 6.3ns
M = Minimum Phase
NM = Non-Minimum Phase
$\eta = 1 - \exp(-0.2 P_0^{0.75})$ (multipath activity parameter)
$P_0 = p_w / 100$ (Fade occurrence factor %)

TERRAIN ROUGHNESS

$w =$

$20 \le w \le 140$ ft

$20 \le w \le 140$

$20 \le 140 \le 140$

F = frequency (GHz)
d = path distance (km)
P_0 = Fade occurrence factor %
$P_0 = p_w$ / 100 (Fade occurrence factor %)
p_w = Worst Month Flat Fading Probability
FM = fade margin (dB)
$V = |G_{xmt}^{dBi} \cdot G_{rcv}^{dBi}|$
G_{xmt} = transmit antenna gain (dBi)
G_{rcv} = receive antenna gain (dBi)

C/I: The ratio of desired signal power to interference power at the receiver

$$C/I\ (dB) = C(dBm) - I(dBm)$$

C = Receive level (dBm)
I = Interference level (dBm)

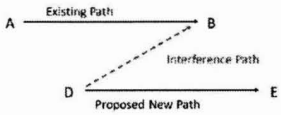

Predicted Carrier to Interference Ratio (C/IPredicted)

$$C/I_{Predicted}\ (dB) = C_B - I_B$$

Receive Signal Level (RSL) at site B (CB)

$$C_B = P_A - L_A + G_A - FSPL_{AB} + G_B - L_B$$

C_B = Receive Signal Level at B (dBm)
P_A = Transmit Power at A (dBm)
L_A = Fixed Losses at A (dB)
G_A = Antenna Gain at A (dBi)
$FSPL_{AB}$ = Free Space Path Loss A to B (dB)
G_B = Antenna Gain at B (dBi)
L_B = Fixed Losses at B (dB)

Interference Level at B (IB)

$$I_B = P_D - L_D + G_D - FSPL_{DB} + G_B - L_B - D_{TOTAL}$$

I_B = Interference Level at B (dBm)
P_D = Transmit Power at D (dBm)
L_D = Fixed Losses at D (dB)
G_D = Antenna Gain at D (dBi)
$FSPL_D$ = Free Space Path Loss D to B (dB)
G_B = Antenna Gain at B (dBi)
L_B = Fixed Losses at B (dB)
D_{TOTAL} = Combined Antenna Discrimination of D and B (dB)

Interference Case Margin

$$\text{Case Margin (dB)} = C/I_{Objective} - C/I_{Predicted}$$

$C/I_{Objective}$ = Carrier to Interference Objective (dB)

External Interference Fade Margin

$$\text{EIFM (dB)} = C/I_{Predicted} - C/N$$

C/N determined from radio specs or waterfall curves (dB)

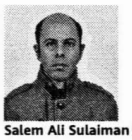

Salem Ali Sulaiman Nasr Al-Ma'amari
Network Quality Management & Development

Planning | External Moderator | Highlighted | Wireless & Microwave | Product & Technology

Like (4) Dislike (0) Favorite (0) Share Report

< **Previous:** Microwave Path Design - Primary Path De... **Next:** Microwave Path Design - Frequency Plann... >

salmaamari MVE Author Created 2024-02-19 05:34:45 (0) (0) 1#

@JOMO# @jonbov @Joshua_Astre **@jothi.krish;** @JuanAcosta @Jul_ang @Iula @kakuye @kalemelak @karladu @Kashif @KasimAbubakr @kenza @Kevin_Thomas @Khuzaima **@Kivanc;** @Koosha @KorayK. @krishnkant @kunthea @Kursat5oyarslan @l2vc @lacsap @Lalheang @Lan59 @Lathesh_Kannoth @Lecky @Lianet @Li15tyfz237 @liqiang185 @little_fish @Litu **@liuxl;** @LordFer @Loti_fa **@LSA;** @Lucas_Zhao @Lucfabrice @lucian2003 @LucianoNhariumbo @lucisherry06 **@Luiza;** @LuizPuppin @m_babar @M_Elsolimany @m3hr4n @maaoulabenbrahim @Macaroni @Mahedi **@Mahesh_Vyas;** @MahtAush @mamoona_4976826 @maithi @Majdi.Chebil @MakubeX @malfaro @Malik3000 @manpham @Maria Abdullah @marwan_cet @Marwan_TE @Matheus_Nunes @Mavee @Maverick @mdasilva @Merra @merwinmp @Mfar53 @MGI @Mglsmn **@Michael256;** @minervaE @MinhMinh **@Miroslav;** @mlairlidis @MJ86 @mkabanov @mmoneebq @MMshaikh @Moemyint18 @Mohamed_Ahmed @Mohamed_Ayed **@Mom;** @Moschino @mounir997 @mourou @Movsarnos @mrom @Muddasar **@Muditverma;** @Muhammad_Danyal @MuhammadIsmailHashmi @MuhammadTalhaSiddiqui @Munsif @Murtaza520 @mytruc @nabet @Nabihazahid @naqu @naqui

@Shameembegum **@Sharif;** @shaus @shayankhanani @shehkh20 @SidzHuawei @simchamnan **@simon_bel;** @slidi @ambq93 @smileymind @smjawad @sofire @sohaib.ansar @Sokrin @Soliman_Mohammed @Somemeow @Sothea_nh @SP1991 @Spas1212 **@SPK;** @Steffy @stephen.xu @ster @Strorry @Sufyan_Ali_Khan @Suhail @suman90pro @Sunil88 @Sven_Alea @sybilann19 @SyedDanyal @Tabish @taha_29four @TaharDZ **@tanjinpeng;**

salmaaman MVE Author Created 2024-02-19 09:35:03 (0) (0) 2#

@mytruc @faysalji @1727 @19muaz19 @77_XiaoHan @aamirkhan @abdelali @abdul_basit7233 @AbidAli1988 @abood_1419 @Adeel U_Awan @AdilHasan786 @Adrhman @Adriale @Ahmed___48 @Ahmed_Israr @Ahmed_Osman @ahmed48420 @AhmedGomaa @ahmedmoharned1212001 @aidnet @Aish1234 @AK47 @Akbar_Sha @Al_amery **@Albert; @AlbertChen;** @ALEXCS **@alexzcong;** @alfresco @Ali_Raza37 @AliBinHussain @AliCeliksu @Alnamany @alopez @Amalia **@Amerigo;** @Amirul_Khan @ammarkhanu @amr_rashedy @Ana_Due @Anas12 @andersoncf1 @Andre_G **@andrej.mitrovic;** @AndresMoreno **@Anees_1104532;** @Anhoang **@Ani39;** @Anno7 @Anzi @aptb88 **@Ariana2019;** @Arquitech2009 @Asad_497 @Ashar_Azeem @ashirhs **@Ashvinkumar;** @astar @ataadmri251 @Atta37924 @atya @awtaerg @Axe_Z @Ayeshaali @azkasaqib @Babar @bagic @Bale **@Bamit;** @barli @Basit786 @BAZ @be_io **@Becky_2019;** @beebz @Beelzebub @bek7 **@BetterMing; @BIGBANG** @Bitaites @bubliu666 @bo2la @bobi @Brooklynoranges **@BruceG;** @Buntheng @BWGAPM **@Cajaandj;** @cantona1976 **@Captain,T;** @carlosalcosta @Caroline_Herrera @cataleyagonzc @Chanbora @channarcus @chanitha @chavdar @che_ram @chencici @chenhui **@Chenwei;** @Chenxintao @chika_emeche @Chris_J @ChrisKA @cmarban **@Conway_Itis; @CostinelC; @CPR;** @csk99 @ctismehmetbulut **@CursedMind;** @CyberTec **@Cyndi.Bear; @DaljitSingh;** @Daniel_Gilbert11 @DawoodShah @DAYOH @Ddkompik @DDSN **@Dee_Hoa;** @Deja_vu @Desiree @dictator @Didi @Diego.Silva @dilber @Dimon1976 @dinesh.tamba @DinoRe @DKetrari @doxt_waxir @dr.wow @dragos_v @DrDoom @E.DR_91 @Edward1 @EhsanulHaq @EL.BODO @elena_z @emjay5071 @Engr_Shakeel @ernesto_cupet6 @ertas @Esra @EsraBilgin @Estelle_Bright @ExpionKu **@F84129404;** @faiza.hamza92 @faojen @fargat @Faridrani @Farinaahmed **@Farkhod_Ganiev;** @Fathy_jr @fatt @Fernando_Ag @firdousfodhi @Five **@fms; @Fr33m4n; @Freaks_J;** @Fuchsia @Funstuff @futurework **@fuzi_yao;** @gabo.ir @Gary1668 @GDCP @Geek69 @GhaziAsad @ghbacala **@Guennadi; @qululu;** @Gustavo.HdezF **@qzzz;** @H.Mansoor @h89151

View More

PuiAlex Moderator Author Created 2024-03-14 11:17:25 (1) (0) 3#

Thanks for sharing

user_4578151 Created 2024-03-25 04:27:54 (1) (0) 4#

Prompt: the author is forbidden or deleted. The content is automatically shielded

Comment

You need to log in to comment to the post Login | Register

Notice: To protect the legitimate rights and interests of you, the community, and third parties, do not release content that may bring legal risks to all parties, including but are not limited to the following:

- Politically sensitive content
- Content concerning pornography, gambling, and drug abuse
- Content that may disclose or infringe upon others ' commercial secrets, intellectual properties, including trade marks, copyrights, and patents, and personal privacy

Do not share your account and password with others. All operations performed using your account will be regarded as your own actions and all consequences arising therefrom will be borne by you. For details, see "User Agreement".

Contact Us: e_online@huawei.com Copyright © 2024 Huawei Technologies Co., Ltd. All rights reserved.

Building Type	E_M
Wood	15 dB
Brick	30 dB
Concrete	30 dB
Metal	40 dB

Solving for building attenuation:

$$L_b = \frac{d_e \times E_M}{15}$$

BUILDING MULTIPATH PROPAGATION LOSS

Losses due to multipath transmission because of buildings can be computed by the formula:

Lmb = 20 Log (*f^MHZ*)

Solution : Based on the table for 150% first freznel clearance, even if there are the 3 diffraction points crossing the 150% clutter clearance, none of these points are within the near field zone of both antennas.

Computing for the near and far field distances:

12.82 Ghz	13.08 Ghz
$\lambda_1 = \frac{3 \times 10^8}{12.82 \times 10^9}$ $\lambda_1 = 0.0234$ meters $\lambda_1 = 0.07677$ foot	$\lambda_2 = \frac{3 \times 10^8}{13.08 \times 10^9}$ $\lambda_2 = 0.0229$ meters $\lambda_2 = 0.07513$ foot
$d_1 = 2.4$ meters $d_1 = 7.874$ feet	$d_2 = 2.4$ meters $d_2 = 7.874$ feet
$D_{NF} = \frac{\pi \times 7.874^2}{8 \times 0.07677}$ $D_{NF} = 317.147$ feet $D_{NF} = 96.667$ meters	$D_{NF} = \frac{\pi \times 7.874^2}{8 \times 0.07513}$ $D_{NF} = 324.069$ feet $D_{NF} = 98.776$ meters
$D_{FF} = \frac{2 \times 7.874^2}{0.07677}$ $D_{FF} = 1615.211$ feet $D_{FF} = 492.319$ meters	$D_{FF} = \frac{2 \times 7.874^2}{0.07513}$ $D_{FF} = 1650.469$ feet $D_{FF} = 500.066$ meters

NEAR

FAR

In addition, the three building top diffraction at the point 26/27 Km from site A has already been computed with the diffraction loss.

Alternative Solution : If you wish the omit the computation of clutter loses, increases the antenna height until they clear the 150% first freznel radius margin.

$$D_{FF} = \frac{\pi \cdot 7.874_{ft}^2}{8 \cdot \lambda_{ft}}$$

ATMOSPHERIC LOSSES

TO BE ADDED THE THERMAL FADE MARGIN

Step 21 : Compute for Atmospheric Losses.

OXYGEN ABSOPTION LOSS

Attenuation is due to the absorption of radio frequency energy by oxygen molecules in the atmosphere is given by the formula :

For Frequencies below 57 Ghz

For Frequencies below 57 Ghz

$$A_O = \left[7.19 \times 10^{-3} + \frac{6.09}{f^2 + 0.227} + \frac{4.81}{(f - 57)^2 + 1.5} \right] \times f^2 \times 10^{-3} \quad \text{dB/Km}$$

For Frequencies between 57 Ghz and 63 Ghz

$A_O = 15$ dB/Km

For Frequencies above 63 Ghz

$$A_O = \left[3.79 \times 10^{-7} + \frac{0.265}{(f - 57)^2 + 1.59} + \frac{0.028}{(f - 118)^2 + 1.47} \right] \times (f + 198)^2 \times 10^{-3} \quad \text{dB/Km}$$

Frequency f in Ghz.

The Reason as that Ao is a constant set for frequencies between 57Ghz to 63 Ghz is the complex spectrum analysis of these frequencies which is dependent on the height of the transmitting and receiving antennas. The result however, would still around the area of 15 dB/Km.

Solution : Computing for oxygen absorption loss at a path length of 30 Km:

For 12.82 Ghz

$$A_O = \left[7.19 \times 10^{-3} + \frac{6.09}{12.82^2 + 0.227} + \frac{4.81}{(12.82 - 57)^2 + 1.5} \right] \times 12.82^2 \times 10^{-3} \quad \text{dB/Km}$$

$A_O = 7.668 \times 10^{-3}$ dB/Km

.007668 dB/1cm

A_O for 30 Km = 0.23 dB

For 13.08 Ghz

$$A_O = \left[7.19 \times 10^{-3} + \frac{6.09}{13.08^2 + 0.227} + \frac{4.81}{(13.08 - 57)^2 + 1.5} \right] \times 13.08^2 \times 10^{-3}$$

$A_O = 7.738 \times 10^{-3}$ dB/Km

WATER VAPOR LOSS

Attenuation due to the absorption of radio frequency energy by water vapor in the atmosphere is given by the formula:

$$A_{H2O} = \left[0.067 + \frac{3}{(f-22.3)^2+7.3} + \frac{9}{(f-183.3)^2+6} + \frac{4.3}{(f-323.8)^2+10}\right] \times f^2 \times a \times 10^{-4} \text{ dB/Km}$$

f in Ghz.

a is Water Vapor Density in gm/m^3 should be below 12 gm/m^3

This formula applies for frequencies below 350 Ghz.

Solution : Coputing for water vaporloss at a path length of 30 Km:

$f = 12.82$ Ghz

$$A_{H2O} = \left[0.067 + \frac{3}{(12.82-22.3)^2+7.3} + \frac{9}{(12.82-183.3)^2+6} + \frac{4.3}{(12.82-323.8)^2+10}\right] \times 12.82^2 \times 12 \times 10^{-4} \text{ dB/Km}$$

$A_{H2O} = 0.0194$ dB/Km

A_{H2O} for 30 Km = 5812 dB

$f = 13.08$ Ghz

$$A_{H2O} = \left[0.067 + \frac{3}{(13.08-22.3)^2+7.3} + \frac{9}{(13.08-183.3)^2+6} + \frac{4.3}{(13.08-323.8)^2+10}\right] \times 13.08^2 \times 12 \times 10^{-4} \text{ dB/Km}$$

$A_{H2O} = 0.00205$ dB/Km

A_{H2O} for 30 Km = .615 dB

Step 22: Arrange all computed data into a systematic table.

The given and calculated data can then be arranged according to the fade margins they result into:

1. Basic Thermal Fade Margin
2. Thermal Fade Margin with Atmospheric Loss Considerations
3. Dispersive Fade Margin
4. Thermal Fade Margin with Rain Considerations (Rain Fade Margin)
5. Thermal Fade Margin with Diffraction Considerations (Diffraction Fade Margin)

From these fade margins, a Flat Margin can then be calculated.

The Flat fade Margin and Composite Fade Margin take into consideration all the fade margins calculated.

Computation for Low Band Frequency – Tx = 12.62 Ghz

PARAMETER	FUNCTION	VALUE	UNIT
Microwave Radio Output Power	*Given*	18.00	dB
Connector Loss	*Subtracted*	0.50	dB
Waveguide Loss	*Subtracted*	0.59	dB
Connector Loss	*Subtracted*	0.50	dB
Antenna Gain	*Added*	47.00	dB
Free Space Loss	*Subtracted*	144.00	dB
Atmospheric Losses (Oxygen Absorption)	*Subtracted*	0.23	dB
Atmospheric Losses (Water Vapor Absorption	*Subtracted*	0.58	dB
Antenna Misalignment Loss	*Subtracted*	0.50	dB
Antenna Gain	*Subtracted*	47.00	dB
Connector Loss	*Subtracted*	0.50	dB
Waveguide Loss	*Added*	0.59	dB
Connector Loss	*Subtracted*	0.50	dB
Power Input to Receiver (RSL)	*Computed*	-36.49	dB
Minimum Receiver Threshold	*Given*	-78.00	dB
THERMAL FADE MARGIN	***COMPUTED***	**41.51**	**dB**

Computation for Low Band Frequency – Tx = 13.08 Gh

PARAMETER	FUNCTION	VALUE	UNIT
Microwave Radio Output Power	*Given*	18.00	dB
Connector Loss	*Subtracted*	0.50	dB
Waveguide Loss	*Subtracted*	0.59	dB
Connector Loss	*Subtracted*	0.50	dB
Antenna Gain	*Added*	47.00	dB
Free Space Loss	*Subtracted*	144.32	dB

Atmospheric Losses (Oxygen Absorption)	*Subtracted*	0.23	dB
Atmospheric Losses (Water Vapor Absorption	*Subtracted*	0.62	dB
Antenna Misalignment Loss	*Subtracted*	0.50	dB
Antenna Gain	*Subtracted*	47.00	dB
Connector Loss	*Subtracted*	0.50	dB
Waveguide Loss	*Added*	0.59	dB
Connector Loss	*Subtracted*	0.50	dB
Power Input to Receiver (RSL)	*Computed*	-36.85	dB
Minimum Receiver Threshold	*Given*	-78.00	dB
THERMAL FADE MARGIN	***COMPUTED***	**41.16**	**dB**

Calculation of the Rain Fade Margin is the difference between the Thermal Fade Margin less Rain Losses. Calculation of the Diffraction Fade Margin is the difference between the Thermal Fade Margin less Diffraction & Clutter Losses.

Rain Fade Margin is treated separately up to the calculation of reliability.

Other Fade Margins may be given such as External Interference Fade Margin and Adjacent Channel Fade Margin. These are computed together along with the Thermal Fade Margin and Diffraction Fade Margin.



FLAT MADE MARGIN

Step 23: Calculate Flat Fade Margin

Calculation for the Flat Fade Margin is given by the formula:

$$FM_{FLAT} = -10 \text{ Log} \left[10^{\left[\frac{-FM_{THERMAL}}{10}\right]} + 10^{\left[\frac{-FM_{ADJ.CHAN}}{10}\right]} + 10^{\left[\frac{-FM_{INT}}{10}\right]} + 10^{\left[\frac{-FM_{DIFF}}{10}\right]} \right]$$

In cases when External Interference Fade Margin (FMint) and Adjacent Channel Fade Margin (FMadj.chan) is not given, then the terms which contains these values in the exponent are omitted.

Solution : Computing for Flat Fade Margin:

Diffraction Fade Margin = Thermal Fade Margin – Diffraction Loss – Clutter Loss

For 12.82 Ghz

Diffraction Fade Margin (FM^DIFF) = 41.52 dB – 2.658 dB

Diffraction Fade Margin (FM^DiFF) = 38.852 dB

$$FM_{FLAT} = -10 \text{ Log} \left[10^{\left[\frac{-41.51}{10}\right]} + 10^{\left[\frac{-38.852}{10}\right]} \right]$$

$$FM_{FLAT} = 36.97 \text{ dB}$$

For 13.08 Ghz

Diffraction Fade Margin (FM_{DIFF}) = 41.16 dB - 2.658 dB

Diffraction Fade Margin (FM_{DIFF}) = 38.502 dB

$$FM_{FLAT} = -10 \text{ Log} \left[10^{\left[\frac{-41.16}{10}\right]} + 10^{\left[\frac{-38.502}{10}\right]} \right]$$

$$FM_{FLAT} = 36.62 \text{ dB}$$

COMPOSITE FADE MARGIN

Step 24: Calculate the composite or effective Fade Margin using the following equation :

$$FM_{EFF} = -10 \text{ Log} \left[10^{\left[\frac{-FM_{FLAT}}{10}\right]} + R_D \, 10^{\left[\frac{-FM_{DSP}}{10}\right]} \right]$$

Where R^D is the Fade Occurrence Factor

Solution : Considering a Dispersive Fade Margin of 40dB with an average fade occurrence factor (R^D = 3), we can compute for the Effective Fade Margin.

For 12.82 Ghz

$$FM_{EFF} = -10 \text{ Log} \left[10^{\left[\frac{-36.97}{10}\right]} + 3 \times 10^{\left[\frac{-40}{10}\right]} \right]$$

$$FM_{EFF} = 33.002 \text{ dB}$$

For 13.08 Ghz

$$FM_{EFF} = -10 \text{ Log} \left[10^{\left[\frac{-36.62}{10}\right]} + 3 \times 10^{\left[\frac{-40}{10}\right]} \right]$$

$$FM_{EFF} = 32.859 \text{ dB}$$

RELIABILITY CALCULATIONS

Step 25: Based on the Effective Fade Margin of the Link, the Link Reliability can be calculated.

In calculating Reliability, Several Models can be used.

1. KQ Factor
2. KQ Factor with Terrain Roughness
3. Vigants Barnett
4. CCIR Recommendations 530

Each method having a different calculation approach and different formula.

TERRAIN ROUGHNESS FACTOR

In the Calculation of the reliability using the KQ factor with Terrain Roughness and Vigants-Barnett method, it is important to initially establish the roughness of the terrain. This is done by taking the standard deviation of regular increments of the path.

The given formula is :

M = Average Elevation above MSL

$$M = \frac{1}{n} \sum_{i=1}^{n} x_i$$

S = Standard Deviation of the Elevations in the path

$$S = \sqrt{\left[\frac{1}{n} \sum_{i=1}^{n} x_i^2\right] - M^2}$$

n is the number of path length subdivisions between the 2 end stations.

M is the average Elevations within the path

S the standard deviation of the elevation within the path;

Notes:

The end points of the path are not taken into consideration with the roughness terrain factor.

The greater he value of n, the more accurate the terrain roughness factor value is calculated.

Solution: Calculating the average terrain elevation. Since we are not to consider the elevation at the end, there are 29 segments at increments of 1 kilometer:

Path Elevations do not include site elevations

	Path Elevations	Path Elevations Squared
1	225.00	50625.00
2	200.00	40000.00
3	175.00	30625.00
4	150.00	22500.00
5	150.00	22500.00
6	150.00	22500.00
7	75.00	5625.00
8	50.00	2500.00
9	25.00	625.00
10	25.00	625.00
11	50.00	2500.00
12	75.00	5625.00
13	100.00	10000.00
14	95.00	9025.00
15	85.00	7225.00
16	70.00	4900.00
17	55.00	3025.00
18	35.00	1225.00
19	25.00	625.00
20	25.00	625.00
21	25.00	625.00
22	75.00	5625.00
23	125.00	15625.00
24	125.00	15625.00
25	150.00	22500.00
26	175.00	30625.00
27	200.00	40000.00
28	210.00	44100.00
29	220.00	48400.00
SUM	3145.00	466025.00
AVE	108.45	16069.83
STANDARD DEVIATION		65.64

STANDARD DEVIATION = $\sqrt{16069.83 - 108.45^2}$

Average Terrain Elevation = M = 108.45

Standard Deviation of the elevations = S = 65.6414

65.64

K-Q Reliability Calculation

The Calculations for the fade probability in the K-Q method is given by the formula:

$$U = \text{K-Q} \times f^{b} \times d^{c} \times 10^{\left(\frac{-FM_{EFF}}{10}\right)}$$

Where:

K-Q – Regional K-Q Value

f – Frequency in Ghz

d – Path Length in Kilometres

b, c – Regional Climatic Factor

FM^EFF – Effective Fade Margin

To get the values of K-Q, b and c, use the following table:

K-Q		
Maritime Temperate, Mediterranean, Coastal or High Humidity and Temperature		
	b = 1.2	2×10^{-5}
Continental Temperate Climate or mid Latitude Island Climate with Average Rolling Terrain		
	b = 1.2 (Asia)	1×10^{-9}
	b = 1.0 (Europe)	1.4×10^{-8}
	b = 1.5 (Continental)	4.1×10^{-4}
Temperate Climate, Coastal Regions with Fairly Flat Terrain		
	b = 1.2 (Asia)	$9.9 \times 10^{-8} / H$
	b = 1.5 (Continental)	2.3×10^{-5} to 4.9×10^{-5}
High Dry Mountainous Region		
	b = 1.2 (Asia)	3.9×10^{-10}
Temperate Climates, Inland Regions with Fairly Flat Terrain		
	b = 1.2 (Continental)	7.6×10^{-5} to 2×10^{-5}

When b=1.2 or b=1.0 then c=3.5, otherwise c = 2.0

$$H = \sqrt{h1 \cdot h2}$$

h1, h2 Antenna heights above ground level

Solution : Using a K-Q value of 1×10^{-9}, b = 1.2 and c = 3.5, the unavilability for link can be calculated.

$$U_{LB} = 1 \times 10^{-9} \times 12.82^{1.2} \times 30^{3.5} \times 10^{\left[\frac{-33.002}{10}\right]}$$
$$U_{LB} = 1.58 \times 10^{-6}$$

$$U_{HB} = 1 \times 10^{-9} \times 13.08^{1.2} \times 30^{3.5} \times 10^{\left[\frac{-32.859}{10}\right]}$$
$$U_{HB} = 1.68 \times 10^{-6}$$



Unfaded Reliability is then computed as 1-Unavailability:

$$R_{LB} = (1 - 1.58 \times 10^{-6}) \times 100\%$$
$$R_{LB} = 99.999842\ \%$$

$$R_{HB} = (1 - 1.68 \times 10^{-6}) \times 100\%$$
$$R_{HB} = 99.999832\ \%$$

Using the same value for K-Q of 1 x 10^-9 , b = 1.2 and c = 3.5, the unavailability and reliability for link due to rain can be calculated.

Rain Fade Margin = Effective Fade Margin – Rain Atenuation

For 12.82 Ghz

Rain Fade Margin = 33.002 dB -26.34 dB

Rain Fade Margin = 6.68 dB

For 13.08 Ghz

Rain Fade Margin = 32.859 dB -25.44 dB

Rain Fade Margin = 7.419 dB

$$U_{LB} = 1 \times 10^{-9} \times 12.82^{1.2} \times 30^{3.5} \times 10^{\left(\frac{-6.68}{10}\right)}$$

$$U_{LB} = 6.78 \times 10^{-4}$$

$$U_{HB} = 1 \times 10^{-9} \times 13.08^{1.2} \times 30^{3.5} \times 10^{\left(\frac{-7.419}{10}\right)}$$

$$U_{HB} = 5.86 \times 10^{-4}$$

$$R_{LB} = (1 - 6.78 \times 10^{-4}) \times 100\%$$

$$R_{LB} = 99.9322\%$$

$$R_{HB} = (1 - 5.86 \times 10^{-4}) \times 100\%$$

$$R_{HB} = 99.9414\%$$

K-Q Reliability with Terrain Roughness

The calculation for the fade probability using the K-Q method and considering the roughness of the terrain is given by the fomula:

$$U = \frac{K\text{-}Q}{S^{1.3}} \times f^{b} \times d^{c} \times 10^{\left(\frac{-FM_{EFF}}{10}\right)}$$

Where:

K-Q – Regional K-Q Value

f – Frequency in Ghz

d – Path Length in Kilometres

b, c – Regional Climatic Factor

FM^EFF – Effective Fade Margin

S – Standard Deviation of the Terrain Elevation (also called roughness Facotr)

Using the same values of K-Q, b and c:

$$U_{LB} = \frac{1 \times 10^{-9}}{65.6414^{1.3}} \times 12.82^{1.2} \times 30^{3.5} \times 10^{\left[\frac{-33.002}{10}\right]}$$

$$U_{LB} = 6.86 \times 10^{-9}$$

$$U_{HB} = \frac{1 \times 10^{-9}}{65.6414^{1.3}} \times 13.08^{1.2} \times 30^{3.5} \times 10^{\left[\frac{-32.859}{10}\right]}$$

$$U_{HB} = 7.294 \times 10^{-9}$$

Unfaded Reliability is then computed as:

$$R_{LB} = (1 - 6.86 \times 10^{-9}) \times 100\%$$
$$R_{LB} = 99.999999\ \%$$

$$R_{HB} = (1 - 7.294 \times 10^{-9}) \times 100\%$$
$$R_{HB} = 99.999999\ \%$$

And computing for the Rain Outage in the same manner:

Rain Fade Margin = Effective Fade Margin – Rain Attenuation

For 12.82 Ghz

Rain Fade Margin = 33.002 dB -26.34 dB

Rain Fade Margin = 6.68 dB

For 13.08 Ghz

Rain Fade Margin = 32.859 dB -25.44 dB

Rain Fade Margin = 7.419 dB

$$U_{LB} = \frac{1 \times 10^{-9}}{65.6414^{1.3}} \times 12.82^{1.2} \times 30^{3.5} \times 10^{\left[\frac{-6.68}{10}\right]}$$

$$U_{LB} = 2.944 \times 10^{-6}$$

$$U_{HB} = \frac{1 \times 10^{-9}}{65.6414^{1.3}} \times 13.08^{1.2} \times 30^{3.5} \times 10^{\left[\frac{-7.419}{10}\right]}$$

$$U_{HB} = 2.544 \times 10^{-6}$$

$$R_{LB} = (1 - 6.78 \times 10^{-4}) \times 100\%$$
$$R_{LB} = 99.9997\ \%$$

$$R_{HB} = (1 - 5.86 \times 10^{-4}) \times 100\%$$
$$R_{HB} = 99.9997\ \%$$

Note the extreme difference, between both K-Q reliabilities with and without taking into consideration terrain Roughness.

Vigants - Barnette Calculation

C FACTOR

The C factor in the Vigants – Barnette method of solving for unavailability takes into consideration bot the terrain roughness and climatic conditions:

$$C = c_f \times \left[\frac{S}{15.2}\right]^{-1.3}$$

Where:

C –C-Factor Value

c^f - Climate factor

S – Roughness Factor

This formula is applicable if S is greater or equal to 6 meters but less than or equal to 42 meters. Values of S which are outside these limits may assume the minimum or maximum value.

c^f– Climate factor may have the typical values :

c^f = 0.5 Good Propagation Conditions, used for mountainous and dry conditions

c^f = 1 Average Propagations Conditions, used for Average terrain and climatic conditions

c^f = 2 Difficult Propagations Conditions, used for over water paths, gulf or coastal areas

Solution. Using the Vigants-Barnette method, we can set the climatic factor to be 1 and the Roughness Factor to be 42.

$$C = 1 \times \left[\frac{42}{15.2}\right]^{-1.3}$$

$$C = 0.2668$$

Note the computed C factor value is for good propagation conditions as the typical C-factor values are:

C = 0.25	Good Propagation Condition
C = 1	Average Propagation Conditions
C = 4	Difficult Propagation Conditions

The Vigants – Barnette unavailability formula is given as:

$$U = 6.0 \times 10^{-7} \times C \times f \times d^3 \times 10^{\left[\frac{-FM_{EFF}}{10}\right]}$$

Where:

C – C – Factor Value

f – Frequency in Ghz

d – Path Length in Kilometres

Solution: The computation for the unavailability using the Vigants-Barnette Method is:

For 12.82 Ghz

$$U_{LB} = 6.0 \times 10^{-7} \times 0.2668 \times 12.82 \times 30^3 \times 10^{\left[\frac{-33.002}{10}\right]}$$
$$U_{LB} = 2.7747 \times 10^{-5}$$

For 13.08 Ghz

$$U_{HB} = 6.0 \times 10^{-7} \times 0.2668 \times 13.08 \times 30^3 \times 10^{\left[\frac{-32.859}{10}\right]}$$
$$U_{HB} = 2.9268 \times 10^{-4}$$

Reliability can then be calculated:

$$R_{LB} = (1 - 2.7747 \times 10^{-5}) \times 100\%$$
$$R_{LB} = 99.9972\ \%$$

$$R_{HB} = (1 - 2.9268 \times 10^{-4}) \times 100\%$$
$$R_{HB} = 99.9971\ \%$$

Calculations for the unavailability due to rain is also done:

Rain Fade Margin = Effective Fade Margin – Rain Attenuation

For 12.82 Ghz

Rain Fade Margin = 33.002 dB -26.34 dB

Rain Fade Margin = 6.68 dB

For 13.08 Ghz

Rain Fade Margin = 32.859 dB -25.44 dB

Rain Fade Margin = 7.419 Db

For 12.82 Ghz

$$U_{LB} = 6.0 \times 10^{-7} \times 0.2668 \times 12.82 \times 30^3 \times 10^{\left(\frac{-6.68}{10}\right)}$$

$$U_{LB} = 0.0119$$

For 13.08 Ghz

$$U_{HB} = 6.0 \times 10^{-7} \times 0.2668 \times 13.08 \times 30^3 \times 10^{\left(\frac{-7.419}{10}\right)}$$

$$U_{HB} = 0.0102$$

The Availability during rain:

$$R_{LB} = (1 - 0.0119) \times 100\%$$
$$R_{LB} = 98.81\ \%$$

$$R_{HB} = (1 - 0.0102) \times 100\%$$
$$R_{HB} = 99.98\ \%$$

CCIR Recc. 530 Calculation

When using the CCIR Recc. 530 Unavailability calculation, it is important to determine 3 factors, the Path Inclination, the Average Grazing Angle and the Geoclimatic Factor.

PATH INCLINATION

Path inclination is given by the formula:

$$\varepsilon = 1000 \times \tan^{-1}\left(\frac{|h_1 - h_2|}{1000 \times d}\right) \text{ milliradians}$$

NOTE: CALCULATION DONE IN RADIANS

Where :

h1 and h2 – antenna height above MSL in meters

d – Path Length in Kilometres

solution: Solving for the Path Inclination:

$$\varepsilon = 1000 \times tan^{-1}\left(\frac{|260 - 250|}{1000 \times 30}\right)$$

$$\varepsilon = 0.3333 \text{ milliradians}$$

$a_e = 8500$

AVERAGE GRAZING ANGLE

The following are the necessary formula need to solve for the average grazing angle:

$$m = \frac{30^2}{34000 \times (250+260)}$$

$$c = \frac{|h1 - h2|}{h1+h2}$$

$$b = 2 \times \left(\sqrt{\frac{m+1}{m \times 3}}\right) \times \cos\left(\frac{\pi}{3} + \left(\frac{1}{3} \times \cos^{-1}\left(\frac{3c}{2}\sqrt{\frac{3m}{(m+1)^3}}\right)\right)\right)$$

NOTE: CALCULATION DONE IN RADIANS

$$m = \frac{d^2}{4 a_e (h_1 + h_2)}$$

$$\frac{30^2}{34000 \cdot (250+260)}$$

Where :

h1 and h2 – antenna height above MSL in meters

d – Path Length in Kilometres

$$c = \frac{|h_1 - h_2|}{(h_1 + h_2)}$$

solution: Solving for the factors needed to solve average grazing angle

$$m = \frac{30^2}{34000 \times (.25+.26)}$$

$$m = 0.52$$

$$c = \frac{|0.25 - 0.26|}{0.25 + 0.26}$$

$$c = 0.0196$$

$$b = 2 \times \left(\sqrt{\frac{0.52+1}{0.52 \times 3}}\right) \times \cos\left(\frac{\pi}{3} + \left(\frac{1}{3} \times \cos^{-1}\left(\frac{3(0.0196)}{2}\sqrt{\frac{3 \times 0.52}{(0.52+1)^3}}\right)\right)\right)$$

$$b = 0.01289$$

$c =$

$$m = \frac{900}{34000 \cdot (250+260)}$$

$$\frac{900}{17,344,000}$$

Average Grazing Angle is given by the formula:

$$\theta = \frac{h1+h2}{d} \times \left(1 - m \times (1 + b^2)\right) \text{ milliradians}$$

Where this time, h1 and h2 are expressed in meters above MSL and d in the kilometres. This will result in a value whose unit is in milliradians.

Solution: Solving for the average grazing angle

$$\theta = \frac{250 + 260}{30} \times (1 - 0.52 \times (1 + 0.01289^2)) \text{ milliradians}$$

$$\theta = 8.1585 \text{ milliradians}$$

GEOCLIMATIC FACTOR

This is the percent of time when the refractivity gradiant of a specific place goes below 100 N units per Kilometre. This value changes from month to month. In path calculations, the worst fading month is taken. The variable P^L is used to solve for the geoclimatic factor K. P^L is taken from refractivity maps while K, being a factor of P^L is calculated by the use of the following formula:

$$K = 10^{-5.4} \times P_L^{1.5} \quad \text{for over land paths}$$

$$K = 10^{-6.0} \times P_L^{1.5} \quad \text{for mountainous paths}$$

$$K = 10^{-4.9} \times P_L^{1.5} \quad \text{for over water paths}$$

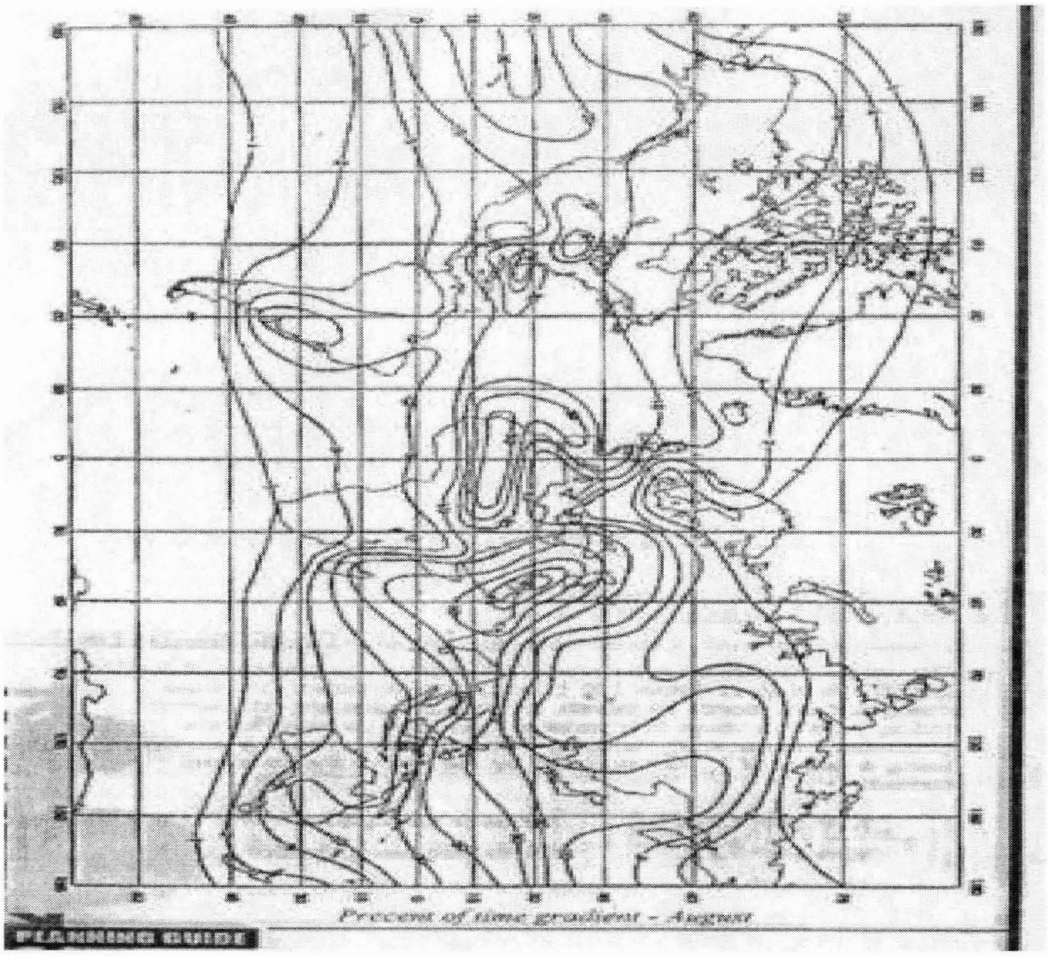

Solution : From the graph (August was chosen as it provided the worst month for the Philippines), we can solve for the value of K given the value of P to be 30. Choosing a Mountainous path :

$$K = 10^{-6} \cdot P_L^{1.5}$$

K = 10^-6.0 x 30^1.5

K = 1.643 x 10^-14

CCIR Rec. 530 UNAVAILABILITY

Having established the particular factors, unavailability can now be computed:

$$U = K \times (1+\varepsilon)^{-1.1} \times \theta^{-1.2} \times f^{0.93} \times d^{3.3} \times 10^{\left(\frac{-FM_{eff}}{10}\right)}$$

Where :

F – Frequency in Ghz

D – Path Length in Kilometers

Solution : Solving for Unavailability using CCIR Recc. 530:

For 12.82 Ghz

$$U_{LB} = 1.643 \times 10^{-4} \times (1 + 0.3333)^{-1.1} \times 8.1585^{-1.2} \times 12.82^{0.93} \times 30^{3.3} \times 10^{\left(\frac{-33.002}{10}\right)}$$

$$U_{LB} = 3.8808 \times 10^{-3}$$

For 13.08 Ghz

$$U_{HB} = 1.643 \times 10^{-4} \times (1 + 0.3333)^{-1.1} \times 8.1585^{-1.2} \times 13.08^{0.93} \times 30^{3.3} \times 10^{\left(\frac{-32.859}{10}\right)}$$

$$U_{HB} = 4.0863 \times 10^{-3}$$

Solving got the corresponding availability

$$R_{LB} = (1 - 3.8808 \times 10^{-3}) \times 100\%$$

$$R_{LB} = 99.6119\ \%$$

$$R_{HB} = (1 - 4.0863 \times 10^{-3}) \times 100\%$$

$$R_{HB} = 99.5914\ \%$$

As seen here, the CCIR Recc. 530 gives the lowest unfaded reliability calculation so far.

Microwave System Equations

Q: How is microwave reliability and outage time computed?

Q: Several types of equations are used for microwave calculations. These are described below:

Free Space Loss

The free space loss is computed based on the path length and frequency using the equation:

(1) A = 96.6 + 20 LOG(F) + 20 LOG(D)

where:

A is the attenuation in dB.

F is the frequency in GHz.

D is the distance in miles.

Rain Attenuation

The rain attenuation due to rainfall can be entered directly or computed by several different methods (see Ryde & Ryde, Medhurst, and CCIR).

When you direct TAP to calculate rain attenuation, you will enter a rainfall rate (in either inches or millimeters per hour) and the portion of the path affected by rain attenuation entered in the current units (miles or kilometers), or as a percentage of the total path.

After entering all of the required values, the attenuation values computed for the three models are displayed. When you select the desired value and return to the microwave link budget program the selected attenuation is incorporated in the fade margin and reliability calculations performed in this program.

TAP keeps track of the source of the rain attenuation value. If you accept the Medhurst value as described above, the Loss Mode will be marked "MED" in the link budget program to remind you of the attenuation model used to generate attenuation. However, if you enter any value directly, the mode will be marked "SPEC" (for specified).

Atmospheric Absorption

The loss from atmospheric absorption can be entered directly or computed by pressing the "Calculate Loss" button for the Absorption Loss field.

Absorption loss is computed as a function of the frequency using the complete length of the path. The loss value is determined from curves based on van Vleck (1947), providing separate values for and water vapor losses. The absorption loss is the sum of these two

Terrain/Humidity Factor

The terrain and humidity factor used in the reliability calculation can be entered directly, or the value can be computed from humidity and terrain roughness information.

Lenkurt (1970) suggests the following values:

4 for very smooth terrain, including over water.

1 for average terrain, with some roughness.

.25 for mountainous, very rough, or very dry areas.

The terrain and humidity factor can be computed using the formula (from Roelofs, 1986):

(2) $a = K \times (W/50)^{-1.3}$

where:

K is a constant based on local area humidity:

2 for coastal humid areas.

1 for average or temperate areas.

.5 for dry areas.

W is the roughness of the terrain. This is the standard deviation of the path elevations taken at one mile intervals, not including the end points.:

(3) $W = \sqrt{\left[\left(1/A\right) \times \sum (E - A)^2\right]}$

where:

A is the average of the terrain at one mile intervals (excluding the end points).

E is the elevation of each of the terrain points at one mile intervals (excluding the end points).

$\Sigma (E - A)^2$ is the sum of the square of differences between each elevation point and the average elevation.

TAP keeps track of the source of the terrain/humidity value. If you calculate the value as described above, the Loss Mode will be marked "CALC". However, if you enter any value directly, the mode will be marked "SPEC" (for specified).

Climate Factor

The climate factor used in the reliability calculation can be entered directly or computed from average annual temperature information.

Lenkurt suggests the following values:

.5 for gulf coast or similar hot, humid areas.

.25 for normal interior temperate or northern areas.

.125 for mountainous or very dry areas.

The climate factor can be computed using the formula (from Roelofs):

(4) B = T/50 x 3/12

$$B = \frac{T}{50} \cdot \frac{3}{12}$$

where:

T is the average annual temperature in degrees Fahrenheit.

If you calculate the value as described above, the value will be marked "CALC" on printed output, and the temperature will be included. However, if you enter any value directly, the value will be marked "SPEC" (for specified).

Composite Fade Margin

The TAP fixed facility data base includes fields for digital fade margin values. These values can be used in addition to the computed thermal fade margin to compute a composite fade margin value.

The additional fade margins included are:

- Dispersive Fade Margin (DFM) is the "contribution to outage that accounts for in-band distortion that can at times cause a digital system to fail when the AGC or flat fade is less than that required to reach the thermal noise threshold." ("Digital Radio Path Fade Margin Calculations", p.32, MDR-2000 Series Product Description, Rockwell International)

- Adjacent Channel Interference Fade Margin (AIFM) is the contribution to system outage resulting "from the broad transmit spectra of digital systems that have sufficient energy that spills over into adjacent channel digital receivers." ("Digital Radio Path Fade Margin Calculations", p.32, MDR-2000 Series Product Description, Rockwell International)

- External Interference Fade Margin (EIFM) is the "contribution to system outage from intersystem (foreign route) cochannel interference. Such interference can come from transmitters on the desired route (overreach, for example) or from transmitters from other routes in the vicinity." ("Digital Radio Path Fade Margin Calculations", p.32, MDR-2000 Series Product Description, Rockwell International).

EIFM is computed using the following equation:

(5) EIFM = RSL - T +(T/I) - (C/I)

where:

RSL is the unfaded received signal level in dBm. Since the RSL is not known until later in the program, the computed EIFM value will not be displayed on the Receive Site screen.

T is the receiver threshold for 10^{-6} BER in dBm.

(T/I) is the threshold to interference ratio in dB.

(C/I) is the carrier to interference ratio in dB.

The fade margin values are entered in the fixed facility lookup or fixed facility data base editor. If you want to exclude any of the fade margin values from the composite fade margin calculation, enter a value of zero (0) or 99.9 for that fade margin value.

The composite fade margin is computed using the equation:

(6) CFM =
$-10 \text{ LOG } (10^{-DFM/10} + 10^{-TFM/10} + 10^{-AIFM/10} + 10^{-EIFM/10})$

Where:

CFM is the Composite Fade Margin.

DFM is the Dispersive Fade Margin.

TFM is the computed Thermal Fade Margin.

AIFM is the Adjacent Channel Interference Fade Margin.

EIFM is the External Interference Fade Margin.

Frequency Diversity

The TAP fixed facility data base includes a field for frequency diversity. If frequency diversity is not employed, set the "Diversity Frequency" field to zero (0). If frequency diversity is used, enter the second frequency in MHz.

The improvement factor for frequency diversity is computed from the following equations, depending on the frequency of the system:

1.000 0.5

2 1.00
4 0.50
6 0.25

(7) $Ifd_{[2\ GHz]} = 1.0000\ (df / f)\ 10^{F/10}$

(8) $Ifd_{[4\ GHz]} = 0.5000\ (df / f)\ 10^{F/10}$

(9) $Ifd_{[6\ GHz]} = 0.2500\ (df / f)\ 10^{F/10}$

(10) $Ifd_{[7\text{-}8\ GHz]} = 0.1250\ (df / f)\ 10^{F/10}$

(11) $Ifd_{[11\text{-}12\ GHz]} = 0.0833\ (df / f)\ 10^{F/10}$

where:

f is the frequency in GHz

df is the diversity spacing in GHz

F is the thermal or composite fade margin

The constant coefficient of the equation is interpolated linearly for intermediate frequencies. Frequencies above or below the specified ranges use the coefficients for the highest or lowest range, respectively.

If both spatial and frequency diversity are employed, the combined improvement factor is the product of the two values.

Reliability

The reliability of a system based on the computed fade margin is calculated based on the following equation (from Lenkurt)

(12) $Undp = a \times b \times 2.5 \times 10^{-6} \times f \times D^3 \times 10^{-F/10}$

where:

Undp is the non-diversity outage probability.

a is the terrain factor.

b is the climate factor.

f is the frequency in GHz.

D is the path length in miles.

F is the fade margin in dB. For systems which include a space antenna, a fade margin is computed for each receive antenna (primary and diversity). The values will be different if the two receive systems have different antenna gains, transmission line lengths, or other losses. The higher value fade margin ("best case") is used for this non- outage calculation. The other fade margin value is used to compute the diversity as described below.

The percent reliability is computed from the outage probability by:

(13) $\%R = 100 \times (1 - Undp)$

The reliability of the system generally can be improved by the use of a second receiving antenna located at a different height ("space diversity"). Both antennas (primary and diversity) feed the receiver through appropriate switching devices.

The space diversity improvement factor for vertically separated receive antennas is computed as:

(14) $I = (7 \times 10^{-5} \times f \times s^2 \times 10^{F2/10}) / D$

where:

I is the space diversity improvement factor

f is the frequency in GHz.

s is the vertical antenna spacing in feet.

D is the path length in miles.

F2 is the lower fade margin in dB. (In space diversity systems, fade margins are computed for both antennas. The larger fade margin value is used to compute the non-diversity reliability, and the smaller fade margin value is used to compute the space diversity improvement.)

The overall reliability with space diversity is computed by dividing the non-diversity outage probability by the improvement factor:

(15) Udiv = Undb/I

References:

Engineering Considerations for Microwave Communications Systems, 1975, GTE Lenkurt Incorporated.

Bullington, Kenneth, "Radio Propagation for Vehicular Communications", *IEEE Transactions on Vehicular Technology*, November 1977.

Roelofs, Stan, "Fade Margin Requirements for Microwave Systems", *Microwave Reference Guide*, 1986, Motorola.

"Digital Radio Path Fade Margin Calculations", p.32, MDR-2000 Series Product Description, Rockwell International

I'm interested!
Please click here to jump to an online form which helps us better understand your needs. Then we will be able to respond to your request with information that is most useful to you.

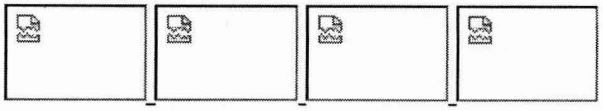

Copyright 1999 by SoftWright LLC

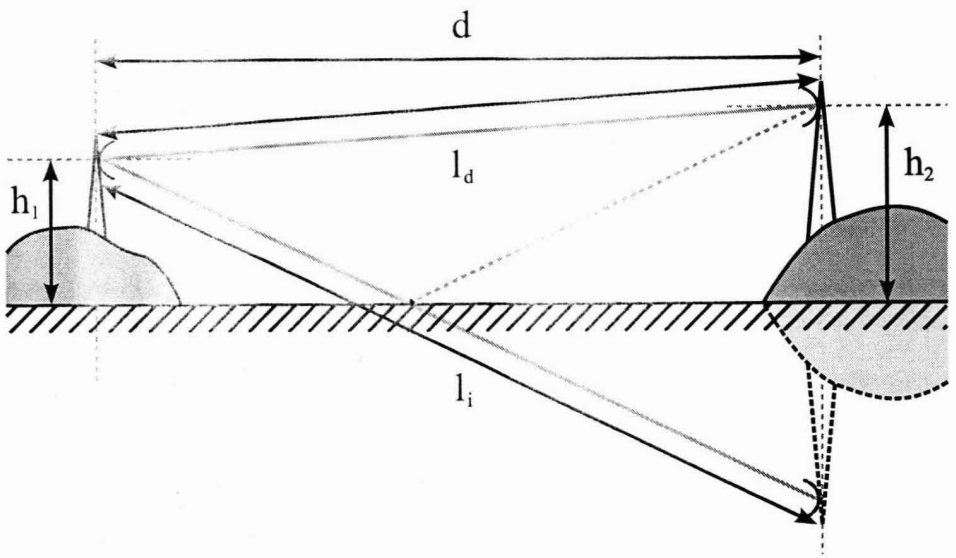

Figure 10: The two ray model, annotated to show the antenna heights (h_1, h_2), horizontal span (d) and the lengths of the direct (l_d) and indirect (l_i) paths.

Appendix: Geometric Model Description

Given link geometry of two antenna heights above sea level (h_1, h_2) and the horizontal distance between the two antennas (d) as shown in Figure 10 we can determine the length of the direct (l_d) and indirect (l_i) rays by calculating the hypotenuse as follows:

$$l_d = \sqrt{d^2 + (h_1 - h_2)^2} \tag{1}$$

$$l_i = \sqrt{d^2 + (h_1 + h_2)^2} \tag{2}$$

The triangle establishing the direct ray is trivial, the triangle establishing the indirect ray can be found by intuiting the distance to the virtual image of the receiving dish, reflected in the water plane.

The path difference is trivially found:

$$l_\Delta = l_i - l_d \tag{3}$$

Assuming propagation at the speed of light, wavelength is given by:

$$\lambda = \frac{c}{f} \tag{4}$$

Given the difference in path length l_Δ and the wavelength λ we can determine the phase difference in radians as follows:

$$\theta_\Delta = \frac{l_\Delta}{\lambda} 2\pi \tag{5}$$

The above two equations are trivially composed to calculate phase difference directly from path length difference and frequency:

$$\theta_\Delta = \frac{f \cdot l_\Delta}{c} 2\pi \tag{6}$$

Now that we have the phase difference we can calculate the amplitude of the received signal using vectors. The direct ray will be a vector with an magnitude of 1, while the indirect ray will have an amplitude equal to the reflection coefficient and an angular difference of θ_Δ.

The magnitude of the sum of two arbitrary vectors is given by:

$$|\mathbf{c}| = \sqrt{(|\mathbf{a}|\cos\theta_{\mathbf{a}} + |\mathbf{b}|\cos\theta_{\mathbf{b}})^2 + (|\mathbf{a}|\sin\theta_{\mathbf{a}} + |\mathbf{b}|\sin\theta_{\mathbf{b}})^2} \quad (7)$$

However, for the direct ray $\mathbf{a}$, $|a| = 1$ and $\theta_a = 0$, so when calculating the relative amplitude of the received signal compared to propagation in free space A_{rx} given a phase difference θ_Δ and a reflection coefficient Γ the above equation simplifies to:

$$A_{rx} = \sqrt{(1 + \Gamma cos\theta_\Delta)^2 + (\Gamma sin\theta_\Delta)^2} \quad (8)$$

When A_{rx} is 1, the received signal strength (RSS) is identical to the expected received signal strength in free space. When A_{rx} is less than 1, the RSS will be diminished. A null occurs when A_{rx} approaches 0. Signal enhancement occurs when A_{rx} increases above 1.

For convenience, A_{rx} can be expressed in dB by taking the logarithm and multiplying by 10. This allows easy calculation in link budget analysis by indicating the "depth of the fade" that the link will experience.

Tide is easily factored into this model by recomputing with changing values for h_1 and h_2. We simply observe that as the tide rises, the antenna height with respect to sea level effectively decreases.

References

[1] Wireless Networking in the Developing World. http://wndw.net/index.html, Dec 2007. Second Edition.

[2] G Bernardi, P Buneman, and M Marina. Tegola Tiered Mesh Network Testbed in Rural Scotland. In *Proc. ACM MobiCom 2008 Workshop on Wireless Networks and Systems for Developing Regions (WiNS-DR'08)*, Sep 2008.

[3] A Sheth, S Nedevschi, R Patra, S Surana, E Brewer, and L Subramanian. Packet Loss Characterization in WiFi-based Long Distance Networks. In *Proc. IEEE Infocom*, 2007.

[4] D Gokhale, S Sen, K Chebrolu, and B Raman. On the Feasibility of the Link Abstraction in (Rural) Mesh Networks. In *Proc. IEEE Infocom*, 2008.

[5] West Highland Free Press. ConCom: Growing Tide of Dissatisfaction, Feb 2008.

[6] Pathloss 4.0, Oct 2009. (Online) http://www.pathloss.com/p4/index.html.

[7] P Bahl, R Chandra, and J Dunagan. SSCH: Slotted Seeded Channel Hopping for Capacity Improvement in IEEE 802.11 Ad-Hoc Wireless Networks. In *Proc. ACM MobiCom*, 2004.

[8] P Rice and A Longley. Prediction Of Tropospheric Radio Transmission Loss Over Irregular Terrain. A Computer Method, Jan 1968.

[9] A LaGrone, A Straiton, and H Smith. Synthesis Of Radio Signals on Overwater Paths. *IRE Transactions on Antennas and Propagation*, 3(2):48–52, 1955.

[10] N Fuke, K Sugiyama, and H Shinonaga. Long-range Oversea Wireless Network Using 2.4 GHz Wireless LAN Installation and Performance. In *Proc. ICCCN*, 2003.

[11] C Haslett. *Essentials of Radio Wave Propagation*, chapter 4 Reflection, scatter and penetration, pages 95–98. Cambridge University Press, 2008.

[12] J McPetrie, B Starnecki, and H Jarkowski. Oversea Propagation on Wavelengths of 3 and 9 Centimeters. In *Proceedings of the IRE*, Jan 1949.

[13] T Inoue and T Akiyama. Propagation Characteristics on Line-of-sight Over-sea Paths in Japan. *IEEE Trans. Antennas Propag.*, 22(4):557–565, 1974.

[14] D Siddle, E Warrington, and S Gunashekar. Signal Strength Variations at 2 GHz for Three Sea Paths in the British Channel Islands: Observations and Statistical Analysis. *Radio Sci.*, 42(4):RS4019, Aug 2007.

[15] W Lam and A Webster. Microwave Propagation on Two Line-of-sight Oversea Paths. *IEEE Trans. Antennas Propag.*, 33(5):510–516, 1985.

[16] S Sen and B Raman. Long Distance Wireless Mesh Network Planning: Problem Formulation and Solution. In *Proc. World Wide Web (WWW) Conference*, 2007.

[17] M Cave, C Doyle, and W Webb. *Essentials of Modern Spectrum Management*. Cambridge University Press, 2007.

[18] S Saunders and A Aragon-Zavala. Antennas And Propagation For Wireless Communication Systems, chapter 3.2.3 Typical Reflection and Transmission Coefficients, page 546. John Wiley & Sons, Ltd, second edition, 2007.

[19] J Bauer, Sep 2009. private communication.

[20] Y Xiao. IEEE 802.11n: Enhancements For Higher Throughput in Wireless LANs. *IEEE Wireless Commun. Mag.*, 12(6):8291, Dec. 2005.

Link Design Examples

The following examples are intended to be used with the stand alone PL50L application. The files are located in the examples directory in the Pathloss program directory. The default installation directory is C:\Program files\Pathlss 5.

PROBLEM PATH

This example uses the file examples/problem/problem.pl5

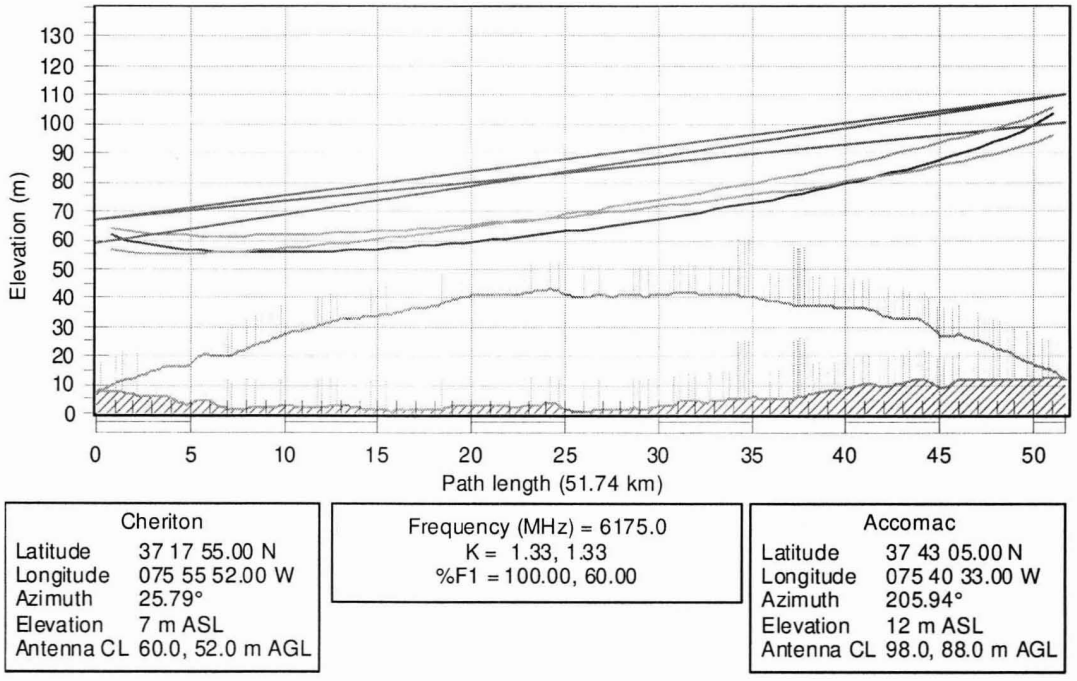

The design frequency is 6175 MHz and the pertinent performance data is given in the table below

Table 1: Multipath performance calculations

TX power (dBm)	32.00		32.00
RX threshold level (dBm)	-76.50		-76.50
Main receive signal (dBm)	-36.90		-36.90
Diversity receive signal (dBm)	-38.80		-38.80
Thermal fade margin (dB)	39.60		39.60
Climatic factor		2.00	
Terrain roughness (m)		6.10	
C factor		6.58	
Average annual temperature (°C)		14.28	

Table 1: Multipath performance calculations

Annual multipath availability (%)	99.99976		99.99984
Annual multipath unavailability (sec)	76.79		51.71
Annual 2 way multipath availability (%)		99.99959	
Annual 2 way multipath availability (sec)		128.50	

The overall performance objective for this path is 99.999% annual availability which has been met based on the above calculations; however in practice the actual path performs poorly.

Given that rain attenuation is not significant at 6 GHz, and that multipath fading mainly occurs under super refractive conditions, this leaves sub-refraction as the most likely cause of the problem. This situation will be analysed as a surface duct and as obstruction of K fading.

Surface duct

In the *Multipath - reflections* design section, select the *Method - Variable gradient ray trace* menu item. Then click

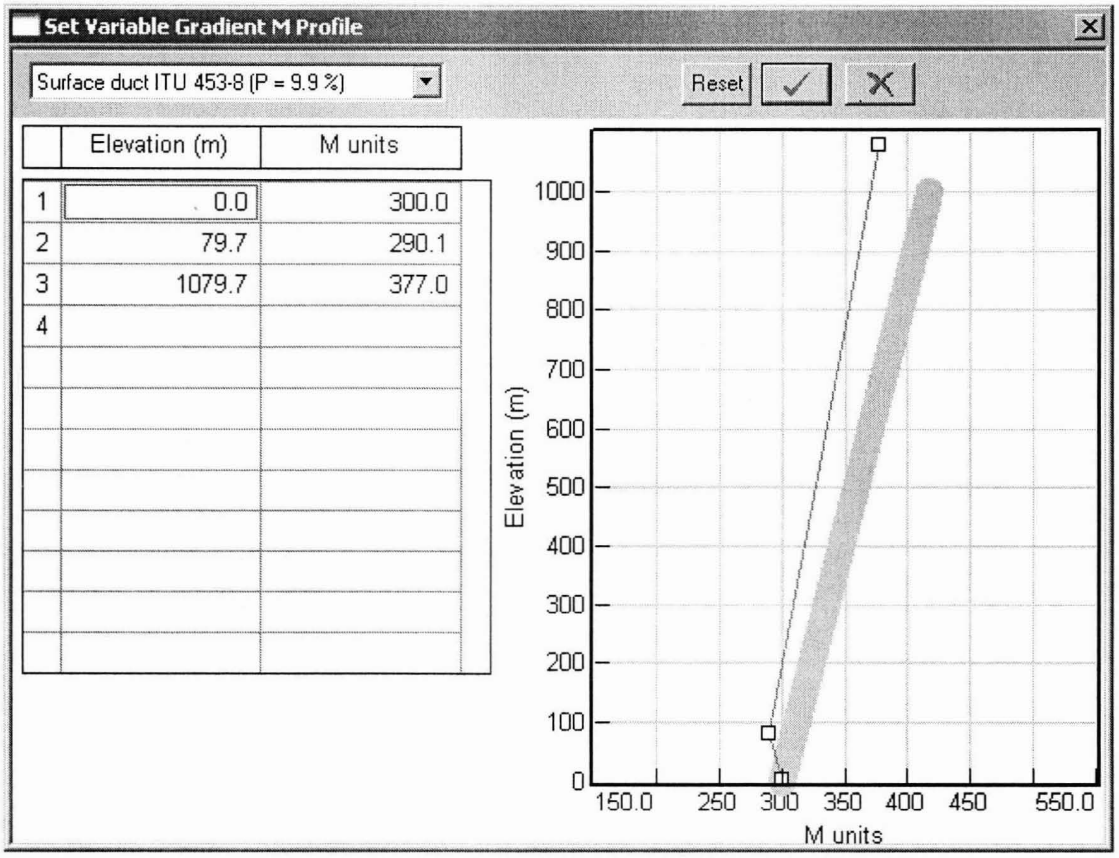

the *Set M profile* button. Select the Surface duct ITU 453-8 M profile. The data for this M profile is taken from the ITU 453-8 data base based on the path center coordinates of this problem path. The "P = 9.9%" term means that the probability of occurrence is 9.9% of the time.

Set the *Number of rays* and the *Total display angle* as shown on the right. Set the *Ground reflections* to *None* to simplify the overall ray trace display.

The resulting display shows that the rays are bent above and below the receive site. In this condition there would be a signal null.

If the profile is reversed using the *Operations - Reverse profile menu item*, it is apparent that the same signal null occurs in both directions

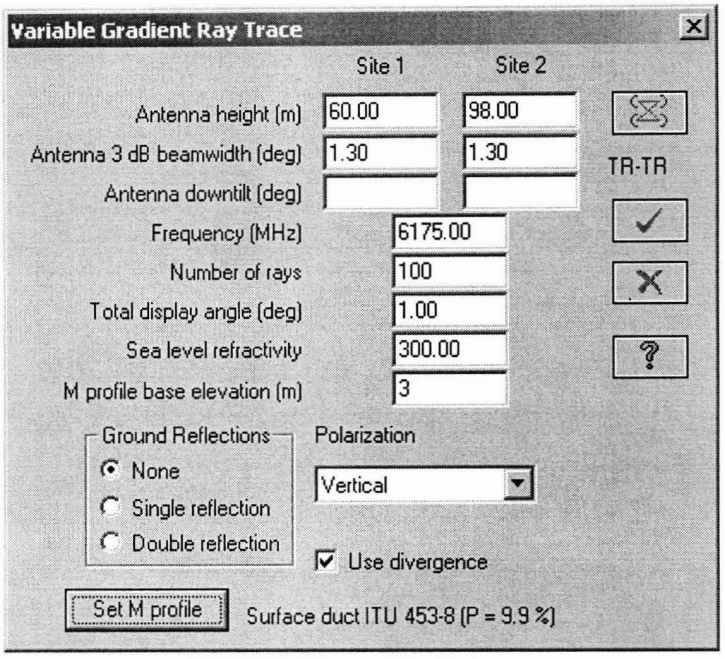

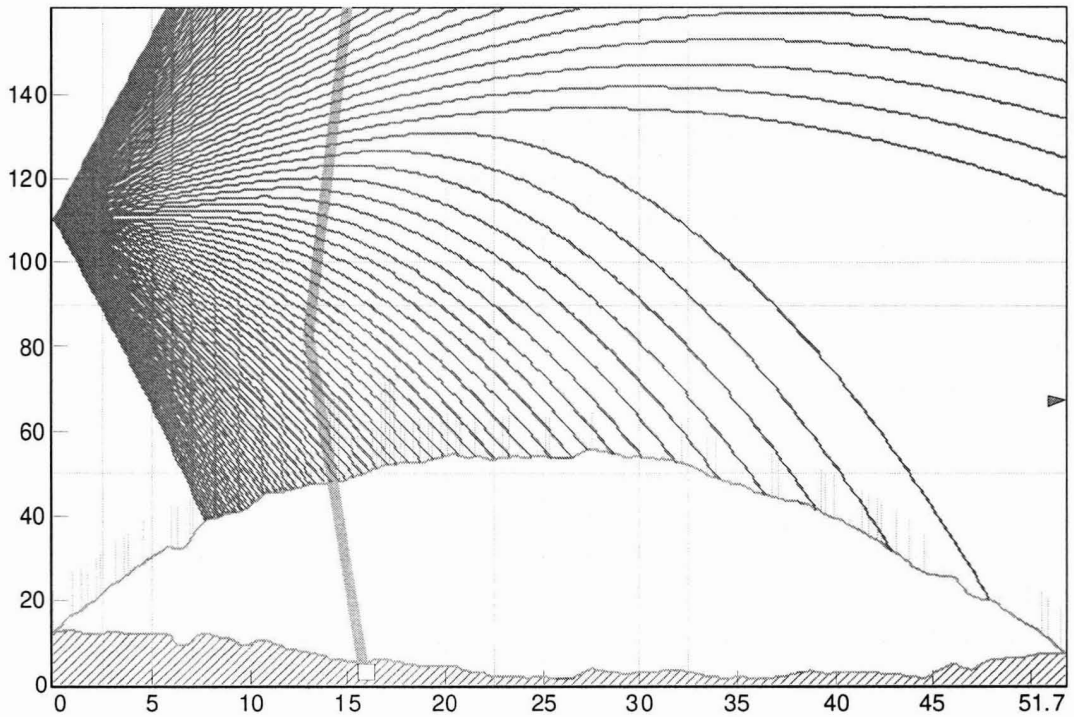

Obstruction (K) fading

Select the *Transmission analysis* design section and then select the *Operations - Obstruction fading* menu item.

Obstruction (K) fading - Public obstruction fading data

Obstruction fading method	Iterative diffraction loss calculations
Diffraction algorithm	Pathloss
Path center latitude	37 30 30.00 N
Path center longitude	075 48 12.50 W
Critical value of dN/dh (K)	171.25 (K = 0.48)
February - Median value of dN/dh (K)	-40.30 (K = 1.35)
February - Standard deviation (N units/km)	45.00
February - Fade probability (%)	1.29E-004
May - Median value of dN/dh (K)	-48.60 (K = 1.45)
May - Standard deviation (N units/km)	45.00
May - Fade probability (%)	5.16E-005
August - Median value of dN/dh (K)	-51.50 (K = 1.49)
August - Standard deviation (N units/km)	66.30
August - Fade probability (%)	0.04
November - Median value of dN/dh (K)	-49.10 (K = 1.46)
November - Standard deviation (N units/km)	70.00
November - Fade probability (%)	0.08
Annual obstruction fade probability (%)	0.03035
Annual obstruction fade outage (sec)	9572.29

Set the *Obstruction fading method* to Iterative diffraction loss calculations and the *Diffraction algorithm* to Pathloss. The thermal fade margin on this path is 39.6 dB. The program determines the value of K which results in a diffraction loss of 39.6 dB (i.e. the thermal fade margin). The example show uses the Public obstruction fading data. This data consists of a median value of dN/dh (K) and its standard deviation for four different time periods. This is used in a normal distribution to determine the probability or the value of K actually occurring. At this location, the months of August and November have high standard deviation values. The overall result is that the total outage time due to obstruction fading is 9572.29 seconds which reduces the annual availability to 99.969%

Corrective Action

In the case of obstruction fading, increasing the antenna heights will reduce the outage; however this will not have any appreciable effect on ducting.

CLEARANCE CRITERIA

This example uses the file examples\clearance_criteria\clearance_criteria.pl5 to illustrate the adverse effects of using the classic heavy route clearance criteria on long paths.

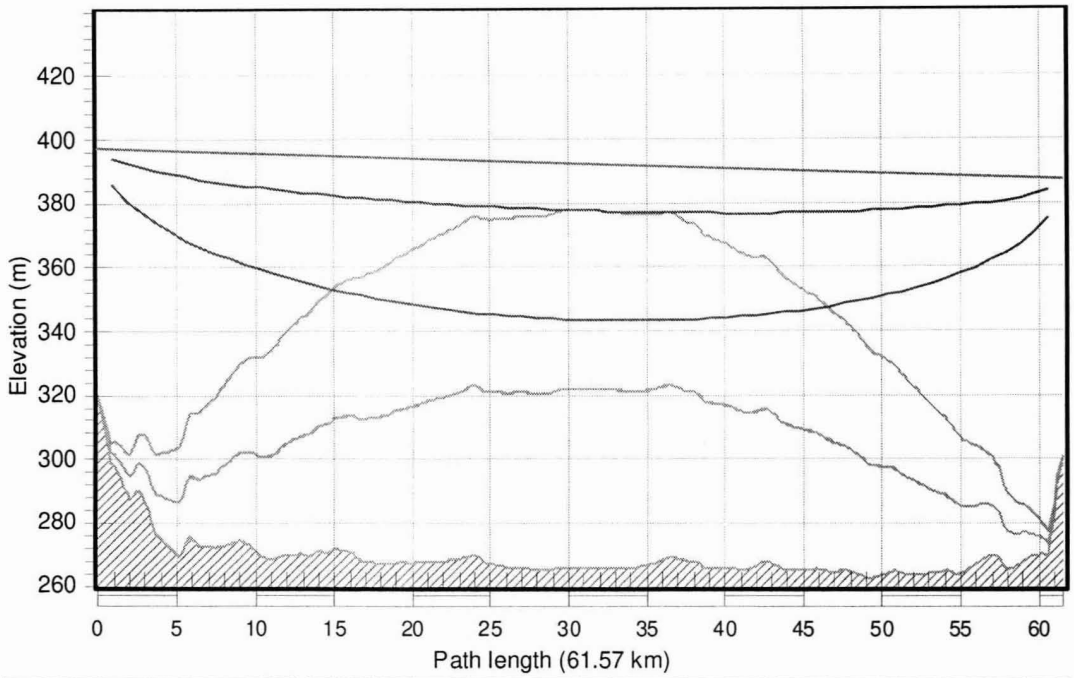

Site 1	
Latitude	53 59 28.29 N
Longitude	103 08 01.82 W
Azimuth	94.25°
Elevation	320 m ASL
Antenna CL	77.7 m AGL

Frequency (MHz) = 1925.0
K = 1.33, 0.67, 1.33
%F1 = 100.00, 30.00

Site 2	
Latitude	53 56 47.58 N
Longitude	102 11 55.19 W
Azimuth	275.01°
Elevation	301 m ASL
Antenna CL	86.0 m AGL

The antenna heights were calculated using the clearance criteria shown. The second criteria (30%F1 at K = 2/3) is the controlling clearance criteria. The original intent of a second clearance criteria was to provide some clearance at a low value of K and therefore prevent signal loss due to diffraction or obstruction fading. The effect of this second clearance criteria will result in excess clearance a the median value of K

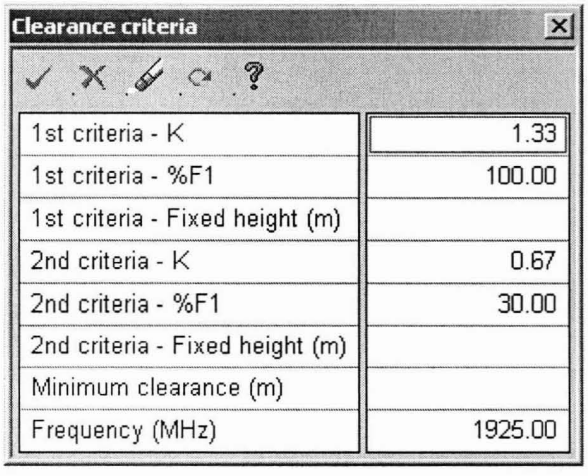

1st criteria - K	1.33
1st criteria - %F1	100.00
1st criteria - Fixed height (m)	
2nd criteria - K	0.67
2nd criteria - %F1	30.00
2nd criteria - Fixed height (m)	
Minimum clearance (m)	
Frequency (MHz)	1925.00

The first and second clearance criteria are shown in the *Antenna heights* design section display below. The red Fres-

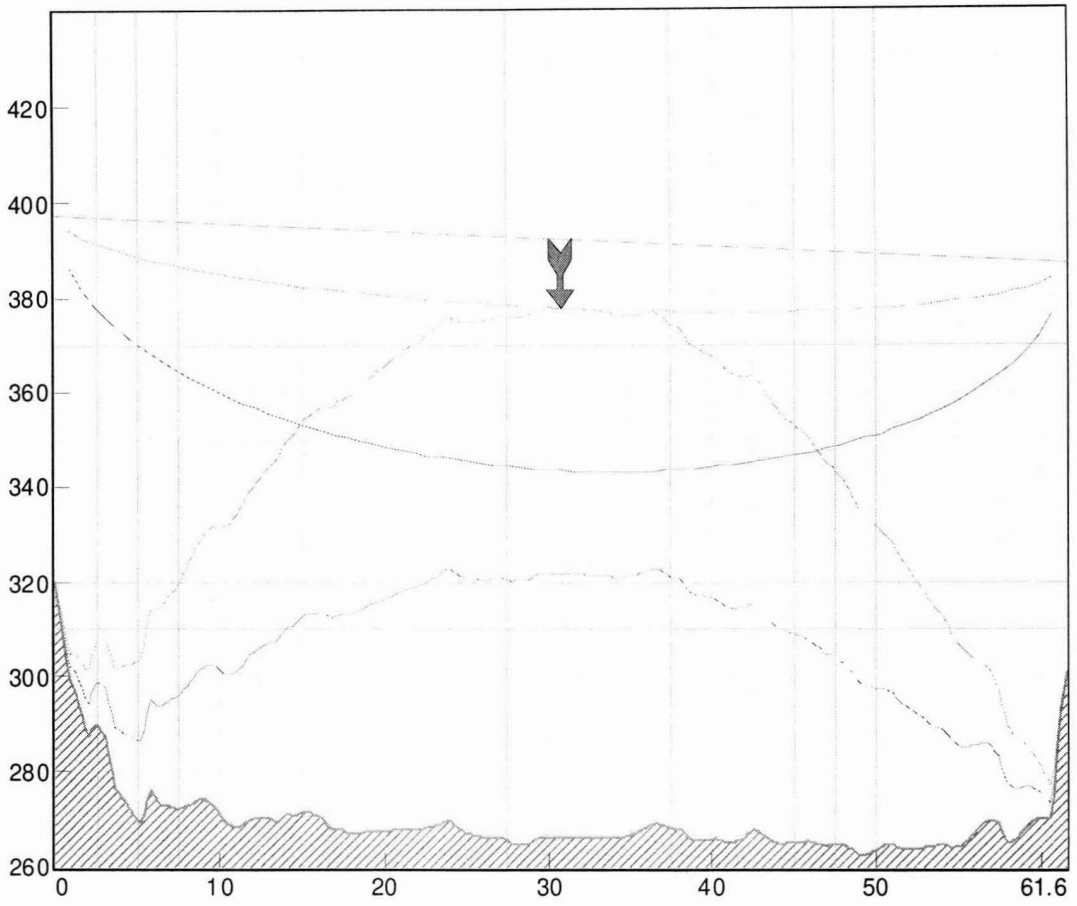

nel zone and effective earth radius profile represent the first clearance criteria (100% F1 at K = 1.33). The corresponding green curves represent the second clearance criteria.

An estimate of the outage due to obstruction fading is available in the transmission analysis design section. Select the *Operations - Obstruction fading* menu item. The annual outage is shown to be 0.26 seconds based on a fade margin of 40.8 dB and can be safely neglected.

The effects of the excess clearance will be analysed in the *Multipath - reflections* design section. Select the *Operations - Fresnel zones* menu item. Select the *Fresnel number 2* reference and click the *Apply* button. Reflected signal along the F2 Fresnel radius will arrive out of phase with the main signal and result in signal cancellation. It is important to note that F2 does not equal 200% F1.

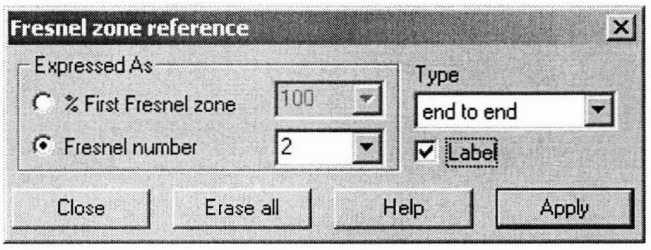

The display shows that the path has second Fresnel zone clearance at the median value of K.

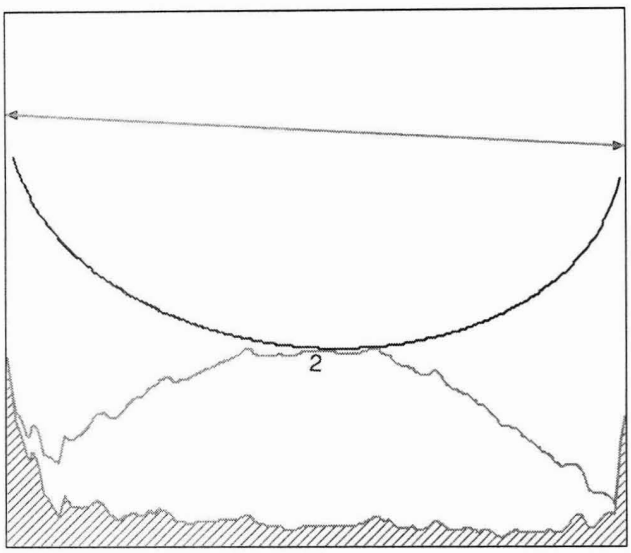

Two methods are available to analyze the effects of a reflected signal on a path. The first method uses a reflective plane definition. This is a highly idealized method when the actual path profile is replaced by the plane. In this case, the analysis is based on a single reflected signal

The second method uses ray tracing on the actual path profile All reflected signals on the path are considered in the analysis and provides a more realistic representation or the actual situation.

Select the *Variable - Analyze using ray tracing* menu item. This method uses the actual path profile and does not require a reflective plane. The results below show a the effects of the main reflected signal with smaller reflected signals superimposed on the trace.

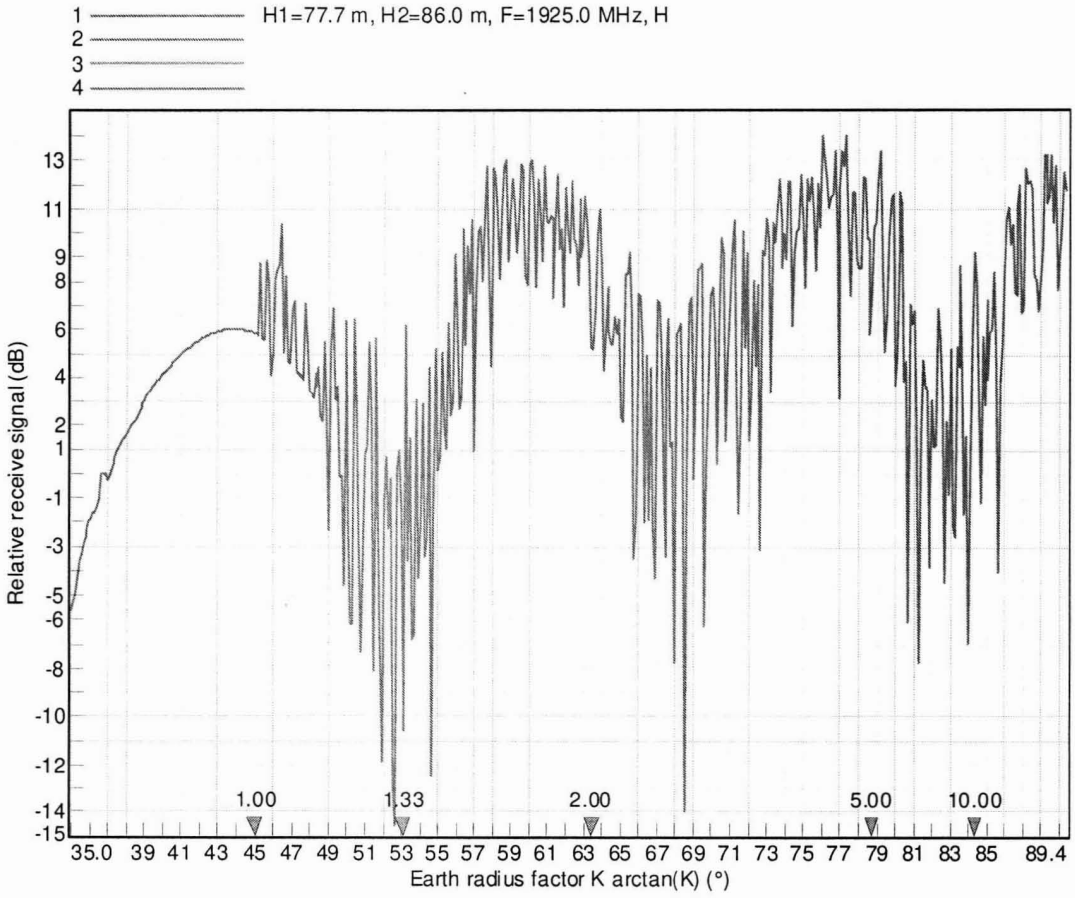

At the median K or 1.33, the operation would be problematic.

Corrective action

The antenna heights were recalculated using a single clearance criteria of 100% F1 at K = 4/3. The ray trace results are shown below. Signal enhancement now occurs at the median K of 1.33.

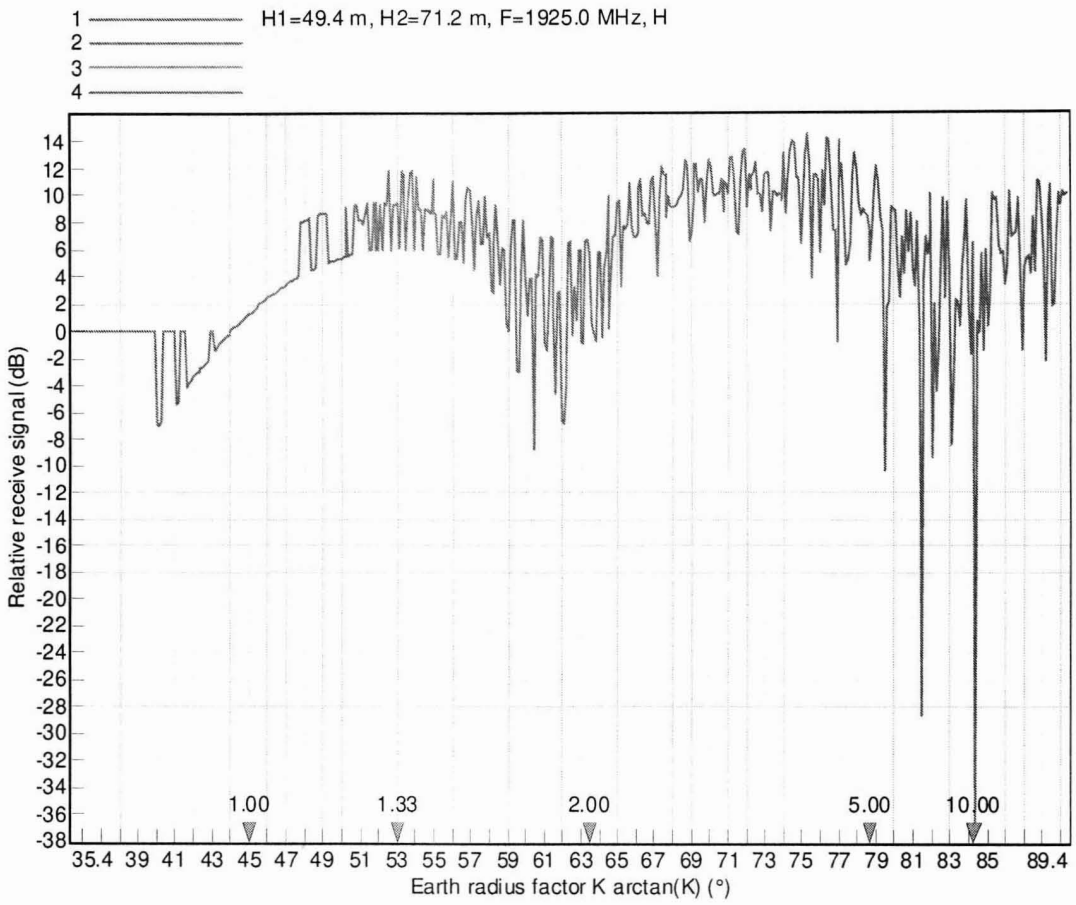

With the same fade margin, the obstruction outage increases from 0.26 seconds to 18 seconds.If the transmission line lengths are reduced for the new antenna heights, the performance using the different clearance criteria is summarized in the table below.

Table 2:

Clearance criteria	Antenna heights	Fade margin	Obstruction outage	Multipath outage
100% F1 at K = 4/3 30% F1 at K = 2/3	78 and 86 meters	40.8 dB	0.26 seconds	854 seconds
100% F1 at K = 4/3	50 and 71 meters	43.6 dB	2 seconds	454 seconds

In this example, the overall performance improved using the lower antenna heights; however, this is not always the case. This path is in a northern climate. Results in a temperate climate will be different. The purpose of this example is to provide a method of analysing excess clearance on a path.

A clearance criteria must specify both a value of K and a percent of the first Fresnel zone. If the Fresnel zone is left out the path will be grazing at the specified value of K and will result in loss in the order of 6 dB.

SPACE DIVERSITY - SPECULAR REFLECTIONS

This example uses the file examples\refelect\refelect.pl5. The path will be analysed for a specular reflection. Space

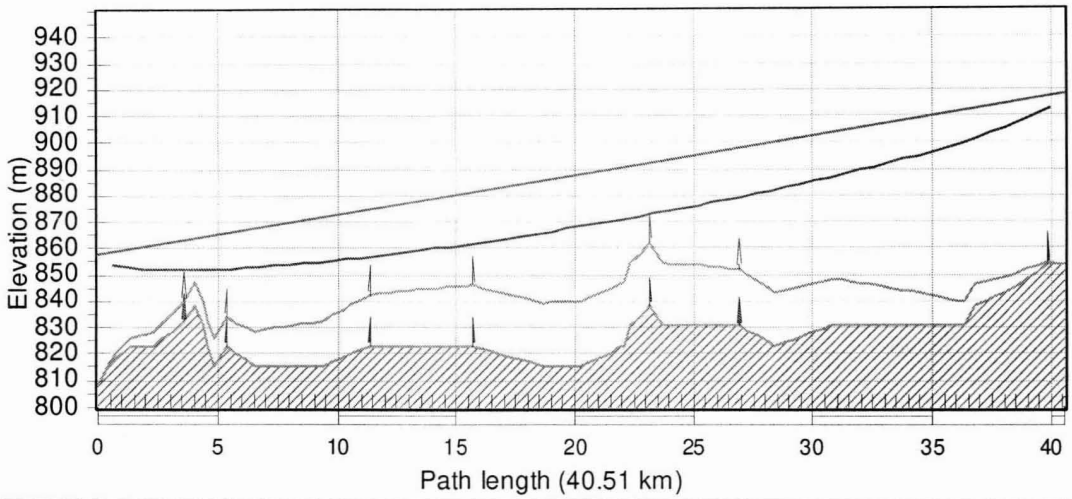

TAU Nevis	
Latitude	52 23 04.00 N
Longitude	113 01 35.00 W
Azimuth	112.68°
Elevation	808 m ASL
Antenna CL	50.0, 44.0 m AGL

Frequency (MHz) = 7590.0
K = 1.33
%F1 = 100.00

Lonepine	
Latitude	52 14 34.00 N
Longitude	112 28 45.00 W
Azimuth	293.12°
Elevation	853 m ASL
Antenna CL	65.0, 55.0 m AGL

diversity will be implemented and the antenna spacings will be determined to minimize the effects of the specular reflection. The analysis will be carried out in the *Multipath - reflections* design section

Constant gradient ray trace

A constant gradient ray trace is used to determine if the path profile geometry can support a specular reflection. From an inspection of the path, it is not evident whether this is the case Select the Method - Constant gradient ray trace menu item. Set all parameters as shown in the dialog on the right and click the green check button to generate the ray trace.

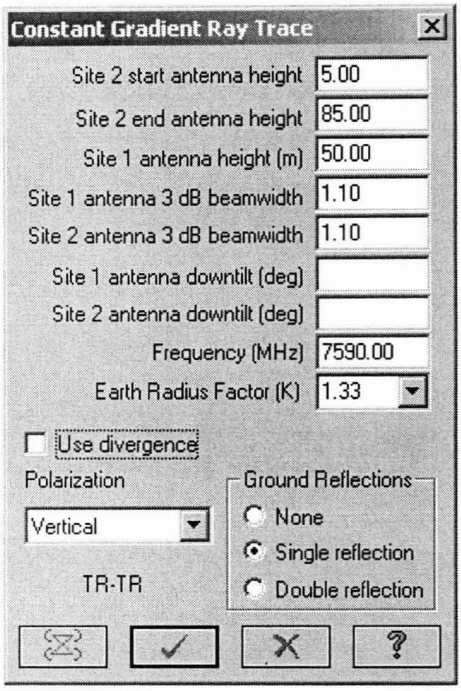

In the description below, the rays are transmitted fro site 1 on the left side of the display. The rays are receive at site 2 on the left site of the display

The ray trace shows that there is a section along the path profile where the reflected rays arrive at site 2 above and below the elevation of the site 2 antenna. There is a the possibility of a specular reflection on this path. The actual ground cover along the reflective section will determine the severity of the problem.

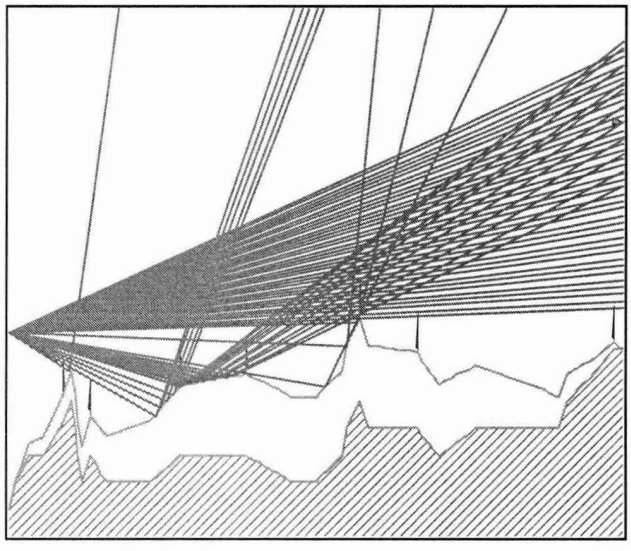

Another simple test for a reflection points on the path

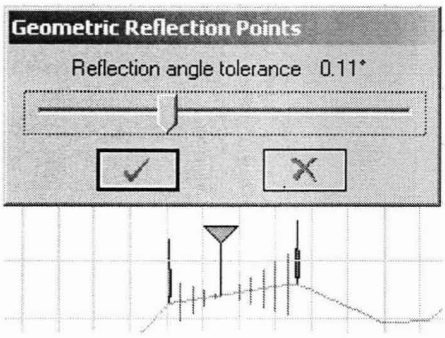

profile is available under the *Method - Mark reflection points* menu item The profile is scanned from site 1 to site 2. At each point, the angle of incidence and the angle of reflection is calculated. The angle of incidence / reflection is the angle formed by the line to the site 1 / site 2 antenna and the actual terrain. If the difference between these two angles is less than the *Reflection angle tolerance* then a green mark is drawn on the profile with an amplitude proportional to the magnitude of the difference. This line drawing process continues and if the difference between angles changes sign, then this indicates that a geometric reflection point has been passed over. The location of the reflection point is interpolated and marked on the profile.

The ray trace can be used to calculate the receive signal variation at site 2 a as a function of height. Select the *Method - Site 2 height - gain* menu item.The results show that there is no signal variation below 45 meters as there are no reflected rays below this elevation. The remainder of the display shows the addition of main and reflected rays in the classic peak and null pattern. The vertical blue line marks the site 2 antenna height. This is properly located near the peak of the curve.

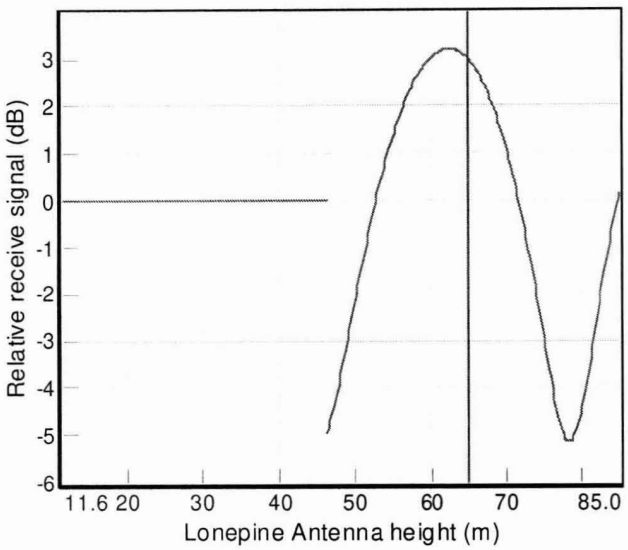

Space diversity implementation

Space diversity will be used on this path and the diversity antenna spacing will be set based on a reflective plane definition.

To clear the display, select the *Method - Constant gradient ray trace* menu item and then click the red X to cancel the operation.

Select the *Operations - Define plane* menu item. Click the *Calculate* button several times and note the calculation method used at the bottom of the display. The first calculation using the standard deviation of the points which are visible to each antenna does not result in a valid plane. The second calculation uses the first range in the ray tracing display and produces the correct plane definition. Note that there may several ranges in the ray trace and each successive click of the calculation button produces a different result.

The *Space diversity planning* feature is only enabled for a space diversity antenna configuration. Select the *Configure - Set antenna configuration* and then check the *TRDR - TRDR* configuration

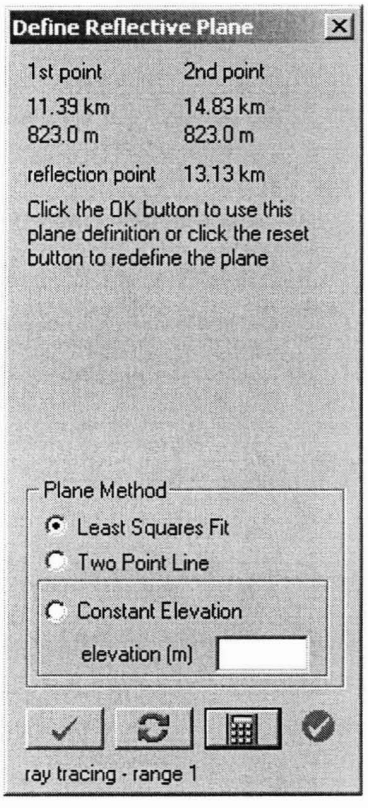

Select the *Variable - Analyse using reflective plane* menu item. The default variable parameter is the earth radius

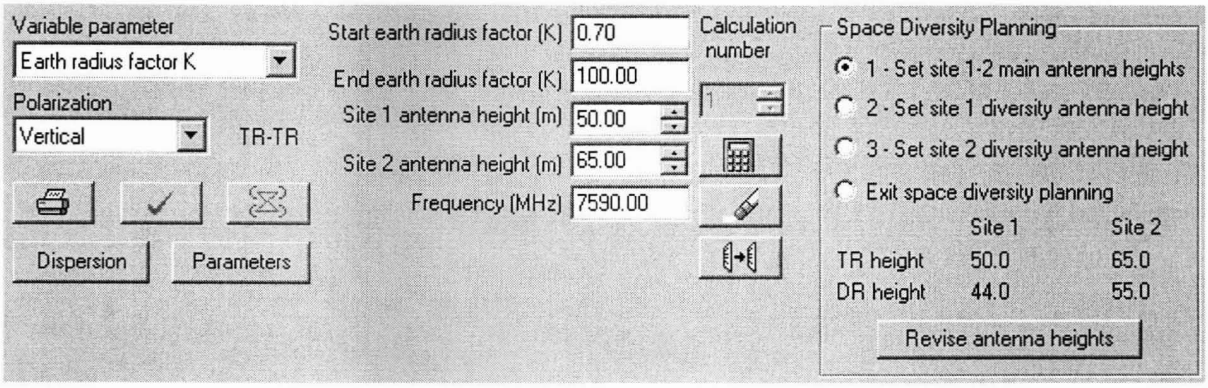

factor K. The start and end values are 0,70 and 100. The values for the site 1 and site 2 main antenna heights are set. Note the up-down controls on these values. The space diversity antenna heights will be set using the three step procedure in the *Space diversity planning* group box using the criteria:

- Simultaneous nulls on the main and diversity antennas do not occur at any value of K.
- At the median value of K (4/3), a signal null does not occur on either the main or diversity antenna.

Click the *1 - Set site 1-2 main antenna heights* button. The receive signal versus K is calculated and displayed. Note the effect of moving the up/down controls on either the *Site 1 or 2 antenna heights*. The distance is incremented and the graph is recalculated. The effect is to slide the curve along the horizontal axis. If necessary, set the main antenna heights for a receive signal peak at K = 1.33

Click the *2 - Set site 1 diversity antenna height*. The *Site 1 antenna height* edit - up/down box is set to the site 1 diversity antenna height and the *Site 2 antenna height* up/down - edit box is set to the site 2 main antenna height and inhibited. The receive signal versus K is calculated for the site 1 diversity to site 2 main antenna combination and displayed. Set the site 1 diversity antenna height so that the signal nulls are not coincident with the main to main nulls and the relative signal level at K = 1.33 is greater than 0.

Click the 3 - *Set site 2 diversity antenna height*. The configuration is the reverse of that in step 2. Set the site 2 diversity antenna height so that the signal nulls are not coincident with the main to main nulls and the relative signal level at K = 1.33 is greater than 0.

If the radio configuration does not allow diversity to diversity transmission, it does not matter if simultaneous nulls occur on the diversity antenna combinations; otherwise, the final antenna heights should take this requirement into consideration.

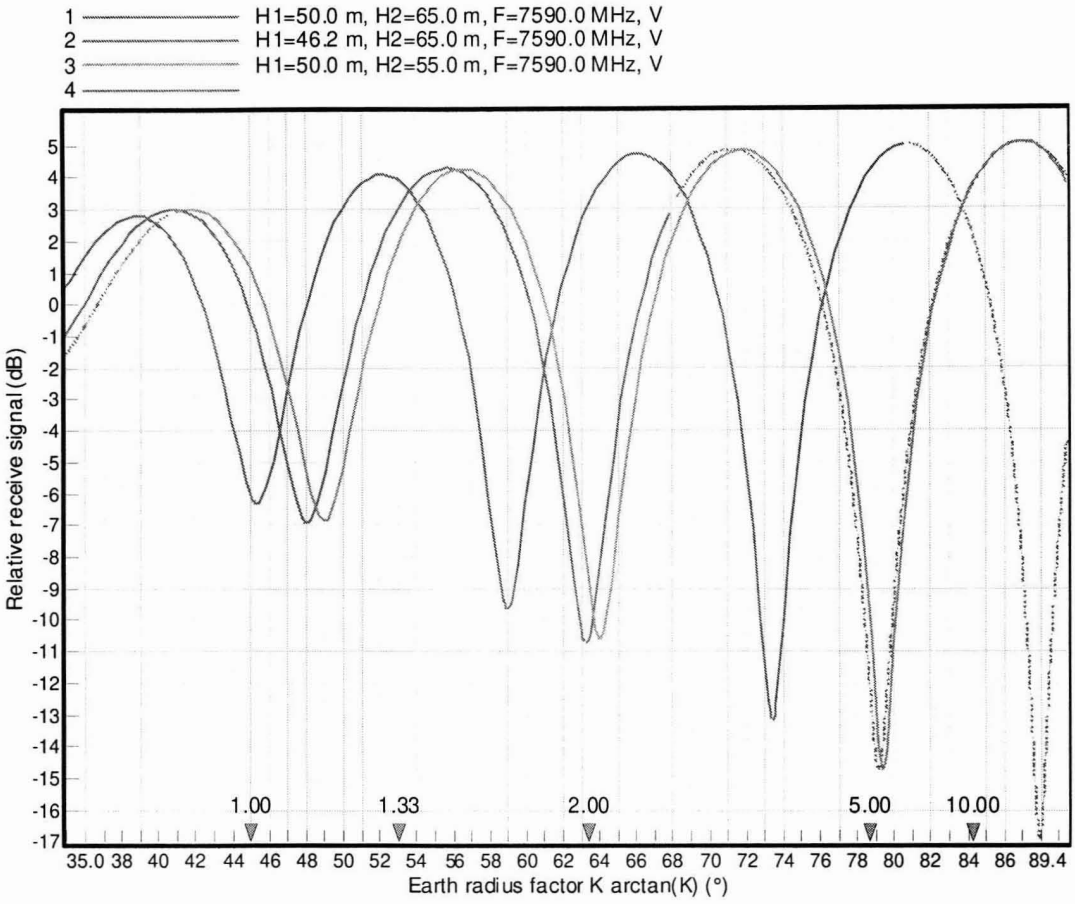

Note the dotted lines on the curves at the high end of the K values. This means that the reflection point has moved outside the reflective plane definition range. Depending on the path geometry this could mean that the curve is not valid in this area and can be ignored.

Dispersion

The final check on any reflection analysis is made on the relative time delay and amplitude of the reflected signal. Click the *Dispersion* button to access the *Dispersion analysis* data entry form.

Any of the parameters in black print can be varied without affecting the file data. The reflection loss and delay are critical performance parameters.

If the reflection delay approaches the data symbol rate, the path will not be workable

The dispersive fade margin measurement is made with a time delay of 6.3 nanoseconds. If the reflection delay is significantly greater than this, then serious performance impairments will occur unless the reflection loss is correspondingly high.

The reflection delay is completely determined from the path geometry. The reflection loss is affected by the antenna discrimination, terrain roughness and ground cover - clearance loss.

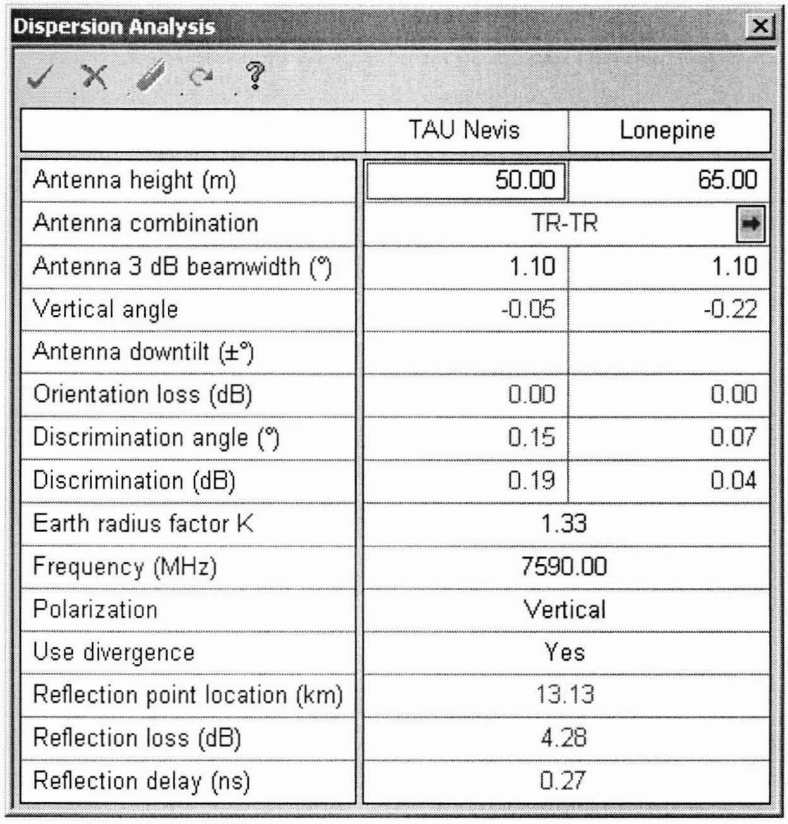

	TAU Nevis	Lonepine
Antenna height (m)	50.00	65.00
Antenna combination	TR-TR	
Antenna 3 dB beamwidth (°)	1.10	1.10
Vertical angle	-0.05	-0.22
Antenna downtilt (±°)		
Orientation loss (dB)	0.00	0.00
Discrimination angle (°)	0.15	0.07
Discrimination (dB)	0.19	0.04
Earth radius factor K	1.33	
Frequency (MHz)	7590.00	
Polarization	Vertical	
Use divergence	Yes	
Reflection point location (km)	13.13	
Reflection loss (dB)	4.28	
Reflection delay (ns)	0.27	

ANTENNA ORIENTATION

This example illustrates the differences in the vertical plane antenna orientation in land mobile and microwave /adaptive modulation applications. The file orient.pl5 is located in the examples/orient directory.

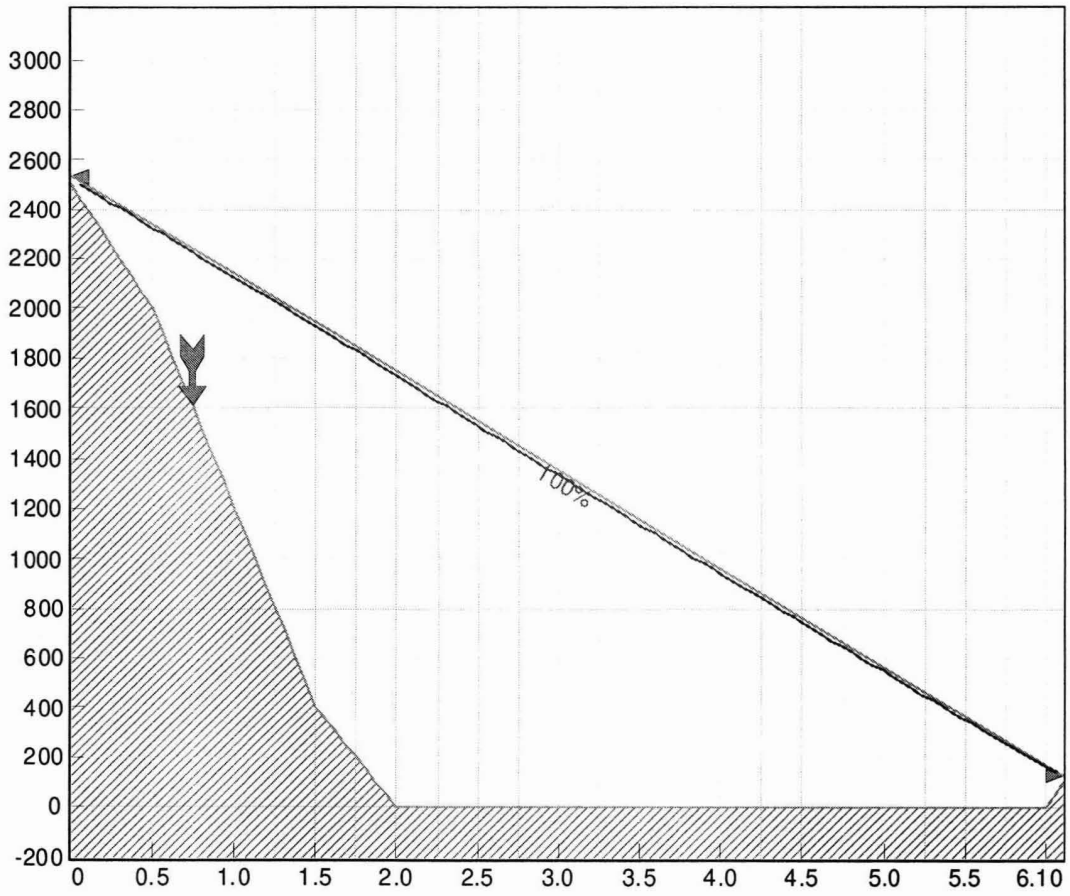

This is a short path with an extreme elevation change.In the *Transmission analysis* design section, note that the status bar shows that this is a microwave application.

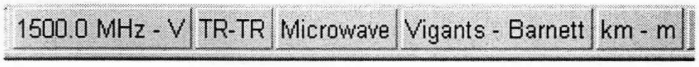

Click on an antenna icon to bring up the antenna data entry form

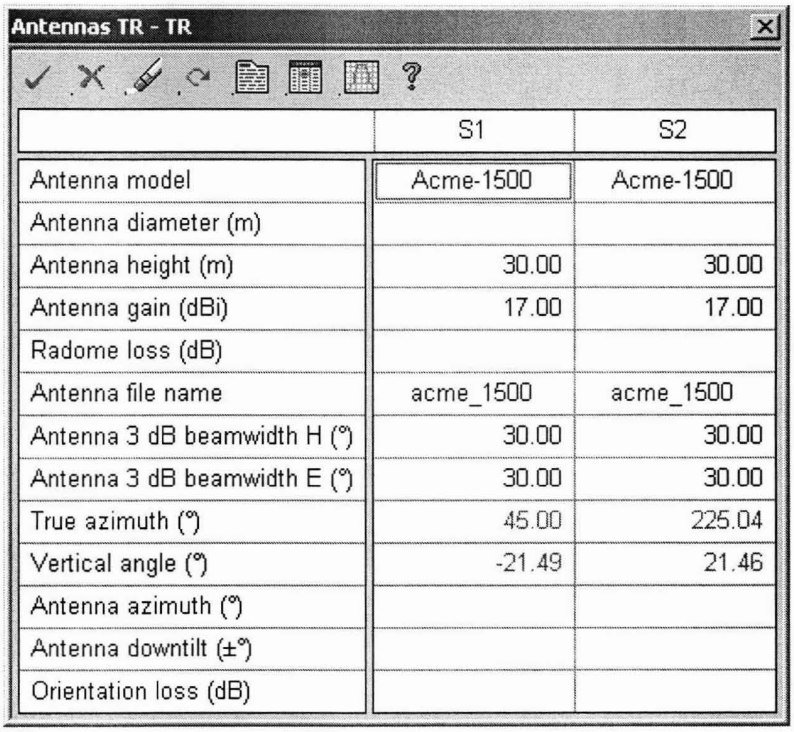

	S1	S2
Antenna model	Acme-1500	Acme-1500
Antenna diameter (m)		
Antenna height (m)	30.00	30.00
Antenna gain (dBi)	17.00	17.00
Radome loss (dB)		
Antenna file name	acme_1500	acme_1500
Antenna 3 dB beamwidth H (°)	30.00	30.00
Antenna 3 dB beamwidth E (°)	30.00	30.00
True azimuth (°)	45.00	225.04
Vertical angle (°)	-21.49	21.46
Antenna azimuth (°)		
Antenna downtilt (±°)		
Orientation loss (dB)		

The vertical angles are 21 degrees; however there is no orientation loss shown. In microwave and adaptive modulations, it is assumed that the antennas are perfectly orientated in the horizontal and elevation planes.

Click the *View antenna data* button. The click the elevation option and note that the orientation loss at an elevation angle of 21.5 degrees is 16.2 dB

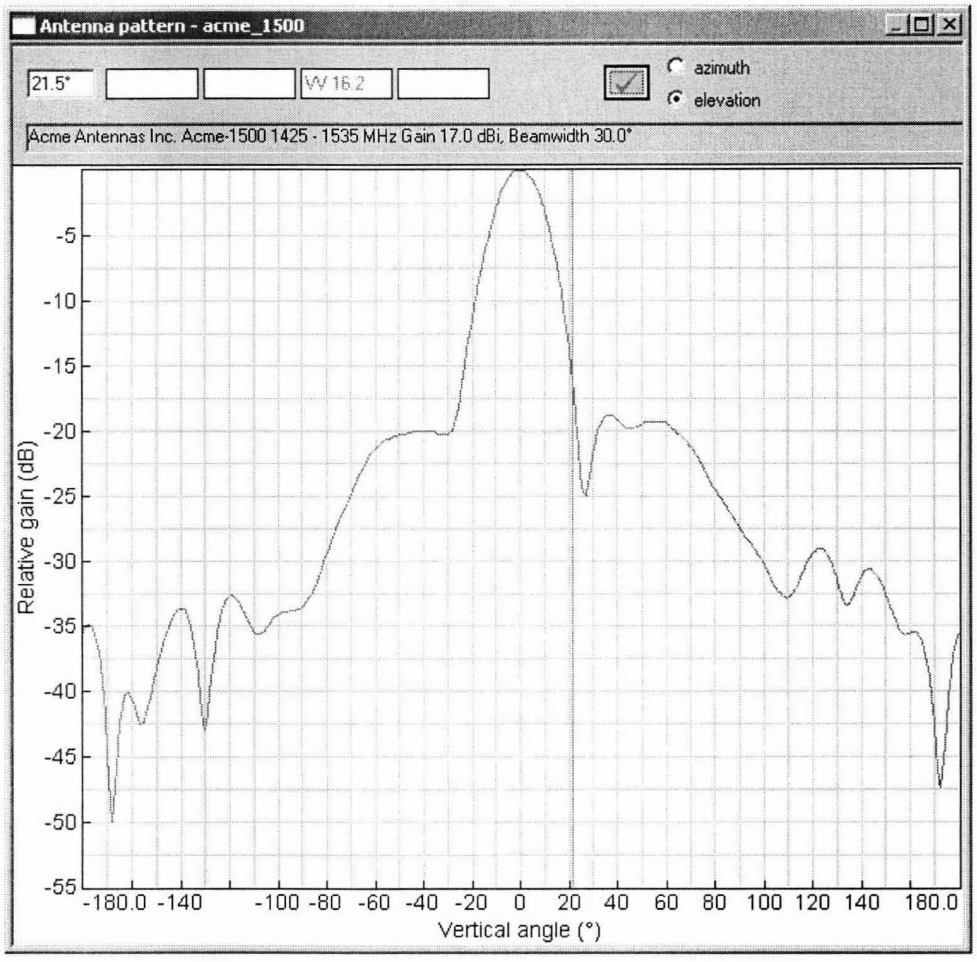

Close the antenna pattern view and then close the *Antenna data* entry form.

Click on the *Microwave* box on the status bar. This is a short cut to the calculation options

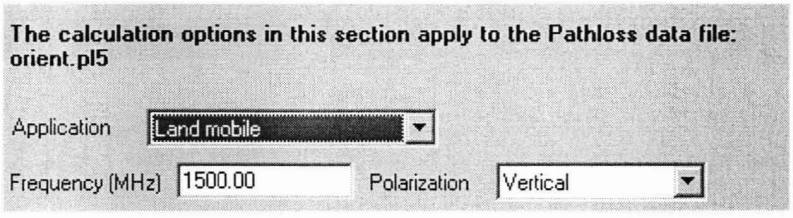

Now set the *Application* to Land mobile. Click the green check to close the calculation options. Note that the status bar now shows a Land mobile application. Click on the antenna icon and not that the orientation loss is now 13 dB at S1 and 16 dB at S2.

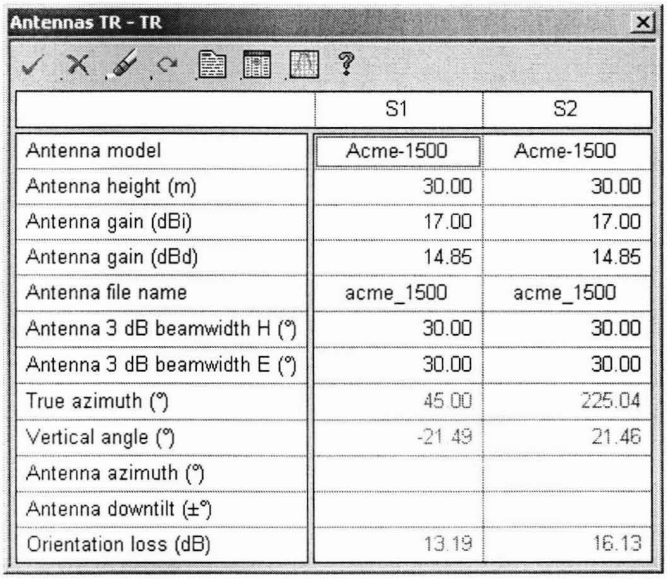

	S1	S2
Antenna model	Acme-1500	Acme-1500
Antenna height (m)	30.00	30.00
Antenna gain (dBi)	17.00	17.00
Antenna gain (dBd)	14.85	14.85
Antenna file name	acme_1500	acme_1500
Antenna 3 dB beamwidth H (°)	30.00	30.00
Antenna 3 dB beamwidth E (°)	30.00	30.00
True azimuth (°)	45.00	225.04
Vertical angle (°)	-21.49	21.46
Antenna azimuth (°)		
Antenna downtilt (±°)		
Orientation loss (dB)	13.19	16.13

In land mobile applications, it is assumed that the antenna boresight is in a horizontal plane. To correct this situation it would be necessary to downtilt the antenna at S1 by 21.49 degrees and uptilt the antenna at S2 by 21.46 degrees as shown below.

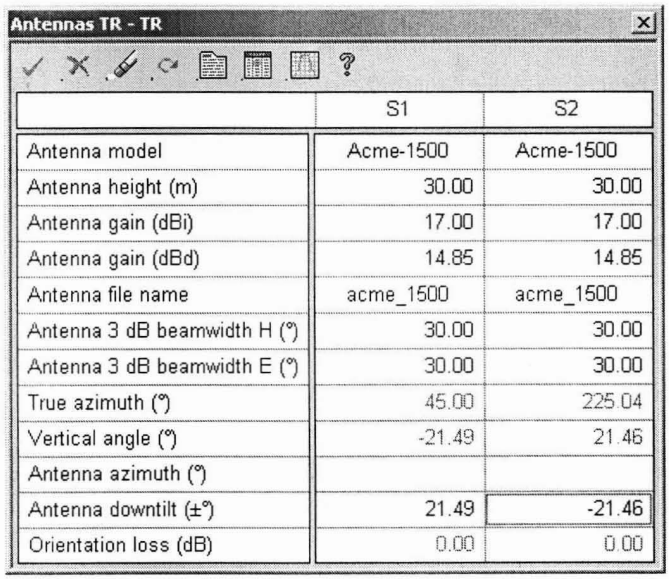

	S1	S2
Antenna model	Acme-1500	Acme-1500
Antenna height (m)	30.00	30.00
Antenna gain (dBi)	17.00	17.00
Antenna gain (dBd)	14.85	14.85
Antenna file name	acme_1500	acme_1500
Antenna 3 dB beamwidth H (°)	30.00	30.00
Antenna 3 dB beamwidth E (°)	30.00	30.00
True azimuth (°)	45.00	225.04
Vertical angle (°)	-21.49	21.46
Antenna azimuth (°)		
Antenna downtilt (±°)	21.49	-21.46
Orientation loss (dB)	0.00	0.00

Chapter 3

The effect of the Earth's surface on propagation: line of sight paths

The Earth's surface is involved in wave propagation by either reflection in the case of line of sight links or diffraction phenomena. Wave propagation within the Earth's surface (e.g. communications with submarines or mine working) is also important. Diffraction phenomena are studied in Chapter 7.

3.1. Electric characteristics of the Earth's surface

As already described in Chapter 2 the characteristics of a non-magnetic medium are defined by its complex permittivity:

$$\eta = \varepsilon - j\,60\,\sigma\lambda\,. \tag{3.1}$$

In the case of the Earth's surface ε and σ depend almost entirely on the degree of humidity at the surface: in the radio wave range, ε is of the order of a few units for most rock types but it is about 80 for water. The value of σ is generally very low for rock. For pure water conductivity is roughly proportional to frequency (dipole conductivity). However, the presence of humidity in the ground produces solutions of the salts which can considerably increase conductivity at low frequencies (ionic conductivity). Beyond about 10GHz the total conductivity of water has reached a limit, whereas permittivity decreases rapidly. This information is given in Fig. 3.1 (CCIR).

It can be seen from Equation (3.1) that for any given type of ground there is a transition frequency for which the real and imaginary parts of η are equal. Below this frequency, the ground behaves for all practical purposes like a conductor, while above it, it behaves like a dielectric medium. The transition frequency is shown in the curves in Fig. 3.1, and is 30GHz for pure water and 1GHz for sea water. For any non-maritime surface it is between 0.6 and 6MHz and for ice it is around 100kHz.

3.2. Surface reflectivity

If we assume that the Earth's surface is plane and homogeneous, its reflectivity will be as defined and calculated in Chapter 2. We know that it depends on the wave's polarization and on the angle of reflection and can be expressed by:

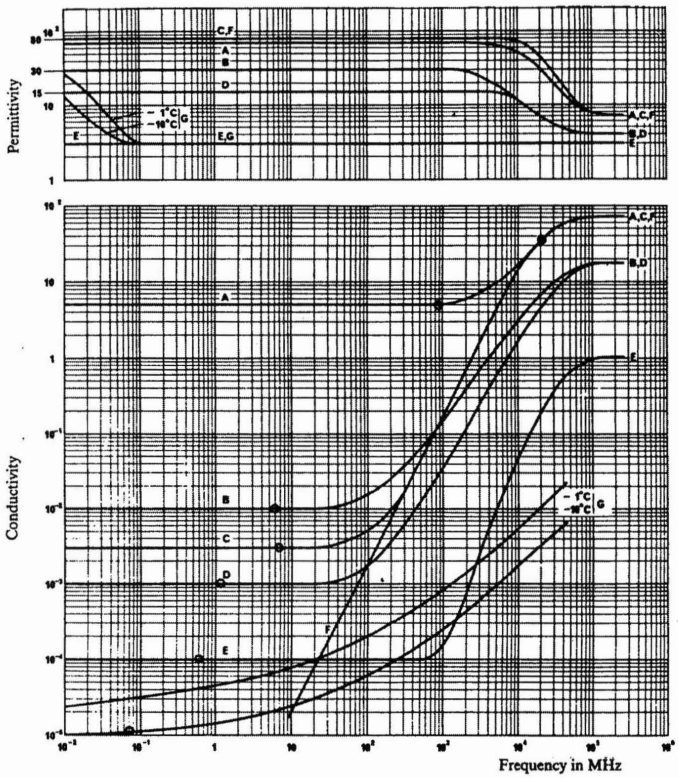

Fig. 3.1 Permittivity ε and conductivity σ of the Earth's surface: A: sea water (mean salinity), 20°C; B: humid soil; C: fresh water, 20°C; D: moderately dry soil; E: very dry soil; F: pure water, 20°C; G: ice (fresh water); ring: transition frequency.

$$R = \frac{\sin\varphi - \sqrt{C}}{\sin\varphi + \sqrt{C}} \tag{3.2}$$

if we introduce a complex function C depending on polarization, which has the two following values:
for horizontal polarization

$$C_H = \eta - \cos^2\varphi\,, \tag{3.3}$$

for vertical polarization

$$C_V = \frac{\eta - \cos^2 \varphi}{\eta^2}. \qquad (3.4)$$

Figures 3.2 and 3.3 give reflectivity as a function of φ for two interesting practical cases, sea water (Fig. 3.1, curve A) and moderately dry soil (Fig. 3.1, curve D). It is

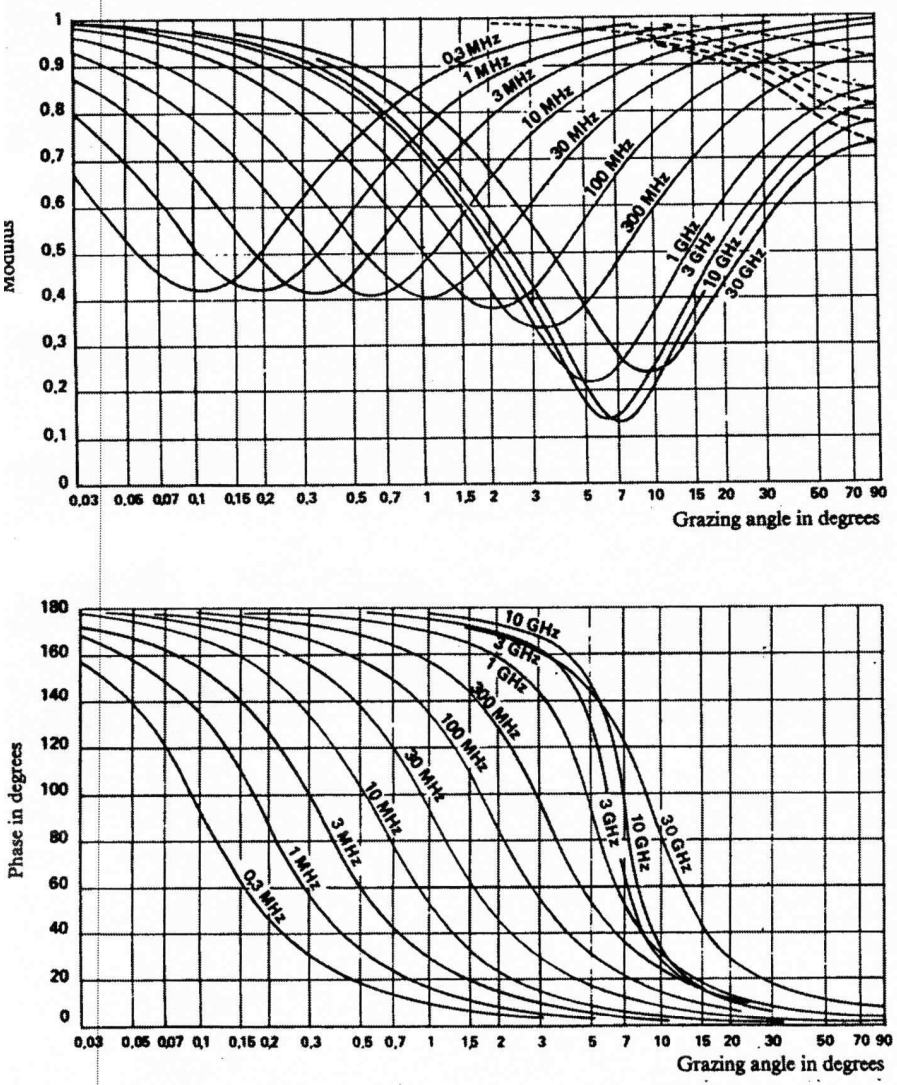

Fig. 3.2. Sea water reflectivity: – horizontal; —— vertical polarization.

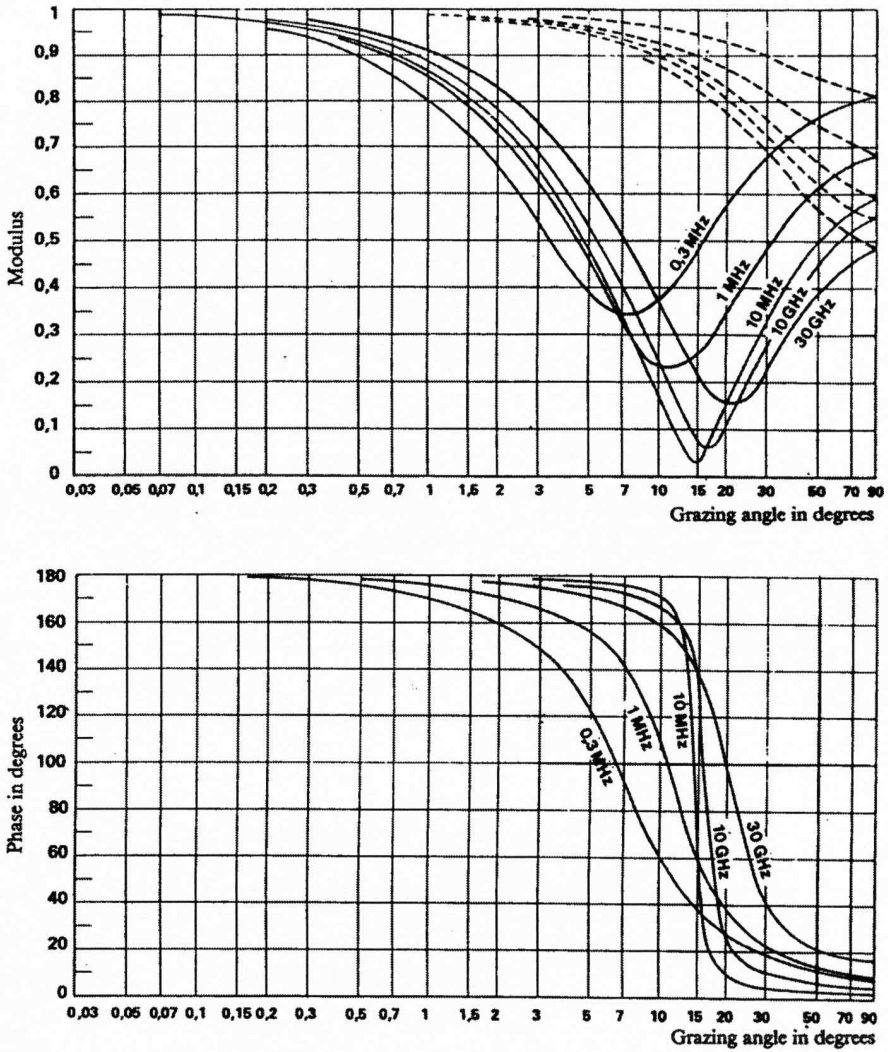

Fig. 3.3. Soil reflectivity (moderately dry soil): – horizontal polarization; —— vertical polarization.

clear that for very small values of φ, the reflectivity is around –1 (modulus 1, phase 180°) whatever the degree of polarization or the nature of the surface. In other words, when φ approaches zero, reflection involves phase inversion.

(The reflection factor is associated with a plane wave, and not, for example, with radiation from an antenna vertical to the ground. See Equation (3.34) and the note at the of Section 3.5)

For horizontal polarization reflectivity remains around –1 even for relatively

large grazing angles. Phase does not appear in Figs 3.2 and 3.3, as it is around 180°.

For vertical polarization reflectivity varies considerably and its modulus reaches a minimum for the pseudo-Brewster angle of incidence (see Chapter 2). This minimum is accompanied by rapid variation in phase. When frequency increases the modulus becomes independent of frequency, particularly for small values of φ, and depends for all practical purposes only on φ and ε, according to the following asymptotic relation, where φ is in radians:

$$R \simeq \frac{1 - \varphi\sqrt{\varepsilon}}{1 + \varphi\sqrt{\varepsilon}}. \tag{3.5}$$

This approximate relationship gives an overestimated value. It may be applied below the Brewster angle of incidence and for frequencies above the transition frequency shown in Fig. 3.1.

3.3. Propagation near a smooth spherical surface

Reflectivity has been defined on the assumption that the Earth's surface is flat. In fact, Earth's curvature cannot be neglected, except for very short links. Some geometrical analysis is therefore necessary. The elements to take into account are shown in Fig. 3.4. It should be borne in mind that for most practical cases this figure is not drawn to scale. Heights h_1 and h_2 are generally very small compared with the distance, and the distance is very small with respect to the radius of the Earth.

The Earth's radius to be taken into account is not the true radius of the Earth (a = 6360km) but an effective radius Ka which takes into account refraction in the atmosphere. The coefficient K depends on the vertical gradient of the refractive index (see Chapter 4). Its mean value is around 4/3, which gives an effective radius of 8500km. It is this value which is generally used in calculations, in the absence of more accurate information on atmospheric refraction conditions. However, K can vary over a wide range and even take negative values in cases of ducted propagation (see Section 4.2.2).

For the triangles *TPO*, *TPR* and *OPR*, the following standard relationships exist:

$$\frac{l_1}{\sin \alpha_1} = \frac{Ka + h_1}{\cos \varphi} = \frac{Ka}{\cos(\varphi + \alpha_1)}, \tag{3.6}$$

$$\frac{l_2}{\sin \alpha_2} = \frac{Ka + h_2}{\cos \varphi} = \frac{Ka}{\cos(\varphi + \alpha_2)}, \tag{3.7}$$

$$d_1 = Ka\alpha_1, \tag{3.8}$$

$$d_2 = Ka\alpha_2, \tag{3.9}$$

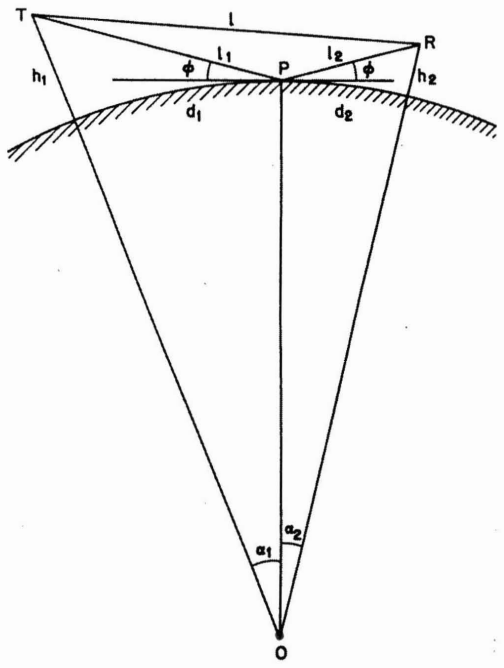

Fig. 3.4. Geometric factors affecting a reflected ray.

$$l^2 = l_1^2 + l_2^2 + 2\, l_1\, l_2 \cos 2\varphi. \tag{3.10}$$

Equation (3.10) can be rewritten to include a term showing the path difference Δ between the direct and the reflected ray:

$$\Delta = l_1 + l_2 - l = \frac{4\, l_1\, l_2 \sin^2 \varphi}{l_1 + l_2 + l}. \tag{3.11}$$

Let us take the general case where α_1, α_2, and φ are small angles. The geometric relations then become:

$$\frac{h_1}{Ka} = \alpha_1 \varphi + \frac{\alpha_1^2}{2}, \tag{3.12}$$

$$\frac{h_2}{Ka} = \alpha_2 \varphi + \frac{\alpha_2^2}{2}, \tag{3.13}$$

$$l_1 = d_1 = Ka\alpha_1, \tag{3.14}$$

$$l_2 = d_2 = Ka\alpha_2, \tag{3.15}$$

$$\Delta = \frac{2 d_1 d_2}{d} \varphi^2. \tag{3.16}$$

To complete these calculations three dimensionless quantities are introduced:

$$b = \frac{d_1 - d_2}{d_1 + d_2} = 1 - 2\frac{d_2}{d} = 2\frac{d_1}{d} - 1, \tag{3.17}$$

$$c = \frac{h_1 - h_2}{h_1 + h_2}, \tag{3.18}$$

$$m = \frac{d^2}{4\,Ka(h_1 + h_2)}. \tag{3.19}$$

3.3.1. Location of the point of reflection

The point of reflection can be determined by eliminating φ from Equations (3.12) and (3.13). Given Equations (3.17) to (3.19) the reasoning here reduces to determining b, which is given by the cubic equation:

$$c = b + bm(1 - b^2). \tag{3.20}$$

Quantities b and c always have a modulus less than 1 and they can be assumed to be positive if we call the greater of the heights h_1. Quantitity m is always less than 1 if the points are in line of sight. Its value is given by the nomogram in Fig. 3.5. Equations (3.20) can be solved using the nomogram in Fig. 3.6.*

N.B. These calculations must be carried out, even if we do not need to know the position of the point of reflection, since the value of b (or d_1/d) is used in all later calculations.

3.3.2. Angle of incidence

This angle is given by the relation:

$$\varphi = \frac{h_1 + h_2}{d}\left[1 - m(1 + b^2)\right]. \tag{3.21}$$

The first term in this expression is the value of angle φ_0 corresponding to a flat Earth, and can be obtained from the nomogram in Fig. 3.5. The second term is therefore a reduction factor Z, due to the curvature of the Earth, given by nomogram in Fig. 3.7. If the distance between transmitter and receiver is sufficiently short, only the first term needs to be taken into account.

* This equation may also be solved by the following expression, valid for m positive:

$$b = 2\sqrt{\frac{m+1}{3m}}\cos\left[\frac{\pi}{3} + \frac{1}{3}\operatorname{Arc}\cos\left(\frac{3c}{2}\sqrt{\frac{3m}{(m+1)^3}}\right)\right]$$

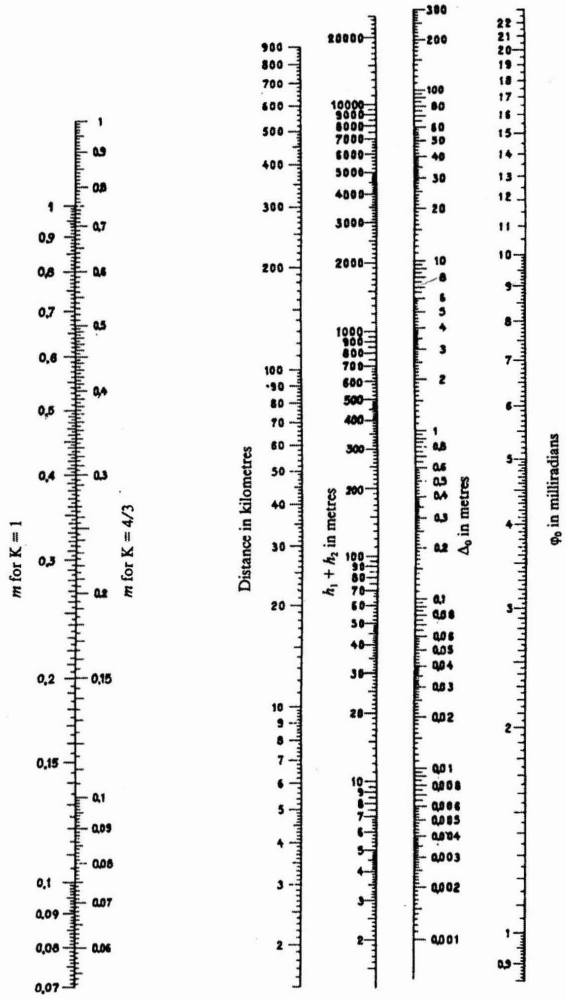

Fig. 3.5. Calculation of m, Δ_0 and φ_0.

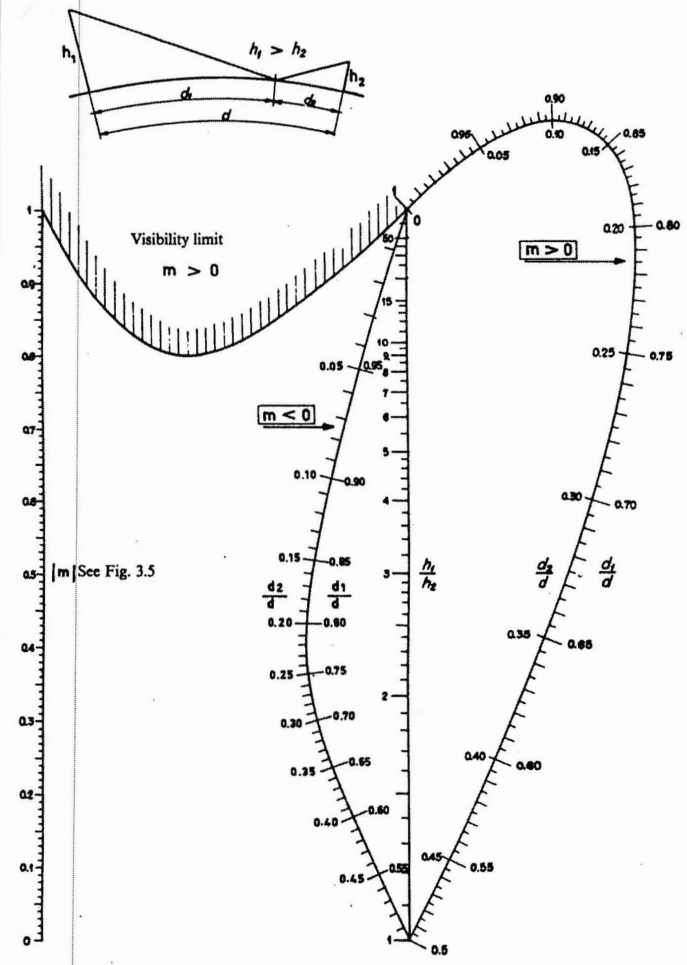

Fig. 3.6. Determining the point of reflection.

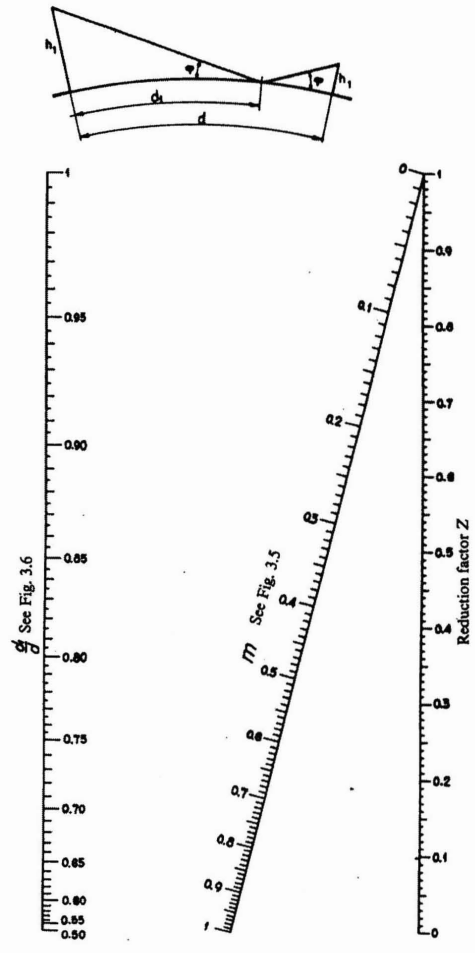

Fig. 3.7. Grazing angle reduction factor on a spherical Earth.

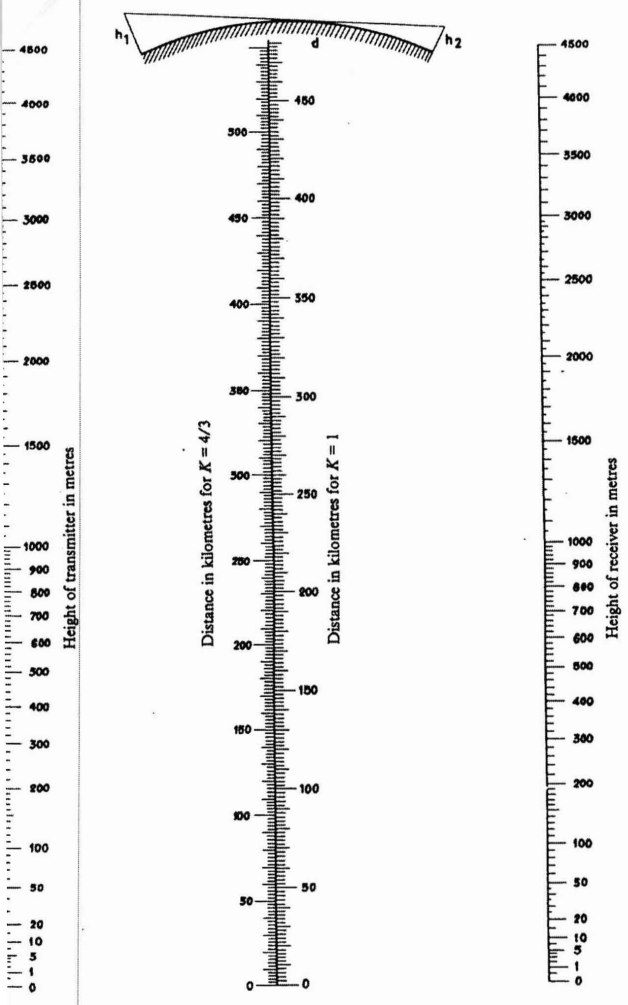

Fig. 3.8. Maximum line of sight distance.

3.3.3. Distance giving a tangent link

This distance is obtained when angle φ becomes zero:

$$m(1 + b^2) = 1 . \tag{3.22}$$

If geometric quantities are considered again, we obtain the standard equation, which can also be deduced directly:

$$d_t = \sqrt{2\,Ka}(\sqrt{h_1} + \sqrt{h_2}) . \tag{3.23}$$

If heights h_1 and h_2 are expressed in metres and the distance d in kilometres, and if the atmospheric conditions are assumed to be normal, i.e. $Ka = 8500$km, we obtain the following practical formula, which can be calculated by the nomogram in Fig. 3.8:

$$d_{t(\mathrm{km})} = 4.1\,[\sqrt{h_{1\,(\mathrm{m})}} + \sqrt{h_{2\,(\mathrm{m})}}] . \tag{3.24}$$

3.3.4. Path difference between the direct and reflected rays

Path differences are given by Equation (3.16), which can be re-written:

$$\Delta = 2\,d\,\frac{d_1}{d}\,\frac{d_2}{d}\,\varphi^2 , \tag{3.25}$$

this expression allows us to calculate the difference once we know φ and the position of the point of reflection. To calculate the difference by nomogram we write:

$$\Delta = \frac{(h_1 + h_2)^2}{2\,d}(1 - b^2)\,[1 - m(1 + b^2)]^2 = \Delta_0\,q \tag{3.26}$$

with:

$$\Delta_0 = \frac{(h_1 + h_2)^2}{2\,d} \quad \text{and} \quad q = (1 - b^2)\,[1 - m(1 + b^2)]^2 \tag{3.27}$$

Δ_0 is given by Fig. 3.5 and q by Fig. 3.9.

If the Earth can be considered as flat, i.e. if K is very large or d is sufficiently small:

$$\Delta \simeq \frac{2\,h_1\,h_2}{d} . \tag{3.28}$$

The path difference varies if we move vertically or horizontally, and consequently the reflected ray will sometimes reinforce and sometimes diminish the direct ray. Therefore this is an interference phenomenom which is particularly apparent if reflection takes place from the surface of the sea.

1. If the receiver moves vertically, a series of regularly spaced maxima and minima is traced (Fig. 3.10). The distance between two consecutive maxima

(or minima) is equal to:

$$\delta h_2 = \frac{\lambda d}{2 d_1 \varphi} = \frac{\lambda d}{2 h_1} \cdot \frac{1 + m(1 - b^2)}{1 - m(1 + b^2)}. \tag{3.29}$$

If the distance is short enough, the Earth can be assumed to be flat, and Equation (3.29) reduces to:

$$\delta h_2 = \frac{\lambda d}{2 h_1}. \tag{3.30}$$

2. If the receiver moves horizontally, as would be the case in an aircraft,

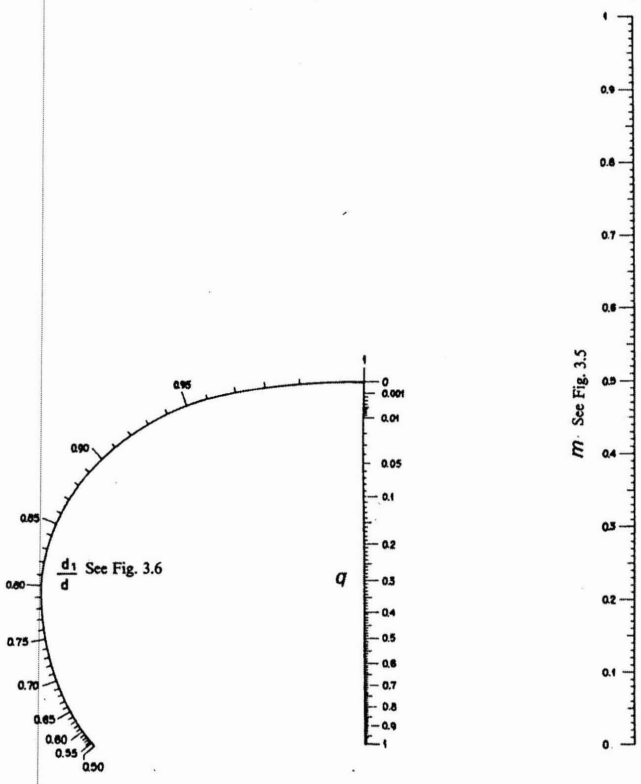

Fig. 3.9. Path difference between the direct and the reflected rays.

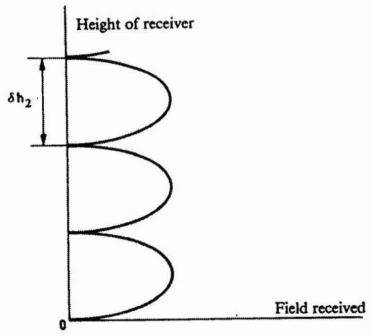

Fig. 3.10. Interference lobes.

maxima and minima are no longer regularly spaced, but close up as the transmitter is approached. The distance between two consecutive maxima or minima is approximately equal, assuming the Earth to be flat, to:

$$\delta d = \frac{\lambda d^2}{2 h_1 h_2}. \tag{3.31}$$

This relation is obviously inadequate as the horizon is approached, since it only applies on a flat Earth. On a spherical Earth the last maximum appears a little before the horizon, after which the field decreases very rapidly. But the method derived from optics, which we are using here, then ceases to apply. To go further the diffraction theory described in Chapter 7 must be used.

3.3.5. Divergence factor

If the area of the earth's surface involved is so large that it can no longer be regarded as flat, reflectivity has to be corrected. This is because a beam broadens after reflection from a convex spherical surface, leading to an apparent reduction in reflectivity. This means that reflectivity must be multiplied by a coefficient less than 1 called the divergence factor.

A beam of solid angle Ω_1 produces a beam of solid angle Ω_2 greater than Ω_1 after reflection (Fig. 3.11). The two beams are of area Σ_1 and Σ_2 in the plane of the receiver. As power per unit area is inversely proportional to area, the received field is multiplied by a factor D less than 1 called the divergence factor.

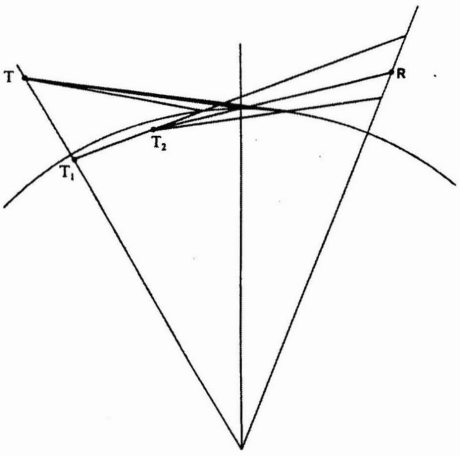

Fig. 3.11. Divergence of a beam of rays.

$$D = \sqrt{\frac{\Sigma_1}{\Sigma_2}} = \left(1 + \frac{2}{Ka \sin \varphi} \frac{l_1 l_2}{l_1 + l_2}\right)^{-1/2}. \tag{3.32}$$

Using the quantities already calculated the divergence factor is given by the following expressions:

$$D = \frac{1}{\sqrt{1 + \frac{2d}{Ka} \frac{d_1}{d} \frac{d_2}{d} \frac{1}{\varphi}}} = \sqrt{\frac{1 - m(1 + b^2)}{1 + m(1 - 3b^2)}} \tag{3.33}$$

and the factor can be either calculated directly, or derived from the nomogram in Fig. 3.12. It can be seen in particular for $m = 0.5$ that D takes the value $1/\sqrt{3}$ independently of b. This expression, which vanishes when the grazing angle becomes zero, is not however applicable to grazing incidence, as it does not take diffraction phenomena into account. The minimum grazing angle below which calculation by optics methods is no longer possible is given by the approximate relation:

$$\varphi_{(\text{mrad})} = \left(\frac{2\,100}{F_{(\text{MHz})}}\right)^{1/3} = (7\,\lambda_{(\text{m})})^{1/3} \tag{3.34}$$

which, by way of example, gives a limiting angle of 2.76mrad at 100MHz and 0.59mrad at 10GHz.

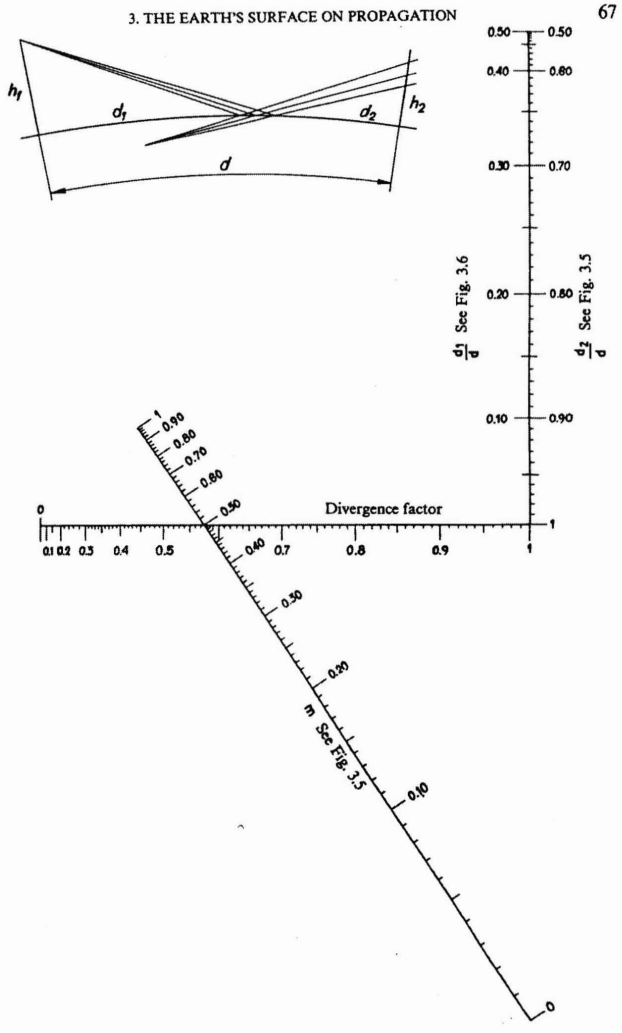

Fig. 3.12. Divergence factor.

3.4. Resultant field

We have only to add the reflected field, taking account of relative phases and amplitudes to obtain the resultant field. Complex notation is used:

$$\frac{E}{E_0} = 1 + \rho D \exp \mathrm{j}\left(\psi + 2\pi \frac{\Delta}{\lambda}\right), \tag{3.35}$$

where:

E_0 is the field in free space;
ρ and ψ are the modulus and argument of reflectivity, and can be taken to equal 1 and π respectively for grazing incidence, except when dealing with vertical polarization over the sea for relatively low frequency (see Fig. 3.2);
D is the divergence factor;
Δ is the difference in length between the direct and reflected rays.

If we are only concerned with the modulus, we have:

$$\left|\frac{E}{E_0}\right| = \sqrt{1 + (\rho D)^2 + 2\rho D \cos\left(\psi + 2\pi \frac{\Delta}{\lambda}\right)}. \tag{3.36}$$

This expression, all of whose factors we can calculate, gives the resultant field. The nomogram in Fig. 3.13 can be used to replace R by ρD and φ by $\psi + 2\pi\Delta/\lambda$.

Particular case: if the Earth is assumed to be flat (short distance) and reflectively equal to –1 (very small grazing angle):

$D=1$ $\rho=1$ $\psi=\pi$

From which we can conclude that:

$$\left|\frac{E}{E_0}\right| = 2\left|\sin\frac{\pi\Delta}{\lambda}\right| = 2\left|\sin\frac{2\pi h_1 h_2}{\lambda d}\right|. \tag{3.37}$$

the field oscillates between zero and twice the free space field.
Moving away at constant altitude, we find a final maximum for:

$$d = \frac{4 h_1 h_2}{\lambda}, \tag{3.38}$$

and beyond this point the field decreases constantly. Very far away from the last maximum the arc can be taken to be equal to the sine and:

$$\frac{E}{E_0} \simeq \frac{4\pi h_1 h_2}{\lambda d}. \tag{3.39}$$

As the field in free space E_0 decreases with $1/d$, the resultant field E decreases with $1/d^2$.

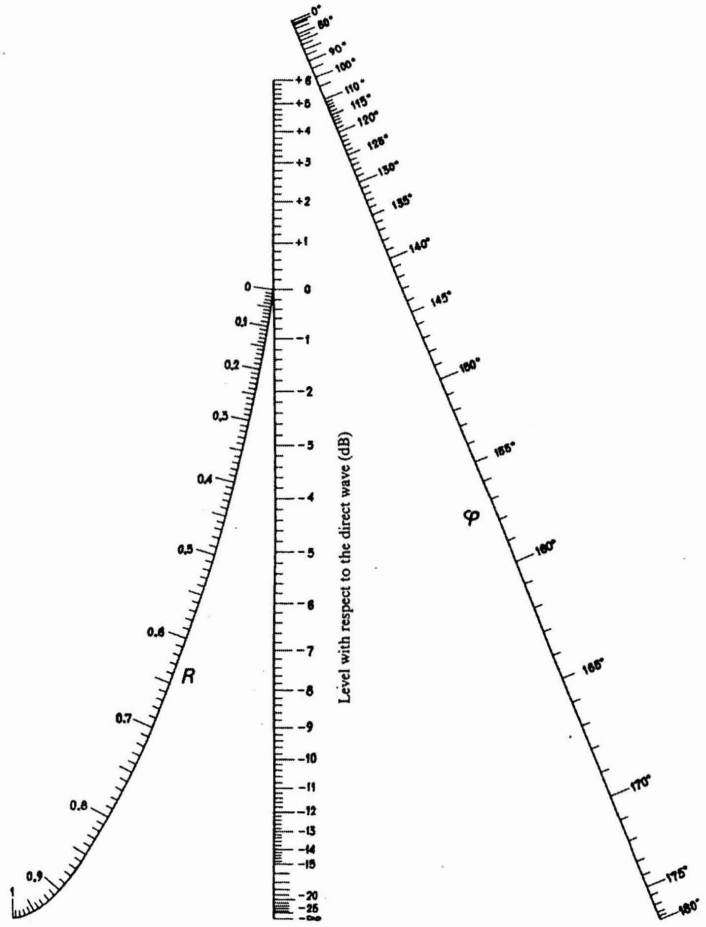

Fig. 3.13. Interference between two waves: resultant field.

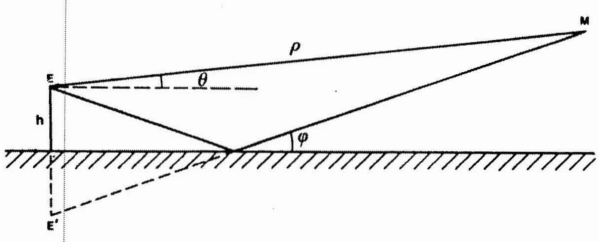

a) Flat Earth and finite distance.

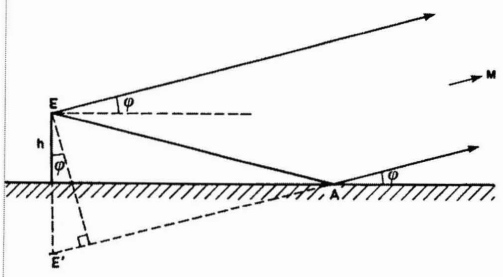

b) Flat Earth and infinite distance.

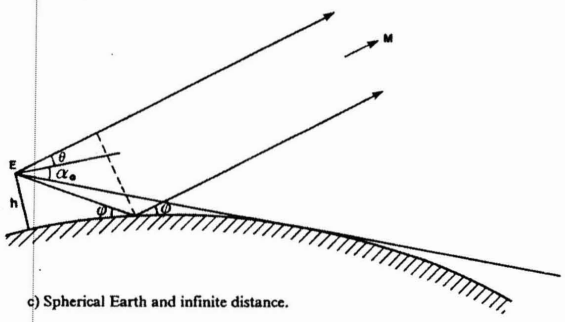

c) Spherical Earth and infinite distance.

Fig. 3.14. Influence of the Earth on a link with a moving aircraft.

3.5. Apparent radiation pattern of an antenna taking the Earth's surface into account: links with aircraft or spacecraft, target detection using radar

Reflection from the Earth's surface profoundly alters antenna patterns, which can have extremely important consequences, e.g. for links with aircraft or for target detection using radar. The effect of the Earth's surface can be calculated, where appropriate, in different ways. We consider the case of radar, but the same calculations can be applied to other radio links (Fig. 3.14).

a) In general, the results obtained previously can be used (Section 3.3), but the calculations are relatively long.

b) If the Earth's surface is treated as a plane, i.e. in particular if the height of the radar above the ground is relatively small, the image method can be used. This is based on the fact that the antenna pattern in the presence of the Earth's surface is the same as the pattern that would be obtained for the real antenna, with an image antenna symmetric to it with respect to the ground, if the ground itself is ignored. Note that currents in the image antenna have the same amplitude as in the real antenna, the same direction for components normal to the Earth's surface and opposite directions for components parallel to the Earth's surface (the Earth is assumed to be perfectly conducting).

If the height of the radar above the plane is equal to h and if ρ and θ denote the polar coordinates of a target in a vertical plane with the radar at its origin, the path difference between the direct and reflected rays can be obtained using a simple geometric calculation:

$$\Delta = \sqrt{\rho^2 + 4h\rho \sin\theta + 4h^2} - \rho \tag{3.40}$$

and the angle of incidence φ on the ground is given by:

$$\tan\varphi = \frac{2h + \rho\sin\theta}{\rho\cos\theta}. \tag{3.41}$$

If the target is at an infinite distant from the radar, Δ and φ tend towards their limiting values, which can then be obtained directly:

$$\varphi \to \theta \qquad \Delta \to 2h\sin\theta. \tag{3.42}$$

This gives the pattern at infinity of the radar antenna in the presence of the Earth's surface, which is assumed to be flat. If the reflectivity of the Earth's surface, for the angle considered, is expressed by:

$$R = |R|\,e^{j\delta} \tag{3.43}$$

the ratio of the resultant field E to field E_0 in the absence of reflection is given by:

$$\frac{E}{E_0} = 1 + |R|\,e^{j\left(2\pi\frac{\Delta}{\lambda}+\delta\right)}. \tag{3.44}$$

If we now assume that the grazing angle φ is relatively small, we can make a first approximation:

$$|R| = 1 \qquad \delta = \pi \tag{3.45}$$

and under these conditions, the modulus of the resultant field is given by:

$$\frac{E}{E_0} = 2\left|\sin\frac{2\pi h\varphi}{\lambda}\right|. \tag{3.46}$$

If the antenna used has a radiation pattern represented by function $f(\varphi)$ in the vertical plane, the situation is the same as if following an antenna whose pattern is represented by the following function was used:

$$2f(\varphi)\left|\sin\frac{2\pi h\varphi}{\lambda}\right|. \tag{3.47}$$

At very high frequencies the quantity h/λ is very large and the function $\sin\frac{2\pi h\varphi}{\lambda}$ oscillates very rapidly. Each lobe of the antenna diagram is then broken down into a certain number of very narrow lobes and there is a zero in the direction of the horizon, which explains the difficulty of detecting low targets.

c) In certain applications terrestrial curvature must be taken into account but we are still interested in the antenna pattern at infinity. Calculations can be carried out as described in Section 3.3 but there lengths l_2 and h_2 are infinite. Equation (3.11) becomes:

$$\Delta = 2l_1\sin^2\varphi. \tag{3.48}$$

Relatively simple geometrical calculation makes it possible to express the path length differences Δ and the divergence factor D as a function of the grazing angle incidence φ and height h:

$$\Delta = \frac{4h\sin^2\varphi}{\sqrt{\sin^2\varphi + \frac{2h}{Ka}} + \sin\varphi} \tag{3.49}$$

$$\frac{1}{D^2} = 2\sqrt{1 + \frac{2h}{Ka\sin^2\varphi}} - 1. \tag{3.50}$$

It is, however, preferable to express these quantities as a function of the angle of elevation θ of the target seen by the radar. Unfortunately, the calculations become far more complicated if we do, and we only consider the case where the height h of a radar is relatively small, and where we are only concerned with small values of θ. If we write α_0 or the absolute value of the (negative) angle of elevation of the horizon seen from the radar:

$$\alpha_0^2 = \frac{2h}{Ka}, \tag{3.51}$$

we obtain the following expressions, where angles are expressed in radians:

$$\Delta = \frac{4h\alpha_0}{27}\left[\left(\left(\frac{\theta}{\alpha_0}\right)^2 + 3\right)^{3/2} - \frac{\theta}{\alpha_0}\left(\left(\frac{\theta}{\alpha_0}\right)^2 - 9\right)\right], \tag{3.52}$$

$$D^2 = \frac{1}{3}\left[1 + \frac{2\frac{\theta}{\alpha_0}}{\sqrt{\left(\frac{\theta}{\alpha_0}\right)^2 + 3}}\right]. \tag{3.53}$$

Having calculated the values of Δ and D, and using the approach described in Section 3.3.5, we can calculate the effective antenna pattern, taking into account the free space pattern. An example is given in Fig. 3.15, where we only consider the main lobe of the antenna. It can be seen that for very low elevation angles the divergence factor plays a major role.

N.B. In the hectometre wave range (MF) and longer waves for antennas on the Earth's surface the radiation characteristics of the antennas can only be defined taking the presence of the Earth's surface into account. But in this case we can no longer talk of line of sight paths (see Section 2.3).

3.6. The influence of the size and position of a reflecting area of the Earth's surface

All the calculations above are based on the assumption that there is no limitation to the extent of the reflecting area. They are therefore directly applicable to paths over the sea. For terrestrial paths it is often the case that only part of the surface between the transmitter and the receiver can be regarded as reflecting. If that

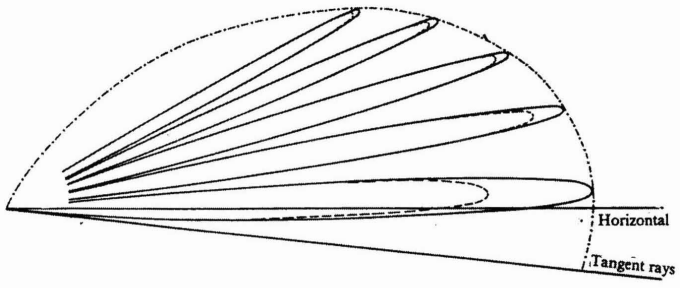

Fig. 3.15. Influence of the Earth's surface on the antenna radiation pattern: Height of antenna 20m. Gain 40dB; λ = 10cm. Heights scale multiplied by 50. —— not taking into account the divergence factor. – taking into account the divergence factor. –.–.– main lobe of the antenna in free space.

SECTION 940-310-102
Issue 2, January 1976

LLF

RADIO ENGINEERING
MICROWAVE RADIO PROPAGATION
SELECTIVE FADING

CONTENTS PAGE

1. INTRODUCTION 1
A. General 1
B. Conditional Qualifications 2
C. Description of Fading 2
2. BASICS—PHYSICS OF MULTIPATH PROPAGATION 4
A. Refraction and Reflection 4
B. Multipath Propagation 6
3. THE RAYLEIGH DISTRIBUTION 7
4. ESTIMATING OUTAGE TIME DUE TO FADING 10
A. Rationale 10
B. Definitions and Estimation of Fading 10
C. Terrain Roughness Modification . . 11
5. DETERMINATION OF NEED FOR PROTECTION 12
A. General 12
B. Short-Haul Objectives 13
C. Short-Haul Appraisal 16
D. Long-Haul Considerations 16
E. Length of Fading Season 16

CONTENTS PAGE

6. SELECTIVE FADING AND NARROWBAND SYSTEMS 18
A. General 18
B. Narrowband Radio and Wired Carrier Systems 18
INTRACHANNEL PHENOMENA 20
A. General 20
B. Experiment Structure 20
C. Definitions and Methodology . . . 20
D. Characteristics of Inband Fading and Distortion 21
E. Conclusions 23

1. INTRODUCTION

A. General

1.01 Time variation in the level of received radio signals is called "fading." Fading is the combined effect of many mechanisms which are associated with meteorological variations in the earth's lower atmosphere. The most common, and potentially the most troublesome to microwave transmission, is the type of fading resulting from wave interference among several components, or rays, of a transmitted signal. Ordinarily, only a small portion of the transmitted beam—the direct ray—reaches the receiving antenna. However, sometimes the atmosphere redirects portions of the remainder by the process of refraction so that the redirected portion also reaches the receiver.

NOTICE
Not for use or disclosure outside the
Bell System except under written agreement

Printed in U.S.A.

There the redirected ray combines with the normal direct ray and either enhances or diminishes the resultant, depending on their phase relationships. This phenomenon is called "multipath propagation," and its effect, "multipath fading." Multipath propagation can also be caused by reflections from the earth or from objects along the path. However, in this section it will be assumed that such reflections are reduced to negligible proportions by proper site layout; the problem of reflections is discussed in detail in Sections 940-310-103 and 940-310-104.

1.02 This section is being reissued to improve and expand the methods of calculation applicable to multipath phenomena, to extend coverage to 40 GHz, and to include narrowband AM systems. The nature and extent of this change precludes the use of change arrows.

B. Conditional Qualifications

1.03 Certain formulas and derived graphic illustrations applicable to the quantification of multipath phenomena (contained essentially in Parts 4 and 5 of this section) have been evolved with respect to systems having standard clearance conditions. Clearance in such systems is not excessive; it normally does not exceed the radius of the first Fresnel zone when K, the equivalent earth radius factor, equals 2/3. Since the standard clearance conditions tend to typify 4- and 6-GHz system design and since ground-related atmospheric effects contribute significantly to multipath propagation, the fade occurrence factor (r), as described in paragraph 4.07, is derived with respect to these standard systems. For this reason, graphic representations such as Fig. 9 (multipath occurrence factor) as well as Fig. 10 and 11 (both of which involve r in the quantification of "time below level") should be considered most accurate in terms of the curves representing 4 and 6 GHz. The 11-GHz curves, for example, were similarly derived. However, 11-GHz systems are extensively employed in mountainous regions of the United States where, by locating microwave towers on mountain tops, midpath clearance hundreds of feet in excess of the first Fresnel zone may be achieved. Such special case paths affording clearances several hundred feet in excess of the first Fresnel zone will experience significantly less selective fading than that implied by the curves of the aforementioned illustrations or otherwise derived in terms of r as defined herein. Design under high clearance conditions will therefore require different equations. Additionally, while it is known that fading activity increases with increasing microwave frequency, additional measurements may yield improved data for the higher frequency ranges (above 11 GHz). Again, as before, extrapolating from current formulas to the 18-, 29-, and 40-GHz regions might yield values subject to improvement when refined data become available.

C. Description of Fading

1.04 An analysis of selective fading as a result of multipath propagation is perhaps best begun with reference to Fig. 1, which illustrates the variations in the envelope levels of two received signals during heavy fading. The graphs represent two 4-GHz microwave signals transmitted over the same path at the same time and having a frequency separation of 100 MHz (about 2.5 percent in this case). The signal levels in decibels relative to their normal unfaded levels are indicated on the ordinate scales. Several characteristics of heavy fading are apparent on these graphs and are discussed below.

1.05 Even though the two signals are observed at the same time and travel over the same paths, their levels do not vary in quite the same way, particularly in regard to the deeper fades. That is, most of the deeper fades do not occur simultaneously. Because these disparities occur between signals of different frequencies, this type of fading is said to be frequency selective; hence the alternate term "selective fading." Although it happens that none of the deeper fades in this example have entered the -40 dB region, the improvement offered by frequency diversity protection can still be demonstrated. For example, the first half-hour (two left-hand columns) of the top chart contains several relatively deep fades which are not present on the lower chart.

1.06 Multipath fading is spatially selective, too. To illustrate, assume a single signal transmitted under conditions similar to those producing the fading shown in Fig. 1. Also assume the signal to be received by two receivers having their antennas vertically separated by a distance of about a hundred wavelengths. Under these conditions, the received signals would have fade relationships resembling those of the frequency-separated signals in Fig. 1. Horizontally-separated antennas would yield similar results, but the distances would have to be many times greater

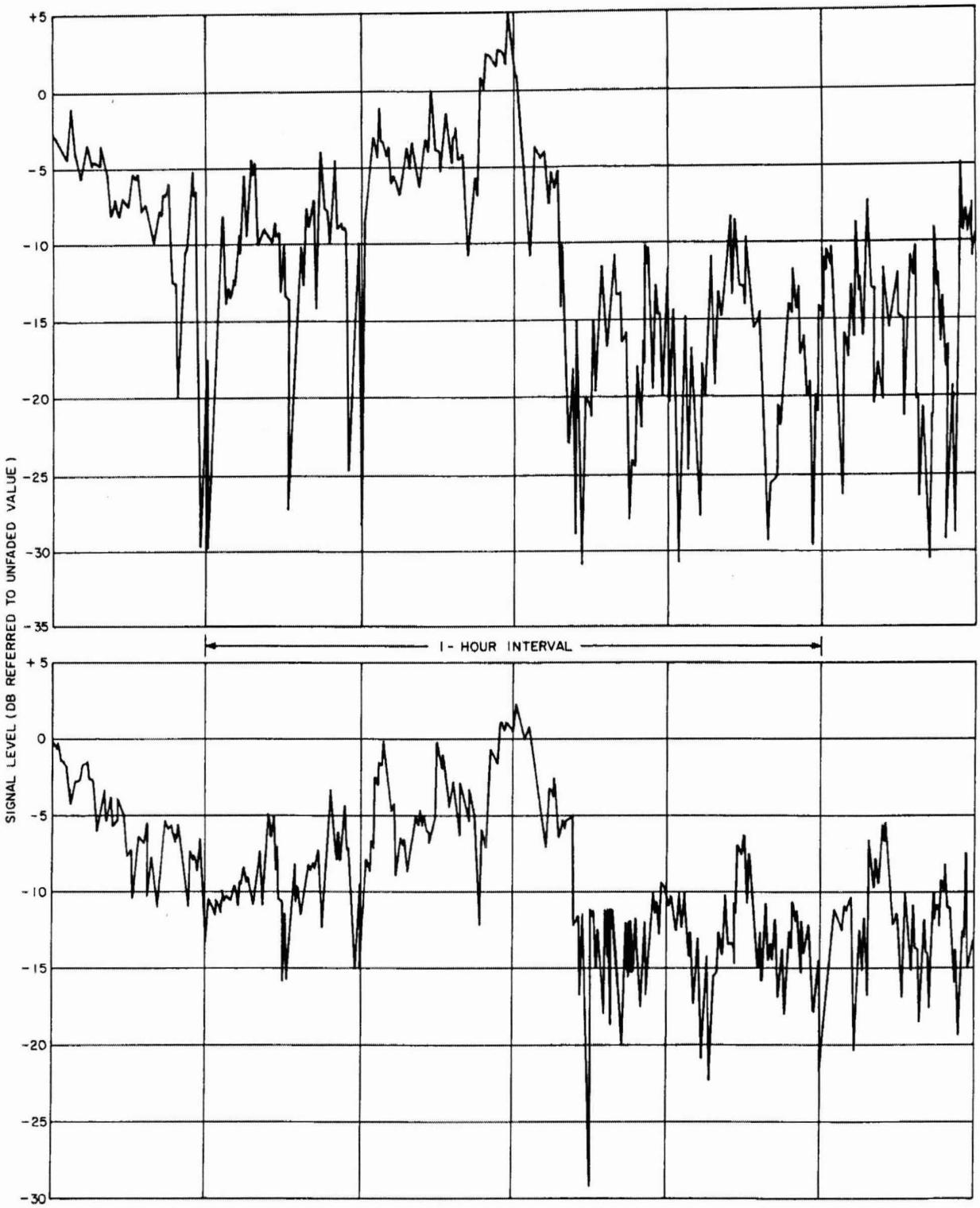

Fig. 1—Heavy Fading on Two Microwave Channels (100-MHz Separation Over the Same Path)

because the structure boundaries in the refractive index tend to be in nearly horizontal layers.

1.07 Also suggested by Fig. 1 is that the number of occurrences and the average duration of the fades are inversely proportional to their depths. That is, there are fewer of the deeper fades, and they are generally of shorter duration than the more shallow ones. While an accurate appraisal cannot be made from this graph, these parameters are elaborated and quantified in Part 4 of this section. Another aspect of multipath fading which is not apparent in Fig. 1 is the fact that the number of fades is related to carrier frequency, although average fade duration, at a given level, remains independent of frequency. These facts are also subsequently considered and quantified.

1.08 Fading activity is variable with the time of day and with the seasons. The late night and early morning hours are usually more conducive to selective fading because the decreased wind activity allows the atmosphere to form into the stratifications which produce multipath propagation. Fading tends to diminish with the morning sun, reaching a minimum at or near noon. On a longer term basis, increased fading activity is generally experienced during the summer months largely because the water vapor content of the atmosphere is at its peak then; the absolute humidity is a major factor in multipath propagation.

1.09 Figure 2 shows typical daily and seasonal variations in fading activity. In it, the vertical lines represent the extremes in signal level received over a 17-mile 4-GHz hop during the 24-hour periods from noon to noon. Signal variations on it are somewhat restricted, owing to the shortness of the hop; however, the preponderance of fading activity during the late summer months, usual in this country, is evident here.

2. BASICS—PHYSICS OF MULTIPATH PROPAGATION

A. Refraction and Reflection

2.01 Radio signals and visible light are both forms of electromagnetic radiation and thus have many properties in common. These similarities are more pronounced as the wavelengths of the radio signals approach that of light. Thus radio signals at microwave frequencies (or wavelengths) behave more like light waves than do those, for example, in the standard AM broadcast band. Two of these properties are refraction and reflection, both of which are deflections of the energy rays from their original paths. A brief discussion of these properties, based on theory and empirical evidence, follows.

2.02 Light and microwave energy may be reflected, or thrown back, from the surfaces of objects in the path. One rule associated with this ***specular***, or "mirror-type," reflection is that the angle of reflection is equal to the angle of incidence; that is, the angle formed by the incident, or arriving, ray and the line. Figure 3 illustrates these angles as well as those concerned with refraction, as discussed later. The other rule is that the incident and reflected rays and the normal to the surface are all in the same plane.

2.03 Several conditions are necessary for reflection of this type. One is that the reflecting surface be "smooth." That is, the average depth of the irregularities must be substantially less than the wavelength of the incident ray. Otherwise

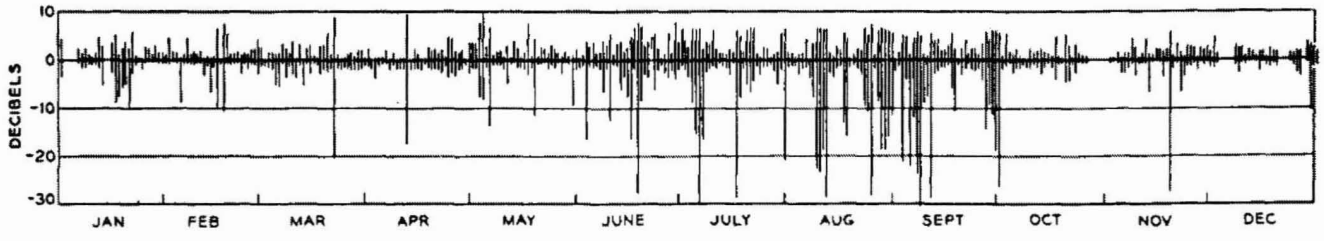

NOTE:
EACH VERTICAL LINE REPRESENTS THE EXTREMES OF RECEIVED SIGNAL STRENGTH DURING ONE DAY.

Fig. 2—Typical Seasonal Variations in Fading Activity

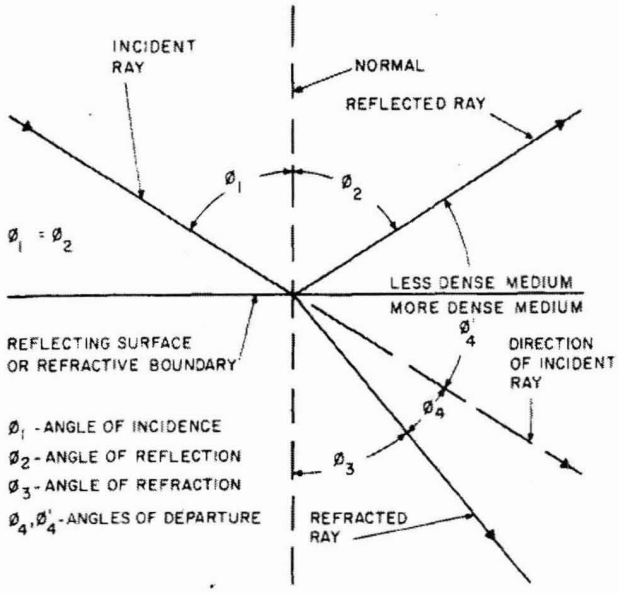

Fig. 3—The Angles and Rays of Reflection and Refractions

the energy will be scattered (also called diffusely reflected). An example of this is that the bottom of a cast-iron skillet makes a good reflector for microwave energy, but not for light. This is because the irregularities in the surface of the skillet are large compared to the wavelengths of light, but small compared to those of microwave energy. Thus, a surface may be "smooth" for one wavelength and "rough" for another. (The wavelengths of light and microwave energy differ by about five orders of magnitude.)

2.04 Another requirement is that the transverse surface dimensions be substantially larger than the wavelength of the incident ray. If this condition is not also met, the ray will tend to be scattered. This type of scattering is called diffraction and will not be discussed here (a dime will reflect light energy, but diffract microwave energy).

2.05 A ray of electromagnetic energy may be either reflected or refracted if it encounters a medium of different density than that of the one through which it has been traveling. ***Refraction*** results in only a slight departure of the beam from the previous path (always less than 90°), whereas the path of a ***reflected*** beam may depart any amount between 0° and 180° from its previous direction. As shown in Fig. 3, the angles of departure referred to here are different from the angles of reflection or refraction. For the purpose of this section, the term "deflection" will be used to include the effect of both refraction and reflection on the direction of the electromagnetic rays.

2.06 The basis for refraction is the fact that electromagnetic energy propagates at different velocities in different media, or in the same medium, if its density varies. This propagation velocity is maximum in a vacuum (the "speed of light") and is lesser in any other medium. Also, it is a constant value for ***all*** wavelengths in a vacuum, whereas it is dependent on wavelength in other media. The ratio of the velocity in a vacuum to the velocity in a particular medium is called its "index of refraction" and is consequently also a function of wavelength. This frequency dependence, although responsible for the light spectrum produced by a prism and that of a rainbow, is of small magnitude and little importance in selective fading at microwave frequencies.

2.07 Figure 4 is a representation of a microwave beam being refracted by an atmospheric discontinuity. Here, the discontinuity is a boundary between two air masses of different density. As each wavefront of the microwave beam crosses the boundary, the part that has entered the less dense air begins traveling slightly faster than the portion still in the more dense mass. When all of a wavefront has crossed the boundary, it is then traveling in a different direction and thus has been refracted. If the air masses in the figure were interchanged, the beam would be bent in the opposite direction. This is a rather simplified explanation, based on Huygens' principle. Huygens' principle is given broader treatment in Section 940-310-105 and in many texts covering basic optics.

2.08 Both the angle of deflection and the energy in the deflected beam depend upon the angle at which the beam approaches the boundary. If the beam encounters the boundary at a 90° angle, no refraction occurs and almost all of the energy crosses it; a small amount will be reflected, depending on the relative indices of refraction. As the angle is changed from 90°, a larger fraction of energy is reflected and the refracted beam is deflected from the incident direction a greater amount. If the incident beam is in the medium of higher density, an angle will be reached, well short of a grazing angle, after which all of the energy will be reflected. This phenomenon does not exist for

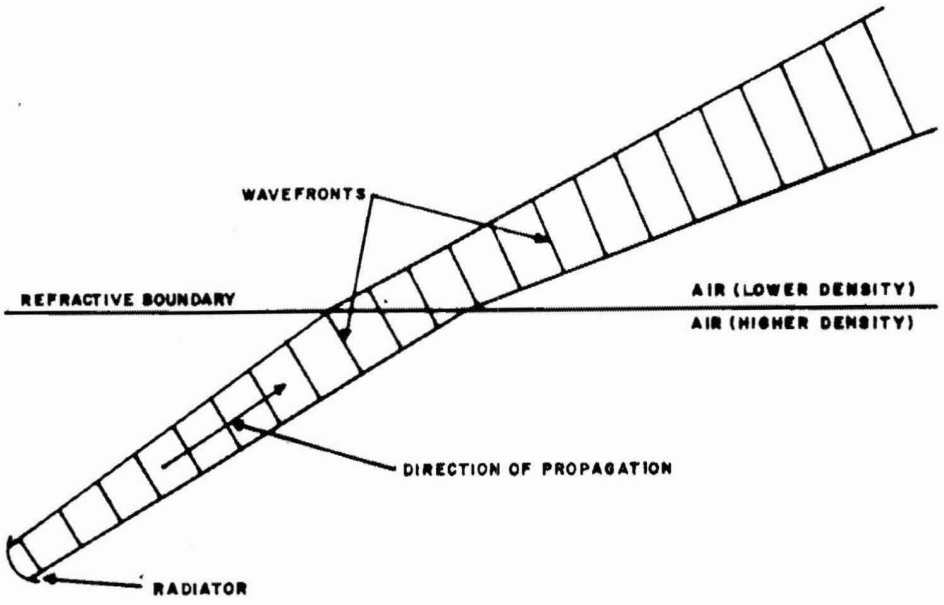

Fig. 4—Refraction of a Microwave Beam Upon Crossing an Atmospheric Discontinuity (Higher-to-Lower Density)

beams originating in the less dense medium; in this case, total reflection is only ***approached*** as the incident beam approaches a grazing angle.

2.09 A microwave signal during propagation through the earth's atmosphere rarely encounters such well-defined boundaries as suggested by Fig. 4. Rather, the variations in density are more gradual, as in the case of humid air masses merging into dry ones, or cold ones into warm ones. In these cases, the bending is more gradual, forming curves instead of sharp angles.

B. Multipath Propagation

2.10 Ordinarily the refractive index of the lower atmosphere has a constant vertical gradient; that is, it decreases with altitude in a rather constant manner. Sometimes, however, relatively abrupt changes in the gradient exist at random altitudes due to temperature inversions (the temperature begins increasing, rather than decreasing, with altitude) or to sharp changes in humidity. These discontinuities usually form horizontal layers, or strata, and cause part of the transmitted beam to be refracted down to the receiver as diagrammed in Fig. 5. It is this propagation by multiple paths which is considered to be the principal source of selective fading. Discontinuities at altitudes of more than a mile can potentially be involved in multipath propagation. The height at which discontinuities continue to be influential will depend on antenna beam width, which determines the energy with which the higher altitudes are illuminated.

2.11 The components of a transmitted beam propagating over these multiple paths may be received in different phases because the path lengths are usually different. They can have different amplitudes, too, according to the effects of absorption and scattering and to the refraction efficiencies of the discontinuities. At the receiver, these components will add vectorially; and thus the normal signal level will be reduced or enhanced, depending on this vector sum.

2.12 Consider a 6-GHz signal reaching the receiver by the direct (line-of-sight) path and one of the additional paths in Fig. 5. Since one wavelength at 6 GHz is about 2 inches, a difference in path length of merely 1 inch (or an odd multiple thereof) will cause the two components to be completely out of phase at the receiver. There they will tend to cancel, reducing the signal to a level determined by their relative amplitudes. Such a 2-component signal will produce a very deep fade if the amplitudes are nearly equal.

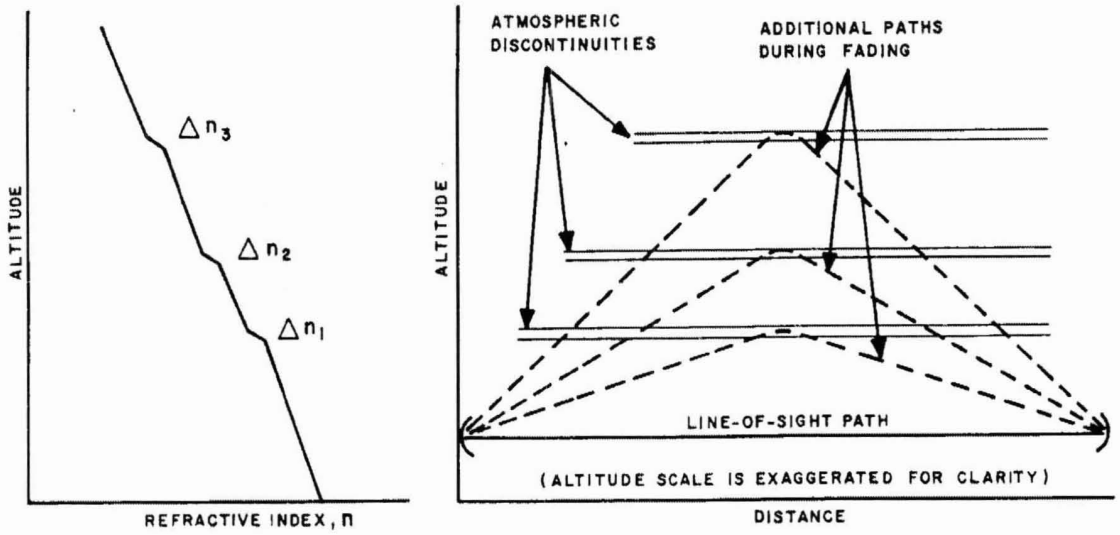

Fig. 5—Multipath Propagation From Refractive Discontinuities in the Atmosphere

2.13 Cosider next an additional signal at a frequency only a few percent different (e.g., another channel in the 6-GHz band) but propagated at the same time and over the same two paths. Because this second signal has a different wavelength, its two components will probably not have the same phase relationship as those of the first (i.e., not 180°). They might actually reach the receiver in phase, thus enhancing the signal, while the first signal is reduced. This combination of wavelength and path-length differences is the primary reason for the frequency-selective characteristic of multipath fading.

2.14 Consider further an additional receiver and antenna for the signal of the first example, except at a different location. Depending on the direction and distance of separation, the difference in path lengths to the second receiver would probably be different from that to the first. Therefore, the resultant signal levels would similarly be different at the two receivers. Thus, the fading produced by multipath propagation is spatially selective.

2.15 In practice, the relationships are less simple than these examples, and often many more than two signal paths are involved. Also, the multipath conditions are variable with the seasons, the time of day, and with the meteorological conditions and the quality of terrain (smooth or rough); all of these variables make any precise prediction of fading impossible. Because of the random nature of fading conditions and their ultimate effect on the received signal, any further analysis is best approached from a statistical point of view. The discussion of the Rayleigh distribution which follows affords such a frame of reference and provides insight regarding the methods used in quantifying multipath phenomena for practical application in improving performance.

3. THE RAYLEIGH DISTRIBUTION

3.01 Lord Rayleigh, the British physicist, formulated a probability distribution function for "the resultant of a large number of vibrations of the same pitch and of arbitrary phase." Expressed somewhat more elaborately, the "Rayleigh" function gives the probability (or time) distribution of the resultant (sum) of a large number of vectors of roughly equivalent size which are constantly and randomly varying in phase. It involves only the magnitude (envelope) of the resultant, the phase distribution being uniform. Because of the similarities between Lord Rayleigh's problem and that of selective fading, the Rayleigh distribution has found use in predicting the fading severity of microwave signals during multipath conditions. The descriptive and predictive power of the Rayleigh curve results in occasional reference to selective fading as "Rayleigh" fading.

3.02 The mathematical expression for the Rayleigh distribution is

$$\Pr (E < E_1) = 1 - \exp [- (E_1/E_{rms})^2].$$

It expresses the probability Pr that the received signal level E is less than any arbitrary voltage E_1. E_{rms}, the root-mean-square value of the distribution, is the so-called "free-space" value which represents the normal received signal envelope in the absence of fading. If this probability distribution is considered over an extended period of time, it expresses the fraction of time the received signal E can be expected to fall below the arbitrary voltage E_1. Figure 6 shows the Rayleigh distribution plotted on a Rayleigh graph scale. The time-fraction is expressed as a percentage, and the ratio E_1/E_{rms} is given in decibels. Inspection of the main (Rayleigh) curve of Fig. 6 reveals that the actual received signal can be expected to fall below the free-space value (0 dB) 60 percent of the time, while a level depressed below −40 dB from normal could be anticipated 0.01 percent of the time.

3.03 Actual microwave reception does not act in strict accordance with the Rayleigh distribution. This is exemplified by the inclusion in Fig. 6 of curves for 4, 6, 11, and 40 GHz, each normalized to its own unfaded level. The curves for 4, 6, and 11 GHz were empirically determined from data taken during two summer months on a hop of 28.5 miles. The curve representing 40 GHz, which serves to extend the example, was generated according to formulae presented in Part 4. Average terrain and climate were assumed, and the path length was also set at 28.5 miles. In practice, paths of this length would not be employed above 11 GHz due to the severe attenuation contributed by rain and fog in the higher frequency ranges.

3.04 During light fading, the criterion of "a large number of vectors of roughly equivalent size" does not usually exist. That is, at these times usually at least one of the components is steady and significantly stronger than the others and/or the number of components is too few to result in a Rayleigh distribution. For a reasonable approximation of the Rayleigh distribution over its whole range, the magnitude of any individual component must be considerably less than the sum of the others' magnitudes and at least several components must be present. Since these conditions are not fulfilled during light fading, empirical curves depart even more from the Rayleigh distribution. For this reason and because heavy fading is of more concern to the study of performance degradation, the empirical curves are limited to fades deeper than 20 dB.

3.05 The augmented Rayleigh distribution of Fig. 6 serves to reveal several significant characteristics of multipath fading. First, and most apparent, is the fact that the time during which a signal can be expected to fall below a given level decreases with increasing fade margin. Second, the added curves demonstrate that fading activity increases with increasing carrier frequency. While an exact mathematical model of this phenomenon is still being developed, a moment's consideration reveals that at a relatively low frequency of, say, 1 MHz, delays approaching 150 meters (one-half wavelength) are required to produce fading. At a typical microwave path length of 26 miles, it is unlikely that atmospheric aberrations sufficient to cause such delays will exist. If, however, the frequency is increased to 1 GHz, delays in the order of the 15-centimeter half-wavelength become increasingly possible. Finally, if we limit our concern to the region representing fade depths below −20 dB, the slope of the Rayleigh distribution is an almost constant 10 dB per decade of probability or time. Taken at face value, Fig. 6 does not show that fading is a function of path length, that average fade duration at a predefined level is frequency independent, nor does it account for other variables such as terrain and climate.

3.06 As stated above, the slope of the Rayleigh distribution in the region below −20 dB is, for all practical purposes, a constant decade of time per 10 dB. Fortunately, the region below −20 dB is also the area of practical concern regarding fade-produced transmission outages. For this reason, it is possible to develop a simplified, flexible method of quantifying anticipated fading activity.

3.07 If the ratio E_1/E_{rms} is expressed as a fade depth F in dB

$$F = -20 \log (E_1/E_{rms}),$$

the Rayleigh distribution may be closely approximated by the simpler expression

$$\Pr (E < E_1) = 10^{-F/10}.$$

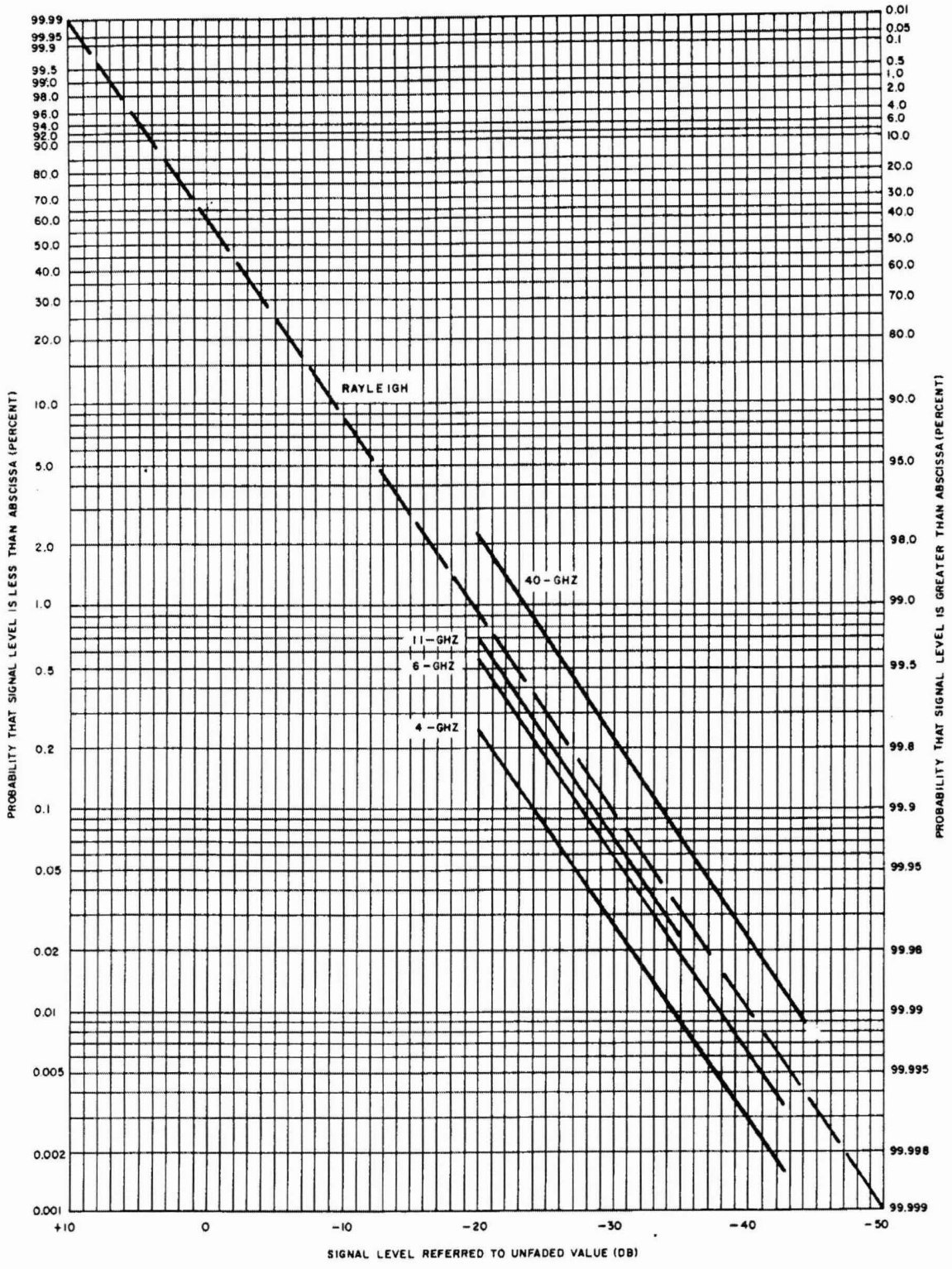

Fig. 6—Probability Distributions (Rayleigh and Empirical Samples)

6300 Sec

If the free-space value (E_{rms}) of the received signal is normalized to 1 and fade depths below this level are represented as L (see Fig. 7), the fade depth F in dB becomes

$$F = -20 \log L$$

which permits the probability function to be expressed as

$$Pr = 10^{\frac{-(-20 \log L)}{10}}$$

which simplifies to L^2 as follows:

$$Pr = 10^{(2 \log L)}$$

$$Pr = 10^{\log(L^2)}$$

$$Pr = L^2.$$

Thus, the characteristic decade of time per 10-dB slope is described as having an L^2 functional dependence. If a finite period of time is multiplied by L^2, it will then yield the proportionate time during which the received signal can be expected to fall below that level. It is then only necessary to modify this time fraction with a factor representing local situational variables (frequency, distance, climate, length of fading season, etc.) to obtain an accurate appraisal of anticipated failure.

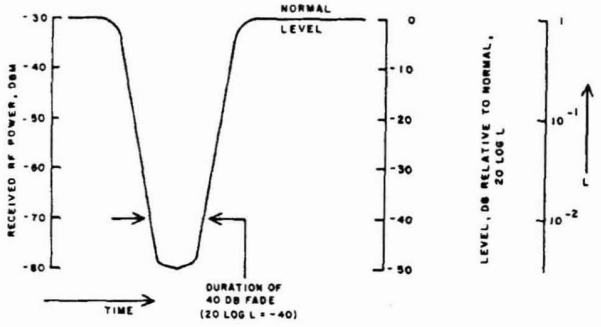

Fig. 7—Definitions of L and Fade Duration (−30 dBm Assumed Normal)

4. ESTIMATING OUTAGE TIME DUE TO FADING

A. Rationale

4.01 Bell System microwave facilities (both long- and short-haul) are designed with a reliability objective of 99.98 percent. Stated differently, they are engineered with an average outage goal of less than 0.02 percent (about 6300 seconds or 1-3/4 hours per year). This overall objective is based on 2-way service and includes outages from all types of fading as well as equipment malfunction, power failure, and other causes. Also, since it is specified for end-to-end service, it implies different per-hop requirements for long- and short-haul systems. The time during which the received signal is below level at a fade depth equal to the receiver fade margin represents potential service failure time. If reliability objectives are to be met, it becomes necessary to appraise and quantify anticipated multipath fading activity on a per-hop basis. The value thus obtained can then be added to the value of outage time allocated to other causes (equipment failure, obstruction or "earth bulge" fading, rain attenuation, etc.) to arrive at a net value of outage time. If this value is excessive or if the value of multipath fading exceeds that value apportioned to multipath effects in terms of overall transmission availability objectives, compensation becomes necessary. Compensation for multipath degradation is typically achieved by means of space or frequency diversity.

4.02 It has been previously stated, and empirically demonstrated, that while average fade duration is independent of frequency and inversely proportional to fade depth, the rate of fading activity and therefore the total time below a given level increases with frequency. Part 4, expanding upon the equivalence of probability (Pr) and L^2 as discussed in Part 3, provides definitions and methods of procedure for the initial quantification of anticipated fading activity.

B. Definitions and Estimation of Fading

Free-Space Value

4.03 The RF power received over a microwave radio hop is least subject to multipath influence at or near noon, when the atmosphere has reached its most stable condition. Even here, however, there can be fractional dB excursions within a period of seconds (scintillations) as well as slower excursions of a dB or two. The normal value of the received signal is therefore obtained as an average over at least one-half hour at or near noon. This so-called free-space value of the received signal is determined repeatedly at least once a week to identify and exclude periods during

which there have been enhanced or depressed signals due to relatively steady atmospheric focusing or defocusing and which therefore cannot be regarded as normal.

Definitions of L and Fade Duration

4.04 During fading, the received RF power can be practically zero for seconds at a time. The terminology to describe this is introduced in Fig. 7 via an example where the free-space value is −30 dBm and a single (idealized) fade decreases the received power temporarily to −80 dBm. Levels in dB relative to normal are denoted by 20 log L, where L represents the antenna voltage during a fade, as compared to the normal or free-space value. The time during which a signal is below a level is called the duration of fade of that level, which is illustrated in Fig. 7 by the duration of a 40-dB fade. Since this illustration is intended to define terms, the relative durations as implied by the curve are not proportioned to scale but are defined below.

Average Fade Duration

4.05 Average durations of fades are independent of microwave frequency and are proportional to L or depth of fade. Typical numerical values are given by: t (typical) = 410 L seconds, where $L < 0.1$. This is graphically illustrated in Fig. 8. As an example, the average duration of a 40-dB fade ($L = 10^{-2}$) is 4.1 seconds at all microwave frequencies.

Time Below Level

4.06 The sum of durations of all fades of a particular depth is called "time below level" (T). It is proportional to L^2 since, in addition to fade duration, the number of fades is also proportional to L. The numerical value of time below level is given by:

$$T = T_o L^2, L < 0.1.$$

In this expression, T_o is the time period (a summer month, for example) over which the summation of fade durations is made. The units of T are also those of T_o with seconds normally being used (one 31-day month = 2.68×10^6 seconds). A realistic evaluation of time below level must, however, account for local situational parameters; thus the practical expression for time below level is

$$T = r T_o L^2, L < 0.1$$

where r, the fade occurrence factor, accounts for situational variables.

4.07 The fade occurrence factor r accounts for frequency, distance, climate, the occasional nature of fading, and, ultimately, terrain roughness (if this latter quantity requires separate consideration). Figure 9 serves to illustrate the multipath occurrence factor as a variable of path length and frequency. The significance of the curves for 18, 29, and 40 GHz is confined to academic interest, since at these frequencies path lengths are sufficiently short to avoid serious multipath fading. The fade occurrence factor r, for a heavy fading month, is expressed as:

$$r = c(f/4)D^3 10^{-5}$$

where

c = 4 over-water and Gulf coast,

= 1 average terrain and climate,

= 1/4 mountains and dry climate,

f = frequency in GHz,

D = path length in miles.

As an example, values of time below level (T) as a function of fade depth for a 26-mile (typical length) path and average terrain and climate (c=1) are shown in Fig. 10 for a heavy fading month. The lines have the decade of time per 10-dB slope typical of multipath fading, specified by the L^2 functional dependence. The values of T at −40 dB are 47, 71, and 129 seconds at 4, 6, and 11 GHz, respectively. Based on an average fade duration of 4.1 seconds as determined previously, this corresponds to 11 fades of 40 dB at 4 GHz, 17 fades at 6 GHz, and 31 fades at 11 GHz.

C. Terrain Roughness Modification

4.08 The coefficient c, as described above, is simplified in that it incorporates and ties together the effects of both terrain and humidity. While this is adequate for first estimates of expected fading in many cases, differentiation between paths having identical climate but differing terrain can be done via modification of c for specific terrain

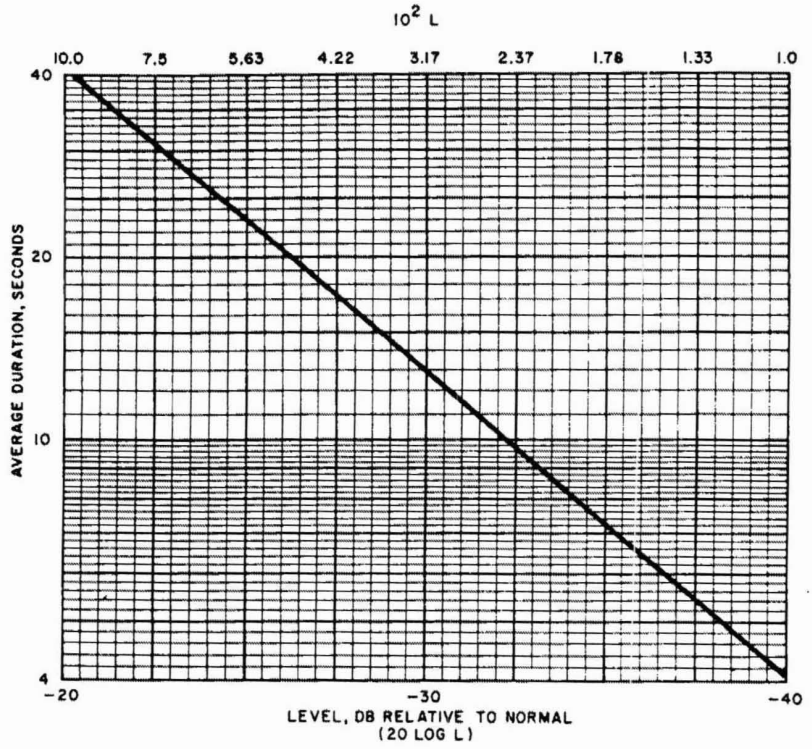

Fig. 8—Average Fade Durations ($<t>$ = 410L, L < 0.1)

roughness. The terrain roughness parameter introduced for this purpose serves to quantify common knowledge that paths over rough terrain fade less than paths over smooth terrain, presumably because stable atmospheric layering is less likely to occur over rough terrain.

4.09 Terrain roughness is calculated from terrain heights above a reference level (sea level, for example) obtained from the path profile at 1-mile intervals, with the ends of the path excluded. The standard deviation of the resulting set of numbers is the terrain roughness, denoted by w. Table A demonstrates the method of calculation used to obtain values of w. The path length in this example is 19 miles. Applicable values of w range from 20 feet (considered as smooth) to 140 feet (rough). These values of 20 and 140 should be used when calculated values of w are less than 20 or larger than 140. A value of 50 has been defined as normal, and in this case, the value of c will remain at 1 for average climate. Modified for roughness, the equations for c become:

$$c = 2\,(w/50)^{-1.3}, \text{ coastal areas}$$

$$= (w/50)^{-1.3}, \text{ average climate}$$

$$= 0.5\,(w/50)^{-1.3}, \text{ dry climate.}$$

5. DETERMINATION OF NEED FOR PROTECTION

A. General

5.01 In Part 4, the overall reliability objective for Bell System microwave facilities was established at less than 0.02 percent or about 6300 seconds per year or less. The practical realization of this goal requires that each hop in a particular system be examined to assure that the proportionate outage time assigned to multipath fading is not exceeded. In Part 5 of this section, the concepts of Part 4 are applied to a per-hop analysis in terms of short- or long-haul system requirements. As herein described, a somewhat simplifying assumption is made regarding the occurrence of simultaneous fading; i.e., it is assumed that simultaneous fading on distinct hops does not occur. Since two or more simultaneous outages translate as a single outage, the slight error thus introduced is conservative in that it overestimates the outage. Design

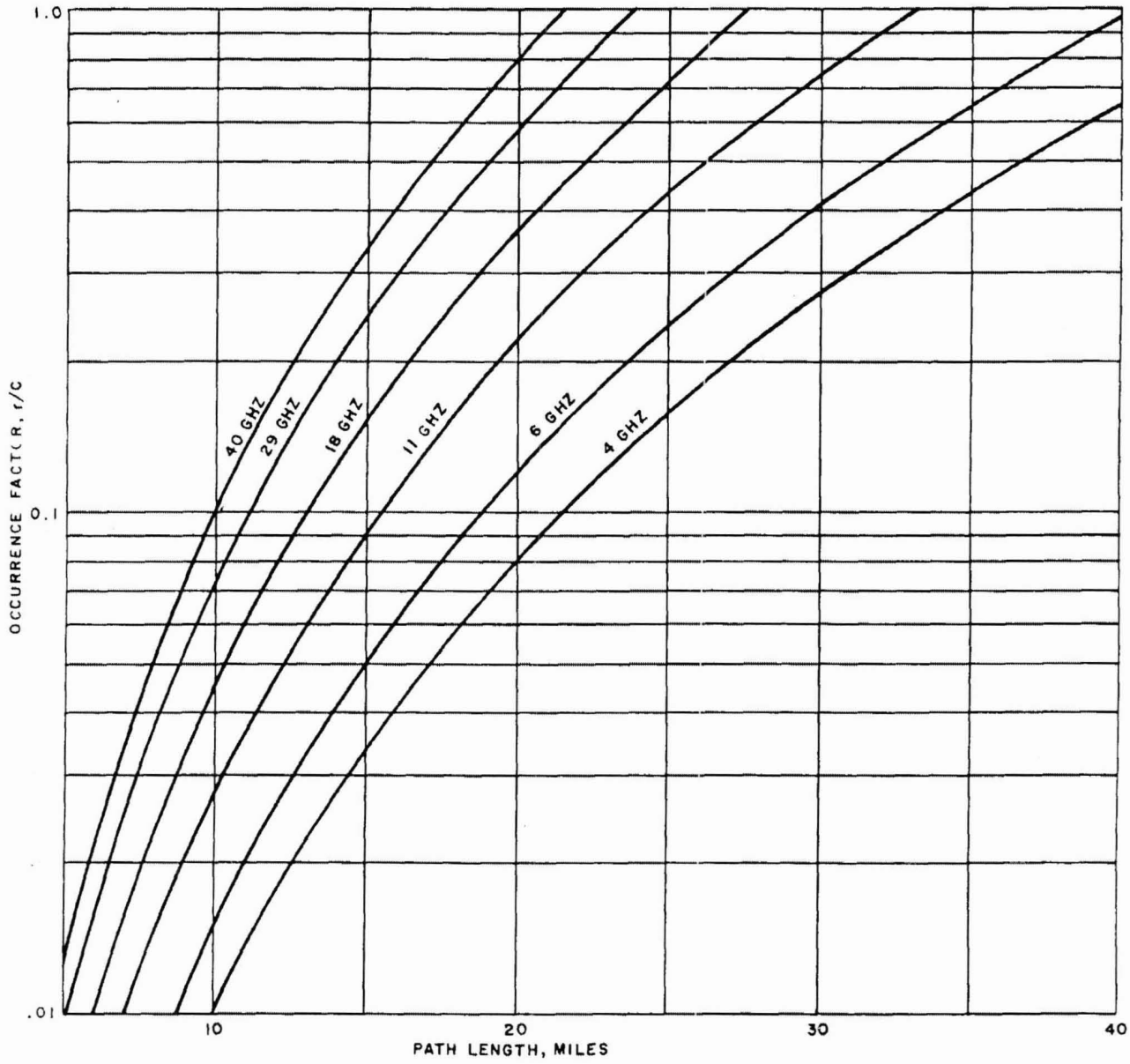

Fig. 9—Multipath Occurrence Factor for a Heavy Fading Month

objectives will therefore tend to exceed actual requirements. In the 18-, 29-, and 40-GHz microwave bands, attenuation from condensed atmospheric moisture (rain and fog) is severe. For this reason, hop lengths are sufficiently short to preclude the need for multipath compensation. The 11-GHz band is also subject to rain attenuation. Here, however, hop lengths can be sufficiently long to result in selective fading. Consequently, that percentage of total outage time allocated to rain fading must be offset by additional reduction of the effects of selective fading. The subject of rain fading is covered in Section 940-310-106 and should be considered in any 11-GHz design effort.

B. Short-Haul Objectives

5.02 Short-haul objectives limit service failure time to 0.02 percent, 2-way annual, on a 250-mile route due to all causes. Of this amount,

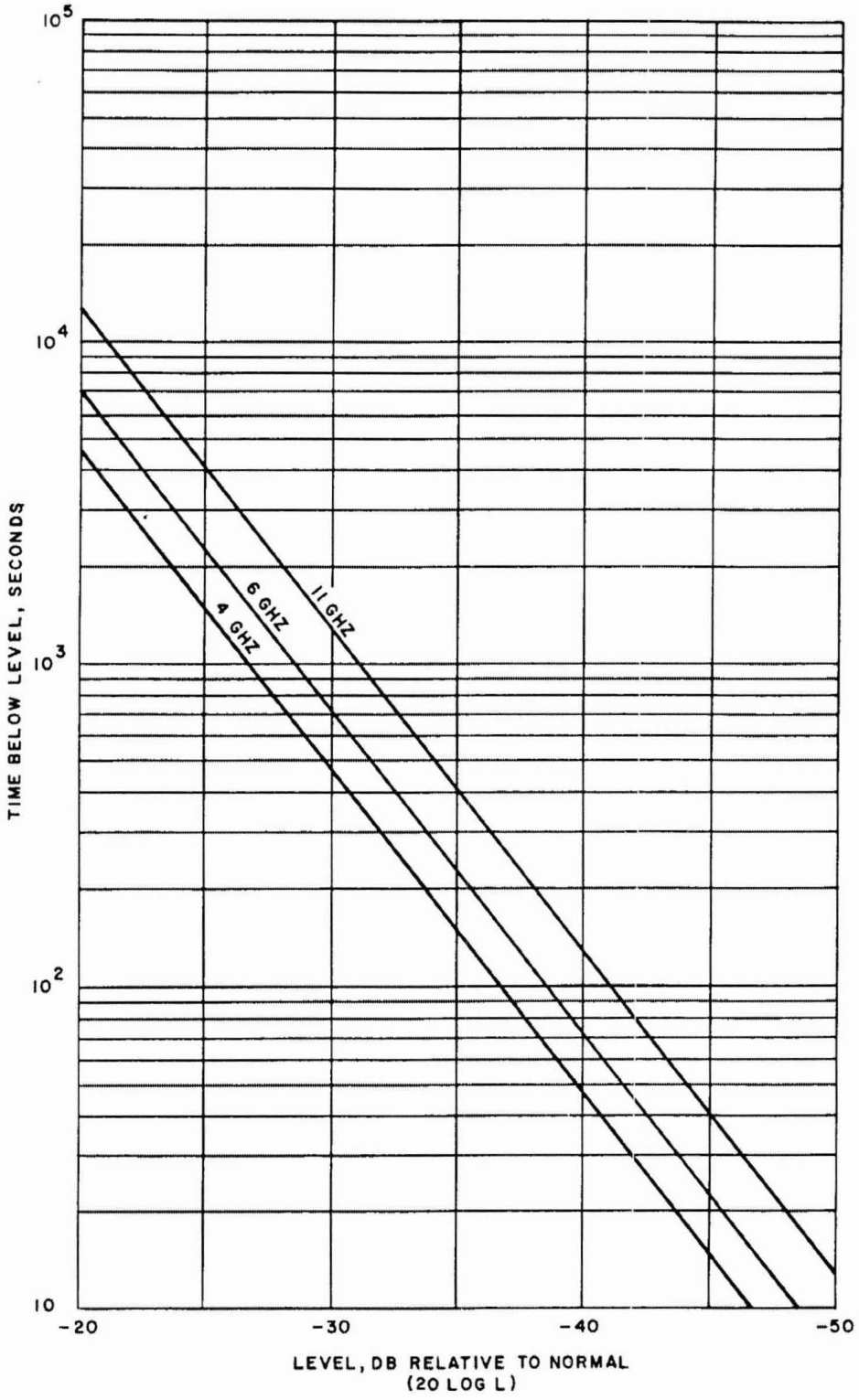

Fig. 10—Time Below Level in a Heavy Fading Month (D = 26 Miles, c = 1, T_o = 31 Days = 2.68 × 10^6 Seconds)

TABLE A

COMPUTATION OF THE TERRAIN ROUGHNESS FACTOR

The terrain roughness factor (w) is, as stated in 4.09, the standard deviation of the path profile (σ). Expressed mathematically,

$$w = \sigma = \left[\frac{\Sigma\,(x - M)^2}{n}\right]^{1/2},$$

where "x" is the vertical distance in feet of the path profile as measured from some horizontal reference at one-mile intervals, excluding the station locations; "n" is the number of such measurements; and "M" is the arithmetic mean, or average, of the measurements.

The above equation for "w" may be altered so that the number of subtractions will be greatly reduced at the expense of larger squared terms:

$$w = \sigma = \left[\frac{\Sigma\,(x^2)}{n} - M^2\right]^{1/2}.$$

It should be noted that $\Sigma\,(x^2) \neq (\Sigma\,x)^2$.

Thus, for the 19-mile hop "A" in the sample calculations, w is computed as follows; preparation of a table similar to that below helps keep computations under control.

NUMBER OF MEASUREMENT	DISTANCE MEASUREMENT	SQUARE OF DISTANCE MEASUREMENT
(n)	(x) feet	(x^2) feet^2
1	600	360,000
2	625	390,625
3	515	265,225
4	440	193,600
5	480	230,400
6	450	202,500
7	400	160,000
8	420	176,400
9	460	211,600
10	420	176,400
11	450	202,500
12	480	230,400
13	450	202,500
14	420	176,400
15	390	152,100
16	480	230,400
17	520	270,400
18	550	302,500
A $\Sigma = 18$	B $\Sigma = 8,550$	C $\Sigma = 4,133,950$

$$M = \Sigma\frac{x}{n} = \frac{8,550}{18} = 475 \text{ ft}$$

$$w = \sigma = \left[\frac{4,133,950}{18} - (475)^2\right]^{1/2} = 63.5$$

$$\sqrt{\frac{C}{A} - \left(\frac{B}{A}\right)^2}$$

one-half is allocated to causes associated with equipment, maintenance, and plant errors. The allocation to fading is therefore 0.01 percent, 2-way annual. There can be, however, obvious exceptions to this. For example, unavailability on a route where all hops are exceptionally short will be due mainly to equipment outages and may be so allocated.

5.03 In the past, it was customary to further apportion the 0.01-percent, 2-way annual value assigned to fading between multipath and obstruction fading—otherwise known as "earth bulge" fading. However, the occurrence of intolerable obstruction fading can be decreased by increasing clearance (higher towers or shorter hops) or by increasing the system gain margin. Reliability records show that there has been a gradual decrease in the occurrence of obstruction fading over the years. In the construction of new hops or in the upgrading of older ones in locations where obstruction fading is known to occur (or by related experience is expected to occur), increased clearances (or limits on path lengths) are assumed to be used. Consequently, no allocation to obstruction fading is made; the entire 0.01-percent, 2-way annual fading allocation is applied to multipath fading. The one-way annual multipath fading allocation for 250 miles becomes 0.005 percent or approximately 26 minutes per year (1600 seconds per year). The corresponding allocation to a hop D miles long is $1600 \times D/250$ seconds per year or 165 seconds per year one way for an average 26-mile hop.

C. Short-Haul Appraisal

5.04 The estimated annual time below level for comparison with the 165-second objective is obtained from the equation for T ($T = r\, T_o\, L^2$, $L < 0.1$) in paragraph 4.06, with T_o describing the length of the fading season. As a geographic average, the value of T_o in this estimate is equal to the number of seconds in three months. This assumes that all significant fading is contained in two heavy- and two medium-fading months, which is equivalent to three heavy-fading months or 8.04×10^6 seconds. Figure 10, presented in conjunction with paragraph 4.07, provides the time below level for a typical heavy fading month. Continuation of this example provides the annual time below level curves of Fig. 11. Examination of Fig. 11 reveals that at −40 dB, the annual average case values are now 142, 212, and 387 seconds at 4, 6, and 11 GHz, respectively, or three times the 47-, 71-, and 129-second values of T obtained in 4.07. Figure 11 also includes the per-hop annual objectives for both short haul (165 seconds) and long haul (20 seconds). Examination of the short-haul objective at a −35 dB fade reveals that the time below level exceeds the 165-second objective by factors of 2.7, 4, and 7.3 at 4, 6, and 11 GHz, respectively. Protection against multipath fading is therefore needed when the fade margin is −35 dB. At a fade margin of −40 dB, the 4-GHz channel in the example can, however, get by without protection.

5.05 The above example assumed T_o as the geographic average of three heavy-fading months. The length of the fading season is, however, influenced by temperature and is essentially a warm weather phenomenon. The value of T_o must therefore be modified as a function of average annual temperature which, in turn, is related to geographic location. Paragraph 5.07 provides the procedure, together with a contour map of the United States, for specific computation of T_o.

D. Long-Haul Considerations

5.06 For long-haul radio the overall objective is also 0.02 percent, but the route length is 4000 miles. Previously, the recommended long-haul multipath allocation to a hop D miles long was $1600 \times D/2000$ seconds per year or 20 seconds per year for the average 26-mile hop. This was based on the assumption of significant fading on only half of the hops. Better estimates of fading can now be made, and the recommended allocation now is $1600 \times D/4000$ or 10 seconds per year for the average 26-mile hop.

E. Length of Fading Season

5.07 Multipath fading is a warm weather phenomenon. Assuming that the length of the warm portion of the year is proportional to the average annual temperature, the value of T_o to be used to estimate the annual time below level is

$$T_o = (t/50)\, 8 \times 10^6 \text{ sec}, \quad 35 \leq t \leq 75$$

where t denotes the average annual temperature of the locality in question given in °F, as determined from Fig. 12. In the average case (Fig. 11), T_o is equal to the number of seconds in three months, and T_o reduces to this when t is 50°F. The temperature contours in Fig. 12 show that 50°F is appropriate for middle latitudes in the United

$3M_o = 8.04 \times 10^6$

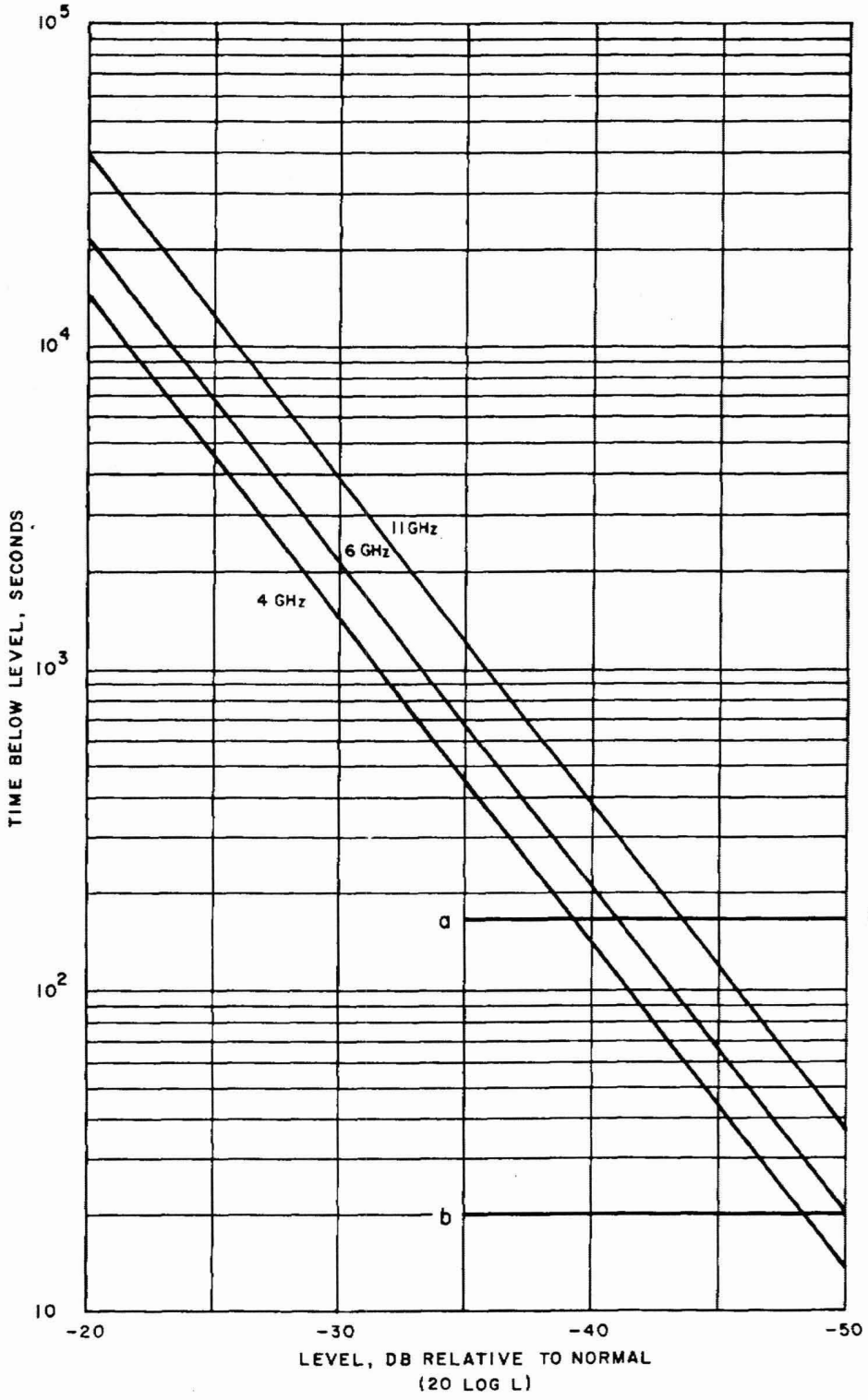

Fig. 11—Annual Time Below Level (Average Case) Objectives: (a) Short Haul, 165 Seconds/Year (b) Long Haul, 20 Seconds/Year

States and for Ohio in particular. Data from Ohio have often been used to describe average fading. The range of average annual temperatures (Fig. 12) is from 35°F in northern North Dakota to 75°F in southern Florida. The corresponding fading season lengths range from 70 percent to 150 percent of average. The adjusted value of T_o therefore ranges from 2 months to 4-1/2 months.

6. SELECTIVE FADING AND NARROWBAND SYSTEMS

A. General

6.01 The emphasis of this section has, thus far, been directed to conventional FM systems which, at the time of writing, characterize microwave transmission media. The use of frequency modulation in microwave radio systems arises primarily from difficulties related to the design of linear amplifiers having adequate gain and power output to handle wideband AM signals at microwave frequencies. The application of a complex amplitude-modulated signal to an amplifier having inherent amplitude nonlinearity results in the generation of spurious frequencies or modulation products which will be present in the output and which cannot be tolerated. A constant amplitude FM signal is, however, relatively insensitive to this type of nonlinear distortion and can thus be transmitted through amplifiers which have compression or amplitude nonlinearity with little penalty.

6.02 The IF bandwidth employed in existing microwave radio systems is typically 20 or 30 MHz. In an FM system, a 30-MHz bandwidth is required in order to carry 1800 telephone message channels or three L-carrier mastergroups. (One mastergroup contains 600 4-kHz voice channels and occupies 2.4 MHz.) Three mastergroups is the per-channel loading in TH-1, TH-3, and TN-1 systems. The need for spectrum conservation together with ever-increasing communications demands has necessitated the development of alternatives to current FM systems having increased information-carrying capacity. A new method, known as the AR-6A (analog radio, 6 GHz, type A) system, employs an amplitude-modulated single-sideband technique wherein a baseband multimastergroup signal is translated to a 6-GHz radio channel. The narrowband terminology, incidentally, refers to the nature of the intelligence (as contained in 4-kHz, AM, SSB channels) within the microwave channel, which again is 20 or 30 MHz wide as in existing FM systems. (The AR-6A channel will be 30 MHz wide, while a later version, operating at 4 GHz, will utilize a 20-MHz channel width.)

B. Narrowband Radio and Wired Carrier Systems

6.03 The use of multiplexed, up-converted groups of AM sidebands to amplitude-modulate a microwave carrier (which is itself transmitted as a single sideband) results in an increased similarity between radio systems and conventional wired carrier telephone systems such as type "L" carrier. With the application of similar techniques to microwave radio, it becomes possible to realize the increased information-carrying capacity of wired carrier systems. The L-3 and L-4 carrier systems, using coaxial cable as the transmission medium, require a bandwidth of only 8 MHz to carry 1800 message channels, as compared to the aforementioned 20 MHz in FM radio. Thus, in the narrowband system, it is possible to contain six mastergroups (3600 message channels) together with necessary guard bands, noise slots, and pilot signals in a single 20-MHz channel, thereby doubling the capacity of the system. A 30-MHz channel will contain ten mastergroups (6000 message channels), resulting in an improvement in excess of three (6000/1800) times that of current FM systems.

6.04 The analogy between carrier systems and narrowband radio is not limited to a coincidence of message capacity and modulation methods, but also includes a commonality of problems. One of the major problems associated with transmission lines is attenuation-versus-frequency distortion, which results in level misalignments of information-carrying frequencies within the band. Inasmuch as the distortion-producing parameters of a transmission line can change with time or be influenced by environmental factors such as temperature, equalizing and regulating networks can be inserted which compensate for nonlinearity. The resultant "flat" line prevents loss of information in the otherwise attenuated portion of the frequency spectrum.

6.05 Selective multipath fading within a 20- or 30-MHz channel carrying AM narrowband information is analogous to attenuation-versus-frequency distortion of a transmission line. The difference rests in the essential predictability (attenuation is known to vary as the square root of frequency) of wired carrier systems as opposed to the compounded problems created by the unpredictability

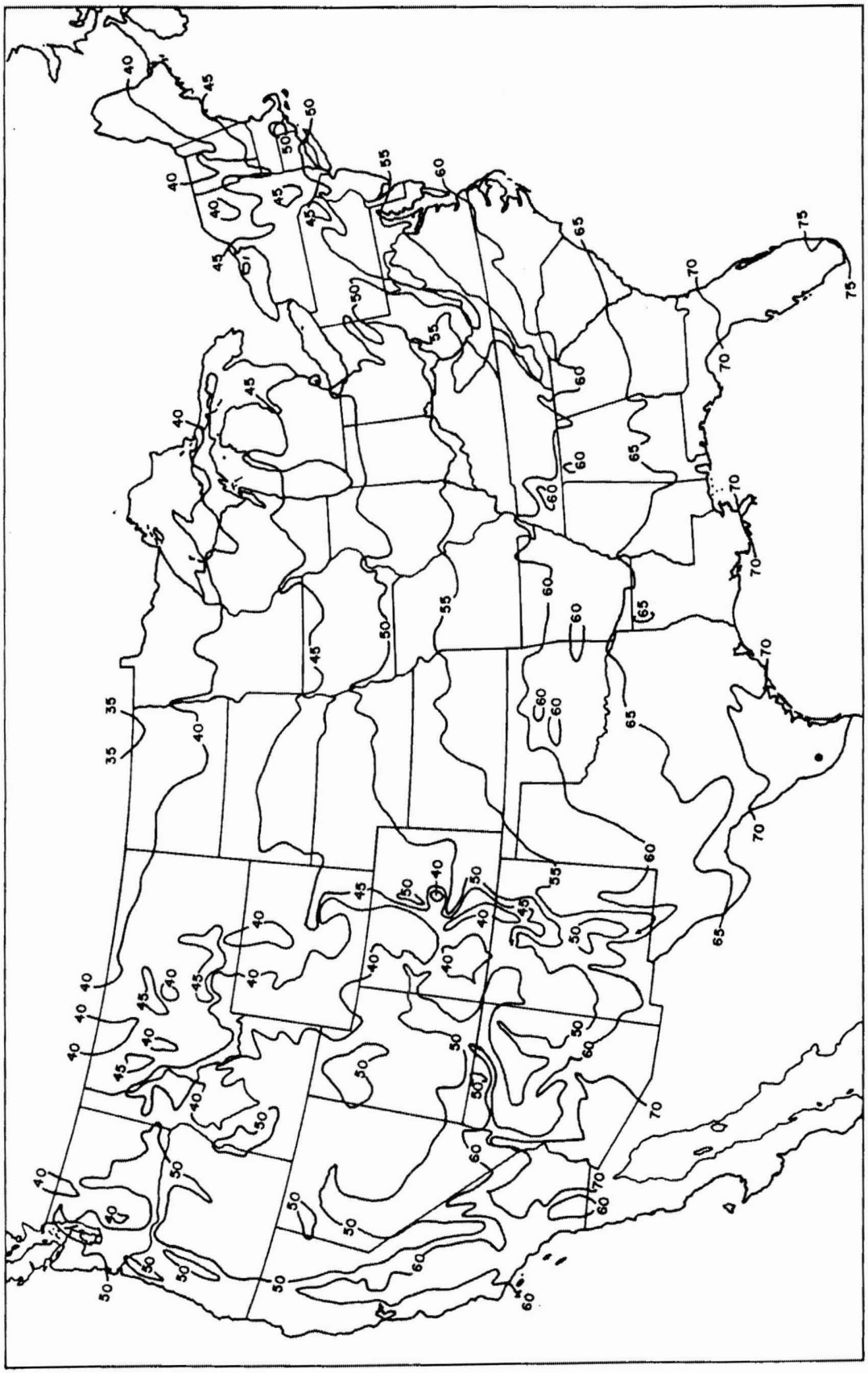

Fig. 12—Average Annual Temperatures in °F

of a radio link. Selective fading can occur randomly at any point in the band; it can remain fixed for a given period or sweep across the band spectrum. Its level will also be changing. Whatever the case, the desired uniform transmission characteristic will be corrupted. The nature of an FM signal, which among other factors contains both sidebands of information, is such that it is less susceptible to intrachannel distortion of this type. For such an FM system during deep fades, a single pilot tone (or noise slot) is sufficient to monitor channel conditions and indicate when a switch to a diversity antenna or protection channel should take place; i.e., the entire channel can be regarded as a singular entity. In a narrowband AM system, selective fading can result in loss of message channels within the affected portion of the main channel spectrum or can distort the channel profile from its ideal flat attenuation-versus-frequency characteristic.

6.06 In dealing with narrowband radio propagation, two major factors attributable to multipath phenomena must be considered and offset. The first results from relatively deep inband selective fading, causing those message channels in the faded portion of the channel spectrum to be reduced in signal level. The second is time-variant deviation of the channel amplitude-versus-frequency characteristic which, because it is continually changing, must be dynamically compensated. Deep fading is monitored by the use of three separate pilot tones (and associated noise slots) located approximately at band center and 2.4 MHz (one mastergroup) in from the respective band edges. Under conditions of deep fading, protection switching of the entire channel will take place if any one of the three band segments has failed. Dynamic equalization, driven by special tones separated from message frequencies, will correct for level misalignments.

INTRACHANNEL PHENOMENA

A. General

6.07 The following discussion provides a characterization of radio channel loss variations as typical of a microwave channel assigned to narrowband service. The data herein presented was extracted from that obtained during two experiments conducted, respectively, in 1970 and 1971. The objective of the first experiment was directed toward the quantification of spectral and temporal behavior of amplitude distortion occurring within a channel as a result of distructive multipath interference. The 1971 experiment demonstrated the realizable advantages of a space diversity system in counteracting these deleterious effects. To the extent that the second experiment duplicated conditions of the first, confirmation of initial results was also obtained. Since the purpose of this discussion is the exposition of salient facts and conclusions, graphic data found most illustrative in support of given topics will be selected from either experiment, except in cases requiring strict parametric continuity.

B. Experiment Structure

6.08 Experimental data was obtained by the generation, transmission, and continuous recording of a tone field consisting of 62 coherent tones. The tones, which were uniformly spaced at 550-kHz intervals, spanned a bandwidth of 33.55 MHz. The tone field, centered at 70.4 MHz, was used to amplitude-modulate a 6-GHz microwave carrier which was transmitted as a single sideband having an essentially flat envelope over a 26.4-mile radio path. At the receiver, the amplitudes of selected tone subsets were continuously monitored and recorded together with timing and tone identification data by means of a multiple input data acquisition system. The data base, compiled during a 59-day period in the case of the first experiment and three summer months in the second, was held within manageable limits by restricting the highest recording rate (five samples per second) to periods of heavy fading, as well as by other methods. By selectively operating upon this large volume of information, significant aspects of multipath behavior were extracted and characterized. Additional objectives of the initial experiment were to prove the feasibility of defining intrachannel distortion selectivity by means of a 3-tone amplitude difference technique and to determine the adequacy of this analysis in terms of level misalignments for the parameters of bandwidth and fade depth.

C. Definitions and Methodology

6.09 In order to reveal the variety and nature of selective fading acting upon a channel, a series of time-sequential amplitude-frequency plots were made across the 33.55-MHz bandwidth. An examination of these sequential scans established that the distortion profiles most frequently exhibited simple slopes, simple curvatures, or combinations of the two. Higher-order structures (cusps, for example) which exceeded second-order analysis

occurred only for the deeper fades. Ideally, the form chosen to represent such selective fading events should be characterized by simplicity and generality. Therefore, the detailed variation across the amplitude-frequency characteristic was defined in terms of linear and quadratic distortion. These could be parameterized by monitoring the amplitudes of three symmetrically spaced reference tones $A(f_1)$, $A(f_2)$, and $A(f_3)$ across a channel of $2\Delta f$ as illustrated in Fig. 13. The bandwidth ($2\Delta f$) was 20.35 MHz in the first (1970) experiment and 19.8 MHz during the second. Again referring to Fig. 13, linear or first-order amplitude distortion (ΔA) is defined as

$$\Delta A = A(f_3) - A(f_1)$$

and represents the ***slope*** in dB across a channel of width $f_3 - f_1 = 2\Delta f$. Quadratic amplitude distortion, so called since its expression contains second-order terminology ($\Delta^2 A/2$), is defined as

$$\frac{\Delta^2 A}{2} = \frac{A(f_1) + A(f_3)}{2} - A(f_2)$$

and represents the component of curvature or ***bow*** in dB across the $2\Delta f$ channel. For the example shown in Fig. 13, the fade depth $A(f_2)$ is -34 dB, and $A(f_3)$ and $A(f_1)$ are respectively -23 dB and -33 dB. Consequently, the channel, for this brief instant, had 10 dB of slope and 6 dB of bow. The observed experimental distributions for slope $|\Delta A|$ and bow $|\Delta^2 A/2|$ were accumulated for various ranges of center channel fade depth as well as for seven different bandwidths. Conditional data, i.e., conditioned on the faded level in dB of $A(f_2)$, serve to more clearly demonstrate at what fade depth the slope and bow mathematical representations applied.

D. Characteristics of Inband Fading and Distortion

Overview and Time Below Level

6.10 Following initialization procedures during which calibration reference levels based on normal or free-space path loss were established, an overview of daily fading activity was generated and is presented in Fig. 14. The lower half of the figure shows the daily distributions of the fraction of total time the received amplitude was faded 20 dB for tones 1, 25, and 62. The upper half of this figure is for the 30-dB level. (Tone 25 was used rather than tone 32 to avoid certain spurious modulation effects which were detected earlier.) Several observations can be made from Fig. 14. First, as is typical of line-of-sight fading, the deep fading at these levels occurred in unpredictable bursts. Second, higher fading activity occurred in more concentrated bursts and for deeper fades. Finally, individual tones exhibited increasingly different fading activity for the deeper fades. This tone dispersion is an indication of the increasing frequency selectivity of deep fades as contrasted to the relatively flat (across the band) fading at levels of 20 dB or less.

6.11 Figure 15 shows the actual fade depth distributions for tones 3, 24, and 60 for the month of August. The tones display the same characteristic decade of time per 10-dB slope as described previously in Part 3 of this section. A question which arises at this time is how the division of a channel into three segments, each of which is now subject to fading, alters the concepts previously set forth in Part 4 of this section. The formula for time below level ($T = r\ T_o\ L^2$) given in paragraph 4.06 is applicable to any of the three tones. It has been demonstrated that mutual exclusivity is not an unreasonable assumption for deep fades having a frequency separation of 5 to 10 MHz, which applies to the three pilot tones of a narrowband channel. Thus, for the limiting case, the total time below level within the channel becomes 3T or, expressed as a time fraction in accordance with the three tones of Fig. 15, $3 \times 2.0 \times 10^{-5} = 6.0 \times 10^{-5}$ at 40 dB. Experience arising from additional experimental work, however, indicates that a more realistic or practical value for tones having 5- to 10-MHz separation and fade margins slightly above, i.e., less deep than, those typical of FM systems was actually 2.6. Thus the practical formula for time below level becomes 2.6T. Another way of viewing this is to say that the number of requests for protection switching will now increase by this amount.

The Space Diversity Improvement

6.12 An additional consideration here is the degree of improvement in outage time offered by a space diversity protection system as envisioned for narrowband systems. This is best illustrated by Fig. 16, which represents a permutation of the three band segments represented by three frequencies F_1, F_2, and F_3 as received simultaneously on the main (top) and diversity (bottom) antennas. As an example, assume a hop having an outage time of 100 seconds per month protected by a space diversity system providing an available improvement

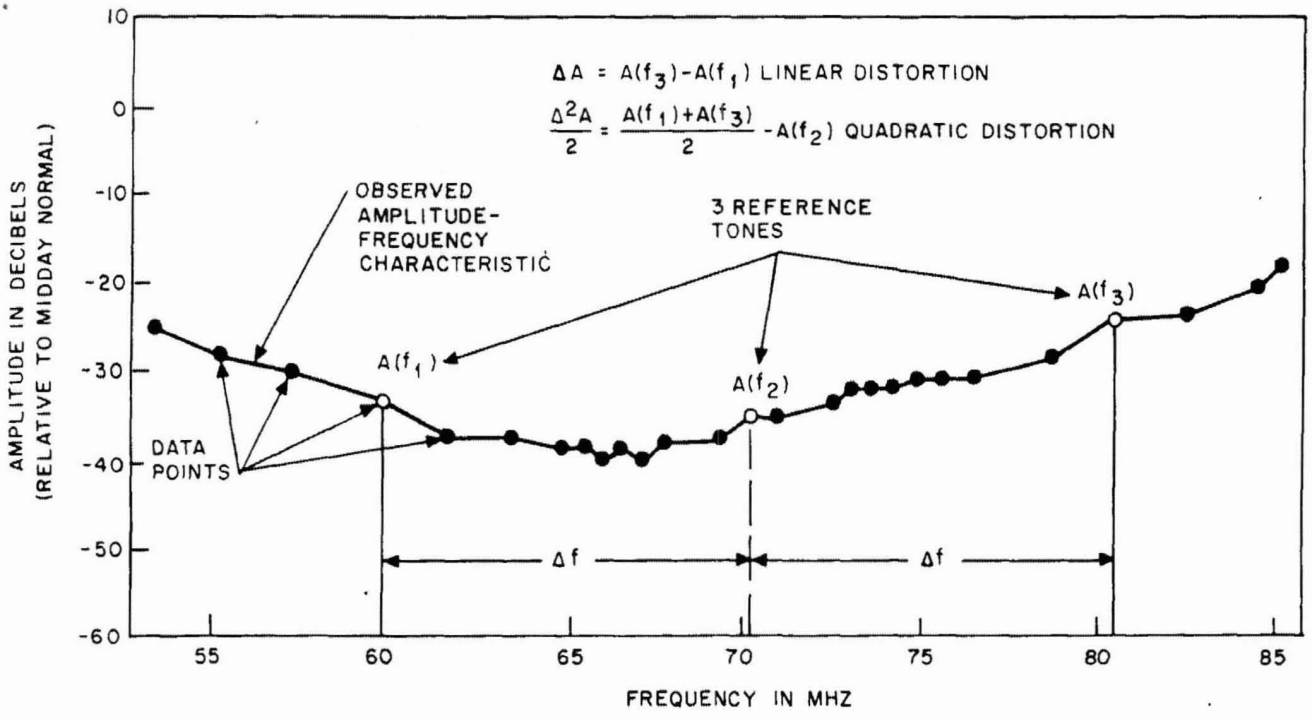

Fig. 13—Selectivity Characterization of the Observed Amplitude-Frequency Characteristic

or I_o (see Section 940-310-115) of 100 in terms of an FM system. This states that the probability of a single frequency experiencing a simultaneous fade on both antennas exists for only 1/100 of the total time. Thus the actual failure time of each single frequency with respect to itself is reduced to 1 second. Since there are now three frequencies, the possibility exists that one of the two additional frequencies might be faded below level on the secondary antenna when a switch is made for the first. Thus each column of Fig. 16 provides the failure time for each frequency with respect to itself and the remaining two, yielding an outage probability of 3 seconds. The sum of the three columns reveals that the limiting case failure time increase will be nine times that of a conventional FM system having the same I_o.

Linear and Quadratic Distributions

6.13 The distributions for slope and bow (linear and quadratic) distortions occurring across a 19.8-MHz channel width are shown in Fig. 17. The abscissa is the amount of distortion in dB, and the ordinate is the fraction of time (2.6784×10^6 seconds, representing the month of August). The distributions exhibit slopes of a decade of probability of occurrence per 10-dB change in distortion, with the linear distortion $\Delta A \geq 18.5$ dB and the quadratic distortion $\Delta^2 A/2 \geq 7$ dB for 10^{-5} of the time or about 27 seconds. The significance of 10^{-5} rests in its approximation of relevant time fractions for high-quality single-hop propagation considerations.

6.14 The linear and quadratic distortion distributions conditioned on the fade depth of the midchannel tone $A(f_2)$ are shown in Fig. 18 and 19, respectively. Note that the time base for each curve is different and is the total time the middle tone was faded the indicated amount. The bandwidth is again 19.8 MHz—Fig. 17, 18, and 19 all being derived from the 1971 experimental data base. Figures 18 and 19 reveal the increase in distortion values with increasing fade depth.

6.15 The increase in distortion as a variable of bandwidth is indicated in Fig. 20 and 21. Figure 20 provides a summary of the linear distortion distributions, while Fig. 21 summarizes the quadratic distributions. The unusual (crossover) behavior of the quadratic distortion for the 33.5-MHz bandwidth

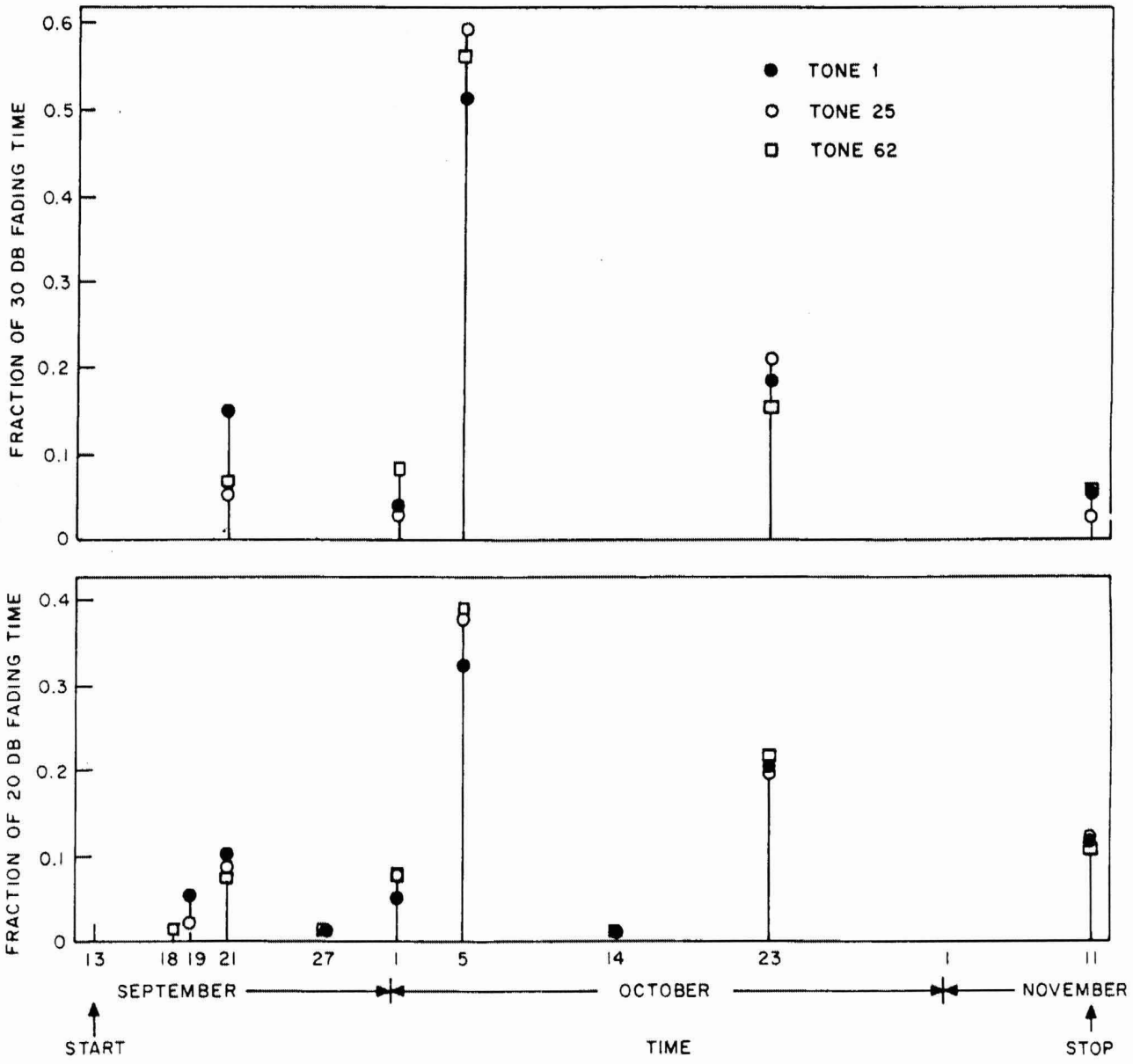

Fig. 14—Daily History of 20- and 30-dB Fading Activity for Tones 1, 25, and 62 During the Entire 1970 Measurement Period

indicates that definition of the selective fading amplitude characteristic by means of three tones becomes inadequate when bandwidths as large as this are spanned. Here again it will be noted that the slopes of the linear and quadratic distortion curves for the larger bandwidths exhibit a decade decrease in probability for 10-dB increase in distortion.

E. Conclusions

6.16 The following conclusions provide a summary of pertinent information discussed in Part 6 of this section or otherwise derived from the experimental data.

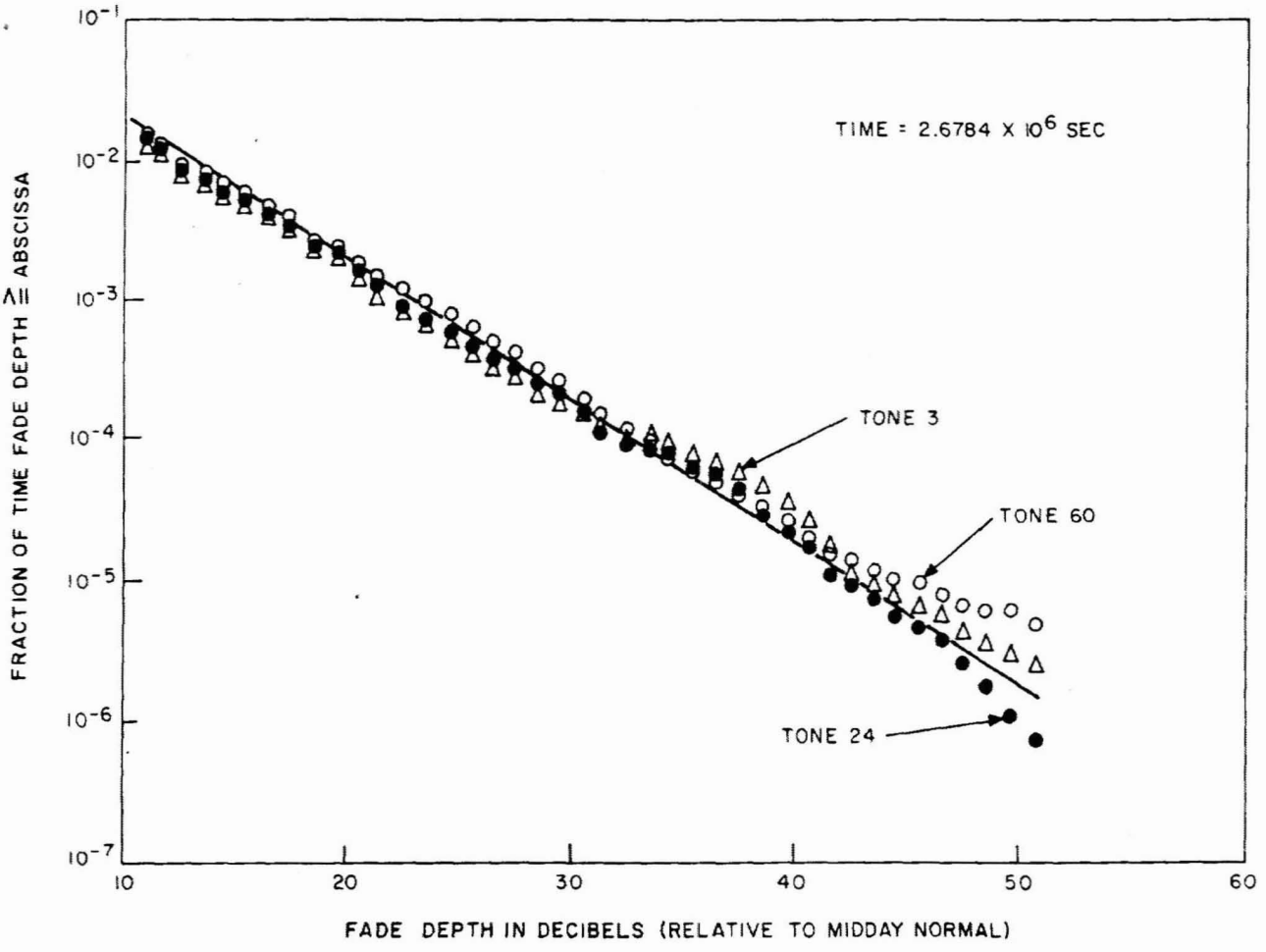

Fig. 15—Fade Depth Distributions for Tones 3, 24, and 60 for the Month of August

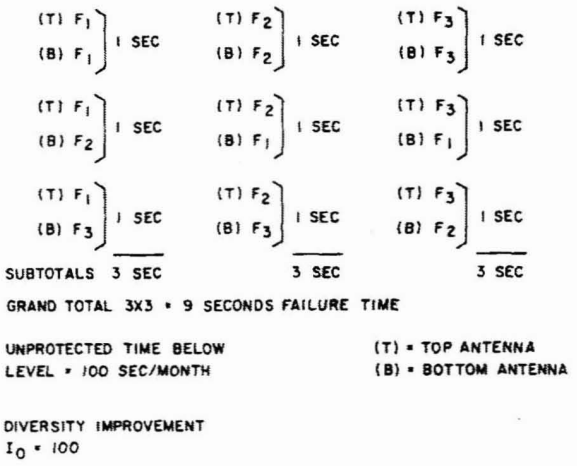

Fig. 16—Increase in Failure Time Resulting From Permutation of Three Independent Frequencies Protected by a Space Diversity System

(a) The practical value of time below level for narrowband channel failure considerations is 2.6 times the value of time below level (T) as calculated in paragraph 4.06 for standard systems. The degree of improvement in failure time offered by a space diversity system was shown to have a worst case value of $I_o/9$ when compared to an FM system.

(b) For fade depths less than 30 dB and bandwidths from 5 to 20 MHz, the distortion frequency selectivity is described (within 2 dB) by linear and quadratic components of amplitude distortion.

(c) For fade depths greater than 30 dB occurring within bandwidths greater than 5 MHz, the amplitude distortion (bow) exceeds second-order components of frequency selectivity.

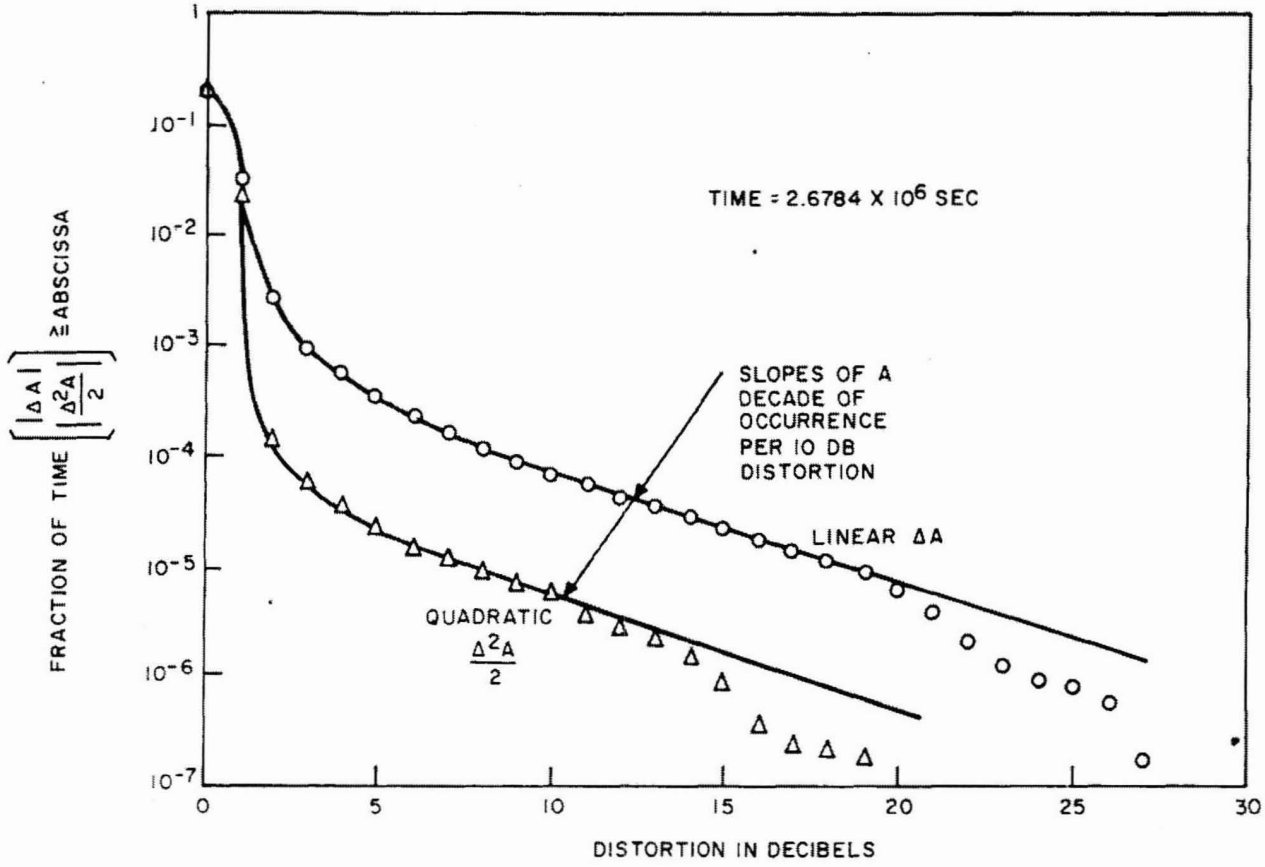

Fig. 17—Unconditional Linear and Quadratic Distortion Distributions for the 19.8-MHz Channel

(d) For bandwidths greater than 5 MHz, the derived statistical distributions of linear and quadratic distortion parameters exhibit slopes of a decade decrease in probability of occurrence per 10-dB increase in distortion.

(e) For a channel bandwidth of 19.8 MHz, the linear and quadratic distortion exceeded 18.5 dB and 7 dB, respectively, for 10^{-5} of the observation time.

(f) The maximum rates of change for the linear and quadratic distortion were 90 and 60 dB per second, respectively.

The information concerning the influence of selective fading on a narrowband channel was derived primarily from experimental descriptions appearing in the *Bell System Technical Journal*. If desired, reference may be made to the following:

> Babler, G. M., "A Study of Frequency Selective Fading for a Microwave Line-of-Sight Narrowband Radio Channel," *Bell System Technical Journal*, March, 1972, pp. 731-757.
>
> Babler, G. M., "Selectively Faded Nondiversity and Space Diversity Narrowband Microwave Radio Channels," *Bell System Technical Journal*, February, 1973, pp. 239-261.

The incipient nature of narrowband technology at the time of writing suggests that increasingly formalized and refined data will become available as experience is gained. Revisions to this section may be anticipated when improved information becomes available.

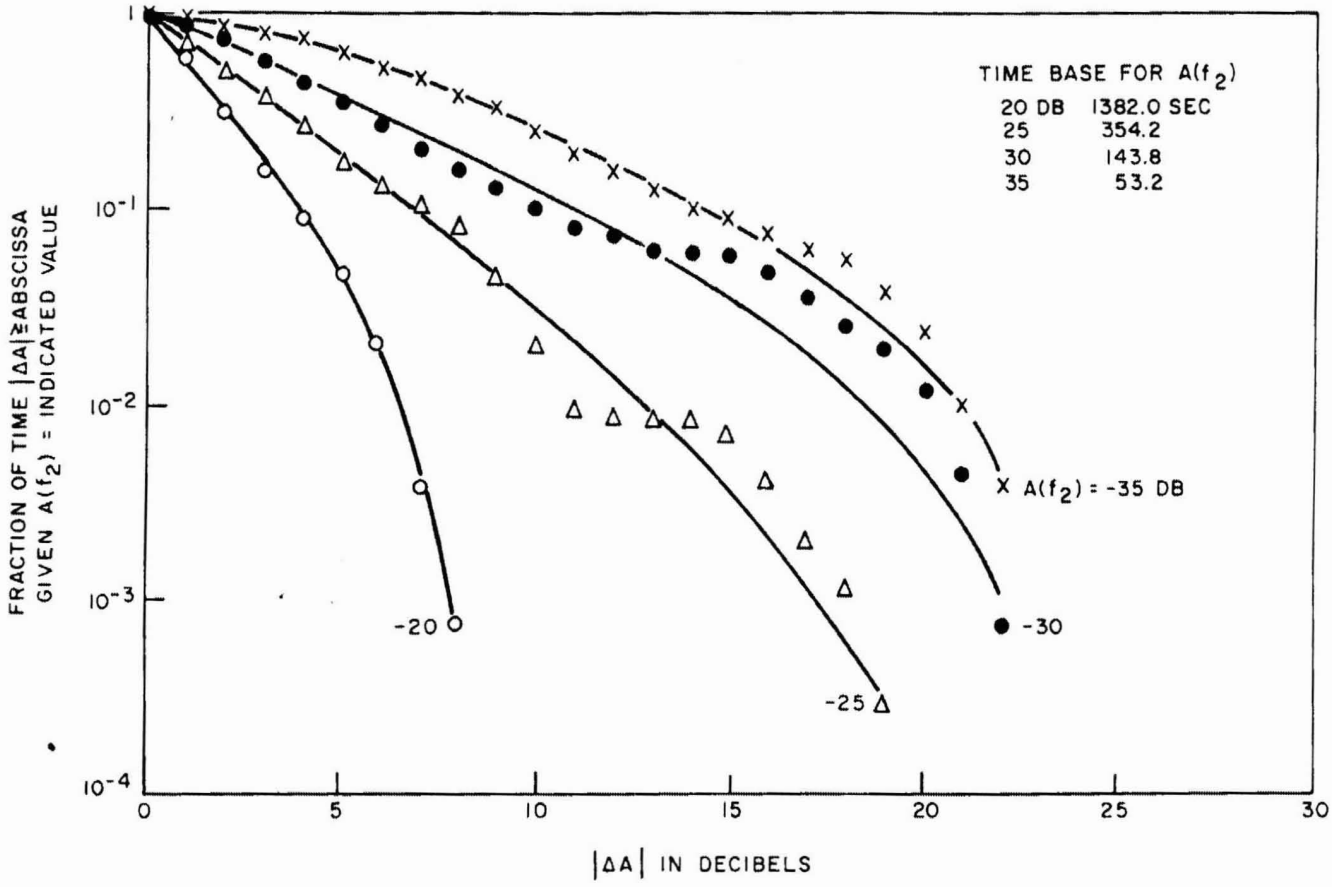

Fig. 18—Conditional Linear Distortion Distributions for the 19.8-MHz Channel

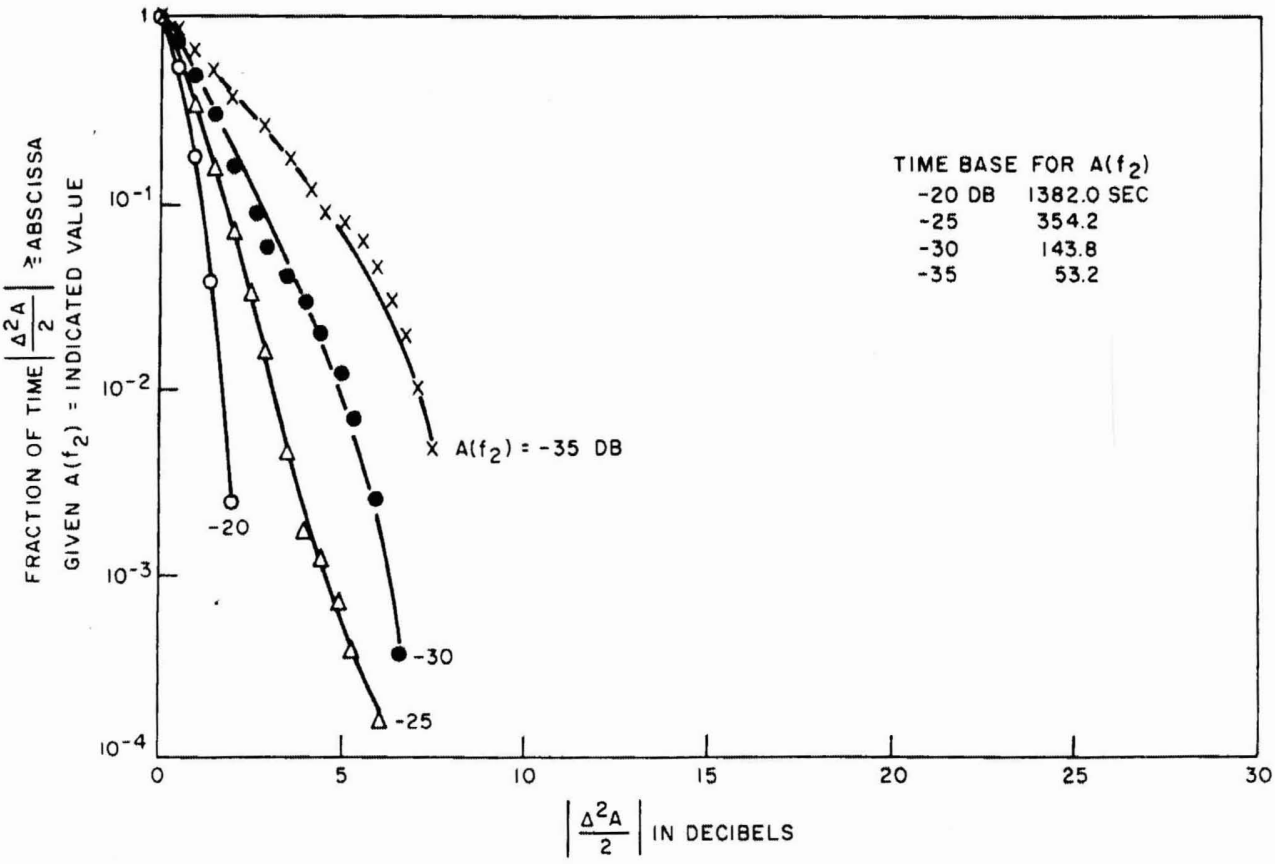

Fig. 19—Conditional Quadratic Distortion Distributions for the 19.8-MHz Channel

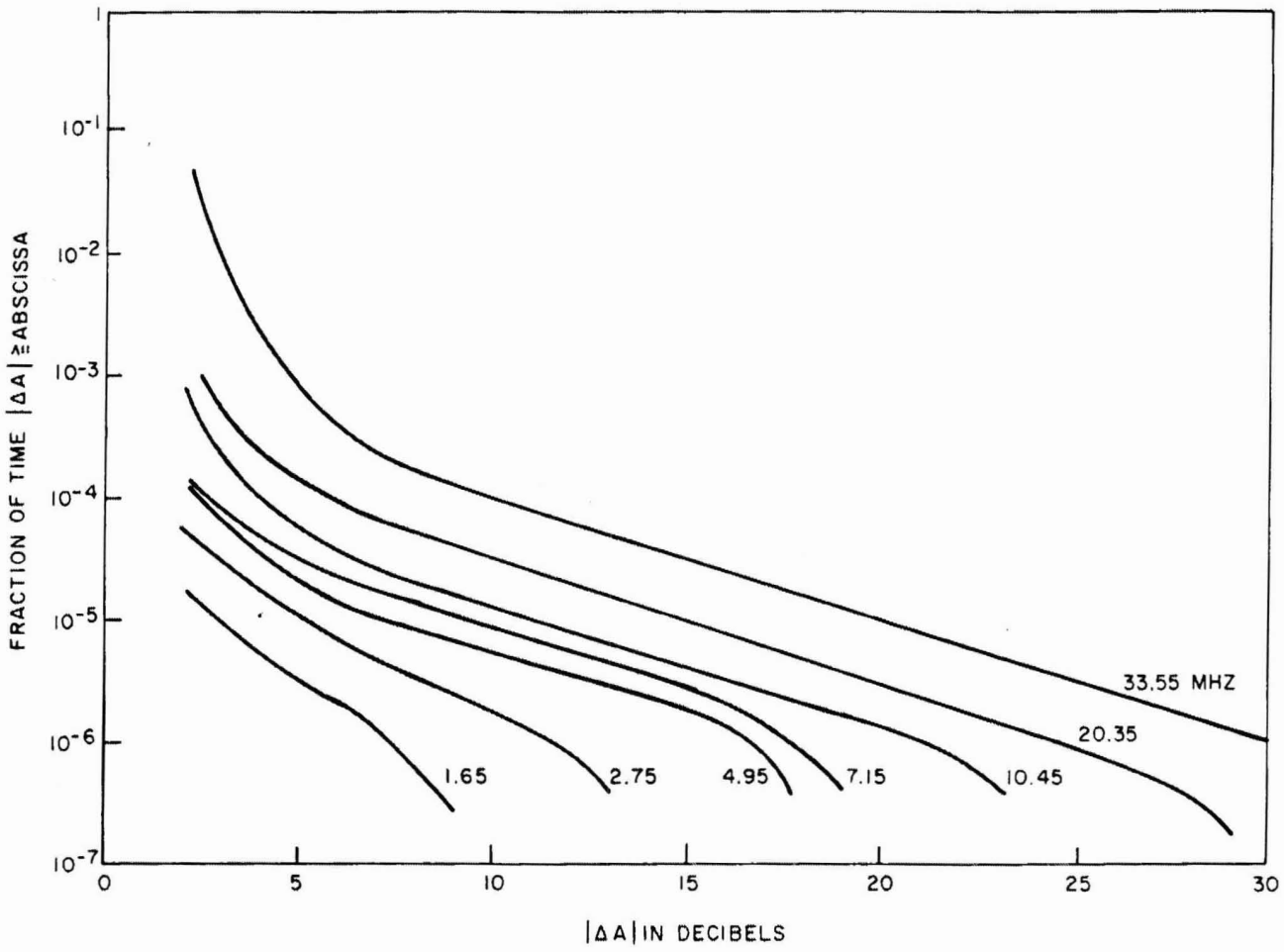

Fig. 20—Summary of Unconditional Linear Distortion Distributions for Different Bandwidths

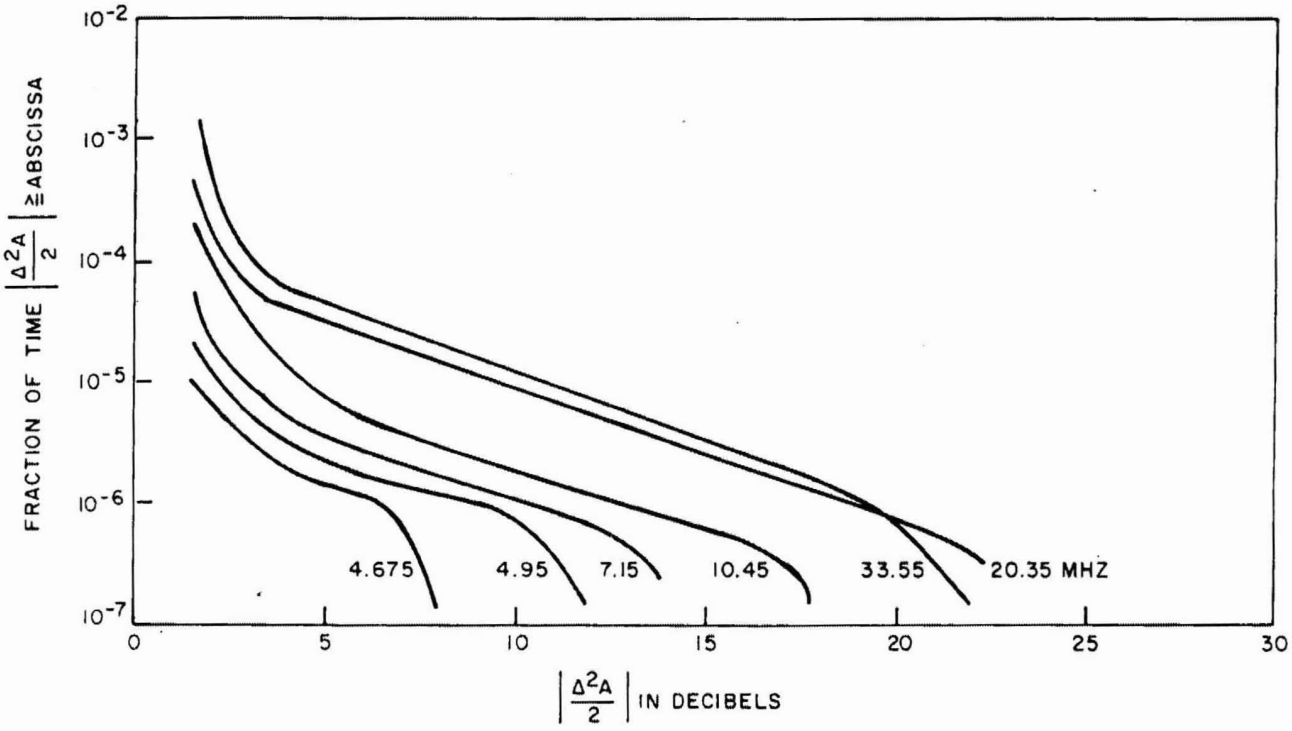

Fig. 21—Summary of Unconditional Quadratic Distortion Distributions for Different Bandwidths

Land Use Data

Q: How do I use the Land Use data in TAP?

A: The TAP Land Use Module is based on the USGS Land Use and Land Cover (LULC) data from 1:250,000 scale maps.

The Land Use data can be used with TAP Area Coverage studies, as well as Path Profiles, Single-Point Field calculations, the Field Preview function and other TAP functions. The Land Use module enables you to find the land classification and apply it to many parts of TAP.

General Concepts

The USGS LULC files categorize land use in 200 square meter cells, with each cell assigned an attribute, such as Urban, Agricultural, Forest, etc. (For a complete listing of the categories and subcategories, see National Mapping Program Data Users Guide 4, *Land Use and Land cover Digital Data from 1:150,000- and 1:100,000-scale Maps*.) When the files are imported into the TAP format, TAP can determine the classification at a given set of coordinates.

In addition, TAP includes a Land Use Loss Database that correlates the land classification with a loss value as a function of frequency. When TAP is used for an area coverage study or single-point field calculation, the environment of the receiver location can be determined from the Land Use data, and a user-specified loss value can be applied. For example, if you want to include an additional loss of 3dB in your frequency band whenever a receiver location is in a forest area, and 6db when in an urban area, the Land Use Loss Database enables you to specify that condition. At the same time, you can specify a loss of 7dB for forest and 12dB for urban in a different frequency band. This approach gives you great flexibility in applying the effects of the land use information to your coverage studies.

The Land Use Loss Database also includes an option to specify an Area Type for the Okumura propagation model for each land use classification and frequency range. This enables the Okumura model to be much more adapted to the actual environment for a study in a given area.

Configuration

The TAP Land Use files are one-degree square areas, and follow a naming convention similar to the SoftWright topographic elevation data files.

For the Land Use files, the convention is

```
LwwwnnNW.LUC
```

Where

- **nn** is the latitude of the SE corner of the degree area
- **N** is either N or S for the latitude direction
- **W** is either W or E for the longitude direction

To specify in TAP where the files are located, use the Land Use selection in the Configuration menu:

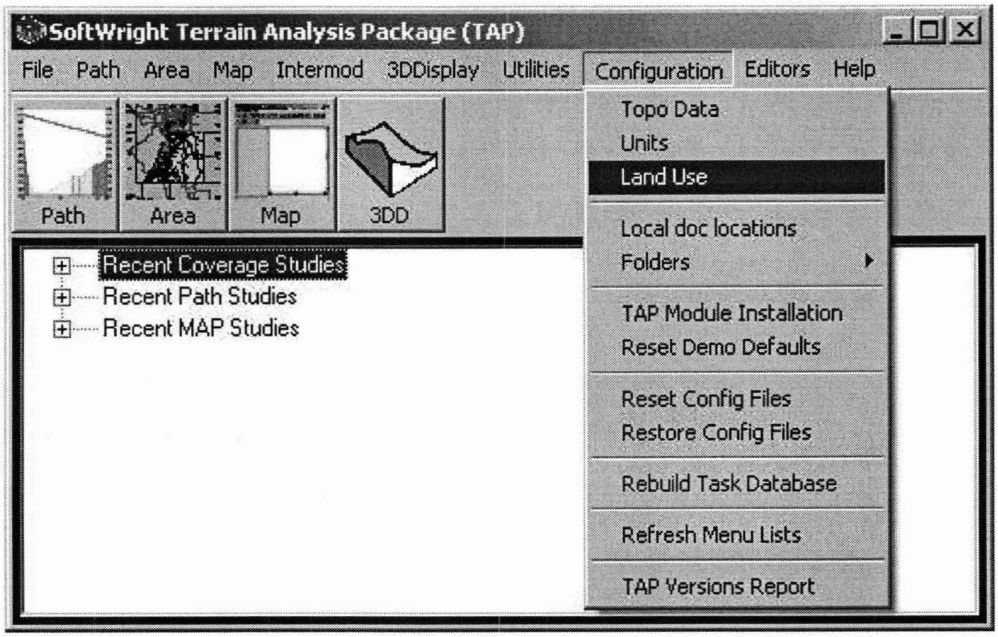

The Land Use Data File Path(s) form will be displayed:

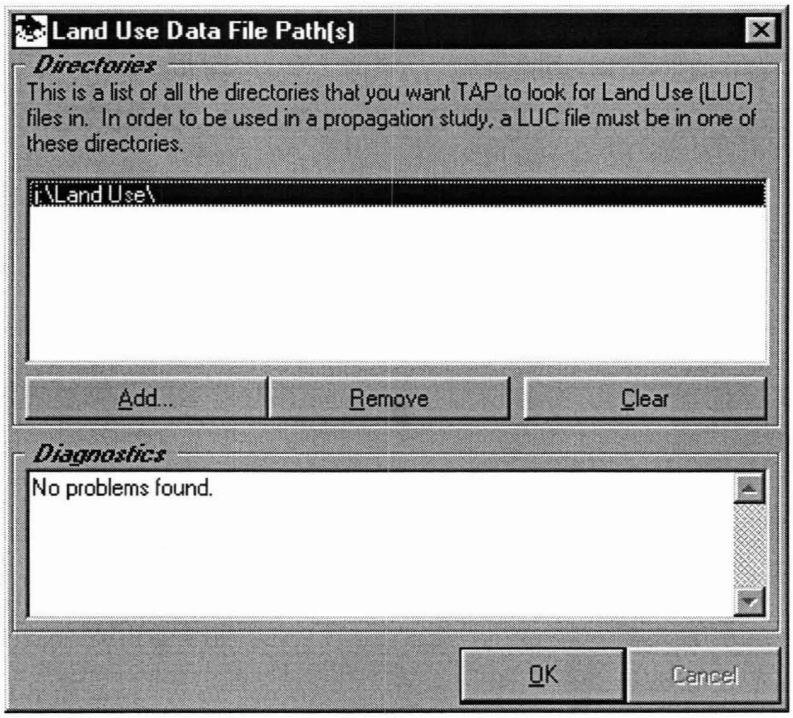

Use the Add and Remove buttons to specify any path(s) where you install the Land Use files. The Diagnostics section reports several potential problems, such as a directory that does not contain any Land Use files, duplicate land use files in multiple directories, etc.

As with the TAP Topographic Data configuration, once this configuration has been

you want TAP to look for the files.

Land Use Loss Database

In order to associate loss values with the various combinations of frequency and land use categories, the Land Use Loss Database can contain numerous configurations, or "templates". Each template contains a set of loss values as a function of frequency and land use, and you can select which template to use for a particular coverage study.

The default templates supplied with the TAP Land Use Module are:

- **FCC R&O 00-11** based on the FCC Report and Order in Docket 00-11, released in May 2000
- **TIA TR8 (May 20, 1977)** based on the Telecommunications Industry Association report of that date
- **TIA TR8 (Revised)** based on a proposed revision of TIA TR8

Note that these are representative samples only. You must verify the applicability of the Land Use Loss values based on frequency and land classifications that are most appropriate to your application.

The Loss Database Editor enables you to modify these templates, or to add your own. The editor is accessible from the Editors menu under Land Use data:

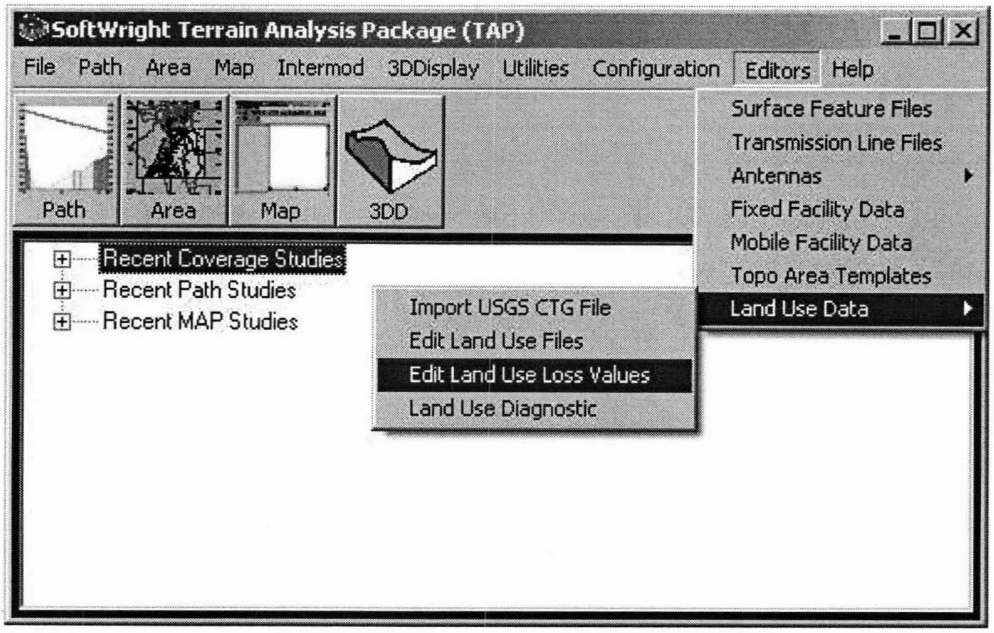

The Loss DB Editor form is displayed:

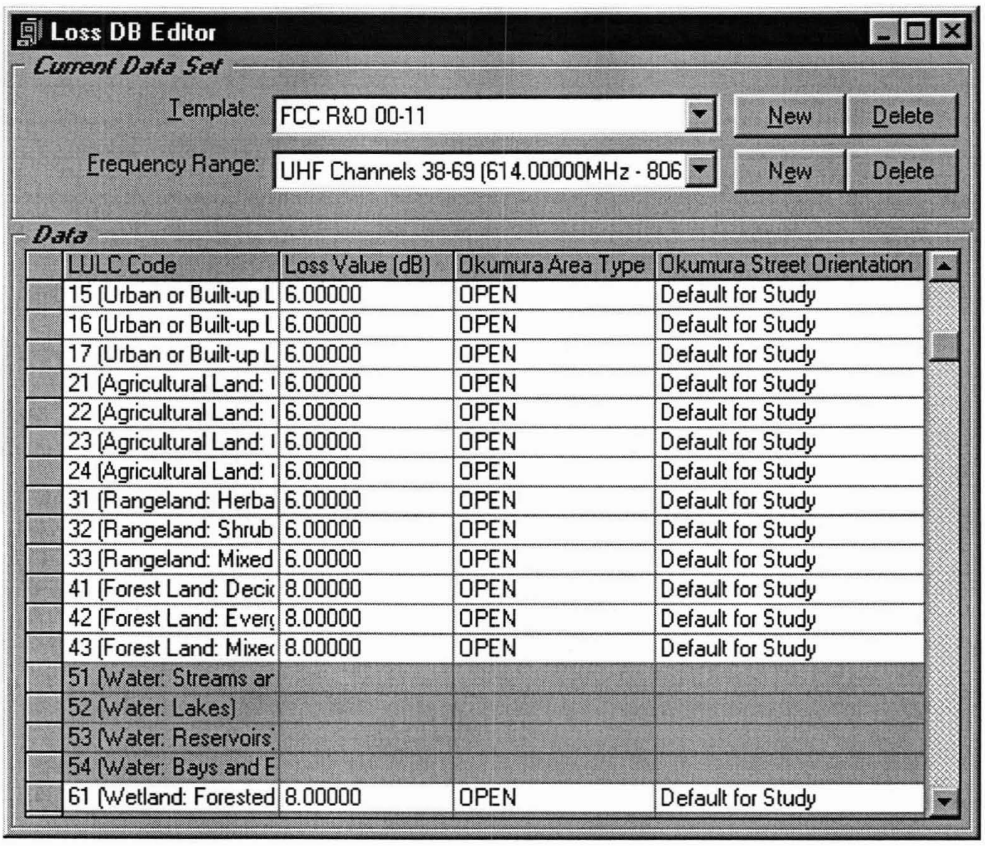

LULC Code	Loss Value (dB)	Okumura Area Type	Okumura Street Orientation
15 (Urban or Built-up L	6.00000	OPEN	Default for Study
16 (Urban or Built-up L	6.00000	OPEN	Default for Study
17 (Urban or Built-up L	6.00000	OPEN	Default for Study
21 (Agricultural Land: I	6.00000	OPEN	Default for Study
22 (Agricultural Land: I	6.00000	OPEN	Default for Study
23 (Agricultural Land: I	6.00000	OPEN	Default for Study
24 (Agricultural Land: I	6.00000	OPEN	Default for Study
31 (Rangeland: Herba	6.00000	OPEN	Default for Study
32 (Rangeland: Shrub	6.00000	OPEN	Default for Study
33 (Rangeland: Mixed	6.00000	OPEN	Default for Study
41 (Forest Land: Decic	8.00000	OPEN	Default for Study
42 (Forest Land: Everg	8.00000	OPEN	Default for Study
43 (Forest Land: Mixec	8.00000	OPEN	Default for Study
51 (Water: Streams ar			
52 (Water: Lakes)			
53 (Water: Reservoirs			
54 (Water: Bays and E			
61 (Wetland: Forested	8.00000	OPEN	Default for Study

You can select the Template, and the Frequency Range in the pulldown lists near the top of the form, or create a new Template or Frequency Range with the New buttons.

In this example, note that some of the categories (51-54) have not been specified. In such cases, those land use classifications will be ignored in a coverage study.

You can also use the Loss Database Editor to specify the Okumura categories to associate with each land use category for each frequency range. The options are available in a pulldown list for the Area Type and Street Orientation columns:

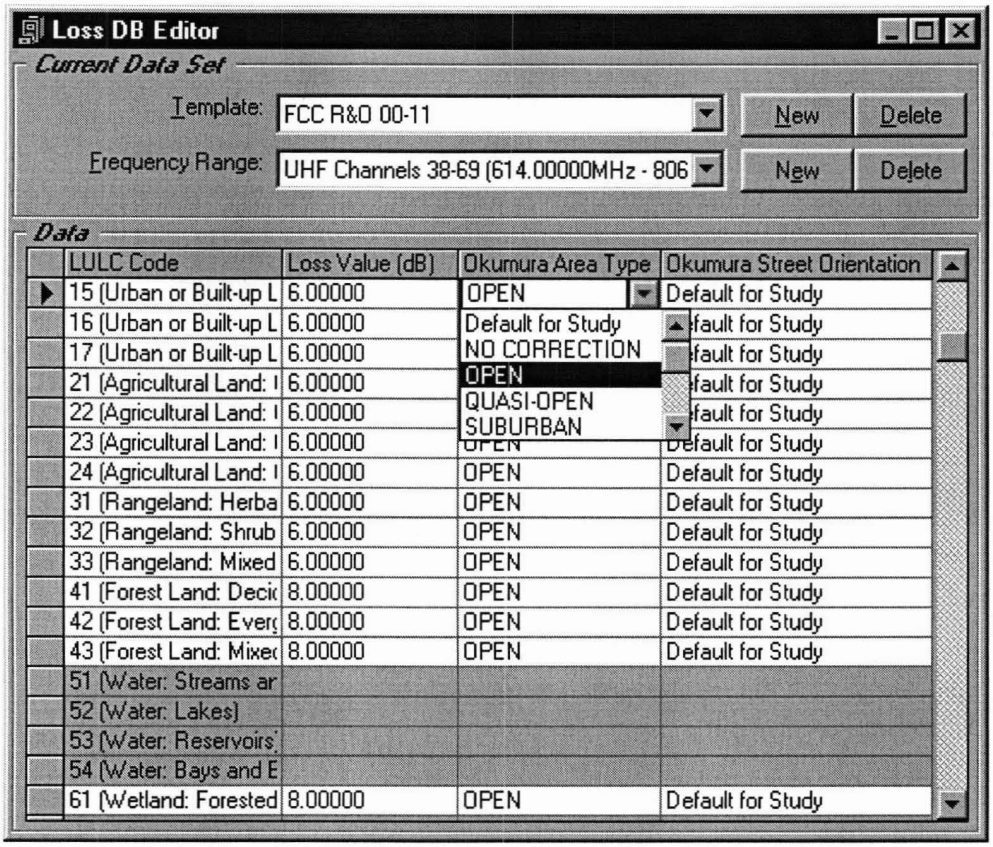

The "Default for Study" option forces the program to use whatever default is set when the Okumura study is set up, ignoring the land use association.

Note that these are representative samples only. You must verify the applicability of the Okumura values based on frequency and land classifications that are most appropriate to your application.

As mentioned above, the Loss Database permits you to set up multiple templates for different conditions. For example, selecting another of the sample templates and finding a similar frequency range shows different loss values will be applied using that template:

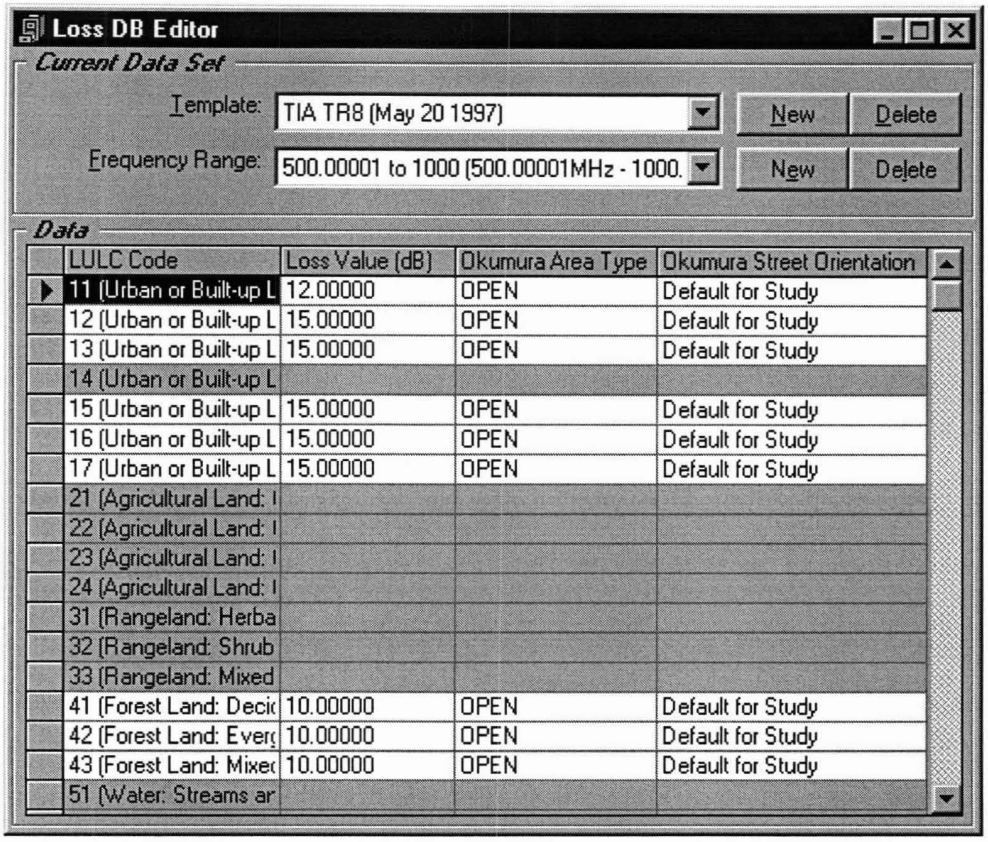

	LULC Code	Loss Value (dB)	Okumura Area Type	Okumura Street Orientation
▶	11 (Urban or Built-up L	12.00000	OPEN	Default for Study
	12 (Urban or Built-up L	15.00000	OPEN	Default for Study
	13 (Urban or Built-up L	15.00000	OPEN	Default for Study
	14 (Urban or Built-up L			
	15 (Urban or Built-up L	15.00000	OPEN	Default for Study
	16 (Urban or Built-up L	15.00000	OPEN	Default for Study
	17 (Urban or Built-up L	15.00000	OPEN	Default for Study
	21 (Agricultural Land: I			
	22 (Agricultural Land: I			
	23 (Agricultural Land: I			
	24 (Agricultural Land: I			
	31 (Rangeland: Herba			
	32 (Rangeland: Shrub			
	33 (Rangeland: Mixed			
	41 (Forest Land: Deci	10.00000	OPEN	Default for Study
	42 (Forest Land: Ever	10.00000	OPEN	Default for Study
	43 (Forest Land: Mixe	10.00000	OPEN	Default for Study
	51 (Water: Streams ar			

Area Coverage Studies

To include Land Use data in an Area Coverage study, you must select the Advanced parameters by checking the "Use Land Use Data" checkbox on the HDCoverage form:

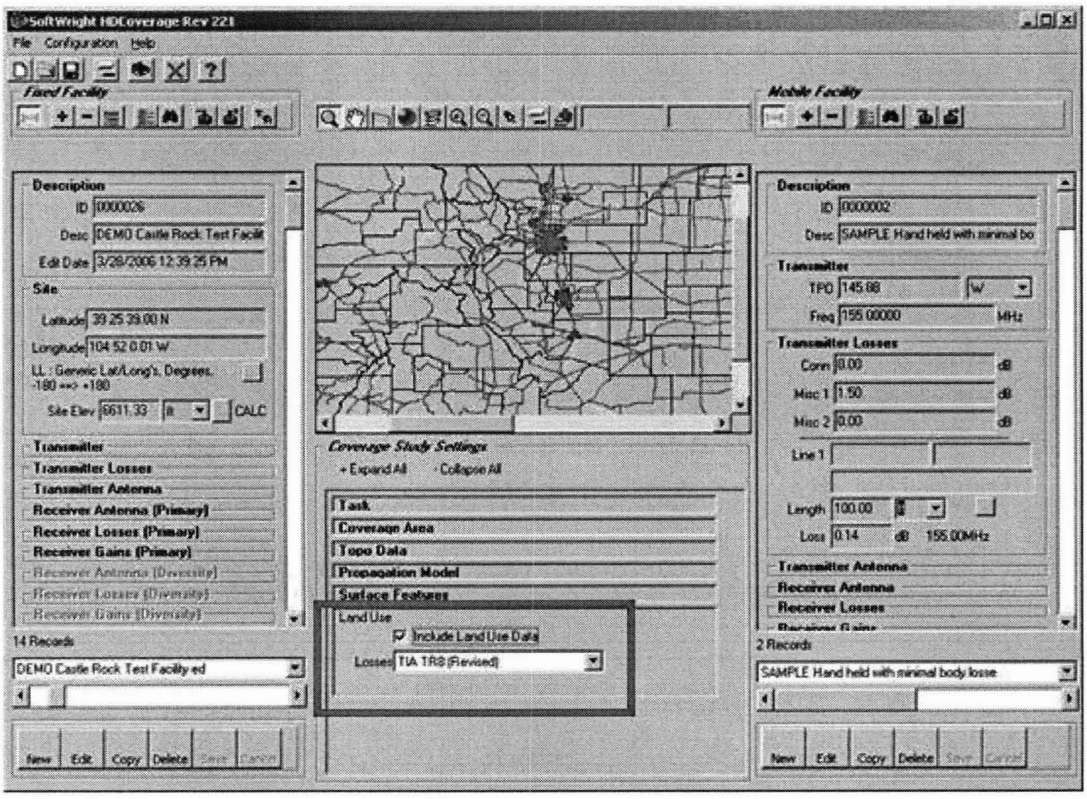

Mark the "Include Land Use Data" checkbox, and select the template to use.

When the area coverage study is executed, the land use values will be included in the

calculation of the field strength at each receiver location if the needed .LUC file for that area is found.

Path Profiles

To use the Land Use data with a path profile, click the Include Land Use Data checkbox:

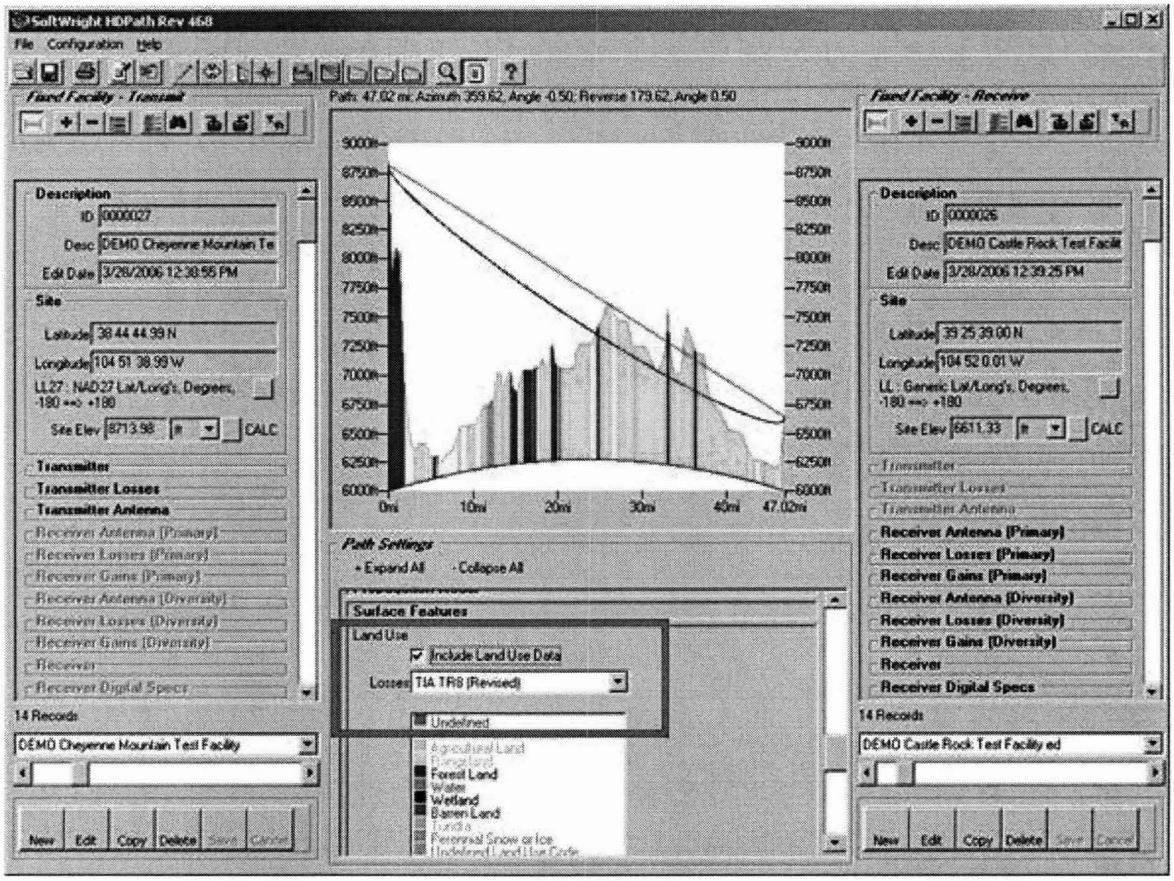

The Land Use legend will be displayed showing the colors used for each land use category. The land use values will be displayed on the profile below the terrain.

The land use category and associated loss value will be displayed in the Mouse Location window as you move the mouse on the profile graphic.

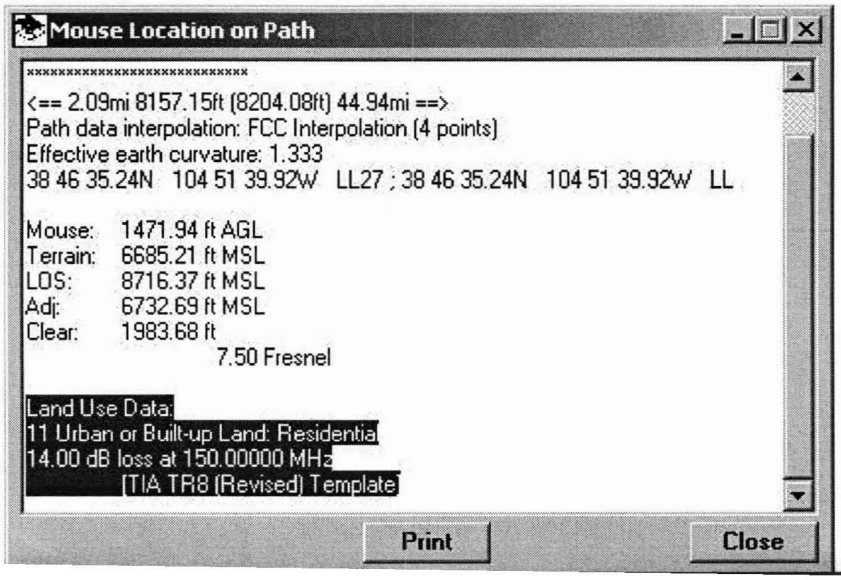

This can be useful in getting a better idea of what the conditions are along the path, such as vegetation and man-made obstructions.

You can also use the USGS Land Use data as a guideline for creating TAP Surface Feature files. The Land use data on the profile can give you an idea of the surface obstacles (vegetation, buildings, etc.) and you can create Surface Feature files to represent those obstructions.

Search SoftWright Website

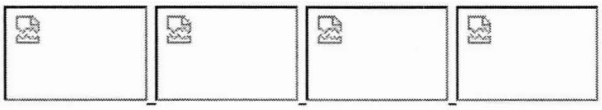

Copyright 2000 by SoftWright LLC

OET BULLETIN No. 69

Longley-Rice Methodology

for

Evaluating TV Coverage and Interference

February 06, 2004

I. INTRODUCTION

This Bulletin provides guidance on the implementation and use of Longley-Rice methodology for evaluating TV service coverage and interference in accordance with Sections 73.622, 73.623 and 74.704 of the FCC rules, 47 C.F.R. §§ 73.622, .623, and 74.704. Bulletin No. 69 explains technical details of the *Sixth Report and Order* in MM Docket No. 87-268, FCC 97-115, adopted April 3, 1997. The Longley-Rice radio propagation model is used to make predictions of radio field strength at specific geographic points based on the elevation profile of terrain between the transmitter and each specific reception point. A computer is needed to make these predictions because of the large number of reception points that must be individually examined. Computer code for the Longley-Rice point-to-point radio propagation model is published in an appendix of NTIA Report 82-100, *A Guide to the Use of the ITS Irregular Terrain Model in the Area Prediction Mode*, authors G.A. Hufford, A.G. Longley and W.A. Kissick, U.S. Department of Commerce, April 1982. Some modifications to the code were described by G.A. Hufford in a memorandum to users of the model dated January 30, 1985. With these modifications, the code is referred to as Version 1.2.2 of the Longley-Rice model. This version is used by the FCC for its evaluations.

The Bulletin is divided into three parts. Part 1 provides information on evaluating TV service area or coverage. Part 2 provides information on evaluating interference to the service areas of both analog NTSC and digital television (DTV) stations. Part 3 provides information on implementation of the FCC's Longley-Rice Computer program.

The present document updates the previous version that was published on July 2,1977. Internet references point to currently available FCC web pages. Certain adjacent-channel D/U ratios have been corrected as indicated in Table 5A. Otherwise, the changes are of an editorial nature, and the program parameters given here are exactly those used by the Media Bureau in processing applications for new or modified stations.

II. PART 1: EVALUATION OF SERVICE

The Area Subject to Calculation

Under the FCC's rules, computation of a TV station's service area or coverage using the Longley-Rice methodology is limited to the areas within certain specific geographic contours.

For analog TV, computations are made inside the conventional Grade B contour defined in Section 73.683 of the FCC rules, 47 C.F.R. § 73.683, with the exception that the defining field for UHF channels is modified by subtracting a dipole factor equal to 20 log[615/(channel mid-frequency in MHz)]. Thus the area subject to calculation for analog TV consists of the geographic points at which the field strength predicted for 50% of locations and 50% of time by FCC curves is at least as great as the values given in Table 1 below. The relevant curves for predicting these fields are the F(50, 50) curves found in Section 73.699 of FCC rules, 47 C.F.R. § 73.699.

Table 1

Field Strengths Defining the Area Subject to Calculation for Analog Stations

Channels	Defining Field Strength, dBu, to be predicted using F(50, 50) curves
2 - 6	47
7 - 13	56
14 - 69	64 - 20 log[615/(channel mid-frequency in MHz)]

For digital television stations, service is evaluated inside contours determined by DTV planning factors in combination with field strength curves derived for 50% of locations and 90% of the time from curves which are also found in Section 73.699 of FCC rules. The family of FCC propagation curves for predicting field strength at 50% of locations 90% of the time is found by the formula F(50, 90) = F(50, 50) - [F(50, 10) - F(50, 50)]. That is, the F(50, 90) value is lower than F(50, 50) by the same amount that F(50, 10) exceeds F(50, 50).

The defining field strengths for DTV service are shown in Table 2. They are determined from the DTV planning factors identified in Table 3. They are used first to determine the area subject to calculation using FCC curves, and subsequently to determine whether service is present at particular points within this area using Longley-Rice terrain-dependent prediction.

Table 2

Field Strengths Defining the Area subject to Calculation for DTV Stations

Channels	Defining Field Strength, dBu, to be predicted for 50% of locations, 90% of time
2 - 6	28
7 - 13	36
14 - 69	41 - 20 log[615/(channel mid-frequency in MHz)]

For digital TV three different situations arise:

1) For DTV stations of the initial allotment plan located at the initial reference coordinates, the area subject to calculation extends in each direction to the distance at which the field strength predicted by FCC curves falls to the value identified in Table 2. The bounding contour is identical, in most cases, to that of the analog station with which the initial allotment is paired. The initial allotment plan and reference coordinates are set forth in Appendix B of the *Sixth Report and Order* in MM

Docket No. 87-268 concerning Digital Television Allotments, adopted April 3, 1997, 12 FCC Rcd 14588 (1997).

2) For new DTV stations, the area subject to calculation extends from the transmitter site to the distance at which the field strength predicted by FCC curves falls to the value identified in Table 2.

3) In the case where a DTV station of the initial allotment has moved, the area subject to calculation is the combination (logical union) of the area determined for the initial allotment and the area inside the contour which would apply in the case of a new DTV station.

Planning Factors

The planning factors shown in Table 3 lead to the values of field strength given above in Table 2 to define the area subject to calculation for DTV stations. These planning factors are assumed to characterize the equipment, including antenna systems, used for home reception. They determine the minimum field strength for DTV reception as a function of frequency band and as a function of channel number in the UHF band.

Table 3

Planning Factors for DTV Reception

Planning Factor	Symbol	Low VHF	High VHF	UHF
Geometric mean frequency (MHz)	F	69	194	615
Dipole factor (dBm-dBu)	K_d	-111.8	-120.8	-130.8
Dipole factor adjustment	K_a	none	none	see text
Thermal noise (dBm)	N_t	-106.2	-106.2	-106.2
Antenna Gain (dBd)	G	4	6	10
Downlead line loss (dB)	L	1	2	4
System noise figure (dB)	N_s	10	10	7
Required Carrier to Noise ratio (dB)	C/N	15	15	15

The adjustment, $K_a = 20 \log[615/(\text{channel mid-frequency in MHz})]$, is added to K_d to account for the fact that field strength requirements are greater for UHF channels above the geometric mean frequency of the UHF band and smaller for UHF channels below that frequency. The geometric mean frequency, 615 MHz, is approximately the mid-frequency of channel 38.

The modified Grade B contour of analog UHF stations is determined by applying this same adjustment factor to the Grade B field strength given in Section 73.683 of the rules. With this

dipole factor modification, the field strength defining the Grade B of UHF channels becomes 64 - 20 log[615/(channel mid-frequency in MHz)] dBu, in place of simply 64. Thus the modified Grade B contour for channel 14 is determined by a median field strength of 61.7 dBu, and the value for channel 51 is 66.3 dBu. This modified Grade B contour bounds the area subject to Longley-Rice calculations for analog stations.

The values appearing in Table 2 follow from the planning factors. They are found from Table 3 by solving the equation: Field + K_d + K_a + G - L - N_t - N_s = C/N.

For a new DTV station with a particular authorized set of facilities, the values given in Table 2 will determine the contour within which the FCC will make all subsequent calculations of service and interference.

Reference Value of ERP for DTV Operation

The initial allotment plan, set forth in Appendix B of the *Sixth Report and Order*, establishes a reference value for the effective radiated power (ERP) of DTV stations. This ERP is the maximum of the values needed to match the service contour of the paired analog station in each direction supposing that the new station operates at the same location with the same antenna height. The reference ERP was calculated using the following methodology:

The distance to the existing analog grade B contour was determined in each of 360 uniformly spaced compass directions starting from true north using linear interpolation of available data as necessary. This determination was made using information in the FCC engineering database of April 3, 1997, including directional antenna data, and from terrain elevation data at points separated by 3 arc-seconds of longitude and latitude. FCC curves (Section 73.699 of FCC rules) were applied in the usual way, as described in Section 73.684 of the rules, 47 C.F.R. § 73.684, to find this grade B contour distance, with the exception that dipole factor considerations were applied to the field strength contour for UHF.

Height above average terrain was determined every 45 degrees from terrain elevation data in combination with the height of the transmitter radiation center above mean sea level, and by linear interpolation for compass directions in between. In cases where the Media Bureau Consolidated Database System (CDBS) indicates that a directional antenna is employed, the ERP in each specific direction was determined through linear interpolation of the relative field values describing the directional pattern. (The directional pattern stored in the CDBS provides relative field values at 10 degree intervals and may include additional values in special directions. The result of linear interpolation of these relative field values is squared and multiplied by the overall maximum ERP listed for the station in the CDBS to find the ERP in a specific direction.)

The corresponding values of ERP for DTV in each direction were then calculated by a further application of FCC curves, with noise-limited DTV coverage defined as the presence of the field strengths identified in Table 2 at 50% of locations and 90% of the time. These ERP values were computed for all 360 azimuths using the same radial-specific height above average terrain as for the analog TV case, but now in conjunction with F(50, 90) curves.

Finally, the ERP for DTV was modified so that it does not exceed 1 megawatt and is not less than 50 kilowatts. This was been done by scaling the azimuthal power pattern rather than by truncation. Thus if replication by FCC curves as described above requires an ERP of 2 megawatts, the power pattern is reduced by a factor of 2 in all directions. The resulting ERP is the reference value cited in Section 73.622 of the rules.

DTV Transmitting Antenna Patterns

In general, these computations of DTV power to match the distance to the grade B contour of an analog station result in ERP values which vary with azimuth. For example, the azimuthal ERP pattern which replicates in UHF the grade B contour of an omnidirectional VHF operation will be somewhat distorted because terrain has a different effect on propagation in the two bands. In addition, the 90% time variability allowance for DTV has an effect on the DTV pattern. Thus the procedure described above effectively derives a new directional antenna pattern wherever necessary for a precise match according to FCC curves.

These DTV azimuthal patterns may be calculated using the procedure outlined above. In addition, these patterns are retained in the CDBS. They are available for downloading at http://www.fcc.gov/mb/databases/cdbs, and searches can be made for particular antennas at http://www.fcc.gov/mb/video. The format for describing DTV transmitting antenna patterns is identical to the historical format for analog stations. Relative field values are given at intervals of 10 degrees, and supplemental values are given at special azimuths. For DTV patterns, special azimuths are included where the pattern factor is unity but both bracketing factors at 10-degree azimuths are less.

Application of the Longley-Rice Methodology

The area subject to calculation is divided into rectangular cells, and the Longley-Rice point-to-point propagation model Version 1.2.2 is applied to a point in each cell to determine whether the predicted field strength is above the value found in Table 1 or Table 2, as appropriate. The values identified in those tables are considered to be thresholds for reception in the absence of interference. For cells with population, the point chosen by the FCC computer program is the population centroid; otherwise it is the geometric center; and the point so determined represents the cell in all subsequent service and interference calculations. The station's directional transmitting antenna pattern, if any, is taken into account in determining the ERP in the direction of each cell. Cells 2 kilometers on a side were used to produce the service and interference data appearing in Appendix B of the *Sixth Report and Order*.

Those desiring to implement the Longley-Rice model in their own computer program to make these calculations should consult NTIA Report 82-100, *A Guide to the Use of the ITS Irregular Terrain Model in the Area Prediction Mode*, authors G.A. Hufford, A.G. Longley and W.A. Kissick, U.S. Department of Commerce, April 1982. The report may be obtained from the U.S. Department of Commerce, National Technical Information Service, Springfield, Virginia, by requesting Accession No. PB 82-217977.

Parameter values set in the Longley-Rice Fortran code as implemented by the FCC are given in Table 4. In addition to these parameters, execution of the code requires a specification of the percent of time and locations at which the predicted fields will be realized or exceeded, and a third percentage identifying the degree of confidence desired in the results. To predict DTV service at cells of the area subject to calculation, the FCC sets the location variability at 50% and the time variability at 90%. The percent confidence is set at 50% indicating that we are interested in median situations. All of these values are the same as the ones used in the computer program developed in the years 1996-1997 by an industry group, the Broadcasters' Caucus, to evaluate various DTV allotment tables.

Table 4

Parameter Values Used in FCC Implementation of the Longley-Rice Fortran Code

Parameter	Value	Meaning/Comment
EPS	15.0	Relative permittivity of ground.
SGM	0.005	Ground conductivity, Siemens per meter.
ZSYS	0.0	Coordinated with setting of EN0. See page 72 of NTIA Report.
EN0	301.0	Surface refractivity in N-units (parts per million).
IPOL	0	Denotes horizontal polarization.
MDVAR	3	Code 3 sets broadcast mode of variability calculations.
KLIM	5	Climate code 5 for continental temperate.
HG(1)	see text	Height of the radiation center above ground.
HG(2)	10 m	Height of TV receiving antenna above ground.

HG(1) in Table 4 is the height of the radiation center above ground. It is determined by subtracting the ground elevation above mean sea level (AMSL) at the transmitter location from the height of the radiation center AMSL. The latter is found in the CDBS while the former is retrieved from the terrain elevation database as a function of the transmitter site coordinates also found in the CDBS. If the coordinates are wrong, the antenna may be seen as under ground. This shouldn't happen, but if it does the FCC computer program replaces the radiation center height AMSL with the ground elevation at the given coordinates plus the height above average terrain found for the station in the CDBS.

Finally, terrain elevation data at uniformly spaced points the between transmitter and receiver must be provided. The FCC computer program is linked to a terrain elevation database with values every 3 arc-seconds of latitude and longitude. The program retrieves elevations from this database at regular intervals with a spacing increment which is chosen at the time the program is compiled; the

computer runs that evaluated service and interference for the *Sixth Report and Order* used a spacing increment of 1 kilometer. The elevation of a point of interest is determined by linear interpolation of the values retrieved for the corners of the coordinate rectangle in which the point of interest lies.

Evaluations of service coverage and interference using finer spacing increments are expected to be consistent with those using 1 kilometer. Evaluations using cells smaller than 2 km on a side are also expected to be consistent with the evaluations given in Appendix B of *Sixth Report and Order.*

III. PART 2: EVALUATION OF INTERFERENCE

The presence or absence of interference in each grid cell of the area subject to calculation is determined by further application of Longley-Rice. Radio paths between undesired TV transmitters and the point representing each cell are examined. The undesired transmitters included in the analysis of each cell are those which are possible sources of interference at that cell, considering their distance from the cell and channel offset relationships. For each such radio path, the Longley-Rice procedure is applied for median situations (that is, confidence 50%), and for 50% of locations, 10% of the time.

The interference analysis examines only those cells that have already been determined to have a desired field above the threshold for reception given in Table 1 for analog stations and Table 2 for DTV stations. A cell being examined is counted as having interference if the ratio of the desired field to that of any one of the possible interference sources is less than a certain critical minimum value. The comparison is made after applying the discrimination effect of the receiving antenna. The critical value is a function of the channel offset relationship.

Cells of the area subject to calculation for an analog station are examined first as to whether the desired signal is above the threshold for reception, second with regard to whether there is interference from another analog station, and finally as to whether there is interference from DTV stations. Thus a DTV station does not cause interference to analog stations in places where there is no service because of a weak desired signal, or in places where interference from other analogue stations already exists.

D/U Ratios

Criteria for the ratio of desired to undesired field strength are specified in Section 73.623 of FCC rules for interference involving DTV stations as desired or undesired. These criteria are summarized in Tables 5A, 5B, and 5C.

Tables 5A, 5B, and 5C also include the criteria for interference between analog stations used in preparing the service and interference evaluation in Appendix B of the *Sixth Report and Order.* The FCC continues to apply an analog-into-analog interference analysis using these criteria for consistency with the *Sixth Report and Order.* DTV stations are therefore allowed to modify their facilities without consideration of possible interference to analog stations where interference from other analog stations already exists.

Table 5A

Interference Criteria for Co- and Adjacent Channels[1]

Channel Offset	D/U Ratio, dB			
	Analog into Analog	DTV into Analog	Analog into DTV	DTV into DTV
-1 (lower adjacent)	-3	-14	-48	-28
0 (co-channel)	+28	+34	+2	+15
+1 (upper adjacent)	-13	-17	-49	-26

The evaluation of service and interference in Appendix B of the *Sixth Report and Order* considered taboo channel relationships for interference into DTV. However, the D/U ratios (approximately -60 dB) were such that they rarely if ever had an effect on the results, and the FCC rules adopted in the *Sixth Report and Order* do not require attention to UHF taboo interference to DTV stations.

The D/U ratios for co-channel interference to DTV service in Table 5A are only valid at locations where the signal-to-noise ratio is 28 dB or greater for interference from DTV and 25 dB or greater for interference from analog TV service. At the edge of the noise-limited service area, where the signal-to-noise (S/N) ratio is 16 dB, the co-channel D/U ratios are 21 dB and 23 dB for interference from analog TV and DTV, respectively. At locations where the S/N ratio is greater than 16 dB but less than 28 dB, D/U values for co-channel interference to DTV are as follows:

To protect DTV reception from DTV co-channel interference, minimum D/U ratios are computed from the following formula:

$$D/U = 15 + 10\log_{10}[1.0/(1.0-10^{-x/10})], \qquad \text{where } x = S/N - 15.19 \text{ dB}.$$

The quantity x is the amount by which the actual desired S/N exceeds the minimum required for DTV reception.

To protect DTV reception from analog co-channel interference, minimum D/U ratios are found from Table 5B. Use linear interpolation for S/N values between those given in the table.

[1] The adjacent-channel D/U ratios given in this table for interference from DTV transmissions are corrections of those published with the July 1997 version of this bulletin. The values given here agree with those used in the *Sixth Report and Order* and with the computer program now used by the Media Bureau to evaluate applications for new and modified stations as well as predecessors of that program.

Table 5B

Minimum Co-channel D/U Ratios for Analog Interference to DTV

DTV Signal-to-Noise Ratio (S/N) in the Absence of Interference, dB	Desired-to-Undesired Ratio to Protect DTV reception from Co-channel Analog Transmissions, dB
16.00	21.00
16.35	19.94
17.35	17.69
18.35	16.44
19.35	7.19
20.35	4.69
21.35	3.69
22.35	2.94
23.35	2.44
25.00	2.00

Receiving Antenna Pattern

The receiving antenna is assumed to have a directional gain pattern which tends to discriminate against off-axis undesired stations. This pattern is a planning factor affecting interference. The specific form of this pattern was chosen by a working group of the FCC Advisory Committee for Advanced Television Service. It is built into the service and interference computer program developed by the Broadcasters' Caucus and also used in the FCC program.

The discrimination, in relative volts, provided by the assumed receiving pattern is a fourth-power cosine function of the angle between the lines joining the desired and undesired stations to the reception point. One of these lines goes directly to the desired station, the other goes to the undesired station. The discrimination is calculated as the fourth power of the cosine of the angle between these lines but never more than represented by the front-to-back ratios identified in Table 6. When both desired and undesired stations are dead ahead, the angle is 0.0 giving a cosine of unity so that there is no discrimination. When the undesired station is somewhat off-axis, the cosine will be less than unity bringing discrimination into play; and when the undesired station is far off axis, the maximum discrimination given by the front-to-back ratio is attained.

Table 5C

Interference Criteria for UHF Taboo Channels

(NC means Not Considered)

Channel Offset Relative to Desired Channel N	D/U Ratio, dB			
	Analog into Analog	DTV into Analog	Analog into DTV	DTV into DTV
N - 8	-32	-32	NC	NC
N - 7	-30	-35	NC	NC
N - 4	NC	-34	NC	NC
N - 3	-33	-30	NC	NC
N - 2	-26	-24	NC	NC
N + 2	-29	-28	NC	NC
N + 3	-34	-34	NC	NC
N + 4	-23	-25	NC	NC
N + 7	-33	-43	NC	NC
N + 8	-41	-43	NC	NC
N + 14	-25	-33	NC	NC
N + 15	-9	-31	NC	NC

Table 6

Front-to-Back Ratios Assumed for Receiving Antennas

TV Service	Front-to-Back Ratios, dB		
	Low VHF	High VHF	UHF
Analog	6	6	6
DTV	10	12	14

IV. PART 3: THE FCC LONGLEY-RICE COMPUTER PROGRAM

The FCC computer program is available as Fortran code. It is complex, and many of its options are available only by recompilation for each case of interest. The individual installing it should have computer programming skills and experience as a system administrator of the computer system on which it is to be installed because linking the data files, which occupy 1.6 gigabytes of disk space, will be a site-specific task. The FCC compiles and runs the program on Sun Microsystem Enterprise 3500 and UltraSPARC computers. The Fortran code currently used by the Media

Bureau to evaluate new proposals is available for downloading from the FCC internet site at http://www.fcc.gov/oet/dtv, and the code used to produce the information presented in Appendix B of the *Sixth Report and Order* is also available there.

Outline of Evaluation Procedure

The examination of each station proceeds as follows:

1) The area subject to calculation is boxed in latitude and longitude. This is performed by proceeding around the compass and finding the latitude and longitude of points at 5 degree azimuth increments on the bounding contour. The maxima and minima of the resulting list of latitudes and longitudes determine a coordinate box.

2) The coordinate box is divided into square cells of a chosen size which should be 2 km on a side or smaller, adjusting the coordinate box to be slightly larger if necessary to accommodate an integer number of cells. The cells must be an integer number of latitude seconds high and an integer number of longitude seconds wide.

3) The coordinates of census blocks falling inside each cell are retrieved along with the population of each block. From this information the total population and the coordinates of the cell centroid are determined for each cell.

4) The Longley-Rice propagation model is then applied as in Part 1, Evaluation of Service, and Part 2, Evaluation of Interference. The output information is organized as shown in Figure 1.

Longley-Rice Parameters

See Table 4 and accompanying text.

Identification of Potentially Interfering Stations

Stations that may be a source of interference are identified as a function of distance and channel relationships. This is performed independently for each cell. Only those stations whose distance from the cell of interest is less than the value given in Table 7 are considered as potential sources of interference.

Figure 1

Form of FCC Longley-Rice Program Output

```
   Analysis of Analog Station IL SOME CITY, Channel 9
                                  POPULATION    AREA (sq km)
within Noise Limited Contour         610288        14667.4
not affected by terrain losses       604312        14165.4
lost to NTSC IX                           0            0.0
lost to additional IX by DTV              0            4.0
lost to all IX                            0            4.0

    Analysis of DTV Station IL SOME CITY, Channel 32
                                  POPULATION    AREA (sq km)
within Noise Limited Contour         610288        14667.4
not affected by terrain losses       606241        14378.2
lost to NTSC IX                        1347           84.3
lost to additional IX by DTV            425           44.2
lost to DTV IX only                     425           44.2
lost to all IX                         1772          128.5
```

Table 7

Culling of Undesired Stations

(NC means Not Considered; it is presumed that stations at the indicated offset do not cause interference even though they may be close in distance to the cell of interest.)

Offset Relative to Desired Channel N	Undesired Channel	Maximum Distance from Cell to Undesired Stations, km			
		Analog Into Analog	Digital into Analog	Analog into Digital	Digital into Digital
-8	N - 8	35.0	35.0	NC	NC
-7	N - 7	100.0	35.0	NC	NC
-4	N - 4	NC	35.0	NC	NC
-3	N - 3	35.0	35.0	NC	NC
-2	N - 2	35.0	35.0	NC	NC
-1	N - 1	100.0	100.0	100.0	100.0
0	N	300.0	300.0	300.0	300.0
+1	N + 1	100.0	100.0	100.0	100.0
+2	N + 2	35.0	35.0	NC	NC
+3	N + 3	35.0	35.0	NC	NC
+4	N + 4	35.0	35.0	NC	NC
+7	N + 7	100.0	35.0	NC	NC
+8	N + 8	35.0	35.0	NC	NC
+14	N + 14	100.0	35.0	NC	NC
+15	N + 15	125.0	35.0	NC	NC

Transmitting Antenna Patterns

The vertical patterns used in the FCC computer program are shown in Table 8. They represent typical patterns. These patterns were used in computing the evaluation of service and interference in Appendix B of the *Sixth Report and Order* and continue to be used in the Media Bureau computer program for evaluating applications for new and modified stations.

Table 8

Vertical Pattern Assumed for Transmitting Antennas

ANGLE, Degrees	Gain in Vertical Plane (expressed as relative field strength)				
	Low VHF Analog and DTV	High VHF		UHF	
		Analog	DTV	Analog	DTV
0.75	1.000	1.000	1.000	1.000	1.000
1.50	1.000	0.950	0.970	0.740	0.880
2.00	0.990	0.860	0.940	0.520	0.690
2.50	0.980	0.730	0.890	0.330	0.460
3.00	0.970	0.600	0.820	0.220	0.260
3.50	0.950	0.470	0.730	0.170	0.235
4.00	0.930	0.370	0.650	0.150	0.210
5.00	0.880	0.370	0.470	0.130	0.200
6.00	0.820	0.370	0.330	0.110	0.150
7.00	0.740	0.370	0.280	0.110	0.150
8.00	0.637	0.310	0.280	0.110	0.150
9.00	0.570	0.220	0.280	0.110	0.150
10.00	0.480	0.170	0.250	0.110	0.150

Notes on Longley-Rice Propagation

Notes on The Prediction of Tropospheric Radio Transmission Loss Over Irregular Terrain (the Longley-Rice Model)

Overview

This document describes the assumptions and methods used in SoftWright's implementation of the "Longley-Rice" point-to-point model for radio propagation in the Terrain Analysis Package (TAP).

The Longley-Rice model predicts long-term median transmission loss over irregular terrain relative to free-space transmission loss. The model was designed for frequencies between 20 MHz and 40 GHz and for path lengths between 1 km and 2000 km.

Note that SoftWright has implemented the "point-to-point" mode rather than the "area" mode because required path-specific parameters can be determined from detailed terrain path profiles available in TAP. The point-to-point mode implemented by SoftWright uses detailed terrain profiles to determine the distances to radio horizons, the horizon elevation angles and effective antenna heights needed by the model. As with other SoftWright propagation models, coverage studies of large areas are accomplished using a large number of individual path studies to multiple points along multiple radials from the central transmitting site.

This implementation is based on Version 1.2.2 of the model, dated September 1984. A later series (beginning with Version 2.0, dated May 1970) uses "considerably modified diffraction calculations" and is "not now recommended and is no longer maintained by its developers." ("A Guide to the Use of the ITS Irregular Terrain Model in the Area Prediction Mode", NTIA Report 82-100, page 17). Note also that the version 1.2.2 implemented by SoftWright does not utilize several other corrections to the model proposed since the method was first published (see A. G. Longley, "Radio propagation in urban areas," OT Rep. 78-144, Apr. 1978; and A. G. Longley, "Local variability of transmission loss- land mobile and broadcast systems," OT Rep., May 1976).

Technical Foundation

TAP users should consult the following technical publications for a detailed discussion of the theoretical and empirical bases of the model:

"Tech Note 101": P. L. Rice, A. G. Longley, K. A. Norton, and A. P. Barsis, "Transmission loss predictions for tropospheric communication circuits," U.S. Government Printing Office, Washington, DC, NBS Tech. Note 101, issued May 1965; revised May 1966 and Jan. 1967.

"Longley-Rice": A. G. Longley and P. L. Rice, "Prediction of Tropospheric radio transmission over irregular terrain, A Computer method-1968." ESSA Tech. Rep. ERL 79-ITS 67, U.S. Government Printing Office, Washington, DC, July 1968.

ITS irregular terrain model in the area prediction mode," NTIA Rep. 82-100, Apr. 1982.

"ITS Report": "Telecommunications Analysis Services Reference Guide", Institute for Telecommunications Services, Spectrum Division, Dec 7, 1983.

A brief but helpful overview of the model, as well as a comparison to other models, is found in IEEE publication "Coverage Prediction for Mobile Radio Systems Operating in the 800/900 MHz Frequency Range," IEEE Trans. Vehicular. Technology, vol. VT-37, p. 21, 27-35, 1988.

Implementation

The SoftWright implementation of the Longley-Rice model preserves the methods and calculations of the original Version 1.2.2 source code, and, as much as possible, integrates the model into the existing Terrain Analysis Package (TAP) software system. However, as described, below, certain constraints imposed by the Longley-Rice model require slight modifications in the use of the TAP system. These modifications are thoroughly discussed below.

General Parameters

Like the other models available in the TAP system (e.g., Carey, Bullington, Okumura) the Longley-Rice model requires the input of certain general parameters to set up the program for propagation calculations:

- Frequency The nominal frequency range for the Longley-Rice model is listed as 20 MHz to 40 GHz in the original paper. The upper limit is modified to 20 GHz in some later documentation.
- ERP Effective Radiated Power is entered in the units set by the user in the System Configuration Screen (mW, W, kW, dBm, dBW, dBk).
- Antenna Omni-directional transmitter operation is assumed unless a directional antenna is specified.
- Heights Antenna heights above ground for transmit and receive facilities are entered in the user-specified units (feet or meters). The program will compute the effective heights needed for Longley-Rice calculations.

Longley-Rice Parameters

The nature of the Longley-Rice model requires certain additional parameters:

Polarization: Either horizontal or vertical polarization must be specified. The Longley-Rice model assumes that both antennas have the same polarization, either vertical or horizontal.

Refractivity: The refractivity of the atmosphere determines the amount of "bending" of the radio waves. In other TAP models, the effect of refractivity is

entered as effective earth curvature, typically "4/3 earth" (1.333). In the Longley-Rice model, there are three ways of specifying refractivity:

You can enter the "Surface Refractivity" value directly, typically in the range of 250 to 400 N-units (corresponding to earth curvature values from 1.232 to 1.767). An effective earth curvature of 4/3 (=1.333) corresponds to a surface refractivity value of approximately 301 N-units. Longley and Rice recommend an Ns equal to 301 N-units for average atmospheric conditions.

You can enter the effective earth curvature value K (such as 1.333 for 4/3 earth) and the surface refractivity Ns will be computed from:

$$N_s = 179.3 \cdot Ln\left[\frac{1}{0.046665}\left(1 - \frac{1}{K}\right)\right]$$

You can enter the refractivity referenced to sea level No and the surface refractivity Ns will be computed based on the elevation of the path. Values of No can be read from maps, such as Figure 1 on page 5 of the 1968 Longley-Rice paper.

Permittivity: The relative permittivity (ε) or dielectric constant of the ground. Typical values are shown below.

Conductivity The soil conductivity (in Siemens per meter) of the ground. Typical values are shown below.

	Relative Permittivity	Conductivity (Siemens per meter)
Average ground	15	0.005
Poor ground	4	0.001
Good ground	25	0.020
Fresh water	81	0.010
Sea water	81	5.000

Climate Seven climate codes are categorized in the Longley-Rice model as

shown:

1	Equatorial (Congo)
2	Continental Subtropical (Sudan)
3	Maritime Subtropical (West coast of Africa)
4	Desert (Sahara)
5	Continental Temperate
6	Maritime Temperate, over land (United Kingdom and continental west coasts)
7	Maritime Temperate, over sea

According to Longley & Rice, "The Continental Temperate climate is common to large land masses in the temperate zone. It is characterized by extremes of temperature and pronounced diurnal and seasonal changes in propagation. In mid-latitude coastal areas where prevailing winds carry moist maritime air inland, a Maritime Temperate climate prevails. This situation is typical of the United Kingdom and of the west coasts of the United States and Europe. For paths that are less than 100 km long, there is little difference between the Continental and Maritime Temperate climates, but for longer paths the greater occurrence of super refraction and ducting in maritime areas may result in much higher fields for periods of 10 percent or less of the year." (see NTIA Report)

Variability: Longley-Rice defines four modes of variability. The mode selected determines the meaning of the reliability and confidence values used in the model. The mode of variability can be considered the "point of view" for considering the meaning of "reliability" and "confidence" in the calculations.

The modes of variability defined by Longley-Rice are: Single message mode, Individual mode, Mobile mode, and Broadcast mode. These modes are defined in more detail in NTIA, p. 37.

In earlier versions of the SoftWright implementation (up to and including TAP 4.0) all calculations use the point-to-point mode of Longley-Rice to compute the field at individual locations (multiple points along multiple radials from a transmitter site). Therefore, the mode of variability was fixed as "Individual" mode (called "Accidental" mode in some of the literature). Furthermore, since we are exactly defining the receive location for each calculation, the program did not consider location variability. Beginning with TAP 4.1, both the mode of

variability and the option for location variability can be selected by the user. The default values for these parameters are "Individual" and "Ignore Location Variability" for compatibility with the earlier versions of TAP.

The types of variability described in Longley-Rice are time, location, and situation variability. These three "dimensions of variability" were developed to account for and categorize variations in measured median signal levels (see NTIA Report, pp. 28-31): (Note that short term variability of the type associated with multipath propagation is not covered by the model.)

Time variability accounts for variations of hourly median values of attenuation due to, for example, slow changes in atmospheric refraction or in the intensity of atmospheric turbulence. The computed field strength value is an hourly median value; the actual field strength at the receiver location would be expected to be above that value during half of each hour and below that value for half of each hour. Time variability describes the effects of these changes over time. The time variability for the calculation is expressed as a percentage from 0.1% to 99.9%. This value gives the fraction of time during which actual received field strength is expected to be equal to or higher than the hourly median field computed by the program. This variable allows you to specify how you want to deal with the time variability of changing atmospheric (and other) effects as described above. Entering higher percentage reliability values effectively reduces the variability resulting from these factors. The resulting field strength predicted by the program will be lower, but with increased reliability that the actual field that could be measured would equal or exceed the computed value at any given time.

Location variability accounts for variations in long-term statistics that occur from path to path due to, for example, differences in the terrain profiles or environmental differences between the paths. The location variability for the calculation is expressed as a percentage from 0.1% to 99.9%. This value gives the fraction of locations where actual received field strength is expected to be equal to or higher than the median field computed by the program. This variable allows you to specify how you want to deal with the location variability. Entering higher percentage reliability values effectively reduces the variability resulting from these factors. The resulting field strength predicted by the program will be lower, but with increased reliability that the actual field that could be measured would equal or exceed the computed value at any given time.

Situation variability accounts for variations between "like appearing" (NTIA, p. 30) systems with the same system parameters and environmental conditions, including differences in the ability of individuals to accurately take field strength readings. "It is at this point that 'hidden variables' enter, variables whose effects we do not understand or which we simply have not

differ between what would otherwise be identical situations. The effects of these differences produce the changes in observed statistics" (NTIA, p.30). Situation variability describes the effects of the changing conditions resulting from these "hidden variables." The situation variability for the calculation is expressed as a percentage from 0.1% to 99.9%. This value gives the fraction of "identical" paths on which actual received field strength is expected to be equal to or higher than the field computed by the program. This variable allows you to specify how you want to deal with the "hidden variables" that are "at the whim of nature" as described above. Entering higher percentage confidence values effectively reduces the variability resulting from these factors. The resulting field strength predicted by the program will be lower, but with increased confidence that the actual field that could be measured would equal or exceed the computed value.

In the default settings of the SoftWright implementation of Longley-Rice, these dimensions of variability are expressed in terms of "reliability" and "confidence". The terms are introduced in the NTIA Report at 36. According to this report, reliability refers to a measure of the variability that a radio system will observe during its use. Confidence refers to the variability that remains after specifying reliability, measurable in the aggregate of a large number of radio systems.

Terrain Profile Characteristics

The Longley-Rice model, as implemented by SoftWright, uses the elevation values to create a detailed profile of a path for analysis by the program. In the case of the Longley-Rice program, the elevation values are read from the TAP elevation data base. As with other propagation models in the TAP system, the file can contain multiple radials and path studies can be performed for multiple points along each radial.

Note that the model as it was originally designed expects terrain profile information at equal increments along a specific path. Although other propagation models available in the TAP system permit unequal elevation point spacing (such as when a radial elevation data file is edited to insert a particular peak or ridge), such files pose a potential problem for the Longley-Rice program. Elevation data extraction parameters that are specified for use with the Longley-Rice field calculation program are first read to determine compliance with the uniform spacing requirement. (The spacing of elevation points on different radials does not have to be the same, but the spacing between points on any given radial must be uniform.) The spacing between points is assumed to be the distance from the site to the first elevation point on the radial. Any intermediate points (i.e., successive points spaced at less than that distance from the preceding point) that are found are ignored. If the spacing between successive points is greater than the determined uniform spacing any remaining elevation data on the radial cannot be processed by the model and that portion of the radial is skipped. The program will compute field strength values out to the last uniformly spaced point on the radial.

1. Effective Antenna Heights: Effective antenna height is defined as the height of the antenna above the "effective reflecting plane" (see IEEE at 28). The model first determines a "range of interest" based upon above ground elevation and the horizon distance of each antenna, and then uses one of two methods to determine the effective heights from the ground levels and least squares elevation values.

2. Horizon Distances and Elevation Angles: The horizon elevation angle refers to the angle by which the horizon rays are elevated or depressed relative to the horizontal at each antenna (see Longley-Rice at 3-1). Using detailed terrain profile information, the model calculates horizon elevation angles as a function of antenna heights above sea level, the effective earth's radius and the great circle distances from each antenna to its horizon.

3. Terrain Irregularity: The model first uses linear interpolation to fit a straight line within the range of interest and then determines an interdecile range Δ h(d) above and below this line (see IEEE at 28). The terrain irregularity parameter Δ h is then computed.

4. Reference Attenuation: The horizon elevations and distances generated by the model are used to calculate transmission loss relative to free space. The model divides total transmission loss into "free-space basic transmission loss" and reference attenuation relative to free space. The free-space basic transmission loss is calculated as a function of frequency and distance. The net received field at any point is computed from the free-space field reduced by the computed reference attenuation relative to free space. One of three prediction methods described in Annex 3 of Longley-Rice is used to calculate the reference attenuation based upon the distance from the transmitting antenna.

- Line of Sight Attenuation: Within radio line of sight, attenuation relative to free space is calculated using two-ray optics formulas.
- Diffraction Attenuation: A diffraction method is used just beyond line of sight that computes a weighted average of estimates of diffraction attenuation over a double knife edge and over irregular terrain.
- Forward Scatter Attenuation: Forward scatter attenuation is computed when the path length and/or the angular distance exceeds certain limits determined by the model.

Parameter Checking

The Longley-Rice programs described in NTIA and other literature include validation of various parameters. The warnings are categorized into four "levels" according to the severity of the error:

Level	Description (NTIA, p. 70)
1	Caution, parameters are close to limits

2	Impossible parameters; default values have been substituted
3	Internal calculations show parameters out of range
4	Parameters out of range

The level recorded by the program is cumulative in the sense that if both a level 1 error and a level 3 error are encountered, the error reported is level 3.

Examples of the warnings detected in the Longley-Rice model help to illustrate these levels:

Level	Example of the warning
1	A specified frequency below 40MHz is "close to limits" of stated Longley-Rice range of 20 - 40GHz.
2	A climate code of -1 is an "impossible parameter" since the range is 1-7. A default value of 5 ("continental temperate") will be substituted.
3	Internal calculations based on the path elevation data can show that a horizon elevation angle is beyond the range considered valid for the Longley-Rice calculations.
4	A specified frequency below 20MHz is "out of range" since the stated Longley-Rice range is 20 - 40GHz.

The original Longley-Rice programs include the following messages for the warnings:

Level	Message
1	`**WARNING - SOME PARAMETERS ARE NEARLY OUT OF RANGE. RESULTS SHOULD BE USED WITH CAUTION.`

2	**NOTE - DEFAULT PARAMETERS HAVE BEEN SUBSTITUTED FOR IMPOSSIBLE ONES.
3	**WARNING - A COMBINATION OF PARAMETERS IS OUT OF RANGE. RESULTS ARE PROBABLY INVALID.
4	**WARNING - SOME PARAMETERS ARE OUT OF RANGE. RESULTS ARE PROBABLY INVALID.

These rather brief and general messages represent a number of different conditions. The SoftWright implementation of the Longley-Rice model expands these messages to include more information about the specific condition that resulted in the warning level set by the program. If more than one warning or error was encountered, all messages will be recorded as described later in this section. The SoftWright messages are listed below.

Detailed Message	Level
Horizon distance(s) may be too short.1	3
Horizon distance(s) may be too long.2	3
Horizon elevation angle greater than 11.5 degrees.3	3
Frequency below 40 MHz.	1
Frequency above 10 GHz.	1
Antenna height(s) less than 1 meter AGL.	1
Antenna height(s) greater than 1000 meters AGL.	1
Surface refractivity below 250.	4
Surface refractivity above 400.	4
Earth curvature less than 75E-9.	4
Earth curvature greater than 250E-9.	4
Real surface transfer impedance less than imaginary part.	4
Frequency below 20 MHz.	4
Frequency above 20 GHz	4

Antenna height(s) less than .5 meter AGL.	4
Antenna height(s) greater than 3000 meters AGL.	4
Distance for calculation is greater than 1000 km.	1
Distance less than 5x difference between eff ant heights.4	3
Distance for calculation is less than 1 km.	4
Distance for calculation is greater than 2000 km.	4
Invalid climate code; climate code set to 5.	2
Invalid variability mode; mode set to 0.	2
Time probability set less than 0.1%.	1
Location probability set less than 0.1%.	1
Situation probability set less than 0.1%.	1

Notes:

1 This condition occurs in Longley-Rice if the computed horizon distance is less than:

$$0.1 \bullet \sqrt{\frac{2 \bullet HE}{GME}}$$

where HE is the computed effective antenna height of the antenna
GME is the effective earth curvature

2 This condition occurs in Longley-Rice if the computed horizon distance is less than:

$$3.0 \bullet \sqrt{\frac{2 \bullet HE}{GME}}$$

where HE is the computed effective antenna height of the antenna
GME is the effective earth curvature

3 This condition occurs in Longley-Rice if the computed horizon elevation angle is greater than 0.2 radians (11.5°).

4 This condition occurs in Longley-Rice if the distance for the computed field strength is

$$\left|\frac{HE(1) - HE(2)}{.2}\right|$$

where HE(1) is the computed effective antenna height of the TX antenna
HE(2) is the computed effective antenna height of the TX antenna

Whenever the Longley-Rice program encounters any of these conditions the warning(s) are recorded in the TAP Results Data Base file for the study.

Conclusion

The discussion in this article is intended to be a cursory overview of the model's treatment of the parameters and statistics of radio propagation as treated by the Longley-Rice model. You are encouraged to refer to the literature to develop your own understanding and interpretation of the Longley-Rice concepts.

Given your system parameters and statistical choices that you have supplied in TAP's Longley-Rice module, our implementation of the model will generate a file of field strength values computed from the long-term median transmission losses at each increment and along each radial you have selected. This file can then be used just as other TAP field strength files with TAP's graphical features (such as the threshold plotting).

Ordering Information For Longley-Rice Propagation Model Documentation

The following documents are available from National Technical Information Service (phone 1-800-553-6847, or 1-703-487-4656). The abbreviated titles refer to the notation used for the documents in the Terrain Analysis Package (TAP)™ *Technical Reference Manual* section on the Longley-Rice model.

"Tech Note 101": P. L. Rice, A. G. Longley, K. A. Norton, and A. P. Barsis, "Transmission loss predictions for tropospheric communication circuits," U.S. Government Printing Office, Washington, DC, NBS Tech. Note 101, issued May 1965; revised May 1966 and Jan. 1967.

Volume 1: **Order Number AD687820**
Volume 2: **Order Number AD687821**

"Longley-Rice": A. G. Longley and P. L. Rice, "Prediction of Tropospheric radio transmission over irregular terrain, A Computer method-1968." ESSA Tech. Rep. ERL 79-ITS 67, U.S. Government Printing Office, Washington, DC, July 1968.

Order Number AD676874

"NTIA Report": G. A. Hufford, A. G. Longley, and W. A. Kissick, "A guide to the use of the ITS irregular terrain model in the area prediction mode," NTIA Rep. 82-100, Apr. 1982.

Order Number PB 82 217 977



I'm interested!
Please click here to jump to an online form which helps us better understand your needs. Then we will be able to respond to your request with information that is most useful to you.

Search SoftWright Website

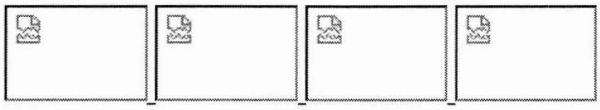

Copyright 2000 by SoftWright LLC

1. Quality of a Microwave Link

For a well-designed path which is not subject to diffraction fading or surface reflections, multipath propagation is the dominant factor in fading below 10 GHz. Above this frequency, the effects of precipitation tend increasingly to determine the permissible path length through the system availability objectives. In principle, the necessary reduction in path length with increase in frequency, reduces the severity of multipath fading. These two main causes of fading are normally mutually exclusive.

ITU defines both "error performance objective" and "availability" to represent the quality of a microwave link. Their related terms are defined in the recommendations ITU-T G.826, ITU-R F1491, and ITU-R F1493. Following is a brief description of them.

The error performance events defined are

- ES (Errored second): a one second period during which one or more EB's (errored block) occurs.
- SES (Severely errored second): a one second period during which 30% or more of EBs occurs.
- BBE (Background block error): an errored block not occurring as part of SES.

Error performance parameters defined are severely errored second ratio (SESR), background block errored ratio (BBER), and errored second ratio (ESR). It is generally agreed that SER and BBER will also be satisfied once SESR meets the objective. The error performance objective of SESR is used and is defined as follows.

Long haul

Rate (Mbps)	1.5 to 5	5 to 15	15 to 55	55 to 160	160 to 3500
Severely errored second ratio (SESR)	0.002 × A	0.002 × A	0.002 × A	0.002 × A	0.002 × A

where $A = (A_1 + 0.01)\, L_{link} / 500$ for 50 km $\leqq L_{link} \leqq$ 500 km

$A = A_1 + 2 \times 10^{-5}\, L_{link}$ for $L_{link} >$ 500 km

A_1 is provisionally been agreed to be in the range of 1% to 2%.

Short haul

Rate (Mbps)	1.5 to 5	5 to 15	15 to 55	55 to 160	160 to 3500
Severely errored second ratio (SESR)	0.002 × B	0.002 × B	0.002 × B	0.002 × B	0.002 × B

Where B is provisionally been agreed to be in the range of 7.5% to 8.5%. B = 0.075 is used unless otherwise specified by the customer.

Access

Rate (Mbps)	1.5 to 5	5 to 15	15 to 55	55 to 160	160 to 3500
Severely errored second ratio (SESR)	0.002 × C	0.002 × C	0.002 × C	0.002 × C	0.002 × C

Where C is provisionally been agreed to be in the range of 7.5% to 8.5%. C = 0.075 is used unless otherwise specified by the customer.

Note that A_1% + B% + C% shall not exceed 17.5%, while B% + C% shall be in the range of 15.5% and 16.5%.

For example, error performance objective for SDH (155 Mbps, link: 50 km) = $0.02 \times (0.01 + 0.01) \times 50 / 500 \times 60 \times 60 \times 24 \times 30$ = 10 sec/month.

A path fails to satisfy this Recommendation if any parameter exceeds the allocated objective in either direction at the end of the given evaluation period. The suggested evaluation period is 1 month.

On the other hand, "availability" is the ratio of the time that the link is available to the total time. This serves as a guideline to the service that can be expected on average over a period of one year. Table 2.1 shows how percentage availability relates to outage time per year.

Availability	Outage Time	Outage per year
99.9%	0.1%	9 hours
99.99%	0.01%	1 hour
99.999%	0.001%	5 minutes
99.9999%	0.0001%	30 seconds

Table 2.1 Link Availability and outage time

Availability is largely a function of fade margins and the amount of signal fading and is best determined by field measurement. The availability parameters defined are

- UR (Unavailability Ratio): unavailability of a 3000S system may be due to propagation effects, equipment failures, human intervention and interference or other causes.
- AR (Availability Ratio): AR = 1 – UR. If a period of SES occurs that is longer than 10 consecutive seconds, the system will change from an available state to an unavailable state. To change back to available, it requires a period of 10 consecutive seconds with non-SES.

The availability objective is defined as follows.

$AR = 1- (B_j \times L_{link} / L_R + C_j)$ where

j: section of national portion, j = {1 = access network, 2 = short haul, 3 = long haul}

L_R: reference length = 2500 km.

The lower limit of L_{link} used to scale the objectives is L_{min} = 50 km.

Access portion		Short haul portion		Long haul portion	
B1	C1	B2	C2	B3	C3
0	5×10^{-4}	0	4×10^{-4}	3×10^{-3} for 250 km $\leqq L_{link} < 2500$ km 1.9×10^{-3} for 50 $\leqq L_{link} <$ 250km	0 for 250km $\leqq L_{link} <$ 2500km $1. \times 10^{-4}$ for 50 $\leqq L_{link} <$ 250km

For example, availability objective for SDH (155 Mbps, link: 50 km) = 1 – ($1.9 \times 10^{-3} \times 50 / 2500 + 1.1 \times 10^{-4}$) = 0.999852. Therefore, unavailability = (1-0.999852) × 60 + 24 × 365 = 77 min/year.

It is stated in ITU-R F1093 that, given the split between availability and error performance objectives, precipitation effects contributes mainly to unavailability and multipath propagation mainly to error performance.

For the purpose of designing a radio network, NEC has adopted the following approaches to measure its equipment against the criteria set forth above.

1. Total Outage Probability

   The total outage probability that is specified in ITU-R P.530-8 is calculated against the error performance objectives.

- If diversity techniques are not employed, the total outage probability is the sum of the probability of outage due to non-selective frequency fading, the probability of outage due to selective frequency fading, and the probability of outage due to XPD (cross polar discrimination).
- If diversity techniques are employed, the total outage probability is the sum of the probability of outage when frequency diversity is used, the probability of outage when space diversity is used, the probability of outage when both space and frequency diversity are used with 2 receivers, and the probability of outage when both space and frequency diversity are used with 4 receivers.

2. Rain attenuation

For the system at frequency above 10 GHz (above 6 GHz if rain intensity is higher than 100 mm/h), rain attenuation has to be considered. The outage probability due to rain attenuation that is specified in ITU-R P.530-8 is calculated against the availability objectives.

However, NEC and TEKOMSEL agreed that the outage probability due to rain attenuation is also calculated against the error performance objectives.

2. Link Budget Analysis

Fade Margin

A signal degrades as it moves through free space – in other words, the loss would occur in a region, which is free of all objects that might absorb or reflect radio energy. It is calculated for miles or kilometers using one of the following formulas.

$L_{fs} = 96.6 + 20*\log_{10} F + 20* \log_{10} D$ where

L_{fs} = free space loss in dB

F = frequency in GHz

D = path length, in miles

or

$L_{fs} = 32.4 + 20*\log_{10} F + 20* \log_{10} D$ where

L_{fs} = free space loss in dB

F = frequency (GHz)

D = path length, in kilometers

Free space loss can also cause data errors referred to as inter-symbol interference (ISI). It is essential to provide adequate link margin to overcome this loss. The amount of extra RF power radiated to overcome this phenomenon is referred to as fade margin. Fade margin is one of the more important factors in determining the availability of the microwave link. The higher the fade margin, the more reliable the link is. The two main events that cause the desired signal to fade are multipath clear air fading (flat fading) and rain fading. Rain fading will be discussed in section 1.6. Here,

Flat fade margin = Receive signal level – Receiver sensibility threshold

At first, a very important step in the link budget is to determine the minimum signal strength required at the receiver input to successfully receive a signal. It is referred to as receiver sensibility threshold (Prx) and is denoted in dBm. It is a function of modulation technique, which dictates the required system bandwidth, and thus contributes to the noise power, and the desired BER.

Receiver Signal Level (RSL) is the expected strength of a signal when it reaches the receiving radio. It can be calculated as follows.

Receiver Signal Level = $P_{tx} – L_{tx} + G_{tx} – L_{fs} + G_{rx} – L_{rx}$

P_{tx}: transmitter output power

L_{fs}: free space path loss

G_{tx}: transmitter antenna gain

G_{rx}: receiver antenna gain

L_{tx}: transmitter feeder loss

L_{rx}: receiver feeder loss

Note that RSL does not account for antenna alignment errors or path fading phenomena, such as multipath reflections, signal distortions, variable atmospheric conditions, and obstructions in the path.

In addition, system gain is obtained through the following formula:

System Gain = P_{tx} – Prx

P_{tx}: transmitter output power

Prx: receiver sensibility threshold

Propagation Loss

In the design of line-of-sight radio relay system, in addition to the free space loss mentioned above, the transmitted signal suffers other types of path loss as it propagates through the air. They are

- Fading due to multipath arising from surface reflection;
- Attenuation due to atmospheric gases;
- Diffraction fading due to obstruction of the path by terrain obstacles;
- Attenuation due to precipitation;

Radio signals are reflected over smooth surfaces, such as a body of water, a flat stretch of earth, or a metal roof that they cancel out the direct signal and bring down the radio link. See figure below.

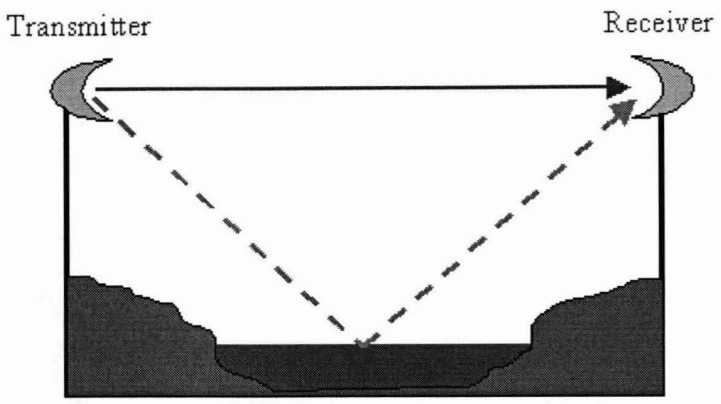

To avoid such failure, a path should be designed so that the reflected signal is dispersed by an uneven surface before it reaches the receiver and cancels out the direct wave. *Reflection Point analysis* will quickly determine, for example, whether there is a significant risk of signal destruction due to reflection off the terrain and where such areas are likely to be. Armed with such information, the System Designer can avoid site deployment in those areas, or in extreme cases, take special precautions to minimize the deleterious effects. Typically, this may take the form of adjusting the height or changing the position of one or both of the antennas to deliberately shift the reflection point from the area of risk to another, less problematic point along the link path.

Attenuation due to Atmospheric Gases

Combinations of irregularities and fluctuations in atmospheric temperature, humidity, and pressure cause more than one and often many propagation paths to exist between the transmitting antenna and the receiving antenna. As the atmospheric conditions vary, the routes and distances of paths also vary, causing signals of differing phases and amplitudes to arrive at the receiving antenna at the same instant.

The attenuation on a path of length d (km) is given by

$A_a = \Upsilon_a * d$ where

$\Upsilon_a = \Upsilon_0 + \Upsilon_w$

Υ_0: attenuation due to dry air absorption

Υ_w: attenuation due to water vapor; Υ_0 and Υ_w values can be obtained in ITU-R P676. Note that for frequency below 10GHz, the Υ_0 and Υ_w values are small enough that they can be disregarded. For frequency higher than 10GHz these values are significant and should be taken into account in the propagation loss calculation.

Diffraction Fading

Diffraction is a propagation phenomenon that allows radio waves to propagate beyond obstructions via secondary waves created by the obstruction. This type of fading is the factor that determines the antenna height. In other words, by allowing sufficient clearance from obstacles along the path, correct performance of the link can be assured. Clearance requirements are usually stated as a combination of a percentage of the first Fresnel zone radius and a K factor (the ratio of the effective Earth radius to the actual Earth radius). For example, a common requirement is that 100% of the first Fresnel zone radius should be clear of all obstructions at a K factor of 4/3.

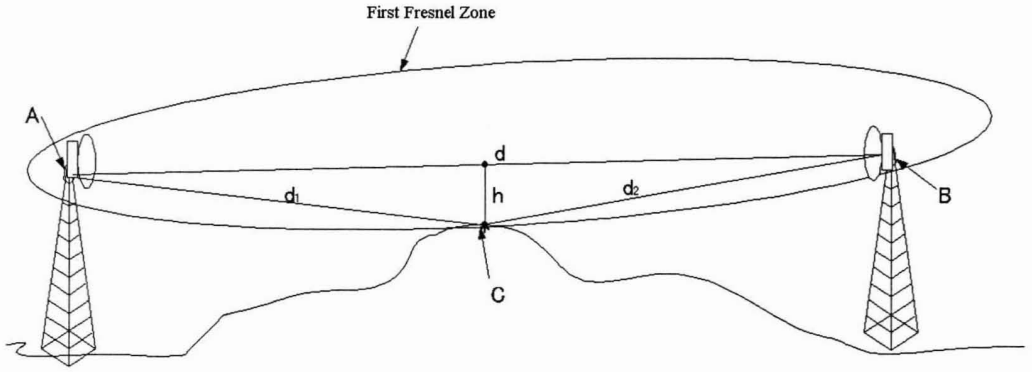

Figure 2.1 Fresnel zone for a radio link

In Figure 2.1, what is called Fresnel zone is shown. It is the volume of space enclosed by an ellipsoid, which has the two antennas at the ends of a radio link at its foci. When the ellipsoid just touches the tip of the diffracting object as demonstrated at point C, such area is occupied by the strongest radio signal and is called the First Fresnel Zone.

The following formula is used to calculate the path clearance of the First Fresnel Zone.

h (in meter) = $17.3 (d_1 * d_2 / f * (d_1 + d_2))^{1/2}$ where

f = frequency (GHz)

d_1 = path length between A and C, in kilometers

d_2 = path length between B and C, in kilometers

or

h (in feet) = $72.1 (d_1 * d_2 / f * (d_1 + d_2))^{1/2}$ where

f = frequency (GHz)

d_1 = path length between A and C, in miles

d_2 = path length between B and C, in miles

A general rule of thumb is that the link is very close to the free space value if 60% of the First Fresnel Zone is clear of obstructions. However, different countries with the different climate may specify a more precise value. For example, Radio Agency in UK specifies $0.577F_1$ for minimum path clearance.

Example. We have a 10 km LOS path over which we wish to establish a link in the 13 GHz band. The path profile indicates that the highest point on the path is 3 km from one end, and the direct path clears it by about 5 meters (16.4ft) – do we have adequate Fresnel zone clearance?

From the equation above, with d_1 = 3 km, d_2 = 7 km, and f = 13 GHz, we have h = 6.95 m for first Fresnel Zone clearance. A clearance of 5 m is about 71% of this, so it is sufficient to allow negligible diffraction loss.

Note that for the zero clearance, which is at a position level with the top of the obstacle, the signal power density is down by some 6 dB. If

necessary, this could be overcome with, for example, an additional 3 dB of antenna gain at each end of the link.

Therefore, the effective value of K-factor, which is obtained in accordance with the path length, and the Fresnel zone clearance radii are the essential elements in determining the antenna height.

In addition, when planning for paths longer than seven miles, the curvature of the earth might become a factor in path planning and require antenna be located higher off the ground. The additional antenna height needed can be calculated using the following formula:

$h = d^2 / 8$ where

h = height of earth bulge (in feet)

d = distance between antennas (in miles)

Therefore, the minimum antenna height at each end of the link for paths longer than seven miles (for smooth terrain without obstructions) needs to take into account path loss due to both diffraction fading and earth bulge.

Flat Fading

When multiple copies of the transmitted signal arrive at the receiver via different path, "multipath" effect occurs. Since each arriving wave can combine destructively or constructively depending on their phase, multipath propagation causes certain areas to have low signal power and vice versa. This is known as multipath fading, which can be categorized as either flat fading or frequency selective fading.

In the case of flat fading, the received signal spectrum remains a close replica of the transmitted signal spectrum except for a change in amplitude. It is also referred to as non-frequency selective fading. Flat fading occurs when the Root Mean Square delay spread of the channel is much smaller than the symbol period of the transmitted signal. According to ITU-R 530-8, the method for predicting the percentage of time (P_W) that fade margin (A) corresponding to a specified bit error ratio (BER) is exceeded in the average worst month is as follows

$$P_W(\%) = K\, d^{3.6} f^{0.89} (1 + |\varepsilon_p|)^{-1.4} \times 10^{-A/10} \text{ where}$$

d: path length in km

f: frequency in GHz

K, referred to as geoclimatic factor is derived as follows in the case of inland links. The definition of inland links and coastal links of various types are defined in pp. 130-131 of the ITU-R P.530-8 recommendation.

$$K = 5.0 * 10^{-7} * 10^{-0.1(C0 - CLat - CLon)} * PL^{1.5} \text{ where}$$

Co

Altitude of lower antenna and type of link terrain	Co (dB)
Low altitude antenna (0 – 400m) - Plains	0
Low altitude antenna (0 – 400m) - Hills	3.5
Medium altitude antenna (400 – 700m) - Plains	2.5
Medium altitude antenna (400 – 700m) - Hills	6
High altitude antenna (> 700m) - Plains	5.5
High altitude antenna (> 700m) - Hills	8
High altitude antenna (> 700m) - Mountains	10.5

Where the type of terrain is unknown, the following values are used.

Altitude of lower antenna (in the range above mean sea level)	Co (dB)
Low altitude antenna (0 – 400m)	1.7
Medium altitude antenna (400 – 700m)	4.2
High altitude antenna (> 700m)	8

CLat

atitude	CLat (dB)
Latitude ≤ 53°N or 53°S	0
53°N or 53°S < Latitude < 60°N or 60°S	-53+ Latitude
Latitude ≥ 60°N or 60°S	7

CLon

ongitude	CLon (dB)
Europe and Africa	3
North and South America	-3
All others	0

The value of the climatic variable PL is estimated by taking the highest value of the –100N units/km gradient exceedance from the maps for the four seasonally representative months of February, May, August and November in Figure 7 to 10 of recommendation ITU-R P.453. An exception to this is that only the maps for May and August should be used for latitude greater than 60°N or 60°S.

Path inclination ε_p is calculated as

$|\varepsilon_p|$ (mrad) = $|ht - hr| / d$ where

d: path length in km

ht, hr: antenna height in meters above sea level

Thereafter, the probability of outage P_{ns} due to the non-selective component of the fading is $P_{ns} = P_W / 100$. Note that the outage probability is here defined as the probability that BER is larger than a given threshold.

Frequency Selective Fading

When the RMS delay spread of the channel is more than about 10% of the symbol period, the wireless channel alters the received signal spectrum. This is referred to as frequency selective fading. In frequency selective fading, the channel is dispersive and the received waveform has intersymbol interference (ISI). Note that unlike analogue systems, an increase in fade margin will not improve the performance of digital system due to frequency selective fading. The outage probability is here defined as the probability that BER is larger than a given threshold.

According to ITU-R 530-8, the method for predicting the selective outage probability is as follows.

$$P_s = 2.15\eta \left(W_M \times 10^{-B_M/20} \tau_m^2 / |T_{r,M}| + W_{NM} \times 10^{-BNM/20} \tau_m^2 / |T_{r,M}|\right)$$

η: Multipath activity parameter = $1 - \exp(-0.2 * Po^{0.75})$

Po : Multipath occurrence factor = Pw (%) /100, A = 0

τ_m: mean time delay = $0.7 * (d / 50)^{1.3}$ (ns)

d : Propagation Distance (km)

Wx: Signature width (GHz)

B_M: Minimum signature (phase notch) depth (dB)

B_{NM}: Non-minimum signature (phase notch) depth (dB)

$\tau_{r,x}$: Reference delay (ns) used to obtain the signature, with x denoting either minimum phase ($_M$) or non-minimum phase ($_{NM}$) fades.

Techniques for Alleviating Propagation Effects

The effects of slow relatively non-frequency selective fading (i.e. flat fading) due to beam spreading, and faster frequency-selective fading due to multipath propagation can be reduced by both non-diversity and diversity techniques.

Techniques without Diversity

In order to reduce the effects of multipath fading without diversity there are several options that can be employed. The guidance is divided into three groups: reduction of the levels of ground reflection, increase of path inclination, and reduction of path clearance.

Link should be sited where possible to reduce the level of surface reflections thus reducing the occurrence of multipath fading and distortion. One of the techniques is to tilt the antenna slightly upwards. A trade-off must be made between resultant loss in antenna directivity and the improvement in multipath fading conditions.

Increase of path inclination is known to reduce the effects of beam spreading, surface multipath fading and atmosphere multipath fading. Therefore, the positions of the antennas on the radio link towers should be chosen to give the largest possible inclinations, particular for the longest links.

Reduction of path clearance to improve multipath effect is less known. However, for the space diversity configuration one antenna might be positioned with low clearance.

Diversity Techniques

Diversity is a technique to reduce the effect of fading by selecting or combining the outputs of two or more receivers which has less correlation than each other in terms of the quality of received signals. Diversity techniques include space and frequency diversity. Frequency diversity should be avoided whenever possible simply because of limited availability of valuable radio frequency resources together with the increasing demand for transmission capacity in public networks.

- Space Diversity

  When two antennas are placed more than a wavelength or so apart, correlation factor between the two received signals can be reduced and the diversity can be increased. The only tradeoff is the physical placement of another antenna. The outage probability for a space diversity system is calculated as follows.

  Step 1:

  Calculate the square of non-selective correlation coefficient,

$k_{ns(s)}^2 = 1 - I_{ns} * P_{ns} / \eta$

P_{ns}: Outage Probability due to flat fading

η: Multipath activity parameter = $1 - \exp(-0.2 * Po^{0.75})$

$I_{ns(s)}$: Vertical space diversity improvement factor

$I_{ns(s)} = \{1 - \exp(-3.34 * 10^{-4} S^{0.87} f^{-0.12} d^{0.48} Po^{-1.04})\} * 10^{(A-V)/10}$

A: Fading margin

Po: $Pw * 10^{A/10} / 100$ fading occurrence factor

Pw: percentage of time fade depth A is exceeded in the average worst month

S: Vertical separation (Centre to Centre) of receiving antennas

f: Frequency (GHz)

d: Path length (km)

V : |G1 – G2|

G1, G2: gains of two antennas (dBi)

Step 2:

Calculate the square of selective correlation coefficient, $k_{s(s)}^2$

0.8238 for $r_w \leqq 0.5$

$k_{s(s)}^2 = 1 - 0.195 (1 - r_w)^{0.109 - 0.13 \log (1-rw)}$ for $0.5 < r_w \leqq 0.5$

$1 - 0.3957 (1 - r_w)^{0.5136}$ for $r_w > 0.9628$

where the correlation coefficient of the relative amplitudes is

$r_w = 1 - 0.9746 (1 - k_{ns(s)}^2)^{2.170}$ for $k_{ns(s)}^2 \leqq 0.26$

$= 1 - 0.6921 (1 - k_{ns(s)}^2)^{1.034}$ for $k_{ns(s)}^2 > 0.26$

Step 3:

Calculate non-selective outage probability for space diversity

$$P_{dns} = P_{ns} / I_{ns(s)}$$

Step 4:

Calculate selective outage probability for space diversity

$$Pds = Ps^2 / \{\eta (1 - ks_{(s)}^2)\}$$

P_s: outage probability due to dispersive fading

η: Multipath activity parameter = $1 - \exp(-0.2 * Po^{0.75})$

Step 5:

Total outage probability due to space diversity is

$$P_{d(s)} = (P_{ds}^{0.75} + P_{dns}^{0.75})^{1.33}$$

This equation is good for both 1+0 with SD and hot standby with SD systems.

- Frequency Diversity

To increase the frequency diversity one could send half of the symbol energy in one frequency band and the other half in another band. By doing this the probability that both frequency bands are heavily faded is less than if there is only one frequency, therefore the probability of guessing a correct symbol at the receiver can increase. The drawback of frequency diversity is that more bandwidth is needed to transmit the same amount of information.

The outage probability for a frequency diversity system $P_{d(f)}$ is calculated using the same procedure as for space diversity except that in Step 1 $I_{ns(f)}$ is calculated differently.

$$I_{ns(f)} = 80 / f * d (\Delta f / f) * 10^{F/10}$$

Δf: Frequency Separation (GHz) If $\Delta f > 0.5$ GHz, use $\Delta f = 0.5$

f: carrier frequency (GHz)

d: path length (km)

F: Flat fade margin

This equation is good for 1+1, Twin-path, N+0 and N+1 systems.

- Space and Frequency Diversity with 2 receivers ($P_{d(s,f)}$)

Step 1:

The non-selective correlation coefficient is found from

$k_{ns} = k_{ns(s)} * k_{ns(f)}$ where $k_{ns(s)}$ and $k_{ns(f)}$ are the non-selective correlation coefficients computed for space diversity and frequency diversity respectively.

The next steps are the same as those for space diversity.

- Space and Frequency Diversity with 4 receivers

Step 1:

Calculate the diversity parameter m_{ns}

$m_{ns} = \eta^3 * (1 - k_{ns(s)}^2) * (1 - k_{ns(f)}^2)$

Step 2:

Calculate the non-selective outage probability employing SD and FD

$P_{dns} = P_{ns}^4 / m_{ns}$

P_{ns}: outage probability due to flat fading

Step 3:

Calculate the square of the equivalent non-selective correlation coefficient k_{ns}^2

$$k_{ns}^2 = 1 - \eta^{0.5} * (1 - k_{ns(s)}^2) * (1 - k_{ns(f)}^2)$$

Step 4:

Calculate the square of selective correlation coefficient, Ks^2 using the same procedure as for space diversity in Step 2.

Step 5:

Selective outage probability with SD + FD is calculated as follows.

$$P_{ds} = \{ P_s^2 / \eta (1 - k_s^2) \}^2$$

P_s: Outage Probability due to dispersive fading

η: Multipath activity parameter = $1 - \exp(-0.2 * Po^{0.75})$

Step 6:

Total outage probability ($P_{d4(s,f)}$) is calculated using the same procedure as for space diversity Step 5.

- Total outage probability using diversity techniques

$$P_d = P_{d(s)} + P_{d(f)} + P_{d(s,f)} + P4_{d(s,f)}$$

XPD Deterioration

Electromagnetic waves are vector quantities, i.e. they are polarized. The preferred (desired) polarization radiated by an antenna is termed co-polarization; the orthogonal polarization is termed cross-polarization. If

polarization can be made pure enough, orthogonally polarized waves can travel together without interference and be separated by properly designed receiving antennas. The ability of antennas to discriminate in this manner is measured by the cross-pol ratio, or polarization isolation and, is called Cross Polarization Discrimination (XPD). For example, transmitting two OC3 signals on the same frequency pair by using opposite polarity can increase XPD, and thus double system capacity.

However, due to the combined effect of multipath and cross-polarization patterns, the XPD can also deteriorate sufficiently to cause co-channel interference and, to a lesser extent, adjacent channel interface for small percentage of time. The reduction in XPD can occur during both clear-air and precipitation conditions and should be dealt with separately. The prediction of outage due to precipitation will be discussed in section 3.12. The calculation of outage due to clear-air effect is as follows.

Step 1:

XPDg + 5 for XPDg $\leqq$ 35

XPD_0 =

40 for XPDg > 35

where XPDg is the NEC's guaranteed minimum XPD at bore sight for both the transmitting and receiving antennas.

Step 2:

Next evaluate the multipath activity parameter. Refer to section 3.6.4.

Step 3:

Determine the parameter Q

$Q = -10 * \log (k_{xp} \times \eta / Po)$

where

0.7 for one transmit antenna

k_{xp} =

$1 - 0.3 * \exp\{-4 * 10^{-6} * (s_t / \lambda)^2\}$ for two transmit antenna

Po : Multipath occurrence factor = Pw (%) /100, A = 0

In the case where two orthogonally polarized transmissions are from different antennas, the vertical separation is s_t (m) and carrier wavelength is λ (m).

Step 4:

Derive the parameter C from

$C = XPDo + Q$

Step 5:

The probability of outage P_{xp} due to clear-air cross polarization can be calculated from

$$P_{xp} = P_0 * 10^{-M_{XPD}/10}$$

Po : Multipath occurrence factor = Pw (%) /100, A = 0

C - Co / I without XPIC

XPD margin M_{XPD} =

C - Co / I + XPIF with XPIC

Co / I : carrier to interference ratio for a reference BER

XPIF : laboratory-measured cross-polarization improvement factor

(XPIF for PASOLINK series 64QAM is 18 dB, 128QAM is 20dB).

Rain Attenuation

The attenuation becomes significant as the size of the raindrops becomes comparable to the wavelength of the signal. Rain attenuation increases as raindrops become larger, more frequent, and the frequency of the link becomes higher (the wavelength becomes smaller). Typically, rain outages are only a concern in frequency bands above 10 GHz.

Step 1:

Obtain the rain rate $R_{0.01}$ exceeded for 0.01% of the time. If not available, an estimate can be obtained from the information given in ITU-R P.837.

Step 2:

Compute the specific attenuation γ_R (dB/km)

$\gamma_R = kR^{\alpha}$ (dB/km) where

$R = R_{0.01}$ (mm/h)

$k = [k_H + k_V + (k_H - k_V)\cos^2\theta \cos 2\tau] / 2$

$\alpha = [k_H \alpha_H + k_V \alpha_V + (k_H \alpha_H - k_V \alpha_V) \cos^2\theta \cos 2\tau] / 2k$

θ is the path elevation angle ($\theta = 0$ in most severe case)

τ is the polarization tilt angle relative to the horizontal.

($\tau = 0^{\circ}$ for horizontal polarization and $\tau = 90^{\circ}$ for vertical polarization)

k_H, k_V, α_H, and α_V is listed in Table 1 of ITU-T P.838-1.

Step 3:

Compute the distance factor

$r = 1 / (1 + d / do)$

d : effective path length

$do = 35 \exp(-0.015 * R_{0.01})$ for $R_{0.01} \leqq 100$ mm/h

$do = 35 \exp(-1.5)$ for $R_{0.01} > 100$ mm/h

Step 4:

An estimate of the path attenuation exceeded for 0.01% of the time is given by:

$A_{0.01} = \gamma_R * deff = \gamma_R * d * r$ (dB) where

$\gamma_R : kR^{\alpha}$ (dB/km)

d : effective path length

γ: 1 / (1 + d / do)

Step 5:

For the links located in the latitudes equal to or greater than 30˚, the attenuation exceeded for other percentage of time in the range of 0.001% and 1% may be deducted from the following.

$Ap / A_{0.01} = 0.12 * p^{-(0.546 + 0.043 \log_{10} p)}$ where

$p = \{ -0.546 + \{(0.298116 - 0.172 * \log \{Ap / (0.12 * A_{0.01})\}^{0.5}) / 0.086$ (%)

This formula has been determined to give factors of 0.12, 0.39, 1 and 2.14 for 1%, 0.1%, 0.01% and 0.001% respectively.

Step 6:

For the links located in the latitudes below 30˚, the attenuation exceeded for other percentage of time in the range of 0.001% and 1% may be deducted from the following.

$Ap / A_{0.01} = 0.07 * p^{-(0.855 + 0.139 \log_{10} p)}$ where

$p = \{ -0.855 + \{(0.731025 - 0.556 * \log \{Ap / (0.07 * A_{0.01})\}^{0.5}) / 0.278$ (%)

This formula has been determined to give factors of 0.07, 0.36, 1 and 1.14 for 1%, 0.1%, 0.01% and 0.001% respectively.

Step 7:

If worst-month statistics are desired, calculate the annual time percentages p corresponding to the worst-month time percentages p_w using climate information specified in ITU-R P.841.

$$p_w = (p / 0.3)^{1/1.15} (\%)$$

P_{rain} is the percentage of time that rain attenuation exceeds flat fade margin for the specified BER in the average year.

$$p_{rain} = (p / 100)$$

The reduction of XPD during precipitation affects the total availability of the system and should be taken into account in outage calculation.

Step 1:

Determine the path attenuation, $A_{0.01}$ exceeded for 0.01% of the time from equation (41).

Step 2:

Determine the equivalent path attenuation, Ap

$$Ap = 10^{((U - Co/I + XPIF)/V)} (dB)$$

$$U = Uo + 30 \times \log f \ (dB)$$

f = Carrier Frequency （GHz）

Uo＝15 dB

Co / I : carrier to interference ratio at reference BER

XPIF: laboratory-measured cross-polarization improvement factor （8dB if 64QAM is used; 20dB if 128QAM is used.）

If XPIC is not used, XPIF = 0

$V(f) = 12.8 \times f^{0.19}$ for $8 \leqq f \leqq 20$GHz

$V(f) = 22.6$ for $20 < f \leqq 35$GHz

Step 3:

Determine the following parameters m and n:

$23.6 \times \log (Ap / 0.12 \times A_{0.01})$ if $m \leqq 40$

m =

40 Otherwise

$n = (-12.7 + (161.23 - 4 \times m)^{0.5}) / 2 - 3 \leqq n \leqq 0$

Step 4:

$P_{XPR} = 10^{(n-2)}$

Total Outage Probability

The total outage probability due to clear-air effects is calculated from

$Pns + Ps + P_{XP}$

P t =

$Pd + P_{XP}$ if diversity is used

The total outage probability due to rain is calculated from taking the larger of P_{rain} (outage probability due to precipitation) and P_{XPR} (outage probability due to precipitation in the case of XPD).

The outage prediction methods given for digital radio systems have been developed by ITU from a definition of outage as BER above a given threshold. The outage due to clear-air effects is apportioned mostly to performance and the outage due to precipitation, predominantly to availability.

Interference Assessment

Longer multipath delay spreads have another consequence: overlap of received data symbols with adjacent symbols, known as intersymbol interference (ISI).

The most usual types of interference for microwave systems are co-channel interference and adjacent channel interference. The cause of it can be either external, or within the system.

- Co-channel Interference

Co-channel interference is caused by other signal residing at the same frequency as the desired signal.

Digital modulations such as 64 QAM, 16 QAM, and QPSK require significantly different specifications with respect to signal to noise and co channel interference. For example, in the modulation characteristics of 64QAM, it requires a co-channel interference rejection of at least 32.6dB. This means that to prevent receive sites from having interference generated within the system at the point of transmission, the antennas must have more than 32.6dB of transmit power. On the other hand, the same station operating at QPSK would only require an antenna with 19.6dB of rejection in the opposite station.



It is imperative to co-ordinate with all other neighboring links to allow minimal physical separation from each other to avoid co-channel interference from nearby RF equipment that operates at the same frequency. In this case, interference to and from the proposed link is

assessed taking into account the path profile between the two stations. Use is made of antenna radiation patterns to obtain the gain of antennas in the direction of unwanted signals.

- Adjacent Channel Interference

Adjacent channel interference is caused by RF leakage on the operational channel from a neighboring RF equipment using an adjacent frequency. This can occur when an adjacent channel user is operating in close proximity to the user's receiver, or when the user's signal is much weaker than that of the adjacent channel user.

Imperfect receiver filters which allow nearby frequencies to leak into the passband. A near-far effect could happen if near-by transmitter captures receiver in wrong band. To cure this problem, better filtering, sufficient guard band, clever channel assignment and maximize frequency separation between channels are the few techniques used today.

- Interference Limits

The interference limits are derived as follows.

Interference limit = Reference sensibility for BER ($=10^{-6}$) – D/U ratio.

The maximum co-channel and adjacent channel interference limits, at the receiver input, from a single unwanted source should be available at the local RF authority.

EIRP

What makes RF equipment work is to deliver RF signal over the air to the opposite station, which can recover and restore the signal back to its

original form. That means at the receiver, a certain level of input signal strength has to be maintained while the signal traveled through the air.

Effective (Equivalent) Isotropically Radiated Power (EIRP) is the measured power of a radio signal radiating from a transmitter antenna 'as if it were radiating from a point-source uniformly in all directions' (isotropic). EIRP calculation is important as it is related to possible undue interference to the adjacent channel, which is used by other operators. Determining the amount of power the radio uses to transmit and receive signals also relates to operating costs. It represents the combined result of the transmitter's RF power plus any antenna gain (any focusing of the power), as compared to a radiating antenna (with no reflector) in space. It is calculated as follows.

EIRP = RSL + Lrx– Grx + Lp

RSL: Receiver signal level

Lrx = Receiver feeder loss

Grx = Receiver antenna gain

Lp = Path loss

Blank This page.

Chapter 5

Measurements Results and Conclusion

In this chapter, propagation data statistics are calculated from Power Delay Profiles (PDPs) recorded at 38GHz and 60GHz bands of frequencies. The data processing software is used to process the PDP data files and quantitatively characterize path loss and rain attenuation statistics. The data processing software, referred to as the "Channel Imaging Analysis Suite", is explained thoroughly in Appendix A. Source code of the Analysis Suite is also included in Appendix A. Chapters 1 and 2, respectively, elaborate on the motivation and purpose of the proposed propagation measurement campaigns. Chapters 3 presents comprehensive details pertaining to measurement locations and channel sounding equipment, while Chapter 4 describes sequence of measurements performed to record wideband propagation characteristics of the radio channel.

Excess signal attenuation (relative to clear-sky path loss) during moderate to heavy rainfall is referred to as the *rain attenuation*. The path loss and rain attenuation statistics, calculated from PDP data files recorded during Path Loss measurement campaigns performed at 38GHz and 60GHz during clear sky and rain conditions, are presented in the first half of the chapter. The results show that the path loss exponent values calculated from data files are close to two for clear-sky PDP measurements. Comparison of rain attenuation values with the Crane Rain Model and the Simplified Attenuation Model (SAM) indicates that measured attenuation values relate better to SAM Model as compared to the Crane Model in a pico-cell scenario. Results from Frequency Diversity measurement campaigns, performed at 38GHz and 60GHz bands of frequencies during clear-sky conditions, are also discussed.

5.1 Propagation Data Recording

The Spread Spectrum Sliding Correlator System, described in Chapter 3, is capable of recording four different types of propagation measurements in the form of PDPs. Each of these four measurement types namely, calibration, spin, track and antenna pattern, record the time delay and the magnitude of signal power reaching the receiver and facilitate characterization of propagation of electromagnetic waves in a local area. Appendix A explains all four measurement data types. The data recording process involves real-time PDP data acquisition into a dedicated laptop computer in a specific file format. Irrespective of the type of data, the recorded PDP is manipulated and converted to text file format for further processing. The following aspects of PDP data recording are rigorously treated in Appendix A:

1. Different Measurement Types & Data Analysis (calibration, spin, track and antenna pattern)
2. Data File Naming Conventions
3. Data File Content Restrictions
4. Directory Structure for Data Recording

After converting the recorded PDP files to text format, the 'Channel Imaging Analysis Suite' is used to compute the desired set of statistics for characterization of the radio channel. The functionality, salient features, data analysis techniques and the underlying computational logic of the data processing software are also explained in Appendix A.

5.2 Path Loss Measurement Results

The term "path loss" is generally used to predict the power transfer between a transmitter and a receiver over a propagation path. It primarily quantifies the basic transmission loss (in dB) between the transmitting and the receiving antennas due to atmospheric attenuation and multipath scattering. The path loss exponent is an empirical constant that is often measured, but can also be derived theoretically in some environments. It varies depending upon the radio

propagation environment and characterizes the rate at which path loss increases with distance for a given propagation scenario. In Equation 5.1, the path loss exponent is expressed by letter 'n'. The variable d represents actual radio link length and d_0 represents reference distance in meters.

$$PathLoss(dB) = 10\log_{10}\left(\frac{d}{d_0}\right)^n \qquad \textbf{Equation 5.1}$$

The path loss and rain attenuation results, derived from Path Loss measurement campaigns discussed in Chapter 4, are classified on the basis of antenna polarization, the frequency of operation and the propagation weather conditions prevalent during channel sounding, as follows:

1. Path Loss statistics during clear-sky at 38 GHz [for all three locations[§]]
2. Path Loss statistics during clear-sky at 60 GHz [for all three locations[§]]
3. Rain Attenuation at 38 GHz with Horizontal Antenna Polarization [for third location[§]]
4. Rain Attenuation at 38 GHz with Vertical Antenna Polarization [for third location[§]]
5. Rain Attenuation at 60 GHz with Vertical Antenna Polarization [for third location[§]]

[§] The three measurement locations are described in detail in Chapter 4. It is important to note that the path loss statistics, calculated by the data processing software, do not represent absolute path loss values. Instead, as explained in Section 3.3.2.4 of Chapter 3, the post-processing software can only calculate path loss value relative to the free-space (FS) calibration distance. Throughout this research, FS calibration is performed at a distance of separation of 4 meters and hence, the path loss attenuation values calculated by the software are relative to a FS calibration distance of 4 meters. The fact that calibration measurements are done in a benign, free-space environment, devoid of any reflected multipath component, allows addition of theoretical path loss value for a 4 m radio link to the software-calculated relative path loss values and hence proposes absolute path loss statistics. The sample link budget for a typical propagation measurement setup is described below for 38GHz and 60GHz configurations. Expected received power values for each measurement configuration are also presented.

As mentioned in Section 3.1.1, the maximum input power to the up-conversion unit is -29dBm and the overall gain of the up-conversion unit is 50dBm. Consequently, the total received power at the output of the receiver antenna can be calculated using Equation 5.0.

$$P_R = P_T + G_T - PL_D + G_R \qquad \textbf{Equation 5.0}$$

In Equation 5.0,

P_R = Total Received Power at the output of the receiving antenna

P_T = Total Power at the input of the transmitting antenna = 21dBm

G_T = Antenna Gain value for the transmitter

G_R = Antenna Gain value for the receiver

PL_D = Absolute Path Loss over distance 'D' meters given by Equation 3.9.

Using Equation 5.0, the expected received power values, fed into the receiver subsystem, can be calculated for different distances of separation. The results for 4m, 161m, 418m, and 531m distance of separation are tabulated in Table 5.0. For complete details about FS calibration process, refer to Sections 3.2 & 3.3.

Table 5.0 Expected received power at 38GHz & 60GHz for typical system parameters.

P_T (dBm)	G_T (dB)	G_R (dB)	Freq. (GHz)	Distance D meters	Path Loss (dB)	Received Power at Antenna Output P_R (dBm)
21	19	39	37.8	4 m	76.03	2.97
21	19	39	37.8	161 m	108.13	-29.13
21	19	39	37.8	418 m	116.42	-37.42
21	19	39	37.8	531 m	118.49	-39.49
21	29	29	59.4	4 m	79.96	-0.96
21	29	29	59.4	161 m	112.05	-33.05
21	29	29	59.4	418 m	120.34	-41.34
21	29	29	59.4	531 m	122.42	-43.42

5.2.1 Clear-sky Path Loss Measurements at 38GHz

This section presents the path loss statistics at 38GHz, as calculated by the Data Analysis Suite, from the PDPs recorded during clear-sky conditions over three LOS wideband wireless links.

The absolute path loss values are expressed in decibels (dB). In addition, average absolute path loss values for each measurement location and antenna polarization configuration are also included. Note that log (or dB) values can not be averaged directly and hence absolute path loss values must be converted to linear scale before performing the averaging operation. Table 5.1 presents absolute path loss values for each of the three measurement locations.

Table 5.1 Absolute Path Loss values at 38GHz during clear-sky conditions.

Clear-sky Line of Sight (LOS) Path Loss Measurements performed at 38GHz at Location 1 (531m radio link), Location 2 (418m radio link) and Location 3 (161m radio link)

Location 1 Vertical Polar.		Location 2 Horizontal Polar.		Location 2 Vertical Polar.		Location 3 Horizontal Polar.		Location 3 Vertical Polar.	
	PathLoss (in dB)		PathLoss (in dB)		PathLoss (in dB)		PathLoss (in dB)		PathLoss (in dB)
1	120.56	1	122.04	1	118.27	1	116.12	1	110.23
2	120.57	2	121.98	2	118.18	2	116.12	2	110.24
3	120.56	3	122.09	3	118.33	3	116.12	3	110.24
4	120.54	4	122.14	4	118.16	4	116.13	4	110.25
5	120.62	5	121.95			5	116.13	5	110.26
6	120.89					6	116.14	6	110.26
7	120.87							7	110.28
8	120.92							8	110.28
9	120.90								
10	120.91								
Av.	**120.74**	**Av.**	**122.04**	**Av.**	**118.24**	**Av.**	**116.13**	**Av.**	**110.26**

The 38GHz transmitting and the receiving antennas are vertically polarized. Therefore, two separate 90-degree waveguide twists are introduced at the antenna units to facilitate polarization rotation of propagating electromagnetic waves. The cumulative excess signal attenuation introduced by the polarization converter waveguides is measured to be 4.43dB during back-to-back FS calibration measurements, as explained in Chapter 3. Therefore, for all propagation measurements performed with horizontal antenna polarization configurations, true absolute path loss values must be calculated by subtracting the waveguide excess attenuation loss value from the corresponding measured absolute path loss values expressed in Table 5.1.

Equation 5.2 presents the desired expression as follows:

$$PL_{true\_abs} = PL_{meas\_abs} - W_{Loss} \qquad \textbf{Equation 5.2}$$

where, W_{Loss} = cumulative waveguide loss

PL_{true_abs} = corrected absolute path loss value

PL_{meas_abs} = measured absolute path loss value

For example, the average measured absolute path loss value for Location 2 (*Horztl. Polarization*) is 122.04dB. The corresponding true absolute path loss value, using Equation 5.2, is 117.61dB.

The path loss exponent value is calculated for vertical antenna polarization and horizontal antenna polarization configurations as shown in Figures 5.1 and 5.2, respectively. For vertical antenna polarization configuration, the path loss exponent value is 2.02 and for horizontal antenna polarization path loss measurements, the value is 2.04.

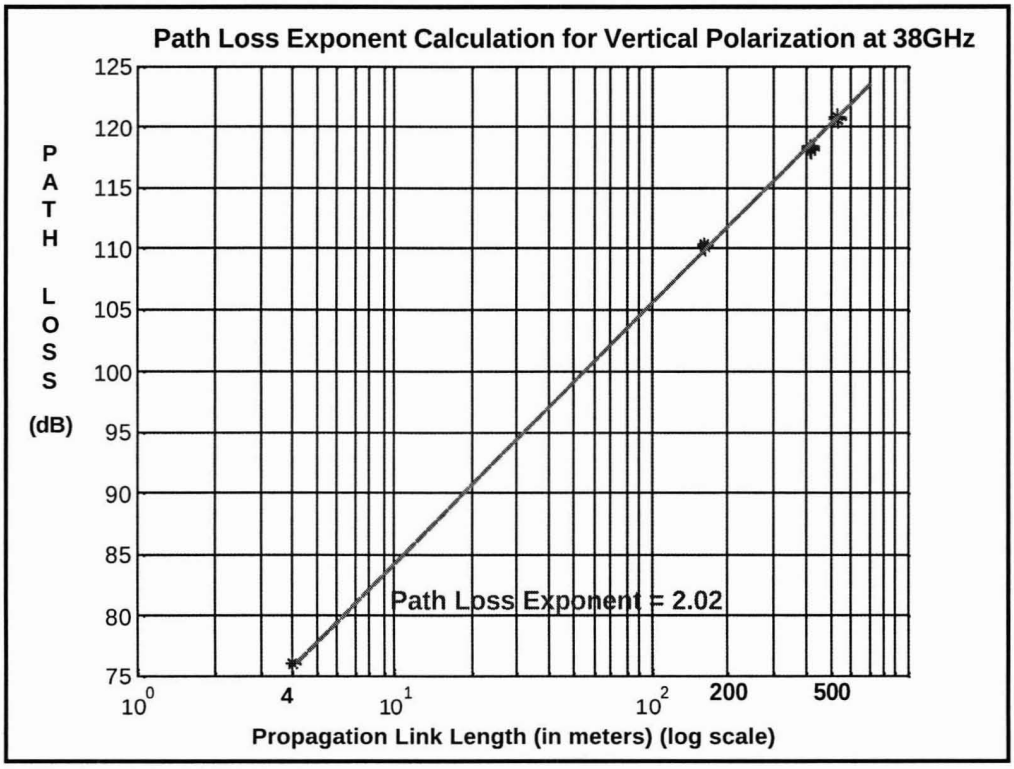

Figure 5.1 The figures shows clear-sky path loss data points and facilitates calculation of path loss exponent value for vertical antenna polarization configuration at 38GHz.

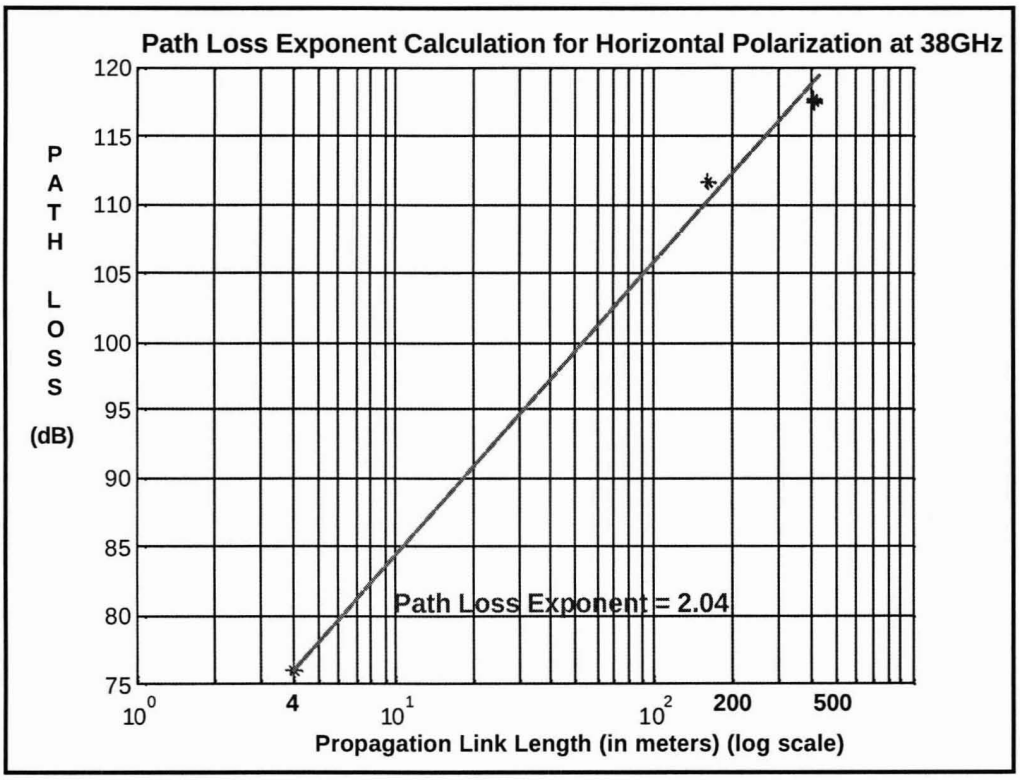

Figure 5.2 The figures shows clear-sky path loss data points and facilitates calculation of path loss exponent value for horizontal antenna polarization configuration at 38GHz.

For a free-space, unobstructed line-of-sight (LOS) links, the expected path loss exponent value, n, is equal to 2. The value is higher in a multipath rich environment or when obstructions are present in the LOS. Results show that average path loss experienced over radio links that represent pico-cell scenarios is slightly higher for horizontal antenna polarization configuration. However, a small difference in the path loss exponent values suggests that average path loss values for pico-cell radio links are largely independent of the antenna polarizations. Also, as expected for an unobstructed LOS radio link, for both antenna polarization configurations, the path loss exponent values are significantly close to the free-space path loss exponent value. The functionality of the channel sounder hardware and the 'Channel Analysis Imaging Suite' is thus verified and validated.

5.2.2 Clear-sky Path Loss Measurements at 60GHz

This section presents the path loss statistics at 60GHz, as calculated by the Data Analysis Suite, from the PDPs recorded during clear-sky conditions over three LOS wideband wireless links. At 60GHz, only vertical antenna polarization clear-sky path loss measurements are performed due to system hardware limitations. Table 5.2 presents quantitative path loss values for each of the three measurement locations. Average path loss values (in dB) are also included. Figure 5.3 plots the path loss values (relative to FS calibration) and allows calculation of approximate path loss exponent value to facilitate characterization of propagation channel at 60GHz.

Table 5.2 Recorded and average path loss values recorded at 60GHz during clear-sky conditions

Clear-sky LOS Path Loss Measurements at 60GHz					
Location 1 (531m) Vertical Polar.		Location 2 (418m) Vertical Polar.		Location 3 (161m) Vertical Polar.	
	PathLoss (in dB)		PathLoss (in dB)		PathLoss (in dB)
1	131.26	1	126.52	1	115.33
2	131.22	2	126.56	2	115.35
3	131.00	3	126.61	3	115.35
4	131.20	4	126.27	4	115.36
5	131.23	5	126.29	5	115.46
6	131.29	6	126.32	6	115.39
Av	**131.20**	**Av**	**126.43**	**Av**	**115.37**

At 60GHz band of frequencies, specific signal attenuation due to oxygen absorption is significant. Figure 5.4 shows that excess signal attenuation due to oxygen absorption is as high as 11dB/km [FCC97]. Consequently, one can expect significantly higher path loss values over long radio links. Statistics from Table 5.2 also indicate that calculated path loss values differ significantly for Locations 1, 2 and 3. This can be attributed to the fact that oxygen absorption respectively contributes approximately 5.5, 4.5 and 1.7dB to path loss values for Locations 1, 2 and 3. Needless to mention, one must also expect path loss exponent values to be appreciably greater than 2 even though all PDP data files are recorded during clear-sky conditions over unobstructed LOS radio links. Figure 5.3 shows the path loss exponent value as 2.12.

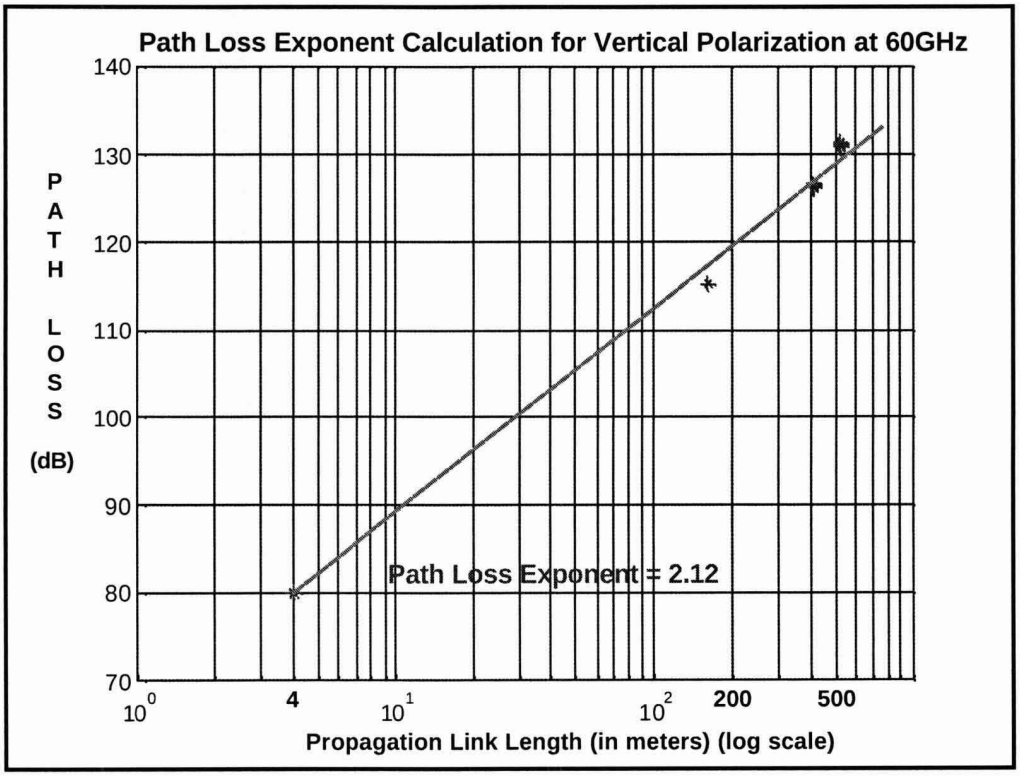

Figure 5.3 The figure shows clear-sky path loss data points and facilitates calculation of path loss exponent value for vertical antenna polarization configuration at 60 GHz.

5.2.3 Rain Models

Most rain attenuation models are based on statistical data of rain rate. This section briefly presents two popular rain models, discussed in detail in Section 2.1.2. The two rain models are:

1. Crane Global Rain Attenuation Model
2. Modified CCIR/SAM (Simplified Attenuation Model) Rain Model

The "Crane" models, after Robert K. Crane, are popular for satellite-earth links but also have terrestrial models. The Global Crane model, developed in 1980, is rigorously treated in [Cra96]. The theoretical prediction model, based on the aR^b rain attenuation model, can be summarized by Equations 5.3 through 5.8. In these Equations, A_R is the rain attenuation in dB, R is the point rain

rate in mm/hr, and d is the distance in km. Constants 'a' and 'b' are rain attenuation coefficients that are functions of frequency and polarization and are tabulated in [Ols78].

$$A_R = aR^b\left[\frac{e^{ubd}-1}{ub}\right] \quad (for\ 0 \le d \le D_0) \qquad \textbf{Equation 5.3}$$

$$A_R = aR^b\left[\frac{e^{ubD_0}-1}{u.b} - \frac{B^b e^{cbD_0}}{c.b} + \frac{B^b e^{cbd}}{cb}\right] \quad (for\ D_0 \le d \le 22.5km) \qquad \textbf{Equation 5.4}$$

where,

$$D_0 = 3.8 - 0.6\ln(R) \qquad \textbf{Equation 5.5}$$

$$B = 2.3R^{-0.17} \qquad \textbf{Equation 5.6}$$

$$u = \frac{\ln[Be^{cD_0}]}{D_0} \qquad \textbf{Equation 5.7}$$

$$c = 0.026 - 0.03\ln(R) \qquad \textbf{Equation 5.8}$$

For paths longer than 22.5 km, the attenuation A_R is calculated for a 22.5 km path, and the resulting rain attenuation is multiplied by a factor of (d /22.5).

The Simplified Attenuation Model (SAM/CCIR) was developed for NASA to provide a simplified technique for hand calculation. This model [Pra86] is based on nominal water droplet sizes and distribution and allows calculation of attenuation rate (dB/km) due to a specified rainfall rate. The attenuation rate can be approximately expressed by Equation 5.9, where R represents the rainfall rate in millimeters per hour and parameters 'a' and 'b' are approximated by Equations 5.10 and 5.11, respectively.

$$\kappa_{rain} = aR^b \qquad \textbf{Equation 5.9}$$

$a = 4.21 \times 10^{-5} f^{2.42}$ (for $2.9GHz \le f \le 54GHz$) **Equation 5.10.(a)**

$a = 4.09 \times 10^{-2} f^{0.669}$ (for $54GHz \le f \le 180GHz$) **Equation 5.10.(b)**

$b = 1.41 f^{-0.0779}$ (for $8.5GHz \le f \le 25GHz$) **Equation 5.11.(a)**

$b = 2.63 f^{-0.272}$ (for $25GHz \le f \le 164GHz$) **Equation 5.11.(b)**

It is important to note that in Equations 5.10 and 5.11, the frequency f is expressed in GHz.

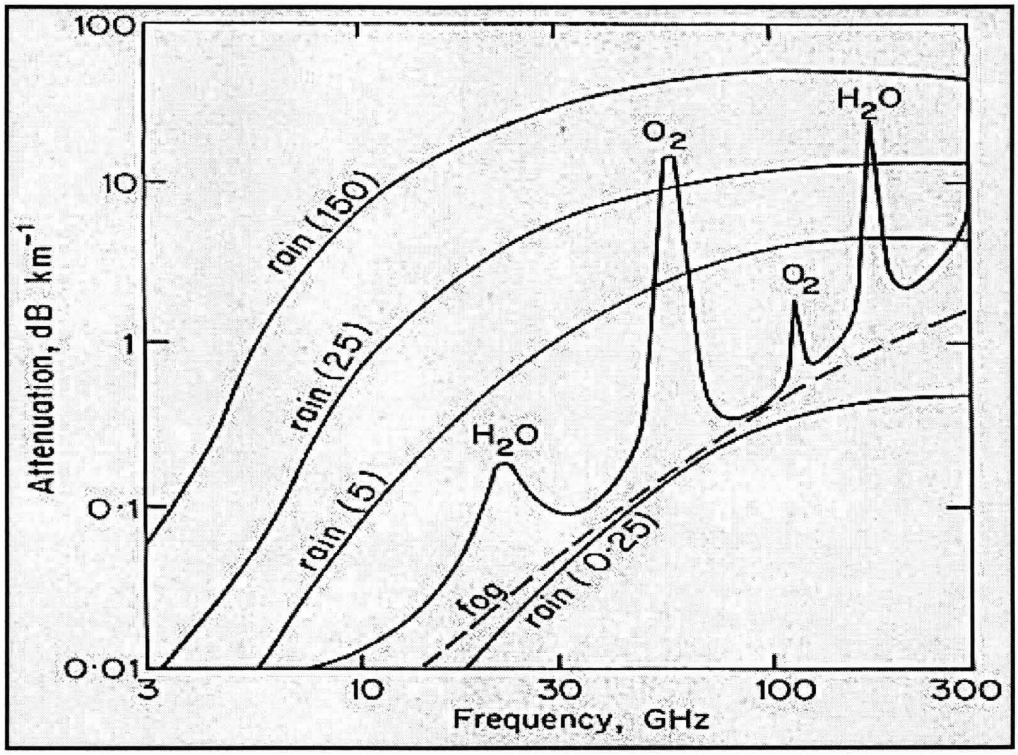

Figure 5.4. Specific Attenuation due to Oxygen absorption at different frequencies [FCC97].

5.2.4 Rain Attenuation Measurements at 38GHz

In this research, in addition to recording more than 1300 PDP data files during clear-sky weather conditions over LOS radio links, PDP data files are also recorded during moderate to heavy rain events. This section presents rain attenuation statistics calculated from as many as 2000 PDP data files, recorded during rain events over an unobstructed 161-meter LOS radio link. The propagation measurement location (Location 3) and general test equipment setup guidelines are, respectively, explained in Chapters 3 and 4. Details related to configuration of Rain Gauge hardware & software, and guidelines for recording rain data are included in Section 4.2.3.

Rain propagation measurements at 38GHz are performed for both horizontal and vertical antenna polarization configurations. The Rain Attenuation, defined as the additional loss of radio signal strength during rain events, is calculated from the recorded PDP data files using the 'Channel

Imaging Analysis Suite'. These statistics, calculated in excess of clear-sky free-space path loss values, are presented separately for horizontal and vertical antenna polarization configurations. The absolute path loss statistics measured during rain events are also tabulated next to rain attenuation values. Table 5.3 presents path loss and rain attenuation values, calculated from PDP data files, for horizontal antenna polarization configuration at 38GHz. Similarly, path loss and excess attenuation values for vertical antenna polarization configuration at 38GHz are tabulated in Table 5.4(a). Note that the path loss values are absolute values, presented in dB.

Table 5.3 Absolute path loss & rain attenuation values at 38GHz *(for Horizontal Polarization).*

LOS Rain Attenuation Measurements at 38GHz (Horizontal Polarization) and (161 meter LOS Radio Link)					
Average Rain Rate (in mm/hr)	**PathLoss (in dB)**	**Rain Atten. (in dB)**	**Average Rain Rate (in mm/hr)**	**PathLoss (in dB)**	**Rain Atten. (in dB)**
	117.36	1.24		117.51	1.39
30.48	117.38	1.26		117.51	1.39
	117.44	1.32	33.1	117.51	1.39
	117.45	1.33		117.65	1.53
	117.45	1.33		117.80	1.68
	117.46	1.34		117.81	1.69
	117.47	1.35		117.81	1.70
	117.47	1.35		117.81	1.70
	117.47	1.35		117.83	1.71
	117.47	1.35		117.83	1.71
	117.48	1.36		117.85	1.73
	117.49	1.37	42.21	118.03	1.91
	117.49	1.37		118.20	2.08
	117.49	1.37		118.20	2.08
	117.49	1.37		118.26	2.14
	117.49	1.37		118.26	2.14
33.1	117.50	1.38	51.8	118.32	2.20

The path loss and rain attenuation values, presented in Tables 5.3 and 5.4, show a clear trend. At lower rain rates, total excess signal attenuation experienced by the propagating electromagnetic (EM) wave is relatively small. With an increase in rain rate, the signal attenuation increases linearly. The receiver subsystem of the channel sounder can accurately record even the slightest fluctuation in the signal strength of the propagating EM waves.

Table 5.4(a) Absolute path loss and rain attenuation values at 38GHz *(for Vertical Polarization).*

LOS Rain Attenuation Measurements at 38GHz (Vertical Polarization) and (161 meter LOS Radio Link)					
Average Rain Rate (in mm/hr)	PathLoss (in dB)	Rain Atten. (in dB)	Average Rain Rate (in mm/hr)	PathLoss (in dB)	Rain Atten. (in dB)
	110.33	0.10		111.77	1.54
	110.43	0.20		111.83	1.60
	110.43	0.20		111.83	1.60
3.81	110.47	0.24		111.86	1.63
	111.26	1.03		111.86	1.63
	111.44	1.21		111.86	1.63
	111.47	1.24		111.86	1.63
	111.49	1.26	37.34	111.86	1.63
	111.52	1.29		112.02	1.79
30.48	111.56	1.33		112.05	1.82
	111.64	1.41		112.07	1.84
	111.73	1.50		112.13	1.90
37.34	111.75	1.52	45.72	112.13	1.90

5.2.4.1 Comparison with Rain Models

In this section, the rain attenuation values, calculated from PDPs files, are compared with rain models described in Section 5.2.3. For a given distance of separation between the transmitting and receiving antennas, Figure 5.5 compares the rain attenuation values (Table 5.3), measured for horizontal polarization configuration, with corresponding values predicted by the Global Attenuation Model for different rain rates. Similarly, Figure 5.6 compares the same set of rain attenuation values (Table 5.3) with the SAM Rain Model. Note that Global Crane Attenuation models for horizontal and vertical polarization configurations are different. Table 5.4(b) presents the values for empirical constants 'a' and 'b' for horizontal and vertical polarization.

Table 5.4(b). Empirical Constants at 38GHz

Antenna Polarization	a	b
Vertical	0.280	0.943
Horizontal	0.315	0.955

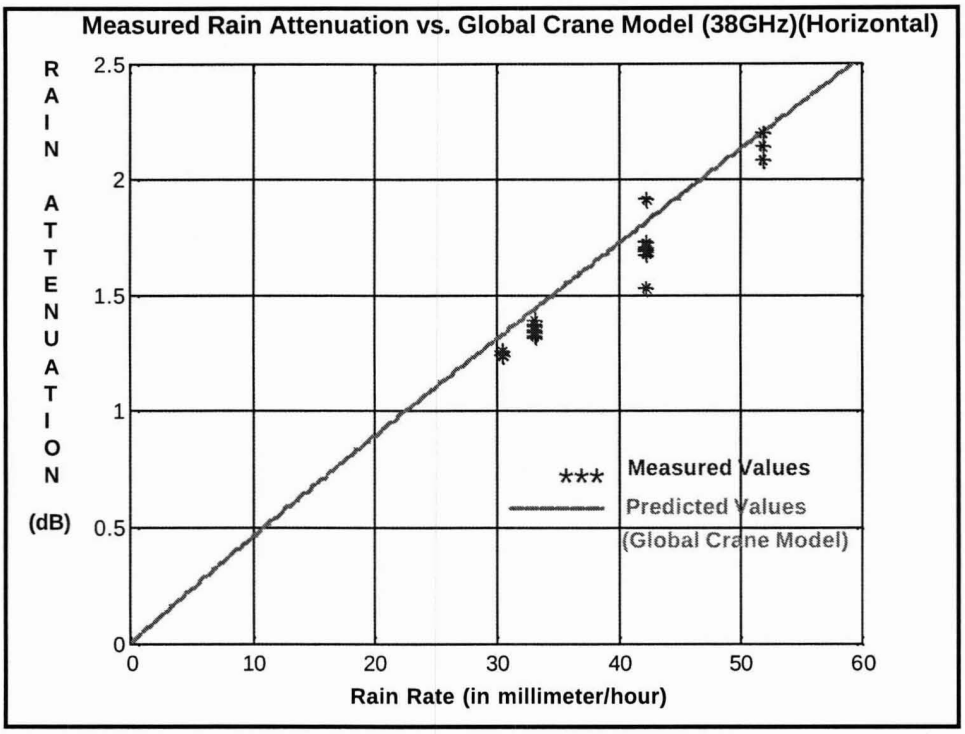

Figure 5.5 Measured Rain Attenuation vs. Global Attenuation Model. (38GHz) (Horizontal)

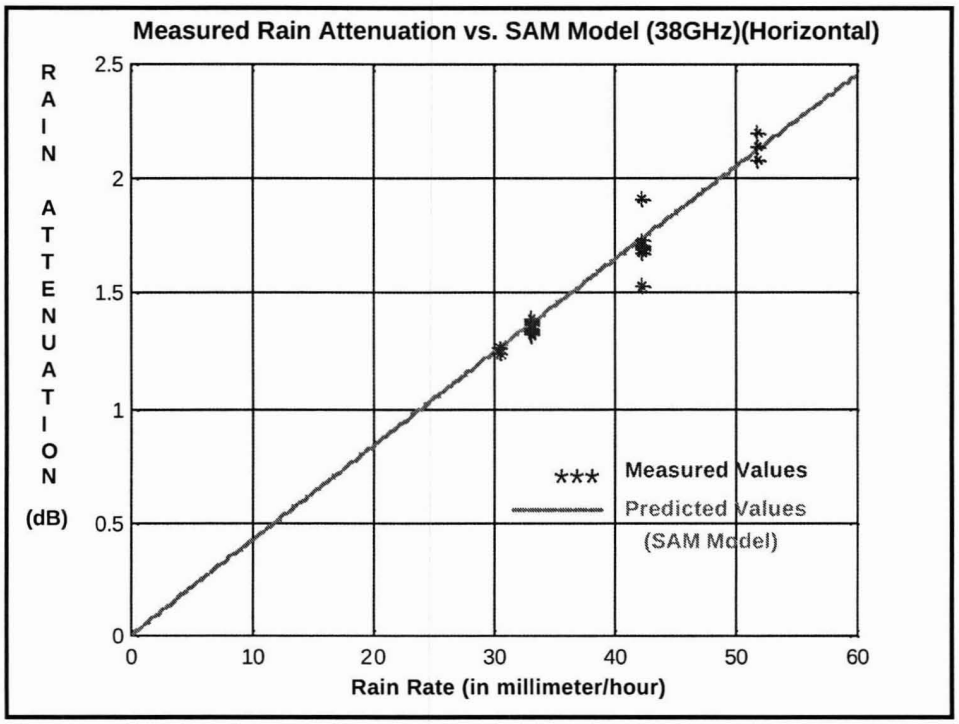

Figure 5.6 Measured Rain Attenuation vs. SAM /CCIR Model. (38GHz) (Horizontal)

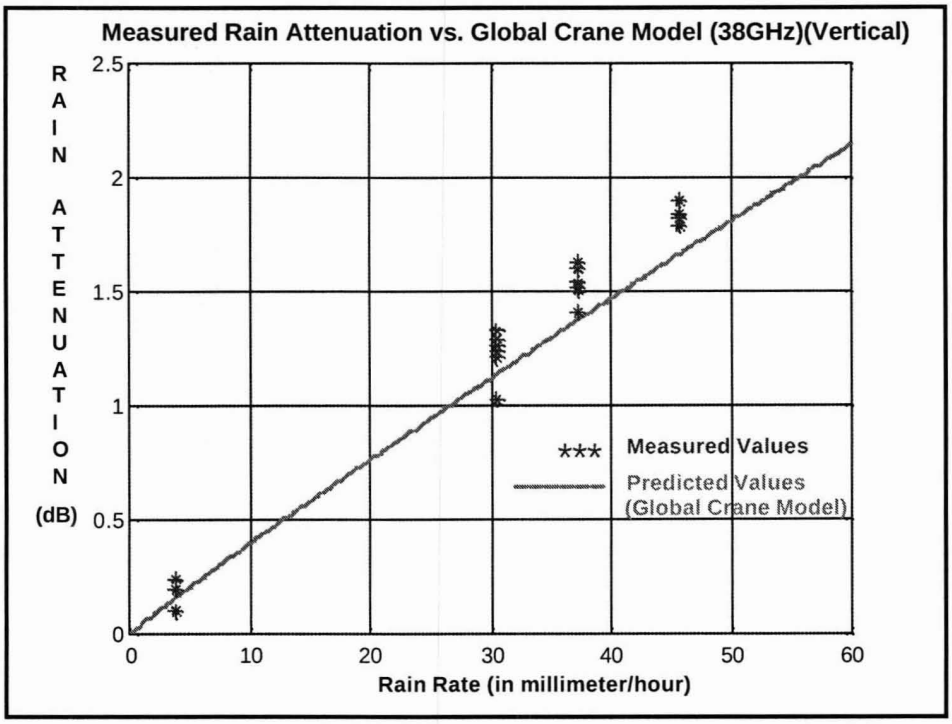

Figure 5.7 Measured Rain Attenuation vs. Global Attenuation Model. (38GHz) (Vertical)

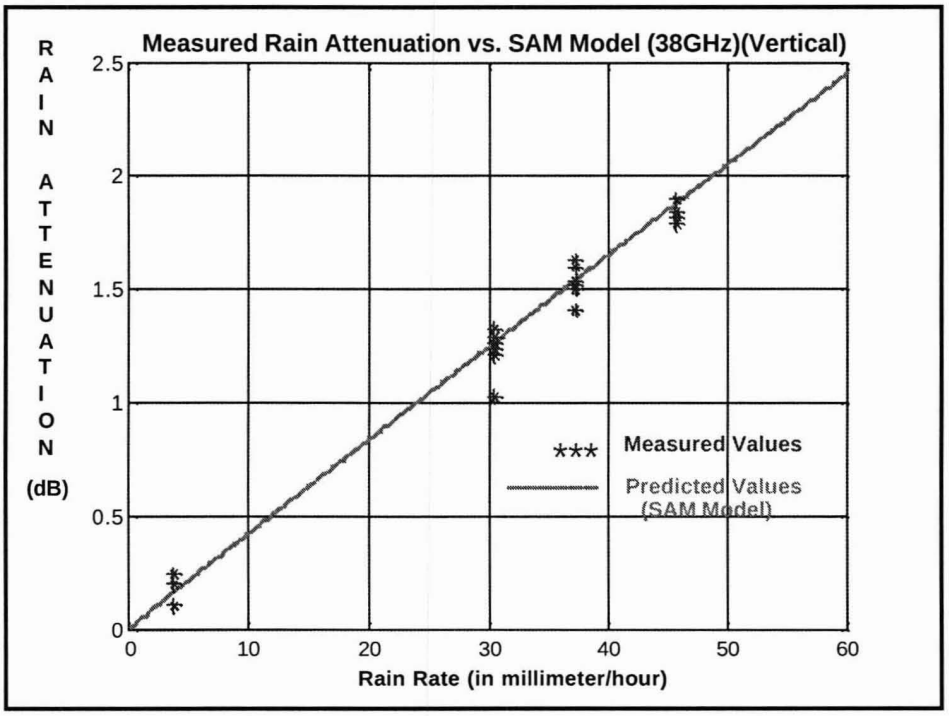

Figure 5.8 Measured Rain Attenuation vs. SAM /CCIR Model. (38GHz) (Vertical Polarization)

The set of expressions from Equation 5.4 through 5.8 completely characterize the Global Rain Attenuation Model. Equations 5.9 through 5.11 facilitate calculation of empirical constant values and the specific attenuation for the SAM/ CCIR Model. Unlike the Crane Model, the empirical constant values for horizontal and vertically polarized electromagnetic waves remain the same for the SAM Model. In other words, there are no separate SDAM Models for propagating electromagnetic waves that have different polarizations. In Figures 5.7 and 5.8, measured rain attenuation values (Table 5.4(a)) for vertical antenna polarization configurations are compared with values predicted by the Global Crane Model and the SAM Model, respectively.

From Figures 5.6 and 5.8, it is evident that the measured rain attenuation values, for horizontal and vertical antenna polarization configurations, are in close agreement with the corresponding attenuation values predicted by the SAM/ CCIR Attenuation Model. Note that for this model, the values of the empirical constants are independent of the antenna polarizations. Consequently, it can be inferred from Figures 5.6 and 5.8 that rain attenuation experienced by horizontally or vertically polarized waves is almost the same for pico-cell radio links. Figure 5.5 indicates that the Global Crane model for horizontal polarization tends to overestimate rain attenuation at low and moderate rain levels over pico-cell radio links. On the other hand, the Global Crane model for vertical polarization tends to underestimate the rain attenuation values. However, in either case, the difference between the measured rain attenuation values and the predicted values is at the most half a decibel (dB).

5.2.5 Rain Attenuation Measurements at 60GHz

As mentioned before, rain attenuation statistics are calculated from the recorded PDP data files using the 'Channel Imaging Analysis Suite'. This section presents rain attenuation values calculated from PDP data files recorded at 60GHz during moderate to heavy rain events. In this research, due to hardware limitations of the channel sounding equipment, only vertical antenna polarization PDP measurements are performed at 60GHz. The respective absolute path loss and rain attenuation values from recorded PDP data files are included in Table 5.5. The statistics

from Table 5.5 clearly indicate a linear increase in path loss values and rain attenuation values with increase in rain rate. The rain attenuation is as high as 3.5dB during heavy rain events with rain rates on the order of 60 mm/hr. The highest recorded rain attenuation value is 3.90dB for a rain rate of 76.20 mm/hr.

Table 5.5 Absolute path loss and rain attenuation values at 60GHz *(for Vertical Polarization)*.

LOS Rain Attenuation Measurements at 60GHz (Vertical Polarization) and (161 meter LOS Radio Link)		
Average Rain Rate (in mm/hr)	**PathLoss (in dB)**	**Rain Atten. (in dB)**
	115.61	0.28
7.62	115.98	0.65
	116.77	1.44
	116.89	1.56
	116.92	1.59
	116.93	1.60
	116.96	1.63
	117.00	1.67
	117.01	1.68
24.76	117.03	1.70
	117.77	2.44
	118.14	2.81
45.72	118.21	2.88
	118.39	3.06
	118.41	3.08
	118.59	3.26
	118.70	3.37
54.86	118.76	3.43
76.20	119.30	3.97

5.2.5.1 Comparison with Rain Models

The statistics presented in Table 5.5 are compared with the values predicted by the Global Crane Attenuation Model and the Simplified Attenuation (SAM/ CCIR) Model. Figure 5.9 compares the rain attenuation values presented in Table 5.5 for vertical antenna polarization measurements at 60GHz with the corresponding predicted values from the Global Crane Attenuation Model. Similarly, in Figure 5.10, the rain attenuation values are compared with values predicted by the SAM/ CCIR Model.

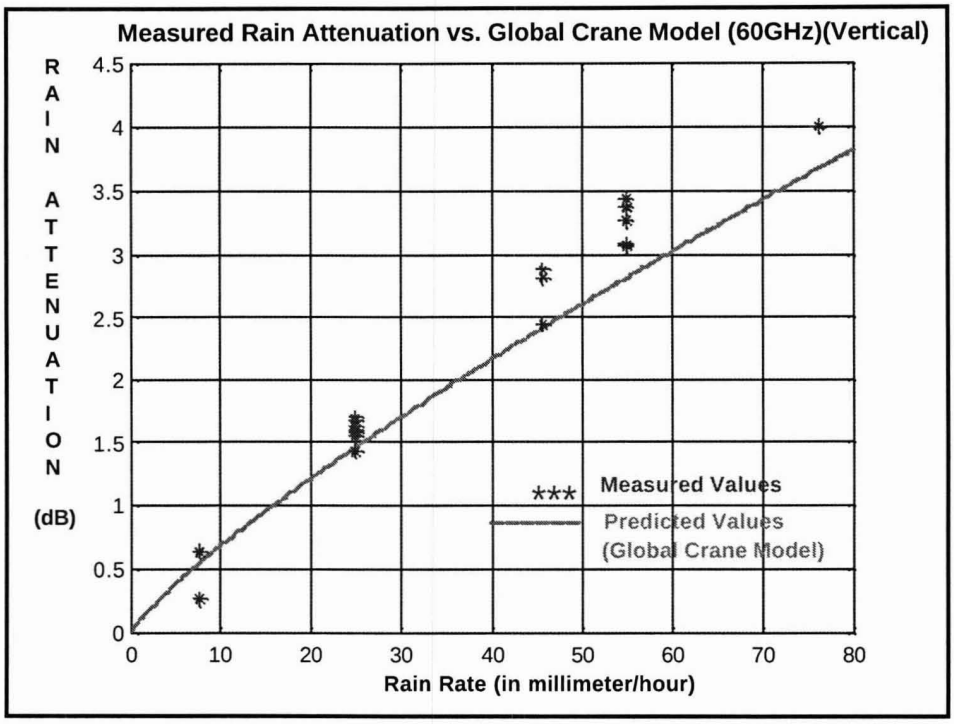

Figure 5.9 Measured Rain Attenuation vs. Global Attenuation Model. (60GHz) (Vertical)

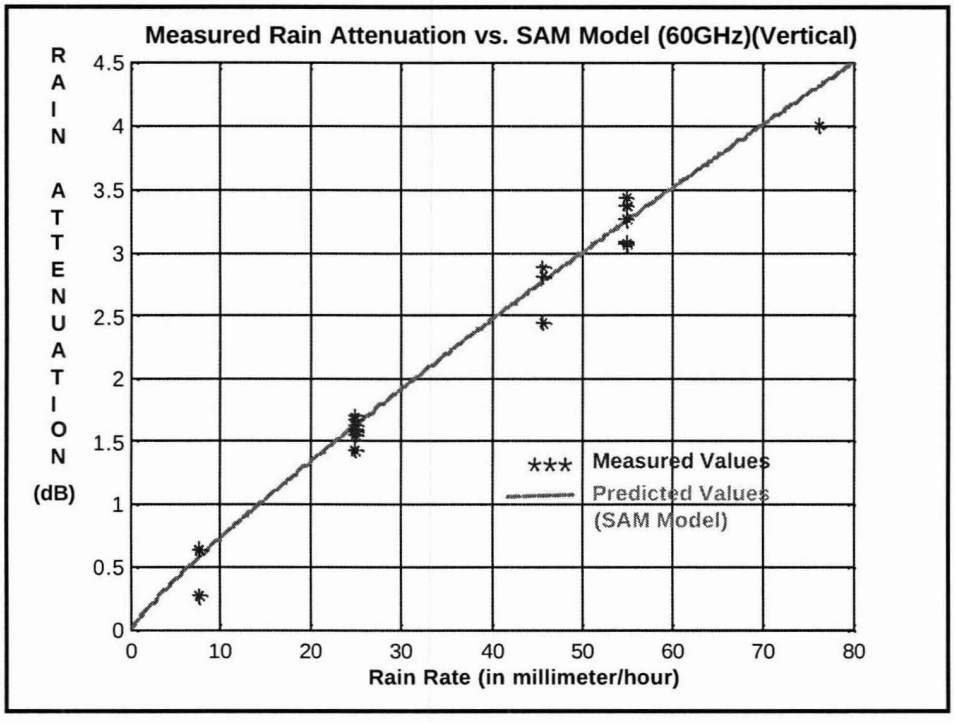

Figure 5.10 Measured Rain Attenuation vs. SAM /CCIR Model. (38GHz) (Vertical Polarization)

For Global Crane Model, the values of empirical constants, 'a' and 'b' are 0.642 and 0.824, respectively, for vertical polarization and 60GHz operational frequency. For the SAM Model, the values of empirical constants are calculated from Equations 5.10 and 5.11. Comparison of measured rain attenuation values with values predicted by Crane and SAM Models indicates that both models propose rain attenuation values that are appreciably close to the actual measured values. However, the SAM/ CCIR Model serves as a better fit for the values as compared to the Global Crane Model. The measured rain attenuation values are almost in complete agreement with the predicted rain attenuation values of the SAM Model. The Crane Model, on the other hand, tends to underestimate the rain attenuation values by a small fraction. The difference between average rain attenuation values and the values predicted by the Global Crane Model is less than 0.5 dB.

5.3 Frequency Diversity Measurement Results

In this research, Frequency Diversity propagation measurements are performed at 38GHz and 60GHz bands of frequencies. In these measurement campaigns, performed at Locations 1 and 2 during clear-sky conditions, Power Delay Profile (PDP) data files are recorded to capture path loss statistics at 12 different frequencies in the 38GHz and 60GHz frequency band. The carrier frequencies used during frequency-diversity propagation measurements at 38GHz and 60GHz are respectively presented in Tables 5.6 and 5.7.

The Sliding Correlator Channel Sounder was designed and developed for operation at 37.8GHz and 59.4GHz carrier frequencies. However, as mentioned above, during frequency diversity propagation measurements, the channel sounder is operated at as many as 24 different carrier frequencies. In order to completely verify and quantitatively characterize the functioning of the channel sounder, it is vital to perform calibration measurements at all the carrier frequencies of interest. Details relevant to these measurement campaigns are introduced in Section 2.3 while Chapter 3 elaborates on the back-to-back as well as the free-space (FS) calibration measurement sequences. Underlying concepts and relevant equations are elaborately explained in Chapter 3.

5.3.1 Frequency Diversity Measurements at 38GHz

These measurements are performed during clear-sky weather conditions over unobstructed LOS radio links that are 531 and 418 meters long. The path loss values calculated from PDP data files recorded at each of the 12 different carrier frequencies in the 38GHz frequency band are presented in Table 5.6. The primary reason for performing FS calibration measurements at all carrier frequencies is to be able to record any non-uniform gain behavior of the channel sounder front end at these frequencies of interest. The path loss statistics recorded to each carrier frequency must be compared with each other in order to evaluate the performance of the channel sounding system over a pico-cell scenario radio link operated at different carrier frequencies. However, at the same time it is necessary to discount any non-uniform gain behavior of the channel sounder front end from the path loss values measured at different carrier frequencies, before these statistics may be compared. This is achieved by manipulating measured absolute path loss statistics at different carrier frequencies to propose path loss values that are relative to corresponding FS calibration path loss values. The path loss statistics hence derived are largely independent of the non-uniform gain behavior of the channel sounder front end. The underlying concept and relevant mathematical equations are included in Chapter 3.

Table 5.6 Frequency Diversity relative path loss statistics at 38GHz frequency band.

Frequency Diversity Measurements at 38GHz frequency band (relative to FS calibration path loss value for 4m free-space LOS radio link)		
Propagation Frequency values (in GHz)	**Location 1 (531m) Relative Path Loss values (in dB)**	**Location 2 (418m) Relative Path loss values (in dB)**
37.2		43.80
37.3		44.00
37.4		43.66
37.5	44.37	43.80
37.6	44.31	43.79
37.7	44.63	43.81
37.8	44.74	43.82
37.9	44.77	44.20
38.0	44.59	44.03
38.1	44.80	44.11
38.2	44.88	44.29
38.3		44.20

Accordingly, the path loss values in Table 5.6 are presented relative to free-space (FS) calibration path loss over a 4 m free-space radio link. These values are also presented in a graphical format in Figure 5.11.

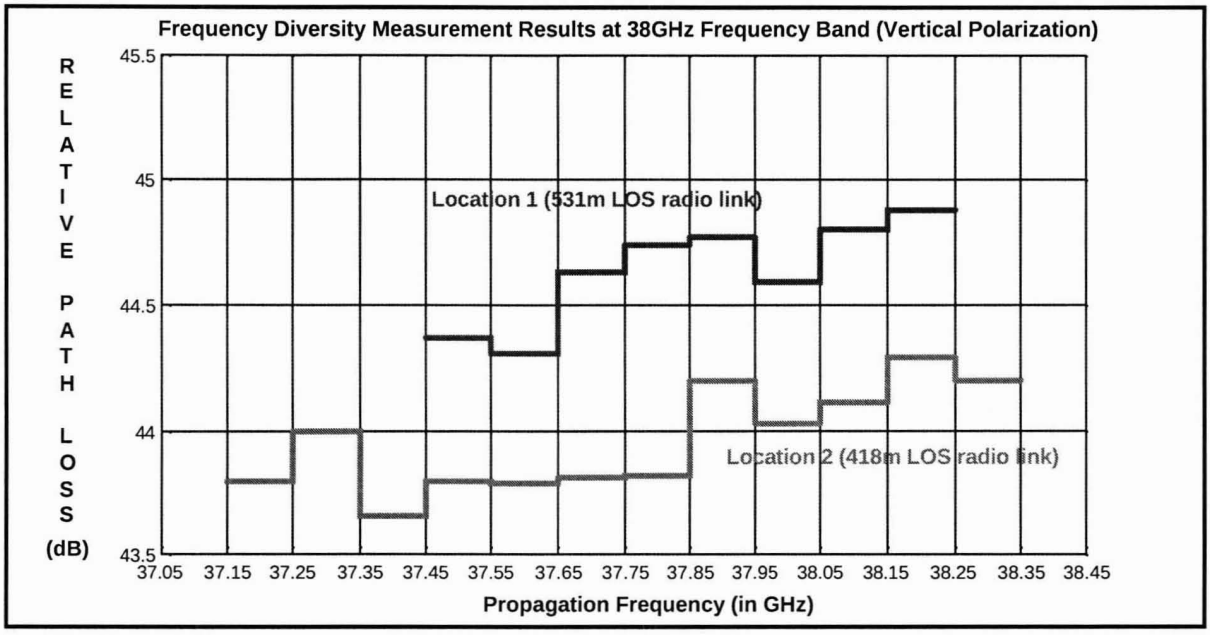

Figure 5.11 Plot of Frequency Diversity relative path loss measurements recorded during clear-sky conditions at 38GHz frequency band for vertical polarization configuration.

The relative path loss statistics, calculated from Frequency Diversity measurements at 38GHz band of frequencies, indicate that the received signal power is fairly constant at all 12 carrier frequencies. The maximum difference between received signal power levels at all carrier frequencies is limited to 0.5 dB. This is expected because the channel sounding hardware makes use of highly directional antennas and these propagation measurements are performed over unobstructed LOS radio links. Consequently, all reflected multipath components are discounted at the receiver. In the absence of any multipath component at the receiver, frequency diversity effects could not be recorded. In a multipath rich LOS environment, frequency selectivity at LMDS band of frequencies usually introduces signal fades on the order of 4 to 6dB. For a NLOS environment, signal fading due to multipath components may be as high as 8dB [Cor94_1].

5.3.2 Frequency Diversity Measurements at 60GHz

This section presents measurements performed at different carrier frequencies in the 60GHz frequency band during clear-sky weather conditions and vertical antenna polarization. As in the previous case, measurements are performed over unobstructed LOS radio links that are 531 and 418 meters long. The path loss values calculated from PDP data files recorded at each of the 12 carrier frequencies in the 60GHz frequency band are presented in Table 5.7. Note that the path loss values presented in Table 5.7 are relative to free-space (FS) calibration distance of 4 meters. Figure 5.12 presented the relative path loss statistics from Table 5.7 in a graphical format.

Table 5.7 Frequency Diversity relative path loss statistics at 60GHz frequency band.

Frequency Diversity Measurements at 60GHz frequency band (relative to FS calibration path loss value for 4m FS LOS radio link)		
Propagation Frequency values (in GHz)	**Location 1 (531m) Relative Path Loss Values (in dB)**	**Location 2 (418m) Relative Path loss Values (in dB)**
58.8	51.93	46.76
58.9	51.81	46.73
59.0	51.68	46.37
59.1	51.32	46.41
59.2	51.27	46.40
59.3	51.20	46.19
59.4	51.22	46.17
59.5	51.70	46.36
59.6	51.29	46.30
59.7	51.38	46.30
59.8	51.36	46.61
59.9	51.63	46.69

As expected for an unobstructed LOS radio link with extremely directional antennas, frequency diversity measurements performed at 60GHz band of frequencies do not exhibit any frequency selectivity in the absence of multipath components. The maximum difference between received signal power level at all carrier frequencies is limited to 0.7 dB as shown in Figure 5.11.

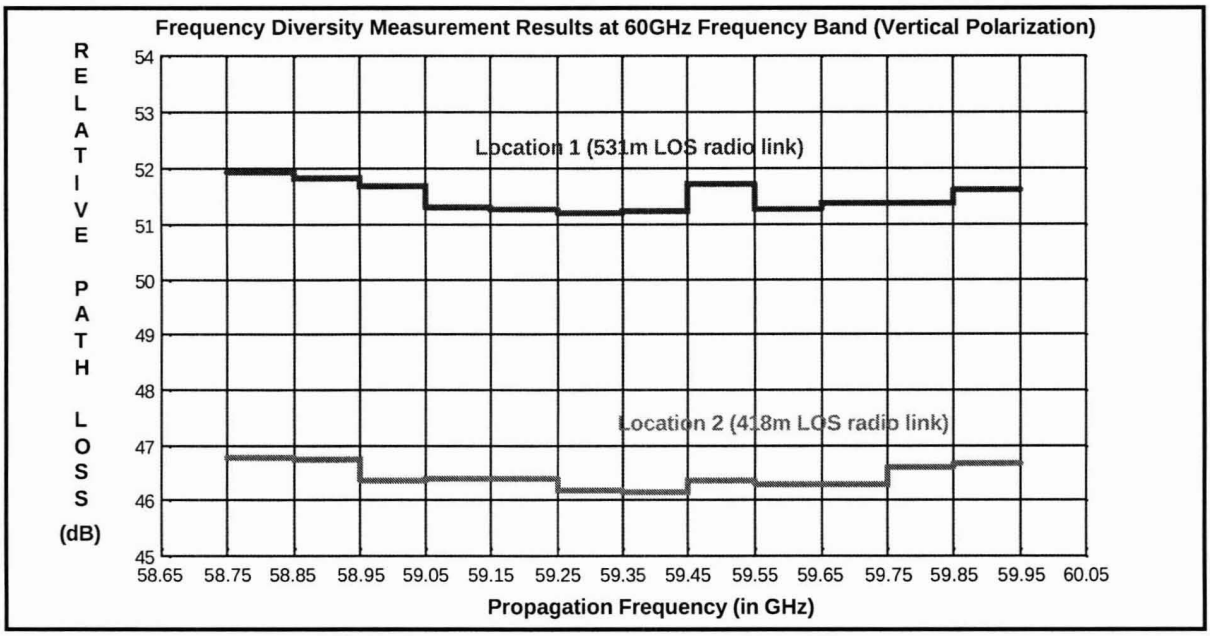

Figure 5.12 Plot of Frequency Diversity relative path loss values measured during clear-sky conditions at 60GHz frequency band.

5.4 Summary

The dissertation primarily focuses on radio wave propagation measurements performed at millimeter-wave frequencies. Extensive Power Delay Profile (PDP) measurements were recorded over three cross-campus radio links at 38GHz frequency band for Local Multipoint Distribution Service (LMDS) applications, and at 60GHz frequency band for Next Generation Internet (NGI) applications. These wideband propagation measurement campaigns, planned and executed as a part of this research, served two purposes. First, the PDP data recorded at different measurement locations reveal basic path loss characteristics of a wideband wireless channel during clear-sky and rain weather conditions. Additionally, the measurement campaign successfully verified the functionality of the channel sounder hardware and validated the 'Channel Imaging and Analysis Suite' software used for PDP data processing.

Local Multipoint Distribution Services (LMDS) are bound to play an important role as the underlying technology for Next Generation Wireless Internet systems. A technological overview

on LMDS systems is presented in Chapter 1. Free Space Optics (FSO) is another promising technology that can revolutionize the high-speed wireless networking world. The chapter also provides an introduction to the FSO technology, and explicit details related to system network architecture and atmospheric propagation issues. Significance of broadband wireless networks for Next Generation Internet (NGI) application is also discussed.

In Chapter 2, fundamentals of radio propagation mechanisms are discussed. Impairments to radio propagation, path loss models, small-scale fading, and free-space mm-wave propagation issues are some of the key aspects included in the discussion. Effects of rain on radio wave propagation and popular rain attenuation prediction models are also addressed. The second part of the chapter presents an extensive literature survey on outdoor mm-wave propagation measurements performed at 38GHz and 60GHz frequency bands.

A wideband direct-sequence spread spectrum (DSS) channel sounding system that is extensively used throughout the measurement campaigns is presented in Chapter 3. In addition to discussing the operation of the channel sounder hardware and significance of various test equipment, relevant details of the transmitting and receiving antennas (operating at 38GHz and 60GHz) used in measurement campaigns are also included. The significance and relevance of calibration measurements are explained in detail. Finally, the chapter presents a technical analysis of the elaborate calibration process and its applicability in the end-to-end link budget analysis.

Chapter 4 describes the hardware, methodology and logistics of all propagation measurement campaigns executed in this research. A comprehensive measurement plan for actual fieldwork during propagation measurements is presented. The measurement plan documents comprehensive details of the three point-to-point wireless links, chosen for propagation measurement campaigns. In addition, the measurement plan elaborates on the sequence of calibration and propagation measurements performed to record Power Delay Profile (PDP) statistics during different weather events. The second half of the chapter elaborates on the rain gauge setup and real-time rainfall recording. Significance of strict time synchronization between propagation measurements and weather monitoring software are also explained.

PDP data recorded during Path Loss measurement campaigns and Frequency Diversity measurement campaigns are presented in Chapter 5. The data files from measurement campaigns are thoroughly analyzed using the 'Channel Imaging Analysis Suite' and calculated Path Loss and Rain Attenuation statistics are discussed. Path Loss Exponent values are calculated for PDP measurements recorded during clear-sky conditions at 38GHz and 60GHz over all radio links. Rain Attenuation values, calculated from relevant PDP data files, are tabulated and compared with popular rain models. Results from Frequency Diversity measurement campaigns are also presented.

Verification and validation of the 'Channel Imaging Analysis Suite' was an important part of this research. The functionality and underlying computational logic of the post-processing software is explained in detail in Appendix A. In addition to a basic introduction to the operation of the data conversion and analysis software, graphical user interfaces (GUI's) that can be used to process the recorded data, are explained.

RADIO SCIENCE, VOL. 42, RS5006, doi:10.1029/2007RS003618, 2007

Rain attenuation prediction and modeling for line-of-sight links on terrestrial paths in South Africa

M. O. Fashuyi[1] and T. J. Afullo[1]

Received 3 January 2007; revised 6 July 2007; accepted 30 July 2007; published 20 October 2007.

[1] The different rain attenuation prediction models proposed by different authors on terrestrial paths are studied in this paper. Subsequently, for paths not exceeding 22 km, the rain attenuation exceeded for 0.01% of the time for these four geographical locations is estimated for South Africa using the ITU-R Model, the Crane Global model, and the Moupfouma model, at different frequencies. Finally, the predicted attenuation values are compared on a monthly basis, as well with the measured upper and lower attenuation bounds for a 6.73-km line-of-sight link operating at 19.5 GHz in Durban.

Citation: Fashuyi, M. O., and T. J. Afullo (2007), Rain attenuation prediction and modeling for line-of-sight links on terrestrial paths in South Africa, *Radio Sci.*, *42*, RS5006, doi:10.1029/2007RS003618.

1. Introduction

[2] Rainfall is a natural and time varying phenomenon that varies from location-to-location and from year-to-year. Above a certain threshold of frequency, attenuation due to rainfall becomes one of the most important limits of the performance of line-of-sight (LOS) microwave links [*Moupfouma*, 1984; *Green*, 2004]. In the temperate climates this frequency threshold is about 10 GHz, while in the tropical climates and in equatorial climate particularly, the incidence of rainfall on radio links becomes important for frequencies as low as about 7 GHz, since raindrops are larger than in the temperate climate [*Moupfouma*, 1984; *Moupfouma and Tiffon*, 1982]. Therefore, in the planning of terrestrial line-of sight systems, accurate prediction of rain induced attenuation on propagation paths is vital [*Segal*, 1986].

[3] The estimate of rain attenuation on terrestrial radio path is usually derived from observed rain rates in the geographical area considered [*Moupfouma*, 1984; *Ajayi et al.*, 1996]. Most of the methods proposed for predicting rain induced attenuation make use of the rainfall cumulative distribution measured at a point [*Moupfouma*, 1984]. Certain authors have used the concept of equivalent path average rain rate which is obtained by multiplying the point rain rate for the time percentage of interest by a reduction factor, while other authors use an effective path length, the value of which is obtained by multiplying the actual path length by a reduction coefficient [*Moupfouma*, 1984].

[4] In our previous paper [*Fashuyi et al.*, 2006], the cumulative distribution of rainfall-rate in South Africa has been estimated using 1-hour rainfall rate statistics measured by the South African Weather Services (SAWS) in different climatic regions for the years 2000–2004 for 12 different meteorological stations. This data has been processed and converted to the ITU-R recommended integration time of 1-minute for Durban [*Fashuyi et al.*, 2006].

[5] For the purpose of this paper, three established attenuation models have been utilized for the prediction of rain attenuation in South Africa. These are: the ITU-R model, the Crane Global model, and the Moupfouma model. This is effected by using $R_{0.01}$, defined as the rain rate value that is exceeded in a region only 0.01% of the time, with a 1-minute integration time, averaged over a period of 5-years, for the different geographical locations in South Africa (Table 1).

2. Specific Rain Attenuation

[6] A fundamental quantity in the calculation of rain attenuation statistics for terrestrial and earth-space paths is the specific attenuation γ or attenuation per unit distance [*Olsen et al.*, 1978]. Two general approaches have been used to calculate γ by various authors: (1) a theoretical method employing a uniform distribution of raindrops modeled as water spheres or more complex shapes; and (2) an empirical procedure based on the approximate relation between γ and rain rate R given as [*Olsen et al.*, 1978]:

$$\gamma = kR^{\alpha} \tag{1}$$

[1]School of Electrical, Electronic, and Computer Engineering, University of KwaZulu-Natal, Durban, South Africa.

Copyright 2007 by the American Geophysical Union.
0048-6604/07/2007RS003618

Table 1. Annual and Averaged $R_{0.01}$ Statistics for Each Geographical Location

Location	2000, mm/h	2001, mm/h	2002, mm/h	2003, mm/h	2004, mm/h	2000–2004, mm/h	ITU-R P.837-1, mm/h	ITU-R P.837-4, mm/h
Durban	108.75	88.82	138.83	139.66	121.84	119.58	95	63
Cape Town	47.7	69.96	57.03	44.5	87.04	61.25	22	25
Pretoria	159.45	114.90	100.73	106.09	113.15	118.86	42	50
Brandvlei	41.25	105.2	67.02	13.67	42.34	53.90	19	20

Equation (1) is known as the power-law form of rain specific attenuation [*Zhang and Moayeri*, 1999], where R is the rain rate in mm/h, k and α are power law parameters, which depend on frequency, raindrop size distribution, rain temperature, and polarization. This form is the method adopted in this paper to compute the specific attenuation. Values for k and α for the frequency range 1–400 GHz were calculated for raindrops with the assumed shape of oblate spheroids, at the temperature of 20°, using the drop size distribution proposed by *Laws and Parsons* [1943], terminal velocity following *Gunn and Kinzer* [1949], and refractive index values according to the model of Ray. These values were adopted by the ITU-R recommendation 838-2 [*ITU-R*, 2003].

[7] To find the total path attenuation due to rain, it is necessary to know the specific attenuation or the rain rate exceeded for the percentage of time of interest and the raindrop size distribution upon which the coefficient k and α depend [*Ajayi et al.*, 1996].

3. Existing Attenuation Prediction Models

3.1. ITU-R Rain Attenuation Model

[8] The ITU-R P.530-10 [*ITU-R*, 2001] gives a simple technique that may be used for estimating the long-term statistics of rain attenuation. The path attenuation is obtained from:

$$A_{0.01} = \gamma_R d_{eff} = \gamma_R r d \quad dB \tag{2}$$

Here d_{eff} is the effective path length of the link by multiplying the actual path length d by a distance factor r, given by:

$$d_{eff} = rd \tag{3}$$

r is a factor which reduces in magnitude as d increases. It is given by:

$$r = \frac{1}{1 + d/d_0} \tag{4}$$

d_0 is a rainfall-rate-dependent factor, introduced to reflect the fact that the greater the intensity of rainfall in a storm, the smaller the physical dimensions of the storm are. It is given by [*ITU-R*, 2001; *Hall et al.*, 1996; *Pozar*, 1988]:

$$d_0 = 35e^{-0.015}R_{0.01} \tag{5}$$

This is valid for $R_{0.01} \leq 100$ mm/h. For $R_{0.01} > 100$ mm/h, the value 100 mm/h is used in place of $R_{0.01}$. The prediction procedure outlined above is considered to be valid in all parts of the world at least for frequencies up to 40 GHz and path lengths up to 60 km.

3.2. Moupfouma Rain Attenuation Model

[9] *Moupfouma* [1984] proposed an empirical model for predicting rain-induced attenuation on terrestrial paths from the knowledge of 1-minute rain intensities recorded in a broad range of geographical areas and the corresponding percentages of time p during which these rain rates are exceeded. The rain induced attenuation on a line-of-sight path can be expressed as [*Moupfouma*, 1984]:

$$A(dB) = kR^{\alpha}d_{eff} \tag{6}$$

with d (km) the actual path length, d_{eff} the effective path length, and r a reduction factor coefficient, here taking the form:

$$d_{eff} = rd \tag{7}$$

$$r = \frac{1}{1 + Cd^m} \tag{8}$$

The attenuation $A(dB)$ and the 1-min rain rate R (mm/h) are calculated for the same time percentage, k and α are the regression coefficients depending on frequency and polarization. To derive C and m, experimental data obtained were used. It was found that C depends on probability level p (in percentage) of interest for which data are available, and m depends on the radio link path length and its frequency. The resultant formula for the path length reduction factor is given by:

$$r = \frac{1}{1 + 0.03\left(\frac{p}{0.01}\right)^{-\beta}d^m} \tag{9}$$

19447799x, 2007, 5, Downloaded from https://agupubs.onlinelibrary.wiley.com/doi/10.1029/2007RS003618. By AGU Journals, Wiley Online Library on [02/12/2024]. See the Terms and Conditions (https://onlinelibrary.wiley.com/terms-and-conditions) on Wiley Online Library for rules of use; OA articles are governed by the applicable Creative Commons License

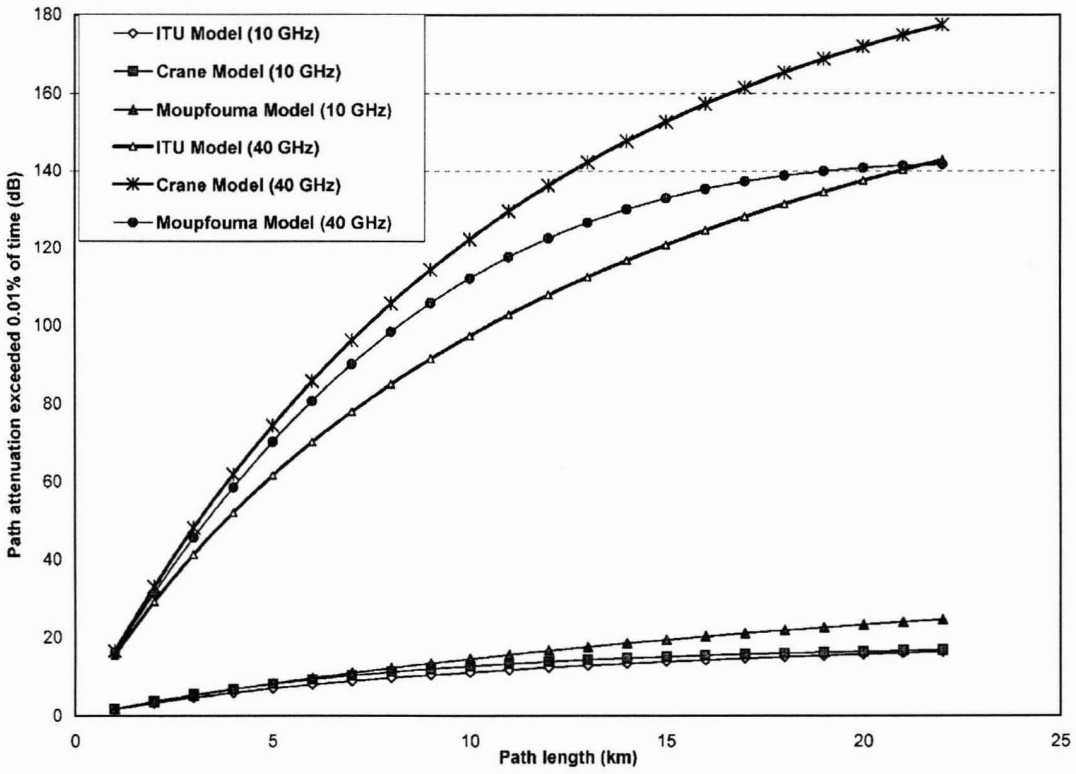

Figure 1. Rain attenuation prediction models for terrestrial line-of-sight links for Cape Town.

with

$$m(F,d) = 1 + \Psi(F)\log_e d \tag{10}$$

$$\Psi(F) = 1.4 \times 10^{-4} F^{1.76} \tag{11}$$

[10] Here F is the frequency in GHz. The β coefficient is given as a result of a best fit by:

$$\left.\begin{array}{l} d < 50 \text{ km} \\ \quad \beta = 0.45 \quad \text{for} \quad 0.001 \le p \le 0.01 \\ \quad \beta = 0.6 \quad \text{for} \quad 0.01 \le p \le 0.1 \\ d \ge 50 \text{ km} \\ \quad \beta = 0.36 \quad \text{for} \quad 0.001 \le p \le 0.01 \\ \quad \beta = 0.6 \quad \text{for} \quad 0.01 \le p \le 0.1 \end{array}\right\} \tag{12}$$

3.3. Crane's Global Rain Attenuation Model

[11] The Crane Global attenuation model was developed for use on either Earth-space or terrestrial paths. It is based entirely on geophysical observations of rain rate, rain structure, and the vertical variation of atmospheric temperature [*Crane*, 1996, 2003]. Rain is characteristically inhomogeneous in the horizontal, and a statistical model is required to provide an estimate of the effect of the homogeneity on the estimation of attenuation [*Crane*, 1996; *De Miranda et al.*, 1998]. Crane accomplished this model by a piecewise representation of the path profile by exponential functions. An adequate model results when two exponential functions are used to span the 0 to 22.5 km distance range, one from 0 to $\delta(R)$ km, the other from $\delta(R)$ to 22.5 km [*Crane*, 1996; *De Miranda et al.*, 1998]. The resulting attenuation model for a given rain rate is given by [*Crane*, 1996]:

$$\begin{aligned} A_T(R,d) &= \gamma(R)\left(\frac{e^{y\delta(R)}-1}{y} + \frac{e^{zd}-e^{y\delta(R)}}{z}e^{\alpha B}\right) \\ &\quad \cdot \delta(R) < d < 22.5 \\ A_T(R,d) &= \gamma(R)\left(\frac{e^{y\delta(R)}-1}{y}\right) \quad 0 < d < \delta(R) \end{aligned} \tag{13}$$

where

A_T = horizontal path attenuation (dB);
R = rain rate (mm/hr);
$\gamma(R)$ = specific attenuation = kR^{α} (*dB*/km).

1944799x, 2007, 5, Downloaded from https://agupubs.onlinelibrary.wiley.com/doi/10.1029/2007RS003618. By AGU Journals, Wiley Online Library on [02/12/2024]. See the Terms and Conditions (https://onlinelibrary.wiley.com/terms-and-conditions) on Wiley Online Library for rules of use; OA articles are governed by the applicable Creative Commons License

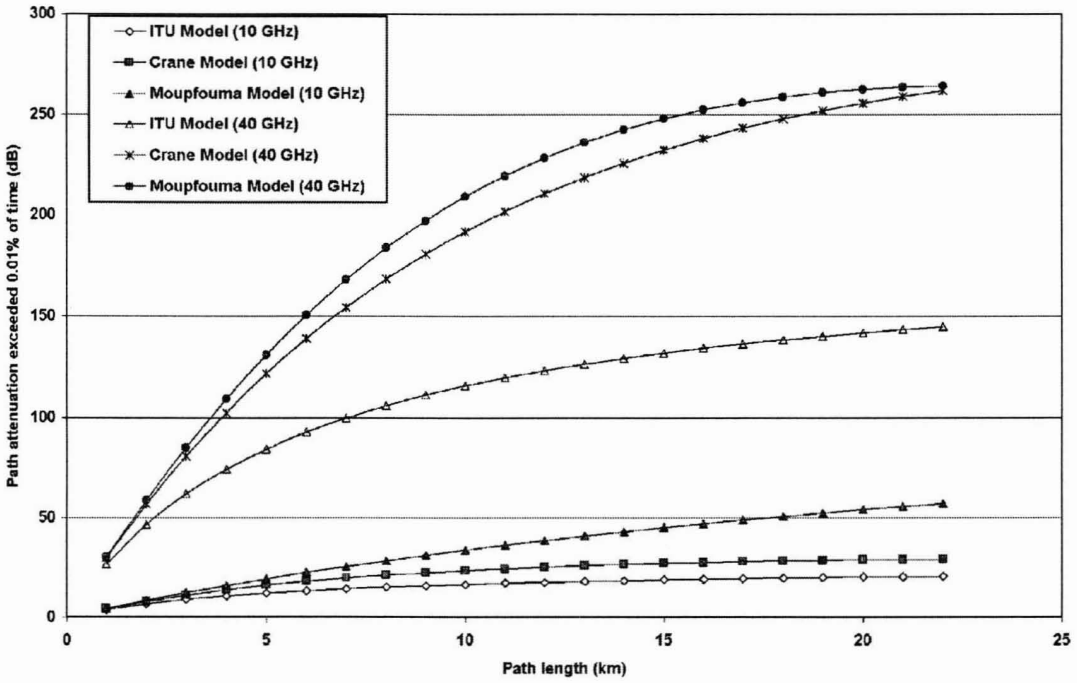

Figure 2. Rain attenuation prediction models for terrestrial line-of-sight links for Pretoria.

The remaining coefficients are the empirical constants of the piecewise exponential model:

$$\left.\begin{aligned} B &= \ln(b) = 0.83 - 0.17\ln(R) \\ c &= 0.026 - 0.03\ln(R) \\ \delta(R) &= 3.8 - 0.6\ln(R) \\ u &= \frac{B}{\delta(R)} + c \\ y &= \alpha u \\ z &= \alpha c \end{aligned}\right\} \quad (14)$$

4. Estimation of Path Attenuation Using Existing Models

[12] The specific rain attenuation predicted for the 4 climatic regions above may not be too adequate for the estimation of attenuation along a radio link path [*Crane*, 1996, 1980]. This is because of the nonuniformity of rain along a radio link and the spatial inhomogeneity present in rain. This makes it unlikely that the reference rainfall rate will extend uniformly over the length of the transmission path, unless this is very short [*ITU-R*, 2001]. The longer the path, the less likely it is that rain will extend over the full length of the path [*Crane*, 1996; *Moupfouma*, 1984; *Crane*, 1980].

[13] In this section, an estimation of the rain induced attenuation on a line-of-sight (LOS) path is calculated using existing models based on the value of $R_{0.01}$. This gives path attenuation $A_{0.01}$ (in dB) for radio path lengths of up to 22 km. This is tested at different frequencies for all the twelve geographical areas [*Fashuyi*, 2006]. In this paper, only a lower frequency of 10 GHz and a higher frequency of 40 GHz will be shown for 4 locations situated at different climatic regions in South Africa. This is to really observe how these models behave at different rain rate values and different frequencies.

[14] Figure 1 shows the plots of rain attenuation for Cape Town. Cape Town is located in Mediterranean region of South Africa with an average $R_{0.01}$ of 61.25 mm/h over a period of 5-years. Out of these three models, the ITU-R model gives the lowest attenuation values at both frequencies (10 GHz and 40 GHz). At 10 GHz, the ITU-R and Crane Global curves get closer as the path length increases while that of Moupfouma increases. Looking at the 40 GHz plots, the Moupfouma model behaves in a different way: as the path length increases, while the ITU-R model and the Moupfouma

1944799x, 2007, 5, Downloaded from https://agupubs.onlinelibrary.wiley.com/doi/10.1029/2007RS003618. By AGU Journals, Wiley Online Library on [02/12/2024]. See the Terms and Conditions (https://onlinelibrary.wiley.com/terms-and-conditions) on Wiley Online Library for rules of use; OA articles are governed by the applicable Creative Commons License

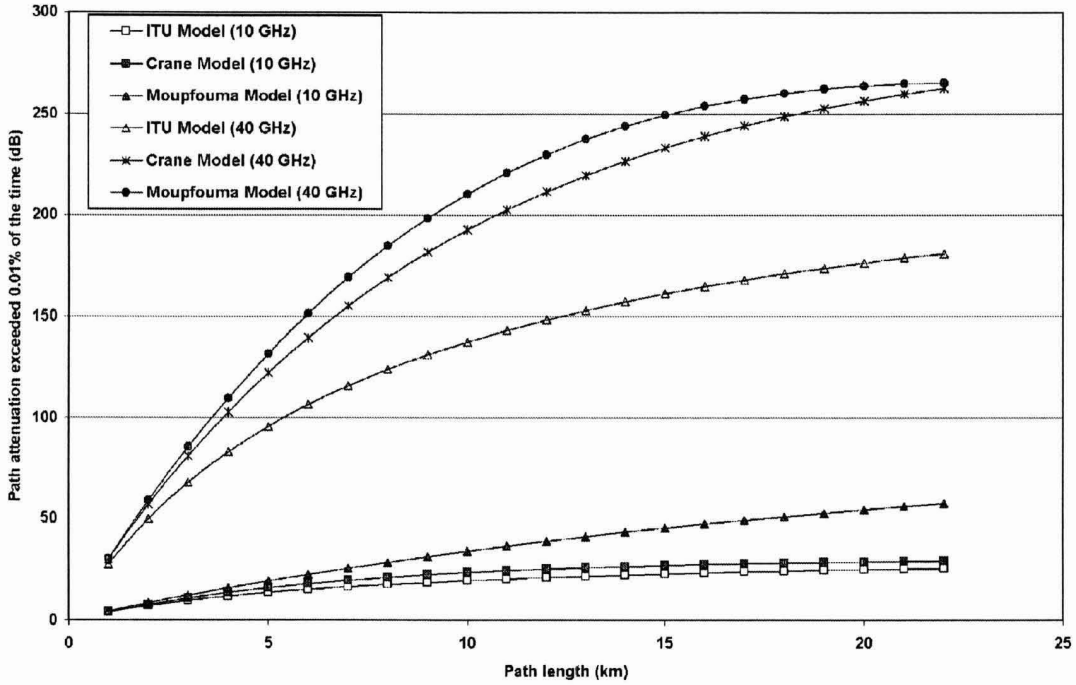

Figure 3. Rain attenuation prediction models for terrestrial line-of-sight links for Durban.

model plots get closer the Crane plot gives the highest rain attenuation along the radio link paths.

[15] Figure 2 shows the $A_{0.01}$ plots for Pretoria, which is situated in the temperate region of South Africa. At 10 GHz and 40 GHz, ITU-R model gives the lowest attenuation values over the propagation path. At 40 GHz, ITU-R attenuation values are still very low as compared to the other two remaining models, while the Moupfouma model gives the highest attenuation values for Pretoria, and the results of the Crane Global model tend to be very close to the Moupfouma model.

[16] Figure 3 shows the attenuation plots for Durban which lies in the Coastal Savannah region of South Africa with an average $R_{0.01}$ of 119.58 mm/h. At both frequencies (10 GHz and 40 GHz), the ITU-R model gives the lowest attenuation values, while the Moupfouma model gives the highest attenuation prediction along the propagation paths. Finally, Figure 4 shows the plots for Brandvlei which is in the desert region of South Africa, with an average $R_{0.01}$ of 53.9 mm/h. At 10 GHz, the ITU-R model gives the lowest attenuation values along the propagation path. The Crane Global model (which tends to give the highest attenuation values here) intersects with that of the Moupfouma model at path lengths of 11 and 12 km, and bends a little bit more downward than that of the Moupfouma plots. At 40 GHz, the Crane Global gives the highest attenuation values along the entire propagation length. The ITU-R model gives the lowest attenuation plots up to a path length of 18 km.

5. Prediction of Rain Attenuation Model for South Africa From Measurements

[17] In this section, the signal attenuation measurements over a period of one year in Durban by *Naicker* [2006] are utilized to model rain attenuation on a terrestrial line-of-sight links in South Africa.

5.1. Link Setup

[18] The line-of-sight link was established between the Howard College and the Westville campuses of the University of KwaZulu-Natal, Durban. The transmitter station was setup on the roof of the Science building at the Westville campus on the azimuth angle of 30.980° and about 178 m above sea level and the receiver station on the roof the Electrical Engineering building at Howard College campus on the azimuth angle of 30.943° and about 145 m above sea level [*Naicker*, 2006; *Naicker and Mneney*, 2006]. These heights were able to provide sufficient clearance for the link. The path clearance from the first Fresnel ellipsoid and the line-of-

19447799x, 2007, 5, Downloaded from https://agupubs.onlinelibrary.wiley.com/doi/10.1029/2007RS003618. By AGU Journals, Wiley Online Library on [02/12/2024]. See the Terms and Conditions (https://onlinelibrary.wiley.com/terms-and-conditions) on Wiley Online Library for rules of use; OA articles are governed by the applicable Creative Commons License

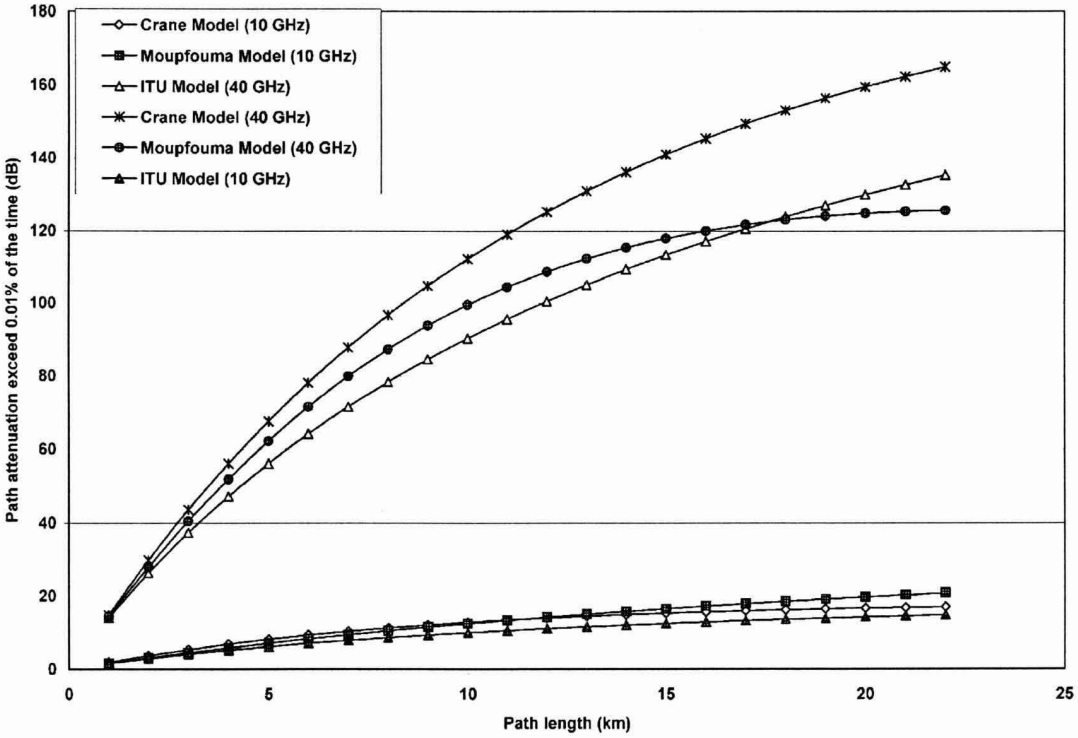

Figure 4. Rain attenuation prediction models for terrestrial line-of-sight links for Brandvlei.

sight path are shown in Figure 5, with an effective earth radius factor value of 4/3.

[19] The link is horizontally polarized and centred at an operating frequency of 19.5 GHz. The length of the link is 6.73 km and two Oregon Scientific WMR928N wireless professional weather stations were used along the path at both the receiver and the transmitter end to record the 1-minute rainfall rate, outdoor temperature, relative outdoor humidity, outdoor dew point temperature, outdoor pressure, wind speed and wind direction under the link [*Naicker*, 2006; *Naicker and Mneney*, 2006].

[20] A valuline® WR42/R220 parabolic antennae of diameter 0.6 m are used at both the receiving and the transmitting stations. The antennae can operate within the 17.7–19.7 GHz and 21.2–23.6 GHz bands and provide a gain of 38.6 dBi and a 3 dB beam width of 1.9 degrees at 19.5 GHz [*Naicker*, 2006; *Naicker and Mneney*, 2006]. These parabolic antennae are protected by a weatherproof material called radome which prevents ice and freezing rain from accumulating directly onto the metal surface of the antenna (see http://en.wikipedia.org/wiki/Radome). (A radome allows a relatively unattenuated electromagnetic signal between the antenna inside the radome and outside equipment.) The cabling consists of FSJ1-50A superflexible coaxial cable which produces an attenuation of 22 dB per 100 m. At the transmitter, an agilent E8251A signal generator is used to provide the source signal and this can operate between 250 KHz-20 GHz. This is used in conjunction with an agilent 83018A microwave system amplifier which can operate from 0.5 GHz to 25 GHz and provide a gain of up to 27 dB (see http://www.home.agilent.com/USeng/nav/-536900735.536879154/pd.html). This setup produces unmodulated continuous wave signals at the operating frequency of 19.5 GHz.

[21] At the receiver, another agilent 83018A power amplifier is used to produce additional gain before feeding the signal into the Rhodes & Schwarz FS1Q40 spectrum analyser. More details on the link setup at the receiver and the transmitter end can be seen in [*Naicker*, 2006; *Naicker and Mneney*, 2006]. The terrestrial link parameters are shown in Table 2.

[22] The expected noise power in the receiver when no signal is transmitted lies between −80.5 to −80.2 dBm. This defines the noise floor. This is determined from the noise temperature of the antenna T_A of 206°K (with an estimated efficiency of 63.4%, equivalent background temperature of 150°K [*Pozar*, 1988], and a maximum physical temperature of 303°K), the transmission line

19447799x, 2007, 5, Downloaded from https://agupubs.onlinelibrary.wiley.com/doi/10.1029/2007RS003618. By AGU Journals, Wiley Online Library on [02/12/2024]. See the Terms and Conditions (https://onlinelibrary.wiley.com/terms-and-conditions) on Wiley Online Library for rules of use; OA articles are governed by the applicable Creative Commons License

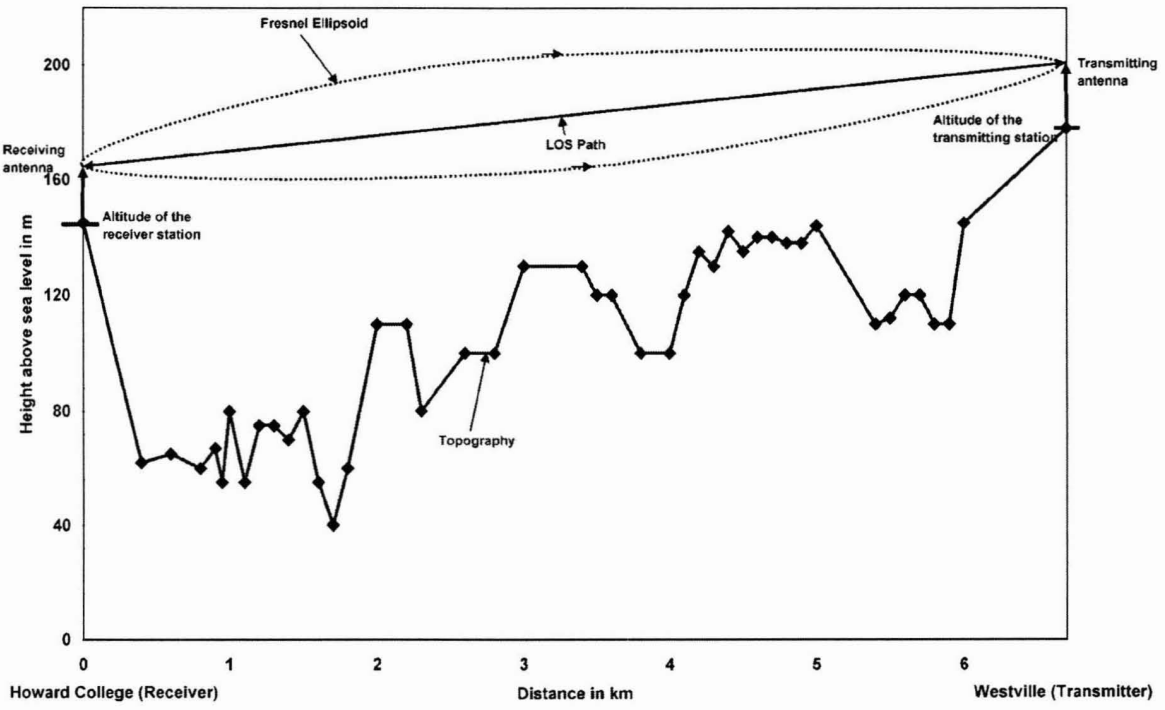

Figure 5. The path profile for the 6.73 km terrestrial line-of-sight link from the Howard College campus to the Westville campus [*Naicker*, 2006; *Naicker and Mneney,* 2006].

noise temperature of 93.4°K (with an attenuation of 22 dB per 100 m); 83018A Agilent Amplifier (with a gain of 27 dB, and noise figure of about 9.5 dB at 19.5 GHz (see http://www.home.agilent.com/USeng/nav/-536900735.536879154/pd.html) with noise temperature of 2398.5°K; thus resulting in total receiver noise temperature of 3470.4°K, or a noise power of −80.2 dBm [*Pozar*, 1988]. At the lower temperature of 287°K, the noise power is −80.5 dBm. In the measurements, this value varied from −79.5 dBm to −82 dBm.

[23] Calculating for the power received P_r we have:

$$\begin{aligned} P_r &= P_t - FSL + G_{rant} + G_{\tan t} - Losses \\ &= 20\ \text{dBm} - 135\ \text{dB} + 38.6\ \text{dBi} \\ &\quad - 2.2\ \text{dB} - 1\ \text{dB} \\ &= -41\ \text{dBm} \end{aligned} \tag{15}$$

where

P_t = Power transmitted (taken as 100 mW = 20 dBm);
FSL = Free space loss;
G_{rant} = Receive antenna gain;
$G_{\tan t}$ = Transmit antenna gain.

Thus the power received P_r expected at the receiver end of the link when a transmitting power of 100 mW is employed between Howard College and Westville campuses should be −41 dBm when there is no rain to cause any rain attenuation.

Table 2. Terrestrial Link Parameters for the LOS SHF System[a]

Parameter	Description
Path length	6.73 km
Height of transmitting antenna above the ground	24 m
Altitude of transmitter station	178 m
Height of receiving antenna above the ground	20 m
Altitude of receiver station	145 m
Carrier frequency	19.5 GHz
Bandwidth under investigation	200 MHz
Transmitting power	10–100 mW
Transmitting/receiver antenna gain	38.6 dBi
Transmitting/receiver antenna beam width[b]	1.9 degrees
Free space loss	135 dBm
Total cabling and connection losses	≈2.2 dB
Clear air attenuation	≈1 dB
Receiver bandwidth	100 kHz–1 GHz

[a]From *Naicker* [2006].

[b]The beam width of an antenna is the angle enclosing the main lobe or twice the angle between the boresight direction and a reference power on the main lobe of the antenna pattern [*Pozar*, 1988].

19447799x, 2007, 5, Downloaded from https://agupubs.onlinelibrary.wiley.com/doi/10.1029/2007RS003618. By AGU Journals, Wiley Online Library on [02/12/2024]. See the Terms and Conditions (https://onlinelibrary.wiley.com/terms-and-conditions) on Wiley Online Library for rules of use; OA articles are governed by the applicable Creative Commons License

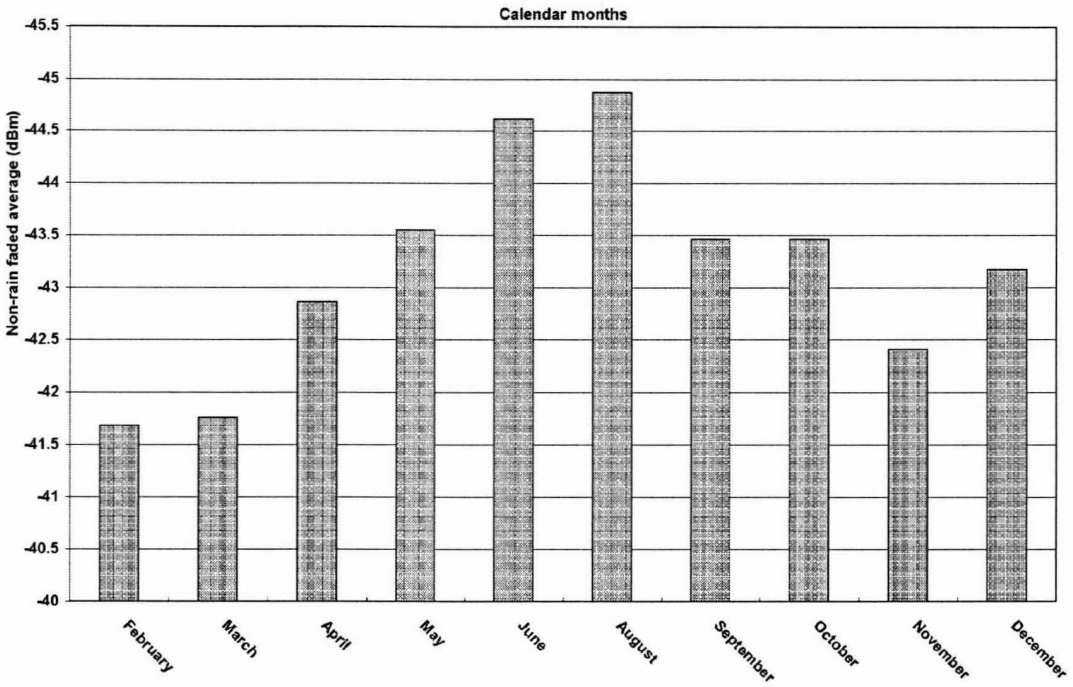

Figure 6. The average nonrain faded signal values for 10 months in 2004.

5.2. Rain Rate and Signal Level Measurements Recorded Along the 6.73 km Link

[24] The signal level measurement and its corresponding 1-minute rain rate statistics were recorded along the 6.73 km link at 19.5 GHz over a period of ten calendar months in Durban for the year 2004: February, March, April, May, June, August, September, October, November and December. This data was analyzed, processed and the average signal level for the nonrainy days for each month was determined. There were no rains in the months of May, June, and August, (which are winter months in Durban) therefore, the signal variations recorded for those three months are assumed to be due to other attenuating factors like k-factor fading, multipath fading, water vapor, and fog.

[25] The nonrain faded average was determined from all the received signal level data for nonrainy days in each month and averaged over the month in question. Figure 6 shows the monthly values of the average signal level for the nonrainy days, which can also be referred to as the nonrain faded average values. It is seen that the actual signal levels are 1–4 dB below the expected free-space level of −41 dBm. Several factors contribute to this; k-factor fading arises due to the fact that the value of the k used in the design is 1.33, while the median value of k-factor for Durban is 1.21, with a value of k = 0.5, exceeded 99.9% of the time [see *Odedina and Afullo*, 2005; *Afullo and Odedina*, 2006]. The "worst" month for k-factor fading is February (with value of $k \approx 0.2$ exceeded 99.9% of the month), while the month of August has k-factor value exceeded 99.9% of the time of 0.9. Note also that the median value of k for August is 1.27 as opposed to the 1.21 for February [*Afullo and Odedina*, 2006]. Thus, this type of fading may contribute 1–1.5 dB over the path (see clearance of the first Fresnel zone, Figure 5, and results in *Odedina and Afullo* [2005] and *Afullo and Odedina* [2006]).

[26] On the other hand, due to the rugged, hilly, and nonflat nature of the intervening terrain, multipath fading need not be a major contributor to signal variation, and may be limited to below 1 dB. Water vapor attenuation is another contributor with highest contribution in summer with an average pressure of about 27 mb (see Table 3), giving an average attenuation of 0.34 dB/km, or 2.2 dB over the 6.7 km path. On the other hand in winter, the average water vapor pressure is about 13 mb (see Table 3), resulting in attenuation of about 0.13 dB per km, and 0.9 dB over the 6.7 km path [*Ajayi et al.*, 1996]. Thus, water vapor attenuation contributes about 1 dB in winter and 2.2 dB in summer. Due to the coastal nature of Durban, as well as the industries, fog attenuation is also a

1944799x, 2007, 5, Downloaded from https://agupubs.onlinelibrary.wiley.com/doi/10.1029/2007RS003618. By AGU Journals, Wiley Online Library on [02/12/2024]. See the Terms and Conditions (https://onlinelibrary.wiley.com/terms-and-conditions) on Wiley Online Library for rules of use; OA articles are governed by the applicable Creative Commons License

Table 3. Average Water Vapor Recorded for Durban in 2004 at 19.5 GHz

Months	Water Vapor, mb
Feb	25.57
Mar	23.29
Apr	23.67
May	15.93
Jun	11.71
Jul	11.62
Aug	15.87
Sep	19.14
Oct	21.76
Nov	22.45
Dec	29.26
Average over the year	20.03 mb

contributor. At the operating frequency of the link of 19.5 GHz, an average attenuation of 0.1 dB/km is expected, resulting in a value of 0.7 dB along the propagation path [*Hall et al.*, 1996]. This thus accounts for the attenuation during nonrainy days.

5.3. Rain Attenuation Prediction Models Along the 6.73 km at 19.5 GHz

[27] The rain attenuation was modeled for the months that had rains in the year 2004. This was done for the months of February, March, April, September, October, November and December. The actual rain attenuation measurements recorded for these months are plotted for varying rain rates. Logarithmic and power estimation models are then used to obtain an analytical fit for the measurement data. The three rain attenuation models, namely, ITU-R model, Crane Global model and the Moupfouma model, are also applied on the link for d = 6.73 km and f = 19.5 GHz. The predicted attenuation values for each month are then compared with the measurements, as displayed in Figures 7–13, where y refers to path attenuation (in dB) and x refers to the rain rate (in mm/h).

[28] Figure 7 shows the rain attenuation plots for February in Durban. The attenuation values predicted from these other models tend to be lower than the ones from the actual measurements for this month. From the measurements, the path attenuation is seen to increase as the rain rate increases until it gets to a rain rate of above 20 mm/h, and at this point, there is slight downward trend of the actual attenuation measurement curve. The highest rain rate measured in this month is 21 mm/h and its corresponding signal attenuation value is 14.93 dB. Similarly, in Figure 8 which shows the attenuation plots for the month of March, it is seen that the maximum rain rate recorded is 19 mm/h, and the attenuation measured at this point is 11.48 dB. For this month, the attenuation predicted by the Crane model is close to the measured

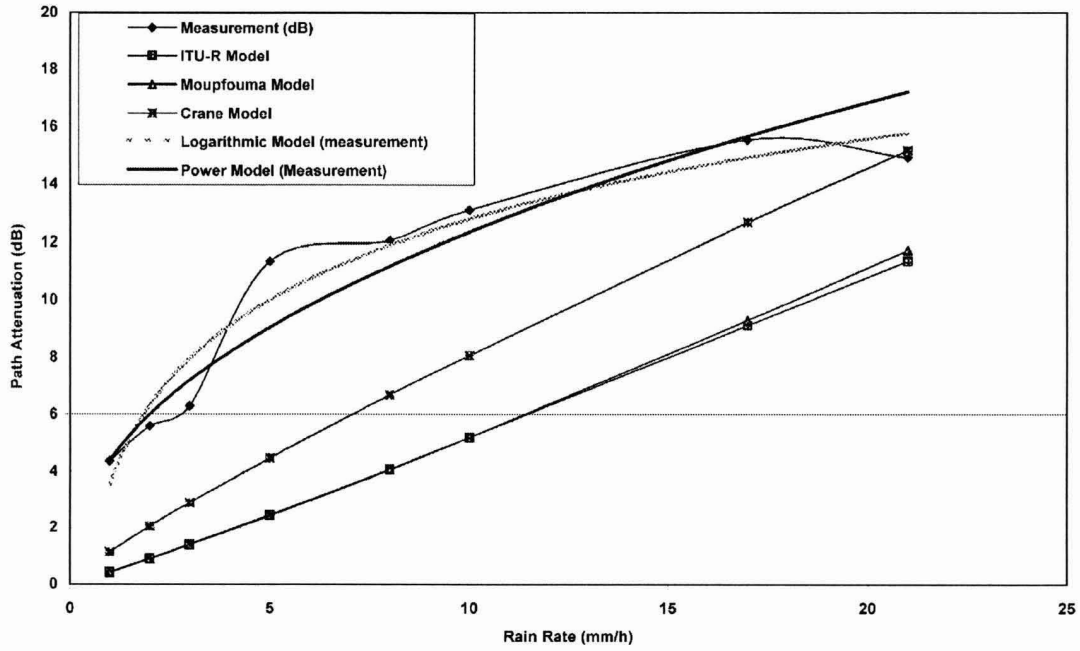

Figure 7. Rain attenuation for Durban in February: measurement and models at 19.5 GHz.

19447799x, 2007, 5, Downloaded from https://agupubs.onlinelibrary.wiley.com/doi/10.1029/2007RS003618. By AGU Journals, Wiley Online Library on [02/12/2024]. See the Terms and Conditions (https://onlinelibrary.wiley.com/terms-and-conditions) on Wiley Online Library for rules of use; OA articles are governed by the applicable Creative Commons License

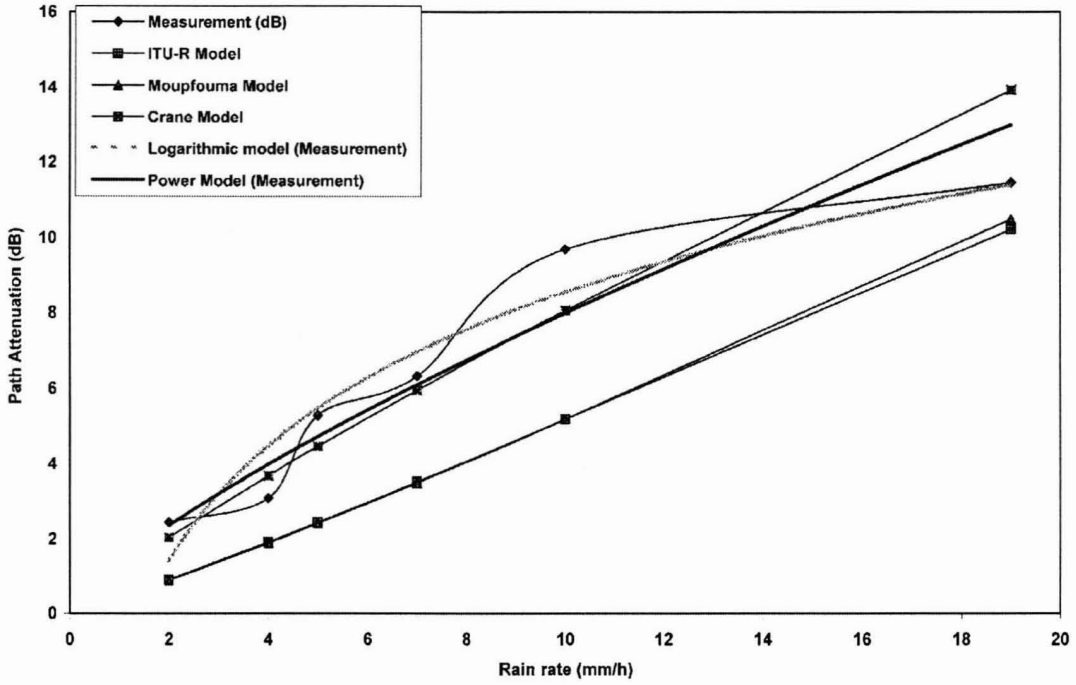

Figure 8. Rain attenuation for Durban in March: measurement and models at 19.5 GHz.

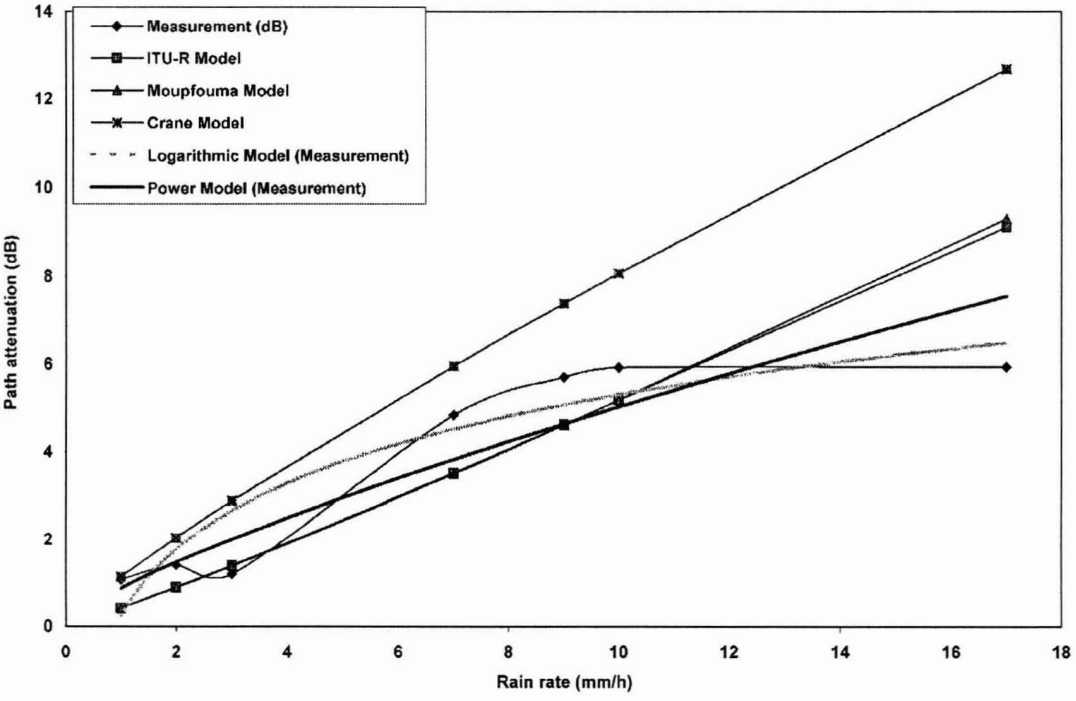

Figure 9. Rain attenuation for Durban in April: measurement and models at 19.5 GHz.

19447799x, 2007, 5, Downloaded from https://agupubs.onlinelibrary.wiley.com/doi/10.1029/2007RS003618. By AGU Journals, Wiley Online Library on [02/12/2024]. See the Terms and Conditions (https://onlinelibrary.wiley.com/terms-and-conditions) on Wiley Online Library for rules of use; OA articles are governed by the applicable Creative Commons License

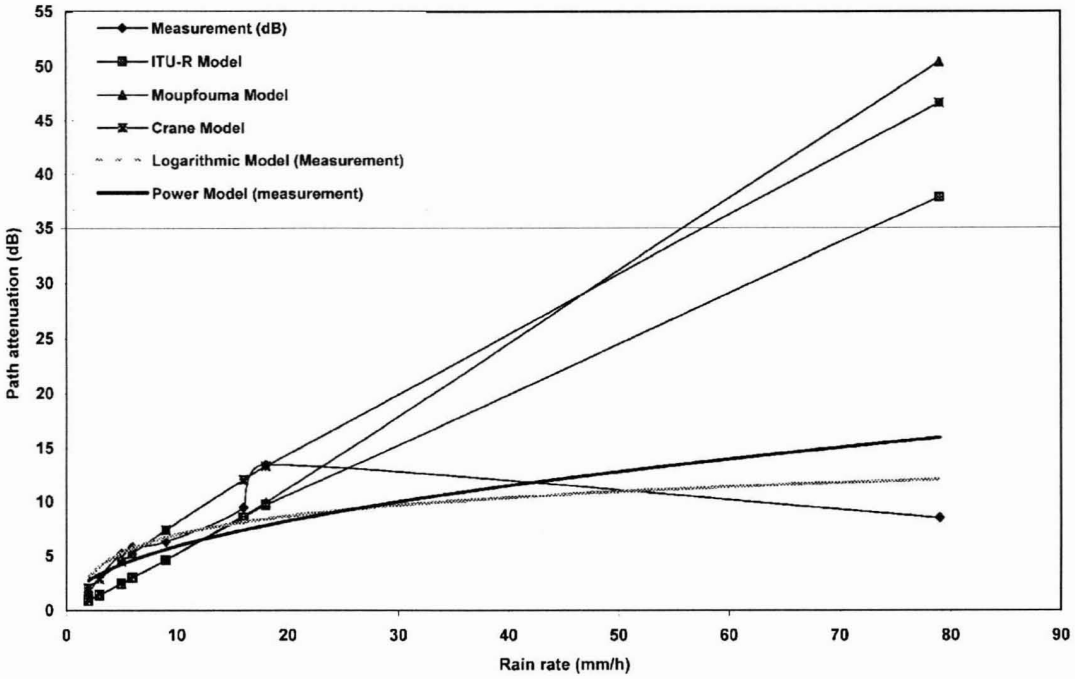

Figure 10. Rain attenuation for Durban in September: measurement and models at 19.5 GHz.

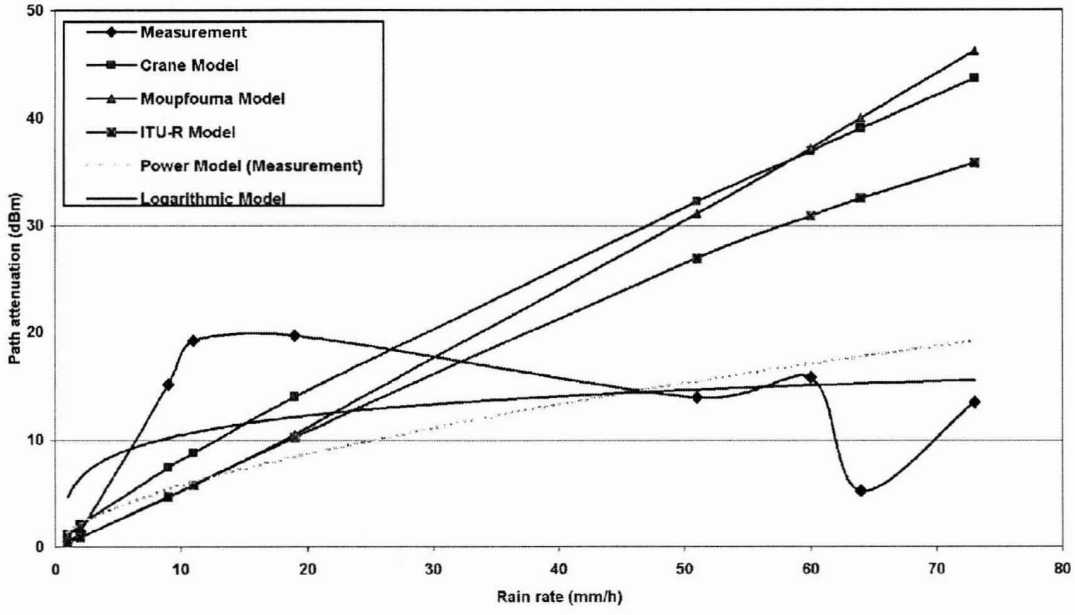

Figure 11. Rain attenuation for Durban in October: measurement and models at 19.5 GHz.

1944799x, 2007, 5, Downloaded from https://agupubs.onlinelibrary.wiley.com/doi/10.1029/2007RS003618. By AGU Journals, Wiley Online Library on [02/12/2024]. See the Terms and Conditions (https://onlinelibrary.wiley.com/terms-and-conditions) on Wiley Online Library for rules of use; OA articles are governed by the applicable Creative Commons License

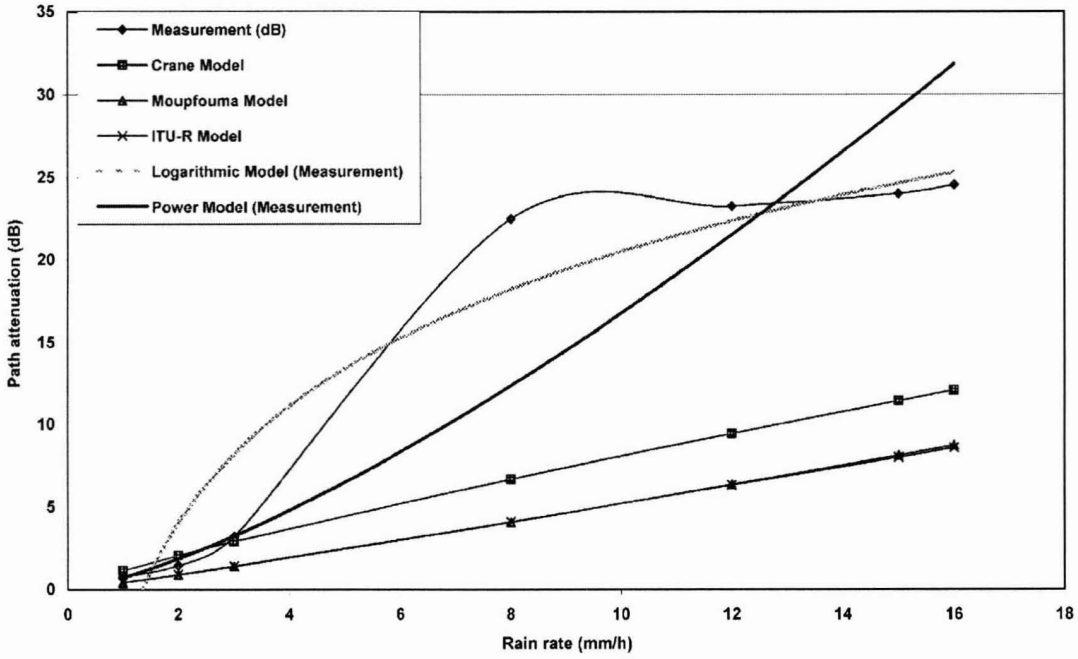

Figure 12. Rain attenuation for Durban in November: measurement and models at 19.5 GHz.

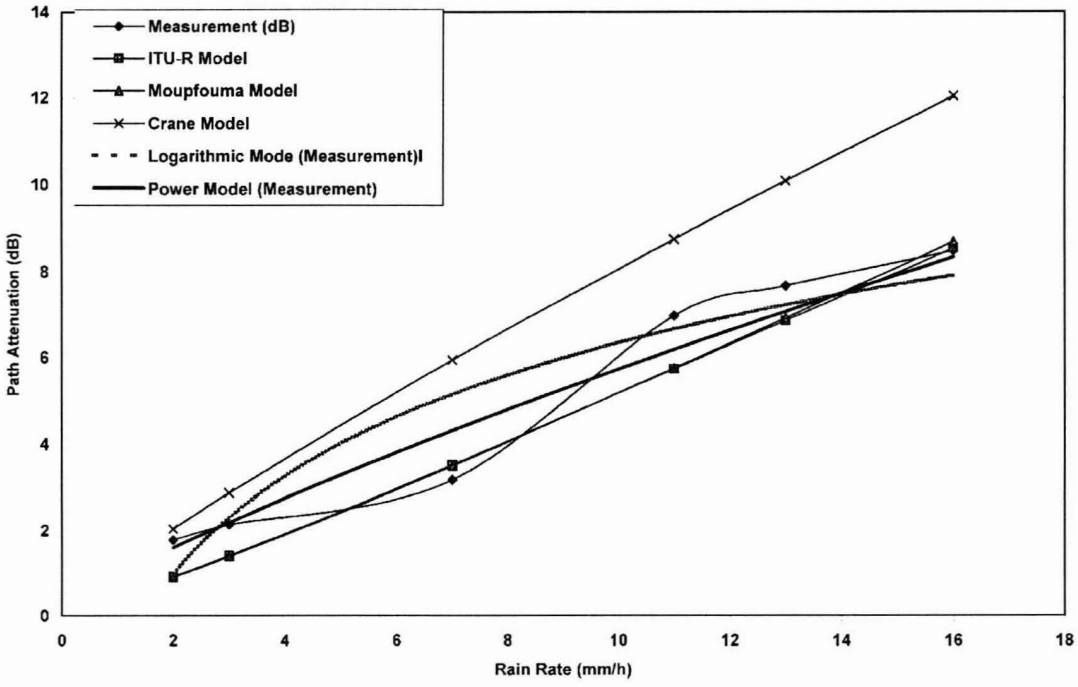

Figure 13. Rain attenuation for Durban in December: measurement and models at 19.5 GHz.

1944799x, 2007, 5, Downloaded from https://agupubs.onlinelibrary.wiley.com/doi/10.1029/2007RS003618. By AGU Journals, Wiley Online Library on [02/12/2024]. See the Terms and Conditions (https://onlinelibrary.wiley.com/terms-and-conditions) on Wiley Online Library for rules of use; OA articles are governed by the applicable Creative Commons License

Table 4. Rain Attenuation Models for the Rainy Months in the Year 2004 in Durban, South Africa, for a 6.73 km Path

Calendar Months	Predicted Model
Feb	$A = 4.0216\text{Ln}(R) + 3.5364$
Mar	$A = 1.399R^{0.7572}$
Apr	$A = 0.8719R^{0.7617}$
Sep	$A = 2.4543\text{Ln}(R) + 1.3125$
Nov	$A = 10.215\text{Ln}(R) - 3.0463$
Dec	$A = 0.9175R^{0.7967}$

attenuation, while the ITU-R and Moupfouma models underestimate the attenuation. The power estimation model and the logarithmic estimation model derived from the measurements overlap the Crane model curve.

[29] The other plots are shown for April (Figure 9); September (Figure 10); October (Figure 11); November (Figure 12); and December (Figure 13). The corresponding best-fit models (based on chi-square statistic) are given in Table 4. From the measurements, one observes that the highest rain rate recorded during the attenuation measurements occurred in the summer months of September and October in Durban, with rain rates of 79 mm/h and 73 mm/h, respectively. It is also observed that, as the rain rate goes above 18 mm/h, a drop in the signal attenuation is observed. That is, as the rain rates exceed about 18 mm/h, the rain attenuation no longer increases, but rather decreases. This is to say, the lower rain rates extend uniformly along the 6.73 km propagation path, but at higher rain rate, the rain may not be able to cover the entire propagation path length. The reason behind this may be explained by the fact that the higher the rain rate, the smaller the rain cell radius, as experimentally determined by Bonati [*Pawlina-Bonati*, 1999; *Pawlina and Binaghi*, 1998]. Therefore, the rain attenuation recorded at these high rain rates reflects a corresponding diminution of the effective path length. Note that, the effective path length is introduced to incorporate the effect of nonuniformity of rain along any propagation path length. The longer the path, the less likely it is that rain will extend the full length of the propagation path. Thus the effective length d_{eff}, decreases as the rain rate rises above 18 mm/hr, due to the corresponding decrease in rain cell radius. This therefore reduces the actual signal attenuation due to rain.

[30] Figure 14 shows the measured maximum, average, and minimum rain attenuation values per rain rate for the entire year along the 6.73 km path at 19.5 GHz. The maximum and minimum plots define an attenuation bound for the given rain rates. In this figure, it is

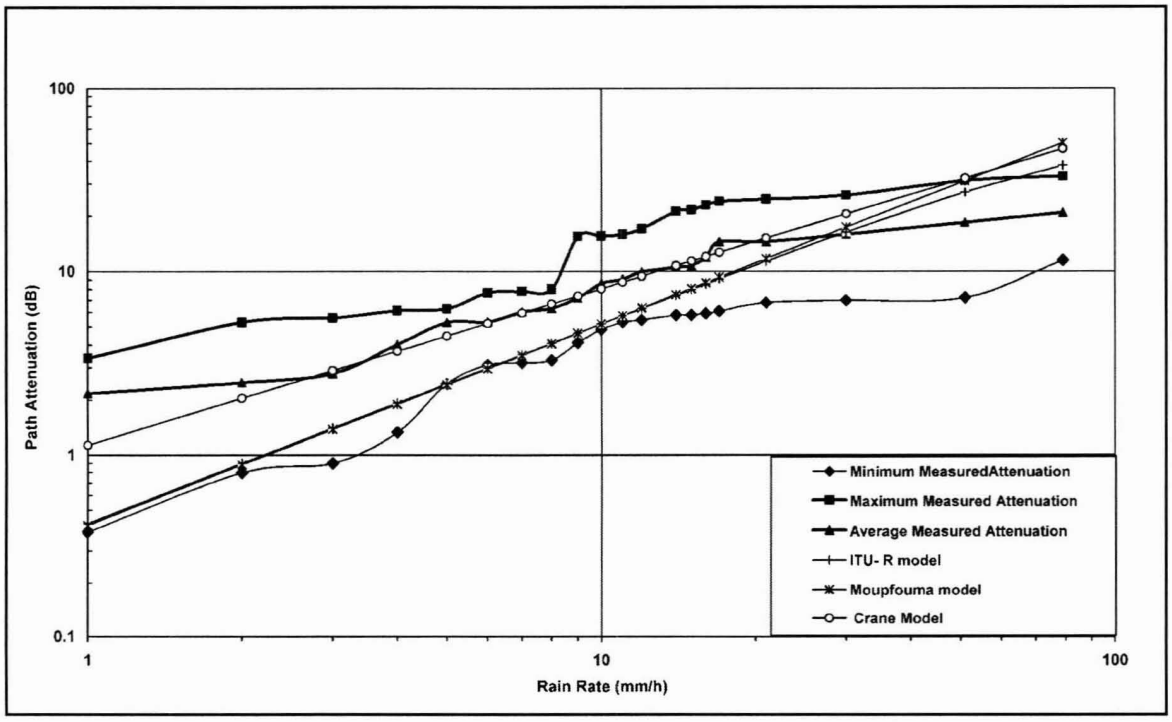

Figure 14. Rain attenuation for Durban along the 6.73 km link at 19.5 GHz for the year 2004: Maximum, minimum and average measured values versus the three models.

1944799x, 2007, 5, Downloaded from https://agupubs.onlinelibrary.wiley.com/doi/10.1029/2007RS003618. By AGU Journals, Wiley Online Library on [02/12/2024]. See the Terms and Conditions (https://onlinelibrary.wiley.com/terms-and-conditions) on Wiley Online Library for rules of use; OA articles are governed by the applicable Creative Commons License

observed that the Crane, Moupfouma and ITU-R attenuation curves all fall within the maximum and minimum bounds up to a rain rate of 50 mm/h. Beyond this, only the ITU-R prediction stays within the bound up to 65 mm/h, while the Crane and Moupfouma plots exit and overpredict the expected attenuation. For rain rates below 30 mm/h, the Moupfouma and ITU-R plots overlap but fall below the measured average; while the Crane plot falls on the measured average plot up to 20 mm/h. Thus while on a month-to-month basis the three attenuation models appear inaccurate, on a yearly or longer-term basis, they fall within the measurement bounds for low to medium rain rates.

6. Conclusions

[31] The different existing attenuation models for predicting rain induced attenuation on terrestrial line-of-sight links are studied in this paper. From the path rain attenuation predictions obtained from the ITU-R model, Crane Global model, and the Moupfouma models at different frequencies and propagation path lengths, ITU-R model gives the lowest attenuation values on all the geographical locations in South Africa, for all frequencies between 10 and 40 GHz. The Moupfouma model gives the highest attenuation prediction for the lower frequency of 10 GHz for the four regions, while the Crane Global model gives high attenuation predictions for the lower rainfall regions of Cape Town and Brandvlei at the higher frequency of 40 GHz.

[32] From the measurement over 19.5 GHz along the 6.73 km link, it is seen that while there are different models depicting month-to-month attenuation variability, the final plot over the entire year indicates that, for rain rates up to 50 mm/h, all the three attenuation models fall within the measured attenuation bounds. They can thus be used to reasonably estimate rain attenuation for low to medium rain rates. However, beyond this, only the ITU-R model stays within the bound. Longer measurements are therefore needed to further buttress this conclusion.

References

Afullo, T. J., and P. K. Odedina (2006), On the k-factor distribution and diffraction fading for southern Africa, *SAIEE Res. J.*, *97*(2), 172–181.

Ajayi, G. O., S. Feng, S. M. Radicella, and B. M. Reddy (Eds.) (1996), *Handbook on Radiopropagation Related to Satellite Communications in Tropical and Subtropical Countries*, pp. 2–14, ICTP Press, Trieste.

Crane, R. K. (1980), Prediction of attenuation by rain, *IEEE Trans. Commun.*, *28*(9), 1717–1733.

Crane, R. K. (1996), *Electromagnetic Wave Propagation Through Rain*, chap. 1–4, John Wiley, New York.

Crane, R. K. (2003), *Propagation Handbook for Wireless Communication System Design*, chap. 2, CRC Press, New York.

De Miranda, E. C., M. S. Pontes, and L. A. R. da silva Mello (1998), Statistical modelling of the cumulative probability distribution function of rainfall rate in Brazil, in *Proceedings of URSI CLIMPARA, April*, pp. 77–80, Ottawa, Ont., Canada.

Fashuyi, M. O. (2006), A study of rain attenuation on terrestrial paths at millimetric wavelengths in South Africa, MSc. thesis, Univ. of KwaZulu-Natal, Durban, S. Africa, Feb.

Fashuyi, M. O., P. A. Owolawi, and T. J. O. Afullo (2006), Rainfall rate modelling for LOS radio systems in South Africa, *SAIEE Res. J.*, *97*(1), 74–81.

Green, H. E. (2004), Propagation impairment on Ka-band SATCOM links in tropical and equatorial regions, *IEEE Antennas Propag. Mag.*, *46*(2), 31–44.

Gunn, R., and G. D. Kinzer (1949), The terminal velocity of fall for water droplets in stagnant air, *J. Meteorol.*, *6*, 243–248.

Hall, M. P. M., L. W. Barclay, and M.T. Hewitt (1996), *Propagation of Radiowaves*, chap. 1–4, IEE Press, London.

ITU-R (2001), Propagation prediction techniques and data required for the design of terrestrial line-of-sight systems, *Recommend. 530-10, ITU-R P Ser.*, pp. 271–295, Int. Telecommun. Union, Geneva.

ITU-R (2003), Characteristics of precipitation for propagation modelling, *Recommend. 837-1, 2, 3, 4, ITU-R P Ser.*, Int. Telecommun. Union, Geneva.

Laws, J. O., and D. A. Parsons (1943), The relationship of raindrop size to intensity, *Eos Trans. AGU*, *24*, 452–460.

Moupfouma, F. (1984), Improvement of rain attenuation prediction method for terrestrial microwave links, *IEEE Trans. Antennas Propag.*, *32*(12), 1368–1372.

Moupfouma, F., and J. Tiffon (1982), Raindrop size distribution from microwave scattering measurements in equatorial and tropical climates, *Electron. Lett.*, *18*, 1012–1014.

Naicker, K. (2006), Rain attenuation modelling for line-of-sight terrestrial links, MSc. thesis, Univ. of Kwazulu-Natal, Durban, Sept.

Naicker, K., and S. H. Mneney (2006), Propagation of measurements and multipath channel modelling for line-of-sight links at 19.5 GHz, *SAIEE Res. J.*, *97*(2), 162–171.

Odedina, P. K., and T. J. Afullo (2005), Effective Earth radius factor determination and its application in southern Africa, in *Proceedings of IASTED International Conference on Antennas, Radar, and Wave Propagation, July*, pp. 222–225, Banff, Canada.

Olsen, R. L., D. V. Rogers, and D. B. Hodge (1978), The aR^b relation in the calculation of rain attenuation, *IEEE Trans. Antennas Propag.*, *26*(2), 547–556.

Pawlina, A., and M. Binaghi (1998), Rain distribution along the path: New statistics of cells and cells separations from radar data, in *Proceedings of URSI Commission F Open Symposium on Climatic Parameters in Radiowave Propagation Prediction*, pp. 81–84, Ottawa, Canada.

Pawlina-Bonati, A. (1999), Essential knowledge of rain structure for radio applications based on available data and models, in *Proceedings of* 3rd *Regular Workshop on Radio Communi-*

1944799x, 2007, 5, Downloaded from https://agupubs.onlinelibrary.wiley.com/doi/10.1029/2007RS003618. By AGU Journals, Wiley Online Library on [02/12/2024]. See the Terms and Conditions (https://onlinelibrary.wiley.com/terms-and-conditions) on Wiley Online Library for rules of use; OA articles are governed by the applicable Creative Commons License

cation in Africa, 25–29 October, edited by J. S. J. Daka and T. J. O. Afullo, pp. 96–106, Gaborone, Botswana.

Pozar, D. M. (1988), *Microwave Engineering*, 2nd ed., chap. 12, John Wiley, New York.

Segal, B. (1986), The Influence of Rain-gage Integration Time on Measured Rainfall-Intensity Distribution Functions, *J. Atmos. Oceanic Technol.*, *3*, 662–667.

Zhang, W., and N. Moayeri (1999), Power-Law Parameters of Rain Specific Attenuation, *Rep. IEEE, 802.16 WG*, 1–8.

T. J. Afullo and M. O. Fashuyi, School of Electrical, Electronic, and Computer Engineering, University of KwaZulu-Natal, Durban, 4000 South Africa. (afullot@ukzn.ac.za)

1944799x, 2007, 5, Downloaded from https://agupubs.onlinelibrary.wiley.com/doi/10.1029/2007RS003618. By AGU Journals, Wiley Online Library on [02/12/2024]. See the Terms and Conditions (https://onlinelibrary.wiley.com/terms-and-conditions) on Wiley Online Library for rules of use; OA articles are governed by the applicable Creative Commons License



Rikio Maruta was born on May 15, 1943. He graduated from the Nippon Electric Institute of Technology in 1967, where he majored in electrical engineering. From 1968 to 1969, he was a research student at the University of Tokyo.

He has been an employee of Nippon Electric Company, Ltd. since 1962. His principal job has been research and development of high-speed PCM multiplexers and digital signal processing terminals such as digital speech interpolation equipment and TDM/FDM transmultiplexers. He was awarded the 1976 Conference Paper Award by the Institute of Electronics and Communication Engineers (IECE) of Japan, and the 1978 Kanto Regional Invention Award by the Japan Institute of Invention and Innovation. He is presently Supervisor, Communication Research Laboratory, Central Research Laboratories, Nippon Electric Company, Ltd.

Mr. Maruta is a member of the Institute of Electric Engineers (IEE) of Japan and the Institute of Electronics and Communication Engineers (IECE) of Japan.



Atsushi Tomozawa was born in Tokuyama, Yamaguchi, Japan, on January 6, 1938. He received the B.S. degree in electrical communication engineering from the Kyushu University in 1960.

He joined the Nippon Electric Company, Ltd. in 1960, and has worked on research and development of PCM systems including delta modulation, high-speed codecs, and digital multiplexers at the Central Research Laboratories. From 1971 through 1974, he was engaged in system studies on TDMA and digital signal processing at COMSAT Laboratories. He was awarded the 1965 Inada Prize by the Institute of Electronics and Communication Engineers (IECE) of Japan. He is presently Assistant Manager, Digital Systems Development Department, Transmission Division, Nippon Electric Company, Ltd.

Mr. Tomozawa is a member of the Institute of Electronics and Communication Engineers (IECE) of Japan.

Prediction of Attenuation by Rain

ROBERT K. CRANE, FELLOW, IEEE

Abstract—**A new model is presented for the prediction of attenuation by rain on either terrestrial or slant earth-to-space propagation paths. The model was developed using geophysical observations of the statistics of point rain rate, of the horizontal structure of rainfall, and of the vertical temperature structure of the atmosphere. The model was tested by comparison with attenuation distribution observations. The results show excellent agreement; the observations differ from model predictions by less than the rms deviations predicted by the model.**

I. INTRODUCTION

RAIN has long been recognized as one of the principal causes of unwanted signal loss on centimeter or millimeter wave propagation paths through the lower atmosphere. Rain is not the only cause. Variations in water vapor along a path or the occurrence of liquid water clouds or fog on the path will also cause variations in signal strength. Fig. 1 displays the relative magnitude of the variations (attenuation) due to water vapor (gaseous absorption), a liquid water cloud, and rain that is expected to be exceeded during less than 2 percent of the year on a zenith path. Specifically, the curves for gaseous absorption display the estimated global variation (two standard deviations) of attenuation about the global and seasonal mean value of attenuation and the variation about the attenuation value computed for a given surface temperature and water vapor density; the cloud values are for a 2 km thick cloud with a 0.2 g/m^3 liquid water content; and the rain curve is for a 2.5 km high rain region of 1 mm/h, conditions typical of the rain rate to be exceeded 2 percent of the year at 38°N latitude along the eastern United States. With the exceptions of the frequency bands about the 22 GHz water vapor absorption line and the 60 GHz complex of oxygen lines, the attenuation exceeded less than 2 percent of the year is caused by rain or cloud. The model cloud produces an attenuation estimate comparable to rain at 2 percent of the year. At the smaller percentages of the year of interest to the communication system designer, rain is the sole cause of increased attenuation.

Early recognition of the importance of rain to systems designed for service reliabilities in excess of 0.99 led to a number of theoretical and experimental studies of the effects of rain. By the early 1970's, a firm theoretical basis had been established for the calculation of attenuation if the rainfall intensity was known along the path [1], [2]. In recent years, the emphasis has been on establishing predictive techniques for the statistical estimation of the attenuation probability distribution for a particular path. Two different approaches to the

Paper approved by the Editor for Communication Theory of the IEEE Communications Society for publication without oral presentation. Manuscript received October 2, 1979; revised January 30, 1980. This work was supported by contracts from the NASA Goddard Space Flight Center, Western Union Telegraph Company, and M.I.T. Lincoln Laboratory.

The author is with Environmental Research & Technology, Inc., Concord, MA 01742.

0090-6778/80/0900-1717$00.75 © 1980 IEEE

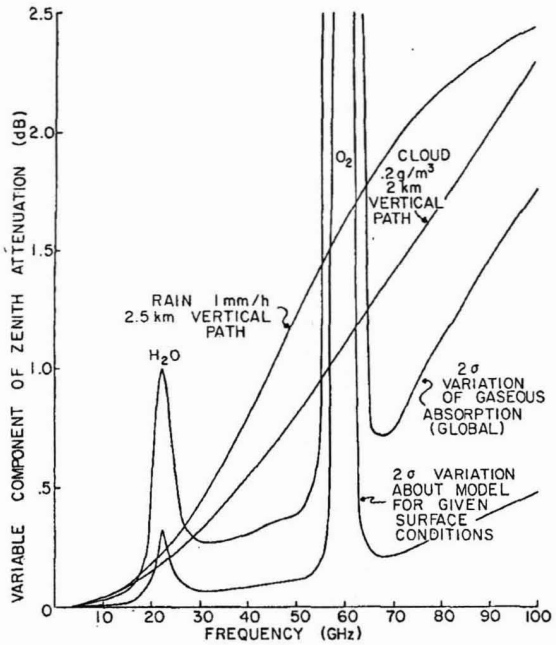

Fig. 1. Zenith attenuation values expected to be exceeded 2 percent of the year at midlatitudes.

estimation problem are possible, one based solely on the use of a large number of attenuation observations at differing frequencies, locations, and path geometries, and the other based on the synthesis of attenuation values from meteorological data. The latter is most promising at the current time because a considerably larger database is available for use in estimating the distribution functions required for modeling path attenuation.

The statistical variations of rainfall intensity, specific attenuation, and attenuation along a path depend in a complex way on the number, type, and intensity of rainstorms that traverse the path each year. No theoretical basis exists for the calculation of the desired rainfall statistics; they must be obtained empirically. Rice and Holmberg [3] performed a statistical analysis of all the then available U.S. National Weather Service rain accumulation observations to provide estimates of instantaneous rain rate distributions. Lee [4] has since published a similar, although less extensive, analysis of the same data. He described the available data and proposed a procedure for the estimation of the desired rain rate statistics. Dutton and Dougherty [5] have extended the work of Rice and Holmberg to provide estimates of the year-to-year variability of the rain rate distribution.

More than an estimate of the surface point rain rate distribution is required for the prediction of attenuation on terrestrial or earth-to-space (slant) communication paths. Rain displays significant spatial and temporal variation along a horizontal path, and procedures are required to statistically estimate the instantaneous rain rate profile along the path. Battesti *et al.* [6], Lin [7], Stutzman and Bostian [8], Rogers [9], and a number of others have proposed models for the calculation of attenuation along a path given the equal probability rain rate value at a point. The models are based either on a direct empirical relationship between surface rain rate and an effective path length which, when multiplied by the specific attenuation value for the surface rain rate, produces the desired attenuation value [6] or on a synthetic storm profile which is used to represent the variation of rain along the path. Most of the models were developed using point rain rate and path attenuation measurements; the free parameters in the model are set to provide the best match between the attenuation estimated using the prediction procedure and the observed values. Model rainstorms have also been developed from analyses of weather radar data for the conversion of point rainfall statistics to path attenuation estimates [9].

Finally, for the prediction of attenuation on a slant path, the vertical variation in rain intensity and in ice or a water state must be modeled. At frequencies below 60 GHz, the attenuation caused by frozen particles such as snow or ice crystals is very small and may be neglected [10]. Only the contribution of the liquid raindrops is important. Observations of the variation of specific attenuation with height reveal that the region producing significant attenuation lies below the height of the bright band (0°C isotherm) [11]; comparisons between radar-based attenuation predictions and simultaneous path attenuation measurements also indicate that only the rain below the bright band contributes to the attenuation [12], [13]. Weather radar observations show that, on average, the rain intensity does not vary with height between the surface and the base of the bright band [14], [15]. On the basis of this evidence, the specific attenuation may be modeled as being constant from the surface to a height near the 0°C isotherm level which must also be statistically estimated.

An attenuation prediction model based upon the use of geophysical data incorporates predictions of the surface point rain rate, the point-to-path variation in rain rate or specific attenuation given the surface point rain rate, and the height dependency of specific attenuation given the surface point rain rate or the percentage of the year the attenuation value is exceeded. This paper presents such a model for use on either slant or terrestrial paths. It is based entirely on geophysical observations of rain rate, rain structure, and the vertical variation of atmospheric temperature. None of the model constants was obtained from attenuation measurements. This procedure was used to amass as large a database as possible from pooled observations at a number of locations. Crane [10] showed that over 10 years of observation at a point are required to estimate the surface rain rate to be exceeded 0.001 percent of the year on the average with an uncertainty (1 standard deviation or 67 percent bound) of less than 10 percent of the estimated value. No equivalent long term attenuation data are currently available from a single location for use in generating a prediction model.

An attenuation prediction model should also provide estimates of the expected year-to-year and the expected station-to-station variation as well as the expected attenuation at the same exceedence probability. The model presented in this paper includes such estimates for either terrestrial or slant paths. Comparisons between model predictions and available attenuation observations made on a number of propagation paths show agreement within the expected uncertainty. The predic-

tion procedure for point rain rate is developed in Section II, the horizontal variation in rain rate and specific attenuation in Section III, the vertical variation of specific attenuation in Section IV and the expected variation of the estimated values in Section V. Comparisons with observations are presented in Section VI.

II. PREDICTION OF SURFACE POINT RAIN RATE

Distribution at Fixed Location

No physical theory exists for the calculation of a surface point rain rate distribution. Consequently, distribution estimates are empirical and must be developed from the available long-term observations of rain accumulation. Two types of rain accumulation data exist: the long duration hourly, daily, and annual accumulation tabulations available for a large number of geographical locations, and the excessive precipitation data available from a limited number of locations [4]. Nearly instantaneous rain rate data are available for an extremely limited number of locations and for limited time durations, typically of a few years or less. The instantaneous data have generally been taken in conjunction with attenuation observations, and provide a comparison for model evaluation, but not a database suitable for establishing the expected rain rate distribution.

A larger database of nearly instantaneous observations is potentially available in the archives of the U.S. National Weather Service in the form of unanalyzed strip chart recordings. Bodtmann and Ruthroff [16] obtained and analyzed data for five years of observations at 20 locations in the United States. The time resolution of the data, however, was limited; the observations represented rain rate values averaged over time intervals on the order of 2–4 min. For the estimation of attenuation along a path, the specific attenuation at each point along the path is required. The specific attenuation is theoretically related to the instantaneous rain rate using measured or modeled raindrop size distributions. Because of the instantaneous/point nature of the data fields needed for the nonlinear rain rate to specific attenuation conversion, it is often assumed that only instantaneous rain rate distributions are useful in the prediction of attenuation. Truly instantaneous rain rate measurements are contaminated by fluctuations caused by atmospheric turbulence and, if the sampling area is small, by the stochastic variation produced by counting a number of raindrops of different sizes and fall velocities. Rain rate averages are needed to remove the variations due to gauge limitations and to turbulence.

The amount of averaging desirable in the preparation of a rain rate distribution estimate depends upon its application. Bussey [17] noted the equivalence between temporal and spatial averaging for translating rain cells and recommended the use of hourly averages for the estimation of attenuation on 50 km terrestrial paths. Radar observations show that rain cells defined by regions of high rain rate which cause significant attenuation have an average dimension of 3 km measured at 60 percent of the peak rain rate value [18]. Assuming an average translation velocity of 15 m/s, a rain cell will pass over a rain gauge in less than 4 min. A rain gauge with a 1–2 min time resolution will resolve the small but significant cells; gauges with longer averaging times will miss the peaks of the cells. For the prediction of attenuation on a variety of terrestrial or slant paths, a 1 min accumulation or averaging time is optimum.

Except for a very limited number of recorded "instantaneous" rain rate distribution observations, 1 min accumulation data are not available. Rice and Holmberg [3] and Lee [4] have devised approximation procedures for the estimation of instantaneous rain rates from the available excessive precipitation data. The excessive precipitation data reported through 1972 consist of the highest 5 min, 10 min, and longer accumulations from each storm with an average 5 min rain rate in excess of 76.2 mm/h, an average 10 min rain rate in excess of 45.7 mm/h, and lower thresholds for longer accumulation periods. In 1972, the excessive precipitation criteria were changed to record only the highest accumulation event each month. If two occurrences of excessive precipitation happen within a storm, only the highest is recorded. Currently, if two events occur within the same month, only the highest is recorded. These data are useful for estimating the highest 5 min accumulation per month and per year, but are of limited use for the direct estimation of annual rain rate statistics valid at 10 min per year or longer. Both Rice and Holmberg and Lee devised models for the use of the data. Comparisons between the Rice-Holmberg model predictions and available instantaneous data show that their model tends to overestimate the rain rates at 0.01 percent and smaller percentages of the year [15].

Measured and modeled rain rate distributions for Washington, DC are presented in Fig. 2. The measured distributions are for one year of data as reported by Bussey [17] and for two years of data measured in Greenbelt, MD [19]. The instantaneous data obtained by Bodtmann and Ruthroff for their location nearest to Washington, DC is also plotted, as is the model prepared by Lee and used by Lin [7]. The Lin-Lee model was empirically adjusted during its development to match the Bodtmann and Ruthroff observations. The model predictions produced by Rice and Holmberg and as refined by Dutton and Dougherty are also presented. As noted above, the Rice-Holmberg model overestimated the rain rate at 0.01 percent of the year.

Rice and Holmberg processed both the excessive precipitation data and the hourly data available from the National Weather Service, Experience with varying the integration interval for processing instantaneous rain rate data has shown that averaging affects only the higher rain rates at the smaller percentages of the year [9], [10], [20]. In the 0.1–1 percent of the year interval, the distribution function for hourly observations provides a good estimate of the distribution function for 1 min averaged rain rate. The Rice-Holmberg model, therefore, should provide a good estimate of the rain rate distribution in the 0.1–1 percent range, a result which is evident in Fig. 2.

The highest 5 average rain rate value in the figure was obtained from the excessive precipitation data for the 26 year period from 1950 through 1976. These data were processed to provide estimates of the mean and standard deviation of the

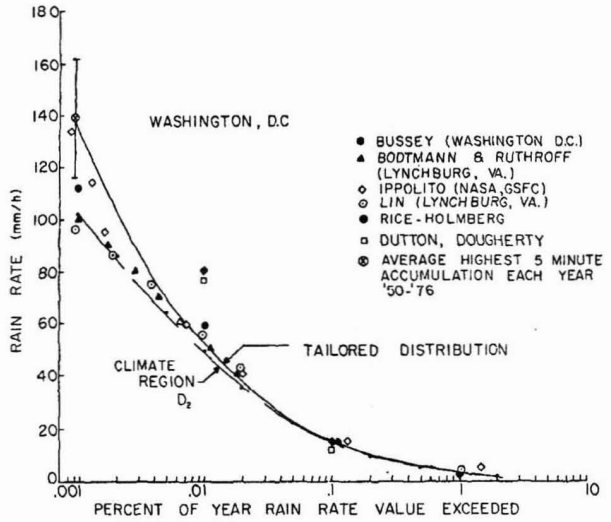

Fig. 2. Measured and modeled instantaneous rain rate distribution for Washington, DC.

rain rate to be exceeded 5 min of the year (~0.001 percent). Analysis of instantaneous rain rate distributions have shown that the highest 5 min average rain rate is usually from an excessive precipitation event that includes the five highest 1 min averaged rain rate values. Assuming this equivalence, the rain rate distribution is known at 0.00095 percent of the year (5 minutes) and in the 0.1–1 percent range (from the Rice-Holmberg model). The tailored distribution plotted in Fig. 2 is a smooth curve that passes through the known values. This curve represents the best estimate available based upon a long data sample. At 0.001 of the year, the observed standard deviation of rain rate values for Washington, DC was 17 percent. The measured distribution reported by Bussey falls just outside this range and the distribution reported by Ippolito falls within this range (rms) about the tailored distribution. Similar agreement is obtained at the other probability of occurrence extreme, 1 percent of the year: the measurements are within the expected 17 percent rms of the tailored and the climate region D_2 model distributions.

Regional Model

Data for the preparation of tailored distributions are only available from First Order Weather Stations in the United States [4] and at a limited number of additional stations throughout the rest of the world. Attenuation predictions are generally required for locations different from the limited number of stations with sufficient long-term data. Crane [10], in processing excessive precipitation data from 15 stations in New England and Eastern New York State, found that the mean and variance of data pooled from seven years and 15 stations were statistically identical with the mean and variance for 24 years at one of the stations (Boston). The mean rain rate was 100 mm/h and the standard deviation was 35 percent for the 15 station sample, and the mean rain rate was 91 mm/h and the standard deviation was 48 percent for Boston. The distribution function for the highest 5 min average rain rate accumulation per year for Boston was applicable to the New England, Eastern New York region. This result implies that regional maps are useful for the representation of rain rate distribution data for application to locations removed from the observing station. The result also suggests the use of data pooled from a region to provide improved statistical estimates for the distribution function.

Rice and Holmberg [3], in the development of the empirical parameters and their dependences on total rain accumulation and thunderstorm rain accumulation, pooled data from stations within each of the 10 climate regions defined by Barry and Chorely [21] for the United States. The climate regions were defined on the basis of temperature, terrain height, average rain accumulation, and vegetation type, not on the basis of similarity in rain rate distribution. A subsequent comparison of the model distribution functions produced for each climate region resulted in the reduction of the number of rain climate regions required to describe the pooled rain rate distributions to five, the five climate regions currently employed by the CCIR [22]. These climate regions, although fashioned for the United States, were subsequently employed to describe rain climate regions for the entire globe. Dutton [23] has since expanded the number of rainfall zones in the United States to 19 based upon mappings of the independent parameters in the Rice-Holmberg model.

The global model currently used by the CCIR represents rain climates typical of those found within the United States, but does not adequately represent the much more intense rain rate regime found in the wet tropical regions of Africa, South America, and Indonesia or the much less intense regime found in the Arctic. In the development of a new global rain climate model for use in communication system design, the number of regions chosen to represent the variation in rain rate was expanded from five to eight to better emphasize variation with latitude. The newly developed rain rate climate model is presented in Figs. 3 and 4. The United States is still spanned by five regions, although one of the regions is divided into three subregions to better describe the within-region climate variation for design application.

The climate region boundaries were established using total rain accumulation and the number of thunderstorm day maps provided by the World Meteorological Organization as published in the *World Survey of Climatology* series edited by Landsberg [24]. In data-sparse regions, guidance was taken from the Köppen world climate classification [25] which, although heavily based upon vegetation type, represents major variations in rain climate. The ranges of the total rain accumulation and thunderstorm day values used for the definition of the rain climate regions were obtained from an initial analysis using the Rice-Holmberg model for Europe and North America. The initial intent was to define rain rate regions with rain rate distributions for adjacent regions approximating the expected bounds for the temporal (year-to-year) and spatial variation of the rain rate distribution within a region; the median rain rate distribution values for each climate region were to differ by approximately 40 percent at 0.001 percent of the year.

The boundaries for each of the climate regions were adjusted

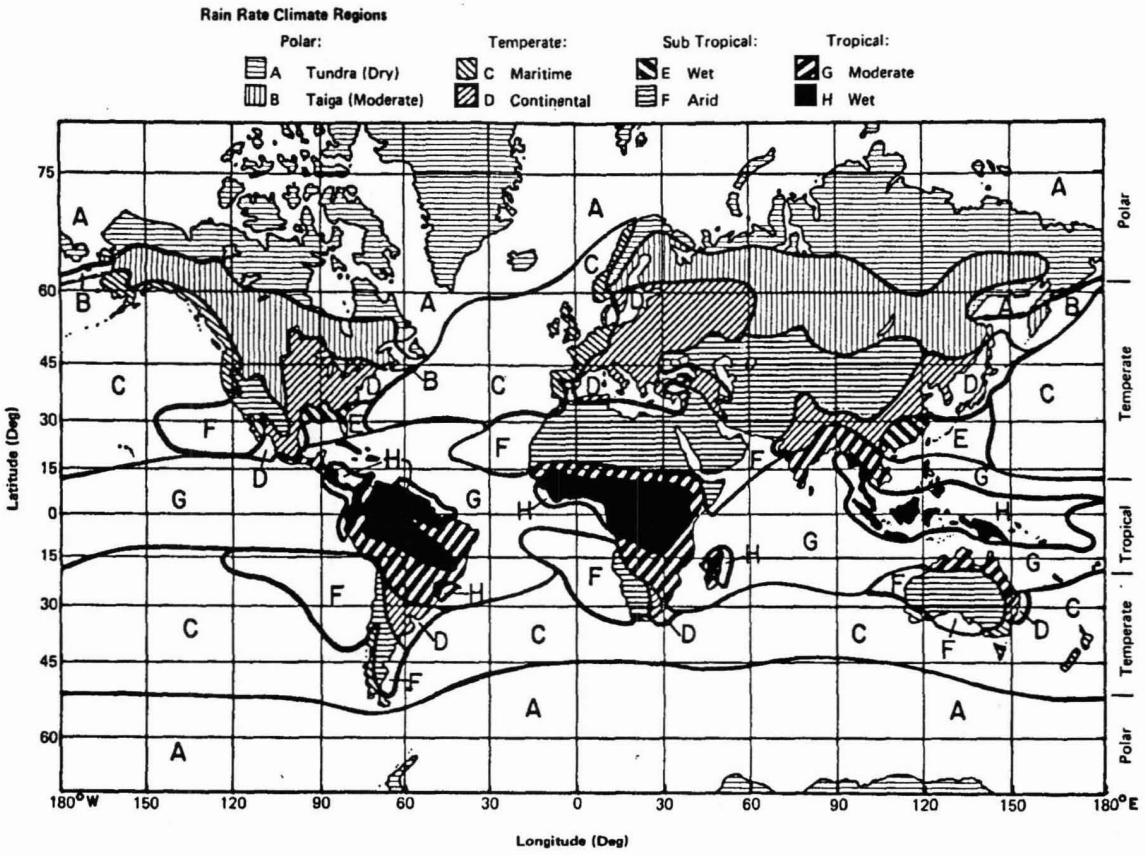

Fig. 3. Rain rate climate regions.

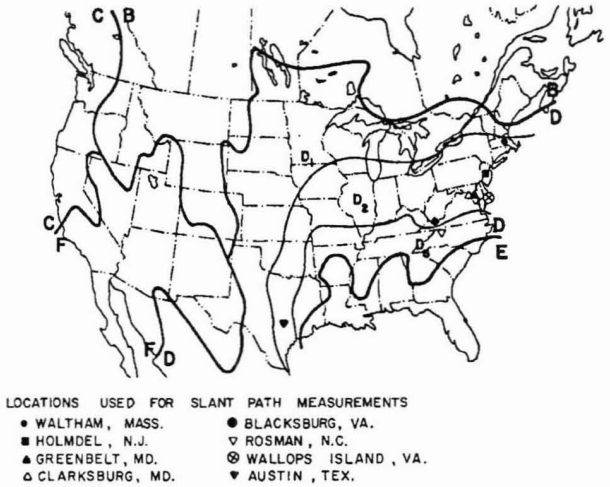

Fig. 4. Rain rate climate regions within the United States.

to compensate for the expected variations caused by terrain, variations in the predominant storm type, storm motion, and general circulation of the atmosphere, and the dominant latitude variation in rain climate. In addition, satellite cloud data, microwave radiometer observations of rain rate [26], and precipitation frequency data [27] were used to extend the rain climate regions out over the oceans.

The available measured instantaneous rain rate distributions were pooled for each of the climate regions defined in Fig. 3 and used to construct a median rain rate distribution for the region. No data were available for Region A, 132 station-years of data were available for Region D_2, and intermediate numbers of station-years were available for the other regions (see Table I). The resulting distributions for each of the eight climate regions are depicted in Fig. 5; the empirical distribution function for Region H together with the measured distributions used for the preparation of the model distribution are presented in Fig. 6. The rain rate distributions are also given in Table I for convenient reference.

Region D, as a result of the refinements used to prepare the final distributions, spans a large range of rain rates at a given exceedence probability. For application within the United States, Region D is bounded by Region E to the southeast and by Regions B or F to the north and west. At 0.001 percent of the year, the expected rain rates range from 64 to 164 mm/h, +61 to −37 percent relative to the 102 mm/h value for Region D. This range is too large for system design, although it is in reasonable accord with the expected standard deviation of 33 percent for one year of observations calculated using 26 years of excessive precipitation data from eight First Order Weather Stations within climate Region D. Region D was divided into three subregions, as shown in Fig. 7, to provide an interpolation of the expected rain rate distributions within the climate

TABLE I
POINT RAIN RATE (R_p) DISTRIBUTION VALUES (mm/h) VERSUS PERCENT OF YEAR RAIN RATE IS EXCEEDED

Percent of Year	Rain Climate Region									
	A	B	C	D_1	D_2	D_3	E	F	G	H
0.001	28	54	80	90	102	127	164	66	129	251
0.002	24	40	62	72	86	107	144	51	109	220
0.005	19	26	41	50	64	81	117	34	85	178
0.01	15	19	28	37	49	63	98	23	67	147
0.02	12	14	18	27	35	48	77	14	51	115
0.05	8.0	9.5	11	16	22	31	52	8.0	33	77
0.1	5.5	6.8	7.2	11	15	22	35	5.5	22	51
0.2	4.0	4.8	4.8	7.5	9.5	14	21	3.2	14	31
0.5	2.5	2.7	2.8	4.0	5.2	7.0	8.5	1.2	7.0	13
1.0	1.7	1.8	1.9	2.2	3.0	4.0	4.0	0.8	3.7	6.4
2.0	1.1	1.2	1.2	1.3	1.8	2.5	2.0	0.4	1.6	2.8
Number of Station Years of Data	0	25	44	15	99	18	12	20	2	11

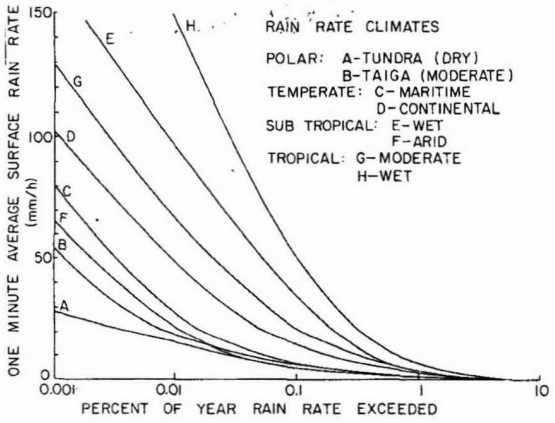

Fig. 5. Model rain rate distribution functions for the climate regions of Fig. 3.

region. The Region D_2 measurements displayed in Fig. 7 were not used in the derivation of the D_1, D_2, or D_3 model curves, but are provided for an independent evaluation of the subregion distribution bounds.

Further subdivision is possible, but depends upon the availability of adequate rain rate data and upon a better understanding of the local effects of terrain and of regional storm types and motions. Further subdivision, while producing better average values for system design, would not simultaneously display the approximate year-to-year variation in the values. The year-to-year variability is modeled as 30 percent of the expected value at the distribution extremes, 0.001 and 1 percent of the year (see Fig. 7). At the intermediate values, 0.01 and 0.1, the uncertainty is reduced to 20 percent to match the results reported by Harden *et al.* [28]. The spatial and temporal variability reported by Harden *et al.* for the United Kingdom (UK), together with the climate Region *C* model curve and bounds, are presented in Fig. 8. The UK data summarized in Fig. 8 were not used in the derivation of the climate Region *C* distribution function. These data show reasonable agreement with the model, although the model tends to overpredict the rain rate in the UK at 0.001 percent of the year. Since the data reported by Harden *et al.* were obtained from gauges with a 2 min time resolution, the discrepancy may be due to the climate or due to gauge limitations.

The rain climate model presented in Figs. 3, 4, 5, and 7 provide the rain rate distribution data needed for the estimation of attenuation. The regions were chosen to span areas with roughly identical year-to-year and location-to-location variations in rain rate distribution values. For a better representation of the rain rate distribution to be expected on the average at a point, a tailored distribution can be prepared (within the United States) using excessive precipitation data from nearby First Order Weather Stations for 0.001 percent of the year and the model calculations prepared by Rice and Holmberg [3] for percentages of the year greater than 0.1 percent. Care should be exercised in using a tailored model since local variations may compromise the expected increase in model precision. Refinement using measured instantaneous rain rate distributions is not recommended due to the expected year-to-year variation in the measured values and the current lack of measurements spanning time intervals of 10 or more years.

III. PREDICTION OF RAIN RATE AND SPECIFIC ATTENUATION ALONG A PROPAGATION PATH

A model for the prediction of surface point rain rate is only the first step in a model for the prediction of attenuation. Rain is characteristically inhomogeneous in the horizontal, and a statistical model is required to provide an estimate of the effect of the inhomogenity on the estimation of attenuation. For application to attenuation modeling, rain is often divided into two classes, stratiform and convective. Weather radar observations reveal that stratiform or widespread rain generally contains regions of imbedded convection and convective cells that are often surrounded by more stratiform regions of lighter rain [14]. Crane [18] has found a marked similarity in the underlying structure of both widespread and showery rain. The rain cell sizes and spacings observed by radar in widespread and isolated shower conditions on the Kansas high plains are identical to those observed in widespread rain in Coastal Virginia. The cell sizes also match those observed in Switzerland, France, Japan, and Malaysia [22].

In the semi-empirical modeling of fluid flow, similar results are expected for situations characterized by the identical values of nondimensional parameters such as the Prandlt number, the Reynolds number, the Rayleigh number, etc. In application to convection in the atmosphere, the fluid dynamical parameters used to characterize the flow are only weakly dependent on climate; hence, the horizontal structure of rain should not depend on climate region. Data on rain cell size, spacing, and the conditional point-to-path variation in rain rate, therefore, can be pooled from different geographic locations and rain climate regions.

Although radar provides the ideal tool for observing the spatial structure of rain [10], insufficient radar data are available to provide a conditional point-to-path relationship. Suf-

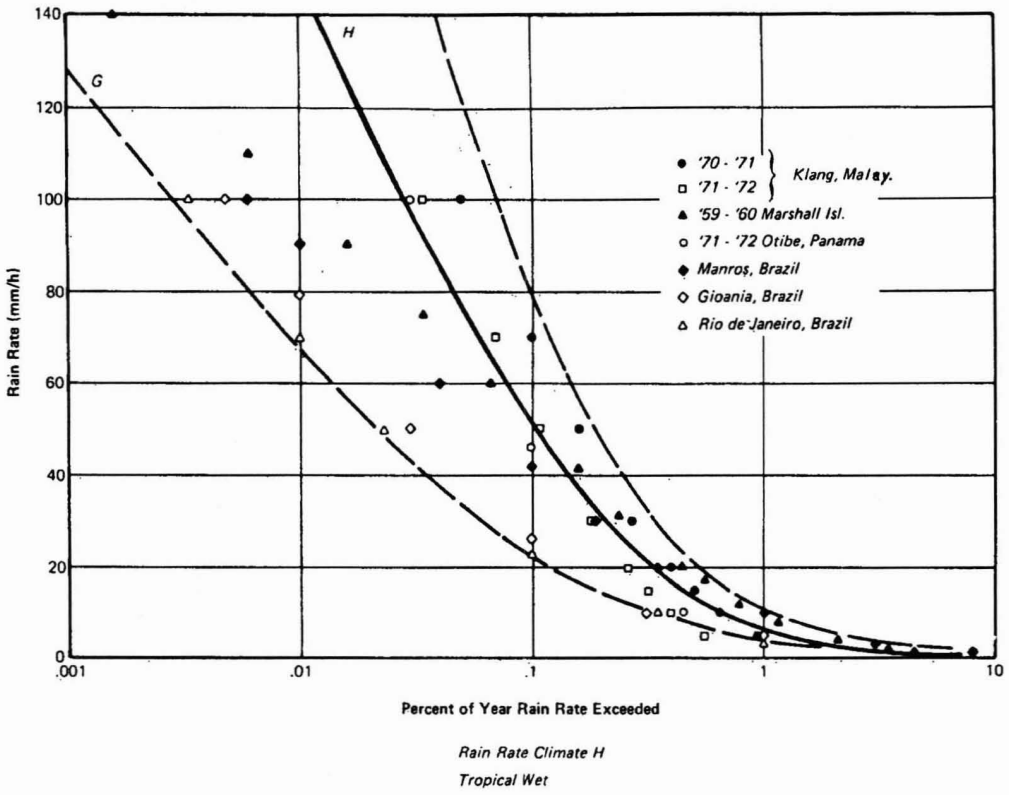

Fig. 6. Rain rate distribution observations for climate Region *H*.

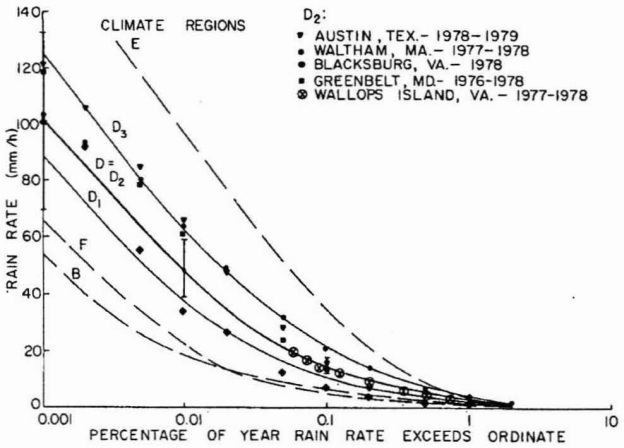

Fig. 7. Rain rate distributions for climate Region *D* within the United States (Fig. 4).

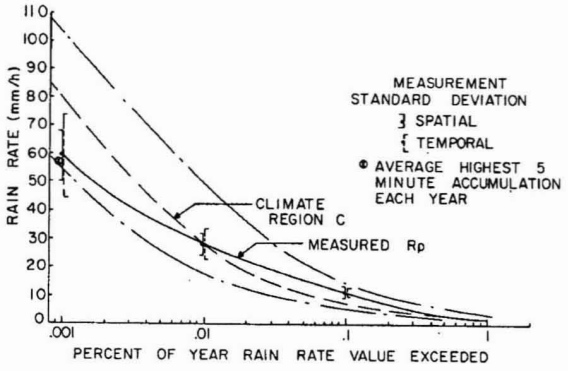

Fig. 8. Rain rate distribution observations in the United Kingdom [28].

ficient data, however, are available from a limited number of rain gauge networks. Jones and Sims [20] reviewed the Thunderstorm Project rain gauge network measurements (obtained in 1946) and more recent data from England to obtain relationships between point and path averaged rain rate values at equal exceedence probabilities. Data were also available from a dense rain gauge network operated for a limited time period by Bell Laboratories in New Jersey [29] and from a line of gauges along a 20 km path in the Rhine Valley of West Germany [30]. These data were pooled to provide an empirical relationship between point and path average rain rate as depicted for a distance of 5 km in Fig. 9.

The path averaged rain rate was plotted versus surface point rain rate for equal exceedence probabilities. Surface rain rate was used as the independent variable rather than probability because the rain rate values are a better measure of rain intensity (hence the dynamics of the meteorological situation that produced the rain) than is percentage of the year when the data are pooled from a number of climate regions. The path average value is expressed as an effective path average factor r where

$$r = \bar{R}/R_p$$

where $\bar{R}$ is path averaged rain rate and R_p is the surface-point

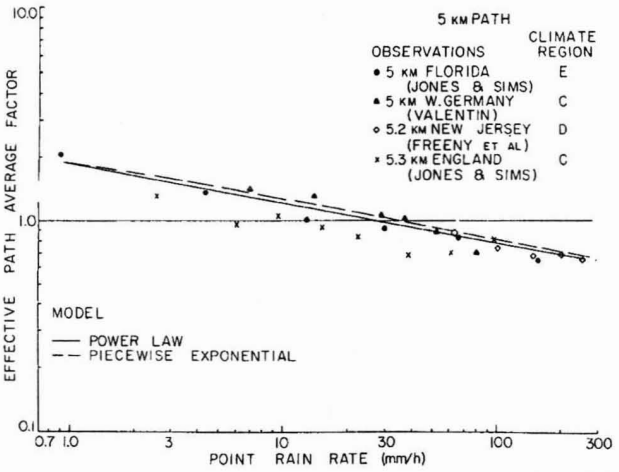

Fig. 9. Path averaged rain rate observations and point-to-path model.

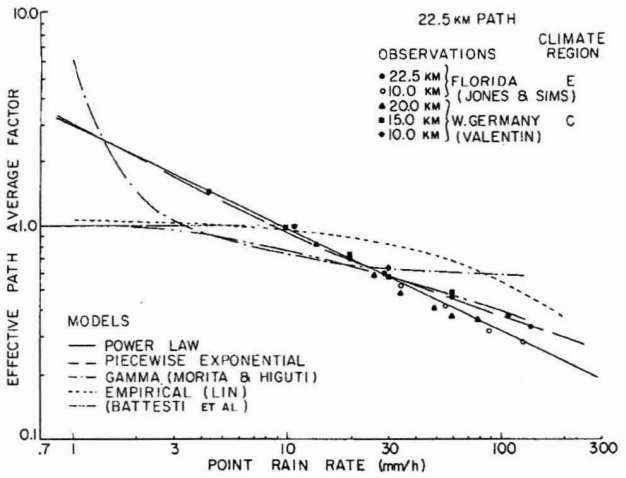

Fig. 10. Path averaged rain rate observations transformed to a 22.5 km path using the spatial independence assumption and model estimates.

rain rate. The data from Florida, New Jersey, and West Germany form an approximate power law relationship; the power law curve is the median of these data. Data for other observation path lengths also displayed approximate power law relationships.

Data were analyzed for path lengths of 5, 10, and 22.5 km. To obtain a sufficient sample size at 22.5 km, it was assumed that, for point rate rates in excess of 25 mm/h, their occurrence probabilities were independent over distances greater than 10 km. This is a reasonable assumption based upon experience with weather radar data. The assumption also produced agreement between observations at path lengths of 10, 15, 20, and 22.5 km and with the power law approximation as displayed in Fig. 10. In using the independence assumption, the path integrated rain rate value ($\bar{R}D$) for a path of length D_2 is equal to the value for a path of length D_1 when the exceedence probability is adjusted by the relative lengths of the paths:

$$P(\bar{R}_1 D_1) = P(\bar{R}_2 D_2) \cdot \left[\frac{D_1}{D_2}\right], \qquad \bar{R}D = \bar{R}_1 D_1 = \bar{R}_2 D_2 \tag{1}$$

where $P(\bar{R}D)$ is the probability of $\bar{R}$ being exceeded on a path of length D and the subscripts identify the path.

The power law relationship parameters were empirically established for distances from 0 to 22.5 km. The power law is expressed by

$$r = \gamma(D) R_p^{\,\delta(D)}; \quad \bar{R} = rR_p = \gamma R_p^{\,(1+\delta)} \tag{2}$$

where $\gamma(D)$ is given in Fig. 11(a) and $\delta(D)$ in Fig. 11(b). For paths D longer than 22.5 km, the value $\bar{R}D = rR_pD$ is identical to the $r'R_p'D_0$ value for a $D_0 = 22.5$ km path, but the R_p' value to be used for the 22.5 km path calculation is obtained from the rain rate distribution function at the probability of occurrence P', $P' = (22.5/D) \cdot P$ where P is the probability of interest.

This path average model produces the desired relationship between the rain rate at a point and the rain rate averaged over a horizontal path of length D. The specific attenuation, however, is a nonlinear function of point rain rate; hence, the model is not adequate for the estimation of attenuation. A statistical model of the profile of instantaneous rain rate along the path is required which then can be integrated to produce the desired attenuation value.

The simplest path profile for rain rate which, when integrated produces the observed median power law relationship, is the derivative of the power law relationship with respect to path length. The data in Fig. 11 were numerically differentiated to obtain this simplest profile model. The results are presented in Fig. 12. These data display the expected behavior. At high point rain rates, the intense rain occurs close to the origin or sampling point location. At low point rain rates, higher rain rates are more likely at distances in excess of 6 km from the sampling location. The latter value is half the average spacing between significant cells observed by Crane [18]. The path profile is still not in a form useful for attenuation modeling because it cannot be readily incorporated into an integral expression for attenuation. This last step is accomplished by a piecewise representation of the curves (Fig. 12) by exponential functions. An adequate model results when two exponential functions are used to span the 0-22.5 km distance range, one from 0 to d km, the other from d to 22.5 km. The resultant model for attenuation (or path integrated rain rate) is given by

$$A(R_p, D) = \alpha R_p^{\,\beta}\left[\frac{e^{u\beta d} - 1}{u\beta} - \frac{b^\beta e^{c\beta d}}{c\beta} + \frac{b^\beta e^{c\beta D}}{c\beta}\right]; \qquad d \leqslant D \leqslant 22.5\ km$$

$$A(R_p, D) = \alpha R_p^{\,\beta}\left[\frac{e^{u\beta D} - 1}{u\beta}\right]; \qquad 0 < D \leqslant d \tag{3}$$

where A is in dB, R_p in mm/h, the specific attenuation in

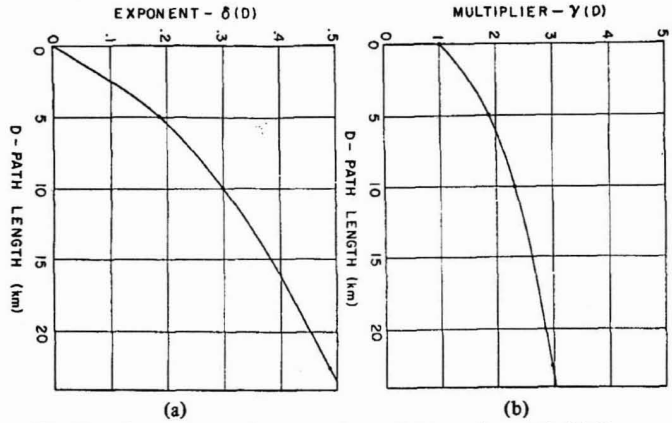

Fig. 11. (a) Multiplier in power law point-to-path model. (b) Exponent in power law point-to-path model.

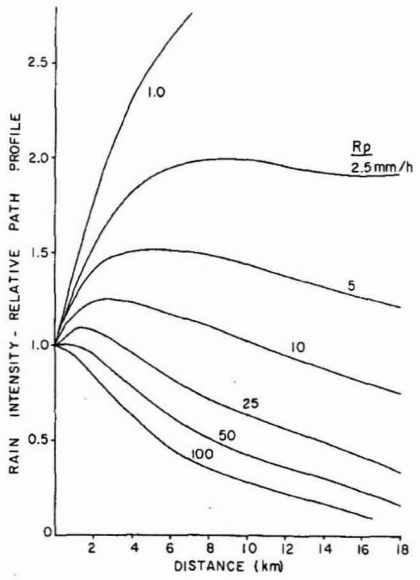

Fig. 12. Relative path rain rate profile, power law model.

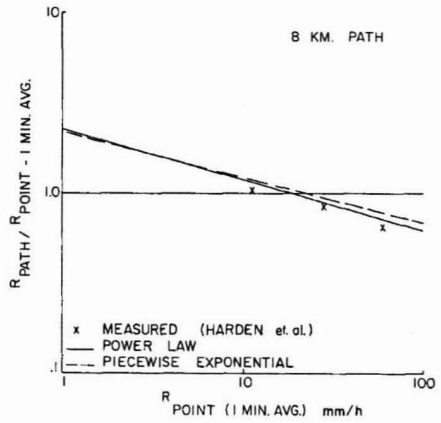

Fig. 13. Comparison between observations and model for data from the United Kingdom (after Harden *et al.* [28]).

dB/km is related to point rain rate by αR^{β} [32], and the remaining coefficients are empirical constants of the piecewise exponential model,

$$u = \frac{\ln [be^{cd}]}{d}; \qquad d \text{ in km} \tag{4}$$

$$b = 2.3\, R_p^{-0.17}; \qquad R_p \text{ in mm/h} \tag{5}$$

$$c = 0.026 - 0.03 \ln R_p \tag{6}$$

$$d = 3.8 - 0.6 \ln R_p. \tag{7}$$

The expression for path attenuation reduces to an expression for the path integrated rain rate when $\alpha = \beta = 1$. The use of this model for the estimation of the effective path average factor is illustrated by the dashed curves in Figs. 9 and 10.

A number of other path average models have been developed using either simultaneous attenuation observations [6], [7] or an assumed Gamma distribution and the observed spatial correlation properties between point rain gauge observations to model the rain rate distribution [31]. Several of these models are also displayed in Fig. 10. With the exception of the Gamma distribution model, the models do not portray the increase in the effective path average factor shown by the data at low rain rates. The Gamma distribution does not adequately represent the observed dependence of effective path average factor on point rain rate at rain rates below 20 mm/h.

Harden *et al.* [28], in their consideration of attenuation estimation for terrestrial communication systems, presented the results of additional point-to-path conversion measurements which were not used in the development of the power law and piecewise exponential models. Their data are presented in Fig. 13 together with the model predictions. The power law model predicts the experimental results with 10 percent of the observed values; the piecewise exponential model is within 20 percent. On the basis of the variations of all the observations including those used for the preparation of the model and other observations that have since become available, the piecewise exponential model will predict the observed path average rain rate given the equal exceedence

probability point rain rate with an rms uncertainty of 17 percent.

IV. PREDICTION OF THE VERTICAL VARIATION OF SPECIFIC ATTENUATION

The point-to-path model predicts the variation of rain rate along a horizontal (surface) path and is suitable for use in the design of terrestrial communication systems. For slant paths, the variation of specific attenuation in the vertical is also important. Theoretical analyses indicate that frozen precipitation in the form of ice and snow do not produce significant attenuation [10]. Water, when present in the form of raindrops or water coatings on raindrop size ice particles, produces significant attenuation.

At one time, the bright band or so-called melting layer evident in radar observations of widespread rain was thought to be caused by melting snow modeled as large water-coated snow particles that could produce significant attenuation [11]. Recent linearly polarized radar measurements of the change in cross section with the orientation of the polarization vector indicate that the bright band is in a region that is still predominantly snow, and that significant melting takes place below the bright band and at a height near the 0°C isotherm [33]. Microphysical observations further suggest that the bright band is produced by snowflake aggregation at about −2°C, and the melting process produces small liquid droplets at the extremities of the snowflakes which subsequently enlarge until the flake collapses into a raindrop. In this version of the melting process, increased attenuation due to large, uniformly wet structures will not occur; the attenuation will be proportional to the melted portion of the snow liquid water content until the larger collapsed drop is formed, at which time the theoretical specific attenuation, rain rate relationship obtains. The simultaneous radar and attenuation observations reported by McCormick [12] and by Goldhirsh [13] support the contention that only the melted raindrops produce attenuation and the regions of ice, snow, and aggregated snow crystals (bright band) do not cause significant amounts of attenuation.

Radar observations also show that rain is characterized on the average by a constant reflectivity from the surface to the height of the 0°C isotherm [15]. Based upon drop size distribution analyses, the constancy of the reflectivity value implies constancy in the value of specific attenuation. A useful model for the vertical structure of specific attenuation therefore assumes a constant value from the surface to the height of the 0°C isotherm. The specific attenuation value is deduced from the surface-point rain rate using a theoretically derived relationship based upon the analysis of drop size distribution data [32], [34].

The height of the 0°C isotherm varies with meteorological conditions. The seasonally and zonally averaged (averaged in longitude at a constant latitude) height of the 0°C isotherm varies from 4.7 km in the tropics to 3.1 km at 40° latitude to the surface at 61° latitude [35]. The height of the 0°C isotherm displays a marked seasonal dependence which, when coupled with the seasonal variation in the occurrence of the higher rain rates, indicates that the 0°C height to be used for the prediction of attenuation should have both a latitude and probability of occurrence dependence.

The dependence of the 0°C isotherm height on latitude and general rain conditions was established for seven locations within the United States using upper air sounding data, surface maps to establish the occurrence of precipitation, and excessive precipitation data to establish the correlation between 0°C height and the occurrence of excessive precipitation events. A high correlation between the average 0°C height and the height at which liquid raindrops exist should not be expected for the higher rain rates because large liquid water droplets are carried aloft above the 0°C height in the strong updraft cores of intense rain cells. Large drops can often be observed up to heights corresponding to temperatures near −5°C. As a model for the prediction of attenuation, the average height of the 0°C isotherm for days with rain was taken to correspond to the height to be expected 1 percent of the year. The highest height observed with rain was assumed to correspond to the value to be expected 0.001 percent of the year. Since the latter value corresponds to the average summer height of the −5°C isotherm, additional support is gained for its use. The latitude dependences of the heights to be expected for surface-point rain rates exceeded 1 percent of the year and 0.001 percent of the year were obtained from the latitude dependences provided by Oort and Rasmussen [35]. The resultant curves are presented in Fig. 14. For the estimation of model uncertainty, the seasonal rms uncertainty in the 0°C isotherm height was 500 m or roughly 13 percent of the average estimated height. The value of 13 percent is used to estimate the expected uncertainties to be associated with Fig. 14.

The correspondence between the 0°C isotherm height values and the excessive precipitation events showed a tendency toward a linear relationship between R_p and H where H is the 0°C isotherm height for high values of R_p. Since, at high rain rates, the rain rate distribution function displays a nearly linear relationship between R_p and $\log P$ (P is probability), the interpolation model used for the estimation of H for P between 0.001 and 1 percent is assumed to have the form

$$H = a + b \log P. \tag{8}$$

This relationship was used to provide the intermediate values displayed in Fig. 14.

The complete model for the estimation of attenuation on a slant path starts with the determination of the vertical distance between the height of the earth station and the 0°C isotherm height ($H - H_0$ where H_0 is station height) for the percentage of the year (or R_p) of interest. The surface projection of the path between the surface and the 0°C isotherm is used to calculate D:

$$\begin{aligned} D &= (H - H_0)/\tan\theta; \qquad \theta \geq 10^\circ \\ &= E\psi, \quad \psi \text{ in radians}; \quad \theta < 10^\circ \end{aligned} \tag{9}$$

where

$$\psi = \sin^{-1}\left[\frac{\cos\theta}{(H+E)} \cdot \left(\sqrt{(H_0+E)^2\sin^2\theta + 2E(H-H_0) + H^2 - H_0^2} - (H_0+E)\sin\theta\right)\right]$$

E is the effective earth's radius (8500 km) and θ is the elevation angle.

The surface-projected attenuation is calculated from (3), and finally, the value for the slant path A_s is estimated using the constancy of specific attenuation below H by

$$A_s = \frac{LA(D)}{D} \tag{10}$$

where

$$L = D/\cos\theta;\ \theta \geq 10^\circ$$
$$= \sqrt{(E+H_0)^2 + (E+H)^2 - 2(E+H_0)(E+H)\cos\psi};\quad \theta < 10^\circ.$$

V. PREDICTION OF VARIATION ABOUT THE ESTIMATED VALUE

The expected value of attenuation to be exceeded a specified percentage of the year is obtained from a four-step procedure requiring: 1) the estimation of the surface-point rain rate, 2) the specific attenuation given the point rain rate, 3) the physical extent of the attenuating region, and 4) the attenuation along the path. The procedure is empirical in nature; each step utilizes a median value derived from a pooled set of observations. The uncertainties claimed for each step are likewise empirical, being obtained from the observed variance of the pooled data. The uncertainties are summarized and combined in this section to provide an overall estimate of the uncertainty in attenuation prediction. The values are expressed as percentages and are to be used for all rain climate regions.

The rain rate climate regions were initially established to span a 40 percent range in rain rate between the empirical distribution functions for adjacent regions at a specified probability value. Distribution functions were pooled from each region to establish the median values of the distribution function at specified probability levels. The standard deviations of the distribution function values were independently obtained at selected probability levels from excessive precipitation data and from the observations reported by Harden *et al.* [28] for climate Region *C*. The resultant standard deviation estimates for the distribution function were 30 percent (in rain rate) at 0.001 and 1.0 percent of the year and 20 percent at 0.01 and 0.1 percent of the year. As an independent evaluation of the uncertainty estimate, the mean and standard deviation of the pooled region D_2 distribution functions were calculated at 0.01 percent of the year. The resultant values were 53 mm/h and 24 percent for the mean and standard deviation (as percent of mean), respectively. These values are in good agreement with the 49 mm/h and 20 percent model values.

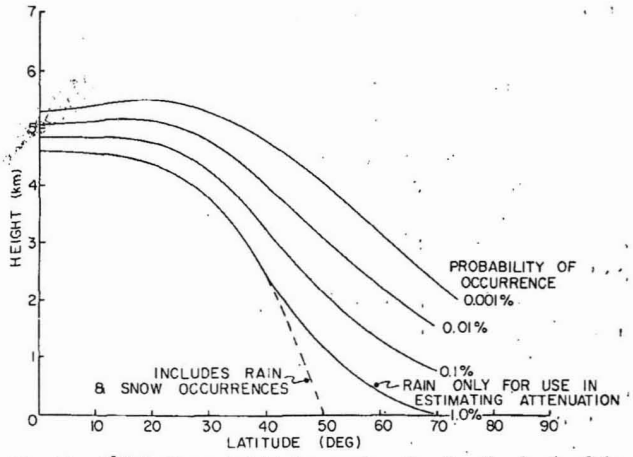

Fig. 14. 0°C isotherm height for use in estimating the depth of the attenuating region on a slant path.

The value of specific attenuation used in the model calculations is obtained from the point rain rate value using a power law relationship to approximate computations employing the Laws and Parsons drop size distribution [32], [34], [36]. Crane [10] found that differences between calculated values of specific attenuation obtained from the Laws and Parsons distribution and from a large number of observed drop size distributions were not statistically significant for frequencies up through 50 GHz. At higher frequencies, the drop size distribution measurement errors in the small drop size range, characteristic of currently available disdrometers, affects the accuracy of the specific attenuation, rain rate relationship. At frequencies up through 50 GHz, the power law relationship matches the calculations based on the Laws and Parsons distribution within an uncertainty of five percent over the 0.25–150 mm/h rain rate range of interest. The additional uncertainties associated with sampling the drop size distribution are negligible and may be ignored [10].

The physical extent of the attenuating region is defined without any uncertainty for a terrestrial path, but depends upon the vertical extent of the rain region for a slant path. In the latter case, the standard deviation associated with the estimate of rain region height was 13 percent.

The point-to-path relationship was obtained from a median best fit curve to the observed variation of the effective path average factor with point rain rate for data pooled from three separate rain climate regions. The data show statistical variation (Figs. 9 and 10) about the piecewise exponential model curve. The spread is associated with both the intrinsic variability of the relationship within and between climate regions and the statistical uncertainties in the estimate of the distribution functions used for the calculation of the effective

TABLE II
EXPECTED STANDARD DEVIATION OF MEASUREMENTS ABOUT MODEL IN PERCENT

Path Type \ Percent of Year	1	.1	.01	.001
Terrestrial Path	36	28	28	36
Slant Path	39	32	32	39

path average factor and point rain rate values due to the limited (a year or less) duration of the observations. Ignoring the latter problem, the data show a 17 percent (rms) deviation about the model curve.

In summary, the several steps of the attenuation prediction model are based on the use of median values of statistically variable quantities. The statistical processes associated with each step can be assumed to be independent of each other and the variances combined on that basis. The terms in the attenuation prediction equation (3) corresponding to each step are multiplicative; hence, we use the percent values for the standard deviations. The variances of the logarithms of the individual bounds were combined to produce the final variance estimate (again expressed in percent). The resultant standard deviation estimates are presented in Table II. These values apply to the estimate of the year-to-year variability in attenuation on a single path or within-the-region variability of similar paths.

VI. APPLICATION OF THE MODEL

Terrestrial Paths

The attenuation prediction model may be used for terrestrial or slant paths operating at any elevation angle. The model was developed solely on the basis of geophysical rain rate and rain structure data, not on the use of simultaneous attenuation observations. The utility of the model, however, can only be established by comparison with attenuation observations.

Harden *et al.* [28] reported on the variation of observed attenuation distributions with distance at fixed percentage of occurrence values obtained on a number of terrestrial paths in the UK. These data are depicted in Figs. 15–17 for frequencies of 11.0, 20.0, and 36.5 GHz, respectively. Two model results are presented: one for the rain rate distribution for rain climate Region *C*, the other for the average measured rain rate distribution R_p (Fig. 8). In calculating the attenuation values, the α and β coefficients in Figs. 18 and 19 and Table III were used. These values were obtained for a Laws and Parsons [36] drop size distribution and a 0°C drop temperature using the procedure described by Crane [34].

At 11.0 GHz, the data are clustered about the model curves for 0.01 percent of the year and about the model results based upon the use of the average measured distribution at 0.001 percent of the year. The one standard deviation bounds (from Table II) are plotted about the model calculation made using the average measured rain rate distribution. Seventy percent of the observations are within the one standard deviation bounds at 0.01 percent of the year, 90 percent at 0.001 percent of the year. These results show excellent agreement between prediction and calculation based on the average observed rain rate distribution. The observed variation about the model calculation is caused by the within-region change in the rain rate distribution. The model calculations using the climate Region *C* rain rate distribution are also in good agreement with the observations; 70 percent of the observations are within the one standard deviation bounds at 0.01 percent of the year and 59 percent are within the bounds at 0.001 percent of the year. The model does well at all distances well into

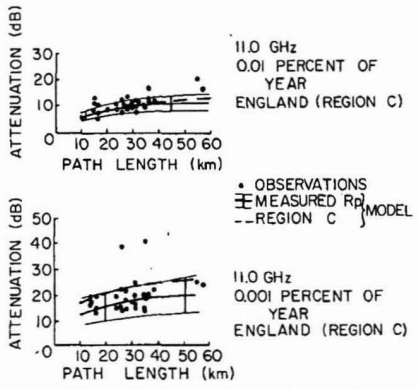

Fig. 15. Terrestrial path observations at 11.0 GHz in the United Kingdom [28].

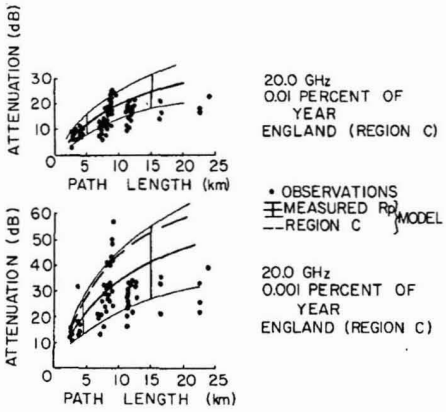

Fig. 16. Terrestrial path observations at 20.0 GHz in the United Kingdom [28].

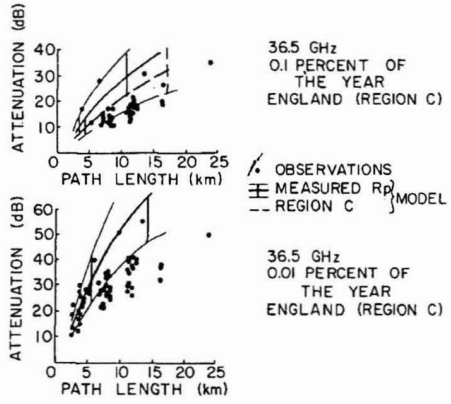

Fig. 17. Terrestrial path observations at 36.5 GHz in the United Kingdom [28].

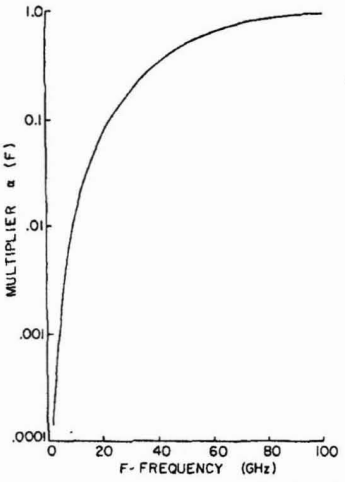

Fig. 18. Multiplier in the power law relationship between specific attenuation and frequency.

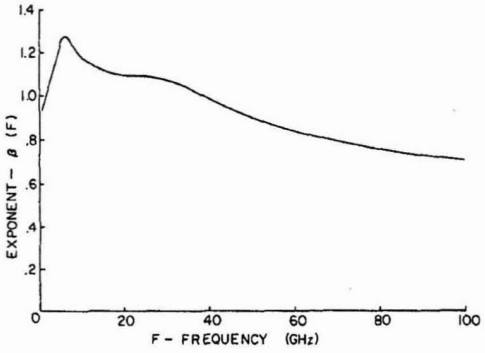

Fig. 19. Exponent in the power law relationship between specific attenuation and frequency.

TABLE III
PARAMETERS FOR COMPUTING SPECIFIC ATTENUATION
$a = \alpha R_p^{\beta}$ (dB/km)

Frequency F – GHz	Multiplier α (F)	Exponent β(F)
1	0.00015	0.95
4	0.00080	1.17
5	0.00138	1.24
6	0.00250	1.28
7.5	0.00482	1.25
10	0.0125	1.18
12.5	0.0228	1.145
15	0.0357	1.12
17.5	0.0524	1.105
20	0.0699	1.10
25	0.113	1.09
30	0.170	1.075
35	0.242	1.04
40	0.325	0.99
50	0.485	0.90
60	0.650	0.84
70	0.780	0.79
80	0.875	0.753
90	0.935	0.730
100	0.965	0.715

the region requiring the application of the independence assumption of Section III. It is noted that the measurements and model agree at a frequency where the nonlinearity in the αR^{β} relationship is relatively important.

At 20 GHz (Fig. 16) reasonable agreement is again evident between the model calculations employing the average measured rain rate distribution R_p. At 0.01 percent of the year, 68 percent of the observations are within one standard deviation of the model prediction (using either R_p or climate Region C); at 0.001 percent of the year, 71 percent are within the one standard deviation bound for the model employing R_p, but only 45 percent are within the bounds for calculations based on the use of the rain climate C distribution. At 0.001 percent of the year, all the out-of-bounds points relative to the Region C calculation show less attenuation than predicted, a result consistent with the difference between R_p and the Region C curve shown in Fig. 8. In general, the impression gained from Fig. 16 is a tendency for the model to underestimate the attenuation for longer paths, a result that could be due to a limited dynamic range of the observing equipment.

At 36.5 GHz, the rain climate Region C distribution curve provides a better fit to the observations; at 0.1 percent of the year, 51 percent of the obervations are within the one standard deviation bounds of the climate Region C curve, while only 14 percent are within the plotted bounds about the R_p calculation. In this case, the rain climate region model provides a better match to the observations. Again, the effect of poor instrument dynamic range is evident at the longer ranges. At 0.01 percent of the year, 78 percent of the observations are within the plotted bounds for paths with lengths shorter than 6 km or expected attenuation values less than 30 dB; 55 percent are within bounds for ranges less than 10 km; but only two observations (11 percent) are within bounds for ranges greater than 10 km (observations which require dynamic ranges in excess of 50 dB).

Measurements on paths having an expected attenuation values of less than 30 dB show excellent agreement between model prediction and observation, particularly when reliable rain rate distribution estimates are available. The success of the prediction method did not depend upon path length for the data shown except where attenuation values in excess of 30 dB are expected. These results confirm the use of the model on terrestrial paths.

Slant Paths

Recent observations using the CTS, COMSTAR, and ATS-6 satellite beacons allow the evaluation of the model at a number of frequencies and locations in Regions D_2 and D_3 of the United States. An example of observations of CTS at 11.7 GHz [37] together with model predictions is given in Fig. 20. The observations match (within 1 dB) the Region D_2 model between 0.2 and 1.0 percent of the year and are within the one standard deviation bounds of the Region D_2 model for percentages of the year less than 0.03. Since agreement between measurements and model calculations is best expressed on a percentage basis, the data are replotted in Fig. 21. The measurements show generally good agreement with the model

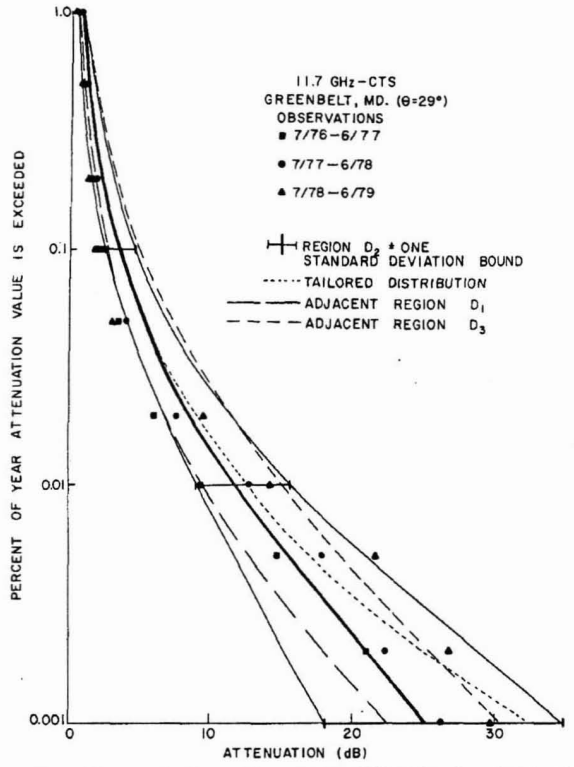

Fig. 20. Slant path observations at 11.7 GHz (after Ippolito [37]).

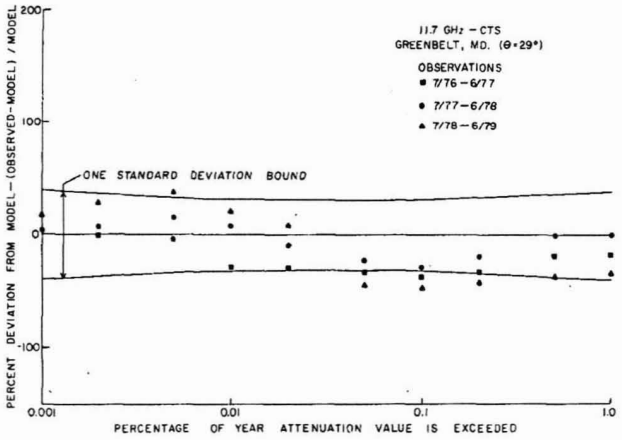

Fig. 21. Slant path observations as percent deviation from the model estimate; same data as Fig. 20.

predictions; 79 percent of the observations lie within the one standard deviation bounds shown in the figure.

Comparisons between a larger sample of observations and model calculations are presented in Fig. 22. The data presented in this figure include the comparison already presented in Fig. 21 plus 11.7 GHz CTS observations from Waltham, MA [38] (see Fig. 4 for location), Holmdel, NJ [39], Blacksburg, VA [8], and Austin, TX [40]; 19.04 and 28.56 GHz–COMSTAR observations from Holmdel, NJ [41], Clarksburg, MD [42], Wallops Island, VA [43], and Blacksburg, VA [8]; and 20 and 30 GHz–ATS-6 measurements from Rosman, NC

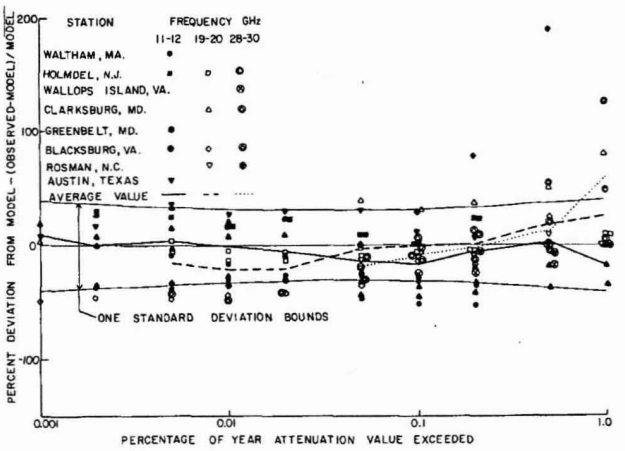

Fig. 22. Slant path observations as percent deviation from the model estimate for seven locations and three frequencies. The locations are given in Fig. 4.

[44]. These data show excellent agreement between measurement and model for percentages of the year less than 0.1 and for all percentages at locations other than Blacksburg, VA. For all the data plotted in Fig. 22, 76 percent of the observations were within the one standard deviation bound about the model prediction. The model is also well supported on average as shown in Fig. 23. In this figure, the mean deviation and standard deviation of the measurements about model predictions are displayed for the data averaged (over frequency and years) at each observation site. The mean deviation is not statistically different from zero (at one standard deviation), indicating that the model predicts attenuation without bias. The standard deviation of the observations about the model is also in good agreement with the predicted value.

Elevation Angle Dependence

The slant path attenuation model provides attenuation estimates for all elevation angles. The sun tracker observations made in the early 1970's provide data for comparison with elevation angle dependence estimates. Kinase and Kinpara [45] provided data on the elevation angle variation of 11.7 GHz attenuation observations for Klang, Malaysia (climate Region *H*; see Fig. 6). The model calculations for 10 and 20 mm/h (0.66 and 0.33 percent of the year, respectively) are presented as a function of elevation angle in Fig. 24 together with the observations for the same probabilities of exceedence. The model results and measurements show definite departures from a simple cosecant of the elevation angle dependence at both high and low elevation angles. The model agrees with observation at the rms deviation expected for observations which vary in elevation angle in synchronism with the sun (~53 percent rms). The data for all elevations and both probabilities of occurrence have a 48 percent rms deviation about the model predictions; at elevation angles above 10°, the rms deviation is less than 36 percent.

These data show excellent agreement between the prediction model and observations.

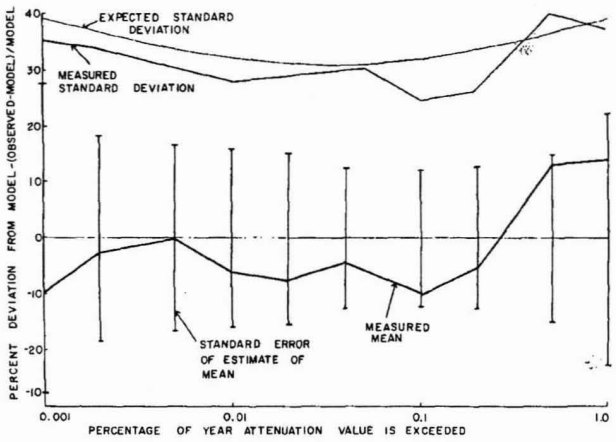

Fig. 23. Mean and standard deviation of the differences between observation and prediction averaged (over time and frequency) at each site.

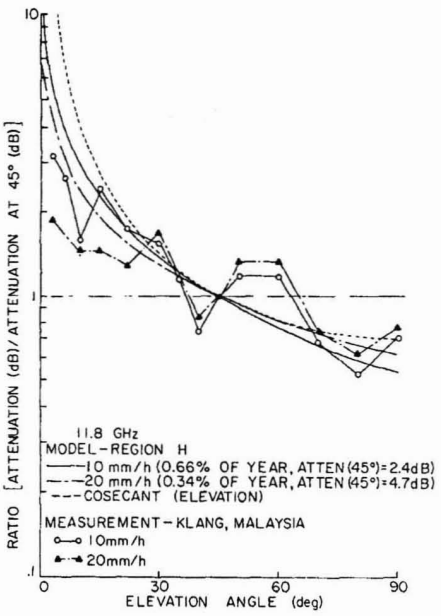

Fig. 24. Elevation angle dependence of 11.8 GHz Suntracker observations at Klang, Malaysia (climate region H; after Kinase and Kinpara [45]).

VII. CONCLUSIONS

A new model for the prediction of attenuation due to rain for use on either terrestrial or slant propagation paths has been prepared and tested against terrestrial system measurements from paths of different length and satellite observations on slant paths of differing elevation angle. For measurements of acceptable quality, the measurements and predictions agree within the predicted one standard deviation bounds for measurements about the model. The average behavior of the predictions is also excellent; the mean deviations between measurement and model are smaller than 14 percent.

The model provides both the outline of a general prediction procedure and a set of detailed steps for making a prediction. The step-by-step procedure is summarized in the Appendix. The model was developed for easy application; the results presented in this paper were all obtained by the author's teenage daughter using a pocket calculator.

Some of the steps in the model deserve additional consideration. The model for the 0°C isotherm height was generated using data from a limited number of upper air stations in the United States, all of which have station heights within 300 m of mean sea level. The model was extended globally on the basis of zonal averages. Application has been successful for stations in low mountains near the coast, but no consideration was made of the general modification of the vertical tempera ture structure caused by large regions of high terrain such as the high plains of Kansas or other similar regions.

Additional refinement in the rain rate climate description is also possible, but requires high quality data spanning more than 10 years at each location. More work is also required on understanding the local variations in rain rate climate, but again, long duration records are required for analysis. Noting the assumed correspondence between measurements made at one point in space over a long time period and over a larger spatial area over much shorter periods, say of a year or two, well-calibrated weather radar observations may provide the data required to extend the model and establish the effects of local terrain variations.

The model should be extended to provide seasonal and monthly predictions. For many system applications, the problem is to establish the design for the worst month to be expected in a number of years. A useful definition of a worst month has been established [46], but the procedures presented in this paper must be modified and expanded to provide a means to estimate worst month performance statistics.

APPENDIX

STEP-BY-STEP APPLICATION OF THE ATTENUATION PREDICTION MODEL

Step 1–Determine Rain Rate Distribution R_p.

1a) Locate path endpoints (terrestrial) or earth station on map (Figs. 3 or 4) and determine rain climate region, A-H.

1b) Obtain rain rate distribution from Table I (or Fig. 5 or 7).

Note that a tailored distribution may be prepared for special locations (see text) and in some instances measured distributions may be available. Caution is recommended in the use of measured instantaneous (1 min average) rain rate distributions if the observations are for a period of less than 10 years.

Step 2–Establish Surface Projected Path Length D.

2a) For terrestrial paths, D is the separation between antennas.

2b) For slant paths, the distance D is calculated from

$$D = (H(P) - H_0)/\tan\theta; \qquad \theta \geqslant 10^\circ$$

$$= E\psi, \text{ see (9)}; \qquad \theta < 10^\circ$$

where θ is the elevation angle, H_0 is the station height, and $H(P)$ is the 0°C isotherm height obtained by interpolation in Fig. 14 for the percentage of time P of interest. To interpolate, plot $H(P)$ versus log P and use a straight line to relate H to log P.

2c) If $D > 22.5$ km, use both $D_0 = 22.5$ km and a new point rain rate R_p' for the modified probability of occurrence,

$$P' = P\left[\frac{D_0}{D}\right]$$

for subsequent calculations.

Step 3–Determine α and β for the frequency of interest from Table II or Figs. 18 and 19.

Step 4–Calculate the surface projected attenuation value A from the R_p and D (or R_p' and D_0). R_p is the rain rate obtained from the rain rate distribution for the probability of occurrence of interest P:

$$A(R_p, D) = \alpha R_p{}^{\beta}\left[\frac{e^{u\beta d} - 1}{u\beta} - \frac{b^{\beta}e^{c\beta d}}{c\beta} + \frac{b^{\beta}e^{c\beta D}}{c\beta}\right]; \qquad d \leqslant D \leqslant D_0$$

$$A(R_p, D) = \alpha R_p{}^{\beta}\left[\frac{e^{u\beta D} - 1}{u\beta}\right]; \qquad D < d$$

$$A(R_p, D) = (H(P) - H_0)\alpha R_p{}^{\beta}; \qquad D = 0(\theta = 90°)$$

where

$$u = \frac{\ln\,[be^{cd}]}{d},$$

$$b = 2.3\,R_p{}^{-0.17},$$

$$c = 0.026 - 0.03 \ln R_p, \quad \text{and}$$

$$d = 3.8 - 0.6 \ln R_p.$$

Step 5–Adjust for height along a slant path (do not perform this step for terrestrial application).

See (10) for $\theta < 10°$:

$$A_s = \frac{LA(R_p, D)}{D} = \frac{A(R_p, D)}{\cos\theta}; \qquad \theta \geqslant 10°$$

where A_s is the slant path attenuation.

ACKNOWLEDGMENT

The measurements used for model evaluation were made available to the author by contractors working for NASA, by Bell Laboratories, and by GTE. The author wishes to acknowledge the help of D. Blood in the preparation of the manuscript and of his daughter, Kathy, who calculated the slant path attenuation estimates during a vacation from high school.

REFERENCES

[1] R. K. Crane, "Propagation phenomenon affecting satellite communication systems operating in the centimeter and millimeter wavelength bands," *Proc. IEEE*, vol. 59, pp. 173–188, 1971.

[2] ——, "Attenuation due to rain—A mini review," *IEEE Trans. Antennas Propagat.*, vol. AP-23, pp. 750–752, 1975.

[3] P. L. Rice and N. R. Holmberg, "Cumulative time statistics of surface-point rainfall rates," *IEEE Trans. Commun.*, vol. COM-21, pp. 1131–1136, 1973.

[4] W. C. Y. Lee, "An approximate method for obtaining rain rate statistics for use in signal attenuation estimating," *IEEE Trans. Antennas Propagat.*, vol. AP-27, pp. 407–413, 1979.

[5] E. J. Dutton and H. T. Dougherty, "Year-to-year variability of rainfall for microwave applications in the USA," *IEEE Trans. Commun.*, COM-27, pp. 829–832, 1979.

[6] J. Battesti, L. Boithias, and P. Misme, "Determination de l'affaiblissement dês a la pluie pour les frequences superieures a 10 GHz," *Ann des Telecommun.*, vol. 26, pp. 439–444, 1971.

[7] S. H. Lin, "Nationwide long-term rain statistics and empirical calculation of 11 GHz microwave rain attenuation," *Bell Syst. Tech. J.*, vol. 56, pp. 1581–1604, 1977.

[8] W. L. Stutzman and C. W. Bostian, "A millimeter wave attenuation and depolarization experiment using the COMSTAR and CTS satellite," Final Rep. SATCOM-79-2, Virginia Polytechnic Inst. and State Univ., Blacksburg, VA; U.S. Army Res. Office, Grant PAAG 29-77-G-0083, 1979.

[9] R. R. Rogers, "Statistical rainstorm models: Their theoretical and physical foundations," *IEEE Trans. Antennas Propagat.*, vol. AP-24, pp. 547–566, 1976.

[10] R. K. Crane, "Prediction of the effects of rain on satellite communication systems," *Proc. IEEE*, vol. 65, pp. 456–474, 1977.

[11] J. R. Joss, R. Cavalli, and R. K. Crane, "Good agreement between theory and experiment for attenuation data," *J. de Recherches Atmosph.*, vol. 8, pp. 299–318, 1974.

[12] K. S. McCormick, "A comparison of precipitation attenuation and radar backscatter along earth-space paths," *IEEE Trans. Antennas Propagat.*, vol. AP-20, pp. 745–755, 1972.

[13] J. Goldhirsh, "Predictive methods for rain attenuation using radar and in-situ measurements tested against the 28-GHz COMSTAR beacon signal," *IEEE Trans. Antennas Propagat.*, vol. AP-27, pp. 398–406, 1979.

[14] T. W. Harrold and P. M. Austin, "The structure of precipitation systems—A review," *J. de Recherches Atmosph.*, vol. 8, pp. 41–57, 1974.

[15] J. Goldhirsh and I. Katz, "Useful experimental results for earth-satellite rain attenuation modeling," *IEEE Trans. Antennas Propagat.*, vol. AP-27, pp. 413–415, 1979.

[16] W. F. Bodtmann and C. L. Ruthroff, "Rain attenuation on short radio paths: Theory, experiment, and design," *Bell Syst. Tech. J.*, vol. 53, pp. 1329–1349, 1974.

[17] H. E. Bussey, "Microwave attenuation statistics estimated from rainfall and water vapor statistics," *Proc. IRE*, vol. 38, pp. 781–785, 1950.

[18] R. K. Crane, "Automatic cell detection and tracking," *IEEE Trans. Geosci. Electron.*, vol. GE-17, pp. 250–262, 1979.

[19] L. J. Ippolito, "11.7 GHz attenuation and rain rate measurements with the Communications Technology Satellite (CTS)," NASA Tech. Memo. 80283, NASA/Goddard Space Flight Center, Greenbelt, MD, 1979.

[20] D. M. A. Jones and A. L. Sims, "Climatology of instantaneous rainfall rates," *J. Appl. Meteorol.*, vol. 17, pp. 1135–1140, 1978.

[21] R. C. Barry and R. J. Chorely, *Atmosphere, Weather, and Climate*. New York: Holt, Rinehart, and Winston, 1970.

[22] CCIR, "Radiometeorological data," CCIR Study Group 5 Rep. 563-1 ITU, Geneva, Switzerland, 1978.

[23] E. J. Dutton, "Precipitation variability in the U.S.A. for microwave terrestrial system design," OTR77-134, NTIS, Springfield, VA, 1977.

[24] H. E. Landsberg, Ed., *World Survey of Climatology*, Vols. 1–15. Amsterdam, The Netherlands: Elsevier, 1974.

[25] B. Haurwitz and J. Austin *Climatology*. New York: McGraw-Hill, 1944.

[26] M. S. V. Rao, W. V. Abbott, III, and J. S. Theon, "Satellite-derived global oceanic rainfall atlas (1973 and 1974)," NASA-SP-410 NASA/Goddard Space Flight Center, Greenbelt, MD, 1976.

[27] H. L. Crutcher and O. M. Davis, "U.S. Navy Marine climate atlas of the World, vol. VIII," NAVAIR 50-1C-54, Naval Weather Service Command, U.S. Navy, 1969.
[28] B. N. Harden, J. R. Norbury, and W. J. K. White, "Estimation of attenuation by rain on terrestrial radio links in the UK at frequencies from 10 to 100 GHz," *Microwave, Optics and Acoustics*, vol. 2, pp. 97–104, 1978.
[29] A. E. Freeny and J. D. Gabbe, "A statistical description of intense rainfall," *Bell Syst. Tech. J.*, vol. 48, pp. 1789–1851, 1969.
[30] R. Valentin, "Statistiken der Regendämpfung für Richtfunkverbindungen uber 10 GHz," Deutsche Bundespost Forschungsinstitet beim FTZ, Rep. 455-TB-62, 1977.
[31] K. Morita and I. Higuti, "Statistical studies in electromagnetic wave attenuation due to rain," *Rev. Elect. Comm. Lab. (Japan)*, vol. 19, pp. 798–842, 1971.
[32] R. L. Olsen, D. V. Rogers, and D. B. Hodge, "The aR^b relation in the calculation of rain attenuation," *IEEE Trans. Antennas Propagat.*, vol. AP-26, pp. 318–329, 1978.
[33] R. K. Crane, "Evaluation of uncertainties in the estimation of hydrometeor mass concentrations using SPANDAR data and aircraft measurements," Scientific Rep. 1., Environmental Res. Tech., Inc., Air Force Contract F19628-76-C-0069; AFGL-TR-78-0018, Air Force Geophys. Lab., Hanscom AFB, MA, 1978.
[34] R. K. Crane, "Microwave scattering parameters for New England rain," Tech. Rep. 426, Massachusetts Inst. Tech. Lincoln Lab., Lexington, MA, 1966.
[35] A. H. Oort and E. M. Rasmusson, *Atmospheric Circulation Statistics*, NOAA Professional Paper 5, U.S. Dept. of Commerce, 1971.
[36] J. O. Laws and D. A. Parsons, "The relation of raindrop-size to intensity," *Am. Geophys. Union Trans.*, vol. 24, pp. 452–460, 1943.
[37] L. J. Ippolito, private communication, 1979.
[38] D. Nackoney, "CTS 11.7 beacon data," Tech. Note TN78-471.3, GTE Lab., Inc., 1978.
[39] A. J. Rustako, Jr., "Measurement of rain attenuation and depolarization of the CTS satellite beacon signal at Holmdel, New Jersey," USNC-URSI Meeting, Seattle, WA, abstract only, 1979.
[40] W. J. Vogel, "CTS attenuation and cross polarization measurements at 11.7 GHz," Final Rep. Cont. NAS5-22576, Elec. Eng. Res. Lab., Univ. of Texas at Austin, Austin, TX, 1979.
[41] H. W. Arnold, D. C. Cox, H. H. Hoffman, and R. P. Leck, "Rain attenuation statistics from a 19 and 28 GHz COMSTAR beacon propagation experiment: One year cumulative distributions and relationships between two frequencies," *IEEE Trans. Commun.*, 1979.
[42] J. M. Harris and G. Hyde, "Preliminary results of COMSTAR 19/29 GHz beacon measurements at Clarksburg, Maryland," *COMSAT Tech. Rev.*, vol. 7, pp. 599–623, 1977.
[43] J. Goldhirsh, "Cumulative slant path rain attenuation statistics associated with the COMSTAR beacon at 28.56 GHz for Wallops Island, Virginia," *IEEE Trans. Antennas Propagat.*, vol. AP-27, 1979.
[44] L. J. Ippolito, "20 and 30 GHz millimeter wave experiments with ATS-6 satellites," NASA TND-8197, NASA Goddard Space Flight Center, Greenbelt, MD, 1976.
[45] A. Kinase and A. Kinpara, "Statistics of attenuation due to precipitation of radio waves in 12 GHz band at higher angles of elevation," Note 101, NHK Tech. Res. Labs., Tokyo, Japan, 1973.
[46] R. K. Crane and W. E. Debrunner, "Worst month statistics," *Electron. Lett.*, vol. 14, pp. 38–40, 1978.

★



Robert K. Crane (SM'71–F'80) received the B.S., M.S., and Ph.D. degrees in electrical engineering from Worcester Polytechnic Institute, Worcester, MA.

He was employed by The MITRE Corporation, where he worked on radar inputs to the SAGE system and on the effects of refraction on radar measurement accuracy. He then became a staff member of the M.I.T. Lincoln Laboratory where he conducted basic and applied research on radio wave propagation through the ionosphere and lower atmosphere, the structure of precipitation systems, and on turbulence in the clear atmosphere. He also served as principal investigator on programs to investigate bistatic scattering from rain and the statistics of weather radar echos conducted for NASA. Other experience includes the observation and analysis of the effects of rain, atmospheric turbulence, and ionospheric irregularities on radar, microwave radiometer, and satellite communication systems. During 1970, 1971 and 1974, he was a U.S. delegate to the International Radio Consultative Committee (CCIR) Meetings and to the World Administrative Radio Conference in 1971 as a Propagation Specialist. He is presently Division Senior Scientist, Earth Resources and Atmospheric Physics Division, Environmental Research & Technology, Inc. (ERT), Concord, MA. He is responsible for remote sensing studies of the earth's atmosphere, basic research in cloud physics, weather modification, radar meteorology, clear air turbulence, atmospheric dynamics, and basic research in radio wave propagation through the atmosphere.

Dr. Crane is a member of the American Meteorological Society, the American Geophysical Union, the International Union of Radio Science (Commission F), Sigma Xi, and Eta Kappa Nu.

Dispersive Fade Margin: A Physical Layer Performance Metric

John Liebetreu
SICOM, Incorporated

Introduction

The study of channel distortions during periods of multipath fading has a history extending to early deployments of microwave long-haul radio links. Early researchers found intersymbol interference to be the main source of channel-induced degradation in emerging digital radio links, so it made little sense to consider traditional flat fade margin as a performance metric.

In these early deployments, the need was recognized for estimating link performance during periods of frequency selective (multipath) fading. In addition, a metric was needed that provided good correlation between laboratory tests and field measurements, to enable assessment of the performance of a radio design prior to its field installation.

Early research by Lundgren and Rummler[1] formed the basis of a statistical model for the transfer function of the dispersive channel, which can cause severe intersymbol interference in digital radio systems. In addition to their statistical channel characterization, Lundgren and Rummler related this model to the probability of outage due to selective fading; this outage probability can be computed with data that is easily generated from a simple and direct set of digital radio performance measurements.

This paper describes a radio equipment "signature," a means of comparing different digital radio designs in their sensitivity to multipath fading, and reviews the concept of DFM, dispersive fade margin, as a measure of the expected outage due to selective fading.

Digital radio signatures: W-curves

Computation of DFM relies on measurement of the robustness of the digital radio and modem to frequency selective fading to obtain a "signature" for the digital radio and modem combination These signatures, known as W-curves (or dispersion signatures), measure the robustness of a communications system to frequency selective fading as a function of frequency. The tests for robustness are based on a two-ray multipath model (Rummler model) with 6.3 ns delay between the main (stronger) and secondary path rays. Note that no loss of generality results from using a fixed value for ray delay, and it has no associated physical interpretation, although signatures can be measured for values other than 6.3 ns. A simple scaling rule relates signatures created with different ray delay values: the width of the signature is independent of ray delay, and the amplitude of the signature is proportional to the ray delay value[2].

In the Rummler model, the main path may either lead or lag the secondary path. The case where the main path leads the secondary path is referred to as the minimum-phase multipath case, and the case where the main path lags the secondary path is referred to as the non-minimum-phase multipath case. Both the non-minimum phase W-curve and the minimum-phase W-curve signatures must be measured to obtain a true picture of a digital radio's robustness to frequency-selective multipath fading.

The procedure used to construct the W-curve signature for a digital radio requires that a notch be created at a given frequency offset from the carrier frequency; the notch depth is increased until

a specified BER is attained (typically between 10^{-3} and 10^{-6}). The depth of the notch is then plotted at this frequency offset. The shape of the resulting plot of notch depths versus frequency offset is responsible for its name. Two typical examples of the W-curve are depicted in figure 1; one of these W-curves corresponds to a BER specification of 10^{-3}, and one corresponds to a BER of 10^{-4}; both W-curves are for the minimum phase multipath case. Both the minimum dispersion signature and the non-minimum-phase dispersion signature are used to compute DFM, since some equalizers behave very differently under minimum-phase conditions than for non-minimum-phase conditions.

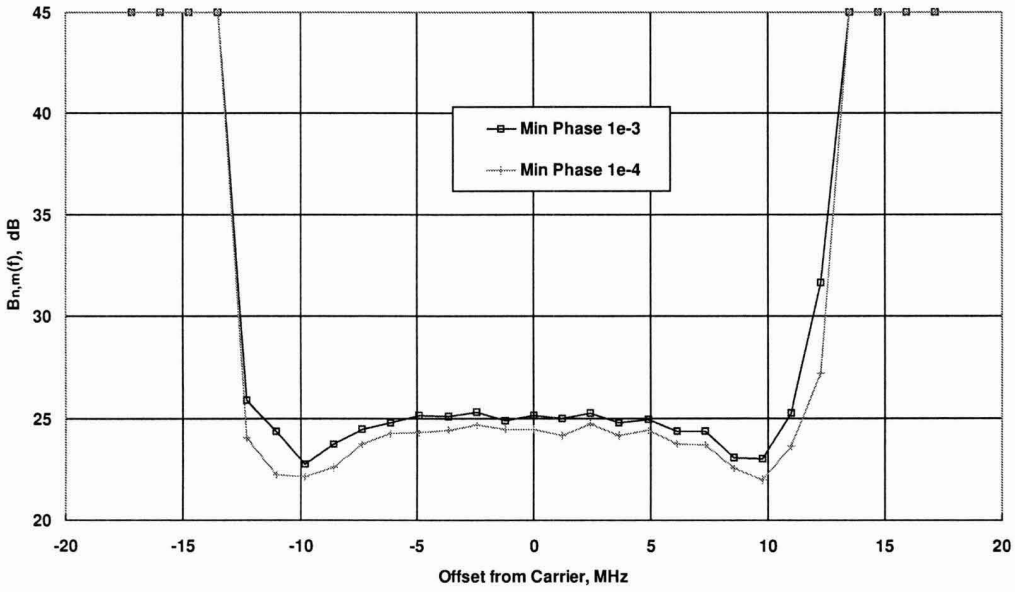

Figure 1. Tyical dispersion signatures

Dispersive fade margin definition

DFM (Dispersive Fade Margin) is defined to be the fade depth exceeded for the same number of seconds at a threshold error rate (the threshold error rate is defined to reside at the value of interest for which the dispersion signatures were created).

DFM is calculated based on the W-curves using the computation[3]

$$DFM = 17.6 - \log_{10}\left(\frac{S_w}{158.4}\right)$$

where,

$$S_w = \int_{-f_1}^{f_1}\left(e^{\frac{-B_n(f)}{3.8}} + e^{\frac{-B_m(f)}{3.8}}\right)df$$

where $B_n(f)$ is the W-curve for non-minimum phase fade, $B_m(f)$ is the W-curve for minimum phase fade, and f_1 sets the signal-occupancy bandwidth, which is the bandwidth of interest. Notice that the expression for S_w is that of a statistical expectation, computed with the assumptions that the distribution of the notch frequency is statistically independent of the other parameters and of uniform distribution over frequency, and the notch depth is exponentially-

distributed.[4] In this expression, it is assumed that minimum-phase and non-minimum-phase fades occur with equal probability; thus the two signatures are given equal weighting in computing DFM. In general, a digital radio with a dispersion signature that falls above that of another radio will result in less outage.

Conclusion

Since dispersive fade margin accounts for all contributions to sensitivity of a digital radio operating in a frequency-selective fading environment, it provides an ideal metric for comparing digital radios with one another. It also serves as a valuable tool in evaluating the effects modem signal processing techniques, such as adaptive equalization, have on link performance in selective fading. Finally, DFM serves as a means of comparing the relative robustness of single-carrier and multi-carrier modulation systems in selective fading environments. It is unlikely to be productive to attempt to standardize on any specific equalization technique, or even on any particular value of DFM. However, it would be of considerable value to the service providers to standardize on a single metric which facilitates comparison of modems using alternative methods to deal with signal distortion induced by propagation in the millimeter-wave bands.

[1] C.W. Lundgren and W.D. Rummler, "Digital radio outage due to selective fading—observation vs. prediction from laboratory simulation," Bell System Technical Journal, pp.1073-1100, May-June 1979.

[2] M. Emshwiller, "Characterization on the performance of PSK digital radio transmission in the presence of multipath fading," ICC'78 Conference Record, Toronto, Ontario, CANADA, Paper 47.3.

[3] Microwave digital radio systems criteria, Bellcore Technical Reference TR-TSY-000752, October 1989.

[4] W.D. Rummler, R.P. Coutts, and M. Linger, "Multipath fading channel models for microwave digital radio," IEEE Communications Magazine, November 1986, pp.30-42.

New techniques for predicting the multipath fading distribution on VHF/UHF/SHF terrestrial line-of-sight links in Canada

Méthodes nouvelles pour la prédiction de la distribution de l'affaiblissement multivoie sur les liaisons terrestres VHF/UHF/SHF en ligne de vue au Canada

R.L. Olsen *and* B. Segal, *Communications Research Centre, Department of Communications, P.O. Box 11490, Station H, Ottawa, Ont. K2H 8S2*

New methods are presented for predicting the signal fading distribution due to multipath propagation for the average worst month on VHF/UHF/SHF terrestrial line-of-sight links in Canada. One method for the deep fading range does not require detailed path profile information and is designed for preliminary planning or licensing purposes. A second method which does employ the path profile is intended for more detailed design purposes. A third method, complementary to the other two, is given for predicting the distribution in the shallow fading range. All three methods are presented in step-by-step form for ease of application. The detailed bases of the methods, and their relationship to earlier methods, are also presented. These methods are the first to employ refractivity gradient statistics in the predictions and to cover the VHF/UHF bands in addition to the SHF band. Some guidance is also given to the designer on the path clearances required to minimize the effects of multipath fading.

De nouvelles méthodes sont présentées pour la prédiction de la distribution de l'affaiblissement du signal due à la propagation multivoie pour les mois moyen le plus difficile sur les liaisons terrestres en ligne de vue au Canada. Une première méthode pour les affaiblissements profonds ne requiert pas une information détaillée sur le profil à l'étude et elle est conçue pour les ébauches préliminaires et l'émission d'autorisations. Une seconde méthode nécessite la connaissance du profil détaillé du parcours et elle est destinée aux conceptions plus élaborées. Une troisième méthode, complémentaire aux deux premières, est adaptée à la prédiction de la distribution des affaiblissements moins profonds. Les trois méthodes sont présentées étape par étape pour que leur application soit plus facile. Les détails sur lesquels reposent ces méthodes et leurs relations avec les méthodes disponibles précédemment sont également présentés. Ces méthodes sont les premières à utiliser les statistiques sur le gradient de l'indice de réfraction dans les prédictions et à couvrir les bandes VHF/UHF en plus de le bande SHF. Quelques conseils sont aussi donnés sur le dégagement des parcours requis pour minimiser les effets de l'affaiblissement multivoie.

Introduction

For over fifteen years, designers of terrestrial microwave line-of-sight links in Canada have almost universally used the techniques of Barnett [1] and Vigants [2] developed in the United States for predicting the deep fading range of the multipath fading distribution for individual hops. More recently, link designers in British Columbia [3] have used the technique of Morita [4] developed in Japan. The basis for this change is a fairly extensive set of measurements carried out in British Columbia [5], and comparisons with both the methods for the US and Japan which showed the Japanese method to be more accurate for this similarly mountainous province. Although the forms of the empirical equations are very similar, the "geoclimatic factor" model for Japan results in the prediction of significantly less severe fading in the average worst month than does that for the US.

In the planning and design of line-of-sight hops in the VHF/UHF bands, even less satisfactory prediction approaches have been applied. The best of these have been the Barnett-Vigants technique [2] for the upper UHF band and the curves of Bullington [6] for both the VHF and the UHF bands. The Barnett-Vigants technique, however, was based on data for the SHF band, and there has been no experimental or theoretical justification for its use at UHF. The Bullington curves were based on few observational data, with no allowance for geoclimatic variability. In the prediction of the shallow fade depth range of the clear-air fading distribution for the average worst month, there has been no technique available for any band that allowed for geoclimatic variability.

This paper presents two methods for predicting the deep fading range of the average worst-month multipath fading distribution on line-of-sight links in the upper VHF, UHF, and SHF bands in Canada. Method 1 does not require detailed path profile information and is best suited for preliminary planning or licensing purposes. In fact, an earlier, nearly identical version has already been adopted by the Department of Communications for licensing purposes in the VHF/UHF bands. It requires only path length, frequency and path inclination as input variables. Method 2, which is more appropriate for link design, also requires the "average" grazing angle of the wave specularly reflected from the ground, and therefore the path profile must be known. In addition to these two methods for the deep fading range, a compatible method is presented for the shallow fading range that also allows for geoclimatic variability. All three methods are first presented in step-by-step form for ease of application. The detailed bases of the methods, and their relationship to earlier methods, are then discussed following the step-by-step presentation. Some guidance is also given to the link designer on path clearances required to minimize the effects of multipath fading. It is suggested, for example, that a rigid application of standard path clearances rules may not be necessary or desirable in some cases.

The systematic analysis of a large British-French SHF data base that led to the development of the empirical prediction equations at

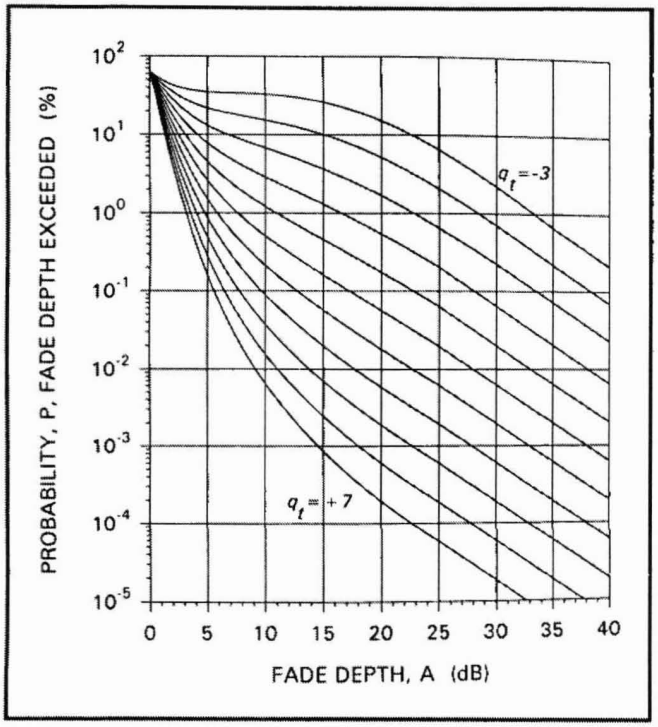

Figure 1: *Family of cumulative distributions of multipath fading typical for the average worst month (fade depth A exceeded for P per cent of the time) that results from an application of Methods 1 and 2 for the deep fading range (A > 25 dB if the shape factor $q_t > 0$, and A > 35 dB if $q_t < 0$), and the procedure for the shallow fading range (curves in increments of 1 for q_t).*

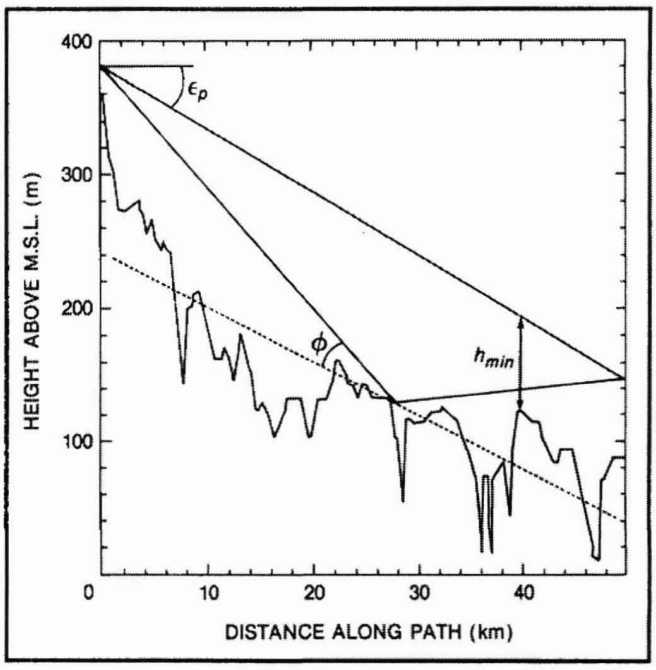

Figure 2: *Illustration of the link variables ϵ_p and ϕ for a typical path, with path profile shown on a flat-earth plot.*

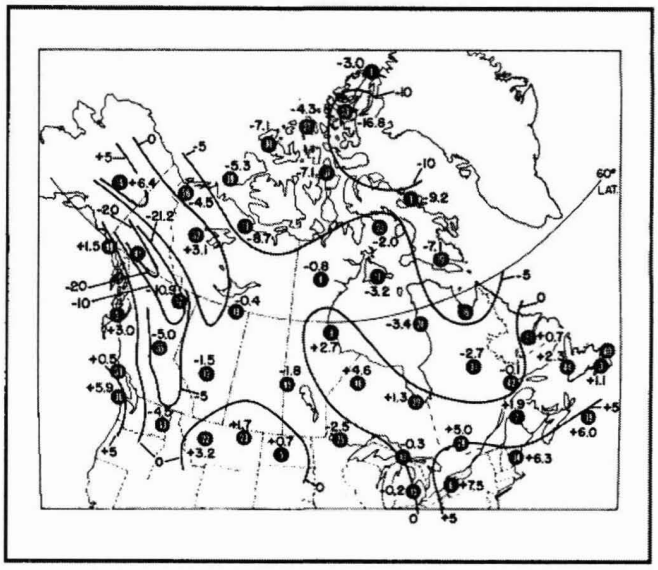

Figure 3: *Contour map indicating logarithmic geoclimatic factor G for Canada. The locations for which specific values of G are indicated are listed in Table III-1 of CRC Report 1315 [29].*

the heart of Methods 1 and 2 has been discussed by Tjelta et al. [7], and in somewhat less detail in three earlier publications [8]-[10]. Besides presenting Methods 1 and 2 in step-by-step form for Canadian link designers, the current paper concentrates on the means of extending the basic prediction equations (developed from the British-French data) to both the Canadian land mass using Canadian fading and meteorological data, and the VHF/UHF bands.

Earlier, almost identical, unpublished versions of Methods 1 and 2 developed for Canada and based on essentially the same British-French-Canadian data base have been recently extended for worldwide application and adopted by the International Radio Consultative Committee (CCIR) [11]. These worldwide CCIR versions employ refractivity gradient maps that, although giving worldwide coverage, do not have the high resolution available from the Canadian refractivity gradient data base and maps used here. Another paper [12] describes the means by which the initial versions of Methods 1 and 2 were extended worldwide, and presents the results of tests on the methods using data for several countries around the world. The detailed basis of the prediction method for shallow fade depths has been presented by Martin [13], and the results of comparisons of predictions with experimental data have been given elsewhere as well [12], [14].

Step-by-step procedures

A family of cumulative distributions of multipath fading typical for the average worst month (fade depth A exceeded for P per cent of the time) that results from an application of the step-by-step procedures that follow is illustrated in Fig. 1. Methods 1 and 2, which are used for predicting the deep fading range of the distribution ($A > 25$ dB or $A > 35$ dB, depending on the value of the "shape factor," q_t), are presented first, followed by the method for the shallow fading range. Both Methods 1 and 2 use a "logarithmic geoclimatic factor," G, in the prediction process, which is a measure of the statistical occurrence of "ducts" near the surface in an average worst month for the link in question [7]. In addition, Method 1 uses the link variables of path length, d (km); frequency, f (GHz); and path inclination, ϵ_p (mrad). Besides G and these three link variables, Method 2 also requires the grazing angle, ϕ (mrad), of the wave specularly reflected from the "average" path profile. The method for the shallow fading range employs the shape factor, q_t, which is a function of the other prediction variables. The link variables, ϵ_p and ϕ, are illustrated in Fig. 2 for a typical path.

Method for initial planning or licensing purposes (Method 1)

This method, which is for predicting the large fade depth range of the fading distribution for the average worst month, should normally be used for planning or licensing purposes or when the path profile is not known. The step-by-step procedure is as follows:

i) For the path location in question, obtain the logarithmic geoclimatic factor G (in dB) for the average worst month, from the map in Fig. 3. This map shows contours of constant G, as well as

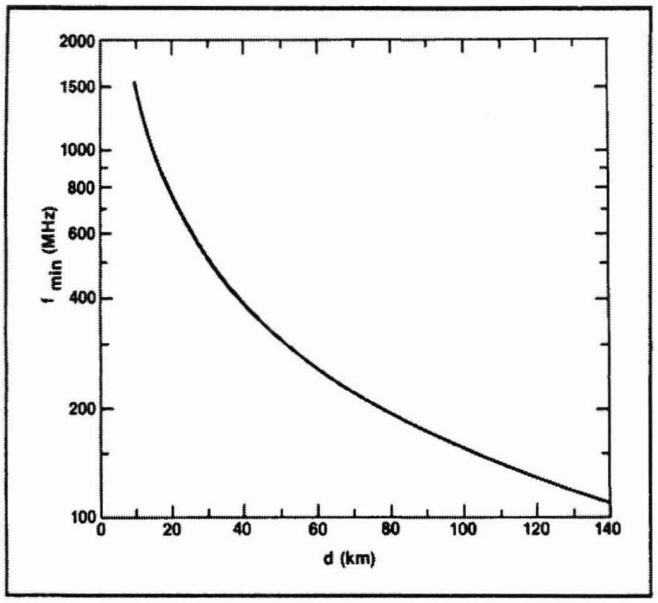

Figure 4: *Frequency below which the prediction methods are expected to be inaccurate, as a function of path length for $h_{min} \geq 77$ m.*

estimated values for 47 radiosonde sites across Canada and adjacent parts of the US. An approximate value for the path can be estimated by interpolation. If the path is above 60° latitude, add 5 dB to the value obtained from the map. If the path is over a medium-sized body of water (e.g. Bay of Fundy, Strait of Georgia, Frobisher Bay, Lake Ontario, Lake Erie), add 6 dB to the value of G obtained from the map (i.e., 5 + 6 dB above 60° latitude). Finally, if the path is over a large body of water, particularly one for which there are no adjacent hills that might give rise to duct-inhibiting turbulence (e.g., Hudson Strait, Viscount Melville Sound, Hecate Strait, Cabot Strait, Lake Superior, Lake Huron, and perhaps Lake Michigan), add 14 dB to the value obtained from the map (5 + 14 dB above 60° latitude). In cases of uncertainty as to the size of the body of water in question, a 10 dB correction factor could be employed. (Particularly for over-water paths or paths above 60°, it may be useful to refer to the later section on limitations and accuracy of the models.)

ii) If the transmitting and receiving antenna heights, h_e and h_r (in metres above some reference height such as mean sea level), are known for the path of length d (km), calculate the magnitude of the path inclination $|\epsilon_p|$ in milliradians from

$$|\epsilon_p| = 1000 \text{ Arctan}[\,|h_r - h_e|/1000d] \approx |h_r - h_e|/d. \quad (1)$$

If the antenna height difference has not yet been established, assume $|\epsilon_p| = 0$ or some other appropriate value.

iii) Calculate the percentage of time, P (%), that fade depth A (dB) is exceeded in the average worst month from the power-law expression

$$P = Kd^{3.6}f^{0.89}(1 + |\epsilon_p|)^{-1.4} \cdot 10^{-A/10}, \quad (2)$$

where K is the geoclimatic factor given by

$$K = 10^{((G/10)-5.7)}. \quad (3)$$

Alternatively, calculate the fade depth A (dB) exceeded for P per cent of the time in the average worst month from

$$A = G - 57 + 36 \log d + 8.9 \log f - 14 \log(1 + |\epsilon_p|) - 10 \log P. \quad (4)$$

Depending on the value of G and the three link variables d, f, and $|\epsilon_p|$, (2) and (4) are valid for $A > 25$ dB or $A > 35$ dB. To determine which is the case, the interpolation procedure for shallow fade depths described below must be applied. A less stringent criterion [11], but one that need not be of concern if this procedure is applied, is that (2) and (4) are valid for $A > 15$ dB or the value exceeded for 0.1% of the worst month, whichever is greater.

Equations (2) and (4) were developed using data for path lengths in the range of 7.5 to 95 km, and frequencies in the range of 2 to 37 GHz. The results of measurements and analysis discussed later, however, suggest that they are valid at least down to the frequency indicated as a function of path length in Fig. 4 (see also (24), particularly for minimum path clearances $h_{min} < 77$ m). The same analysis provides a minimum path length for validity at a given frequency (here, (24) or Fig. 4 must be inverted). As indicated in a later discussion of one set of multifrequency results, (2) and (4) may be valid also for path lengths at least as large as 189 km. Path clearances contained in the data base covered a range of values [7] that resulted from the application of standard clearance rules for the SHF band in France and the UK [11]. As discussed later, (2) and (4) are likely to be conservative (fade depths overpredicted) for clearances either significantly less or significantly greater than normal. Some guidance on setting path clearance is given in the second last section.

Method requiring path profile (Method 2)

This method is best suited for link design applications. In addition to the path length, d (km); frequency, f (GHz); and path elevation angle, ϵ_p (mrad), it requires that the grazing angle, ϕ (mrad), of the wave specularly reflected from the "average" path profile be known. This necessitates the availability of the actual path profile. The step-by-step procedure is as follows:

i) Obtain the logarithmic geoclimatic factor G as in Method 1, including the over-water and/or Arctic correction factors if required.

ii) Obtain the magnitude of the path inclination, $|\epsilon_p|$ (mrad), as in Method 1.

iii) From the profile of the terrain along the path, obtain the terrain heights, h, at intervals of 1 km, beginning 1 km from one terminal and ending 1 km to 2 km from the other. Using these heights, carry out a linear regression with the "method of least squares" to obtain the linear equation of the "average" profile:

$$h(x) = a_0 + a_1 x, \quad (5)$$

where x is the distance along the path from the transmitter. The coefficients can be calculated from the relations [15],

$$a_0 = (\Sigma h - a_1 \Sigma x)/n, \quad (6)$$

$$a_1 = \frac{\Sigma xh - (\Sigma x \cdot \Sigma h)/n}{\Sigma x^2 - (\Sigma x)^2/n}, \quad (7)$$

where the summations are over the number, n, of profile height samples. From (5), calculate $h(0)$ and $h(d)$, the heights of the average profile at the ends of the path, and the heights of the antennas above the average path profile:

$$h_1 = h_e - h(0), \quad (8.1)$$

$$h_2 = h_r - h(d). \quad (8.2)$$

For paths where the point of specular reflection is fairly obvious (such as on paths over water, partially over water, or partially over flat, level terrain), the height above the reflecting surface should be

used for h_1 and h_2. Also, on paths where a rigid application of the regression interval indicated above (i.e., to within 1 km of the ends of the path) would give obvious errors in the calculation of the "average" grazing angle (even though it is known to apply statistically [7]), it is suggested that a smaller regression interval over the path profile be chosen. On long paths, an increase in the profile sample distance to 2 km or more might be acceptable. After some experience with these more rigorous procedures involving linear regression, on some paths it may be possible to draw by eye a fairly accurate mean path profile in the vicinity of the reflection point.

If the path is so rough that it is obvious the main wave interaction with the ground would be one of diffraction from irregular mountain peaks rather than reflection from relatively flat surfaces, it may be meaningless to attempt to determine an appropriate value for the average grazing angle. For such a path, it is suggested that Method 1 be applied, and that the value of G estimated from the map of Fig. 1 be reduced by 2 dB.

iv) Calculate the "average" grazing angle, ϕ (mrad), corresponding to a 4/3-earth radius model for refraction (i.e., $a_e = 8500$ km) from

$$\phi = \frac{h_1 + h_2}{d}\,[1 - m(1 + b^2)\,], \tag{9}$$

where

$$m = \frac{d^2}{4a_e(h_1 + h_2)}, \tag{10}$$

$$\varsigma = \frac{|h_1 - h_2|}{h_1 + h_2}, \tag{11}$$

$$b = 2\sqrt{\frac{m+1}{3m}}\cos\left[\pi/3 + \frac{1}{3}\,\mathrm{Arcos}\left(\frac{3\varsigma}{2}\sqrt{\frac{3m}{(m+1)^3}}\right)\right]. \tag{12}$$

Assume a minimum value for ϕ of 1 mrad. In calculation of the coefficients m and ς, the variables a_e, d, h_1 and h_2 must be in the same units. The grazing angle ϕ will be in the desired units of milliradians if h_1 and h_2 are in metres and d in kilometres. If desired, the distances d_e and d_r from terminals e and r to the point of specular reflection on the average profile can be determined from

$$d_e = (1 \pm b)d/2 \begin{cases} h_1 > h_2 \\ h_1 < h_2 \end{cases} \tag{13.1}$$

and

$$d_r = (1 \mp b)d/2 \begin{cases} h_1 > h_2 \\ h_1 < h_2 \end{cases}. \tag{13.2}$$

Such calculations can be useful in choosing a suitable regression interval on the path profile.

v) Calculate the percentage of time, P, that the fade depth, A (dB), is exceeded in the average worst month from

$$P = Kd^{3.3}f^{0.93}(1 + |\epsilon_p|)^{-1.1}\phi^{-1.2} \cdot 10^{-A/10}, \tag{14}$$

where K is the geoclimatic factor given by

$$K = 10^{((G/10)-4.6)}. \tag{15}$$

Alternatively, calculate the fade depth, A (dB), exceeded for P per cent of the time from

$$a = G - 46 + 33\log d + 9.3\log f - 11\log(1 + |\epsilon_p|) - 12\log\phi - 10\log P. \tag{16}$$

The minimum ranges of variables over which (14) and (16) should apply are the same as those indicated with (2) and (4), with the addition of the range $\phi < 14$ mrad [7].

Interpolation procedure for shallow fade depths

This empirical procedure has been designed to predict that portion of the fading distribution for the average worst month between 0 dB and the deep fading levels predicted by Methods 1 and 2. In step-by-step form, it is as follows:

i) Using Method 1 or 2 as appropriate, calculate the percentage of time, P (35 dB), that a fade depth of 35 dB is exceeded in the "tail" of the distribution (i.e., (2) or (14)).

ii) Calculate the value of the parameter q' corresponding to the fade depth $A = 35$ dB and $P = P(35\text{ dB})$ from

$$q' = -\frac{20}{A}\log_{10}\left[-\ln\left(\frac{100 - P}{100}\right)\right]. \tag{17}$$

iii) Calculate the value of the shape factor q_t from

$$q_t = (q' - 2)/[\,(1 + 0.3 \cdot 10^{-A/20}) \cdot 10^{-0.016A}] - 4.3(10^{-A/20} + A/800). \tag{18}$$

iv) If $q_t > 0$, repeat steps i) to iii) for $A = 25$ dB.

v) For $0 < A < 25$ dB or $0 < A < 35$ dB, as appropriate, calculate the percentage of time, P, that A is exceeded from

$$P = 100[1 - \exp(-10^{-qA/20})\,], \tag{19}$$

where q is also a function of A given by

$$q = 2 + 10^{-0.016A}[1 + 0.3 \cdot 10^{-A/20}] \times [q_t + 4.3(10^{-A/20} + A/800)\,]. \tag{20}$$

Alternatively, calculate the fade depth, A (dB), exceeded for P per cent of the time from

$$A = -\frac{20}{q}\log_{10}\left[-\ln\left(\frac{100 - P}{100}\right)\right]. \tag{21}$$

The method is valid for values of q_t greater than about -3, which covers virtually all the combined ranges of G, d, f, $|\epsilon_p|$, and ϕ values likely to arise under operational circumstances in Canada. For values of q_t less than about -3, the shape of the model distribution becomes nonphysical.

Background to the methods

The basic microwave tail models

Equations (2) and (14) (or (4) and (16)) are three- and four-variable models (four and five variables with the geoclimatic factor) based on microwave data for the large fade depth tail portion of the fading distribution for the average worst month. The tail portion of the distribution as expressed by these equations has the Rayleigh slope of 10 dB/decade and occurs for fade depths greater than about 15 dB on average. It is believed to be caused by a combination of atmospheric fading (largely beam spreading of the direct wave, commonly referred to as defocussing) and surface reflection [16]-[17].

With the possible exception of minor variations discussed by Tjelta et al. [7], these three- and four-variable models [10] are believed to be the most accurate "tail" models currently available [12], [18]. They were developed as part of an effort by Interim Working Party 5/2 (now WP 5C) of CCIR Study Group 5 [19] to improve prediction methods for microwave frequencies [9]. They

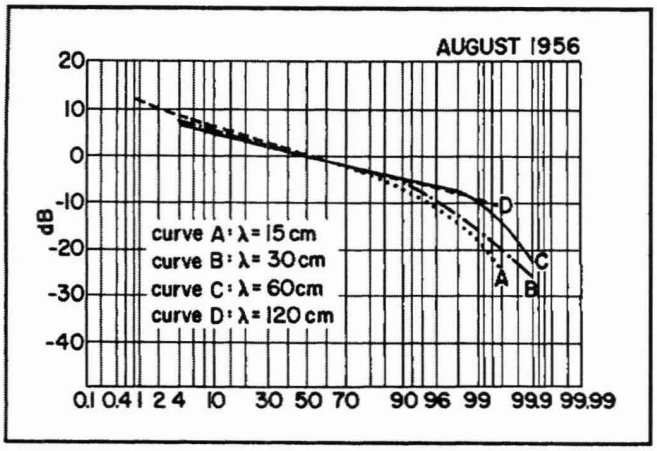

Figure 5: *Worst-month fading distributions in 1956 for 189 km path, Mount Cimone-Milan, Italy, at 250 MHz, 500 MHz, 1 GHz and 2 GHz (after Carassa and Quarta [24]).*

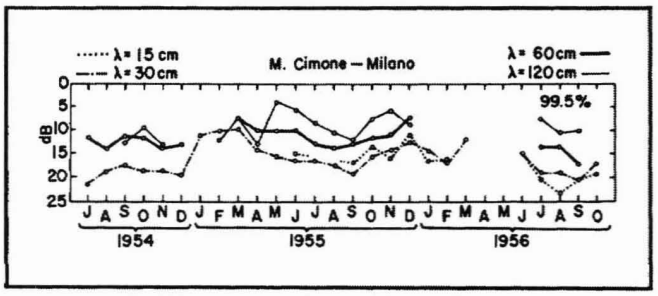

Figure 6: *Monthly fade depths exceeded for 99.5% of the time for the three-year period 1954-1956 on the path indicated (after Carassa and Quarta [24]).*

were based on a fading data base for 47 links in France and the UK, considerably larger than the number used in the Barnett-Vigants model [1]-[2] for the US, the Doble model [11], [20] for the UK, or the old regional model for North-Western Europe [21] still cited by the CCIR [11].

The new models also incorporate improved analytical procedures [7]. The earlier models were based on fits at either constant probability or constant fade depth levels of the distribution. Errors were caused by the fact that for some links, these levels were not in the tail of the fading distribution. In developing the new "tail" models, the fade depths were chosen specifically so that they would be in the distribution tails and have the highest exceedance probabilities possible within this constraint, in order to maximize statistical stability. These minimum tail fade depths were then scaled to a fixed probability level using the average 10 dB/decade Rayleigh slope, before the model fitting was carried out.

Another improvement in the modelling is that worst-month fading distributions are treated with greater statistical consistency. In some previous analyses, for example, the worst one-month distributions over different measurement durations were mixed (i.e., worst-month distributions for one year were combined with those for two years, three years, etc., in the fitting). Such mixed statistics have a bias with respect to each other (i.e., four-year worst-month fade depths tend to be larger than three-year fade depths, etc.), and those associated with the longest overall durations of measurement have very large standard errors. The approach employed in the new analysis [7], [9]-[10] was to use the average worst-month distribution envelope [22], whatever the number of years. Clearly, with this approach the standard error of one-year worst-month statistics is greater than that of two-year averages, etc., but there is no bias. The fit is therefore more accurate.

The major improvements in the new models have resulted from the use of multiple regression and multiple iteration [7], [9]-[10] in fitting the power-law equations to the fading data. Multiple regression gives the most accurate relationship between the exponents in the power law, and multiple iteration allows the geoclimatic factor to vary from one region to another, at the same time increasing the accuracy of the multiple regression.

Various other statistical tests and correlation analyses of errors were used to determine the most significant prediction variables [7], [10]. One major finding of these analyses is that the path inclination is a more significant variable than the surface roughness variable originally introduced by Pearson [23] and later employed by Vigants [2]. The relevance of surface roughness in the Barnett-Vigants model [2] is explained by two factors: a) a large component of the surface roughness is often the average terrain inclination, which is highly correlated with the path inclination; and b) there is a tendency for the roughest paths to have the largest path inclinations. Another important outcome of the analysis is that the "average" grazing angle, ϕ, of the ground-reflected wave is a significant prediction variable. The physical bases of all the prediction variables have been considered in some detail elsewhere [7], [16].

Extrapolation of the microwave tail models to VHF/UHF

There are not enough VHF and UHF data available anywhere in the world to allow the direct development of empirical models for these bands giving close to the same degree of confidence as those for the SHF band. After some investigation, it was felt that the best prediction approach for the VHF and UHF bands would be to extrapolate downwards in frequency from the basic microwave tail models discussed earlier. There are enough data available for testing, and the physical mechanisms that cause fading at both SHF and VHF/UHF are sufficiently well understood [16]-[17], to lend confidence to this approach.

The most useful data are those that have been obtained at multiple frequencies within the VHF/UHF/SHF bands. The frequency term in the prediction equations can then be evaluated without the need to know the geoclimatic factor. A particularly good set of measurements at four frequencies (250 MHz, 500 MHz, 1 GHz, 2 GHz) was obtained over a six-year period on a 189 km path in Italy [24]-[25]. The fading distributions for the worst month in this six-year period are reproduced in Fig. 5, and the month-by-month 99.5% (tail) levels for a three-year period, in Fig. 6. As is evident from Fig. 5, the distributions for the three higher frequencies have tails beginning at about 10 dB. (The dynamic range of the receiver at the lowest frequency was insufficient for the tail to be observed.) More importantly, both Figs. 5 and 6 suggest that for the summer months, there is an average difference of approximately 2.8 dB between the distribution tails at adjacent frequencies for a given percentage of time. This is the approximate difference predicted by Method 2. As a second check, the appropriate geoclimatic factor was calculated from the 2 GHz data for August 1956, by working backwards from the three-variable model of (2); the result was found to be identical to the average value for the adjacent Dijon area of France [7]. (This check also suggests that Methods 1 and 2 are at least approximately valid for path lengths at least as large as 189 km.)

Another important set of multifrequency measurements (45.1 MHz, 474 MHz and 2.81 GHz) was obtained for a 68 km path on New York's Long Island [26]. At 0.1% of the worst month, which is in the distribution tails at both 47[illegible] nd 2.8 GHz, the measured difference in fade depth at these [illegible]ies is 8.5 dB as compared to a predicted value of 7.2 dB wit[illegible] 12. Such agreement is very good. The 45.1 MHz distributio[illegible]t exhibit a tail for the fade depths measured, and the median level suggests that there is considerable destructive interference between the direct and ground-reflected waves even under normal conditions. A calculation from the 2.8 GHz distribution using the three-variable model (4) gives $G = 10.6$ dB, and a calculation using the four-variable model (6) gives [illegible] for this region of the US (see Fig

1 34903 SCI: JRS
50 U/A 05/04/95 187-

Table 1
Data and characteristics of experimental links in Canada

Link [Reference] (Path coordinates)	Ant. Ht. (m) Above Ground Tx	Rx	d (km)	f (GHz)	$\lvert\epsilon_p\rvert$ (mrad)	ϕ (mrad)	Measurement period (Worst month)	Tail A (dB)	Tail P (%)	Observ. G (dB) (Eqn. 4)	Observ. G (dB) (Eqn. 16)	Predict. G (dB) (Fig. 3)	Remarks
1. Corkery-Shirley Bay, Ont. [32] (45°16'16"N, 77°3'44"W-45°20'52"N, 76°52'58"W)	18	40	16.3	10.8	3.55	3.8	May-Sep 1979	25.8	0.001	9.8	7.3	5.0	Reference link.
2. Corkery-Shirley Bay, Ont. [32]	18	40	16.3	11.08	3.55	3.8	May-Sep 1979	29.3	0.001	13.1	10.7	5.0	Reference link.
3. Corkery-Shirley Bay, Ont. [32]	18	40	16.3	16.53	3.55	3.8	May-Sep 1979	18.0	0.001	0.3	−2.2	5.0	Reference link.
4. Corkery-Shirley Bay, Ont. [32]	18	40	16.3	16.81	3.55	3.8	May-Sep 1979	19.9	0.001	2.2	−0.4	5.0	Reference link.
5. Kingsmere-Shirley Bay, Ont. [32] (45°29'17"N, 75°51'21"W-45°20'52"N, 76°52'58"W)	18	40	15.7	11.35	15.5	22.2	May-Sep 1979	12.0	0.001	4.2	9.6	5.0	Surface reflection on Ottawa River. Reference link.
6. Kingsmere-Shirley Bay, Ont. [32]	18	40	15.7	17.71	15.5	22.2	May-Sep 1979	15.3	0.001	5.8	11.1	5.0	Surface reflection on Ottawa River. Reference link.
7. Kemptville-Avonmore, Ont. [36] (44°59'57"N, 75°33'18"W-45°08'47"N, 74°56'48"W)	63	78	50.5	3.65	0.326	2.1	11 Jun-29 Jul 1985	16.2	0.311	4.1	1.8	5.0	Reference link.
8. Kemptville-Avonmore, Ont. [36]	63	65	50.5	3.65	0.079	1.9	11 Jun-29 Jul 1985	16.4	0.424	4.5	1.7	5.0	Reference link.
9. Kemptville-Avonmore, Ont. [31]	63	78	50.5	8.05	0.326	2.1	9 Aug-12 Sep 1977	16.0	1.95	8.9	6.4	5.0	Reference link.
10. Kemptville-Avonmore, Ont. [31]	63	65	50.5	8.05	0.079	1.9	9 Aug-12 Sep 1977	16.0	1.35	6.7	3.9	5.0	Reference link.
11. Kemptville-Avonmore, Ont. [31]	63	25	50.5	8.05	0.730	1.0	9 Aug-12 Sep 1977	22.0	0.14	5.1	−1.4	5.0	0.6 Fresnel zone clearance. G value not included in average for Ottawa.
12. Firth-Tabor, B.C. [5] (54°48'45"N, 122°46'11"W-53°54'44"N, 122°27'01"W)	6	6	102.3	7.5	1.98	3.9	Jul 1981-Oct 1982 (Sep 1982)	15.0	0.197	−7.8	−7.0	−5.0	Reference link.
13. McEwan-Tabor, B.C. [5] (54°24'11"N, 122°29'45"W-53°54'44"N, 122°27'01"W)	11	9	54.7	3.8	2.5	18.7	Jul 1981-Oct 1982 (Sep 1982)	15.0	0.0077	−8.6	−0.5	−5.0	Reference link.
14. Hixon-Tabor, B.C. [5] (53°28'43"N, 122°38'00"W-53°54'44"N, 122°27'01"W)	53	57	49.8	3.9	9.3	5.5	Jul 1981-Oct 1982 (Sep 1982)	20.0	0.0011	−4.0	−3.7	−5.0	Reference link.
15. Cluculz-Frazer, B.C. [5] (53°54'54"N, 123°27'25"W-54°01'51"N, 124°37'21"W)	15	27	77.8	7.2	2.63	6.0	Apr 1980-May 1981 (July 1980)	20.0	0.0119	−9.3	−6.4	−5.0	Reference link.
16. Cluculz-Frazer, B.C. [5]	15	27	77.8	7.5	2.63	6.0	Apr 1980-May 1981 (Sep 1980)	20.0	0.0085	−11.0	−8.1	−5.0	Reference link.

Another early set of multifrequency measurements (9.4 GHz, 4.6 GHz, 3 GHz and 714 MHz) was obtained by Durkee [27] over a 64 km path, also in New York state. Although the 714 MHz data were not obtained over exactly the same period as the higher frequency data, the differences in the distributions are reasonably consistent with the model. The differences between distributions measured during two different time periods at 300 MHz and 3 GHz on a 160 km path in Switzerland [28] are also reasonably consistent with the model.

An important consideration in applying the Rayleigh tail models ((2) and (14)) is the minimum frequency for which they are valid. As discussed elsewhere [16], the tail is believed to result primarily from the combination of atmospheric fading due to ducts in proximity to the path, and surface reflections. The most likely situation to cause atmospheric fading such that the atmospheric signal and the surface-reflected signals can interfere sufficiently destructively with one another occurs when the centre of the duct is located just below the path [16]. Here the atmospheric fading and the phase shift between the direct and surface-reflected waves are simultaneously greatest for a duct of given intensity.

This "relative maximum" phase shift can be estimated [16] from

$$\Delta\phi_m = 2\pi f(\Delta\tau_1 + \Delta\tau_2) + \pi, \tag{22}$$

where $\Delta\tau_1$ is the geometric delay difference within a normal atmosphere, $\Delta\tau_2$ is the additional contribution due to the presence of a duct just below the path, and π is the phase shift introduced in surface reflection. The duct contribution, $\Delta\tau_2$, is normally much larger than $\Delta\tau_1$ and can be estimated [16] from

$$\Delta\tau_2 \approx 0.8(|\Delta N| \cdot 10^{-6})d/c, \tag{23}$$

where $|\Delta N|$ is the intensity of the duct (i.e., the difference in refractivity between the bottom and the top of the duct) in N units, d is the path length, and c is the speed of light.

Ignoring the usually small value of $\Delta\tau_1$ and assuming a duct intensity of 12.1 N units over a path whose minimum clearance, h_{min}, under ducting conditions (obtained from a flat-earth plot such as that in Fig. 2, with exclusion intervals of at least 1 km at the ends of the path to avoid hills on which the antennas are situated) is greater than 77 m (i.e., intensity due to a duct threshold gradient of -157 N units/km over a duct thickness of 77.3 m, the average surface duct thickness in Canada [29]), we obtain $\Delta\phi_m \approx 2\pi(9.7 \cdot 10^{-6})fd/c + \pi$. Furthermore, for a path with $h_{min} < 77$ m, we obtain $\Delta\phi_m \approx 2\pi(9.7 \cdot 10^{-6})fdh_{min}/77c + \pi$. If the minimum value of $\Delta\phi_m = 2\pi$ is taken, allowing for a relatively uniform distribution of the phase between direct and surface-reflected waves, this gives a quasi-minimum frequency of

$$f_{min} = \begin{cases} \dfrac{1.6 \cdot 10^4}{d}\ \text{(MHz)} & \text{for } h_{min} \geq 77\ \text{m} \\ \dfrac{1.2 \cdot 10^6}{dh_{min}}\ \text{(MHz)} & \text{for } h_{min} < 77\ \text{m} \end{cases}, \tag{24}$$

Table 1 *(cont'd)*
Data and characteristics of experimental links in Canada

Link [Reference] (Path coordinates)	Ant. Ht. (m) Above Ground Tx	Rx	d (km)	f (GHz)	$\|\epsilon_p\|$ (mrad)	ϕ (mrad)	Measurement period (Worst month)	Tail A (dB)	Tail P (%)	Observ. G (dB) (Eqn. 4)	Observ. G (dB) (Eqn. 16)	Predict. G (dB) (Fig. 3)	Remarks
17. Creston-Salmo, B.C. [5] (49°05'35"N, 116°22'45"W-49°04'18"N, 117°04'56"W)	17	15	51.4	4.1	0.89	–	Feb-Oct 1982 (Feb 1982)	25.0	0.0006	−11.2	–	−4.5*	Rough, mountainous terrain.
18. Rossland-Salmo, B.C. [5] (49°05'35"N, 117°47'50"W-49°04'18"N, 117°04'56"W)	6	13	52.3	6.9	17.1	–	Feb-Oct 1982 (Oct 1982)	15.0	0.0022	−5.5	–	−5.0*	Rough, mountainous terrain.
19. Santa Rosa-Salmo, B.C. [5] (49°01'27"N, 118°03'31"W-49°04'18"N, 117°04'56"W)	11	15	71.6	4.1	6.5	–	Feb-Oct 1982 (Oct 1982)	20.0	0.0105	−2.0	–	−5.0*	Rough, mountainous terrain.
20. Blackwall-Hope, B.C. [5] (49°06'05"N, 120°45'25"W-49°24'35"N, 121°33'28"W)	18	11	67.6	3.8	8.2	–	Feb 1981-May 1982 (Dec 1981)	15.0	0.0038	−9.0	–	−2.0*	Rough, mountainous terrain.
21. Hope-Chilliwack, B.C. [5] (49°24'35'N, 121°33'28"W-49°06'52"N, 121°54'07"W)	26	46	41.4	7.8	29.2	40.0	Feb 1981-Oct 1982 (Jul 1982)	15.0	0.0012	−1.9	7.2	2.0	
22. Uniondale-London, Ont. [37] (43°13'42"N, 81°02'18"W-43°00'25"N, 81°16'28"W)	46	25	30.7	16.65	3.16	1.9	11 Jul-1 Nov 1986	7.5	5.0	16.4	11.2	5.0	P value reduced by 6% to account for rain attenuation [40].
23. Otter Lake, N.B.-Nictaux S, N.S. [38] (45°22'10"N, 65°46'23"W-44°52'00"N, 65°02'10"W)	69	81	80.4	9.5	0.684	5.7	31 Jul-3 Sep 1981	27.5	0.315	6.1	9.1	11.0 (5.0)	Oversea path with partial blockage of sea reflection.
24. Big Sicker-Vancouver, B.C. [5] (48°51'38"N, 123°45'20"W-49°16'52"N, 121°33'28"W)	15	72	66.1	4.2	9.6	6.7	Jul-Oct 1979 (Oct 1979)	20.0	0.0961	10.9	12.5	10.0 (4.0)	60% oversea path.
25. Vancouver-Big Sicker, B.C. [5]	70	15	66.1	8.2	9.6	6.7	Jul-Oct 1980 (Jul 1980)	20.0	0.0352	4.0	5.5	10.0 (4.0)	60% oversea path.
26. Lowther Peak-Martyr Peak, N.W.T. [39] (74°31.8'N, 97°27.2'W-74°41.2'N, 95°2.9'W)	7	7	72.0	0.468	0.125	3.0	2 Sep 1983-22 Apr 1984 4 Jun 1984-7 Jan 1985 (Oct 1983)	22.8	0.1	7.2	2.4	11.9 (−7.1)	Arctic oversea path.
27. Schomberg Peak-Cockburn Peak, N.W.T. [39] (75°33.7'N, 105°35.1'W-75°1.8'N, 100°15.1'W)	7	7	91.0	0.463	0.231	1.1	4 Jun 1984-7 Jan 1985 (Jul 1984)	36.9	1.0	28.3	24.1	11.9 (−7.1)	Arctic oversea path with <0.6 Fresnel zone clearance.
28. Cockburn Peak-Lowther Peak, N.W.T. [39] (75°1.8'N, 100°15.1'W-74°31.8'N, 97°27.2'W)	7	7	98.8	0.453	0.253	0.7†	2 Sep 1983-10 Nov 1983 4 Jun 1984-7 Jan 1975 (Jul 1984)	41.5	0.1	21.8	14.7	11.9 (−7.1)	Arctic oversea path with <0.6 Fresnel zone clearance.
29. Cockburn Lake-Lowther Peak, N.W.T. [39] (75°1.6'N, 100°10.0'W-74°31.8'N, 97°27.2'W)	7	5	96.5	0.458	1.05	0.0†	2 Sep 1983-20 Oct 1983 3 Aug 1984-7 Jan 1985 (Sep 1983)	42.5	0.01	16.1	10.7	11.9 (−7.1)	Grazing oversea path in Arctic.
30. Cape Warwick-Lacy, N.W.T. [30] (61°36'N, 64°38'W-60°41'N, 64°35'W)	6	6	101.7	0.465	1.24	2.87	Dec 1986-Nov 1987 (Jun 1987)	23.0	1.0	16.4	16.4	12.1 (−6.9)	Acrtic oversea path.
31. Cape Warwick-Cape Cracroft, N.W.T. [30] (61°36'N, 64°38'W-62°44'N, 65°18'W)	6	6	131.9	0.453	0.48	2.11	Dec 1986-Nov 1987 (Jul 1987)	14.4	3.0	6.1	5.3	12.0 (−7.0)	Arctic oversea path.
32. Cape Cracroft-Vanderbilt, N.W.T. [30] (62°44'N, 65°18'W-63°04'N, 67°39'W)	6	6	125.7	0.466	0.72	3.81	Dec 1986-Nov 1987 (Sep 1987)	12.6	2.0	4.1	6.2	3.9 (−7.1)	Arctic oversea path.
33. Cape Vanderbilt-Iqaluit, N.W.T. [30] (63°04'N, 67°39'W-63°45'N, 68°32'W)	6	6	89.6	0.450	5.45	2.00	Dec 1986-Nov 1987 (Sep 1987)	10.5	0.1	2.4	−0.9	3.9 (−7.1)	Actic oversea path.

Notes: The predicted G values in parentheses are values from Fig. 3 uncorrected for over-water and Arctic paths.
* The predicted G values for the mountainous paths indicated by an asterisk must be reduced by 2 dB for Method 2, as discussed in the step-by-step procedure.
† In the two paths noted, ϕ = 1mrad assumed in observed G calculations for 4-variable model (16), as discussed in the procedure for Method 2.

for threshold duct conditions, with d in kilometres and h_{min} in metres. A plot of f_{min} as a function of path length is given in Fig. 4 for $h_{min} \geq 77$ m. It must be emphasized that f_{min} will be smaller for larger duct intensities, and therefore distribution tails (i.e., with Rayleigh slope) will exist at lower frequencies. The limit expressed by (24) and Fig. 4 is meant only to give some indication of the frequency below which the accuracy of the Rayleigh tail model must be seriously questioned on physical grounds. (For the purposes of determining a minimum path length, d_{min} (km), for approximate validity of the Rayleigh tail model at a given frequency f (MHz), the independent and dependent variables in (24) or Fig. 4 can be inverted.)

Interpolation procedure for shallow fade depths

The basis of the method for low fade depths is described in more detail elsewhere [12]-[14]. It is essentially an empirical interpolation procedure which generates a smooth transition between the large fade depth Rayleigh tail range of the distribution described by Methods 1 and 2, and the fade depth of 0 dB. Tests on the method using extensive microwave data available for France and the UK show it to have mean residual errors of less than 1 dB and standard deviations of error of less than 3.2 dB in the exceedance probability range of 0.01% to 1% of the average worst month [12], [14]. There is no reason to believe that it would not perform as well in Canada. Once sufficient data for VHF/UHF links in Canada become available, including overland links, the accuracy of the method should be verified for this part of the spectrum. Since it is an interpolation procedure tied to the two tail methods, however, it is reasonable to expect, as observed for the British-French data [7], [14], that the errors for the tail methods are upper bounds on average to the errors of the interpolated curves.

Radio-meteorological considerations

Basis for geoclimatic factor variation

The propagation of radio waves through the troposphere is influenced by gradients in the refractive index. These gradients determine the curvature of the signal "rays" as they travel, and extreme values of gradients are responsible for anomalous propagation during clear-air conditions. The refractivity, N, defined as the difference between the actual refractive index at a point in the atmosphere and the refractive index *in vacuo* multiplied by 10^6, is determined by the values of temperature, pressure and absolute humidity. A vertical refractivity gradient of approximately -39 N units/km over the lowest 100 m is average for Canada [29]. Larger lapse rates (i.e., gradients < -39 N units/km) are referred to as being "superrefractive." Gradients less than -157 N units/km are designated as "ducting" gradients, while the overall height limits between which this condition prevails constitute the actual "duct."

Although the vertical structure of refractivity is known to be crucial to the tropospheric propagation of microwave signals far beyond the line of sight, its importance in terms of multipath on line-of-sight links is not yet as well appreciated. Two important considerations weight heavily on this problem. First of all, while low-lying superrefractive or ducting layers (i.e., below the level of the antennas) may give rise to abnormal spreading, or "defocussing," of the energy in the direct wave between the two antennas, and at the same time to an enhanced surface-reflected wave that interferes destructively with the direct wave [16]-[17], there is no precise point at which these conditions occur. Depending on the geometry of the situation, a duct may not be necessary at all for multipath propagation to occur. In other instances a rather large or very intense duct might be required.

The second consideration arises out of the practical limitations of most of the tropospheric refractivity statistics available. These statistics are generally derived from analysis of meteorological observations obtained using radiosondes, typically those launched by weather balloons for synoptic weather information. At the very low altitudes of concern to VHF-SHF radio links, these data are seriously lacking in both resolution and sensitivity. The net result is that many low-lying refractive structures are not recorded by the radiosonde system. In addition, the severity of rapidly varying layers is underestimated. Where a realistic estimate of the probability of duct occurrence is needed, it is actually likely to be more accurately approximated by the recorded incidence of superrefractive layers than by the noted occurrence of ducting gradients themselves. Coupled with these problems of spatial resolution and sensitivity are the additional limitations arising from the fact that the routine radiosonde measurements are taken only every 12 hours, with different local measurement times in each time zone.

Choice of a suitable climatic variable to characterize fading

In view of the uncertainty regarding both the identity of the fundamental radio-meteorological variable of consequence and the lack of reliability in existing data, several possible predictor variables were examined. The results were then considered for meteorological significance and for consistency with available propagation data. The three-year data base used for this purpose was the same as that employed in a tabulation of duct occurrences contained in an earlier report [29], and includes all sites listed in Table III-1 of that report except St. John's, Nfld. These locations cover all of Canada, albeit thinly, and adjacent parts of the US.

The occurrences of both ducts and surface-based superrefractive layers were calculated. The data for surface ducts and elevated-surface ducts were merged, as it was felt that these conditions are likely to produce very similar progagation effects. Furthermore, since it was felt that data for a single worst month might be unreliable (because of normal fluctuations over a few years and the fact that one month might provide too small a sample), data were also examined for the worst two and the worst three calendar months. These were not necessarily successive months, nor the same months for ducts and superrefractive layer occurrences.

The superrefractive layer occurrences were found to provide a smooth pattern of variation across the country with very similar results for one-, two-, or three-calendar-month data. The duct probabilities also yielded geographically similar maps for one-, two-, or three-month averages. Perhaps because of the reduced number of occurrences, however, the duct probability maps displayed a less gradual or consistent pattern of variation over the entire land mass, particularly in the high Arctic.

From a climatological point of view, the superrefractive layer occurrence provided a more convenient variable for classifying anomalous refractivity conditions in Canada. On the other hand, when a regression relation was sought (see following section) between the different refractive parameters and the known fading characteristics at selected locations, it was found that the superrefractive layer occurrence predicted more extreme fading for southwestern Ontario and the northeastern corner of the US than seemed reasonable on the basis of the small sample of fading data available. The worst three-calendar-month average probability of occurrence of surface plus elevated-surface ducts was therefore used in the present model.

Relationship between the geoclimatic factor and duct occurrence probability

Fortunately, enough fading data exist for various paths around the country so that prediction equations can be obtained in terms of the combined occurrence probability of surface and elevated-surface ducts. Table 1 presents these data and the associated path parameters. The fade depths, A, and time percentages, P, given correspond to the first points (i.e., highest percentage of time and lowest fade depth) that can reasonably be considered to be in the distribution tail (i.e., the deep fading portion with a slope of approximately 10 dB/decade) [7]. In most cases, either the complete distribution or enough points in it were available to permit these tail points to be determined relatively easily.

As far as possible, these data are for the worst calendar month of the overall measurement period, both of which are indicated in Table 1. The four paths for which this is not strictly true are Corkery-Shirley Bay, Kingsmere-Shirley Bay, Kemptville-Avonmore, and Otter Lake-Nictaux South. The first two are so short and the tail-point percentage so low (0.001%) that five-month averages were used. Furthermore, the fading for the Corkery-Shirley Bay path was fairly uniform throughout this five-month period. The data for the Kemptville-Avonmore and Otter Lake-Nictaux South paths should be effectively worst-month data because of the time intervals in which they were obtained.

The procedure followed in establishing a relationship between the logarithmic geoclimatic factor G and duct occurrence, was to work backwards from the fading data to calculate G for each link. This was done using both the three-variable equation (4) and the four-variable equation (16). Table 1 lists both sets of values, except for four paths in British Columbia where only the three-variable calculations are given. These paths are so rough that an accurate value for the "average" grazing angle, ϕ, could not be established. Table 1 also lists the values of G for the over-water and Arctic paths before and after the corrections indicated previously were applied. These are discussed in the next section.

The three paths in the Ottawa area (Corkery-Shirley Bay, Kingsmere-Shirley Bay, Kemptville-Avonmore) and the four

paths in the Prince George area (Firth-Tabor, McEwan-Tabor, Hixon-Tabor, Cluculz-Fraser) currently provide the best basis on which to establish the relationship between the logarithmic geoclimatic factor G and the duct occurrence probability, P_d (%). An important aspect of these paths is that there are several in each vicinity, with more than one link in some cases (i.e., different frequencies and antenna heights), allowing average values of G to be established for each region. Another is that duct occurrence statistics are available from radiosonde stations in the vicinities of each of these two groups of paths (Maniwaki, Que., and Prince George, B.C.). Finally, a third important point is that the two groups of paths represent close to the two extremes of most frequent and least frequent ducting occurrences that are possible over the Canadian land mass.

The average "observed" G values obtained using the four-variable model of (16) for the Ottawa and Prince George areas are 5 dB and −5 dB, respectively. (The constant in (16) (viz. −46 dB) was adjusted to give an average of 0 dB between these two "extremes," but the 10 dB difference was coincidental.) The corresponding combined occurrences of surface and elevated-surface ducts in the worst-three-month periods are $P_d = 11.9\%$ for Maniwaki (Ottawa) and 2.5% for Prince George. Since the most plausible relationship between these two variables is a logarithmic one, as between A and P, the transformation equation established from these two sets of values is

$$G = -10.9 + 14.8 \log P_d. \tag{25}$$

The "two-region fit" of (25) was used to establish the logarithmic geoclimatic factor map of Fig. 3. This map was then used to predict G values for all the other experimental paths in question, and these are listed in Table 1.

Discussion of fading measurements

Several observations can be made from the data of Table 1 to aid in the prediction process. The presentation of both three- and four-variable calculations of G demonstrates the importance of using the four-variable model (Method 2) wherever possible. The calculated fade depths based on the three-variable model (4) can differ by several decibels from those based on the four-variable model (16). There is a tendency for the three-variable model to underpredict the fade depth when the average path clearance is unusually large, and to overpredict when it is unusually small. It is for this reason that the average values of G for the Ottawa and Prince George regions were determined using the four-variable model.

The use of G values directly from the map of Fig. 3 for the over-water paths clearly results in an underprediction of the fading levels for these paths. This is not surprising since ducts are more prevalent over relatively large bodies of water such as those involved in the current data base. Moreover, it appears that, by and large, the Arctic paths that are over large bodies of water suffer from the greatest underprediction. It is interesting that the observed decreasing severity of the fading with distance northward on the UHF links in the Hudson Strait area [30] is consistent with this fact, since Frobisher Bay is considerably smaller and probably more subject to duct-inhibiting turbulence from surrounding mountainous terrain than Hudson Strait itself. This is the assumption that has been made in setting the two correction factors for over-water paths in Methods 1 and 2, these factors being chosen to give reasonable agreement with the admittedly small sample of data currently available for such paths in Table 1.

The "observed" G values for the two groups of Arctic UHF paths (i.e., those in the vicinities of Hudson Strait and Viscount Melville Sound) are about 14 and 20 dB higher, on average, than the values predicted from the map of Fig. 3. This could be due entirely to the fact that the paths are all over water, but it is felt that differences in the diurnal patterns of duct occurrence in the Arctic and further south are more likely mostly responsible. For much of the year, the diurnal or nocturnal periods have much longer duration in the Arctic. It is therefore likely that ducts would persist for longer periods of time than is typical in the South. The statistical significance of a duct observation in the Arctic would thus be greater than that inferred from the observations at temperate latitudes.

A small part of the large difference between observed and predicted G values in the Arctic could also be due to radiosonde resolution errors in measuring the occurrence of ducts, as noted earlier; ducts in the Far North tend to be somewhat thinner, on average, than those occurring at lower latitudes [29]. A small part could even be due to an error in the frequency extrapolation from SHF to UHF, although it should be quite small in view of the multifrequency results discussed previously. To be on the safe side for predictions above 60° latitude (i.e., approximately the latitude of the Hudson Strait measurements), a correction factor of 5 dB has been assumed for overland paths, and additional factors of 6 and 14 dB for paths over medium and large bodies of water, respectively.

One of the interesting and perhaps important results indicated by the data for both the Kemptville-Avonmore links and the links in the high Arctic is that deep fading appears to be less severe in some cases when path clearance is reduced. On the "near-grazing" Kemptville-Avonmore link, which has 0.6 Fresnel zone clearance [31], the improvement in the deep fading range of the distribution is 6.6 dB over the average of the other two links at 8 GHz with normal clearances. At UHF on the "grazing" Cockburn Lake-Lowther Peak link, the improvement is 13.4 dB over the Schomberg Peak-Cockburn Peak link, which has higher, but still less than 0.6 Fresnel zone, clearance. This is believed to be due to the fact that the direct wave for such links passes entirely below most ducts or else is launched from within the duct and suffers less loss due to beam spreading (defocussing) than if the duct were situated below the direct path [16]-[17]. In these particular examples, the effect appears to more than offset any tendency for the fading to be increased as a result of the smaller grazing angle involved, or as a result of earth diffraction during periods of subnormal refractivity gradients. However, it is important to note that the Lowther Peak-Martyr Peak link with its clearance of greater than 0.6 Fresnel zone still appears to show better performance (8.3 dB from the four-variable model) in deep fading conditions than the "grazing" Cockburn Lake-Lowther Peak link. (Note, however, that the original data for the latter path [32] do not clearly indicate the beginning of a tail, and the tail statistics in Table 1 may give larger observed values of G than the actual values.) Thus, reducing path clearance does not necessarily lead to improved performance during multipath fading conditions.

The results for the high Arctic paths suggest, in fact, that there may be a clearance for which the fading is maximum. Maximum fading occurs on the Schomberg Peak-Cockburn Peak path with a minimum path clearance of about 55 m under normal conditions. This may have some relation to the fact that the mean thickness of surface ducts observed at Resolute was 61 m [29]. No such dependence of fading on path clearance (other than the effect of path clearance on grazing angle) has been observed for temperate climates [7], which may be due to a greater tendency for surface ducts to become elevated (or vice versa) as the solar elevation angle changes, or just to a lack of data for varying path clearance. Since there was some difference in the measurement periods for the high Arctic paths, the worst months for the two with the least fading occurring in 1983 and the worst months for the two with the most fading, in 1984, a degree of uncertainty remains. In any case, the result seems physically plausible, since fading would be reduced at low clearances for the reason noted above and at large clearances because of the combined lower occurrence of ducts and higher grazing angles. The likelihood that it may also occur in warmer climates needs further investigation. Some guidance on the setting of path clearance is given in a later section.

Table 2
Summary of mean (*m*), standard deviation (*s*), and maximum (*max*) of prediction errors* (in dB) for various groupings of links

Link grouping	No. of links	Method 1			Method 2		
		m	*s*	*max*	*m*	*s*	*max*
All links	33	−0.1	5.5	16.4	0.1	5.0	12.2
Reference**	15	0.4	3.9	8.1	0.0	4.1	7.2
Overland†, not including reference	6	0.6	7.0	11.4	−1.4	5.1	6.2
Overland†	21	0.5	4.8	11.4	−0.4	4.3	7.2
Southern†	24	0.8	4.7	11.4	−0.1	4.2	7.2
Mountainous	10	3.1	3.3	7.0	−0.1	3.9	5.2
Over-water	11	−1.2 (−8.6)	7.1 (8.4)	16.4	0.4 (−10.0)	6.1 (7.8)	12.2
Arctic	8	−2.9 (−10.8)	7.5 (8.7)	16.4	0.1 (−11.9)	7.0 (8.2)	12.2

* Predicted minus observed values of *G*.
** Includes all links in Ottawa area (excluding Kemptville-Avonmore "near grazing" link).
† Excluding Kemptville-Avonmore "near grazing" link.
Note: Means and standard deviations using uncorrected values of *G* indicated in parentheses.

The fairly large variability in the observed geoclimatic factors for the Corkery-Shirley Bay and Kingsmere-Shirley Bay paths results from the very low percentage of time (0.001%) for the tail point on such short paths. Although the fading indicated for the Corkery-Shirley Bay path is worse at 11 GHz than at 17 GHz – the inverse of the result normally expected – no statistical significance should be attached to this result, since it was due to only a single eight-minute fading event that occurred at 11 GHz and not at 17 GHz. Nevertheless, the large number of links involved serves to improve the reliability of the average *G* estimated for the Ottawa region.

Limitations and accuracy of Methods 1 and 2

Estimated means, standard deviations and maxima of the prediction error for Methods 1 and 2 are given in Table 2 for different groups of data. These were obtained from the differences between the predicted and observed values of *G* in Table 1. Results for the over-water and Arctic links are shown both with and without the correction factors for such links, those for the Arctic links, which are all over water, including both.

The first grouping of overland links outside the two reference regions (Ottawa and Prince George) was included because it gives some measure of how well the "two-region fit" applies to overland links in other temperate regions of the country. The grouping of all southern links does somewhat the same thing, but includes the results for the three over-water links which contain the 6 dB correction for links over medium-sized bodies of water. Comparisons with the results for all reference links suggest that the fit is indeed accurate for other temperate regions.

The grouping for mountainous links in British Columbia includes the five reference links in the Prince George area (nos. 12-16), those in the Salmo region (nos. 17-19), and those in the Hope region (nos. 20-21). The lower standard deviations for Method 1 with respect to Method 2, and for mountainous links with respect to all overland links, cannot be considered as statistically significant because of the small number of links involved. However, they do suggest that the predictions for mountainous links should be as accurate as, or at least not significantly less accurate than, predictions for links over flatter terrain.

The results for the grouping of over-water paths show the effect of the respective 6 and 14 dB corrections for medium-sized and large bodies of water. Since seven of these paths are in the Arctic, they also include the effect of the 5 dB correction for paths above 60° latitude. However, since the correction was derived from these results, they cannot be considered a true test of the accuracy of the over-water correction. Additional results for an independent set of over-water links would likely show larger errors, but these could then be used to improve the over-water correction. An obvious extension to the simple 6 and 14 dB over-water corrections is to use the suggested 10 dB correction factor in cases of uncertainty as to the size of the body of water.

The results for the Arctic links show the effect of the correction for links above 60° latitude and those for medium-sized and large bodies of water combined, since they are all over-water paths. Again, since the correction factors were based on the results themselves, the results cannot be considered as a true measure of the accuracy of Methods 1 and 2 in the Arctic. However, the fact that the mean error for the group of paths in the vicinity of Hudson Strait is close to that for the group in Viscount Melville Sound, and the fact that the uncorrected *G* values for these two groups of paths based on the radiosonde data are almost identical, lend some confidence to the prediction for over-water paths in the Arctic. Since there are no results yet for overland Arctic paths, the 5 dB correction factor (which was based on the results for the three links in or at the entrance to Frobisher Bay (nos. 31-33) using the 6 dB correction for links over medium-sized bodies of water) remains to be fully tested.

A comparison of the standard deviations of error of 4.8 and 4.3 dB on overland links for Methods 1 and 2, respectively, with the corresponding values of 3.4 and 2.9 dB for the 47 overland links in France and the UK [7] might suggest that some accuracy has been lost in "transporting" the basic prediction equations to Canada. However, it must be remembered that the Canadian figures are all based on one-year worst-month fade depths, whereas the European figures are based on a mixture of one-year statistics and averages taken over two, three and four years. Such a mixture will inevitably reduce the standard deviation of error, since a finite but unknown component of the error is due to year-to-year statistical variability and not to intrinsic errors in the prediction equations. Furthermore, the proportion of unusual paths (i.e., very short or very rough) is larger in the Canadian data base. Considering that the predictions for six of the 21 overland paths are also based on geoclimatic factors scaled from refractivity gradient data, it is satisfying that the errors are as small as they are.

It must be emphasized that the small improvement in the standard deviations of error in Method 2 with respect to Method 1 does not adequately highlight the fact that the former method gives much greater accuracy for specific paths which have above- or below-average clearances. This is better shown by a comparison of the maximum errors for the two methods.

The British-French paths on which the model coefficients were based had an average clearance at midpath of 106 m (standard deviation of 70 m), and average clearance to dominant obstacles of 31 m under 4/3-earth refractivity conditions. Although the ϕ variable in Method 2 allows accuracy to be maintained over large clearance ranges, some inaccuracy is introduced when clearances are outside the range in the data base. This is seen in the results for the "near grazing" and "grazing" paths (nos. 11 and 29) discussed in the preceding section.

Comparison with other methods

Three prediction methods particularly merit comparison with the new methods presented in this paper: the Bullington curves [6] sometimes used for the VHF and UHF bands; the Barnett-Vigants method [1]-[2] developed for the US, and used previously for paths in the SHF and upper UHF bands in Canada; and the version of the new methods for France and the UK [7].

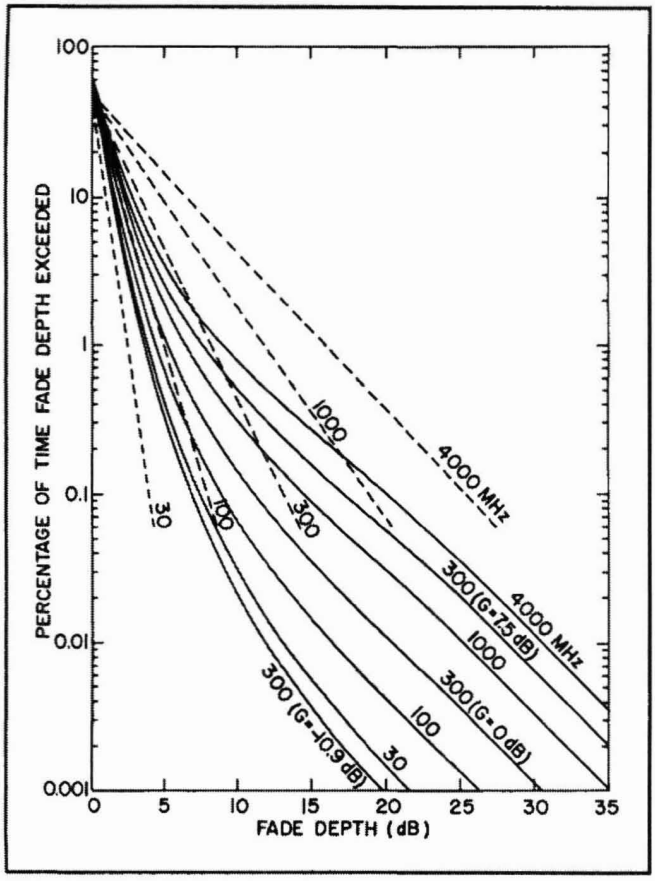

Figure 7: *Comparison of Bullington's curves (– – –) with results for Method 1 (——) for a 56 km (35 mi) horizontal path (results for Method 1 are for G = 0 dB, unless otherwise indicated at 300 MHz).*

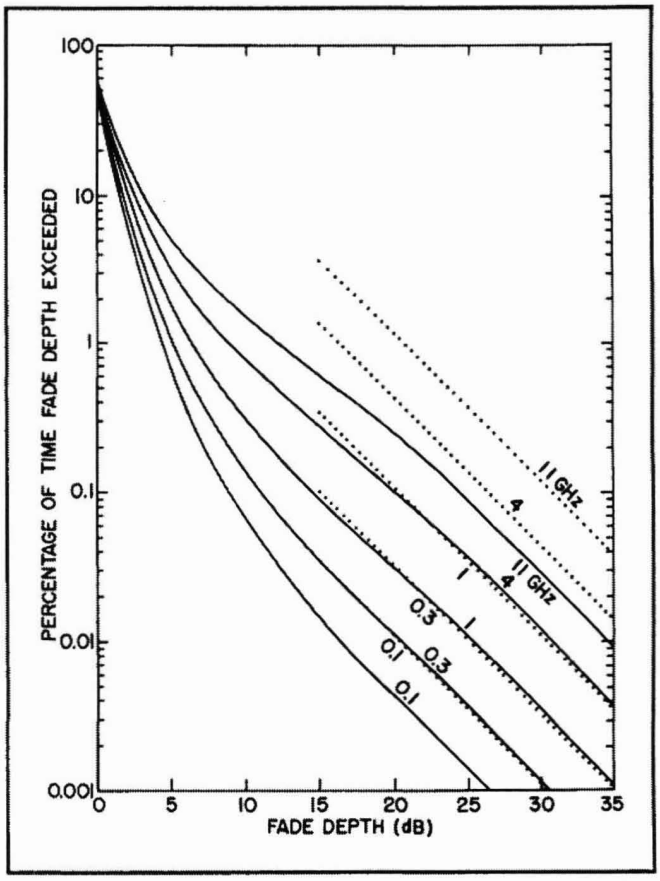

Figure 8: *Comparison of results for Barnett's method (· · · · , C = 1) and Method 1 (——, G = 0) for a 56 km (35 mi) horizontal path in average fading conditions.*

A graphical comparison of the results of Method 1 (interpolation procedure for shallow fade depths) with the curves of Bullington is given in Fig. 7. For this comparison, a horizontal path ($|\epsilon_p| = 0$) with a length of 56 km (35 mi) was assumed, corresponding to the average of the 30-40 mi range specified by Bullington. Curves are presented for five frequencies ranging from 30 MHz to 4 GHz for an assumed value of geoclimatic factor, $G = 0$ dB. For 300 MHz, curves are also given for the two most extreme values of G below the 60th parallel, 7.5 dB and -10.9 dB, corresponding respectively to Port Erie, Ont. (Buffalo, N.Y.) and Fort Nelson, B.C.

The Bullington curves were based on experimental data, but unfortunately the author did not specify which data or frequency-dependence model were employed. Presumably some of the data used were those discussed in the section on extrapolation of the microwave tail models to VHF/UHF. One major limitation of the Bullington curves is that they show path variability only in terms of frequency. A less important limitation for the percentages of time typically of interest, is that they do not extend to the Rayleigh tail region.

It is perhaps a fortunate coincidence that the best agreement between the results of Method 1 (along with the interpolation procedure for shallow fade depths) and of Bullington occurs near 100 MHz, placing Bullington's curves on the conservative side for the 150 MHz and 450 MHz bands which have been used in Canada, at least under average fading conditions. Obviously Bullington's curves contain a larger frequency variability in the non-tail portion of the distribution, but with the limited data available, it is difficult to know which is the more accurate. However, it is important to note that the advantage of much greater path variability gained in the new methods (i.e., through the additional variables of geoclimatic factor, path length, path inclination and grazing angle) by far outweighs any possible loss of accuracy in the frequency dependence. This is illustrated in part by the curves in Fig. 7 for the "extreme" geoclimatic factors.

A graphical comparison of results from Method 1 and the method of Barnett [1] is given in Fig. 8, again for "average" climatic conditions in each case, and a path length of 56 km. The curves for Barnett's method are cut off at 15 dB, which is the limit of its applicability. Expressed in the same form as (4) and (16), the Barnett method is

$$A = 10 \log C - 42 + 30 \log d + 10 \log f - 10 \log P \quad (26)$$

for d in km, f in GHz, and P in per cent. Here, C is a factor that takes the value 1 for average climate and terrain conditions in the US, 4 for the Gulf of Mexico coast, and 1/4 for dry mountains, giving a variation in 10 log C of ± 6 dB. Vigants [2] extended the method by expressing C in terms of surface roughness, which increased the total geoclimatic variability from 12 to 17 dB.

Some of the advantages of the new methods over those of Barnett and Vigants have already been discussed. Fig. 8 illustrates another: average fading conditions in the US, at least as expressed by the Barnett model, are more severe than in Canada. This is not surprising, in view of the greater likelihood of extreme refractivity gradients in the US [33]. However, some of the difference apparent in Fig. 8 disappears for longer paths because of the large coefficient for path length in Methods 1 and 2. The difference becomes greater for paths shorter than 56 km.

As noted previously, the constants in (4) and (16) were adjusted to give $G = 0$ for "average" fading conditions in Canada (i.e., midway between those for Ottawa and Prince George). In fact, the actual average value of G for the 47 locations on the map of Fig. 3 (including the Arctic correction factor of 5 dB for the 16 locations above 60°N) is 0.1 dB.

The relationship between the logarithmic geoclimatic factor for France and the UK [7], here denoted by G_E, and that for Canada, is $G = G_E + 8$ (dB). This means that observed "average" fading conditions in France and the UK are more severe than those in Canada. This is partly due to the fact that few mountainous paths were included in the British-French data base. Indeed, an initial analysis of data for several paths in Switzerland [34] gives some very low values for the geoclimatic factor, similar to those in B.C. Another factor is that the average value of G_E is further weighted towards high values by the extreme results from the East Anglia region of the UK [7], a region that appears to have more severe fading ($G_E = 8$ dB, or $G = 16$ dB) than even the Niagara peninsula region of Ontario.

Implications for determining suitable path clearances

On the basis of the data for the Kemptville-Avonmore links and the earlier discussion, it is suggested that, in order to minimize tower heights and maximize link performance in multipath fading conditions, the antenna heights on the lower link in an SHF space-diversity configuration should be chosen, if possible, to give a 0.6 Fresnel zone path clearance from the terrain surface under 4/3-earth refractivity conditions (i.e., no diffraction loss). The upper link should still be designed to give a path clearance of at least that obtained from the design criteria for temperate climates cited in CCIR Report 338-6 [11]. To avoid increasing the height of existing towers, it would even seem appropriate to allow the lower link in a space-diversity configuration to graze the terrain surface in normal refractivity conditions, at least on paths with one or two isolated obstacles. The approximately 6 dB of extra diffraction loss (i.e., flat fading) incurred under normal refractivity conditions on a path having an obstacle approaching the shape of a "knife edge" would be well within link fade margins. The data for the Lowther Peak-Martyr Peak path in the Arctic would suggest that a grazing-clearance design for the lower link in a space-diversity configuration might be acceptable even for a relatively smooth path profile if the increased diffraction loss in both normal refractivity conditions (17 dB, for example, for the Lowther Peak-Martyr Peak path) and subrefractive conditions can be tolerated. A compromise solution would be to set the diversity antenna height to give a clearance of 0.3 Fresnel zone for either a path with one or two isolated obstacles or one in which the obstruction is extended along a portion of the path profile (i.e., a relatively smooth path). Again, the maximum 6 dB of extra diffraction loss incurred under normal refractivity conditions in the latter case [11] should be acceptable.

On the basis of the data for the links in Viscount Melville Sound, it is suggested that links in the 450 MHz band without diversity be designed for at least 0.6 Fresnel zone path clearance under 4/3-earth refractivity conditions. If tower costs are prohibitive, which might normally be the case unless they can be located on hilltops, it is suggested that grazing clearance under 4/3-earth refractivity conditions might be the next best alternative if fade margins are sufficiently large to make the increased diffraction loss under both 4/3-earth and subrefractive conditions acceptable. In a space-diversity configuration, it would certainly seem appropriate to design the lower link for grazing clearance of the terrain profile under 4/3-earth conditions as long as the increased diffraction loss in subrefractive conditions is acceptable. In the absence of other information, these procedures might also be used for other frequency bands in the upper VHF/UHF range of the spectrum.

The diffraction calculations required can be carried out using the computer program "PREDICT," resident at the Communications Research Centre.* In these calculations, the estimated value of the effective earth's radius factor, $k_{eff}(P\%)$, exceeded for P per cent of the time (over a path of length d) that is necessary for estimating the diffraction loss exceeded for $100 - P$ per cent of the time can be obtained from

$$k_{eff}(P\%) = k(P\%) \quad d \leq 20 \text{ km}, \tag{27.1}$$

$$k_{eff}(P\%) = k(P\%) + 0.53 \log(d/20) \quad 20 < d \leq 70 \text{ km}, \tag{27.2}$$

$$k_{eff}(P\%) = k(P\%) + 0.29[1 + \log(d/70)] \quad 70 \text{ km} < d, \tag{27.3}$$

where $k(P\%)$ is the point statistic estimated from the Tropospheric Refractivity Atlas for Canada [29]. Equations (27.1)-(27.3), which are based [35] on the curve for effective earth's radius versus path length given in CCIR Report 338-6 [11], are likely to be most accurate for exceedance percentages near 99.9%, but should be applicable over at least the range $99\% < P < 99.99\%$.

Discussion and conclusions

Three new methods have been presented for predicting the average worst-month multipath fading distributions on VHF/UHF/SHF line-of-sight links in Canada. Method 1 does not require detailed path profile information and is best suited for preliminary planning or licensing purposes. Method 2 requires the path profile and should normally be employed in detailed link design. The interpolation procedure is used in combination with either Method 1 or 2 to predict the shallow fading range of the distributions. All methods make use of radioclimatological data on the map of Fig. 3. They have been presented in step-by-step form for ease of application.

These methods are considerably more accurate than the Barnett-Vigants and Bullington methods normally used previously in Canada for the SHF/upper UHF and VHF/UHF bands, respectively. This improved accuracy is mainly the result of four factors: the use of more statistically significant prediction variables; the use of one more prediction variable than the Barnett-Vigants method in the case of Method 2; the use of radioclimatological and propagation data specifically related to the Canadian environment; and the extrapolation of the accurate microwave models downwards in frequency.

Several improvements to the new methods are envisaged in the future. These include possible modifications to the basic tail models resulting from analysis of a larger data base [34] for several countries including Canada. Of particular importance would be inclusion of data for mountainous paths.

Further improvements to the radioclimatological statistics employed to determine geoclimatic variability may also be possible. These include the use of longer-term refractivity gradient statistics than the three-year statistics employed here, the use of average worst-month statistics rather than average worst-three-month statistics, and the use of statistics for gradients other than the ducting threshold. If more radio data become available for paths in the vicinity of radiosonde stations, improvement in the regression equation (25) relating the logarithmic geoclimatic factor G to the refractivity gradient statistics may also be possible. Particularly lacking are suitable overland radio data for the Arctic from which to construct a more accurate Arctic correction factor, or preferably a new map with a more accurate relation between G and refractivity gradient statistics as a function of latitude.

Similarly, improvements to the correction factor for over-water paths are envisaged once more over-water data become available. One approach to this problem is likely to be the pooling of data for more than one country at temperate latitudes. Extension of the interpolation method for shallow fade depths or development of a separate prediction technique for the enhancement range of the clear-air fading distribution would also be desirable, but is hampered by lack of data. Again, pooling of data for more than one country is likely to produce the quickest results.

* On-line access or purchase available from the Radio Propagation Directorate, Communications Research Centre, Department of Communications, P.O. Box 11490, Station H, Ottawa, Ont. K2H 8S2.

Acknowledgements

The extrapolation of the basic microwave model to VHF/UHF was undertaken at the request of the DOC Spectrum Engineering section. The authors are grateful to Mr. Ted Devey for bringing this problem to their attention. Grateful thanks go to Mr. Mike Caskey of BNR for furnishing data and information on the Kemptville-Avonmore path, to Mr. Dwight Chang and Mr. Nev Owen of the B.C. Telephone Company for information on the paths in B.C., to Prof. Alan Webster of the University of Western Ontario (UWO) and Mr. Tim Merritt (formerly of UWO) for data and information on the Uniondale-London path, and to Mr. Claude Bilodeau of the Communications Research Centre (CRC) and Dr. Richard Butler (formerly of the CRC) for information on the Arctic paths. Thanks are also due to Dr. David Rogers, Dr. Jim Whitteker, and the three referees for their valuable suggestions in reviewing the manuscript. Finally, in the development of the basic microwave models, the first author would like to acknowledge the joint efforts of colleagues M. Louis Martin of the Centre National d'Études des Télécommunications (CNET) in France, and Mr. Terje Tjelta of Norwegian Telecom, and the helpful discussions with various CCIR colleagues. Much of this basic work was done while the first author was on an exchange visit to CNET in Lannion, France.

References

[1] W.T. Barnett, "Multipath propagation at 4, 6, and 11 GHz," *Bell Syst. Tech. J.*, vol. 51, Feb. 1972, pp. 321-361.

[2] A. Vigants, "Space diversity engineering," *Bell Syst. Tech. J.*, vol. 54, Jan. 1975, pp. 103-142.

[3] N. Owen, B.C. Telephone Company Ltd., Vancouver, B.C., private communication, 1982.

[4] K. Morita, "Prediction of Rayleigh fading occurrence probability of line-of-sight microwave links," *Rev. Electr. Comm. Lab. (Japan)*, vol. 18, Nov.-Dec. 1970, pp. 810-821.

[5] N. Owen, E. Lee and M. Kharadly, "Analysis of microwave fading observations on certain microwave paths in British Columbia," in *Proc. URSI Commission F Symposium on Wave Propagation and Remote Sensing*, ESA Report SP-194, European Space Agency, Paris, France, April 1983, pp. 3-12.

[6] K. Bullington, "Radio propagation fundamentals," *Bell Syst. Tech. J.*, vol. 36, May 1957, pp. 593-626.

[7] T. Tjelta, R.L. Olsen and L. Martin, "Systematic development of new multi-variable techniques for predicting the distribution of multipath fading on terrestrial microwave links," *IEEE Trans. Antennas and Propagation*, vol. AP-38, Oct. 1990, pp. 1650-1665.

[8] L. Martin, R.L. Olsen and T. Tjelta, "Initial analyses of multipath fading measurements for various geographical conditions in France," in *Proc. Int. Symp. on Antennas and Propagation*, Kyoto, Japan, 1985, pp. 1067-1070.

[9] R.L. Olsen, T. Tjelta, L. Martin and J.E. Doble, "Towards a more accurate method of predicting the distribution of multipath fading on terrestrial microwave links," *Electron. Lett.*, vol. 22, Aug. 14, 1986, pp. 902-903.

[10] T. Tjelta, R.L. Olsen and L. Martin, "An investigation of terrain related variables for predicting the multipath fade depth distribution on terrestrial microwave links," in *Proc. NATO/AGARD Conf. on 'Terrestrial Propagation Characteristics in Modern Systems of Communication, Surveillance, Guidance and Control,'* Conf. Proc. No. CP-407, National Technical Information Service, Springfield, Va., Nov. 1987, pp. 1/1-9.

[11] CCIR Report 338-6, "Propagation data and prediction methods required for line-of-sight radio-relay systems," in *Proc. XVIIth Plenary Assembly, annex to vol. V*, International Telecommunication Union, Geneva, Switzerland, 1990, pp. 355-420.

[12] R.L. Olsen, T. Tjelta, L. Martin and B. Segal, "New worldwide techniques for predicting the multipath fading distribution on terrestrial line-of-sight links in the VHF/UHF/SHF bands," to be submitted for publication.

[13] L. Martin, "Une expression analytique pour la représentation de lois de probabilité théoriques et experimentales," Centre National d'Études des Télécommunications, Lannion, France, Note Technique NT/LAB/MER/314, 1988.

[14] R.L. Olsen, T. Tjelta and L. Martin, "Results of tests on a new method for predicting the distribution of multipath fading for various percentages of time," International Telecommunication Union, Geneva, Switzerland, CCIR IWP 5/2 Doc. 89/59, Apr. 3, 1989.

[15] N.R. Draper and H. Smith, *Applied Regression Analysis*. New York: John Wiley and Sons, 1981.

[16] R. Olsen, L. Martin and T. Tjelta, "A review of the role of surface reflection in multipath propagation over line-of-sight terrestrial microwave links," in *Proc. NATO/AGARD Conference on 'Terrestrial Propagation Characteristics in Modern Systems of Communications, Surveillance, Guidance and Control,'* Conf. Proc. No. CP-407, National Technical Information Service, Springfield, Va., Nov. 1987, pp. 2/1-23.

[17] R.L. Olsen, "The role of atmospheric stratification and surface effects in multipath propagation over terrestrial line-of-sight links: a review of some recent results," in *Proc. SBMO International Microwave Symp.*, Sao Paulo, Brazil, July 1989, pp. 401-408.

[18] T. Tjelta, R.L. Olsen and L. Martin, "Results of tests on methods for predicting the distribution of multipath fading at large fade depths," International Telecommunication Union, Geneva, Switzerland, CCIR IWP 5/2 Doc. 89/60, Apr. 27, 1989.

[19] M.P.M. Hall, "Activities in CCIR study group 5," *J. IERE*, vol. 58 (supplement), Sept.-Dec. 1988, pp. S244-S247.

[20] J.E. Doble, "Prediction of multipath delays and frequency selective fading on digital radio links in the U.K.," *IEE Colloqium Digest*, no. 62, 1979.

[21] L. Boithias, *Propagation des Ondes Radioélectriques*, Paris: Dunod, 1983, p. 139.

[22] CCIR Recommendation 581-1, "The concept of worst month," in *Proc. XVIth Plenary Assembly, vol. V*, International Telecommunication Union, Geneva, Switzerland, 1986, p. 230.

[23] K.W. Pearson, "Method for the prediction of the fading performance of a multisection microwave link," in *Proc. IEE*, vol. 112, July 1965, pp. 1291-1300.

[24] F. Carassa and P. Quarta, "Propagation tests at 250, 500, 1000, 2000 Mc/s on a 189 km path," in *Electromagnetic Wave Propagation*, M. Desirant and J.L. Michiels, Eds. London: Academic Press, 1960, pp. 471-478.

[25] F. Carassa, "Prove di propagazione con le frequenze di 250, 500, 1000 MHz," *Alta Frequenza*, vol. 25, May 1956, pp. 378-390.

[26] G.S. Wickizer and A.M. Braaten, "Propagation studies on 45.1, 474, and 2800 Megacycles within and beyond the horizon," in *Proc. IRE*, July 1947, pp. 670-680.

[27] A.L. Durkee, "Results of microwave propagation tests on a 40-mile overland path," in *Proc. IRE*, vol. 36, Feb. 1948, pp. 197-205.

[28] W. Klein and L.J. Libois, "Essais de transmission par faisceaux hertziens sur un long parcours en visibilité optique entre la France et la Suisse," *Onde Électr.*, vol. 33, 1953, pp. 665-677.

[29] B. Segal and R.E. Barrington, "The radio climatology of Canada: tropospheric refractivity atlas for Canada," Communications Research Centre, Department of Communications, Ottawa, Ont., CRC Report No. 1315, Dec. 1977.

[30] C. Bilodeau, "Measurements of UHF radio propagation on the Baffin and Labrador coasts," Communications Research Centre, Department of Communications, Ottawa, Ont., CRC Report No. 1430, July 1988.

[31] M. Caskey, Bell-Northern Research, Ottawa, Ont., private communication, 1987.

[32] R.S. Butler, "Measurements at 11 and 17 GHz of terrestrial microwave fading and depolarization," Communications Research Centre, Department of Communications, Ottawa, Ont., CRC Report No. 1358, Sep. 1982.

[33] B.R. Bean, B.A. Cahoon, C.A. Samson and G.D. Thayer, "A world atlas of radio refractivity," U.S. Department of Commerce, Washington, D.C., Monograph 1, 1966.

[34] CCIR Report 1144, "Data banks to support evaluation of prediction methods," in *Proc. XVIIth Plenary Assembly, annex to vol. V*, International Telecommunication Union, Geneva, Switzerland, 1990, pp. 1-25.

[35] CCIR Doc. 5/8, "Effects of refractivity on path clearance and on angle-of-arrival for line-of-sight radio-relay links," International Telecommunication Union, Geneva, Switzerland, Mar. 29, 1983.

[36] P.A. Kennard, J.D. McNicol and M.D. Caskey, "Fading dynamics in high spectral efficiency digital radio," in *Proc. IEEE Int. Conf. on Communications*, Toronto, Ont., 1986, pp. 1487-1492.

[37] T. Merritt, Centre for Radio Science, University of Western Ontario, London, Ont., private communication, 1987.

[38] W.I. Lam and A.R. Webster, "Microwave propagation on two line-of-sight oversea paths," *IEEE Trans. Antennas and Propagation*, vol. AP-33, May 1985, pp. 510-516.

[39] R.S. Butler, "The Northwest Passage propagation experiment: report of the 1983-1984 measurement program," Communications Research Centre, Department of Communications, Ottawa, Ont., CRC Report No. 1391, Sep. 1985.

[40] B. Segal, "Rain attenuation statistics for terrestrial microwave links in Canada," Communications Research Centre, Department of Communications, Ottawa, Ont., CRC Report No. 1351, Jan. 1982.

RECOMMENDATION ITU-R P.676-3

ATTENUATION BY ATMOSPHERIC GASES

(Question ITU-R 201/3)

(1990-1992-1995-1997)

The ITU Radiocommunication Assembly,

considering

a) the necessity of estimating the attenuation by atmospheric gases on terrestrial and slant paths,

recommends

1 that, for general application, the procedures in Annex 1 be used to calculate gaseous attenuation at frequencies up to 1 000 GHz. (Software code in MATLAB is available from the Radiocommunication Bureau);

2 that, for approximate estimates of gaseous attenuation in the frequency range 1 to 350 GHz, the simpler procedure given in Annex 2 be used.

ANNEX 1

Line-by-line calculation of gaseous attenuation

1 Specific attenuation

The specific attenuation at frequencies up to 1 000 GHz due to dry air and water vapour, can be evaluated most accurately at any value of pressure, temperature and humidity by means of a summation of the individual resonance lines from oxygen and water vapour, together with small additional factors for the non-resonant Debye spectrum of oxygen below 10 GHz, pressure-induced nitrogen attenuation above 100 GHz and a wet continuum to account for the excess water vapour-absorption found experimentally. Figure 1 shows the specific attenuation using the model, calculated from 0 to 1 000 GHz at 1 GHz intervals, for a pressure of 1 013 hPa, temperature of 15° C for the cases of a water-vapour density of 7.5 g/m^3 (Curve A) and a dry atmosphere (Curve B).

Near 60 GHz, many oxygen absorption lines merge together, at sea-level pressures, to form a single, broad absorption band, which is shown in more detail in Fig. 2. This Figure also shows the oxygen attenuation at higher altitudes, with the individual lines becoming resolved at lower pressures.

For quick and approximate estimates of specific attenuation at frequencies up to 350 GHz, in cases where high accuracy is not required, simplified algorithms are given in Annex 2 for restricted ranges of meteorological conditions.

FIGURE 1

Specific attenuation due to atmospheric gases, calculated at 1 GHz intervals

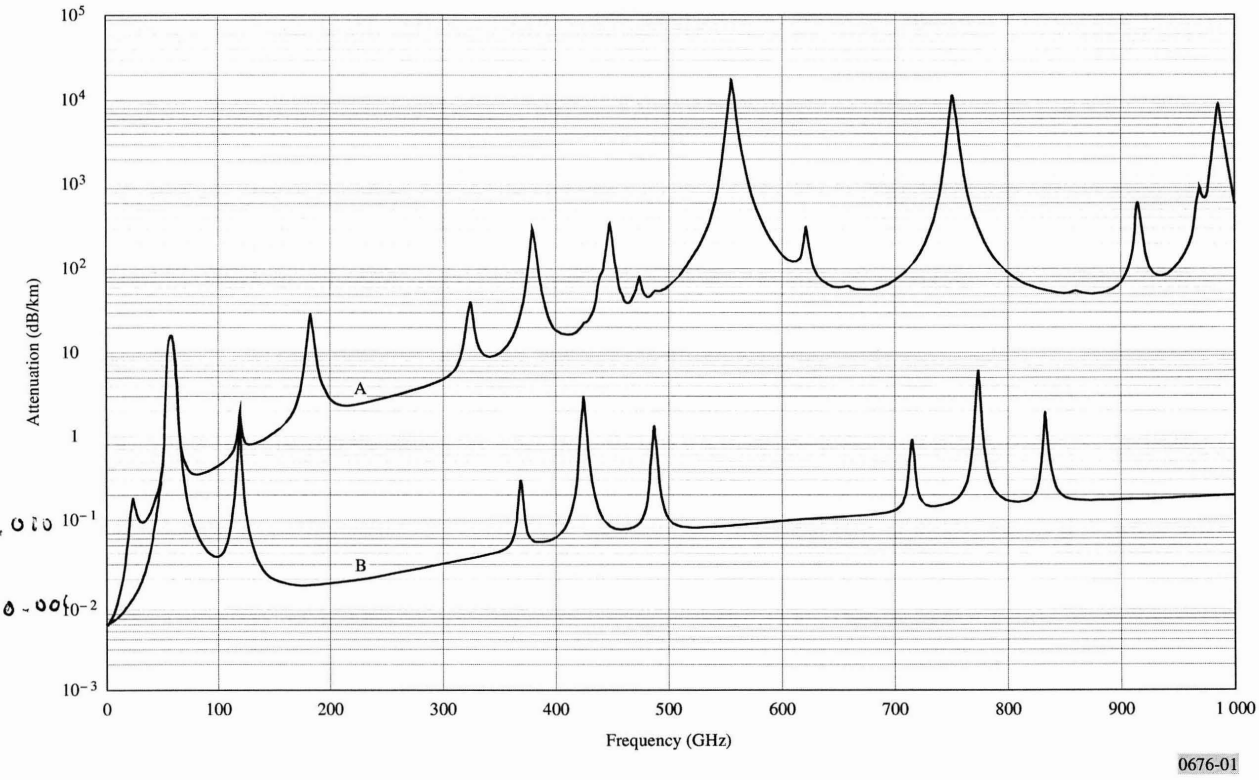

Curves A: standard atmosphere (7.5 g/m^3)

B: dry atmosphere

FIGURE 2

Specific attenuation in the range 50-70 GHz at the altitudes indicated

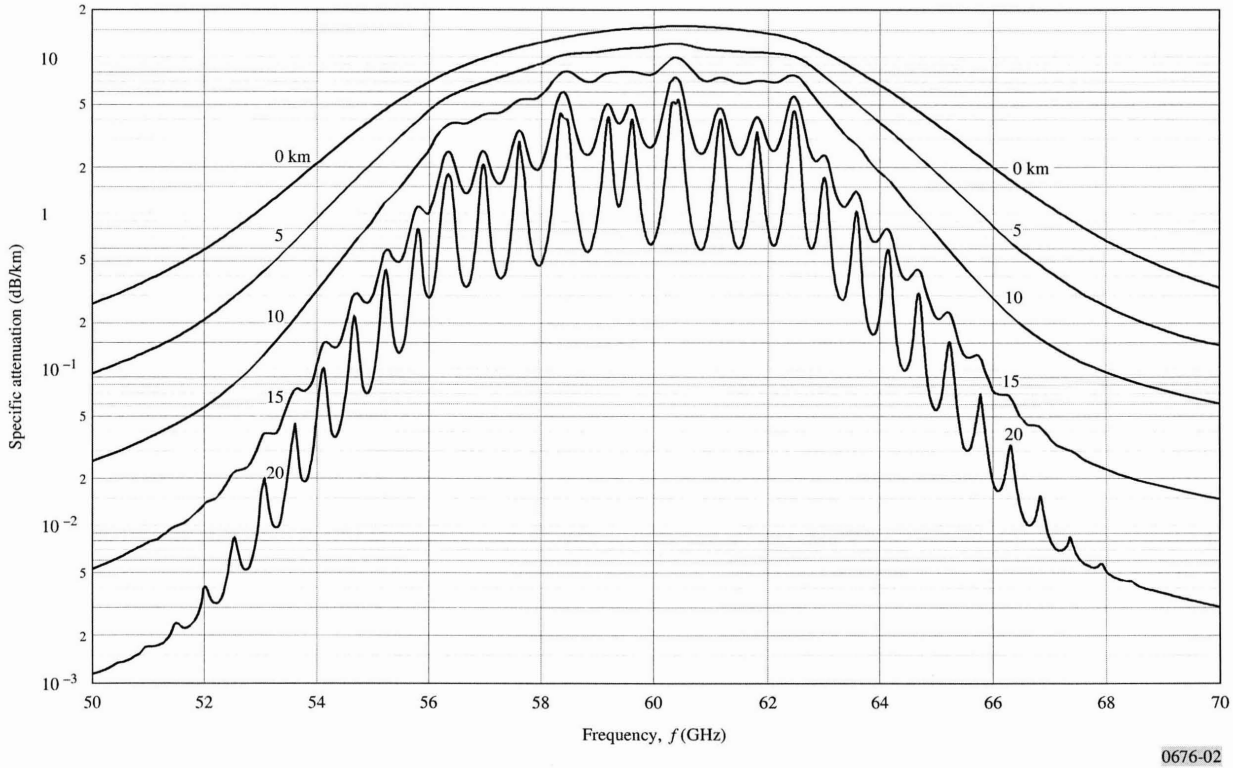

The specific gaseous attenuation is given by:

$$\gamma = \gamma_o + \gamma_w = 0.1820 f N''(f) \quad \text{dB/km} \tag{1}$$

where γ_o and γ_w are the specific attenuations (dB/km) due to dry air and water vapour, respectively, and where f is the frequency (GHz) and $N''(f)$ is the imaginary part of the frequency-dependent complex refractivity:

$$N''(f) = \sum_i S_i F_i + N''_D(f) + N''_W(f) \tag{2}$$

S_i is the strength of the ith line, F_i is the line shape factor and the sum extends over all the lines; $N''_D(f)$ and $N''_W(f)$ are dry and wet continuum spectra.

The line strength is given by:

$$\begin{aligned} S_i &= a_1 \times 10^{-7}\, p\, \theta^3 \exp\left[a_2 (1 - \theta)\right] \quad \text{for oxygen} \\ &= b_1 \times 10^{-1}\, e\, \theta^{3.5} \exp\left[b_2 (1 - \theta)\right] \quad \text{for water vapour} \end{aligned} \tag{3}$$

where:

p: dry air pressure (hPa)

e: water vapour partial pressure in hPa (total barometric pressure $P = p + e$)

$\theta =$ $300/T$

T: temperature (K).

Local values of p, e and T measured profiles (e.g. using radiosondes) should be used; however, in the absence of local information, the Reference Standard Atmospheres described in Recommendation ITU-R P.835 should be used.

The water-vapour partial pressure, e, may be obtained from the water-vapour density ρ using the expression:

$$e = \frac{\rho T}{216.7} \tag{4}$$

The coefficients a_1, a_2 are given in Table 1 for oxygen, those for water vapour, b_1 and b_2, are given in Table 2.

The line-shape factor is given by:

$$F_i = \frac{f}{f_i}\left[\frac{\Delta f - \delta (f_i - f)}{(f_i - f)^2 + \Delta f^2} + \frac{\Delta f - \delta (f_i + f)}{(f_i + f)^2 + \Delta f^2}\right] \tag{5}$$

where f_i is the line frequency and Δf is the width of the line:

$$\begin{aligned} \Delta f &= a_3 \times 10^{-4} (p\, \theta^{(0.8 - a_4)} + 1{,}1\, e\, \theta) \quad \text{for oxygen} \\ &= b_3 \times 10^{-4} (p\, \theta^{b_4} + b_5\, e\, \theta^{b_6}) \quad \text{for water vapour} \end{aligned} \tag{6}$$

and δ is a correction factor which arises due to interference effects in oxygen lines:

$$\begin{aligned} \delta &= (a_5 + a_6 \theta) \times 10^{-4} p\, \theta^{0.8} \quad \text{for oxygen} \\ &= 0 \quad \text{for water vapour} \end{aligned} \tag{7}$$

The spectroscopic coefficients are given in Tables 1 and 2.

TABLE 1

Spectroscopic data for oxygen attenuation

f_0	a_1	a_2	a_3	a_4	a_5	a_6
50.474238	0.94	9.694	8.60	0	1.600	5.520
50.987749	2.46	8.694	8.70	0	1.400	5.520
51.503350	6.08	7.744	8.90	0	1.165	5.520
52.021410	14.14	6.844	9.20	0	0.883	5.520
52.542394	31.02	6.004	9.40	0	0.579	5.520
53.066907	64.10	5.224	9.70	0	0.252	5.520
53.595749	124.70	4.484	10.00	0	−0.066	5.520
54.130000	228.00	3.814	10.20	0	−0.314	5.520
54.671159	391.80	3.194	10.50	0	−0.706	5.520
55.221367	631.60	2.624	10.79	0	−1.151	5.514
55.783802	953.50	2.119	11.10	0	−0.920	5.025
56.264775	548.90	0.015	16.46	0	2.881	−0.069
56.363389	1 344.00	1.660	11.44	0	−0.596	4.750
56.968206	1 763.00	1.260	11.81	0	−0.556	4.104
57.612484	2 141.00	0.915	12.21	0	−2.414	3.536
58.323877	2 386.00	0.626	12.66	0	−2.635	2.686
58.446590	1 457.00	0.084	14.49	0	6.848	−0.647
59.164207	2 404.00	0.391	13.19	0	−6.032	1.858
59.590983	2 112.00	0.212	13.60	0	8.266	−1.413
60.306061	2 124.00	0.212	13.82	0	−7.170	0.916
60.434776	2 461.00	0.391	12.97	0	5.664	−2.323
61.150560	2 504.00	0.626	12.48	0	1.731	−3.039
61.800154	2 298.00	0.915	12.07	0	1.738	−3.797
62.411215	1 933.00	1.260	11.71	0	−0.048	−4.277
62.486260	1 517.00	0.083	14.68	0	−4.290	0.238
62.997977	1 503.00	1.665	11.39	0	0.134	−4.860
63.568518	1 087.00	2.115	11.08	0	0.541	−5.079
64.127767	733.50	2.620	10.78	0	0.814	−5.525
64.678903	463.50	3.195	10.50	0	0.415	−5.520
65.224071	274.80	3.815	10.20	0	0.069	−5.520
65.764772	153.00	4.485	10.00	0	−0.143	−5.520
66.302091	80.09	5.225	9.70	0	−0.428	−5.520
66.836830	39.46	6.005	9.40	0	−0.726	−5.520
67.369598	18.32	6.845	9.20	0	−1.002	−5.520
67.900867	8.01	7.745	8.90	0	−1.255	−5.520
68.431005	3.30	8.695	8.70	0	−1.500	−5.520
68.960311	1.28	9.695	8.60	0	−1.700	−5.520
118.750343	945.00	0.009	16.30	0	−0.247	0.003
368.498350	67.90	0.049	19.20	0.6	0	0
424.763124	638.00	0.044	19.16	0.6	0	0
487.249370	235.00	0.049	19.20	0.6	0	0
715.393150	99.60	0.145	18.10	0.6	0	0
773.839675	671.00	0.130	18.10	0.6	0	0
834.145330	180.00	0.147	18.10	0.6	0	0

TABLE 2

Spectroscopic data for water-vapour attenuation

f_0	b_1	b_2	b_3	b_4	b_5	b_6
22.235080	0.1090	2.143	28.11	0.69	4.80	1.00
67.813960	0.0011	8.735	28.58	0.69	4.93	0.82
119.995941	0.0007	8.356	29.48	0.70	4.78	0.79
183.310074	2.3000	0.668	28.13	0.64	5.30	0.85
321.225644	0.0464	6.181	23.03	0.67	4.69	0.54
325.152919	1.5400	1.540	27.83	0.68	4.85	0.74
336.187000	0.0010	9.829	26.93	0.69	4.74	0.61
380.197372	11.9000	1.048	28.73	0.69	5.38	0.84
390.134508	0.0044	7.350	21.52	0.63	4.81	0.55
437.346667	0.0637	5.050	18.45	0.60	4.23	0.48
439.150812	0.9210	3.596	21.00	0.63	4.29	0.52
443.018295	0.1940	5.050	18.60	0.60	4.23	0.50
448.001075	10.6000	1.405	26.32	0.66	4.84	0.67
470.888947	0.3300	3.599	21.52	0.66	4.57	0.65
474.689127	1.2800	2.381	23.55	0.65	4.65	0.64
488.491133	0.2530	2.853	26.02	0.69	5.04	0.72
503.568532	0.0374	6.733	16.12	0.61	3.98	0.43
504.482692	0.0125	6.733	16.12	0.61	4.01	0.45
556.936002	510.0000	0.159	32.10	0.69	4.11	1.00
620.700807	5.0900	2.200	24.38	0.71	4.68	0.68
658.006500	0.2740	7.820	32.10	0.69	4.14	1.00
752.033227	250.0000	0.396	30.60	0.68	4.09	0.84
841.073593	0.0130	8.180	15.90	0.33	5.76	0.45
859.865000	0.1330	7.989	30.60	0.68	4.09	0.84
899.407000	0.0550	7.917	29.85	0.68	4.53	0.90
902.555000	0.0380	8.432	28.65	0.70	5.10	0.95
906.205524	0.1830	5.111	24.08	0.70	4.70	0.53
916.171582	8.5600	1.442	26.70	0.70	4.78	0.78
970.315022	9.1600	1.920	25.50	0.64	4.94	0.67
987.926764	138.0000	0.258	29.85	0.68	4.55	0.90

The dry air continuum arises from the non-resonant Debye spectrum of oxygen below 10 GHz and a pressure-induced nitrogen attenuation above 100 GHz.

$$N''_D(f) = f\ p\ \theta^2 \left[\frac{6.14 \times 10^{-5}}{d\left[1 + \left(\frac{f}{d}\right)^2\right]} + 1.4 \times 10^{-12} (1 - 1.2 \times 10^{-5} f^{1.5})\ p\ \theta^{1.5} \right] \tag{8}$$

where d is the width parameter for the Debye spectrum:

$$d = 5.6 \times 10^{-4} (p + 1.1\ e)\ \theta \tag{9}$$

The wet continuum, $N''_W(f)$, is included to account for the fact that measurements of water-vapour attenuation are generally in excess of those predicted using the theory described by equations (2) to (7), plus a term to include the effects of higher-frequency water-vapour lines not included in the reduced line base:

$$N''_W(f) = f(3.57\ \theta^{7.5}\ e + 0.113\ p)\ 10^{-7}\ e\ \theta^3 \tag{10}$$

2 Path attenuation

2.1 Terrestrial paths

For a terrestrial path, or for slightly inclined paths close to the ground, the path attenuation, A, may be written as:

$$A = \gamma r_0 = (\gamma_o + \gamma_w) r_0 \quad \text{dB} \tag{11}$$

where r_0 is path length (km).

2.2 Slant paths

This section gives a method to integrate the specific attenuation calculated using the line-by-line model given above, at different pressures, temperatures and humidities through the atmosphere. By this means, the path attenuation for communications systems with any geometrical configuration within and external to the Earth's atmosphere may be accurately determined simply by dividing the atmosphere into horizontal layers, specifying the profile of the meteorological parameters pressure, temperature and humidity along the path. In the absence of local profiles, from radiosonde data, for example, the reference standard atmospheres in Recommendation ITU-R P.835 may be used, either for global application or for low (annual), mid (summer and winter) and high latitude (summer and winter) sites.

Figure 3 shows the zenith attenuation calculated at 1 GHz intervals with this model for the global reference standard atmosphere in Recommendation ITU-R P.835, with horizontal layers 1 km thick and summing the attenuations for each layer, for the cases of a moist atmosphere (Curve A) and a dry atmosphere (Curve B).

The total slant path attenuation, $A(h, \varphi)$, from a station with altitude, h, and elevation angle, φ, can be calculated as follows when $\varphi \geq 0$:

$$A(h.\varphi) = \int_h^\infty \frac{\gamma(H)}{\sin \Phi} \, dH \tag{12}$$

where the value of Φ can be determined as follows based on Snell's law in polar coordinates:

$$\Phi = \arccos\left(\frac{c}{(r + H) \times n(H)}\right) \tag{13}$$

where:

$$c = (r + h) \times n(h) \times \cos \varphi \tag{14}$$

where $n(h)$ is the atmospheric radio refractive index, calculated from pressure, temperature and water-vapour pressure along the path (see Recommendation ITU-R P.835) using Recommendation ITU-R P.453.

On the other hand, when $\varphi < 0$, there is a minimum height, h_{min}, at which the radio beam becomes parallel with the Earth's surface. The value of h_{min} can be determined by solving the following transcendental equation:

$$(r + h_{min}) \times n(h_{min}) = c \tag{15}$$

This can be easily solved by repeating the following calculation, using $h_{min} = h$ as an initial value:

$$h'_{min} = \frac{c}{n(h_{min})} - r \tag{16}$$

Therefore, $A(h, \varphi)$ can be calculated as follows:

$$A(h,\varphi) = \int_{h_{min}}^\infty \frac{\gamma(H)}{\sin \Phi} \, dH + \int_{h_{min}}^h \frac{\gamma(H)}{\sin \Phi} \, dH \tag{17}$$

FIGURE 3

Zenith attenuation due to atmospheric gases, calculated in 1 GHz intervals

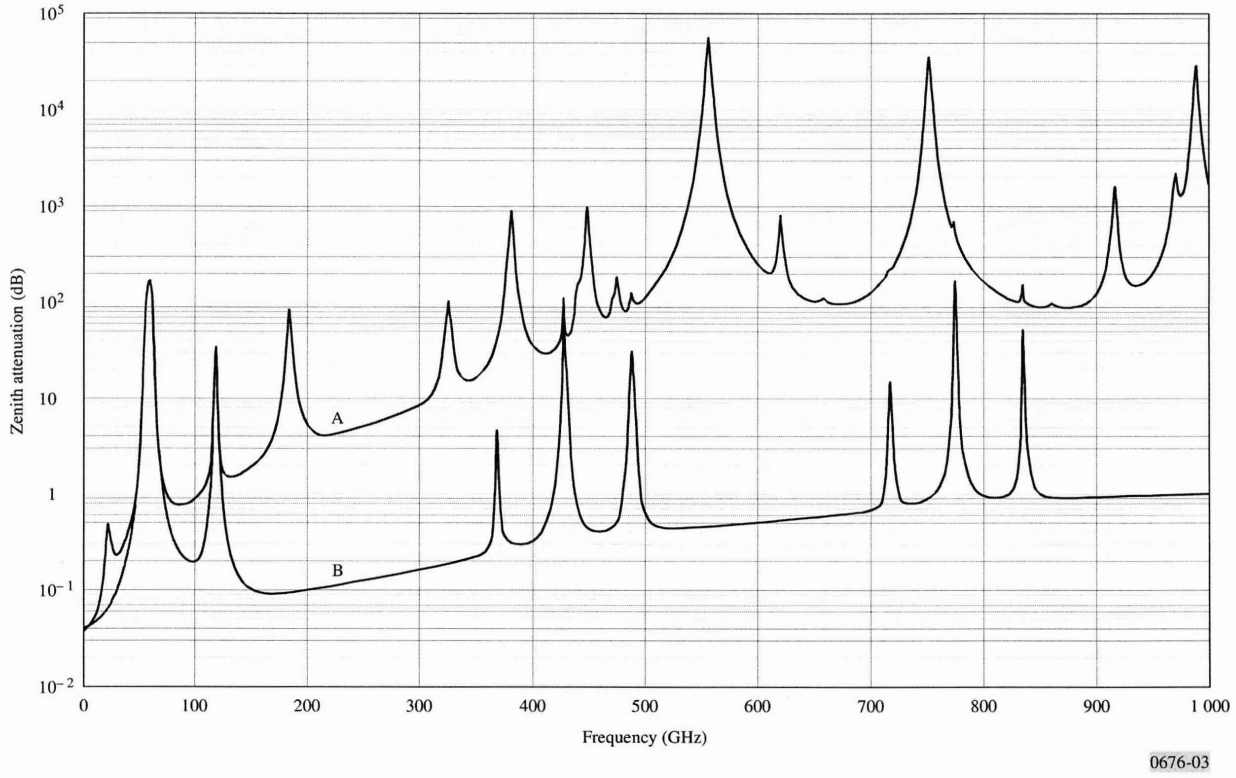

Curves A: standard atmosphere (7.5 g/m^3)

B: dry atmosphere

In carrying out the integration of equations (12) and (17), care should be exercised in that the integrand becomes infinite at $\Phi = 0$. However, this singularity can be eliminated by an appropriate variable conversion, for example, by using $u^4 = H - h$ in equation (12) and $u^4 = H - h_{min}$ in equation (17).

A numerical solution for the attenuation due to atmospheric gases can be implemented with the following algorithm.

To calculate the total attenuation for a satellite link, it is necessary to know not only the specific attenuation at each point of the link but also the length of path that has that specific attenuation. To derive the path length it is also necessary to consider the ray bending that occurs in a spherical Earth.

FIGURE 4

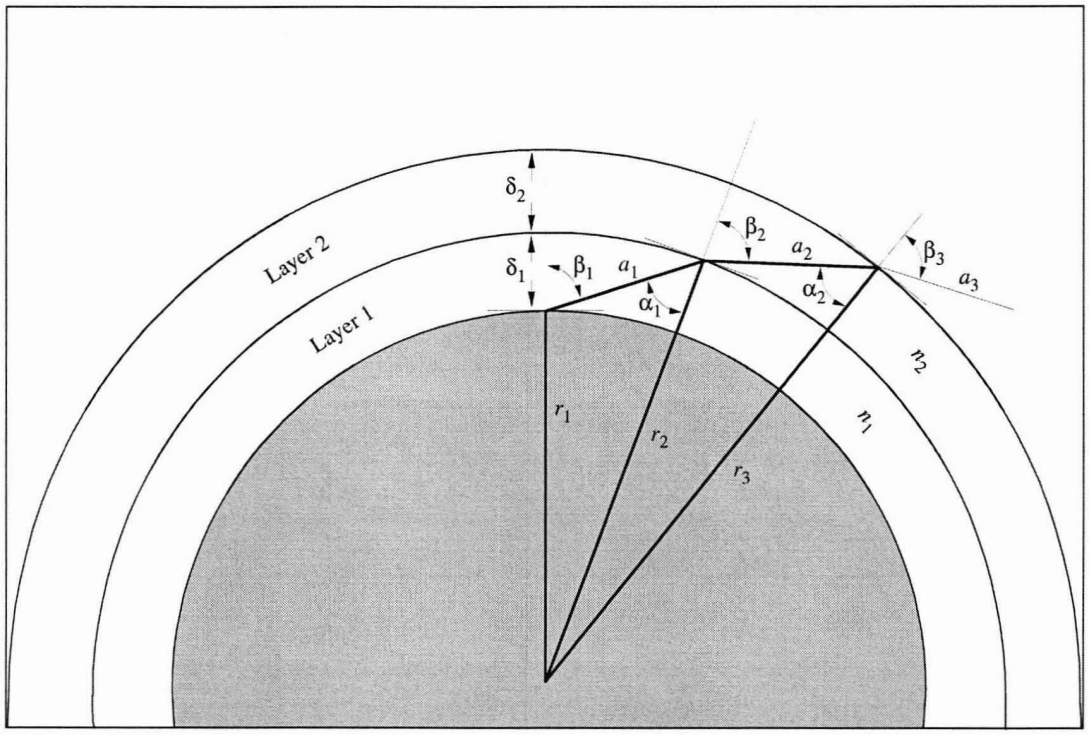

0676-04

Using Fig. 4 as a reference, a_n is the path length through layer n with thickness δ_n that has refractive index n_n. α_n and β_n are the entry and exiting incidence angles. r_n are the radii from the centre of the Earth to the beginning of layer n. a_n can then be expressed as:

$$a_n = -r_n \cos\beta_n + \frac{1}{2}\sqrt{4 r_n^2 \cos^2\beta_n + 8 r_n \delta_n + 4\delta_n^2} \tag{18}$$

The angle α_n can be calculated from:

$$\alpha_n = \pi - \arccos\left(\frac{-a_n^2 - 2r_n \delta_n - \delta_n^2}{2a_n r_n + 2a_n \delta_n}\right) \tag{19}$$

β_1 is the incidence angle at the ground station (the complement of the elevation angle θ). β_{n+1} can be calculated from α_n using Snell's law that in this case becomes:

$$\beta_{n+1} = \text{arc sin}\left(\frac{n_n}{n_{n+1}} \sin\alpha_n\right) \tag{20}$$

where n_n and n_{n+1} are the refractive indexes of layers n and $n + 1$.

The remaining frequency dependent (dispersive) term has a marginal influence on the result (around 1%) but can be calculated from the method shown in the ITU-R Handbook on Radiometeorology.

The total attenuation can be derived using:

$$A_{gas} = \sum_{n=1}^{k} a_n \gamma_n \quad \text{dB} \tag{21}$$

where γ_n is the specific attenuation derived from equation (1).

To ensure an accurate estimate of the attenuation, the thickness of the layers should increase exponentially with height. Accurate results can be obtained with layer thickness that increases from 10 cm for the lower layer to 1 km at an altitude of 100 km.

For Earth-to-space applications the integration should be performed at least up to 30 km.

3 Dispersive effects

The effects of dispersion are discussed in the ITU-R Handbook on Radiometeorology, which contains a model for calculating dispersion based on the line-by-line calculation. For practical purposes, dispersive effects should not impose serious limitations on millimetric terrestrial communication systems operating with bandwidths of up to a few hundred MHz over short ranges (for example, less than about 20 km), especially in the window regions of the spectrum, at frequencies removed from the centres of major absorption lines. For satellite communication systems, the longer path lengths through the atmosphere will constrain operating frequencies further to the window regions, where both atmospheric attenuation and the corresponding dispersion are low.

ANNEX 2

Approximate estimation of gaseous attenuation in the frequency range 1-350 GHz

This Annex contains simplified algorithms for quick, approximate estimation of gaseous attenuation for a limited range of meteorological conditions and a limited variety of geometrical configurations.

1 Specific attenuation

The specific attenuation due to dry air and water vapour, from sea level to an altitude of 5 km, can be estimated using the following simplified algorithms, which are based on curve-fitting to the line-by-line calculation, and agree with the more accurate calculations to within an average of about ±15% at frequencies removed from the centres of major absorption lines. The absolute difference between the results from these algorithms and the line-by-line calculation is generally less than 0.1 dB/km and reaches a maximum of 0.7 dB/km near 60 GHz. For altitudes higher than 5 km, and in cases where higher accuracy is required, the line-by-line calculation should be used.

For dry air, the attenuation γ_o (dB/km) is given by:

$$\gamma_o = \left[\frac{7.27\ r_t}{f^2 + 0.351\ r_p^2\ r_t^2} + \frac{7.5}{(f - 57)^2 + 2.44\ r_p^2\ r_t^5} \right] f^2\ r_p^2\ r_t^2 \times 10^{-3} \quad (22a)$$

for $f \leq 57$ GHz

$$\gamma_o = \left[2 \times 10^{-4}\ r_t^{1.5} \left(1 - 1.2 \times 10^{-5}\ f^{1.5}\right) + \frac{4}{(f-63)^2 + 1.5\, r_p^2\, r_t^5} + \frac{0.28\, r_t^2}{(f - 118.75)^2 + 2.84\, r_p^2\, r_t^2} \right] f^2\, r_p^2\, r_t^2 \times 10^{-3} \quad (22b)$$

for 63 GHz $\leq f \leq$ 350 GHz

$$\gamma_o = \frac{(f - 60)(f - 63)}{18}\ \gamma_o(57) - 1.66\ r_p^2\ r_t^{8.5} (f - 57)(f - 63) + \frac{(f - 57)(f - 60)}{18}\ \gamma_o(63) \quad (22c)$$

for 57 GHz $\leq f \leq$ 63 GHz.

where:

f: frequency (GHz)

$r_p = p/1013$

$r_t = 288/(273 + t)$

p: pressure (hPa)

t: temperature (°C).

For water vapour, the attenuation γ_w (dB/km) is given by:

$$\gamma_w = \left[\begin{array}{l} 3.27 \times 10^{-2}\ r_t + 1.67 \times 10^{-3}\ \dfrac{\rho\ r_t^7}{r_p} + 7.7 \times 10^{-4}\ f^{0.5} + \dfrac{3.79}{(f - 22.235)^2 + 9.81\, r_p^2\ r_t} \\ + \dfrac{11.73\ r_t}{(f - 183.31)^2 + 11.85\, r_p^2\ r_t} + \dfrac{4.01\ r_t}{(f - 325.153)^2 + 10.44\, r_p^2\ r_t} \end{array} \right] f^2\ \rho\ r_p\ r_t \times 10^{-4} \quad (23)$$

for $f \leq$ 350 GHz

where ρ is the water-vapour density (g/m^3).

Figure 5 shows the specific attenuation from 1 to 350 GHz at sea-level for dry air and water vapour with a density of 7.5 g/m^3. This figure was derived using the line-by-line calculation as described in Annex 1.

2 Path attenuation

2.1 Terrestrial paths

For a horizontal path, or for slightly inclined paths close to the ground, the path attenuation, A, may be written as:

$$A = \gamma\, r_0 = (\gamma_o + \gamma_w) r_0 \quad \text{dB} \quad (24)$$

where r_0 is the path length (km).

FIGURE 5

Specific attenuation due to atmospheric gases

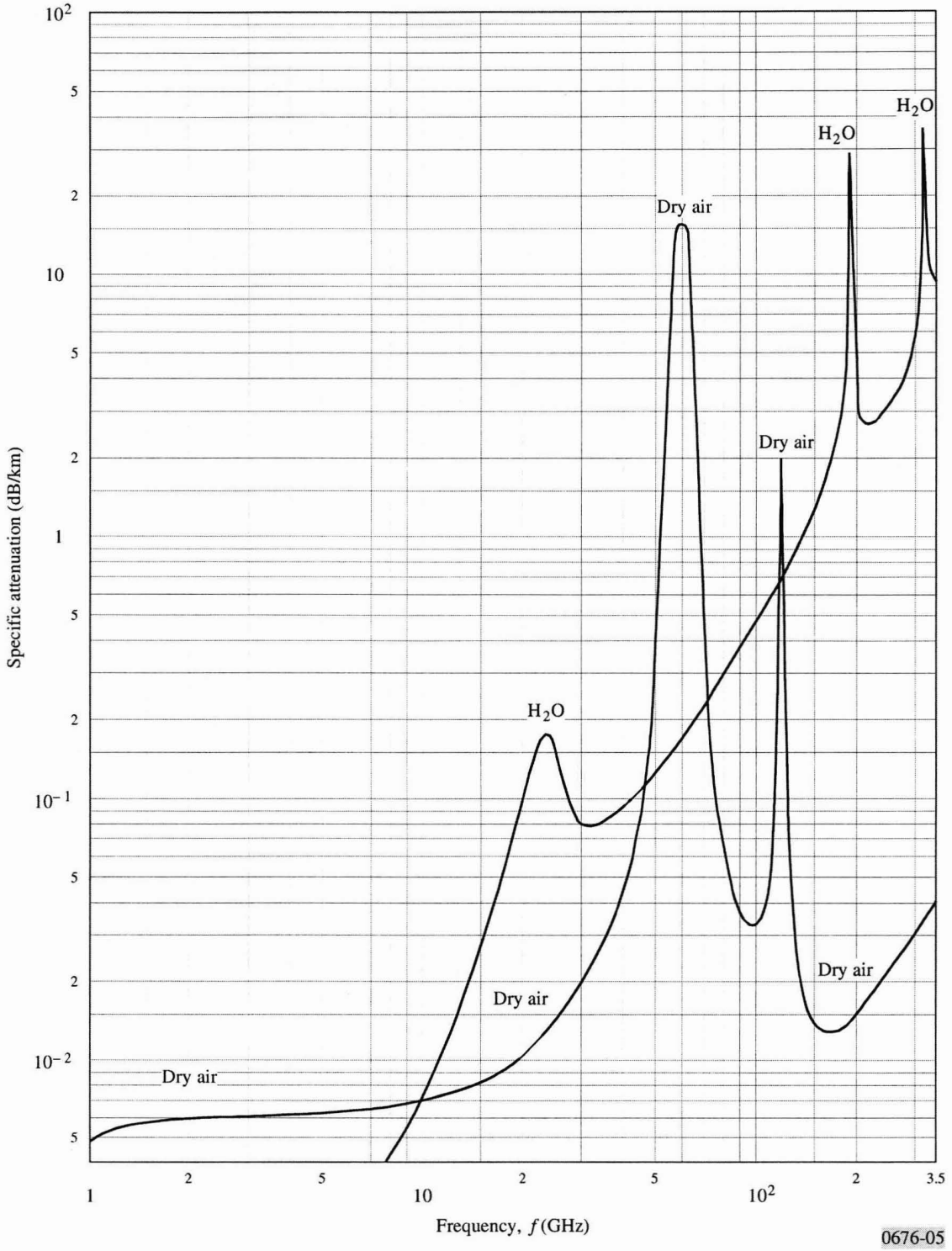

Pressure: 1 013 hPa
Temperature: 15° C
Water vapour: 7.5 g/m^3

2.2 Slant paths

This section contains simple algorithms for the calculation of gaseous attenuation along slant paths through the Earth's atmosphere, by defining an equivalent height by which the specific attenuation calculated in § 1 may be multiplied to obtain the zenith path attenuation, from sea level up to altitudes of about 2 km. The path attenuation at elevation angles other than the zenith may then be determined using the procedures described later in this section.

For dry air, the equivalent height is given by:

$$h_o = 6 \quad \text{km} \quad \text{for} \quad f < 50 \ \text{GHz} \tag{25}$$

$$h_o = 6 + \frac{40}{(f - 118.7)^2 + 1} \quad \text{km} \quad \text{for } 70 < f < 350 \ \text{GHz} \tag{26}$$

and for water-vapour, the equivalent height is:

$$h_w = h_{w0} \left\{ 1 + \frac{3.0}{(f - 22.2)^2 + 5} + \frac{5.0}{(f - 183.3)^2 + 6} + \frac{2.5}{(f - 325.4)^2 + 4} \right\} \quad \text{km} \tag{27}$$

For $f < 350$ GHz

where:

h_{w0}: water vapour equivalent height in the window regions

= 1.6 km in clear weather

= 2.1 km in rain.

These equivalent heights for water vapour were determined at a ground-level temperature of 15° C. For other temperatures the equivalent heights may be corrected by 0.1% or 1% per °C in clear weather or rain respectively, in the window regions, and by 0.2% or 2% in the absorption bands (height increasing with increasing temperature).

The concept of equivalent height is based on the assumption of an exponential atmosphere specified by a scale height to describe the decay in density with altitude. Note that scale heights for both dry air and water vapour may vary with latitude, season and/or climate, and that water vapour distributions in the real atmosphere may deviate considerably from the exponential, with corresponding changes in equivalent heights. The values given above are applicable up to an altitude of 2 km.

The total zenith attenuation is then:

$$A = \gamma_o h_o + \gamma_w h_w \quad \text{dB} \tag{28}$$

Figure 6 shows the total zenith attenuation at sea level for two cases: (A) the dry reference standard atmosphere in Recommendation ITU-R P.835 and (B) including the water-vapour model atmosphere in Recommendation ITU-R P.835. Between 50 and 70 GHz greater accuracy can be obtained from the 0 km curve in Fig. 7. This figure was derived using the line-by-line calculation as described in Annex 1.

2.2.1 Elevation angles between 10° and 90°

For elevation angles between 10° and 90°, the path attenuation is obtained using the cosecant law:

$$A = \frac{h_o \gamma_o + h_w \gamma_w}{\sin \varphi} \quad \text{dB} \tag{29}$$

where φ is the elevation angle.

FIGURE 6

Total zenith attenuation at ground level

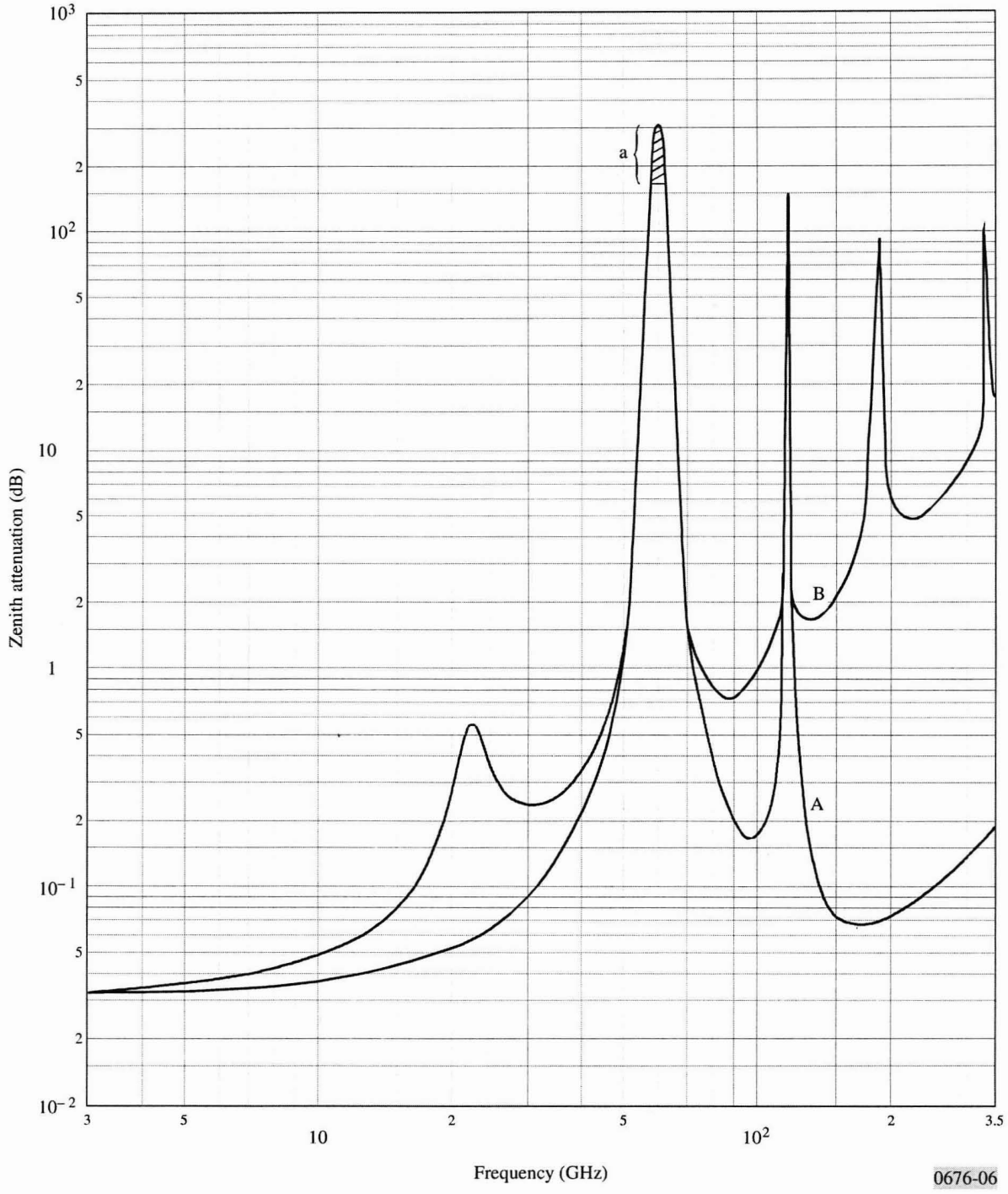

Pressure: 1 013 hPa

Temperature: 15° C

a: range of values (see Fig. 7)

Curves A: for a dry atmosphere

B: with an exponential water-vapour atmosphere of 7.5 g/m^3 at ground level, and a scale height of 2 km

FIGURE 7

Zenith oxygen absorption from the altitudes indicated

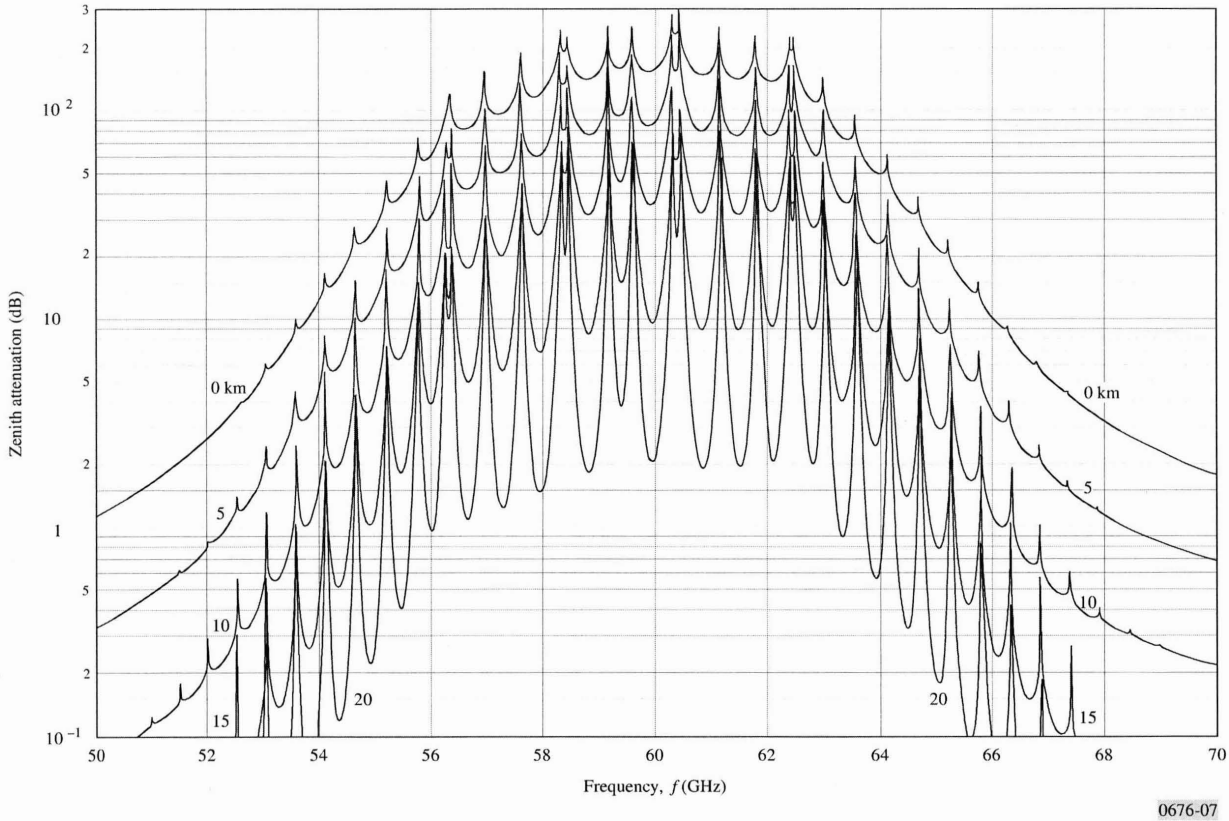

These formulae are applicable to cases of inclined paths between a satellite and an earth station situated at sea level. To determine the attenuation values on an inclined path between a station situated at altitude h_1 and another at a higher altitude h_2, the values h_o and h_w in equation (29) must be replaced by the following h'_o and h'_w values:

$$h'_o = h_o \left[e^{-h_1 / h_o} - e^{-h_2 / h_o} \right] \quad \text{km} \tag{30}$$

$$h'_w = h_w \left[e^{-h_1 / h_w} - e^{-h_2 / h_w} \right] \quad \text{km} \tag{31}$$

it being understood that the value ρ of the water vapour density used in equation (23) is the hypothetical value at sea level calculated as follows:

$$\rho = \rho_1 \times \exp(h_1 / 2) \tag{32}$$

where ρ_1 is the value corresponding to altitude h_1 of the station in question, and the equivalent height of water vapour density is assumed as 2 km (see Recommendation ITU-R P.835).

Equations (30), (31) and (32) use different normalizations for the dry air and water vapour equivalent heights. While the mean air pressure referred to sea level can be considered constant around the world (equal to 1 013 hPa), the water vapour density not only has a wide range of climatic variability but is measured at the surface (i.e. at the height of the ground station). For values of surface water vapour density, see Recommendation ITU-R P.836.

2.2.2 Elevation angle between 0° and 10°

In this case, the relations (29) to (32) must be replaced by more accurate formulae allowing for the real length of the atmospheric path. This leads to the following relations:

$$A = \frac{\sqrt{R_e}}{\cos\varphi} \left[\gamma_o \sqrt{h_o}\, F\left(\tan\varphi \sqrt{\frac{R_e}{h_o}} \right) + \gamma_w \sqrt{h_w}\, F\left(\tan\varphi \sqrt{\frac{R_e}{h_w}} \right) \right] \quad \text{dB} \tag{33}$$

where:

R_e: effective Earth radius including refraction, given in Recommendation ITU-R P.834, expressed in km (a value of 8 500 km is generally acceptable for the immediate vicinity of the Earth's surface)

φ: elevation angle

F: function defined by:

$$F(x) = \frac{1}{0.661\, x + 0.339 \sqrt{x^2 + 5.51}} \tag{34}$$

The formula (33) is applicable to cases of inclined paths between a satellite and an earth station situated at sea level. To determine the attenuation values on an inclined path between a station situated at altitude h_1 and a higher altitude h_2 (where both altitudes are less than 1 000 km above m.s.l.), the relation (33) must be replaced by the following:

$$A = \gamma_o \sqrt{h_o} \left[\frac{\sqrt{R_e + h_1} \cdot F(x_1)\, e^{-h_1/h_o}}{\cos\varphi_1} - \frac{\sqrt{R_e + h_2} \cdot F(x_2)\, e^{-h_2/h_o}}{\cos\varphi_2} \right]$$

$$+ \gamma_w \sqrt{h_w} \left[\frac{\sqrt{R_e + h_1} \cdot F(x'_1)\, e^{-h_1/h_w}}{\cos\varphi_1} - \frac{\sqrt{R_e + h_2} \cdot F(x'_2)\, e^{-h_2/h_w}}{\cos\varphi_2} \right] \quad \text{dB} \tag{35}$$

where:

φ_1 : elevation angle at altitude h_1

$$\varphi_2 = \arccos\left(\frac{R_e + h_1}{R_e + h_2}\cos\varphi_1\right) \tag{36a}$$

$$x_i = \tan\varphi_i \sqrt{\frac{R_e + h_i}{h_o}} \qquad \text{for } i = 1, 2 \tag{36b}$$

$$x'_i = \tan\varphi_i \sqrt{\frac{R_e + h_i}{h_w}} \qquad \text{for } i = 1, 2 \tag{36c}$$

it being understood that the value ρ of the water vapour density used in equation (23) is the hypothetical value at sea level calculated as follows:

$$\rho = \rho_1 \cdot \exp(h_1 / 2) \tag{37}$$

where ρ_1 is the value corresponding to altitude h_1 of the station in question, and the equivalent height of water vapour density is assumed as 2 km (see Recommendation ITU-R P.835).

Values for ρ_1 at the surface can be found in Recommendation ITU-R P.836. The different formulation for dry air and water vapour is explained at the end of § 2.2.

For elevation angles less than 0°, the line-by-line calculation in Annex 1 must be used.

2.3 Slant path water-vapour attenuation

The above method for calculating slant path attenuation by water vapour relies on the knowledge of the profile of water-vapour pressure (or density) along the path. In cases where the total columnar water vapour content along the path, V, is known, an alternative method may be used. The total water-vapour attenuation in the zenith direction can be expressed as:

$$A_w = a_v V \qquad \text{dB} \tag{38}$$

where V (kg/m^2 or mm) and a_v (dB/kg/m^2 or dB/mm) is the water-vapour mass absorption coefficient. The mass absorption coefficient can be calculated from the specific attenuation coefficient γ_w, divided by the water-vapour density ρ, which may be obtained from the water-vapour pressure using equation (4).

Values for the total columnar content V can be obtained either from radiosonde profiles or radiometric measurements. Statistics of V are given in Recommendation ITU-R P.836. For elevation angles other than the zenith, the attenuation must be divided by sin θ, where θ is the elevation angle, assuming a uniform horizontally-stratified atmosphere, down to elevation angles of about 10°.

Copyright © 1975 American Telephone and Telegraph Company
THE BELL SYSTEM TECHNICAL JOURNAL
Vol. 54, No. 1, January 1975
Printed in U.S.A.

Space-Diversity Engineering

By A. VIGANTS

(Manuscript received March 14, 1974)

Vertically separated antennas are recommended to increase the transmission availability of line-of-sight microwave links by reducing the duration and frequency of multipath fading events. The emphasis is on application to the 4- and 6-GHz bands on links with negligible ground reflections. Necessary signal processing, links utilizing passive repeaters (reflectors), and overwater links are also treated. Some new experimental data are presented.

I. INTRODUCTION

Bell System microwave radio relay routes consist of links (paths, hops) that have an average length of about 26 miles. Transmission on most hops is along the line of sight, with antennas mounted on towers that are typically 250 feet high. In some cases, when line-of-sight transmission between towers is not practical, large reflectors on prominent points of terrain (passive repeaters) are used. Tower locations are selected to avoid ground reflections, but inevitable exceptions, such as transmission across a lake, do occur.

Multipath propagation during anomalous atmospheric conditions can give rise to destructive interferences at the receiving antenna; the resultant signal fluctuates (fades) and may be reduced to practically zero for seconds at a time. The corresponding interruptions to service, if permitted to occur, would be unacceptable. Interruptions to operation can be avoided by switching from an unserviceable radio channel to a protection channel operating at a different radio frequency, since multipath fading, being an interference phenomenon, is frequency selective. Use of such protection (frequency diversity) has been restricted to conserve the frequency spectrum.[1]

Space diversity is an alternative or additional form of protection from the effects of multipath fading.[2–8] Its effectiveness depends upon the fact that multipath propagation results in vertical structure of the electromagnetic fields at the receiving tower. Selection between two vertically separated antennas receiving at the same frequency is com-

parable in effect to a frequency-diversity system with a protection channel for every working channel (switched on a per-hop basis). Unfamiliarity with the principles of operation and unavailability of space-diversity equipment, as well as costs, have inhibited use of space diversity in the past. Currently, use of space diversity is increasing. One reason for this (apart from spectrum conservation) is that, in areas of high fading, frequency diversity alone cannot provide the desired transmission availability.

Space-diversity engineering, as presented here, encompasses estimation of fading, determination from transmission availability objectives of the need for protection, and calculation of the antenna separation needed to obtain the required transmission availability. The effects of signal processing on the improvement available from an antenna pair are discussed, with particular attention given to threshold switching. Space diversity through passive repeaters and on over-water paths is also discussed. Clearance requirements are summarized in the last section; current work on antennas placed so low as to lack clearance under normal propagation conditions is discussed in Appendix A.

The emphasis in this paper is on application in the 4- and 6-GHz frequency bands, although the expressions for the estimation of the amount of fading and the diversity improvement apply to other microwave frequencies. However, transmission in the 11-GHz band is also affected by rain, and this must be taken into account by additional reduction of the effects of multipath fading. This design aspect belongs more properly in a treatment of 11-GHz radio system design and is not discussed here.

II. DESCRIPTION OF FADING

The RF power received after transmission over a microwave radio hop is never absolutely constant; even at noon, when the atmosphere has "stabilized," there can be fractional dB excursions (scintillations recurring a few times per second), as well as slower excursions of a dB or two. In propagation experiments, the normal value of the received signal is determined from the peak in a signal-level histogram obtained over at least one-half hour at or near noon. This so-called free-space value of the received signal is determined repeatedly at least once a week to identify periods during which enhanced or depressed signals have resulted from the relatively steady atmospheric focusing or defocusing. These periods, therefore, are not "normal."

During fading, the received RF power can be practically zero for seconds at a time. The terminology to describe this is introduced in Fig. 1 through an example in which the free-space value is -30 dBm and a single, idealized fade decreases the received power temporarily

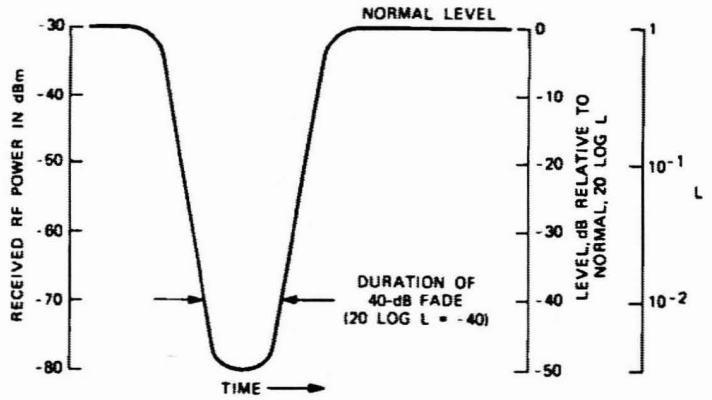

Fig. 1—Definitions of L and fade duration (−30 dBm assumed normal as an example).

to −80 dBm; levels in dB relative to normal are denoted by 20 log L. The time during which a signal is below a level is called the duration of fade of that level (the duration of a 40-dB fade is illustrated in Fig. 1). Average durations of fades are independent of microwave frequency* and are proportional to L; typical numerical values are given by (see also Fig. 2)[9–11]

$$\langle t \rangle = 410\, L \text{ seconds}, \quad L < 0.1. \tag{1}$$

As an example, the average duration of a 40-dB fade ($L = 10^{-2}$) is 4.1 seconds, both at 4 and 6 GHz.

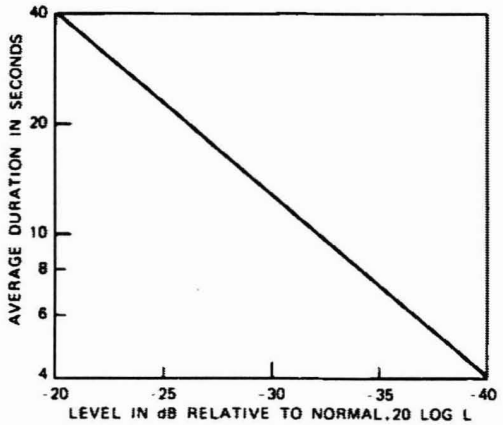

Fig. 2—Average fade durations ($\langle t \rangle = 410L$, $L < 0.1$).

* An underlying assumption throughout this work is that antenna sizes and path lengths are as encountered most often in practice: antenna diameters are between about 4 and 16 feet, and path lengths are between about 14 and 40 miles.

The sum of the durations of all fades of a particular depth is called "time below level." It is proportional to L^3, since the number of fades is proportional to L, and its numerical values are given by[9]

$$T = rT_0L^3, \quad L < 0.1, \tag{2}$$

where T_0 is the time period over which the summation of fade durations is made (a month, for example); the units of T are those of T_0 (seconds are normally used). The fade occurrence factor r for heavy fading months (see Fig. 3) is[9]

$$r = c(f/4)D^3 10^{-5}, \tag{3}$$

where

$$\begin{aligned} c &= 4 \text{ over water and Gulf coast,} \\ &= 1 \text{ average terrain and climate,} \\ &= \tfrac{1}{4} \text{ mountains and dry climate,} \\ f &= \text{frequency in GHz,} \end{aligned} \tag{4}$$

and

D = path length in miles.

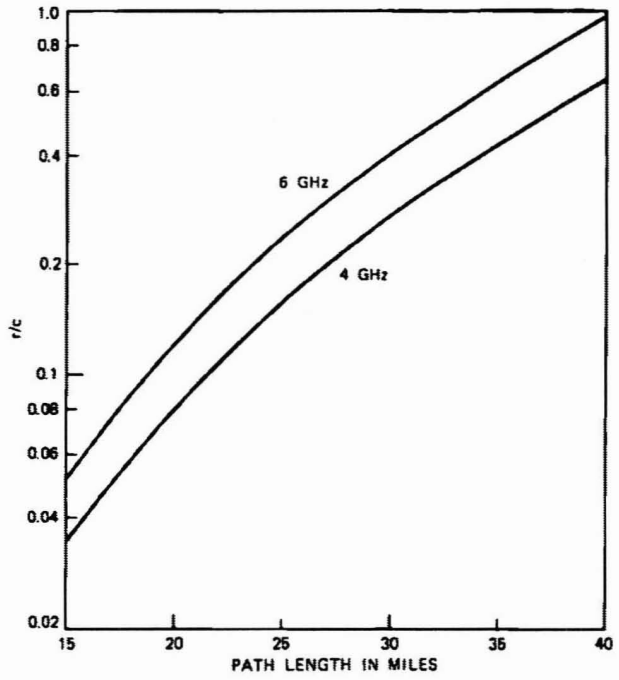

Fig. 3—Multipath occurrence factor.

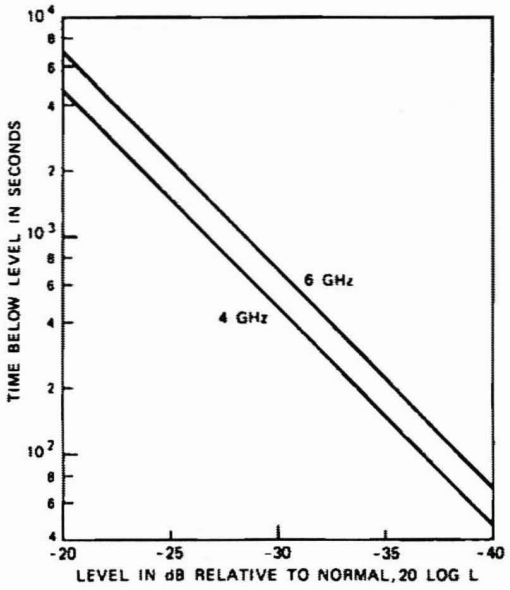

Fig. 4—Time below level in a heavy fading month (D = 26 miles, c = 1, T_0 = 31 days = 2.68×10^6 seconds).

As an example, values of T as a function of fade depth for a 26-mile path (average length) and average terrain and climate are shown in Fig. 4 for a heavy fading month. The lines have the decade of time per 10-dB slope typical of multipath fading, specified by the L^3 functional dependence. The values of T at -40 dB are 47 and 71 seconds at 4 and 6 GHz, respectively. Based on an average duration of 4.1 seconds, this corresponds to 11 fades of 40 dB at 4 GHz.

The coefficient c in (4) incorporates the effects of both terrain and humidity and is adequate for first estimates of expected fading in many cases. Differentiation between paths of identical climate but differing terrain can be done by introducing a terrain roughness parameter[12] quantifying common knowledge that paths over rough terrain fade less than paths over smooth terrain, presumably because stable atmospheric layering is less likely to occur over rough terrain. Terrain roughness is calculated from terrain heights above a reference level (sea level, for example) obtained from the path profile at one-mile intervals, with the ends of the path excluded. The standard deviation of the resulting set of numbers is the terrain roughness, denoted by w (see sample calculation in Appendix B). Applicable values of w range from 20 feet ("smooth") to 140 feet ("rough"); values of 20 and 140 should be used when calculated values of w are less than 20 or larger than 140.

Modified for roughness, the equations for c become:

$$\begin{aligned} c &= 2\ (w/50)^{-1.3}, \text{ coastal areas,} \\ &= (w/50)^{-1.3}, \text{ average climate,} \\ &= 0.5\ (w/50)^{-1.3}, \text{ dry climate,} \end{aligned} \tag{5}$$

where a roughness of 50 feet has been defined as "normal."

III. PERFORMANCE OBJECTIVES

The time below level of the received signal, at a fade depth equal to the receiver fade margin, represents potential service-failure time. Protection is needed if this exceeds the value set by transmission-availability objectives.

Bell System short-haul objectives limit service failure time to 0.02 percent (two-way) annually on a 250-mile route due to all causes. One-half of this is allocated to causes associated with equipment, maintenance, and plant errors. There are obvious exceptions to this; for example, unavailability on a route where all hops are exceptionally short will be due mainly to equipment outages, and may be so allocated.

The allocation to fading, therefore, is 0.01 percent (two-way) annually. In the past, this allocation had been apportioned between multipath and obstruction fading ("earth-bulge" fading). However, the occurrence of intolerable obstruction fading can be decreased by increasing clearance (higher towers or shorter hops) or by increasing system gain margin; reliability records show that there has been a gradual decrease in the occurrence of obstruction fading over the years.[13] In the construction of new hops or in the upgrading of older ones in locations where obstruction fading is known to occur (or by related experience is expected to occur), increased clearances (or limits on path lengths) are assumed to be used. Consequently, no allocation to obstruction fading is made in space-diversity engineering; the entire 0.01 percent two-way annual fading allocation is applied to multipath fading. The one-way annual multipath fading allocation for 250 miles becomes 0.005 percent or approximately 26 minutes per year (1600 seconds per year). The corresponding allocation to a hop D miles long is $1600 \times D/250$ seconds per year (165 seconds per year for the average 26-mile hop).

Estimated annual time below level (for comparison with the objective) is obtained from the equation for T in the previous section, with T_0 describing the length of the fading season. As a geographic average, the value of T_0 in this estimate is equal to the number of seconds in three months; this assumes that all significant fading is contained in two heavy and two medium fading months, which is equivalent to

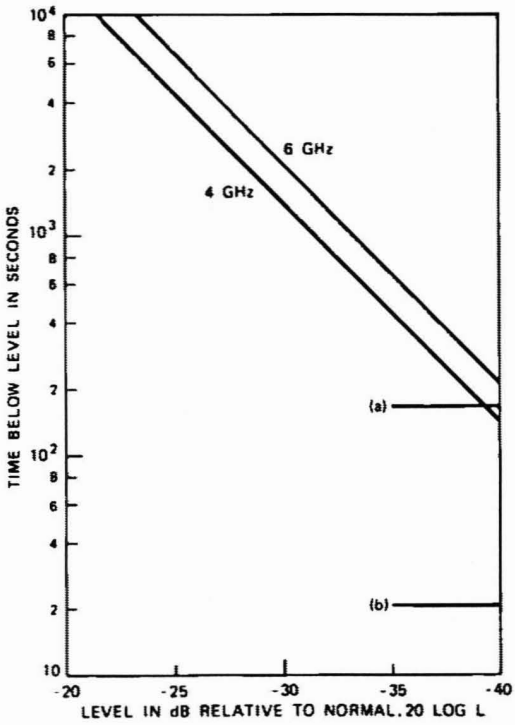

Fig. 5—Annual time below level (average case). Objectives: (a) short haul = 165 seconds/year, (b) long haul = 20 seconds/year.

three heavy fading months.[14] Estimation of the length of the fading season as a function of geographic location is discussed in Appendix C.

Continuation of the example of Fig. 4 provides the annual time-below-level curves in Fig. 5 (142 and 212 seconds below −40 dB at 4 and 6 GHz, respectively). For a fade margin of 35 dB, considered here for the purposes of discussion, the time below level is too large, compared to the 165-second objective, by factors of 2.7 and 4 at 4 and 6 GHz, respectively; protection against multipath fading (space or frequency diversity) is needed when the fade margin is 35 dB. At a fade margin of 40 dB, the 4-GHz channel in the example can get by without protection.

For long-haul radio the overall objective is also 0.02 percent, but the route length is 4000 miles. However, long-haul transmission models assume that half of the hops never experience significant fading.[14] With the addition of this assumption to those previously made in this section, the long-haul multipath allocation to a hop D miles long becomes $1600 \times D/2000$ seconds per year (20 seconds per year for the average 26-mile hop). In practice, long-haul radio has at least one protection

channel, which is required for equipment protection and maintenance and is used to provide frequency-diversity protection. Such use modifies the need for space-diversity protection (see Appendix D). Use of frequency diversity in short-haul radio can be expected to be infrequent because of regulatory restrictions.[1]

IV. THE SPACE-DIVERSITY EFFECT

During periods of multipath fading, deep fades of signals received on two vertically separated receiving antennas rarely overlap in time. The relatively few that do overlap give rise to simultaneous time below level (sum of durations of simultaneous fades, see Fig. 6), which is proportional to L^4 and can be expressed as[7,8,15]

$$T_s = T/I_0, \tag{6}$$

where T is the time below level of the signal received on the main antenna and I_0 is the available improvement, given numerically in practical units by the following (see also nomogram in Fig. 7):[7,8]

$$I_0 = 7 \times 10^{-5} v^2 s^2 f/DL^2, \quad s \leqq 50, \tag{7}$$

where

v = relative gain parameter (gain of secondary antenna relative to main antenna in dB is $20 \log v$),
s = vertical separation of receiving antennas in feet, center-to-center,
f = frequency in GHz,
D = path length in miles,

and

L = level parameter (level in dB relative to normal is $20 \log L$).

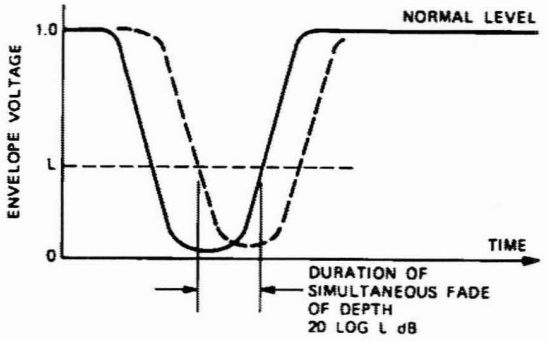

Fig. 6—Definition of simultaneous fade.

20·log·v

[0·log v²

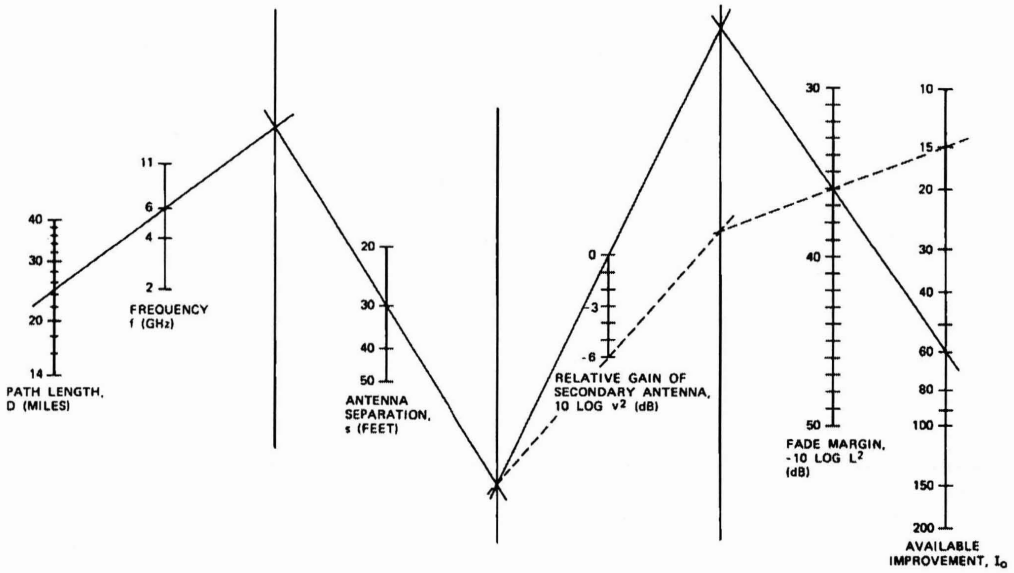

Fig. 7—Nomogram for available improvement I_0.

VIGANTS SPACE

D = 14 - 40 miles

F = 2 - 11 GHz

SP = 10 - 50 ft

FADE: 30 - 50 dB

V: 0 - -6

Equation (7) applies only for the ranges of variables indicated on the nomogram in Fig. 7. Extrapolation of the scales may lead to errors. For example, under some conditions the increase in improvement due to an increase in separation over 50 feet may be small. Separations for which the available improvement is less than 10 should not be used; if possible, separations of at least 30 feet should be used.

The example of Fig. 5 is continued in Fig. 8 to demonstrate drawing of a curve for T_s; the secondary antenna in the example has the same gain as the main antenna ($v^2 = 1$) and the vertical center-to-center separation of the antennas is 30 feet ($s = 30$). The values of I_0 at -40 dB are 145 and 97 for the 6- and 4-GHz channels, respectively. The values of T_s at -40 dB are $212/145 = 1.46$ seconds and $142/97 = 1.46$ seconds, identical for 6 and 4 GHz. This comes about because both T and I_0 are proportional to frequency. Having established one point (1.46 seconds at -40 dB) for T_s, we draw through it a line with a slope of a decade of time per 5 dB, as specified by the L^4 functional dependence. When I_0 becomes less than about 5, terms in addition to that proportional to L^4 are needed to describe T_s, which is why the line for T_s in Fig. 8 is not extended all the way to the left into the region (normally not of practical interest) where T_s approaches T.

The simultaneous time below level in Fig. 8 is smaller than the 165-seconds-per-year short-haul objective for fade margins larger than about 30 dB; it is smaller than the 20-seconds-per-year long-haul objective for fade margins larger than about 34 dB.

V. COMPARISON OF SPACE AND FREQUENCY DIVERSITY

Space diversity in its most common form provides a protection channel for every working channel (1×1 protection) on a per-hop basis. Frequency diversity usually provides one or two protection channels for m working channels ($1 \times m$ or $2 \times m$ protection) on the basis of switching sections that can contain as many as 10 hops in extreme cases. The most effective form of frequency diversity is, of course, 1×1 on a per-hop basis (now restricted in use at 4 and 6 GHz because of spectrum conservation); this can readily be compared to space diversity.

For equal performance the available improvements, I_0, are equated. A convenient form for I_0 is

$$I_0 = v^2 q L^{-2}, \tag{8}$$

where for space diversity (from the previous section)

$$q = 7 \times 10^{-5} s^2 f/D, \quad s \leqq 50 \tag{9}$$

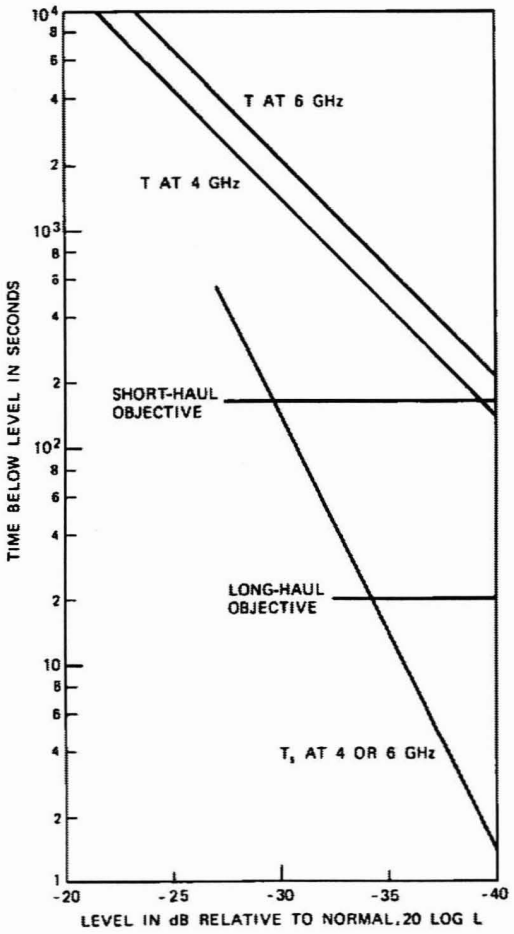

Fig. 8—Annual simultaneous time below level for 30-foot separation of antennas (continuation of average-case example from Fig. 5).

and for frequency diversity[16]

$$q = 50(\Delta f/f)/fD, \quad \Delta f < 0.5 \text{ GHz}, \tag{10}$$

where f is the frequency in GHz (4 or 6), and Δf is the difference of radio channel center frequencies, also in GHz; D is the path length in miles. Values of separations in space and frequency providing equal performance (for antennas of equal size; $v^2 = 1$) are obtained by eliminating q from (9) and (10):

$$\begin{aligned} s &= 106\sqrt{\Delta f}, \text{ in the 4-GHz band,} \\ &= 57.5\sqrt{\Delta f}, \text{ in the 6-GHz band,} \end{aligned} \tag{11}$$

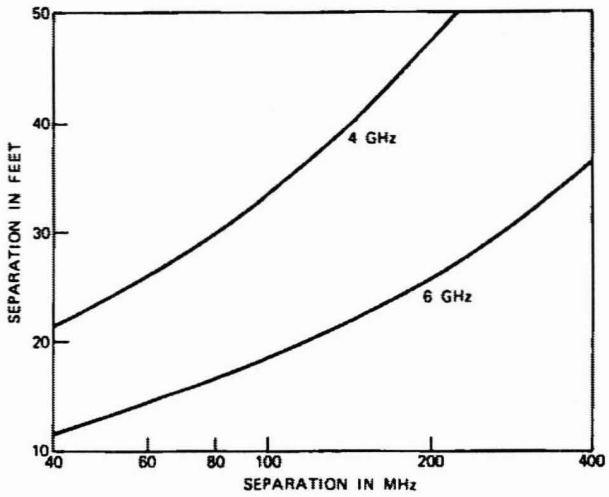

Fig. 9—Separations in space and frequency providing equal protection (one-for-one switching on a per-hop basis; antennas of equal size, $v^2 = 1$).

where s is in feet. A 30-foot separation is equivalent to a Δf of about 0.08 GHz in the 4-GHz band and about 0.27 GHz in the 6-GHz band (Fig. 9).

VI. SIGNAL PROCESSING

The signals received by the two antennas must be processed to obtain a diversity signal. Static addition at RF is not practical, since the duration of one-half cycle at, say, 4 GHz is $\frac{1}{8}$ nanosecond, and delay changes of this magnitude in the relative arrival times of the two signals arise easily because of daily angle-of-arrival variations. Without dynamic phase compensation, such changes would lead to signal cancellations during normal daytime operation, even when multipath fading is not present. The cost of dynamic phase compensation has so far been prohibitive.

Addition at baseband without dynamic phase compensation has been used (duration of a half cycle at 10 MHz is 50 nanoseconds). In some implementations, the weaker signal is dropped from the sum, when the relative signal strength ratio exceeds some 4 dB, to improve the signal-to-noise ratio of the diversity signal. Simultaneous time below level can be used to approximate the time below level of the diversity signal.

Switching, particularly at RF, permits an economically advantageous configuration of equipment. The simultaneous time-below-level curves (Fig. 8) describe the performance of an idealized comparator (switch),

where the diversity signal is, at every instant, the stronger of the two received signals. The switching activity, accompanied by undesirable step phase changes, is high. This can be reduced by introducing hysteresis, but at the cost of reduced performance. Suppose switching occurs only when the ratio of the received powers is larger than a number b^2 ($10 \log b^2$ in dB). The improvement realized becomes

$$I = \eta I_0, \tag{12}$$

where an estimate of the efficiency factor η (see Appendix E) is

$$\eta = 2/(b^2 + b^{-2}). \tag{13}$$

As an example, when $10 \log b^2$ is 6 dB, η is 0.47, and an available improvement of 100 becomes a realized improvement of 47.

A different approach must be used when only one receiver per radio channel is available, which is the case in long-haul radio. The diversity implementation utilizes an RF waveguide switch activated by the AGC voltage when the receiver input falls below a threshold (one example of switching logic is shown in Table I). Switching of this sort has been referred to as threshold or "blind" switching, since at the instant of switching there is no assurance that a stronger signal will be available at the other antenna. Most of the time, a stronger signal *is* found, since few of the deep fades on the two receiving antennas overlap in time. The time below level T_t for threshold switching is calculated (see Appendix F) in Fig. 10 for a 4-GHz channel (in continuation of the example from Fig. 8); the threshold is at -35 dB relative to normal. The values of T_t and T_s are identical at the threshold. Above threshold, T_t approaches T rapidly, since the switch does not act for fades during which the minimum signal does not drop below -35 dB. The part of T_t of importance in space-diversity engineering is the straight-line section below threshold. This straight-line section is parallel to T, since it represents an average of the two single-antenna statistics by virtue of the continued cycling of the switch due to failure

Table I — Switching logic of a threshold switch

Switch Output Relative to Switch Threshold	Switch Connected to	Action
High	Main antenna	Stay on main antenna
High	Secondary antenna	Switch to main antenna after 15 minutes
Low	Main antenna	Switch to secondary antenna after 0.1 second
Low	Secondary antenna	Switch to main antenna after 0.1 second

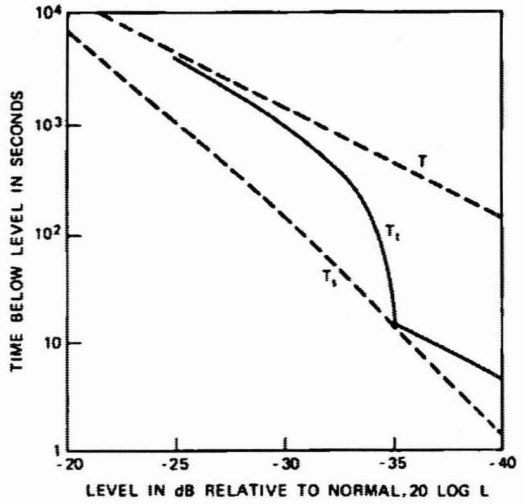

Fig. 10—Time below level in threshold switching—continuation of average-case example (4 GHz, threshold at −35 dB, 30-foot separation of antennas).

of the receiver to locate a signal stronger than the threshold value, which is −35 dB relative to normal in the example.

A suitable value of the threshold is about 2 dB above the fade margin. The −35 dB threshold in the example would be appropriate for a fade margin of 37 dB. The improvement ($I_t = T/T_t$) is constant below threshold (about 30 in the example) and equal to the value of I_0 at

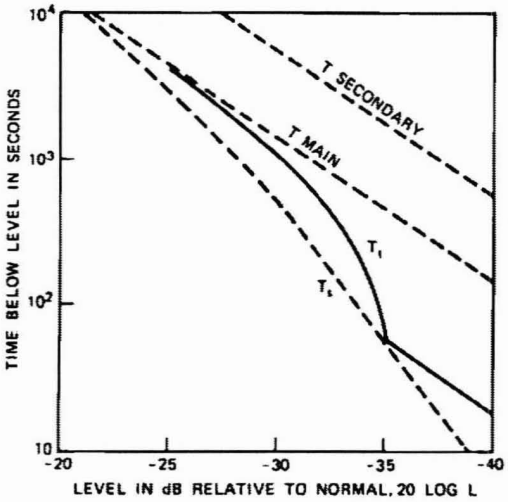

Fig. 11—Example of reduced performance due to smaller secondary antenna (10 log $v^2 = -6$, other parameters as in Fig. 10).

the threshold. This is one reason for placing the threshold close to the fade margin, since a threshold at -30 dB, for example, would provide an I_t of only about 10. A second reason is to limit the occurrence of the phase steps due to the cycling of the switch to occasions when the signals border on the unusable (actually, the chance is small that the signals remain for prolonged periods in the 2-dB corridor between the threshold and the fade margin, and many of the phase steps will occur, therefore, when the signals are unusable). The cycling should occur at a rate of at least five times per second; at much slower rates, a good signal is not found fast enough and performance deteriorates. Corridors smaller than 2 dB should be avoided, since signal drifts caused by aging of equipment or noise accumulation from hop to hop in a switching section can frustrate design intentions and require frequency diversity action before space diversity.

Use of a smaller secondary antenna reduces performance, as illustrated in Fig. 11, where the only change from Fig. 10 is that a secondary antenna with 6 dB less gain ($v^2 = 0.25$) has been used. The improvement I_t has decreased to about 8 ($\approx 30/4$) from about 30 in the equal-size-antenna case.

VII. SPACE-DIVERSITY TRANSMISSION

Space diversity for microwave radio is usually envisioned as diversity reception; i.e., the system consists of a single antenna which transmits to two vertically separated receiving antennas. Since the path loss from antenna to antenna does not depend on the direction of transmission, an arrangement of two vertically separated transmitting antennas and a single receiving antenna can also be used.

Combined use of transmitting and receiving diversity can reduce tower work; on a long route only alternate towers would be affected. A single bad hop can be corrected by additional installation at one end only. On hops where additional installation at one end is impossible because of economics or zoning, use of both transmitting and receiving diversity at the other end provides full diversity protection in both directions.

A drawback to transmitting diversity is the vulnerability of the control signal. In diversity reception, the signals from both antennas are always available at the switching site, to be processed in any desired manner. In transmitting diversity, only one antenna can transmit at a given frequency at a given time (dynamic phase correction for control of the two transmitters does not appear feasible or desirable). The required control information must be fed back from the receiving to the transmitting end, since control must be based—because of the frequency selectivity of deep fades (see Appendix G)—on fading in

the controlled channel. The feedback link increases both the cost of control and the possibility for failure of control.

VIII. FIELD EXPERIENCE

The basic experimental data on simultaneous fading on vertically separated receiving antennas were obtained in Ohio and Texas in 1966. The variation of the improvement as the square of the vertical separation of the antennas was further verified experimentally in Georgia in 1968 (Appendix H). Field followup in terms of monitoring performance of in-service space diversity was carried out in 1972 in California and Florida. The monitoring was made possible by the development of Portable Propagation Recorders (PPR), the first installation of which was at Brawley, California, in May 1972.

Space diversity in the California case was installed by Pacific Telephone and Telegraph Co. to improve transmission availability of two hops (Salton-Brawley and Brawley-Glamis traversing Imperial Valley) on the Dallas-Los Angeles route. Extensive irrigation and high temperatures with little wind combine to create severe fading on the two hops in question. Measured and calculated values of I_0 are compared in Table II (Fig. 12 is an example of measured data). RF threshold switching was used, and the comparison was made at the threshold value (-35 dB relative to normal) where I_t and I_0 are equal.[17] The agreement of calculated and measured values is good, showing that the equation for I_0 is applicable under diverse climatic conditions.

Two hops monitored in Florida (Andytown South-Andytown North and Andytown North-Okeelanta in Northern Everglades) were equipped with secondary receiving antennas and RF threshold switches as part of a program to improve transmission availability of hops that fade heavily. The measured results and the predictions for Andytown

Table II — Comparison of calculated and measured values of I_0 (Salton-Brawley and Brawley-Glamis, California)*

Antenna Spacing (feet)	Frequency (GHz)	Path Length (miles)	Relative Gain of Secondary Antenna (v^2)	I_0 at 20 log $L = -35$	
				Calculated from Equation (7)	Measured
30	4	42.6	0.41	7.6	8.0†
15	4	42.6	0.41	1.9	1.5‡
15	4	37.1	0.41	2.2	2.5§

* Antenna configurations were dictated by circumstances; generally, configurations providing an improvement of at least 10 would be used.
† Brawley to Glamis, 7/7–8/14, 1972.
‡ Glamis to Brawley, 5/11–7/3, 7/7–8/14, 1972.
§ Salton to Brawley, 8/17–8/29, 1972.

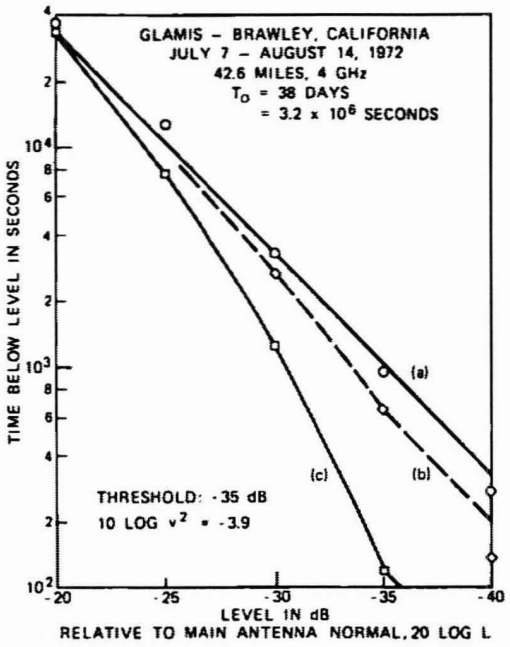

Fig. 12—Threshold switching, Glamis to Brawley, California. Reception at (a) Glamis, main antenna (unprotected), (b) Brawley, 15-foot separation, (c) Glamis, 30-foot separation.

South to Andytown North are summarized in Fig. 13.[18] At −47 dB (bottom level of the PPR for this case), the predicted time below level in the 148-day test period was insignificant (only a few seconds), and none was measured. Diversity performance thus conformed to expectations and the needed improvement in transmission availability was obtained.

IX. PATHS WITH PASSIVE REPEATERS

Use of passive repeaters (large reflectors of, say, 40 by 48 feet) on ridges or hilltops is sometimes dictated by terrain or by the undesirability of active repeaters in remote locations (power and maintenance-access problems). Tests on a Mountain Bell hop (Lusk-Wendover, Wyoming) in 1973 established that space diversity is operative through passive repeaters.[19] A design procedure for practical cases, based on the Wyoming results, is:

(*i*) Determine reflector size to obtain reasonable fade margin.
(*ii*) Estimate unprotected time below level (T) as the sum of the values of T for the individual legs (distances from reflector to ends of hop).

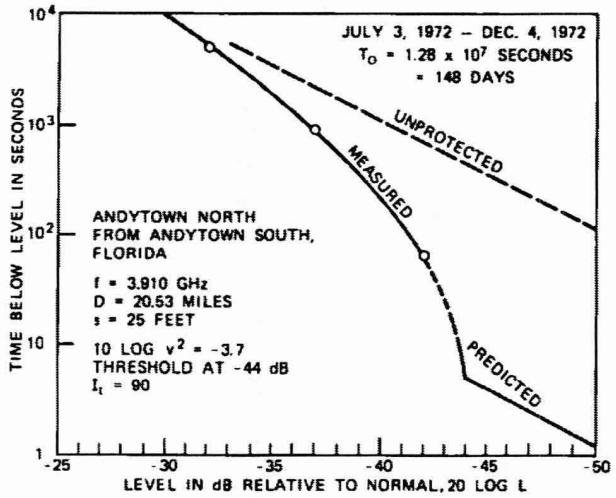

Fig. 13—Threshold switch operation at Andytown North, Florida.

(*iii*) Determine improvement needed to meet transmission availability objectives.

(*iv*) If improvement is needed, determine vertical spacing based on longest leg (use at least 20 or 30 feet); use this vertical spacing at both ends of hop.

(*v*) If an antenna pair is in the near field of a reflector, ensure that projected reflector height is not less than the distance from the bottom edge of the bottom antenna to the top edge of the top antenna.

The experimental data obtained at Wendover and Lusk are summarized in Figs. 14 and 15 (the parameters of the experiment are summarized in Table III).[19] Time-below-level differences for individual antennas in a pair arise from gain differences in instrumentation chains; curves fitted to the points have the standard decade of time per 10-dB multipath slope in the deep-fade region. The curves fitted to the simultaneous fading points have the standard decade of time per 5-dB slope in the deep-fade region. Space-diversity reception at Lusk *is* effective (Fig. 15), which is a result that could not be predicted using present methods. Successful space-diversity operation at Wendover could be predicted beforehand by viewing the transmitting antenna at Lusk as a feed illuminating a large aperture (the double reflectors), since little fading would be generated on the short Lusk-to-reflectors leg.

The measured improvements at −35 dB, 50 at Wendover and 30 at Lusk, are larger than the calculated values of 40 and 16, respectively.

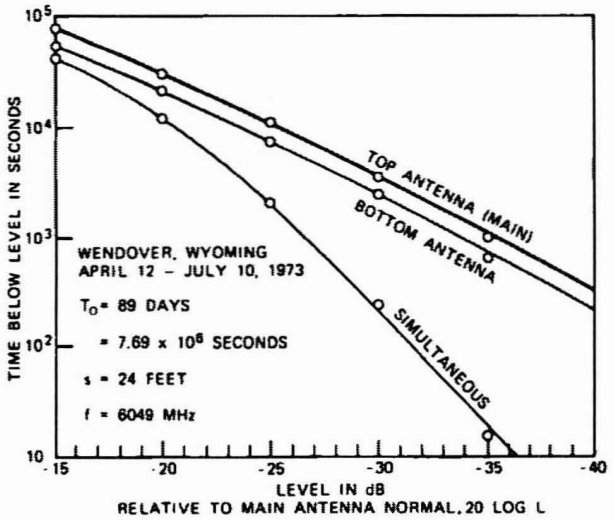

Fig. 14—Space diversity on path containing passive repeater; reception at Wendover, Wyoming.

The difference arises partly because use of the longest leg in the calculations is a simple approximation of a complex situation and partly because some scattering of measured points around the averages predicted by the equation for I_0 can be expected.

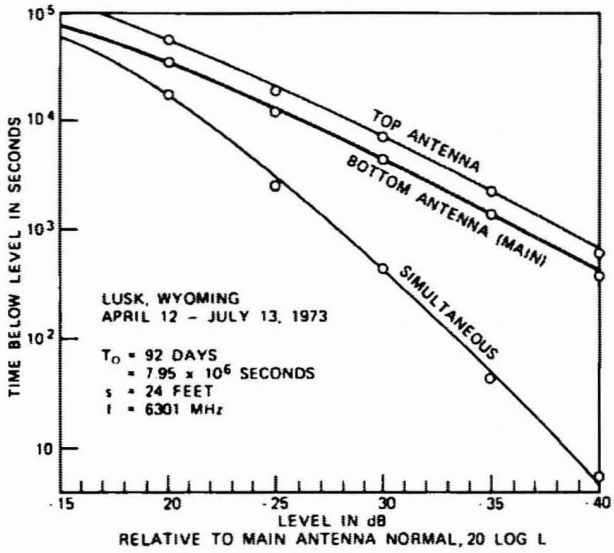

Fig. 15—Space diversity on path containing passive repeater; reception at Lusk, Wyoming.

Table III — Parameters of Lusk Radio test—Lusk to Wendover, Wyoming

Reflectors	Two 40- by 48-ft reflectors separated by 138.5 ft
Path lengths from reflectors:	
To Wendover	31.5 miles
To Lusk	9.5 miles
Antenna separations at Wendover and Lusk	24 ft (nominal) vertical center to center
Frequencies:	
Wendover	6049 MHz received
Lusk	6301 MHz received
Calculations:	
Values of v^2 arising from gain differences in instrumentation chains:	
Wendover	$v^2 = 1.6$
Lusk	$v^2 = 0.63$
Calculated improvement at −35 dB based on 31.5-mile path length	
Wendover ($v^2 = 1.6$)	$I_0 = 40$
Lusk ($v^2 = 0.63$)	$I_0 = 16$
Allocation to multipath fading from performance objectives for 41 miles (31.5 + 9.5)	1600 × 41/250 = 262 seconds per year

The multipath objective for the Wendover-Lusk link is 262 seconds per year one way (see Table III). Even allowing the annual time below level to increase by a factor of two due to late summer and fall fading, the objective can be met comfortably with receiver fade margins in the 35- to 40-dB range.

X. OVER-WATER PATHS

Over-water paths, undesirable because of reflections, are sometimes unavoidable. When the over-water area is too large to permit shifting the reflection point off it via a high-low antenna combination, space diversity can be used to reduce reflection fading. A procedure for determining antenna spacing is discussed in terms of the geometry shown in Fig. 16, in which the reference plane coincides with the surface of the water during "flat-earth" propagation conditions (i.e., those obtaining when K, the ratio of equivalent to actual earth radius, is infinity). The "bulge" height h of the surface reflection point A is

$$h = d_1 d_2 / 1.5\, K, \tag{14}$$

where h is in feet when d_1 and d_2 are in miles. If the height h_2 of the receiving point were changed, then the relative phase of the rays arriving via the paths TR and TAR would also change. For a fixed

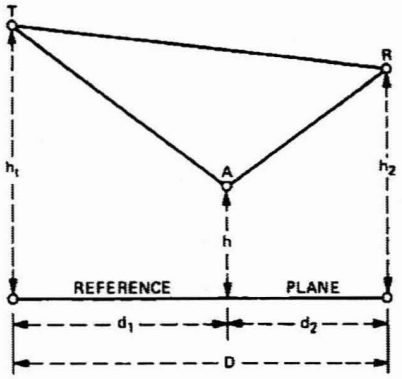

Fig. 16—Geometry for discussion of over-water paths.

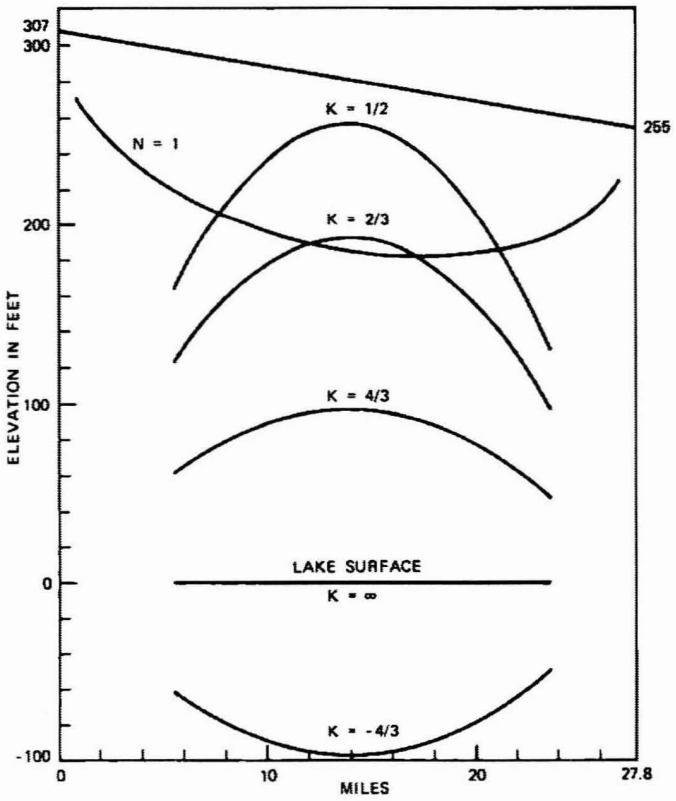

Fig. 17—Lake surface at various K values in over-water path example (N denotes boundary of Nth Fresnel zone at a frequency of 4 GHz).

transmitting antenna height h_t, the increment in h_2 for a change from an in-phase to an out-of-phase condition (half interference fringe spacing) is approximately (for large K), in feet,

$$\Delta h_2 \approx 1300D/f(h_t - h), \tag{15}$$

where h_t and h are in feet, D is the path length in miles, and f is the frequency in GHz.

The desired antenna separation for good diversity, therefore, would be equal to Δh_2, but this is possible for one value of K only, since Δh_2 increases as h increases (an increase of h results from a decrease of K). For protection over a large range of K, a suitable initial choice for the antenna separation is

$$s = 1300D/fh_t, \tag{16}$$

which corresponds to Δh_2 for $K = \infty$. The appropriateness of this

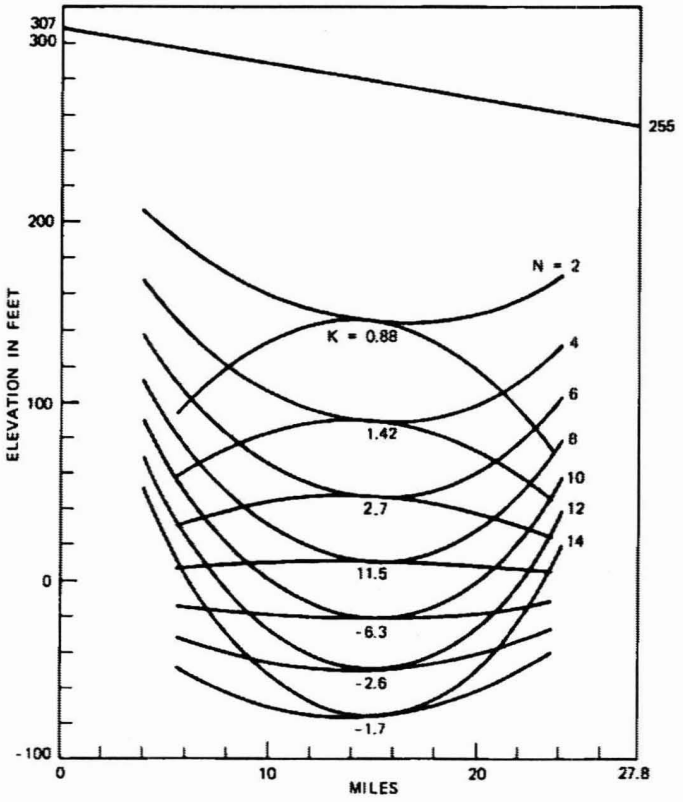

Fig. 18—Values of K at which lake surface is tangent to even Fresnel zone boundaries at a frequency of 4 GHz.

choice must be verified. In a recently examined situation (shown in Fig. 17) the path length D is 27.8 miles, the transmitting antenna height h_t is 307 feet, and the receiving antenna height h_2 is 255 feet; since the planned hop is on the Gulf coast, the antennas are placed high to avoid obstruction fading. Protection from fading created by reflections from the lake surface is desired for values of K ranging from $\frac{1}{2}$ to about $-\frac{1}{3}$ (Fig. 17 and the subsequent drawings were generated very easily on an xy-plotter driven by a programmable desk calculator). Values of K for which the lake surface is tangent to even Fresnel zone boundaries (determined by trial and error) are shown in Fig. 18; at these values of K, signal minima occur at the 255-foot height. For 4-GHz transmission, a first choice for diversity antenna separation would place the second receiving antenna at the 225-foot height $[(1300 \times 27.8)/(4 \times 307) \approx 30; 255 - 30 = 225]$. Simultaneous sig-

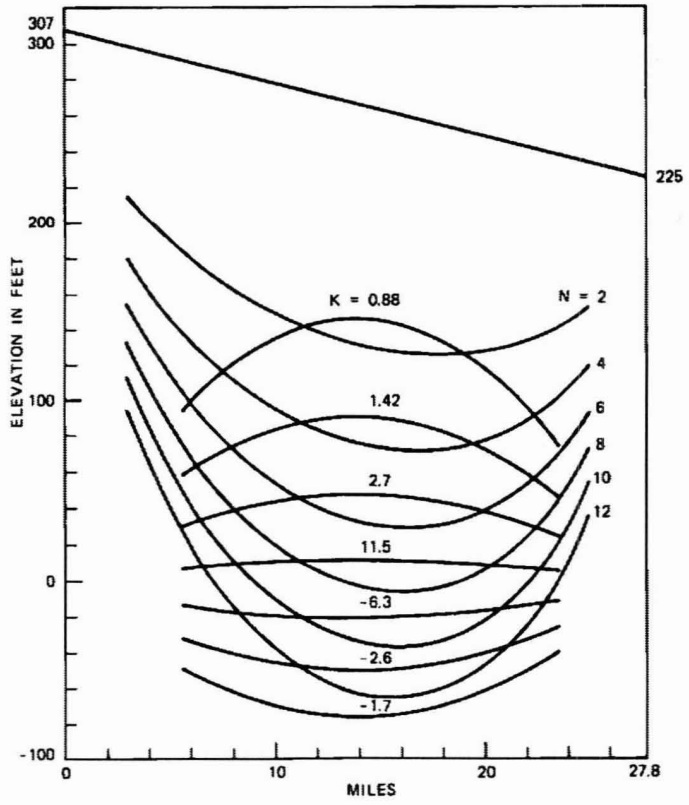

Fig. 19—Even Fresnel zone boundaries at 225-foot height for bottom receiving antenna at a frequency of 4 GHz.

nal minima will not occur on the two antennas because even Fresnel zone boundaries for the 225-foot height are not tangent to the lake surface at K values that correspond to signal minima on the top receiving antenna (see Fig. 19). The question of optimization now arises. It would be desirable to place the bottom antenna somewhat lower to move the boundary of F_2 down, further away from the lake surface at $K = 0.88$; this would bring the boundary of F_{12} closer to the lake surface at $K = -1.7$ and, therefore, is not desirable. If the design requirements were relaxed to cover values of K between $\frac{1}{2}$ and ∞ only, then the bottom antenna could be brought further down to make the separation closer to the value of Δh_2 at $K = \frac{4}{3}$.

A possible alternative location of the bottom antenna, foreground clearance permitting, is the 85-foot height (see Fig. 20). This has some

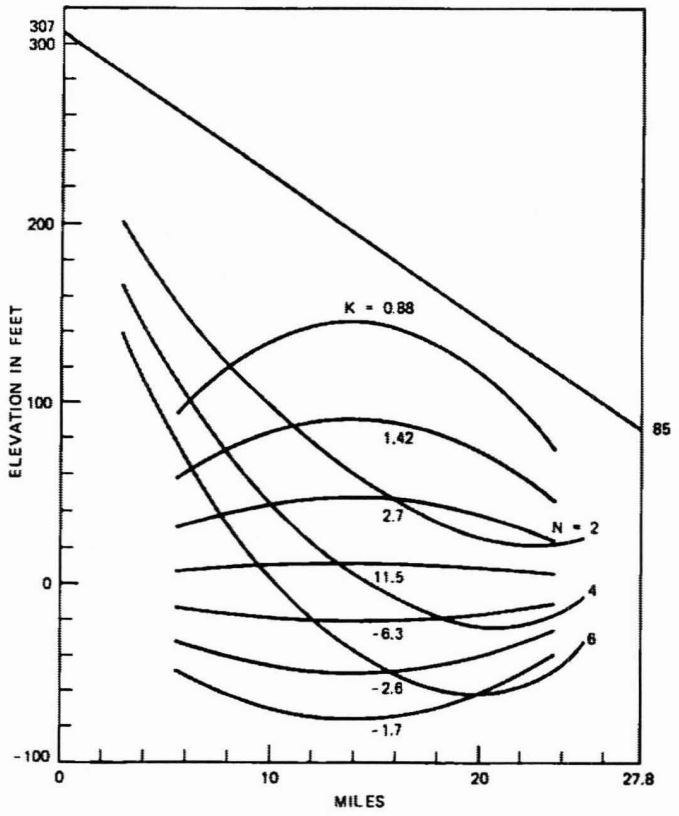

Fig. 20—Even Fresnel zone boundaries at 85-foot height for bottom receiving antenna at a frequency of 4 GHz.

of the properties of a high-low shot, and the even Fresnel zone boundaries are well placed.

A final observation on space-diversity design for protection from reflections is that the antenna spacings often are suitable, fortunately, for protection from atmospheric multipath fading.

XI. CLEARANCE RULES

Operating experience indicates that propagation conditions in various sections of the United States can be classified, in broad terms, as good, average, or difficult as shown on the map in Fig. 21. Desired clearances for transmission between main antennas are summarized in Table IV. In addition, hop lengths in coastal areas of the southern United States are sometimes restricted to 20 miles to reduce obstruction fading.

Clearance requirements for antennas added to provide space-diversity protection from multipath fading are less stringent: 0.6 F_1 at $K = \frac{4}{3}$, with a foreground clearance of 10 feet in the first 500 feet from the antenna. In many cases, this permits placement of the secondary antenna below the main antenna.

It appears (from recent results discussed in Appendix A) that it may be possible to relax the secondary-antenna clearance require-

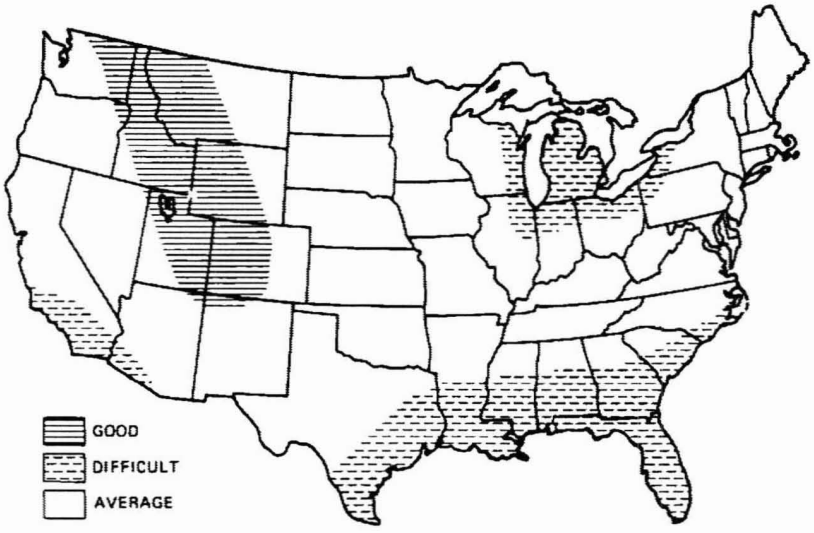

Fig. 21—Geographic occurrence of good, average, and difficult propagation conditions.

Table IV — Clearance rules for top antennas

Propagation Conditions	Clearance
Good	0.6 F_1 at $K = 1$ (but not less than grazing at $K = \frac{2}{3}$)
Average	The larger of 0.3 F_1 at $K = \frac{2}{3}$ and F_1 at $K = \frac{1}{2}$
Difficult	Grazing at $K = \frac{1}{2}$

ments; however, results of further tests (now in progress) must be evaluated before general recommendations on this can be made.

XII. ACKNOWLEDGMENTS

We are indebted to W. T. Barnett and E. E. Muller for useful discussions. The Multiple Input Data Acquisition System (MIDAS) and Portable Propagation Recorder (PPR) were designed by G. A. Zimmerman.

APPENDIX A

Effects of Reduced Clearance

The purpose of the bottom antenna in a space-diversity pair is to provide protection from multipath fading; its clearance therefore need not be based on requirements for protection from obstruction fading. Placement of secondary antennas lower than currently permitted would reduce tower costs because of reduced wind loading.

An investigation of multipath fading as a function of antenna height was undertaken at Palmetto, Georgia in 1972 at 4.198 GHz on a 26.4-mile path from Atlanta, Georgia.[20] The path profile (Fig. 22; arrows denote trees) shows that the controlling obstruction is located some 6 miles from the receiving antennas at Palmetto. Lines of sight that graze the obstruction are shown in Fig. 22 for three kinds of atmospheric conditions. Under normal conditions the gradient of the index of refraction is -39 N units per kilometer,* and the ratio K of the equivalent-to-actual earth radius is $\frac{2}{3}$. When the gradient becomes -157 N units per kilometer, the so-called flat-earth condition exists ($K = \infty$) and clearance is substantial. For changes of the gradient in the opposite direction, clearance becomes reduced; in path design the value of interest is $K = \frac{2}{3}$, which corresponds to a positive gradient of 79 N units per kilometer.

The projections of the grazing lines on the Palmetto tower are given by the tops of the three bars on the right-hand side of Fig. 23, at 30,

* The radio refractive index of air, n, is frequently expressed as $n = 1 + N \times 10^6$, where N describes the refractive index in "N units."

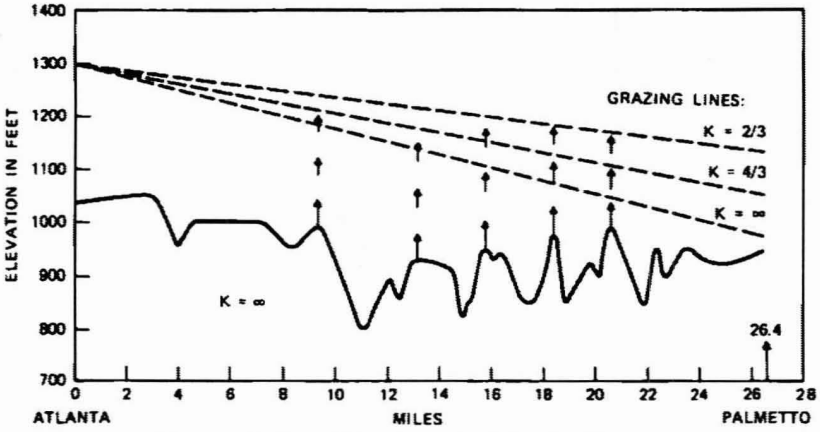

Fig. 22—Path profile, Atlanta to Palmetto, Georgia.

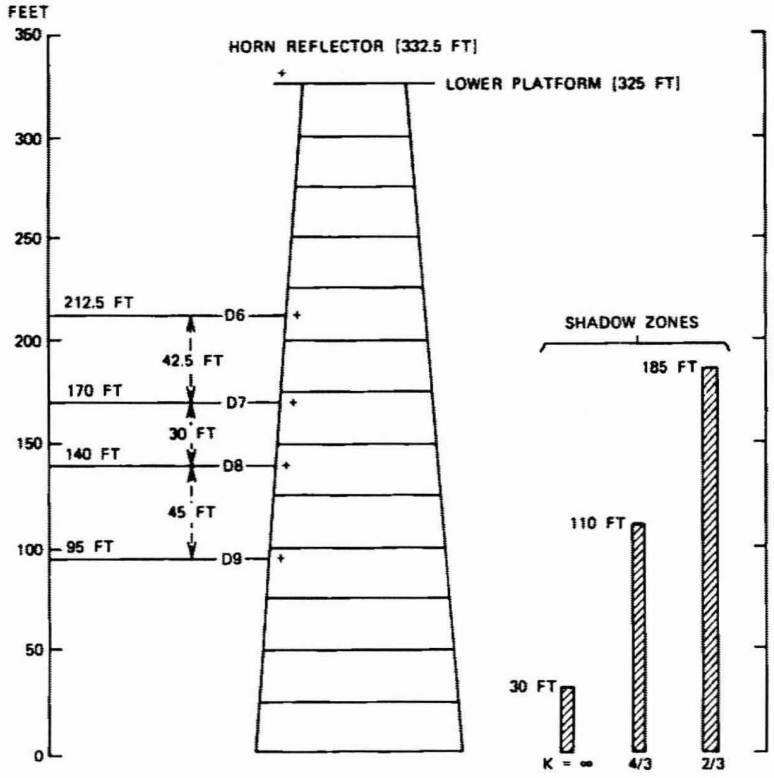

Fig. 23—Receiving antennas at Palmetto, Georgia in 1972.

110, and 185 feet from ground. The center line of the horn-reflector receiving antenna is 332.5 feet from ground. The center lines of the antennas added for test purposes are labeled D6 through D9. The antenna at D7 was a small 15-dB-gain horn; the other three are 4-foot-diameter parabolic reflectors. The normal antenna height for reception from Atlanta would be at about D6; the tower is much higher because clearance on another path controls its height.

The antenna of interest is the bottom 4-foot parabolic reflector at D9, with center line 95 feet above ground. The center line is 15 feet below the point where the grazing line under normal conditions ($K = \frac{4}{3}$) projects on the tower. The clearance in Fresnel zones is about $-0.2F_1$. The center line of the bottom antenna falls on the grazing line when K is about 1.72, which corresponds to an index of refraction gradient of about -66 N units per kilometer, which is 27 N units per kilometer higher than the gradient of -39 N units per kilometer under normal $K = \frac{4}{3}$ conditions.

The below-grazing location of the bottom antenna was further verified by noting that there was a signal loss of 14 dB when it was moved from its previous (higher) location on March 14, 1972. A theoretical loss of about 8 dB would occur if the obstruction were a knife edge; diffraction over a tree-covered hilltop accounts for the additional 6-dB loss.

Data were analyzed on received power (recorded by MIDAS[21]) during time intervals containing deep fading (more than 20 dB) on any of the five receiving antennas in April, May, and June of 1972. The total of such time intervals was about 13 hours during which the amount of fading was similar for the top four antennas. The *a priori* expectation was that the bottom antenna would fade more, since its signal level during normal daytime conditions was 14 dB low because of a lack of clearance. The opposite occurred: the signal received by the bottom antenna faded *less* than signals received by the four upper antennas.

The measured time-below-level data (during the 13 hours of deep-fading activity) for the bottom antenna (D9) and the one above it (D8) are shown in Fig. 24 (fading on the other antennas, after adjustment for gain differences, was the same as that on D8). The single antenna curves have the normal slope (decade of time per 10 dB) for deep multipath fades. Time below level for the bottom antenna is smaller than that for D8 by about a factor of three in the deep-fade region.

Diversity performance of the combination of D8 and D9 was excellent. Simultaneous fades on the two antennas were never deeper than about 18 dB from normal (see Fig. 24).

These results relate to aspects of radio propagation not covered by previous experience or theory. Physically, the observations can per-

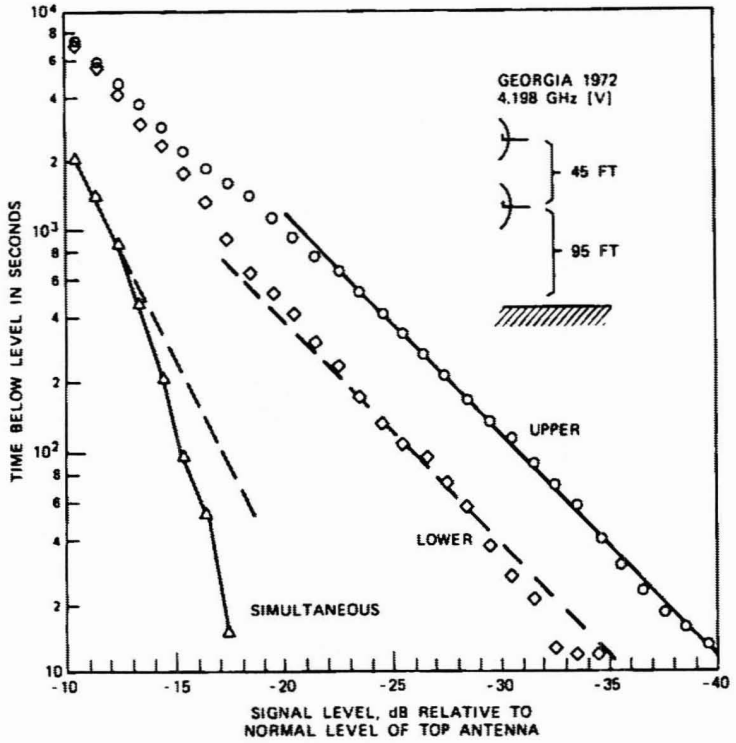

Fig. 24—Fading measured at Palmetto, Georgia.

haps be explained by the presence of layers with strong negative gradients in the index of refraction that create fading but offset the normal lack of clearance for the bottom antenna. Furthermore, since the bottom antenna is relatively close to the ground, the terrain blocks some of the potentially interfering rays, which would also tend to reduce the amount of fading.

A tentative conclusion is that protection from multipath fading can be obtained by placing the bottom antenna somewhat below grazing under normal atmospheric conditions (diffraction loss of perhaps 10 dB). It must be established that antennas placed in such a manner perform well consistently; results from tests at Culver, Indiana (1973–1974) are encouraging.

APPENDIX B

Example of Roughness Calculation

The terrain heights (denoted by x_i, terminal ends omitted) for the 19-mile path in the example of Fig. 25 are provided in Table V. The roughness (standard deviation) is the square root of the average

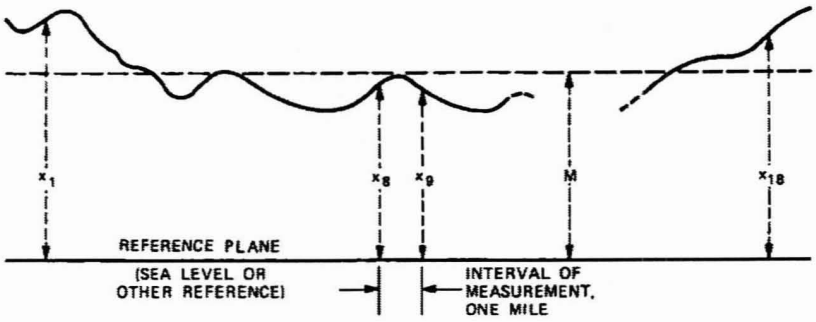

Fig. 25—Determination of terrain roughness.

Table V — Example of terrain heights for 19-mile path (see Fig. 25)

i	x_i (ft)	i	x_i (ft)	i	x_i (ft)
1	600	7	400	13	450
2	625	8	420	14	420
3	515	9	460	15	390
4	440	10	420	16	480
5	480	11	450	17	520
6	450	12	480	18	550

square of the deviation from the mean:

$$w = \sqrt{\frac{1}{18}\sum_{i=1}^{18}(x_i - M)^2}$$

$$= \sqrt{\left[\frac{1}{18}\sum_{i=1}^{18} x_i^2\right] - M^2} \tag{17}$$

$$M = \frac{1}{18}\sum_{i=1}^{18} x_i = 8550/18 = 475 \tag{18}$$

$$w = \sqrt{(4133950/18) - (475)^2} = 63.5 \text{ feet.} \tag{19}$$

APPENDIX C

Length of Fading Season

Multipath fading is a warm-weather phenomenon. Assuming that the length of the warm portion of the year is proportional to the average annual temperature, the value of T_0 to be used in eq. (2) to esti-

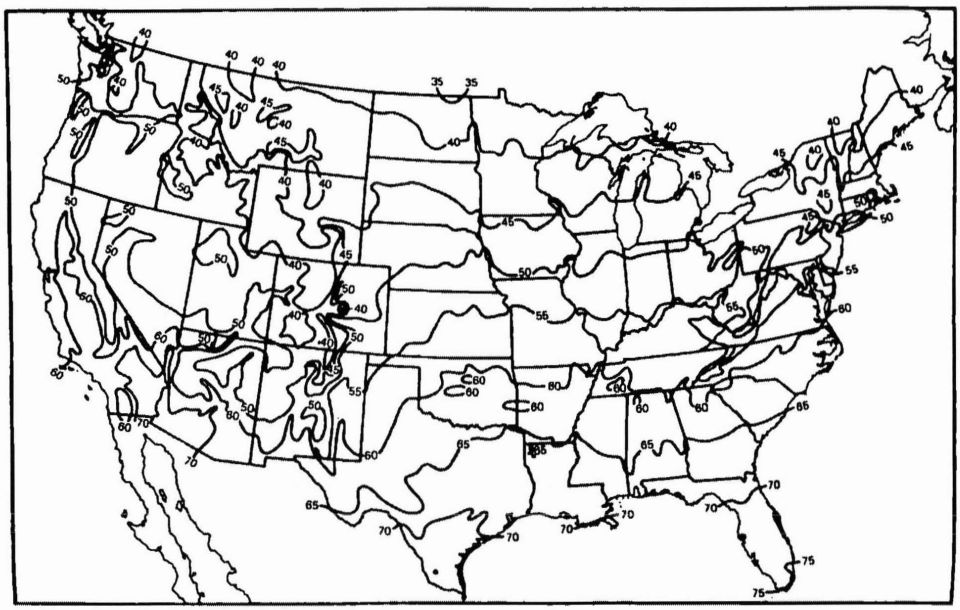

(Reprinted from the 1963 *Weather Handbook*, p. 194, by permission of the publisher, Conway Research, Inc., Atlanta, Georgia. No further reproduction is authorized.)

Fig. 26—Average annual temperatures in °F.

mate the annual time below level is

$$T_0 = (t/50)8 \times 10^6 \text{ sec}, \quad 35 \leqq t \leqq 75, \tag{20}$$

where t denotes the average annual temperature of the locality in question in °F as determined from Fig. 26.

In the average case (Figs. 5 and 8), T_0 is equal to the number of seconds in three months; eq. (20) reduces to this when t is 50°F. The temperature contours in Fig. 26 show that 50°F is appropriate for middle latitudes in the United States and for Ohio in particular; data from Ohio have often been used to describe average fading.

The range of average annual temperatures (Fig. 26) is from 35°F in northern North Dakota to 75°F in southern Florida. The corresponding fading season lengths range from 70 percent to 150 percent of average (T_0 ranges from 2 months to 4½ months).

APPENDIX D

Addition of Space Diversity to Frequency Diversity

In the Bell System, fully loaded long-haul routes with radio channels in both the 4- and 6-GHz bands will utilize cross-band frequency-diversity protection with two protection channels—18 working channels in a 2 × 18 system.[14] Expectations are that space diversity in 2 × 18 protection systems will be needed only when problem hops are encountered—exceptionally high fading activity or unavoidable ground reflections—that will have to be treated on an individual basis. The need for space-diversity protection will arise on long-haul routes that have radio channels in one frequency band only, 4 or 6 GHz; the single frequency-diversity channel permitted on such routes[1] may not provide adequate protection in geographic areas where fading activity is above average.

The time below level at the fade margin of an average working channel in a frequency-diversity system with one protection channel and m working channels (a 1 × m system) is approximately equal to the simultaneous time below level of channels in an equivalent 1 × 1 system in which the separation of the center frequencies of the two channels is

$$\Delta f_{eq} = m/[\sum_k (1/\Delta f_k)], \tag{21}$$

where the sum contains $\frac{1}{2}m(m+1)$ terms, extending the summation over frequency separations of all channel pairs in the 1 × m system. The equivalent 1 × 1 system (introduced to simplify calculations) is derived from the first term in the alternating series describing transmission unavailability[14] under the assumption that equipment works

perfectly during fading (equipment failures are accounted for via the allocation of transmission availability objectives).

The simultaneous time below level of the two channels in the equivalent 1 × 1 system is

$$T_{eq} = T/I_{eq}, \tag{22}$$

where T is the time below level in an unprotected channel and

$$I_{eq} = q_{eq}L^{-2}, \tag{23}$$

with q_{eq} determined by using Δf_{eq} in eq. (10). As an example, in a 1 × 3 system with 60 MHz between channels

$$\Delta f_{eq} = \frac{3}{(3/60) + (2/120) + (1/180)} = 41.5 \text{ MHz}. \tag{24}$$

Similarly, in a 1 × 7 system with 30 MHz between channels,

$$\Delta f_{eq} = 15.3 \text{ MHz}. \tag{25}$$

The use of these values of Δf_{eq} to calculate T_{eq} for one hop is illustrated in the example in Table VI and Fig. 27. In a multihop switching section, T_{eq} would be determined by adding values of T_{eq} determined for each hop.

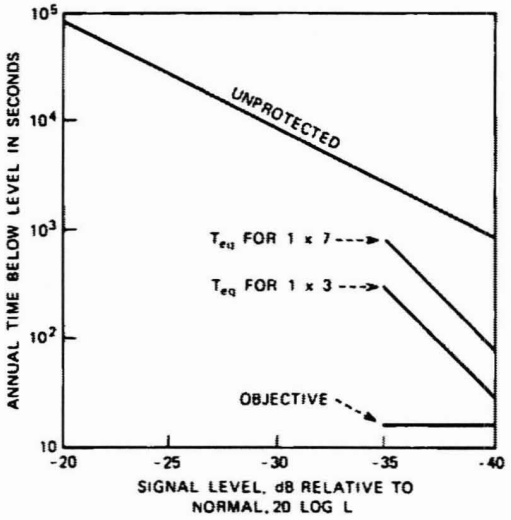

Fig. 27—Example of need for space-diversity protection (see Table VI for path parameters and calculations).

Table VI — Sample calculations

Path parameters	D = 20 miles (southern coastal area) f = 6 GHz w = 20 feet t = 70°F
Fading in an unprotected channel	$c = 2(w/50)^{-1.3} = 6.58$ $r = c(f/4)D^3 10^{-5} = 0.79$ $T_0 = (t/50)8 \times 10^6 = 1.12 \times 10^7$ seconds $T = rT_0L^3 = 8.8 \times 10^6\ L^3$ seconds/year
Long-haul objective	$1600 \times D/2000 = 16$ seconds/year
Equivalent 1 × 1 system replacing 1 × 3	$\Delta f_{eq} = 41.5$ MHz $q_{eq} = (50/6 \times 20) \times (41.5/6000) = 0.0029$ $I_{eq} = 0.0029\ L^{-1}$
Equivalent 1 × 1 system replacing 1 × 7	$\Delta f_{eq} = 15.3$ MHz $q_{eq} = (50/6 \times 20) \times (15.3/6000) = 0.0011$ $I_{eq} = 0.0011\ L^{-1}$

The long-haul objective (using D_s to denote the length of the switching section) is

$$T_{ob} = 1600D_s/2000 \text{ sec}, \tag{26}$$

in terms of which the recommendations for the application of space diversity are:

$$T_{eq} < T_{ob}, \text{ space diversity not needed}, \tag{27}$$

$$T_{eq} > 1.5\ T_{ob}, \text{ space diversity needed}. \tag{28}$$

Use of space diversity is optional in the tolerance band ($T_{ob} \leqq T_{eq} \leqq 1.5\ T_{ob}$), which reflects parameter uncertainties and the fact that the approximation used to determine T_{eq} overestimates the unavailability. According to the above criteria, space diversity is needed in the example in Fig. 27 (assuming a one-hop switching section with 40-dB fade margin).

If space-diversity protection is needed, then it should first be applied to the worst hop in a switching section. In subsequent calculations, T_s from eq. (6) should replace T_{eq} for space-diversity-equipped hops, since improvement due to space diversity is normally dominant.

APPENDIX E

Comparative Switching With Hysteresis

The analysis is carried out in terms of the envelope voltages (R_1 and R_2) of the signals from the two receiving antennas. The antennas are

assumed to be of the same size and R_1 and R_2 are normalized to be unity in the absence of fading. The envelope R of the diversity signal is a composite of R_1 and R_2 obtained by switching; R becomes R_1 when $R_1 > bR_2$ and R becomes R_2 when $R_2 > bR_1$. The parameter b ($b \geqq 1$) describes the hysteresis of the switch.

The probability of a fade of 20 log L dB is the probability that $R < L$. Regions in the R_1, R_2-plane over which the joint probability density function $p(R_1, R_2)$ has to be integrated to obtain this probability are shown in Fig. 28. This shows that

$$\Pr(R < L) = \int_0^L dR_2 \int_0^L dR_1 p(R_1, R_2) + \frac{1}{2}\int dR_2 \int dR_1 p(R_1, R_2) \quad \text{over triangle 1,} \quad + \frac{1}{2}\int dR_2 \int dR_1 p(R_1, R_2) \quad \text{over triangle 2.} \tag{29}$$

For deep fades and antennas of equal size,[8]

$$p(R_1, R_2) \cong 4q^{-1}R_1R_2. \tag{30}$$

Substitution and integration gives

$$\Pr(R < L) \cong q^{-1}L^4 \frac{b^2 + b^{-2}}{2}. \tag{31}$$

In the absence of hysteresis, b is unity. When hysteresis is introduced, b becomes larger than unity, and the probability of fading is increased by a factor of $0.5(b^2 + b^{-2})$.

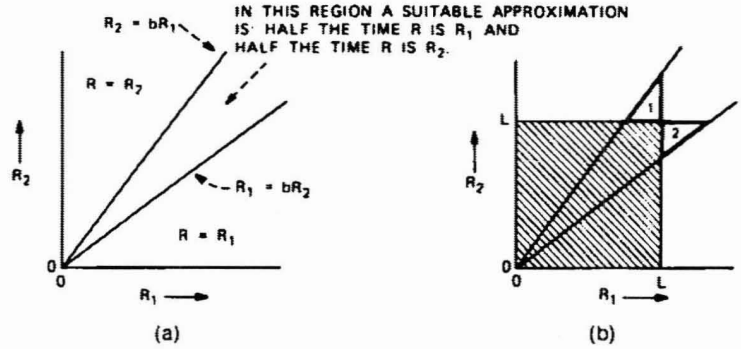

Fig. 28—Comparative switching with hysteresis. (a) Switching diagram. (b) Areas in which $R < L$.

APPENDIX F

Threshold Switching Calculations

Below threshold the switch cycles, and R is R_1 or R_2 in equal amounts of time; the below-level probability for below-threshold operation is, with A denoting the threshold value,

$$\Pr(R < L) = \tfrac{1}{2}\Pr(R_1 < L, R_2 < A) + \tfrac{1}{2}\Pr(R_1 < A, R_2 < L), L < A. \quad (32)$$

Because of symmetry in the joint probability density function, this simplifies to

$$\Pr(R < L) = \int_0^L dR_1 \int_0^A dR_2 p(R_1, R_2), \quad L < A \quad (33)$$

for antennas of equal size. The below-level probability in above-threshold operation is (invoking symmetry as above) the sum of two terms. The first term describes the situation when R is R_1, the second when R has become R_2 upon R_1 dropping below threshold:

$$\Pr(R < L) = \Pr(A < R_1 < L) + \Pr(R_1 < A, R_2 < L), \quad L > A. \quad (34)$$

These equations are based on results obtained for correlated Rayleigh distributed variables.[2] Use of the probability density function from eq. (30) in (33) gives a deep fade approximation:

$$\Pr(R < L) \cong q^{-1}A^2L^2, \quad L < A, \quad (35)$$

which shows the L^2 behavior below threshold.

The curves in Figs. 10 and 11 were calculated (as outlined above) for correlated Rayleigh-distributed variables with q determined from the empirical expression for I_0 (machine computation was necessary because the integrals cannot be evaluated in closed form). The Rayleigh distribution was used in the theoretical calculations because its previous uses have provided insights valuable to the statistical description of space-diversity operation. The theoretically predicted functional forms have been verified by using actual fading records as inputs to computer-simulated threshold switches.[22]

APPENDIX G

Common Control Switching

Space-diversity switching is normally implemented on a per-channel basis: each radio channel has its own switch, and switching decisions for a channel are based, in FM systems, on carrier levels received on

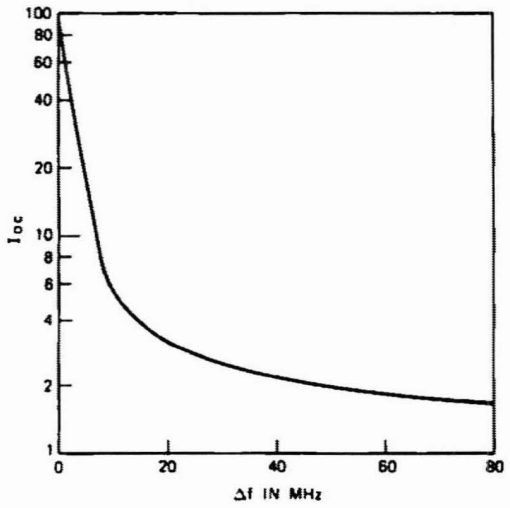

Fig. 29—Improvement in a controlled channel as a function of frequency separation from controlling channel (4-GHz band, 30-foot antenna separation, 26-mile path, 40-dB fade margin).

the upper and lower antennas. Use of the carrier in one channel (controlling channel) to control switching of other channels (controlled channels) would reduce costs. For example, diversity transmission could be controlled by the received carrier in another channel, thus eliminating the feedback link; similarly, a single broadband switch could be used to switch a number of radio channels. Unfortunately, the improvement obtained in such common control schemes is too small to be of practical value.

The available improvement I_{oc} in a controlled channel depends on Δf, the frequency separation of the carriers in the controlling and controlled channels. When Δf is zero, I_{oc} is equal to the available improvement I_0 in the controlling channel, with I_0 given by (7). In the limit, as Δf increases and becomes large, I_{oc} approaches unity as fading at the two frequencies becomes independent. Theoretical estimates[23] show that the initial decrease in I_{oc} as Δf increases from zero is rapid. As an example, the approximate behavior of I_{oc} as a function of Δf in the 4-GHz band is shown in Fig. 29 for a 30-foot antenna separation on a 26-mile path and with a fade margin of 40 dB. The value of I_{oc} at $\Delta f = 0$ is about 100. At one channel separation, $\Delta f = 20$ MHz, I_{oc} has decreased to about 3. Clearly, the improvement in the controlled channels is too small to be of practical value. The lack of performance in common control switching is simply a consequence of the fact that deep multipath fades are highly frequency selective.

APPENDIX H

Results of Palmetto, Georgia, Experiments in 1968

Power received at 4.198 GHz on five vertically separated antennas (Fig. 30) was measured on a 24.6-mile path from Atlanta to Palmetto, Georgia over a 72-day period in 1968 (August 16–October 27). Five inputs of MIDAS[21] (Multiple Input Data Acquisition System) were used to acquire the data. A power reading from the horn reflector on top was obtained first; about 2 milliseconds later, a reading from the top dish was obtained, and so on down the tower. This scanning was repeated at a rate of five times per second. The readings were converted to a logarithmic scale and recorded in digital form (nominally 1 dB quantizing) on magnetic tape for subsequent computer processing. In the absence of fading, to conserve tape, the recording rate was less than the sampling rate.

Improvement as a function of fade depth for the ten antenna pairs, with separations ranging from 4 to 60 feet center-to-center, was obtained by dividing at a given fade depth the measured time below level for an antenna (T) by the measured simultaneous time below level (T_s). The equation for improvement,

$$I_0 = qL^{-2}, \tag{36}$$

was fitted to the points in the deep-fade region to determine a value of q for each antenna separation ($v^2 = 1$, since gains were set to equalize free-space levels). The values of q so obtained are shown in Fig. 31 as a function of antenna separation; because of random differences in

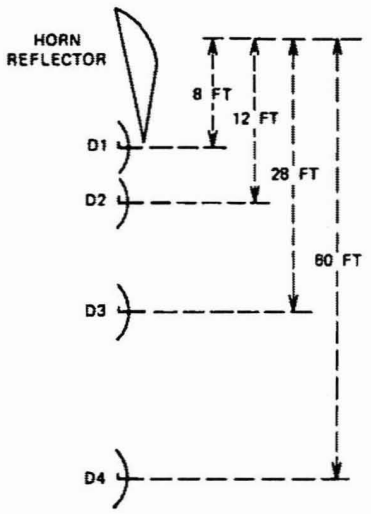

Fig. 30—Receiving antennas at Palmetto, Georgia in 1968. D1 to D4 are 4-foot-diameter parabolic reflectors.

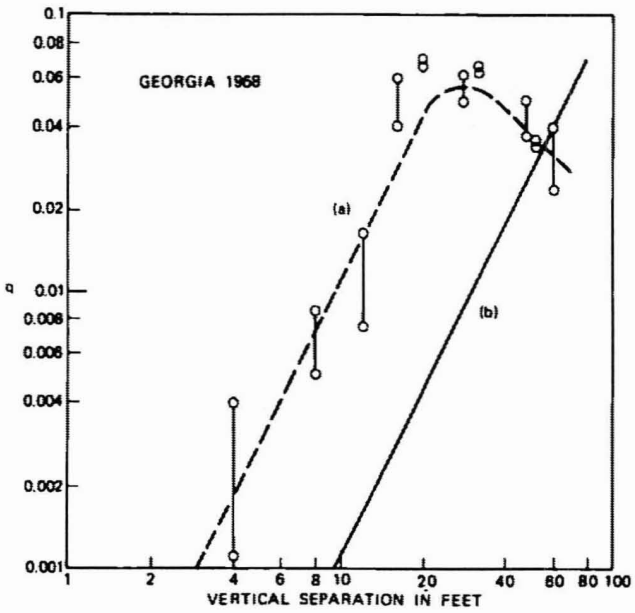

Fig. 31—Variation of correlation parameter q: (a) Georgia 1968, and (b) eq. (9). Increasing values of q denote increasing decorrelation.

T from antenna to antenna, there are two values of q for each antenna separation, depending on whether T for the upper or the lower antenna was used to form the ratio T/T_s.

As a function of antenna separation, the correlation parameter q first increases as the square of the antenna separation, but then levels off and decreases (dotted line in Fig. 31); the presence of a small dominant component in the multipath spectrum is the most likely cause of this. Compared to eq. (9) (see also solid line in Fig. 31), q is enhanced for smaller separations, but is reduced for separations over about 50 feet. Dominant components being random on paths designed for negligible ground reflections, the enhancement cannot be counted upon when choosing an antenna separation; however, the possibility that q may decrease for large separations must be provided for. This is the reason why the applicability (for design purposes) of (7) has been limited to antenna separations of 50 feet or less.

REFERENCES

1. FCC First Report and Order (Docket 18920), June 3, 1971.
2. E. Henze, "Theoretische Untersuchungen über einige Diversity-Verfahren," Archiv Elektrischen Übertragung, *11*, No. 5 (May 1957), pp. 183–194.
3. H. Makino and K. Morita, "The Space Diversity Reception and Transmission Systems for Line-of-Sight Microwave Link," Rev. Elec. Comm. Lab (Japan), *13*, No. 1-2 (January–February 1965), pp. 111–129.

4. H. Makino and K. Morita, "Design of Space Diversity Receiving and Transmitting Systems for Line-of-Sight Microwave Links," IEEE Trans. Commun. Tech., *COM-15*, No. 4 (August 1967), pp. 603–614.
5. R. F. White, "Space Diversity on Line-of-Sight Microwave Systems," IEEE Trans. Commun. Tech., *COM-16*, No. 1 (February 1968), pp. 119–133.
6. R. F. White, *Engineering Considerations for Microwave Communications Systems*, San Carlos, Calif.: Lenkurt Electric Co., June 1970.
7. A. Vigants, "Space-Diversity Performance as a Function of Antenna Separation," IEEE Trans. Commun. Tech., *COM-16*, No. 6 (December 1968), pp. 831–836.
8. A. Vigants, "The Number of Fades in Space-Diversity Reception," B.S.T.J., *49*, No. 7 (September 1970), pp. 1513–1530.
9. W. T. Barnett, "Multipath Propagation at 4, 6, and 11 GHz," B.S.T.J., *51*, No. 2 (February 1972), pp. 321–361.
10. S. H. Lin, "Statistical Behavior of a Fading Signal," B.S.T.J., *50*, No. 10 (December 1971), pp. 3211–3270.
11. A. Vigants, "Number and Duration of Fades at 6 and 4 GHz," B.S.T.J., *50*, No. 3 (March 1971), pp. 815–841.
12. K. W. Pearson, "Method for the Prediction of the Fading Performance of a Multisection Microwave Link," Proc. IEE (London), *112*, No. 7 (July 1965), pp. 1291–1300.
13. A. Vigants, "Observations of 4 GHz Obstruction Fading," Proc. IEEE Int. Conf. on Commun., *8*, 1972, pp. 28-1 to 28-2.
14. W. Y. S. Chen, "Estimated Outage in Long-Haul Radio Relay Systems with Protection Switching," B.S.T.J., *50*, No. 4 (April 1971), pp. 1455–1485.
15. S. H. Lin, "Statistical Behavior of Deep Fade of Diversity Signals," IEEE Trans. Commun., *COM-20*, No. 6 (December 1972), pp. 1100–1107.
16. W. T. Barnett, unpublished work.
17. W. T. Barnett, unpublished work.
18. A. Vigants, "Threshold-Switched LOS Space-Diversity Reception in the Everglades," Conf. Record, pages 12C-1 to 12C-3, IEEE Int. Conf. Commun., June 17–19, 1974 Minneapolis, Minnesota; Institute of Electrical and Electronics Engineers, 1974.
19. A. Vigants, "Space Diversity on a 6-GHz Path with Billboard Reflectors," Conference Record, pages 12B-1 to 12B-4, International Conference on Communications, June 17–19, 1974, Minneapolis, Minnesota; Institute of Electrical and Electronics Engineers, 1974.
20. A. Vigants, "Variation of Fading with Antenna Height and Size," URSI/IEEE G-AP Int. Symp., Williamsburg, Va., December 11–15, 1972.
21. K. Bullington, "Unlocking the Secrets of Microwave Propagation," Bell Laboratories Record, *50*, No. 1 (January 1972), pp. 8–13.
22. M. V. Pursley, unpublished work.
23. A. Vigants, unpublished work.

```
100 REM     PROGRAM          ****RADLNK****          MICROWAVE RADIO PREDICTIONS
105 REM  A. SCOPE
110 REM     THE PROGRAM CALCULATES  1 - PATH LOSS  (UNOBSTRUCTED)
115 REM                             2 - RAIN ATTENUATION       2GHZ<F<99GHZ
120 REM                             3 - RAIN OUTAGE TIMES
125 REM                             4 - AMPLITUDE DISPERSION FADING
130 REM                             5 - FADE MARGIN GIVEN EQUIPMENT SPEC'S
135 REM                             6 - BEARINGS & DISTANCES OF STATIONS
140 REM                             7 - FREQUENCY & SPACE DIVERSITY DATA
145 REM                             8 - FRESNEL ZONE SIZE & EARTH BULGE
150 REM                             9 - RADIO HORIZON    FOR INTERFERENCE
155 REM                            10 - REFLECTION POINTS ALONG THE ROUTE
160 REM
165 REM     THE PROGRAM OUTPUTS     1 - SYSTEM DETAILS
170 REM                             2 - TERRAIN DATA       (FOR PATH PLOT)
175 REM                             3 - LINK SIGNAL LEVELS
180 REM                             4 - RAIN OUTAGE TIMES
185 REM                             5 - NORMAL FADING OUTAGE TIMES
190 REM                             6 - SYSTEM AVAILABILITY,   NO HARDWARE
195 REM                             7 - PATH PLOT (A3 & A4 PLOT SIZES)
200 REM                             8 - PATH REFLECTIVITY AT 3 K VALUES
205 REM                             9 - RECOMMENDED SPACE DIVERSITY SEP
210 REM                            10 - EQUIPMENT DATABASE HANDLER.
215 REM  B. OPERATION
220 REM     FOR THE INITIAL RUN, IT IS NECESSARY TO LOAD THE PROGRAM WITH
225 REM     DATA. THIS IS PERFORMED BY SELECTING ALL MAIN MENU OPTIONS
230 REM     (IN ANY SEQUENCE) PRIOR TO PRINTING THE REPORT (5).
235 REM     THE OPTION 'PATH GEOMETRY' AND IT'S SUB-MENU ITEMS DOES NOT
240 REM     HAVE TO BE USED INITIALLY AS DEFAULT VALUES ARE SET.
245 REM     SUBSEQUENT CHANGES CAN BE MADE BY SELECTING ANY OF THE MAIN
250 REM     MENU OPTIONS AND THEN PRINTING THE NEW REPORT (OR PLOT).
255 REM     THE PATH PROFILE PLOT OPTION IS INDEPENDANT OF THE REST OF THE
260 REM     PROGRAM. THREE VARIABLES ARE INTERLINKED, REFER TO 2.1 PROGRAM
265 REM     OPERATION. THIS ALLOWS THE USER TO EVALUATE THE PATH OBSTACLES.
270 REM     MINIMIZATION OF RADIO OVERSHOOT WILL ALSO REDUCE POSSIBLE
275 REM     INTERFERENCE.
280 REM
285 REM  C. PROGRAM CAN BE RESET BY EXITING AND RESTARTING. PATH GEOMETRY
290 REM     DATA CAN BE RESET WITHIN IT'S OWN SELECTION.     ALTERNATIVELY
295 REM     PROGRAM DATA MAY BE OVER-WRITTEN.
300 REM
305 REM  D. THE PROGRAM ASSUMES UNOBSTRUCTED PATHS FOR THE RADIO RAYLINE.
310 REM     REFER TO FRESNEL ZONE CLEARANCE RULES IN 1.1.1 DESIGNING LINKS
315 REM
320 REM  E. RAIN RATES ARE FOR 0.05% PROBABILITY FOR THE WORST MONTH.
325 REM     REF:  CCITT REP 563  AND HANDBOOK RAIN CONTOURS CHARTS.
330 REM
335 REM  F. CONVERSION OF UNITS:   DBM=10*LOG(WATTS/0.001)
340 REM                            DBI=DBD + 2.12
345 REM
350 REM  G. PROGRAM WRITTEN BY: DAVID BURGER     JULY 1985
355 REM
360 DIM X(101),Y(101),XD(101),YD(101),RF(101)
365 T46=27:KF=1.3333:R2=13:R3=1:R44=.05:R4$="M"      'DEFAULT VALUE SET
```

R2 = RAIN RATE
R3 = CLIMATE FACTOR
KF = IC FACTOR
T46 = RMS ROUGHNESS
R44 = RAIN PERCENT

GW BASIC

KF = 1.33
R2 = 13
R3 = 1

```
500 CLS:PRINT"PROGRAM       ***RADLNK***                    MICROWAVE LINK PREDICTI
ONS"
505 SOUND 88,4:SOUND 151,3:SOUND 88,2
510 PRINT TAB(44)"D.BURGER VS 2.4":PRINT:PRINT:PRINT:PRINT
515 PRINT TAB(22)"1 - INPUT  SYSTEM   DETAILS"
520 PRINT TAB(22)"2 - PATH  PROFILE  GEOMETRY"
525 PRINT TAB(22)"3 - INPUT  RAIN INTENSITIES"
530 PRINT TAB(22)"4 - EQUIPMENT    PARAMETERS"
535 PRINT TAB(22)"5 - LINK PERFORMANCE REPORT":PRINT TAB(22)"6 - DEFAULT PARAMET
ERS":PRINT TAB(22)"7 - EXIT"
540 KEY OFF
545 QX$=INKEY$:IF QX$="" THEN 545
550 IF VAL(QX$)>7 OR VAL(QX$)<1 THEN 545
555 SOUND 88,3
560 ON VAL(QX$) GOSUB 700,3800,1000,1200,2000,4700,7500
565 GOTO 500
570 END
```

```
700 REM      **************************SYSTEM DETAILS
705 CLS:PRINT"PROGRAM       ***RADLNK***          SYSTEM DETAILS INPUT"
710 PRINT:PRINT:PRINT"TO RETURN TO MAIN MENU  <EXIT>":PRINT
715 PRINT"<CURRENT DATA>":PRINT"STATION  A ";N1$
720 PRINT"STATION  B ";N2$
725 PRINT
730 INPUT"TERMINAL  A  NAME ";QX$
735 IF QX$="" THEN 745
740 IF QX$="EXIT" THEN RETURN ELSE N1$=QX$
745 INPUT"TERMINAL  B  NAME ";QX$
750 IF QX$="" THEN 760
755 IF QX$="EXIT" THEN RETURN ELSE N2$=QX$
760 FLAG2=0:PRINT:PRINT"ENTER GRID COORDINATES   Y/N"
765 QX$=INKEY$:IF QX$="" THEN 765
770 IF QX$="Y" THEN 3500
775 PRINT"DISTANCE BETWEEN TERMINALS   KM ";P1;"   ";:INPUT QX$
780 IF QX$="" THEN 795
785 IF QX$="EXIT" THEN RETURN ELSE P1=VAL(QX$)
790 IF P1<=0 THEN PRINT"<ERROR>":SOUND 88,3:GOTO 775
795 PRINT:PRINT"1 - NO DIVERSITY":PRINT"2 - SPACE DIVERSITY"
800 PRINT"3 - FREQUENCY DIVERSITY":PRINT:PRINT"INPUT DIVERSITY OPTION"
805 QX$=INKEY$:IF QX$="" THEN 805
810 IF QX$="EXIT" THEN RETURN ELSE FLAG3=VAL(QX$)
815 IF FLAG3<2 OR FLAG3>3 THEN 860
820 IF FLAG3=2 THEN 825 ELSE 845
825 PRINT"VERTICAL  SEPARATION    (M) ";SD1;:INPUT "  ";QX$
830 IF QX$="" THEN 835 ELSE SD1=ABS(VAL(QX$))
835 IF SD1<.01 THEN PRINT"<ERROR>":SOUND 88,3:GOTO 825
840 GOTO 860
845 PRINT"FREQUENCY SEPARATION  (MHZ) ";FD1;:INPUT "  ";QX$
850 IF QX$="" THEN 855 ELSE FD1=ABS(VAL(QX$))
855 IF FD1<7 THEN PRINT"<ERROR>":SOUND 88,3:GOTO 845
860 RETURN
```

MODE

FLAG3

1 NO DIV

2 SPACE DIV

3 FREQ DIV

```
1200 REM      ************************EQUIPMENT PARAMETERS CONTROL
1205 CLS:PRINT"PROGRAM       ***RADLNK***              EQUIPMENT PARAMETERS INPUT"
1210 PRINT:Z$="NOT IN DATABASE"
1215 PRINT:PRINT:PRINT
1220 PRINT TAB(17)"KEYBOARD INPUT":PRINT TAB(22)"1 - SPECIFY  DATA":PRINT
1225 PRINT TAB(17)"FILE INPUT":PRINT TAB(22)"2 - VIEW DATA BASE"
1230 PRINT TAB(22)"3 - MODIFY EQUIPMENT DATABASE":PRINT TAB(22)"4 - WRITE NEW EQ
PT. DATABASE"
1235 PRINT TAB(22)"5 - PRINT EQUIPMENT LIST":PRINT:PRINT TAB(17)"EXIT":PRINT TAB
(22)"6 - EXIT TO MAIN MENU"
1240 QX$=INKEY$:IF QX$="" THEN 1240
1245 IF VAL(QX$)<1 OR VAL(QX$)>6 THEN 1240
1250 IF VAL(QX$)=6 THEN RETURN
1251 IF VAL(QX$)=1 THEN 1265
1252 PRINT"CURRENT EQUIPMENT FILES"
1253 FILES "*.EQP"
1255 PRINT:INPUT"INPUT EQUIPMENT MANUFACTURER ";Z$
1260 Z$=LEFT$(Z$,5)+".EQP"
1265 ON VAL(QX$) GOSUB 1500,2500,3000,2600,2800
1270 GOTO 1205
```

```
1500 REM      **************************SPECIFY EQUIPMENT PARAMETERS
1505 CLS:PRINT"PROGRAM      ***RADLNK***          SPECIFY EQUIPMENT PARAMETERS"
1510 PRINT"EQUIPMENT MANUFACTURER FILE: ";Z$
1515 PRINT:PRINT" ";N3$:PRINT" FREQUENCY     ";F1:PRINT" TX POWER      ";P2
1520 PRINT" RX THRESHOLD ";R1:PRINT" TX ANT GAIN  ";G1:PRINT" RX ANT GAIN  ";G2
1525 PRINT" WAVEGUIDE LOSS ";G3
1530 INPUT"EQUIPMENT  TYPE         ";QX$
1535 IF QX$="" THEN 1545
1540 IF QX$="EXIT" THEN RETURN ELSE N3$=QX$
1545 INPUT"SIGNAL  FREQUENCY  GHZ ";QX$
1550 IF QX$<>"" THEN F1=ABS(VAL(QX$))
1555 INPUT"TRANSMIT  POWER    DBM ";QX$
1560 IF QX$<>"" THEN P2=VAL(QX$)
1565 INPUT"RECEIVE THRESHOLD  DBM ";QX$
1570 IF QX$<>"" THEN R1=VAL(QX$)
1575 INPUT"TOTAL WAVEGUIDE LOSSES ";G3
1580 PRINT:PRINT"<INPUT DISH SIZE  (M)   Y/N"
1585 QX$=INKEY$:IF QX$="" THEN 1585
1590 IF QX$="Y" THEN 1625
1595 INPUT"TRANSMIT ANTENNA  GAIN (DBI)";QX$
1600 IF QX$<>"" THEN G1=VAL(QX$)
1605 INPUT"RECEIVE  ANTENNA  GAIN (DBI)";QX$
1610 IF QX$<>"" THEN G2=VAL(QX$)
1615 N5$=" "
1620 RETURN
1625 INPUT"SIZE OF BOTH DISH ANTENNAS  (M) :";DD
1630 G1=10*LOG(4.78*(ABS(DD)*F1/.3)^2)/LOG(10)       'DISH ANTENNA GAIN
1635 N5$=" +"+STR$(DD)+"M DISH"
1640 G2=G1
1645 RETURN
```

```
2000 REM      **************************LINK PERFORMANCE REPORT
2005 IF P1<=0 OR F1<=0 THEN PRINT"<NO DATA>":SOUND 88,3:GOSUB 4100:RETURN
2010 P9=92.5+20*LOG(P1)/LOG(10)+20*LOG(F1)/LOG(10)
2013 GOSUB 3300                                        'ATMOSPHERIC ATTENUATION
2015 R9=P2+G1+G2-P9-G3-ATMOS
2020 F9=R9-R1
2025 GOSUB 3200                                        'AMPLITUDE DISP FADING
2030 T44=P1*P1/(KF*50.96)
2035 T48=17.34*SQR(P1/(4*F1))
2040 O2=O1
2045 IF FLAG3=3 THEN 2050 ELSE 2060
2050 IF O1>=.05 THEN X=SQR(O1)/(.18*FD1/F1) ELSE X=O1/(.035*FD1/F1)
2055 GOTO 2065
2060 IF FLAG3=2 THEN X=830*P1*10^(-F9/10)/(F1*SD1*SD1) ELSE 2070
2065 O2=O1*X/SQR(1+X*X)
2070 CLS
2075 GOSUB 3240                                        'RAIN FADING
2080 O8=100-O2-PRY
2085 O9=100-O2-PRM
2090 F8=F9-A8
2095 IF O1>100 THEN O1=100
2100 IF O2>100 THEN O2=100
2105 IF O9<0 THEN O9=0
2110 IF O8<0 THEN O8=0
2115 PRINT"SUBROUTINE     *LINK PERFORMANCE PRINTOUT*"
2120 LPRINT"PROGRAM        ***RADLINK***          MICROWAVE LINK PREDICTIONS"
2125 LPRINT:LPRINT"SYSTEM DETAILS"
2130 LPRINT USING "      Frequency                    ###.###";F1;:LPRINT" GHz"
2135 LPRINT USING "      Path Length                  ###.###";P1;:LPRINT" Km"
2140 IF FLAG2=1 THEN LPRINT USING"     Bearing of STATION B          ###.#";H;:LP
RINT"  DEG"
2145 LPRINT"      STATION  A                    ";N1$
2150 IF FLAG2=1 THEN LPRINT"               Latitude & Longitude ";
2155 IF FLAG2=1 THEN LPRINT USING"  ####.##  ";AA1,AA2
2160 LPRINT"      STATION  B                    ";N2$
2165 IF FLAG2=1 THEN LPRINT"               Latitude & Longitude ";
2170 IF FLAG2=1 THEN LPRINT USING"  ####.##  ";BB1,BB2
2175 LPRINT"      Equipment Type                ";N3$+N5$
2180 LPRINT:LPRINT"TERRAIN DATA";TAB(36)"PERFORMED AT K = ";KF
2185 LPRINT USING "      Earth Bulge                  ###.#";T44;:LPRINT" m"
2190 LPRINT USING "      RMS Roughness                ###.#";T46;:LPRINT" m"
2195 LPRINT USING "      Fresnel Zone Radius          ###.#";T48;:LPRINT" m"
2200 LPRINT:LPRINT"LINK SIGNAL LEVELS"
2205 LPRINT USING "      Free Space Path Loss        ####.#";P9;:LPRINT" dB"
2210 LPRINT USING "      Transmit Antenna Gain        ###.#";G1;:LPRINT" dBi"
2215 LPRINT USING "      Receive  Antenna Gain        ###.#";G2;:LPRINT" dBi"
2220 LPRINT USING "      Transmit Power               ###.#";P2;:LPRINT" dBm"
2225 LPRINT USING "      Waveguide + Other Losses     ###.#";G3;:LPRINT" dB"
2227 LPRINT USING "      Atmospheric Attenuation     ####.#";ATMOS;:LPRINT" dB"
2230 LPRINT:LPRINT USING "      MEDIAN RECEIVE LEVEL         ####.#";R9;
2235 LPRINT" dBm"
2240 LPRINT USING "      Receive Threshold            ###.#";R1;:LPRINT" dBm"
2245 LPRINT:LPRINT USING "      FADE MARGIN                  ####.#";F9;
2250 LPRINT" dB"
2255 LPRINT:LPRINT:LPRINT"RAIN ATTENUATION OUTAGES"
2260 LPRINT USING "      Climate Factor                 #.#";R3
```

```
2800 REM      *************************PRINT EQUIPMENT LIST
2805 LPRINT"PROGRAM          ***RADLNK***            EQUIPMENT LIST"
2810 LPRINT:LPRINT"Manufacturer ";Z$
2815 LPRINT"    TYPE";TAB(28);"F GHz";TAB(35);"Tx POW";TAB(45);"Rx THRES";TAB(55
);"ANT Gain";TAB(65);"RF Loss's"
2820 OPEN Z$ FOR INPUT AS #1
2825 INPUT #1,N3$,G3,P2,R1,G1,F1
2830 IF LEFT$(N3$,3)="END" THEN 2855
2835 LPRINT TAB(5);N3$;TAB(26);:LPRINT USING"###.###";F1;
2840 LPRINT USING"   ###.#";P2;:LPRINT USING"      ####.#";R1;
2845 LPRINT USING"     ###.#";G1;:LPRINT USING"      ###.#";G3
2850 GOTO 2825
2855 CLOSE #1
2860 LPRINT:LPRINT
2865 RETURN
```

```
3000 REM      **************************MODIFY EQUIPMENT FILE
3005 CLS:FLAG5=0
3010 OPEN "DUMP.EQP" FOR OUTPUT AS #2
3015 OPEN Z$ FOR INPUT AS #1
3020 INPUT #1,N3$,G3,P2,R1,G1,F1
3025 IF LEFT$(N3$,3)="END" THEN FLAG5=1
3030 GOSUB 1500                                          'SPECIFY EQUIPMENT
3035 WRITE #2,N3$,G3,P2,R1,G1,F1
3040 PRINT:PRINT"<MORE DATA ?     Y/N >"
3045 QX$=INKEY$:IF QX$="" THEN 3045
3050 IF QX$="N" THEN 3055 ELSE IF FLAG5=1 THEN 3030 ELSE 3020
3055 IF FLAG5=0 THEN 3060 ELSE 3075
3060 INPUT #1,N3$,G3,P2,R1,G1,F1
3065 WRITE #2,N3$,G3,P2,R1,G1,F1
3070 IF LEFT$(N3$,3)="END" THEN 3080 ELSE 3060
3075 WRITE #2,"END",G3,P2,R1,G1,F1
3080 CLOSE #2
3085 CLOSE #1
3090 REM  SWAP FILES
3095 OPEN Z$ FOR OUTPUT AS #1
3100 OPEN "DUMP.EQP" FOR INPUT AS #2
3105 INPUT #2,N3$,G3,P2,R1,G1,F1
3110 WRITE #1,N3$,G3,P2,R1,G1,F1
3115 IF LEFT$(N3$,3)="END" THEN 3120 ELSE 3105
3120 CLOSE #1:CLOSE #2
3125 KILL"DUMP.EQP"
3130 RETURN
```

T4 = RMS Roughness

F9 - FADE MARGIN

```
3200 REM    ***********AMPLITUDE DISPERSION FADING
3205 IF T46<6 THEN T4=6
3210 IF T46>42 THEN T4=42 ELSE T4=T46
3215 O1=.002088*(10^(-F9/20))^2*F1*(P1^3)*(T4^-1.27)*R3
3220 IF O1>=99 THEN 3230
3225 RETURN
3230 O1=100-2.37*(T4^-1.27)*R3*10^(F9/7.88)/LOG(P1/10)
3235 RETURN
```

R2 = 13 R4 = 0.05

F1 = FRQ, GHz

R2 = RAIN RATE

R4 = RAINRATE PERCENT

```
3240 REM    ***********RAIN FADING
3245 IF F1>75 THEN DU=75+.3*(F1-75) ELSE DU=F1
3250 A8=.495*LOG(R2)-1.931+(2.847-.1911*LOG(R2))*LOG(.4344*LOG(DU))
3255 A8=P1*10^A8
3260 IF R4$="M" THEN R4=R44^1.15*.29 ELSE R4=R44
3265 IF A8<F9 THEN PRY=R4*(ABS(A8/F9))^3.2 ELSE PRY=R4*(ABS(A8/F9))^2.6
3270 PRM=(3.45*PRY)^.87
3275 RETURN
```

YR

M = MONTH

R4 = RAIN RATE % .05

57-63 = 14.9 dB/km

```
3300 REM    ***********ATMOSPHERIC ATTENUATION
3305 IF F1>57 THEN 3320
3310 A8=(6.6/(F1^2+.33)+9/((ABS(F1-57))^2+1.96))*F1^2*.001
3315 GOTO 3335
3320 IF F1<63 THEN A8=14.9:GOTO 3335 ELSE 3325
3325 IF F1>350 THEN A8=100:GOTO 3335
3330 A8=(4.13/(ABS(F1-63)^2+1.1)+.19/(ABS(F1-118.7)^2+2))*F1^2*.001
3335 ATMOS=P1*A8
3340 RETURN
```

NOT USED

AMP DISP FADE

$$O1 = 0.002088 \cdot \left(10^{\left(\frac{-F9}{20}\right)}\right)^2 \cdot F1 \cdot P1^{3} \cdot T4^{-1.27} \cdot R3$$

F9 = FADE MARGIN

F1 = FRQ = GHz

P1 = PATH, km

T4 = ROUGHNESS, m

R3 = CLIMATE FACTOR LO

```
3500 REM   ***********BEARINGS & DISTANCE
3505 REM OUTPUT    H=HEADING(DEGREES)      P1=DISTANCE(KILOMETERS)
3510 PRINT:PRINT"            *BEARINGS & DISTANCE*"
3515 PRINT"     SOUTH LATITUDES ENTER AS -VE"
3520 PRINT"     EAST LONGITUDES ENTER AS -VE"
3525 PI#=3.1415927#:FLAG2=1
3530 INPUT"     TERMINAL A    LAT,LONG :";AA1,AA2
3535 A1#=AA1/360*2*PI#
3540 A2#=AA2/360*2*PI#
3545 INPUT"     TERMINAL B    LAT,LONG :";BB1,BB2
3550 B1#=BB1/360*2*PI#
3555 B2#=BB2/360*2*PI#
3560 A3#=B2#-A2#
3565 A4#=SIN(A1#)*SIN(B1#)+COS(A1#)*COS(B1#)*COS(A3#)
3570 A5#=SQR(1-A4#*A4#)
3575 A6#=A5#/A4#:A7#=ATN(A6#)
3580 IF A6#<0# THEN 3585 ELSE 3590
3585 A7#=PI#+A7#
3590 D#=60*360*A7#/(2*PI#)
3595 P1=D#*1.853:S=D#*1.152
3600 H1#=(SIN(B1#)-SIN(A1#)*COS(A7#))/(SIN(A7#)*COS(A1#))
3605 IF H1#*H1#=1# THEN H2#=0# ELSE H2#=SQR(1#-H1#*H1#)
3610 H3#=H2#/H1#
3615 H4=ATN(H3#)
3620 IF H3<0 THEN 3625 ELSE 3630
3625 H4=PI+H4
3630 H5=H4*57.2957795#
3635 IF SIN(A3)<0 THEN H=H5 ELSE H=360-H5
3640 GOTO 795
```

```
3800 REM    ****B*U*R*G*E*R*****PATH GEOMETRY
3805 CLS:PRINT"PROGRAM       ***RADLNK***          PATH GEOMETRY & EVALUATION"
3810 PRINT:PRINT:PRINT:PRINT:PRINT TAB(22)"1 - ENTER PATH PROFILE"
3815 PRINT TAB(22)"2 - ENTER SUPPORT HEIGHTS"
3820 PRINT TAB(22)"3 - PLOT A3 SIZE":PRINT TAB(22)"4 - PLOT A4 SIZE"
3825 PRINT TAB(22)"5 - PRINT PATH INFORMATION":PRINT TAB(22)"6 - GROUND/SEA REFL
ECTION ANALYSIS"
3830 PRINT TAB(22)"7 - EXIT TO MAIN MENU":PRINT:PRINT
3835 QX$=INKEY$:IF QX$="" THEN 3835
3840 IF VAL(QX$)<1 OR VAL(QX$)>7 THEN 3835
3845 SOUND 100,1:IF VAL(QX$)=7 THEN RETURN
3850 IF VAL(QX$)=3 THEN U5=80:U6=80 ELSE U5=35:U6=50
3860 ON VAL(QX$) GOSUB 4200,4000,5200,5200,5000,6500
3865 GOTO 3805
```

```
4000 REM  ********************SUPPORT HEIGHTS
4005 CLS:PRINT"PROGRAM       ***RADLNK***          STATION SUPPORT HEIGHT [AGL]"
4010 PRINT:PRINT"EXISTING SUPPORT HEIGHT AT  ";N1$;TAB(44);" =";D1;" M   [A]"
4015 PRINT"EXISTING SUPPORT HEIGHT AT  ";N2$;TAB(44);" =";D2;" M   [B]"
4020 PRINT:INPUT"HEIGHT OF STATION  [A]  SUPPORT      (M)";QX$
4025 IF QX$="" THEN 4030 ELSE D1=ABS(VAL(QX$))
4030 INPUT"HEIGHT OF STATION  [B]  SUPPORT      (M)";QX$
4035 IF QX$="" THEN 4040 ELSE D2=ABS(VAL(QX$))
4040 RH2=4.12*(SQR(D1)+SQR(D2))
4045 PRINT"<RADIO HORIZON  (SMOOTH EARTH) =";RH2;" KM"
4050 GOSUB 4100                                        WAIT
4055 RETURN
```

```
4100 REM       *************************WAIT
4105 FOR COUNT=1 TO 655:NEXT COUNT
4110 RETURN
```

Horizon Smooth ~~Some~~

$$4.12\left(\sqrt{D1}+\sqrt{D2}\right)$$

```
4200 REM ******************PATH PROFILE ENTRY
4205 CLS:PRINT"PROGRAM       ***RADLNK***          CONTOUR PROFILE ENTRY  [ASL]"
4210 PRINT:PRINT:PRINT"THE HEIGHT OF EACH STATION (ABOVE DATUM) IS ENTERED"
4215 PRINT"AT ZERO DISTANCE FROM STATION [A]. STATION [B] DATUM HEIGHT"
4220 PRINT"IS ENTERED AT THE ACTUAL PATH LENGTH DISTANCE":PRINT
4225 IF P1<=.0003 THEN INPUT"DISTANCE BETWEEN TERMINALS   (KM) ";P1 ELSE PRINT"P
ATH DISTANCE = ";P1;" KM"
4230 PRINT:PRINT"<EDIT PATH DATA >   Y/N"
4235 QX$=INKEY$:IF QX$="" THEN 4235
4240 IF QX$="Y" THEN GOSUB 4500
4245 PRINT:PRINT"TYPE 'EXIT' WHEN ALL DATA POINTS ARE ENTERED":PRINT
4250 PRINT"DATA POINT ";N+1:INPUT"     DISTANCE  FROM  [A]   KM ";QX$
4255 IF QX$="" THEN 4250
4260 IF QX$="EXIT" THEN 4290
4265 IF VAL(QX$)<0 OR VAL(QX$)>(P1+.001) THEN PRINT"<ERROR>":SOUND 88,3:GOTO 425
0 ELSE N=N+1
4270 XD(N)=VAL(QX$)
4275 INPUT"     HEIGHT AT THIS POINT   M ";YD(N)
4280 PRINT:PRINT
4285 GOTO 4250
4290 FOR J=1 TO N                                   'ORDER INPUT DATA
4295 FOR I=2 TO N
4300 IF XD(I)>XD(I-1) THEN 4320
4305 DUMPX=XD(I-1):DUMPY=YD(I-1)
4310 XD(I-1)=XD(I):YD(I-1)=YD(I)
4315 XD(I)=DUMPX:YD(I)=DUMPY
4320 NEXT I
4325 NEXT J
4330 RETURN
```

```
4500 REM  ****************PATH DATA EDITOR
4505 CLS:PRINT"PROGRAM       ***RADLNK***          PATH PROFILE DATA EDITOR"
4510 PRINT:PRINT"POINT","DIST","HEIGHT"
4515 FOR I=1 TO N:PRINT I,XD(I),YD(I):NEXT I
4520 PRINT:PRINT"(E)DIT  (R)ESET  E(X)IT"
4525 QX$=INKEY$:IF QX$="" THEN 4525
4530 IF QX$="R" THEN 4560
4535 IF QX$="E" THEN INPUT"INPUT POINT,DIST,HEIGHT";J,XJ,YJ ELSE 4290
4540 IF J>N OR J<0 THEN PRINT"<ERROR>":SOUND 88,4:GOTO 4505
4545 IF XD(J)>P1+.0001 THEN PRINT"<ERROR>":SOUND 88,4:GOTO 4505
4550 IF XD(J)<0 THEN PRINT"<ERROR>":SOUND 88,4:GOTO 4505 ELSE XD(J)=XJ:YD(J)=YJ
4555 GOTO 4505
4560 FOR I=1 TO N
4565 XD(I)=0:YD(I)=0
4570 NEXT I
4575 FOR I=1 TO 101
4580 X(I)=0:Y(I)=0:RF(I)=0
4585 NEXT I
4590 N=0
4595 RETURN
```

```
4700 REM  ***************DEFAULT  VALUES
4705 CLS:PRINT"PROGRAM       ***RADLNK***          DEFAULT PARAMETERS SET"
4710 PRINT:PRINT:PRINT"RMS ROUGHNESS (M) ";TAB(40);T46;TAB(55);
4715 INPUT QX$
4720 IF QX$="" THEN 4725 ELSE T46=ABS(VAL(QX$))
4725 PRINT:PRINT"K FACTOR           ";TAB(40);KF;TAB(55);
4730 INPUT QX$
4735 IF QX$="" THEN 4740 ELSE KF=VAL(QX$)
4740 IF KF<.4 THEN KF=.6
4745 IF KF>10 THEN KF=10
4750 PRINT:PRINT"RAINFALL RATE PERCENTILE DATA ";TAB(40);R44;TAB(55);
4755 INPUT QX$
4760 IF QX$="" THEN 4765 ELSE R44=ABS(VAL(QX$))
4765 PRINT:PRINT"RAINFALL BASED MONTH OR YEAR  M/Y ";TAB(42);R4$;TAB(55);
4770 INPUT QX$
4775 IF QX$="" THEN 4785
4780 IF QX$="Y" OR QX$="M" THEN R4$=QX$:GOTO 4785 ELSE PRINT"<ERROR>":SOUND 88,3
:GOTO 4765
4785 RETURN
```

```
5500 REM    **********DOT JOINING - DATA FILL
5505 PRINT              'NYQUIST SAMPLING OF INPUT DATA
5510 FOR I=1 TO 101:X(I)=0:Y(I)=0:RF(I)=0:NEXT I:PRINT"<WAIT>"
5515 FOR I=1 TO U5+1
5520 KN=0
5525 FOR J=1 TO N
5530 X(I)=R*(I-1)
5535 IF ABS(XD(J)-X(I))<.51*R AND KN=0 THEN Y(I)=YD(J):KN=1:GOTO 5545
5540 IF ABS(XD(J)-X(I))<.51*R AND KN=1 THEN Y(I+1)=YD(J)
5545 NEXT J
5550 NEXT I
5555 I=0
5560 REM    DOT JOINING
5565 I=I+1
5570 IF I>U5+1 THEN PRINT"<DOT    JOINING      COMPLETE>":RETURN
5575 IF Y(I)=0 THEN 5565
5580 J=I
5585 J=J+1
5590 IF J>U5+1 THEN 5600
5595 IF Y(J)=0 THEN 5585
5600 FOR K=I TO J-2
5605 Y(K+1)=Y(K)-(Y(I)-Y(J))/(J-I)
5610 NEXT K
5615 I=J-1
5620 GOTO 5565
```

```
5700 REM    ********************EARTH BULGE
5705 REM    PERFORMED AT  K
5710 FOR I=2 TO U5
5715 DS=P1/U5*(I-1)
5720 Y(I)=Y(I)+(DS*P1-DS*DS)/(KF*12.74)
5725 NEXT I
5730 PRINT"<EARTH BULGE ADJUSTMENT COMPLETE>"
5735 RETURN
```

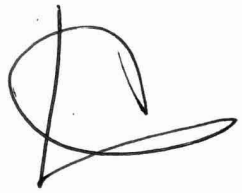

```
5800 REM    ******************RMS ROUGHNESS
5805 M=0:B=0:C=0:T=0
5810 FOR I=2 TO U5
5815 RF(I)=D1+(D1-D2)/(I/U5)-Y(I)
5820 NEXT I
5825 FOR I=2 TO U5
5830 C=C+RF(I):B=B+RF(I)*RF(I)
5835 NEXT I
5840 M=C/U5:V=(B-U5*M*M)/(U5-1):T46=SQR(V)
5845 PRINT"<RMS   ROUGHNESS   COMPLETE> ";T46
5850 REM    ******************RAYLINE CLEARANCE
5855 FOR I=1 TO 101:RF(I)=0:NEXT I
5860 RF(1)=D1:RF(U5+1)=D2
5865 FOR I=2 TO U5
5870 RF(I)=I*(D2+Y(U5+1)-D1-Y(1))/U5+D1+Y(1)-Y(I)
5875 NEXT I
5880 PRINT"<RAYLINE CLEARANCE COMPLETE>"
5885 RETURN
```

U5 = NUMBER OF X VALUE IN PLOT

D1 =
D2 = SUPPORT HEIGHT

RF = SURFACE ROUGH

Y = PLOTTER DATA

RMS

```
6000 REM   ********************SCALING PLOT
6005 Y1=Y(1):Y2=Y(1)
6010 FOR I=1 TO U5+1
6015 IF(Y1-Y(I))<=0 THEN 6030 ELSE 6020
6020 Y1=Y(I)                                          'MINIMUM Y DATA
6025 GOTO 6040
6030 IF (Y2-Y(I))<0 THEN 6035 ELSE 6040
6035 Y2=Y(I)                                          'MAXIMUM Y DATA
6040 NEXT I
6045 IF Y2<(Y(1)+D1) THEN Y2=Y(1)+D1
6050 IF Y2<(Y(U5+1)+D2) THEN Y2=Y(U5+1)+D2
6055 IF (Y2-Y1)>120 THEN KK=.04 ELSE KK=.2
6060 Y1=INT(KK*(Y1-2.6))/KK
6065 Y2=CINT(KK*(Y2+2.6)+.85)/KK
6070 YD=Y2-Y1
6075 PRINT"<PLOT   SCALING    COMPLETE>"
6080 RETURN
```

```
5200 REM    ********************PLOTTER
5205 IF Y2>850 THEN Z$="#####." ELSE Z$="###.# "
5210 L=YD/U6:WIDTH "LPT1:",100
5215 OPEN "LPT1:" FOR OUTPUT AS #1
5220 W=1:PRINT"<PLOTTING   PATH    PROFILE>"
5225 PRINT #1,"TERRAIN PROFILE  ";N1$;" TO ";N2$
5230 PRINT #1," ":PRINT #1,TAB(10);"HEIGHT (M)";TAB(U6+14);"CLR"
5235 FOR U=0 TO U6/10:PRINT #1,TAB(U*9+8+U-1);:PRINT #1,USING Z$;U*10*L+Y1;
5240 NEXT U:PRINT #1," "
5245 PRINT #1,TAB(10);:FOR I=1 TO U6/5:PRINT #1,"+----";:NEXT I:PRINT #1,"+"
5250 FOR I=1 TO U5+1
5255 GOSUB 4100                                          'WAIT
5260 PRINT #1,MID$("KILOMETERS",W,1);:PRINT #1,TAB(2);:PRINT #1,USING "###.##";X
(I);:
5265 IF I=1 THEN 6310
5270 IF I=U5+1 THEN 6325
5275 PRINT #1,TAB(9)"I";TAB((Y(I)-Y1)/L+10.5);">";TAB(U6+11);"I";
5280 PRINT #1,USING Z$;RF(I)
5285 W=W+1:NEXT I
5290 PRINT #1,TAB(10);:FOR I=1 TO U6/5:PRINT #1,"+----";:NEXT I:PRINT #1,"+"
5295 PRINT #1,USING "          K FACTOR = ##.##";KF;:PRINT #1,USING "    RMS ROUG
HNESS = ####.##";T46
5300 PRINT #1," ":PRINT #1," ":PRINT #1," ":CLOSE #1:WIDTH "LPT1:",80
5305 RETURN
5310 PRINT #1,TAB(9)"I";TAB((Y(I)-Y1)/L+10.5);">";TAB((Y(I)+D1-Y1)/L+11.5);"*";T
AB(U6+11);"I";
5315 PRINT #1,USING Z$;RF(I)
5320 GOTO 6285
5325 PRINT #1,TAB(9)"I";TAB((Y(I)-Y1)/L+10.5);">";TAB((Y(I)+D2-Y1)/L+11.5);"*";T
AB(U6+11);"I";
5330 PRINT #1,USING Z$;RF(I)
5335 GOTO 6285
```

```
7000 REM  **************************PROFILE SCAN FOR ILLUMINATED REGION
7005 Z$="ILLUMINATED PATH"
7010 ALF=SQR(30000/10^(G1/10))/2                    'HALF 3DB BEAMWIDTH
7015 BET=SQR(30000/10^(G2/10))/2                    'HALF 3DB BEAMWIDTH
7020 HA=SIN(P1*8.980001E-03)*(6380.43+Y(1)+D1)
7025 HB=SIN(P1*8.980001E-03)*(6380.43+Y(U5+1)+D2)
7030 HA=ATN(HA/SQR(ABS(1-HA*HA)))*180/3.14159
7035 HB=ATN(HB/SQR(ABS(1-HB*HB)))*180/3.14159
7040 FOR I=1 TO U5+1
7045 THET1=ATN(X(I)/(Y(1)+D1-Y(I)))                 'ANGLE TO GND POINT
7050 IF THET1>HB-BET THEN 7060
7055 X1=I+1
7060 THET2=ATN((P1-X(I))/(Y(U5+1)+D2-Y(I)))         'ANGLE TO GND POINT
7065 IF THET2<HA-ALF THEN 7075
7070 X2=I-1
7075 NEXT I
7080 IF X1>=X2 THEN X1=0:X2=0:Z$="NON EXISTANT"
7085 PRINT"<ANT PROFILE SCAN COMPLETE>"
7090 RETURN

7500 REM  **************************END
7505 CLS:SOUND 88,6:END
```

G1 = ANT GAIN dBI

Dispersive Fade Margin

Dispersive fade margin (DFM) is a measure of the robustness of a digital microwave radio receiver to spectrum distortions ("standing waves") caused by the interaction of refractive or reflective multipath signals with the direct (desired) signal. For uniformity, the DFM for all digital microwave radios marketed in the U.S. are characterized using Rummler's model, a multipath signal delayed 6.3 nsec (about 6.3 ft. longer) compared to the direct signal.

As a general rule, a link DFM > 50 dB will have not impact upon path performance (outage or quality). However, if geometry calculations from the path profile reveal multipath (reflective) signal longer than about 10-20 nsec, as between mountain top sites with excessive clearance, the DFM rapidly lowers with multipath delay. This will degrade performance (increase RBER, ESs, and outage SESs) unless the amplitude of the multipath signal is lowered with adequate antenna discrimination. For example, if the multipath signal is delayed 30 nsec, the radio DFM degrades to 33 dB and a total of about 20 dB (10 dB at each end) of antenna discrimination is required to optimize path performance (link DFM = radio DFM + antenna discriminations). The multipath delay on most "flat land" microwave paths is < 2 nsec, equating to an inconsequential > 60 dB DFM

If the DFM is > 50 dB, it is power added to the thermal fade margin (TFM, to 10^-3 BER) to derive the composite fade margin of the link in the absence of interference. Assuming TFM = 40 dB and DFM = 45 dB (10 nsec echo),

$$\begin{aligned} CFM &= -\log(10^{(-TFM/10)} + 10^{(-DFM/10)}) \\ &= -\log(10^{(-40/10)} + 10^{(-45/10)}) \\ &= 39 \text{ dB} \end{aligned}$$

Good engineering practice aims to obtain the largest possible dispersive fade margin without countermeasures and to add them as required and as consistent with a favorable trade-off between transmission performance and cost-effectiveness.

Source: Harris - Farinon Division

$$CFM = -\log \cdot 10^{\frac{-TFM}{10}} + 10^{\frac{-DFM}{10}}$$

$$= -\log \cdot 10^{\frac{-40}{10}} + 10^{\frac{-45}{10}}$$

$$= 39 \text{ dB}$$

TFM = 40
DFM = 45

meters = feet * 0.3048
6371.22 kms = earth radius
PI = 4 * atn(1) = 3.14159265358979

Source: ESSA Technical Report ERL 79-ITS 67, Page 3-1

Fade Margin

Fade margin is the dB difference between the receiver threshold level and the unfaded received signal level (RSL). RSL is the sum of transmitter and receiver system gains and losses including free space path loss. Typical fade margins are 20 dB for VHF / UHF links and 35 to 40 dB for microwave links.

Example: Receiver Threshold: -113 dBm
Unfaded RSL: -88.57 dBm
Fade Margin = -88.57 + -113
= 24.43 dB Fade Margin

Free Space Path Loss (Propagation loss between isotropic antennas)

The Free Space Path loss calculation assumes the use of a theoretical point-source or isotropic antenna at each end of the path. Radio frequency (RF) energy is radiated uniformly in all directions at the transmitting end while the receiving antenna provides no directivity.

The basic transmission loss in free space is:

$L = 20 \log (4\pi r / \lambda)$
$= 32.45 + 20 \log f + 20 \log r$ dB

R in miles:	Lfs	= 20 log R	+ 20 log Freq	+ 36.6
R in miles:	Lfs	= 20 log R	+ 20 log Freq	+ 96.6
R in kilometers:	Lfs	= 20 log R	+ 20 log Freq	+ 32.4
R in kilometers:	Lfs	= 20 log R	+ 20 log Freq	+ 92.4

The constant 32.45 is derived from $20 \log (4\pi r / \lambda)$:

$20 \log (4\pi r / \lambda) = 20 \log (12.56637061 / 0.2997925)$
$= 32.447782$

where the antenna separation r is expressed in kilometers and the free space wavelength λ equals 0.2997925 / f kilometers for a radio frequency in megahertz. Free space propagation velocity equals 299.8 x 10^6 meters/second (0.2998 x 10^-3 meters/nanosecond).

Therefore:

where frequency = gigahertz
distance = kilometers
$20 \log (4\pi r / \lambda) = 20 \log (12.56637061 / 0.0002997925)$
$= 92.44779649$
$= 92.45$

where frequency = megahertz
distance = miles
0.186291059 = 0.2997925 * 0.6214

A value of K = 2/3 produces a larger earth bulge than does a value of K = 4/3

Elevation Angle - Horizon

The Horizon Elevation Angle of an obstruction may be determined using the following equations:

e1 = ((0.001 * (hL1 - hS1) / dL1) - (dL1 / (2 * a)) radians

e2 = ((0.001 * (hL2 - hS2) / dL2) - (dL2 / (2 * a)) radians

where:

a is the effective earth's radius in kilometers
hS1, hS2 are the antenna heights above sea level in meters
hL1, hL2 are the heights in meters above sea level of the horizon obstacles
dL1, dL2 are the great circle distances in kilometers from each antenna to its' horizon

Example:

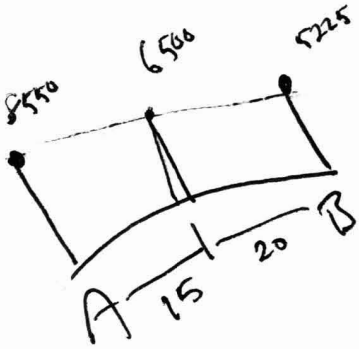

a = 6371.22		earths radius -kms
hS1 = 8550 * 0.3048		Site A antenna height - AMSL - meters
hL1 = 6500 * 0.3048		Distant obstacle height - AMSL - meters
hS2 = 5225 * 0.3048		Site B antenna height - AMSL - meters
hL2 = 6500 * 0.3048		Distant obstacle height - AMSL - meters
dL1 = 15 * 1.609		Path distance - kms - Site A to obstacle
dL2 = 20 * 1.609		Path distance - kms - Site B to obstacle

From Site A to Obstacle

```
if dL1 >= 0.9 then
  e1 = ((0.001 * (hL1 - hS1)) / dL1) - (dL1 / (2 * a))   radians
  e1 = e1 * 180 / PI                                     convert radians to
degrees
else
  e1 = 90

e1 = -1.591874 degrees
```

From Site B to Obstacle

```
if dL2 >= 0.9 then
  e2 = ((0.001 * (hL2 - hS2)) / dL2) - (dL2 / (2 * a))   radians
  e2 = e2 * 180 / PI                                     convert radians to
degrees
else
  e2 = 90

e2 = 0.5472335 degrees
```

Conversions and constants
kms = miles * 1.609

dBu (Field Intensity - Field Strength)

Electric field intensity or field strength is measured in free space (***independent*** of a receiver's antenna gain) in a linear scale in microvolts per meter. Electric field intensity is often expressed in the unit of dBu which stands for dB relative to a field intensity of 1 microvolt per meter; it does not mean dB below 1 microvolt of rms voltage (which equals -106.98 in a 50-ohm system). (Source: Land-Mobile Radio System Engineering)

Electric field intensity in dBu (decibels referenced to 1 μV/m):

dBu = EIRP - 20 log Distance + 106.92 in a 50-ohm system

Digital Radio Noise Figure (NF) and Noise Levels

N = Digital receiver thermal noise floor, dBm
= -114 + 10 log BW + NF

where BW = Receiver noise bandwidth, MHz (Symbol or baud rate, Mbaud)
= Data rate / modulation efficiency (6 bps / Hz for 64 QAM)
= 47 Mbps / 6 bps/Hz = 7.8 MHz (Mbaud)

NF = 5 dB (from radio specifications)

Example: -100 = -114 + 10 log 7.8 + 5

BW: Bandwidth in MHz
NF: Noise figure at the antenna port, dB

(Source: Harris - Farinon Division)

DATA RATE = 47 Mbps
MODULATION EFF = 6 bps/Hz

$\frac{47 \times 10^6 \text{ bps}}{6 \times 10^0 \frac{\text{bps}}{\text{Hz}}} = \frac{47 \text{ Mbps}}{6 \frac{\text{bps}}{\text{Hz}}} \approx 7.8 \text{ MHz}$ (Mbaud)

$7.8 \times 10^6 \frac{1}{\text{Hz}}$

Earth Curvature - K

The degree and direction of bending of a radio wave can be defined by an equivalent earth radius factor, K. This factor, K, multiplied by the actual earth r;radius, R, is the radius of a fictitious earth curve. The curve is equivalent to the relative curvature of the radio beam with respect to the curvature of the earth. K is equal to the curvature of the actual earth minus the curvature of the actual beam of radio frequency energy. K = 1 is the true earth's radius.

The curvature for various values of K can be calculated from the following relationship:

h = (d1 * d2) / (1.5 * K)

Where

h = the change in vertical distance from a horizontal reference line, in feet
d1 = the distance from a point to one end of the path, in miles
d2 = the distance from the same point to the other end of the path, in miles
K = the equivalent earth radius factor

Some common values of K are:

K = Infinity - a completely flat earth
K = 4/3 - a generally flat earth with some curvature
K = 1 - curved earth representing the earth's true radius
K = 2/3 - a smaller curved earth

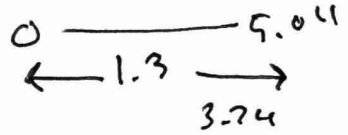

Formulas

Antenna Transmission Line Loss and Efficiency

Attenuation of RF power along an transmission line varies with the frequency and the type of transmission line. Transmission line loss is expressed as Loss / 100 feet or Loss / 100 meters. The efficiency of a transmission line is expressed as Efficiency (%) = 100 / (10 ^(Loss / 10))

Loss = Line Length (feet or meters) * Line Loss / 100

Example: Line Length = 78 feet
Line Loss per 100 feet = 0.951

Loss = 78 * 0.951 / 100
Loss = 0.74178

Efficiency = 100 / (10^(0.74178 / 10))
Efficiency = 84.298

Antenna Beam Tilt - Microwave

The upward and downward beam tilt of a microwave antenna (parabola) can be calculated using the following equation:

Beam Tilt (degrees) = Atn(ABS(Hs1 - Hs2) / Pd)

where:

Hs1, Hs2 are the antenna heights above sea level in meters or feet
Pd is the path distance in feet or meters



Example:

Hs1 = 8480 + 70	Site A elevation - AMSL + antenna height AGL - feet
Hs2 = 5170 + 55	Site B elevation - AMSL + antenna height AGL - feet
Pd = 33.79	Path distance between Site 1 and Site 2 - Miles

1.07 (degrees) = Atn (3325 / (33.79 * 5280))

Beam Tilt at Site 1: -1.07 degrees
Beam Tilt at Site 2: +1.07 degrees

dBd

Antenna gain referenced to a half-wave dipole. Antenna gain (Gt or Gr) is expressed in units of dBi or dBd. Antennas used in land mobile radio applications often have their gain expressed in units of dBd. Microwave radio communications often use antenna gains expressed in units of dBi.

Note: Free space path loss is in units of dBi. This means antenna gains must be referenced to an isotropic antenna when calculating system gains and losses. Common FCC practice references antenna gains to a half-wave dipole (dBd). When an antenna gain is in units of dBd, the antenna has a gain of 2.15 dB over an isotropic antenna, assuming equal antenna efficiencies. Thus, path loss must be decreased by 4.30 dB when using dBd gain units because two antennas are involved, one for transmitting and one for receiving. (Source: Land-Mobile Radio System Engineering)

dBi = dBd + 2.15
dBd = dBi - 2.15

Example: Transmitter Antenna Gain (Gt) = 10 dBd
Gt = Gt + 2.15
Gt = 12.15 dBi

---

dBi

Antenna gain referenced to an isotropic radiator. A theoretical antenna that radiates the same energy level in all directions. Antenna gain (Gt or Gr) is expressed in units of dBi or dBd. Antennas used in land mobile radio applications often have their gain expressed in units of dBd. Microwave radio communications often use antenna gains expressed in units of dBi.

Note: Free space path loss is in units of dBi. This means antenna gains must be referenced to an isotropic antenna. Common FCC practice references antenna gains to a half-wave dipole (dBd). When an antenna gain is in units of dBd, the antenna has a gain of 2.15 dB over an isotropic antenna, assuming equal antenna efficiencies. Thus, path loss must be decreased by 4.30 dB when using dBd gain units because two antennas are involved, one for transmitting and one for receiving. (Source: Land-Mobile Radio System Engineering)

dBi = dBd + 2.15
dBd = dBi - 2.15

Example: Receiver Antenna Gain (Gr) = 10 dBi
Gr = Gr - 2 .15
Gr = 7.85 dBd

---

dBm to Microvolts (rms)

dBm = -106.98
*uV = SQRT(EXP((dBm - 30) / 10) * R) / 0.000001*

Example: dBm = 30 (1 watt)
R = 50 ohms
*uV = SQRT(EXP((30 - 30) / 10) * 50) / 0.000001*
uV = 7,071,169.076

In Visual Basic, this formula would be written as:
uV = SQR(EXP((dBm - 30) / 10 * log(10)) * R) / 0.000001

20 log (4πr / λ) = 20 log (12.56637061 / 0.186291059)
= 36.58035705
= 36.60

where frequency = gigahertz
distance = miles
0.186291059 = 0.2997925 * 0.6214 * .001
20 log (4πr / λ) = 20 log (12.56637061 / 0.000186291059)
= 96.58035705
= 96.60

Fresnel Zone - F

A cigar-shaped shell of circular cross section surrounding the direct path between a transmitter and a receiver. For the first Fresnel zone, the distance from the transmitter to any point on this shell and on to the receiver is one-half wavelength longer than the direct path, for the second Fresnel zone, two half-wavelengths, etc.

For the first Fresnel zone: Fe = 72.1 * (SQRT(d1 * d2) / (f * D))

For any Fresnel zone directly: Fn = 72.1 * n * (SQRT(d1 * d2) / (f * D))

where
F(1)(n)= first or nth Fresnel zone radius in feet
d1 = distance from one end of the path to reflection point in miles
D = total length of path in miles
d2 = D - d1
f = frequency in GHz

$$72.1 \cdot n \cdot \sqrt{\frac{d_1 \cdot d_2}{f_{GHz} \cdot D}}$$

Kilometers to Miles

miles = kms * 0.6214

Microvolts (rms) to dBm

P = E^2 / R
P = 10 log (E^2 / R) + 30

Example: E = 1μV (rms)
R = 50 ohms
P = 10 log ((1^-12) / 50) + 30
P = -106.9897

$1\mu V = 1 \times 10^{-6}$

$$10 \cdot \log\left[\frac{(1\times10^{-6})^2}{50}\right] + 30$$

$$10 \cdot \log\left[\frac{1\times10^{-12}}{50}\right] + 30$$

Microvolts / meter (μV/m) - Electric Field Intensity or Field Strength

Electric field intensity or field strength is measured in free space (***independent*** of a receiver's antenna gain) on a linear scale in microvolts per meter. Electric field intensity is often expressed in the unit of dBu which stands for dB relative to a field intensity of 1 microvolt per meter; it does not mean dB below 1 microvolt of rms voltage (which equals -106.98 in a

50-ohm system). (Source: Land-Mobile Radio System Engineering)

Electric field intensity in dB (decibels referenced to 1 μV/m):

dBu = $EIRP_{dBk}$ - 20 log Distance + 106.98 in a 50-ohm system

Field strength and received voltage may also be expressed as a function of received voltage, receiver antenna gain, the receiver antenna impedance, and frequency.

$\mathcal{E}_{(dB\mu V/m)}$ = 20 log μV - Gr + 20 log F - 29.8 in a 50-ohm load
$\mathcal{E}_{(dB\mu V/m)}$ = 20 log μV - Gr + 20 log F - 31.4 in a 72-ohm load
$\mathcal{E}_{(dB\mu V/m)}$ = 20 log μV - Gr + 20 log F - 37.3 in a 300-ohm load

Received voltage is calculated as:

$E_{(dB\mu V)}$ = 20 log μV/m + Gr - 20 log F + 29.8 in a 50-ohm load
$E_{(dB\mu V)}$ = 20 log μV/m + Gr - 20 log F + 31.4 in a 72-ohm load
$E_{(dB\mu V)}$ = 20 log μV/m + Gr - 20 log F + 37.3 in a 300-ohm load

Field strength and Received Voltage is calculated as:

$P_{(dBm)}$ = $E_{(dB\mu V)}$ - 106.98 in a 50-ohm load

$P_{(dBm)}$ = 20 log μV/m + Gr - 20 log F - 106.98 + 29.8 in a 50-ohm load
$P_{(dBm)}$ = 20 log μV/m + Gr - 20 log F - 108.57 + 31.4 in a 72-ohm load
$P_{(dBm)}$ = 20 log μV/m + Gr - 20 log F - 114.77 + 37.3 in a 300-ohm load

For different antenna impedances, use the following formula:

10 log (antenna impedance) + 12.8

Example: 29.78 = 10 log 50 + 12.8 (antenna impedance = 50 ohms)

Miles to Kilometers

kms = miles * 1.609
kms = miles * 1.853

Watts (watts, milliwatts, kilowatts, dBW, dBm, dBk)

Radio frequency output of a transmitter (P) or the power output at the transmitter antenna terminals (Pt).

$P_{(dBW)}$	= 10 log $P_{(watts)}$	Power in dB relative to one watt
$P_{(dBm)}$	= 10 log $P_{(milliwatts)}$	Power in dB relative to one milliwatt
$P_{(dBm)}$	= 10 log $P_{(watts)}$ + 30	Power in dB relative to one milliwatt
$P_{(dBk)}$	= 10 log $P_{(kilowatts)}$	Power in dB relative to one kilowatt
$P_{(dBk)}$	= 10 log $P_{(watts)}$ - 30	Power in dB relative to one kilowatt

Radio Propagation for Vehicular Communications

KENNETH BULLINGTON, FELLOW, IEEE

Abstract—Radio propagation is affected by many factors including the frequency, distance, antenna heights, curvature of the earth, atmospheric conditions, and the presence of hills and buildings. The influence of each of these factors at frequencies above about 30 MHz is discussed with most of the quantitative data being presented in the series of nomograms. By means of three or four of these charts an estimate of the received power and the received field intensity for a given point-to-point radio transmission path ordinarily can be obtained in a minute or less. The theory of propagation over a smooth spherical earth is presented in a simplified form that is made possible by restricting the frequency range to above about 30 MHz where variations in the electrical constants of the earth have only a secondary effect. The empirical methods used in estimating the effects of hills and buildings and of atmospheric refraction are compared with experimental data on shadow losses and on fading ranges.

I. INTRODUCTION

METHODS of calculating ground-wave propagation over a smooth spherical earth have been given by Burrows and Gray and by Norton for all values of distance, frequency, antenna height, and ground constants [1], [2]. These two methods are different in form but they give essentially the same results. Both methods are relatively simple to use at the lower frequencies where grounded antennas are in common use, but their complexity increases as the frequency increases. At frequencies above 30 or 40 MHz, elevated antennas are in common use and the radio path loss between two horizontal antennas tends to be equal to the loss between two vertical antennas. In addition, both types of transmission tend to be independent of the electrical constants of the ground so that considerable simplification is possible. This paper presents a series of nomograms that have been found useful in solving radio propagation problems in the very-high-frequency range and above. These charts are arranged so that radio transmission can be expressed in terms of either the received field intensity or the received power delivered to a matched receiver. The field-intensity concept may be more familiar, but the power-transfer concept becomes more convenient as the frequency is increased.

In addition to the smooth earth theory an approximate method is included for estimating the effects of hills and other obstructions in the radio path. The phenomena of atmospheric refraction (bending away from straight-line propagation), atmospheric ducts (tropospheric propagation), and atmospheric absorption are discussed briefly, but the principal purpose is to provide simplified charts for predicting radio propagation under average weather conditions. It is expected that normally the nomograms will provide the desired answer directly without any additional computation except the addition of the dB values obtained from three or four individual charts. The basic formulas are presented as an aid to understanding the principles involved and as a more accurate method should one be required. This paper does not consider sky-wave propagation although ionospheric reflections may occur at frequencies above 30 MHz and may cause occasional long-distance interference between systems operating on the same frequency.

A convenient starting point for the theory of radio propagation is the condition of two antennas in free space, which is discussed in terms of both received field intensity and received power. Since most radio paths cannot be considered to be free-space paths the next step is to determine the effect of a perfectly flat earth, and this is followed by the effect of the curvature of the earth. After the basic smooth-earth theory is completed there is a discussion of the variations in received power caused by atmospheric conditions and by irregularities on the earth surface, but the methods used in predicting these factors are necessarily less exact than the data for a smooth spherical earth in a uniform atmosphere.

II. FREE-SPACE FIELD

A free-space transmission path is a straight-line path in a vacuum or in an ideal atmosphere and sufficiently removed from all objects that might absorb or reflect radio energy. The free-space field intensity E_0 at a distance d meters from the transmitting antenna is given by

$$E_0 = \frac{\sqrt{30 g_1 P_1}}{d} \text{ V/m} \tag{1}$$

where P_1 is the radiated power in watts and g_1 is the power-gain ratio of the transmitting antenna. The subscript 1 refers to the transmitter and the subscript 2 will refer to the receiver. For an ideal (isotropic) antenna that radiates power uniformly in all directions $g = 1$. For any balanced antenna in free space (or located more than a quarter-wavelength above the ground) g is the power-gain ratio of the antenna relative to the isotropic antenna. A small doublet or dipole whose overall physical length is short compared with a half-wavelength has a directivity gain of $g = 1.5$ (1.76 dB), and a half-wave dipole has a gain of $g = 1.64$ (2.15 dB) in the direction of maximum radiation. In other directions of transmission the field is reduced in accordance with the free-space antenna pattern obtained from

Manuscript received January 3, 1977. This invited paper consists of selections from two earlier papers written by the author. Only minor changes have been made in keeping with uniformity and standardized methods of expressing parameters, e.g., MHz, dBW, and μV/m. The papers are "Radio Propagation at Frequencies Above 30 Megacycles," PROCEEDINGS OF THE IRE, vol. 35, no. 10, pp. 1122-1136, October 1947 (also presented at National Electronics Conference, October 1946), and "Radio Propagation Fundamentals," *Bell System Technical Journal*, vol. 36, no. 3, 593-626, May 1957. Reprinting is by permission of the IEEE, the *Bell System Technical Journal*, and the National Electronics Conference, an activity of National Engineering Consortium, Inc.

The author is with Bell Laboratories, Holmdel, NJ 07733.

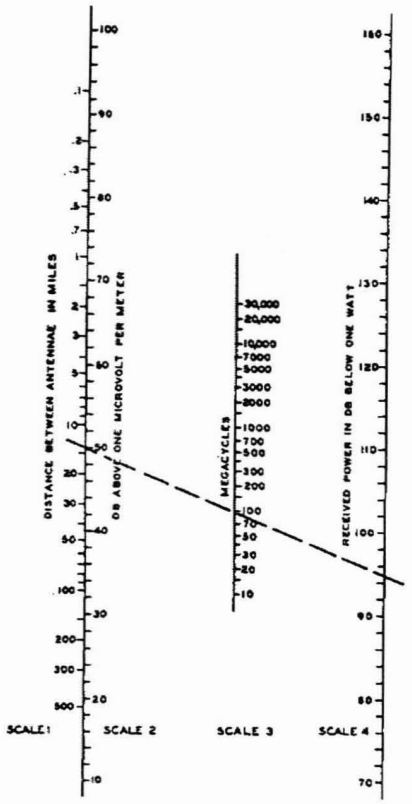

Fig. 1. Free-space field intensity and received power between half-wave dipoles, 1 W radiated.

theory or measurement. Consequently, the freespace field intensity in a direction perpendicular to a half-wave dipole is

$$E_0 = \sqrt{\frac{30 \times 1.64 P_1}{d}} \sim 7\sqrt{\frac{P_1}{d}}. \tag{2}$$

This field intensity in μV/m for 1 W of radiated power is shown on scale 2 of Fig. 1 as a function of the distance in miles shown on scale 1. For radiated power of P W the correction factor to apply to the field intensity or power is 10 log P (dB). For example, the free-space field intensity at 100 mi from a half-wave dipole radiating 1 W is 33 dBμV/m (about 45 μV/m). When the radiated power is 50 W (17 dBW) the received field intensity is 33 + 17 = 50 dBμV/m (about 315 μV/m). It will be noted that the field intensity is related to the energy density of the radio wave at the receiving antenna but is independent of the type of the receiving antenna.

The directivity gain of an array of n dipoles (sum of driven and parasitic elements) of optimum design is approximately equal to n times the gain of one dipole although some allowance should be made for antenna power losses. The theoretical power-gain ratio of a horn, paraboloid, or lens antenna whose aperture has an area of B m^2 is $g = 4\pi B/\lambda^2$; however, the effective area is frequently taken as one-half to two-thirds of the actual area of the aperture to account for antenna inefficiencies.

III. RELATION BETWEEN THE RECEIVED POWER AND THE RADIATED POWER

Before discussing the modifications in the free-space field that result from the presence of the earth, it is convenient to show the relation between the received field intensity (which is not necessarily equal to the free-space field intensity) and the power that is available to the receiver. The maximum useful power P_2 that can be delivered to a matched receiver is given by

$$P_2 = \left(\frac{E\lambda}{2\pi}\right)^2 \frac{g_2}{120} \text{ W} \tag{3}$$

where

- E received field intensity in volts per meter,
- λ wavelength in meters = $300/F$,
- F frequency in megacycles,
- g_2 power-gain ratio of the receiving antenna.

This relation between received power and the received field intensity is shown by scales 2-4 in Fig. 1 for a half-wave dipole. For example, the maximum useful power at 100 MHz that can be picked up by a half-wave dipole in a field of 50 dBμV/m is -95 dBW.

A general relation for the ratio of the received power to the radiated power obtained from (1) and (3) is

$$\frac{P_2}{P_1} = \left(\frac{\lambda}{4\pi d}\right)^2 g_1 g_2 \left(\frac{E}{E_0}\right)^2. \tag{4}$$

When both antennas are half-wave dipoles, the power transfer ratio is

$$\frac{P_2}{P_1} = \left(\frac{1.64\lambda}{4\pi d}\right)^2 \left(\frac{E}{E_0}\right)^2 = \left(\frac{0.13\lambda}{d}\right)^2 \left(\frac{E}{E_0}\right)^2 \tag{4a}$$

and is shown in Fig. 1 for free-space transmission ($E/E_0 = 1$).

When the antennas are horns, paraboloids, or multi-element arrays, a more convenient expression for a ratio of the received power to the radiated power is given by

$$\frac{P_2}{P_1} = \frac{B_1 B_2}{(\lambda d)^2} \left(\frac{E}{E_0}\right)^2 \tag{4b}$$

where B_1 and B_2 are the effective areas of the transmitting and receiving antennas, respectively. This relation is obtained from (4) by substituting $g = 4\pi B/\lambda^2$ and is shown in Fig. 2 for free-space transmission when $B_1 = B_2$. For example, the free-space loss at 4 GHz between two antennas of 10 ft^2 effective area is about 72 dB for a distance of 30 mi.

IV. TRANSMISSION OVER PLANE EARTH

The presence of the ground modifies the generation and the propagation of the radio waves so that the received field inten-

sity is ordinarily less than would be expected in free space. The ground acts as a partial reflector and as a partial absorber, and both of these properties affect the distribution of energy in the region above the earth. The principal effect of plane earth on the propagation of radio waves is indicated by the following equation [4], [5]:

$$E = E_0[\underbrace{1}_{a)} + \underbrace{Re^{j\Delta}}_{b)} + \underbrace{(1-R)Ae^{j\Delta}}_{c)} + \underbrace{\cdots}_{d)}]. \tag{5}$$

where a) is the direct wave, b) is the reflected wave, c) is the surface wave, and d) is the induction field and secondary effects of the ground. R is the reflection coefficient of the ground and is approximately equal to -1 when the angle θ between the reflected ray and the ground is small. The commonly used concept of a *perfectly conducting* earth, for which the reflection coefficient for vertical polarization is $+1$ for any angle of incidence, may cause some misunderstanding at this point. In practice the principal interest is in low angles, and as the angle θ approaches zero the reflection coefficient approaches -1 for any finite value for the conductivity of the earth, even if it were made of solid copper. The magnitude and phase of the reflection coefficient can be computed from the following equation[1]:

$$R = \frac{\sin\theta - z}{\sin\theta + z} \tag{6}$$

where

$z = \sqrt{\epsilon_0 - \cos^2\theta}/\epsilon_0$ for vertical polarization,

$z = \sqrt{\epsilon_0 - \cos^2\theta}$ for horizontal polarization,

$\epsilon_0 = \epsilon - j60\sigma\lambda$,

[1] It will be noted that for vertical polarization this expression agrees with the data given by Burrows and subsequently included in [20], but for horizontal polarization it is the negative of that given in these references. This change was necessary in order to make (5) and (6) independent of polarization. The pseudo-Brewster angle frequently mentioned in the literature occurs when the reflection coefficient is a minimum and is approximately equal to the value of θ for which $\sin\theta = |z|$; this occurs with vertical polarization only, since $z > 1$ for horizontal polarization. The reflection coefficient is sometimes modified by a divergence factor to give a first approximation of the effect of the curvature of the earth, but this additional complication does not seem essential here. The effect of the curvature of the earth is discussed in the next section, and for conditions of frequency and antenna height where some interpolation is required the possible variations due to atmospheric conditions are usually greater than the error introduced by the omission of the divergence factor. The measured data on the plane-earth reflection coefficient agrees reasonably well with the theoretical values at frequencies below about 1000 MHz. At higher frequencies the magnitude of the reflection coefficient is sometimes less than 1 presumably due to multiple reflections from the irregularities on the earth's surface. Measured values as low as -0.2 at 10 000 MHz over rolling country have been reported by W. M. Sharpless. The low value of reflection coefficient is not expected to be important for ground-to-ground transmission, but it tends to smooth the lobes that occur in the high-angle radiation, hence, may be important in air-to-ground transmission.

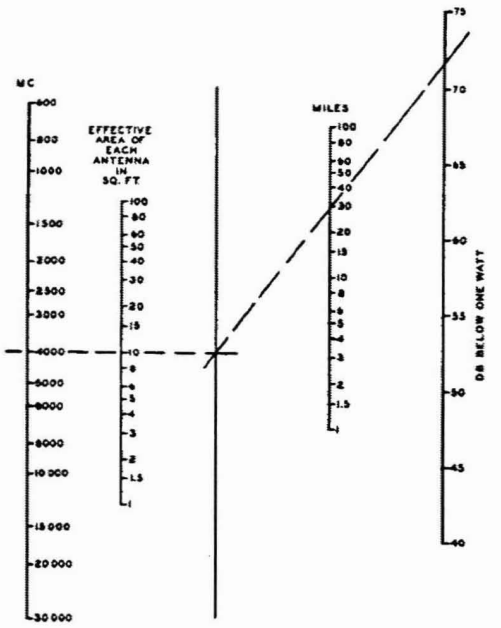

Fig. 2. Received power in free space between two antennas of equal effective areas, 1 W radiated.

ϵ dielectric constant of the ground relative to unity in free space,

σ conducitivity of the ground in mhos per meter,

λ wavelength in meters,

$j = \sqrt{-1}$,

$e^{j\Delta} = \cos\Delta + j\sin\Delta$.

The surface-wave attenuation factor A depends upon the frequency, ground constants, and type of polarization. It is never greater than unity and decreases with increasing distance and frequency as indicated by the following approximate equation[2]:

$$A \cong \frac{-1}{1 + j\dfrac{2\pi d}{\lambda}(\sin\theta + z)^2}. \tag{7}$$

The angle Δ used in (5) is the phase difference in radians resulting from the difference in the length of the direct and reflected rays. It is equal to $4\pi h_1 h_2/\lambda d$ radians when the distance d between antennas is greater than about five times the sum of the two antenna heights h_1 and h_2.

The effect of the ground shown in (5) indicates that ground-wave propagation may be considered to be the sum of three principal terms; namely, the direct wave, the reflected wave, and the surface wave. The first two types correspond to our common experience with visible light, but the surface

[2] This approximate expression is sufficiently accurate as long as $A < 0.1$, and it gives the magnitude of A within about 2 dB for all values of A. However, as A approaches unity, the error in phase approaches 180 deg. More accurate values are given by Norton, where in his nomenclature $A = f(P, B)e^{i\phi}$.

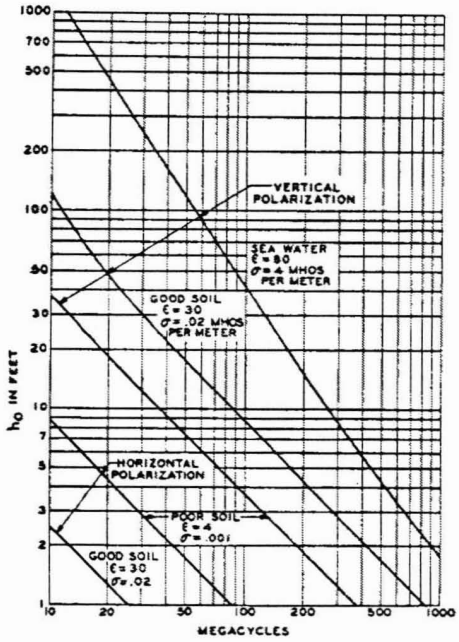

Fig. 3. Minimum effective height.

wave is less familiar. Since the earth is not a perfect reflector some energy is transmitted into the ground and is absorbed. As this energy enters the ground it sets up ground currents, which is another way of saying that the distribution of the electromagnetic field in the region near the surface of the earth is distorted relative to what it would have been over an ideal perfectly reflecting surface. The surface wave is defined as the vertical electric field for vertical polarization, or the horizontal electric field for horizontal polarization that is associated with these ground currents.[3]

The practical importance of the surface wave is limited to a region above the ground of about one wavelength over land or five to ten wavelengths over sea water since for greater heights the sum of the direct and reflected waves is larger in magnitude. Thus the surface wave is the principal component of the total ground wave at frequencies less than a few megahertz, but it is of secondary importance in the very high-frequency range (30 to 300 MHz) and it usually can be neglected at frequencies above 300 MHz.

A physical picture of the various components of the ground wave can be obtained from (5), but an equivalent expression which is more convenient for this discussion, is

$$\frac{E}{E_0} = 2 \sin \frac{\Delta}{2} + j[(1+R) + (1-R)A]e^{j(\Delta/2)}. \tag{8}$$

When the angle $\Delta = 4\pi h_1 h_2/\lambda d$ is greater than about 0.5 radian the terms inside the brackets (which include the surface wave) are usually negligible, and a sufficiently accurate approximation is given by

$$\frac{E}{E_0} = 2 \sin \frac{2\pi h_1 h_2}{\lambda d}. \tag{8a}$$

In this case, the principal effect of the ground is to produce interference fringes or lobes so that the field intensity, at a given distance and for a given frequency, oscillates around the free-space field as either antenna height is increased.

When the angle Δ is less than about 0.5 rad the receiving antenna is below the maximum of the first lobe, and the surface wave may be important. A sufficiently accurate approximation for this condition is[4]

$$\left|\frac{E}{E_0}\right| = \left|\frac{4\pi h_1' h_2'}{\lambda d}\right|. \tag{8b}$$

In this equation $h' = h + jh_0$ where h is the actual antenna height and $h_0 = \lambda/2\pi z$ has been designated as the minimum effective antenna height. The magnitude of the minimum effective height $|h_0|$ is shown in Fig. 3 for sea water and for "good" and "poor" soil. "Good" soil corresponds roughly to clay, loam, marsh, or swamp while "poor" soil means rocky or sandy ground.

The surface wave is controlling for antenna heights less than the minimum effective height, and in this region the received field or power is not affected appreciably by changes in the antenna height. For antenna heights that are greater than the minimum effective height, the received field or power is increased approximately 6 dB every time the antenna height is doubled until free-space transmission is reached. It is ordinarily sufficiently accurate to assume that h' is equal to the actual antenna height or the minimum effective antenna height, whichever is the larger.

The ratio of the received power to the radiated power for transmission over plane earth is obtained by substituting (8b) into (4), resulting in

$$\frac{P_2}{P_1} = \left(\frac{\lambda}{4\pi d}\right)^2 g_1 g_2 \left(\frac{4\pi h_1' h_2'}{\lambda d}\right)^2 = \left(\frac{h_1' h_2'}{d^2}\right)^2 g_1 g_2. \tag{9}$$

This relation is independent of frequency and is shown in Figure 4 for half-wave dipoles ($g = 1.64$). A line through the two

[3] Another component of the electric field associated with the ground currents is in the direction of propagation. It accounts for the success of the wave antenna at lower frequencies, but it is always smaller in magnitude than the surface wave as defined above. The components of the electric vector in three mutually perpendicular coordinates are given by Norton.

[4] This approximate expression is obtained from (8) by assuming

$$\sin\theta = \frac{h_1 + h_2}{d} \ll z \tag{a}$$

$$\sin \frac{2\pi h_1 h_2}{\lambda d} = \frac{2\pi h_1 h_2}{\lambda d} \tag{b}$$

$$A = \frac{\lambda}{j2\pi d z^2}. \tag{c}$$

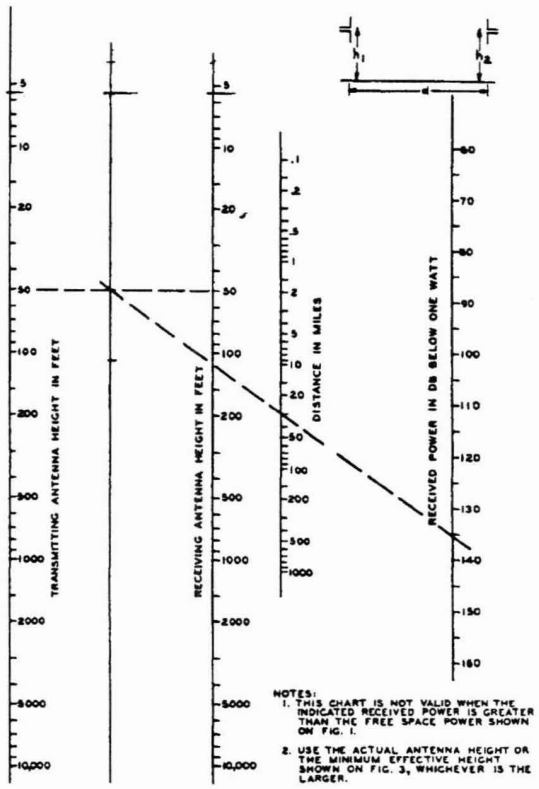

Fig. 4. Received power over plane earth between half-wave dipoles, 1 W radiated.

scales of antenna height determines the point on the unlabeled scale between them, and a second line through this point and the distance scale determines the received power for 1 W radiated. When the received field intensity is desired, the power indicated on Fig. 4 can be transferred to scale 4 of Fig. 1, and a line through the frequency on scale 3 indicates the received field intensity on scale 2. The results shown in Fig. 4 are valid as long as the value of received power indicated is lower than shown in Fig. 1 for free-space transmission. When this condition is not met, it means that the angle Δ is too large for (8b) to be accurate, and that the received field intensity or power oscillates around the free-space value as indicated by (8a).

As an example, consider a 250-W 30-MHz transmitter with both transmitting and receiving dipoles mounted 50 ft above the ground and separated by a distance of 30 mi over plane earth. The transmission loss is shown in Fig. 4 to be 135.5 dB. Since 250W is 24 dBW, the received power is $24 - 135.5 = -111.5$ dBW. (The free-space power transfer shown in Fig. 1 indicates a received power of $24 - 91 = -67$ dBW, so Fig. 4 is controlling.) The received field intensity can be obtained from Fig. 1, which shows that a received power of -111.5 dBW corresponds to a received field intensity of about 23 dBuV/m at a frequency of 30 MHz. Should one antenna be only 10 ft above "good" soil, rather than 50 ft, the minimum effective height of 30 ft shown in Fig. 3 should be used on one of the height scales in Fig. 4 in determining the transmission loss. It will be noted that this example assumes a perfectly flat earth. The curvature of the earth introduces an additional loss of about 4 dB, as discussed in the next section.

In addition to the effect of plane earth on the propagation of radio waves, the presence of the ground may affect the impedance of an antenna and thereby may have an effect on the generation and reception of radio waves. This effect usually can be neglected at frequencies above 30 MHz except where whip antennas are used. The impedance in the presence of the ground oscillates around the free-space value, but the variations are unimportant as long as the center of the antenna is more than a quarter-wavelength above the ground. A convenient method of showing the effect of the change in impedance of a balanced antenna near the ground is to replace the directivity gain g in the preceding formulas by the arbitrary factor of $g' = g/r$ where r is the ratio of the input resistance in the presence of the ground to the input resistance of the same antenna in free space. This assumes an impedance match between the antenna and the transmitting equipment with proper tuning to balance out any reactance.

For horizontal dipoles less than a quarter-wavelength above the ground the ratio r is less than unity. It approaches zero as the antenna approaches a perfectly conducting earth, but in practice it does not reach zero at zero height because of the finite conductivity of the earth. The wave antenna and the top-loaded antenna frequently used at lower frequencies are sometimes called horizontal antennas, but since they are used to radiate or receive vertically polarized waves they are not horizontal antennas in the sense used here.

For vertical half-wave dipoles the factor r is approximately equal to unity since the height of the center of the antenna can never be less than a quarter-wavelength above the ground. For very short vertical dipoles, however, the ratio r is greater than unity, and it approaches a value of $r = 2$ for antennas very near to the ground. This means that, whereas a short vertical dipole whose total length $2l$ is small compared with the wavelength that has an input radiation resistance of $80(\pi l/\lambda)^2$ Ω in free space, it has a resistance of $160(\pi l/\lambda)^2$ Ω near the ground.

Correct results for a vertical whip antenna working against a perfectly counterpoise are obtained by using $r = 2$. This means that a vertical whip antenna of length l is 3 dB less efficient than a dipole of length $2l$ (located more than a quarter-wavelength above the ground) for either transmitting or receiving. The poorer efficiency at the receiver is not important when external noise is controlling.

V. FADING PHENOMENA

Variations in signal level with time are caused by changing atmospheric conditions. The severity of the fading usually increases as either the frequency or path length increases. Fading cannot be predicted accurately, but it is important to distinguish between two general types: (1) inverse bending and (2) multipath effects. The latter includes the fading caused by interference between direct and ground reflected waves as well as interference between two or more separate paths in the atmosphere. Ordinarily, fading is a temporary diversion of energy to some other than the desired location.

The path of a radio wave is not a straight line except for the ideal case of a uniform atmosphere. The transmission path

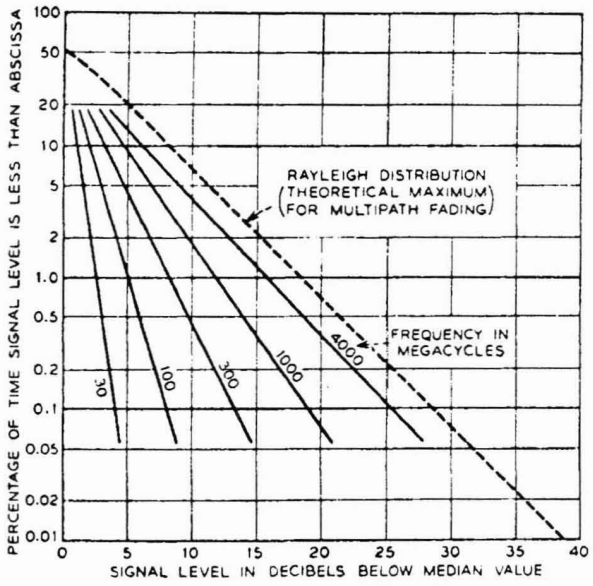

Fig. 5. Typical fading characteristics in the worst month on 30 to 40 mile line-of-sight paths with 50 to 100 ft clearance.

may be bent up or down depending on atmospheric conditions. This bending may either increase or decrease the effective path clearance and inverse bending may have the effect of transforming a line of sight path into an obstructed one. This type of fading may last for several hours. The frequency of its occurrence and its depth can be reduced by increasing the path clearance, particularly in the middle of the path.

Severe fading may occur over water or on other smooth paths because the phase difference between the direct and reflected rays varies with atmospheric conditions. The result is that the two rays sometimes add and sometimes tend to cancel. This type of fading can be minimized, if the terrain permits, by locating one end of the circuit high while the other end is very low. In this way the point of reflection is placed near the low antenna and the phase difference between direct and reflected rays is kept relatively steady.

Most of the fading that occurs on "rough" paths with adequate clearance is the result of interference between two or more rays traveling slightly different routes in the atmosphere. This multipath type of fading is relatively independent of path clearance, and its extreme condition approaches the Rayleigh distribution. In the Rayleigh distribution, the probability that the instantaneous value of the field is greater than the value R is exp $[-(R/R_0)^2]$ where R_0 is the rms value.

Representative values of fading on a path with adequate clearance are shown in Fig. 5. After the multipath fading has reached the Rayleigh distribution, a further increase in either distance or frequency increases the number of fades of a given depth, but it decreases the duration so that the product is the constant indicated by the Rayleigh distribution.

VI. TROPOSPHERIC TRANSMISSION BEYOND LINE OF SIGHT

A basic characteristic of electromagnetic waves is that the energy is propagated in a direction perpendicular to the surface of uniform phase. Radio waves travel in a straight line only as long as the phase front is plane and is infinite in extent.

Energy can be transmitted beyond the horizon by three principal methods: reflection, refraction, and diffraction. Reflection and refraction are associated with either sudden or gradual changes in the direction of the phase front, while diffraction is an edge effect that occurs because the phase surface is not infinite. When the resulting phase front at the receiving antenna is irregular in either amplitude or position, the distinctions between reflection, refraction, and diffraction tend to break down. In this case the energy is said to be scattered. Scattering is frequently pictured as a result of irregular reflections although irregular refraction plus diffraction may be equally important.

The following paragraphs describe first the theories of refraction and of diffraction over a smooth sphere and a knife edge. This is followed by empirical data derived from experimental results on the transmission to points far beyond the horizon, on the effects of hills and trees, and on fading phenomena.

Refraction

The dielectric constant of the atmosphere normally decreases gradually with increasing altitude. The result is that the velocity of transmission increases with the height above the ground, and on the average the radio energy is bent or refracted toward the earth. As long as the change in dielectric constant is linear with height, the net effect of refraction is the same as if the radio waves continued to travel in a straight line but over an earth whose modified radius is

$$ka = \frac{a}{1 + \frac{a}{2}\frac{d\epsilon}{dh}} \tag{10}$$

where

a true radius of earth,
$d\epsilon/dh$ rate of change of dielectric constant with height.

Under certain atmospheric conditions the dielectric constant may increase ($0 < k < 1$) over a reasonable height, thereby causing the radio waves in this region to bend away from the earth. Since the earth's radius is about 2.1×10^7 ft (6.4×10^6 m), a decrease in dielectric constant of only 2.4×10^{-8}/ft (7.9×10^{-8}/m) of height results in a value of $k = 4/3$, which is commonly assumed to be a good average value [6]. When the dielectric constant decreases about four times as rapidly (or by about 10^{-7} per foot (3.3×10^{-7}/m of height), the value of $k = \infty$. Under such a condition, as far as radio propagation is concerned, the earth can then be considered flat, since any ray that starts parallel to the earth will remain parallel.

When the dielectric constant decreases more rapidly than 10^{-7}/ft (3.3×10^{-7}/m) of height, radio waves that are radiated parallel to or at an angle above the earth's surface may be bent downward sufficiently to be reflected from the earth. After reflection the ray is again bent toward the earth, and the path of

a typical ray is similar to the path of a bouncing tennis ball. The radio energy appears to be trapped in a duct or waveguide between the earth and the maximum height of the radio path. This phenomenon is variously known as trapping, duct transmission, anomalous propagation, or guided propagation [7], [8]. It will be noted that in this case the path of a typical guided wave is similar in form to the path of sky waves, which are lower frequency waves trapped between the earth and the ionosphere. However, there is little or no similarity between the virtual heights, the critical frequencies, or the causes of refraction in the two cases.

Duct transmission is important because it can cause long distance interference with another station operating on the same frequency; however, it does not occur often enough nor can its occurrence be predicted with enough accuracy to make it useful for radio services requiring high reliability.

Diffraction over a Smooth Spherical Earth and Ridges

Radio waves are also transmitted around the earth by the phenomenon of diffraction. Diffractions is a fundamental property of wave motion, and in optics it is the correction to apply to geometrical optics (ray theory) to obtain the more accurate wave optics. In other words, all shadows are somewhat "fuzzy" on the edges, and the transition from "light" to "dark" areas is gradual rather than infinitely sharp. Our common experience is that light travels in straight lines and that shadows are sharp, but this is only because the diffraction effects for these very short wavelengths are too small to be noticed without the aid of special laboratory equipment. The order of magnitude of the diffraction at radio frequencies may be obtained by recalling that a 1000-MHz radio wave has about the same wavelength as a 1000-Hz sound wave in air so that these two types of waves may be expected to bend around absorbing obstacles with approximately equal facility.

The effect of diffraction around the earth's curvature is to make possible transmission beyond the line-of-sight. The magnitude of the loss caused by the obstruction increases as either the distance or the frequency is increased, and it depends to some extent on the antenna height [1]. The loss resulting from the curvature of the earth is indicated by Fig. 6 as long as neither antenna is higher than the limiting value shown at the top of the chart. This loss is in addition to the transmission loss over plane earth obtained from Fig. 4.

When either antenna is as much as twice as high as the limiting value shown in Fig. 6, this method of correcting for the curvature of the earth indicates a loss that is too great by about 2 dB with the error increasing as the antenna height increases. An alternate method of determining the effect of the earth's curvature is given by Fig. 7. The latter method is approximately correct for any antenna height, but it is theoretically limited in distance to points at or beyond the line-of-sight assuming that the curved earth is the only obstruction. Fig. 7 gives the loss relative to free-space transmission (and hence is used with Fig. 1) as a function of three distances: d_1 is the distance to the horizon from the lower antenna, d_2 is the distance to the horizon from the higher antenna, and d_3 is the distance beyond the line-of-sight. In other words, the total distance between antennas is $d = d_1 + d_2 + d_3$. The dis-

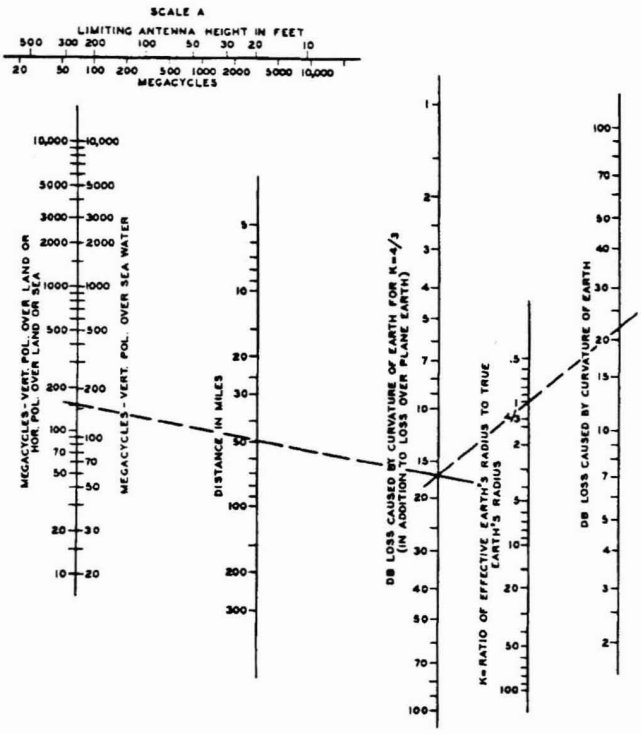

Fig. 6. Diffraction loss caused by curvature of the earth assuming neither antenna height is higher than shown on scale A.

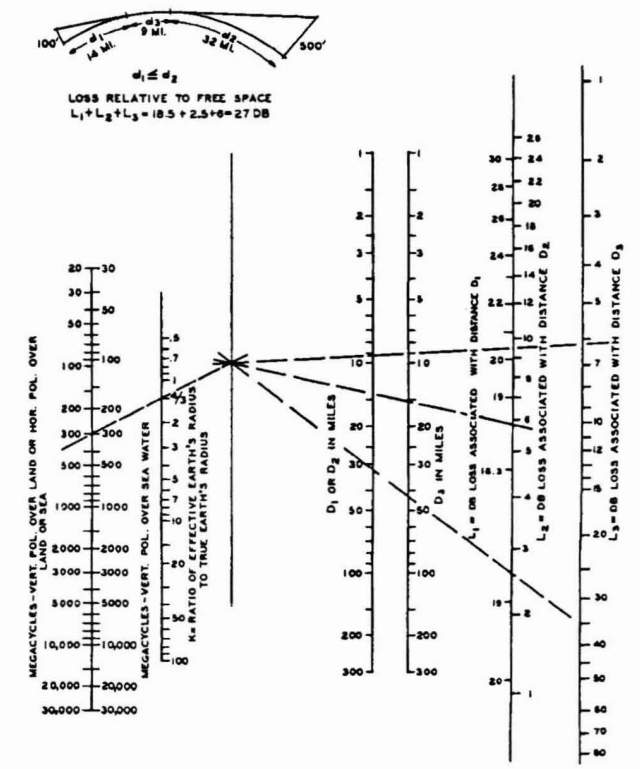

Fig. 7. Decibel loss relative to free-space transmission at points beyond line-of-sight over a smooth earth.

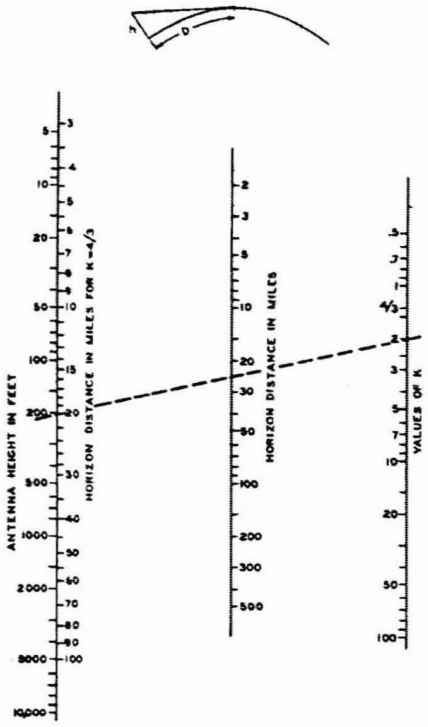

Fig. 8. Distance to horizon.

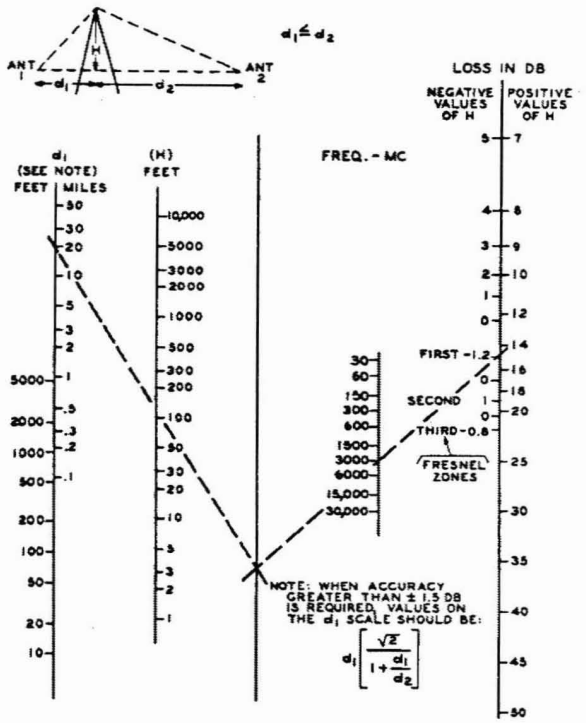

Fig. 9. Knife-edge diffraction loss relative to free space.

tance to the horizon over smooth earth is shown in Fig. 8 and is given by

$$d_{1,2} = \sqrt{2kah_{1,2}} \tag{11}$$

where $h_{1,2}$ is the appropriate antenna height and ka is the effective earth's radius.

The preceding discussion assumes that the earth is a perfectly smooth sphere, and the results are critically dependent on a smooth surface and a uniform atmosphere. The modification in these results caused by the presence of hills, trees, and buildings is difficult or impossible to compute, but the order of magnitude of these effects may be obtained from a perfectly absorbing knife edge.

The diffraction of plane waves over a knife edge or screen causes a shadow loss whose magnitude is shown in Fig. 9 The height of the obstruction H is measured from the line joining the two antennas to the top of the ridge. It will be noted that the shadow loss approaches 6 dB as H approaches 0 (grazing incidence), and that it increases with increasing positive values of H. When the direct ray clears the obstruction H is negative, and the shadow loss approaches 0 dB in an oscillatory manner as the clearance is increased. In other words, a substantial clearance is required over line-of-sight paths in order to obtain "free-space" transmission. The knife edge diffraction calculation is substantially independent of polarization as long as the distance from the edge is more than a few wavelengths.

At grazing incidence the expected loss over a ridge is 6 dB, (Fig. 9) while over a smooth sperical earth Fig. 7 indicates a loss of about 20 dB. More accurate results in the vicinity of the horizon can be obtained by expressing radio transmission in terms of path clearance measured in Fresnel zones as shown in Fig. 10. In this representation the plane earth theory and the ridge diffraction can be represented by single lines, but the smooth sphere theory requires a family of curves with a parameter M that depends primarily on antenna heights and frequency. The big difference in the losses predicted by diffraction around a perfect sphere and by diffraction over a knife edge indicates that diffraction losses depend critically on the assumed type of profile. A suitable solution for the intermediate problem of diffraction over a rough earth has not yet been obtained.

The problem of two or more knife-edge obstructions between the transmitting and receiving antennas such as shown in Fig. 11(a) has not been solved rigorously. However, graphical integration indicates that the shadow loss for this case is equivalent within 2 or 3 dB to the shadow loss for the knife edge represented by the height of the triangle composed of a line joining the two antennas and a line from each antenna through the top of the peak that blocks the line-of-sight from that antenna.

Thus far it has been assumed that the transmission between the two antennas would be approximately the same as in free space if the obstacles could be removed. This assumption is usually valid only at centimeter wavelengths, and at lower frequencies it is necessary to include the effects of waves reflected from the ground. This results in four paths, namely, MOQ, MOQ' $M'OQ$, and $M'OQ'$ shown in Fig. 11(b) for a single obstruction. Each of these paths is similar in form to the single path illustrated by Figure 11(a). The sum of the field intensi-

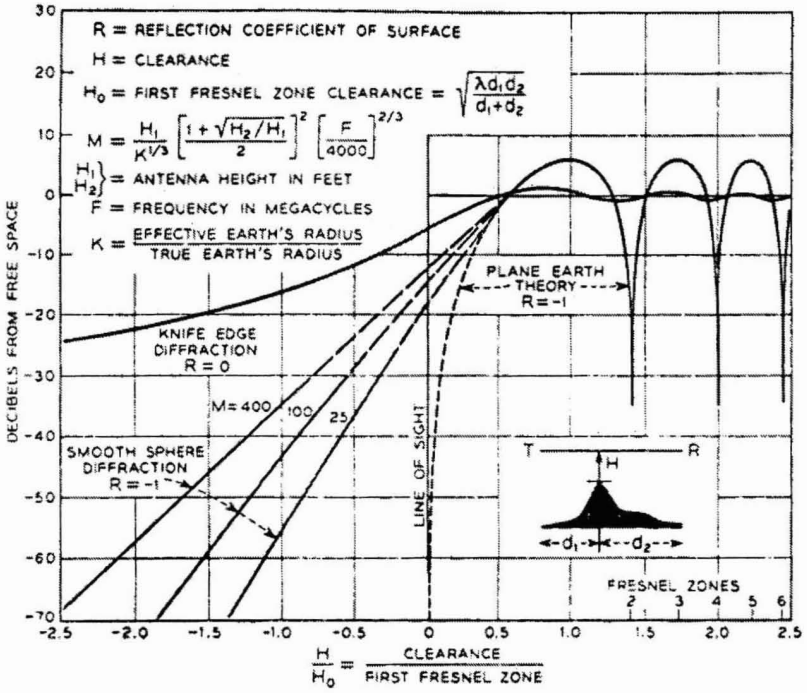

Fig. 10. Transmission loss versus clearance.

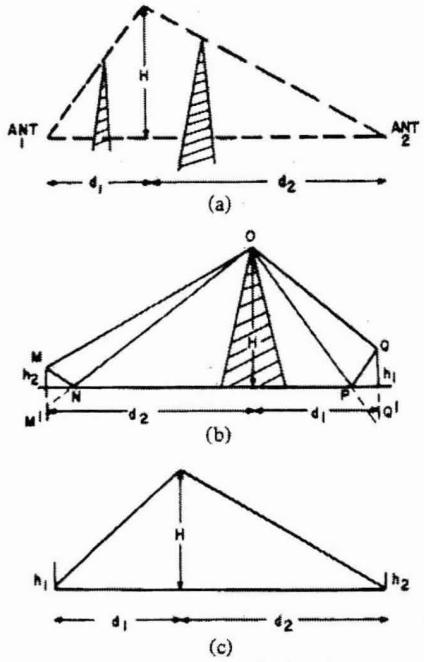

Fig. 11. Ideal profiles used in developing theory of diffraction over hills.

ties over these four paths, considering both magnitude and phase, is given by the following equation:

$$\left|\frac{E}{E_0}\right| = S_1\left[1 - \frac{S_2}{S_1}e^{-j(\Delta+b)} - \frac{S_3}{S_1}e^{-j(\Delta+c)} + \frac{S_4}{S_1}e^{-j(b+c)}\right] \tag{12}$$

where

E received field intensity,
E_0 free-space field intensity,
S_1 magnitude of the shadow loss over path MOQ,
S_2 magnitude of the shadow loss over path MOQ',
S_3 Magnitude of the shadow loss over path $M'OQ$,
S_4 Magnitude of the shadow loss over path $M'OQ'$,
Δ $=4\pi h_1 h_2/\lambda(d_1 + d_2)$ radians,
b approximately equal to $4\pi h_2 H/\lambda d_2$ rad,
c approximately equal to $4\pi h_1 H/\lambda d_1$ rad.

This equation assumes that the reflection coefficient is -1 and that the actual antenna heights are greater than the minimum effective antenna height h_0. This means that the surface wave is neglected, and the equation fails when either antenna height approaches zero. The angles b and c are phase angles associated with the diffraction phenomena, and the approximate values given above assume that H is greater than h_1 or h_2. This assumption permits the shadow losses to be averaged so that $S_1 = S_2 = S_3 = S_4 = S$. After several algebraic manipulations (12) can be reduced to

$$\left|\frac{E}{E_0}\right| = 2(2S)\left|\sin\frac{\Delta}{2}\cos\frac{b-c}{2} + j\left(\sin^2\frac{b+c}{4} - \sin^2\frac{b-c}{4}\right)e^{j(\Delta/2)}\right| \tag{13}$$

where S is the average shadow loss for the four paths. This means that the shadow triangle should be drawn from a point

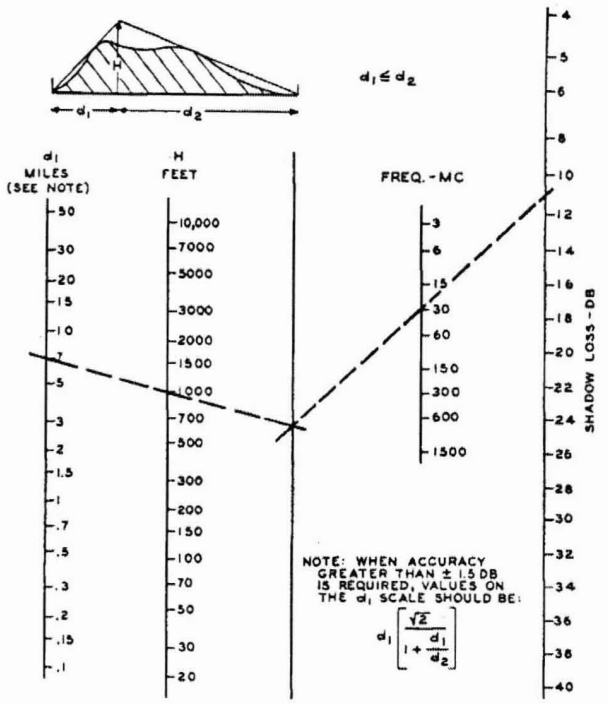

Fig. 12. Shadow loss relative to smooth earth.

midway between the location of the actual antenna and the image antenna as shown in Fig. 11(c). For small values of H this equation is approximately equal to

$$\left|\frac{E}{E_0}\right| = 2(2S)\sin\frac{\Delta}{2} \tag{14}$$

Since the field intensity over plane earth (assuming that the antenna heights are greater than the minimum effective height h_0) is $2E_0 \sin \Delta/2$, the first-order effect of the hill is to add a loss of 20 log $2S$ which is shown by the nomogram in Fig. 12. The complete expression given in (12) indicates that, under favorable conditions, the field intensity behind sharp ridges may be greater than over plane earth. This result has been found experimentally in a few cases, but the correlation between theory and experiment is not complete. In general, the field intensity predicted by either (12) or (13) tends to be too high; that is, shadow losses rather than gains occur on most of the paths on which measured data are available. The less-approximate expression given in (14) agrees more closely with experimental data, is more conservative, and is easier to use. Consequently, it is usually assumed that the effect of obstructions to line-of-sight transmission (at least in the 30- to 150-MHz range) is to introduce the loss shown in Fig. 12 in addition to the normal loss over smooth earth for the antenna heights and distances involved. Measured results on a large number of paths in the 30- to 150-MHz range indicate that about 50 percent of the paths are within 5 or 6 dB of the values predicted on this basis. The correlation on 10 percent of the paths is no better than 10 to 12 dB, and an occasional path may differ by 20 dB.

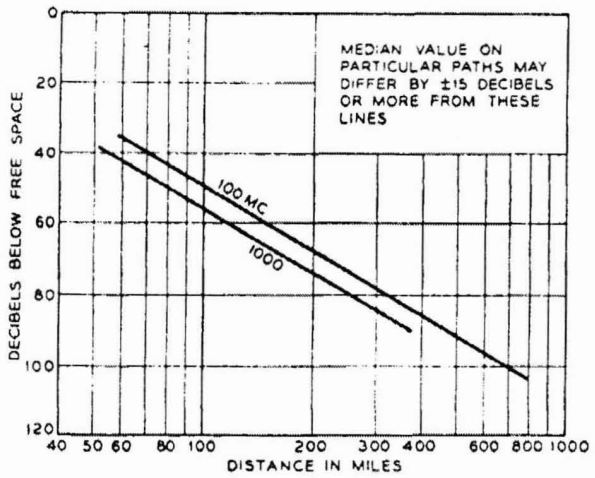

Fig. 13. Beyond-horizon transmission; median signal level versus distance.

VII. EXPERIMENTAL DATA FAR BEYOND THE HORIZON

Most of the experimental data at points far beyond the horizon fall in between the theoretical curves for diffraction over a smooth sphere and for diffraction over a knife edge obstruction. Various theories have been advanced to explain these effects, but none has been reduced to a simple form for every day use [9]. The explanation most commonly accepted is that energy is reflected or scattered from turbulent air masses in the volume of air that is enclosed by the intersection of the beamwidths of the transmitting and receiving antennas [10].

The variation in the long term median signals with distance has been derived from experimental results and is shown in Fig. 13 for two frequencies [11]. The ordinate is in decibels below the signal that would have been expected at the same distance in free space with the same power and the same antennas. The strongest signals are obtained by pointing the antennas at the horizon along the great circle route. The values shown in Fig. 13 are essentially annual averages taken from a large number of paths, and substantial variations are to be expected with terrain, climate, and season as well as from day to day fading.

Antenna sites with sufficient clearance so that the horizon is several miles away will on the average provide a higher median signal (less loss) than shown in Fig. 13. Conversely, sites for which the antenna must be pointed upward to clear the horizon will ordinarily result in appreciably more loss than shown in Fig. 13. In many cases the effects of path length and angles to the horizon can be combined by plotting the experimental results as a function of the angle between the lines drawn tangent to the horizon from the transmitting and receiving sites [12].

When the path profile consists of a single sharp obstruction that can be seen from both terminals, the signal level may approach the value predicted by the knife edge diffraction theory [13]. While several interesting and unusual cases have been recorded, the knife edge or "obstacle gain" theory is not applicable to the typical but only to the exceptional paths.

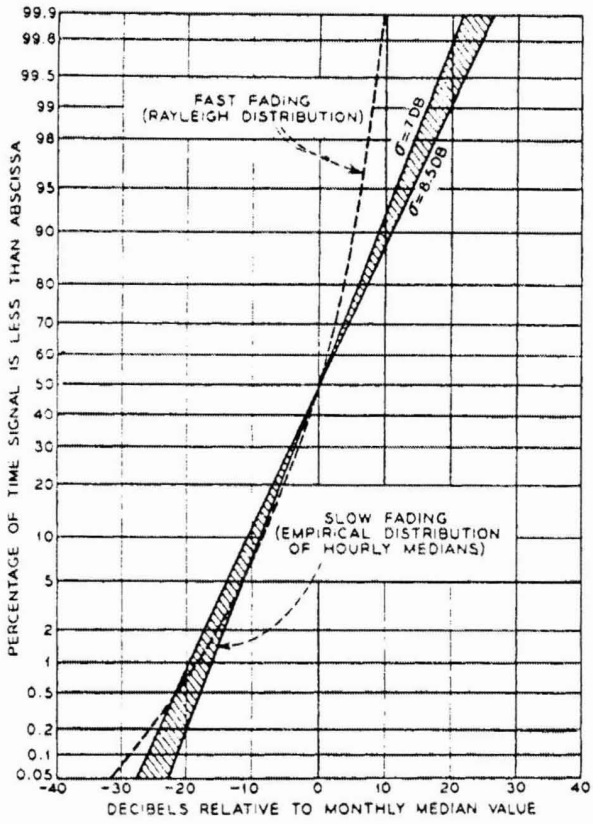

Fig. 14. Typical fading characteristics at points far beyond horizon.

As in the case of line-of-sight transmission the fading of radio signals beyond the horizon can be divided into fast fading and slow fading. The fast fading is caused by multipath transmission in the atmosphere, and for a given size antenna the rate of fading increases as either the frequency or the distance is increased. This type of fading is much faster than the maximum fast fading observed on line-of-sight paths, but the two are similar in principle. The magnitude of the fades is described by the Rayleigh distribution.

Slow fading means variations in average signal level over a period of hours or days, and it is greater on beyond horizon paths than on line-of-sight paths. This type of fading is almost independent of frequency and seems to be associated with changes in the average refraction of the atmosphere. At distances of 150 to 200 mi the variations in hourly median value around the annual median seem to follow a normal probability law in decibels with a standard deviation of about 8 dB. Typical fading distributions are shown in Fig. 14. The median signals levels are higher in warm humid climates than in cold dry climates, and seasonal variations of as much as ±10 dB or more from the annual median have been observed [14].

Since the scattered signals arrive with considerable phase irregularities in the plane of the receiving antenna, narrow-beamed (high gain) antennas do not yield power outputs proportional to their theoretical area gains. This effect has sometimes been called loss in antenna gain but it is a propagation effect and not an antenna effect. On 150- to 200-mi paths this loss in received power may amount to 1 or 2 dB for a 40-dB gain antenna, and perhaps 6 to 8 dB for a 50-dB antenna. These extra losses vary with time, but the variations seem to be uncorrelated with the actual signal level.

The bandwidth that can be used on a single radio carrier is frequently limited by the selective fading caused by multipath or echo effects. Echoes are not troublesome as long as the echo time delays are very short compared with one cycle of the highest baseband frequency. The probability of long delayed echoes can be reduced (and the rate of fast fading can be decreased) by the use of narrow beam antennas both within and beyond the horizon [13], [15]. Useful bandwidths of several megahertz appear to be feasible with the antennas that are needed to provide adequate signal-to-noise margins. Successful tests of television and of multichannel telephone transmission have been reported on a 188-mi path at 5 000 MHz [16].

The effects of fast fading can be reduced substantially by the use of either frequency or space diversity. The frequency or space separation required for diversity varies with time and with the degree of correlation that can be tolerated. A horizontal (or vertical) separation of about 100 wavelengths is ordinarily adequate for space diversity on 100- to 200-mi paths. The corresponding figure for the required frequency separation for adequate diversity seems likely to be more than 20 MHz.

VIII. EFFECTS OF NEARBY HILLS—PARTICULARLY ON SHORT PATHS

The experimental results on the effects of hills indicate that the shadow losses increase with the frequency and with the roughness of the terrain [17]. An empirical summary of the available data is shown in Fig. 15. The roughness of the terrain is represented by the height H shown on the profile at the top of the chart. This height is the difference in elevation between the bottom of the valley and the elevation necessary to obtain line-of-sight from the transmitting antenna. The right-hand scale in Fig. 15 indicates the additional loss above the expected over plane earth. Both the median loss and the difference between the median and the 10 percent values are shown. For example, with variations in terrain of 500 ft, the estimated median shadow loss at 450 MHz is about 20 dB, and the shadow loss exceeded in only 10 percent of the possible locations between points A and B is about $20 + 15 = 35$ dB. It will be recognized that this analysis is based on large-scale variations in field intensity and does not include the standing-wave effects which sometimes cause the field intensity to vary considerably within a few feet.

IX. EFFECTS OF BUILDINGS AND TREES

The shadow losses resulting from buildings and trees follow somewhat different laws from those caused by hills. Buildings may be more transparent to radio waves than the solid earth, and there is ordinarily much more back scatter in the city than in the open country. Both of these factors tend to reduce the shadow losses caused by the buildings, but on the other hand

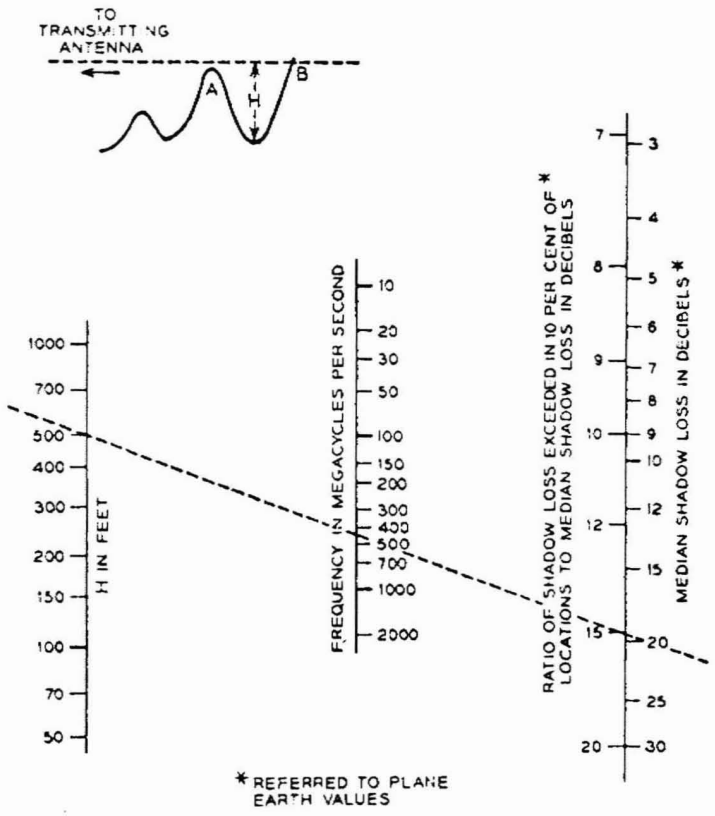

Fig. 15. Estimated distribution of shadow losses.

the angles of diffraction over or around the buildings are usually greater than for natural terrain. In other words, the artificial canyons caused by buildings are considerably narrower than natural valleys, and this factor tends to increase the loss resulting from the presence of buildings. The available quantitative data on the effects of buildings are confined primarily to New York City. These data indicate that in the range of 40 to 450 Mhz there is no significant change with frequency, or at least the variation with frequency is somewhat less than that noted in the case of hills [18]. The median field intensity at street level for random locations in Manhattan (New York City) is about 25 dB below the corresponding plane earth value. The corresponding values for the 10 percent and 90 percent points are about 15 and 35 dB, respectively. Typical values of attenuation through a brick wall are from 2 to 5 dB at 30 MHz and 10 to 40 dB at 3000 MHz depending on whether the wall is dry or wet. Consequently, most buildings are rather opaque at frequencies of the order of thousands of megahertz.

When an antenna is surrounded by moderately thick trees and below tree-top level, the average loss at 30 MHz resulting from the trees is usually 2 or 3 dB for vertical polarization and is negligible with horizontal polarization. However, large and rapid variations in the received field intensity may exist within a small area, resulting from the standing-wave pattern set up by reflections from trees located at a distance of several wavelengths from the antenna. Consequently, several nearby locations should be investigated for best results. At 100 MHz the average loss from surrounding trees may be 5 to 10 dB for vertical polarization and 2 or 3 dB for horizontal polarization. The tree losses continue to increase as the frequency increases, and above 300 to 500 MHz they tend to be independent of the type of polarization. Above 1000 MHz trees that are thick enough to block vision are roughly equivalent to a solid obstruction of the same overall size.

X. MINIMUM ALLOWABLE INPUT POWER

The effective use of the preceding data for estimating the received power requires a knowledge of the power levels needed for satisfactory operation since the principal interest is in the signal-to-noise ratio. The signal level required at the input to the receiver depends on several factors including the noise introduced by the receiver (called first-circuit or set noise), the type and magnitude of any external noise, the type of modulation, and the desired signal-to-noise ratio. A complete discussion of these factors is beyond the scope of this paper, but the fundamental limitations are listed below in order to show the order of magnitude. The theoretical minimum noise level is that set by the thermal agitation of the electrons, and its root-mean-square power in dBW is -204 dB plus 10 log (bandwidth) where (bandwidth) is approximately equal to twice the audio (or video) bandwidth [19]. The set noise of a typical receiver may be 5 to 15 dB higher than the theoretical minimum noise. The lower values in this range of "excess" noise are more likely to be met in the VHF range while the higher values are more probable in the SHF range. This means that the set noise in a 3000-Hz audio band

TABLE I
FIGURES TO USE

Type of Terrain	Both Antennas Lower in Height than Shown on Fig. 6	One or Both Antenna Heights Higher than Shown on Fig. 6	
		Within Line-of-Sight	Beyond Line-of-Sight
Plane earth	Fig. 4 or 1	Figs. 4 or 1 or 2	Figs. 1 or 2 and 7
Smooth earth	Figs. 4 and 6	Figs. 4 or 1 or 2	Figs. 1 or 2
Irregular terrain	Figs. 4, 6, 7 and 12	Figs. 4 and 12 or 1 or 2 and 9	Figs. 1 or 2, 7 and 12

may be −151 to −161 dBW. Measured data indicate that the carrier power needs to be 12 to 20 dB higher than the noise power to provide an average signal-to-noise ratio that is sufficient for moderate intelligibility. This assumes that the modulation level has been adjusted so that most of the peaks of speech power can be transmitted without causing overmodulation in the transmitter. It follows that the required input power for a single-channel voice circuit is of the order of −140 dBW, which is roughly equivalent to 1 μV across a 70 Ω input resistance. This limiting input power is approximately correct (within 3 or 4 dB) for both amplitude and frequency modulation since the radio-frequency signal-to-noise ratio must be above that required for marginal operation before the use of frequency modulation can provide appreciable improvement in the audio signal-to-noise ratio.

The input power must be greater than −140 dBW when circuits of above marginal quality or greater bandwidth are desired and when external noise rather than set noise is controlling. Man-made noise is frequently controlling at 30 MHz, but is less serious at 150 MHz. Above 500 MHz set noise is almost always controlling. For circuits requiring a high degree of reliability a margin should also be included for the fading range to be expected during adverse weather conditions.

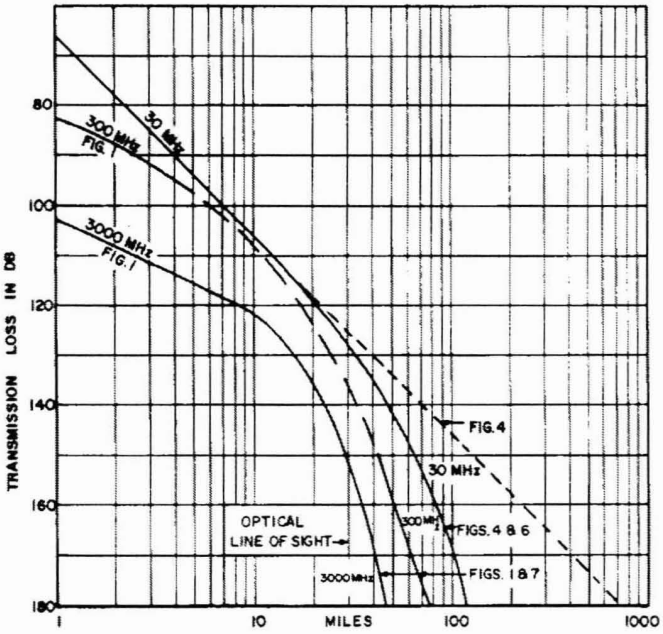

Fig. 16. Transmission over smooth earth at 30, 300, and 3000 MHz; half-wave dipoles at 250 and 30 ft.

XI. SUMMARY AND EXAMPLES

In any given radio propagation problem some of the factors described above are important, while others can be neglected. Table I indicates the figures that apply to any given situation.

Whenever Fig. 4 is used, reference should be made to Figs. 1 and 3 as a check on its proper use. When Fig. 12 is used in determining the effects of hills, the profile is usually drawn on rectangular coordinates (neglecting the earth's curvature), and the shadow triangle is drawn to the base of the antenna halfway between the antenna and its image). Curved coordinates are sometimes used, but they are not necessary since the loss caused by the curvature of the earth is either negligible or has already been considered in Figs. 6 or 7. Fig. 9 is used for determining the first-zone clearance and for estimating the shadow losses when the transmission without the obstruction is expected to be the same as in free space. In the latter case, the shadow triangle is drawn from the actual antennas, and curved coordinates are useful since the curvature of the earth should be included in the profile.. Various examples of the use of these figures have been given during the discussion of each individual chart, but further examples may help to illustrate the relations between the various figures. Assume a transmitting dipole located 250 ft above the ground and a receiving dipole on a 30 ft mast. The estimated transmission losses at 30, 300, and 3000 MHz over smooth earth are shown in Fig. 16 for $k = 4/3$ for various distances between these two dipoles. The solid lines indicate values obtained from the figures, and the dashed lines show the region where some interpolation is required.

The received power depends on the radiated power and the antenna-gain characteristics as well as on the transmission loss between dipoles. A typical 30-MHz transmitter may radiate 250 W so that at a distance of 30 mi the received power is 10 log 250 − 129 = −105 dBW. (The value of 129 dB is obtained from Fig. 16.) Similarly, a 300-MHz transmitter may radiate 50 W from a 5-dB gain antenna, and when a 5-dB gain receiving antenna is used the estimated received power at 30 mi is 10 log 50 + 5 + 5 − 137 = −110 dBW. At 3000 MHz the radiated power may be 0.1 W and antenna gains of 28 dB each are not uncommon, so the received power at 30 miles is 10 log 0.1 + 28 + 28 − 152 = −106 dBW. (The values of radiated power used in this example are not the maximum continuous-wave powers that can be obtained but the down-

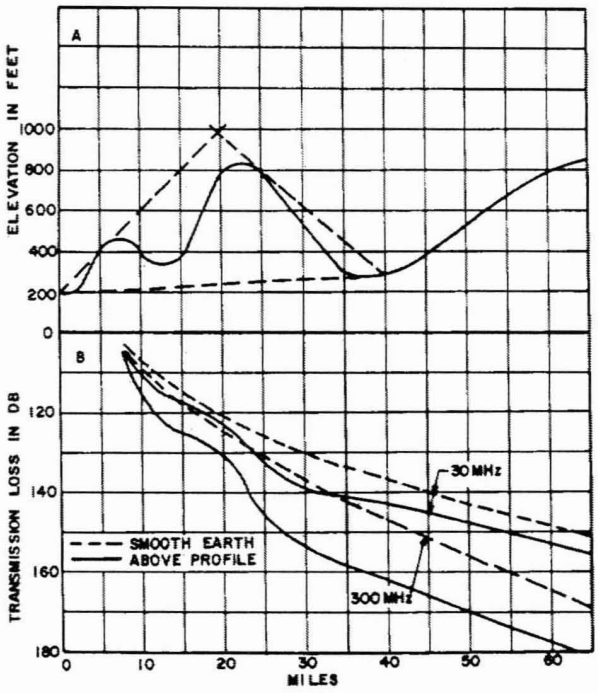

Fig. 17. Transmission loss over irregular terrain at 30 and 300 MHz; half-wave dipoles of 250 and 30 ft.

TABLE II
SHADOW-LOSS COMPUTATIONS

Miles from Transmitter	H (feet)	dl (miles)	Shadow Loss in dB Obtained from Fig. 12	
			30 MHz	300 MHz
12.5	200	4.5	3.5	9
20	70	6.5	2	4
25	310	4.5	5.5	13
35	750	14.5	7	16
40	760	20	6	14
50	610	18	5	12
60	490	16.5	4.5	11

ward trend with increasing frequency is a characteristic of the available tubes.)

Over irregular terrain it is assumed that the shadow loss based on knife-edge diffraction theory is to be added to the transmission loss obtained from smooth-earth theory. The computation of shadow losses for the profile shown in Fig. 17 (a) is given in Table II.

The estimated transmission loss for 30 and 3000 MHz including the shadow loss from Table II is shown by the solid lines on Fig. 17(b), while the dashed lines are the corresponding values over smooth earth taken from Fig. 17. Superimposed on these average values will be unpredictable variations of ±6 to 10 dB resulting from the effects of trees and buildings and from profile irregularities that were smooth out in drawing the profile shown in Fig. 17(a).

REFERENCES

[1] C. W. Burrows and M. C. Gray, "The Effect of the earth's curvature on ground wave propagation," in *Proc. I.R.E.*, vol. 29, pp. 16–24, Jan. 1941.
[2] K. A. Norton, "The calculation of ground-wave field intensities over a finitely conducting spherical earth," in *Proc. I.R.E.*, vol. 29, pp. 623–639. Dec. 1941.
[3] E. W. Allen, "Very-high frequency and ultra-high frequency signal ranges as limited by noise and co-channel interference," in *Proc. I.R.E.*, vol. 35, pp. 128–136, Feb. 1947.
[4] C. R. Burrows, "Radio propagation over plane earth-field strength curves, *Bell Syst. Tech. J.*, vol. 16, pp. 45–75, Jan. 1937.
[5] K. A. Norton, "The propagation of radio waves over the surface of the earth and in the upper atmosphere, Part II, in *Proc. I.R.E.*, vol. 25, pp. 1203–1236, Sept. 1937.
[6] J. C. Schelleng, C. R. Burrows, and E. G. Ferrell, "Ultra-Short Wave Propagation," *Bell Syst. Tech. J.*, vol. 12, pp. 125–161, April 1933.
[7] MIT Radiation Laboratory Series, L. N. Ridenour, Editor-in-Chief, Volume 13, *Propagation of Short Radio Waves*, D. E. Kerr, Ed., New York: McGraw Hill, 1951.
[8] Summary Technical Report of the Committee on Propagation, National Defense Research Committee, Volume 1, Historical and Technical survey. Volume 2, Wave Propagation Experiments. Volume 3, Propagation of Radio Waves. Stephen S. Attwood, Ed., Washington, D.C., 1946.
[9] K. Bullington, "Characteristics of beyond-horizon radio transmission," in *Proc. I.R.E.*, vol. 43, p. 1175, Oct. 1955.
[10] W. E. Gordon, "Radio scattering in the troposphere," in *Proc. I.R.E.*, vol. 43, p. 23, Jan. 1955.
[11] K. Bullington, "Radio transmission beyond the horizon in the 40- to 4,000 MC band, in *Proc. I.R.E.*, vol. 41, pp. 132–135, Jan. 1953.
[12] K. A. Norton, P. L. Rice, and L. E. Vogler, "The use of angular distance in estimating transmission loss and fading range for propagation through a turbulent atmosphere over irregular terrain," in *Proc. I.R.E.*, vol. 43, pp. 1488–1526, Oct. 1955.
[13] F. H. Dickson, J. J. Egli, J. W. Herbstreit, and G. S. Wickizer, Large reductions of VHF transmission loss and fading by presence of mountain obstacle in beyond line-of-sight paths," in *Proc. I.R.E.*, vol. 41, pp. 967-969, Aug. 1953.
[14] K. Bullington, W. J. Inkster, and A. L. Durkee, "Results of propagation tests at 505 MC and 4090 MC on beyond-horizon path," in *Proc. I.R.E.*, vol. 43, pp. 1306–1316, Oct. 1955.
[15] H. G. Booker and J. T. deBetterncourt, "Theory of radio transmission by tropospheric scattering using very narrow beams," in *Proc. I.R.E.*, vol. 43, pp. 281–290, Mar. 1955.
[16] W. H. Tidd, "Demonstration of bandwidth capabilities of beyond-horizon tropospheric radio propagation," in *Proc. I.R.E.*, vol. 43, pp. 1297–1299, Oct. 1955.
[17] K. Bullington, "Radio propagation variations at VHF and UHF," in *Proc. I.R.E.*, vol. 38, pp. 27–32, Jan. 1950.
[18] W. R. Young, "Comparison of mobile radio transmission at 150, 450, 900 and 3700 MC, *Bell Syst. Tech. J.*, vol. 31, pp. 1068–1085, Nov. 1952.
[19] Harald T. Friis, "Noise figures of radio receivers," in *Proc. I.R.E.*, vol. 32, 419–422, July 1944.
[20] Terman, *Radio Engineer's Handbook*, 1st ed., p. 699.

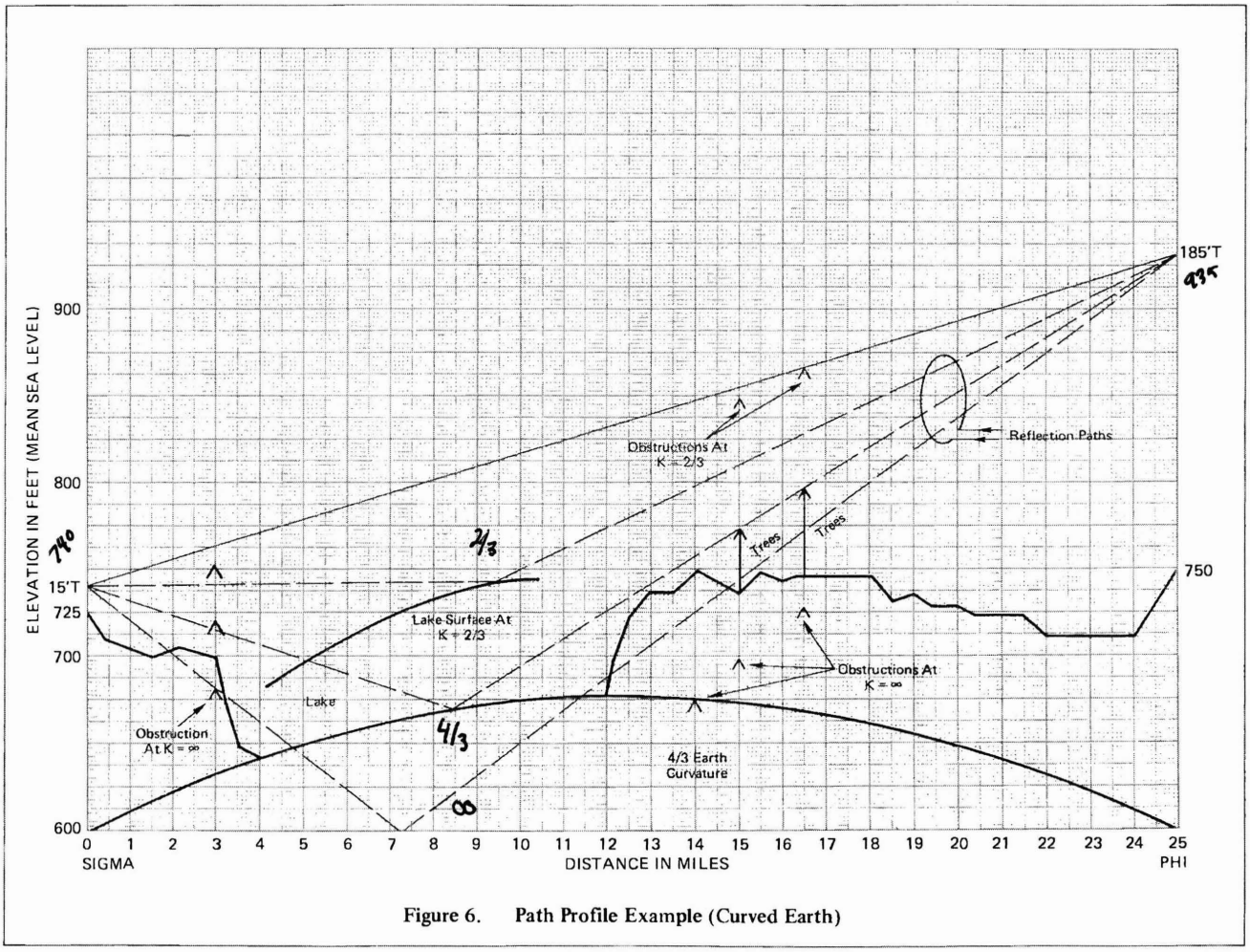

Figure 6. Path Profile Example (Curved Earth)

World Radio History

11.04 mi
K = ∞
h_1 = 740
h_2 = 995
D = 25

on Page 51, separate calculations and separate points must be marked for each set, over each obstruction, and again all points must be cleared by the line between antennas.

A skilled transmission engineer can usually reduce the number of points for which calculations need to be made to a relative few. For example, in the path of Figure 5 it is obvious that only five points are potential obstructions.

Though this method at first glance appears to be tedious, in practice it can be done very quickly and easily for most paths. It has the great advantage that any kind of rectilinear graph paper can be used, and that the most convenient scales can be chosen for each axis individually, since there is no interacting effect between the two scales. This method also provides a very useful means of double-checking, at critical points, the clearances as determined by any of the other methods.

4. Reflection Point Calculations

When K = ∞ (flat earth condition) there is a very simple relationship between the antenna heights and the distances from the respective ends to the reflection point (in miles). The relationship is:

$$\frac{h_1}{h_1 + h_2} = \frac{d_1}{d_1 + d_2} = \frac{d_1}{D}$$

where h_1 is the elevation of the lower antenna and h_2 the elevation of the higher antenna in feet above the reflecting surface, d_1 the distance in miles from the h_1 end to the reflecting point, and $d_1 + d_2 = D$ the path length in miles. This leads to the following expression:

For K = ∞

$$d_1 = nD, \text{ where } n = \frac{h_1}{h_1 + h_2} \qquad (2A)$$

For values of K other than infinity, and for unequal antenna elevations, the geometric relation involves cubic equations whose solution is somewhat cumbersome. However, graphical solutions have been worked out and are found in the literature in several different forms. A nomographic solution for the condition K = 2/3 is given in Figure 7A, and a similar solution for K = 4/3 in Figure 7B. By the use of these charts, an approximate value of n for each condition can be determined and the corresponding values of d_1 calculated. These values, together with the calculated value for K = ∞ can then be used to plot the reflection point range on the path profile, as shown in the example of Figure 6.

Reflective path analysis can be carried out equally well and in somewhat simpler fashion using the flat earth, curved beam approach as depicted in Figure 5. With flat earth profiles, the reflection points for the three significant values of K are calculated and marked along the bottom line of the profile. The appropriate curved beam template for each of these values is then used to trace the beam path and determine whether the paths from antenna to reflective point are clear or obstructed.

The nomograph solution provides accuracy adequate for most work. Where greater accuracy is desired, the following relationships are useful:

For K = 2/3

$$\frac{h_1}{d_1} - d_1 = \frac{h_2}{d_2} - d_2 \qquad (2B)$$

After determining the approximate values of d_1 and d_2 by means of Figure 7A, substitute them in the above equation, together with h_1 and h_2. If the reflection point location is correct, the two sides will be equal. If they are not equal, increase d_1 by a small amount and decrease d_2 by the same amount. If this change causes the inequality to increase, reverse the procedure. Continue by iteration until a value is reached for which the two sides are equal or very closely so.

For K = 4/3

$$\frac{h_1}{d_1} - \frac{d_1}{2} = \frac{h_2}{d_2} - \frac{d_2}{2} \qquad (2C)$$

Use Figure 7B to determine the approximate values of d_1 and d_2 then proceed as described above to determine a more exact value.

The small shaded area in the lower left hand corner of each chart represents conditions for which the path would be below grazing and a true reflection point would not exist.

The parameters X and Y from Figure 7 can also be used to determine the value of K for which the path would be at grazing clearance. For this condition the relation is given by the expression:

$$y = \frac{h}{D^2} = \frac{2700}{30^2} = 3$$

$$K = \frac{1}{1.5\,(X + Y + 2\sqrt{XY})}$$

They can also be used to determine the location of the reflection point for the grazing condition from the expression:

$$n = \frac{1}{1 + \sqrt{Y/X}}$$

The range of 0 to 3.0 for the Y parameter and 0 to 2.0 for the X parameter on Figures 7A and 7B will cover most situations where location of the reflection point is needed. For example, on a path of 30 miles, a value of 3.0 for Y would correspond to a height of 2700 feet above the reflecting surface for h_2, and a value of 2.0 for X to a height of 1800 feet above the surface for h_1.

In some special situations it may be necessary to calculate reflection points for paths where one or both of these values are exceeded. Since the charts are rectilinear and all of the lines are straight, it is relatively simple to extrapolate beyond the chart to determine an appropriate value for n. The iterative process described above can be used to improve the accuracy, if desired.

5. Preliminary Map Survey

The preliminary map survey has for its objective the planning of one or more routes which might appear to be possible between the terminal points given, based on available data, and the plotting of profiles which are necessarily preliminary, for all of the indicated paths and alternates determined from the study.

Use of Maps

The prospects of arriving at the best possible route and sites are enhanced by the study of the greatest numbers of alternate possibilities. It is recommended that all available information bearing on the proposed route be first assembled. Large scale maps, such as the aeronautical charts, are suggested for the beginning of the study, and for keeping track of its progress and the site locations.

It is recommended that the terminal locations be first plotted on the aeronautical charts, if these are available, or on a large scale map. At this point it is advisable to make a determination of the maximum, minimum and possible average length of path to be considered. This will depend to a considerable extent on the frequency band to be used, type of service to be assigned to the system and the topography. Having made these determinations, it is suggested arcs be drawn representing these values from the first terminal, and the areas between the arcs be searched for possible first sites. The search at this point will include the topographic maps and any other maps or photography which can be searched for additional information. Having selected one or more possible sites for the first repeater point, preliminary profiles should be drawn. These will furnish a check of the practicability of using the sites selected.

Limitations

The ideal situation obtains when all of the topographic maps for a given path can be assembled on the same scale and spliced together accurately so that a straight line can be drawn between the plotted adjacent sites. An accurate scale in miles is then marked on the line and, following the line over the contours, it is then possible to tabulate the elevations with their appropriate mileages. It is essential that the tabulated elevations and mileages be sufficient to fully describe the profile when plotted. Where the line crosses a hilltop, it is reasonable to assume in the preliminary map study that the ultimate height, unless specifically marked, is half the contour interval higher than the nearest lower contour line.

Cases of Incomplete Mapping

Where some maps in a given path are to a different scale than others, a useful technique is to splice plain white paper to each map where the scale changes and project, by geographic coordinates, a known point or the next adjacent site so that the proper line can be drawn on the available map. The tabulated data should then be plotted on the type of profile desired. For the paths with incomplete topographic survey, it is desirable to plot the profile showing that portion of the elevations which is available. If the path appears to be a good one in the field survey, the profile may be completed from field data. The tentative regular and alternate sites should also be plotted by geographic coordinates on the large scale map, to show their relative position, and to assist in the interference and frequency coordination study.

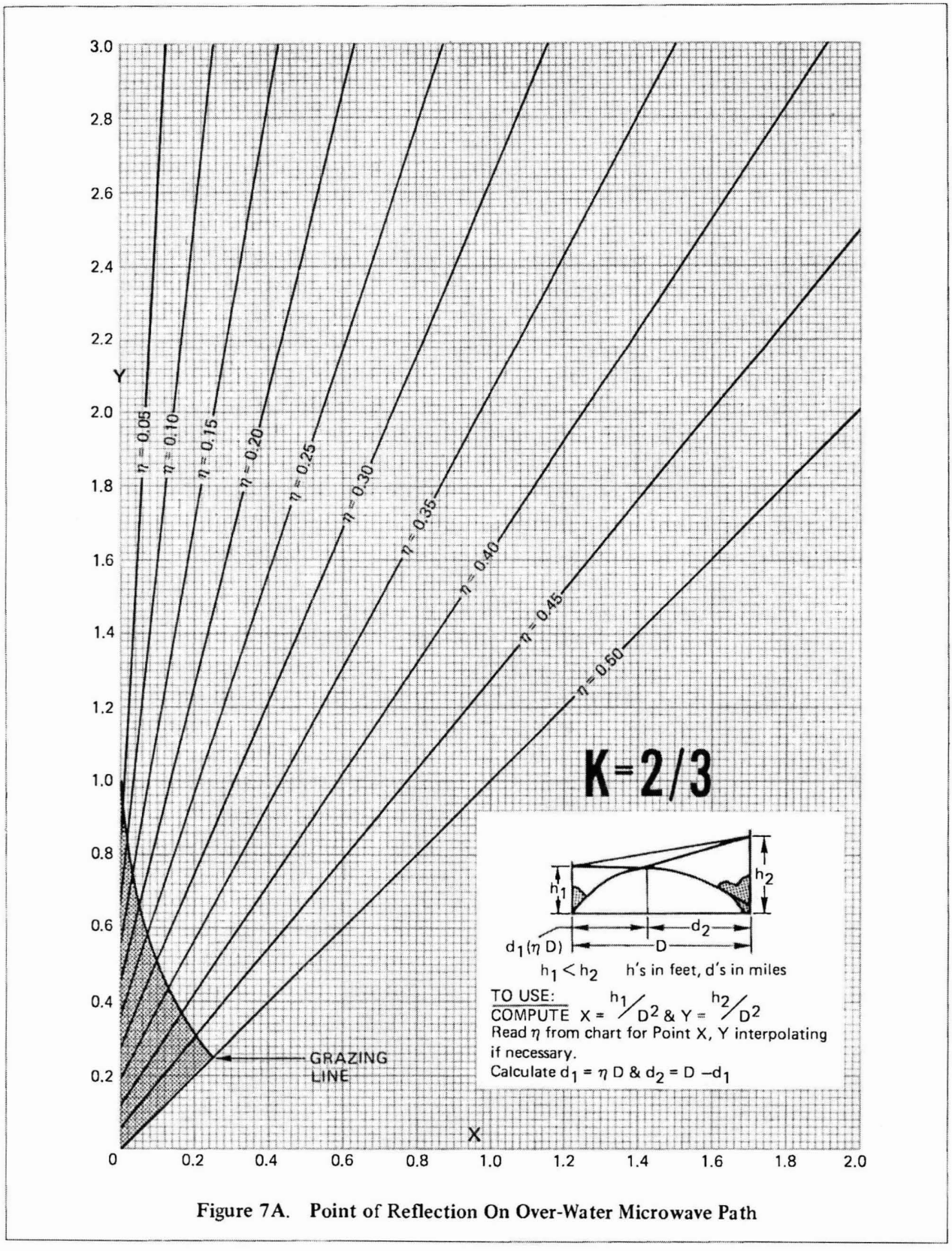

Figure 7A. Point of Reflection On Over-Water Microwave Path

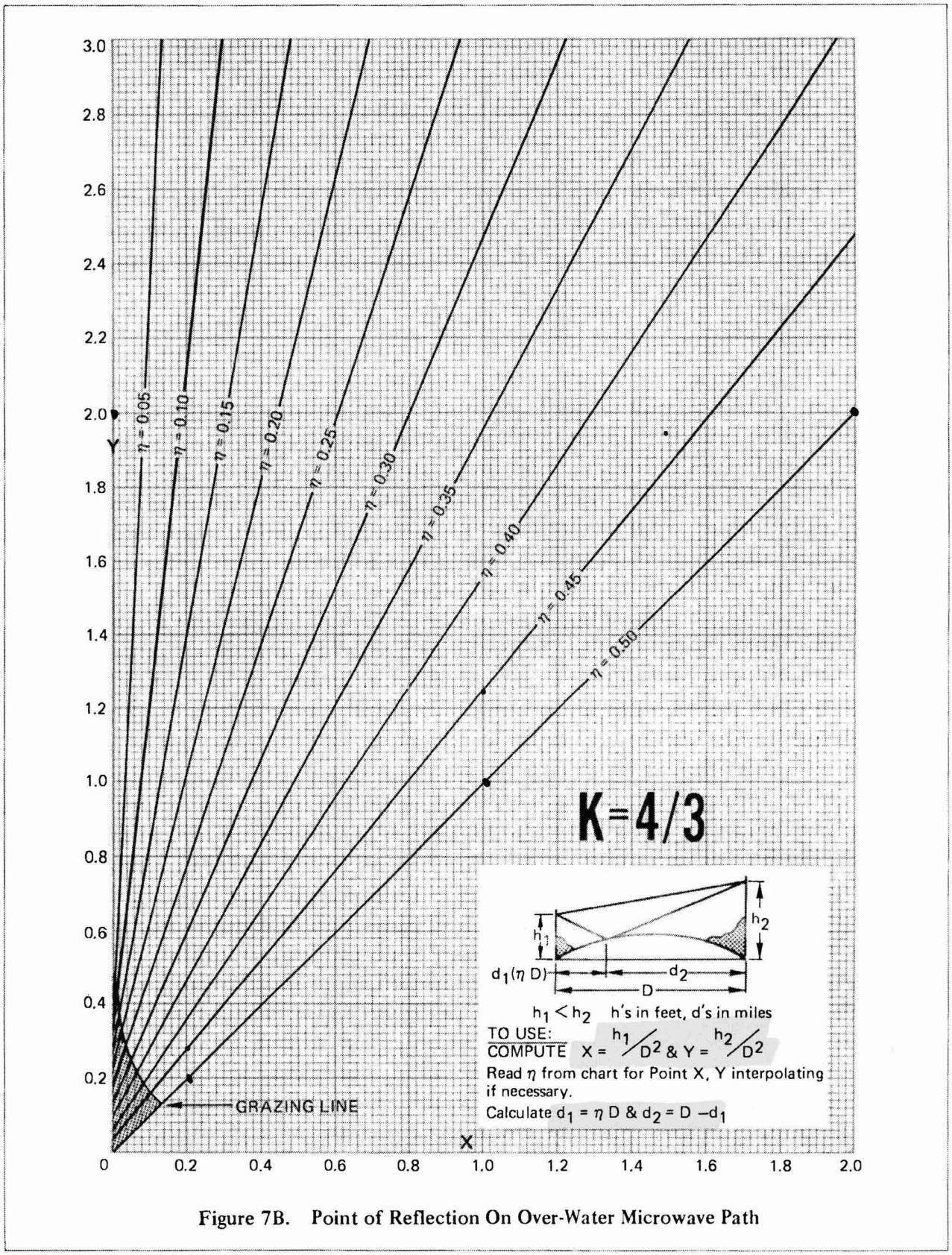

Figure 7B. Point of Reflection On Over-Water Microwave Path

HDPath Reflection Analysis

Q: How do I use HDPath™ to compute possible reflection points along a path?

A: The method described in *Engineering Considerations for Microwave Communications Systems* (Lenkurt, 1970) is used

TAP systems (Version 5.0.1056 and later) with a Maintenance Subscription date of June 30, 2005 or later, and that include the Reflection Analysis module can use HDPath to compute the possible reflection points.

Reflection Point Location

The reflection point locations are determined from the topographic elevation values along the path. For each point along the path, the antenna heights and path elevation at the point are used with Figures 7A and 7B from Lenkurt. The reflection point distance for that path elevation is determined for both 2/3 (Figure 7A) and 4/3 earth curvature (Figure 7B). This range of distance defines the portion of the path where a point of the specified elevation could be a reflection problem within the 2/3 to 4/3 range of possible earth curvature values.

If the distance of the path point under consideration is within that range, then the location on the path is considered a possible reflection point. In other words, for the elevation of the point at the distance of the point, an effective earth curvature value exists between 2/3 and 4/3 that would make the point a potential reflection point. (If the distance of the point along the path is outside of the distance range determined from the 2/3 and 4/3 Lenkurt curves, the assumption is that the point is not a potential reflection point for any reasonable effective earth curvature value.)

The earth curvature value is interpolated between 2/3 and 4/3 earth based on the relative location within the computed distance range. This gives the approximate earth curvature value at which a point at that distance and that elevation would present a reflection concern.

For example, consider a path 39.9 miles long, with antennas at each end with elevation values of 3855 feet and 4809 feet. A point along the path at a distance of 9.2 miles has an elevation of 3626 feet. Based on Lenkurt's Figure 7A and 7B for that path elevation and antenna height configuration, the reflecting point distance at 2/3 earth curvature is 9.43 miles, and for 4/3 earth the distance is 7.83 miles. Since the point under consideration (at 9.2 miles) lies in that distance range, it must be considered as a potential reflecting point.

Reflected Ray Line of Sight

The reflection effects of the point are only of concern if both ends of the path have clear line of sight to the potential reflecting point. Any obstruction in the path would block the reflected ray. Therefore, the next step is to see if this line of sight exists. Two paths are considered: from the transmitting antenna to the point under consideration (at ground level), and from that point to the receiving antenna.

The line of sight from that point to each end-point antenna is checked. If either path is blocked then the ray reflecting from that point on the path will be blocked, preventing a complete reflecting path and the point will be ignored. The line of sight is checked at the

earth curvature value computed for the point as described above.

Earth Curvature Values

The location of the potential reflection point as determined from Figure 7A/B in Lenkurt indicates the possibility of a reflected ray at the point somewhere in the range of effective earth curvature values in the range from 2/3 to 4/3 earth. The line of sight for the reflecting ray can be checked for a total of four possible values of effective earth curvature:

- 2/3 earth: This is the case that would provide the highest amount of obstruction along the path, i.e., the most amount of effective "bending" of the topography upward, giving the highest probability that some of that topography will obstruct one or both paths of the reflected ray. Hence, this is the most "optimistic" modeling, showing the maximum likely amount of terrain shielding of the reflected rays.
- 4/3 earth: This is the upper limit of the Lenkurt modeling, often used for typical atmospheric bending.
- Infinity: This is the case with no adjustment of the topography for earth curvature (effectively a "flat earth" approach). This is the case that would provide the least amount of obstruction along the path, i.e., the highest probability that the reflected ray would indeed have a clear path and be a potential problem. This can be considered the most "pessimistic" modeling, showing the least amount of shielding of the reflected rays.
- The interpolated value, based on the range of distances determined from Lenkurt. For example, in the path described above, the reflecting point distance at 9.43 miles corresponds to an earth curvature of 2/3 (0.666), and the distance of 7.83 miles corresponds to an earth curvature of 4/3 (1.333). Interpolating linearly, 9.2 miles (the actual distance of the point under), would correspond to an earth curvature value of 1.239.

Interpretation

Suppose the shadowing of the terrain *blocks* either part of the reflected ray path at an effective earth curvature of infinity (the most likely to have a *clear* path). Then the assumption can be made that the reflected ray at that point will not affect the received signal at the end of the path. Any consideration of earth curvature effects that would "bend" the topography upward along the path would only result in more effective blocking of the reflected ray.

At the other extreme, suppose the shadowing of the terrain allows a clear path for the reflected ray even at 2/3 earth curvature (the maximum "bending" effect considered). In this case, the potential reflecting point is of concern, since any reflected signal has the potential to reach the receiving antenna and cause interference or cancellation.

In the event that neither of the extreme conditions are met, the two shadowing evaluation studies (at 4/3 earth and at the interpolated effective curvature value) will give a relative idea of the potential severity of the reflection point.

The prediction of a reflection point does not ensure that a reflection will actually occur.

Other factors, such as the topography at the point and the type of surface will also have significant effect on the actual reflection. The determination of the reflection point location assumes a level surface at the reflecting point (in order for the angle of incidence and the equal angle of reflection to result in a continuous path between the antennas). The reflection coefficient at the point will determine how much of the signal energy is reflected toward the end point antenna. Smooth surfaces (relative to the wavelength) result in the most reflection. A large lake would generally present a serious concern, while heavy vegetation would significantly reduce the likelihood of reflection. A physical inspection of possible reflection point locations is important to determine the realistic probability of actual destructive reflections along the path.

Program Operation

For example, suppose you have a profile plotted in HDPath:

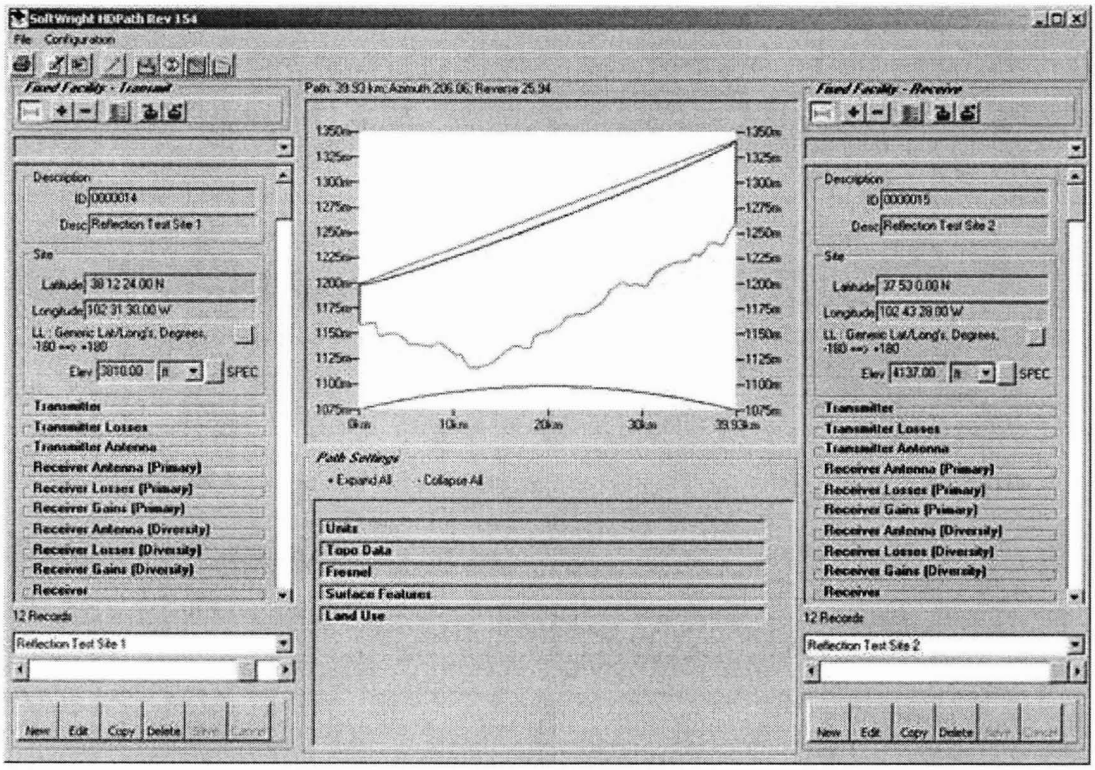

While the path has a clear line-of-sight, you can use HDPath to check for possible reflection points.

Click the Reflection Analysis button on the toolbar in the upper left portion of the HDPath form:

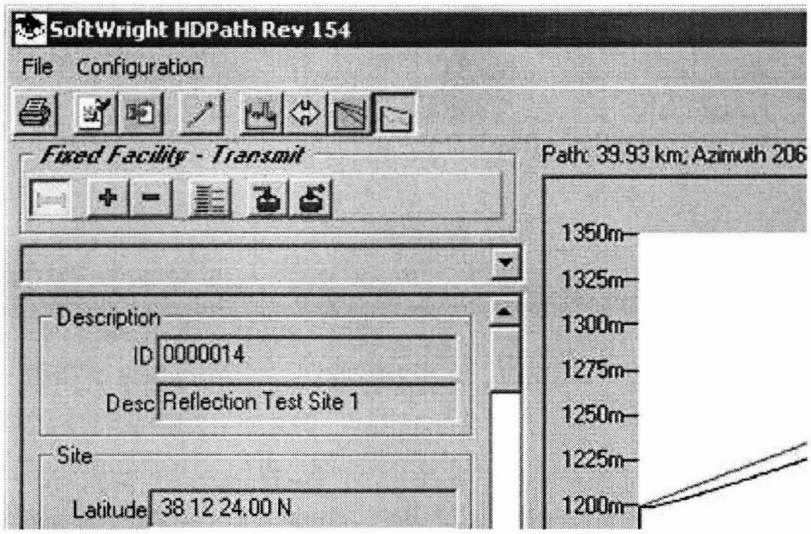

The Path Reflection Analysis form will be displayed with the results of the calculation:

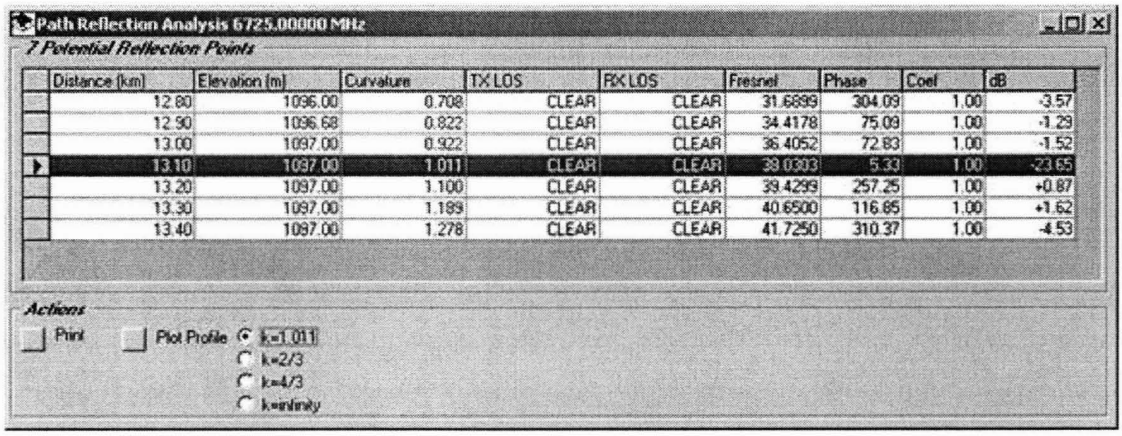

The form is displayed with the worst-case reflection point highlighted.

You can click the Print button to display a summary of the computed reflection analysis for all the points. The summary is written to a temporary file and opened in Notepad:

SWReflPt.TXT - Notepad

File Edit Format View Help

```
5/12/2005 12:35:00 PM
Reflection Analysis


From:  Reflection Test Site 1
38 12 24.0N   102 31 30.0W   LL
Site: 3810.00 ft MSL; 125.00 ft AGL

To : Reflection Test Site 2
37 53 00.0N   102 43 28.0W   LL
Site: 4137.00 ft MSL; 269.00 ft AGL


12.80km 1096.00m
k=0.708; Fresnel 31.69; Phase 304.09°; Ref Coef 1.00; Gn/Ls    -3.57dB

12.90km 1096.68m
k=0.822; Fresnel 34.42; Phase 75.09°; Ref Coef 1.00; Gn/Ls    -1.29dB

13.00km 1097.00m
k=0.922; Fresnel 36.41; Phase 72.83°; Ref Coef 1.00; Gn/Ls    -1.52dB

13.10km 1097.00m
k=1.011; Fresnel 38.03; Phase 5.33°; Ref Coef 1.00; Gn/Ls   -23.65dB

13.20km 1097.00m
k=1.100; Fresnel 39.43; Phase 257.25°; Ref Coef 1.00; Gn/Ls    +0.87dB

13.30km 1097.00m
k=1.189; Fresnel 40.65; Phase 116.85°; Ref Coef 1.00; Gn/Ls    +1.62dB

13.40km 1097.00m
k=1.278; Fresnel 41.73; Phase 310.37°; Ref Coef 1.00; Gn/Ls    -4.53dB
```

You can click the Plot button to draw the reflection paths on the profile:

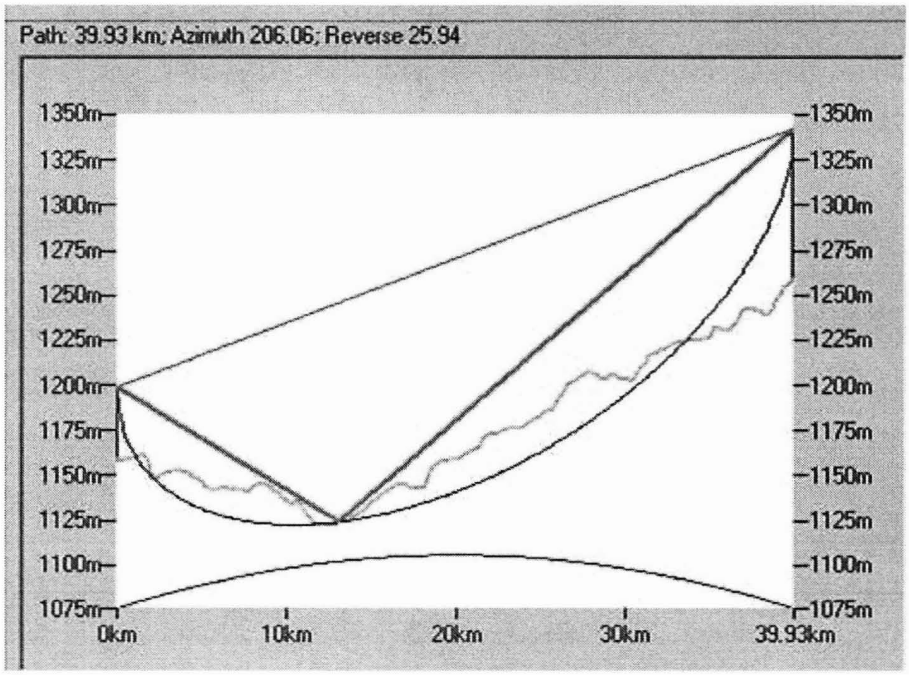

As indicated on the Reflection Point Analysis form and on the profile plot, this point would be of concern since both of the reflected rays are unobstructed.

The nature of the terrain at the reflection point should also be considered. If your TAP system includes the Land Use module, you can add land use information to the profile to determine the USGS Land Use Land

The Land Use information is added by checking the box in the Land Use section of the form:

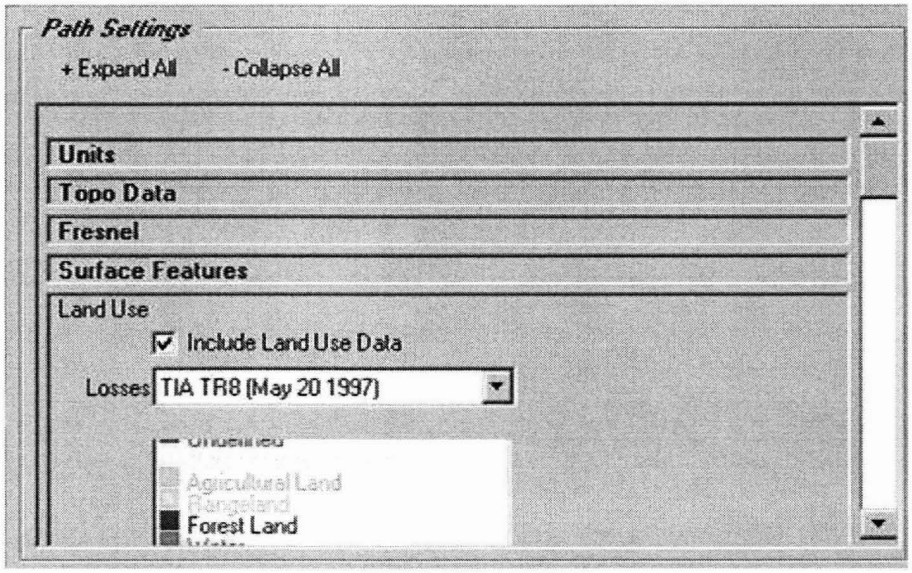

When you redraw the path and the reflection point information, you can see the Land Use information near the reflection point:

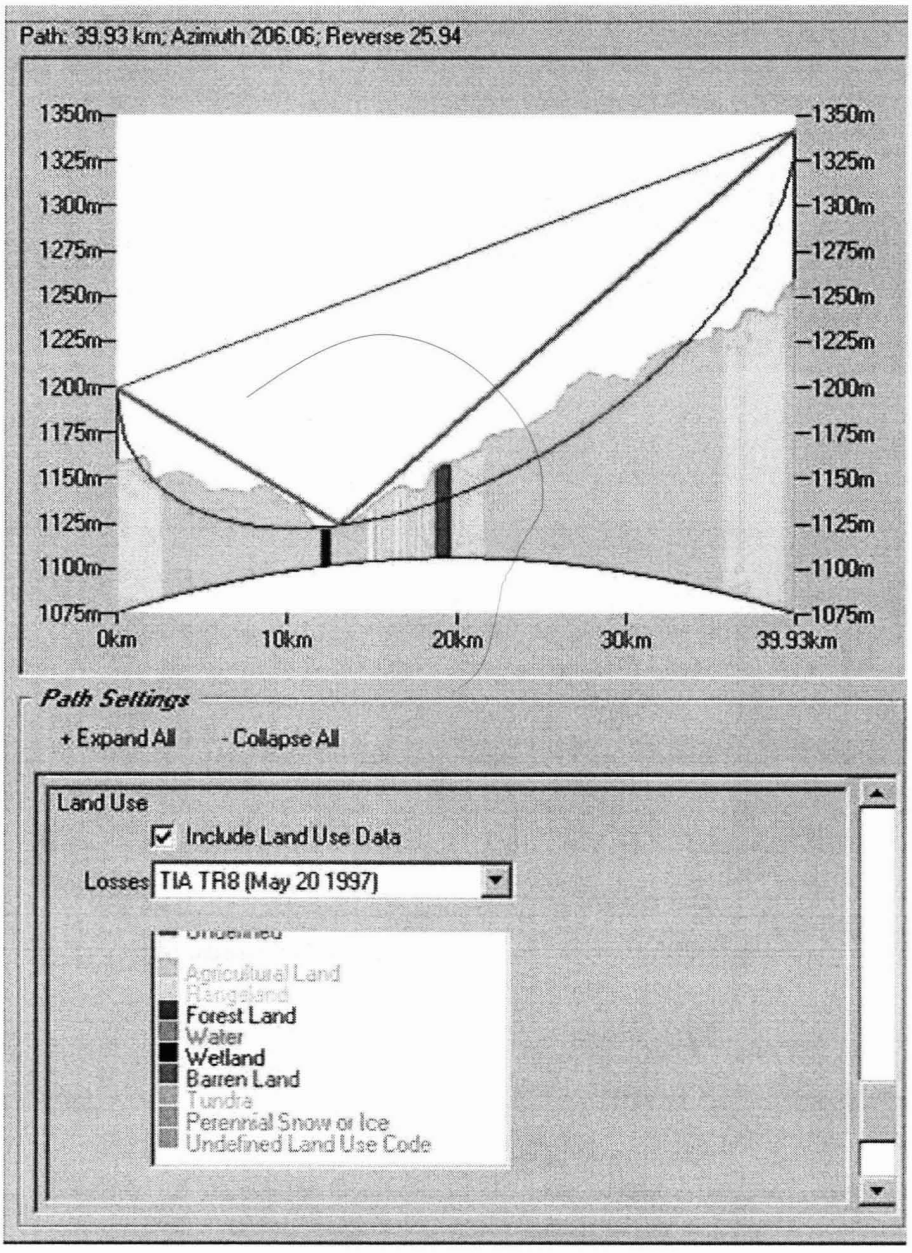

In this example, note that there is an area of "Wetland" (listed in the Land Use legend) very near the

that the actual area of wetland extended into the area of the reflection point and was actually cause a signal problem on the path. Move the antenna heights relocated potential reflection points away from the wetland into agricultural areas and eliminated the problem.

Search SoftWright Website

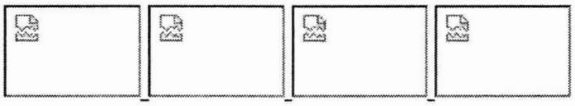

Copyright 2005 by SoftWright LLC

RECOMMENDATION ITU-R P. 835-2

REFERENCE STANDARD ATMOSPHERES

(Question ITU-R 201/3)

(1992-1994-1997)

The ITU Radiocommunication Assembly,

considering

a) the necessity for a reference standard atmosphere for use in calculating gaseous attenuation along an Earth-space path,

recommends

1 that the standard atmospheres in Annex 1 be used to determine temperature, pressure and water-vapour pressure as a function of altitude, for calculating gaseous attenuation, except when more reliable local data are available.

ANNEX 1

1 Mean annual global reference atmosphere

The following reference standard atmosphere reflects the annual mean profiles when averaged across the globe.

1.1 Temperature and pressure

The reference standard atmosphere is based on the United States Standard Atmosphere, 1976, in which the atmosphere is divided into seven successive layers showing linear variation with temperature, as given in Fig. 1.

The temperature T at height h is given by:

$$T(h) = T_i + L_i (h - H_i) \qquad \text{K} \tag{1}$$

where:

$$T_i = T(H_i) \tag{2}$$

and L_i is the temperature gradient starting at altitude H_i and is given in Table 1.

TABLE 1

Subscript, i	Altitude, H_i (km)	Temperature gradient, L_i (K/km)
0	0	–6.5
1	11	0.0
2	20	+1.0
3	32	+2.8
4	47	0.0
5	51	–2.8
6	71	–2.0
7	85	

FIGURE 1

Reference profile of atmospheric temperature

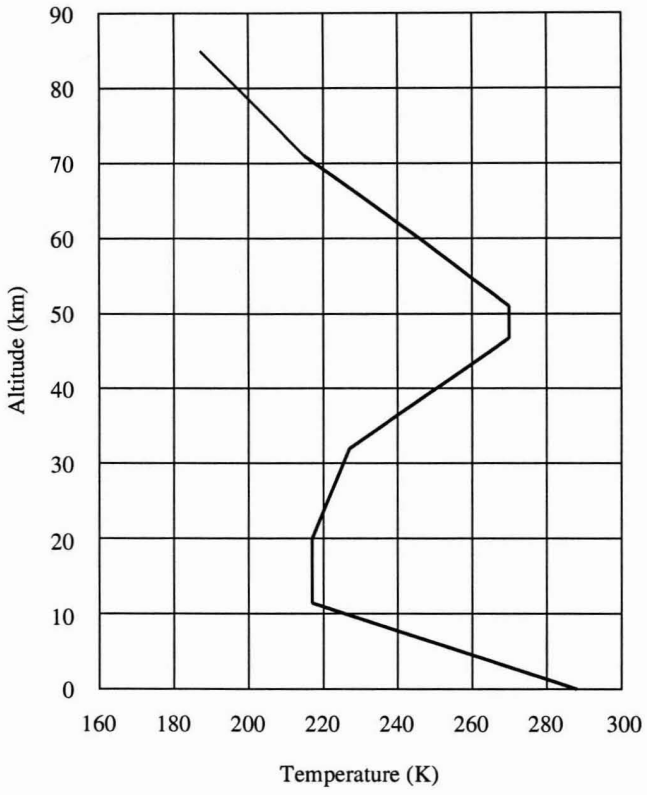

When the temperature gradient $L_i \neq 0$, pressure is given by the equation:

$$P(h) = P_i \left[\frac{T_i}{T_i + L_i (h - H_i)} \right]^{34.163 / L_i} \quad \text{hPa} \tag{3}$$

and when the temperature gradient $L_i = 0$, pressure is obtained from the equation:

$$P(h) = P_i \exp\left[\frac{-34.163 (h - H_i)}{T_i} \right] \quad \text{hPa} \tag{4}$$

The ground-level standard temperature and pressure are:

$$\begin{aligned} T_0 &= 288.15 \quad \text{K} \\ P_0 &= 1\,013.25 \quad \text{hPa} \end{aligned} \tag{5}$$

Note that above about 85 km altitude, local thermodynamic equilibrium of the atmosphere starts to break down, and the hydrostatic equation, on which the above equations are based, is no longer valid.

1.2 Water-vapour pressure

The distribution of water vapour in the atmosphere is generally highly variable, but may be approximated by the equation:

$$\rho(h) = \rho_0 \exp(-h / h_0) \qquad g/m^3 \tag{6}$$

where the scale height $h_0 = 2$ km, and the standard ground-level water-vapour density is:

$$\rho_0 = 7.5 \qquad g/m^3 \tag{7}$$

Vapour pressure is obtained from the density using the equation (see Recommendation ITU-R P.453):

$$e(h) = \frac{\rho(h)\, T(h)}{216.7} \qquad hPa \tag{8}$$

Water-vapour density decreases exponentially with increasing altitude, up to an altitude where the mixing ratio $e(h)/P(h) = 2 \times 10^{-6}$. Above this altitude, the mixing ratio is assumed to be constant.

1.3 Dry atmosphere for attenuation calculations

The profile of the density of atmospheric gases other than water vapour (the "dry atmosphere") may be found from the temperature and pressure profiles given in § 1.1.

For attenuation calculations, this density profile may be approximated by an exponential profile according to equation (6) with:

$$h_0 = 6 \text{ km} \tag{9}$$

2 Low-latitude annual reference atmosphere

For low latitudes (smaller than 22°) the seasonal variations are not very important and a single annual profile can be used.

The temperature T (K) at height h (km) is given by:

$T(h) = 300.4222 - 6.3533\, h + 0.005886\, h^2$ for $0 \le h \le 17$

$T(h) = 194 + (h - 17)\, 2.533$ for $17 \le h \le 47$

$T(h) = 270$ for $47 \le h \le 52$

$T(h) = 270 - (h - 52)\, 3.0714$ for $52 \le h \le 80$

$T(h) = 184$ for $80 \le h \le 100$

while the pressure P (hPa):

$P(h) = 1012.0306 - 109.0338\, h + 3.6316\, h^2$ for $0 \le h \le 10$

$P(h) = P_{10} \exp[-0.147\, (h - 10)]$ for $10 \le h \le 72$

$P(h) = P_{72} \exp[-0.165\, (h - 72)]$ for $72 \le h \le 100$

where P_{10} and P_{72} are the pressures at 10 and 72 km respectively.

For water vapour (g/m^3)

$\rho(h) = 19.6542 \exp[-0.2313\, h - 0.1122\, h^2 + 0.01351\, h^3 - 0.0005923\, h^4]$ for $0 \le h \le 15$

$\rho(h) = 0$ for $h > 15$

3 Mid-latitude reference atmosphere

For mid-latitudes (between 22° and 45°) the following profiles may be used for the summer and winter.

3.1 Summer mid-latitude

The temperature T (K) at height h (km) is given by:

$T(h) = 294.9838 - 5.2159\ h + 0.07109\ h^2$ for $0 \le h \le 13$

$T(h) = 215.5$ for $13 \le h \le 17$

$T(h) = 215.5 \exp [\ (h - 17)\ 0.008128]$ for $17 \le h \le 47$

$T(h) = 275$ for $47 \le h \le 53$

$T(h) = 275 + \{1 - \exp [\ (h - 53)\ 0.06]\ \}\ 20$ for $53 \le h \le 80$

$T(h) = 175$ for $80 \le h \le 100$

while the pressure P (hPa):

$P(h) = 1012.8186 - 111.5569\ h + 3.8646\ h^2$ for $0 \le h \le 10$

$P(h) = P_{10} \exp [-0.147\ (h - 10)]$ for $10 \le h \le 72$

$P(h) = P_{72} \exp [-0.165\ (h - 72)]$ for $72 \le h \le 100$

where P_{10} and P_{72} are the pressures at 10 and 72 km respectively.

For water vapour (g/m^3):

$\rho(h) = 14.3542 \exp [-0.4174\ h - 0.02290\ h^2 + 0.001007\ h^3]$ for $0 \le h \le 10$

$\rho(h) = 0$ for $h > 10$

3.2 Winter mid-latitude

The temperature T (K) at height h (km) is given by:

$T(h) = 272.7241 - 3.6217\ h - 0.1759\ h^2$ for $0 \le h \le 10$

$T(h) = 218$ for $10 \le h \le 33$

$T(h) = 218 + (h - 33)\ 3.3571$ for $33 \le h \le 47$

$T(h) = 265$ for $47 \le h \le 53$

$T(h) = 265 - (h - 53)\ 2.0370$ for $53 \le h \le 80$

$T(h) = 210$ for $80 \le h \le 100$

while the pressure P (hPa):

$P(h) = 1018.8627 - 124.2954\ h + 4.8307\ h^2$ for $0 \le h \le 10$

$P(h) = P_{10} \exp [-0.147\ (h - 10)]$ for $10 \le h \le 72$

$P(h) = P_{72} \exp [-0.155\ (h - 72)]$ for $72 \le h \le 100$

where P_{10} and P_{72} are the pressures at 10 and 72 km respectively.

For water vapour (g/m^3):

$\rho(h) = 3.4742 \exp [-0.2697\ h - 0.03604\ h^2 + 0.0004489\ h^3]$ for $0 \le h \le 10$

$\rho(h) = 0$ for $h > 10$

4 High latitude reference atmosphere

For high latitudes (higher than 45°) the following profiles may be used for the summer and winter.

4.1 Summer high latitude

The temperature T (K) at height h (km) is given by:

$T(h) = 286.8374 - 4.7805\ h - 0.1402\ h^2$ for $0 \le h \le 10$

$T(h) = 225$ for $10 \le h \le 23$

$T(h) = 225 + \exp\ [\ (h - 23)\ 0.008317]$ for $23 \le h \le 48$

$T(h) = 277$ for $48 \le h \le 53$

$T(h) = 277 - (h - 53)\ 4.0769$ for $53 \le h \le 79$

$T(h) = 171$ for $79 \le h \le 100$

while the pressure P (hPa):

$P(h) = 1008.0278 - 113.2494\ h + 3.9408\ h^2$ for $0 \le h \le 10$

$P(h) = P_{10} \exp\ [-0.140\ (h - 10)]$ for $10 \le h \le 72$

$P(h) = P_{72} \exp\ [-0.165\ (h - 72)]$ for $72 \le h \le 100$

where P_{10} and P_{72} are the pressures at 10 and 72 km respectively.

For water vapour (g/m^3):

$\rho(h) = 8.988 \exp\ [-0.3614\ h - 0.005402\ h^2 - 0.001955\ h^3]$ for $0 \le h \le 15$

$\rho(h) = 0$ for $h > 15$

4.2 Winter high latitude

The temperature T (K) at height h (km) is given by:

$T(h) = 257.4345 + 2.3474\ h - 1.5479\ h^2 + 0.08473\ h^3$ for $0 \le h \le 8.5$

$T(h) = 217.5$ for $8.5 \le h \le 30$

$T(h) = 217.5 + (h - 30)\ 2.125$ for $30 \le h \le 50$

$T(h) = 260$ for $50 \le h \le 54$

$T(h) = 260 - (h - 54)\ 1.667$ for $54 \le h \le 100$

while the pressure P (hPa):

$P(h) = 1010.8828 - 122.2411\ h + 4.554\ h^2$ for $0 \le h \le 10$

$P(h) = P_{10} \exp\ [-0.147\ (h - 10)]$ for $10 \le h \le 72$

$P(h) = P_{72} \exp\ [-0.150\ (h - 72)]$ for $72 \le h \le 100$

where P_{10} and P_{72} are the pressures at 10 and 72 km respectively.

For water vapour (g/m^3):

$\rho(h) = 1.2319 \exp\ [0.07481\ h - 0.0981\ h^2 + 0.00281\ h^3]$ for $0 \le h \le 10$

$\rho(h) = 0$ for $h > 10$

BIBLIOGRAPHY

BRUSSAARD, G., DAMOSSO, E. and STOLA, L. [October, 1983] Characterisation of the 50-70 GHz band for space communications. CSELT Rapporti Tecnici, Vol. XI, **5**.

2.5.5- Select your radio according to Type (3000S , Pasolink , Pasolink+ , …..) , Frequency ban (7G , 8G , 11G, …….) Modulation (16 QAM , 32 QAM , 128 QAM,….) Capacity (PDH x E1 , STM-0 , STM-1) then click Both to set same Radio for both stations then Press OK as shown in Fig. 2.5.5

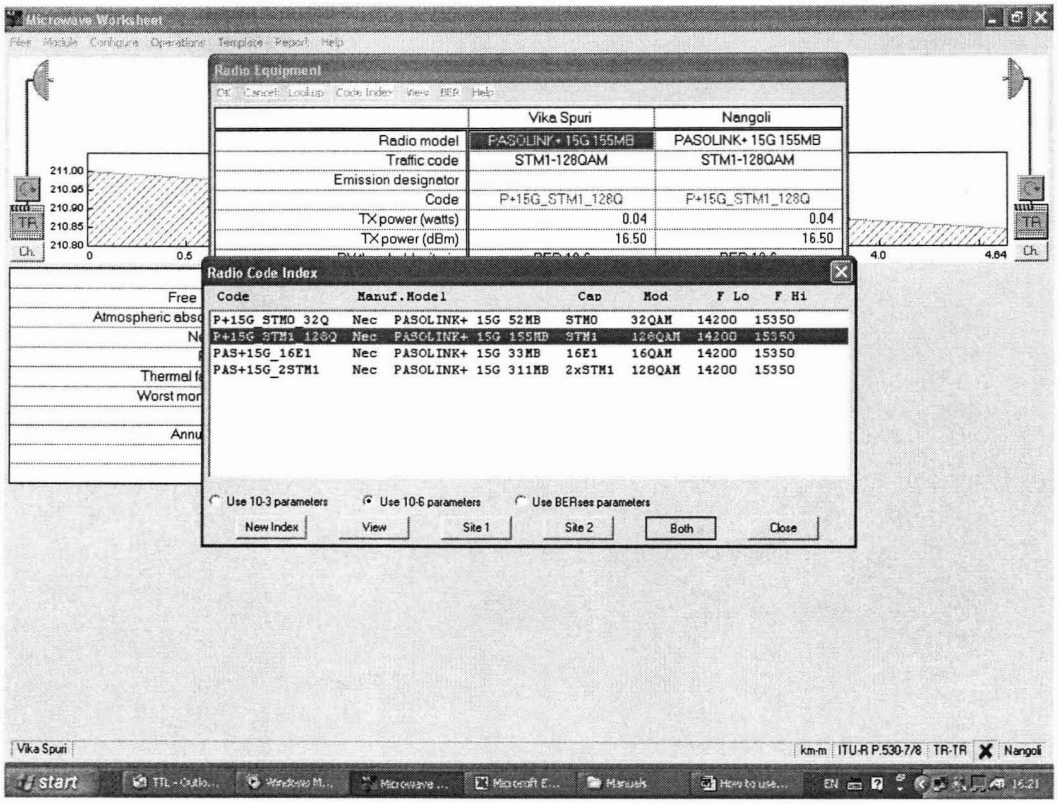

Fig. 2.5.5

2.5.6- Set Branching Circuit or Hybrid Loss by clicking on its Symbol (above TR) then press OK as shown in Fig. 2.5.6

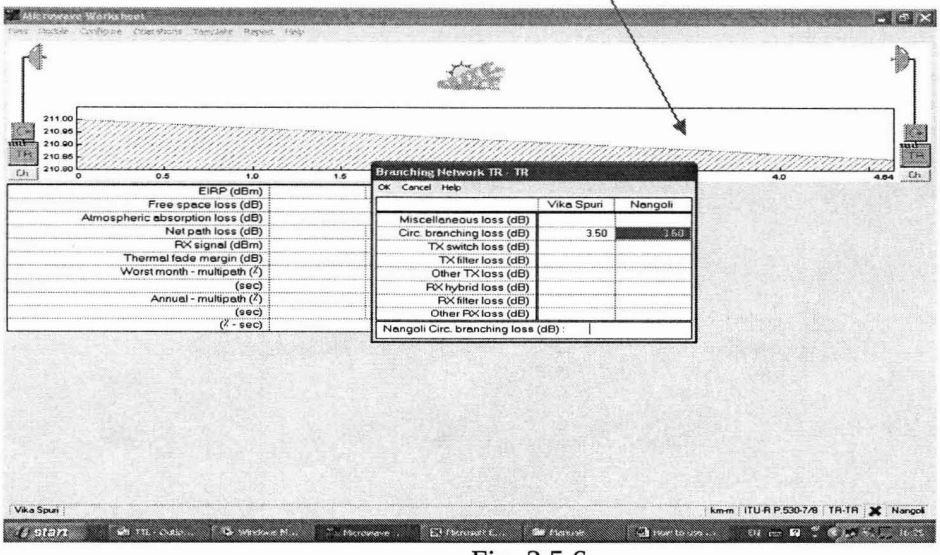

Fig. 2.5.6

2.5.3- Select Radio Equipment type by clicking on TR you will get Radio Equipment page as shown in Fig. 2.5.3

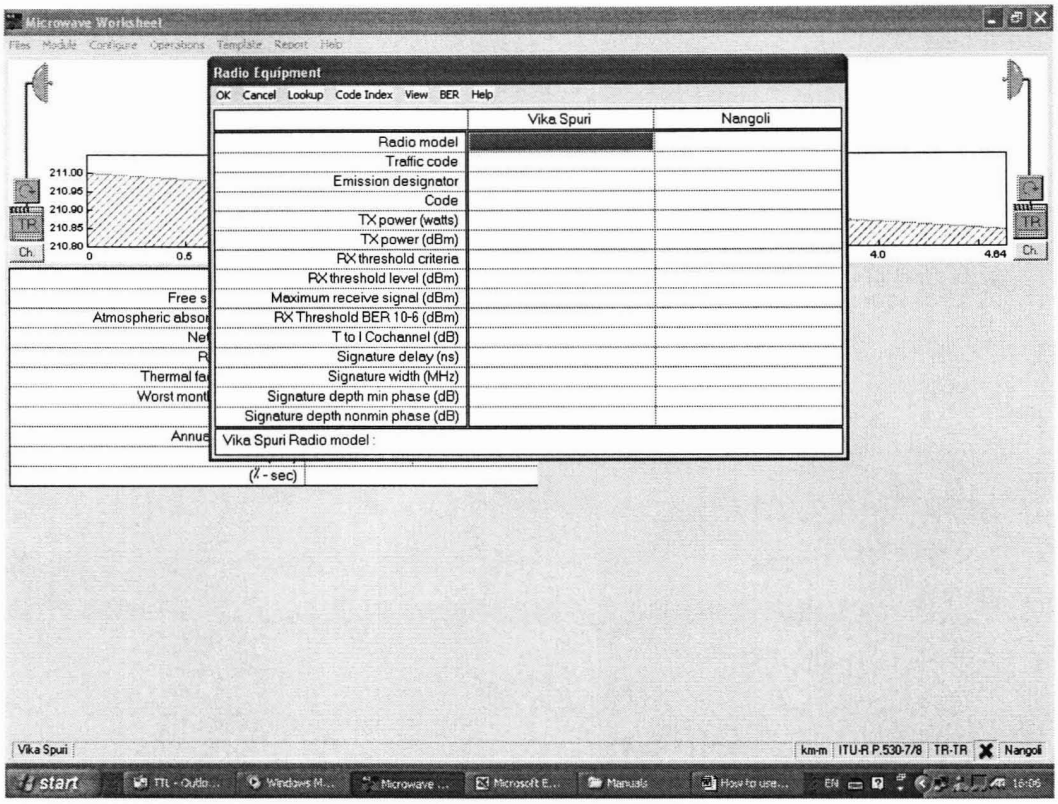

Fig. 2.5.3

2.5.4- click on Code Index then New Index. Go to your pathloss folder – Equipment – MRS – NEC (where you placed NEC equipment folder) as shown in Fig. 2.5.4

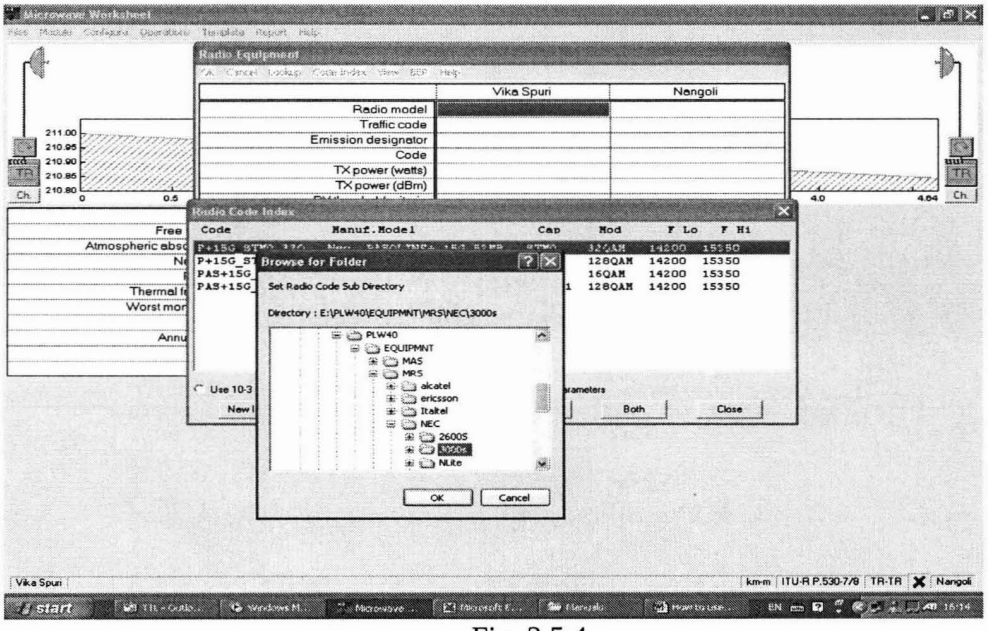

Fig. 2.5.4

2.5- Link Budget Calculations

After we already decided antenna heights for each link we should calculate link budget for each link to find antenna diameter, link RX & Availability as the following steps

2.5.1- Go to Worksheets from Modules menu or by pressing ctrl W. you get work sheet page as shown in Fig. 2.5.1

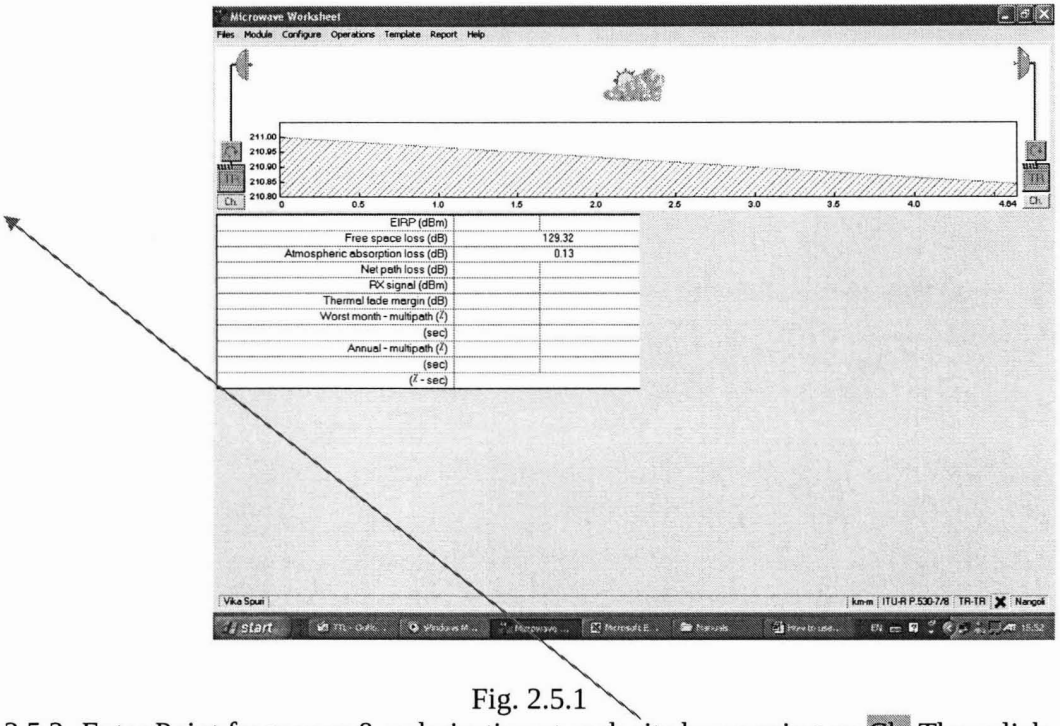

Fig. 2.5.1

2.5.2- Enter Point frequency & polarization at each site by pressing on Ch. Then click OK As shown in Fig. 2.5.1 & 2.5.2

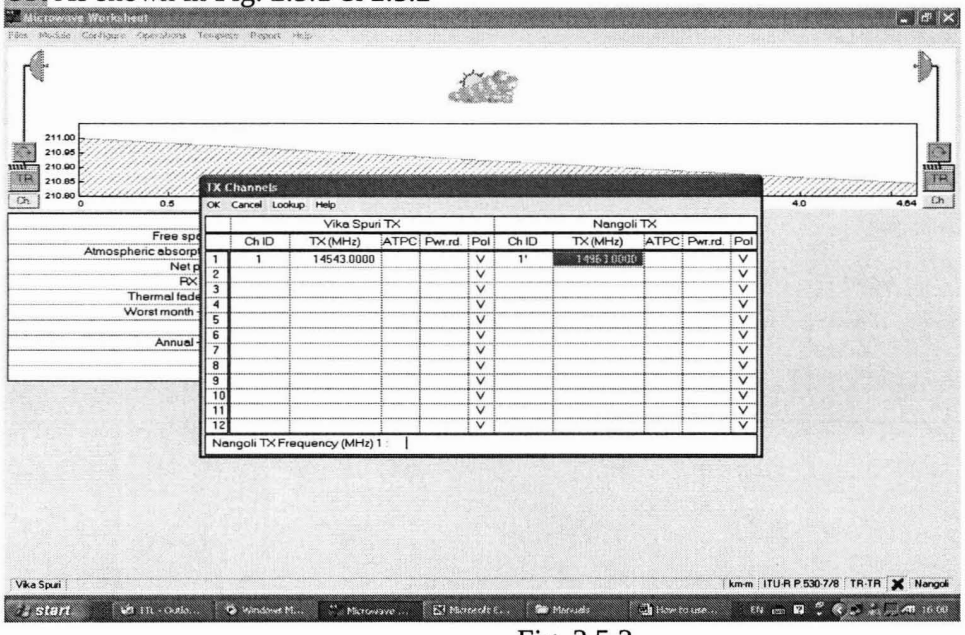

Fig. 2.5.2

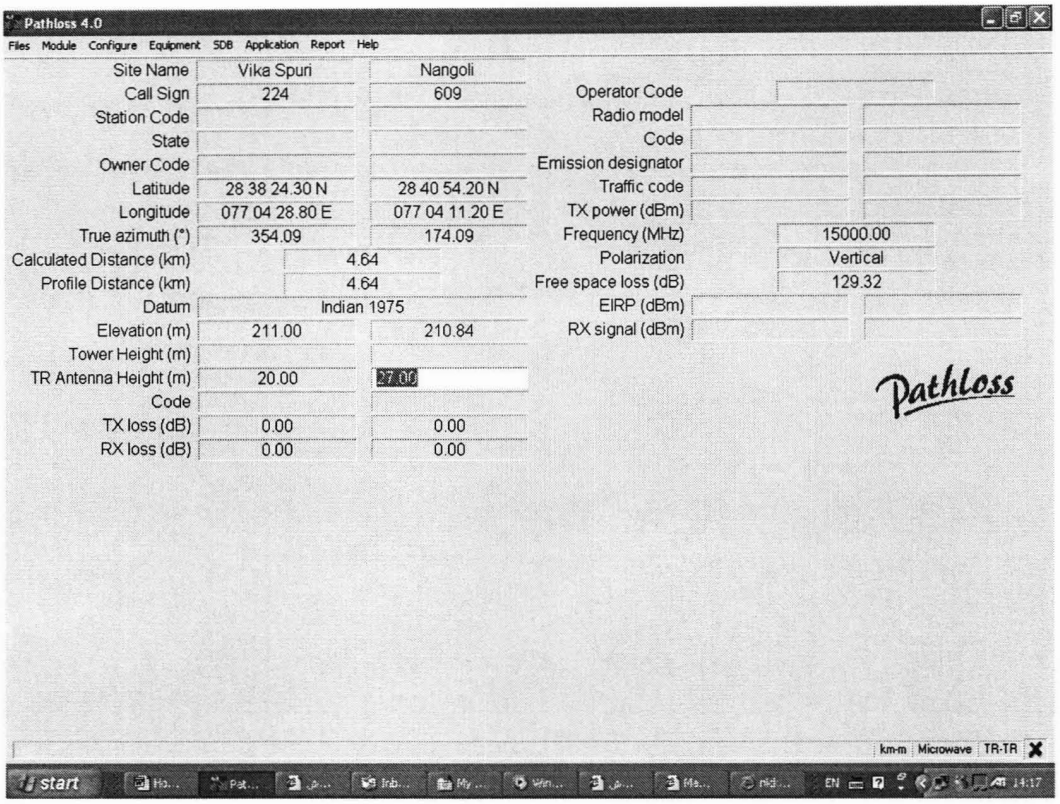

Fig. 2.4.3

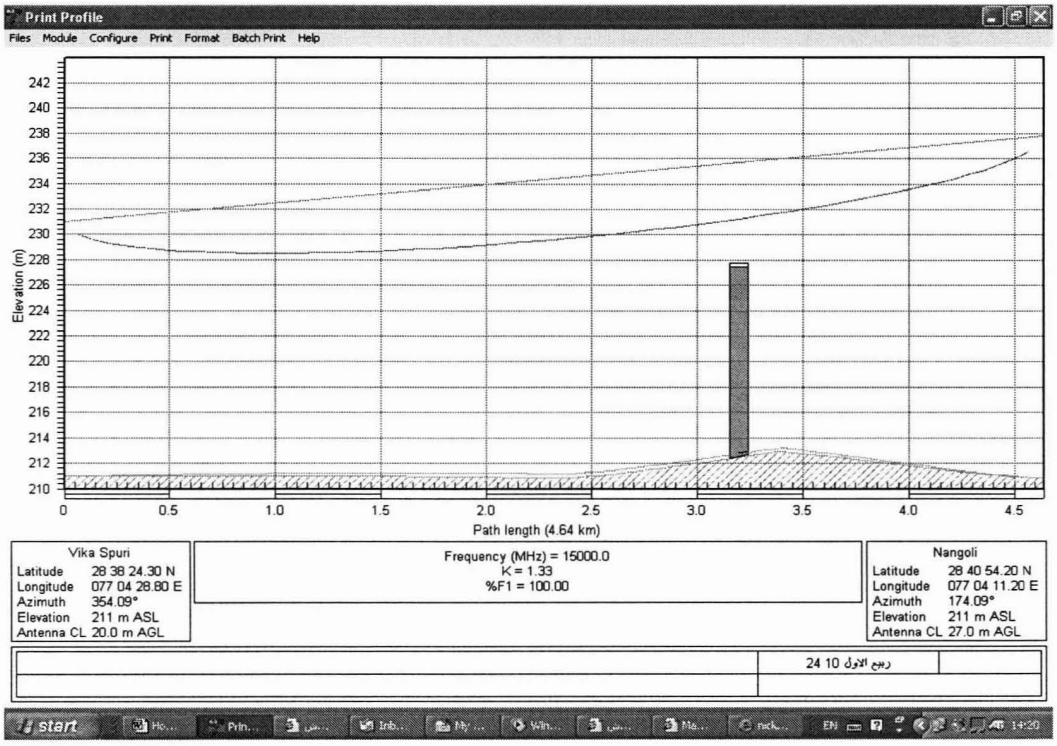

Fig. 2.4.5

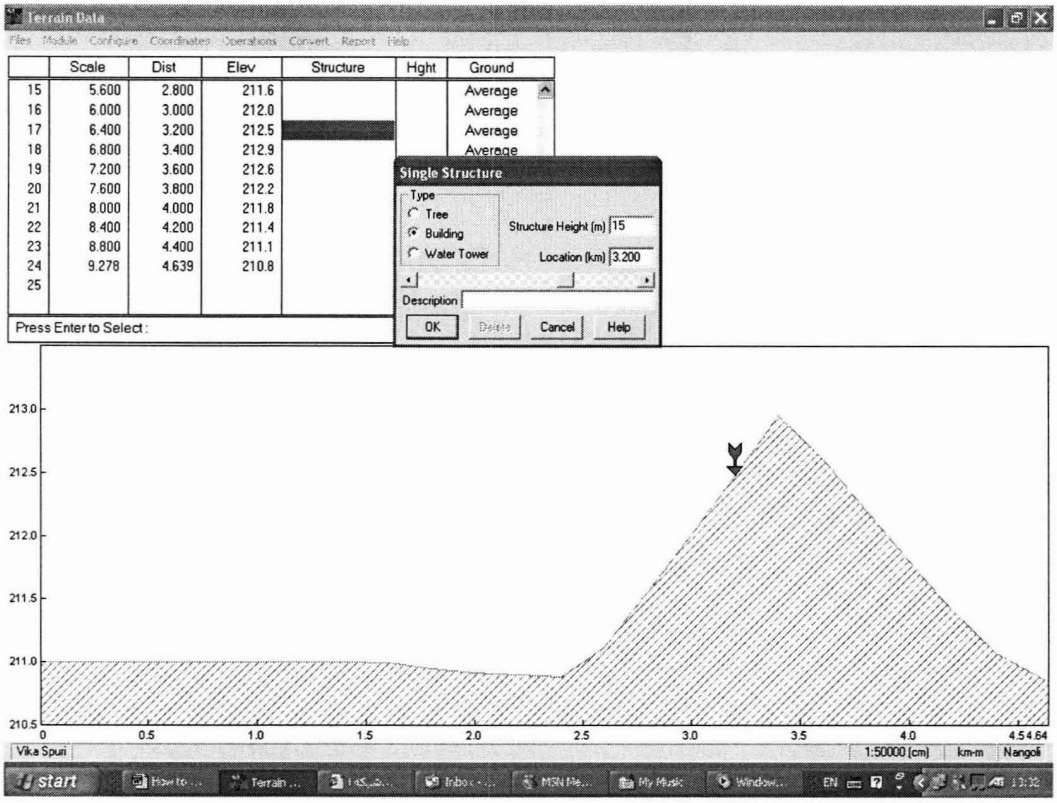

Fig. 2.3.3

2.4- Finding Suitable Antenna Heights

After we entered Terrain Data & Obstacles Heights we have to find the suitable Antenna heights in each sites to grantee clear Line Of Sight (LOS) as the following steps

2.4.1- Go to Antenna Height page from Modules menu or by pressing ctrl A as shown in Fig. 2.4.1

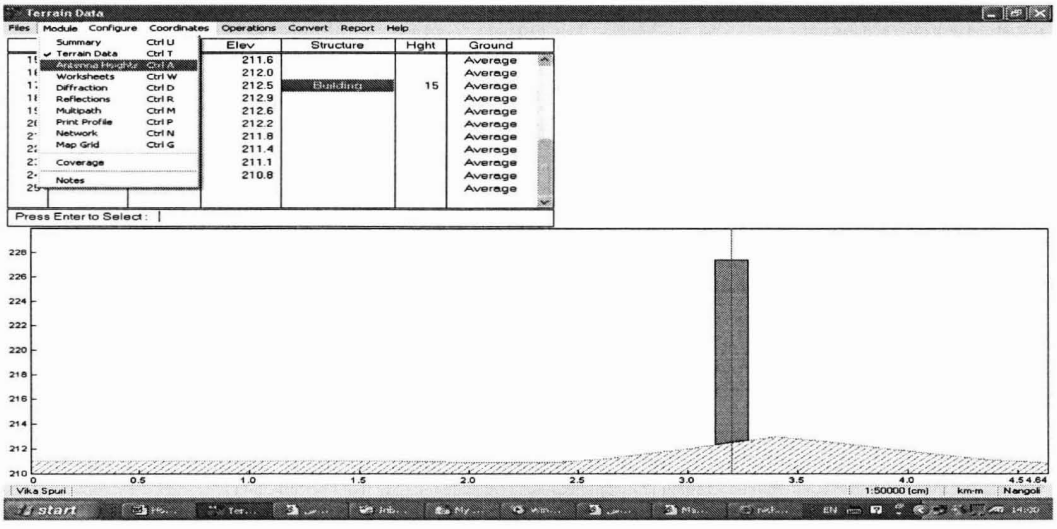

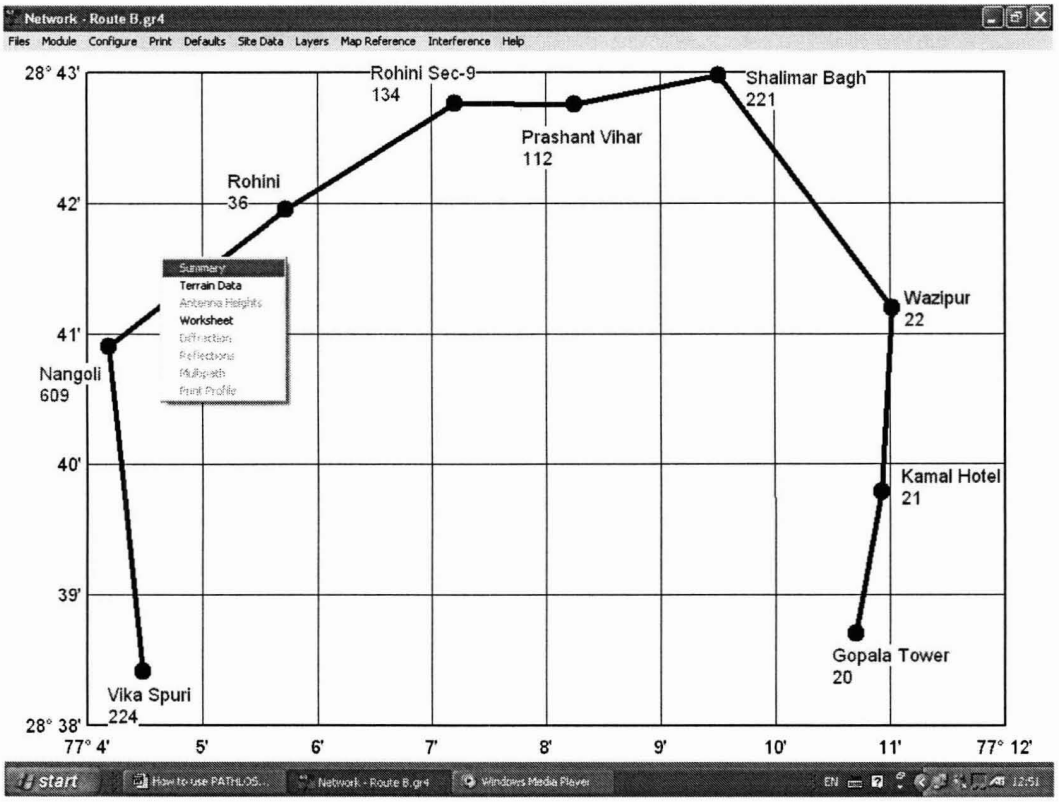

Fig. 2.2.1

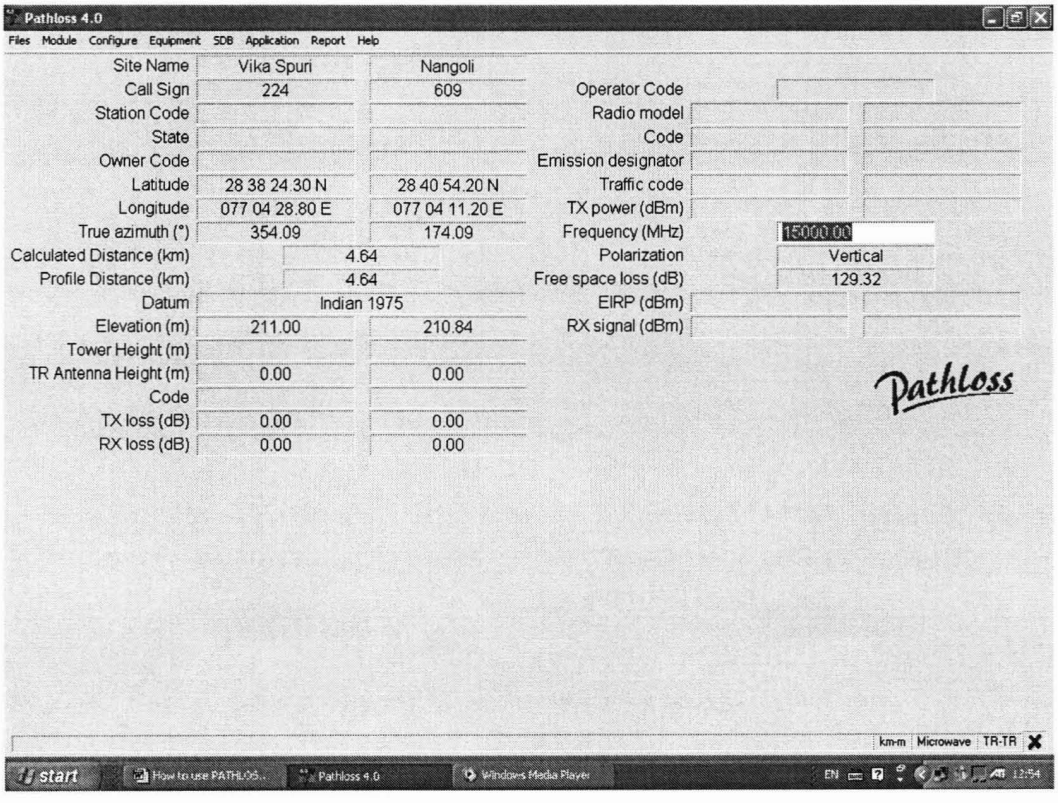

Fig. 2.2.2

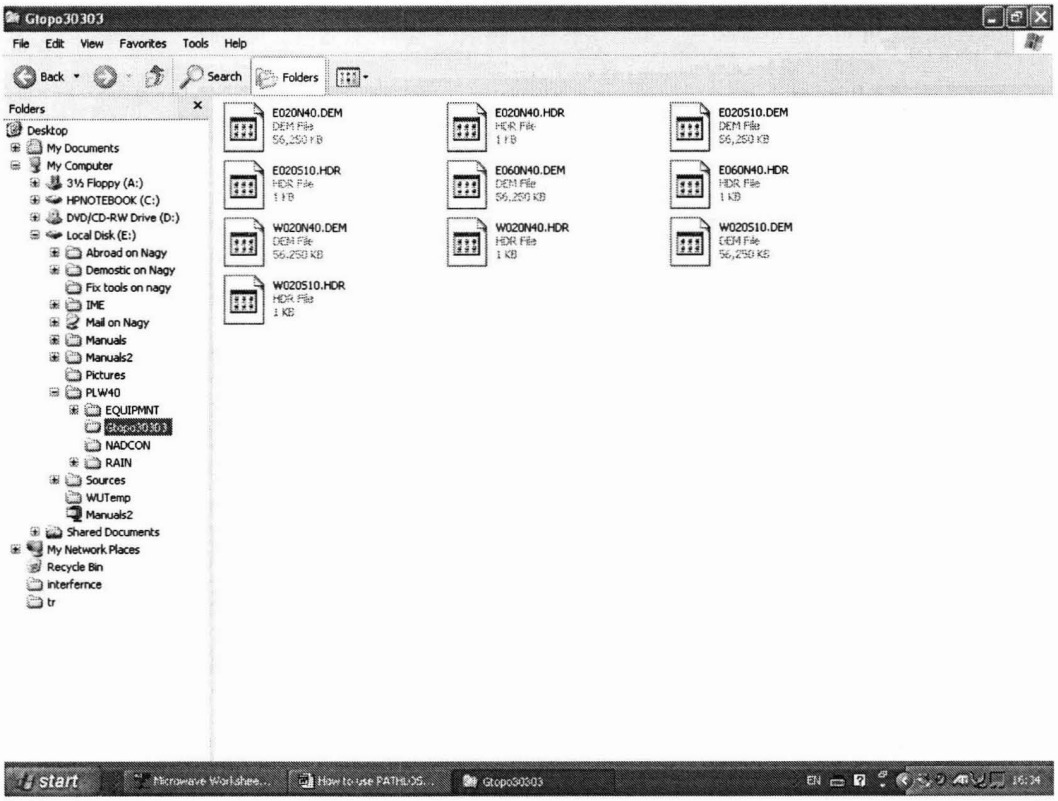

Fig. 1.2.6

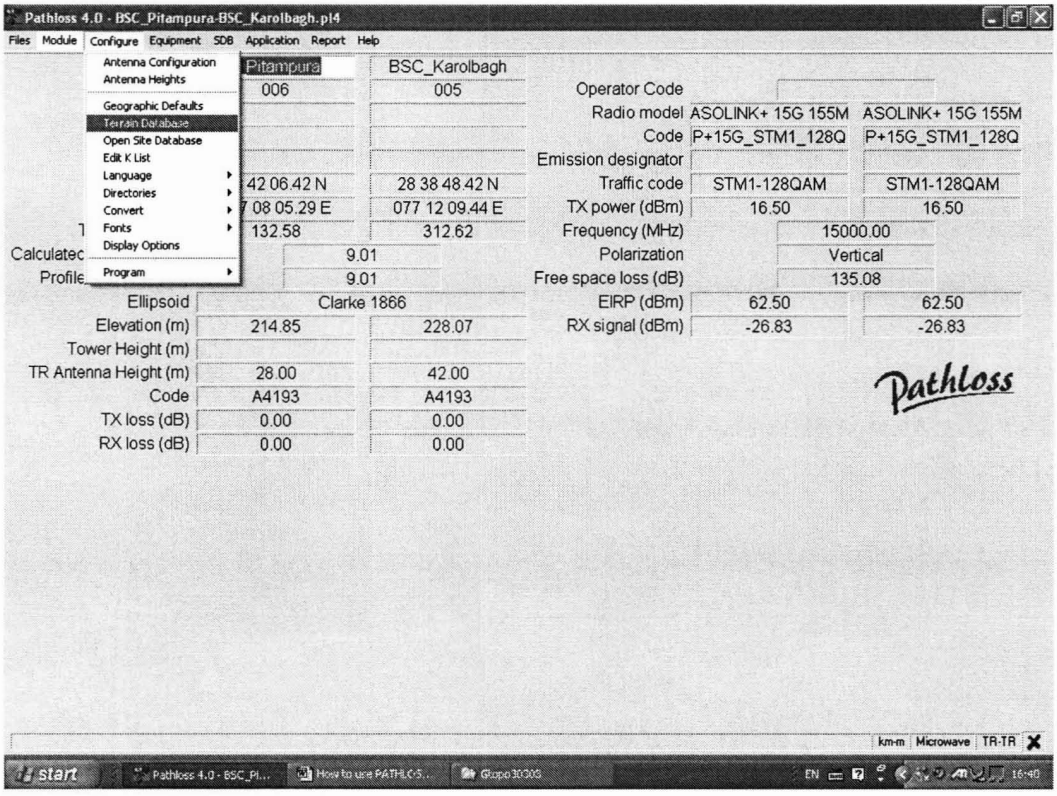

Fig. 1.2.7

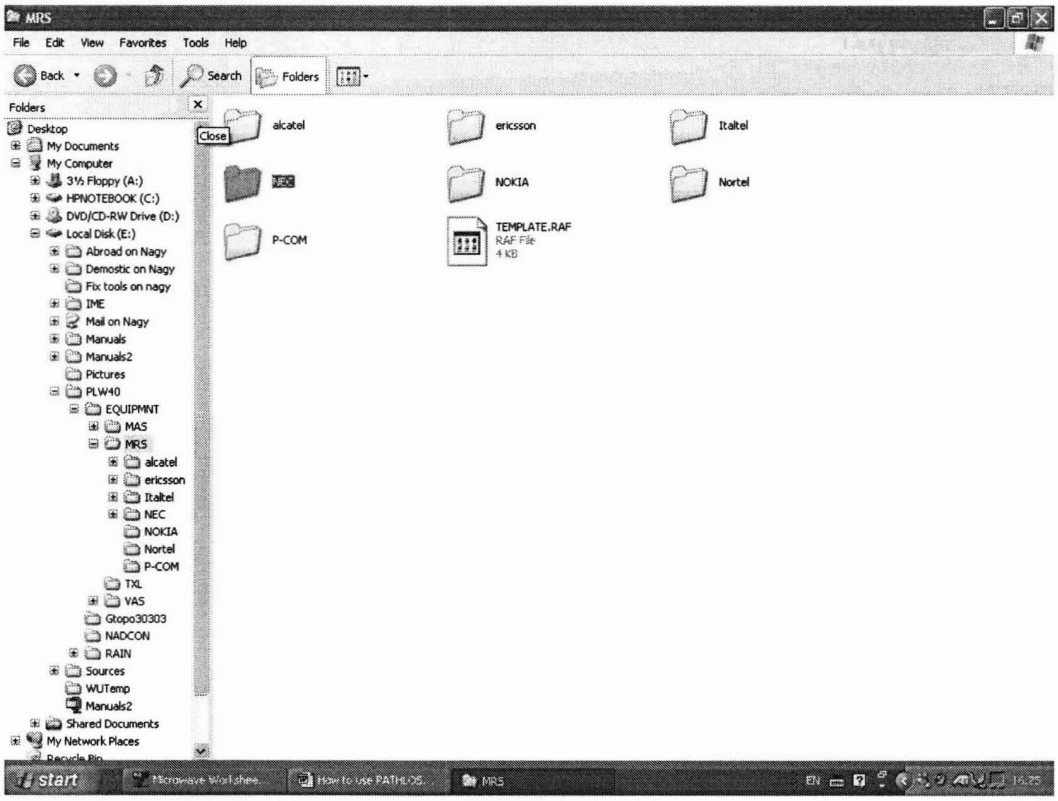

Fig. 1.2.5

3- Gopo30303 (Terrain Data File)

This folder contents the Terrain data for all the world but this data is very big size so it will be better if you take only some areas where you expected to do your survey as shown in Fig. 1.2.6

WARNING

This data is not accurate so we usually get terrain data from contours maps or from path survey.
Just we use this data for reference
So it isn't allowed to use this data to create path profile

How to set this data?

1- Create new folder in your PATHLOSS folder & name it as Gopo30303
2- Copy inside it the necessary area files (each area has 2 files)
3- Run pathloss program
4- Go to configure menu & click terrain database as shown in fig. 1.2.7
5- Set Primary (No Selection) & Secondary (GTopo30 Global 30sec) as shown in Fig. 1.2.8
6- Click Set Up Secondary – Set Directory – choose Gtopo30303 folder then kick OK – click Close – click OK as shown in Fig.1.2.9

2.5.7- Enter Feeder Data & connection losses by pressing on Wave Guide symbol then kick OK as shown in Fig. 2.5.7

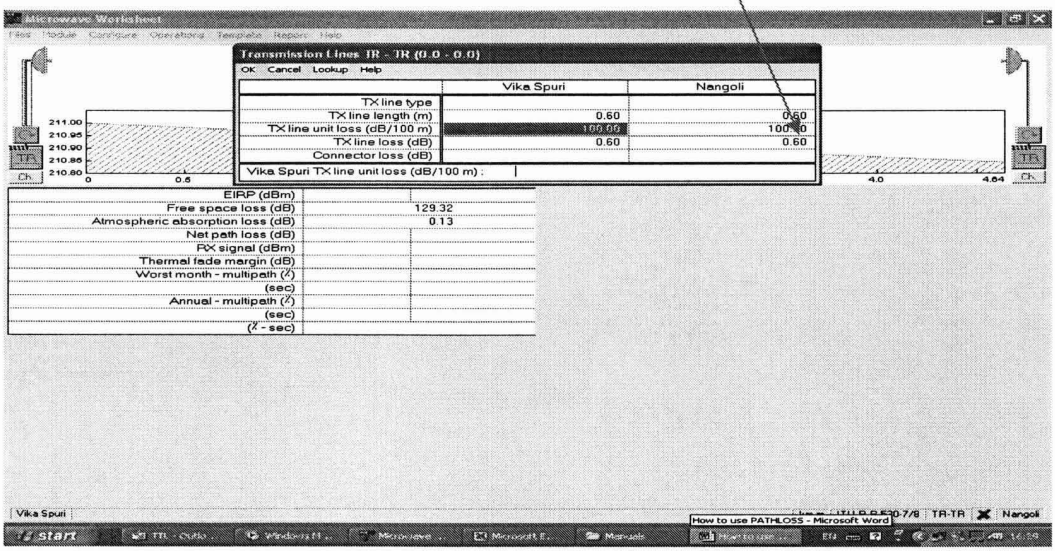

Fig. 2.5.7

2.5.8- Select antenna type for each station by clicking on antenna symbol then press as shown in Fig. 2.5.8

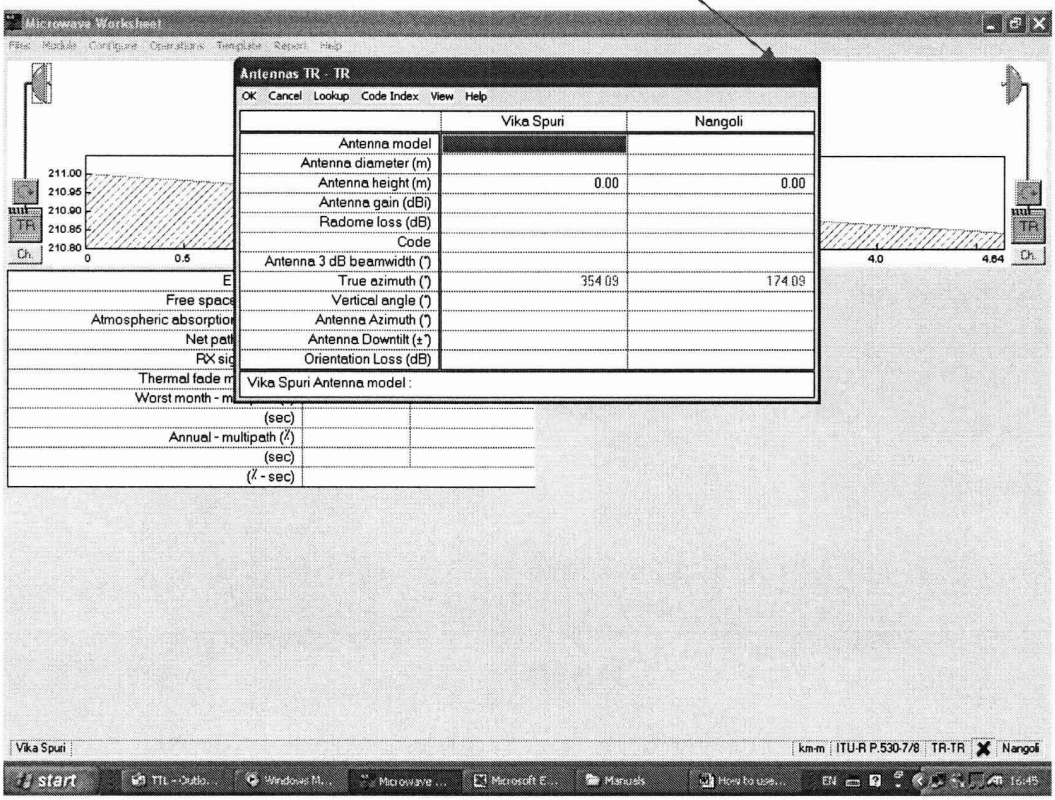

Fig. 2.5.8

2.5.9- Press on Code Index then New Index then brows for pathloss folder (where you placed it) – Equipment – MAS – Antenna manufacturer (Andrew, RFS, …..) – Frequency Range (102-132 , 122 – 132 , 142 – 153 , …….)then press OK as shown in Fig. 2.5.9

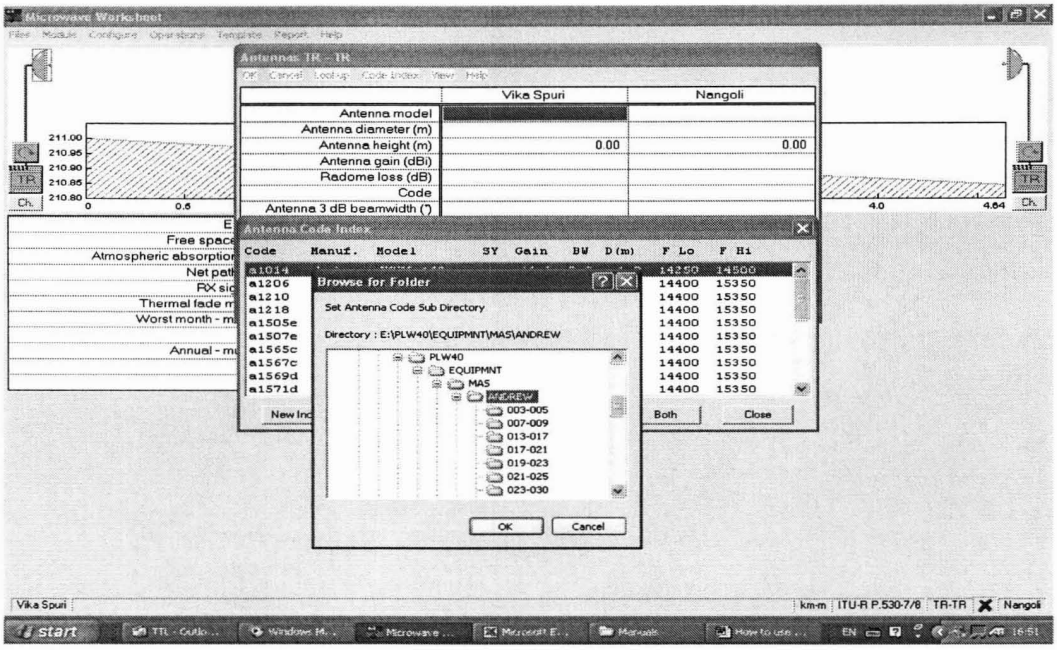

Fig. 2.5.9

2.5.10- Select antenna for site 1 & press on Site 1 & select antenna for site 2 & press Site 2 or in case of both sites have same antenna press on Both. The press Close – OK as shown in Fig. 2.5.10

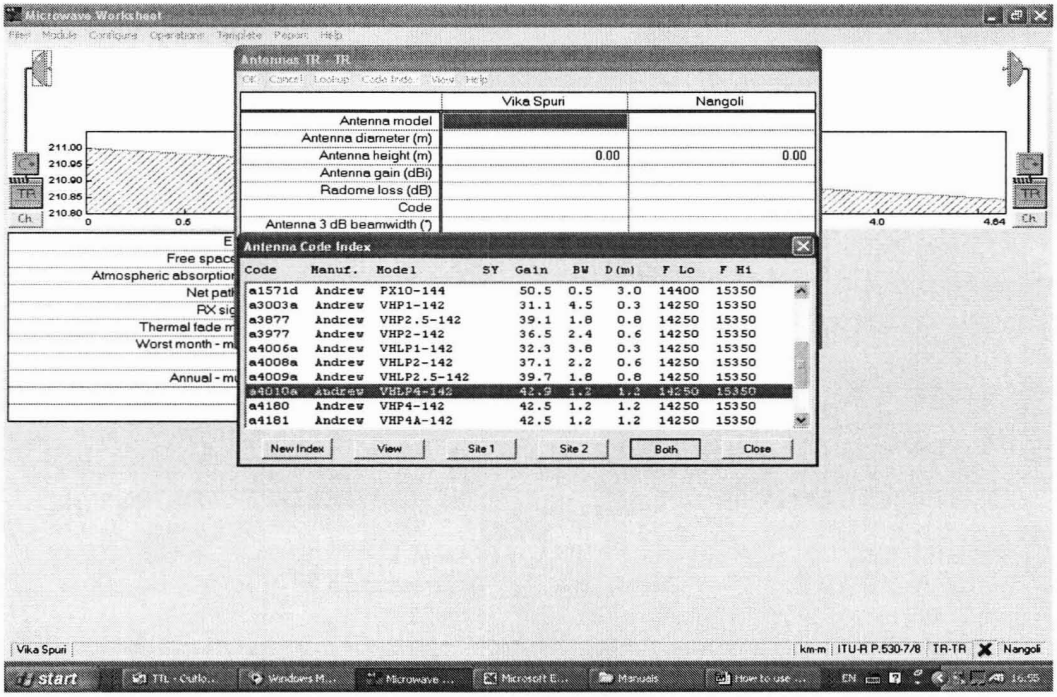

Fig. 2.5.10

2.5.11- Set Reliability Method

In worksheet page go to Operation Menu – reliability Methods as per attached in Fig. 2.5.11

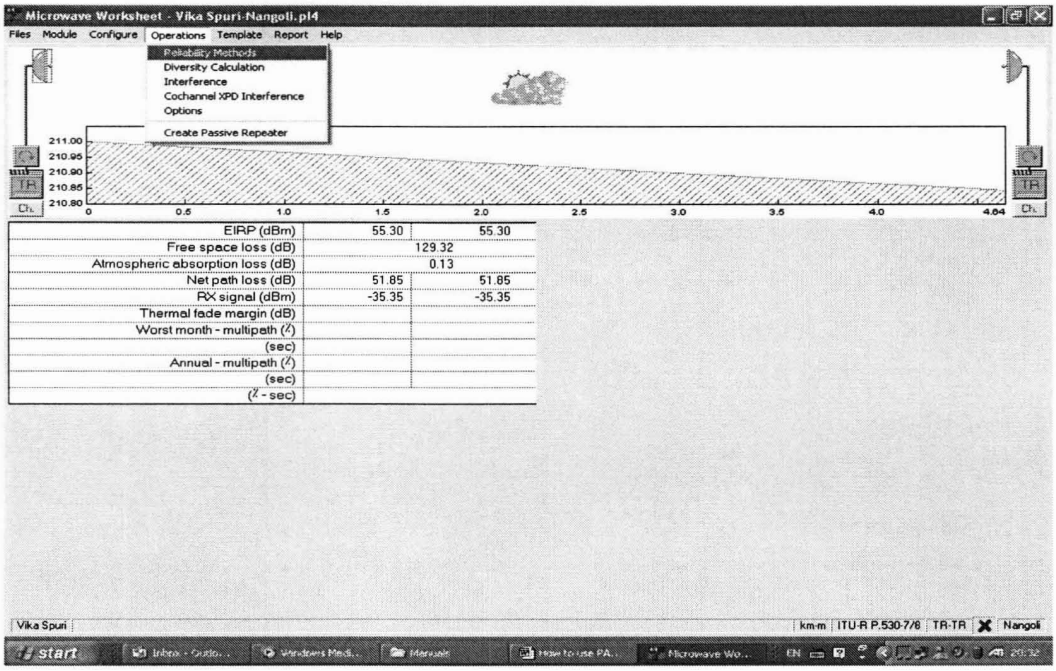

Fig. 2.5.11

Set Reliability criteria as per shown in Fig. 2.5.11-1 for SDH or as Project & Customer requirement & press OK

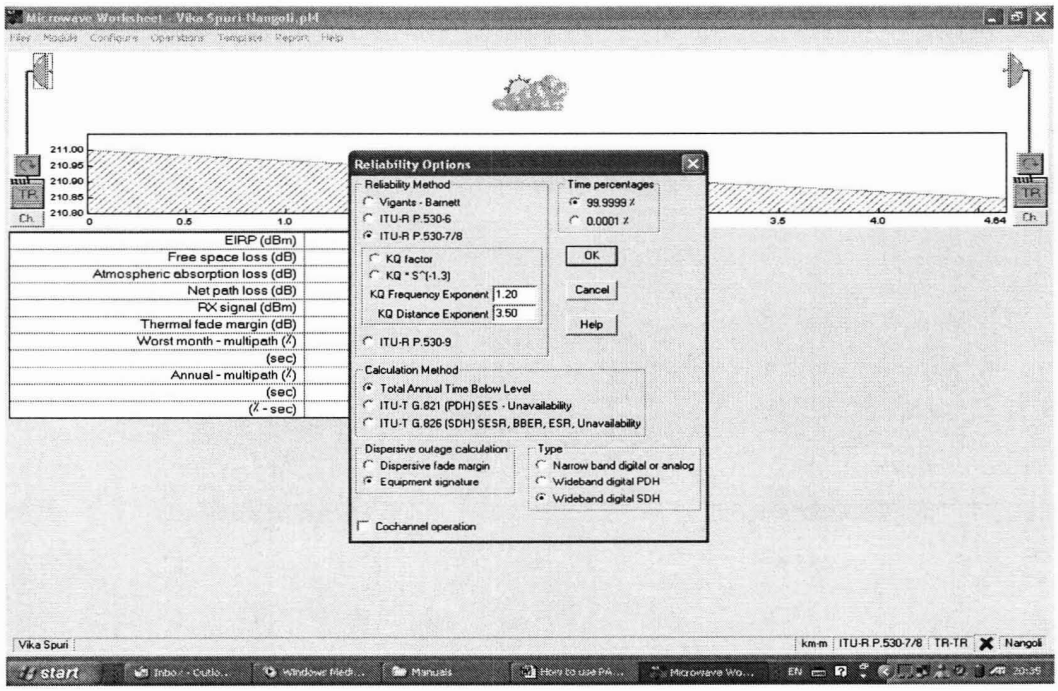

Fig. 2.5.11.1

2.5.12- Set of Rain factor

Press on Rain symbol – select ITU-R-P-530. 6/8 – press Load Rain File – Select Rain area according to ITU-530 Map Fig. 1.2.3 (Rain Files are placed in Pathloss folder – Rain) – Press Close as per shown in Fig. 2.5.12

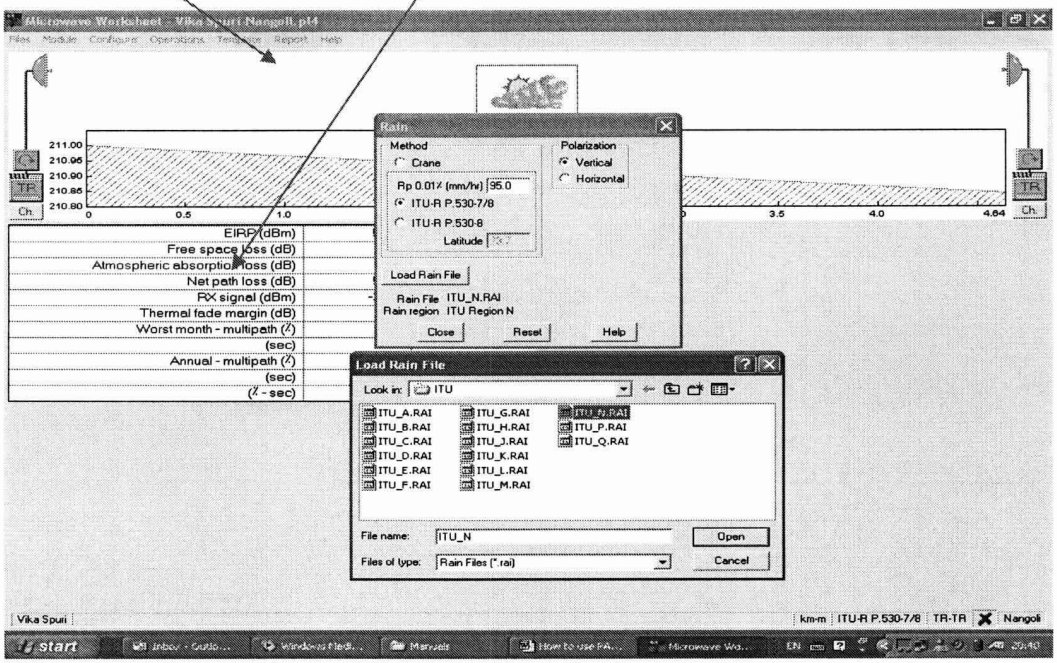

Fig. 2.5.12

2.5.13- Set Geoclimatic Factor

Press on the Ground Symbol (as shown in Fig. 2.5.13-1) – Set Geoclimatic Factor according to ITU-R-P-453 as Shown in Fig. 2.5.13-2)

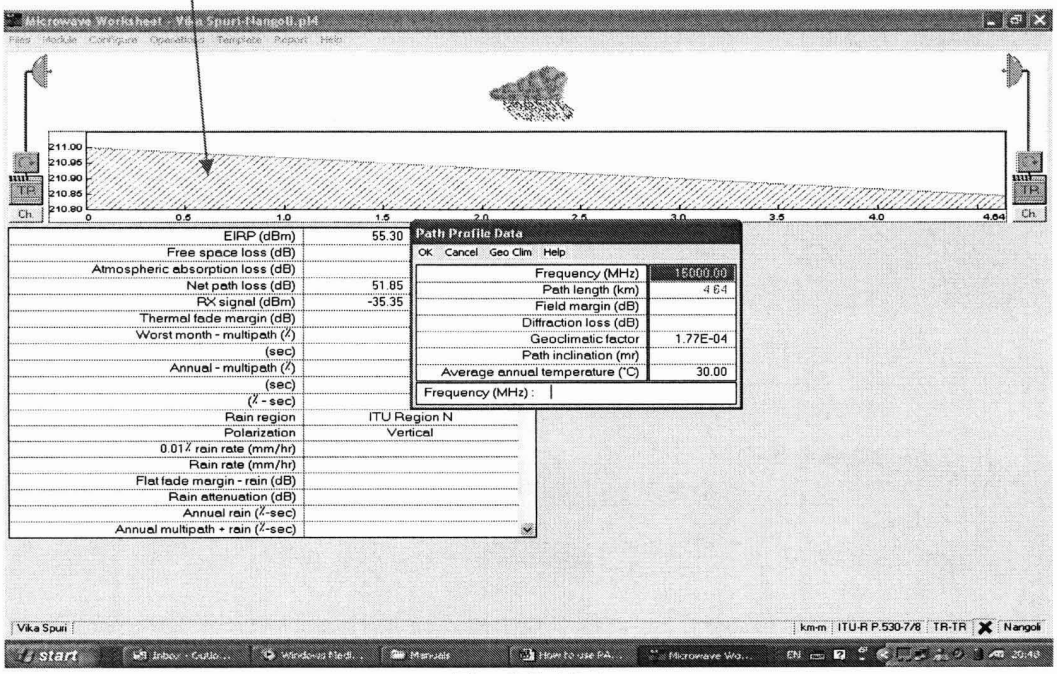

Fig. 2.5.13-1

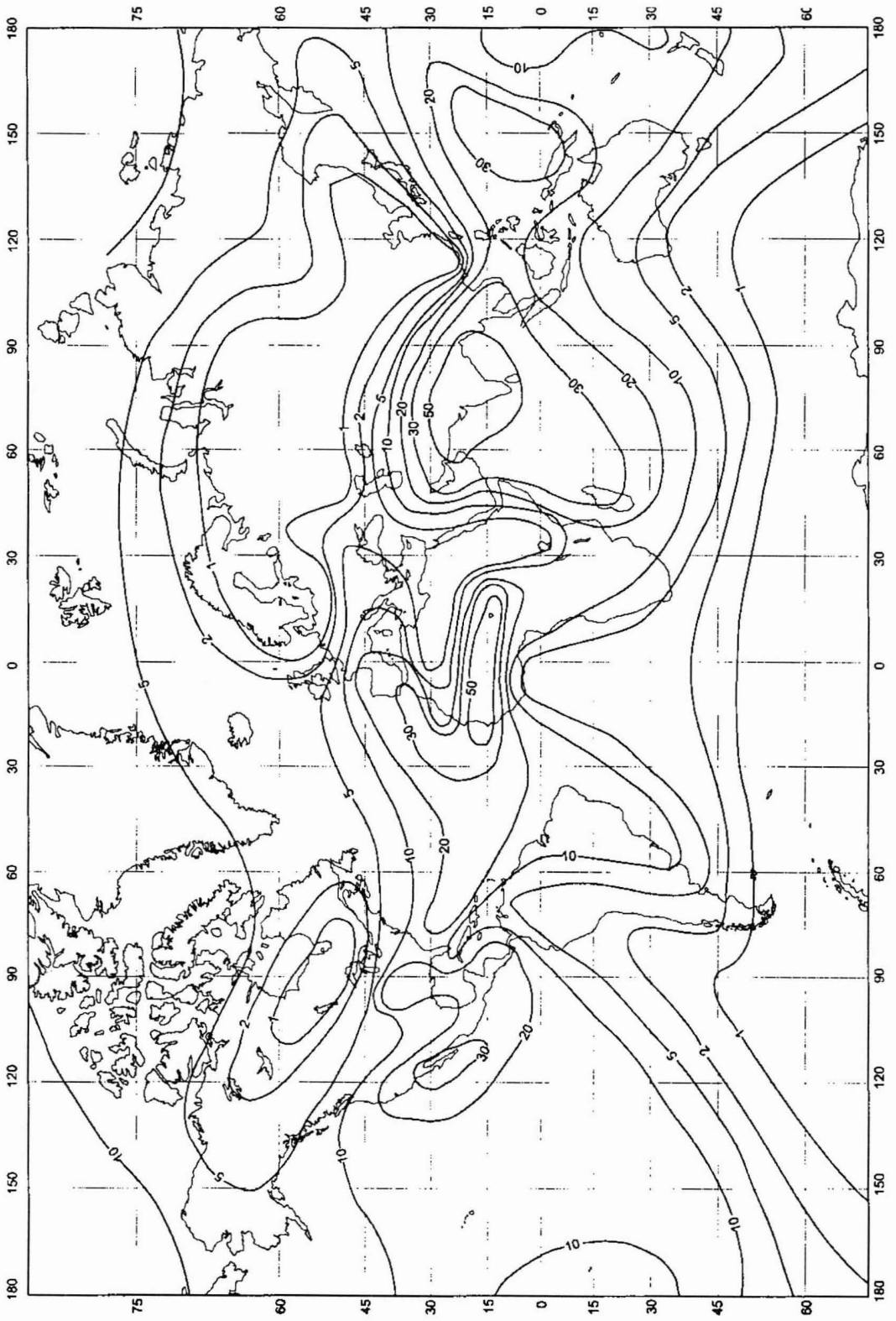

Percent of Time Gradient ≤ 100 N units / km - November

Fig. 2.5.13-2

2.5.14- Make sure of either our Path Calculation is correct or we need to revise again. To do that please check the followings

- Make sure that your worksheet page has Green Correct sign in Right Bottom of screen. If it is wrong sign that's mean there are some data mistake
- Have a look to RX Signal, Fade Margin & (Annual Availability with rain) Percentage as per shown in Fig. 2.5.14

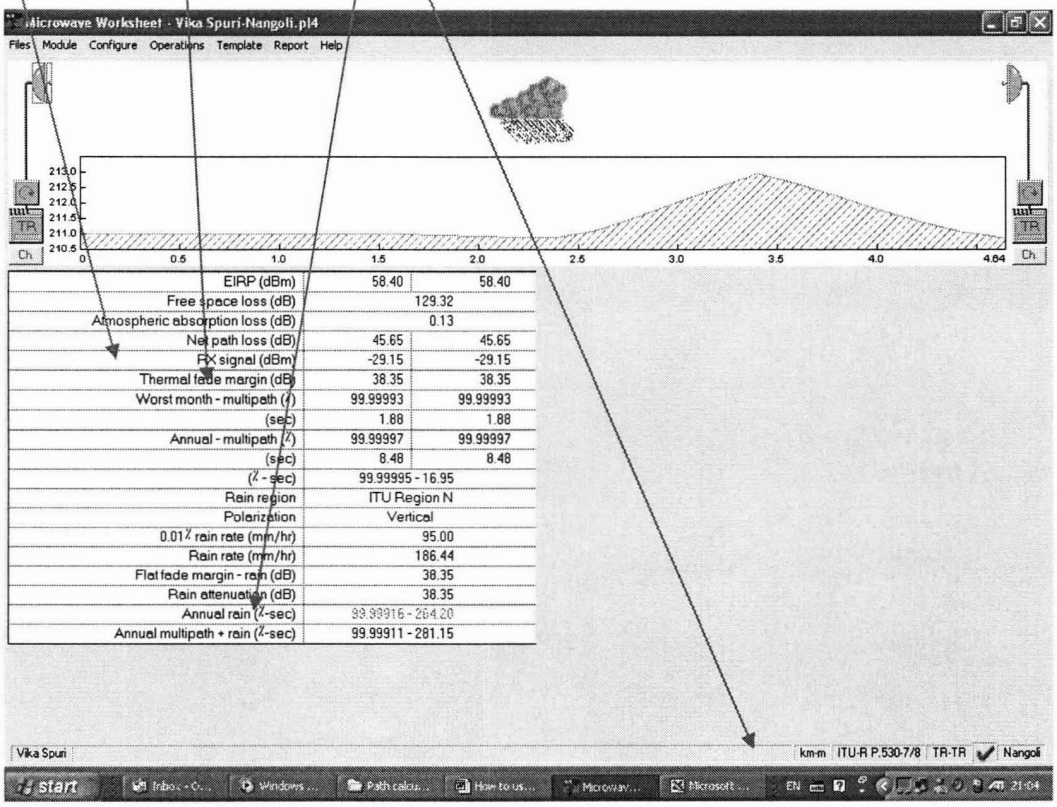

Fig. 2.5.14

- If any of (RX, Margin, Availability) is less than the required to meet the Spec. & recommendations. You have to increase antenna diameter or add Space Diversity Radio to reach to the required Spec.
- So you go to step 2.5.10 again & select new antennas

2.5.15- After finish of path calculations go to Report Menu in Worksheet page – click Full Report

You will get full path calculation report as below one. You can copy it to Word or Excel sheet & save it for reference & submitting with your survey report

Microwave Worksheet - Vika Spuri-Nangoli.pl4

	Vika Spuri	Nangoli
Elevation (m)	211.00	210.84
Latitude	28 38 24.30 N	28 40 54.20 N
Longitude	077 04 28.80 E	077 04 11.20 E
True azimuth (°)	354.09	174.09
Vertical angle (°)	-0.02	-0.01
Antenna model	VHP6-142	VHP6-142
Antenna height (m)	0.00	0.00
Antenna gain (dBi)	46.00	46.00
TX line length (m)	0.60	0.60
TX line unit loss (dB /100 m)	100.00	100.00
TX line loss (dB)	0.60	0.60
Circ. branching loss (dB)	3.50	3.50
Frequency (MHz)	15000.00	
Polarization	Vertical	
Path length (km)	4.64	
Free space loss (dB)	129.32	
Atmospheric absorption loss (dB)	0.13	
Net path loss (dB)	45.65	45.65
Radio model	PASOLINK+ 15G 155MB	PASOLINK+ 15G 155MB
TX power (watts)	0.04	0.04
TX power (dBm)	16.50	16.50
EIRP (dBm)	58.40	58.40
TX Channels	1 14543.0000V	1' 14963.0000V
RX threshold criteria	BER 10-6	BER 10-6
RX threshold level (dBm)	-67.50	-67.50
RX signal (dBm)	-29.15	-29.15
Thermal fade margin (dB)	38.35	38.35
Geoclimatic factor	1.77E-04	
Path inclination (mr)	0.03	
Average annual temperature (°C)	30.00	
Worst month - multipath (%)	99.99993	99.99993
(sec)	1.88	1.88
Annual - multipath (%)	99.99997	99.99997
(sec)	8.48	8.48
(% - sec)	99.99995 - 16.95	
Rain region	ITU Region N	
0.01% rain rate (mm/hr)	95.00	
Flat fade margin - rain (dB)	38.35	
Rain rate (mm/hr)	186.44	
Rain attenuation (dB)	38.35	
Annual rain (%-sec)	99.99916 - 264.20	
Annual multipath + rain (%-sec)	99.99911 - 281.15	

ÇáÇÍÏ, ÑÈíÚ ÇáÇæá 10 1424
Reliability Method - ITU-R P.530-7/8
Rain - ITU-R P530-7

2.6- Frequency Interference Calculations for the Network

After completing all the above processes for all the link you should calculate if there will be any frequency interference cases in the designed Network (if there are any existing links working with the same frequency band you have to add it to your network before calculating interference)

How to Calculate frequency Interference

2.6.1- Go to Network Page by clicking ctrl N – Defaults menu – Link Label
Select TX Frequency & Polarization – Press Rest All as per shown in Fig. 2.6.1

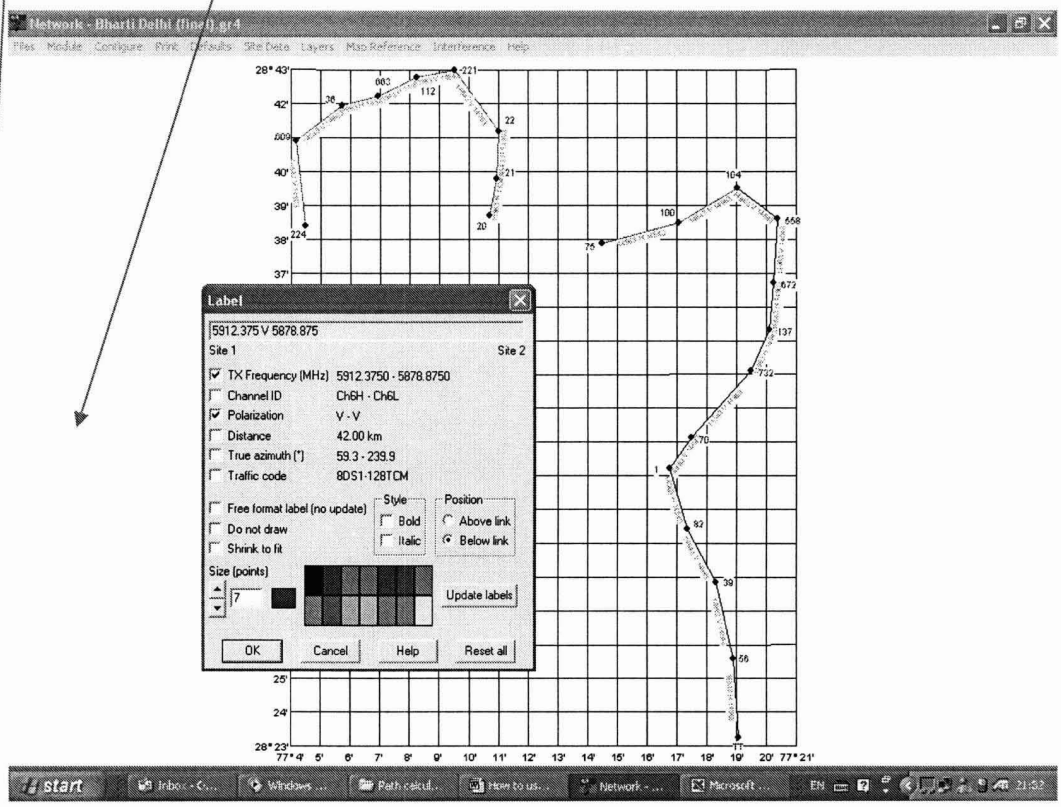

Fig. 2.6.1

Have a look to your network & make sure that all links Frequencies & Polarizations are correct according to your plan. If there is any mistake in any link please go to its work sheet & make it correct

2.6.2- Go to Interference Menu & Click Calculate Intra as per shown in Fig. 2.6.2

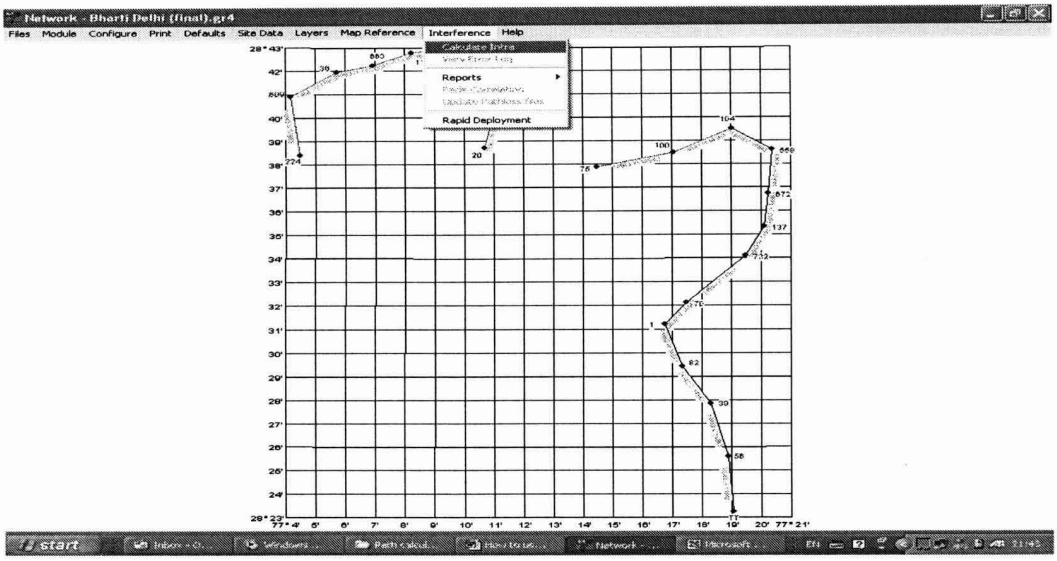

Fig. 2.6.2

2.6.3- Set the Interference Calculation criteria according to Specs. & press Calculate as per shown in Fig. 2.6.3

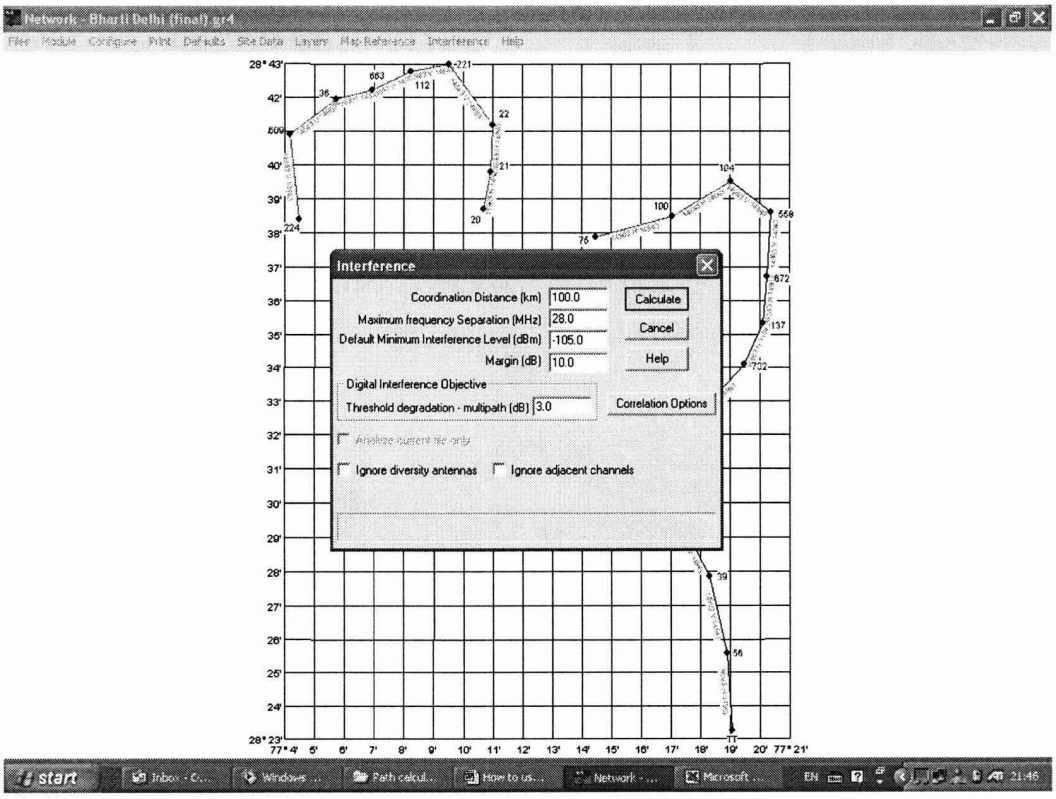

Fig. 2.6.3

2.6.4- Go to Interference Menu – Report – Cross Reference as shown in Fig. 2.6.4

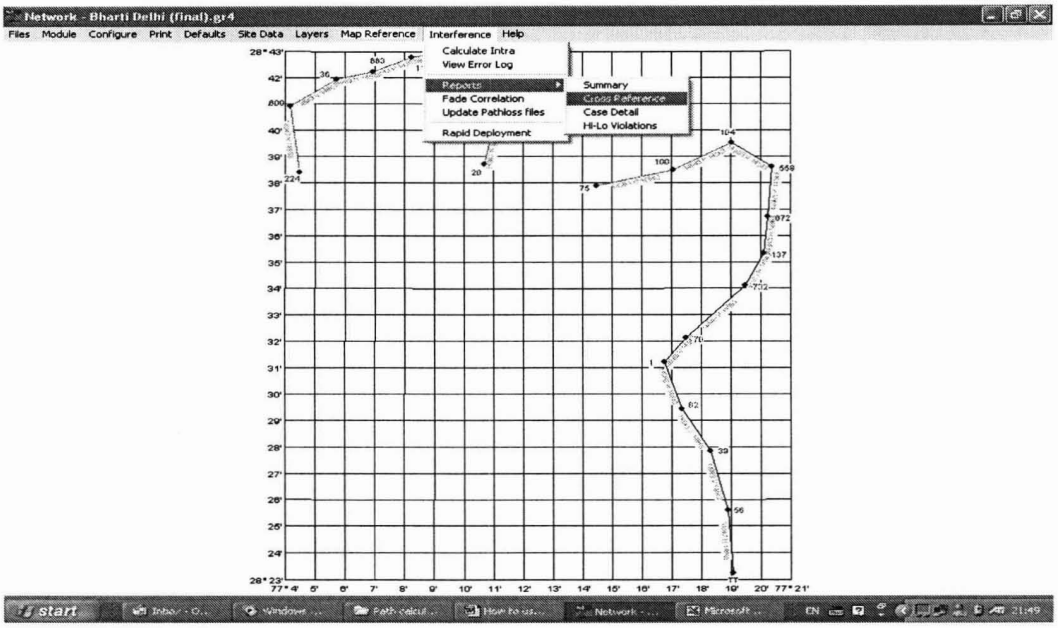

Fig. 2.6.4

2.6.5- You will get Interferences cases as below example.

Study carefully those interference cases & if any one of them is dangerous case please re-plan you network frequencies or change your antenna type to higher XPD antennas. Also you can use ATPC function to keep lower TX power which will help to avoid some interference cases

Interference Cross Reference - Bharti Delhi (final).gr4

Coordination Distance (km)	100.00	obj	Interference level objective (dBm)
Maximum frequency Separation (MHz)	28.00	v-i	Victim to interferer path length (km)
Default Minimum Interference Level (dBm)	-105.00	tad	Total antenna discrimination (dB)
Margin (dB)	10.00	ifl	Interfering Signal (dBm)
Threshold degradation objective (db)	3.00	td	Threshold Degradation (dB)
Total number of cases calculated	87	*	OHLOSS

Calculation made on ÇáÇÍÏ, ÑÈíÚ ÇáÃæá 10 1424 09:46:00 ã

Case 1 Charmwood (Okhla), VHP4A-142, 14963.0000H, STM1-128QAM, obj = -98.6
1-1 Faridabad (Charmwood), VHP2-142, 14963.0000V, STM1-128QAM, v-i = 3.3, tad = 70.0 (i 0.0° v -191.9°), ifl = -102.0 (3.5), td = 1.6
1-2 Okhla (Sarita Vihar), VHP2-142, 14963.0000V, STM1-128QAM, v-i = 3.5, tad = 68.0 (i 128.8° v 0.0°), ifl = -100.2 (1.7), td = 2.2

Case 2 Okhla (Charmwood), VHP2-142, 14543.0000H, STM1-128QAM, obj = -98.6
2-1 Charmwood (Faridabad), VHP4A-142, 14543.0000V, STM1-128QAM, v-i = 3.5, tad = 67.0 (i 191.9° v 0.0°), ifl = -99.1 (0.5), td = 2.7
2-2 Faridabad19 (Faridabad), VHP2-142, 14543.0000V, STM1-128QAM, v-i = 11.0, tad = 52.2 (i -5.7° v -2.3°), ifl = -100.3 (1.7), td = 2.2 *

2-3 Sarita Vihar (Okhla), VHP2-142, 14543.0000V, STM1-128QAM, v-i = 2.0, tad = 68.0 (i 0.0° v -128.8°), ifl = -101.4 (2.9), td = 1.8

Case 3 Faridabad (Charmwood), VHP2-142, 14543.0000V, STM1-128QAM, obj = -98.6
3-1 Charmwood (Okhla), VHP4A-142, 14543.0000H, STM1-128QAM, v-i = 3.3, tad = 70.0 (i -191.9° v 0.0°), ifl = -101.8 (3.2), td = 1.7
3-2 Faridabad19 (Faridabad), VHP2-142, 14543.0000V, STM1-128QAM, v-i = 4.2, tad = 62.0 (i 0.0° v -164.7°), ifl = -102.0 (3.4), td = 1.6
3-3 Shalimar Bagh (Wazipur), VHP4A-142, 14543.0000V, STM1-128QAM, v-i = 31.4, tad = 30.1 (i 9.4° v 1.0°), ifl = -81.5 (-17.0), td = 17.1 *
3-4 Kamal Hotel (Gopala Tower), VHP2-142, 14543.0000H, STM1-128QAM, v-i = 25.2, tad = 48.3 (i -38.8° v -0.5°), ifl = -103.8 (5.2), td = 1.1 *

Case 4 Charmwood (Faridabad), VHP4A-142, 14963.0000V, STM1-128QAM, obj = -98.6
4-1 Okhla (Charmwood), VHP2-142, 14963.0000H, STM1-128QAM, v-i = 3.5, tad = 67.0 (i 0.0° v 191.9°), ifl = -99.3 (0.8), td = 2.6
4-2 Faridabad (Faridabad19), VHP2-142, 14963.0000V, STM1-128QAM, v-i = 3.3, tad = 62.0 (i 164.7° v 0.0°), ifl = -94.1 (-4.4), td = 5.7

Case 5 Faridabad19 (Faridabad), VHP2-142, 14963.0000V, STM1-128QAM, obj = -98.6
5-1 Okhla (Charmwood), VHP2-142, 14963.0000H, STM1-128QAM, v-i = 11.0, tad = 52.2 (i -2.3° v -5.7°), ifl = -100.5 (2.0), td = 2.1 *
5-2 Faridabad (Charmwood), VHP2-142, 14963.0000V, STM1-128QAM, v-i = 4.2, tad = 62.0 (i -164.7° v 0.0°), ifl = -102.2 (3.7), td = 1.6
5-3 Touch Tel (Faridabad19), VHP4A-142, 14963.0000H, STM1-128QAM, v-i = 4.4, tad = 68.0 (i 0.0° v -170.3°), ifl = -102.5 (3.9), td = 1.5
5-4 Mayur Vihar Ph-3 (Noida Sec10), VHP2-142, 14963.0000H, STM1-128QAM, v-i = 20.6, tad = 50.3 (i 1.3° v -341.0°), ifl = -104.2 (5.6), td = 1.0 *

Case 6 Faridabad (Faridabad19), VHP2-142, 14543.0000V, STM1-128QAM, obj = -98.6
6-1 Charmwood (Faridabad), VHP4A-142, 14543.0000V, STM1-128QAM, v-i = 3.3, tad = 62.0 (i 0.0° v 164.7°), ifl = -93.9 (-4.7), td = 5.9
6-2 Faridabad19 (Touch Tel), VHP2-142, 14543.0000H, STM1-128QAM, v-i = 4.2, tad = 68.0 (i 170.3° v 0.0°), ifl = -108.0 (9.4), td = 0.5

Case 7 Touch Tel (Faridabad19), VHP4A-142, 14543.0000H, STM1-128QAM, obj = -98.6
7-1 Faridabad19 (Faridabad), VHP2-142, 14543.0000V, STM1-128QAM, v-i = 4.4, tad = 68.0 (i -170.3° v 0.0°), ifl = -102.2 (3.7), td = 1.5
7-2 Vaishali (Mayur Vihar Ph-3), VHP4A-142, 14543.0000V, STM1-128QAM, v-i = 28.5, tad = 50.7 (i 0.7° v -352.4°), ifl = -95.1 (-3.5), td = 5.1 *

Case 8 Faridabad19 (Touch Tel), VHP2-142, 14963.0000H, STM1-128QAM, obj = -98.6
8-1 Faridabad (Faridabad19), VHP2-142, 14963.0000V, STM1-128QAM, v-i = 4.2, tad = 68.0 (i 0.0° v 170.3°), ifl = -108.2 (9.7), td = 0.4

The Effect of Terrain Roughness in the Microwave Line-of-Sight Multipath Fading Estimation Based on Rec. ITU-R P.530-15

Polat Göktaş[*1], *Ayhan Altıntaş* [1,2], *Satılmis Topçu*[2], and *Ezhan Karaşan*[1]
[1] Department of Electrical and Electronics Engineering, Bilkent University, Ankara 06800, Turkey
pgoktas@ee.bilkent.edu.tr, altintas@ee.bilkent.edu.tr and ezhan@ee.bilkent.edu.tr
[2] Bilkent University - ISYAM, Ankara 06800, Turkey
topcu@ee.bilkent.edu.tr

Abstract

Multipath fading is an important constraint on the prediction of path loss for terrestrial line-of-sight microwave links. The International Telecommunication Union - Radiocommunication (ITU-R) Rec. P.530 [1] is one of the most widely used methods providing guidelines for the design of terrestrial line-of-sight links. The purpose of the study presented in this paper is to make an investigation of the effect of both terrain roughness and geoclimatic factor parameters in the path loss characteristics of microwave line-of-sight (LOS) propagation in NATO Band 3+ (1350 - 2690 MHz) and NATO Band 4 (4440 - 5000 MHz) frequency ranges. The two parameters led to significantly different results for the link availability due to multipath fading as a function of the fade margin.

1. Introduction

The estimation of path loss and link availability is necessary for the design of line-of-sight radio-relay systems. A worldwide path loss prediction model has been recommended by the Radiocommmunication Sector of the International Telecommunication Union (ITU-R) in Recommendation ITU-R P.530 [1]. This recommendation is used to predict both path loss and link availability in the average worst month for microwave links. Rec. ITU-R P.530 [1] path loss prediction model is composed of four significant clear-air and rainfall propagation mechanisms on terrestrial line-of-sight links: fading or enhancement due to multipath effects, diffraction loss over terrain obstruction, attenuation due to hydrometeors and depolarization (XPD). This paper focuses on multipath propagation model in clear-air environment for terrestrial line-of-sight links.

In this paper, we first analyse the theoretical prediction method of flat fading (such as worst month outage probability) based on Rec. ITU-R P.530. Then, we define how to find out the standart deviation of terrain height and investigate the effect of terrain roughnesss on the worst month outage probability for an example link in Istanbul, Turkey.

2. Mathematics of Multipath Fading Model

Link unavailability due to multipath fading in the average worst month depends on the effects of climate and terrain data. S_a [1] is defined as the standard deviation of terrain heights (m) within a 110 km × 110 km area in Rec. ITU-R P.530. The worldwide data for this parameter is provided by ITU-R Study Group 3.

Another parameter needed to calculate the link availability of terrestrial line-of-sight links is the geoclimatic factor. There are two ways to calculate this parameter: a quick calculation (QC) method and a detailed link design (DLD) method.

- The quick calculation (QC) method uses only, dN_1 [1, 2], point refractivity gradient in the lowest 65 m of the atmosphere not exceeded for 1% of an average year as shown in Equation (1). The worst month outage probability, p_w, is calculated by using Equations (2) and (3) in the quick calculation (QC) method.

ITU-R P.530-15 [1] Quick Calculation Method

$$\mathrm{K} = 10^{-4.6-0.0027dN_1} \tag{1}$$

$$p_o = Kd^{3.1}(1+|\varepsilon_p|)^{-1.29} f^{0.8} \times 10^{-0.00089h_L} \tag{2}$$

$$p_w = p_o \times 10^{\frac{-A}{10}} \tag{3}$$

978-1-4673-5225-3/14/$31.00 ©2014 IEEE

- The detailed link design (DLD) method uses both dN_1 and S_a parameters as shown in Equation (4). The percentage of time that fade depth A (in decibels) is exceeded in the average worst month is calculated by using Equations (5) and (6).

ITU-R P.530-15 [1] Detailed Link Design Method

$$K = 10^{-4.4-0.0027dN_1}(10 + S_a)^{-0.46} \tag{4}$$

$$p_o = Kd^{3.4}(1 + |\varepsilon_p|)^{-1.03} f^{0.8} \times 10^{-0.00076h_L} \tag{5}$$

$$p_w = p_o \times 10^{\frac{-A}{10}} \tag{6}$$

The parameters dN_1, S_a, $|\varepsilon_p|$ and h_L significantly affect the fade occurrence factor, p_o and unavailability due to multipath fading probability, p_w. Equations (3) and (6) are used for a deep-fading prediction method (for small percentage of time) but for all percentage of time A must be replaced by A_t, the fade depth at which the transition occurs between deep-fading and shallow-fading distribution.

3. Impact of Terrain Roughness Parameter in Multipath Fading Estimation

We calculate the standard deviation of terrain heights, S_a which is a parameter in the performance prediction of the microwave radio links. The method calculates the mean of the terrain heights in a specified window around the point of interest as shown in Equation (7).

$$\bar{x} = \frac{\sum_{i=1}^{n} x_i}{n} \tag{7}$$

Then, the standard deviation of the terrain heights (σ) is calculated according to the following equation

$$\sigma = \sqrt{\sum_{i=1}^{n} \frac{(x_i - \bar{x})^2}{n-1}} \tag{8}$$

where n= number of path profile points
x_i= height (above sea level) of the i-th profile point

The worldwide S_a data provided by ITU-R is too coarse such that the distance between grid points is 110 km. If the path distance between transmitter and receiver sites is less than 110 km, S_a parameter is computed by using bi-linear interpolation of four gridpoints. We change the resolution of terrain roughness data and investigate its effect on the link availability. The path profile between transmitter and receiver sites is constructed by using a Digital Map in DTED format that has a resolution of 3×3 seconds (approximately 100 meters). Terrain roughness data is provided with the different moving window sizes. Different resolutions of S_a and the number of terrain points used in the calculation of S_a are given in Table 1.

Table 1. Different resolutions of S_a and number of terrain points in S_a data file

Resolution	Number of terrain gridpoints
30 seconds	121 × 121
1 minutes	61 × 61
5 minutes	13 × 13
10 minutes	7 × 7

To confirm this observation on the link availability, we applied simulation on terrestrial line-of-sight link located in Istanbul, Turkey. Figure 1 shows base station sites for microwave links studied in Istanbul. The path length of the Çataltepe - Beylikdüzü radio link is 55.448 km. The main parameters of this link are summarized in Table 2. As illustrated in Figure 2, clearance of the first Fresnel zone is investigated in the microwave link analysis. The path profile of the link is used in the analysis considering the curvature of the Earth.

Table 2. Terrestrial link parameters for Çataltepe - Beylikdüzü microwave LOS link

Parameter	Description
Transmitter Station	Çataltepe 41° N $02^{'}$ $58.00^{"}$ 29° E $17^{'}$ $48.00^{"}$
Receiver Station	Beylikdüzü 41° N $01^{'}$ $06.00^{"}$ 28° E $38^{'}$ $17.00^{"}$
Altitude of transmitter station (a.s.l)	300 m
Altitude of receiver station (a.s.l)	150 m
Height of receiving antenna (a.g.l)	20 m
Radio Frequency	2 GHz
Path Length	55.448 km
Path Inclination	2.69 mrad
dN_1	-451.5 N-units/km
Free Space Loss	133.4 dB

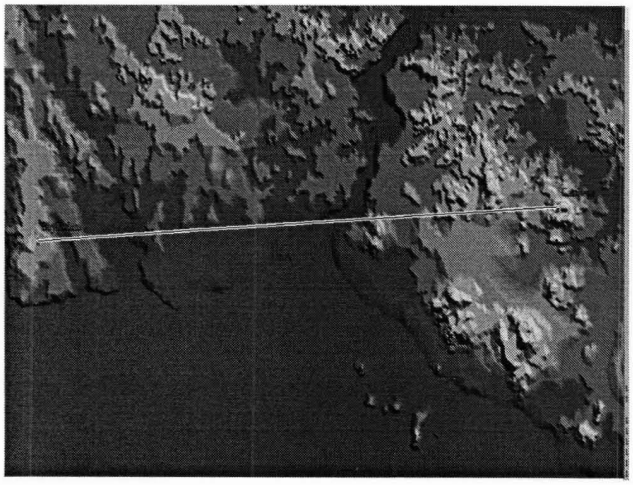

Figure 1. Location of sites used for microwave link simulation in Istanbul, Turkey

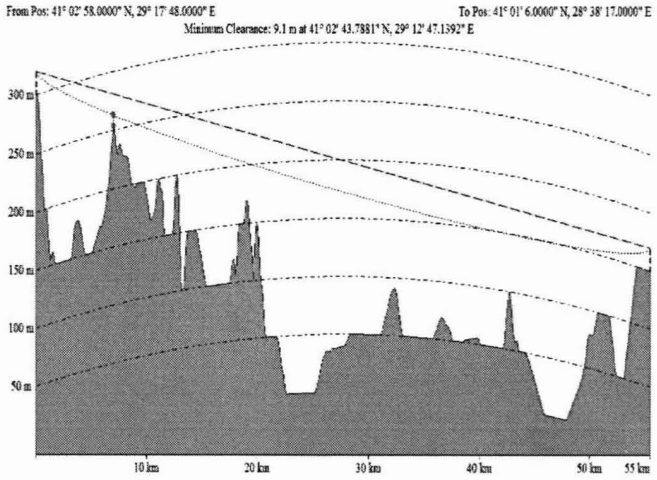

Figure 2. Cataltepe - Beylikdüzü Radio Link LOS Analysis, first Fresnel zone is indicated by the curve under the LOS path

In this paper, there are two different ways to calculate terrain roughness parameter: mean and midpoint path profile point. In the first case, the associated latitude and longitude of each profile point is determined along the Çataltepe - Beylikdüzü path using a fixed distance increment. Terrain roughness data is found at each profile point in this radio link. Another investigation parameter is the impact of the midpoint terrain roughness on the link availability in example radiolink. The coordinates of the midpoint is obtained from the average of transmitter and receiver site coordinates. If the location coordinates along the path are different from the gridpoints, the standard deviation of terrain heights at the desired location is computed by performing a bi-linear interpolation on the values at the four closest gridpoints. The results are summarized in Table 3. The comparison of the results are presented on Figure 3(a) to Figure 3(b) in terms of predicted worst month unavailability.

Table 3. Terrain roughness data (S_a) for different window size in Çataltepe - Beylikdüzü microwave LOS link

30 second moving window size		1 minutes moving window size		5 minutes moving window size		10 minutes moving window size		S_a given by ITU	
Mean	Midpoint	Mean	Midpoint	Mean	Midpoint	Mean	Midpoint	Mean	Midpoint
10.7	6.1	16.7	10.3	36.3	21.1	47.5	38.7	134.4	128.0

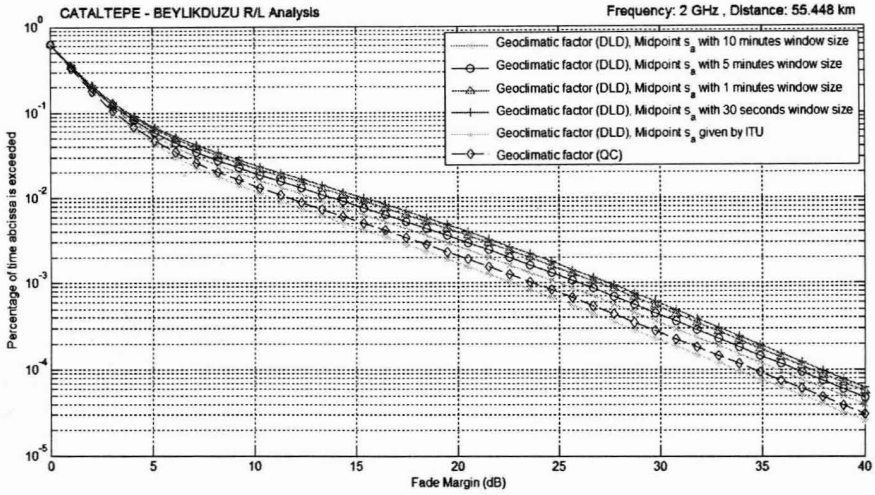

(a) Predicted worst month unavailability as function of midpoint terrain roughness value

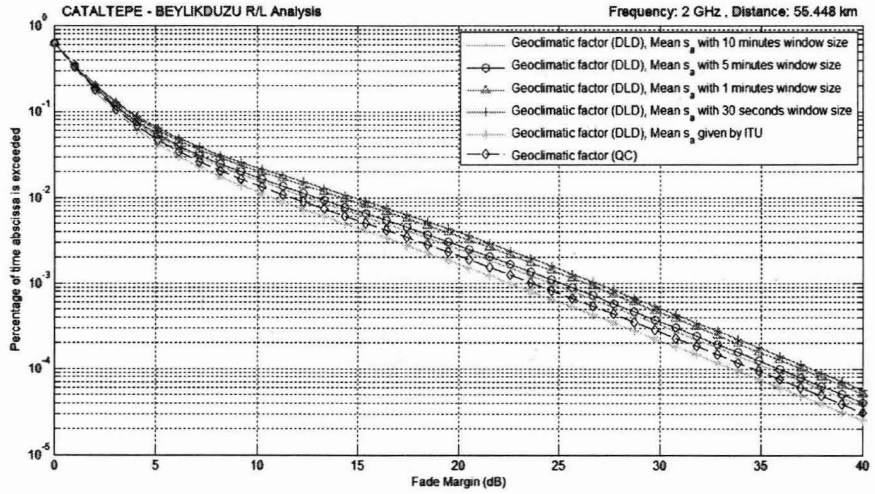

(b) Predicted worst month unavailability as function of mean terrain roughness value

Figure 3. Percentage of time (p_w) that fade depth (A) is exceeded in an average worst month

4. Conclusion

The multipath fading outage prediction method proposed by Recommendation ITU-R P.530 [1] is studied. We compared two methods of terrain roughness calculation on terrestrial microwave line-of-sight links. The effect of geoclimatic factor and different resolutions of terrain roughness data is investigated on the worst month link unavailability in Çataltepe - Beylikdüzü microwave radio link. At the fixed unavailability (p_w=10^{-3}), fade margin can change up to 5 dB as shown in Figure 3. It can be seen that multipath fading prediction model with the terrain roughness data provided by ITU is optimistic. The future work will be focused on field measurements which will be used for better comparison of simulation results.

5. References

1. International Telecommunication Union, "Propagation data and prediction methods required for the design of terrestrial line-of-sight systems," Recommendation ITU-R P. 530-15, 2013.

2. International Telecommunication Union, "The radio refractive index: its formula and refractivity data," Recommendation ITU-R P. 453-10, 2012.

100 Ft 38 44 44.96

104 51 40.89

30 Ft 39 25 39

104 52 0.01

TAP
WC
[illegible]

21228
W135F

Professional Path Analysis Using a Spreadsheet

Use any common spreadsheet application to do your path-analysis number crunching.

By James Lawrence Sr, WB5HVH

Modern spreadsheet programs have the power to compute and to present line-of-sight radio-path analyses. The accuracy of the predictions and the quality of the presentations can exceed that obtained with commercial software. By developing your own spreadsheet application, you can supplement or replace your current path-analysis application. Capable spreadsheet programs can be obtained for a modest price or even free of charge.[1]

The formulas and methods required to build a path-analysis spreadsheet application are in the public domain and are readily discovered using the Internet or your public library. Virtually any modern spreadsheet program has the horsepower to handle the straightforward math. The only thing remaining is "elbow grease" and ingenuity. This paper will explain the math and the graphics required to build your own application for frequencies ranging from VHF to G-band microwave. It is based on a working application with field-proven results. The resulting application is accurate, inexpensive, simple to use and easily transportable.

[1]Notes appear on page 44.

2506 Radcliffe Dr
Sugar Land, TX 77478
wb5hvh@arrl.net

Cover Sheet

Having come from a telecom and control-systems engineering background, I prefer the "data sheet" format for presentation. This format lends itself nicely to the path analysis application. Also, I prefer a "3D" spreadsheet approach. That is, multiple "sheets" within a "book," with each sheet having a specific purpose. Fig 1 shows the cover sheet of my multi-sheet example application. Notice the datasheet format.

The "cover sheet" provides for user input, and it presents the numeric and graphic results. At the top of the sheet, there is a typical data-sheet area for title, revision history and other documentation. Both ends of the path (the sites) are documented in parallel columns. Just below the user input, there is a section for the numeric results. At the bottom, there is the obligatory visual representation of the path complete with ground elevation, foliage and Fresnel clearances.

Only the cells for user input are left unprotected. All other cells are protected for the purpose of document integrity. Calculation formulas may be hidden if desired. This portion of the document can be left austere or embellished with "pull-down" choices for user input if desired.

The example presented in this paper calculates path loss from site "A" to site "B" only. If there are separate transmit and receive antennas at the sites,

WIDGET LOGO HERE	REV	BY / DATE	REVISION DESCRIPTION	FILE NAME: S-Path.xls	REV: A
	A	J.R. Lawrence / 29-May-02	EXAMPLE	HOP NAME: SITE A to SITE B	
WiDGi-CORP COMUNICATIONS DEPARTMENT				HOP TYPE: 2.4 GHz Spread Spectrum	
RADIO HOP DATA SHEET				BY: jrl	CHKD: / APRVD:

GEN	01	SITE NAME			SITE ALPHA				SITE A	SITE BETA									SITE B
	02	ADDRESS			#1 ALPHA DRIVE					#2 BETA COURT									
	03	CITY, STATE, ZIP			ALPHA HILLS, TEXAS 78957					BETA VALLEY, TEXAS 77478									
	04	NORTH LATITUDE	NAD 27		32 DEG	26 MIN	52.0 SEC	*32.448* DEG		32 DEG	20 MIN	23.0 SEC	*32.340* DEG						
	05	WEST LONGITUDE			87 DEG	46 MIN	5.0 SEC	*87.768* DEG		87 DEG	55 MIN	1.0 SEC	*87.917* DEG						
TOWER	06	ELEVATION	TOWER HEIGHT	HEIGHT AGL	195 FT	360 FT	*555* FT			310 FT	270 FT	*580* FT							
	07	CALCULATED IN METERS			*59.4* M	*109.7* M	*169.2* M			*94.5* M	*82.3* M	*176.8* M							
	08	MANUFACTURER			ROHN					ALLIED									
	09	MODEL			TYPE 45					BETA									
	10	FCC/FAA TOWER NUMBER			87654321					12345678									
	11	OTHER INFO			GUYED TOWER W/STROBE AND DIAL-UP ALARM					SELF SUPPORTING W/STROBE AND TOWER WATCHER									
ANTENNA	12	TYPE			SOLID DISH W/RADOME					GRID DISH									
	13	MANUFACTURER	MODEL																
	14	SIZE	BEAMWIDTH	GAIN	6 FT	*1.8* M	4.8 DEG	30.8 dBd		8 FT	*2.4* M	3.6 DEG	33.3 dBd						
	15	HEIGHT AGL	BEARING		350 FT	*106.7* M	***229.4*** DEG A to B			260 FT	*79.2* M	***49.4*** DEG B to A							
	16	OTHER INFO		POLARIZATION				HORIZ					HORIZ						
FEED LINE	17	TYPE																	
	18	MANUFACTURER																	
	19	MODEL		SIZE															
	20	LENGTH 1	FREQ	ATTEN. / 100 FT	360 FT	2455.0 MHz	2.22 dB / 100 FT			270 FT	2455.0 MHz	2.22 dB / 100 FT							
	21	LENGTH 2	FREQ	ATTEN. / 100 FT	30 FT	2455.0 MHz	5.93 dB / 100 FT			30 FT	2455.0 MHz	5.93 dB / 100 FT							
	22	OTHER INFO																	
RADIO	23	MANUFACTURER																	
	24	MODEL		SERIAL NO.															
	25	TRANSMITTER	FREQ	GAIN	2455.0 MHz	27.0 dBm				2455.0 MHz	27.0 dBm								
	26	RECEIVER	SENS		-94.0 dBm					-94.0 dBm									
	27	OTHER INFO																	
RESULTS	28	HOP DISTANCE	HOP FACTORS		***11.46*** MILES	*18.44* KM	0.40 (0.125 DRY to 0.500 HUMID)			1.00 (4.0 SMOOTH to 0.25 MOUNTAINS)									
	29	SYSTEM GAINS: SITE A TO SITE B			*27.0* dB XMIT	*94.0* dB XCEIVE	*30.8* dB "A" ANT			*33.3* dB "B" ANT	*185.2* TOTAL								
	30	SYSTEM LOSSES			*131.1* dB PATH	*9.8* dB COAX "A"	*7.8* dB COAX B			*2.8* dB OTHER	*151.4* TOTAL								
	31	FADE MARGIN	AVAILABILITY	DOWNTIME	***33.8*** dB	***99.99985%***	***49*** SEC / YR or	0.8 MIN / YR or		0.014 HR / YR									

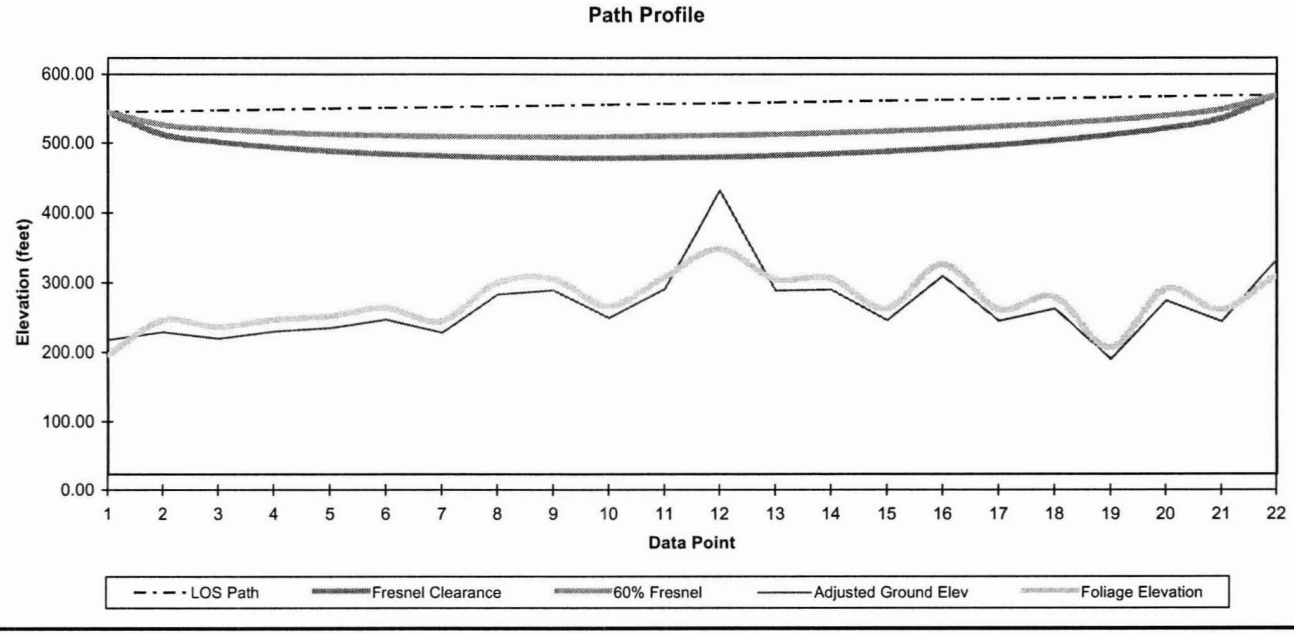

Fig 1—The author's cover sheet for his path-analysis spreadsheet.

it may be desirable to calculate from site B to site A also. Creating another instance of the file and swapping the site A and B parameters can easily do this. One could also get crafty and enhance the application to calculate both cases. Also, path diversity is not covered but can be readily handled if required.

As previously stated, my approach is to place the logical calculation groupings on separate sheets. This breaks the problem down into easy-to-manage sections. Each separate calculation sheet pulls data from the cover sheet, completes the calculations as required and pushes the result back up to the cover sheet. Examples of discrete calculation sheets are "Bearing and Distance," "Path Loss" and "Availability."

Bearing and Distance

For the bearing-and-distance calculations, you will need the latitude and the longitude of each site as input. The required output is the bearing from site A to site B, the bearing from site B to site A, and the distance between the sites in various units including Earth surface arc.

The latitude and longitude are available from user input on the cover sheet. The calculation will require these values in decimal format. Here is a method for making the latitude/longitude conversion to decimal.

=Cover!R24+((Cover!V24)+(Cover!Z24/60))/60

In this example, the values for "Degrees," "Minutes" and "Seconds" reside on the cover sheet in cells R24, V24 and Z24 respectively. Error checking can be implemented to ensure that the user does not enter values outside the valid range, that is "61 seconds."

Now that we have the latitudes and longitudes from user input and we have made the conversion to decimal, let us look at the distance calculation. The distance between any two points on the surface of a sphere can be determined with the formula:

$$\cos D = \sin A \sin B + \cos A \cos B \cos L \quad \text{(Eq 1)}$$

where

D = distance in degrees of arc
A = site A latitude in decimal degrees
B = site B latitude in decimal degrees
L = site A longitude minus site B longitude

Since A, B and L are known, the value for distance is easy to calculate. Although "degrees of arc" will be required to find the bearing, it is not very useful from the human perspective. To resolve this, here are some useful conversions:

111.23 km = degree of arc (for this planet only)
0.621371 mi = 1 km

Now, let's consider the bearing calculation. The bearing from site A to site B can be obtained with the following formula:

$$\cos C = (\sin B - \sin A \cos D) / (\cos A \sin D) \quad \text{(Eq 2)}$$

where

C = bearing from North
D = distance of arc between the sites, in degrees of arc (from the distance calculation above)

Again, this is a simple calculation, but there are caveats. First, the raw result only works half of the time. Second, know your spreadsheet's result format (degrees or radians) and make the necessary conversion when required. Knowing the sine of L allows you to resolve the "half the time" problem. Here is a way to work it all out:

=IF(E40 < 0, 360 – E46, E46)

confirms the raw bearing calculation from site A to site B. This means, "If the sine of L is less than zero, subtract the raw bearing from 360°, otherwise the answer is good.

In this calculation, cell E40 contains sin L and cell E46 contains the raw bearing in degrees,

=IF(E47 > 180, E47 – 180, E47 + 180)

derives the bearing from site B to site A. If the confirmed bearing is greater than 180°, subtract 180°, otherwise add 180°. Where cell E47 contains the confirmed bearing from site A to site B.

Please note that this calculation example works in north latitude and west longitude. It may require tweaking for the rest of the planet. This completes the bearing and distance calculations.

Path Loss

Next, we will tackle path loss. Path loss is loosely defined as the loss in signal associated with the line-of-sight or free-space distance between sites A and B. The formula for free-space path loss is readily available in textbooks and vendor catalogs.

$$L_{fs} = K + 20 \log f + 20 \log D \quad \text{(Eq 3)}$$

where

L_{fs} = loss in decibels
K = pseudo constant (based on frequency)
f = frequency in gigahertz
D = distance in miles

We have already calculated the distance between the sites. The frequency of the hop is known from user input. The only thing remaining is the constant, K. In general, K is equal to 96.6 dB plus some small frequency-dependent amount or addend. This would be a good application for a "pull-down" pick-list. My path-analysis application was only used within a known range of frequencies, so I simply interpolated between the lowest and the highest "frequency addend." The results came out very close to those obtained with a commercial application.

Availability

Another required calculation sheet is that of availability. There are several mathematical models for availability. I chose Barnett's:[2]

$$Av = (1 - a \times b \times 10^{-5} \times f/4 \times d^3 \times 10^{-FM/10}) \times 100\% \quad \text{(Eq 4)}$$

Where

Av = availability (uptime) expressed in percent
a = terrain roughness factor
b = climate factor
f = frequency in gigahertz
d = distance between sites in miles
FM = fade margin

This one is not tough, but it requires a bit more explanation. Terrain roughness and climate factors are subjective input from the user on the cover sheet. The terrain-roughness factor varies between 0.25 for mountains (rough) and 4.0 for Groom Lake (smooth). The climate factor varies between 0.125 for Groom Lake (dry) and 0.50 for Houston (humid). Again, frequency and distance are known values at this point. The last variable is fade margin. Fade margin is simply the sum of all gains minus the sum of all losses. This reminds me of one of the two "rules of engineering": "Some of it plus the rest of it equals all of it."[3] Fade margin will be discussed in more detail later; but for the sake of this calculation, its value resides in a cell on the cover sheet.

Miscellaneous Gains and Losses

There needs to be a place for the user to apply miscellaneous gains, losses and "guesstimates." This will be the last calculation sheet. It is an exception to the "user input on cover sheet" rule. Examples of losses would be connectors, lighting arrestors and old coaxial cable. Gains could include power amplifiers or receive preamplifiers. Just add it all up and stick the total on this sheet.

Path Profile

The most complex portion of creating this path-analysis application is the graphic presentation of the path profile. As a minimum, the path profile should show the straight line of sight between the two antenna elevations, the 60% Fresnel zone and the ground elevations corrected for earth curvature. I choose to add the full Fresnel zone and average foliage height plus an option for "point addends" to represent buildings or towers that might protrude through foliage and possibly into the Fresnel zone.

Like most graphs, this profile is created from a table of values. Some of the values are borrowed from user input on the cover sheet, some are input by the user into the table and most are calculated. The last exception to "user input on the cover sheet" is elevation data taken from a topographic map. Yes, you need a "topo" map to do a proper path analysis.[4] Even when you use the electronic topographic information from commercial programs, you should check it against actual maps. I have found that electronic three-second data are not suitable for a reliable line-of-sight analysis. Peaks in or near the path are often missed and I have found endpoint elevations to be off by over 100 feet. Fig 2 is an example of a table of values.

In Fig 2, the shaded areas are protected; user input is allowed in the "Ground Elevation" and the "Point Addend" columns. Here is an explanation of the table column by column:

Data Point: Data points A and B represent the elevations at the two sites. I chose to use a total of 20 data points between sites because that provides adequate resolution for most paths of 900 MHz and above.

Distance d1 (miles): This is simply the distance from each data point to site "A." These are equidistant segments of the entire path length, (in this case, 11.46 miles divided by 21 or 0.5457 miles each). Here is the easy way. Data Point 1: "= $^1/_{21} \times$ D36" (where cell D36 contains the path length in miles). Data Point 2: "= $^2/_{21} \times$ D36," and so on. This data column will be used in the earth-curvature calculation.

Ground Elevation: The ground elevations for points A and B come from user input on the cover sheet. Those for the other 20 points are read from a topo map. The user simply draws a line between the two Sites on the topo map (or maps), divides the line into 21 equal parts, and reads the highest elevation at, *or near,* each of the 20 resulting points.

Distance d2 (miles): This is the same data as distance d1 but from site B. This data column will also be used in the earth-curvature calculation.

LOS Path: The line-of-sight path column will draw a straight line between the antenna AGL (above ground level) elevations on the graph. The data for sites A and B are simply the corresponding ground elevation from that data column plus the antenna height (AGL) from the cover sheet. Each of the 20 data points builds on the previous point. For example, the Data Point 1 calculation would be "=F12 + ((F33 – F12) / 21)" where cell F12 represents Data Point A, and cell F33 represents Data Point B. The next calculation for Data Point 2 would be "=F13+((F33-F13)/21)" and so on.

Fresnel Clearance: Fresnel clearance elevation for each data point can be calculated with this series of calculations:

Data Point A: =F12 – 72.1 × SQRT((C12 × (D36 – C12)) / (D35 × D36))

Data Point 1: =F13 – 72.1 × SQRT((C13 × (D36 – C13)) / (D35 × D36))

Where cell D35 contains the frequency in gigahertz, and cell D36 contains the path length in miles.

I leave it to you to research and confirm this calculation

A	B	C	D	E	F	G	H	I	J	K	L
9	Path Information										
10	Data	Distance	Ground	Distance	LOS	Fresnel	60%	Adjusted	Foliage	Earth	Point
11	Point	d1 (miles)	Elevation	d2 (miles)	Path	Clearance	Fresnel	Ground Elev	Elevation	Curvature	Addend
12	A (1)	0.00	195	11.46	**545.00**	**545**	**545**	**195.00**	**195.00**	0	
13	2	0.55	203	10.91	**546.19**	**513**	**526**	**205.98**	**245.98**	2.98	
14	3	1.09	191	10.37	**547.38**	**502**	**520**	**196.66**	**236.66**	5.66	
15	4	1.64	199	9.82	**548.57**	**494**	**516**	**207.04**	**247.04**	8.04	
16	5	2.18	202	9.28	**549.76**	**489**	**513**	**212.12**	**252.12**	10.12	
17	6	2.73	212	8.73	**550.95**	**485**	**511**	**223.91**	**263.91**	11.91	
18	7	3.27	192	8.18	**552.14**	**482**	**510**	**205.40**	**245.40**	13.40	
19	8	3.82	245	7.64	**553.33**	**480**	**509**	**259.59**	**299.59**	14.59	
20	9	4.36	250	7.09	**554.52**	**479**	**509**	**265.48**	**305.48**	15.48	
21	10	4.91	210	6.55	**555.71**	**479**	**509**	**226.07**	**266.07**	16.07	
22	11	5.46	251	6.00	**556.90**	**479**	**510**	**267.37**	**307.37**	16.37	
23	12	6.00	292	5.46	**558.10**	**480**	**511**	**408.37**	**348.37**	16.37	100
24	13	6.55	249	4.91	**559.29**	**482**	**513**	**265.07**	**305.07**	16.07	
25	14	7.09	251	4.36	**560.48**	**485**	**515**	**266.48**	**306.48**	15.48	
26	15	7.64	208	3.82	**561.67**	**488**	**518**	**222.59**	**262.59**	14.59	
27	16	8.18	273	3.27	**562.86**	**492**	**521**	**286.40**	**326.40**	13.40	
28	17	8.73	210	2.73	**564.05**	**498**	**524**	**221.91**	**261.91**	11.91	
29	18	9.28	229	2.18	**565.24**	**504**	**529**	**239.12**	**279.12**	10.12	
30	19	9.82	159	1.64	**566.43**	**512**	**534**	**167.04**	**207.04**	8.04	
31	20	10.37	245	1.09	**567.62**	**522**	**540**	**250.66**	**290.66**	5.66	
32	21	10.91	218	0.55	**568.81**	**536**	**549**	**220.98**	**260.98**	2.98	
33	B(22)	11.46	310	0.00	**570.00**	**570**	**570**	**310.00**	**310.00**	0	

Frequency	2.455	GHz
Path Length	11.46	miles
Curvature Height	h = d1*d2 / 1.5k	feet
k	1.33	4/3 (default)
Foliage Height	40	feet
Beam elevation	0.001900949	radians

Fig 2—The last worksheet of the project accepts user input that is not handled by the cover sheet. User input goes in the areas clear of shading.

method. It is readily verifiable. This data column draws the bottom of the Fresnel zone curve on the path-analysis graph.

60% Fresnel: This is simply the Fresnel data multiplied by 0.6. This data column draws the 60% Fresnel-zone curve on the graph.

Adjusted Ground Elev: This data column is simply the ground-elevation column plus the addend for Earth curvature plus any manual addends from the last column. This data column will draw the ground elevation line between each of the tower bases.

Foliage Elevation: This data column is the ground elevation plus the addend for Earth curvature plus a user-input constant for average foliage height. In this example, an average foliage height of 40 feet was used.

Earth Curvature: The formula for calculating earth curvature is $h = d1 \times d2 / 1.5\ k$. The values for *d1* and *d2* for each data point have previously been calculated. "*k*" is typically 4/3 or 1.333; "*k*" should be set as user input with a default to 1.333.

Point Addend: This data column is for user input. The example shows 100 feet added to data point 11. Notice how this is depicted in the graph; there is a protrusion through the average foliage at a point approximately 6 miles from site "A." This could represent a tower or a building. The example proves that it does not penetrate the Fresnel zone.

This completes the explanation of the data table. All that remains is to define the graph. The process would depend upon the graph application used, but it should be straightforward. Be sure to let the graph adjust the Y-axis automatically. Once this is set up properly, the user only need enter the 20 elevations taken from the topo map. (Note: Spreadsheet programs with integral graphing capabilities are more convenient, but external graphing applications can be used if needed.)

Numeric Results

The last thing that needs to be done is to present the numeric results on the cover sheet. I used the area just above the graph for this purpose. The fade margin and the availability are the "bottom line" so I show them in bold type. As previously mentioned, the fade margin is equal to the system gains less the system losses. This is a good place to calculate and summarize those gains and losses. It is also nice to present the path distance in miles and kilometers.

A spin-off of availability is predicted downtime. This comes in handy when trying to explain costs; for example, $10,000 can buy you maybe 15 seconds a year. There are 31,557,600 seconds in a year.[5] One minus the availability times this number of seconds gives you the predicted downtime.

Conclusion

In summary, this paper provides the basic information required so that readers can create a line-of-sight path analysis application from a spreadsheet. The features and the presentation of your application are left to you. I strongly feel that a spreadsheet program, configured properly, can rival a commercial path-analysis application. A spreadsheet application similar to the one described in this paper has been tested repeatedly against commercial applications for the same path, and it consistently yields comparable results. If anything, the custom spreadsheet application makes more accurate and conservative predictions.

Notes

[1]Open Office, Gnumeric or KSpread for *Linux.*

[2]Barnett's model for outage or unavailability. "Engineering Considerations for Microwave Communications Systems," *AG Communication System*, 4th Edition, 1991, pp 68-69.

[3]The other rule is, "You can't push a rope."

[4]Topographic maps are available from several sources, overnight if necessary. Use the free Legend maps for each state to determine which topo or topos you will need for a path. I don't recommend using anything but the 7.5-minute series of maps. Other scales are too difficult to read. Topo map software is also available from several vendors and there are some topo maps available free of charge on the Internet.

[5]Do not forget leap years.

James received a Bachelors degree in Telecommunications from Texas A&M University, and is employed as a Principal Engineer in the Communications Department of a Fortune 100 corporation. He has been a licensed Amateur for almost 30 years. □□

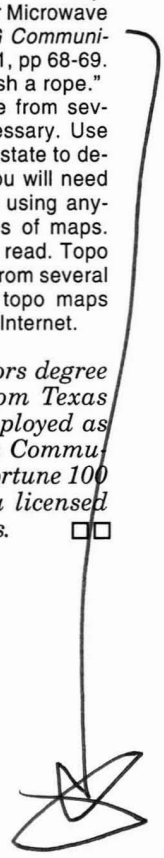

Surface Refractivity Gradient Data for Radio System Design

Steve J. Salamon[1,3], *Hedley J. Hansen*[2], *and Derek Abbott*[1]

[1]School of Electrical and Electronic Engineering, University of Adelaide, South Australia 5005, stephen.salamon@adelaide.edu.au, derek.abbott@adelaide.edu.au

[2]RFT group CEWD, DSTO, PO Box 1500 Edinburgh, South Australia 5111, hedley.hansen@dsto.defence.gov.au

[3]Radio Transport, Telstra Corporation, 30 Pirie St Adelaide, South Australia 5000, steve.salamon@team.telstra.com

Abstract

Reliable information about the cumulative distribution of surface refractivity gradient is often required in the design of radio systems. Strong negative gradients, or super-refraction, may lead to interference between terrestrial stations, both terrestrial links and satellite earth stations. Predicted positive or sub-refractive gradients are taken into account in determining the minimum antenna heights, to ensure terrestrial links achieve their required availability. This paper reviews sources of refractivity gradient data, and considers how refractivity gradient at a point may relate to an effective value over a terrestrial path.

1. Introduction

The radio refractive index, or radio refractivity, can be estimated from the meteorological parameters of air temperature T, pressure P, and water vapour pressure e. Refractivity N, in "N-units", or parts-per-million by which the refractive index exceeds unity, is often estimated by [1]

$$N = N_{\text{dry}} + N_{\text{wet}} = \frac{77.6}{T}\left(P + 4810\frac{e}{T}\right) \tag{1}$$

where P: atmospheric pressure (hPa)

T: absolute temperature (K)

e: water vapour pressure (hPa).

Although T and P can be measured directly, e can be estimated from measured dew-point [1]. Instruments that collect these parameters are carried aloft by balloons. Many of these instruments, known as radiosondes, are released regularly, once, twice or even four times a day, generally at times close to 00 and 12 hours Co-ordinated Universal Time (UTC), and also 06 and 18 hours UTC in the case of stations with ascents every 6 hours.

Experimental measurements of these parameters on fixed towers are sometimes used to obtain surface refractivity gradient distributions [2, 3], and measurements on towers in France have been used to develop an empirical model for gradient distribution as a function of median surface refractivity and median refractivity gradient [4].

Radiosonde data, with a sufficient number of ascents to provide reliable information in the tails of the gradient distribution, are only available from a limited number of stations— so empirical models to estimate the cumulative distribution of surface gradient from surface meteorological data have been developed. The Harvey model [5] predicts the most extreme value of positive refractivity gradient to be expected, while a recent model [6] predicts the refractivity gradient cumulative distribution from surface refractivity data. This paper presents a simplified version of the latter model. It predicts extreme values of the gradient distribution, and then predicts the distribution by interpolation.

Another source of surface gradient data is provided by numerical meteorological models, which implement a numerical solution to the meteorological conservation equations. World-wide models of this type can provide the parameters of (1) at a number of levels in the atmosphere, to produce digital maps of surface gradient distribution [1].

Considering that extreme gradient events may have limited geographic extent, especially in the case of sub-refractive events, this paper describes techniques to estimate the sub-refractive tail of the distribution of mean surface gradient over a radio path of arbitrary length.

2. Radiosonde Data

There are a very limited number of stations regularly providing data from ascents at 6 hourly intervals. These provide very good information about the local surface gradient distribution, as the ascents are spread throughout the day. Many more stations around the world provide radiosonde data at 12 hourly intervals, but caution is required in using data from stations with 24 hourly data, as gradient distributions can vary considerably depending on the local time of day that the ascents occur. Figure 1 illustrates this for a station in India. The data is from the NOAA/ESRL Radiosonde Database [7], processed as described in [6].

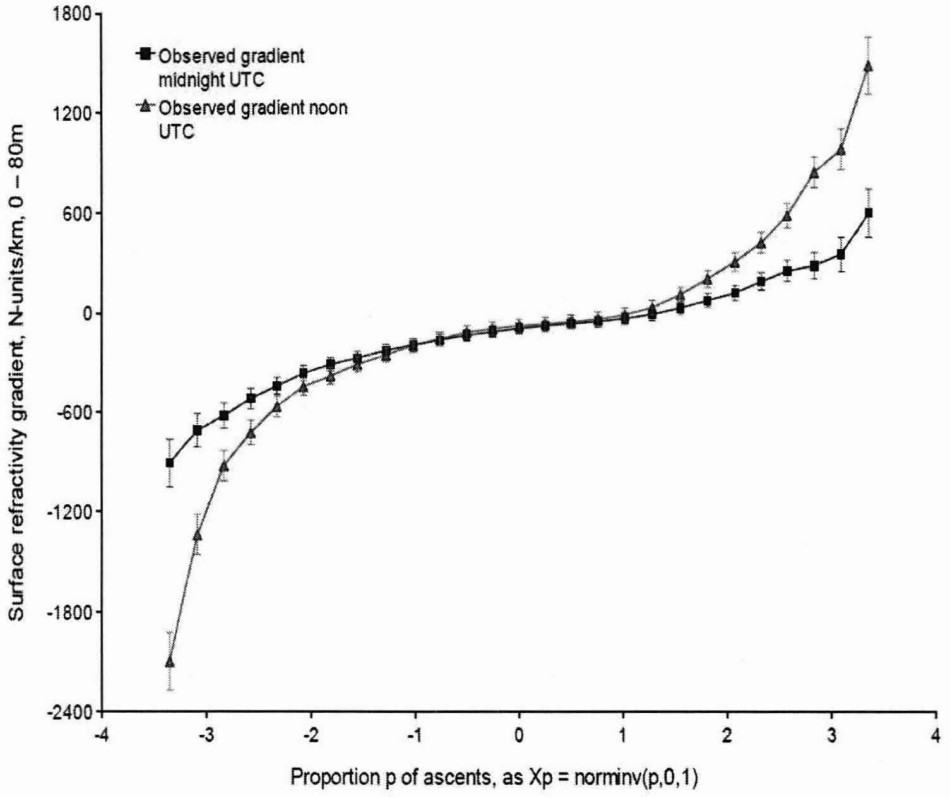

Figure 1. Radiosonde observed gradient distributions for Aurangabad, India, latitude 19.85 degrees, longitude 75.4 degrees, at around midnight UTC (early morning local time) and noon UTC (late afternoon local time).

3. Gradient Prediction from Surface Data

An empirical model has recently been developed [6], which predicts the surface gradient distribution from the distribution of a variable ΔN_s, referred to as "surface refractivity anomaly," which is the difference between surface refractivity N_s and its median value for that season of the year and hour of the day. A simpler model based on this work is obtained by taking only the 0.01% and 99.99% tail-points of the ΔN_s distribution, $\Delta N_{s0.01}$ and $\Delta N_{s99.99}$, to predict the 0.01% and 99.99% tail-points of the 0-80m surface gradient distribution, $G_{80}(0.01\%)$ and $G_{80}(99.99\%)$.

Linear regression analysis of data from 60 radiosonde stations provides the following model, firstly for the super-refractive tail-point, in units of N-units per km,

$$G_{80}(0.01\%) = 216 - 7.86\left(\Delta N_{s99.99} - \Delta N_{s0.01}\right), \tag{2}$$

and the sub-refractive tail-point, in the same units,

$$G_{80}(99.99\%) = -25 + 9.8\max\left(-\Delta N_{s0.01},\ \ 0.75\Delta N_{s99.99}\right). \tag{3}$$

We consider the distribution in terms of an inverse cumulative normal probability variable

$$X_p = \text{norminv}(p,\ 0,\ 1). \tag{4}$$

Denoting the values of X_p corresponding to the 0.01% and 99.99% tail points as $X_{0.01}$ and $X_{99.99}$, the complete cumulative distribution of refractivity gradient can be estimated by interpolation, using a modified sinh function:

$$G_{80}(X_p) = (G_{80}(99.99\%)+1.7C)\exp[A(X_p - X_{99.99})] + (G_{80}(0.01\%)-1.47C)\exp[B(X_{0.01} - X_p)] - 2C\tanh\left(X_p/4\right) + D\left(X_p/X_{99.99} - 1\right)\left(X_p/X_{99.99} + 1\right) \quad (5)$$

$$\text{with} \qquad A = \frac{8000}{5000 + G_{80}(99.99\%)} \qquad \text{and} \qquad B = \frac{4000 - G_{80}(0.01\%)}{8000}, \quad (6)$$

and C, which reduces the slope of the distribution in the region of the median, is given by

$$C = -G_{80}(99.99\%)A\exp(-AX_{99.99}) + G_{80}(0.01\%)B\exp(BX_{0.01}). \quad (7)$$

If the median gradient $G_{80}(50\%)$ is known, or can be predicted, then

$$D = [G_{80}(99.99\%)+1.7C]\exp(-AX_{99.99}) + [G_{80}(0.01\%)-1.47C]\exp(BX_{0.01}) - G_{80}(50\%); \quad (8)$$

alternatively set $D = 0$ if the median gradient is unknown. The value of the median gradient for the lowest 65 metres of the atmosphere, interpolated from the Rec ITU-R P.453 digital map [1], is used as an estimate of $G_{80}(50\%)$ in (8), for the testing of this model described below.

4. Testing the Predicted Gradient Distributions

Tables 1 and 2 below present error statistics for the ITU-R digital maps [1], the model of [6], and the revised version of that model in Section 3 above, when compared with the gradient distributions obtained by interpolating the radiosonde data [6]. Independent radiosonde data from 47 stations, not involved in the development of either of the new models, was used in these tests. Also the geographical distribution was different, with data from 33 Australian stations included in the 60 used to develop the models, but none included in the testing, while stations from China, Korea, Japan, Thailand and Indonesia were included in the testing but not in the development of the models.

Table 1. RMS error , in N-units/km, of empirical gradient models and ITU-R Rec. P.453 digital maps, compared with data from radiosondes for the same heights: 0-80 m for the models and 0-65 m for the maps.

Model under test, RMS error compared to radiosonde data	Percentage of ascents								
	0.01%	*0.1%*	*1%*	*10%*	*50%*	*90%*	*99%*	*99.9%*	*99.99%*
ITU-R P.453 digital maps, 0-65 m [1]	–	–	159	96	36	44	154	–	–
Prediction from surface data, same ascents [6]	204	173	140	90	39	47	102	229	406
Prediction from surface data, same ascents, eq.(5)	231	152	81	47	28	39	96	173	305

Table 2. Mean error, in N-units/km, of empirical gradient models and ITU-R Rec. P.453 digital maps, compared with data from radiosondes for the same heights: 0-80 m for the models and 0-65 m for the maps.

Model under test, mean error compared to radiosonde data	Percentage of ascents								
	0.01%	*0.1%*	*1%*	*10%*	*50%*	*90%*	*99%*	*99.9%*	*99.99%*
ITU-R P.453 digital maps, 0-65 m [1]	–	–	-6	-7	+8	-21	-121	–	–
Prediction from surface data, same ascents [6]	-28	-92	-99	-61	-21	+6	-11	-54	-168
Prediction from surface data, same ascents, eq.(5)	-100	-75	-34	-5	+3	-16	-56	-52	-8

5. Effective Sub-refractive Gradient for a Radio Path

The surface gradient data from radiosondes, or gradient distribution prediction models, as described in [6] or in Section 3 above, estimate the distribution surface gradient at a point, but especially in the case of severe sub-refractive gradients, they may only affect part of a radio path at any point in time. An early treatment [8] of this provides an effective gradient for a path of arbitrary length, for 99.99% of the time, in a "continental temperate" climate. Converting the effective Earth radius factor to refractivity gradient in N-units per km, this curve is accurately replicated by

$$G_{\text{path}}(99.99\%) = -13 + \frac{2670}{d}, \tag{9}$$

where d: path length, km.

Based on observed median depression radio fading events and meteorological measurements in the Julia Creek area of Queensland, Australia, a generally more severe model has been proposed [5], which can be expressed in terms of refractivity gradients G_{point} and G_{path}, in N-units per km, as

$$G_{\text{path}} = 157\left[\left(\sqrt{39/d}\right)\Big/\left(0.17 + \frac{94.2}{157 + G_{\text{point}}}\right) - 1\right]. \tag{10}$$

Refractivity profiles during sub-refractive events can be complex [5]. Extreme surface gradients, as suggested by the tails of the curves in Figure 1, are likely to non-linear, with gradient varying considerably with height. Even in milder cases, increased gradient variation is normally seen at low heights, below 20 metres, as compared with greater heights [2, 3]. The vertical refractivity profile is likely to vary considerably with distance along the path.

6. Conclusion

Reasonably accurate prediction of the cumulative distribution of surface refractivity gradient appears to be possible at locations with long-term automatic weather station data, using the models described above. At any instant in time, refractivity may vary in a complex way with height and distance along a radio path, so a uniform refractivity gradient for the whole path may not adequately describe refractive effects on field strength.

7. References

1. Recommendation ITU-R P.453-10, "The radio refractive index: its formula and refractivity data," Geneva, February 2012.

2. M. Grabner and V. Kvicera, "Statistics of lower atmosphere refractivity in Czechia," Proc. Asia-Pacific Microwave Conference, **4**, 2005, DOI: 10.1109/APMC.2005.1606923.

3. G.S. Zhamsuyeva, "Variation of radiometeorological parameters in the lower atmosphere near Lake Baikal," Proc. URSI Climpara '98, Ottawa April 1998, pp. 116-117.

4. L. Blanchard and H. Szun, "Results of measurements of refractivity on towers in France; improvement of the ITU Rec P.453-6 cumulative distribution model of refractivity gradient," Proc. URSI Climpara '98, Ottawa, April 1998, pp. 112-115.

5. R. A. Harvey, "A subrefractive fading model for microwave paths using surface synoptic meteorological data," *IEEE Trans. Antennas and Propagation*, **AP-35**, no. 7, July 1987, pp. 832-844.

6. S. J. Salamon, H. J. Hansen and D. Abbott, "Prediction of Surface Refractivity Gradient Distributions, from Weather Station Surface Data," European Conference on Antennas and Propagation, April 2014, in press.

7. National Oceanic and Atmospheric Administration, Earth System Research Laboratory, *NOAA / ESRL Radiosonde Database*, http://www.esrl.noaa/raobs/Welcome.cgi

8. L. Boithias and J. Battesti, "Protection contre les évanouissements sur les faisceaux Hertziens en visibilité," *Annales des Telecommunications*, **22**, no. 9-10, 1967, pp. 230-242.

Protection Ratio Calculation Methods for Fixed Radiocommunications Links

C.D.Squires, E. S. Lensson, A. J. Kerans

Spectrum Engineering
Australian Communications and Media Authority
Canberra, Australia

david.squires@acma.gov.au

Abstract

This paper describes three methods of calculating required interference protection ratios for Fixed Link radiocommunications receivers, using ITU-R prediction methods. The Initial Planning Method in common use in Australia can be used to predict the required fade margins for Fixed Links operating at frequencies where the dominant fade mechanism is multipath. The Detailed Link Planning Method can be used to determine more rigorous fade margin requirements for specific Fixed Links with known system and path parameters. The updated ITU-R Method for Small Percentages of Time has the potential to be implemented in a semi-automated way, without reference to topographic information or path profiles. Input of averaged parameters is replaced with specific known parameters at Fixed Link path locations.

1. Introduction

The calculation methods used to determine required levels of protection from noise and interference for microwave fixed services in Australia are given in the Australian Communications and Media Authority (ACMA) document Radiocommunications Assignment and Licensing Instruction No.FX-3 (RALI FX3), Microwave Fixed Services: Frequency Coordination [1, 2]. The methodology and assumptions that underpin the RALI FX-3 Protection Ratios and Correction Factor curves are not well described and have not been updated in accordance with ITU recommendations for a significant period. Anecdotal evidence suggests that in many cases, the protection criteria afforded to Fixed Links are well in excess of that required for their efficient operation. A need also exists for a review and clarification of the calculation methodology.

This paper describes three calculation methods which can be used to determine the required fade margins and levels of protection from noise and interference for point-to-point fixed service receivers (Fixed Links) in the 1.5 GHz band. While the 1.5 GHz band was chosen for this study, the methods are of general application and may be used for interference coordination of Fixed Links for which the dominant fade mechanism is multipath fading. Calculations of protection criteria for links with rain fade as the dominant mechanism are not considered in this paper.

1.1 The commonly used method of Protection Ratio calculation.

Initially, the protection ratios currently defined in RALI FX-3 are described in the context of their derivation from the Initial Planning Method (IPM) as presented in ITU Recommendations and Reports [3]. This method provides a way to determine interference protection ratios for all fixed links operating at frequencies where the dominant fade mechanism is multipath fading. The principal advantage is that protection ratios are simply and easily determined from a graphical perspective over a range of path lengths. The approach does not require complex calculations to be performed and is considered adequate for Fixed Link paths over flat terrain, however it can be shown that, for all other path types the protection ratio allowed is overly conservative for the protection of Fixed Links.

1.2 A more accurate method of Protection Ratio calculation.

The Detailed Link Planning Method (DLPM) as presented in ITU Recommendations and Reports [3] is implemented to determine more rigorous protection ratio requirements for specific Fixed Links, given known path and equipment parameters. Reference to printed topographic maps to calculate an *average grazing angle* along the radio path is required for each Fixed Link calculation. The advantage over the simple (IPM) graphical method is that the resulting protection ratio is typically less conservative for a given Fixed Link. This method has the

potential to allow more efficient use of the available radiofrequency spectrum by increasing the number of possible Fixed Link assignments in a particular band and geographical area. The primary drawback of this method is the time and effort required to determine terrain heights and undertake complex calculations.

1.3 A method for future software implementation

The approach to determining protection ratios as presented in updated ITU Recommendations [4] is investigated with regard to its possible future use as a method of Protection Ratio calculation which can be implemented using software. Such an approach has the potential to significantly reduce the labour-intensive nature of using the DLPM, by using excisions and manipulations of data from a Digital Elevation Model (DEM) to calculate an *area surface roughness factor* for the relevant path in preference to calculating an *average grazing angle*, along with the use of a *refractivity gradient* dataset covering the Australian continent. This updated method allows the input of specific known data in preference to using 'averaged' factors for calculating climate and terrain effects.

2. Initial Planning Method for fixed link receivers

The Initial Planning Method can be used to calculate a value of required fade margin for Fixed Links. The fade margin represents the predicted maximum fade depth exceeded for a specified percentage of time due to anomalous atmospheric attenuation of the signal received at a Fixed Link radiocommunications receiver. It is dependant on the required threshold Bit Error Ratio (BER) in the case of digital receivers, as well as frequency, path length and profile, occupied bandwidth, required time percentage availability and the variability of the refractivity gradient in the lowest section of the troposphere. The algorithms used to calculate fade margin were developed by researchers in a semi-empirical way utilising measurements of received signal degradation due to fading on existing Fixed Links at various locations.

Protection ratios include a fixed margin for noise and interference. This fixed margin is the difference in power level between a wanted minimum signal arriving at a receiver and any unwanted received signals which constitute interference. The reception of a wanted signal at an acceptably high power level allows the receiver to operate at a defined minimum BER which is required for a minimum standard of operation. The level of acceptable interference is normally set at 6dB or 10dB below the calculated noise floor of a given Fixed Link receiver [7]. The calculated fade margin and the fixed margin for noise and interference constitute the required protection ratio for a particular Fixed Link receiver with known path length and profile type.

In this study based on the 1.5 GHz band, the parameters of an AWA RMD1500 receiver [8] were adopted. This receiver type is widely deployed in Australia and can be considered representative in the band. A required BER of 10^{-3} was assumed, requiring a minimum received level of -95 dBm.

Figure 1 is a reproduction of the Protection Ratio Correction Factor curve as presented in RALI FX3 for the 1.5 GHz band. The curve was produced using an adaptation of the semi-empirical algorithm for calculating necessary Fade Margin as presented in ITU Report 338-5 (1986) [3] *equation (1),*

$$FM = 10\log\left[K\ f^{0.89} d^{3.6} \left(1+\left|\varepsilon_p\right|\right)^{-1.4}\right] - 10\log P \quad \textit{(1)}$$

using a conservative ***K*** factor for climate and terrain effects (*overland paths not in mountainous regions*).

$$K = 10^{-6.5} * P_L^{1.5}, \quad (P_L = 20)$$

Where,

f = *frequency in GHz*

d = *Path Length in km*

ε_p = *path inclination in milliRadians*

and taking into account the calculated noise floor of a receiver with 4MHz Bandwidth,

$$kTB\,(dBm) = 10\log\left(1.38^{-23} * 288 * 4 * 10^{6}\right) + 30 = -108\ dBm$$

The acceptable interference level is set to 6dB below the calculated noise floor in order to reproduce the RALI FX3 curve in Figure 1. This setting allows the Protection Ratio Correction Factor (PRCF) to be zero at a nominal path length of 60 km in the 1.5 GHz band. The protection ratio for the nominal path length (10 log *P*) is therefore 60 dB.

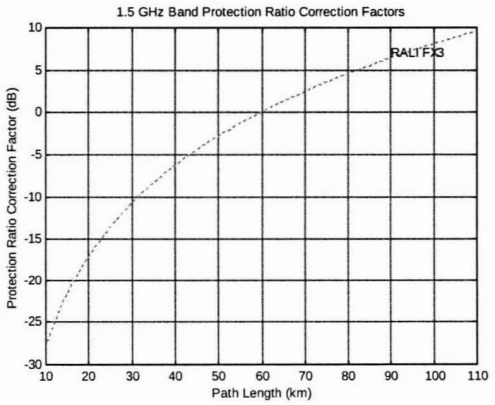

Figure 1. RALI FX3 Protection Ratio Correction Factors for the 1.5 GHz band.

3. Detailed Link Planning Method for selected fixed link receivers

The Detailed Link Planning Method (DLPM) is detailed in Recommendations and Reports of the CCIR Report 338-5 of 1986 [3] and in a modified form in RALI FX-3 of October 1992. [2]

The method can be applied to any fixed link where terrain heights along the path at regular intervals are known. Such data can be obtained from printed topographic maps or from digital elevation models (DEM) such as the Auslig 1:250000 raster. The terrain heights are used to calculate Average Grazing Angle[1] using the method of least squares. Protection Ratios are calculated for a number of apparatus licensed Fixed Links in Australia which are considered to be representative of links operating over 'flat', 'average' and 'mountainous' terrain.[2]

Figure 2 shows a Protection Ratio curve similar to that presented in RALI FX3 for the 1.5 GHz band. The curve was produced using the Initial Planning Method as above.

Specific protection ratios for selected Fixed Links were calculated using the semi-empirical algorithm for Detailed Link Planning Method for calculating necessary Fade Margin *equation (2),*

$$FM = 10\log\left[K\, f^{0.93} d^{3.3}\left(1+\left|\varepsilon_p\right|\right)^{-1.1} \phi^{-1.2}\right] \qquad (2)$$

using a conservative K factor for 'Flat' or 'Average' terrain;

$$K = 10^{-6.5} * P_L^{1.5}, \quad (P_L = 20)$$

for climate and terrain effects (*overland paths not in mountainous regions*).

Or using another K factor for 'Mountainous' terrain;

$$K = 10^{-7.1} * P_L^{1.5}, \quad (P_L = 20)$$

for climate and terrain effects (*overland paths in mountainous regions*).

Where,

f = *frequency in GHz*

d = *path length in km*

ε_p = *path inclination in milliRadians*

ϕ = *average grazing angle*

[1] Average Grazing Angle is calculated at a reflection point along the path, taking into account antenna heights and the terrain profile.

[2] 'Flat' or 'Average' terrain is defined here as analogous to *overland paths not in mountainous regions.*
'Mountainous' terrain is defined here as analogous to *overland paths in mountainous regions.*

and taking into account the calculated noise floor of a receiver with 4MHz Bandwidth.

Figure 2 also depicts the calculated Protection Ratios of various existing Fixed Links over almost 'flat' terrain. In this representation, Protection Ratios can be read directly from the graph for both the Initial Planning Method, (equivalent to the RALI FX3 curve) and the Detailed Link Planning Method. (*ie* no adjustment for Correction Factor is required). The level of acceptable interference into Fixed Link receivers is set at a more conservative level of 10dB below the calculated noise floor of the representative receiver. A control calculation referred to as Hypothetical Flat is used to depict a theoretical fixed link path of 60 km length operating over perfectly flat terrain, with transmit and receive antenna heights both set at 100m above ground level. The calculation result indicates that such a hypothetical link would be under-protected by the provisions of RALI FX3 by approximately 3dB. In practical situations, terrain paths are not perfectly flat and advantage is taken of transmit and receive antenna height differences to decrease the likelihood of fading due to anomalous propagation.

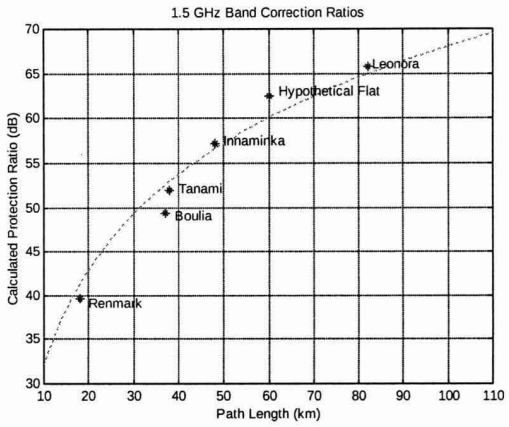

Figure 2. Protection Ratios for Fixed Links over 'Flat' terrain

There is a close correlation between the calculated protection ratios for existing Fixed Links operating over nearly flat terrain using the Detailed Link Planning Method, and the protection afforded to all fixed links by RALI FX3 using the Initial Planning Method. This result indicates that adequate protection is currently provided to fixed links operating over 'flat' terrain. The average level of overprotection afforded to the selected Fixed Links by RALI FX3 is 0.8 dB.

Figure 3 depicts the calculated Protection Ratios of various Fixed Links over 'average' terrain. Average terrain is defined here as terrain which is neither flat nor

mountainous. These links normally have one or both masts and antennas located on a hilltop. The intervening terrain along the path (*the path profile*) may vary from partially flat to undulating.

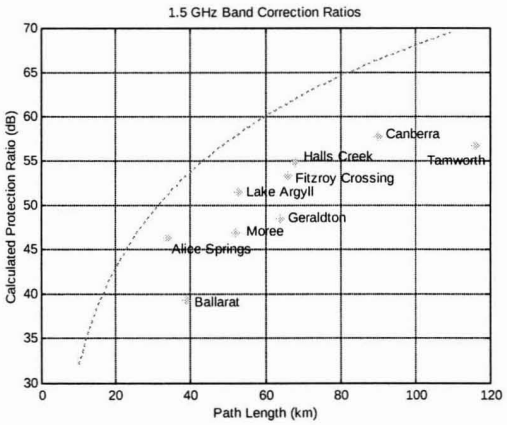

Figure 3. Protection Ratios for Fixed Links over 'Average' terrain

Reference to Figure 3 indicates that Fixed Links operating over 'average' terrain are generally afforded a higher level of protection from interference by the Initial Planning Method than is necessary for their reliable operation. The Fixed Links studied are representative of those operating over average terrain with a range of path lengths and situated in various locations on the Australian continent. The calculated level of over-protection varies between 5dB and 14dB over the range of Fixed Links selected, with an average of 9.25 dB.

Figure 4 depicts the calculated Protection Ratios for various Fixed Links over 'Mountainous' terrain. In all links depicted there is a significant difference in antenna heights above sea level and large variation in terrain height over the path profile.

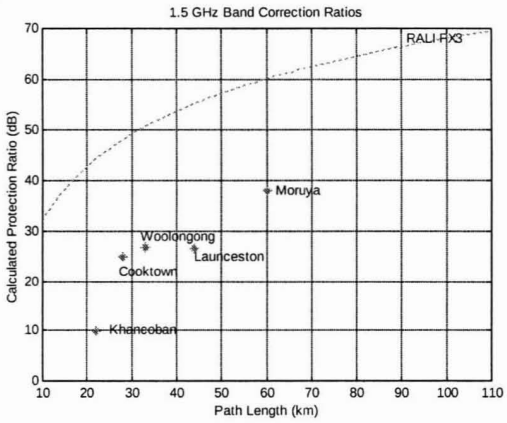

Figure 4. Protection Ratios for Fixed Links over 'Mountainous' terrain

Reference to Figure 4 indicates that Fixed Links over 'Mountainous' terrain are generally afforded a significantly higher level of protection from interference by the Initial Planning Method than is necessary for their reliable operation. The Fixed Links studied are representative of those operating over 'mountainous' terrain with a range of path lengths and situated in various locations on the Australian continent. The calculated level of over-protection varies between 21dB and 28dB over the range of existing fixed links selected, with an average of 24dB. It should be noted that the result for Khancoban at -35 dB is not considered reliable as the path length is very short and the calculated grazing angle due to significant antenna height difference and path profile variation is large, however the grouping of Cooktown, Wollongong , Launceston and Moruya suggests a more realistic outcome.

4. Alternative Protection Ratio Calculation Method

An alternative empirically derived Protection Ratio calculation method, reproduced from ITU-R 530/9 of 2001 (*Fading and enhancement due to multipath and related mechanisms: Method for small percentages of time*) [4] and presented below can be used to determine protection ratios for individual Fixed Links, taking into account their path profiles and point refractivity gradients.

For detailed link design applications, calculate the percentage of time p_w that fade depth A (dB) is exceeded in the average worst month from
equation (3)

$$p_w = K\ d^{3.2}\left(1+\left|\varepsilon_p\right|\right)^{-0.97} 10^{0.032 f - 0.00085 h_L - A/10} \quad \% \qquad (3)$$

where,

f = *frequency in GHz*

d = *Path Length in km*

ε_p = *path inclination in milliRadians*

h_L = *altitude of the lower antenna*

and the geoclimatic factor $\boldsymbol{K}$ *is obtained from equation (4).*

Extract from ITU-R 530.9

equation (4) for the geoclimatic factor K, was derived from multiple regressions on fading data for 251 links in various geoclimatic regions of the world with path lengths $\boldsymbol{d}$ *in the range of 7.5 to 185 km, frequencies* $\boldsymbol{f}$ *in the range of 450 MHz to 37 GHz, path inclinations* $\boldsymbol{\varepsilon_p}$ *up to 37 mrad, lower antenna altitudes* $\boldsymbol{h_L}$ *in the range of 17 to 2 300 m,*

refractivity gradients dN_1 *in the range of –860 to –150 N-unit/km, and area surface roughnesses* s_a *in the range of 6 to 850 m (for* $s_a < 1$ *m, use a lower limit of 1 m).*

$$K = 10^{-3.9 - 0.003\,dN_1}\, s_a^{-0.42} \qquad (4)$$

*s_a (area surface roughness) is defined as the standard deviation of terrain heights (m) within a 110 km * 110 km area with a 30 s resolution.*

The algorithm used to find p_w *(equation 3)* determines the *time percentage that fade depth is exceeded in the average worst month*, given a required fade depth.

Equation 3 can be manipulated to determine the *fade depth*, given a required time percentage that fade depth is exceeded in the average worst month, as follows; *(equation 5)*

$$let \quad a = Pwx \,/\, \left(K\, d^{3.2} \left(1+\varepsilon_p\right)^{-0.97}\right) \qquad where\ Pwx = 0.01\%$$

$$let \quad y = \log_{10}(a) \,/\, \log_{10}(10)$$

$$then, \quad A = \left(y - 0.032\, f + 0.00085 h_L\right) * -10 \qquad (5)$$

Given a required time percentage of 0.01%, the resulting fade margin (***A***) can be calculated for a range of path lengths. The standard deviation of terrain height data extracted from a Digital Elevation Model (the *area surface roughness*) is required for this implementation.

Protection Ratios depicted in Figure 5 are calculated using the updated and modified algorithm, *(equation 5)* with no change in the noise floor calculation or

BER = 10^{-3} receive level applicable to 1.5 GHz Fixed Links using AWA RMD1500 receivers. The maximum allowable level of Interference is set to 6 dB below the noise floor of the receiver. The resulting curve is plotted along with a Protection Ratio curve derived from the Initial Planning Method. *(equation 1).*

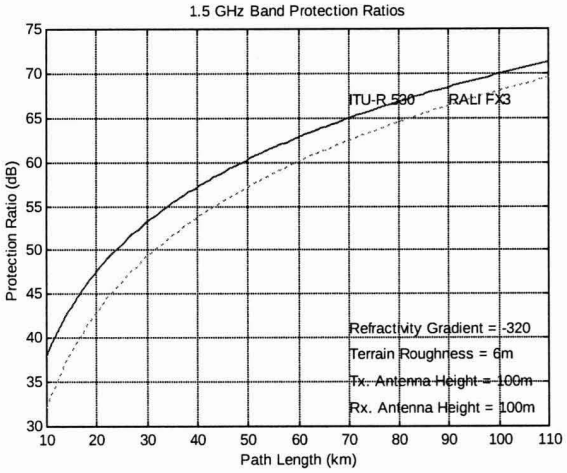

Figure 5. Comparison of 'Flat' Terrain Protection Ratios

Using the modified ITU-R P530 method (*equation 5*) provides an opportunity to enter known parameters specific to terrain roughness, antenna height, and refractivity gradient. It can be seen from figure 5 that using terrain roughness, transmit and receive antenna heights and refractivity gradient as noted on figure 5, the modified ITU-R P530 method produces a similar result to the existing RALI FX3 curve, and passes through the point previously calculated for 'Flat' terrain (Hypothetical Flat) using the Detailed Link Planning Method.

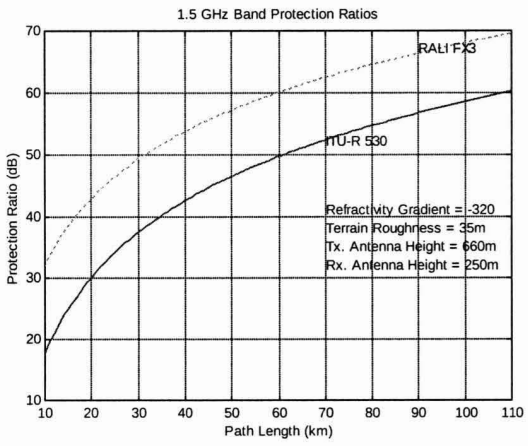

Figure 6. Comparison of 'Average' Terrain Protection Ratios

Figure 6 depicts a Protection Ratio curve specific to 'average' terrain by varying the terrain roughness and antenna elevation parameters to similar values applicable to links over 'average' terrain. (*equation 5*). This curve passes through the region previously calculated for 'average' terrain using the Detailed Link Planning Method.

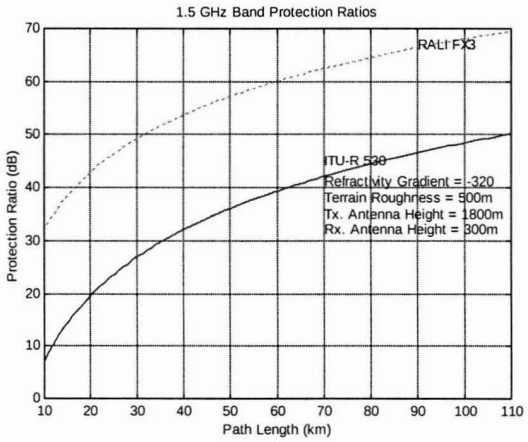

Figure 7. Comparison of 'Mountainous' Terrain Protection Ratios

Figure 7 depicts a Protection Ratio curve specific to 'mountainous' terrain by varying the terrain roughness and antenna elevation parameters to similar values applicable to 'mountainous' terrain links. This curve passes through the region previously calculated for 'mountainous' terrain using the Detailed Link Planning Method. It should be noted that this method is not reliable for very short path lengths with significant antenna height differences.

5. Conclusions

Three significant conclusions have been reached after implementing and comparing the methods of protection ratio calculation for Fixed Links as detailed in this paper.

5.1 The Protection Ratio Correction Factor curves presented in RALI FX3 are derived from the *Initial Planning Method* as presented in Recommendations and Reports of the CCIR, XVI Plenary Assembly, Dubrovnik, 1986, Report 338-5. [3] The curves as currently implemented provide a method to determine an adequate and often conservative protection ratio for all Fixed Links where the dominant fade mechanism is multipath fading.

5.2 The *Detailed Link Planning Method* as presented in Recommendations and Reports of the CCIR, XVI Plenary Assembly, Dubrovnik, 1986, Report 338-5 [3] can be used to calculate protection ratios for Fixed Links with known path and equipment parameters. Use of this method often results in a significantly less conservative protection ratio required for a given Fixed Link. A link that may otherwise fail coordination can often be successfully coordinated using the Detailed Link Planning Method, allowing for the efficient use of the radiofrequency spectrum by Fixed Links.

5.3 The *modified Method for Small Percentages of Time* (*equation 5*), referenced from ITU-R P530/9 of 2001 [4] and detailed in this document can be used to calculate protection ratios for all Fixed Links where the dominant fade mechanism is multipath fading. Algorithms were developed and improved for this semi-empirical method by researchers at multiple locations, taking into account fade measurement statistics on operating Fixed Links. The calculated results are comparable to those produced by the Detailed Link Planning Method. The *modified Method for Small Percentages of Time* has the potential to be implemented in a semi-automated way, without reference to physical topographic maps or charts. It uses data extracted from a *Digital Elevation Model* and takes into account the known values of *Refractivity Gradient* at the location of a Fixed Link.

6. References

[1] **RALI FX3 Microwave Fixed Services: Frequency Coordination** 1992 Sequence No. 12
ACMA Spectrum Planning and Engineering Group

[2] **RALI FX3 Microwave Fixed Services: Frequency Coordination** 1998 Sequence No. 137
ACMA Spectrum Planning and Engineering Group

[3] **REPORTS OF THE CCIR**
XVI Plenary Assembly, Dubrovnik Report 338-5 1986
Propagation Data and Prediction Methods Required for Line-of-Sight Radio-Relay Systems

[4] **RECOMMENDATION ITU-R P.530-9** 2001
Propagation data and prediction methods required for the design of terrestrial line-of-sight systems

[5] **RECOMMENDATION ITU-R P.453-8** 2001
The radio refractive index: its formula and refractivity data

[6] **RECOMMENDATION ITU-R P.452-11** 2003
Prediction procedure for the evaluation of microwave interference between stations on the surface of the Earth at frequencies above about 0.7 GHz

[7] **RECOMMENDATION ITU-R F.758-2** 2000
Considerations in the development of criteria for sharing between the terrestrial fixed service and other services

[8] **AWA RMD1500**
radiocommunications receiver technical specification

2011 6th International Conference on Industrial and Information Systems, ICIIS 2011, Aug. 16-19, 2011, Sri Lanka

Semi-Automated Microwave Radio Link Planning Tool

W.M.D.R. Gunathilaka, H.G.C.P. Dinesh, K.M.M.W.N.B. Narampanawe

Abstract— **Link Budget is a main estimate in telecommunication microwave link planning for accurate and reliable link. This software program is a comprehensive path design tool and it can be used for radio links operating in the microwave frequency range. When a link budget is prepared, many parameters are considered for calculations. Therefore this software program is very essential tool in the telecommunication industry. This paper presents a software tool that can be used to prepare link budgets by providing essential parameters. Moreover this software can be used for applications such as frequency selection according to ITU (International Telecommunication Union) standards, graphical representation of the radio path profile between any two geographical locations on the loaded terrain and generates the Fresnel zone according to the frequency. Furthermore this software tool can be interfaced with a GPS (Global Positioning System) receiver to gather geographical locations and based on this information, microwave frequency band is suggested according to regulatory body guidelines.**

Index Terms— Frequency planning, Link Budget, Link Planning, Microwave Radios, Software Tools

I. INTRODUCTION

A communication system that utilizes the radio frequency band as electromagnetic waves between 3GHz and 30 GHz are called microwaves as their wavelength is smaller. Microwave frequencies are used in telecommunication link designing because they are less prone to accidental damage, links between mountains, over reservoirs and over jungles are more economically and feasible, single point security, single point installation and maintenance and they can quickly be deployed

Microwave link design is a metrological, systematical and lengthy process that includes Loss/attenuation calculations, fading and fades margin calculations, frequency planning and interference calculations and quality (Bit Error Rate-BER) and availability calculations.

As shown in Fig. 1 these four processes are very important in microwave link planning.

W.M.D.R. Gunathilaka is with the Department of Electrical and Electronic Engineering, University of Peradeniya, Peradeniya, Sri Lanka (e-mail: dinusharg@gmail.com).

H.G.C.P. Dinesh is with the Department of Electrical and Electronic Engineering, University of Peradeniya, Peradeniya, Sri Lanka (e-mail: karunaa33@yahoo.com).

K.M.M.W.N.B. Narampanawe is with the Department of Electrical and Electronic Engineering, University of Peradeniya, Peradeniya, Sri Lanka (e-mail: narampanawe@ee.pdn.ac.lk).

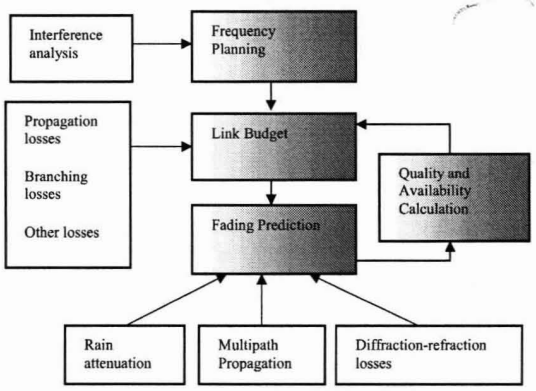

Fig. 1 Steps of link planning

According to quality and availability calculations, it is required to re-calculate link budget to improve reliability and quality of the link. This is the reason for using software to calculate and design Microwave links in telecommunication industry [1] [2].

This developed software is for telecommunication companies and regulators deal with many microwave radio links. This tool can be used store data of each microwave links through user friendly GUI (Graphical User Interface). Further it has tools for frequency planning, calculating link budget, fading prediction and graphically implementation of terrain profile. This software allows any user to perform step by step analysis of all important propagation related phenomena that needed to generate a planning report containing all the data necessary for accurate and reliable implementation of microwave radio links and maintain database about them.

There are some microwave link planning software (ex: Pathloss, Atoll Microwave, Global Mapper) available commercially for link budget and graphically implementations but they are very expensive for some commercial and educational usage. Further they require computer platforms with high-end resources. This developed software has many tools for frequency planning, link budget calculation, fading prediction and graphical implementation of path profile. In addition to that software tool can be used to implement the whole microwave links in a network including link data, tower information of a particular client company.

978-1-61284-0035-4/11/$26.00 ©2011 IEEE

II. LINK DATABASE SYSTEM

One of the key functions of this software is Link Database System. It contains the data of microwave links such as longitude, latitude, elevation of site, antenna height, polarization, transmit/receive frequencies, transmit power, cable losses, antenna gains, receiver sensitivity, received signal strength, free space losses, fade margin and reliability.

According to longitude and latitude, software graphically presents the actual location on terrain map. As shown in Fig. 2, it shows every uploaded microwave radio links which is an inheritable function compared to other commercial software. Detailed information of each microwave link can easily be read by clicking mouse on microwave link or tower position.

As shown in Fig. 3, path profile and Fresnel zone of particular microwave radio link can be obtained by just a mouse click.

III. MICROWAVE RADIO LINK PLANNING

There are two scenario of planning a new Microwave Radio Link with this software.

1.) Two station Planning.

2.) Plan one station respect to database system.

When two stations planning are considered, user has to enter data of both stations. In the second method reference station data are automatically entered to the link budget.

There are several steps involved in planning a new Microwave Radio Link such as Path Distance and Elevation Calculation, Frequency Planning, Link Budget calculation, Path Profile and Fresnel Zone Analysis.

A. Path Distance and Elevation Calculation

First step of planning a microwave link is map study and path profile preparation. Preliminary map studies help to determine the actual topography of the terrain, the height, and obstacles along the desired path for line of sight clearance. Desired stations' longitude and latitude are collected for path profile preparation. Using these longitude and latitude values, path distance is calculated and it is used to select the transmit frequency and other parameters.

There is a unique feature in this software to collect the

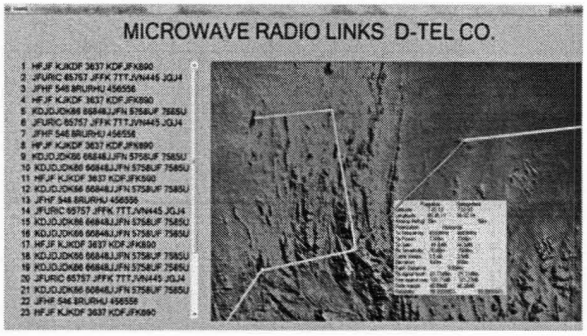

Fig. 2 Microwave Links in Terrain map

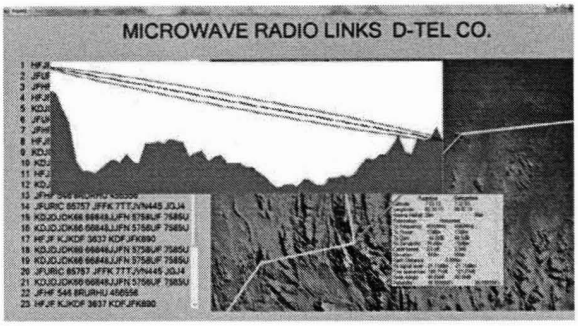

Fig.3 Path profile of a specific radio link

longitude and latitude data from a GPS receiver module as shown in Fig 4. By connecting the GPS receiver to a computer running this software in link planning mode at proposed station location, longitude and latitude data are automatically uploaded to the link budget calculation as shown in Fig 5 [3].

After entering the longitude and latitude values of two sites to this software, the path distance and elevations of two points are calculated automatically [4] [5].

B. Frequency Planning

The second step of the link planning is Frequency Planning. The goal of frequency planning is to allocate microwave frequencies to a radio link as a few frequencies possible so that the availability and the quality of the radio link are less affected by the interference. Path length, site location, terrain topography and atmospheric effects are the basic considerations involved in the assignment of radio frequency when determining a frequency band that is suitable for the specific link [6]. Assigning a microwave frequency channels are authorization given by an authority for an operator to use a microwave frequency channels. It is created in accordance with the series-F recommendation given by the ITU-R (International Telecommunication Union-Radio communications and wireless) [7].

The available frequency band is subdivided in to two

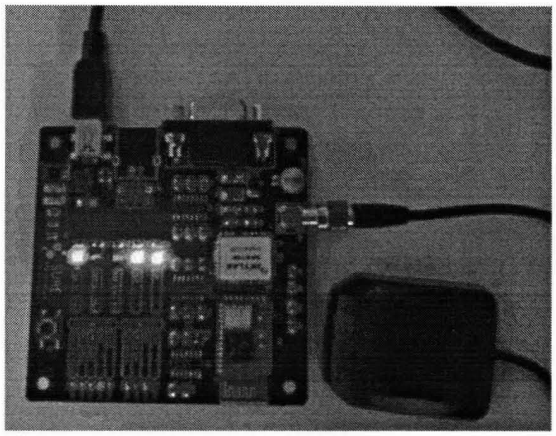

Fig.4 GPS Receiver and Antenna

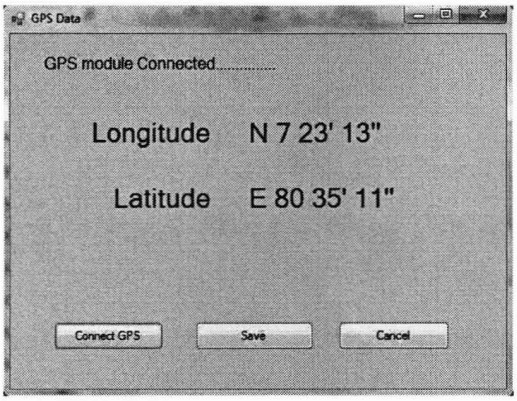

Fig. 5 GPS Data

halves, a lower/go, and an upper/return duplex half. The space between two duplex halves should sufficiently be large such that the radio transceiver can function under minimum interference full duplex operation. The bandwidth of a channel based on the capacity of the radio link and the modulation scheme used. The most important goal of frequency planning is to allocate available channels to a different link in the network without exceeding the quality and availability objectives of the individual links because of the radio frequency interferences [8].

There are two possible methods for frequency selection in this software, namely they are 'Manual' and 'ITU data' as shown in Fig. 6. In Manual frequency selection mode user can assign frequencies to two stations and the software will calculate the link budget for the given frequencies. In ITU data mode, the software indicates frequency sub bands / channels as shown in Fig. 6. After selecting the suitable frequency band, user can choose the site either as high or low frequency.

There is a special feature in this software; it suggests the frequency band according to path distance which is issued by the spectrum governing body of a country as shown in Table 1. This automatically selects the suitable frequency band using a standard frequency vs. distance data guidelines suggested by regulatory body. This special function is useful to choose suitable frequency for a desired link which will be approved by the regulator.

C. *Link Budget*

The link budget is a mathematical calculation involving loss and gain factors related with the transmission lines, antennas and propagation channel, to find the maximum operating distance between a transmitter and a receiver can operate successfully [10]. According to Fig. 7 it can be seen the output power is varying in each step and finally it reduces. The final outcome is fade margin of the link.

To calculate the link budget user has to enter parameters such as Transmit power of antenna, cable Losses, Transmit Gain, Receiver Sensitivity, terrain factor and Climate factor.

1. *Transmit Power*

The transmit power is the RF (Radio Frequency) power coming out of a transmitter. It is measured in 'dBm' and does not include the signal loss of the coaxial cable or the gain of the antenna.

2. *Cable Losses*

Usually cable losses are called as branching losses that come from the hardware used to deliver the transmitter/receiver output to/from the antenna.

3. *Transmit Antenna Gain*

Transmit gain is the quantity that an antenna boosters the RF signal over a specified direction. Antenna achieves 'Gain' simply by focusing RF energy.

4. *Receiver Sensitivity*

The minimum input signal level required to produce a specified signal-to-noise ratio at the output of the receiver to recover the transmitted signal properly.

5. *Terrain Factor*

The terrain factor is used to calculate the availability of a link. , it can either be calculated from terrain roughness and humidity information or be included directly.

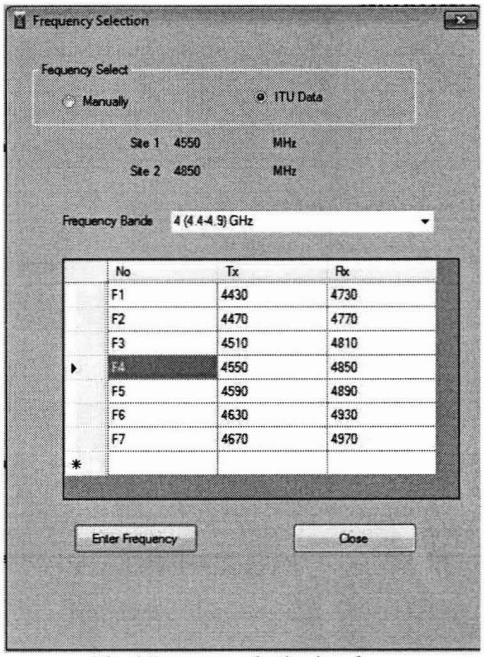

Fig. 6 Frequency selection interface

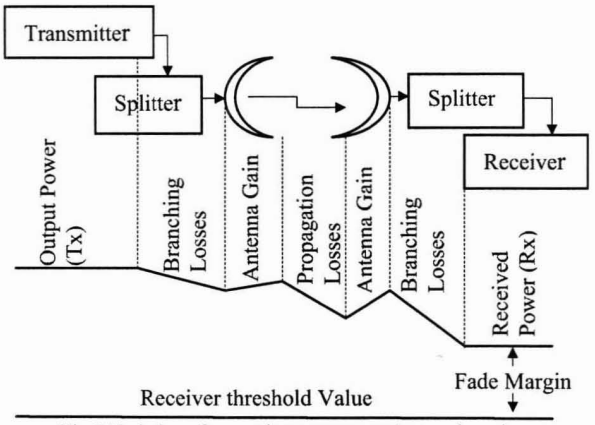

Fig 7 Variation of power between transmitter and receiver

4.00 - Very smooth terrain, including over water.
1.00 - Average terrain, with some roughness.
0.25(1/4) - Mountains, very rough, or very dry areas.

6. Climate Factor

The climate factor is used to calculate the availability of a link; it can either be computed from average annual temperature information or be entered directly.

0.500 (1/2) - gulf coast or similar hot, humid areas.
0.250 (1/4) - normal interior temperate or northern areas.
0.125 (1/8) - mountainous or very dry areas.

According to those parameters link budget is calculated including Receiver Signal Level, EIRP (Effective Isotropic Radiate Power), and Free Space Loss, Fade Margin, Outage probability and Reliability.

Free Space Loss (FSL)

Free Space loss is the theoretical attenuation of a radio signal when it propagates away from the transmitting antenna. When a radio signal radiates from the antenna with the distance it spreads out more and more. As the area covered increases, the amount of power per unit area (the power density) decreases. This effectively weakens the radio signals [11]. FSL is calculated using following equation (1) [12].

$$FSL = 32.44 + 20 \cdot \log(f) + 20 \cdot \log(d) \quad \text{- (1)}$$

Where,

f = frequency, MHz
d = distance between two stations, Km

7. Effective Isotropic Radiated Power (EIRP)

EIRP is the radio frequency power measured at the main focal point of the antenna. It is equal to the sum of the transmit power in the antenna (in dBm) added to the gain (dBi) of the antenna. Since it is a power level that measured in dBm [9], EIRP is calculated using following equation (2).

TABLE I
DISTANCE/ FREQUENCY GUIDELINE

Frequency Band/GHz	Distance/km
4	>20
7	14.4 ~ 20
11	9 ~ 14.4
15	6.5 ~ 9
18	2.5 ~ 6.5
23	< 2.5
26	< 1

$$EIRP = P_{out} + G_t - C_t \quad \text{- (2)}$$

Where,
Pout = Output power of transmitter
Ct = Cable loss in transmitter
Gt = Antenna gain of transmitter

8. Received (Rx) Signal Level

Received signal level is the actual received signal (dBm) presented to the radio receiver at far station. It is calculated using equation (3) [10].

$$\text{Received Signal Level} = EIRP - FSL + G_r - C_r \quad \text{- (3)}$$

Where,
Gr = Antenna gain of receiver
Cr = Cable loss in receiver

9. Fade Margin

The difference between received signal level and the receiver sensitivity threshold is called fade margin, each link must have sufficient fade margin to protect against path padding's, that weakness the microwave radio signal. Fade margin is the insurance against unexpected system outage [13]. Fade margin can be calculated by using equation (4).

$$\text{Fade margin} = \text{Rx signal Level} - \text{Receiver Sensitivity} \quad \text{- (4)}$$

To determine the feasibility of a link, the calculated receive signal level is compared with the Receiver sensitivity threshold. The link is theoretically feasible if,

Received signal Level ≥ Receiver sensitivity.

If the receiver sensitivity threshold is smaller than or equal to the received signal level then the link might be feasible

implement, because the received signal must be strong enough to be interpreted by the receiver demodulator.

10. Reliability

The reliability of a microwave link depends on the calculated fade margin. The reliability is calculated using following equation (5).

$$\text{Re}liability = a \times b \times 2.5 \times 10^{-6} \times f \times D^3 \times 10^{\frac{-F}{10}} \quad \text{- (5)}$$

Where,

a = terrain factor
b = climate factor
f = frequency, GHz
D = path length, miles
F = fade margin, dB

D. Path profile and Fresnel zone

1. Path profile

When the link budget is calculated, it can be feasible theoretically but practically it may not be feasible because the link may not be in line-of–sight. Microwave radio communication strictly required line-of-sight condition and the clear path of first Fresnel zone. Therefore path profile is important in link planning.

Graphical representation of the path traveled by the radio waves between the two radio stations of a link is the path profile. The path profile determines the height of the antennas and the locations at each end of the link, and it insures that the link is out of obstacles.

According to input longitude and latitude the software graphically represent the terrain variation between two stations using height database and the Fresnel zone graph. Fig. 8 shows graphical representation of terrain variation for a given data set. The SRTM (Shuttle Radar Topography Mission) data base is used to obtain path profile. This database indicates the height for an accuracy of 90m. This data base is in UTM (Universal Transverse Mercator) coordinate system with WGS84 datum.

2. Fresnel zone

Radio frequency waves travel along a straight line. When they get away from the transmitting antenna, they spread out the farther.

Fresnel zone is the area that the microwave signal spreads out. When there is an obstacle in the Fresnel zone, part of the microwave radio signal will be diffracted away from the straight-line path. The practical effect is that on a microwave radio link, is reduce the amount of energy that reaching the receive antenna [14].

The radius of the Fresnel zone depends on the frequency of the signal, when smaller the frequency, higher the Fresnel zone [9]. Fig. 9 shows the radius of Fresnel zone. There is special tool in software to calculate the Fresnel zone and

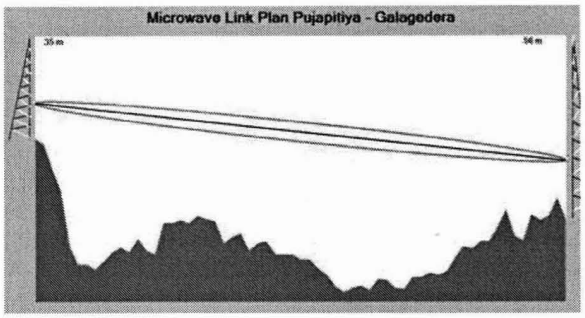

Fig.8 Path Profile and Fresnel zone

graphically represent. Radius of the first Fresnel zone is calculated using equation (6).

$$R = 17.32\sqrt{\frac{x(d-x)}{f \cdot d}} \quad (6)$$

R = Radius of first Fresnel zone, m
x = distance from one point to radius point, Km
d = distance between antenna, Km
f =frequency, GHz

The software represents a terrain map and Fresnel zone graph together as shown in Fig. 8, when the path is not clear for the Fresnel zone, height of the antenna can be increased graphically using software tool. A new antenna height automatically adds to the link budget report.

Final report includes inputs and calculated data as shown in Fig. 10 that can be taken as the final soft/ hard print.

IV. CONCLUSION

To design this software it was required to write some additional software for handling databases of frequency bands and mean sea levels (elevations). It was compared with existing reports of several links to check whether the accuracy of this software. The results were acceptable with those existing reports which conclude that this software works properly according to the standards.

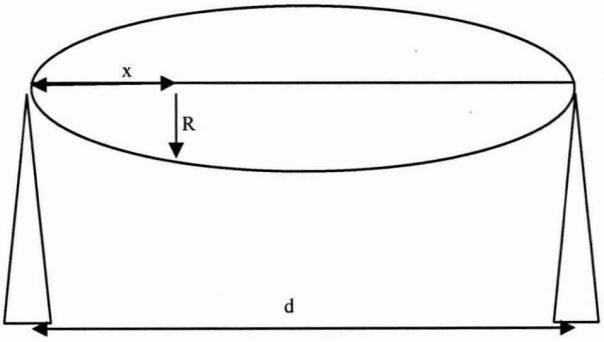

Fig .9 Radius of Fresnel Zone

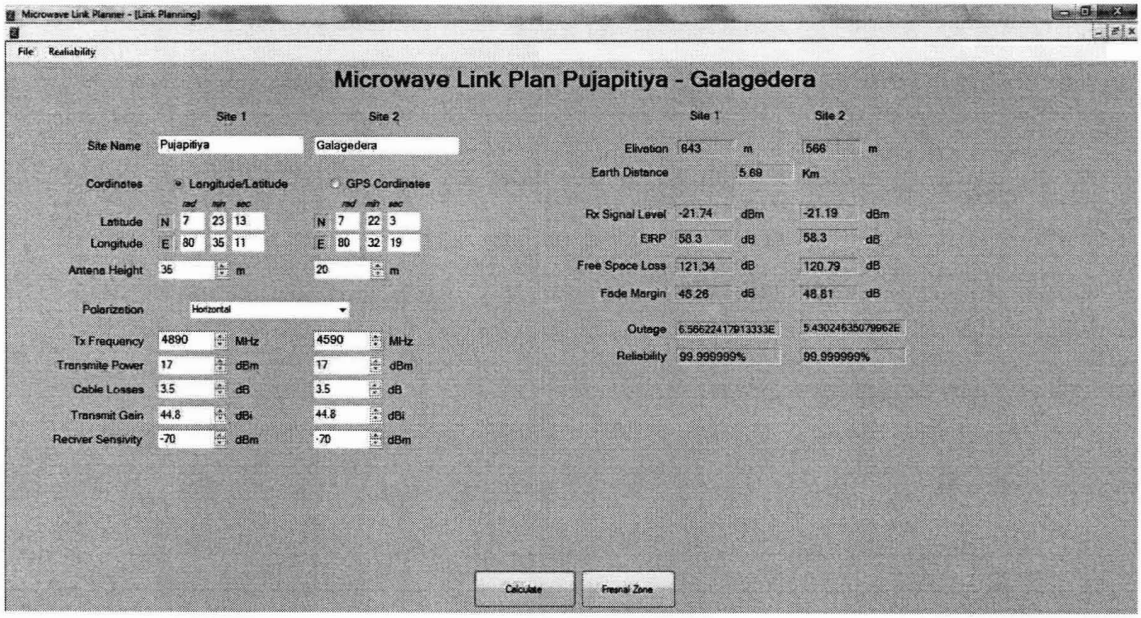

Fig. 10 Final Report

Sometimes calculated values may vary with actual values because of many immeasurable factors and natural phenomena's.

This software is calculating the link budget and path profile as like in other commercially available software's but time taking to calculations and plotting to path profile is less than other software. Accuracy of calculations is under standard of ITU. Further this tool requires only low cost minimal hardware that is a computer and a GPS receiver.

In further this software will be developed to select suitable frequency according to climate and geographical factors. In addition to that 3D terrain and 3D Fresnel views will developed for planning and optimize microwave communication network.

V. REFERENCES

[1] William C.Y.Lee, "Wireless & Cellular Telecommunications", Third Edition, pp 573-586.

[2] S.Ramabhadran, "Telecommunications Principles Circuits Systems and Experiments", pp 841-860.

[3] Mini USB & Bluetooth Interface GPS Demo Board User's Guide.

[4] "Digital Microwave Communication Principals ", Huawei Technologies Co,Ltd,4/4/2007, pp 89-90.

[5] Steven Dutch, "Converting UTM to Latitude and Longitude", National and applied Science, University of Wisconsin-Green Bay, November 16, 2009 [online] Available: http://www.uwgb.edu/dutchs/

[6] A.Michael Noll, "Introduction to Telephones & Telephone Systems", Second Edition, pp 41-44.

[7] ITU-R F-Seris Recommendation www.itu.int/ITU-R/

[8] Udo W.Pocch, Dennis Machel, John McCahn, "Telecommunications and Networking", pp 117-120.

[9] Bhupesh Batra, "Microvawe link-Fudamentals", February 10, 2010 [online] Available: http://www.bhupeshbatra.com/tutorials/

[10] TCIL Bhawn,"Microwave Link Design", presentation, December 10,2009 [online] Available: www.docstoc.com/search/radio-link./3/

[11] "An Introduction to microwave Radio Link Desing",SAF tehnikaA/S 202, December 3,2009 [online] Available : www.saftehnika.com

[12] Nihal Kularathna, Dileeka Dias, "Essentials of Modern Telecommunications System", pp 156.

[13] Michael F.Young, "Planning Microwave Radio Link", November 20, 2009 [online] Available: www.ydi.com/calculation/

[14] "Fresnel Zone Calculator", November 20,2009 [online] Available: www.afar.net/fresnel-zone-calculator/

A Comparison of Experimental and Theoretical Values of Atmospheric Absorption at the Longer Millimeter Wavelengths

EDWARD E. ALTSHULER, FELLOW, IEEE, AND RICHARD A. MARR

Abstract—**The main objective of this paper is to compare experimentally determined values of atmospheric absorption at the longer millimeter wavelengths with theoretical absorptions. The difficulties that arise in attempting to obtain accurate theoretical and experimental results are discussed. The experimental absorptions were obtained from a set of low angle slant path measurements at 15 and 35 GHz using the sun as a source. The surface absorption coefficient, zenith absorption and effective height of the absorbing atmosphere were derived from these data. Regressions of both surface absorption coefficient and zenith absorption were performed as a function of surface absolute humidity; the results were compared with theoretical values obtained by several investigators. Zenith absorptions were found to be in good agreement with theory; however, experimental surface absorption coefficients were consistently lower than calculated values.**

I. Introduction

THE PRINCIPAL ATMOSPHERIC gases which absorb electromagnetic energy in the millimeter-wave region of the spectrum are oxygen and water vapor. This absorption is difficult to calculate in the window regions because the total absorption is the summation of contributions from the wings of hundreds of absorption lines throughout the spectrum, and the shapes of these lines are not precisely known. It is also difficult to measure the absorption in the window regions because it is relatively low (only about 0.1 dB/km at the longer millimeter wavelengths).

Since the absorption is a function of temperature, pressure and humidity, it is necessary that these meteorological parameters be known along the propagation path if the results are to be compared with theory. The dilemma that arises is that although a more controlled experiment can be conducted over a short path, the net absorption is very low; higher absorptions are present for longer terrestrial paths, but meteorological data are more difficult to obtain. In addition, multipath effects and earth curvature limit the length of the path. This limitation may be overcome by using a slant path; but since it is not practical to collect meteorological data along the total path, only surface values are used. The surface absorption coefficient is calculated directly from these values. In order to calculate the zenith absorption, vertical temperature, pressure and humidity profiles must be estimated; profiles similar to the U.S. Standard Atmosphere are often used. Fortunately, past results indicate that the zenith absorption is correlated with the surface parameters.

In this paper, results of atmospheric absorption measurements made over very long slant paths at frequencies of 15 and 35 GHz are reported. The absorption was determined from a set of measurements using the sun as a source. Fifty-eight sets of data were collected at sunrise and sunset during clear sky conditions for a set of elevation angles from near the horizon to 20°. For a normal clear atmosphere (free of inversions) the absorption is directly proportional to the length of the propagation path through the absorbing medium. A linear regression of absorption as a function of distance is performed and the surface absorption coefficient and zenith absorption are determined and then compared with theoretical values.

Manuscript received August 26, 1987; revised February 10, 1988.

The authors are with the Electromagnetics Directorate, Rome Air Development Center, Hanscom AFB, MA 01731-5000.

IEEE Log Number 8822576.

II. Theoretical Considerations

Atmospheric gases absorb energy from electromagnetic waves if the molecular structure of the gas is such that the individual molecules possess electric or magnetic dipole moments. It is known from quantum theory that at specific wavelengths, energy from the wave is transferred to the molecule, causing it to rise to a higher energy level; if the gas is in thermodynamic equilibrium it will then reradiate this energy isotropically as a random process, thus falling back to its prior energy state. Because the incident wave has a preferred direction and the emitted energy is isotropic, the net result is a loss of energy from the wave. The only atmospheric gases with strong absorption lines at millimeter wavelengths are water vapor and oxygen. The absorption lines of O_3, CO, N_2O, NO_2 and CH_2O are much too weak to affect propagation in the window regions.

The oxygen molecule has a magnetic dipole moment with a cluster of resonances near a wavelength of 5 mm (60 GHz) and a single resonance at 2.53 mm (118.75 GHz). Although the more than 30 lines near a wavelength of 5 mm are resolvable at low pressures (high altitudes), they appear as a single pressure-broadened line near sea level, owing to a large number of molecular collisions. Even though the magnetic dipole moment of oxygen is approximately two orders of magnitude weaker than the electric dipole moment of water vapor, the net absorption due to oxygen is still very high, simply because it is so abundant. The fact that the distribution of oxygen throughout the atmosphere is very stable makes it very easy to model. A plot of the approximate oxygen absorption as a function of frequency is shown in Fig. 1.

0018-926X/88/1000-1471$01.00 © 1988 IEEE

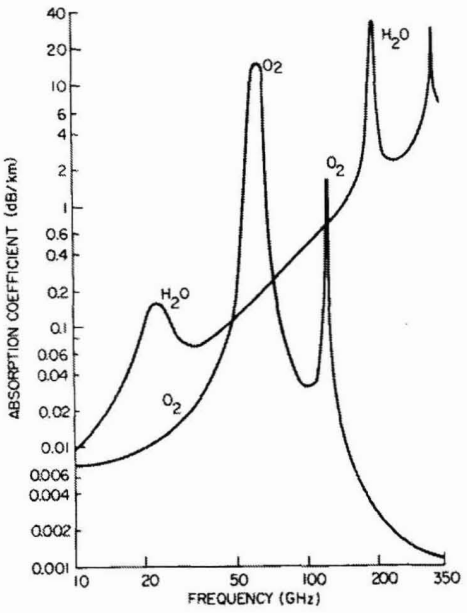

Fig. 1. Absorption coefficients of oxygen and water vapor.

The water vapor molecule has an electric dipole moment with resonances at wavelengths of 13.49, 1.64, and 0.92 mm (22.24, 183.31, and 325.5 GHz) in the millimeter-wave region. In general, the positions of these resonances, their intensities, and their linewidths agree well with experimental data. There are, however, serious discrepancies between theoretical and experimental absorption coefficients in the window regions between these strong lines; experimental attenuations are often a factor of two to three times larger than theoretical values. Although the cause of the discrepancy is not known, indications are that either the line shapes do not predict enough absorption in the wings of the resonance or there is an additional source of absorption that has not yet been identified. It should be mentioned that there are over 1800 water vapor lines in the millimeter wave/infrared spectrum, 28 of which are at wavelengths above 0.3 mm. Because the wings of these lines contribute to the absorption in the window regions, very small errors in the line shapes can significantly affect the overall absorption. In addition to the uncertainty of the absorption coefficient of water vapor, there is also the problem of water vapor concentration. The amount of water vapor in the lower atmosphere is highly variable and has surface densities ranging from a fraction of a gram per cubic meter for very arid climates to more than 30 g/m^3 for hot and humid regions; for this reason it is very difficult to model. A plot of the approximate water vapor absorption as a function of frequency along with that of oxygen is shown in Fig. 1 for a density of 7.5 g/m^3. Because the absorption is assumed to be linearly proportional to the water vapor density, except for very high concentrations, absorptions for other water vapor densities may be calculated.

It is assumed that for clear sky conditions the slant path absorption is proportional to the distance through the absorbing atmosphere. For high elevation angles a flat earth approximation may be used and the distance through the absorbing layer is proportional to the cosecant of the elevation angle. For low elevation angles the following formula, based on a curved earth, has been derived using the law of cosines [1].

$$D(\theta) = [(a_e + h_e)^2 - a_e^2 \cos^2 \theta]^{1/2} - a_e \sin \theta \qquad (1)$$

where

- θ elevation angle
- $D(\theta)$ distance through the absorbing layer
- a_e effective earth radius
- h_e effective height of the absorbing layer.

The elevation angle θ, is recorded at the time of each measurement. The effective earth radius a_e is a function of the refractivity profile. Since this profile cannot be readily obtained in practice, the effective earth radius is estimated from the surface refractivity. The effective earth radius factor k is

$$k = \frac{1}{1 + \frac{a}{n}\frac{dn}{dh}\cos\theta} \qquad (2)$$

where

- a earth radius
- n index of refraction
- dn/dh gradient of index of refraction with height.

For θ close to the horizon and $n \doteq 1$

$$\frac{dn}{dh} = \frac{1-k}{ak}. \qquad (3)$$

Based on a large sample of refractivity data, it has been shown [2]

$$-\Delta N = 7.32 e^{.005577 N_s} \qquad (4)$$

where the surface refractivity $N_s = (n - 1)\cdot 10^6$ and ΔN = refractivity gradient

$$\frac{dn}{dh} \approx \frac{\Delta n}{\Delta h} = \frac{\Delta N \times 10^{-6}}{\Delta h}$$

$$k = \frac{1}{1 - 0.04665 e^{.00557 N_s}}. \qquad (5)$$

The effective earth radius is

$$a_e = ka. \qquad (6)$$

The effective height of the absorbing atmosphere h_e is defined as follows. If all of the oxygen and water vapor in the atmosphere were compressed into a uniform layer having a weighted density equal to that of the oxygen and water vapor at the earth's surface, then the height of that layer is designated as the effective height of the absorbing medium. Since h_e is a function of the vertical distributions of oxygen and water

vapor and since these are not known, a method for estimating h_e must be devised. We have assumed that the absorption $A(\theta)$ is proportional to the distance through the lower atmosphere $D(\theta)$.

$$A(\theta) = \alpha_0 + \alpha_1 D(\theta) \tag{7}$$

where α_0 and α_1 are the regression line coefficients. But as the distance $D(\theta)$ approaches zero, the absorption $A(\theta)$ also approaches zero; therefore α_0 should approach zero.

Thus for $\alpha_0 = 0$ we would like to determine a value for α_1 which produces a best fit for the regression line. Since the set of $D(\theta)$ values is a function of h_e, we select a value of h_e which produces a set of distances that result in a minimum standard error of estimate S_e. To obtain an expression for S_e we define the following statistical parameters.

$$\bar{D} = \frac{\sum_{i=1}^{N} D(\theta_i)}{N} \tag{8}$$

$$\bar{A} = \frac{\sum_{i=1}^{N} A(\theta_i)}{N} \tag{9}$$

$$\hat{A}(\theta_i) = \alpha_1 D(\theta_i) \tag{10}$$

$$S_e = \sqrt{\frac{1}{N-2} \sum_{i=1}^{N} [A(\theta_i) - \hat{A}(\theta_i)]^2} \,. \tag{11}$$

(Note that N is the sample size, not to be confused with the refractivity.)

The value of h_e which minimizes S_e is selected as the effective height of the absorbing layer.

III. Measurement Program

A brief description of the experimental system and the measurement procedure that was used to obtain the absorption data is described in this paper; more details have been provided in a previous paper [3]. All measurements were made at Prospect Hill, Waltham, MA, during sunrise and sunset at elevation angles from 1.0°, in increments of 0.5°, up to 10°, and then in increments of 1° up to 20°. An 8.8 m paraboloidal antenna having beamwidths of approximately 4 and 9 arcmin at 35 and 15 GHz, respectively, was used. Conventional Dicke-switched radiometers with state-of-the-art components were used.

The antenna beam was positioned ahead of the sun and the intensity of the received signal (antenna temperature) was observed as the sun drifted through the beam. The apparent sky temperature, due to atmospheric emission was compensated for by moving the antenna off the sun at each elevation angle to obtain a background reading which was subtracted out. In addition, calibrated noise diodes were turned on at each elevation angle to compensate for radiometer gain changes. The data were thus derived from a series of repeated drift measurements. With this system attenuations of up to approximately 25 dB could be measured. Errors were estimated to be about 0.1 dB for low attenuations but approached 2 dB for attenuations above 20 dB. Since data were collected during a sunspot minimum, solar activity was minimal. The measurement time for each set of data was only about two hours so errors due to solar instability were insignificant. All data were recorded on magnetic tape. The surface temperature, pressure and dew point temperature were recorded at the start and completion of each set of data and then averaged. For the period during which absorption data were collected, 58 sets of data were designated as "clear sky." This meant that the sun could be clearly viewed during the course of the measurements.

IV. Analysis of Data

The surface absolute humidity and surface refractivity were computed from the surface temperature, dew point and pressure. The effective earth radius was then computed from the surface refractivity using (5) and (6). A linear regression of absorption versus distance through the absorbing layer was conducted for a set of effective heights of the absorbing atmosphere ranging from 0.1 to 8 km in 0.1 km intervals. For each set of data the standard error was calculated and plotted as a function of effective height; the effective height which produced the minimum standard error was selected as the effective height of the absorbing atmosphere. With a_e and h_e determined, $A(\theta)$ was then plotted as a function of $D(\theta)$. With (7) a regression line with slope α_1 was computed. The corresponding set of zenith absorptions was computed by multiplying the absorption coefficients by the effective heights.

A. 35 GHz Data

Using the procedure described above an effective earth radius was computed from each surface refractivity. The corresponding k-factors ranged from 1.30 to 1.48, not too different from the often used $k = 4/3$ factor. With the effective earth radius specified, an optimum effective height was determined for each set of data. Plots of the dependence of the standard error of estimate of the regression line on the effective height are shown in Fig. 2 for low, average and high humidity days. It is seen that the standard error, although not too sensitive a function of the effective height, has a minimum value for each set of effective heights.

With the optimum effective heights specified, a linear regression is then performed for each set of data. Typical regression lines for low, average and high humidity days are shown in Fig. 3. It is seen that the correlation coefficients are very high indicating that the absorption is indeed proportional to the distance through an absorbing layer. The slope of the regression line α_1 is the surface absorption coefficient in dB/km. Since the absorbing layer is assumed to consist of a uniform distribution of oxygen and water vapor, the zenith absorption is simply the product of the surface absorption coefficient times the effective height.

The main objective of this experiment was to attempt to establish the dependence of the surface absorption coefficient α_1 and the zenith absorption A_z on surface meterological parameters for clear sky conditions. We have 58 sets of

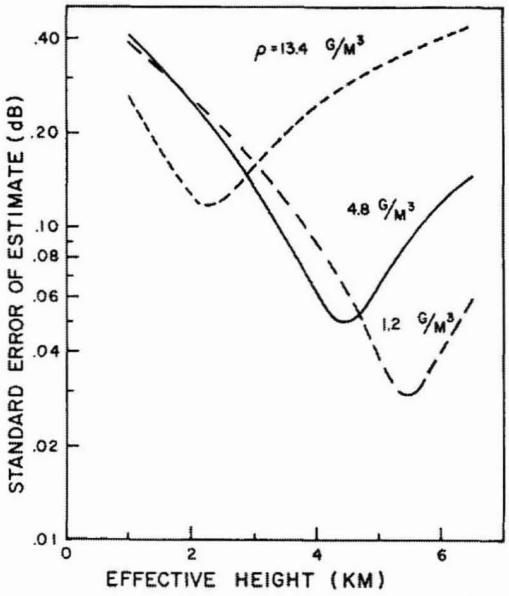

Fig. 2. Optimum effective heights for dry, average and humid days.

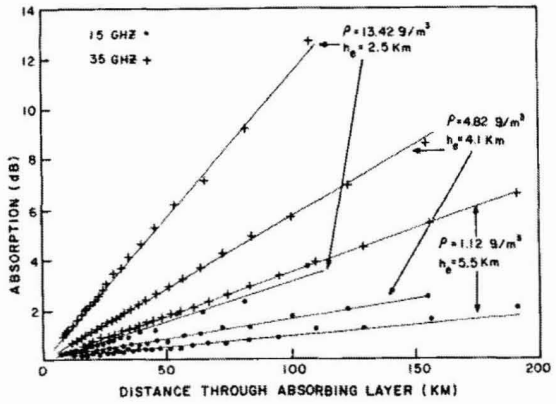

Fig. 3. Atmospheric absorption as a function of distance through an absorbing layer.

surface absorption coefficients, zenith absorptions, surface humidities and temperatures. A multiple linear regression of zenith absorption A_z versus surface absolute humidity ρ and temperature t was performed. The resulting regression line is

$$A_z(\rho, t) = 0.271 + 0.0114\rho - 3.554 \times 10^{-4} t$$

where A_z is in dB, ρ is in g/m^3 and t is in Kelvin units.

The corresponding correlation coefficients are

$$r(A_z; \rho) = 0.8346$$

$$r(A_z; t) = 0.5197$$

$$r(A_z; \rho, t) = 0.8365.$$

It is seen that $r(A_z, \rho)$ is significantly larger than $r(A_z; t)$. Also, the range of temperatures for clear sky conditions was about 30 K; since this corresponds to an absorption range of only about 0.01 dB it was concluded that the surface temperature is not a significant parameter for this study. The regression analysis was repeated again for ρ only and $A_z(\rho) = 0.177 + 0.0093\rho$ with a standard error of estimate $S_e(A; \rho) = 9.46 \times 10^{-4}$. A plot of $A_z(\rho)$ versus ρ is shown in Fig. 4. A correlation coefficient of 0.794 indicates that there is indeed a linear dependence of absorption on surface absolute humidity.

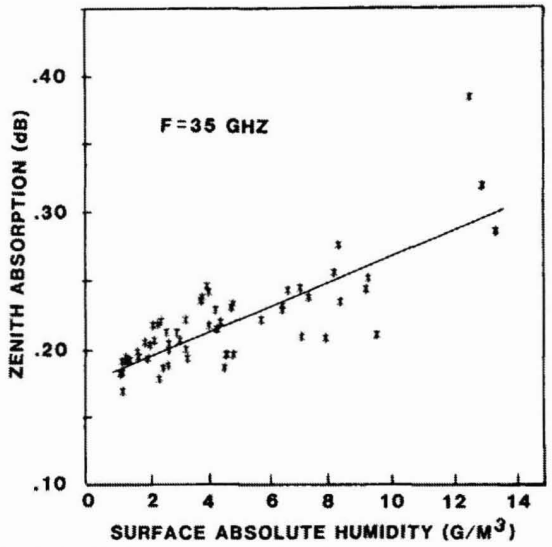

Fig. 4. Zenith absorption versus surface absolute humidity, F = 35 GHz.

A linear regression of the surface absorption coefficient α_1 as a function of surface absolute humidity was also conducted for the same 58 sets of data. This analysis led to the following result.

$$\alpha_1(\rho) = 0.018 + 0.0068\rho$$

$$S_e(\alpha_1; \rho) = 5.13 \times 10^{-4}$$

$$r(\alpha_1, \rho) = 0.872.$$

We note that the correlation coefficient and standard error are comparable to those obtained for zenith absorption. A plot of $\alpha_1(\rho)$ versus ρ is shown in Fig. 5.

There are several reasons why the correlation of absorption with surface absolute humidity is perhaps not higher. We have made the assumption that the surface humidity is representative of the vertical humidity profile. The total precipitable water which is a measure of all of the water vapor along a vertical path through the atmosphere is a more meaningful indicator of humidity than the surface value alone. The correlation of total precipitable water with surface absolute humidity has been studied by several investigators and unfortunately their conclusions are not in agreement. Reber and Swope [4] report correlation coefficients of only about 0.5 based on annual statistics for several regions near Los Angeles. Monthly correlation in some cases dropped below zero. Bolsenga [5] on the other hand reported correlation coefficients of about 0.80 and Reitan [6] has reported correlation coefficients as high at 0.99. Thus there is sufficient

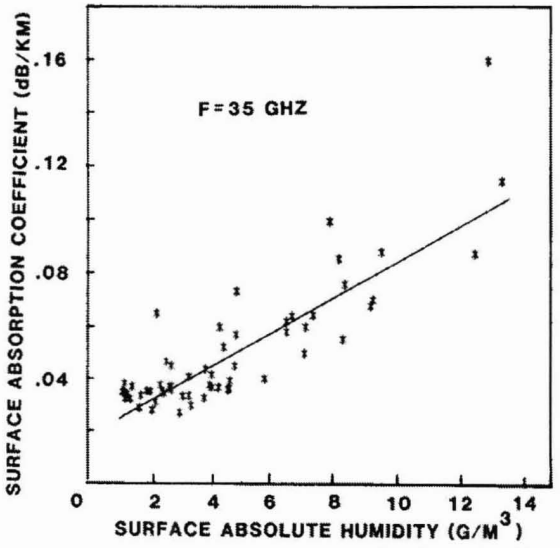

Fig. 5. Surface absorption coefficient versus surface absolute humidity, F = 35 GHz.

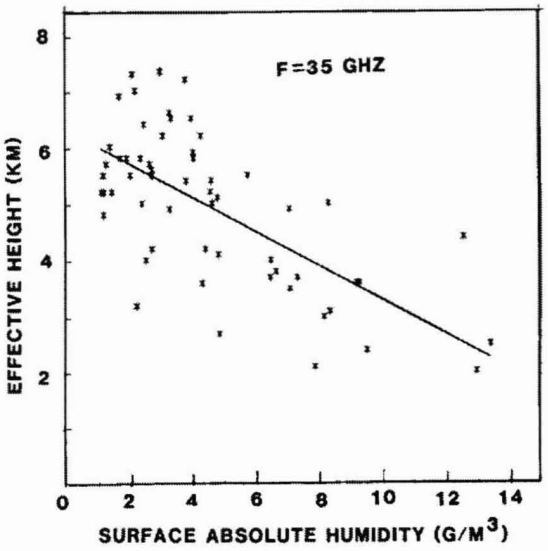

Fig. 6. Effective height versus surface absolute humidity, F = 35 GHz.

uncertainty to conclude that the surface absolute humidity is only a fair indicator of the water vapor aloft. Unfortunately it is very difficult to measure the total precipitable water; surface absolute humidity is the best alternate parameter.

However, even if it were possible to obtain an accurate humidity profile at the location of the radiometer, it would still be necessary to assume that the atmosphere is horizontally stratified in order to infer the humidity over 100 km down range for very low elevation angles. Thus it is not possible from a practical standpoint to determine the humidity along a slant path. Fortunately, the surface absolute humidity is an unbiased estimator of the humidity aloft so the resulting regression should be a good indicator of the approximately linear relationship of absorption as a function of humidity.

Since the effective height of the absorbing layer is a function of the vertical distributions of oxygen and water vapor and since the water vapor is related to the surface absolute humidity, then the effective height should also be a function of the surface absolute humidity. A regression of effective height as a function of the surface absolute humidity was performed, and the results are shown in Fig. 6. For a linear regression the correlation coefficient was 0.668. Only a very slight increase in the correlation resulted when a higher degree polynomial regression was tried. The regression line is

$$h_e = 6.35 - 0.302\rho.$$

The standard errors for the intercept and slope are 0.23 and 0.043, respectively. It is seen that there is only a fair correlation of the effective height with surface absolute humidity. This is not too suprising considering once again the variability of the humidity aloft.

The behavior of the surface absorption coefficient with the effective height was also examined. A plot of these parameters is shown in Fig. 7. Polynomial regressions for absorption as a function of height were performed, and it was found that a second degree polynomial provided a rather good fit (r = −0.916). This result indicates that high absorptions are typically associated with low effective heights; this is consistent with that which would have been expected since a high absorption is produced by a high water vapor density which in turn lowers the effective height of the combined densities of oxygen and water vapor.

B. 15 GHz Data

The 15 GHz absorption data were not as consistent as those measured at 35 GHz. This was due primarily to the fact that the 15 GHz radiometer was noisier than the 35 GHz radiometer. In addition, the absorption at 15 GHz was significantly lower than that at 35 GHz which resulted in a larger percent error. Whereas the 35 GHz absorption decreased monotonically with increasing elevation angle, this was not typically the behavior of the 15 GHz data, particularly at the higher elevation angles for which the absorptions were only a fraction of a dB. Thus it was not possible to use the same procedure as was used with the 35 GHz data for obtaining an optimum effective height for the equivalent absorbing layer.

The effective height of the absorbing layer is a weighted average of the individual oxygen and water vapor absorptions. Since the percent contribution to the absorption is approximately the same for these gases at both 15 and 35 GHz, particularly for surface absolute humidities below about 15g/m^3, the effective heights which were derived from the 35 GHz data were also used for 15 GHz.

As before, the measured absorptions were plotted as a function of distance through the equivalent absorbing layer. Typical plots of $A(\theta)$ versus $D(\theta)$ for the same low, average and high humidity days as for 35 GHz are also plotted in Fig. 3. Note the irregular behavior of the data for distances corresponding to the higher elevation angles.

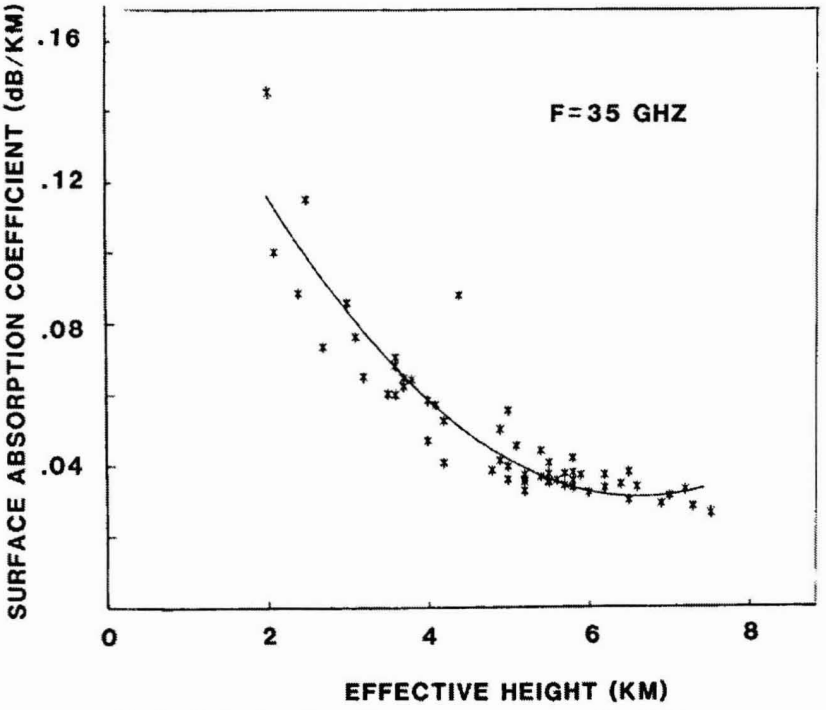

Fig. 7. Surface absorption coefficient versus effective height, $F = 35$ GHz.

Zenith absorptions for 15 GHz were calculated for the same 58 days as was done for the 35 GHz absorptions, and a regression of zenith absorption as a function of surface absolute humidity was performed. The result is

$$A_z(\rho) = 0.048 + 0.0035\rho$$

$$S_e(A_z;\ \rho) = 4.51 \times 10^{-4}$$

and

$$r(A_z,\ \rho) = 0.717.$$

As would be expected the correlation coefficients for the 15 GHz data are poorer than those for the 35 GHz data. A plot of $A_z(\rho)$ versus ρ is shown in Fig. 8.

A regression of the surface absorption coefficient vs surface absolute humidity was done for the same 58 sets of data, and the resulting equation was obtained.

$$\alpha(\rho) = 0.0042 + 0.0023\rho$$

$$S_e(\alpha_1;\ \rho) = 2.45 \times 10^{-4}$$

and

$$r(\alpha_1,\ \rho) = 0.780.$$

A plot of $\alpha_1(\rho)$ versus ρ is shown in Fig. 9.

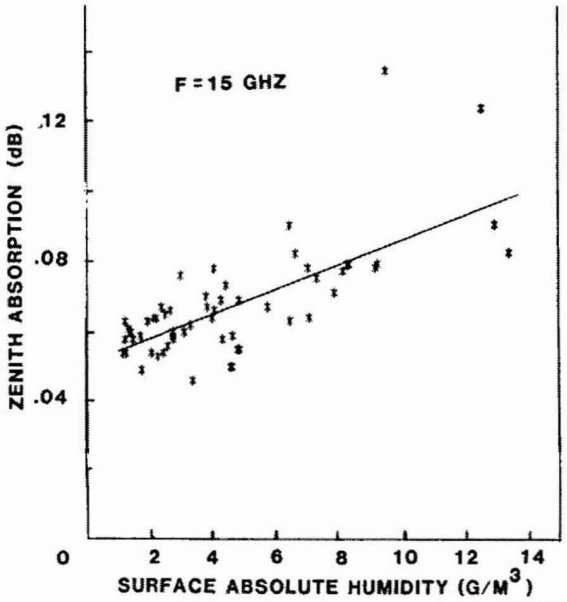

Fig. 8. Zenith absorption versus surface absolute humidity, $F = 15$ GHz.

V. Comparison of Experiment with Theory

Theoretical absorption results have been obtained from four sources; Liebe [7], Clough *et al.* [8], Gibbins [9], and CCIR

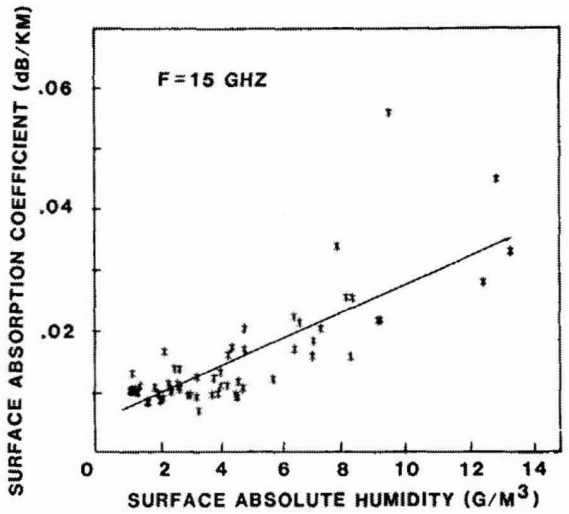

Fig. 9. Surface absorption coefficient versus surface absolute humidity, $F = 35$ GHz.

TABLE I
REGRESSION COEFFICIENTS FOR ABSORPTION VERSUS SURFACE ABSOLUTE HUMIDITY

	Absorption Coefficient (dB/KM) $\alpha_l = \alpha_{l0} + \alpha_{l1}\rho + \alpha_{l2}\rho^2$					Zenith Absorption (dB) $A_z = A_{z0} + A_{z1}\rho + A_{z2}\rho^2\rho$ in g/m^3				
					$F = 15$ GHz					
	Experiment	Liebe	Gibbins	Clough	CCIR		Experiment	Liebe	Clough	CCIR
α_{l0}	0.0045	0.0094	0.0083	0.0082	0.0083	A_{z0}	0.0477	0.0470	0.0400	0.0499
α_{l1}	0.0027	0.0020	0.0025	0.0024	0.0026	A_{z1}	0.0035	0.0039	0.0044	0.0059
α_{l1}		5.62×10^{-5}	4.72×10^{-5}	1.91×10^{-5}		A_{z2}		6.56×10^{-5}	3.63×10^{-5}	
					$F = 35$ GHz					
α_{l0}	.0182	0.0304	0.0270	0.0279	0.0270	A_{z0}	0.1774	0.1530	0.1522	0.1622
α_{l1}	.0068	0.0068	0.0088	0.0091	0.0104	A_{z1}	0.0093	0.0130	0.0171	0.0232
α_{l2}		2.99×10^{-4}	2.57×10^{-4}	4.78×10^{-5}		A_{z2}		3.68×10^{-4}	5.56×10^{-5}	

[10]. Liebe and Clough specially calculated absorptions at 15 and 35 GHz for a range of humidities so that we could make a direct comparison. Gibbins and CCIR results were computed from their respective equations. It was found that the zenith absorptions and surface absorption coefficients of Liebe and Clough could be accurately represented by second degree polynomials of the surface absolute humidity. Gibbins' result was expressed as a second degree polynomial of the surface absolute humidity; he did not, however, provide an algorithm for the calculation of zenith absorption. The CCIR expressions for zenith absorption and surface absorption coefficient were expressed as linear functions of surface absolute humidity. In Table I the regression coefficients for the calculated and measured absorptions are summarized. In Figs. 10–13 the regression lines for zenith absorption and surface absorption coefficient are plotted as a function of surface absolute humidity for frequencies of 15 and 35 GHz, respectively.

It is seen that the experimental zenith absorption at 15 GHz agrees very well with calculations by Clough *et al.* and Liebe. The CCIR result is slightly higher for the higher humidities. At 35 GHz the experimental values are in good agreement with those of Liebe and Clough except for the high humidities. The CCIR results are higher, particularly at the higher humidities. The experimental surface absorption coefficients at 15 GHz are lower than four sets of theoretical values; however, the slopes of experimental and theoretical regression lines are about the same. At 35 GHz the experimental absorption coefficients are also lower than the theoretical values particularly for higher humidities.

The experimental and theoretical effective heights are shown in Fig. 14 as a function of surface absolute humidity. The experimental regression line is that of Fig. 6. The theoretical values were calculated for both 15 and 35 GHz and found to be approximately the same. The Clough values were slightly higher than those of CCIR and Liebe. The experimental values were found to be slightly higher than the theoretical values, particularly for the lower humidities.

Finally, in Fig. 15 the calculated and experimental ratios of the 35 GHz to 15 GHz absorptions are compared. There is a distinct difference in the humidity dependence of the ratios.

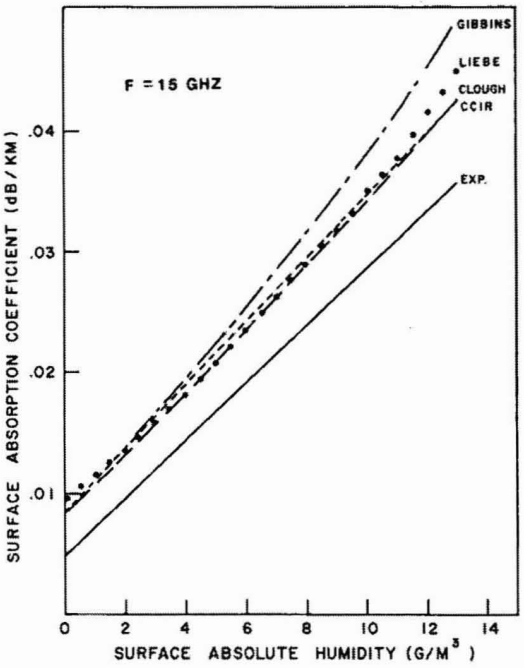

Fig. 10. Calculated and experimental surface absorption coefficients, F = 15 GHz.

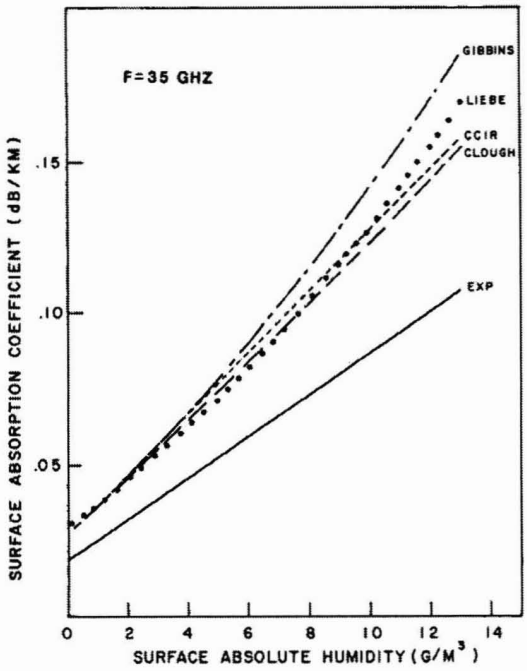

Fig. 12. Calculated and experimental, surface absorption coefficients, F = 35 GHz.

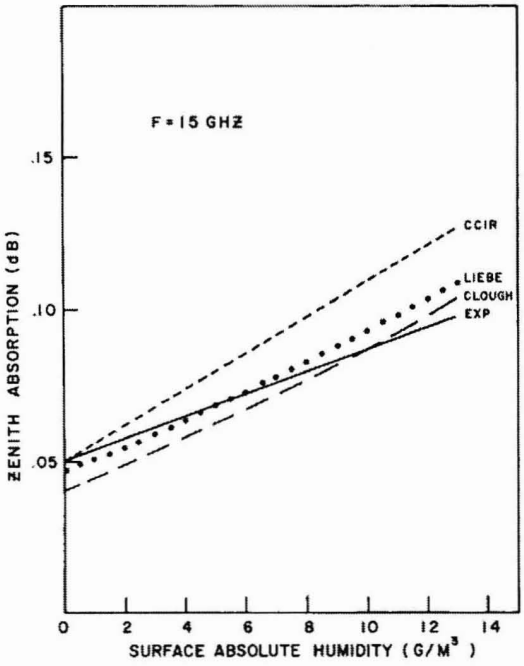

Fig. 11. Calculated and experimental zenith absorptions, F = 15 GHz.

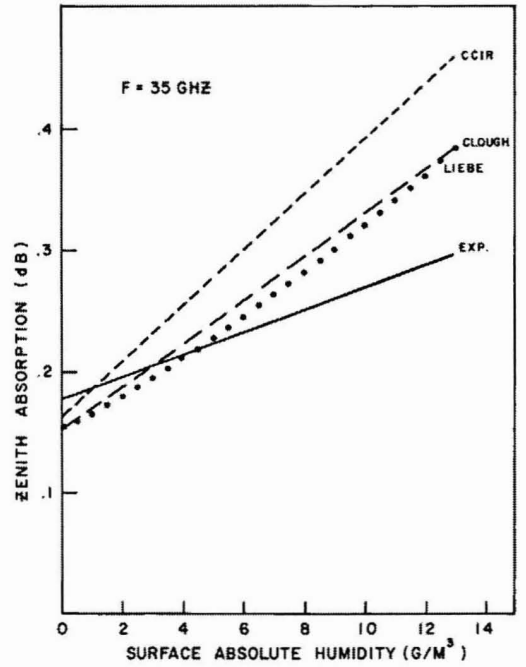

Fig. 13. Calculated and experimental zenith absorptions, F = 35 GHz.

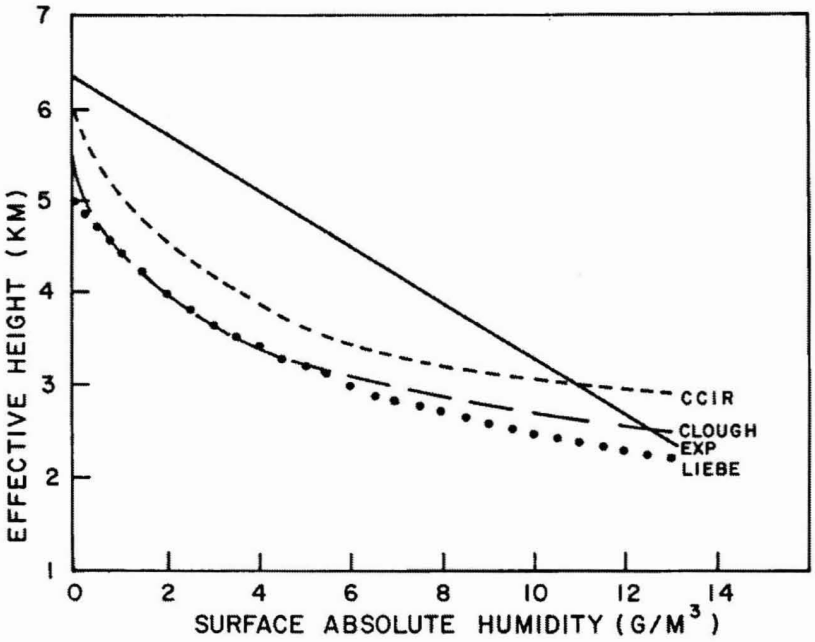

Fig. 14. Calculated and experimental effective heights.

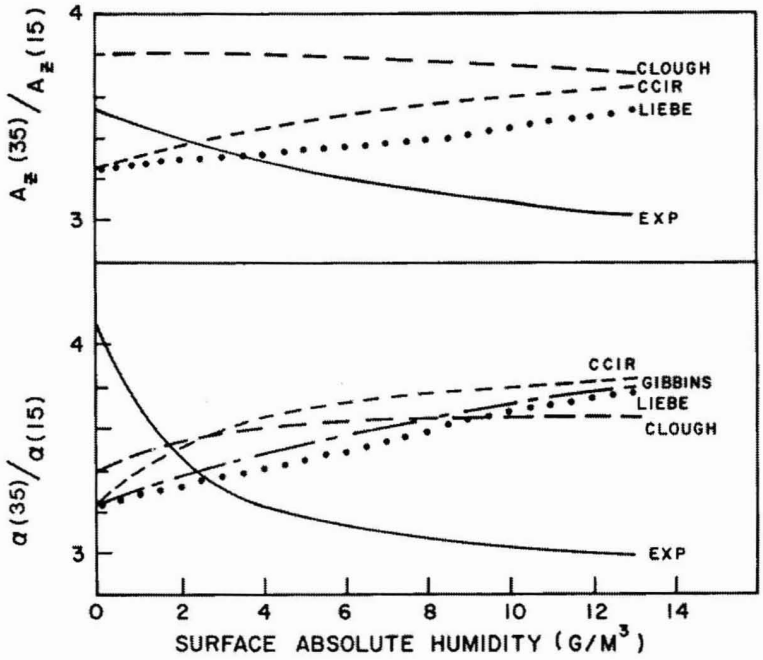

Fig. 15. Calculated and experimental frequency ratios of absorption.

The experimental ratios generally decrease as the surface absolute humidity increases. Only the Clough ratio of zenith absorptions shows a slight decrease with increasing humidity.

VI. Conclusion

An effort has been made to conduct accurate measurements under clear sky conditions of atmospheric absorption at the longer millimeter wavelengths. The absorption was correlated with meteorological data and then compared with the theoretical values. It has been shown experimentally that the absorption is indeed directly proportional to the distance through the absorbing atmosphere. The correlation of absorption with surface absolute humidity has been examined and found to be fair. However, since the water vapor along the

propagation path is not expected to be highly correlated with the surface absolute humidity, it is understandable that the correlation of the absorption with the surface absolute humidity would only be moderate. It would appear, however, that the surface absolute humidity should be an unbiased estimator of the water vapor aloft; that is, there is no reason to believe that the surface absolute humidity should consistently underestimate or overestimate the amount of water vapor aloft. Therefore, from a statistical standpoint, the correlation of absorption with surface absolute humidity should be meaningful.

The theoretical zenith absorptions of Liebe [7] and Clough *et al.* [8], are in good agreement at both 15 and 35 GHz; the CCIR [10] results are significantly higher for the higher humidities. The experimental zenith absorptions agree very well with those of Liebe and Clough *et al.* at 15 GHz; at 35 GHz the agreement is poorer for higher humidities.

Calculated surface absorption coefficients as a function of surface absolute humidity show good agreement at both 15 and 35 GHz; Gibbins' [9] values are slightly higher than the others. The experimental surface absorption coefficients are consistently lower than the theoretical values.

The calculated effective heights as a function of surface absolute humidity are in good agreement with one another. The experimental effective heights are somewhat higher than the corresponding calculated values, particularly for the lower humidities. Since the zenith absorption is the product of the surface absorption coefficient and the effective height, the typically lower experimental surface absorption coefficients combine with typically higher effective heights to produce zenith absorptions which are in good agreement with calculated values.

The calculated ratios of the 35 GHz to 15 GHz zenith absorptions of Liebe and CCIR are in good agreement with one another; corresponding values of Clough *et al.* are somewhat higher. The experimental ratios are higher for the lower humidities and lower for the higher humidities. The calculated ratios of the surface absorption coefficients as a function of surface absolute humidity show good agreement. Once again the experimental values are somewhat higher than the calculated values for low humidities and somewhat lower for high humidities. The most significant difference in the humidity dependence of the absorption ratios is that the calculated ratios generally increase with increasing humidity whereas the experimental ratios decrease with increasing humidity.

In conclusion, we feel that the experimental results that have been presented are very important, since to the best of our knowledge they are the only measured absorption data that have been directly compared with calculated values at the longer millimeter wavelengths. In general, the experimental and theoretical zenith absorptions are in good agreement; the experiment surface absorption coefficients on the other hand, are consistently lower than the calculated values. An explanation for this behavior is not available at this time. Further controlled experiments of absorption as a function of meteorological parameters would be valuable.

References

[1] E. E. Altshuler, "Slant path absorption correction for low elevation angles," *IEEE Trans. Antennas Propagat.*, vol. AP-34, pp. 717–718, May 1986.

[2] B. R. Bean and E. J. Dutton, "Radio meteorology," Nat. Bur. Stand. Monograph 92, Washington, D.C., p. 62, 1966.

[3] E. E. Altshuler, M. A. Gallop, Jr., and L. E. Telford, "Atmospheric attenuation statistics at 15 and 35 GHz for very low elevation angles," *Radio Sci.*, vol. 13, pp. 839–852, Sept.-Oct. 1978.

[4] E. E. Reber and J. R. Swope, "On the correlaiton of total precipitable water in a vertical column and absolute humidity at the surface," presented at Int. Conf. Aerospace and Aeronautical Meteorology, May 22–26, 1972, Washington, DC.

[5] C. H. Reitan, "Surface dew point and water vapor aloft," *J. Appl. Meteor.*, vol. 2, pp. 776–779, 1963.

[6] S. J. Bolsenga, "The relationship between total atmospheric water vapor and surface dew point on a mean daily and hourly basis," *J. Appl. Meteor.*, vol. 4, pp. 430–432, 1965.

[7] H. J. Liebe, "An updated model for millimeter-wave propagation in moist air," *Radio Sci.*, vol. 20, pp. 1069–1089, Sept.-Oct. 1985.

[8] S. A. Clough, F. X. Kneizys, E. P. Shettle, and G. P. Anderson, "Atmospheric radiance and transmittance: FASCOD Z," presented at Sixth Conf. Atmospheric Radiation, May 13–16, Williamsburg, VA.

[9] C. J. Gibbins, "Improved algorithms for the determination of specific attentuation at sea level by dry air and water vapor, in the frequency range 1-350 GHz," *Radio Sci.*, vol. 21, pp. 949–954, Nov.-Dec. 1986.

[10] CCIR, *Propagation in Non-Ionized Medial*, vol. V, pp. 167–177, 1986.



Edward E. Altshuler (S'54-M'55-SM'62-F'84) received the B.S. degree from Northeastern University, Boston, MA, in 1953, the M.S. degree from Tufts University, Medford, MA, in 1954, and the Ph.D. degree from Harvard University, Cambridge, MA, in 1960.

Before joining Air Force Cambridge Research Labs (AFCRL) in 1960 he was employed by Arthur D. Little, MIT and Sylvania. He was Director of Engineering at Gabriel Electronics from 1961 to 1963 and Chief of the Transmission Branch at AFRCL from 1963–1982. He is currently conducting tropospheric propagation research for the Electromagnetics Directorate of RADC (formerly AFCRL). He has been a lecturer in the Graduate School of Engineering at Northeastern University since 1964.

Dr. Altshuler has been Chairman of the IEEE Boston Section Antennas and Propagation Society and served as Chairman of the 1968 IEEE AP-S/URSI Symposium held in Boston. He was Associate Editor for Radio Science from 1976–1978 and is a member of Commissions B and F of the International Union of Radio Science. He has served on the Air Force Scientific Advisory Board and is currently Chairman of the NATO Research Study Group on Millimeter Wave Propagation.

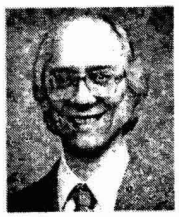

Richard A. Marr received the B.S. degree in engineering and computer science from the University of Massachusetts, MA, in 1969.

In 1973, after serving four years in the Air Force, he joined the Aerospace Instrumentation Laboratory of the Air Force Cambridge Laboratories. There he designed and built instrumentation and telemetry packages for sounding rockets on several research programs. Since 1976 he has been with the Electromagnetics Directorate of the Rome Air Development Center. He is involved in the study of tropospheric limitations on military systems, including millimeter wave target seekers, line-of-sight communication links and troposcatter radios.

APPENDIX 4 : **Fixed service propagation modelling**

Table of Contents

1. INTRODUCTION 1

2. CALCULATING THE BASIC TRANSMISSION LOSS (L_{BF}) 2

3. MODELLING TERRAIN DEPENDENT LOSSES (L_M) 2

3.1 SMOOTH EARTH 3
3.2 SINGLE KNIFE-EDGE 4
3.3 MULTIPLE OBSTACLES 4

4. DETAILED FIXED SERVICE PROPAGATION PREDICTION MODELS ... 5

4.1 WANTED SIGNAL PATH PROPAGATION MECHANISMS 6
4.1.1 Prediction of multi-path fading - initial planning method 7
4.1.2 Prediction of multi-path fading - detailed link design method 8
4.1.3 Prediction of attenuation due to rain 10
4.2 INTERFERENCE PATH PROPAGATION MECHANISMS 11
4.2.1 LOS propagation (including short-term effects) 12
4.2.2 LOS with diffraction losses 13
4.2.3 Clutter losses 13

1. Introduction

The basic method of frequency coordination, detailed under Part 4 of RALI FX 3, requires, in the first instance, the quantification of the basic free-space loss over the wanted and the unwanted signal paths. In order to facilitate a more rigorous assessment of the overall transmission loss, detailed path analysis and the application of appropriate propagation models is often necessary.

This appendix extends the simple transmission loss analysis outlined under the basic method of frequency coordination, through the addition of diffraction models suitable for estimating terrain dependent path losses over the wanted and unwanted signal paths. Guidance is also provided regarding the application of the more commonly used ITU-R terrestrial service propagation prediction methods incorporating statistical analyses based on system specific criteria.

Note: The onus is on the assigner to apply[1] the most appropriate propagation model/s for the given interference environment also noting that the ITU-R prediction models outlined in this document are subject to ongoing development.

[1] All of the fixed service propagation models described in this document may be usefully incorporated as computer program algorithms (integrated with terrain and assignment databases), to facilitate less labour intensive and more efficient frequency assignment practices.

2. Calculating the basic transmission loss (L_{bf})

Recalling that the total transmission loss (L_b) between two ideal antennas, consists of:

- a (time invariant) basic free space loss (L_{bf}); and
- additional attenuation due to terrain, rain and other physical attributes associated with a particular propagation path (L_m).

The total transmission loss is then given by:

$$L_b = L_{bf} + L_m \qquad \text{(dB)}$$

where:

$$L_{bf} = 32.4 + 20\log f + 20\log d \qquad \text{(dB)}$$

where: f - frequency (MHz); and
d - distance (km).

In cases where an initial coordination assessment using the basic free-space attenuation model fails to meet the specified interference management criteria, then more complex propagation analyses may be invoked in order to more accurately characterise the L_m component of the total transmission loss. Subsequent choice of appropriate propagation model/s may be critical in determining the outcome of detailed coordination.

3. Modelling terrain dependent losses (L_m)

A more detailed analysis of the overall transmission loss must include consideration of additional (ie. above free-space) attenuation due to the effects of terrain and diffraction in particular. Thus under the basic method of frequency coordination:

$$L_m \cong L_d$$

where: L_d - attenuation due to diffraction (dB).

The attenuation due to diffraction may be estimated by the propagation models, based on the application of ITU-R Recommendation P.526-4 "*Propagation by diffraction*", described in the following sub-sections. The models are valid for systems operating above about 1 GHz and consider attenuation due to diffraction over:

- a "smooth-earth" propagation path;
- a single knife-edge obstacle; and
- multiple obstacles.

The selection of the appropriate diffraction model(s) is determined by an analysis of the relevant path profile(s). For an initial analysis and under the basic method of coordination, critical path clearance over the wanted signal path is normally assumed since no additional interference protection is mandated for fixed service systems operating over obstructed paths. Propagation models used for link planning purposes typically specify results based on a median signal level (ie. the level exceeded for 50% of the time). For interference calculation purposes, more stringent criteria are normally applied and, for the basic method of frequency coordination, long term (20%) and short term (0.01%) criteria are adopted.

Accordingly, for the path profile analysis, the following k-factors[2] are normally applied:

- k = 4/3 under the median link planning "standard atmosphere" criteria (50%);
- k = 3 under the long term "annual" interference criteria (20%); and
- k = 20 under the short term "worst month[3]" interference criteria (0.01%)

For terrain modelling and path analyses based on digitised data, an elevation model at least equivalent to or better than the ACMA's RadDEM (9 second data) is to be used.

3.1 Smooth Earth

The standard method for calculating the transmission loss due to diffraction over a smooth-earth is defined as follows:

$$L_d = F(X) + G(Y_1) + G(Y_2) \qquad \text{(dB)}$$

where: X - normalised length of the path;

$$X = 2.2 \sqrt[3]{f}\ \frac{d}{\sqrt[3]{a_e^2}}$$

Y_1, Y_2 - normalised antenna heights;

$$Y = 0.0096 \sqrt[3]{f^2}\ \frac{h}{\sqrt[3]{a_e}}$$

a_e - equivalent Earth radius, equal to the product ka
where: a - the actual Earth radius (6370km); and
k - the applicable k-factor[4].
h - antenna height (m);
d - path length (km); and
f - frequency (MHz).

---

[2] Defined in Recommendation P.310-9 as the ratio of the effective Earth radius to the actual Earth radius and related to the vertical refractivity gradient dn/dh (ΔN, see also Recommendation P.453-5).

[3] See Recommendation P.581-2 *"The concept of Worst Month"*.

[4] Note: As $k \rightarrow \infty$ the spherical earth diffraction model is no longer valid and $L_d = 0$.

the distance term is given by:

$$F(X) = 11 + 10 \log(X) - 17.6X$$

with the height gain term:

$$G(Y) \cong \begin{cases} 17.6\sqrt{Y - 1.1} - 5 \log(Y - 1.1) - 8 & \text{for} \quad Y > 2 \\ 20 \log(Y + 0.1Y^3) & \text{for} \quad Y \leq 2 \end{cases}$$

3.2 Single knife-edge

The standard method for calculating the transmission loss due to diffraction over a single knife-edge obstacle is defined as follows:

$$L_d = 6.9 + 20\log(\sqrt{(v - 0.1)^2 + 1} + v - 0.1) \quad \text{(dB)}$$

where: $v = h\left(\sqrt{\frac{fd}{150 d_1 d_2}}\right)$

h - height (m) of the obstacle relative to a straight line joining the path ends;
d1, d2 - distance (km) of the two ends of the path from the top of the obstacle;
d - path length (km); and
f - frequency (GHz).

3.3 Multiple obstacles

The single obstacle diffraction model may be extended to account for multiple obstacles. Path analysis and calculation of the attenuation due to diffraction over multiple obstacles may be determined using the "stretched string analysis" method detailed in ITU-R Recommendation P.526.

This concludes the outline of basic transmission loss calculation and propagation modelling methodologies intended to be incorporated as part of the basic method of frequency coordination. The following sections provide an overview of the commonly used ITU-R fixed service propagation prediction procedures, which take account of the statistical nature of terrestrial radiowave propagation and which can be applied under particular instances of detailed coordination.

4. Detailed fixed service propagation prediction models

The transmission loss calculation procedures incorporated under the basic method of frequency coordination represent a deterministic approach; free-space loss is constant in time and diffraction loss values are calculated for a particular 'k' value of effective Earth radius. In the real world, the k-factor varies with time and location in accordance with complex physical interactions involving the refractivity gradient (dn/dh) in the lowest part of the atmosphere and other mechanisms, as detailed in the propagation "P series" of ITU Recommendations.

An important objective in planning terrestrial microwave link systems is to ensure that outages resulting from these variations are extremely rare events, thus system fade margins, linked to error performance and availability objectives, of the appropriate order are implemented to assure that this is so. Accordingly, in order to take account of the statistical nature of radiowave propagation, the application of appropriate propagation prediction models is necessary.

Performance prediction (related to propagation effects) principally depends upon the assessment of two main propagation mechanisms; multi-path fading and/or attenuation due to rain. Multi-path fading typically gives rise to short outages and thus has the most impact on error performance. For the purpose of modelling multi-path fading, propagation prediction methods have been derived which estimate the probability of single-frequency fading[5]. Rain attenuation events typically give rise to outage durations greater than 10 seconds, therefore directly influencing availability of systems operating in the bands above about 10 GHz. The prediction of rain outages is possible through application of rainfall intensity statistics to modelling methods for rain attenuation.

The following ITU-R recommendations represent the principal ITU-R models used for fixed service propagation modelling:

- Recommendation P.530-6 " *Propagation data and Prediction Methods required for the design of Terrestrial Line-of-Sight Systems"* as typically utilised for link planning purposes; and
- Recommendation P.452-7 *"Prediction Procedure for the Evaluation of Microwave Interference between stations on the Surface of the Earth at frequencies above about 0.7 GHz*", provides methodologies specifically intended for use on interference paths.

Although these models address propagation mechanisms for the wanted signal and the interference path independently, the prediction methods are not exclusive to either path type. The use of these particular ITU-R prediction methods is not mandated and, in cases where a departure from these models can be justified, other (relevant) prediction methods may be applied.

An outline of the application of prediction methods based on the above recommendations, for frequency coordination purposes, is provided in the following

[5] Wideband systems may also suffer frequency selective fading, not addressed in these models.

sections. However, the emphasis in this document is to provide guidance regarding the application of these models in the Australian context, rather than the verbatim reproduction of detailed methodologies. Accordingly, for detailed application, reference must be made to the relevant source recommendations.

4.1 Wanted signal path propagation mechanisms

The wanted signal for microwave fixed services can be modelled using the performance prediction methods presented in ITU-R Recommendation P.530-6, for the following propagation mechanisms:

- diffraction fading due to obstruction or partial obstruction of the path, as already discussed in Section 3 of this Appendix;
- attenuation due to atmospheric gases;
- attenuation due to variation of the angle-of-arrival/launch; and
- fading due to multi-path, beam spreading, scintillation and attenuation due to rain.

For frequency coordination purposes, only the dominant multi-path fading (and related mechanisms) and rain outage mechanisms are considered in this overview. The following subsections outline two methodologies, (Section 4.1.1 "an initial planning method" and Section 4.1.2 "detailed link design method", as detailed in Recommendation P.530-6) suitable for estimating the effects of multipath fading and statistical algorithms (Section 4.2.3) for evaluating rain fade attenuation.

The prediction of the remaining propagation mechanisms (including multipath enhancement modes) as also detailed in Recommendation P.530-6 are part of the detailed link design process and are not considered here.

Note: The prediction methods presented in Sections 4.1.1 and 4.1.2 model single frequency fading (ie. "flat fade margin") and do not account for dispersive effects which may be a concern in detailed planning for wideband (ie. 34/140/155 Mb/s) systems. However, the methods may be considered adequate for frequency coordination purposes and are valid for fade depths greater than approximately 15 dB or the value exceeded for 0.1% of the worst month, whichever is the greater.

4.1.1 Prediction of multi-path fading - initial planning method

For the path location in question, estimate the geoclimatic factor K for the average worst month from p_L[6] and the following empirical relationships, derived for Australia:

$K = 10^{-6.5} p_L^{1.5}$	Overland links for which the lower of the transmitting and receiving antennas is less than 700 m above mean sea level;
$K = 10^{-7.1} p_L^{1.5}$	Overland links for which the lower of the transmitting and receiving antennas is higher than 700 m above mean sea level;
$K = 10^{-5.9} p_L^{1.5}$	Links over medium-sized bodies of water, coastal areas beside such bodies of water, or regions of many lakes; and
$K = 10^{-5.5} p_L^{1.5}$	Links over large bodies of water, or coastal areas beside such bodies of water.

Whilst in most cases selecting the correct empirical relationship "*K*" is straightforward, any ambiguity can be resolved by referring to the notes included in ITU-R Recommendation P.530-6, which provide further guidance regarding the parameters and terminology used in the above-listed relationship criteria.

If the antenna heights are known, calculate the magnitude of the path inclination ($|\varepsilon_p|$) from:

$$|\varepsilon_p| = \frac{1}{d} |h_r - h_e| \qquad \text{(mrad)}$$

where: d - path length (km); and

h_e, h_r - transmit and receive antenna height respectively (metres above sea level or some other reference height).

The fade depth (A) that is exceeded for a percentage of time (p_w) in the average worst month is:

$$A = 10\log(K\, d^{3.6} f^{0.89} (1 + |\varepsilon_p|)^{-1.4}) - 10\log p_w \qquad \text{(dB)}$$

where: f is frequency (GHz).

For the prediction of average year instead of average worst month exceedence percentages, refer to P.530-6 § 2.3.5. and ITU-R Recommendation PN.841[7].

---

[6] p_L (percentage of time that the average refractivity gradient in the lowest 100 m of the atmosphere is less than –100 N units/km) refractivity gradient contour maps are provided in Figure 1, Annex A to Appendix 1 of RALI FX 3.

[7] ITU-R Recommendation P.841 "*Conversion of annual statistics to worst-month statistics*".

4.1.2 Prediction of multi-path fading - detailed link design method

The detailed link design method is an extension of the initial planning method and it accounts for the path profile. The geoclimatic factor K is estimated using the following empirical relationships:

$K = 10^{-5.4} p_L^{1.5}$	Overland links for which the lower of the transmitting and receiving antennas is less than 700 m above mean sea level;
$K = 10^{-6.0} p_L^{1.5}$	Overland links for which the lower of the transmitting and receiving antennas is higher than 700 m above mean sea level;
$K = 10^{-4.8} p_L^{1.5}$	Links over medium-sized bodies of water, coastal areas beside such bodies of water, or regions of many lakes; and
$K = 10^{-4.4} p_L^{1.5}$	Links over large bodies of water, or coastal areas beside such bodies of water.

The path inclination is calculated as described in the initial planning method. From the profile of the terrain along the path, obtain the terrain heights h at intervals of 1.0 km, beginning 1.0 km from one terminal and ending 1-2 km from the other. Using these heights, carry out a linear regression with the "method of least squares" to obtain the linear equation of the "average" profile:

$$h(x) = a_0 x + a_1$$

where x is the distance along the path. The regression coefficients can be calculated from the relations:

$$a_0 = \frac{\sum_n xh - \left(\sum_n x \sum_n h\right) / n}{\sum_n x^2 - \left(\sum_n x\right)^2 / n}$$

$$a_1 = \left(\sum_n h - a_0 \sum_n x\right) / n$$

where n is the number of profile height samples.

Calculate $h(0)$ and $h(d)$, the heights of the average profile at the ends of the path, and the heights of the antennas above the average path profile:

$$h_1 = h_e - h(0)$$

$$h_2 = h_r - h(d)$$

Calculate the "average" grazing angle φ corresponding to a 4/3 Earth radius model (i.e. $a_e = 8\,500$ km) (Refer to Recommendation ITU-R P.834):

$$\varphi = \frac{h_1 + h_2}{d}\left[1 - m\left(1 + b^2\right)\right]$$

where:

$$m = \frac{d^2}{4\,a_e\,(h_1 + h_2)}$$

$$c = |h_1 - h_2| \,/\, (h_1 + h_2)$$

$$b = 2\sqrt{\frac{m+1}{3m}}\cos\left[\frac{\pi}{3} + \frac{1}{3}\arccos\left(\frac{3c}{2}\sqrt{\frac{3m}{(m+1)^3}}\right)\right]$$

In calculation of the coefficients m and c, the variables a_e, d, h_1 and h_2 must be in the same units. The grazing angle φ will be in the desired units of milliradians if h_1 and h_2 are in metres and d in kilometres.

The fade depth (A) that is exceeded for a percentage of time p_w in the average worst month is:

$$A = 10\log(K\,d^{3.3} f^{0.93}(1 + |\varepsilon_p|)^{-1.1}\varphi^{-1.2}) - 10\log p_w \quad \text{(dB)}$$

where: f is frequency (GHz).

4.1.3 Prediction of attenuation due to rain

The specific attenuation due to rain, as based on ITU-R Recommendation P.838 *"Specific Attenuation Model for Rain for use in Prediction Methods"* is given by:

$$\gamma_R = kR^{\alpha} \qquad \text{(dB/km)}$$

where: R - rainfall intensity[8] (mm/hr); and
k, α - frequency dependant coefficients.

The coefficients k and α for linear (H - horizontal, V - vertical) and circular polarisation can be calculated from the following equations:

$$k = 0.5\,[k_H + k_V + (k_H - k_V)\cos^2\theta\cos(2\tau)]$$

$$\alpha = \frac{1}{2k}\,[k_H\alpha_H + k_V\alpha_V + (k_H\alpha_H - k_V\alpha_V)\cos^2\theta\cos(2\tau)]$$

where: $k_H, \alpha_H, k_V, \alpha_V$ - regression coefficients (as specified in Table 1) for estimating specific attenuation;
θ - path elevation angle; and
τ - polarisation tilt angle relative to the horizontal ($\tau = 45°$ for circular).

Frequency (GHz)	k_H	k_V	α_H	α_V
1	0.0000387	0.0000352	0.912	0.880
2	0.000154	0.000138	0.963	0.923
4	0.000650	0.000591	1.121	1.075
6	0.00175	0.00155	1.308	1.265
7	0.00301	0.00265	1.332	1.312
8	0.00454	0.00395	1.327	1.310
10	0.0101	0.00887	1.276	1.264
12	0.0188	0.0168	1.217	1.200
15	0.0367	0.0335	1.154	1.128
20	0.0751	0.0691	1.099	1.065
25	0.124	0.113	1.061	1.030
30	0.187	0.167	1.021	1.000
35	0.263	0.233	0.979	0.963
40	0.350	0.310	0.939	0.929
45	0.442	0.393	0.903	0.897
50	0.536	0.479	0.873	0.868

Table 1. Regression coefficients for estimating specific attenuation

[8] The rainfall intensity for 0.01% of the time can be derived from the rain climate region map in Figure 2, Annex A to Appendix 1, for rainfall intensities at other percentages refer to ITU-R Recommendation P.838.

For any given path the attenuation due to rain is calculated for an effective path length, which accounts for the distribution of the rain intensity rate. The attenuation (A) due to rain, exceeded for 0.01% of the worst month is:

$$A = \gamma_R \left(\frac{d}{1 + \frac{d}{d_0}} \right) \qquad \text{(dB)}$$

where: d - path length (km); and

$$d_0 = 35 e^{(-0.015 R_{0.01})}$$

The attenuation (A_p) due to rain, exceeded for p% ($0.001 < p < 1$) of the worst month is:

$$A_p = 0.12\, p^{-(0.546 + 0.043 \log_{10} p)} \qquad \text{(dB)}$$

4.2 Interference path propagation mechanisms

Interference path transmission losses for microwave fixed service links, including situations where interference levels rise for short periods of time (p%) due to propagation enhancement on the interference path, can be modelled using the prediction models defined in ITU-R Recommendation P.452-7[9], for the following propagation mechanisms:

- line-of-sight (including multi-path and focussing effects and gaseous absorption);
- line-of-sight with sub-path diffraction;
- diffraction due to clutter;
- tropospheric scatter; and
- ducting and other anomalous propagation modes.

Note: The troposcatter and the above-mentioned "anomalous" mode models are not considered here, as interference contribution through these modes to the homogeneous fixed service are not considered significant. However, they may be of significance when considering interference to particularly sensitive systems such as Earth stations of the space services.

Two basic types of interference path are considered when modelling transmission losses for a terrestrial propagation path. These demonstrate either a first Fresnel zone clearance or intrusion into the first Fresnel zone. For a terrestrial path with first Fresnel zone clearance, line-of-sight and clutter loss are the applicable propagation models. The corresponding predicted transmission loss is:

---

[9] Computer programs associated with the prediction procedures described in this Recommendation are available from the ITU.

$$L_b\,(\mathrm{p}) = L_{b0}\,(\mathrm{p}) + A_{ht} + A_{hr} \quad (\mathrm{dB})$$

where: L_{b0} (p) - predicted basic transmission loss not exceeded for p% of time given by the LOS model; and

A_{ht}, A_{hr} - appropriate additional losses due to height-gain effects in local clutter.

For a terrestrial path with (obstacle) intrusion into the first Fresnel zone, the above-mentioned models apply with the addition of a diffraction model. The predicted transmission loss is then:

$$L_b\,(\mathrm{p}) = L_{b0}\,(\mathrm{p}) + L_{ds}\,(\mathrm{p}) + A_{ht} + A_{hr} \quad (\mathrm{dB})$$

where: L_{ds} (p) - prediction for p% of the time given by the sub-path diffraction loss element of the diffraction model.

4.2.1 LOS propagation (including short-term effects)

The basic transmission loss $L_{b0}(p)$ not exceeded for time percentage, p%, due to line-of-sight propagation is given by:

$$L_{b0}\,(p) = 92.5 + 20\log f + 20\log d + E_s(p) + A_g \qquad (\mathrm{dB})$$

where: $E_s(p)$ - correction for multipath and focusing effects:

$$E_s\,(p) = -9.617\,(1 - e^{-d/10}) \qquad (\mathrm{dB}) \text{ for } 0.01\ \% \text{ of the time}$$

$$E_s\,(p) = -1.035\,(1 - e^{-d/10}) \qquad (\mathrm{dB}) \text{ for } 20\ \% \text{ of the time}$$

Total gaseous (atmospheric) absorption is only considered significant at frequencies above approximately 10 GHz. The total gaseous absorption is:

$$A_g = [\gamma_o + \gamma_w(\rho)]\,d \qquad (\mathrm{dB})$$

where:

γ_o, $\gamma_w(\rho)$ - specific attenuation due to dry air and water vapour, respectively, and are found from the equations in Recommendation ITU-R P.676; and

ρ: water vapour density:

$$\rho = 7.5 + 2.5\,\omega \qquad (\mathrm{g/m^3})$$

ω: fraction of the total path over water.

4.2.2 LOS with diffraction losses

The excess loss due to diffraction may be calculated using a diffraction methodology[10], assuming the effective Earth radius to be time-dependant due to the changes in bulk atmospheric radio refractivity lapse rate. ITU-R Recommendation P.452-7 §4.3 describes this time-dependant sub-path refraction loss model.

4.2.3 Clutter losses

The presence of clutter (buildings and vegetation) in the vicinity of the transmit and receive antennas can cause additional transmission losses, A_{ht} and A_{hr}. These losses are dependant upon the height of the clutter. Clutter losses may be calculated using the methodologies described in ITU-R Recommendation P.452-7 §4.6 by a height-gain model which is normalised to the nominal height of the clutter.

---

[10] Derived from ITU-R Recommendation P.526-4.

JAUES

Journal of Al Azhar University Engineering Sector

Vol. 11, No. 41, October, 2016, 1341-1355

DESIGN AND IMPLEMENTATION OF MICROWAVE PLANNING TOOL WITH STUDYING THE EFFECT OF VARIOUS ASPECTS

Mohamed Maher Hanafi, Mohamed Hamza EL-Saba, and Hussein A.Elsayed
Electronics and Communication Eng. Dept, Ain Shams University

ABSTRACT

Microwave Line-of-sight radio is one of most important and common transmission methods in telecommunications networks. As the microwave radio signals are propagated through the lower atmosphere, they are sensitive to terrain, atmospheric, and climatic conditions. The planning and design of a reliable microwave links is very difficult and require a lot of complex computations. Therefore, not only software implementation is required, but studding the effect of all the different design aspects is very crucial for the telecommunication systems. The software then estimates the path profile, link budget, fade margin, and all other parameters at any place.

This paper presents the microwave software planning tool design and implementation with study of all of the design parameters. This software is an engineering tool to aid in the design and planning of the microwave transmission links considering the geography, distance, antenna height, transmit power, frequency, temperature, atmospheric effect, pressure, losses, and other factors which affects on the microwave line-of-sight radio link

I. INTRODUCTION

Microwave radio transmission is the transmission of information by electromagnetic waves with very small wavelengths. A microwave link is a communications system that uses a beam of microwave radio to transmit information between two locations, which ranges from just a few meters to several kilometers. There are some programs that can configure network, estimate path profile to find antenna height in each station, calculate link budget, receiver level, and link availability for microwave sites.

This study is an attempt to design and implement microwave transmission planning tool to enable telecommunication engineers to design the microwave transmission sites based on geography, distance, antenna height, transmit power, frequency, temperature, water vapor, pressure, losses, and other factors to create the best microwave line-of-sight radio link. The tool also connects to online maps servers to draw the path profile and import it into the tool when user creates a new link. It uses the terrain curve and mathematical equations to simulate very accurate radio transmission link between any two sites.

In the implemented microwave planning tool, users can add extra obstacles manually depending on the site survey, then the "path profile chart" page will display if there is a clear line-of-sight or not. The implemented tool doesn't required setup so it allows users to easily and quickly design the microwave transmission networks.

This software is designed to support equipment manufacturers, telecommunications, coordination, and engineering service providers worldwide. It has been taken into account that this software may be used by civil engineers and in site acquisition departments in the mobile service providers. Therefore, the technical idioms in the input parameters and the output results are reduced.

2. MICROWAVE PROPAGATION AND FREE SPACE PROPAGATION

The microwave beam is an electromagnetic wave that propagates in free space as well as material substances. The electromagnetic wave consists of two fields: electric field and magnetic field. In free space they are in phase and mutually perpendicular. If the microwave signal traveled in a vacuum, the

characteristics of the microwave systems are determined by the mechanisms affecting the propagation of radio waves. These characteristics depend on the frequencies used for transmission, the atmospheric effects, and the earth terrain. The received signal can therefore be the resultant of any number of the following ways as shown in Fig. 1:

a) Direct waves (free-space).
b) Reflected waves (reflected from the ground).
c) Sky waves (reflected from ionized layers above the earth and is known as the ionosphere).
d) Surface waves (caused by diffraction around the earth).

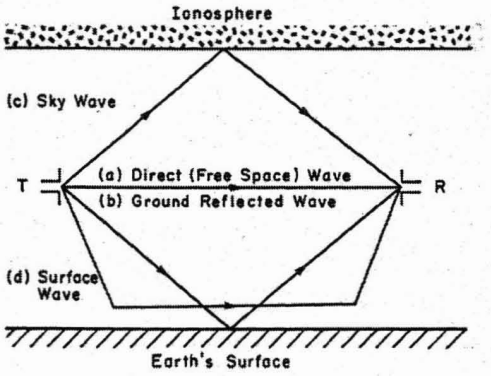

Fig. 1. Transmission paths between the transmitter and receiver.

Microwave radio transmission requires a line-of-sight path between transmitting and receiving antennas. Free space path loss is the loss in signal strength of an electromagnetic wave that would result from a line-of-sight path through free space, it occurs when both transmitting and receiving antennas are located away from the influence of the Earth's surface or other reflecting and absorbing objects. These conditions provide a highly predictable and stable power loss and are considered ideal conditions. Free space loss is expressed as the ratio of the power into an isotropic transmitting antenna to the power output from an isotropic receiving antenna. The Free space loss is given by equation (1).

$$FSL = \left(\frac{4\pi d}{\lambda}\right)^2 = \left(\frac{4\pi df}{c}\right)^2 \quad (1)$$

where λ is free space wavelength, d is the distance between two endpoints is measured in km, and the frequency f in GHz. For simplicity, the path loss equation can be expressed as in equation (2).

$$\text{FSL(dB)} = 20 \log_{10}(d) + 20 \log_{10}(f) + 92.45 \quad (2)$$

3. Path Profile and Fresnel Zone

The radio path profile is a plot of the earth's elevations against the distance between the two endpoints that represent the microwave path. For long distance, map work analysis is essential because physically checking for the Line-of-sight is impossible. The preferred method of doing so is to produce a path profile which is a cross-section of the Earth's surface between the two end points. Digital map is required and the contour line elevations recorded from a straight line are drawn between the two points on the map. The Earth's bulge and the curvature of the radio beam need to be taken into account. Critical obstruction points identified on the path profile should always be physically inspected for additional obstructions such as trees or buildings. The Earth bulge is determined as in equation (3).

$$b = d_1.d_2 / 12.75\, k \quad (3)$$

where b is in meters, d1, d2 are the distances from each end site to a certain point in kilometers, and k is the effective Earth radius factor.The microwave beam between two endpoints is not a straight line but a wave front has a cross-sectional width of which the direct ray is the axis. There are a series of concentric ellipsoidal regions; the measure of beam width on one of them is the first Fresnel zone, which is an ellipsoid containing most of the signal power that reaches the receiving antenna as shown in Figure 2. The clearance required along the path in order not to interfere this wave front along the path. This clearance is a function of the distance between the two end points and the frequency of operation

For a fixed path, the first Fresnel zone becomes narrower with increasing frequency and larger antennas. Path profiles show the clearance of a microwave beam and its Fresnel zones above the ground

with the effective Earth radius factor as the parameter. The required clearance creates a cigar shape between the endpoints and it described by 0.6 of the first Fresnel zone.

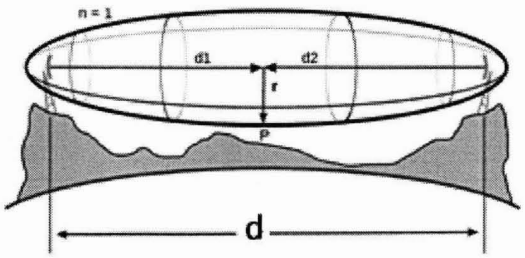

Figure 2 Fresnel Zone

The general equation for calculating the Fresnel zone radius at any point P in between the endpoints of the link is shown in equation (4):

$$F = 17.32 \sqrt{\frac{d_1 * d_2}{fd}} \tag{4}$$

Where F is the radius of the Fresnel Zone in meter, d_1 is the distance to P from one end in Km, d_2 is the distance from P to the other end in Km, f is the operation frequency in GHz and d is the total distance between two endpoints.

4. MULTIPATH FADING

Multipath fading is the drop in the received signal due to phase cancellation between the direct path signal and one or more signals traveling over different paths. The multipath cancellation is caused by reflection or refraction of the microwave beam. The reflection occurs when a portion of the wave front is reflected by the surface of the earth and arrives out of phase with the direct signal. The outages due to multipath fading function of parameters such as frequency, hop length, terrain type and roughness, climatic conditions, path clearance and geoclimatic factor determined from the hop terrain and climatic zone.

Each country has unique parameters; some of these parameters can be obtained by following the various versions of ITU 530. In fact, multipath fading causes a fast and deep signal attenuation that can cause an outage if the fade margin is exceeded. So, when designing a radio link, it is important to know the probability of this event occurring relative to the depth of fading. The formulas and methods presented by ITU are an attempt to define prediction models that allow you to accurately predict the outage time for any given hop. The probability distribution curve follows a Rayleigh distribution [2] for deep fades; the Rayleigh fading is given as:

$$p(F < M) = P_o * 10^{-M/10} \tag{5}$$

That mean the probability of a fade exceeding a set fade margin M is proportional to a set multipath fading occurrence factor Po. Because the fading is caused by multipath, one tries to predict the probability of multiple paths existing. The equation for calculating the geoclimatic factor K [4] is as follows:

$$K = 5.0 * 10^{-7} * 10^{-0.1(C_o - C_{Lat} - C_{Lon})} PL^{1.5} \tag{6}$$

where C_o is the terrain altitude coefficient [4] and takes the values

$$C_0 = \begin{cases} 1.7 & \text{from 0–400m AMSL} \\ 4.2 & \text{from 400m–700m} \\ 8 & \text{above 700m} \end{cases}$$

the coefficient C_{Lat} of latitude ξ [4] is given by:

$C_{Lat} = 0$ (dB) for $\xi \leq 53°$ N or °S

$C_{Lat} = -53 + \xi$ (dB) for $53°$ N or °S $< \xi <$ $60°$ N or °S

$C_{Lat} = 7$ (dB) for $\xi \geq 60°$ N or °S

and the longitude coefficient C_{Lon}, [4] by:

$C_{Lon} = 3$ (dB) for longitudes of Europe and Africa

$C_{Lon} = -3$ (dB) for longitudes of North and South America

$C_{Lon} = 0$ (dB) for all other longitudes

The equation for calculating the path inclination [5] is as follows:

$$\epsilon_P = |h_r - h_e| / d \tag{7}$$

Where h_r and h_e are the heights of the transmitting and receiving antennas above sea level and d is the distance between two endpoints in kilometers. The average worst month fade probability [2], P_w can thus be expressed as:

$$P_w = K * d^{3.6} * f^{0.89} (1 + \epsilon_p)^{-1.4} * 10^{-A/10} \% \tag{8}$$

Where K is the geoclimatic factor, d is the path length in kilometers, f is the frequency in gigahertz, ϵ_p is the path inclination in milliard (max value 24), and A is the fade margin in decibels.

5. ATMOSPHERIC ABSORPTION AND RAIN EFFECT

Due to gases (especially oxygen) and water vapor along the microwave propagation path, a loss in microwave energy occurs. This loss is known as atmospheric attenuation. Most of this lost energy is normally absorbed by gases and water vapor and transformed into heat. The total atmospheric attenuation is the sum of the atmospheric absorption due to oxygen and the atmospheric absorption due to water vapor [2] and is expressed as follows:

$$A_a = (\gamma_{water} + \gamma_{oxygen}) \tag{9}$$

The atmospheric absorption due to oxygen is given by the Van Vleck equation [6] as follows:

$$\gamma_o = \left[0.4909 \frac{P^2}{T^{5/2}} V_1\right] \left\{\frac{1}{1 + 2.904 * 10^{-4} \lambda^2 p^2 T^{-1} V_1^{\,2}}\right\} \left\{1 + \frac{0.5 V_2}{\lambda^2 V_1}\right\} \tag{10}$$

where: γ_o is the atmospheric absorption due to Oxygen dB/km, P is the atmospheric pressure in millibars, T is the atmospheric temperature in Kelvin, λ is the wavelength, V_1 and V_2 constants where V_1= 0.018 cm^{-1}, V_2= 0.05 cm^{-2}. The atmospheric absorption due to water vapor from Van Vleck equation [6] is given by:

$$\gamma_w = 1.852 * 3.165 * 10^{-6} \frac{\rho_w P^2}{T^{3/2}} \left\{ \frac{1}{(1 - 0.742\lambda)^2 + 2.853 * 10^{-6} \lambda^2 P^2 T^{-1}} + \frac{1}{(1 + 0.742\lambda)^2 + 2.853 * 10^{-6} \lambda^2 P^2 T^{-1}} + \frac{3.43}{\lambda^2} \right\} \tag{11}$$

where γ_w is the water vapor density in m^{-3}, Note that the atmospheric temperature for altitude less than 12 km is: T=188-6.5 h, where h is the altitude in km. Assuming that air pressure at sea level is 1015 millibars, then the air pressure in millibars at any altitude for up to 12 km [6] is given by :

$$P = 1015(1 - 0.02257\, h)^{5.2561} \tag{12}$$

To calculate the total Atmospheric absorption along the microwave propagation path [4] the equation will be as follows:

$$A_a = (\gamma_{water} + \gamma_{oxygen}) * d \quad (13)$$

Where d is the distance between two endpoints.

The rain causes a degradation in the receive signal, this degradation is directly proportional to the frequency of the signal. Each particular raindrop contributes to the attenuation of the signal. The actual amount of fading is dependent on the frequency of the signal and the size of the raindrop. The two main causes of rain fading are scattering and absorption. Suitable statistical models are needed to relate the number of raindrops in a rain cell and their size distribution to the rain intensity. These models have been designed on the basis of a large amount of experimental data, coming from different regions in the world. Rain does not occur all times of year and its rate does not remain same all the time when it occurs. An important input to any rain attenuation model is the expected rain activity in the region where the radio hop will operate, as derived from long-term statistics. The rain rate exceeded for 0.01% of the time (in order to achieve 99.999% availability, for a given path length) is the significant parameter, useful to characterize the rainfall activity in a given region. The ITU-R recommendations can be used. In the last release of Rec. P-837 [13] a new approach is reported to estimate the rain rate exceeded for any percentage of time, in any part of the world. This is based on data files (available from the ITU website). These recommendations designed based on world maps with rain regions, Figure 3, each region was labeled with a letter, and each letter is associated with the corresponding rain rate in mm/h as shown in Table 1.



Figure 3 Example for maps with rain regions [13]

Table 1 The rain rate for every rain region according to the ITU-R recommendations.[13]

Percentage of time (%)	A	B	C	D	E	F	G	H	J	K	L	M	N	P	Q
1.0	<0.1	0.5	0.7	2.1	0.6	1.7	3	2	8	1.5	2	4	5	12	24
0.3	0.8	2	2.8	4.5	2.4	4.5	7	4	13	4.2	7	11	15	34	49
0.1	2	3	5	8	6	8	12	10	20	12	15	22	35	65	72
0.03	5	6	9	13	12	15	20	18	28	23	33	40	65	105	96
0.01	8	12	15	19	22	28	30	32	35	42	60	63	95	145	115
0.003	14	21	26	29	41	54	45	55	45	70	105	95	140	200	142
0.001	22	32	42	42	70	78	65	83	55	100	150	120	180	250	170

The specific rain attenuation is the parameter that gives the attenuation that the microwave link facing in each kilometer. The specific rain attenuation γ_R (dB/km) can be expressed as a function of the rain rate R (in mm/h) [7] by the following exponential formula:

$$\gamma_{R} = kR^{\alpha} \quad (14)$$

where the parameters k and α are functions of the signal wavelength and polarization. ITU-R Rec. P-838 [14] gives a table with the k and α value, for Vertical and Horizontal polarizations, in the frequency range 1 to 400 GHz Table 1.

Table 2 the ITU-R Rec. P-838 standards for the k and α value, for Vertical and Horizontal polarizations, in the frequency range 1 to 40 GHz [14].

Frequency GHz	Horizontal polarisation		Vertical polarisation	
	K	α	K	α
1	0.0000387	0.912	0.0000352	0.880
2	0.000154	0.963	0.000138	0.923
4	0.000650	1.121	0.000591	1.075
6	0.00175	1.308	0.00155	1.265
7	0.00301	1.332	0.00265	1.312
8	0.00454	1.327	0.00395	1.310
10	0.0101	1.276	0.00887	1.264
12	0.0188	1.217	0.0168	1.200
15	0.0367	1.154	0.0335	1.128
20	0.0751	1.099	0.0601	1.065
25	0.124	1.061	0.113	1.030
30	0.187	1.021	0.167	1.000
35	0.263	0.979	0.233	0.963
40	0.350	0.939	0.310	0.929

The specific rain attenuation is not sufficient for computing the attenuation of the whole path, because there is a considerable temporal and spatial variation of the rain rate across the link. So, just multiplying the specific attenuation by the actual link path cannot properly give whole path attenuation. Instead, two new parameters are needed: rain cell length d_o which mean the length over which the rain is considered as uniform, and effective path length d_{eff}, which mean the average length of the intersection between cell and link. So , to calculate the effective path length [7], the equation will be as following:

$$d_{eff} = \frac{d}{1 + \frac{d}{d_o}} \tag{15}$$

Where d is the actual length of the terrestrial microwave link, and:

$R_{0.01} \leq 100\text{mm/h}$

$d_o = 35e^{-0.015R_{0.01}}$

And for $R_{0.01} > 100\text{mm/h}$

$d_o = 35e^{-1.5}$

So, an estimate of the path attenuation (required fade margin due to rain) exceeded for 0.01% of the time [8] is given by:

$$A_{0.01} = \gamma_R \, d_{eff} \tag{16}$$

Note that the rain unavailability is predicted as the probability that rain attenuation exceeds the Fade Margin that computed as a result of Link Budget calculation.

6. LINK BUDGET AND FADE MARGIN

A link budget is accounting of all of the gains and losses from the transmitter, through the medium and to the receiver in the microwave radio transmission system which includes the transmitter antenna gain, the receiver antenna gain, the free-space path loss, and any additional losses caused by equipments, waveguides, cables, connectors, etc. Link Budget [2] which is called also Received Signal Level (RSL) equation will be as following:

$$P_{RX} = P_{TX} + G_{TX} - L_{TX} - FSL + G_{RX} - L_{RX} \tag{17}$$

where P_{RX} is the received signal power (dBm) ,P_{TX} is the transmitter output power (dBm), G_{TX} is the transmitter antenna gain (dBi), L_{TX} is the transmitter losses (dB),FSL is the free space loss (dB),G_{RX} is the receiver antenna gain (dBi),L_{RX} is the receiver losses (dB).

The Fade Margin is the difference between the received signal level and the receiver threshold level. It is calculated to use it as a safety margin against fading that may occurs. In other words, it defined as the amount by which a received signal level may be reduced without causing system performance to fall below a specified threshold value.

7. FLOWCHART AND BLOCK DIAGRAM OF THE IMPLEMENTED MICROWAVE PLANNING TOOL

Figure 4 and **Error! Reference source not found.** show the steps that the software follows to design a new line-of-sight radio link. It shows the scenario that the tool flows to collect data from the user, then processing it according to integrated equations, draw path profile, and then provide the user with the results.

At start up, the tool has to check the internet connectivity to get the geographical information from Google API according to the values that have stored from the last use. Next step the tool requires some needed information that set by the user such as: coordinates, Frequency, Antennas diameter, Polarization, Radio type and Tx power. Then, the tool has to check the internet connectivity again. If it is connected, it requests the geographical information from Google API and it draws the Map and the elevation path profile according to the new coordinates that set by the user. After that, the tool requests information such as: the elevation of earth above sea level at sites A and B, K-Factor, antenna height at sites A & B, and if there are any extra obstacles along the path. According to that information and if there is internet connectivity, the tool draws the path profile chart. The tool asks for d1 to calculate the first Fresnel zone. Then the tool asks for the some extra information such as: climate factor, terrain factor, terrain type, geographical region, latitude range, rain region, feeder losses, temperature, water vapor, and pressure. According to all above information, the tool calculates and displays the results. The results is: free space loss, flat fade margin, multipath fading losses, link availability, percentage of link down, atmospheric absorption, required fade margin against rain, specific attenuation due to rain and unavailability percentage due to rain.

The block diagram of the implemented microwave planning tool shows the relations between the equations and input and output parameters. It shows how the tool been built and describe how it relate all parameters together as shown in Figure 5.

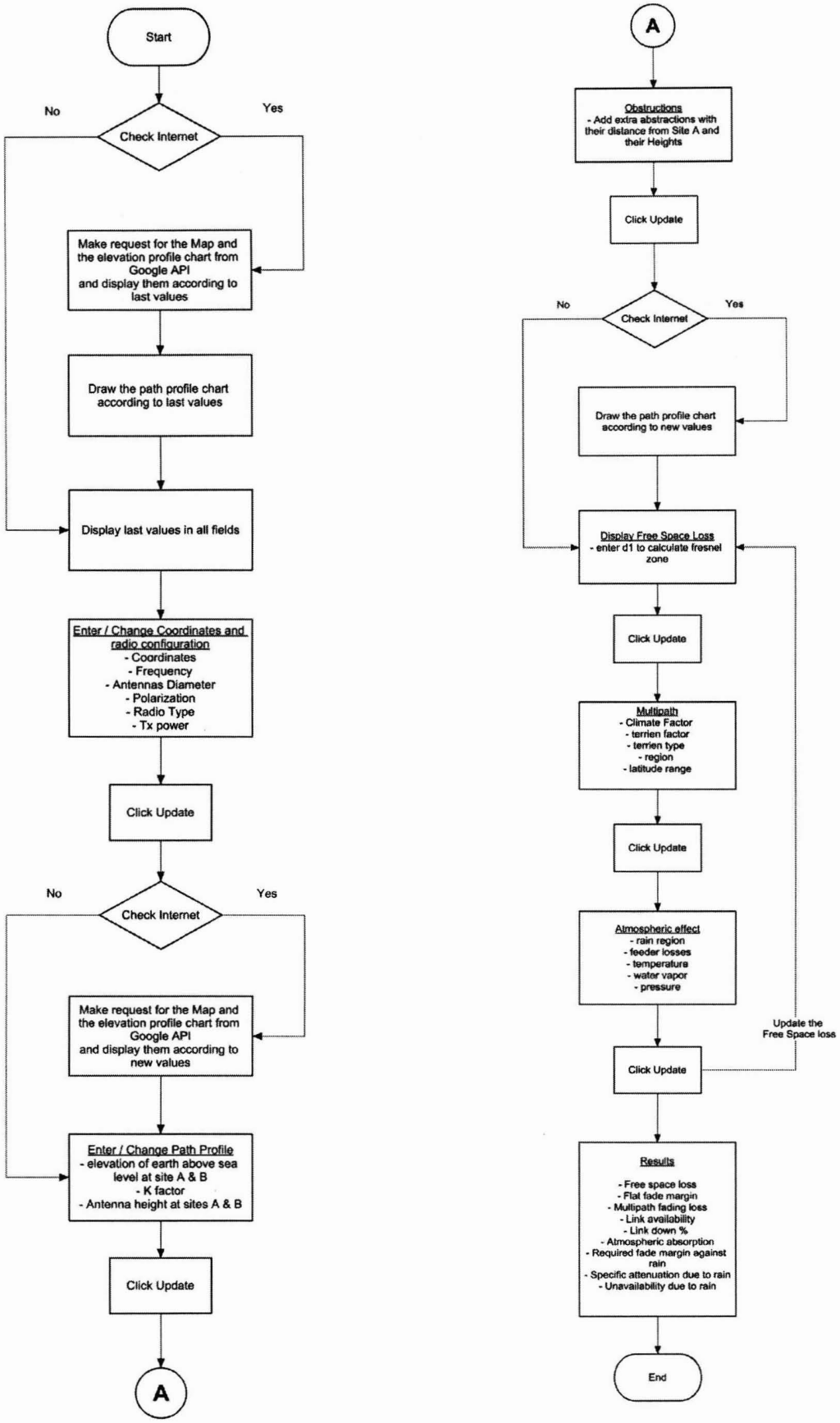

Figure 4 Flowchart of the implemented tool

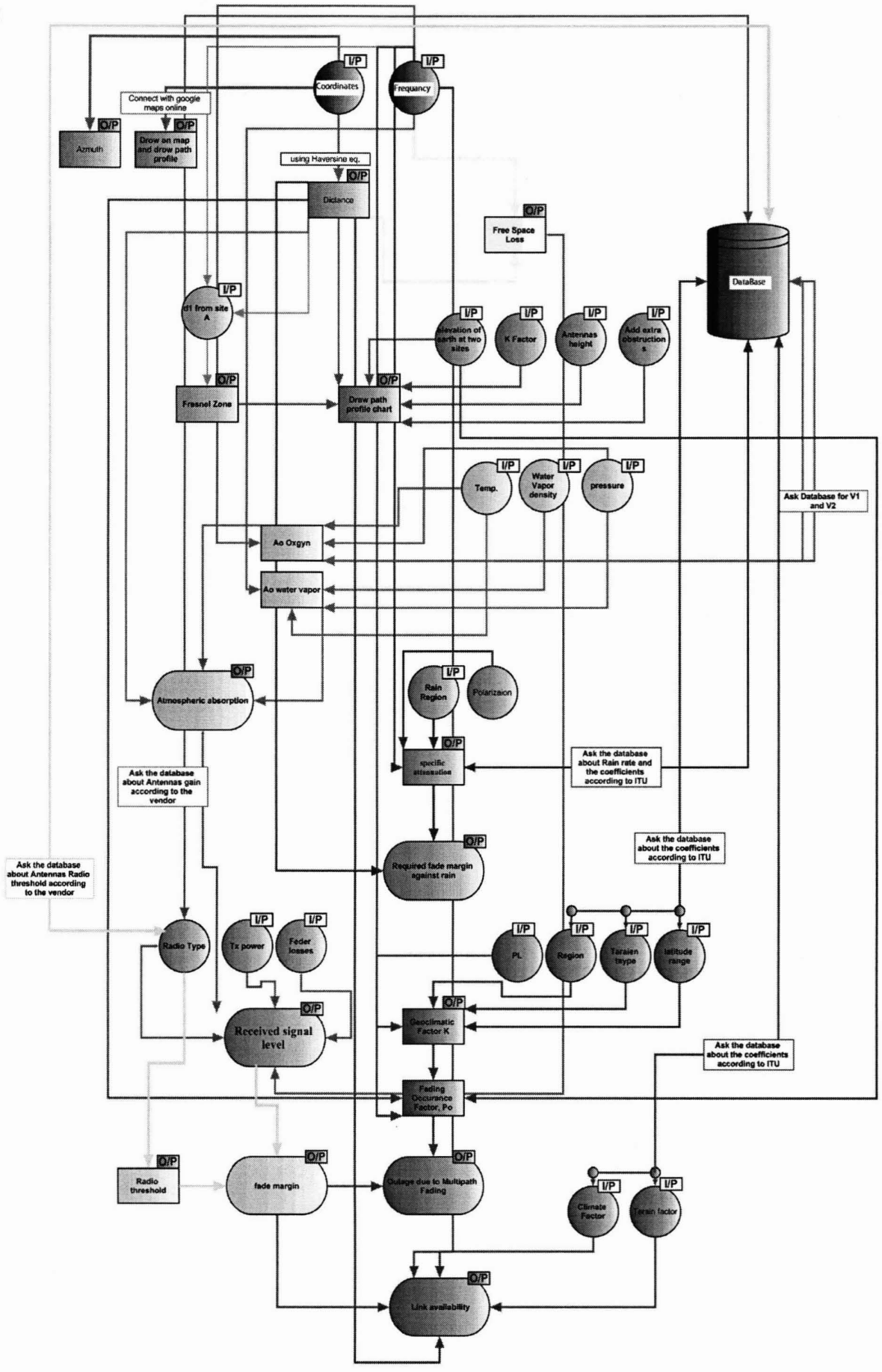

Figure 5 Block diagram of the implemented microwave planning tool.

8. SIMULATION RESULTS FOR THE IMPLEMENTED MICROWAVE PLANNING TOOL

The implemented microwave planning tool is software developed to automatically design microwave point-to-point links. This software has nine parts: Coordinates and radio configuration, Map, Path profile, Obstructions, Path profile chart, Free space loss, Multipath, Atmospheric effect and Results. The following subsections explain those parts.

1) *Coordinates and radio configuration:*

In this part, the user has to add the coordinates and the radio configuration parameters as follows:
Area has been chosen: Sinai
Coordinates -can be obtained using GPS- :
Site A:

- Latitude: 27° 48' 42.2640" N
- Longitude: 33° 34' 16.7520" E

Site B:

- Latitude: 27° 42' 52.9920" N
- Longitude: 33° 30' 2.9880" E

The operation Frequency selected: 7.617 GHz
The radio equipment selected: SIEMENS SRAL XD
Antenna A diameter: 1.2 m
Antenna B diameter: 1.2 m
Polarization: Vertical
Tx Power: 29 dBm

As such, the software will automatically convert the coordinates to the decimal form; it will calculate the distance between site A and B by using **Haversine Formula**. it will calculate the Azimuth from site A to B, and From B to A as shown in Fig. .

Fig. 6. Coordinates and radio configuration.

2) *Map:*

In this part, the software finds the location of the two sites A & B and draw the direct path between them. It also draws the path profile (the elevation profile) for the direct path between site A & B as shown in Fig. .

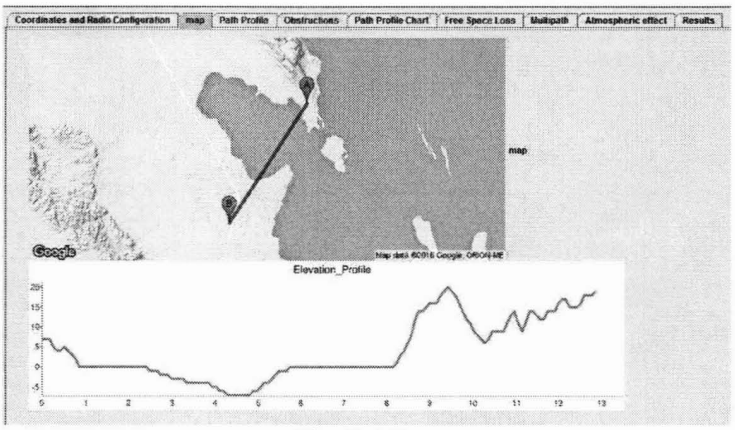

Fig. 7. Map.

3) *Path profile:*

In this part, the user defines the elevation of the earth above sea level at site A&B, selects the curvature of the earth (the effective Earth radius factor), and defines the antennas height for site A & B as shown in Figure . In the introduced case study, the elevation is taken as

- At site A: 5.5 m
- At site B: 17.0 m

and the antennas height as

- At site A: 30 m
- At site B: 35 m

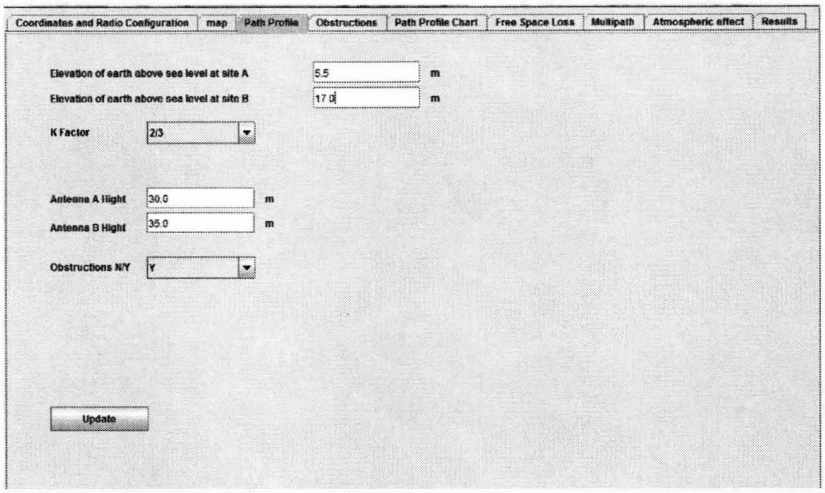

Figure 8 Path profile.

4) Obstructions

If there are any extra obstructions, the user has to add the height of each one in this part, and its name and the distance from site A for each one and the tool will calculate the highest one as in Fig. .

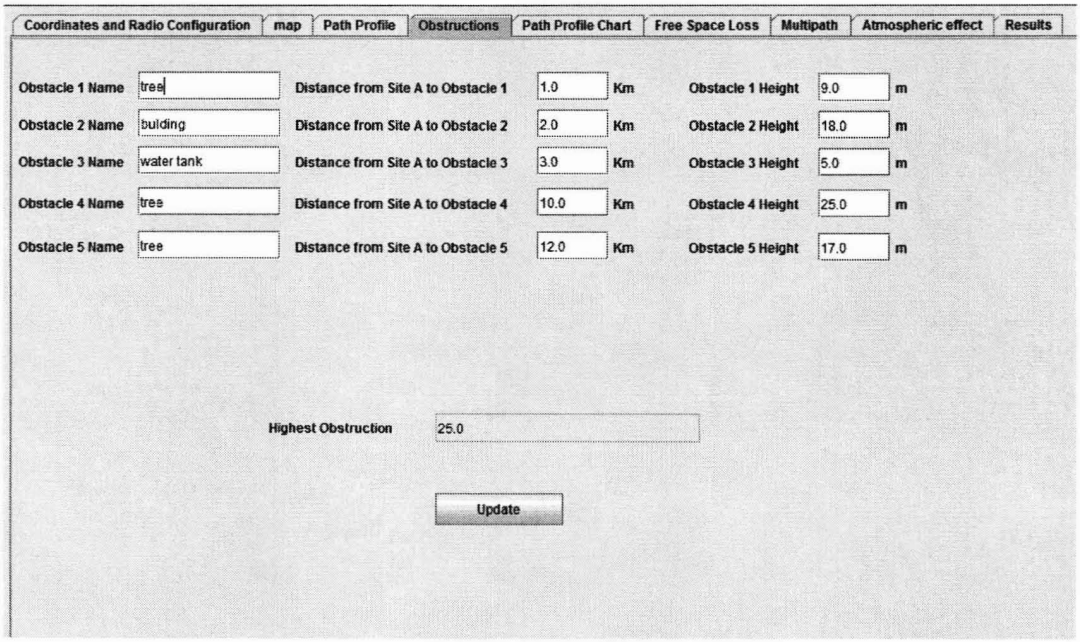

Fig. 9 Obstructions.

5) Path Profile Chart

In this part, the software draws sites A & B, the beam with the freznel Zone, the terrain of the earth and the elevation of the obstacles. Based on the provide information, the tool shows if the line-of-sight path is clear or not Figure .

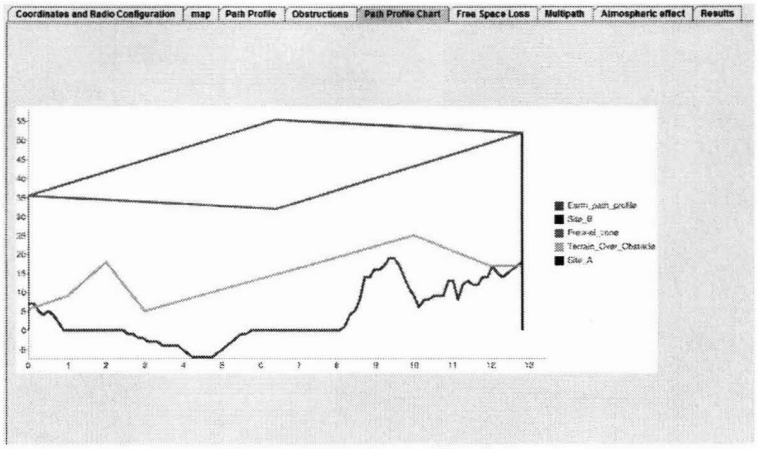

Figure 10 Path profile chart.

6) Free Space Loss

Here, the tool calculates the free space loss and the received signal level from (2). The user can put the distance to calculate the Fresnel Zone radius at it and the tool calculates it automatically from (4) as shown in Fig. .

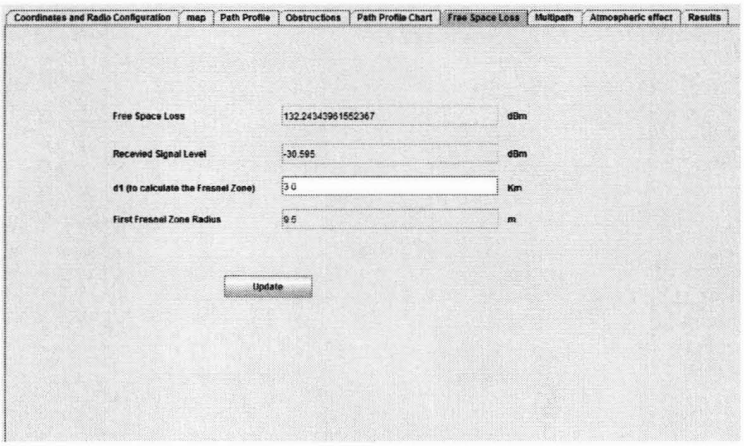

Fig. 11 Free space loss.

7) Multipath

In this part, the user chooses the Climate factor (average, dry, humid), the terrain factor (average, mountains, smooth), the natural of the terrain (Hills, Plains, mountains), the region (Europe and Africa, North and South America, Others), and the Latitude Range. If there is XPIC in the design, the user has to enter Cross polarization discrimination XPD, and Processing gain enhancement XPIF. Then, the software automatically calculates the Geoclimatic Factor (K) from (6) as shown in Fig. .

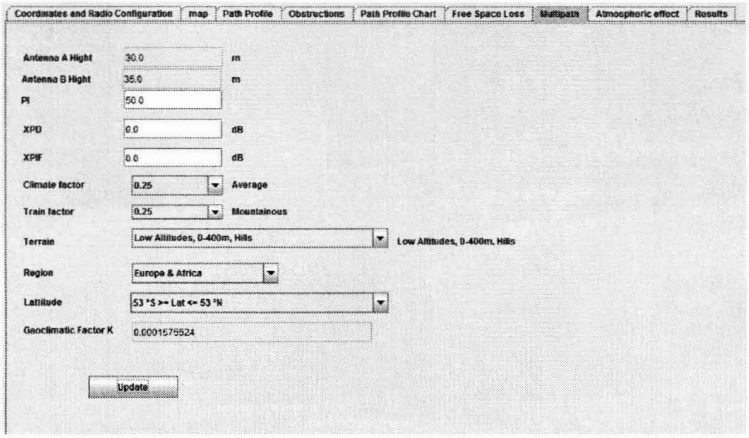

Fig. 12. Multipath.

8) Atmospheric effect

In this part, the user chooses the rain region according to the ITU standards and enters the feeder losses, temperature , water vapor , and pressure as shown in Fig. .

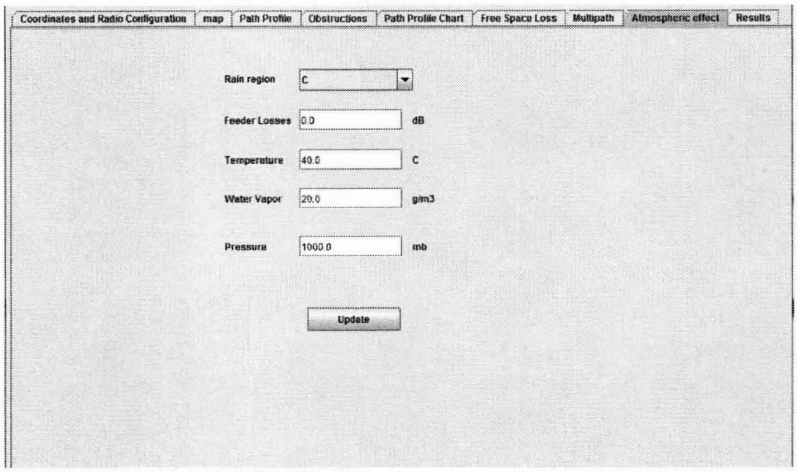

Fig. 13 .Atmospheric effect.

9) Results

Finally the results part displays all the results of this link design as illustrated in Fig. :

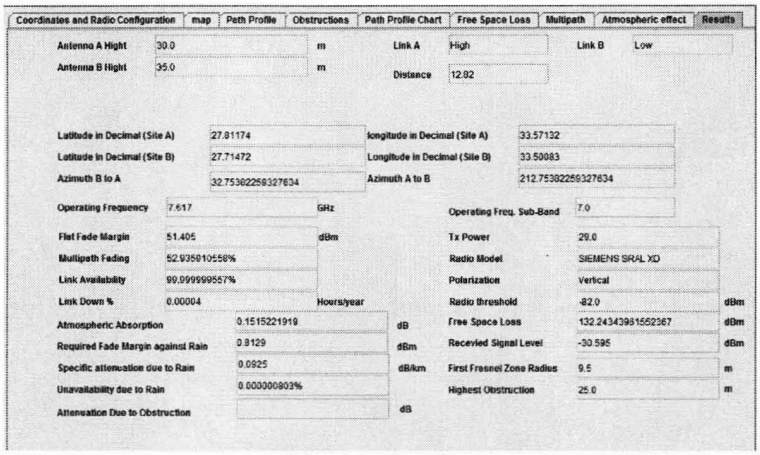

Fig. 14. Results

After defining all of the required design parameters, the implemented tool presents the results of the microwave radio link designed as following:

- **Free space loss:** it is calculated using (2). In the investigated case study, the result of the free space loss is: 132.24343961552367 dBm
- **Flat fade margin:** it is calculated according to the received signal level and the receiver threshold level for the radio equipment selected as the fade margin is equal to the difference between the received signal level and the receiver threshold level. In the investigated case study, the result of the flat fade margin is: 51.405 dBm
- **Multipath fading loss:** it is calculated using (5), (6), (7), (8) and according to the standards of ITU and the data entered in part 7 in the software. In the investigated case study, the result of multipath fading loss is: 52.935910558%
- **Link availability:** it equals 1 - P_w where:

$$P_w = \left([6.10^{-7} C f d^3] 10^{-\frac{FFM}{10}} \right)$$

In the investigated case study, the result of the link availability is: 99.999999557%

- **Link down:** it is the annual outage and it is calculated as follows

[365*24*60 (1- link availability)]/60 Hours/year

In the investigated case study, the result of the annual outage is: 0.00004 Hours/year

- **Atmospheric absorption**: it is calculated using (9), (10), (11), (12), (13) and the data entered in part 8 in the software. In the investigated case study, the result of the Atmospheric absorption is: 0.1515221919 dB
- **Required fade margin against rain**: it is calculated using (14), (15), (16) and the standards of ITU. In the investigated case study, the result of the required fade margin against rain is: 0.8129 dBm
- **Specific attenuation due to rain**: is calculated using (14). In the investigated case study, the result of the specific attenuation due to rain is:0.0925 dBm/km
- **Unavailability due to rain:** it is calculated as following:

  $11.628 \{-0.546 + [0.29812 + 0.172 \log (0.12 \text{ FM due to rain /FFM})]^{1/2}\}$

In the investigated case study, the result of the unavailability due to rain is:0.000000803%

9. PERFORMANCE CONSIDERATIONS

This research evaluated the effect of the different parameters to show which parameters affect which outcome. So, those parameters are changed such as: obstructions effect, multipath fading, atmospheric effect and rain effect. Some of these parameters provide additional fade margins that improve the performance of the link, and some of them reflect directly in the results of the design such as: link availability, outage time and received signal level.

For example without including the atmospheric effect; the results are as following: link availability is 99.999999573, outage time is 0.00004 Hours/year, and received signal level is -30.4434

In another case with ignoring the climate factor (average, dry, humid) and the terrain factor (average, mountains, smooth); the results are as following: link availability is 100.000000000%, outage time is 0.00000 Hours/year, and received signal level is -30.595

Finally, with respect to atmospheric effect, climate factor and terrain factor; the results are as following: link availability is 99.999999557%, outage time is 0.00004 Hours/year, and received signal level is -30.595. Table 3 shows the change in the results in these three cases:

Table 3 Case study changes

Case details	Link availability	Outage time	Received signal level
Without respect to atmospheric effect	99.999999573%	0.00004	-30.4434
Without respect to climate and terrain factors	100.000000000%	0	-30.595
With respect to atmospheric effect, climate and terrain factors	99.999999557%	0.00004	-30.595

It is clear that there are variations in the results depending on the included and ignored parameters. So, take more parameters into consideration leads to more accurate design as shown in considered case study, which is lead to more reliable and stable microwave link. Depending on the required accuracy and complexity of the design, some parameters can be ignored.

10. CONCLUSION

The final product of this work is characterized as software that can design a new microwave radio links. The program can calculate the path length of the link between two endpoints, free space loss, flat fade margin, multipath fading loss, link availability, atmospheric absorption, and unavailability due to rain. This software is developed to help telecommunications engineers to design and simulate a new microwave line-of-sight radio links over varieties of terrain and paths such as hills, mountains, and urban areas; and under varieties atmospheric conditions without going into detailed mathematical equations. The effected of the different system paramours is studied related to the required accuracy of the design.

REFERENCES

[1] Habeeb Khader Shankiti, "MICROWAVE COMMUNICATION SYSTEMS: TRANSMISSION CONSIDERATIONS, MEASUREMENT EQUIPMENT AND MEASURING TECHNIQVES," University Of Riyadh, 1975.

[2] Trevor Manning, "Microwave Radio Transmission Design Guide," ARTECH HOUSE,2009.

[3] Mohamed Jamil Ahmed Mulla," LONG HOP LINE-OF-SIGHT MICROWAVE LINK ACROSS THE RED SEA," University Of Riyadh, 1972.

[4] PROPAGATION DATA AND PREDICTION METHODS REQUIRED FOR THE DESIGN OF TERRESTRIAL LINE-OF-SIGHT SYSTEMS RECOMMENDATION ITU-R P.530-7.

[5] Mike O. Asiyo And Thomas J. O. Afullo , "STATISTICAL ESTIMATION OF FADE DEPTH AND OUTAGE PROBABILITY DUE TO MULTIPATH PROPAGATION IN SOUTHERN AFRICA," Progress In Electromagnetics Research B, Vol. 46, Pp. 251-274, 2013.

[6] Bassem R. Mahafza , "Radar Systems Analysis And Design Using MATLAB Third Edition," CRC Press, 2015.

[7] HOSSAIN Sakir , "Rain Attenuation Prediction For Terrestrial Microwave Link In Bangladesh," Journal Of Electrical & Electronics Engineering;, Vol. 7 Issue 1, Pp.63-68, May2014

[8] Uzma Siddique, Laeeq Ahmad, And Gulistan Raja , "Microwave Attenuation And Prediction Of Rain Outage For Wireless Networks In Pakistan's Tropical Region," International Journal Of Microwave Science And Technology, Volume 2011, 2011.

[9] H. Abdalla Jr, Paulo Carvalho, Luis. F. Molinaro, Carlos Evangelista, L Bermudez, "TOOLS FOR MICROWAVE RADIO COMMUNICATIONS SYSTEM DESIGN," Journal Of Microwaves And Optoelectronics, Vol. 3, N.O 1, Pp.26-38, April 2003.

[10] Saad Abdulaziz Al- Bidnah, "MICROWAVE COMMUNICATION SYSTEM DESIGN IN SAUDI ARABIA," University Of Riyadh, Saudi Arabia, 1972.

[11] Samuel P. Mason, Peter S. Guest, Andreas K. Goroch, "ATMOSPHERIC EFFECTS ON RADIO FREQUENCY (RF) WAVE PROPAGATION IN A HUMID, NEAR-SURFACE ENVIRONMENT," NAVAL POSTGRADUATE SCHOOL, March 2010.

[12] Tom Garlington, "Microwave Line-Of-Sight Transmission Engineering," U.S. Army Information Systems Engineering Command (USAISEC), Transmission Systems Directorate, WP No. AMSEL-IE-TS-06015, June 2006.

[13] Characteristics Of Precipitation For Propagation Modelling , RECOMMENDATION ITU-R P.837-1, (1992-1994).

[14] Specific Attenuation Model For Rain For Use In Prediction Methods, RECOMMENDATION ITU-R P.838-3, (1992-1999-2003-2005).

MICROWAVE LINK PREDICTIONS

PROGRAM DESCRIPTION **RADLNK**

WRITTEN BY: D. BURGER JULY 1985

1. PROGRAMME DESCRIPTION

1.1 INTRODUCTION

The program RADLNK is designed to provide the microwave radio system designer a consistant means of obtaining a realistic evaluation of a microwave radio link. The link performance output can accommodate a basic system with variations such a frequency/space diversity, space grid coordinates, flexible equipment selection etc. Refer to the sample printout attached.

A segment on Path Geometry is included in order for the designer to evaluate path obstructions and tower heights. This is a graphics-style package and affects the link performance with respect to RMS Roughness of the terrain. The Path Geometry segment also shows the radio rayline clearance from the ground.

Part of the Path Geometry block is a section on Ground/Sea reflection analysis. This scans the terrain for potential reflective regions and presents a report detailing these regions. The analysis also recommends a space diversity separation for both ends of the link.

The designer then may examine the reflective region on a site visit and decide if space diversity need by used.

PROGRAM RADLNK is suitable for use on microwave radio equipment of all types, in all terrain areas and all realistic K factors.

The program does have limitations and there are summarized below:

Frequency of operation	0.001 GHz (1MHz) to 150 GHz.
For rain considerations	2 GHz to 99 Ghz.
For atmospheric absorption	2 GHz to 99 GHz
Path Length.	0.001 km (1m) to 999.999 km.

The effect of the K factor on Earth Bulge is always considered. This permits the accurate profiling of a radio path with different K factors expected in regions.

The program is written in GWBASIC for the IBM PC and variants.

1.1.1 DESIGNING MICROWAVE RADIO LINKS

The starting point in a radio communications link is to identify it as an economic and practical means of bridging awkward terrain and flexible expansion of capacity in the future. The planning of a link must take into account, cost, equipment availability and propagation availability.

The designer may adopt "rules" on which to base a link or network. Such rules take the form of:

1. Minimization of cost, spares inventory, maintenance.
2. Propagation availability greater than 99.950% End to End.
3. Hardware availability greater than 99.900%.
4. Terrain clearance of rayline greater than 0.3F at K = 0.66 and F at K = 1.33, where F is Fresnel zone radius.

Program RADLNK can consider points 2) and 4) but it is up to the designer to specify the rules. Point 3) is the subject of another program titled "COMREL; Communications Network Reliability, Hardware Considerations. Point 1) is up to the ingenuity of the designer.

The designer may determine an equipment configuration to meet a specified requirement, or use "standard" equipment and obtain an availability figure to offer a client.

1.1.2 INFLUENCE OF TERRAIN

The microwave beam is influenced by the intermediate terrain between the stations and obstacles in its path. It follows a slightly curved path in the vertical plane, ie, it is refracted in the atmosphere due to the dielectric constant of the atmosphere. The amount of refraction changes with temperature, vapour pressure and relative humidity. In addition to this effect, the microwave beam can be diffracted by obstacles in it path or in the extreme, the scattering effect from the troposphere. It is up to the designer to evaluate any diffraction or troposcatter effects separately from free-space data used in RADLNK. If a path is surveyed using optical means the results would correspond to a K factor of approx 1.16. Obstacles such as trees should be considered as blocking a microwave beam, so adequate clearance should be considered even allowing for their growth.

The consideration of the Fresnel Zone clearance becomes paramount in highly reflective paths, eg over water. Rayline clearance to the 2nd Fresnel zone is important over this type of path.

1.1.3 INFLUENCE OF WEATHER

At microwave frequencies over 2 GHz, rain and preciption can influence the attenuation on a route. Refer to the specific attenuation chart elsewhere in this handbook. The rain attenuation model in program RADLNK is modelled from this information in this chart. The effect of atmospheric absorption is presented, where, at certain frequencies, molecular resonance occurs. This can be significant at frequencies near 21 GHz and 60 GHz which correspond to the water vapour and oxygen resonance frequencies respectively.

1.1.4 SITUATIONS TO BE AVOIDED

Several situations should be avoided when designing a link:



1. Over water paths and paths over low flat terrain. Where they cannot be avoided, the use of space diversity or the High-low placement of antennas to move the reflection point onto rough terrain is recommended.

2. Sites near radar stations. Possible solutions here include RF filters, RF attenuators and utilization of terrain protection, ie placing a terminal in a radar shadow region.



3. Sites on the very top of high mountains or ridges are suseptible to more potential interference from distant links, and the effects of delay distortion from multiple path effects.

4. Having a microwave rayline pass near city buildings or down streets, results in severe reflection situations and increased outage times.

1.2 SUBROUTINES (LINK BUDGET)

1.2.1 SYSTEM DETAILS

A brief description of each subroutine (Block) utilized in the Link Budget calculation follows:

Data Input Block	Inputs station names, path distance, grid bearings, diversity selection, K factor. The option for a link utilizing both space and frequency diversity cannot be directly supported. The program would need to be run twice with each option.

1.2.2 RAIN DATA

Data Input Block	Inputs rain rate data and climate zone. The climate zone is based on the geographic location of the link.

N.B. Rain Data from Rain Contours 0.05% Probability elsewhere in this handbook.

1.2.3 EQUIPMENT

Data Input Block

Inputs type of equipment, allows selection of antenna size and peculiar equipment variations. The equipment shown in the menu is popular for links up to 8 Mb/s (120 channels) capacity. Any equipment may be configured providing specifications are known. Equipment without integral antennas would need some default antenna gains to be entered in the data block. Refer to equipment Data block.

1.2.4 PERFORMANCE REPORT OUTPUT

Calculation/Output Block

Calculation of path loss (free space) fade margin, Fading, 1st Fresnel zone radius and system availabilities. Where options like diversity are not selected, they do not appear on output. It is at the start of this block that all link calculations are performed.

1.2.5 EQUIPMENT DATA

Data Block

Hardware data not directly accessed from user. It is here that the user may enter other equipment as options.

1.2.6 AMPLITUDE DISPERSION FADING

Calculation Block — Fading calculation based on Algorithm from NEC DIGITAL MICROWAVE RADIO HANDBOOK for digital radio links. The fading prediction is applicable to FDM and video links.

1.2.7 RAIN FADING

Calculation Block — Fading calculation based on Algorithm derived from CCIR REP 721-1

1.2.8 STATION DISTANCES & BEARINGS

Calculation Block — Calculates distance between stations given grid coordinates and the bearing of station B from station A. This block operates using the spherical "Great Circle" calculations.

1.3 SUBROUTINE (PATH GEOMETRY)

A brief description of each subroutine (Block) utilized in the Path Geometry calculation follows:

1.3.1 PATH GEOMETRY

Menu Block — SUB-MENU SELECTION

1.3.2 SUPPORT HEIGHTS

Data Input Block — Inputs height of support structures at both stations. Radio Horizon distance shown for smooth earth. The radio horizon distance is presented as a course of station support heights, and suitable in an interference study.

1.3.3 PATH PROFILE ENTRY

Data input Block — Inputs path profile data from map. The number of input points is not critical.

1.3.4 PATH DATA RESET

Calculation Block — Resets path data to zero if a mistake or new data is inputted. Does not affect Link Budget subroutines.

1.3.5 DEFAULT VALUES SET

1.3.6 PATH DATA PARAMETER OUTPUT

Output Block — Dumps path profile data onto printer.

1.3.7 PROFILE DISPLAY

Menu Block — SUB-SUB MENU SELECTION.

1.3.8 DOT JOINING/DATA FILL

Calculation Block — Joins all the path profile data points (linear).

1.3.9 EARTH BULGE CORRECTION

Calculation Block — Modifies the data fill to account for earth Bulge.

1.3.10 RMS ROUGHNESS

Calculation Block — Calculates the RMS roughness of corrected data. This is used in LINK BUDGET. Default values are set.

1.3.11 RAYLINE CLEARANCE

Calculation Block — Calculates the clearance between the rayline and the terrain. This is titled CLR on the plotter output.

1.3.12 PLOT SCALING
Calculation Block — Determines maximum and minimum data and calculates suitable plot dimensions.

1.3.13 PLOTTER
Output Block — Plots data size A3 of A4 or any specified size.

1.4 GROUND/SEA REFLECTION ANALYSIS

A brief description of each subroutine (Block) utilized in the Reflection Analysis follows:

1.4.1 SELECTION AND TESTING REFLECTIONS — Scans through the region selected by the designer, or due to illumination or full path. (Note: Full path testing is time consuming). Testing performed at 3 K values.

1.4.2 ILLUMINATED REGION
Calculation Block — This scans the path profile to determine the illuminated region open for reflections.

2. PROGRAM OPERATION

2.1 DESCRIPTION

Program RADLNK effectively consists of three separate programs with the only interlinked variables P1, KF and T46. The three programs consist of the Link Budget Block, Path Geometry Block, and Ground/sea reflection analysis. All are menu driven for ease of use. The output procedure follows the following steps, for full variable interlinking.

a) Enter all data, no particular order
b) Print Path Data (optional)
c) Ground/sea reflection analysis (optional)
d) Plot Path Profile
e) Print Link Performance report

The output procedure in a different order of operation will operate on default values where they are necessary. The Ground/sea reflection analysis cannot operate without frequency and path profile data.

To obtain the rainfall rate, refer to the contour map of Australian and Fiji. Rainfall data for other regions can be used to calculate the 0.05% or 0.01% levels as required by the program.

2.1.1 LINK BUDGET BLOCK

The link budget block calculates the link signal levels and predicted attenuation and fading due to rain. One-way link availability is calculated for the worst month and annual period. All menu options except path geometry and Ground/sea reflection analysis need be selected to operate this block. Where appropriate, default values are set, pending execution of the other blocks.

At any time, the designer can edit any of the data that has been entered. This allows easy access to results using different equipments for example.

2.1.2 PATH GEOMETRY BLOCK

Input options can be selected on the actual data available. if insufficient data is available for output, RADLNK will advise the user.

Dot joining and earth bulge cannot be disabled under user control. Note, the degree of earth bulge is defined as the K Factor. The K Factor has a theoretical range of 0 thru infinity, however practical values in the program range 0.4 thru 10 (Default at 1.333).

A A3 size output is available with expanded X-Axis and Y-Axis. This provides higher resolution where clearances are marginal.

The CLR heading data, shows the clearance in metres between rayline and ground, the height of trees or buildings would need to be subtracted from the CLR data, if they were not considered in the path profile.

The rayline between stations must be drawn in by hand.

2.2 REFERENCE LIST

"Rain Attenuation Considerations for Satellite Paths in Australia" R.K. Flavin, Telecom Australia.

"Attenuation by Hydrometeors, Preciptation and other Atmospheric Particles" CCIT REP 721-1.

"Propagation data for design Terrestial, Troposcatter, Trans-Horizon and Earth-Space Telecommunication systems CCITT REC 530-1, REP 338-4.

"Antenna Theory. Analysis and Design" C A Balanis, Harper and Row.



"Digital Microwave Radio, Engineering Fundamentals" NEC, Tokyo. MSD-3003 820B-01.

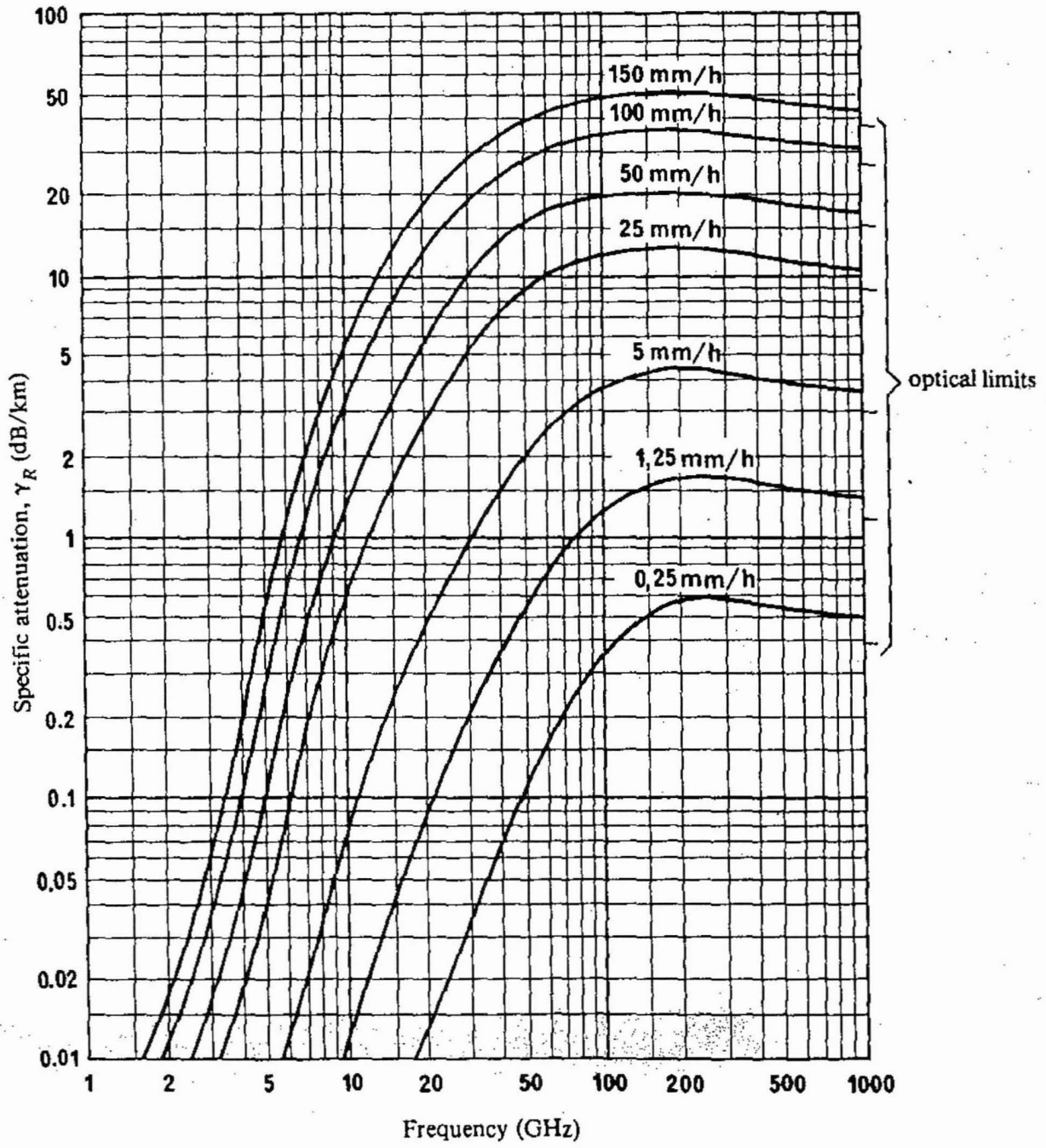

FIGURE 1 – *Specific attenuation γ_R due to rain*

Raindrop size distribution [Laws and Parsons, 1943]
Terminal velocity of raindrops [Gunn and Kinzer, 1949]
Index of refraction of water at 20° C [Ray, 1972]
Spherical drops

PROGRAM ***RADLNK*** MICROWAVE LINK PREDICTIONS

RADIO LINK FROM TERMINAL [A] TO PASSIVE REPEATER

Path Length	5.700 Km
Earth Bulge @ K = 1.33	0.48 m
RMS Roughness @ K = 1.33	82.59 m
Max Fresnel Zone Radius	6.33 m

LINK SIGNAL LEVELS

Frequency	10.680 GHz
Free Space Path Loss	128.2 dB
Stn [A] Antenna Gain	39.4 dBi
Feedline Loss	0.4 dB
Stn [B] Antenna Gain	39.4 dBi
Feedline Loss	0.0 dB
Transmit Power	13.0 dBi
Atmospheric Attenuation	0.0 dB
MEDIAN RECEIVE LEVEL	-36.8 dB
Receive Threshold	-80.0 dBm
FADE MARGIN	43.2 dB

RADIO LINK FROM PASSIVE REPEATER TO TERMINAL [B]

Path Length	1.200 Km
Earth Bulge @ K = 1.33	0.02 m
RMS Roughness @ K = 1.33	80.21 m
Max Fresnel Zone Radius	2.91 m

LINK SIGNAL LEVELS

Frequency	10.680 GHz
Free Space Path Loss	114.7 dB
Stn [A] Antenna Gain	39.4 dBi
Feedline Loss	0.4 dB
Stn [B] Antenna Gain	39.4 dBi
Feedline Loss	0.4 dB
Transmit Power	-36.8 dBi
Atmospheric Attenuation	0.0 dB
MEDIAN RECEIVE LEVEL	-73.5 dB
Receive Threshold	-80.0 dBm
FADE MARGIN	6.5 dB

RAIN ATTENUATION OUTAGES

Climate Factor	1.2
Rain Rate Exceeds 0.050% /M	30.0 mm/H
Rain Attenuation	4.5 dB
RAIN MARGIN	2.1 dB
Rain Outage TIME/MONTH	0.0170 %
Rain Outage TIME/YEAR	0.0027 %

AMPLITUDE DISPERSION OUTAGES

Outage Time (Single Link)	0.0163 %

LINK AVAILABILITY (Excluding Hardware, One Way)

Availability (WORST MONTH)	99.9667 %
Availability (ANNUAL)	99.9810 %

PROGRAM ***RADLNK*** PRINT PROFILE DETAILS

PASSIVE REPEATER Support Height = 35 m
TERMINAL B Support Height = 35 m
Path Length (Km) = 1.2

TERRAIN PROFILE DATA

Data Point	1	DISTANCE From [A]	Km	0
		HEIGHT at this Point	m	760
Data Point	2	DISTANCE From [A]	Km	.5
		HEIGHT at this Point	m	660
Data Point	3	DISTANCE From [A]	Km	1.2
		HEIGHT at this Point	m	630

PROGRAM ***RADLNK*** PRINT PROFILE DETAILS

TERMINAL [A] Support Height = 35 m
PASSIVE REPEATER Support Height = 35 m
Path Length (Km) = 5.7

TERRAIN PROFILE DATA

Data Point	1	DISTANCE From [A]	Km	0
		HEIGHT at this Point	m	848
Data Point	2	DISTANCE From [A]	Km	.5
		HEIGHT at this Point	m	730
Data Point	3	DISTANCE From [A]	Km	1
		HEIGHT at this Point	m	700
Data Point	4	DISTANCE From [A]	Km	1.5
		HEIGHT at this Point	m	710
Data Point	5	DISTANCE From [A]	Km	2
		HEIGHT at this Point	m	650
Data Point	6	DISTANCE From [A]	Km	2.5
		HEIGHT at this Point	m	670
Data Point	7	DISTANCE From [A]	Km	3
		HEIGHT at this Point	m	660
Data Point	8	DISTANCE From [A]	Km	3.5
		HEIGHT at this Point	m	660
Data Point	9	DISTANCE From [A]	Km	4
		HEIGHT at this Point	m	690
Data Point	10	DISTANCE From [A]	Km	4.5
		HEIGHT at this Point	m	700
Data Point	11	DISTANCE From [A]	Km	5
		HEIGHT at this Point	m	630
Data Point	12	DISTANCE From [A]	Km	5.5
		HEIGHT at this Point	m	730
Data Point	13	DISTANCE From [A]	Km	5.7
		HEIGHT at this Point	m	760

PROGRAM ***PRAD*** Engsoft MICROWAVE LINK PREDICTIONS

RADIO LINK FROM PENSHURST TO HAMILTON

Path Length	24.200 Km
Earth Bulge [K = 1.33	8.62 m
RMS Roughness [K = 1.33	70.60 m
Max Fresnel Zone Radius	11.72 m

LINK SIGNAL LEVELS

Frequency	13.250 GHz
Free Space Path Loss	142.5 dB
Stn `A§ Antenna Gain	34.0 dBi
Feedline Loss	0.0 dB
Stn `B§ Antenna Gain	34.0 dBi
Feedline Loss	0.0 dB
Transmit Power	22.0 dBi
Atmospheric Attenuation	0.2 dB
MEDIAN RECEIVE LEVEL	-52.7 dB
Receive Threshold	-80.0 dBm
FADE MARGIN	27.3 dB

RAIN ATTENUATION OUTAGES

Climate Factor	1.0
Rain Rate Exceeds 0.050% /M	15.0 mm/H
Rain Attenuation	11.5 dB
RAIN MARGIN	15.8 dB
Rain Outage TIME/MONTH	0.0046 %
Rain Outage TIME/YEAR	0.0006 %

1988.1288 Sec/yr
33.13 min/yr

AMPLITUDE DISPERSION OUTAGES

Outage Time (Single Link)	0.0063 % →

LINK AVAILABILITY (Excluding Hardware, One Way)

Availability (WORST MONTH)	99.9891 %
Availability (ANNUAL)	99.9931 %

$\frac{0.0063}{100} \cdot 31557600$

Secs per YEAR

0.0063 %
99.9937 %

PROGRAM ***RADLNK*** MICROWAVE LINK PREDICTIONS

SYSTEM DETAILS

FREQUENCY	10.680 GHZ
PATH LENGTH	20.700 KM
STATION A	DARKES FOREST
STATION B	ENGADINE
EQUIPMENT TYPE	MINILINK 10

TERRAIN DATA — PERFORMED AT K = 1.3333

EARTH BULGE	6.3 M
RMS ROUGHNESS	42.0 M
FRESNEL ZONE RADIUS	12.1 M

LINK SIGNAL LEVELS

FREE SPACE PATH LOSS	139.4 DB
TRANSMIT ANTENNA GAIN	32.0 DBI
RECEIVE ANTENNA GAIN	32.0 DBI
TRANSMIT POWER	13.0 DBM
WAVEGUIDE/OTHER LOSSES	0.0 DB
RECEIVE LEVEL	-62.4 DBM
RECEIVE THRESHOLD	-80.0 DBM
FADE MARGIN	17.6 DB

RAIN ATTENUATION OUTAGES

CLIMATE FACTOR	1.0
RAIN RATE EXCEEDED 0.05%	30.0 MM/H
RAIN ATTENUATION	13.5 DB
RAIN MARGIN	4.1 DB
RAIN OUTAGE TIME/MONTH	0.0947 %
RAIN OUTAGE TIME/YEAR	0.0216 %

AMPLITUDE DISPERSION OUTAGES

OUTAGE TIME (SINGLE LINK)	0.0300 %
SPACE DIVERSITY SEPARATION	8.0 M
OUTAGE TIME (DIVERSITY LINK)	0.0120 %

LINK AVAILABILITY (EXCLUDING HARDWARE)

AVAILABILITY (WORST MONTH)	99.8932 %
AVAILABILITY (ANNUAL)	99.9664 %

```
PROGRAM    ***RADLNK***          RADIO PATH DETAILS

DARKES FOREST        SUPPORT HEIGHT =  20  M
ENGADINE             SUPPORT HEIGHT =  15  M
PATH LENGTH  (KM) =  20.7

TERRAIN PROFILE DATA
DATA POINT  1
     DISTANCE FROM    A  (KM)  0
     HEIGHT AT THIS POINT (M)  380
DATA POINT  2
     DISTANCE FROM    A  (KM)  3
     HEIGHT AT THIS POINT (M)  300
DATA POINT  3
     DISTANCE FROM    A  (KM)  4
     HEIGHT AT THIS POINT (M)  300
DATA POINT  4
     DISTANCE FROM    A  (KM)  5
     HEIGHT AT THIS POINT (M)  280
DATA POINT  5
     DISTANCE FROM    A  (KM)  6.3
     HEIGHT AT THIS POINT (M)  310
DATA POINT  6
     DISTANCE FROM    A  (KM)  7.5
     HEIGHT AT THIS POINT (M)  280
DATA POINT  7
     DISTANCE FROM    A  (KM)  8
     HEIGHT AT THIS POINT (M)  260
DATA POINT  8
     DISTANCE FROM    A  (KM)  8.8
     HEIGHT AT THIS POINT (M)  200
DATA POINT  9
     DISTANCE FROM    A  (KM)  10.5
     HEIGHT AT THIS POINT (M)  240
DATA POINT  10
     DISTANCE FROM    A  (KM)  12.6
     HEIGHT AT THIS POINT (M)  200
DATA POINT  11
     DISTANCE FROM    A  (KM)  13.5
     HEIGHT AT THIS POINT (M)  120
DATA POINT  12
     DISTANCE FROM    A  (KM)  14.3
     HEIGHT AT THIS POINT (M)  200
DATA POINT  13
     DISTANCE FROM    A  (KM)  19.5
     HEIGHT AT THIS POINT (M)  100
DATA POINT  14
     DISTANCE FROM    A  (KM)  20.7
     HEIGHT AT THIS POINT (M)  200

RAIN RATE  0.05% PER MONTH =  30
CLIMATE  ZONE              =  1
```

PROGRAM *RADLNK* GROUND/SEA REFLECTION ANALYSIS

REGION FOR CONSIDERATION IS ILLUMINATED PATH
LINK FROM DARKES FOREST TO ENGADINE

K FACTOR 0.600
REFLECTION POINT AT 1.294 KM FROM A. RAY CLEARANCE 36.174 M
SD SEPARATION. STN A 0.8 M
STN B 12.5 M

REFLECTION POINT AT 1.553 KM FROM A. RAY CLEARANCE 39.924 M
SD SEPARATION. STN A 0.9 M
STN B 10.7 M

SCAN FOR CLEARANCE < 2 FRESNEL ZONES
SCAN COMPLETE

K FACTOR 1.333
REFLECTION POINT AT 1.294 KM FROM A. RAY CLEARANCE 37.980 M
SD SEPARATION. STN A 0.8 M
STN B 12.4 M

SCAN FOR CLEARANCE < 2 FRESNEL ZONES
SCAN COMPLETE

K FACTOR 10.000
REFLECTION POINT AT 1.035 KM FROM A. RAY CLEARANCE 34.944 M
SD SEPARATION. STN A 0.1 M
STN B 1.3 M

SCAN FOR CLEARANCE < 2 FRESNEL ZONES
SCAN COMPLETE

TERRAIN PROFILE DARKES FOREST TO ENGADINE

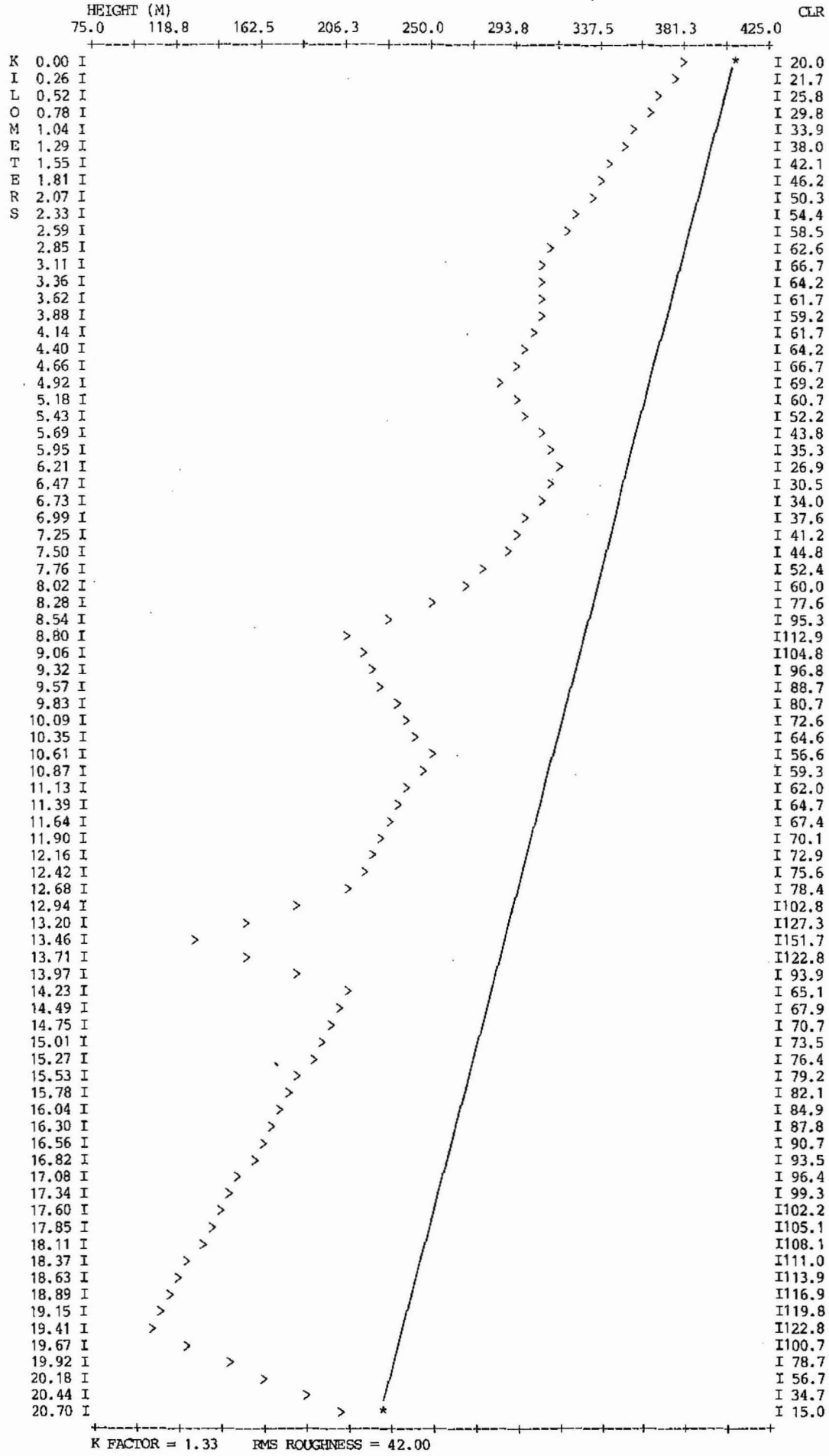

K FACTOR = 1.33 RMS ROUGHNESS = 42.00

TERRAIN PROFILE DARKES FOREST TO ENGADINE

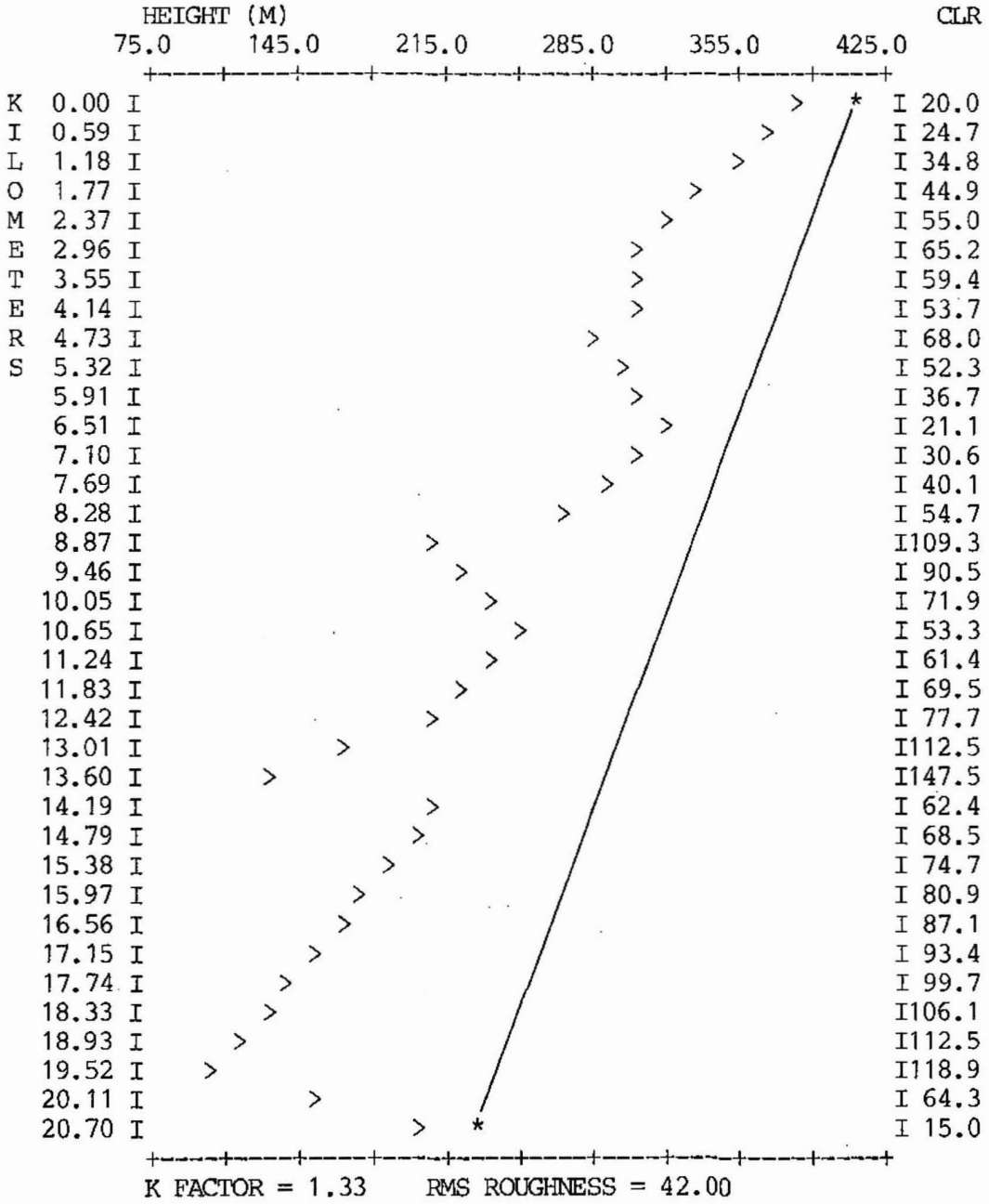

K FACTOR = 1.33 RMS ROUGHNESS = 42.00

1.5 PROGRAM VARIABLES

F1	-	FREQUENCY (GHZ)
P1	-	PATH LENGTH (KM)
P2	-	TRANSMIT POWER (DBM)
P9	-	FREE SPACE PATH LOSS (DB)
G1,G2	-	ANTENNA GAIN (DBI)
G3	-	OTHER ATTENUATION (DB)
F8	-	RAIN MARGIN
F9	-	FADE MARGIN (DB)
R1	-	RECEIVE THRESHOLD (DBM)
R2	-	RAIN RATE EXCEEDED R4% PER MONTH
R3	-	CLIMATE FACTOR
R4	-	RAINFALL RATE PERCENTILE VALUE
R9	-	RECEIVE LEVEL (DBM)
A8	-	RAIN ATTENUATION
PRM	-	RAIN OUTAGE TIME PER MONTH
PRY	-	RAIN OUTAGE TIME PER YEAR
O1	-	AMPLITUDE DISPERSION OUTAGE TIME
O2	-	DIVERSITY LINK OUTAGE TIME
O8	-	SYSTEM AVAILABILITY PER YEAR
O9	-	SYSTEM AVAILABILITY PER MONTH
D1,D2	-	SUPPORT HEIGHTS FOR STATIONS
N1$, N2$	-	STATION NAMES
N3$	-	EQUIPMENT NAMES
QX$	-	INPUT VARIABLE FOR MENU'S
Z $	-	DATA DISPLAY FIELD
AA1,AA2-		COORDINATES OF STATION N1$
BB1,BB2-		COORDINATES OF STATION N2$
H	-	BEARING OF STATION N2$ FROM STATION N1$
XD(101), YD(101)-		MATRIX WHERE INPUT PATH DATA IS ENTERED
X(101), Y(101)	-	PLOTTER DATA
RF(101)-		SURFACE ROUGHNESS CALCULATION DATA
U5	-	NUMBER OF X VALUES IN PLOT

U6	-	NUMBER OF Y VALUES IN PLOT
R	-	PLOTTER X AXIS INCREMENT
L	-	PLOTTER Y AXIS INCREMENT
KN	-	COUNTER FOR DATA X VALUES CLOSER THAN 0.5R
KF	-	K FACTOR
Y1, Y2	-	MINIMUM, MAXIMUM PLOT VALUES
KK	-	NUMBER ROUNDING FACTOR
T44	-	EARTH BULGE (MAXIMUM POINT)
T46	-	RMS ROUGHNESS
T48	-	FRESNEL ZONE RADIUS (MAXIMUM, MID PATH)
SD1	-	SPACE DIVERSITY SEPARATION (M)
FD1	-	FREQUENCY DIVERSITY SEPARATION (MHZ)
ALF	-	ANGULAR VARIABLE FOR REFLECTION CALCULATION
BET	-	ANGULAR VARIABLE FOR REFLECTION CALCULATION
MI$	-	Metric / Imperial units selection.
ME$	-	User message / name

Your Company Logo

Radio Frequency Transmission Design Report

Project Description
City, State

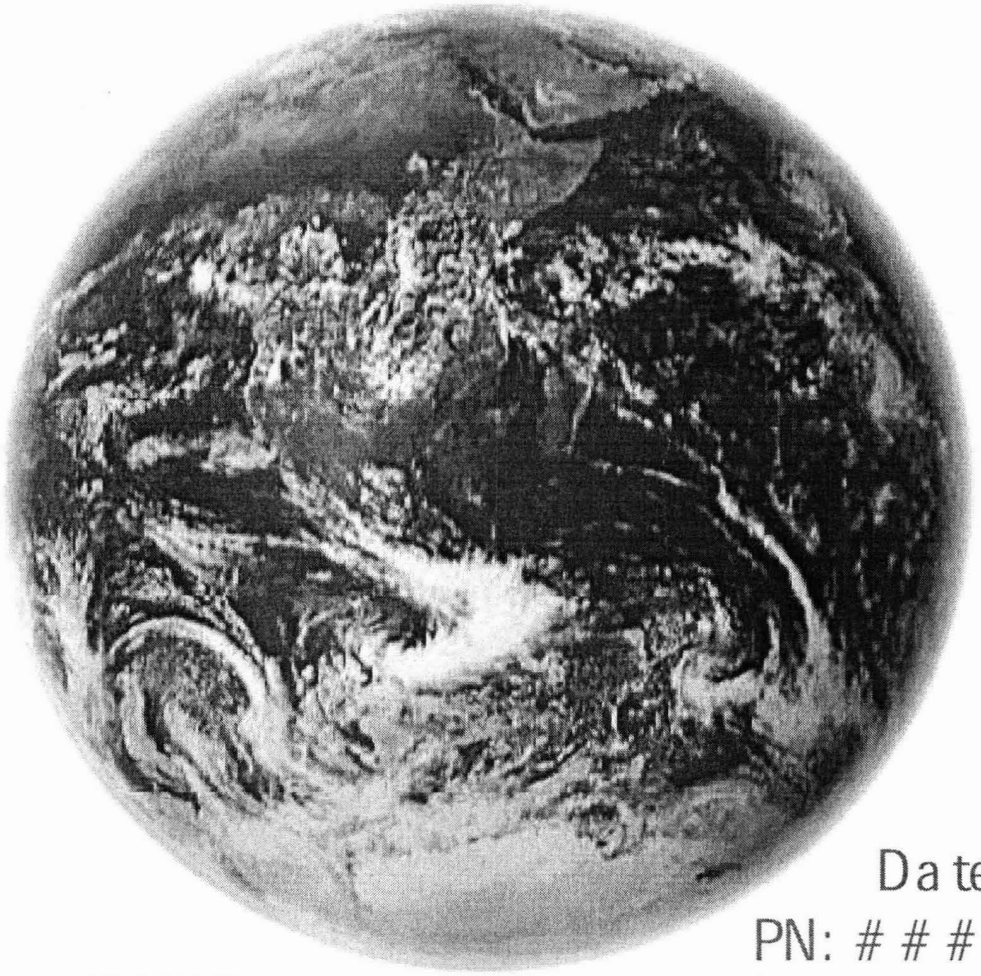

Date

PN: ######

TCS Consultants, Inc.

Wireless Communications Design

PO Box 884 * Montgomery TX, 77356 * (936) 588-3200

System Grid Map:

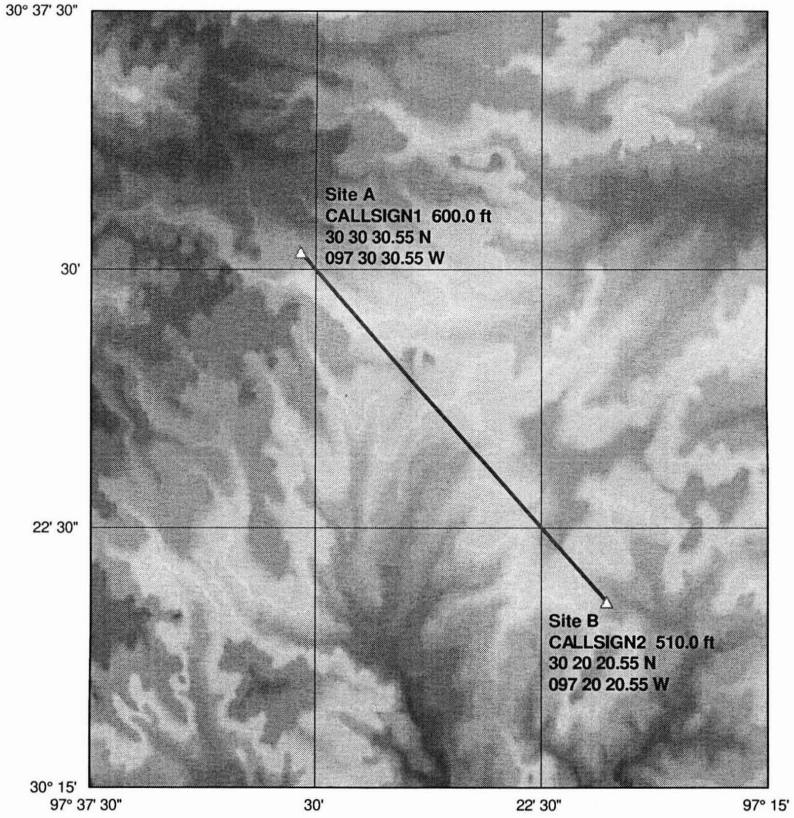

System Highway Map:

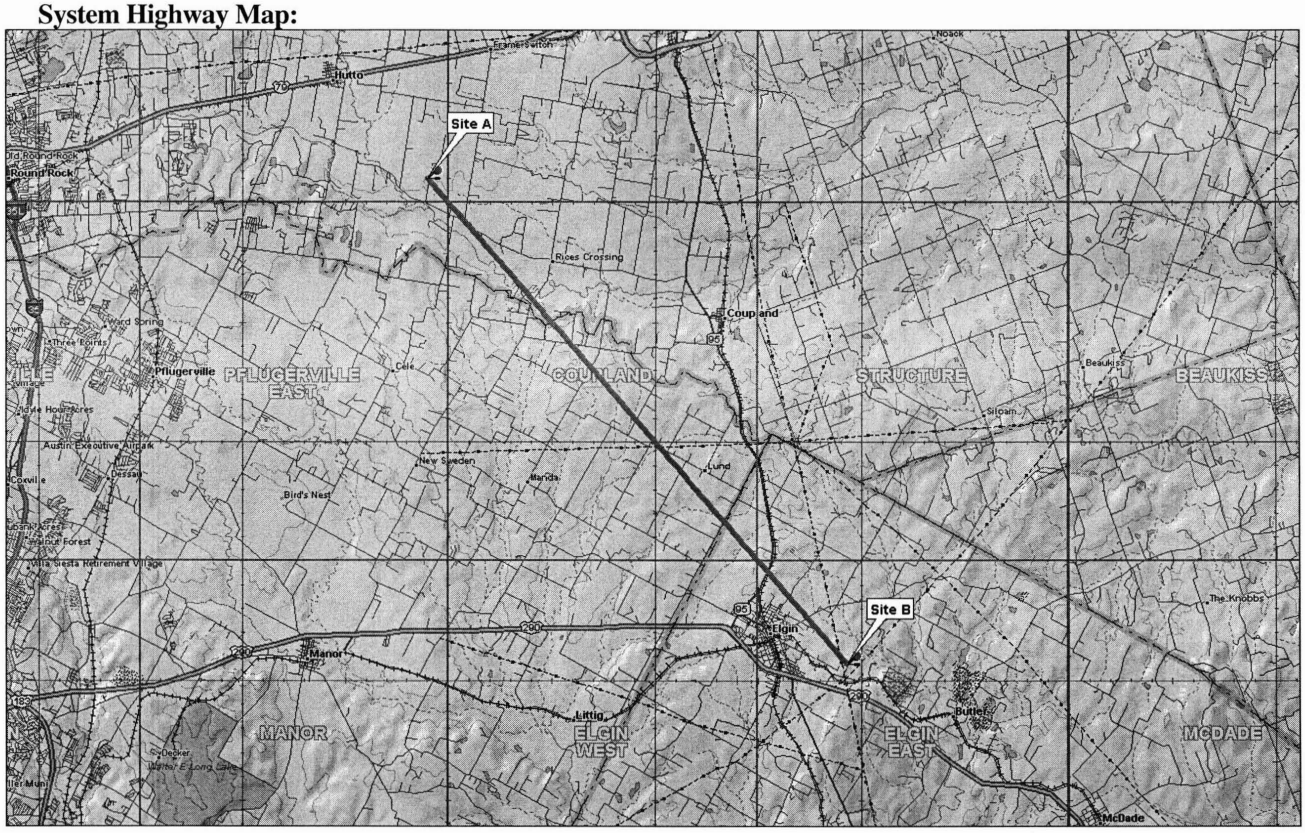

MICROWAVE SYSTEM

ANTENNA CENTERLINES AND CABLE LENGTHS

Site Name A	ACL (AGL)	Waveguide (ft)	Waveguide Type	Frequency (GHz)	Waveguide (ft)	ACL (AGL)	Site Name B
Site A (Main)	200'	240'	EW-52	6.175	180'	140'	Site B (Main)
Site A (Diversity)	180'	220'	EW-52	6.175	140'	120'	Site B (Diversity)

ACL -- Antenna Center Line.
AGL -- Above Ground Level.

DGPS COORDINATES – NAD 1983

SITES	LATITUDE	LONGITUDE	UTM Zone	UTM Easting (km)	UTM Northing (km)
Site A	N 30° 30' 30.55"	W 097° 30' 30.55"	14N	643.122	3376.078
Site B	N 30° 20' 20.55"	W 097° 20' 20.55"	14N	659.659	3357.524

General Scope of Work

Information presented in this report represents data collected during the path survey performed by **TCS Consultants, Inc.** in support of **'Your Company Name Here'** path design effort. This effort was performed during the month of **mm/dd/yyyy**. This report contains information for **1 path / hop** of microwave, operating in the **6.175 GHz** frequency band.

Equipment Description

Radios:

Generic Radios (For Sample Purpose)

Transmit Power:	30.00 dBm
Receiver Threshold at BER @ 10^{-6}:	-69.00 dBm

Antennas:

RFS Cablewave PAD8-59W

Antenna Size:	8 feet diameter
Antenna Gain:	41.60 dB
Radome Loss:	0.50 dB

RFS Cablewave PAD6-59W

Antenna Size:	6 feet diameter
Antenna Gain:	39.10 dB
Radome Loss:	0.40 dB

Transmission Line:

RFS Cablewave (WE61)

Transmission Attenuation @ 6.175 GHz	1.18 dB / 100 feet
Size / Type:	2.25" x 1.33" (Elliptical Waveguide)
Minimum Bending Radius:	(E Plane) 8 inches.
Minimum Bending Radius:	(H Plane) 22 inches.

Method of Survey:

All station sites and all potential path obstructions were located using Differential Global Positioning Satellites (DGPS) and laser distance measurement devices. The path was then traversed and the horizontal and vertical positions and heights of all potential obstructions were recorded. All obstructions were located using real time corrected DGPS recordings, real time corrections were provided by OmniStar Satellite differential service through a Trimble Differential GPS Receiver. The data was then imported into a computer running a survey/mapping program. The survey/mapping program graphically displayed all the survey data and produced the coordinate and height data required for engineering each path.

Path Design Criteria:

Site coordinates were determined by DGPS upon arrival to each site. At the same time the station site coordinates were being surveyed, the near field measurements and elevations were also measured. Heights of all potential obstructions including trees and buildings as well as all offset distance and angular measurements were provided by laser distance measuring devices and/or clinometers / transits.

The processed survey coordinates were then scaled and plotted on USGS 7 ½ minute (1:24,000) topographical quadrangle maps. A line was drawn connecting the path sites. A topographic cross section or

profile was generated from the map contour lines and the path critical points and the locations of potential obstructions were determined.

The proposed path was then traversed and all critical points and potential obstructions were surveyed to determine their coordinates and elevations.

Special Consideration and Findings:

Path – Site A to Site B:

The path from Site A to Site B traverses in a southeasterly direction toward the Site B end of the path. This path is currently configured for space-diversity operation with 8' main antennas and 6' diversity antennas proposed. This path traverses over medium terrain in a C-6 climate factor area and, as such, was deemed critical.

Trees within the path ranged from 5' AGL scrub to 80' residential evergreens. Critical antenna placement control areas are:

(1) 5.6 miles from Site A (80' Trees @ 585' AMSL ground elevation)
(2) 9.0 to 9.2 miles from Site A (80' Tree – Range @ 545' to 550' AMSL ground elevations)

Near Field Obstructions:
45' & 75' Trees @ Site A (Within 1 mile)
65' Trees @ Site B (Within 1 mile)

There is currently space available at both structures for antenna placement (see Site Data section for details)

This path meets or exceeds the customer desired 99.9995% reliability based on the path as designed within this report.

Conclusions:

Minimum centerlines are based on the results of this survey conducted during the month of **mm/dd/yyyy**. For the antenna clearance criteria, the following were used: 60% of the first Fresnel Zone when K-Factor = 1.333 (4/3rd) + 10' or 30% of the first Fresnel zone when K-Factor = 0.667 (2/3rd) + 10' (the greater clearance of the criterion).

Questions or comments:

Surveyor | surveyor@tcstx.com (Path Survey)

Design & Editing | Design@tcstx.com (Report & Design)

TCS Consultants, Inc. | (936) 588-3200 USA

Site Map:


Radio Tower
Well
Boggy Creek
Well
Graves
HUTTO
TAYLOR
PIPELINE
Well
Site A
Saul Cem
Cottonwood Creek
Brushy Creek
Normans Crossing
Kimbro Cem
Grave
Gravel Pit
PFLUGERVILLE EAST
COUPLAND

Site Description:

Site Name:	**Site A**
Site Location:	**FM 1660 1.6 miles northeast of Normans Crossing.**
Address:	**15096-16494 FM 1660**
City / State:	**Hutto, TX 78634**
County:	**Williamson County**

Geodetic Coordinates NAD – 1983

Survey Data:

Latitude:	**N 30° 30' 30.55"**
Longitude:	**W 097° 30' 30.55"**
Method used to derive coordinates:	**Differential Global Positioning Satellites (DGPS)**
Elevation AMSL:	**600' AMSL (182.88 Meters)**
Reference Maps:	**Hutto, TX (USGS 7 ½ Minute Topographical)**
FCC Tower Registration Data:	**FCC# XXXXXXX (Tower Registration)**
Latitude:	**Sample – Tower Doesn't Exist**
Longitude:	**Sample – Tower Doesn't Exist**
Elevation AMSL:	**Sample – Tower Doesn't Exist**
Comments:	

Nearest Airport: **There are no airports within 8 kilometers (5 miles).**

Latitude / Longitude:	**N/A**	**N/A**

Road Information:

General Road Condition:	**Paved**
Type of Vehicle Required to Reach Site:	**Any**
Distance to Main Hwy:	**2.8 miles south of US-79**
Distance to Nearest Town:	**3.2 miles southeast of the town of Hutto, TX**

Equipment Shelter Information:

Equipment Area Type/Status:	**Aggregate Communications Building (New)**
Height / Size:	**10'h x 12'w x 25'l**
Distance between Antenna Structure and Equipment Room:	**15' from tower to building via WG Bridge**
Estimated Distance Inside Building:	**(L + W) = 27'**

Comments: **45' additional waveguide used in the microwave calculations for this site.**

Tower Information:

Existing Tower(s):	**Yes**	Type:	**Guyed**
Height of Structure:	**285' AGL**	Height to Tip:	**289' AGL**

Comment / Restrictions Existing Tower(s):

Antenna Information:

Existing Antenna(s): **Yes – See Structure Elevation Drawing.**

Comments / Restrictions Existing Antenna(s): **None.**

Path To:	Antenna Centerline	Antenna Type	Antenna Size	Forward Azimuth Degrees (T)
Site B (Main)	**200' AGL**	**PAD8-59W**	**8'**	**139.04°**
Site B (Diversity)	**180' AGL**	**PAD6-59W**	**6'**	**139.04°**

Comment at Site:

Prepared By: **Robert A. Simmons** Date: **November 18, 2002**

Structure Elevation Drawing:

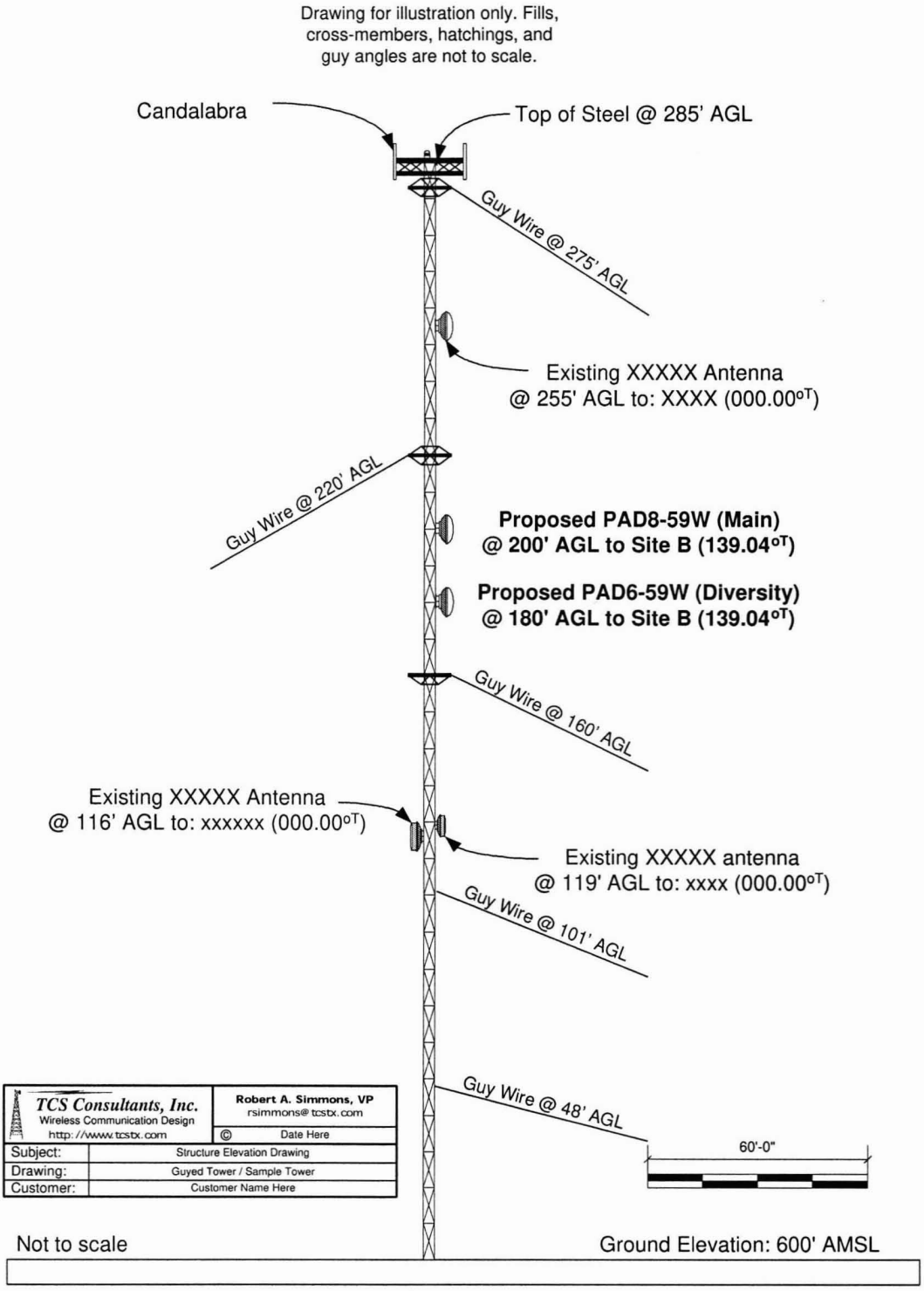

Site Plat / Plot Drawing:

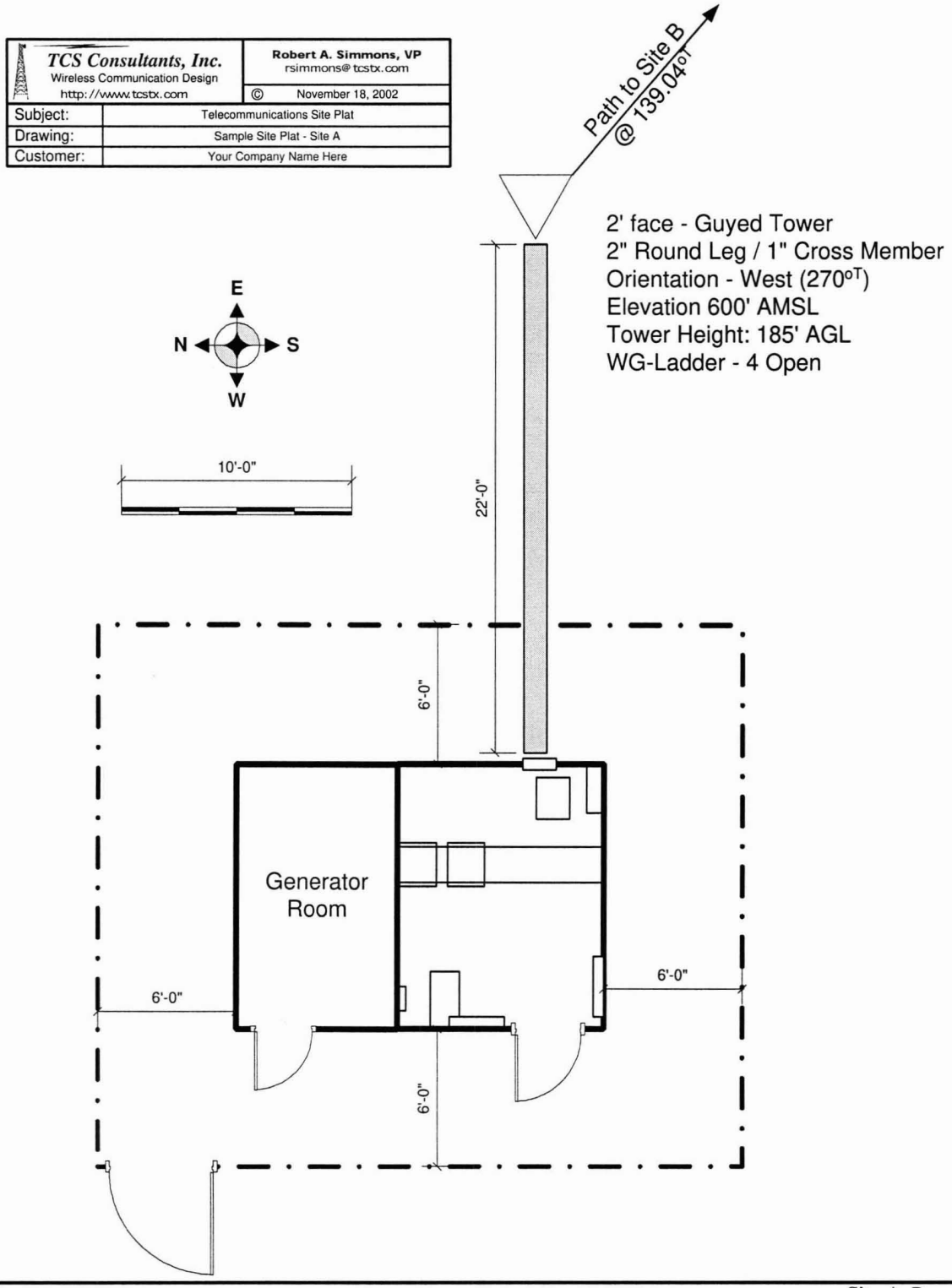

Building Layout Drawing:

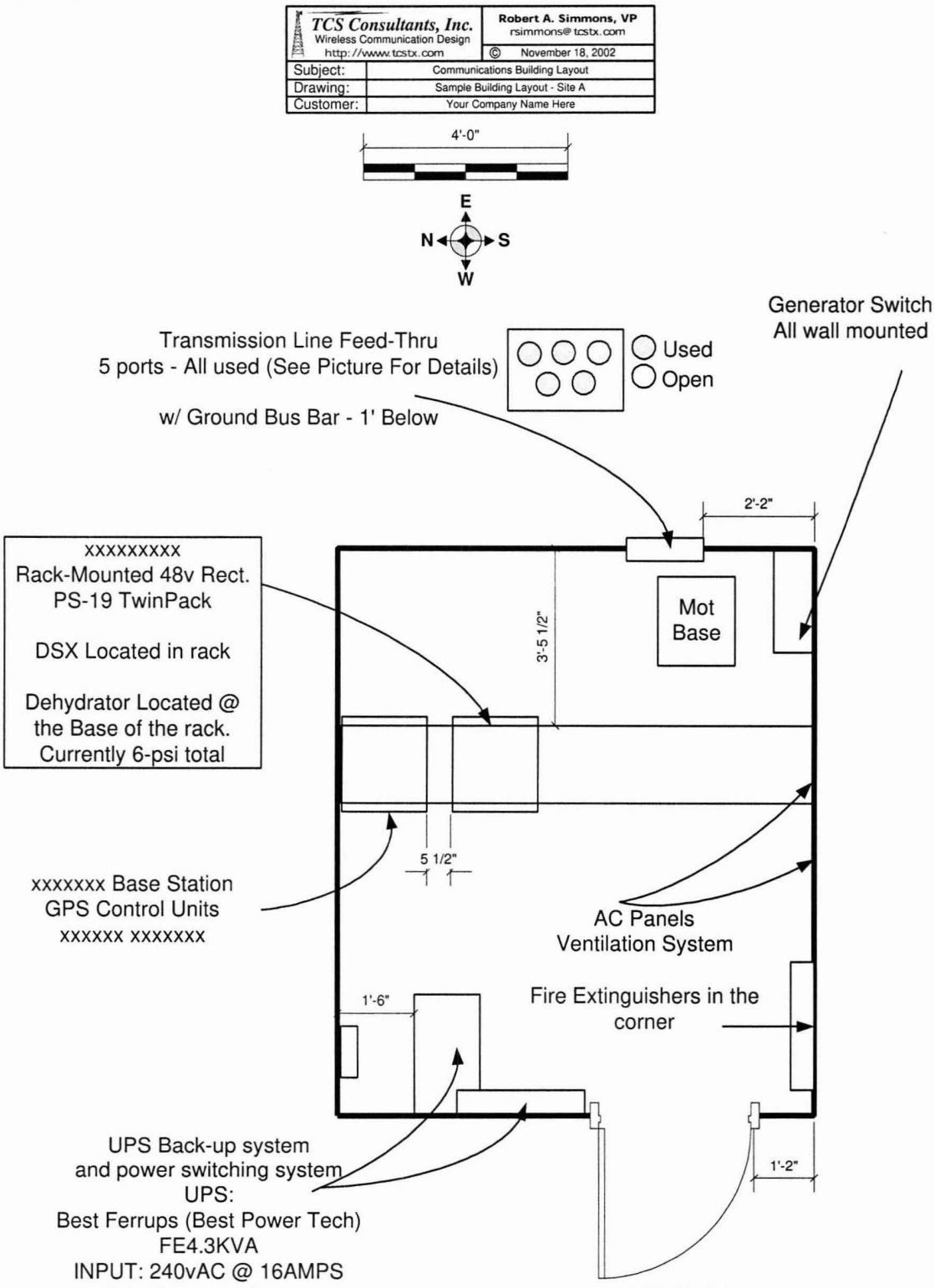

Site Photographs (Sample Pictures – Do not match fictitious site):

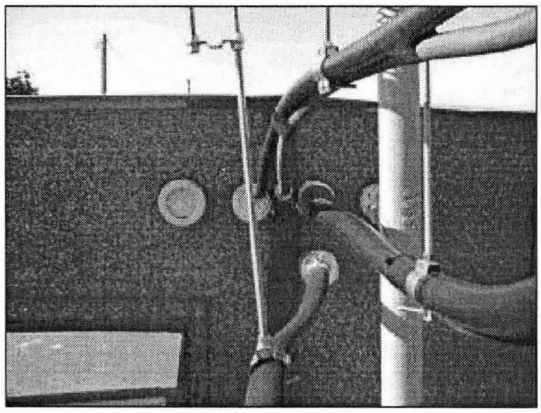

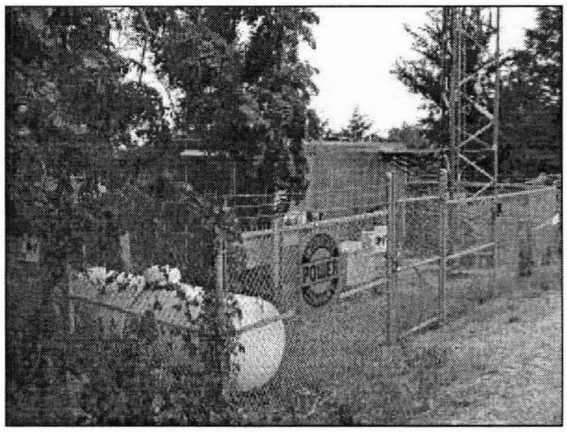

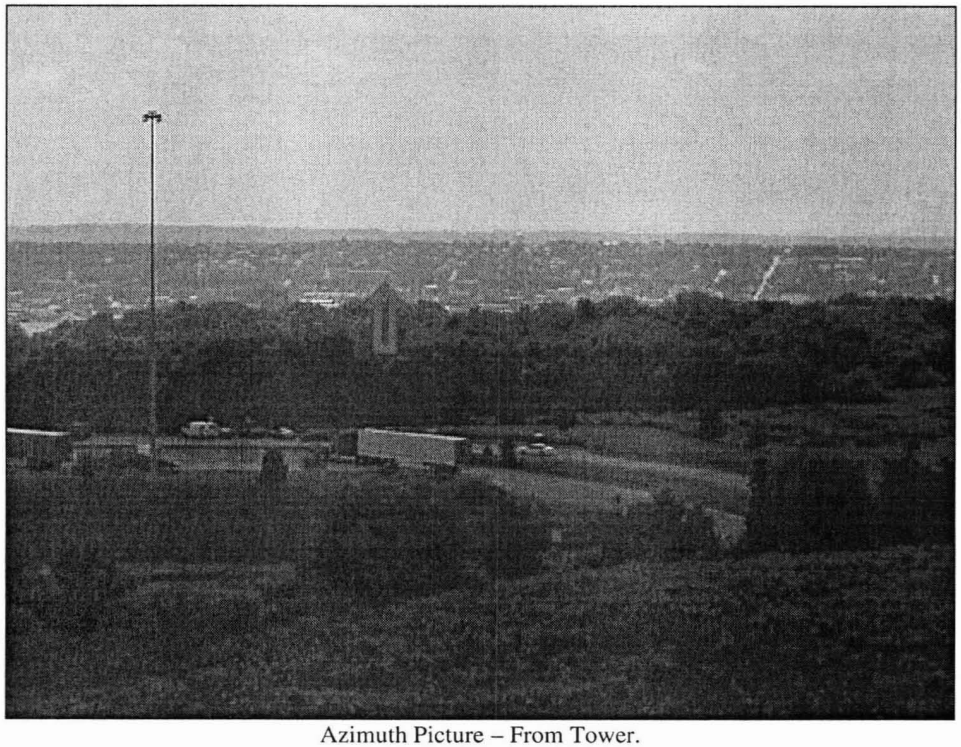

Azimuth Picture – From Tower.

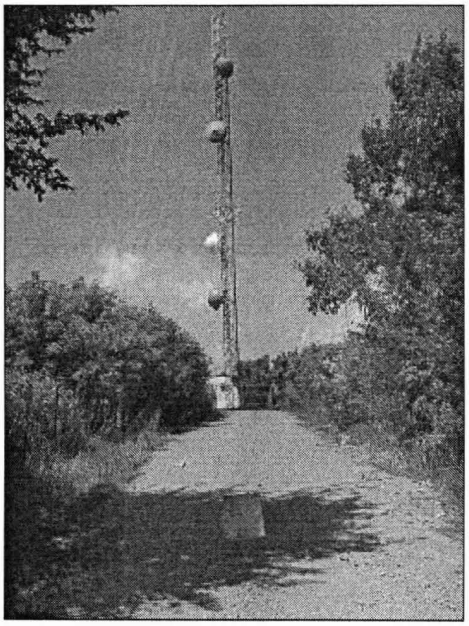

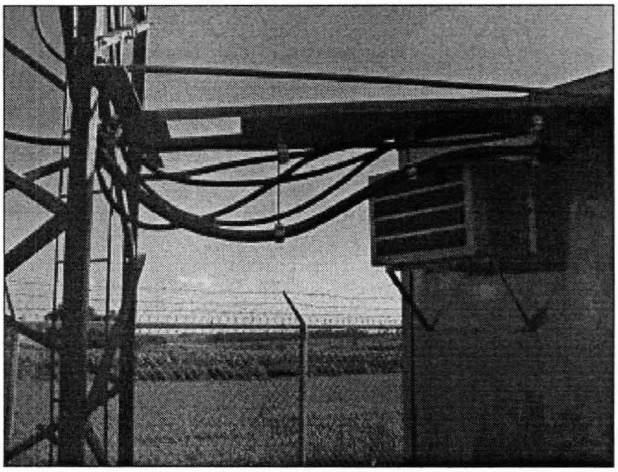

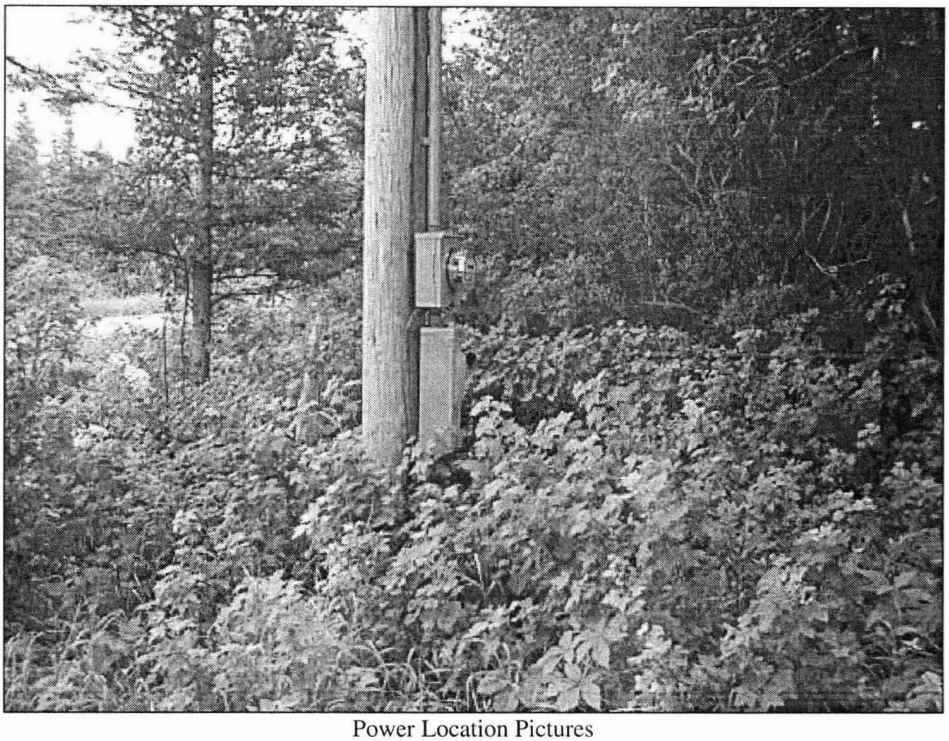

Power Location Pictures

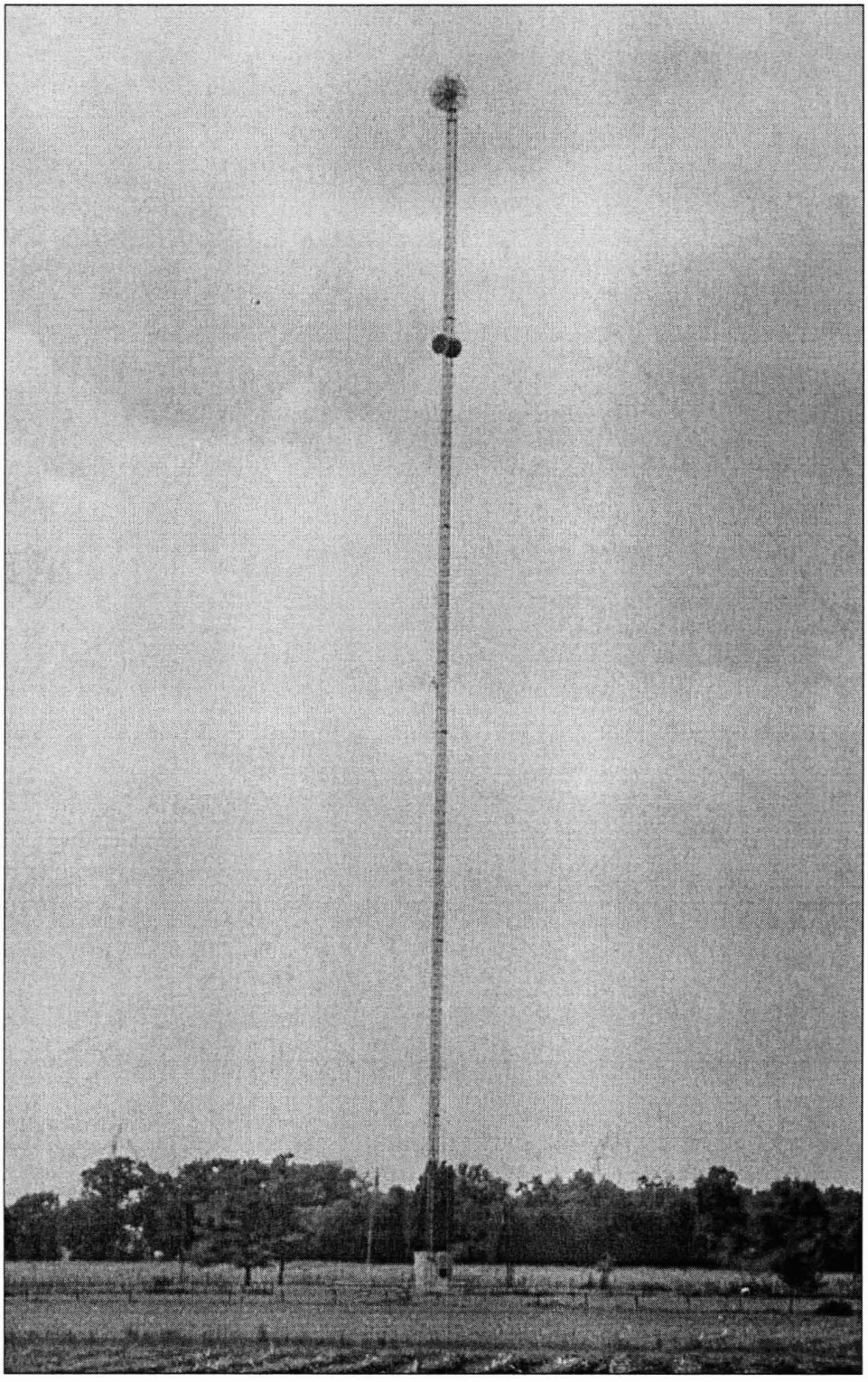



RF Path Loss & Transmission Distance Calculations

By

Walter Debus
Director of Engineering
Axonn, LLC

Technical Memorandum

August 4, 2006

INTRODUCTION

For radio transmission systems that consist of at least one transmitter, plus trans/ceiver antennas and at least one receiver there are two questions that inevitably get asked. The questions are: how far apart can the transmitter and receiver be in distance while maintaining acceptable performance, and what can be changed to increase this separation distance? The simplistic answers to these questions are: use the Free Space Path Loss model in determining trans/ceiver separation, and change the transmitter power to increase separation distance. While these two assumptions work under restricted conditions, in general they are overly optimistic for most situations. This paper presents mathematical transmission models that represent more realistic transmission systems. Furthermore, a better understanding as to what can be changed in the system that result in greater transmission distance. In addition, measured field data is presented that supports the realistic math models.

A typical RF transmission system is shown in Figure 1. The received signal strength (link budget) in Figure 1 is equal to:

(1) $R = P_t + G_{tot} - L$

For a known receiver sensitivity value, the maximum path loss can be derived as shown in (2).

(2) $L = P_t + G_{tot} - R$

Example: for $P_t = 39$ dBm, $G_{tot} = 7.5$ dB, $R = -95$ dBm; the path loss can not exceed $L \approx 142$ dB without violating the receiver sensitivity.

PATH LOSS AND DISTANCE CALCULATIONS

Path Loss is the largest and most variable quantity in the link budget. It depends on frequency, antenna height, receive terminal location relative to obstacles and reflectors, and link distance, among many other factors. Usually a statistical path loss model or prediction program is used to estimate the median propagation loss in dB. The estimate takes into account the situation - - line of sight (LOS) or non-LOS - -and general terrain and environment using more or less detail, depending on the particular model. For example, (3) is the Free Space loss model which only takes into consideration distance and frequency. Hence, this model is very limited in its ability to accurately predict path loss in most environments.

(3) $L_{fs} = 32.45 + 20\text{Log}_{10}(d_{km}) + 20\text{Log}_{10}(f_{MHz})$

By rearranging terms in (3) the maximum distance can be calculated. For instance, using the example above with a Path Loss of 142 dB and assuming $f_{MHz} = 2350$, the maximum distance that can be achieved assuming free space path loss is:

(4) $d_{fs} = \text{antiLog}_{10}[\{142 - 32.45 - 20\text{Log}_{10}(2350)\}/20] \approx 121$ km.

The distance of 121 km can only be achieved under the most optimistic case of LOS with absolutely no other types of distortion or reflections occurring.

The National Institute of Standards and Technology (NIST) have done an excellent job in documenting and comparing several realistic empirical propagation loss models. Based on the NIST study, the remainder of this document examines the following loss models:

- Free Space Model
- CCIR Model
- Hata Models
- Walfisch-Ikegami Models (WIM)

Figure 2 shows the numerous physical environment variables used to some degree by each of the above models in calculating path loss. Subsequently each loss model will be discussed more fully.

FREE SPACE PATH LOSS MODEL (L_{fs}) - The L_{fs} equation is shown in (3). Substituting (3) into (1) and then solving for distance yields the maximum distance equation for Free-space shown in (4).

CCIR PATH LOSS MODEL (L_{ccir}) - An empirical formula for the combined effects of free-space path loss and terrain-induced path loss was published by the CCIR (Comite' Consultatif International des Radio-Communication, now ITU-R) and is given by:

(5) $$L_{ccir} = 69.55 + 26.16\text{Log}_{10}(f_{MHz}) - 13.82\text{Log}_{10}(h_b) - a(h_m) + [44.9 - 6.55\text{Log}_{10}(h_b)]\text{Log}_{10}(d_{km}) - B$$

Where:

$$a(h_m) = [1.1\text{Log}_{10}(f_{MHz}) - 0.7]h_m - [1.56\text{Log}_{10}(f_{Mhz}) - 0.8]$$

$$B = 30 - 25\text{Log}_{10}(\%\text{ of area covered by buildings})$$

Substituting (5) into (1) and solving for distance yields the following CCIR maximum distance equation:

(6) $$d_{ccir} = \text{antiLog}_{10}\{[P_t + G_{tot} - R - 69.55 - 26.16\text{Log}_{10}(f_{MHz}) + 13.82\text{Log}_{10}(h_b) + a(h_m) + B] / [44.9 - 6.55\text{Log}_{10}(h_b)]\}$$

Example: for $P_t = 39$ dBm, $G_{tot} = 7.5$ dB, $R = -95$ dBm, $f_{MHz} = 2350$, $h_b = 8$ meters, $h_m = 1$ meter and $B = 25\%$ area covered by buildings; yields a maximum CCIR distance of:

(7) $$d_{ccir}\,(\text{meters}) \approx 550$$

HATA PATH LOSS MODELS (L_{hata}) – based on the CCIR model and following extensive measurements of urban and suburban radio propagation losses, Okumura published many empirical curves useful for radio system planning. These empirical curves were subsequently reduced to a convenient set of formulas known as the Hata models that are widely used in the industry. The CCIR and Hata models differ only in the effects of the mobile antenna and area coverage. There are four Hata models: Open, Suburban, Small City, and Large City. The basic formula for Hata path loss is:

(8) $$L_{hata} = 69.55 + 26.16\text{Log}_{10}(f_{MHz}) - 13.82\text{Log}_{10}(h_b) - a(h_m) + [44.9 - 6.55\text{Log}_{10}(h_b)]\text{Log}_{10}(d_{km}) - K$$

Where:

Type of Area	$a(h_m)$	K
Open	$[1.1\text{Log}_{10}(f_{MHz}) - 0.7]h_m - [1.56\text{Log}_{10}(f_{Mhz}) - 0.8]$	$4.78[\text{Log}_{10}(f_{MHz})]^2 - 18.33\text{Log}_{10}(f_{MHz}) + 40.94$
Suburban		$2[\text{Log}_{10}(f_{MHz}/28)]^2 + 5.4$
Small City		0
Large City	$3.2[\text{Log}_{10}(11.75h_m)]^2 - 4.97$	0

Substituting (8) into (1) and solving for distance yields the following Hata maximum distance equation:

(9) $$d_{hata} = \text{antiLog}_{10}\{[P_t + G_{tot} - R - 69.55 - 26.16\text{Log}_{10}(f_{MHz}) + 13.82\text{Log}_{10}(h_b) + a(h_m) + K] / [44.9 - 6.55\text{Log}_{10}(h_b)]\}$$

Example: for P_t = 39 dBm, G_{tot} = 7.5 dB, R = -95 dBm, f_{MHz} = 2350, h_b = 8 meters, h_m = 1 meter; yields maximum Hata distances of:

(10) $$d_{hata}(\text{meters}) \approx \begin{cases} 5300, & \text{Open} \\ 1600, & \text{Suburban} \\ 740, & \text{Small City} \\ 740, & \text{Large City} \end{cases}$$

WALFISCH-IKEGAMI PATH LOSS MODELS (L_{wim}) – the WIM has been shown to be a good fit to measured propagation data for frequencies in the range of 800 to 2000 MHz and path distances in the range up to 5 km. The WIM distinguishes between Line Of Sight (LOS) and NLOS propagation situations.

In a LOS situation where the base antenna height is greater the 30 meters ($h_b \geq 30$) and there is no obstruction in the direct path between the transmitter and the receiver, the WIM path loss model for LOS is:

(11) $$L_{wim\text{-}los} = 42.64 + 26\text{Log}_{10}(d_{km}) + 20\text{Log}_{10}(f_{MHz})$$

Substituting (11) into (1) and solving for distance yields the following WIM LOS maximum distance equation:

(12) $$d_{wim\text{-}los} = \text{antiLog}_{10}\{[P_t + G_{tot} - R - 42.64 - 20\text{Log}_{10}(f_{MHz})] / 26\}$$

Example: for P_t = 39 dBm, G_{tot} = 7.5 dB, R = -95 dBm, f_{MHz} = 2350; yields maximum WIM LOS distance of:

(13) $$d_{wim\text{-}los}\ (\text{meters}) \approx 16200$$

For NLOS situations the WIM model uses all the parameters listed in association with Figure 2. The model is the most complex but it has the ability to represent more environments. In the absence of data, building height in meters may be estimated by three times the number of floors, plus 3m if the roof is pitched instead of flat. The model works best for base antennas well above roof height. The NLOS path loss equation is best presented in sections due to its complexity. The high level NLOS path loss equation is:

(14) $$L_{win\text{-}nlos} = \begin{cases} L_{fs} + L_{rts} + L_{msd}, & L_{rts} + L_{msd} \geq 0 \\ L_{fs}, & L_{rts} + L_{msd} < 0 \end{cases}$$

Where:

L_{fs} = Free-Space loss = $32.45 + 20\text{Log}_{10}(d_{km}) + 20\text{Log}_{10}(f_{MHz})$

$L_{rts} = -16.9 - 10\text{Log}_{10}(w) + 10\text{Log}_{10}(f_{MHz}) + 20\text{Log}_{10}(\Delta h_m) + L_{ori}$

Where:

$$L_{ori} = \begin{cases} -10 + 0.354\,\text{Ø}, & 0 \leq \text{Ø} \leq 35° \\ 2.5 + 0.075(\text{Ø}-35°), & 35° \leq \text{Ø} \leq 55° \\ 4.0 - 0.114(\text{Ø}-55°), & 55° \leq \text{Ø} \leq 90° \end{cases}$$

$$L_{msd} = L_{bsh} + K_a + K_d \cdot Log_{10}(d_{km}) + K_f \cdot Log_{10}(f_{MHz}) - 9Log_{10}(b)$$

Where:

$$L_{bsh} = \begin{cases} -18Log_{10}(1 + \Delta h_b), & \Delta h_b > 0 \\ 0, & \Delta h_b \le 0 \end{cases}$$

$$K_a = \begin{cases} 54, & \Delta h_b > 0 \\ 54 + 0.8|\Delta h_b|, & \Delta h_b \le 0 \text{ and } d_{km} \ge 0.5 \\ 54 + 0.8|\Delta h_b|(d_{km}/0.5), & \Delta h_b \le 0 \text{ and } d_{km} < 0.5 \end{cases}$$

$$K_d = \begin{cases} 18, & \Delta h_b > 0 \\ 18 + 15(|\Delta h_b|/h_B), & \Delta h_b \le 0 \end{cases}$$

$$K_f = \begin{cases} 0.7(f_{MHz}/925 - 1), & \text{Small City} \\ 1.5(f_{MHz}/925 - 1), & \text{Large City} \end{cases}$$

Substituting (14) into (1) and solving for distance yields the following WIM NLOS maximum distance equation:

(15) $$d_{wim\text{-}nlos} = antiLog_{10}\{[P_t + G_{tot} - R - 32.45 - (30 + K_f)Log_{10}(f_{MHz}) + 16.9 + 10Log_{10}(w) - 20Log_{10}(\Delta h_m) - L_{ori} - L_{bsh} - K_a + 9Log_{10}(b)]/(20 + K_d)\}$$

Example: for $P_t = 39$ dBm, $G_{tot} = 7.5$ dB, $R = -95$ dBm, $f_{MHz} = 2350$, Small City; yields maximum WIM NLOS distance of:

(16) $d_{wim\text{-}nlos}$ (meters) ≈ 820

USE OF PATH LOSS MODELS

A good question asked is, what is the best path loss model to use? For instance, from the common example used above in each model the calculated distance values range widely. Table (A) shows these calculated example values. What is the correct model?

Table A
Calculated Distance Values for Common Example

Path Loss Model	Calculated Distance Value in Meters
Free-Space	121,000
WIM LOS	16,200
Hata Open	5,300
Hata Suburban	1,600
WIM NLOS	820
Hata Small/Large City	740
CCIR	550

The two extremes (Free-space and CCIR) in Table (A) are further clarified in Figure 3 which is a graph of the various model path losses as a function of distance. At a distance of 1 km the difference in the two extremes is approximately 50 dB and at 10 km this difference grows to approximately 70 dB. Hence, it is extremely important to pick a model that is representative of the environment the RF system is working into or gross errors in system performance will occur.

Measured data offers a means to better understand what path loss model to use in calculating transmission distance. Field strength measurements were conducted on a COFDM[1] system. The transmitter was installed on the roof of a single story building and the receiver was mobile. The system configuration consisted of transmitter power of 39 dBm, antenna gain of 9 dB, connection losses of 1.5 dB, transmitter height of 8 meters, receiver height of 1 meter and transmission frequency of 2350 MHz. At various known GPS location points surrounding the building field strength measurements were made. Figure 4 shows the GPS map and the various signal strength measurements at various points. Also shown are 100 meter rings that are used to average the measurements. Figure 5 is a graph of both the calculated and measured receiver signal strength for the roof mounted system. Note in Figure 5 the good correlation between the Hata small/large city model and the measured data. Also, the WIM-NLOS model closely correlates with the measured data. The CCIR model seems overly pessimistic and the open LOS type models seem overly optimistic. Based on Figure 5, along with ease of use, the Hata small/large city model is recommended for most urban environment path loss calculations.

RULE OF THUMB DOUBLE-THE-DISTANCE ESTIMATOR

A common rule of thumb that is used in RF engineering is: 6 dB increase in link budget results in doubling the transmission distance. This rule is correct for the Free-space path loss model but is overly optimistic and does not hold true for more realistic models. In some cases it may take in excess of 15 dB increase in link budget to double the transmission distance. The increase value is a function of the variables shown in Figure 2 with the transmitter height being the most sensitive. Table (B) lists the dB increase value needed to double the distance for the various path loss models and for the system variables used in the above distance calculation examples. Values are shown for two different transmitter antenna heights. Hence, based on Table (B), a good rule of thumb for urban environments is: 12 dB increase in link budget results in doubling the transmission distance.

Table B
Link Budget Increase Values Needed to Double Transmission Distance

Path Loss Model	dB Increase Value Needed To Double Distance	
	T_x Height = 1m	T_x Height = 15m
Free-Space	6.0	6.0
WIM-LOS	7.8	7.8
Hata Models	13.5	11.2
CCIR	13.5	11.2
WIM-NLOS	15.3	11.4

SENSITIVITY ANALYSIS OF DISTANCE CALCULATIONS

Equations 4, 6, 9, 12 and 15 calculate the maximum transmission distance for the various path loss models. Given these equations exist allows for a maximum distance sensitivity analysis to be performed. The method of analysis is to change a single variable in an equation by a fixed percentage and then calculate the resultant percentage change in maximum distance. Repeating this process for each variable provides the knowledge as to what variable is the most sensitive to change. With this knowledge, focus can be placed on the system elements that will afford the biggest payback in effort expended to increase transmission distance. The Hata model will be used for illustrative purposes. Referring back to (9), the variables that can be changed in the Hata distance equation are: transmit power, total gain, receiver sensitivity, frequency, transmitter height and receiver height. Each of these variables was changed one-at-a-time by ± 2% increments up to ± 10%. The percentage difference in distance was then calculated at each point. Figure 6 is a graph of the resultant Hata sensitivity analysis. As seen, the receiver sensitivity is the most sensitive variable to change that effects transmission distance. A 10% increase in receiver sensitivity results in a 75% increase in transmission distance.

A sensitivity analysis was performed on all path loss models with similar results as found with the Hata model. That is, receiver sensitivity and transmit power are number one and two when it comes to distance sensitivity.

SUMMARY

[1]COFDM - Coded Orthogonal Frequency Division Multiplex

Care must be taken when choosing the path loss model for predicting RF system performance. Serious errors can occur by using the Free-space path loss model for all but the most restricted cases. A more realistic model to use for urban environments is the Hata small/large city model. The Hata model is easy to use and has demonstrated its ability to predict path loss with a good degree of accuracy.

For urban environments, the use of 12 dB is a good rule of thumb for predicting the needed increase in link budget in order to double the transmission distance.

Receiver sensitivity is the first variable in a system that should be optimized in order to increase transmission distance. Other variables in a system also effect distance but must be changed by a greater percentage to equal the effects offered by changing the receiver sensitivity.

Walter Debus
Director of Engineering
Axonn, L.L.C.

Figure 1

Typical RF Transmission System

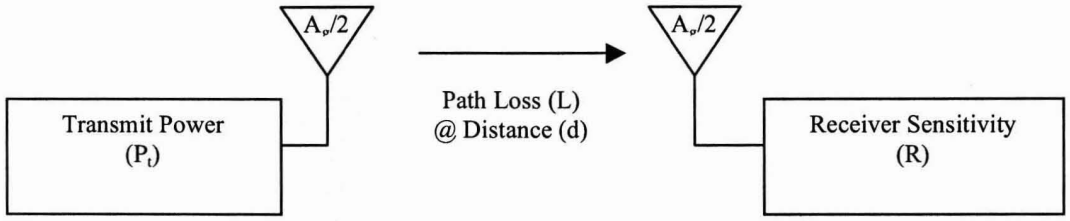

Where:

P_t = Transmitter power in dBm
A_g = Total antenna gain in dB
C_l = Total connection loss in dB
G_{tot} = (A_g - C_l) Total gain in dB
L = Transmission path loss in dB
R = Receiver sensitivity in dBm
d = Distance between transmitter and receiver in meters

Figure 2

Physical Environment Path Loss Variables

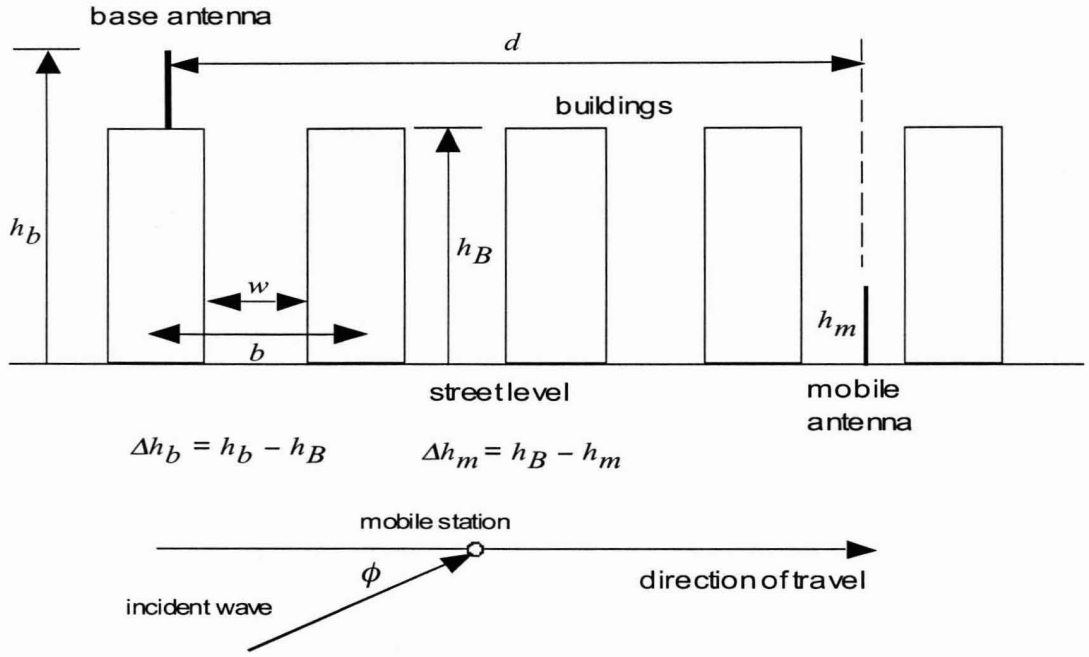

Where:

d = Distance in meters
h_b = Base antenna height over street level in meters
h_m = Mobile station antenna height in meters
h_B = Nominal height of building roofs in meters
Δh_b = hb-h_B = Height of base antenna above rooftops in meters
Δh_m = h_B-h_m = Height of mobile antenna below rooftops in meters
b = Building separation in meters (20 to 50m if no data given)
w = Width of street (b/2 if no data given)
Ø = Angle of incident wave with respect to street (use 90° if no data)

Figure 3

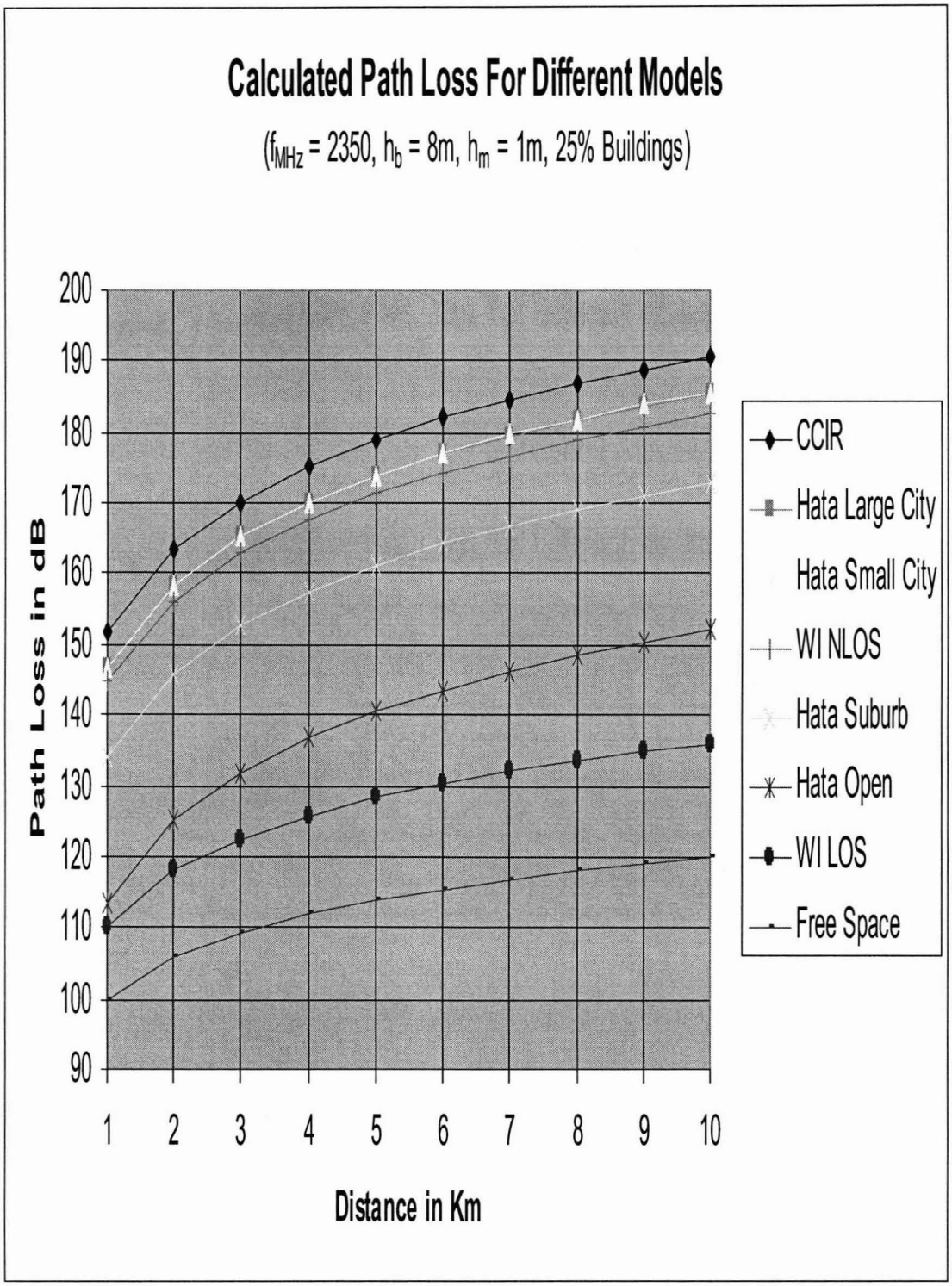
Calculated Path Loss For Different Models
(f_{MHz} = 2350, h_b = 8m, h_m = 1m, 25% Buildings)
Path Loss in dB
200
190
180
170
160
150
140
130
120
110
100
90
1
2
3
4
5
6
7
8
9
10
Distance in Km
CCIR
Hata Large City
Hata Small City
WI NLOS
Hata Suburb
Hata Open
WI LOS
Free Space

Figure 4

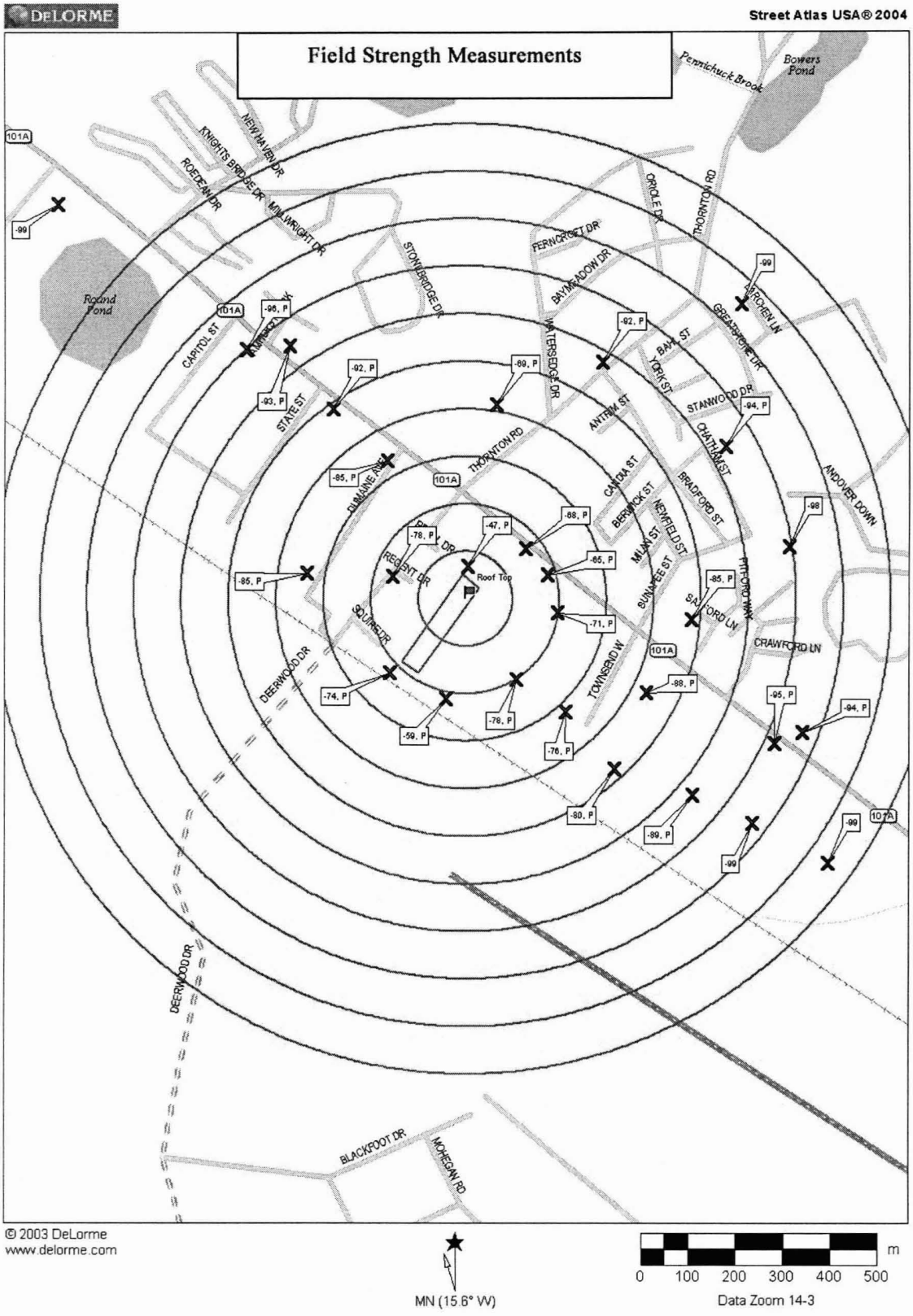
DeLORME
Street Atlas USA® 2004
Field Strength Measurements
Roof Top
Round Pond
Bowers Pond
Pennichuck Brook
101A
-99
-96, P
-93, P
-92, P
-89, P
-85, P
-78, P
-47, P
-88, P
-65, P
-71, P
-74, P
-59, P
-78, P
-76, P
-80, P
-89, P
-99
-85, P
-88, P
-95, P
-94, P
-98
-92, P
-94, P
KNIGHTS BRIDGE DR
NEWPORT DR
ROEDEAN DR
MILLWRIGHT DR
STONEBRIDGE DR
FERNCROFT DR
BAYMEADOW DR
ORIOLE DR
THORNTON RD
ARGYLE LN
GREENSTONE DR
CAPITOL ST
STATE ST
WATERSEDGE DR
ANTRIM ST
YORK ST
BATH ST
STANWOOD DR
CHATHAM ST
ANDOVER DOWN
DUMAINE AVE
CANDIA ST
BERWICK ST
NEWFIELD ST
MILAN ST
BRADFORD ST
BUNNEE ST
SAFFORD LN
PITTSFORD WAY
CRAWFORD LN
REGENT DR
SQUIMSIR
DEERWOOD DR
TOWNSEND W
BLACKFOOT DR
MOHEGAN RD
© 2003 DeLorme
www.delorme.com
MN (15.6° W)
0 100 200 300 400 500 m
Data Zoom 14-3

Figure 5

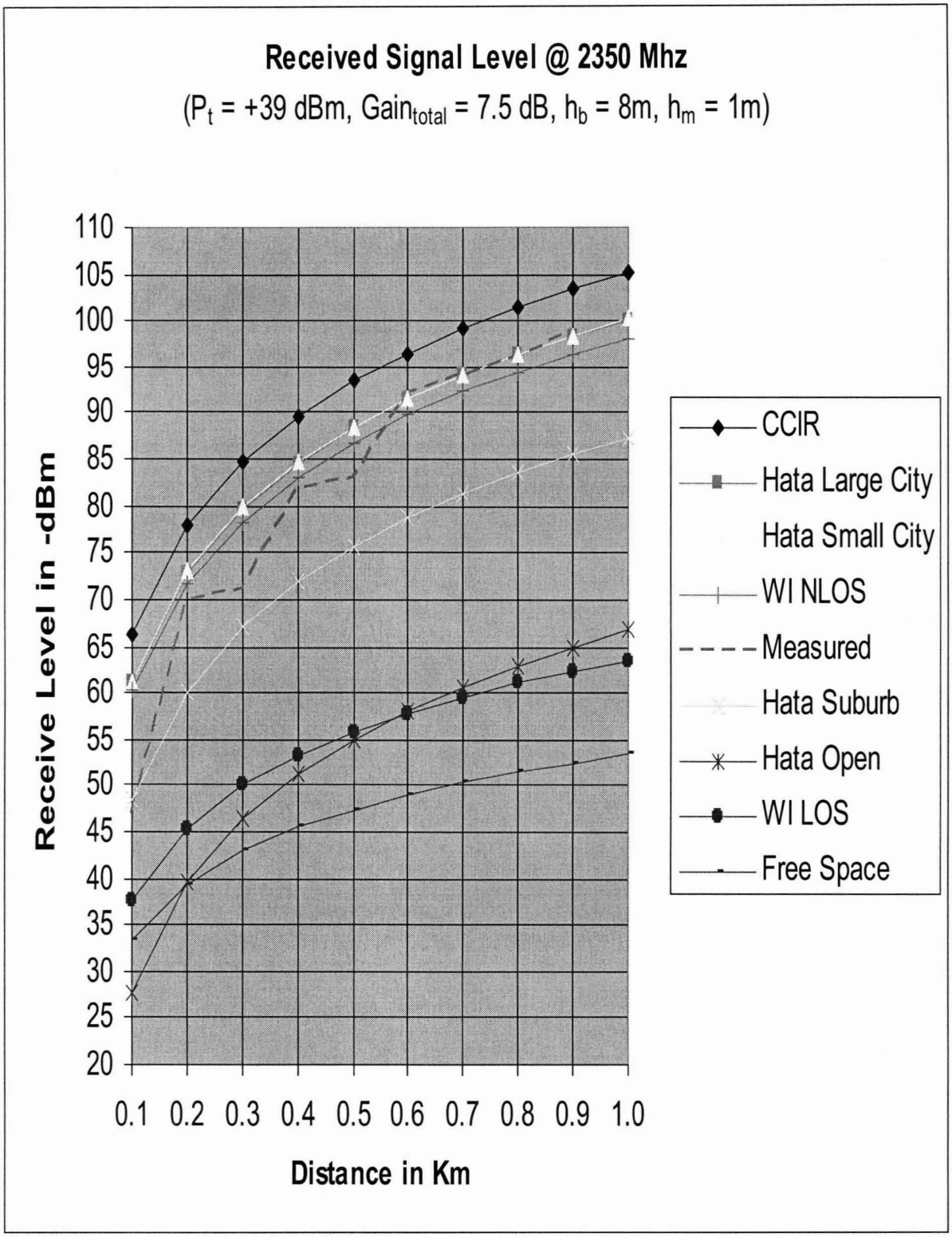
Received Signal Level @ 2350 Mhz
(P_t = +39 dBm, $Gain_{total}$ = 7.5 dB, h_b = 8m, h_m = 1m)
Receive Level in -dBm
110
105
100
95
90
85
80
75
70
65
60
55
50
45
40
35
30
25
20
0.1 0.2 0.3 0.4 0.5 0.6 0.7 0.8 0.9 1.0
Distance in Km
CCIR
Hata Large City
Hata Small City
WI NLOS
Measured
Hata Suburb
Hata Open
WI LOS
Free Space

Figure 6

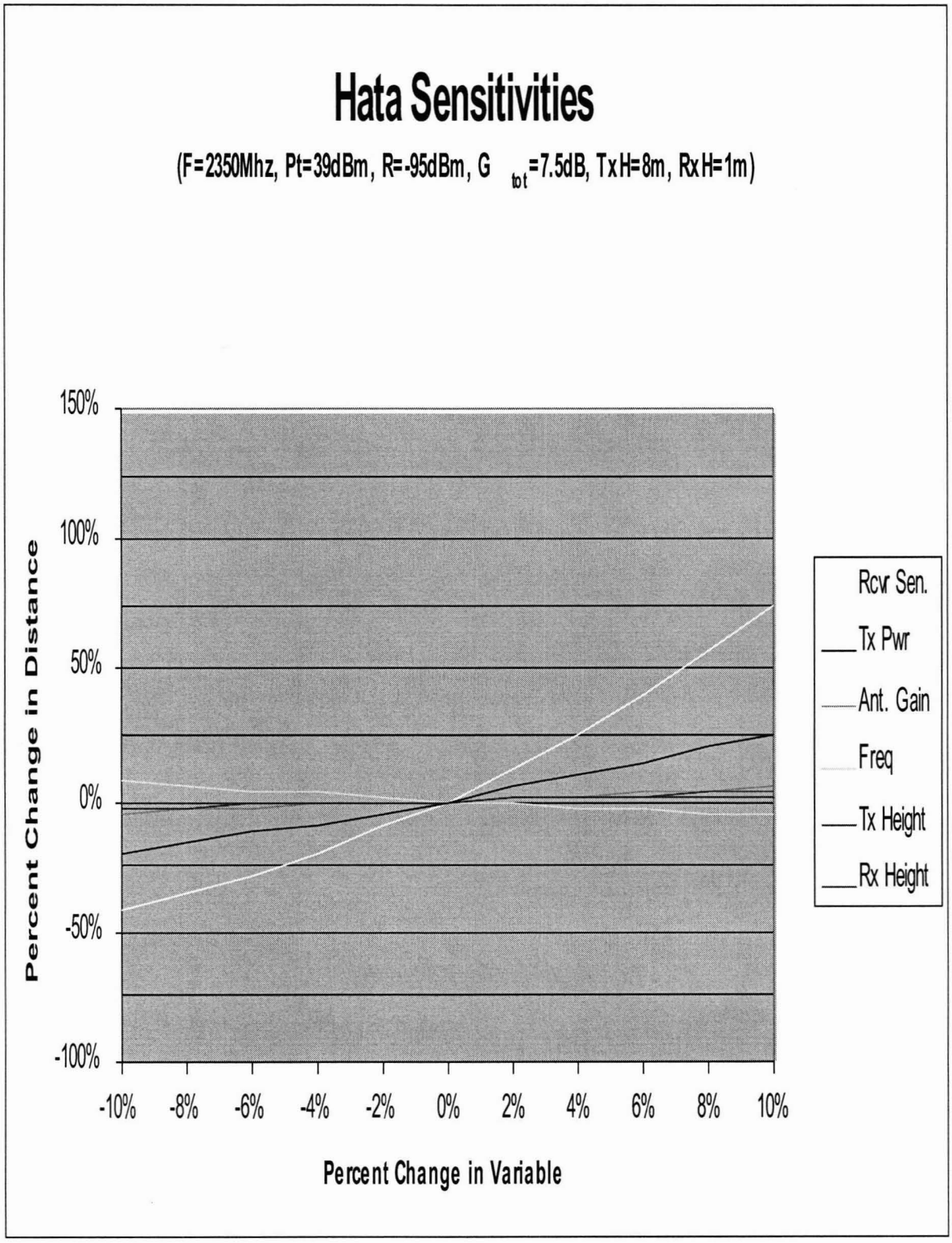
Hata Sensitivities
(F=2350Mhz, Pt=39dBm, R=-95dBm, G tot=7.5dB, TxH=8m, RxH=1m)
150%
100%
50%
0%
-50%
-100%
Percent Change in Distance
-10%
-8%
-6%
-4%
-2%
0%
2%
4%
6%
8%
10%
Percent Change in Variable
Rcvr Sen.
Tx Pwr
Ant. Gain
Freq
Tx Height
Rx Height

Earth Curvature Correction

Q: How is earth curvature correction calculated?

A: TAP software which uses radial elevation data (for plotting radial profiles, computing radio propagation obstruction losses, etc.) allows elevation values to be corrected for earth curvature, including atmospheric diffraction effects.

The formula used for elevation correction is:

(1) $E_{corr} = E + (78.5/k) \times 10^{-3} \times D \times (P-D)$

E_{corr} is the corrected elevation in **meters.**

E is the actual elevation in **meters.**

k is the curvature correction factor to compensate for atmospheric diffraction, typically 4/3 for most radio propagation applications. To ignore atmospheric diffraction, use a value of 1.0 for this factor.

D is the horizontal distance along the path from the primary site to the point being corrected (in **kilometers**).

P is the distance from the site to the end of the path (in **kilometers**).

The equation can also be written using British units as:

(2) $E_{corr} = E + (D \times \{P-D\}) / (1.5 \times k)$

E_{corr} is the corrected elevation in **feet.**

E is the actual elevation in **feet**.

k is the curvature correction factor to compensate for atmospheric diffraction, typically 4/3 for most radio propagation applications. To ignore atmospheric diffraction, use a value of 1.0 for this factor.

D is the horizontal distance along the path from the primary site to the point being corrected (in **miles**).

P is the distance from the site to the end of the path (in **miles**).

Since the term {P-D} is the distance from the point being corrected to the far end of the path, the equation can also be written in terms of the distances

(2) $E_{corr} = E + (D_1 \times D_2) / (1.5 \times k)$

E_{corr} is the corrected elevation in **feet.**

E is the actual elevation in **feet**.

k is the curvature correction factor to compensate for atmospheric diffraction, typically 4/3 for most radio propagation applications. To ignore atmospheric diffraction, use a value of 1.0 for this factor.

D_1 is the horizontal distance along the path from the primary site to the point being corrected (in **miles**).

D_2 is the horizontal distance along the path from the point being corrected to the end of the path (in **miles**).



I'm interested!
Please click here to jump to an online form which helps us better understand your needs. Then we will be able to respond to your request with information that is most useful to you.

Search SoftWright Website

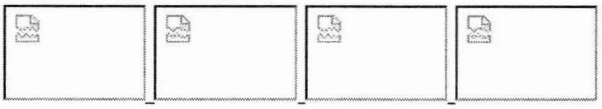

Copyright 1999 by SoftWright LLC

Comparison of Microwave Links Prediction Methods: Barnett-Vigants vs. ITU Models

Basile L. Agba[1], Robert Morin[2], and Germain Bergeron[2]

[1]Institut de Recherche d'Hydro-Québec, 1800 Lionel-Boulet, Varennes, Québec, Canada
[2]Hydro-Québec, 1500 University, Montreal, Québec, Canada

Abstract— Hydro-Québec operates one of the widest electricity networks in the world. The microwave network infrastructure is essential to manage the power grid in Québec and therefore, it is important to meet the reliability criteria that are generally above those accepted by traditional communication operators. In addition, over one third of the existing links has lengths between 70 km and 90 km and operates in extreme weather conditions and all year long. To address these constraints, the microwave links design needs to be as much accurate as possible. The aim of the research presented in this paper is to make a comparative study between two commonly used prediction models for microwave links: Barnett-Vigants and ITU-R P. 530. The first part of this work considers each of the following aspects (unavailability, diversity gain and conversion methods). We analyse each aspect as a function of frequency, fading margin and link length. The two models led to significantly different results for the unavailability due to multipath as a function of the link length, and also for the space diversity as a function of the gain difference between the main antenna and the diversity antenna. Remarkable differences between the two models were also observed when studying the unavailability due to rain as a function of the frequency. The second part of this work compares the overall performance of both models in terms of the total outage probability over ten links with different lengths and different locations. The differences observed for some links are significant.

1. INTRODUCTION

The microwave links deployment, like any other wireless network, requires accurate prediction methods in order to minimize the discrepancies between simulation results and real system performance. Although numerous microwave links are deployed around the world, most of them can be considered as short-range or mean-range links for which the path length is less than 20 km. Hydro-Québec operates one of the widest electricity networks in the world. The microwave network infrastructure is essential to manage the power grid in Québec and therefore, it is important to meet the reliability criteria that are generally above those accepted by traditional communication operators. In addition, over one third of the existing links has lengths between 70 km and 90 km and operates in extreme weather conditions and all year long. To address these constraints, the microwave links design needs to be as much accurate as possible. The aim of the research presented in this paper is to make a comparative study between two commonly used prediction models for microwave links: Barnett-Vigants (B-V) and ITU-R P. 530 [1].

This paper is divided in two parts. The first part analyses some main aspects (such as unavailability, diversity methods and conversion methods) as a function of various parameters, frequency, fading margin and link length. The second part compares the overall performance of both models in terms of the total outage probability over some typical links. Due to space limitation and to reduce the number of figures, we will present only some figures which illustrated significant differences between B-V model and ITU model.

2. BARNETT-VIGANTS VS. ITU: STEP BY STEP COMPARISON

The two models are compared on a step by step basis to illustrate the effect of a given parameter or the combined effect of few parameters. Four main aspects will be analysed: unavailability due to multipath, diversity method with focus on space diversity, worst month to annual conversion methods, and unavailability due to rain.

2.1. Unavailability due to Multipath

The unavailability due to multipath is a key indicator in microwave links design. Indeed, it indicates the outage probability if any engineering techniques (diversity and other engineering techniques) is used to mitigate the propagation effects. The two options for calculating the unavailability in B-V model are respectively "Baseband switching systems" and "IF combining systems". The common

parameters of the two models are flat fade margin ($FFM = A$), frequency (f) and distance (d). One additional parameter is used in B-V model, C factor, while three additional parameters are used in ITU model, geoclimatic K factor, link inclination $|\varepsilon_p|$, and the lowest antenna altitude (above sea level) h_L. The outage probability is expressed in percentage (%) as follows [2, 3].

B-V model:

$$P_w = \left(\left[6 \cdot 10^{-7} C f d^{3.0} \right] 10^{-A/10} \right) \times 100 \tag{1}$$

ITU model:

$$P_w = K d^{3.0} \left(1 + |\varepsilon_p|\right)^{-1.2} \times 10^{0.033 f - 0.001 h_L - A/10} \tag{2}$$

For comparison purposes, real parameters of an existing link are used: $d = 70\,\text{km}$, $f = 7.425\,\text{GHz}$; $FFM = 37\,\text{dB}$; $C = 1$; $K = 1.84E-4$; $|\varepsilon_p| = 0.3\,\text{mrad}$ and $h_L = 150\,\text{m}$ [4]. Link length and frequency are the two parameters which led to significant difference on worst month unavailability due to multipath. In fact, it is obvious that the unavailability increases as the distance increases.

But using the above parameters which represent the real case configuration of a given link, B-V model overestimates worst month unavailability for link length greater than 25 km as illustrated on the Figure 1 (d varying from 5 km to 90 km).

The same observation is valid for any operating frequency used between 7 GHz and 12 GHz. The simulation of Figure 2 is done with $d = 70\,\text{km}$.

A major drawback of B-V model is the choice of C factor which is somewhat subjective. ITU-R P. 530 model is more appropriate to design detailed links. Indeed, there is flexibility to adjust optimally K factor value in contrast to C factor value which is solely based on generic tables or maps.

2.2. Diversity Methods

The frequency diversity calculation for the two models is significantly identical. Only the space diversity gain, I_{sd} is studied first as a function of the gain difference between main and diversity antennas in the receiver side, and second as a function of these two antennas separation. Figures 3 and 4 show that B-V model is also overestimated regardless the system used, "baseband switching" and "IF combining" [5].

B-V baseband switching systems

$$I_{sd} = 1.2 \cdot 10^{-3} \cdot \frac{f}{d} S^2 v^2 10^{A/10} \tag{3}$$

B-V IF combining systems

$$I_{sd} = 1.2 \cdot 10^{-3} \cdot \frac{f}{d} S^2 \frac{16 \cdot v^2}{(1+v)^4} 10^{A/10} \tag{4}$$

where, S is the main and diversity antennas separation; $v \leq 1$ and $v_{\text{dB}} \leq 0$.

Typically the gain difference is $v_{\text{dB}} = -|G_1 - G_2|$.

ITU-R P. 530-12

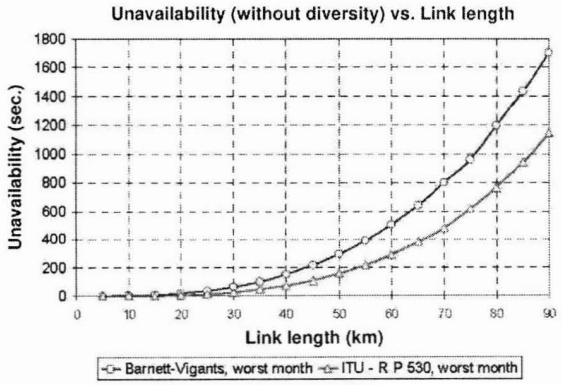

Figure 1: Worst month unavailability due to multipath as function of link length.

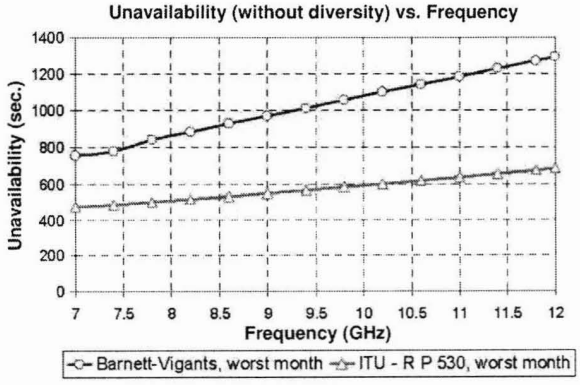

Figure 2: Worst month unavailability due to multipath as function of the operating frequency.

The diversity improvement is calculated differently for non selective and selective fading using radio signature method [2, 6]. The non selective outage probability with space diversity employs a basic formula given by $I_{sd} = I$:

$$I = \left[1 - \exp\left(-0.04 \times S^{0.87} f^{-0.12} d^{0.48} p_0^{-0.104}\right)\right] 10^{\left(\frac{A - |G_1 - G_2|}{10}\right)} \tag{5}$$

where, p_0 is the occurrence factor of multipath propagation.

If there is no propagation problem along the diversity path, it is recommendable to ensure that the gain difference is as small as possible, ideally $|G_1 - G_2| = 0\,\text{dB}$. Although the unavailability based on B-V model is higher compared to the ITU model, all the curves of Figures 3 and 4 follow the same trend. It is also noticeable that the space diversity gain increases very quickly in the B-V model while its variation is slow in the ITU model.

2.3. Conversion Methods for the Multipath Unavailability

For the unavailability due to multipath, the worst month value P_w is calculated first and then is converted to annual value P_{an} using one of the two following methods: mean annual temperature method (generally used in B-V model) and the conversion procedure described in ITU-R P. 530-12 [2, 7]. To show how the conversion method influences the annual value, we consider a typical link with the parameters defined previously. The following simulations are performed:

- Worst month unavailability is calculated by B-V model then converted to annual value using each of the two conversion methods.
- Worst month unavailability is calculated by the ITU model and converted into annual value also using each of the two conversion methods.

The simulation results are summarized in Table 1.

Depending on the conversion method, the annual unavailability values are completely different. But it seems to be more suitable to use ITU method because the formulation is only based on objective parameters such as length, inclination and latitude.

Table 1: Annual mean temperature method vs. ITU-R P. 530-12 method.

		Annual mean temperature	ITU-R P. 530 method
	Worst month unavailability	*Annual unavailability*	*Annual unavailability*
Barnett-Vigants	14.2 min.	30.7 min.	42.8 min.
ITU-R P. 530	13.9 min.	29.6 min.	42.07 min.

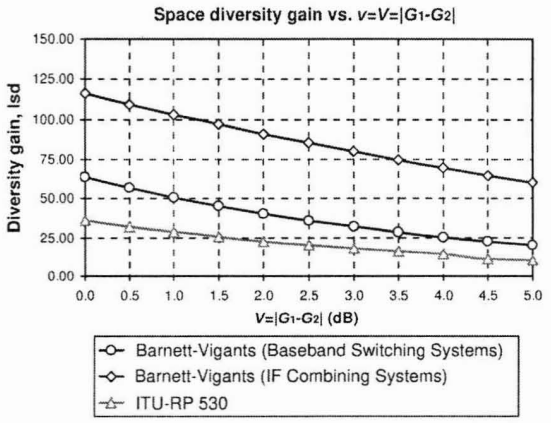

Figure 3: Space diversity gain as function of the gain difference between main and diversity antennas.

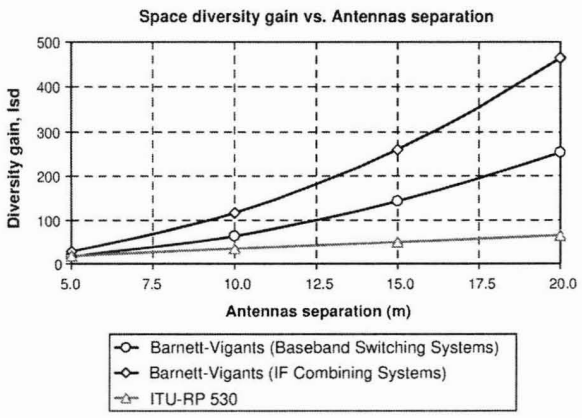

Figure 4: Space diversity gain as function of the main and diversity antennas separation.

2.4. Unavailability due to Rain

The commonly used method in B-V model to calculate the unavailability due to rain is the Crane method [8, 9]. The same calculation is made in ITU-R P. 530 model using the method described in ITU-R P. 838 recommendation [2, 10]. The rain regression coefficients (k and α defined as function of the frequency and the polarization) are essential. Although the two methods are different, the same coefficients are used.

For a given frequency (7.425 GHz), the annual unavailability due to rain increases with the link length. Figure 5 shows that:

- The vertical polarization is better than horizontal polarization for each method.
- For the link length more than 60 km, ITU method, especially in horizontal polarization will reduce the unavailability due to rain about ten seconds.

The unavailability due to rain is largely dependent on the operating frequency. Figure 6 shows that:

- The vertical polarization is better than the horizontal polarization for each method.
- Below 8 GHz and for horizontal polarization, the unavailability due to rain based on the ITU method is lower than the Crane method. Inversely, above 8 GHz, ITU method leads to much higher unavailability. Recall that this observation is valid for 50 km link length.

3. BARNETT-VIGANTS VS. ITU: OVERALL PERFORMANCE COMPARISON

We now present some main results using comparison table. Some main parameters used for simulation are summarized in Table 2. It is important to note that the ITU model includes radio signature method. In this case, we calculate separately the non-selective outage probability P_{ns}

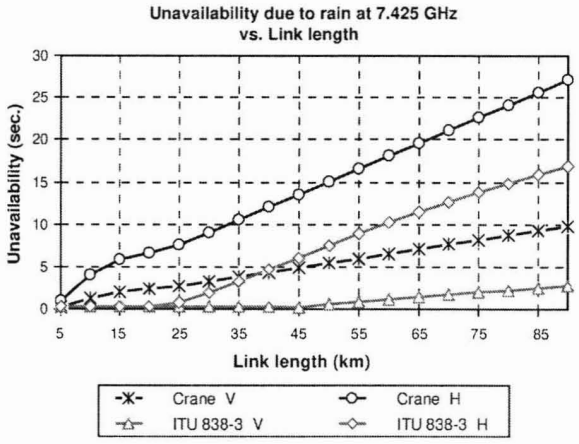

Figure 5: Annual unavailability due to rain as function of the link length.

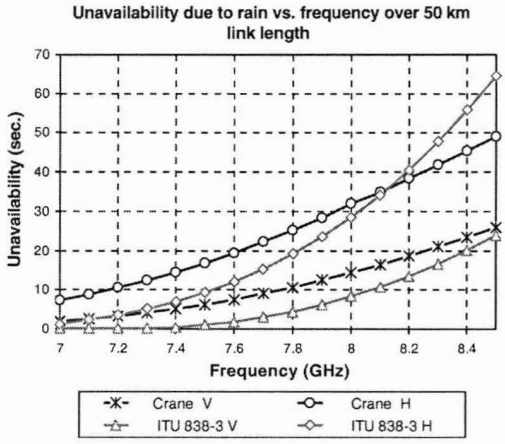

Figure 6: Annual unavailability due to rain as function of the operating frequency.

Table 2: Main parameters used for simulation.

Link	Link length (km)	Flat Fade Margin (dB)	Barnett-Vigants, C factor	ITU-R P. 530, K factor
1	70.00	41.52	0.25	1.24E-04
2	40.10	41.75	1.00	9.70E-05
3	22.30	40.66	3.29	1.55E-04
4	38.70	40.04	3.16	1.48E-04
5	60.30	43.63	0.25	1.11E-04
6	12.70	39.63	0.25	9.60E-05
7	82.30	45.93	0.52	1.41E-04
8	61.30	32.57	0.52	8.30E-05
9	70.10	41.19	0.25	1.06E-04

Table 3: Total bidirectional annual unavailability.

	Bidirectional annual unavailability with space and frequency diversity (sec.)		
Link	Barnett-Vigants, (Pathloss 4.0)	ITU-R P. 530-12 (MWLinkSim 1.0)	ITU improvement %
1	8.77	2.54	71.0%
2	5.15	0.81	84.3%
3*	6.42	6.64	−3.4%
4*	17.47	2.26	87.1%
5	2.20	0.57	74.1%
6	7.00	0.28	96.0%
7	1.28	3.12	−143.8%
8	352.39	43.58	87.6%
9	1.70	0.29	82.9%
The mean improvement % of ITU model over Barnett-Vigants model			48.4%

*ITU method is used without signature parameters

and the selective outage probability P_s. Then the two values are added together to obtain the total outage. The obtained results are also summarized in Table 3.

The analysis of overall performance in terms of worst month unavailability over the nine links shows clearly that the B-V model is oversized compared to the ITU model. This analysis confirms the results of step by step study made previously. The gain when the ITU model is used is rated at 50%.

4. CONCLUSION

The unavailability due to multipath and the unavailability due to rain are the two main phenomena we have studied in this paper. The results can be summarized as follows. The unavailability due to multipath is lower in the ITU model. In addition, the calculation procedure proposed by Recommendation ITU-R P. 530 provides extensive information on the criticality of the link and shows how some parameters affect microwave link design. For rain, the ITU model seems less severe for operating frequencies below 8 GHz while it is much more severe for frequencies above 8 GHz. In addition, the ITU model offers the possibility to take into account the combined effect of rain and wet snow (a phenomenon which may be interesting to consider in Quebec). The ongoing work is focused on in-situ measurements which will be compared to simulation results.

REFERENCES

1. Anderson, H. R., *Fixed Broadband Wireless System Design*, John Wiley & Sons, 2003.
2. International Telecommunication Union, "Propagation data and prediction methods required for the design of terrestrial line-of-sight systems," ITU-R P. 530-12, 2005.
3. Barnett, W. T., "Multipath propagation at 4, 6 and 11 GHz," *Bell System Technical Journal*, Vol. 51, No. 2, 311–361, Feb. 1972.
4. Agba, B. L., "Comparaison des modèles de propagation pour les liaisons hertziennes," IREQ-2008-0180 report, 2008.
5. Vigants, A., "Space-diversity engineering," *Bell System Technical Journal*, Vol. 54, No. 1, 103–142, Jan. 1975.
6. International Telecommunication Union, "Effects of multipath propagation on the design and operation of line-of-sight digital fixed wireless systems," ITU-R F-1093-2, 2006.
7. International Telecommunication Union, "Conversion of annual statistics to worst-month statistics," ITU-R P. 841-4, 2005.
8. Crane, R. K., "Prediction of attenuation by rain," *IEEE Transactions on Communications*, Vol. 28, No. 9, 1717–1732, Sep. 1980.
9. Crane, R. K., *Electromagnetic Wave Propagation through Rain*, John Wiley & Sons, New York, 1996.
10. International Telecommunication Union, "Specific attenuation model for rain for use in prediction methods," ITU-R P. 838-3, 2005.

13

REFLECTIONS AND OBSTRUCTIONS

A radio signal between a transmitter and a receiver usually travels through free space. However, radio transmitters employ practical antennas that emit significant energy in directions other than directly between the transmitter and the receiver. A radio signal traveling near the Earth can be subjected to a number of propagation obstacles. The most common is the earth's surface. The combined effect at the receive antenna of the direct signal and the signal reflected from the Earth can be important.

If the Earth is a smooth flat surface, the reflection from the Earth will appear at the receive antenna along with the direct signal. The interaction of those two signals will cause an increase or decrease in the received signal level that is dependent on the vertical placement of the receive (or transmit) antenna. That can be described as a series of secondary lobes superimposed on the antenna's normal propagation pattern (Fig. 13.1a) or as a variation in received signal level called *obstruction gain* (Fig. 13.1b). (F_1 is the first Fresnel zone defined below.) Figure 13.1b assumes perfect reflection from the obstruction. Obstruction gain is discussed at the end of this chapter.

The effect of the Earth on the radio signal reflected from the Earth is a combination of at least three factors: scattering, divergence, and reflection. The radio engineer must determine, on the basis of transmit and receive antenna patterns and surface conditions, whether not reflected energy is a significant factor. Many sources suggest evaluating only the reflecting earth surface within the first Fresnel zone (see the following). While this is generally accurate, there are cases where it is not true (Beckmann and Spizzichino, 1987). The areas close to the transmit and receive antennas are especially important but other reflective surfaces can be significant. Actual path examination by an experienced person is a practical approach.

13.1 THEORETICAL ROUGH EARTH REFLECTION COEFFICIENT

If the earth's surface is perfectly flat, the angle of the reflected signal is the same as the angle of the incident signal. Snell's law of optical reflection (the angle of incidence is equal to the angle of reflection) applies. The path is symmetric; the path traveled by the incident and reflected signal can be reversed (an incident signal following the original reflected signal's path will be reflected along the original incident signal's path). As the surface becomes rough, the situation begins to change (Rice, 1951). When the incident signal strikes the rough surface, some energy is directed at angles different than predicted by

Digital Microwave Communication: Engineering Point-to-Point Microwave Systems, First Edition. George Kizer.
© 2013 The Institute of Electrical and Electronics Engineers, Inc. Published 2013 by John Wiley & Sons, Inc.

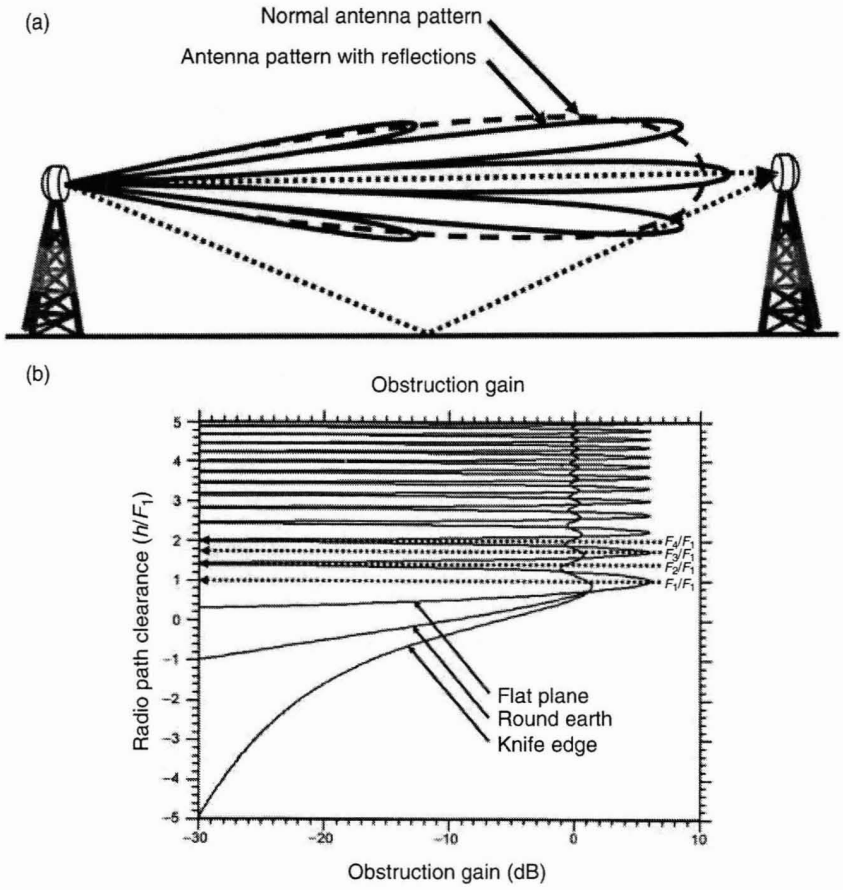

Figure 13.1 (a,b) Reflection lobes and obstruction gain.

Snell's law. As the roughness increases, the potential reflection point diffuses the incident signal and little directed energy is reflected. The potential reflection point is termed a *glistening area*. Under these conditions, path reflection symmetry is totally lost. All signals are diffused regardless of their direction of arrival. If the earth's surface is smooth, the reflected signal is coherent (specular). Scattered signal loss is negligible and the reflected signal power is only a function of divergence and reflection. The criterion for transition from rough to smooth reflection is not well defined. Various sources suggested coherent reflection occurs when surface height irregularities h are shorter than $\lambda/(8 \sin \phi)$ (Ishimaru, 1978; Long, 2001), or $\lambda/(16 \sin \phi)$ (Reed and Russell, 1953) where λ is the wavelength and ϕ is the grazing angle. The Rayleigh criterion, $\lambda/(8 \sin \phi)$, limits reflected path phase differences to no more than $\pi/2$. Landee et al. (1957) suggest that to maintain reflection magnitude within 1 dB of theoretical, parabolic and flat reflectors must maintain RMS surface error less than $\lambda/14$ and $\lambda/28$, respectively. As will be noted below, these commonly used criteria are misleading on microwave paths. Coherent reflection (at reduced levels) occurs for all degrees of terrain roughness (Fig. 13.3).

The energy reflected in the direction of a (coherent) specular reflected signal (a signal that obeys Snell's law of reflection) (Fig. 13.2) is determined by the reflection coefficient (ratio of coherent reflected power to incident power) for the surface. This coefficient is not a function of polarization.

Estimating scattered energy from rough surfaces is complicated (Bullington, 1954; Liao and Sarabandi, 2010; Norton, 1952; Rice, 1951). Accurate estimates of this scattered energy as a function of surface roughness are not known in general. However, limiting cases (Beckmann and Spizzichino, 1987; Boithias, 1987) for the reflection coefficient have been derived. If the surface is perfectly smooth, the

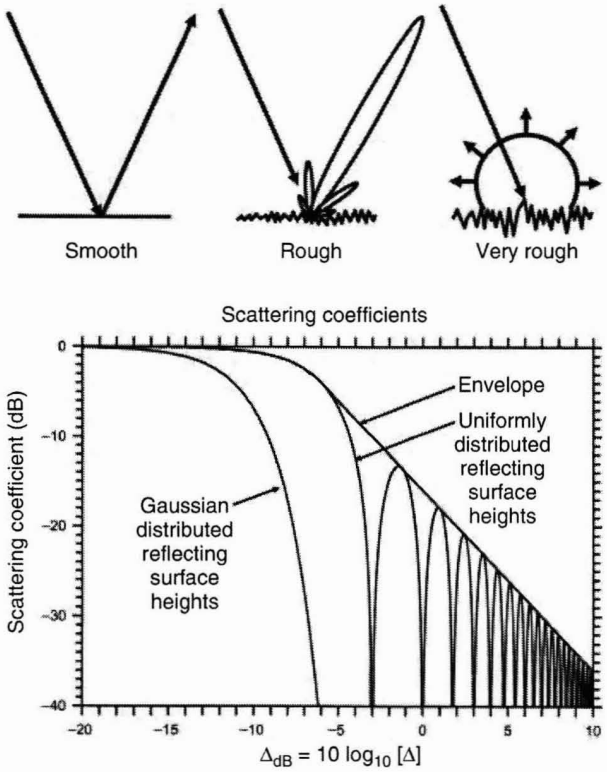

Figure 13.2 Effect of surface roughness and reflection coefficients.

reflection coefficient is 1 (0 dB). If the surface heights near the reflection can be characterized as a group of small areas with a Gaussian height distribution, the Gaussian model applies. If the surface heights near the reflection can be characterized as a group of small areas with a uniformly distributed heights, the uniform model applies.

$$\Delta = \Delta h \ \sin \frac{\phi}{\lambda} \cong 0.01745 \ \frac{\Delta h \ \phi(^\circ)}{\lambda} \quad \text{for small grazing angle } \phi$$

$$\text{since } \sin \phi \cong \phi(\text{rad}) \text{ within 10\% for } \phi \leq 0.785 \ (45^\circ) \text{ or 1\% for } \phi \leq 0.262 \ (15^\circ) \qquad (13.1)$$

Δ = effective surface height;
Δh = surface actual height;
ϕ = grazing angle;
λ = radio wave free space wavelength.

13.1.1 Gaussian Model

Beckmann and Spizzichino (1987) propose the following:

$$C_S \ (\text{dB}) = 10 \ \log \left(e^{-16\pi^2 \Delta^2}\right) = -685.810 \ \Delta^2 \qquad (13.2)$$

C_S (dB) = reflection (scattering) coefficient (dB);
Δh = standard deviation of the normal distribution of reflecting surface heights.

Boithias (1987) proposes the following:

$$C_S\,(\text{dB}) = 10\log\left[I_0\left(16\pi^2\Delta^2\right)\mathrm{e}^{16\pi^2\Delta^2}\right] \approx 5\log\left\{\frac{\left[1+\left(16\pi^2\Delta^2\right)\right]}{\left[1+2.35\left(16\pi^2\Delta^2\right)+2\pi\left(16\pi^2\Delta^2\right)^2\right]}\right\} \tag{13.3}$$

C_S (dB) = reflection coefficient (dB);
I_0 = modified Bessel function of the first kind of order zero.

13.1.2 Uniform Model

Beckmann and Spizzichino (1987) propose the following:

$$C_S\,(\text{dB}) = 10\log\frac{\left[\sin^2(2\pi\Delta)\right]}{(2\pi\Delta)^2} \tag{13.4}$$

C_S (dB) = reflection coefficient;
Δh = maximum difference of uniformly distributed reflecting surface heights.

$$\begin{aligned}\text{Reflection coefficient envelope (dB)} &= 20\log\frac{[\sin(2\pi\Delta)]}{(2\pi\Delta)},\ \Delta_{\text{dB}} \le -5.8\\ \text{Reflection coefficient envelope (dB)} &= -16.0-2\Delta_{\text{dB}},\ \Delta_{\text{dB}} > -5.8\\ \Delta_{\text{dB}} &= 10\log(\Delta)\end{aligned} \tag{13.5}$$

Note that Δh is based on difference in heights and not on absolute height.
In the above sources, the reflection coefficient is called a *scattering coefficient.*
Bullington (1954) noted that variations from complete randomness tend to fill in nulls predicted by theoretical calculations. Rice (1951) observed that mildly rough surface reflections were Rayleigh distributed. Liao and Sarabandi (2010) observed that these approximations were derived for roughness on the order of the radio wavelengths or smaller. They also do not account for the shadowing that occurs for very small grazing angles.

13.2 SCATTERING FROM EARTH TERRAIN

For more general cases, surface roughness can be characterized by the Rayleigh roughness parameter.

$$P = 4\pi\left(\frac{\sigma}{\lambda}\right)\sin\theta \tag{13.6}$$

P = Rayleigh roughness parameter;
= effective terrain roughness;
σ = RMS surface height (measured from crest to trough);
λ = radio wave free space wavelength;
θ = grazing angle of incident signal relative to the mean surface plane.

By convention, if $P \le \pi/2$, the surface is deemed smooth. If $P \ge 2\pi$, the surface is considered rough. The relative reflected signal level is defined by the terrain reflection coefficient.

R = reflection coefficient
= (voltage) amplitude of the reflected signal relative to the amplitude of the incident signal
$20 \log_{10} (R)$ = reflected signal power/incident signal power (dB).

With the exception of large bodies of water, actual earth terrain seldom conforms to any regular shape. The reflection coefficient R is related to the Rayleigh roughness parameter but the relationship is difficult to define. This relationship is usually assumed to conform approximately to one of the following models:

Exponential

$$R = \frac{1}{\left[1 + \left(\frac{P^2}{2}\right)\right]} \tag{13.7}$$

Pseudoexponential

$$R = \frac{1}{\left[1 + \left(\frac{2P^2}{3}\right)\right]^{(3/4)}} \tag{13.8}$$

Normal

$$R = \exp\left(\frac{-P^2}{2}\right) \tag{13.9}$$

$$\exp(x) = e^x$$

Longley–Rice Empirical

$$R = \exp\left(\frac{-P}{2}\right) \tag{13.10}$$

Weiner (1982) summarized the results of various researchers who measured scattering from actual terrain, terrain models, and the ocean. Weiner's data is summarized in Figure 13.3.

The normal model is commonly used in theoretical research papers. The Longley–Rice empirical model is often used in practical, irregular terrain estimations. However, on the basis of the Weiner data, the pseudoexponential model appears to most closely match experimental results. Regardless of the model used, the difference between the model prediction and actual results can be several decibels.

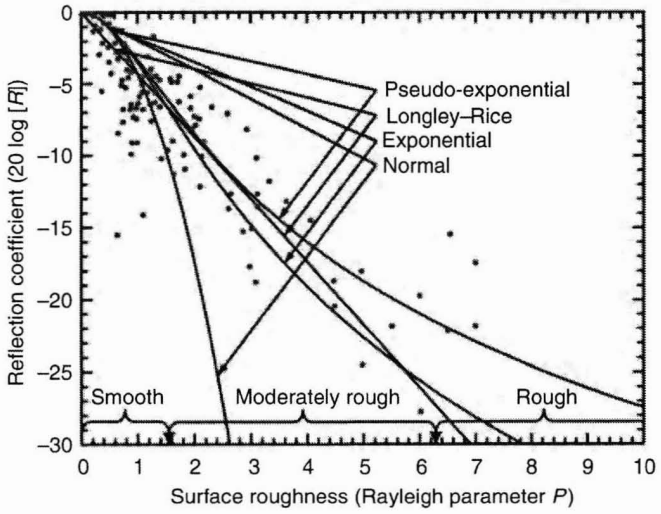

Figure 13.3 Coherent scattered signal power levels.

13.3 PRACTICAL EARTH REFLECTION COEFFICIENT

Flat terrain is highly reflective. As we shall see later in this chapter, all smooth terrain, whether dry dielectric or wet conductor, is reflective. Sometimes, potential reflections can be avoided by tilting one or both antennas (Hartman and Smith, 1977) (recognizing that this degrades CPD) or by placing antennas so that terrain, buildings, or trees block potential reflections. However, most practical situations do not permit a theoretical evaluation of the earth's reflection coefficient. Bullington (1954) observed "... that the antenna heights at which the maxima and minima occur [on a path in central Nebraska] varied with the time of day so no fixed combination could be optimum all of the time. Moreover, it was found that moving the tower only about 100 ft at one terminal reduced the reflection coefficient on this path from 0.72 (−3 dB) to about 0.55 (−5 dB), which indicates that the magnitude of the reflection coefficient cannot be predicted accurately from the gross features of the path profile."

Bullington (1954) continued, "A rigorous determination of the reflection from a rough surface is a difficult problem. In fact, it is virtually impossible except for certain idealized profiles. In general, it is not possible to represent an actual profile by a reasonable number of parameters. Considerable judgment is required in formulating the problem and the end result may be no more than a range of possible answers." This situation was addressed by Laine (1978). He related reflection coefficient to typical earth surface types. Table 14.1 is adapted from his Table 1.

In Table 14.1, the reflection coefficient (E_R/E_S) is the ratio of the reflected signal RMS voltage divided by the normal signal RMS voltage. The signal-to-reflection power is normal signal power (dBm) minus reflected signal power (dBm). The maximum upfade column shows the maximum increase in normal received signal level that can be caused by the level of reflection shown on that line. The maximum downfade column shows the minimum decrease in normal received signal level that can be caused by the level of reflection shown on that line. Note that if the reflected signal is at least 1 dB less than the desired signal, the worst-case downfade is −20 dB. If the reflected signal is 3 dB less than the desired signal, the worst-case downfade is less than −10 dB. If the reflected signal is −20 dB, the downfade will be an insignificant 1 dB.

The objective of the path designer is to recognize the cases where reflections are likely and attempt to reduce (using terrain or antenna discrimination) the reflection power to less than 20 dB of the desired signal at the receive antenna. (If the reflection is stronger, the anticipated free space loss will not be achieved.)

In addition to the surfaces listed in Table 13.1, there are invisible reflective surfaces that sometimes occur. Plants (such as wheat and pine trees) and agricultural area (such as rice paddies and irrigated fields) put out significant moisture that can form an invisible reflective surface when the air is quiet.

For mountaintop-to-mountaintop paths, invisible layers are almost always present over quiet valleys. These layers, if not anticipated, can cause significant reflective fading. As the layers are many Fresnel zones below the main signal path, they are difficult to combat with space diversity. An effective method of reducing their effect is to move the mountaintop antennas far back from the edge of the site, so potential illumination of the layers is blocked.

13.4 REFLECTION LOCATION

If the terrain is relatively smooth, potential reflections must be considered. The location of a reflection on a smooth earth was derived by Boithias (1987) (Fig. 13.4).

$$h_1 \geq h_2$$

h_1 = physical height of the antenna at one end of the path *above the reflection point physical height*;
h_2 = physical height of the antenna at the other end of the path *above the reflection point physical height*.

$$D = d_1 + d_2$$

TABLE 13.1 Lane's Practical Earth Reflection Coefficients

Type of Terrain	Reflection Coefficient (E_R/E_S)	Signal-to-Reflection Power, dB	Maximum Upfade, dB	Maximum Downfade, dB
Smooth Water or	−1.00	0.0	6.0	−∞
Salt Flat or	−0.99	0.1	6.0	−40
Desert	−0.98	0.2	5.9	−34
	−0.97	0.3	5.9	−30.5
	−0.95	0.4	5.8	−26.0
	−0.93	0.6	5.7	−23.1
	−0.91	0.8	5.6	−20.9
Rough Water or	−0.89	1.0	5.5	−19.2
Cotton or	−0.84	1.5	5.3	−15.9
Low Grass	−0.79	2.0	5.1	−13.6
	−0.75	2.5	4.9	−12.0
	−0.71	3.0	4.7	−10.8
Sagebrush or	−0.63	4.0	4.2	−8.6
High Grass	−0.50	6.0	3.5	−6.0
Partially Wooded	−0.40	8.0	2.9	−4.4
	−0.32	10.0	2.4	−3.3
	−0.24	12.0	1.9	−2.4
	−0.20	14.0	1.6	−1.9
	−0.16	16.0	1.3	−1.5
	−0.13	18.0	1.1	−1.2
Heavily Wooded	−0.10	20.0	0.8	−0.9
Forest	−0.05	26.0	0.4	−0.4
	−0.01	40.0	0.1	−0.1

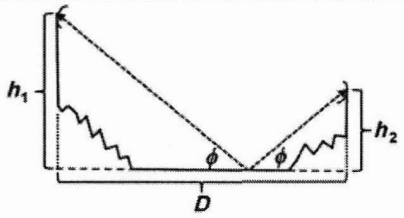

$h_1 \geq h_2$

Figure 13.4 Flat earth path profile reflection geometry (flat earth, $K = \infty$).

D = distance from one end of the path to the other end;
= total path distance;
d_1 = distance from one end of the path to the reflection point;
d_2 = distance from the other end of the path to the reflection point;
B = normalized distance from the center of the path to the reflection point (−1 to 1).

$$C = \frac{(h_1 - h_2)}{(h_1 + h_2)} \geq 0$$

$$M = \frac{D^2}{[4Ka(h_1 + h_2)]}$$

$$d_1 = \left(\frac{D}{2}\right)(1 + B)$$

$$d_2 = D - d_1$$

K = equivalent earth radius factor;
a = physical earth radius $\cong$ 6367 km $\cong$ 3957 (statute) miles.

All the above equations are in the same units of distance. B (reflection location factor) is the solution to the following equation:

$$BM^3 - BM - B + C = 0 \tag{13.11}$$

For ducting conditions ($K \leq 0$), three solutions exist (two near the ends of the path and one near the center). For normal conditions ($K > 0$), only the following solution exists:

$$B = 2\sqrt{\frac{M+1}{3M}}\cos\left\{\left(\frac{\pi}{3}\right) + \left[\frac{1}{3}\text{Arc}\cos\left(\frac{3C}{2}\sqrt{\frac{3M}{(M+1)^3}}\right)\right]\right\} \tag{13.12}$$

$$\phi\,(\text{rad}) = \left[\frac{(h_1 + h_2)}{D}\right]\left[1 - M\left(1 + B^2\right)\right]$$

Boithias's flat earth results apply to overwater paths and paths in dessert terrain where the earth is flat. However, in most other cases, the terrain near the reflection point is inclined relative to the surface of a smooth earth. Boithias's flat earth results can be extended to this case by conceptually rotating the terrain, so the reflecting plane becomes parallel to the Earth. This allows B and ϕ to be calculated using Boithias's formulas. However, for the geometry to be correct, the antenna heights must be adjusted so that they are measured relative to the extension of the flat surface that has been conceptually rotated to be parallel to the earth's surface (Fig. 13.5).

For small angles and short distances (relative to the earth's radius), the flat, inclined terrain case could be rotated (in the vertical plane in line with the path) so as to be congruent to the flat earth case if h_1 and h_2 are redefined as follows:

h_1 = physical height of the antenna at one end of the path *above the extended flat terrain physical height*;
h_2 = physical height of the antenna at the other end of the path *above the extended flat terrain physical height*.

With these h_1 and h_2 redefinitions, the flat terrain reflection results apply to the Boithias flat, inclined terrain case.

As the path profile will have flat terrains of varying sizes, the obvious question is, "What is the minimum size of flat terrain that will produce a significant reflection?" Assume a reflected radio path where we are only concerned with the energy contained within a perpendicular radius (h/F_1) of the main reflected path. F_1 is the first Fresnel zone radius (See the end of this chapter for an explanation of Fresnel zones.) and h is a number yet to be determined. Norton (1952) observed that "... only the curvature of the reflecting surface in the plane of propagation will appreciably influence the intensity of the ground-reflected wave, and we need not even investigate the surface curvature normal to the propagation path."

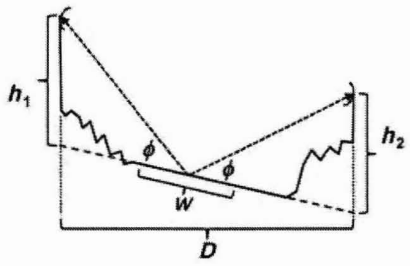

Figure 13.5 Smooth inclined earth path profile reflection geometry (flat earth, $K = \infty$).

In other words, we are only concerned with the energy that would be reflected by the terrain within an ellipse with relatively small off-axis (normal to direction of propagation) total width of 2 (h/F_1) and potentially large on-path (in line with the direction of propagation) total width of $W = 2\left[\left(h/F_1\right)/\sin\phi\right]$, where ϕ is the radio path (launch) angle relative to the flat earth. The reflected path energy contained within the (h/F_1) radius was calculated by Hristov (2000). He showed that if $h \approx 1/2$ the reflected energy is the same as for h infinitely large (full earth reflecting surface). For $h > 1/2$, the power varies up and down but eventually converges to the $h \approx 1/2$ value. Like Norton, Hristov also observed that for an inclined surface, the Fresnel zone radius is stretched along the radio path. From this, we may infer that the minimum flat terrain on path width that has potential for significant effect would be on the order of at least $W = 2[(1/2)(F_1 \sin\phi)] = F_1/\sin\phi$. This essentially indicates that the significant energy in the radio wave is contained within one Fresnel zone of the ray between the transmitter and the receiver. (This region is often called the *Fresnel volume* in other technologies such as seismic imaging and sonar detection.)

Hristov's calculations showed that energy from the area greater than approximately the first Fresnel zone's projection onto the Earth is not significant for uniform terrain. He derived the projected dimensions of the Fresnel zone onto a flat earth ((Hristov, 2000), Eqs. 3.13 and 3.14). They simplify to the following:

$$L_n = \frac{d\sqrt{1 + \frac{(4h_1h_2)}{(n\lambda d)}}}{1 + \frac{(h_1+h_2)^2}{(n\lambda d)}} \tag{13.13}$$

L_n = projected length of Fresnel zone projected onto the smooth earth in the direction of the radio path = 2 (semimajor axis) = $2a_n$ as per the book by Hristov (2000).

$$W_n = \frac{\sqrt{1 + \frac{(4h_1h_2)}{(n\lambda d)}}}{\sqrt{1 + \frac{(h_1+h_2)^2}{(n\lambda d)}}} \tag{13.14}$$

W_n = projected width of Fresnel zone projected onto the smooth earth in the direction of the radio path = 2(semiminor axis) = $2b_n$ as per the book by Hristov (2000);
n = Fresnel zone integer designation (1 for first Fresnel zone);
d = path length between transmitter and receiver;
$\approx d_o + (n\lambda/2) \approx d_o + (1/4)$ as per the book by Hristov (2000);
h_1 = transmit antenna height above reflection point height;
h_2 = receive antenna height above reflection point height;
λ = radio wavelength;
λ(ft) = 0.98357/F (GHz);
λ(m) = 0.29980/F (GHz);
F = radio operating frequency.

D, h_1, h_2, and λ are all in the same distance units.

13.5 SMOOTH EARTH DIVERGENCE FACTOR

The divergence factor accounts for the power divergence of the signal reflected by a round surface (assuming perfect reflection). This coefficient is not a function of polarization and is only significant for small grazing angles. The factor is given by the following formulas (Hall, 1979; Kizer, 1990) for reflection from a smooth earth:

$$C_D = \text{sqrt}\left\{1 + \frac{(2d_1d_2)}{(K\,r\,d\,\sin(\phi))}\right\} \tag{13.15}$$

C_D = reflection coefficient (voltage ratio);
= Abs (reflected signal magnitude/incident signal magnitude);
ϕ = grazing angle at reflection = angle of incidence = angle of reflection;
d_1 = distance from one end of the path to the location of interest;
d_2 = distance from the other end of the path to the location of interest;
$d = d_1 + d_2$;
R_e = earth's equatorial radius = 6378 km = 3963 miles;
R_p = earth's polar radius = 6357 km = 3950 miles;
E^2 = Eccentricity^2 = $(R_e{}^2 - R_p{}^2)/R_e{}^2$;
ψ = latitude at reflection point;
r = Earth's radius at reflection point = R_p/sqrt[1 − (E^2 cos ψ)];
K = equivalent earth radius factor (typically 4/3);
C_D(dB) = 20 log [C_D (voltage ratio)];
$\phi(^\circ) = (\frac{180}{\pi})\phi$(rad).

The above formula, based on optical analogy, was derived by Kerr (1951). For small ϕ, the above divergence factor formula will significantly overestimate reflection loss. Long (2001) suggests that the formula is accurate as long as the difference between the main and reflected signal exceeds $\lambda/4$. This is equivalent to requiring the path to have a minimum first Fresnel zone clearance (h/F_1) of [1/sqrt(2)] where h is the path height above the reflection point, F_1 is the first Fresnel zone height (for the definition of F_1, see below), and sqrt is square root]. Conventional fixed microwave line-of-sight radio path design limits the minimum path clearance (above the Earth) to approximately this value.

Although this formula is commonly available in path calculation programs, in many practical cases, it overestimates reflection path loss (primarily because of path blockage and roughness). Actual microwave paths are rarely smooth reflective surfaces. The use of this formula is only recommended for line-of-sight microwave paths over water or flat terrain.

13.6 REFLECTIONS FROM OBJECTS NEAR A PATH

One of the tasks of the path designer is to determine potential reflections or obstructions along the path between the transmit and receive antennas. Potentially reflecting surfaces on buildings and water towers are fairly common. As buildings are usually composed of flat surfaces, treating them as passive reflectors is relatively easy. However, structures with more complex shapes are much more difficult to analyze.

In theory, if the structure is in the far field of both antennas and is smaller than the first Fresnel zone, it will be uniformly illuminated (in amplitude and phase) by the transmit antenna (If the structure is larger across than the first Fresnel zone, the illumination will have a significant phase change across the surface of the structure and the reflection loss will be greater than calculated by the following method.). "All" that needs to be done is to integrate the E field across the structure accounting for the reflected ray phase change at each point on the surface of the structure, divide the result by the structure area, and take 20 times the common logarithm of the result. This is generally easier said than done.

However, for simple structures this is practical. If a surface is flat, the two-way (reception and retransmission) gain is the following:

$$\text{Two-way flat reflector gain (dB)} = 22.2 + 40 \log F(\text{GHz}) + 20 \log A(\text{ft}^2) + 20 \log \cos\left(\frac{C}{2}\right) \quad (13.16)$$

$$42.9 + 40 \log F(\text{GHz}) + 20 \log A(\text{m}^2) + 20 \log \cos\left(\frac{C}{2}\right)$$

F = frequency of radio wave;
A = reflector area;

C = angle between incoming and outgoing radio signal paths.

If the surface is a simple cylinder or sphere, we can, in principle, calculate the divergence factor to account for the curvature of the object's surface. The object's reflective gain would be the following:

$$\text{Two-way flat reflector gain (dB)} = \text{Two-way flat reflector gain (dB)} + \text{divergence factor (dB)} \quad (13.17)$$

Assume a circular cylinder with normalized radius of R_n = cylinder radius/λ (wavelength). The height of the cylinder is unimportant from a divergence perspective; only its radius of curvature is significant. The divergence factor can be simplified to the following integral:

$$\text{Cylinder divergence factor} = 20 \log \left\{ \int_0^{+1} \cos \left[2\pi \left(2 R_n \sqrt{(1 - x^2)} \right) dx \right] \right\} \quad (13.18)$$

Assume a circular sphere with normalized radius of R_n = sphere's radius/λ (wavelength). The divergence factor can be simplified to the following integral:

$$\text{Sphere divergence factor} = 20 \log \left\{ \int_0^{+1} r \cos \left[2\pi \left(2 R_n \sqrt{(1 - r^2)} \right) dr \right] \right\} \quad (13.19)$$

Both of these integrals are difficult to integrate formally. Likewise, numerical integration is challenging because of the rapid oscillation of the cosine term for large values of R_n. The cylinder divergence factor integral was numerically integrated. The results were a smooth curve that, when curve fitted, resulted in the following equation:

$$\text{Cylinder divergence factor (dB)} = -12 - 10 \log (R_n) \quad (13.20)$$

$$R_n = \frac{\text{cylinder's radius}}{\lambda} \text{ (wavelength)}$$

$$= 1.017 \text{ cylinder's radius (ft) } f \text{ (GHz)}$$

$$= 3.336 \text{ cylinder's radius (m) } f \text{ (GHz)}$$

f = operating frequency

The spherical divergence factor integral was numerically integrated. The results varied widely depending on R_n. If R_n was an integer or an integer plus 1/2, the divergence factor was $-\infty$. If R_n was an integer plus 1/4, a peak value was calculated. If R_n was an integer plus 3/4, a near-peak value was calculated. If we limit the results to just the peak values when R_n was an integer plus 1/4, a smooth curve was generated. Curve-fitting this curve resulted in the following equation:

$$\text{Sphere divergence factor (dB)} = -32 - 40 \log (R_n) \quad (13.21)$$

$$R_n = \frac{\text{sphere's radius}}{\lambda} \text{ (wavelength)}$$

$$= 1.017 \text{ cylinder's radius (ft) } f \text{ (GHz)}$$

$$= 3.336 \text{ cylinder's radius (m) } f \text{ (GHz)}$$

f = operating fequency

These results are graphed in Figure 13.6.